RETINAL DEGENERATION AND THERAPY APPROACHES

EDITED BY: Nicolás Cuenca, Ayse Sahaboglu, Javier Sancho-Pelluz, Jacqueline Reinhard and Miguel Flores-Bellver

PUBLISHED IN: Frontiers in Neuroscience and Frontiers in Immunology

frontiers Research Topics

frontiers

Frontiers eBook Copyright Statement

The copyright in the text of individual articles in this eBook is the property of their respective authors or their respective institutions or funders. The copyright in graphics and images within each article may be subject to copyright of other parties. In both cases this is subject to a license granted to Frontiers.

The compilation of articles constituting this eBook is the property of Frontiers.

Each article within this eBook, and the eBook itself, are published under the most recent version of the Creative Commons CC-BY licence. The version current at the date of publication of this eBook is CC-BY 4.0. If the CC-BY licence is updated, the licence granted by Frontiers is automatically updated to the new version.

When exercising any right under the CC-BY licence, Frontiers must be attributed as the original publisher of the article or eBook, as applicable.

Authors have the responsibility of ensuring that any graphics or other materials which are the property of others may be included in the CC-BY licence, but this should be checked before relying on the CC-BY licence to reproduce those materials. Any copyright notices relating to those materials must be complied with.

Copyright and source acknowledgement notices may not be removed and must be displayed in any copy, derivative work or partial copy which includes the elements in question.

All copyright, and all rights therein, are protected by national and international copyright laws. The above represents a summary only. For further information please read Frontiers' Conditions for Website Use and Copyright Statement, and the applicable CC-BY licence.

ISSN 1664-8714
ISBN 978-2-88974-954-6
DOI 10.3389/978-2-88974-954-6

About Frontiers

Frontiers is more than just an open-access publisher of scholarly articles: it is a pioneering approach to the world of academia, radically improving the way scholarly research is managed. The grand vision of Frontiers is a world where all people have an equal opportunity to seek, share and generate knowledge. Frontiers provides immediate and permanent online open access to all its publications, but this alone is not enough to realize our grand goals.

Frontiers Journal Series

The Frontiers Journal Series is a multi-tier and interdisciplinary set of open-access, online journals, promising a paradigm shift from the current review, selection and dissemination processes in academic publishing. All Frontiers journals are driven by researchers for researchers; therefore, they constitute a service to the scholarly community. At the same time, the Frontiers Journal Series operates on a revolutionary invention, the tiered publishing system, initially addressing specific communities of scholars, and gradually climbing up to broader public understanding, thus serving the interests of the lay society, too.

Dedication to Quality

Each Frontiers article is a landmark of the highest quality, thanks to genuinely collaborative interactions between authors and review editors, who include some of the world's best academicians. Research must be certified by peers before entering a stream of knowledge that may eventually reach the public - and shape society; therefore, Frontiers only applies the most rigorous and unbiased reviews.
Frontiers revolutionizes research publishing by freely delivering the most outstanding research, evaluated with no bias from both the academic and social point of view. By applying the most advanced information technologies, Frontiers is catapulting scholarly publishing into a new generation.

What are Frontiers Research Topics?

Frontiers Research Topics are very popular trademarks of the Frontiers Journals Series: they are collections of at least ten articles, all centered on a particular subject. With their unique mix of varied contributions from Original Research to Review Articles, Frontiers Research Topics unify the most influential researchers, the latest key findings and historical advances in a hot research area! Find out more on how to host your own Frontiers Research Topic or contribute to one as an author by contacting the Frontiers Editorial Office: frontiersin.org/about/contact

RETINAL DEGENERATION AND THERAPY APPROACHES

Topic Editors:
Nicolás Cuenca, University of Alicante, Spain
Ayse Sahaboglu, University of Tübingen, Germany
Javier Sancho-Pelluz, Catholic University of Valencia San Vicente Mártir, Spain
Jacqueline Reinhard, Ruhr-University, Germany
Miguel Flores-Bellver, University of Colorado Anschutz Medical Campus, United States

Citation: Cuenca, N., Sahaboglu, A., Sancho-Pelluz, J., Reinhard, J., Flores-Bellver, M., eds. (2022). Retinal Degeneration and Therapy Approaches. Lausanne: Frontiers Media SA. doi: 10.3389/978-2-88974-954-6

Table of Contents

05 ***Non-photoreceptor Expression of* Tulp1 *May Contribute to Extensive Retinal Degeneration in* Tulp1-/- *Mice***
Arpad Palfi, Adlet Yesmambetov, Pete Humphries, Karsten Hokamp and G. Jane Farrar

22 ***Foveal Therapy in Blue Cone Monochromacy: Predictions of Visual Potential From Artificial Intelligence***
Alexander Sumaroka, Artur V. Cideciyan, Rebecca Sheplock, Vivian Wu, Susanne Kohl, Bernd Wissinger and Samuel G. Jacobson

33 ***Research Models and Gene Augmentation Therapy for* CRB1 *Retinal Dystrophies***
Nanda Boon, Jan Wijnholds and Lucie P. Pellissier

46 ***Novel Therapeutic Approaches for the Treatment of Retinal Degenerative Diseases: Focus on CRISPR/Cas-Based Gene Editing***
Carmen Gallego, Manuel A. F. V. Gonçalves and Jan Wijnholds

61 ***Cerebral Modifications and Visual Pathway Reorganization in Maculopathy: A Systematic Review***
Raffaele Nuzzi, Laura Dallorto and Alessio Vitale

80 ***Mutation-Independent Therapies for Retinal Diseases: Focus on Gene-Based Approaches***
Sabrina Carrella, Alessia Indrieri, Brunella Franco and Sandro Banfi

88 ***Amyotrophic Lateral Sclerosis: A Neurodegenerative Motor Neuron Disease With Ocular Involvement***
Pilar Rojas, Ana I. Ramírez, José A. Fernández-Albarral, Inés López-Cuenca, Elena Salobrar-García, Manuel Cadena, Lorena Elvira-Hurtado, Juan J. Salazar, Rosa de Hoz and José M. Ramírez

104 ***Novel Porcine Retina Cultivation Techniques Provide Improved Photoreceptor Preservation***
Natalie Wagner, Sabrina Reinehr, Maurice R. Gammel, Andrea Greulich, José Hurst, H. Burkhard Dick, Sven Schnichels and Stephanie C. Joachim

119 ***Photoreceptor Degeneration in Pro23His Transgenic Rats (Line 3) Involves Autophagic and Necroptotic Mechanisms***
Kiana Kakavand, Andrew I. Jobling, Ursula Greferath, Kirstan A. Vessey, Robb U. de Iongh and Erica L. Fletcher

138 ***Optogenetic Gene Therapy for the Degenerate Retina: Recent Advances***
Michelle E. McClements, Federica Staurenghi, Robert E. MacLaren and Jasmina Cehajic-Kapetanovic

155 ***Organ Cultures for Retinal Diseases***
José Hurst, Agnes Fietz, Teresa Tsai, Stephanie C. Joachim and Sven Schnichels

163 ***Commentary: Organ Cultures for Retinal Diseases***
Stephen R. Mut and Maribel Vazquez

166 ***Optimized OPA1 Isoforms 1 and 7 Provide Therapeutic Benefit in Models of Mitochondrial Dysfunction***
Daniel M. Maloney, Naomi Chadderton, Sophia Millington-Ward, Arpad Palfi, Ciara Shortall, James J. O'Byrne, Lorraine Cassidy, David Keegan, Peter Humphries, Paul Kenna and Gwyneth Jane Farrar

185 ***An* in vitro *Model of Human Retinal Detachment Reveals Successive Death Pathway Activations***
Jelena Potic, Martial Mbefo, Adeline Berger, Michael Nicolas, Dana Wanner, Corinne Kostic, Alexandre Matet, Francine Behar-Cohen, Alexandre Moulin and Yvan Arsenijevic

195 ***Degeneration-Dependent Retinal Remodeling: Looking for the Molecular Trigger***
Michael Telias, Scott Nawy and Richard H. Kramer

202 ***Gene Therapy to the Retina and the Cochlea***
Ryan Crane, Shannon M. Conley, Muayyad R. Al-Ubaidi and Muna I. Naash

220 ***Functional 3-Dimensional Retinal Organoids:* Technological Progress *and Existing Challenges***
Meimanat Fathi, Cody T. Ross and Zohreh Hosseinzadeh

229 ***Mutant PRPF8 Causes Widespread Splicing Changes in Spliceosome Components in Retinitis Pigmentosa Patient iPSC-Derived RPE Cells***
Ángeles Arzalluz-Luque, Jose Luis Cabrera, Heli Skottman, Alberto Benguria, Arantxa Bolinches-Amorós, Nicolás Cuenca, Vincenzo Lupo, Ana Dopazo, Sonia Tarazona, Bárbara Delás, Miguel Carballo, Beatriz Pascual, Imma Hernan, Slaven Erceg and Dunja Lukovic

245 ***Immunologic Rejection of Transplanted Retinal Pigmented Epithelium: Mechanisms and Strategies for Prevention***
Carson C. Petrash, Alan G. Palestine and M. Valeria Canto-Soler

257 ***Knock-Out of Tenascin-C Ameliorates Ischemia-Induced Rod-Photoreceptor Degeneration and Retinal Dysfunction***
Susanne Wiemann, Aisha Yousf, Stephanie C. Joachim, Carolin Peters, Ana M. Mueller-Buehl, Natalie Wagner and Jacqueline Reinhard

277 ***Effects of Hydrostatic Pressure on Electrical Retinal Activity in a Multielectrode Array-Based* ex vivo *Glaucoma Acute Model***
Claudia Ingensiep, Kim Schaffrath, Peter Walter and Sandra Johnen

frontiers in Neuroscience

ORIGINAL RESEARCH
published: 23 June 2020
doi: 10.3389/fnins.2020.00656

Non-photoreceptor Expression of *Tulp1* May Contribute to Extensive Retinal Degeneration in *Tulp1-/-* Mice

Arpad Palfi†, Adlet Yesmambetov†, Pete Humphries, Karsten Hokamp and G. Jane Farrar*

Department of Genetics, Trinity College Dublin, Dublin, Ireland

Mutations in tubby like protein 1 gene (*TULP1*) are causative of early-onset recessive inherited retinal degenerations (IRDs); similarly, the *Tulp1-/-* mouse is also characterized by a rapid IRD. *Tulp1* mRNA and protein expression was analyzed in wild type mouse retinas and expression data sets (NCBI) during early postnatal development. Comparative histology was undertaken in *Tulp1-/-*, rhodopsin-/- (*Rho-/-*) and retinal degeneration slow-/- (*Rds-/-*) mouse retinas. Bioinformatic analysis of predicted TULP1 interactors and IRD genes was performed. Peak expression of *Tulp1* in healthy mouse retinas was detected at p8; of note, TULP1 was detected in both the outer and inner retina. Bioinformatic analysis indicated *Tulp1* expression in retinal progenitor, photoreceptor and non-photoreceptor cells. While common features of photoreceptor degeneration were detected in *Tulp1-/-*, *Rho-/-*, and *Rds-/-* retinas, other alterations in bipolar, amacrine and ganglion cells were specific to *Tulp1-/-* mice. Additionally, predicted TULP1 interactors differed in various retinal cell types and new functions for TULP1 were suggested. A pilot bioinformatic analysis indicated that in a similar fashion to *Tulp1*, many other IRD genes were expressed in both inner and outer retinal cells at p4–p7. Our data indicate that expression of *Tulp1* extends to multiple retinal cell types; lack of TULP1 may lead to primary degeneration not only of photoreceptor but also non-photoreceptor cells. Predicted interactors suggest widespread retinal functions for TULP1. Early and widespread expression of TULP1 and some other IRD genes in both the inner and outer retina highlights potential hurdles in the development of treatments for these IRDs.

Keywords: retina, degeneration, mouse model, inherited, *Tulp1*, disease, blindness, eye

OPEN ACCESS

Edited by:
Ayse Sahaboglu, University of Tübingen, Germany

Reviewed by:
Oleg Gorbatyuk, The University of Alabama at Birmingham, United States
Michael B. Powner, City, University of London, United Kingdom

****Correspondence:***
Arpad Palfi
palfia@tcd.ie

† These authors have contributed equally to this work

Specialty section:
This article was submitted to Neurodegeneration, a section of the journal Frontiers in Neuroscience

Received: *14 April 2020*
Accepted: *27 May 2020*
Published: *23 June 2020*

Citation:
Palfi A, Yesmambetov A, Humphries P, Hokamp K and Farrar GJ (2020) Non-photoreceptor Expression of Tulp1 May Contribute to Extensive Retinal Degeneration in Tulp1-/- Mice. Front. Neurosci. 14:656. doi: 10.3389/fnins.2020.00656

INTRODUCTION

Mutation in over 300 genes have been identified as causative of inherited retinal degenerations (IRDs) (Duncan et al., 2018; RetNet - Retinal Information Network, 2019) affecting 1 in 3000, or more than 2 million people worldwide (Sahel et al., 2015; Farrar et al., 2017). The impact of IRDs on vision ranges from mild impairment to complete blindness; IRDs represent a significant economic and social burden including devastating psychological and quality-of-life impacts on patients and families (Smith et al., 2015; Retina International, 2019).

Mutations in tubby like protein 1 gene (*TULP1*) are causative of rare, early onset, severe forms of autosomal recessive retinal degeneration, usually diagnosed as Leber congenital amaurosis 15 (LCA15) or retinitis pigmentosa 14 (RP14) (RetNet - Retinal Information Network, 2019). TULP1 is highly specific to photoreceptors in the mouse retina (Hagstrom et al., 1999; Xi et al., 2005; Grossman et al., 2009), although lower levels of TULP1 have been detected in ganglion and progenitor cells in human retinas (Milam et al., 2000). To enhance understanding of *TULP1*-linked IRDs, *Tulp1-/-* mice were generated (Hagstrom et al., 1999; Ikeda et al., 2000). *Tulp1-/-* mice exhibit an early and severe retinal degeneration akin to the human condition; shortening of photoreceptor segments and swollen extruded mitochondria by postnatal day (p)14 (Ikeda et al., 2000); abnormal ribbon synaptic architecture by p13–p16 (Grossman et al., 2009); shortening of bipolar cell dendrites with less branching and compromised b-wave electroretinogram (ERG) by p16 (Grossman et al., 2009); reduced rod and cone ERGs by week 4 (Hagstrom et al., 1999; Ikeda et al., 2000); photoreceptor apoptosis from p18 (Ikeda et al., 2000) resulting in complete loss of the outer nuclear layer (ONL) by week 20 (Hagstrom et al., 1999; Ikeda et al., 2000).

The function of TULP1 has not been clearly established. In photoreceptors, TULP1 is colocalized with f-actin in the inner segments (Xi et al., 2005), where it may be engaged in trafficking of proteins such as rhodopsin (RHO) and cone opsins between the inner and outer segments (Grossman et al., 2011; Hagstrom et al., 2012). TULP1 is also required for normal development of photoreceptor synapses and survival of photoreceptor cells (Grossman et al., 2009). TULP1 interacts with the synaptic ribbon protein (RIBEYE) and mediates localization of the endocytic machinery at the periactive zone of photoreceptor synapses (Wahl et al., 2016). Direct interaction between dynamin-1 (DNM1) and TULP1 highlights the role of TULP1 in synaptic vesicular transport (Xi et al., 2007) (Grossman et al., 2013). TULP1 also interacts with the microtubule associated protein 1b (MAP1B) (Grossman et al., 2014). Additionally, TULP1 is a ligand for MER proto-oncogene tyrosine kinase (MERTK) and facilitates phagocytosis in retinal pigment epithelium (RPE) cells (Caberoy et al., 2010).

As TULP1 has been detected in retinal ganglion and progenitor cells in human retinas (Milam et al., 2000), we hypothesized that likewise, TULP1 may not be exclusively specific to photoreceptors in mice. The *Tulp1-/-* retina may represent a model where aspects of primary photoreceptor and non-photoreceptor degenerations could be studied. Therefore, we explored non-photoreceptor expression of *Tulp1* in the murine retina and assessed the potential impact of lack of TULP1 in non-photoreceptor cells in *Tulp1-/-* mice. We also considered, whether TULP1 may be expressed in the early post-natal retina of mice, which may contribute to the severe retinal degeneration observed in *Tulp1-/-* mice.

The p5–p30 period was selected for analysis, a timeframe which overlaps with a substantial part of postnatal development of the mouse retina and precedes photoreceptor degeneration in *Tulp1-/-* mice. Immunocytochemistry and bioinformatic analysis indicated *Tulp1* expression in both the outer and inner retina in wild type (wt) mice. Using various cellular markers, we evaluated the architecture of *Tulp1-/-* retinas compared to retinas from *Rho-/-* (Humphries et al., 1997) and retinal degeneration slow (*Rds-/-*) (Sanyal et al., 1980) mice, where retinal degeneration is believed to originate from photoreceptors. Significant differences between the inner retina of *Tulp1-/-* versus the *Rho-/-* and *Rds-/-* retinas were identified. We suggest that these may reflect the effects of expression of *Tulp1* in multiple non-photoreceptor cells. Bioinformatic analysis of expression of the predicted TULP1 interactome suggests cell type-specific utility of TULP1 in the retina. Additionally, bioinformatic analysis indicated that a similar profile of expression in both the outer and inner retina is observed for a number of other IRD genes at p4–p7.

MATERIALS AND METHODS

Animals

The following transgenic mice were used in this study; *Tulp1-/-* (B6.129X1-Tulp1tm1Pjn/Pjn; The Jackson Laboratory) (Ikeda et al., 2000), *Rho-/-* (Humphries et al., 1997), and *Rds-/-* (Sanyal et al., 1980). The background strain of these mice was C57BL/6J (except for *Rds-/-*, which was O20/A; this line does not exist anymore); wt C57BL/6J mice were used as controls. Mice were maintained under specific pathogen free (SPF) housing conditions; both sexes were used for experiments. Animal welfare complied with the Directive 2010/63/EU; Protection of Animals Used for Scientific Purposes, Regulations 2012 (S.I. No. 543 of 2012) and the Association for Research in Vision and Ophthalmology (ARVO) Statement for the Use of Animals in Ophthalmic and Vision Research.

Expression Analysis of GEO Data Sets

Tulp1, TULP1 interactor and IRD mRNA expression was analyzed in retinal cell type-specific mouse data sets (GSE71462, GSE19304, GSE127771, GSE80232, GSE81903, GSE33088, GSE86199, GSE115404, GSE90652) downloaded from the Gene Expression Omnibus (GEO) resource. Depending on the microarray platform used, raw CEL files were processed either with GCRMA and Limma (GSE59201) or with the oligo package from Bioconductor (GSE33088) to derive normalized expression values. GSE19304, for which raw expression values were provided, was normalized with the tmm method (Robinson and Oshlack, 2010) in R. Bulk RNA sequencing data were transformed from counts or FPKM/RPKM (fragments/reads per kilobasepairs per million) values to TPM (transcripts per million) values using Perl scripts[1]. Technical and biological replicates in each data set were averaged. Normalization between data sets was carried out by dividing each data point by the average of the housekeeping genes; *Actb*, *B2m*, *Gapdh*, *Gusb*, *Hmsb*, *Hprt*, *Impdh2, Mapk1*, *Oaz1*, *Pgk1*, *Ppia*, *Rpl13a*, *Rplp0*, *Sdha*, *Tbp*, *Tfrc*, and *Ywhaz*.

In our study, we utilized data derived from bulk RNA sequencing or microarray expression analysis (apart from one single cell RNA sequencing data set for ganglion cells). Single

[1]https://github.com/khokamp/Perl-scripts

cell RNA sequencing has become an invaluable technique in gene expression profiling; in the retina, for example, single cell RNA sequencing has been proven extremely beneficial for identifying and clustering retinal cell types or even pinpointing molecular signatures of disease states (Macosko et al., 2015; Shekhar et al., 2016; Daniszewski et al., 2018; Laboissonniere et al., 2019; Lukowski et al., 2019; Menon et al., 2019). In this study, we were interested in measuring expression of a large cohort of IRD genes. Whereas RNA sequencing and microarrays typically detect expression of thousands of genes, single cell RNA sequencing data sets sometimes only cover a few hundred genes. The early stage single cell data sets had particularly low coverage and were not included in this study.

Estimation of Photoreceptor Component in Non-photoreceptor Transcriptomes

Rod photoreceptors comprise ∼80% of retinal cells (Jeon et al., 1998) and represent the major source of contamination in other retinal cell types. To estimate photoreceptor contamination in the transcriptome of non-photoreceptor samples, we used expression level of *Rho* (a highly expressed rod specific gene). The ratio of *Rho* expression in a given sample versus age matched photoreceptor samples was used to estimate the photoreceptor component of the transcriptome in the given sample. To obtain the pure sample component of the non-photoreceptor transcriptomes, the photoreceptor components were taken away.

Immunohistochemistry and TUNEL Stain

Mice were sacrificed, eyes enucleated and fixed in 4% paraformaldehyde in PBS for 4 h at 4°C. Eyes were washed in PBS, cryoprotected in 10, 20, and 30% sucrose in PBS, embedded in OCT (VWR), cryosectioned (12 μm), thaw-mounted onto polysine slides (Thermo Fisher Scientific) and stored at −20°C. Serial sections were taken in the optic nerve area. Immunocytochemistry was performed as described before (Palfi et al., 2016). Sections were incubate with primary antibodies (**Table 1**) overnight at 4°C, then incubated with secondary antibodies conjugated with either FITC, Alexa-Fluor-488, Cy3, and Alexa-Fluor-647 (Jackson ImmunoResearch Laboratories) in 1:400 dilution for 2 h, at RT and nuclei counterstained with DAPI. TUNEL staining was completed using the TMR red in situ cell death detection kit (Roche), as per the manufacturer's protocol. Subsequent to TUNEL staining, sections were processed for immunocytochemistry. Sections were covered using Hydromount (National Diagnostics).

Microscopy and Analysis

Fluorescent microscopy was carried out utilizing an Olympus IX83 inverted motorized microscope (cellSens v1.9 software) equipped with a SpectraX LED light source (Lumencor) and an Orca-Flash4.0 LT PLUS/sCMOS camera (Hamamatsu). Multi-channel fluorescence images were acquired as separate 16 bit gray-value images with fluorescence colors assigned and channels superimposed. In a given observation method, the same settings/operations were applied to all images. Pan-retinal images were produced from 10× magnification (plan fluorite objective) images with lateral frames stitched together in cellSens. Single frame images were taken using 20× and 40× plan super apochromat objectives using enhanced focal imaging (EFI) with 5–8 Z-slices. Sections were taken from areas adjacent (within 200 μm) to the optic nerve and randomly allocated for various analyses.

Measurements were taken in images from the central half of the retinas using comparable areas and similar analysis windows; object numbers were normalized to length of retina. Typically, four sections/eye were analyzed, and four measurements per section were made. All measurements were made using cellSens software (Olympus). Thickness of retinal layers was determined in 10× magnification stitched images from sections stained with COX4 immunocytochemistry. PAX6-positive cells were counted in 10× magnification stitched images using automatic image analysis; 2D deconvolution and Count and Measure tool. Bipolar (CHX10 positive) cells were manually counted in single frame 40× images. TUNEL-positive cells were counted in 10× pan-retinal stitched images using manual counting. For intensity measurements, the area of interest was delineated using the Closed Polygon tool and mean fluorescence intensity, i.e., mean 16-bit gray value determined.

Representative images for figures were exported from cellSens as individual fluorescence channels and post-processed in Photoshop CS6 (Adobe). In a given observation method, the same settings/operations were applied to all images both in cellSens and Photoshop. The only exception from this was in images co-labeled with TUNEL stain and immunocytochemistry, where the aim was to highlight immune-positive cells (independent to their original signal intensity) in order to facilitate localization of TUNEL-positive cells.

TULP1 Interactors

Potential TULP1 interactor genes were predicted with PrePPI (Zhang et al., 2012) and STRING (Szklarczyk et al., 2019) using default settings for PrePPI and medium confidence for STRING and resulted in 182 human (179 mouse) and 68 interactors, respectively (**Supplementary Table 1**); 22 interactors were predicted by both resources (**Supplementary Table 1**). Eleven validated interactors (ACTB, ACTG1, AXL, CTBP2, DNM1, FYN, GRB2, MAP1B, MERTK, NCK1, and TYRO3) were taken from the literature; seven of them were also predicted with PrePPI or SRING (**Supplementary Table 1**). Combined lists of 229 interactors (predicted by at least one resource or validated) and 33 interactors (predicted by both resources or validated) were assembled (**Supplementary Table 1**). Utilizing the GEO open source retinal expression data sets, TULP1 interactors were ranked by normalized expression level for selected retinal cell types and postnatal ages, and the top 20% highest expressed interactors (46) from each cell type selected for analysis. The high confidence list of 33 interactors were also analyzed separately. Heat maps for selected data sets were generated with the pheatmap package in R[2]. Default settings were applied except for scaling in row direction and Pearson correlation as the

[2]https://cran.r-project.org/web/packages/pheatmap/index.html

TABLE 1 | Antibodies used in this study.

Primary antibody target	Number	Species	Dilution	Source
Rhodopsin	4D2	Mouse	1:200	Robert Molday, University of British Columbia, Vancouver, BC, Canada
Arrestin 3	AB15282	Rabbit	1:200	Merck
CRALBP	Ab15051	Mouse	1:200	Abcam
PKCα	P4334	Rabbit	1:2000	Sigma
CHX10	Sc-374151	Mouse	1:200	Santa Cruz
PAX6	PRB-278P	Rabbit	1:200	Biolegend
MAP2	Ab592	Chicken	1:600	Abcam
Calbindin	A85359	Chicken	1:200	Antibodies.com Ltd.
CTBP2	612044	Mouse	1:200	BD Biosciences
RBPMS	ABN1376	Guinea Pig	1:400	Millipore
Tulp1	M-tulp1N antibody	Rabbit	1:200	Stephanie A. Hagstrom Cleveland Clinic, Cleveland, OH
GABA	A2052	Rabbit	1:500	Sigma
COX4	Ab16056	Rabbit	1:200	Abcam

distance matrix. Venn diagrams were constructed using a Venn diagram tool[3].

Statistical Analysis

Datasets were analyzed with Shapiro–Wilk test for normality before applying parametric tests. Paired sample *t*-test or a one-way analysis of variance (ANOVA) with a Tukey's multiple comparison *post hoc* test was used to compare study groups; *n* numbers varied between 3 and 6. Brown–Forsythe test was utilized to determine the robustness of testing equality of means. The homogenous subset test was also included in the measurements in order to establish the likelihood of encountering type I error. A *p*-value of less than 0.05 was considered statistically significant. Statistical analyses were carried out using IBM SPSS and Minitab software; Microsoft Excel was used to plot the charts.

RESULTS

TULP1 Expression in the Mouse Retina

Expression of *Tulp1* has thus far solely been associated with photoreceptors in the mouse retina (Hagstrom et al., 1999; Ikeda et al., 2000). Utilizing TULP1 immunohistochemistry (M-tulp1N antibody) (Hagstrom et al., 1999) in wt mouse retinas, TULP1 expression was observed in both photoreceptor and non-photoreceptor cells. We found evidence of photoreceptor expression by p5, an earlier timepoint than previously analyzed (**Figures 1a,b**). TULP1 was distributed in the perikaryon, inner segment and synapse of developing photoreceptors by p8 (**Figures 1e,f**), which became largely confined to the inner segments and the synaptic ribbons in wt retinas by p14–p30 (**Figures 1i,j,m,n**); reflecting previous studies (Hagstrom et al., 1999; Xi et al., 2005). TULP1 expression in the ONL peaked at p8 ($p < 0.001$) (**Figure 1q**). Notably, weak but consistent TULP1 expression was observed in the neuroblast and inner nuclear layers (NBL/INL) at p5 (**Figure 1b**) and in the INL at p8 (**Figure 1f**) but not at p14 (**Figure 1j**) or p30 (**Figure 1n**). No TULP1 expression was found in *Tulp1-/-* retinas as anticipated (**Figure 1**), although background label was observed in the tips of degenerating outer segments at p14 (**Figure 1k**) and p30 (**Figure 1o**) as also observed in outer segment tips of wt retinas. RT-qPCR analysis from wt retinal RNA (**Figure 1r**) mirrored the TULP1 expression profile in the ONL (**Figure 1q**) with peak expression at p8.

As TULP1 levels in the inner retina were low, to probe the identity of positive cells we explored *Tulp1* mRNA expression. Data mining of public mRNA expression data sets (GSE71462, GSE19304, GSE127771, GSE80232, GSE81903, GSE33088, GSE86199, GSE115404, GSE90652) from purified populations of specific retinal cell types was undertaken employing the NCBI GEO resource. Expression levels were normalized using the average expression of 17 housekeeping genes. Normalized expression of *Tulp1* (and *Rho*, a rod specific gene) in various retinal cell types is given in **Figure 2A**. In photoreceptors (**Figure 2A**), the *Tulp1* expression profile was similar to that found with RTqPCR from whole retinas (**Figure 1r**) and TULP1 immunocytochemistry in the ONL (**Figure 1q**) with peak of expression being observed at p8. Non-photoreceptor retinal cell types also expressed *Tulp1*, although typically at lower levels compared to photoreceptors (**Figure 2A**).

As the majority of retinal cells are rod photoreceptors (from ∼p5 onward) (Jeon et al., 1998), they represent the major source of contamination when separating non-photoreceptor cells. To estimate the photoreceptor component of *Tulp1* expression in non-photoreceptor samples, we utilized expression level of *Rho* (**Figure 2A**). Estimated photoreceptor contamination ranged between ∼2–30% (11.9 ± 10.6%) in the non-photoreceptor samples and accounted for various amounts of *Tulp1* expression (**Figure 2B**). Results from this analysis suggested *bona fide Tulp1* expression in p7 bipolar, p4 Muller, developing and adult ganglion and adult RPE cells (**Figure 2B**). p5–p8 non-photoreceptors (the cells remaining after sorting photoreceptors) were also positive for *Tulp1* expression supporting the cell-specific data (**Figure 2B**). In other cell types, e.g., amacrine cells, it appeared that all *Tulp1* expression was accounted for by the

[3]http://bioinformatics.psb.ugent.be/webtools/Venn/

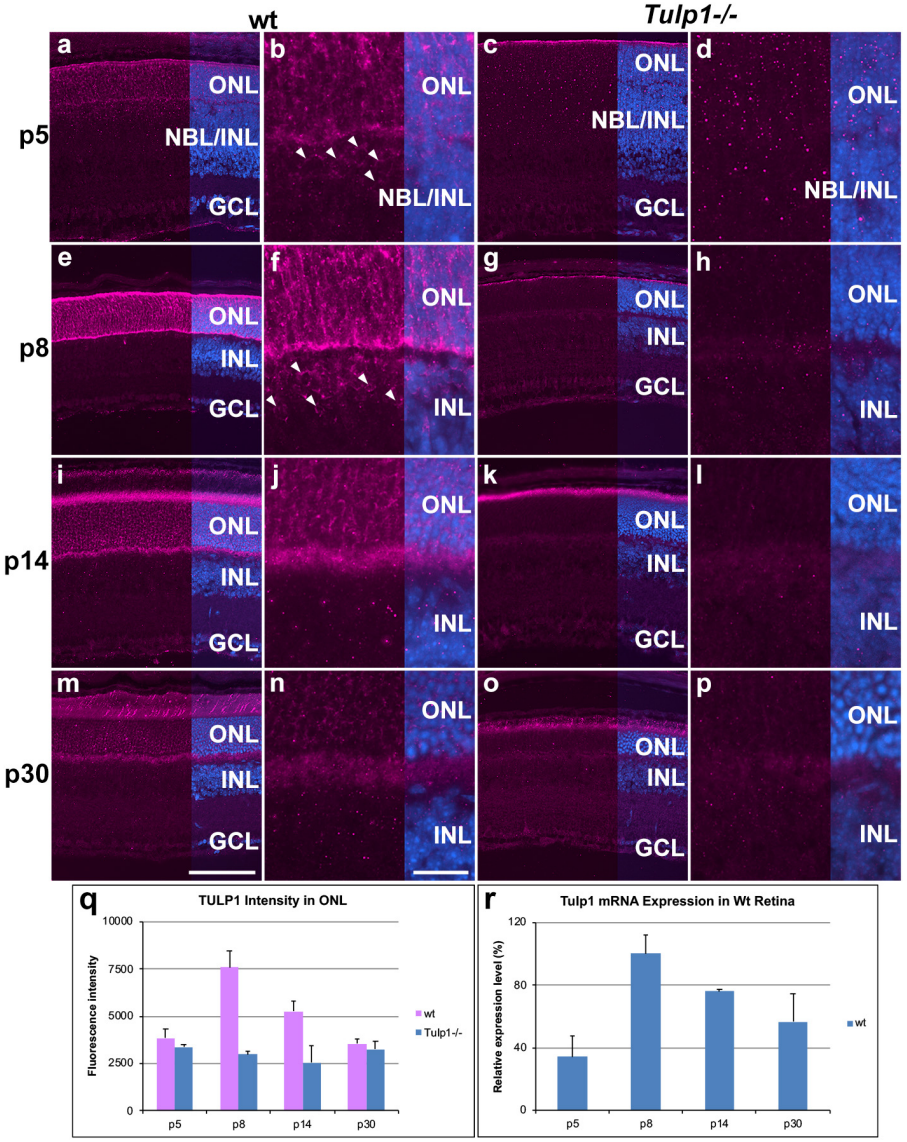

FIGURE 1 | TULP1 expression during postnatal development of the retina. Retinas from wt and *Tulp1-/-* mice were taken at p5, p8, p14, and p30 (n = 4). Sections were labeled with TULP1 (purple) immunocytochemistry and counterstained with DAPI (blue). **(a,c,e,g,i,k,m,o)** low magnification overview; **(b,d,f,h,j,l,n,p)** high magnification view of the ONL/INL boundary. Arrowheads indicate TULP1-positive cells in the NBL/INL **(b)** and INL **(f)**. TULP1 label intensities were quantified in the outer nuclear layer (ONL; **q**) from microscope images using cellSens software and results are given in a bar chart; bars represent mean + SD (n = 4). **(r)** *Tulp1* RTqPCR was carried out using *Actb* control for normalization; data are provided in a bar chart; bars represent mean + SD (n = 3). INL, inner nuclear layer, NBL, neuroblast layer; GCL, ganglion cell layer. Scale bar **(m)**: 100 μm. Scale bar **(n)**: 20 μm.

photoreceptor component suggesting no actual *Tulp1* expression in these cells (**Figure 2B**). *Tulp1* was also expressed in the embryonic retina (**Figure 2A**) but the identity of the positive cell types was unknown.

Development, Degeneration and Remodeling of the *Tulp1-/-* Retina

Our results revealed that TULP1 was present not only in photoreceptors (p5–p30) but in the NBL/INL at p5 and p8 in the mouse retina. Additionally, bioinformatic analysis also suggested *Tulp1* expression in various inner retinal cell types in wt mice. Therefore, we hypothesized, that the *Tulp1-/-* retina could be compromised by primary defects not only in the outer retina as previously described (Hagstrom et al., 1999; Ikeda et al., 2000) but in the inner retina too. Development, degeneration and remodeling in such a retina may differ from retinas affected solely by a primary photoreceptor degeneration, that is driven by a gene whose expression is limited to photoreceptors. To test this hypothesis, we selected two gene knock-out mouse models; *Rho-/-* (Humphries et al., 1997) and *Rds-/-* (Sanyal et al., 1980) as disease controls, where the causative genes are considered to be

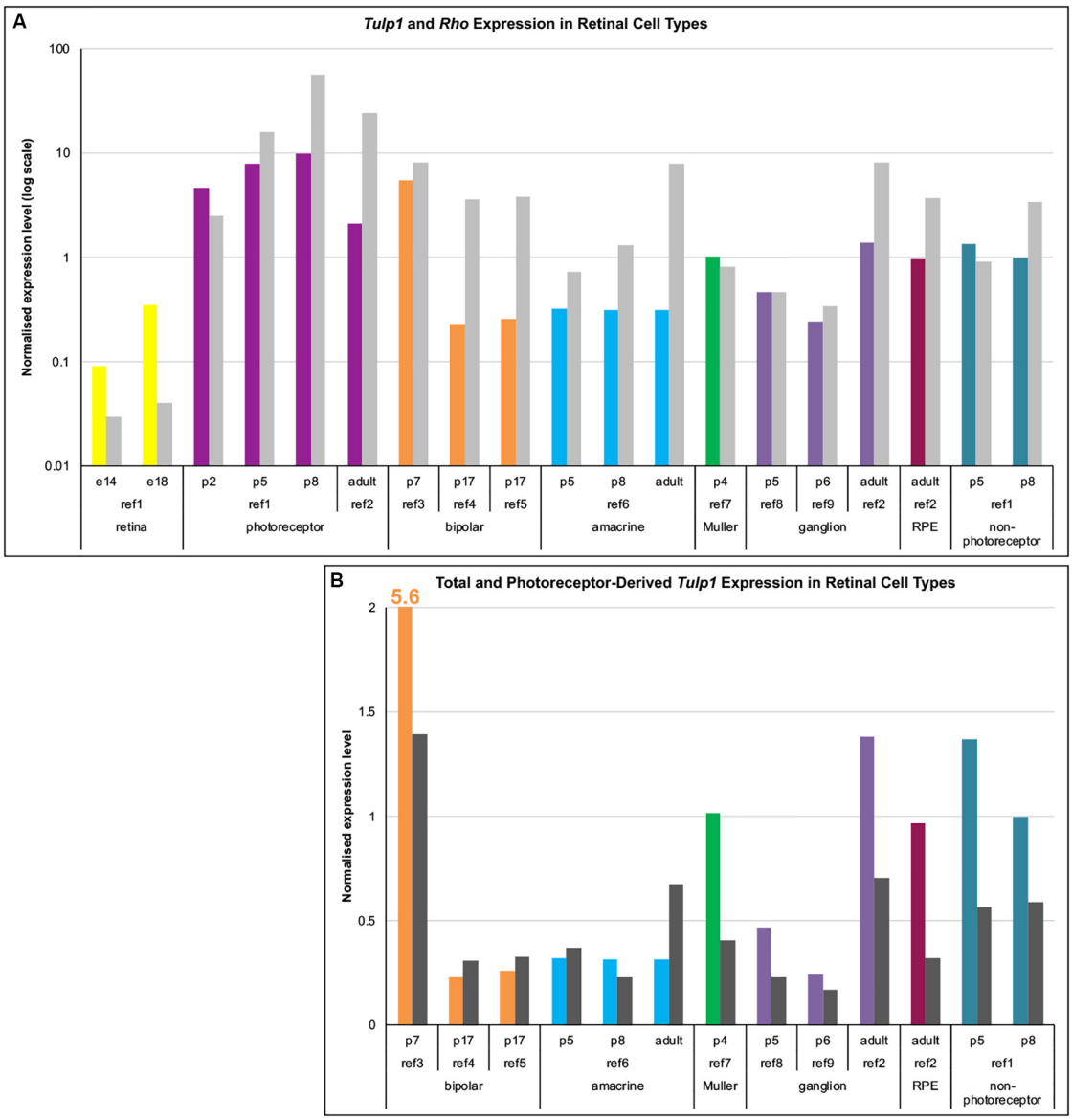

FIGURE 2 | Expression analysis of *Tulp1* in retinal cell types. Raw expression data were obtained from GEO (NCBI) using GSE71462 (ref1), GSE19304 (ref2), GSE127771 (ref3), GSE80232 (ref4), GSE81903 (ref5), GSE33088 (ref6), GSE86199 (ref7), GSE115404 (ref8), GSE90652 (ref9) data sets. Expression levels were normalized using the average expression of 17 housekeeping genes. **(A)** Normalized expression values of *Tulp1* (color coded for different cell types) and *Rho* (gray) from various retinal cell type samples are given in a bar chart. **(B)** The total (color coded for different cell types) and the photoreceptor component (dark gray; estimated using *Rho* expression) of *Tulp1* expression in various samples is given in a bar chart.

specific to photoreceptor cells. We compared the architecture of retinas from *Tulp1-/-*, disease control (*Rho-/-* and *Rds-/-*) and wt mice using a range of cellular markers. Mice were on a C57/BL6J background, except for *Rds-/-*, which was on a O20/A background.

Gross Retinal Architecture and Outer Retina

Detailed findings of the gross retinal architecture and the outer retina are given in Supplementary Results including **Supplementary Figures 1–5**. The overall architecture of IRD (*Tulp1-/-*, *Rho-/-*, and *Rds-/-*) retinas was similar and involved a significant loss of the ONL from p14 (**Supplementary Figure 1**). Regarding the outer retina, significant shortening of photoreceptor segments by p14 (**Supplementary Figure 2**), mislocalization of RHO (**Supplementary Figure 2**), delayed cone development (**Supplementary Figure 3**), thinning of the C-terminal binding protein 2 (CTBP2)-positive synaptic region in the outer plexiform layer (OPL) by p14 (**Supplementary Figure 4**) and ectopic sprouting of horizontal cell neurites at p8–p14 (**Supplementary Figure 5**) were observed. While

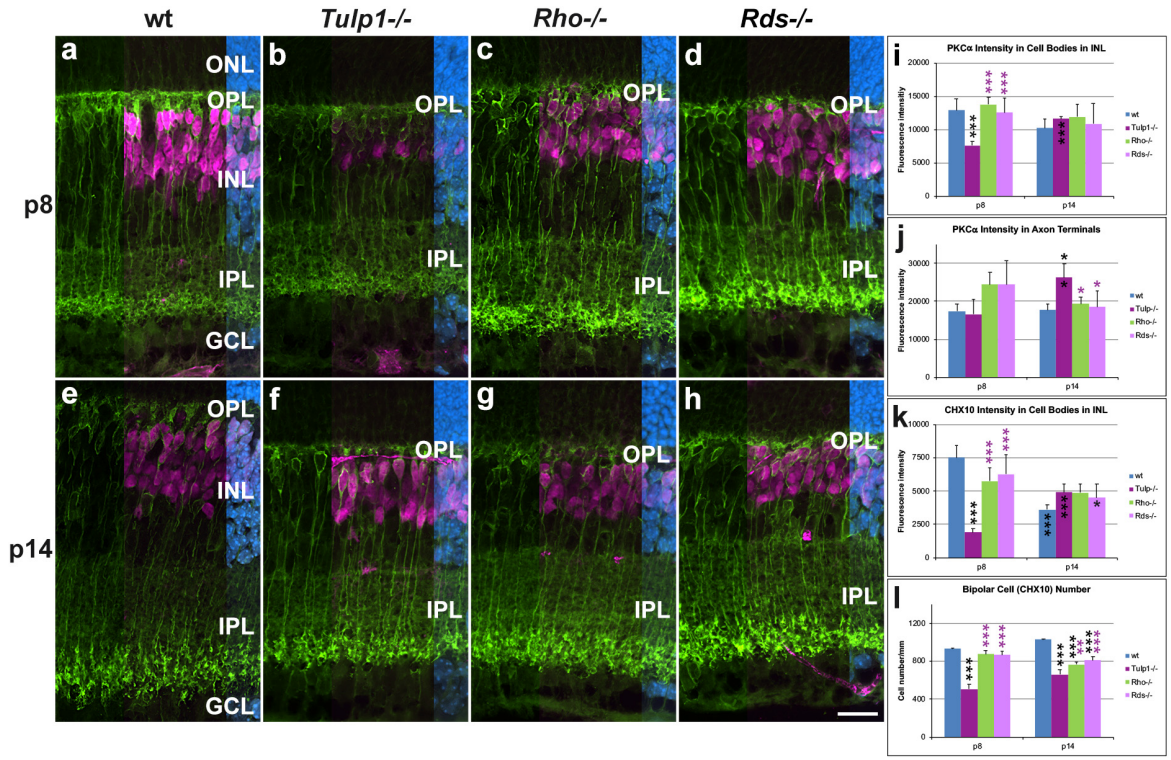

FIGURE 3 | Bipolar cells detected with PKCα and CHX10 immunocytochemistries. **(a–h)** Retinal sections from wt, *Tulp1-/-*, *Rho-/-*, and *Rds-/-* mice at p8 and p14 ($n = 6$) were co-labeled with PKCα (green) and CHX10 (purple, overlaid on the right) and counterstained with DAPI (blue; overlaid on the far right). CHX10 labels all bipolar cell bodies while PKCα labels rod bipolar cells only. Fluorescence label intensities and cell numbers were determined in microscope images using cellSens software and results are given in bar charts; bars represent mean + SD. **(i,j)** PKCα intensity in the cell bodies and in axon terminals in inner plexiform layer (IPL), respectively ($n = 4$). **(k)** CHX10 intensity in cell bodies ($n = 4$). **(l)** Quantification of CHX10-positive cells ($n = 6$). ONL: outer nuclear layer, OPL, outer plexiform layer; INL, inner nuclear layer; GCL ganglion cell layer. Scale bar **(h)**: 20 mm. $^{*}p < 0.05$; $^{**}p < 0.01$; $^{***}p < 0.001$ (ANOVA). Black stars above bars refer to differences between IRD and wt mice, purple stars above bars refer to differences between *Tulp1-/-* and the other IRD mice; black stars within bars refer to a difference compared to the previous time point.

some significant differences between IRD retinas were detected, for example, different CTBP2 expression profiles in the OPL (**Supplementary Figure 4**); most alterations in photoreceptors (**Supplementary Figures 2**, **3**), horizontal cells (**Supplementary Figure 5**) and the OPL (**Supplementary Figure 4**) were similar between IRD retinas.

Inner Retina

Given the interesting observation of *Tulp1* expression in the murine inner retina, a more detailed analysis was undertaken in bipolar, Muller, ganglion, and amacrine cells. Protein kinase Cα (PKCα) (**Figure 3**) labels rod bipolar cells and ceh-10 homeodomain containing homolog (CHX10) labels the cell bodies of all bipolar cells (**Figure 3**). PKCα intensities were measured in cell bodies (INL, **Figure 3i**) and axon terminals (IPL, **Figure 3j**). PKCα expression decreased in *Rho-/-*, *Rds-/-*, and wt retinas, while it increased in *Tulp1-/-* retinas between p8 and p14 (**Figures 3i,j**). Additionally, a marked loss of PKCα-positive dendritic arborization from p8 (**Figures 3a–h**) and compromised axon terminals at p14 (**Figures 3e–h**) were evident in all three IRD models. CHX10 labeling was similar in intensity between wt, *Rho-/-*, and *Rds-/-* (**Figures 3a,c,d,k**) retinas peaking at p8. In contrast, CHX10 expression was significantly less in *Tulp1-/-* (**Figures 3b,k**) compared to wt, *Rho-/-*, and *Rds-/-* retinas at p8. CHX10 intensities increased in *Tulp1-/-* (**Figure 3k**), while decreasing in the other retinas between p8 and p14 (**Figure 3k**). There were significantly fewer CHX10-positive cell bodies in *Tulp1-/-* (**Figures 3a–d,l**) compared to all other retinas at p8 and in the IRD retinas compared to wt p14 (**Figure 3l**). In summary, the above measures of bipolar cells were similar between wt, *Rho-/-*, and *Rds-/-* and significantly different from *Tulp1-/-* retinas.

Paired Box 6 (PAX6) immunocytochemistry labels amacrine and ganglion cells in the developing mouse retina. In the INL and ganglion cell layer (GCL) of wt, Rho-/-, and Rds-/- retinas, expression of PAX6 was low at p5, reached its highest intensity at p8 and decreased by p14 (**Figure 4**). In *Tulp1-/-* retinas, the expression profile differed substantially; expression increased from p5 to p14 and peak expression was delayed from p8 to p14. PAX6-positive cell numbers decreased in all retinas from p5 to p14; IRD retinas had lower numbers compared to wt.

The CTBP2 gene encodes two alternative transcripts producing two distinct proteins; CTBP2 (C-terminal binding protein 2, a transcriptional repressor) and RIBEYE (a major

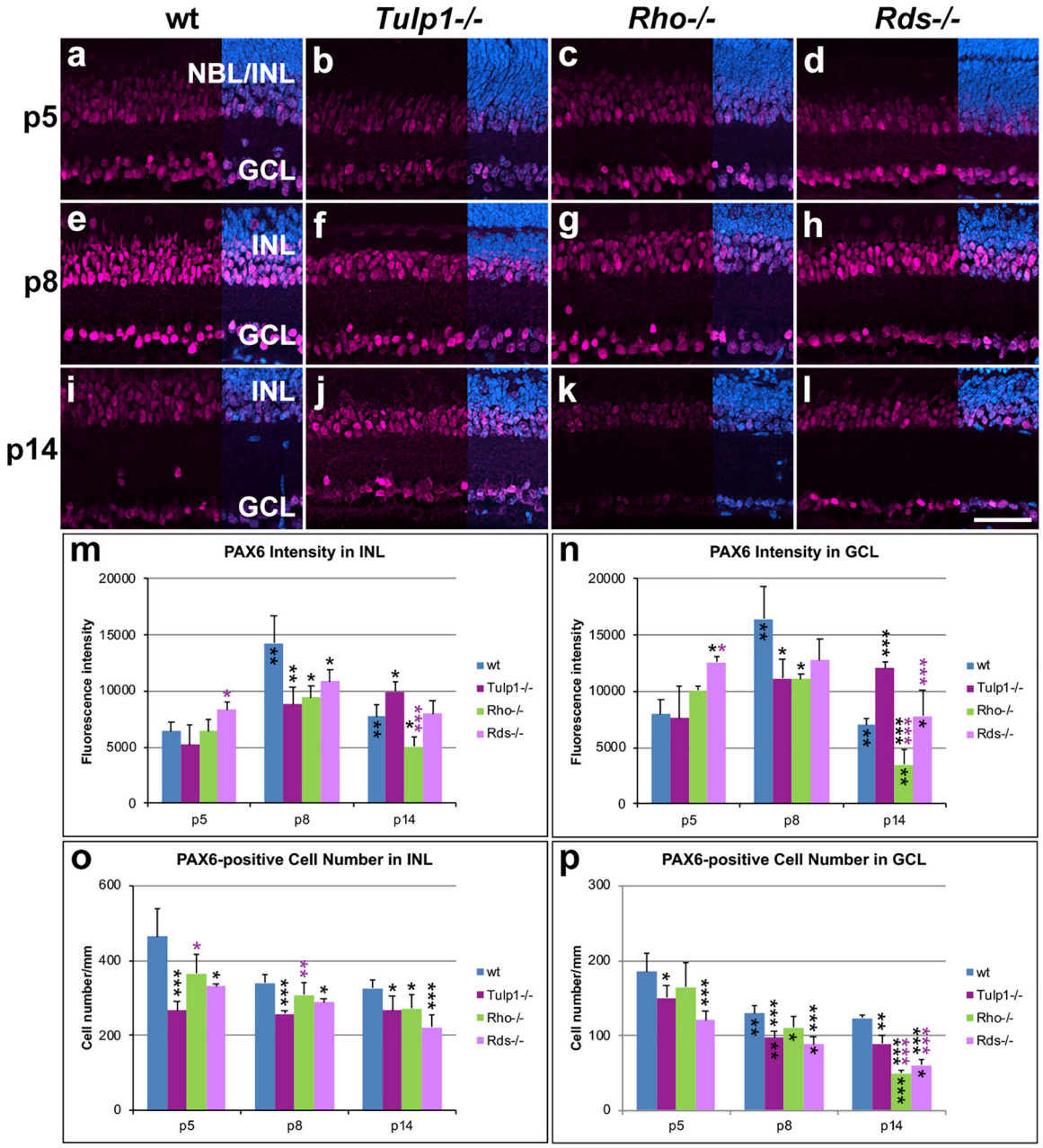

FIGURE 4 | Amacrine and ganglion cells stained with PAX6 immunocytochemistry. Retinas from wt, *Tulp1-/-*, *Rho-/-*, and *Rds-/-* mice were taken at p5, p8, and p14 ($n = 5$–6). **(a–l)** Sections were labeled with PAX6 immunocytochemistry (purple) and counterstained with DAPI (blue; overlaid on right). PAX6 label intensities (**m,n**; $n = 4$) and PAX6-positive cell numbers (**o,p**; $n = 5$) were quantified in the inner nuclear layer (INL) and ganglion cell layer (GCL) from microscope images using cellSens software and results are given in bar charts; bars represent mean + SD. NBL, neuroblast layer. Scale bar **(l)**: 50 mm. $^{*}p < 0.05$; $^{**}p < 0.01$; $^{***}p < 0.001$ (ANOVA). Black stars above bars refer to differences between IRD and wt mice, purple stars above bars refer to differences between *Tulp1-/-* and the other IRD mice; black stars within bars refer to a difference compared to the previous time point.

component of the synaptic ribbons in the retina). The CTBP2 antibody used detects both CTBP2 and RIBEYE. CTBP2 is located in nuclei, while RIBEYE in synaptic regions (OPL and inner plexiform layer /IPL/), hence the two proteins are spatially separated and therefore readily distinguished. CTBP2 labels cell bodies predominantly in the INL and GCL (**Figure 5**). Expression in cell bodies peaked at p8 in wt and *Rds-/-* INLs (**Figure 5m**) and GCLs (**Figure 5n**); in contrast CTBP2 labeling of cell bodies was at its lowest level in *Tulp1-/-* retinas at p8 and peaked at p14 (**Figures 5m,n**). CTBP2 expression intensity levels in cell bodies decreased in *Rho-/-* retinas from p5 to p14 (**Figures 5m,n**). In the IPL, CTBP2 (RIBEYE) is localized to

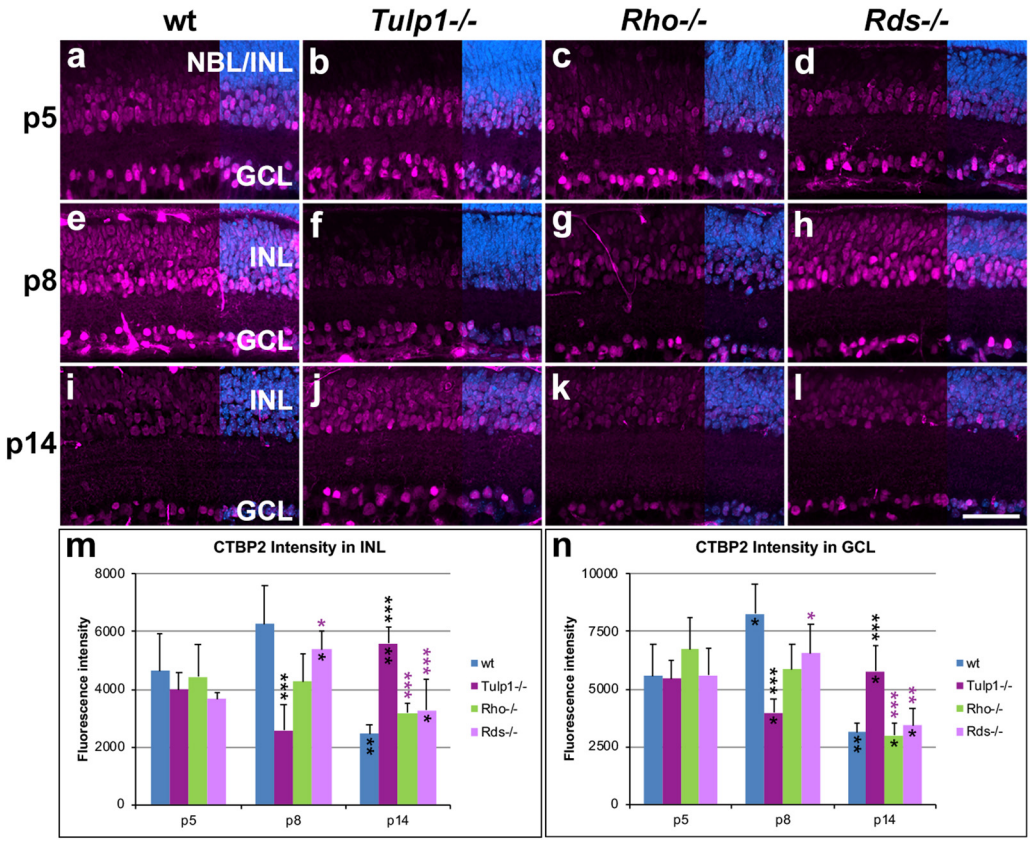

FIGURE 5 | CTBP2 labeling in INL and GCL. Retinas from wt, *Tulp1-/-*, *Rho-/-*, and *Rds-/-* mice were taken at p5, p8, and p14 ($n = 5$–6). **(a–l)** Sections were labeled with CTBP2 immunocytochemistry (purple) and counterstained with DAPI (blue; overlaid on the right). CTBP2 label intensities ($n = 4$) were quantified in the inner nuclear layer (INL; **m**) and ganglion cell layer (GCL; **n**) from microscope images using cellSens software, and results are given in bar charts; bars represent mean + SD. NBL, neuroblast layer, ONL, outer nuclear layer. Scale bar **(l)**: 50 mm. *$p < 0.05$; **$p < 0.01$; ***$p < 0.001$ (ANOVA). Black stars above bars refer to differences between IRD and wt mice, purple stars above bars refer to differences between *Tulp1-/-* and the other IRD mice; black stars within bars refer to a difference compared to the previous time point.

the synaptic ribbons of bipolar cells. CTBP2 labeling in the IPL peaked in wt retinas at p8 (**Figures 6e,n**), while it was lowest in *Tulp1-/-* retinas at this time point (**Figures 6f,n**). CTBP2 label intensities in IPL were similar at all ages in *Rho-/-* and *Rds-/-* retinas (**Figure 6n**).

Muller cells, the primary macroglia in retina were labeled using cellular retinaldehyde-binding protein (CRALBP). CRALBP expression was low in p5 retinas and increased by p8 in all but *Tulp1-/-* (**Supplementary Figure 6**). In wt retinas, Muller processes labeled strongly and spanned the retina radially from the outer limiting membrane (OLM) to the inner limiting membrane (ILM) by p8 (**Supplementary Figure 6e**). In the ONL, the radial processes reached the OLM and formed a CRALBP-positive continuous layer at p8 (**Supplementary Figure 6e** and **Figure 7a**); this pattern was similar at p14 (**Supplementary Figure 6i** and **Figure 7e**). In *Tulp1-/-* retinas, CRALBP labeling was weak in the ONL-IPL region at p8 (**Supplementary Figure 6f** and **Figure 7b**), the radial processes in the ONL did not reach the OLM until p14 (**Figure 7f**). The CRALBP-positive layer in the OLM was weak at p8, and less intense at p14 compared to wt (**Figures 7b,f**). In *Rho-/-* and *Rds-/-* retinas, CRALBP expression in the INL-IPL region was between wt and *Tulp1-/-* at p8 (**Figures 7c,d**). Radial Muller glia processes in the ONL were straight and ran between the columns of photoreceptor nuclei in wt retinas (**Figures 7a,e**); in contrast, they appeared to enclose some photoreceptor cell bodies in IRD retinas (**Figures 7b–d,f–h**). The severity of this phenotype increased from *Tulp1-/-* to *Rho-/-* and to *Rds-/-* and from p8 to p14 (**Figure 7**). These latter findings are in line with (Sakami et al., 2019) suggesting that Muller cells were the primary effectors of photoreceptor phagocytosis in P23H-RHO mice (analyzed at p14). The current study suggests that this event has been initiated in *Tulp1-/-*, *Rho-/-*, and *Rds-/-* retinas by p8. Other studies also reported remodeling of Muller cells but at later time points; for example, glutamine synthetase expression decreased by p20 and GFAP increased from p15 in Muller cells of the rd10 retina (Roche et al., 2016). GFAP increased from p18 to 30 in the rd1 retina (Strettoi et al., 2003).

Ganglion cells were labeled for microtubule associated protein 2 (MAP2) and RNA binding protein mRNA processing factor (RBPMS). MAP2 labeled the dendritic tree of ganglion cells in the IPL (**Figure 6**), while RBPMS predominantly

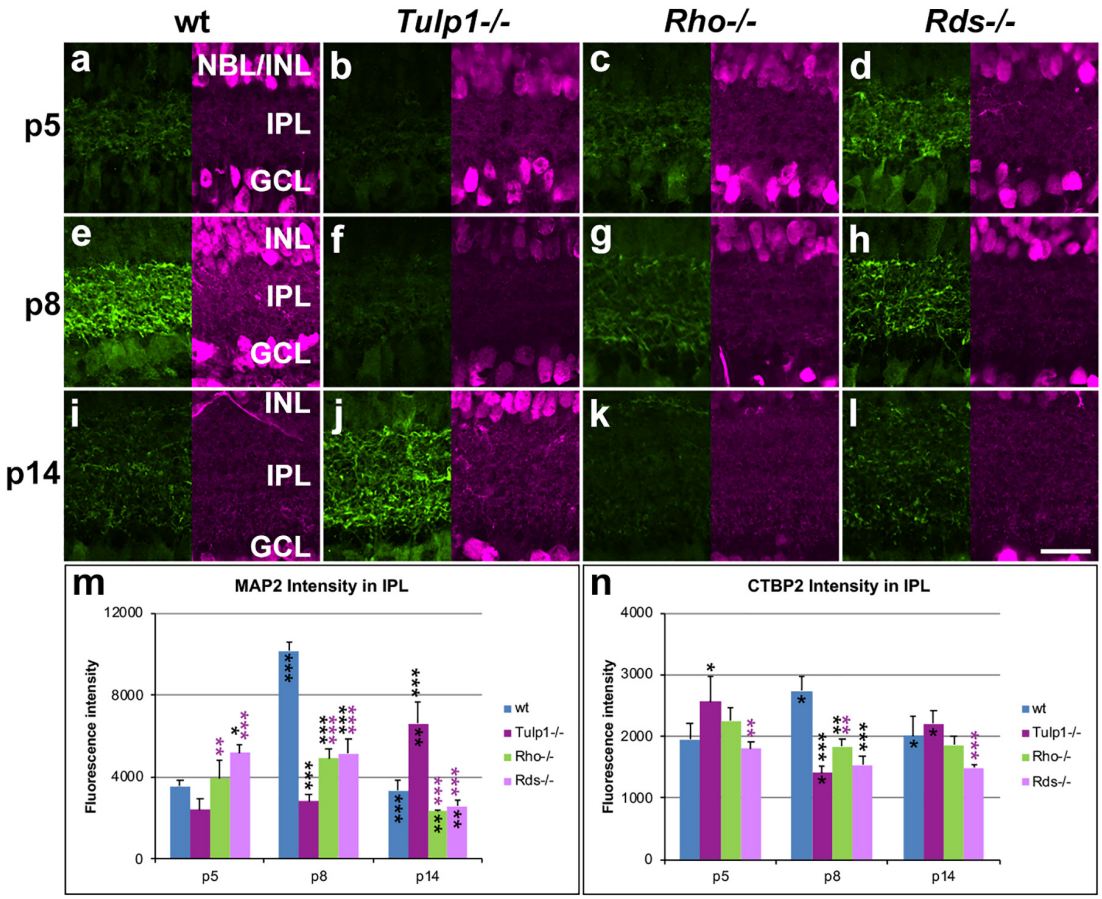

FIGURE 6 | Inner plexiform layer (IPL) and ganglion cells. Retinas from wt, *Tulp1-/-*, *Rho-/-*, and *Rds-/-* mice were taken at p5, p8, and p14 ($n = 5$–6). **(a–l)** Sections were co-labeled with MAP2 (left; green) and CTBP2 (RYBEYE; right; purple) immunocytochemistries. MAP2 ($n = 3$; **m**) and CTBP2 ($n = 3$; **n**) label intensities in the inner plexiform layer (IPL) were quantified from microscope images using cellSens software and results are given in bar charts; bars represent mean + SD. INL, inner nuclear layer; NBL, neuroblast layer. Scale bar **(l)**: 20 mm. $^{*}p < 0.05$; $^{**}p < 0.01$; $^{***}p < 0.001$ (ANOVA). Black stars above bars refer to differences between IRD and wt mice, purple stars above bars refer to differences between *Tulp1-/-* and the other IRD mice; black stars within bars refer to a difference compared to the previous time point.

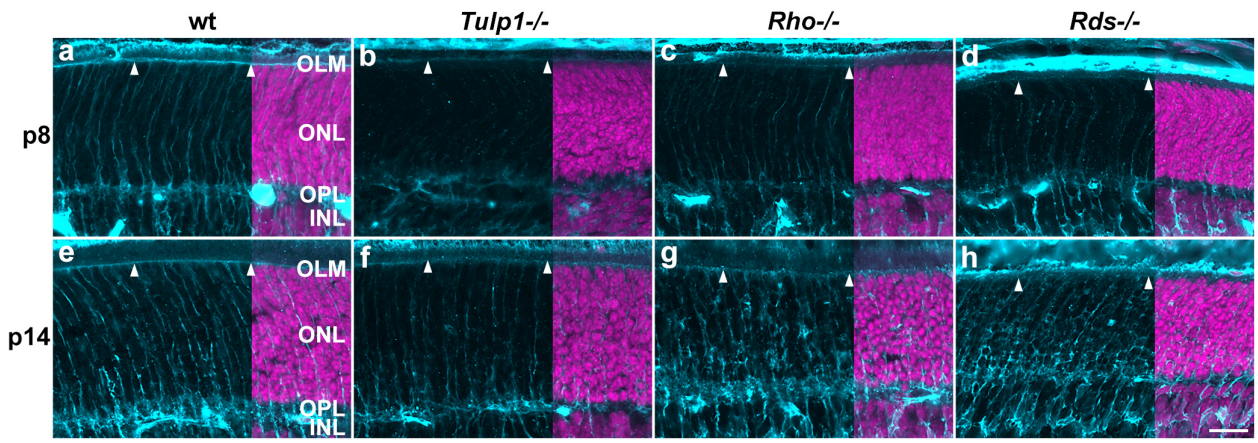

FIGURE 7 | Muller cell labeling (CRALBP) in the outer retina. Retinas from wt, *Tulp1-/-*, *Rho-/-*, and *Rds-/-* mice were taken at p8 and p14 ($n = 5$–6). **(a–h)** Sections were labeled with CRALBP immunocytochemistry (light blue) and counterstained with DAPI (purple; overlaid on the right). ONL, outer nuclear layer; OPL, outer plexiform layer; INL, inner nuclear layer. Arrowheads point to the OLM. Scale bar **(h)**: 20 m.

localized to the cell bodies and main dendritic branches of ganglion cells (**Supplementary Figure 7**). Expression of MAP2 (**Figure 6m**) and RBPMS (**Supplementary Figure 7m**) was similar in wt retinas; expression was low at p5, peaked at p8 and decreased by p14. MAP2 expression was significantly less in IRD compared to wt retinas at p8 (**Figure 6m**). Notably, MAP2 labeling was significantly less at p8 and higher at p14 in *Tulp1-/-* compared to *Rho-/-* and *Rds-/-* retinas (**Figure 6m**). In contrast, less differences were found in RBPMS expression levels between IRD and wt retinas (**Supplementary Figure 7m**), however, the number of RBPMS-positive cells was higher in *Tulp1-/-* retinas at p5 and p8. In summary, the observations suggest that development of ganglion cells, in particular, ganglion cell dendrites in the IPL are altered in IRD retinas, and differ significantly between *Tulp1-/-*, and *Rho-/-* and *Rds-/-* retinas.

In summary, in the inner retina, expression of PKCα, CHX10, CTBP2 (and RYBEYE) and MAP2, increased in *Tulp1-/-* retinas from p8 to p14, while their expression was maintained or decreased in *Rho-/-*, *Rds-/-*, and wt retinas during the same period suggesting an altered development of *Tulp1-/-* retinas compared to the other retinas analyzed.

TUNEL-Positive Cells

TUNEL (terminal deoxynucleotidyl transferase dUTP nick end labeling) staining was performed to enable visualization of apoptotic cells. Cells were co-labeled for CHX10 (**Figure 8**) and PAX6 (**Supplementary Figure 8**) to aid localization of TUNEL-positive cells in the INL. At p5–p8, the majority of TUNEL-positive cells were in the NBL and bipolar cell region of the INL in both wt and IRD retinas (**Figures 8a–h** and **Supplementary Figures 8a–h**). The photoreceptor and GCLs also had TUNEL-positive cells but in lower numbers. The number of TUNEL-positive cells increased in the ONL of *Rho-/-* and *Rds-/-* retinas from p8 and in *Tulp1-/-* retinas from p14 (**Figure 8m**); this was mirrored by significantly decreased ONL thickness in the IRD retinas from p14 (**Supplementary Figure 1q**). Notably, significantly more TUNEL positive cells were found in the INL of *Tulp1-/-* compared to wt, *Rho-/-*, and *Rds-/-* retinas by p14 (**Figure 8n**), however, this was not reflected in decreased *Tulp1-/-* INL thickness at either p14 or p30 (**Supplementary Figure 1r**).

The results indicate a large-scale photoreceptor apoptosis in the three IRD models from p8–p14, timeframes that are somewhat earlier than detected previously in *Rds-/-* retinas from p14 (Portera-Cailliau et al., 1994) and in *Tulp1-/-* retinas from p18 (Ikeda et al., 2000). Interestingly, by p14, apoptosis is largely over in the INL of wt, *Rho-/-*, and *Rds-/-*, but not in *Tulp1-/-* retinas. As the INL thickness did not decrease significantly in *Tulp1-/-* compared to the other retinas by p30, the presence of significant apoptosis at p14 may probably be a sign of a delayed developmental process rather than progressive degeneration of the INL in *Tulp1-/-* retinas at this stage. Lower number of apoptotic cells in *Tulp1-/-* compared to wt INLs at p5-p8 are also suggestive of delayed developmental apoptosis in *Tulp1-/-* retinas.

Cell Type Specific TULP1 Interactomes in the Retina

Our analysis indicated that *Tulp1* was expressed, apart from photoreceptors, in, bipolar, Muller, ganglion, and RPE cells. Additionally, early changes in the *Tulp1-/-* retina exhibited specific, *Tulp1*-linked perturbations in bipolar, Muller, amacrine and ganglion cells. As the function(s) of TULP1 are not clearly established, we aimed to interrogate the potential roles that TULP1 might have in these retinal cell types.

Tubby like protein 1 (TULP1) interactors were predicted with PrePPI (Zhang et al., 2012) and STRING (Szklarczyk et al., 2019) and resulted in 179 and 68 interactors, respectively (**Supplementary Table 1**); 22 interactors were predicted by both resources (**Supplementary Table 1**). Eleven validated interactors were taken from the literature (**Supplementary Table 1**); seven of which were also predicted with PrePPI or SRING. Proteins were merged into a medium confidence list of 229 TULP1 predicted interactors (**Supplementary Table 1**). A high-confidence list of 33 TULP1 interactors from the above list includes interactors validated or predicted by both PrePPI and STRING. Cell type-specific mRNA expression levels of TULP1 predicted interactor genes were determined in retinal cell types where bioinformatic analysis suggested expression of *Tulp1*; GEO expression data sets (GSE97534, GSE59201, GSE115404, GSE127771, GSE86199, GSE19304) were used. Expression levels of high-confidence predicted interactor genes are given in heatmaps for p4–p7 and adult cell types (**Figures 9A,B**), as well as, during postnatal development of cones (**Figure 9C**). A zoom-enabled pdf version of this figure is given in **Supplementary Figure 9**). TULP1 predicted interactor genes from the medium-confidence list were ranked by expression level in retinal cell types and expression of the highest expressed 20% predicted interactor genes from each cell type further analyzed by heat maps and Venn diagrams (**Supplementary Figure 10**).

Significant differences in expression of TULP1 predicted interactor genes between rod, cone, ganglion, bipolar, and Muller cells at p4–p7 (**Figure 9A** and **Supplementary Figures 10a–c**), and between photoreceptor (∼rod), cone, ganglion, and RPE cells from adult retinas (**Figure 9B** and **Supplementary Figures 10d–f**) were determined. During development of cone photoreceptors, few (∼10%) age-specific predicted interactors were found (**Supplementary Figures 10g–i**), although the expression pattern of the predicted interactor genes varied with age (**Figure 9C** and **Supplementary Figure 10g**).

Regarding expression of the high-confidence TULP1 interactor genes (**Figure 9**) in rods and cones, various functional groups were predicted. Cytoskeletal (including intracellular trafficking) interactor genes included *Actb*, *Actg1*, *Map1b*, *Rpgrip1*, *Dnm1*, *Bbs2*, and *Ush2a*. Ctbp2 and *Cabp4* are proteins linked to synaptic function. Outer segment interactors were found in rods and cones; e.g., *Rho*, *Gnat1*, *Pde6b*, and *Cngb1* in rods, and *Guca1b* and *Gucy2d* in cones. As the highest concentration of TULP1 is found in photoreceptor inner segments, TULP1 may be implicated in transport of outer segment proteins, similar to rod and cone opsins (Grossman et al., 2011). Alternatively, low levels of TULP1 may be present in

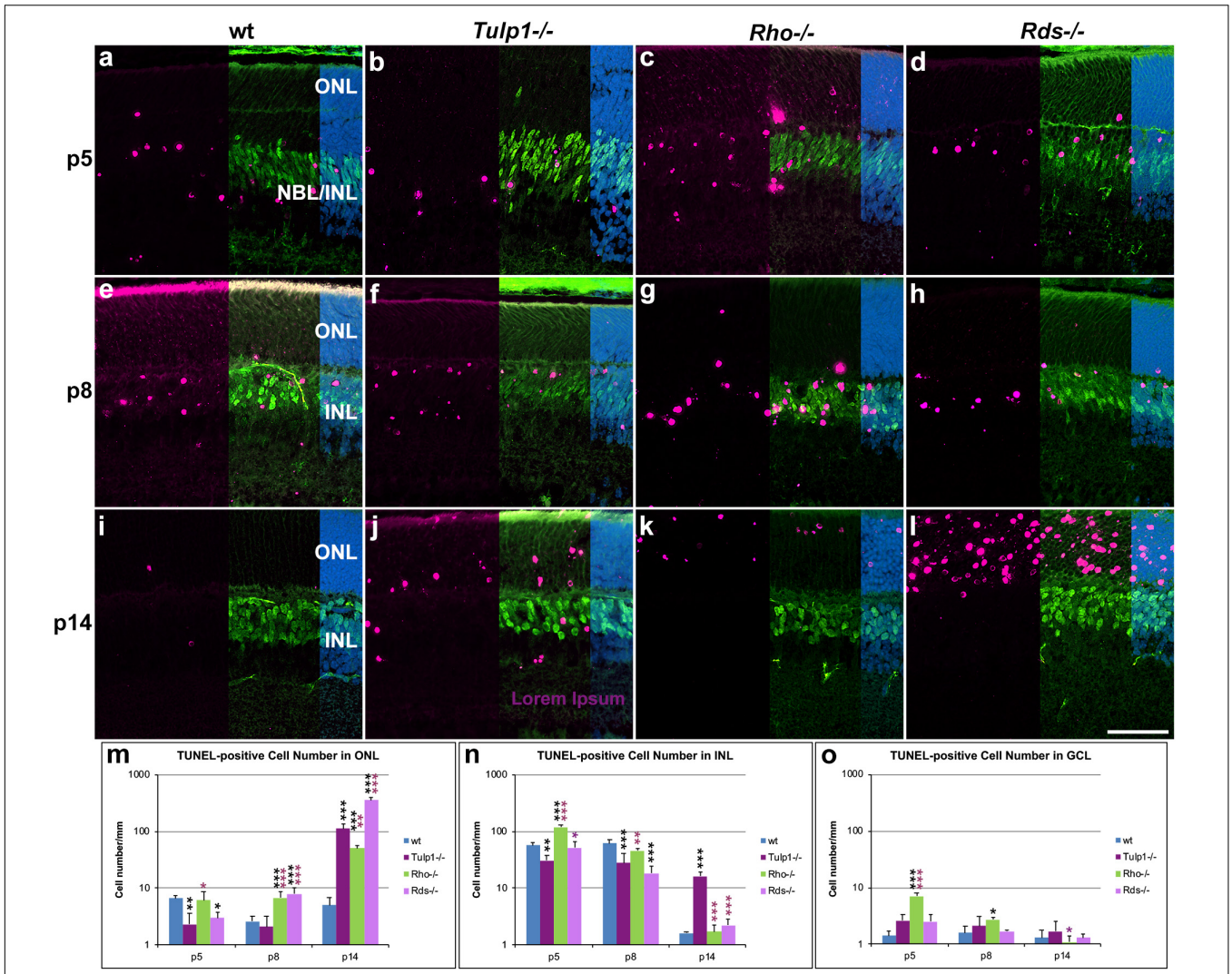

FIGURE 8 | Combined TUNEL stain and CHX10 immunocytochemistry in the ONL – INL region. Retinas from wt, *Tulp1-/-*, *Rho-/-*, and *Rds-/-* mice were taken at p5, p8, and p14 ($n = 3$). **(a–l)** Sections were co-labeled with TUNEL stain (purple) and CHX10 (green) immunocytochemistry (overlaid on the right side), and counterstained with DAPI (blue; overlaid on the far right). Quantification of TUNEL-positive cells in the outer nuclear layer (ONL; **m**), inner nuclear layer (INL; **n**) and ganglion cell layer (GCL; **o**) were carried out from microscope images using cellSens software and results are given in bar charts; bars represent mean + SD. NBL, neuroblast layer. Scale bar **(l)**: 50 mm. $^{*}p < 0.05$; $^{**}p < 0.01$; $^{***}p < 0.001$ (ANOVA). Black stars refer to differences between IRD and wt mice, purple stars refer to differences between *Tulp1-/-* and the other IRD mice.

the outer segments and could interact with predicted interactors *in situ*. Other photoreceptor- or retina-specific TULP1 interactor genes expressed in photoreceptors included transcription factors (*Nrl*, *Crx*, *Nr2e3*) and proteins such as *Rbp3*, *Abca4* (retinoid cycle), *Crb1* and *Aipl1*, often exhibiting differential expression between rod and cone photoreceptors (**Figure 9**).

Of note, expression of two functional groups of TULP1 interactor genes was predicted with high-confidence in retinal ganglion cells (**Figure 9**); some interactors were linked to signal transduction, for example, *Axl*, *Tyrp3*, *Grb2*, and *Nck1*, while others, that is, *Actb*, *Actg1*, *Dnm1*, and *Map1b* represented cytoskeletal interactors. TULP1 predicted interactor genes expressed in bipolar cells at p7, Muller cells at p4 and adult RPE cells (**Figure 9**) belonged to three functional groups; cytoskeleton (*Dnm1* in bipolar, *Actg1* in Muller and *Actb* and *Dnm1* in RPE cells), signal transduction (*Mertk* in bipolar and Muller, *Grb2* in Muller, and *Axl*, *Nck1*, *Tyro3,* and *Mertk* in RPE cells) and retinoid cycle (*Rgr* in RPE, Muller and bipolar, *Rbp3* in Muller and *Abca4* in bipolar and RPE cells).

IRD Gene Expression in Early Postnatal Retinal Cell Types

TULP1 is one of more than 300 genes causative of IRDs (RetNet - Retinal Information Network, 2019). In this study, we found that *Tulp1* was expressed in both photoreceptor and non-photoreceptor cells, in particular during development of the mouse retina. We queried how common this feature

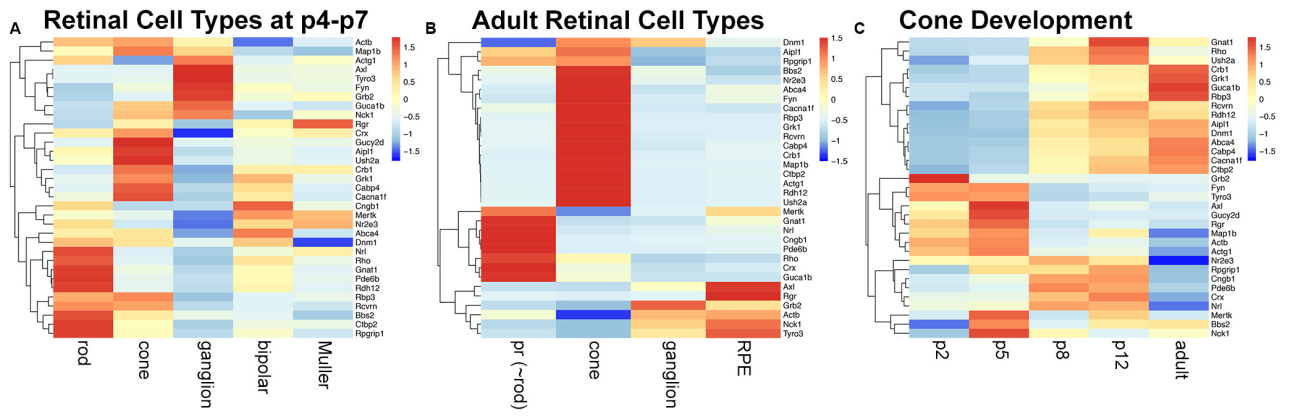

FIGURE 9 | mRNA expression of a high-confidence TULP1 predicted interactome in various retinal cell types. A list of 33 TULP1 interactors were assembled from predicted (by both PrePPI and STRING) and 11 validated interactors. Expression of their corresponding genes in various retinal cell types was determined from Gene Expression Omnibus data sets; GSE97534, GSE59201, GSE115404, GSE127771, GSE86199, GSE19304, and is given in row-scaled clustered heatmap representation in some p4-p7 **(A)** and adult **(B)** retinal cell types and in developing cone cells at p2, p5, p8, p12, and adult **(C)**. Note that in panel **(A)**, rod, cone, and ganglion cells are from p5, bipolar cells are from p7 and Muller cells are from p4 retinas. pr: photoreceptor. A zoom-enabled version of this figure is given as **Supplementary Figure 9**.

may be among other IRD genes. Using retinal expression data sets (GSE59201, GSE97534, GSE71462, GSE33088, GSE127771, GSE86199, GSE115404), normalized expression levels of 235 mouse orthologs of a panel of 251 human IRD genes (Dockery et al., 2017; **Supplementary Table 2**) were determined in selected retinal cell types at p4–p7 (**Figure 10**). The photoreceptor-derived component of the transcriptome was accounted for employing *Rho* expression in non-photoreceptor samples. The analysis suggests widespread expression of IRD genes in various, often multiple (for example, in photoreceptor, amacrine and ganglion cells), retinal cell types at p4–p7 (**Figure 10**; a zoom-enabled pdf version of this figure is given in **Supplementary Figure 11**). Of note, low level of *Rds* expression was detected in Muller cells; while only in these cells and at a low level, this is worth noting given we used *Rds-/-* retinas as disease controls.

DISCUSSION

Tulp1 expression in photoreceptor and non-photoreceptor cells has been explored in the mouse retina and potential TULP1 interactors highlighted. While TULP1 expression has previously only been observed in photoreceptors in mice (Hagstrom et al., 1999; Ikeda et al., 2000; Xi et al., 2005), expression of human TULP1 has been detected in neuroblast, RPE, INL, and ganglion cells (Milam et al., 2000). In the current study, using immunocytochemistry we found evidence of TULP1 expression in the neuroblastic/INL region of the murine retina during the p5–p8 period (**Figure 1**), which has not been reported previously. Expression of TULP1 was also evident in the ONL at all ages analyzed (p5–p30) confirming prior studies (Hagstrom et al., 1999; Ikeda et al., 2000; Xi et al., 2005), but, moreover, demonstrating a developmental expression profile with *Tulp1* expression peaking at ∼p8, again not reported previously (**Figure 1**). While expression of TULP1 was found in occasional ganglion cells in humans (Milam et al., 2000), we did not detect protein expression in these cells in mice during the analyzed period. However, bioinformatic evaluation based on mRNA expression suggested that *Tulp1* was expressed in ganglion cells, as well as in RPE, bipolar and Muller cells in the mouse retina (**Figure 2**). Possibly, the affinity of the TULP1 antibody used in the study, i.e., M-tulp1N (Hagstrom et al., 1999), was not sufficient to detect the level of TULP1 in ganglion cells. Similarly, *Tulp1* expression was also detected in p5 ganglion cells using single cell transcriptome profiling (Rheaume et al., 2018). TULP1 has been implicated in MERTK-dependent phagocytosis in the RPE (Caberoy and Li, 2009), however, TULP1 in the RPE was suggested to originate from shedding of photoreceptor segments (Caberoy et al., 2010). Our bioinformatic analysis indicates that *Tulp1* is expressed in adult mouse RPE, in agreement with transcriptome analysis of human RPE/choroid (Whitmore et al., 2014). According to our study, *Tulp1* is expressed in p7 but not in p17 bipolar cells; no data were available for Muller cells. Notably, peak expression of *Tulp1* overlaps with differentiation, maturation and synaptic development of the mouse retina.

To explore the impact of TULP1 on the inner retina, we analyzed the architecture of the retina in *Tulp1-/-* mice in the p5–p14 window. This period coincides with a major part of postnatal development and peak expression of *Tulp1* in the mouse retina. As comparators we evaluated retinas from *Rho-/-* (Humphries et al., 1997) and *Rds-/-* (Sanyal et al., 1980) mice; *Rho* and *Rds* are believed to be expressed exclusively in photoreceptors in the retina. As such, in these mice, retinopathy is due to loss of photoreceptor-specific proteins. Therefore, any alterations in the inner retina should be the result of the primary photoreceptor degeneration. Notably, we detected an extremely low level of *Rds* expression in Muller cells (**Figure 10**). Most probably this represents photoreceptor contamination of the Muller cells analyzed (*Rho* expression was used to account for photoreceptor contamination). Alternatively, it could be caused by the close

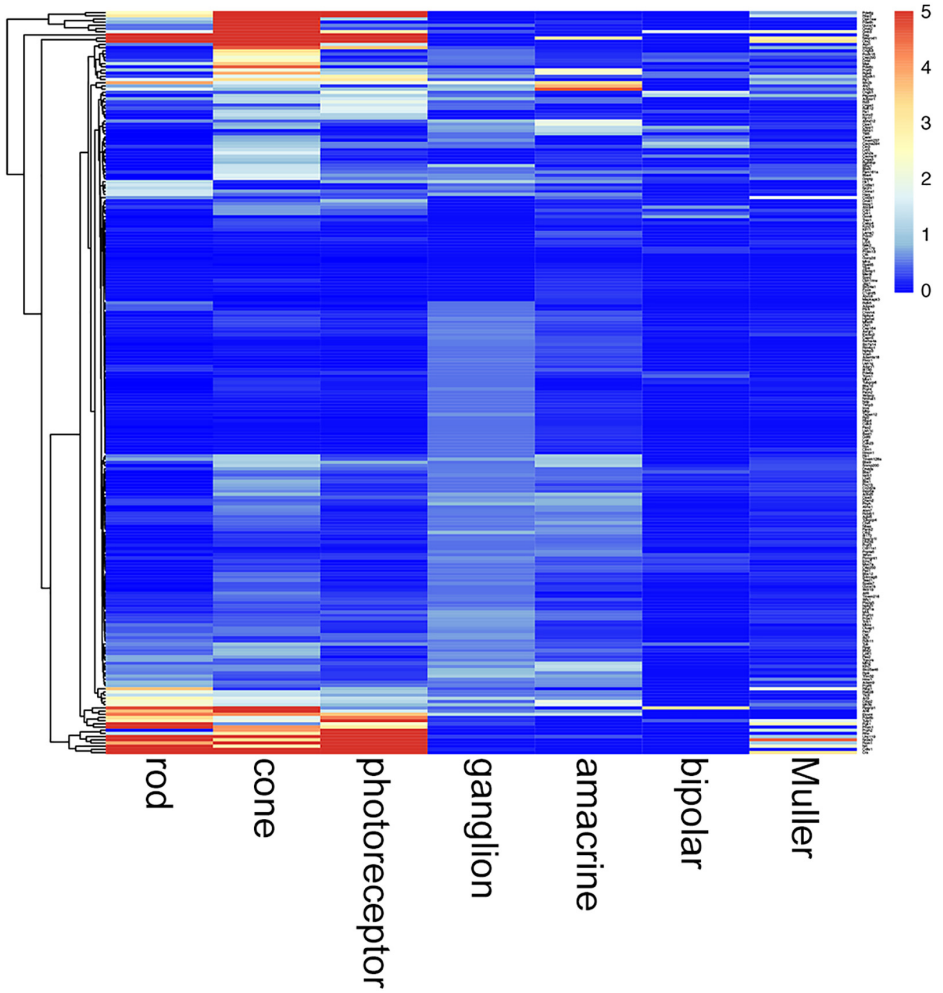

FIGURE 10 | Cell type-specific expression of IRD genes in mouse retina at p4–p7. Retinal cell type-specific gene expression values of 235 mouse orthologs of a panel of 251 human IRD genes (Dockery et al., 2017) were determined using GSE59201, GSE97534, GSE71462, GSE33088, GSE127771, GSE86199, GSE115404 data sets from Gene Expression Omnibus. Photoreceptor contamination of non-photoreceptor samples was determined utilizing Rho expression and corresponding photoreceptor derived IRD gene expression values deducted from these samples. Expression values are given in a clustered heatmap format; pr, photoreceptor. A zoom-enabled version of this figure is given as **Supplementary Figure 11**.

physical and functional contact (Sakami et al., 2019) between photoreceptors and Muller cells. When comparing *Tulp1-/-*, *Rho-/-*, and *Rds-/-* retinas, two main trends were identified.

Common alterations in all IRD retinas were observed including alterations in rod and cone photoreceptors, ectopic sprouting of horizontal cell neurites, distorted Muller glia labeling in the ONL, decreased immunoreactivity of CTBP2 in the OPL, compromised rod bipolar cell dendritic and axon terminal development, decreased bipolar cell numbers (**Supplementary Figures 1–5**) and a significant increase in TUNEL-positive photoreceptors by p8–p14. Similar features of early degeneration and remodeling have been described in other IRD mouse models (Strettoi and Pignatelli, 2000; Strettoi et al., 2002; Gargini et al., 2007; Grossman et al., 2009; Puthussery et al., 2009; Singh et al., 2014; Soto and Kerschensteiner, 2015; Roche et al., 2016).

Of note, we detected alterations in the architecture and development of the inner retina of *Tulp1-/-* mice, which differed from the specific, photoreceptor-driven degeneration observed in *Rho-/-* and *Rds-/-* retinas and were only characteristic of *Tulp1-/-* retinas. These included different expression profiles of CHX10 and PKCα in bipolar cells, of PAX6 and CTBP2 in INL and GCL and of MAP2 in IPL (**Figures 3–7**). Expression of PKCα, CHX10, CTBP2, and MAP2, increased in *Tulp1-/-* retinas from p8 to p14, while expression was maintained or decreased in *Rho-/-*, *Rds-/-*, and wt retinas during the same period. Additionally, there was a significant number of apoptotic cells in *Tulp1-/-* (but not in *Rho-/-*, *Rds-/-*, and wt) INLs at p14 (**Figure 8**).

Delayed peak expression (from p8 to p14) of the above cellular markers in *Tulp1-/-* retinas, may be a sign of altered development and maturation of bipolar, amacrine and ganglion cells. For example, MAP2 is a critical component for dendritic extension,

branching and remodeling (Johnson and Jope, 1992) (Szebenyi et al., 2005) (Wang and Rubel, 2008). MAP2 upregulation is also a hallmark of activity-dependent stabilization of dendrites in cultured sympathetic neurons (Vaillant et al., 2002). Therefore, delayed MAP2 expression in the *Tulp1-/-* IPL may possibly indicate delayed development of synaptic connectivity in the *Tulp1-/-* retina. Delayed apoptosis in the INL also suggests that the normal developmental profile of the inner retina may be compromised in the *Tulp1-/-* retina. Overall, the data suggest that loss of *Tulp1* expression is causative of not only primary photoreceptor degeneration but possibly primary perturbation of inner retinal cells and circuitries.

As noted, the function of TULP1 has not been fully established; most studies have been focused on photoreceptor and RPE cells (see below). Trafficking between inner and outer segments (Hagstrom et al., 2001, 2012; Xi et al., 2005; Grossman et al., 2011), and cytoskeletal functions including vesicular transport in the synaptic region (Xi et al., 2007; Grossman et al., 2009, 2013; Wahl et al., 2016) are known functions in photoreceptor cells. These functions are in line with our analysis of cell type-specific expression of validated (such as *Actb*, *Actg1*, *Map1b*, and *Dnm1*) and predicted (such as *Bbs2*, *Rpgrip1,* and *Ush2a*) TULP1 interactor genes (**Figure 9** and **Supplementary Figure 10**). Indeed, predicted cytoskeletal TULP1 interactor genes were expressed in all retinal cell types analyzed including bipolar, ganglion, Muller, and RPE cells. While TULP1's role in the cytoskeleton has been described in the context of photoreceptors (see above), RPE (Caberoy et al., 2010) and DNM1 expression in the inner retina (Grossman et al., 2013), our study predicts TULP1 as a cytoskeletal interactor in all analyzed retinal cell types.

Notably, the data also highlight the retinoid visual cycle as a potential new TULP1-linked retinal function (**Figure 9** and **Supplementary Figure 10**). Various proteins involved in aspects of the retinoid cycle (*Rbp3*, *Rgr*, and *Abca4*, and *Rpe65* and *Lrat* from the high- and medium-confidence predicted TULP1 interactor lists, respectively) were expressed in a number of retinal cell types, including photoreceptor (*Rbp3* and *Abca4*), bipolar (*Rgr* and *Abca4*), Muller (*Rgr* and *Rbp3*), and RPE cells (*Rgr*, *Abca4*, *Rpe65,* and *Lrat*). Expression of *Rgr* is typically linked to RPE and Muller cells, *Abca4* to photoreceptors and *Rbp3* to photoreceptor and retinoblastoma cells (Entrez). As such, our findings suggest some atypical sites of expression for these genes. However, other studies also detected uncommon expression for some of these genes; *Abca4* has been found expressed in RPE cells (Lenis et al., 2018) and *Rbp3* in bipolar and ganglion cells (Siegert et al., 2012). Additionally, as some of these cells are in close physical contact to each other in the retina, for example, photoreceptor and RPE, or photoreceptor and Muller cells, contamination between these cell types may happen and ultimately influence cell-specific gene expression data.

Signal transduction was another function newly predicted for TULP1 interactor genes in non-photoreceptor cells (**Figure 9** and **Supplementary Figure 10**), for example, in RPE (*Axl*, *Nck1*, *Tyro3*, and *Mertk*), ganglion (*Axl*, *Tyro3*, *Grb2*, *Nck1*), bipolar (*Mertk*) and Muller (*Mertk* and *Grb2*) cells. Additionally, expression of a number of transcription factors that were predicted with high confidence as TULP1 interactors (*Nrl*, *Crx*, and *Nr2e3*) were detected (**Figure 9**). As these transcription factors were expressed in various retinal cell types, TULP1 may possibly be involved in regulation of development and maturation of the retina as indicated previously (Boggon et al., 1999; Milam et al., 2000; Grossman et al., 2009). In summary, cell type-specific expression of validated and predicted TULP1 interactor genes suggest differential utility of TULP1 in various cell types in mouse retina including bipolar and Muller cells, where expression of *Tulp1* was not recognized before. Some predicted TULP1-linked retinal functions, such as the retinoid visual cycle, or non-photoreceptor signal transduction have been highlighted for the first time. These studies were based on bioinformatic analysis of mRNA expression of predicted TULP1 interactor genes and so predicted TULP1 interactors will require validation by proteomic approaches. Nevertheless, our data highlight the potentially diverse roles that TULP1 may play in the retina.

The data suggest that *Tulp1* is expressed in various cell types in the retina; this may explain the severe phenotype of TULP1-linked IRD (Jacobson et al., 2014) and may be relevant from a therapeutic perspective. We interrogated how unique this feature might be among IRD genes (RetNet - Retinal Information Network, 2019). Indeed, expression of a significant proportion of ∼180 mouse IRD genes has previously been detected in adult retinal cell types (Siegert et al., 2012). However, to the best of our knowledge, cell type-specific expression of IRD genes has not been evaluated in the early postnatal mouse retina. As such, we analyzed the expression of 235 mouse orthologs of a panel of 251 human IRD genes (Dockery et al., 2017) in p4–p7 mouse retinal expression data sets and found widespread expression of IRD genes in various, often multiple retinal cell types at p4–p7 (**Figure 10**). Taking *Tulp1* as an example, this gene is primarily expressed in photoreceptor cells. However, it also appears to be expressed in a number of non-photoreceptor cell types as observed using both mRNA expression data and immunocytochemistry in this study. It is possible that restoring TULP1 levels solely in photoreceptors may not provide the level of therapeutic benefit expected. Data from Siegert et al. (2012), Jacobson et al. (2014) and the current analysis suggest more extensive expression in both the outer and inner retina for a significant number of IRD genes.

Current interest in ocular gene therapy is enormous with recent approval, by the FDA/EMA, of Luxturna, the first ocular gene therapy. Results from this study provide significant evidence of expression of *Tulp1* in murine retinal non-photoreceptor cells, in particular, during early postnatal development. These data correlate with human studies (Milam et al., 2000; Caberoy et al., 2010), additionally, they suggest significant roles for TULP1 in both photoreceptor and non-photoreceptor cells. A bioinformatic analysis of IRD genes suggests widespread expression of many other IRD genes in both inner and outer retinal cell types during early development. These findings raise the possibility that gene therapies targeting *TULP1* (Widgren et al., 2016; Chen et al., 2018) (Jacobson et al., 2014; Avela et al., 2019) and other similarly expressed IRD genes, may possibly need to restore expression of these genes in both

photoreceptor and non-photoreceptor cells. Furthermore, early postnatal expression of these genes highlights a potential hurdle for future treatments of some IRDs.

DATA AVAILABILITY STATEMENT

All datasets presented in this study are included in the article/**Supplementary Material**.

ETHICS STATEMENT

The animal study was reviewed and approved by the Animal Research Ethics Committee, University of Dublin, Trinity College.

AUTHOR CONTRIBUTIONS

AP: concept, experimental design, experiments, figures and artwork, writing the manuscript, and grant support. AY: experimental design, experiments, and writing the manuscript. PH: concept and grant support. KH: bioinformatics and writing the manuscript. GF: concept, experimental design, writing the manuscript, and grant support. All authors contributed to the article and approved the submitted version.

FUNDING

Health Research Board of Ireland (HRA-POR-2013-376 and HRAPOR-2015-1140), Science Foundation Ireland (16/IA/4452), Fighting Blindness Ireland – Health Research Charities Ireland (formerly Medical Research Charities Group; MRCG-2016-14), JSC Center for International Programs "Bolashak" (15-1/9842) Republic of Kazakhstan, StarT Marie Curie Innovative Training Network (813490).

ACKNOWLEDGMENTS

The authors thank Dr. Robert Molday (University of British Columbia, Vancouver, BC, Canada) for providing the 4D2 rhodopsin antibody and Stephanie A. Hagstrom (Cleveland Clinic, Cleveland, OH, United States) for providing the M-tulp1N tulp1 antibody.

SUPPLEMENTARY MATERIAL

The Supplementary Material for this article can be found online at: https://www.frontiersin.org/articles/10.3389/fnins.2020.00656/full#supplementary-material

REFERENCES

Avela, K., Salonen-Kajander, R., Laitinen, A., Ramsden, S., Barton, S., and Rudanko, S. L. (2019). The genetic aetiology of retinal degeneration in children in Finland – new founder mutations identified. *Acta Ophthalmol.* 97, 805–814. doi: 10.1111/aos.14128

Boggon, T. J., Shan, W. S., Santagata, S., Myers, S. C., and Shapiro, L. (1999). Implication of tubby proteins as transcription factors by structure- based functional analysis. *Science* 286, 2119–2125. doi: 10.1126/science.286.5447.2119

Caberoy, N. B., and Li, W. (2009). Unconventional secretion of tubby and tubby-like protein 1. *FEBS Lett.* 583, 3057–3062. doi: 10.1016/j.febslet.2009.08.015

Caberoy, N. B., Zhou, Y., and Li, W. (2010). Tubby and tubby-like protein 1 are new MerTK ligands for phagocytosis. *EMBO J.* 29, 3898–3910. doi: 10.1038/emboj.2010.265

Chen, X., Sheng, X., Liu, Y., Li, Z., Sun, X., Jiang, C., et al. (2018). Distinct mutations with different inheritance mode caused similar retinal dystrophies in one family: a demonstration of the importance of genetic annotations in complicated pedigrees. *J. Transl. Med.* 16:145. doi: 10.1186/s12967-018-1522-7

Daniszewski, M., Senabouth, A., Nguyen, Q. H., Crombie, D. E., Lukowski, S. W., Kulkarni, T., et al. (2018). Single cell RNA sequencing of stem cell-derived retinal ganglion cells. *Sci. Data* 5:180013. doi: 10.1038/sdata.2018.13

Dockery, A., Stephenson, K., Keegan, D., Wynne, N., Silvestri, G., Humphries, P., et al. (2017). Target 5000: target capture sequencing for inherited retinal degenerations. *Genes* 8:304. doi: 10.3390/genes8110304

Duncan, J. L., Pierce, E. A., Laster, A. M., Daiger, S. P., Birch, D. G., Ash, J. D., et al. (2018). Inherited retinal degenerations: current landscape and knowledge gaps. *Transl. Vis. Sci. Technol.* 7:6. doi: 10.1167/tvst.7.4.6

Farrar, G. J., Carrigan, M., Dockery, A., Millington-Ward, S., Palfi, A., Chadderton, N., et al. (2017). Toward an elucidation of the molecular genetics of inherited retinal degenerations. *Hum. Mol. Genet.* 26, R2–R11. doi: 10.1093/hmg/ddx185

Gargini, C., Terzibasi, E., Mazzoni, F., and Strettoi, E. (2007). Retinal organization in the retinal degeneration 10 (rd10) mutant mouse: a morphological and ERG study. *J. Comp. Neurol.* 500, 222–238. doi: 10.1002/cne.21144

Grossman, G. H., Beight, C. D., Ebke, L. A., Pauer, G. J. T., and Hagstrom, S. A. (2014). Interaction of tubby-like protein-1 (Tulp1) and microtubule-associated protein (MAP) 1A and MAP1B in the mouse retina. *Adv. Exp. Med. Biol.* 801, 511–518. doi: 10.1007/978-1-4614-3209-8_65

Grossman, G. H., Ebke, L. A., Beight, C. D., Jang, G. F., Crabb, J. W., and Hagstrom, S. A. (2013). Protein partners of dynamin-1 in the retina. *Vis. Neurosci.* 30, 129–139. doi: 10.1017/S0952523813000138

Grossman, G. H., Pauer, G. J. T., Narendra, U., Peachey, N. S., and Hagstrom, S. A. (2009). Early synaptic defects in tulp1-/- mice. *Investig. Ophthalmol. Vis. Sci.* 50, 3074–3083. doi: 10.1167/iovs.08-3190

Grossman, G. H., Watson, R. F., Pauer, G. J. T., Bollinger, K., and Hagstrom, S. A. (2011). Immunocytochemical evidence of Tulp1-dependent outer segment protein transport pathways in photoreceptor cells. *Exp. Eye Res.* 93, 658–668. doi: 10.1016/j.exer.2011.08.005

Hagstrom, S. A., Adamian, M., Scimeca, M., Pawlyk, B. S., Yue, G., and Li, T. (2001). A role for the Tubby-like protein 1 in rhodopsin transport. *Invest. Ophthalmol. Vis. Sci.* 42, 1955–1962.

Hagstrom, S. A., Duyao, M., North, M. A., and Li, T. (1999). Retinal degeneration in tulp1-/- mice: vesicular accumulation in the interphotoreceptor matrix. *Invest. Ophthalmol. Vis. Sci.* 40, 2795–2802.

Hagstrom, S. A., Watson, R. F., Pauer, G. J. T., and Grossman, G. H. (2012). Tulp1 is involved in specific photoreceptor protein transport pathways. *Adv. Exp. Med. Biol.* 723, 783–789. doi: 10.1007/978-1-4614-0631-0_100

Humphries, M. M., Rancourt, D., Farrar, G. J., Kenna, P., Hazel, M., Bush, R. A., et al. (1997). Retinopathy induced in mice by targeted disruption of the rhodopsin gene. *Nat. Genet.* 15, 216–219. doi: 10.1038/ng0297-216

Ikeda, S., Shiva, N., Ikeda, A., Smith, R. S., Nusinowitz, S., Yan, G., et al. (2000). Retinal degeneration but not obesity is observed in null mutants of the tubby-like protein 1 gene. *Hum. Mol. Genet.* 9, 155–163. doi: 10.1093/hmg/9.2.155

Jacobson, S. G., Cideciyan, A. V., Huang, W. C., Sumaroka, A., Roman, A. J., Schwartz, S. B., et al. (2014). TULP1 mutations causing early-onset retinal degeneration: preserved but insensitive macular cones. *Investig. Ophthalmol. Vis. Sci.* 55, 5354–5364. doi: 10.1167/iovs.14-14570

Jeon, C. J., Strettoi, E., and Masland, R. H. (1998). The major cell populations of the mouse retina. *J. Neurosci.* 18, 8936–8946. doi: 10.1523/jneurosci.18-21-08936.1998

Johnson, G. V. W., and Jope, R. S. (1992). The role of microtubule-associated protein 2 (MAP-2) in neuronal growth, plasticity, and degeneration. *J. Neurosci. Res.* 33, 505–512. doi: 10.1002/jnr.490330402

Laboissonniere, L. A., Goetz, J. J., Martin, G. M., Bi, R., Lund, T. J. S., Ellson, L., et al. (2019). Molecular signatures of retinal ganglion cells revealed through single cell profiling. *Sci. Rep.* 9, 1–15. doi: 10.1038/s41598-019-52215-4

Lenis, T. L., Hu, J., Ng, S. Y., Jiang, Z., Sarfare, S., Lloyd, M. B., et al. (2018). Expression of ABCA4 in the retinal pigment epithelium and its implications for Stargardt macular degeneration. *Proc. Natl. Acad. Sci. U.S.A.* 115, E11120–E11127. doi: 10.1073/pnas.1802519115

Lukowski, S. W., Lo, C. Y., Sharov, A. A., Nguyen, Q., Fang, L., Hung, S. S., et al. (2019). A single-cell transcriptome atlas of the adult human retina. *EMBO J.* 38:e100811. doi: 10.15252/embj.2018100811

Macosko, E. Z., Basu, A., Satija, R., Nemesh, J., Shekhar, K., Goldman, M., et al. (2015). Highly parallel genome-wide expression profiling of individual cells using nanoliter droplets. *Cell* 161, 1202–1214. doi: 10.1016/j.cell.2015.05.002

Menon, M., Mohammadi, S., Davila-Velderrain, J., Goods, B. A., Cadwell, T. D., Xing, Y., et al. (2019). Single-cell transcriptomic atlas of the human retina identifies cell types associated with age-related macular degeneration. *Nat. Commun.* 10, 1–9. doi: 10.1038/s41467-019-12780-8

Milam, A. H., Hendrickson, A. E., Xiao, M., Smith, J. E., Possin, D. E., John, S. K., et al. (2000). Localization of tubby-like protein 1 in developing and adult human retinas. *Invest. Ophthalmol. Vis. Sci.* 41, 2352–2356.

Palfi, A., Hokamp, K., Hauck, S. M., Vencken, S., Millington-Ward, S., Chadderton, N., et al. (2016). MicroRNA regulatory circuits in a mouse model of inherited retinal degeneration. *Sci. Rep.* 6:31431. doi: 10.1038/srep31431

Portera-Cailliau, C., Sung, C. H., Nathans, J., and Adler, R. (1994). Apoptotic photoreceptor cell death in mouse models of retinitis pigmentosa. *Proc. Natl. Acad. Sci. U.S.A.* 91, 974–978. doi: 10.1073/pnas.91.3.974

Puthussery, T., Gayet-Primo, J., Pandey, S., Duvoisin, R. M., and Taylor, W. R. (2009). Differential loss and preservation of glutamate receptor function in bipolar cells in the rd10 mouse model of retinitis pigmentosa. *Eur. J. Neurosci.* 29, 1533–1542. doi: 10.1111/j.1460-9568.2009.06728.x

Retina International (2019). *The Socioeconomic Impact of Inherited Retinal Dystrophies (IRDs) in the Republic of Ireland The Socioeconomic Impact of Inherited Retinal Dystrophies (IRDs) in the Republic of Ireland Retina International*. Available online at: http://www.retina-international.org/wp-content/uploads/2019/11/cost-of-illness-final-report-roi.pdf (accessed December 20, 2019).

RetNet - Retinal Information Network (2019). Available online at: https://sph.uth.edu/retnet/ (accessed September 23, 2019).

Rheaume, B. A., Jereen, A., Bolisetty, M., Sajid, M. S., Yang, Y., Renna, K., et al. (2018). Single cell transcriptome profiling of retinal ganglion cells identifies cellular subtypes. *Nat. Commun.* 9:2759. doi: 10.1038/s41467-018-05134-3

Robinson, M. D., and Oshlack, A. (2010). A scaling normalization method for differential expression analysis of RNA-seq data. *Genome Biol.* 11:R25. doi: 10.1186/gb-2010-11-3-r25

Roche, S. L., Wyse-Jackson, A. C., Byrne, A. M., Ruiz-Lopez, A. M., and Cotter, T. G. (2016). Alterations to retinal architecture prior to photoreceptor loss in a mouse model of retinitis pigmentosa. *Int. J. Dev. Biol.* 60, 127–139. doi: 10.1387/ijdb.150400tc

Sahel, J. A., Marazova, K., and Audo, I. (2015). Clinical characteristics and current therapies for inherited retinal degenerations. *Cold Spring Harb. Perspect. Med.* 5:a017111. doi: 10.1101/cshperspect.a017111

Sakami, S., Imanishi, Y., and Palczewski, K. (2019). Müller glia phagocytose dead photoreceptor cells in a mouse model of retinal degenerative disease. *FASEB J.* 33, 3680–3692. doi: 10.1096/fj.201801662r

Sanyal, S., De Ruiter, A., and Hawkins, R. K. (1980). Development and degeneration of retina inrds mutant mice: light microscopy. *J. Comp. Neurol.* 194, 193–207. doi: 10.1002/cne.901940110

Shekhar, K., Lapan, S. W., Whitney, I. E., Tran, N. M., Macosko, E. Z., Kowalczyk, M., et al. (2016). Comprehensive classification of retinal bipolar neurons by single-cell transcriptomics. *Cell* 166, 1308.e30–1323.e30. doi: 10.1016/j.cell.2016.07.054

Siegert, S., Cabuy, E., Scherf, B. G., Kohler, H., Panda, S., Le, Y.-Z., et al. (2012). Transcriptional code and disease map for adult retinal cell types. *Nat. Neurosci.* 15, 487–495. doi: 10.1038/nn.3032

Singh, R. K., Kolandaivelu, S., and Ramamurthy, V. (2014). Early alteration of retinal neurons in aipl1 -/- animals. *Investig. Ophthalmol. Vis. Sci.* 55, 3081–3092. doi: 10.1167/iovs.13-13728

Smith, J., Ward, D., Michaelides, M., Moore, A. T., and Simpson, S. (2015). New and emerging technologies for the treatment of inherited retinal diseases: a horizon scanning review. *Eye* 29, 1131–1140. doi: 10.1038/eye.2015.115

Soto, F., and Kerschensteiner, D. (2015). Synaptic remodeling of neuronal circuits in early retinal degeneration. *Front. Cell. Neurosci.* 9:395. doi: 10.3389/fncel.2015.00395

Strettoi, E., and Pignatelli, V. (2000). Modifications of retinal neurons in a mouse model of retinitis pigmentosa. *Proc. Natl. Acad. Sci. U.S.A.* 97, 11020–11025. doi: 10.1073/pnas.190291097

Strettoi, E., Pignatelli, V., Rossi, C., Porciatti, V., and Falsini, B. (2003). Remodeling of second-order neurons in the retina of rd/rd mutant mice. *Vis. Res.* 43, 867–877. doi: 10.1016/s0042-6989(02)00594-1

Strettoi, E., Porciatti, V., Falsini, B., Pignatelli, V., and Rossi, C. (2002). Morphological and functional abnormalities in the inner retina of the rd/rd mouse. *J. Neurosci.* 22, 5492–5504. doi: 10.1523/JNEUROSCI.22-13-05492.2002

Szebenyi, G., Bollati, F., Bisbal, M., Sheridan, S., Faas, L., Wray, R., et al. (2005). Activity-driven dendritic remodeling requires microtubule-associated protein 1A. *Curr. Biol.* 15, 1820–1826. doi: 10.1016/j.cub.2005.08.069

Szklarczyk, D., Gable, A. L., Lyon, D., Junge, A., Wyder, S., Huerta-Cepas, J., et al. (2019). STRING v11: protein-protein association networks with increased coverage, supporting functional discovery in genome-wide experimental datasets. *Nucleic Acids Res.* 47, D607–D613. doi: 10.1093/nar/gky1131

Vaillant, A. R., Zanassi, P., Walsh, G. S., Aumont, A., Alonso, A., and Miller, F. D. (2002). Signaling mechanisms underlying reversible activity-dependent dendrite formation. *Neuron* 34, 985–998. doi: 10.1016/S0896-6273(02)00717-1

Wahl, S., Magupalli, V. G., Dembla, M., Katiyar, R., Schwarz, K., Köblitz, L., et al. (2016). The disease protein tulp1 is essential for periactive zone endocytosis in photoreceptor ribbon synapses. *J. Neurosci.* 36, 2473–2493. doi: 10.1523/JNEUROSCI.2275-15.2016

Wang, Y., and Rubel, E. W. (2008). Rapid regulation of microtubule-associated protein 2 in dendrites of nucleus laminaris of the chick following deprivation of afferent activity. *Neuroscience* 154, 381–389. doi: 10.1016/j.neuroscience.2008.02.032

Whitmore, S. S., Wagner, A. H., DeLuca, A. P., Drack, A. V., Stone, E. M., Tucker, B. A., et al. (2014). Transcriptomic analysis across nasal, temporal, and macular regions of human neural retina and RPE/choroid by RNA-Seq. *Exp. Eye Res.* 129, 93–106. doi: 10.1016/j.exer.2014.11.001

Widgren, P., Hurme, A., Falck, A., Keski-Filppula, R., Remes, A. M., Moilanen, J., et al. (2016). Genetic aetiology of ophthalmological manifestations in children - A focus on mitochondrial disease-related symptoms. *Acta Ophthalmol.* 94, 83–91. doi: 10.1111/aos.12897

Xi, Q., Pauer, G. J. T., Ball, S. L., Rayborn, M., Hollyfield, J. G., Peachey, N. S., et al. (2007). Interaction between the photoreceptor-specific tubby-like protein 1 and the neuronal-specific GTPase dynamin-1. *Investig. Ophthalmol. Vis. Sci.* 48, 2837–2844. doi: 10.1167/iovs.06-0059

Xi, Q., Pauer, G. J. T., Marmorstein, A. D., Crabb, J. W., and Hagstrom, S. A. (2005). Tubby-like protein 1 (TULP1) interacts with F-actin in photoreceptor cells. *Investig. Ophthalmol. Vis. Sci.* 46, 4754–4761. doi: 10.1167/iovs.05-0693

Zhang, Q. C., Petrey, D., Deng, L., Qiang, L., Shi, Y., Thu, C. A., et al. (2012). Structure-based prediction of protein–protein interactions on a genome-wide scale. *Nature* 490, 556–560. doi: 10.1038/nature11503

Conflict of Interest: The authors declare that the research was conducted in the absence of any commercial or financial relationships that could be construed as a potential conflict of interest.

Copyright © 2020 Palfi, Yesmambetov, Humphries, Hokamp and Farrar. This is an open-access article distributed under the terms of the Creative Commons Attribution License (CC BY). The use, distribution or reproduction in other forums is permitted, provided the original author(s) and the copyright owner(s) are credited and that the original publication in this journal is cited, in accordance with accepted academic practice. No use, distribution or reproduction is permitted which does not comply with these terms.

frontiers in Neuroscience

ORIGINAL RESEARCH
published: 03 August 2020
doi: 10.3389/fnins.2020.00800

Foveal Therapy in Blue Cone Monochromacy: Predictions of Visual Potential From Artificial Intelligence

*Alexander Sumaroka[1], Artur V. Cideciyan[1], Rebecca Sheplock[1], Vivian Wu[1], Susanne Kohl[2], Bernd Wissinger[2] and Samuel G. Jacobson[1]**

[1] Scheie Eye Institute, Department of Ophthalmology, Perelman School of Medicine, University of Pennsylvania, Philadelphia, PA, United States, [2] Molecular Genetics Laboratory, Institute for Ophthalmic Research, Centre for Ophthalmology, University of Tüebingen, Tüebingen, Germany

Novel therapeutic approaches for treating inherited retinal degenerations (IRDs) prompt a need to understand which patients with impaired vision have the anatomical potential to gain from participation in a clinical trial. We used supervised machine learning to predict foveal function from foveal structure in blue cone monochromacy (BCM), an X-linked congenital cone photoreceptor dysfunction secondary to mutations in the *OPN1LW/OPN1MW* gene cluster. BCM patients with either disease-associated large deletion or missense mutations were studied and results compared with those from subjects with other forms of IRD and various degrees of preserved central structure and function. A machine learning technique was used to associate foveal sensitivities and best-corrected visual acuities to foveal structure in IRD patients. Two random forest (RF) models trained on IRD data were applied to predict foveal function in BCM. A curve fitting method was also used and results compared with those of the RF models. The BCM and IRD patients had a comparable range of foveal structure. IRD patients had peak sensitivity at the fovea. Machine learning could successfully predict foveal sensitivity (FS) results from segmented or un-segmented optical coherence tomography (OCT) input. Application of machine learning predictions to BCM at the fovea showed differences between predicted and measured sensitivities, thereby defining treatment potential. The curve fitting method provided similar results. Given a measure of visual acuity (VA) and foveal outer nuclear layer thickness, the question of how many lines of acuity would represent the best efficacious result for each BCM patient could be answered. We propose that foveal vision improvement potential in BCM is predictable from retinal structure using machine learning and curve fitting approaches. This should allow estimates of maximal efficacy in patients being considered for clinical trials and also guide decisions about dosing.

Keywords: machine learning, random forest, optical coherence tomography, chromatic perimetry, retinal degeneration, rods, cones, visual acuity

OPEN ACCESS

Edited by:
Nicolás Cuenca, University of Alicante, Spain

Reviewed by:
David Geoffrey Birch, Retina Foundation of the Southwest, United States
John Gerard Flannery, University of California, Berkeley, United States

***Correspondence:**
Samuel G. Jacobson
jacobsos@pennmedicine.upenn.edu

Specialty section:
This article was submitted to Neurodegeneration, a section of the journal Frontiers in Neuroscience

Received: *25 March 2020*
Accepted: *07 July 2020*
Published: *03 August 2020*

Citation:
Sumaroka A, Cideciyan AV, Sheplock R, Wu V, Kohl S, Wissinger B and Jacobson SG (2020) Foveal Therapy in Blue Cone Monochromacy: Predictions of Visual Potential From Artificial Intelligence. Front. Neurosci. 14:800. doi: 10.3389/fnins.2020.00800

INTRODUCTION

Gene augmentation therapy clinical trials in inherited retinal degenerations (IRDs) have to date mainly delivered vector-gene product by the subretinal route (reviewed in Garafalo et al., 2019). A preferred surgical location for the induced retinal detachment has been the macular region. Among the many reasons for targeting the macula is the realization that, if proven safe, a therapy

that increases or preserves central vision would be noticed and appreciated by patients. Also, monitoring of post-treatment efficacy could occur by common clinical methods such as visual acuity (VA) and central structural parameters using optical coherence tomography (OCT).

Many IRD patients with impaired foveal structure and vision could benefit from gene augmentation delivered to the retina with a less traumatic method than a surgically induced macular detachment which carries the potential risk of further reducing central vision. One potential option is an intravitreal delivery of vector-gene product. Among the caveats associated with intravitreal gene therapy are concerns about potency and inducing uveitis (Miller and Vandenberghe, 2018) and most experimental evidence in non-human primates is that mainly the photoreceptors in the fovea would be able to be targeted with the current viral vectors (Dalkara et al., 2013; Boye et al., 2016; Khabou et al., 2018; Byrne et al., 2020).

A number of IRDs would qualify as diseases in which an improvement in VA, despite foveal photoreceptor abnormalities, would be welcomed by affected patients, even if not accompanied by a gain in expanse of visual field (Garafalo et al., 2019). Among these IRDs is blue cone monochromacy (BCM), the X-linked congenital disorder with loss of red (L, long wavelength sensitive) and green (M, middle wavelength sensitive) cone photoreceptor function secondary to mutations in the *OPN1LW/OPN1MW* gene cluster on chromosome Xq28. There is evidence of retained L/M cones at and around the fovea in BCM, suggesting that this condition may be a candidate for intravitreal gene therapy (Cideciyan et al., 2013; Carroll et al., 2014; Scoles et al., 2016; Sumaroka et al., 2018; Garafalo et al., 2019). Missing to date, however, have been studies that would determine the level of efficacy that could be expected from such therapy, i.e., what is the degree of improvement in foveal function that could occur in the individual BCM patient.

Machine learning techniques have recently been used to predict treatment potential in two forms of Leber congenital amaurosis (LCA) caused by mutations in *CEP290* or *IQCB1* (*NPHP5*), that had little or no measurable vision but some measurable central retinal structure (Sumaroka et al., 2019). The present work uses these methods to try to predict from cross-sectional retinal structure images with OCT in BCM patients of different genotypes the best possible foveal visual outcomes in a clinical trial of intravitreally delivered vector-gene, acknowledging that it would only target foveal cones and not extracentral dysfunctional cones in these retinas.

MATERIALS AND METHODS

Human Subjects

Two groups of patients were included: IRD patients (n = 26; ages 18–72 years; **Supplementary Table S1**) and BCM patients (n = 16; ages 7–52 years; **Supplementary Table S2**). IRD patients had retained visual acuities of at least 20/250 and measurable foveal cone function, determined as sensitivity to a 600-nm light stimulus on a white background light. All IRD patients had retained foveal outer nuclear layer thickness (range, 24–150 μm). We assumed that the cones in this cohort of IRD patients were functioning proportional to their remaining quantum catch and there was no additional de-sensitization beyond the partial loss of photoreceptors and shortening of outer segments (OSs) among the surviving cones (Sumaroka et al., 2019). Patients with cystoid macular edema or foveal atrophy were not included. Data from three normal subjects (N1–3, ages 22–32) were also included in this "training set" to cover the full range of foveal photoreceptor layer parameters. BCM patients included two eight-patient cohorts with different genotypes: those with large deletion mutations and those with the C203R missense mutation in a singular resident *OPN1LW* or *OPN1LW/MW* hybrid gene or in all genes of the *OPN1LW/OPN1MW* gene cluster (Sumaroka et al., 2018). All subjects underwent a complete eye examination as well as specialized tests of visual function and structure. Data from one eye were included for each patient. The research was approved by the institutional review board at the University of Pennsylvania. Previous genetic research testing in addition was approved by the institutional review board at the University of Tuebingen. All subjects were treated in accordance with the tenets of the Declaration of Helsinki; informed consent was obtained from adults, and assent with parental permission for all children.

Foveal Structure: Optical Coherence Tomography (OCT), Data Extraction

Cross-sections along the horizontal meridian through the fovea were obtained with OCT (RTVue-100; Optovue Inc., Fremont, CA, United States). The principles of the method and our recording and analysis techniques have been published (e.g., Sumaroka et al., 2016, 2018). Three 15° wide B-scans composed of 4,091 A-scans or longitudinal reflectivity profiles (LRPs) were selected from each subject. Post-acquisition processing of OCT data was performed with custom programs (MATLAB Release, 2018, MathWork, Natick, MA, United States). All scans were aligned by straightening the major hyperreflective signal believed to originate near the interface between the basal aspect of the retinal pigment epithelium and Bruch's membrane (RPE2/BrM). To increase the signal-to-noise ratio, lateral sampling density of the B-scan was reduced by averaging neighboring LRPs to get 512 A-scans per 15°. All scans were centered at the fovea; the foveola was identified manually as the maximum depression. Six retinal layers were identified and segmented with a computer-assisted algorithm: outer plexiform layer (OPL), external limiting membrane (ELM), inner segment (IS)/OS [also known as ellipsoid zone (EZ)] line, cone OS tips (COST; also known as phagosome zone; Cuenca et al., 2018, 2020), apical aspect of the RPE (RPE1), and RPE2/BrM (**Supplementary Figure S1A**). From this segmentation, ONL thickness, IS and COS length, and RPE thickness were extracted. Data were extracted at seven eccentricities centered at the fovea with 0.25° increments. In addition, the number of negative and positive peaks (extrema) on the gradient of the LRPs between the ELM and RPE2/BrM layers was automatically counted (**Supplementary Figure S1B**). The reflectivity values at each

depth with respect to RPE2/BrM were extracted at the same eccentricity (**Supplementary Figure S1C**). The results of data extraction for ONL, IS, COS, and RPE are shown and the range of the values in the training set overlap with those of the BCM patient set (**Supplementary Figure S1D**).

Foveal Function: Visual Sensitivity and Visual Acuity

Visual sensitivities were measured in the light-adapted state using 600-nm stimuli (size V, 1.7° diameter, 200 ms duration) on a standard 10 cd.m^{-2} white background (Humphrey Field Analyzer, HFA-750i analyzer, Zeiss-Humphrey, Dublin, CA, United States). The method has been described (for example, Charng et al., 2016; Matsui et al., 2016). Best-corrected VA was measured with the Early Treatment Diabetic Retinopathy Study (ETDRS) methodology.

Data Analysis of the Training Set: Relationship of Structure and Function

We used two techniques of regression analysis to predict the possible outcome of treatment. The first technique, a supervised machine learning approach [random forest (RF)], was used to model the relationship between foveal function [foveal sensitivity (FS); VA] and retinal structure. Following our previous data analyses (Sumaroka et al., 2019), two groups of models based on the form of input variables were constructed. The model in each group was applied to predict FS and VA. Group 1 (Model I-FS and I-VA) used the input features derived from segmentation parameters: thicknesses of ONL, IS, COS, and RPE, and the number of distinct layers between ELM and RPE2/BrM. Additionally, the relationship between ONL and COS, and thickness of these layers and retinal eccentricity were accounted for by directly including interaction terms. For models in Group II (Model II-FS and II-VA), only reflectivity values were used as input features. Performance of each model was evaluated by leave-one-out, 29-fold cross-validation. The predicted value was defined as average of prediction at each eccentricity in all three scans based on the remaining subjects in the training set.

The second technique was based on curve fitting using the established relationship between photopigment (and outer retinal structure) and visual-retinal thresholds, measured by psychophysics or electrophysiology (Ripps et al., 1978; Machida et al., 2000; Jacobson et al., 2005, 2014). To implement fitting, we used the relationship between retinal structural data and functional data derived from our training set (**Supplementary Figure S1E**). In this technique, the predicted result was defined as the average of three predictions using foveal ONL (0-eccentricity).

Final RF models were trained using data from all 29 subjects (26 IRD and three normals). Root-mean-square error (RMSE) was used as an indicator of model performance for all methods. The difference between the measured target variable (sensitivity) and the predicted value was calculated first. Difference across all patients was squared, averaged, and square root extracted. Range of predictions were estimated as $\pm$ 1.96*RMSE.

RESULTS

Machine Learning to Predict Foveal Function From Foveal Structure in IRDs

We first asked whether the machine learning algorithm can be trained to predict reliably the foveal cone sensitivity based on co-localized foveal retinal structure in a cohort of patients with different forms of IRD. An RF supervised learning algorithm was used with the foveal structure parameters as input and light-adapted 600 nm sensitivity as output (**Figure 1**). Measured and predicted FSs were compared for all IRD patients. Data from six IRD patients illustrate a range of thicknesses of foveal ONL (**Figures 1A,D**) along with the corresponding measured FS and VA in comparison with predictions by two models for each parameter (I-FS, II-FS and I-VA, II-VA, respectively) (**Figures 1B,C,E,F**). S23 and S3 exemplify milder central retinal disease with normal or near-normal FS and retained IS/OS structure, whereas S24 has more severe disease with greater foveal abnormalities in function and structure (**Figure 1A**). S11, S8, and S20 illustrate abnormal foveae with visible defects of IS/OS (**Figure 1D**) similar to those in some BCM patients. Measured FSs in these patients (especially S20) are further reduced and there is corresponding loss of VA.

Measured and predicted FS were compared for the six IRD patients representing a spectrum of disease severities. The predictions of the models appear to approximate well the measured FS and VA values (**Figures 1B,C,E,F**).

Across all IRD patients, differences between measured and predicted sensitivities were used to calculate RMSE for each model (**Figures 2A,B**).

Curve Fitting to Predict Foveal Function From Foveal Structure in IRDs

Using non-linear regression analysis, we fit a logarithmic curve that assumes the cones were functioning proportional to their remaining quantum catch (following the experimental results in Ripps et al., 1978; Machida et al., 2000; Jacobson et al., 2005, 2014). The function used was y = y0 + a*log(x), where y was either FS in dB or VA in decimal and x was foveal ONL thickness in microns. Coefficients for FS were y0 = −12.01, ($p < 0.01$) a = 17.38 ($p < 0.01$) and for VA were y0 = −1.07, ($p < 0.01$) a = 0.91 ($p < 0.01$) (**Figure 2C**, solid line). Examples of the predicted foveal function by calculating FS (**Figures 1B,E**) and VA (**Figures 1C,F**) using only foveal ONL as input are shown. Calculated versus measured FS and VA are plotted across all IRD patients (**Figure 2D**) and an equality line is superimposed (solid line); RMSE was estimated from the difference between measured and calculated FS and VA (dashed lines, **Figures 2C,D**).

Predicted and Measured Sensitivities in BCM

Predictions of FS and VA from foveal structure were then tested in patients with BCM. The BCM patients had either disease-associated large deletion mutations or the C203R mutation (**Supplementary Tables S1, S2**). The two categories of genotypes were recently found to have different phenotypes in terms of

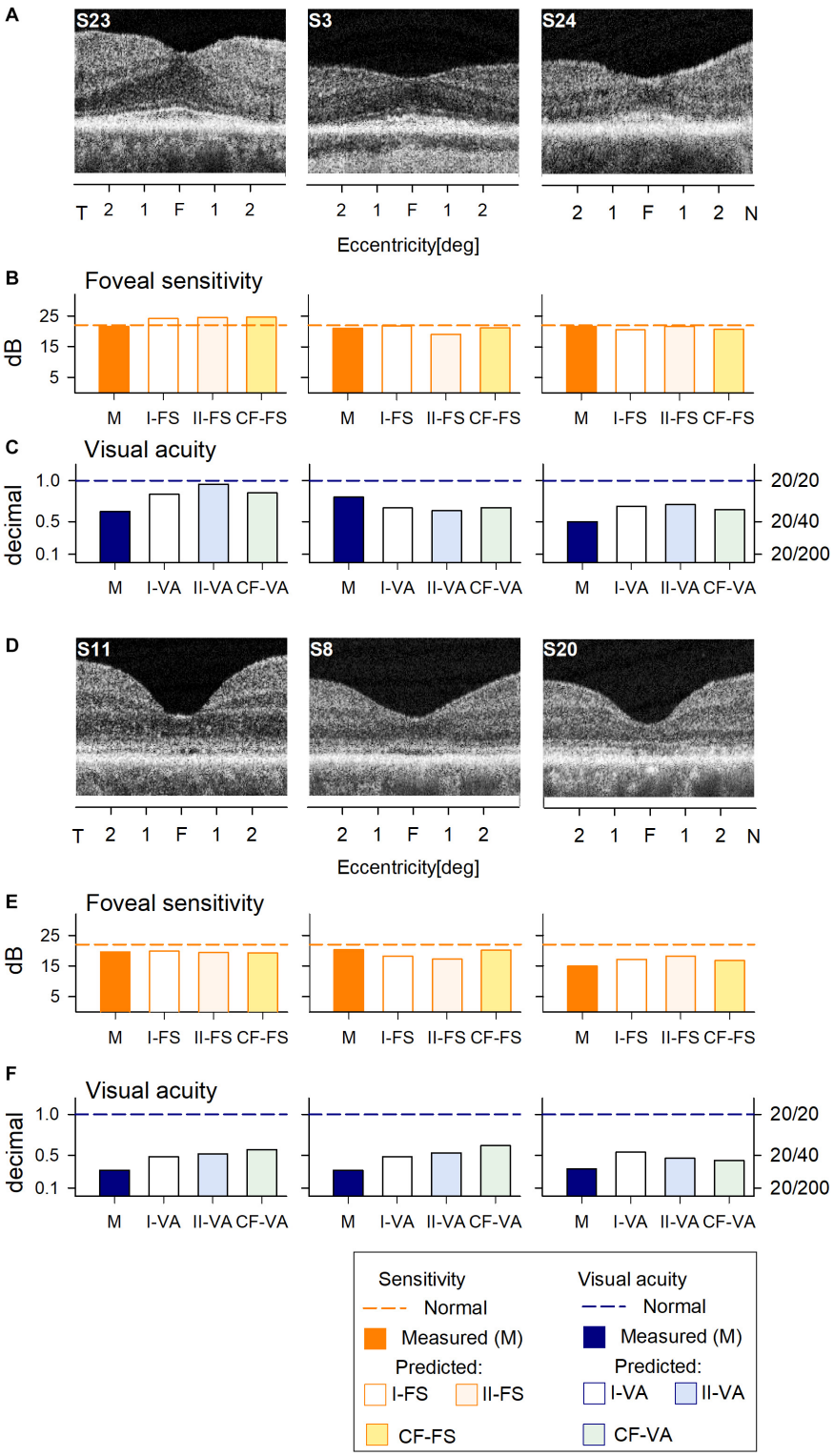

FIGURE 1 | Prediction of foveal sensitivity (FS) and visual acuity (VA) in the IRD training set group. **(A)** Foveal region OCT scans from 3 IRD subjects (S23, S3, S24) representing different ONL thicknesses. **(B)** Comparison of measured FS (M, orange bar) and predicted results by Model I-FS (white bar) and Model II-FS (light orange bar). Yellow bar is FS value calculated by formula extracted from curve fitting (CF-FS). **(C)** Comparison of measured VA (dark blue bar) and predicted by Model I-VA (white bar) and Model II-VA (light blue bar). Light green bar is VA calculated by a formula extracted from curve fitting (CF-VA). **(D–F)** are the same as **(A–C)** but the scans are from 3 IRD subjects (S11, S8, S20) who have visible defects of IS/OS similar to those encountered in some BCM patients. Dashed lines in **(B,C,E,F)** represent lower boundary of normal range.

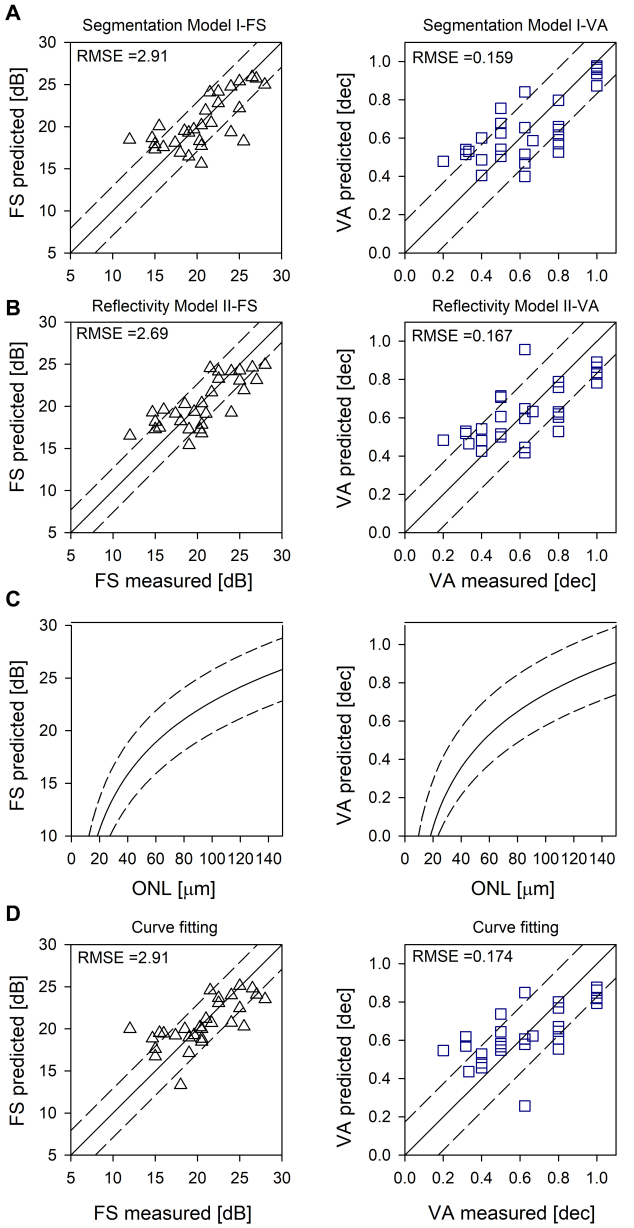

FIGURE 2 | Evaluation of the models. **(A)** Random forest segmentation Model I-FS and I-VA showing predicted versus measured values. **(B)** Random forest Model II-FS and II-VA showing predicted versus measured values. Equality line (y = x) is superimposed (solid line); RMSE are shown as dashed lines **(A,B)**. **(C)** Logarithmic curve [y = y0 + a*log(x)] fitted to FS versus ONL, and VA versus ONL (solid lines). **(D)** Prediction based on curve fitting. Equality line (y = x) is superimposed (solid line). RMSE are shown as dashed lines **(C,D)**.

persistence of foveal structure; patients with large deletions show on average more severe losses of central structure at earlier ages (Sumaroka et al., 2018). The cohort of eight patients with large deletion mutations tended to be younger in age than those with the C203R mutation.

All of the patients with large deletions had no detectable FS at the foveal location. Predicted FS results by the two RF models and the curve fitting were similar and indicated the potential for at least 1.5 log unit FS increases (**Figures 3B,E**). As expected, VA was reduced in all patients; the predicted results by both RF models and curve fitting indicated a comparable level of improvement potential (**Figures 3C,F**). There was no difference between results that explicitly took into consideration cone OS (COS) length (Model I-VA) and the other two approaches (II-VA, CF).

The cohort of C203R BCM patients also had no detectable FS (**Figures 4B,E**) and reduced VA (**Figures 4C,F**). RF models and curve fitting predicted potential increase in FS but some patients (P12, P13, P14) showed slightly greater increases when COS length was not considered (I-FS). This suggests that these BCM foveae with greater ONL thickness but shorter COS than expected had less potential for improvement. This was even more evident in the VA data; Model I-VA tended to predict less improvement than the other two approaches (II-VA, CF).

Comparison of the treatment potential (difference between prediction and measured values) based on data from the three methods is shown for the two BCM genotype groups (**Figure 5**). For the patients with large deletions, all three approaches were, on average, the same. For C203R mutation patients, there was a statistically significant difference between approaches (Kruskal–Wallis one-way ANOVA on Ranks, $P = 0.021$); Model I-FS was on average less than II-FS and CF (Student–Newman–Keuls method $P < 0.05$) (**Figure 5A**). A similar effect was observed with VA predictions with little or no difference for patients with large deletions but considerable difference in the C203R patients (one-way ANOVA, $P < 0.001$, Student–Newman–Keuls method $P < 0.05$ (**Figure 5B**). Plotting ONL versus COS thicknesses for training and BCM sets indicates there is a difference. For the training set, there was strong correlation between COS length and ONL thickness ($r = 0.814$, $P < 0.001$), as has been observed for rod structure by histopathology (Machida et al., 2000). For BCM, there is no correlation of COS and ONL; COS thickness is reduced and independent of genotype. The greater COS thickness for the C203R cohort for the same ONL thickness as in the training set subjects would explain the difference in the prediction between Model I versus Model II as well as CF for the two genotypes (**Figure 5C**).

DISCUSSION

Current understanding of the X-linked human disease BCM was preceded by a lengthy journey of scientific discovery that included the basics of photoreceptor anatomy, biochemistry, physiology, and molecular genetics (for example, Young, 1802; von Helmholtz, 1866; Osterberg, 1935; Nathans et al., 1986a,b, 1989, 1993; Curcio et al., 1990; Saari, 2000; Neitz and Neitz, 2011; Palczewski, 2012). Recent progress in delivery of genes to the retina has prompted discussion of which disease entities would be promising targets for gene therapies (Garafalo et al., 2019). One of the first questions to ask about BCM as a possible candidate for gene augmentation therapy was whether there were sufficient L/M cone photoreceptors present in the retina of these patients, considering the disease manifests as a congenital visual disorder and there is a macular degenerative

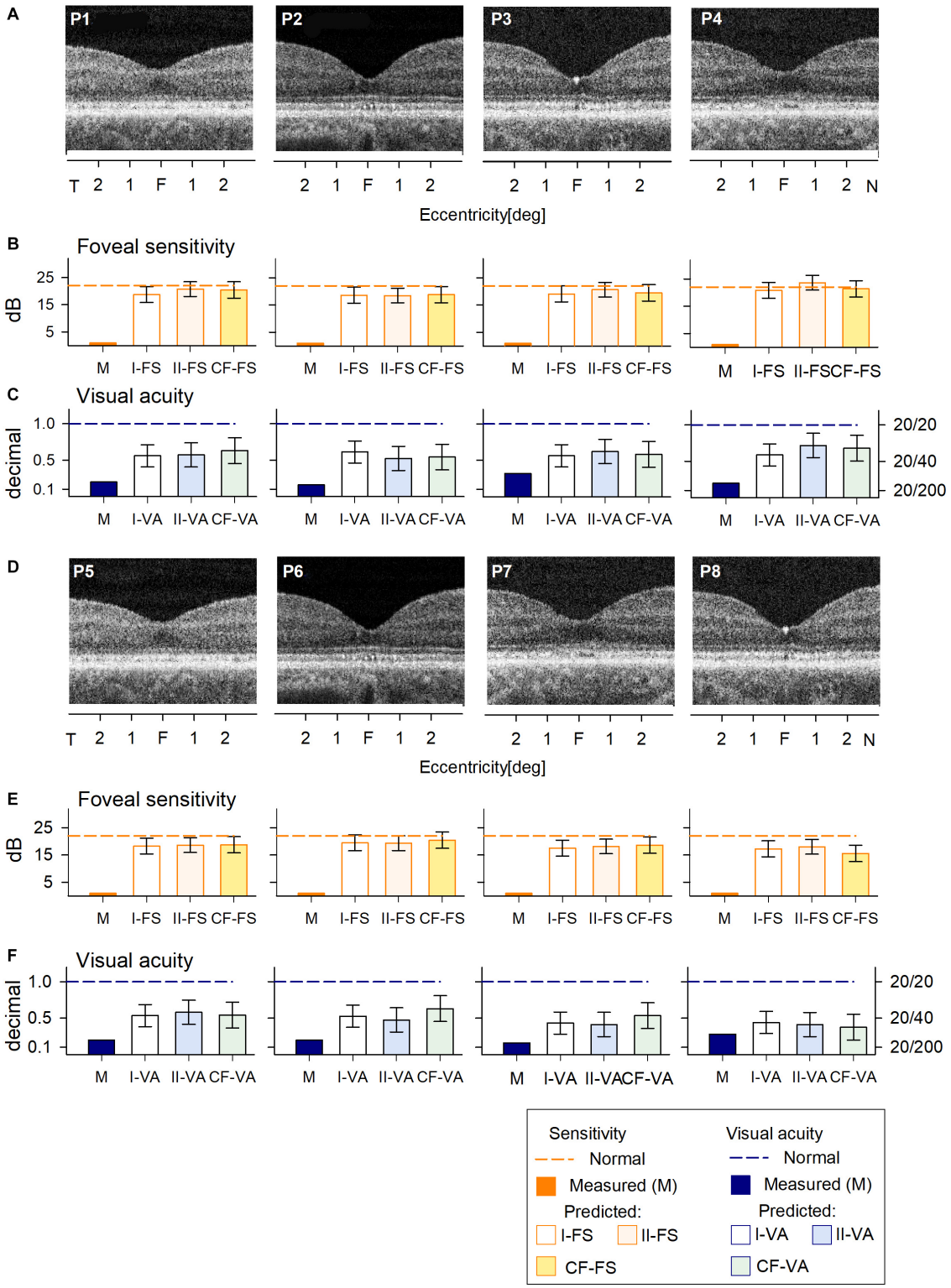

FIGURE 3 | Prediction of FS and VA of BCM patients with large deletion mutations. **(A)** Foveal region OCT scans from four BCM patients (ages 7–13 years). **(B)** Non-detectable sensitivity at foveal location (orange bar) and predicted results by Model I-FS (white bar) and Model II-FS (light orange bar) as in **Figure 1**. Yellow bar is sensitivity value calculated by formula extracted from curve fitting (CF-FS). **(C)** Comparison of measured VA (dark blue bar) and predicted results by Model I-VA (white bar) and Model II-VA (light blue bar). Light green bar is visual acuity calculated by formula extracted from curve fitting (CF-VA). **(D–F)** are the same as **(A–C)** but BCM patients are older (ages 18–35 years); dashed lines in **(B,C,E,F)** represent lower boundary of normal range. Error bars represent RSME for corresponding model.

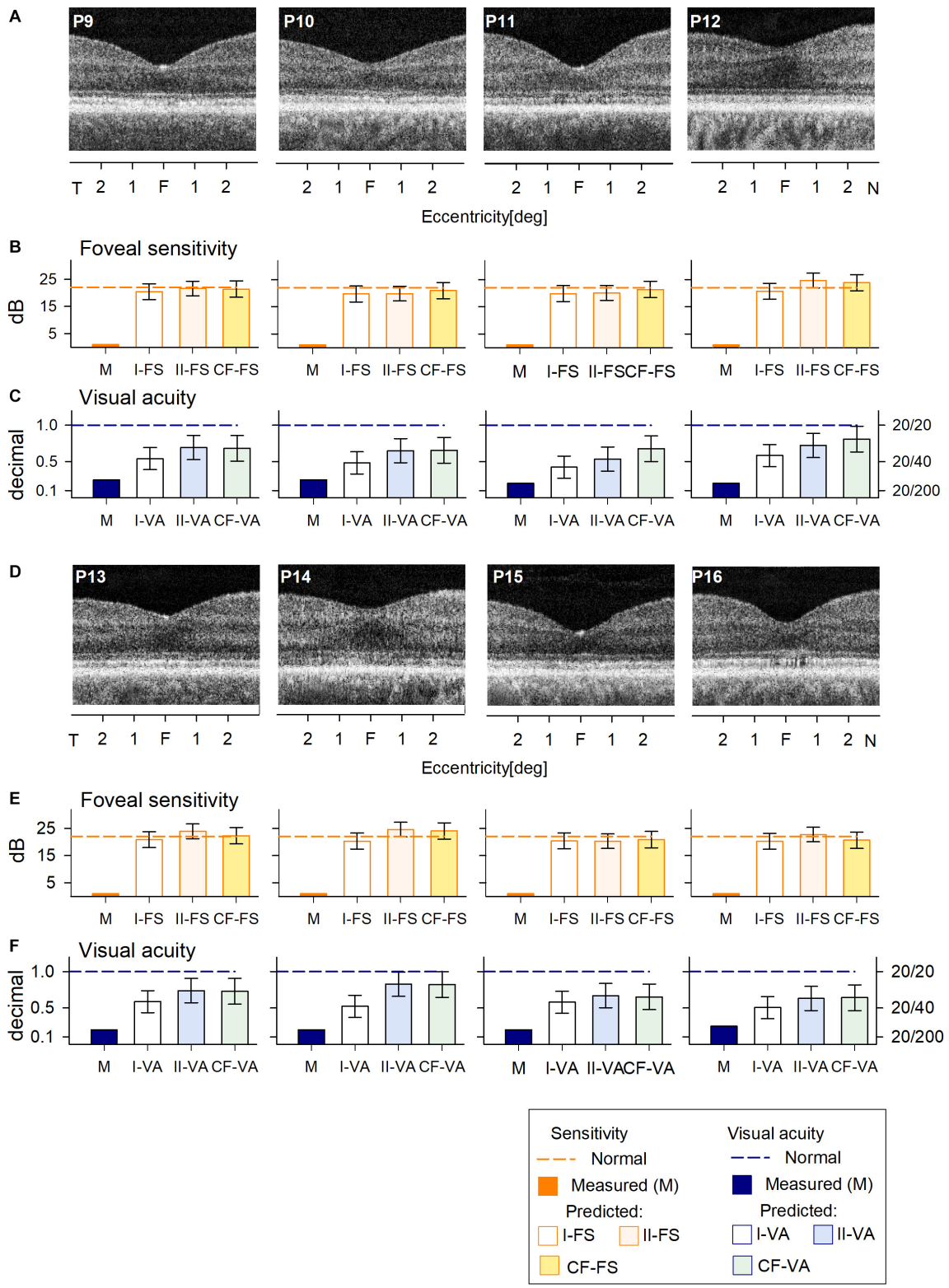

FIGURE 4 | Prediction of FS and VA of BCM patients with the C203R mutation. **(A)** Foveal region OCT scans from four BCM patients (ages 13–35 years). **(B)** Non-detectable sensitivity at foveal location (orange bar) and predicted results by Model I-FS (white bar), Model II-FS (light orange bar), and CF-FS (yellow bar) as in **Figures 1**, **3**. **(C)** Comparison of measured VA (dark blue bar) and predicted and predicted by Model I-VA (white bar), Model II-VA (light blue bar), and CF-FS (light green bar). **(D–F)** are the same as **(A–C)** but BCM patients are older (ages 35–52 years); dashed lines (in **B**,**C**,**E**,**F**) represent lower boundary of normal range. Error bars represent RSME for corresponding model.

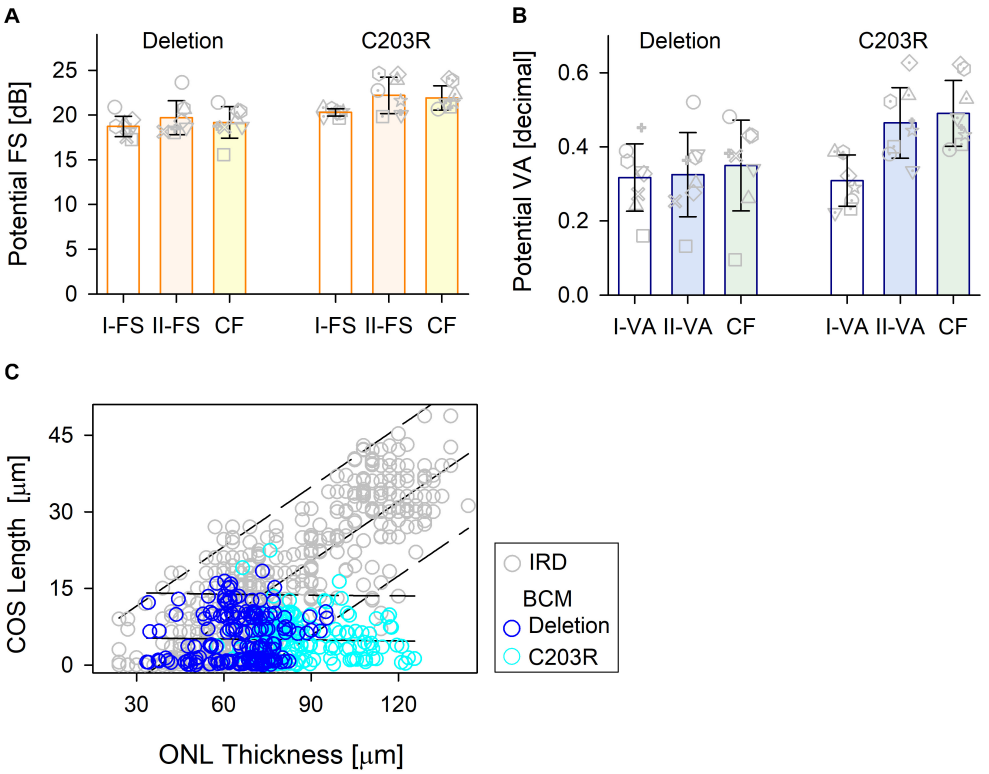

FIGURE 5 | Comparison of the treatment potential (difference between prediction and measured values) for the three methods in the two BCM genotypes. **(A)** Treatment potential for FS in deletion mutations and C203R mutation patients. Model 1, white bar; Model II, light orange bar; CF, light yellow bar. **(B)** Treatment potential for VA in the two groups. Model 1, white bar; Model II, light blue bar; CF, light green bar. Individual subjects, gray unfilled symbols; error bars, standard deviation. **(C)** Relation between ONL thickness and COS length for IRD patients used in the training set (gray circles) and those for BCM patients (deletion, dark blue circle; C203R, cyan circle).

component at later stages (Cideciyan et al., 2013). For BCM due to large deletion or C203R mutations included in the current work, the hypotheses have evolved over time. Earlier work based on adaptive optics (AO) images of waveguiding cones in C203R patients suggested that residual cones were all S cones and there were no L/M cones to be treated (Carroll et al., 2012). In contrast, evaluation of the spatial density of dark (non-waveguiding) cones together with OCT measurements in deletion patients was consistent with partially retained L/M cones (Cideciyan et al., 2013). Similarly retained L/M cones were later found in C203R patients with the use of split-detector AO imaging of their ISs (Carroll et al., 2014; Scoles et al., 2016; Patterson et al., 2020). More recently, the question of genetic heterogeneity and possible phenotypic differences within BCM was addressed with studies of cohorts of patients with large deletions versus patients with missense mutation, specifically C203R. An unexpected observation was that foveal cone structure was more persistent in the cohort of patients with the C203R mutation and the difference in natural history of disease progression could be as much as two to three decades (Sumaroka et al., 2018). Examination of further C203R patients in the sixth and seventh decades of life confirmed the original findings (Sumaroka, unpublished observation). Despite these structural differences in foveal photoreceptor integrity between genotypes at different patient ages, there were no significant differences in central visual function, such as VA (Sumaroka et al., 2018).

Is there progress toward therapy for the visual dysfunction in BCM? Recent murine proof-of-concept studies lend support to the concept that a gene augmentation approach to BCM may be feasible (Zhang et al., 2017; Deng et al., 2018, 2019). What is the expectation for therapeutic efficacy in a patient with BCM? We determined that there are sufficient cone photoreceptors to warrant foveal gene therapy in BCM (Cideciyan et al., 2013) but not until the current study were we able to ask about the potential difference to central visual function that efficacious therapy could make. The opportunity to ask such a question is presented by the considerable progress in technology of non-invasive imaging, and understanding of the anatomical basis of the cross-sectional retinal images with OCT (for example, Huang et al., 1998; Podoleanu and Rosen, 2008; Spaide and Curcio, 2011; Muller et al., 2019). Our first such attempt at predicting vision from retinal structure was done in two forms of LCA caused by *CEP290* and *IQCB1* (*NPHP5*) mutations that retained foveal and extrafoveal cone islands but no evidence of rods. The supervised machine learning approach used data from patients with retinitis pigmentosa with only cone-mediated macular function remaining. The results in these two forms of

severe genetic retinal blindness allowed for prediction of maximal efficacy (Sumaroka et al., 2019).

The present work asked a similar question about prediction of vision from OCT structure but the differences between BCM and the previously studied forms of LCA required changes in strategy. Ideally, any treatment of BCM would target all the L/M cones throughout the retina but that will have to await future advances in gene (or other therapeutic) delivery. There is no evidence that L/M cones in human BCM are structurally intact outside of the fovea; the retinal region feasible to target would be the BCM fovea. BCM gene therapy would preferably be via an intravitreal delivery, and intravitreal gene delivery has been mainly limited to foveal transduction (Dalkara et al., 2013). Therefore, in BCM only the fovea and foveal cone photoreceptor structure would need to be quantified; surrounding extrafoveal retina where rod:cone ratios increase rapidly would not be targeted and, unlike the *CEP290* and *IQCB1* (*NPHP5*) forms of LCA previously analyzed, BCM has evidence of normal rod function and structure (Curcio et al., 1990; Cideciyan et al., 2013). Limiting the targeted retinal area to the fovea is useful in the design of a clinical trial because the functional predictions would best include the time-honored measure of central spatial vision (i.e., VA) as well as a measurement of visual sensitivity at fixation that is dramatically reduced in BCM (e.g., longer wavelength stimuli in the light-adapted state).

Two techniques of regression analysis were used to predict the possible outcome of therapy and the results were compared. A supervised machine leaning approach (RF) was taken to model the relationship between retinal structure and both FS and VA. This followed our previous data analyses: two groups of models based on the form of the input variables were constructed (Sumaroka et al., 2018). The second technique used CF to known foveal function and structural data (ONL) and this was based on an established model assuming photoreceptor function proportional to remaining quantum catch (Ripps et al., 1978; Kemp et al., 1988; Machida et al., 2000; Jacobson et al., 2005, 2014; Rangaswamy et al., 2010); parameters of a mathematical equation describing their relationship were extracted. RF models and CF produced comparable predictions of foveal efficacy in the BCM patients.

How would a BCM clinical trial use the data and analyses from the current study? In the present era of novel therapies, we enter early phase trials with the primary goal of evaluating safety; there is usually a qualitative prediction that there may be some efficacy signal at the doses initially used. A pattern has been that if VA improves (to some degree) compared to baseline, success is announced, and the trial may actually move forward to later phases, given regulatory approval of course. For BCM [and *CEP290*-LCA and *IQCB* (*NPHP5*)-LCA; Sumaroka et al., 2019], we can now advance to quantitative prediction of efficacy outcome. Once a patient has a clinical and molecular diagnosis of BCM, relevant parameters of function and structure would be quantified. The most commonly available measure of central visual function in the clinic is best-corrected VA, and retinal structure would be measured using OCT scans through the fovea. The presence of foveal ONL (by observation of the scan) would likely fulfill an entry criterion for enrollment. Yet, there is a need for quantitation of foveal ONL, and OCT machine algorithms are up to this task. VA and ONL at baseline allow us to estimate efficacy using predicted VA (VA_p) calculated from the following formula: $VA_p = -1.07 + 0.91*\log(ONL)$. From the result, a patient's predicted efficacy from therapy would be determined as VA_p–VA. For example, P13 (C203R mutation, in his fourth decade of life) with a VA of 20/100 (decimal 0.2) and foveal ONL thickness of 90 μm would be predicted to show on average an improvement in VA to 20/25 (decimal 0.71 ± 0.34), equivalent to a six-line positive change (range four to seven lines) on an ETDRS chart. A further example is P5 (deletion mutation, in his second decade of life) with the same VA of 20/100 (decimal 0.2) as P13 but foveal thickness of 59 μm would be predicted to show an improvement in VA to 20/40 (decimal 0.54 ± 0.34), equivalent to a four-line positive change on an ETDRS chart (range zero to six lines). Treatment potential is estimated based on the retinal structure retained by each patient at the time of the intervention. If treatment changed the retinal structure, such as leading to COS lengthening, foveal treatment potential would also be expected to increase accordingly. Results in a recent clinical trial in *CEP290*-LCA suggested that such positive structural changes in the outer retina are possible (Cideciyan et al., 2019).

Other progress using machine learning to predict measures of visual function or retinal structure from various inputs is published and the topic is now being reviewed frequently (for example, Schmidt-Erfurth et al., 2018; Arcadu et al., 2019; Kihara et al., 2019; Wen et al., 2019; Della Volpe-Waizel et al., 2020). For the field of IRDs, next steps would be to research how artificial intelligence-based modeling could be used to analyze conditions with residual rod-mediated vision and structure. Ongoing and future gene-based trials that involve rod photoreceptors would benefit from such predictions.

DATA AVAILABILITY STATEMENT

The raw data supporting the conclusions of this article will be made available by the authors, without undue reservation.

ETHICS STATEMENT

The studies involving human participants were reviewed and approved by the University of Pennsylvania, Institutional Review Board. Written informed consent to participate in this study was provided by the participants' legal guardian/next of kin.

AUTHOR CONTRIBUTIONS

AS, AC, SK, BW, and SJ contributed to the experimental design and performed experiments, data analysis, and manuscript writing. RS and VW performed data analysis and editing.

All authors contributed to the article and approved the submitted version.

FUNDING

This work was supported by the Blue Cone Monochromacy Families Foundation and by funds of the German Research Council (Wi1189/12-1 to BW). The authors declare that the study funding bodies (BCM Families Foundation and German Research Council) had no role in the study design, data collection and analysis, interpretation of data, the writing of the article or the decision to submit for publication.

SUPPLEMENTARY MATERIAL

The Supplementary Material for this article can be found online at: https://www.frontiersin.org/articles/10.3389/fnins.2020.00800/full#supplementary-material

REFERENCES

Arcadu, F., Benmansour, F., Maunz, A., Michon, J., Haskova, Z., McClintock, D., et al. (2019). Deep learning predicts OCT measures of diabetic macular thickening from color fundus photographs. *Invest. Ophthalmol. Vis. Sci.* 60, 854–857. doi: 10.1167/iovs.18-25634

Boye, S. E., Alexander, J. J., Witherspoon, C. D., Boye, S. L., Peterson, J. J., Clark, M. E., et al. (2016). Highly efficient delivery of adeno-associated vital vectors to the primate retina. *Hum. Gene Ther.* 27, 580–597. doi: 10.1089/hum.2016.085

Byrne, L. C., Day, T. P., Visel, M., Strazzeri, J. A., Fortuny, C., Dalkara, D., et al. (2020). I vivo-directed evolution of adeno-associated virus in the primate retina. *JCI Insight* 5:e135112.

Carroll, J., Dubra, A., Gardner, J. C., Mizrahi-Meissonnier, L., Cooper, R. F., Dubis, A. M., et al. (2012). The effect of cone opsin mutations on retinal structure and the integrity of the photoreceptor mosaic. *Invest. Ophthalmol. Vis. Sci.* 53, 8006–8015. doi: 10.1167/iovs.12-11087

Carroll, J., Scoles, D. H., Langlo, S., Neitz, J., Pennesi, M. E., Neitz, M., et al. (2014). Imaging cone structure in patients with OPN1LW and OPN1MW mutations. Invest. *Ophthalmol. Vis. Sci.* 55:4542.

Charng, J., Cideciyan, A. V., Jacobson, S. G., Sumaroka, A., Schwartz, S. B., Swider, M., et al. (2016). Variegated yet non-random rod and cone photoreceptor disease patterns in RPGR-ORF15-associated retinal degeneration. *Hum. Mol. Genet.* 25, 5444–5459. doi: 10.1093/hmg/ddw361

Cideciyan, A. V., Hufnagel, R. B., Carroll, J., Sumaroka, A., Luo, X., Schwartz, S. B., et al. (2013). Human cone visual pigment deletions spare sufficient photoreceptors to warrant gene therapy. *Hum. Gene. Ther.* 24, 993–1006. doi: 10.1089/hum.2013.153

Cideciyan, A. V., Jacobson, S. G., Drack, A. V., Ho, A. C., Charng, J., Garafalo, A. V., et al. (2019). Effect of an intravitreal antisense oligonucleotide on vision in Leber congenital amaurosis due to a photoreceptor cilium defect. *Nat. Med.* 25, 225–228. doi: 10.1038/s41591-018-0295-0

Cuenca, N., Ortuño-Lizarán, I., and Pinilla, I. (2018). Cellular characterization of OCT and outer retinal bands using specific immunohistochemistry markers and clinical implications. *Ophthalmology* 125, 407–422. doi: 10.1016/j.ophtha.2017.09.016

Cuenca, N., Ortuño-Lizarán, I., Sánchez-Sáez, X., Kutsyr, O., Albertos-Arranz, H., Fernández-Sánchez, L., et al. (2020). Interpretation of OCT and OCTA images from a histological approach: clinical and experimental implications. *Prog. Retin. Eye Res.* 3:100828. doi: 10.1016/j.preteyeres.2019.100828

Curcio, C. A., Sloan, K. R., Kalina, R. E., and Hendrickson, A. E. (1990). Human photoreceptor topography. *J. Comp. Neurol.* 292, 497–523. doi: 10.1002/cne.902920402

Dalkara, D., Byrne, L. C., Klimczak, R. R., Visel, M., Yin, L., Merigan, W. H., et al. (2013). In vivo-directed evolution of a new adeno-associated virus for therapeutic outer retinal gene deliver from the vitreous. *Sci. Transl. Med.* 5:189. doi: 10.1126/scitranslmed.3005708

Della Volpe-Waizel, M., Traber, G. L., Maloca, P., Zinkernagel, M., Schmidt-Erfurth, U., Rubin, G., et al. (2020). New technologies for outcome measures in retinal disease: review from the European vision institute special interest focus group. *Ophthalmic Res.* 63, 77–87. doi: 10.1159/000501887

Deng, W. T., Li, J., Zhu, P., Chiodo, V. A., Smith, W. C., Freedman, B., et al. (2018). Human L- and M-opsins restore M-cone function in a mouse model for human blue cone monochromacy. *Mol. Vis.* 24, 17–28.

Deng, W. T., Li, J., Zhu, P., Freedman, B., Smith, W. C., Baehr, W., et al. (2019). Rescue of M-cone function in aged Opn1mw-/- mice, a model for late-stage blue cone monochromacy. *Invest. Ophthalmol. Vis. Sci.* 60, 3644–3651. doi: 10.1167/iovs.19-27079

Garafalo, A. V., Cideciyan, A. V., Heon, E., Sheplock, R., Pearson, A., WeiYang Yu, C., et al. (2019). Progress in treating inherited retinal diseases: early subretinal gene therapy clinical trials and candidates for future initiatives. *Prog. Retin. Eye Res.* 100827. doi: 10.1016/j.preteyeres.2019.100827

Huang, Y., Cideciyan, A. V., Papastergiou, G. I., Banin, E., Semple-Rowland, S. L., Milam, A. H., et al. (1998). Relation of optical coherence tomography to microanatomy in normal and rd chickens. *Invest. Ophthalmol. Vis. Sci.* 39, 2405–2416.

Jacobson, S. G., Aleman, T. S., Cideciyan, A. V., Sumaroka, A., Schwartz, S. B., Windsor, E. A., et al. (2005). Identifying photoreceptors in blind eyes caused by RPE65 mutations: prerequisite for human gene therapy success. *Proc. Natl. Acad. Sci. U.S.A.* 102, 6177–6182. doi: 10.1073/pnas.0500646102

Jacobson, S. G., Cideciyan, A. V., Huang, W. C., Sumaroka, A., Roman, A. J., Schwartz, S. B., et al. (2014). TULP1 mutations causing early-onset retinal degeneration: preserved but insensitive macular cones. *Invest. Ophthalmol. Vis. Sci.* 5, 5354–5364. doi: 10.1167/iovs.14-14570

Kemp, C. M., Jacobson, S. G., and Faulkner, D. J. (1988). Two types of visual dysfunction in autosomal dominant retinitis. *Invest. Ophthalmol. Vis. Sci.* 29, 1235–1241.

Khabou, H., Garita-Hernandez, M., Chaffiol, A., Reichman, S., Jaillard, C., Brazhnikova, E., et al. (2018). Noninvasive gene delivery to foveal cones for vision restoration. *JCI Insight* 3:e96029. doi: 10.1172/jci.insight.96029

Kihara, Y., Heeren, T. F. C., Lee, C. S., Wu, Y., Xiao, S., Tzaridis, S., et al. (2019). Estimating retinal sensitivity using optical coherence tomorography with deep-learning algorithms in macular telangiectasia type 2. *JAMA. Netw. Open* 2:e188029. doi: 10.1001/jamanetworkopen.2018.8029

Machida, S., Kondo, M., Jamison, J. A., Khan, N. W., Kononen, L. T., Sugawara, T., et al. (2000). P23H rhodopsin transgenic rat: correlation of retinal function with histopathology. *Invest. Ophthalmol. Vis. Sci.* 41, 3200–3209.

MATLAB Release (2018). *The Mathworks, Inc.*, Natick, Massachusetts, United States.

Matsui, R., McGuigan, D. B. III, Gruzensky, M. L., Aleman, T. S., Schwartz, S. B., Sumaroka, A., et al. (2016). SPATA7: evolving phenotype from cone-rod dystrophy to retinitis pigmentosa. *Ophthalmic. Genet.* 37, 333–338. doi: 10.3109/13816810.2015.1130154

Miller, J. W., and Vandenberghe, L. H. (2018). Breaking and sealing barriers in retinal gene therapy. *Mol. Ther.* 26, 2081–2082. doi: 10.1016/j.ymthe.2018.08.003

Muller, P. L., Wolf, S., Dolz-Marco, R., Tafreshi, A., Schmitz-Valckenberg, S., and Holz, F. G. (2019). "Ophthalmic diagnostic imaging: retina," in *High Resolution Imaging in Microscopy and Ophthalmology: new Frontiers in Biomedical Optics*, ed. J. F. Bille (Berlin: Springer), 87–106.

Nathans, J., Davenport, C. M., Maumenee, I. H., Lewis, R. A., Hejtmancik, J. F., Litt, M., et al. (1989). Molecular genetics of human blue cone monochromacy. *Science* 245, 831–838. doi: 10.1126/science.2788922

Nathans, J., Maumenee, I. H., Zrenner, E., Sadowski, B., Sharpe, L. T., and Lewis, R. A. (1993). Genetic heterogeneity among blue-cone monochromats. *Am. J. Hum. Genet.* 53, 987–1000.

Nathans, J., Piantanida, T. P., Eddy, R. L., Shows, T. B., and Hogness, D. S. (1986a). Molecular genetics of inherited variation in human color vision. *Science* 232, 203–210. doi: 10.1126/science.3485310

Nathans, J., Thomas, D., and Hogness, D. S. (1986b). Molecular genetics of human color vision: the genes encoding blue, green, and red pigments. *Science* 232, 193–202. doi: 10.1126/science.2937147

Neitz, J., and Neitz, M. (2011). The genetic of normal and defective color vision. *Vis. Res.* 51, 633–651. doi: 10.1016/j.visres.2010.12.002

Osterberg, G. (1935). Topography of the layer of rods and cones in the human retina. *Acta. Ophthal. Suppl.* 6, 1–103.

Palczewski, K. (2012). Chemistry and biology of vision. *J. Biol. Chem.* 287, 1612–1619. doi: 10.1074/jbc.R111.301150

Patterson, E. J., Kalitzeos, A., Singh, N., Kane, T. M., Kasilian, M., Higgins, B. P., et al. (2020). Longitudinal assessment of foveal cone structure in blue cone monochromacy. *Invest.Ophthalmol.Vis. Sci.* 61:5270.

Podoleanu, A. G., and Rosen, R. B. (2008). Combinations of techniques in imaging the retina with high resolution. *Prog. Retin. Eye Res.* 27, 464–499. doi: 10.1016/j.preteyeres.2008.03.002

Rangaswamy, N. V., Patel, H. M., Locke, K. G., Hood, D. C., and Birch, D. G. (2010). A comparison of visual field sensitivity to photoreceptor thickness in retinitis pigmentosa. *Invest. Ophthalmol. Vis. Sci.* 51, 4213–4219. doi: 10.1167/iovs.09-4945

Ripps, H., Brin, K. P., and Weale, R. A. (1978). Rhodopsin and visual threshold in retinitis pigmentosa. *Invest. Ophtalmol. Vis. Sci.* 17, 735–745.

Saari, J. C. (2000). Biochemistry of visual pigment regeneration: the Friedenwald lecture. *Invest. Ophthalmol. Vis. Sci.* 41, 337–348.

Schmidt-Erfurth, U., Sadeghipour, A., Gerendas, B. S., Waldstein, S. M., and Bogunovic, H. (2018). Aritifical intelligence in retina. *Prog. Retin. Eye Res.* 67, 1–29. doi: 10.1016/j.preteyeres.2018.07.004

Scoles, D., Flatter, J. A., Cooper, R. F., Langlo, C. S., Robison, S., Neitz, M., et al. (2016). Assessing photoreceptor structure associated with ellipsoid zone disruptions visualized with optical coherence tomography. *Retina* 36, 91–103. doi: 10.1097/iae.0000000000000618

Spaide, R. F., and Curcio, C. A. (2011). Anatomical correlates to the bands seen in the outer retina by optical coherence tomography: literature review and model. *Retina* 31, 1609–1619. doi: 10.1097/IAE.0b013e3182247535

Sumaroka, A., Garafalo, A. V., Cideciyan, A. V., Charng, J., Roman, A. J., Choi, W., et al. (2018). Blue cone monochromacy caused by the C203R missense mutation or large deletion mutations. *Invest. Ophthalmol. Vis. Sci.* 59, 5762–5772. doi: 10.1167/iovs.18-25280

Sumaroka, A., Garafalo, A. V., Semenov, E. P., Sheplock, R., Krishnan, A. K., Roman, A. J., et al. (2019). Treatment potential for macular cone vision in Leber congenital amaurosis due to CEP290 or NPHP5 mutations: predictions from artificial intelligence. *Invest. Ophthalmol. Vis. Sci.* 60, 2551–2562. doi: 10.1167/iovs.19-27156

Sumaroka, A., Matsui, R., Cideciyan, A. V., McGuigan, D. B. III, Sheplock, R., Schwartz, S. B., et al. (2016). Outer retinal changes including the ellipsoid zone band in Usher syndrome 1B due to MYO7A mutations. *Invest. Ophthalmol. Vis. Sci.* 57, OCT253–OCT261. doi: 10.1167/iovs.15-18860

von Helmholtz, H. (1866). "Concerning the perceptions in general," in *Treatise on Physiological Optics, III*, ed. J. P. C. Southall (New York, NY: Dover), 1–18.

Wen, J. C., Lee, C. S., Keane, P. A., Xiao, S., Rokem, A. S., Chen, P. P., et al. (2019). Forecasting future Humphrey visual fields using deep learning. *PLoS One* 14:e0214875. doi: 10.1371/journal.pone.0214875

Young, T. (1802). The Bakerian lecture: on the theory of light and colours. *Phil. Trans. R. Soc.* 92, 12–48. doi: 10.1098/rstl.1802.0004

Zhang, Y., Deng, W. T., Du, W., Zhu, P., Li, J., Xu, F., et al. (2017). Gene-based therapy in a mouse model of blue cone monochromacy. *Sci. Rep.* 7:6690. doi: 10.1038/s41598-017-06982-7

Conflict of Interest: The authors declare that the research was conducted in the absence of any commercial or financial relationships that could be construed as a potential conflict of interest.

Copyright © 2020 Sumaroka, Cideciyan, Sheplock, Wu, Kohl, Wissinger and Jacobson. This is an open-access article distributed under the terms of the Creative Commons Attribution License (CC BY). The use, distribution or reproduction in other forums is permitted, provided the original author(s) and the copyright owner(s) are credited and that the original publication in this journal is cited, in accordance with accepted academic practice. No use, distribution or reproduction is permitted which does not comply with these terms.

frontiers in Neuroscience

REVIEW
published: 14 August 2020
doi: 10.3389/fnins.2020.00860

Research Models and Gene Augmentation Therapy for *CRB1* Retinal Dystrophies

Nanda Boon[1], *Jan Wijnholds*[1,2] *and Lucie P. Pellissier*[3]*

[1] Department of Ophthalmology, Leiden University Medical Center, Leiden, Netherlands, [2] The Netherlands Institute for Neuroscience, Royal Netherlands Academy of Arts and Sciences (KNAW), Amsterdam, Netherlands, [3] Biology and Bioinformatics of Signalling Systems, Physiologie de la Reproduction et des Comportements INRAE UMR 0085, CNRS UMR 7247, Université de Tours, IFCE, Nouzilly, France

Retinitis pigmentosa (RP) and Leber congenital amaurosis (LCA) are inherited degenerative retinal dystrophies with vision loss that ultimately lead to blindness. Several genes have been shown to be involved in early onset retinal dystrophies, including *CRB1* and *RPE65*. Gene therapy recently became available for young RP patients with variations in the *RPE65* gene. Current research programs test adeno-associated viral gene augmentation or editing therapy vectors on various disease models mimicking the disease in patients. These include several animal and emerging human-derived models, such as human-induced pluripotent stem cell (hiPSC)-derived retinal organoids or hiPSC-derived retinal pigment epithelium (RPE), and human donor retinal explants. Variations in the *CRB1* gene are a major cause for early onset autosomal recessive RP with patients suffering from visual impairment before their adolescence and for LCA with newborns experiencing severe visual impairment within the first months of life. These patients cannot benefit yet from an available gene therapy treatment. In this review, we will discuss the recent advances, advantages and disadvantages of different *CRB1* human and animal retinal degeneration models. In addition, we will describe novel therapeutic tools that have been developed, which could potentially be used for retinal gene augmentation therapy for RP patients with variations in the *CRB1* gene.

Keywords: retinitis pigmentosa, leber congenital amaurosis, crumbs homolog 1, gene therapy, mouse model

OPEN ACCESS

Edited by:
Ayse Sahaboglu,
University of Tübingen, Germany

Reviewed by:
Ilaria Piano,
University of Pisa, Italy
William Anthony Beltran,
University of Pennsylvania, United States
Stephen Tsang,
Columbia University, United States

***Correspondence:**
Lucie P. Pellissier
lucie.pellissier@inrae.fr

Specialty section:
This article was submitted to Neurodegeneration, a section of the journal Frontiers in Neuroscience

Received: *04 June 2020*
Accepted: *24 July 2020*
Published: *14 August 2020*

Citation:
Boon N, Wijnholds J and Pellissier LP (2020) Research Models and Gene Augmentation Therapy for CRB1 Retinal Dystrophies. Front. Neurosci. 14:860. doi: 10.3389/fnins.2020.00860

CRB FAMILY MEMBERS

Crumbs (Crb) is a large transmembrane protein initially discovered at the apical membrane of *Drosophila* epithelial cells (Tepass et al., 1990). Several years later, it was found that mutations in a human homolog of the *Drosophila melanogaster* protein crumbs, denoted as CRB1 (Crumbs homolog 1), was involved in retinal dystrophies in humans (Den Hollander et al., 1999). The human *CRB1* gene is mapped to chromosome 1q31.3, and contains 12 exons, has 12 identified transcript variants so far, three CRB family members, and over 210 kb genomic DNA (Den Hollander et al., 1999)[1]. Canonical CRB1 is, like its *Drosophila* homolog,

[1]http://grch37.ensembl.org/Homo_sapiens/Gene/Summary?db=core;g=ENSG00000134376;r=1:197170592-197447585

a large transmembrane protein consisting of multiple epidermal growth factor (EGF) and laminin-globular like domains in its extracellular N-terminus (**Figure 1A**). The intracellular C-terminal domain contains a FERM and a conserved glutamic acid-arginine-leucine-isoleucine (ERLI) PDZ binding motives. An alternative transcript of CRB1, *CRB1-B*, was recently described and suggested to have significant extracellular domain overlap with canonical CRB1 while bearing unique 5′ and 3′ domains (Ray et al., 2020). In mammals, CRB1 is a member of the Crumbs family together with CRB2 and CRB3 (**Figure 1A**). CRB2 displays almost the same protein structure as CRB1, except a depletion of four EGF domains. CRB3A lacks the entire typical extracellular domain but contains the transmembrane domain juxtaposed to the intracellular part with the FERM-binding motif and a ERLI PDZ sequence. A second protein (isoform CRB3B) arises from the same *CRB3* gene due to alternate splicing of the last exon, resulting in a different C-terminus with a cysteine-leucine-proline-isoleucine (CLPI) amino acid sequence, and thus lacks the PDZ domain (Fan et al., 2007; Margolis, 2018). Interestingly, the CRB3B isoform is found in mammals, but not in zebrafish or *Drosophila* (Fan et al., 2007). Further details about CRB isoform details can be found in Quinn et al. (2017).

CRB LOCALIZATION IN THE RETINA

In mammalian tissue CRB1 and CRB2 are predominantly expressed in the retina, however, CRB2 expression is also found in other tissues such as in kidney podocytes, in the subventricular zone of the brain, and in the spinal cord (Ebarasi et al., 2015; Slavotinek et al., 2015; Dudok et al., 2016; Tait et al., 2020). Within the retina, CRB proteins are localized at the subapical region (SAR) above the adherence junctions between photoreceptor and Müller glial cells (MGCs), multiple photoreceptor cells (PRCs), or between multiple MGCs (Pellikka et al., 2002; van de Pavert et al., 2004). In addition, unlike CRB1, CRB2 also localizes in the retinal pigment epithelium (RPE). Defining the subcellular localization is essential to understand the function of CRB proteins (**Figure 1B**). Mouse studies have shown that full length Crb1 protein is exclusively present in MGC at the SAR while Crb2 and Crb3 are present in both PRC and MGC (van Rossum et al., 2006). Serial tangential cryosectioning of the retina followed by western blotting displays *Crb1-B* transcript expression in outer segments of PRCs in mice (Ray et al., 2020). The first ultrastructural data in postmortem human retina revealed a different localization, where CRB2 is located in MGC at the SAR and at vesicles in photoreceptor inner segments, whereas CRB1 is located in both MGC and PRC at the SAR (Pellissier et al., 2014b, 2015). CRB3A was found in microvilli of MGC at the SAR and in inner segments of PRC (Pellissier et al., 2014b, 2015). However, recently, it was shown that CRB1 and CRB2 are located in MGC and PRC at the SAR in the second trimester of human fetal retina and in human iPSC-derived retinal organoids, whereas in the first trimester only CRB2 was detected (Quinn et al., 2019a). Single-cell RNA sequencing data of human fetal retina and RPE confirms that CRB1 is present in retinal progenitor cells and MGC but not in RPE, which is in accordance with mouse versus primate localization studies (Hu et al., 2019). In addition, similar localization for CRB1, CRB2, and CRB3A were detected in rhesus and cynomolgus macaques (Quinn et al., 2019b). CRB3A was also detected in the inner retina and RPE of both rhesus and cynomolgus macaques (Quinn et al., 2019b). These recent data suggest that, in humans, CRB2 might also be present at the SAR membranes in PRC rather than only in vesicles of photoreceptor inner segments. The discrepancies in CRB2 pattern at the SAR observed in postmortem human retinas versus monkeys, fetal and retinal organoids could be explained by the age of the donors studied, the quality of the samples (processed within 48 h after death), or by technical issues. We could speculate that CRB2 may have a different location in human aged retinas, CRB2 at the SAR might have not been detected, or CRB2 might have been endocytosed from the PRC plasma membrane following donor death. Additional experiments with fresh human retina defining the subcellular localization of CRB1 and CRB2 could potentially resolve these differences. In summary, according to all these evidences, we hypothesize that in primates, including humans, CRB1 and CRB2 are located in both cell types at the SAR. Therefore, both MGC and PRC should be targeted to prevent retinal degeneration in RP patients.

Recently, Crb trafficking to the correct apical location in *Drosophila* epithelium has been further investigated (**Figure 1C**; Li et al., 2007; Pocha et al., 2011; Kraut and Knust, 2019; Aguilar-Aragon et al., 2020). Crb is correctly localized by Rab11-containing endosomes using motor-driven transport along polarized microtubules and F-actin filaments. Interestingly, upon loss of microtubule minus-end director protein dynein, Rab11 endosomes containing Crb are transported basally rather than apically (Aguilar-Aragon et al., 2020). Once Crb is successfully addressed to the apical membrane, it is delivered at the correct localization on the plasma membrane using exocyst-mediated delivery. Mutant clones for sec15 or sec5, subunits of the exocyst, strongly disrupts the apical localization of Crb, confirming the essential requirement of the exocyst in delivery of Crb to the apical membrane (Aguilar-Aragon et al., 2020). In cultured mammalian cells, the exocyst associates with adherens junctions and PAR3 (Ahmed and Macara, 2017; Polgar and Fogelgren, 2018). Because of the known interaction between CRB, PAR6, and PAR3 in mammals, mentioned below, this trafficking model might be conserved among species. Further investigations are required to test whether the mechanisms of epithelial polarization are conserved in humans.

CRB PROTEIN FUNCTION IN MAMMALIAN TISSUES

Various research studies have shown that CRB1 and CRB2 are apical polarity factors, and apical-basal cell polarity is essential for the formation and function of epithelial tissues (Bazellières et al., 2018). More research is required to define the function of the recently described CRB1-B isoform because of its distinct 5′ and 3′ domain. Below, we will describe the canonical function

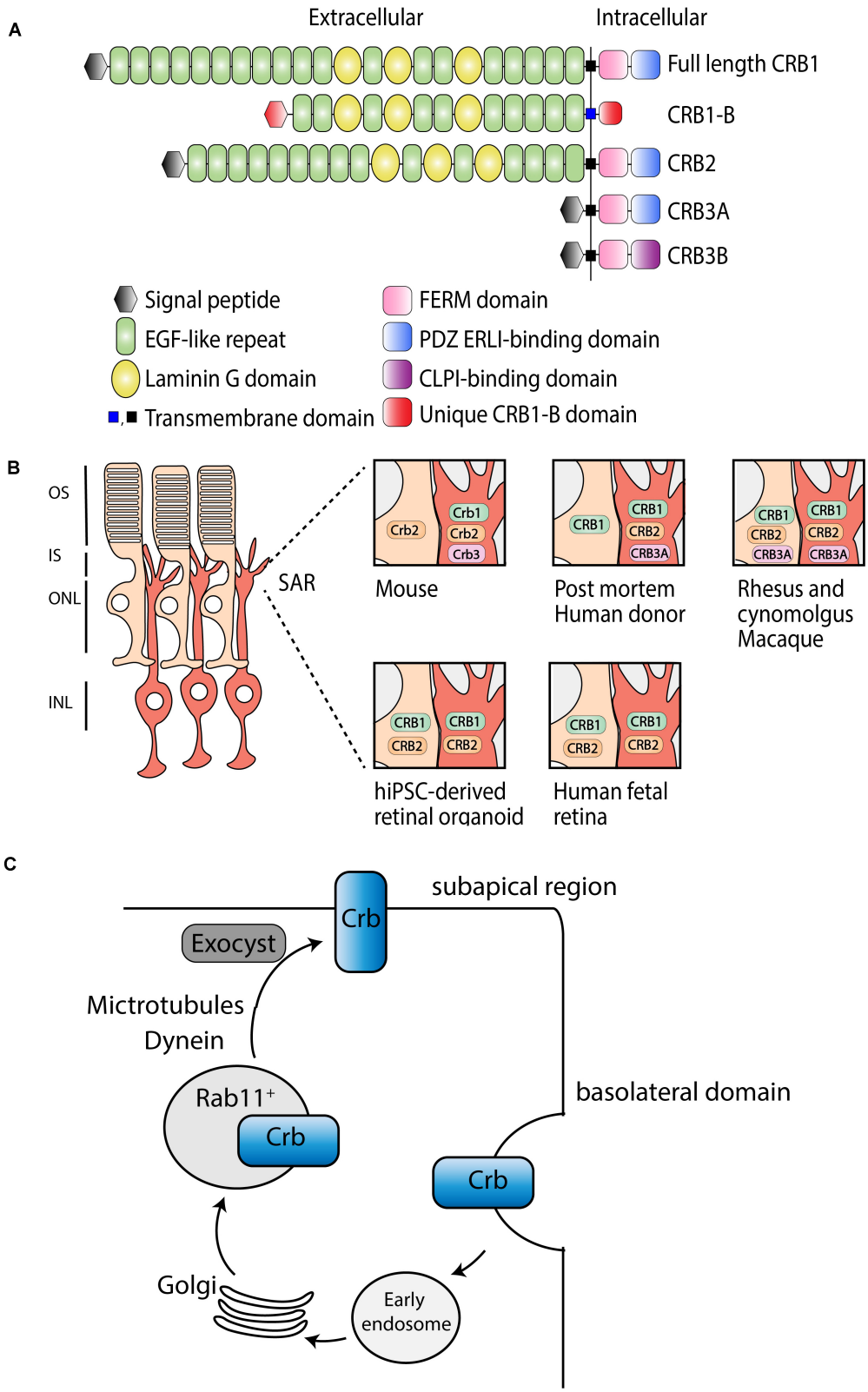

FIGURE 1 | Schematic representation of CRB subcellular localization and proposed trafficking mechanism. **(A)** Schematic overview of full length CRB1 (CRB1-A), CRB1-B, CRB2, CRB3A, and CRB3B proteins. **(B)** Subcellular localization of CRB1, CRB2, and CRB3A in the retina of mouse, post mortem human donor, macaque, hiPSC, and human fetal retina. **(C)** Trafficking mechanism in *Drosophila* suggested to be conserved among species, adapted from Aguilar-Aragon et al. (2020).

of CRB in maintaining cell adhesion and morphogenesis, and its role in cell division and development.

Maintaining Cell Adhesion and Morphogenesis

The prototypic ERLI sequence of CRB proteins is important for interaction with key adaptor proteins. The core CRB complex is formed by interaction of CRB and protein associated with Lin Seven 1 (PALS1), also known as membrane-associated guanylate kinase p55 subfamily member 5 (MPP5), where PALS1 binds to the conserved C-terminal PDZ domain of CRB (Roh et al., 2002; van de Pavert et al., 2004; Margolis, 2018). Ablation of *Mpp5* in mouse RPE causes early onset retinal degeneration, whereas ablation of *Mpp5* in the neural retina does not, suggesting an essential role of PALS1 at the tight junctions of RPE but not in the neural retina (Park et al., 2011). The core CRB complex is evolutionary conserved and regulates apical-basal polarity and maintains cell adhesion (Bulgakova and Knust, 2009). Pals1 can interact with Mpp3 and Mpp4 at the SAR in the mouse retina (**Figure 2A**; Kantardzhieva et al., 2005, 2006; Dudok et al., 2013). *Mpp3* conditional knockout (cKO) mice with Mpp3 specifically ablated in the retina showed disrupted localization and reduced levels of Pals1, indicating that Mpp3 is essential to maintain levels of Pals1 at the SAR near the outer limiting membrane (Dudok et al., 2013).

Additionally, binding of PALS1 and CRB can lead to the recruitment of PATJ or multiple PDZ domain protein 1 (MUPP1) to the apical membrane (**Figure 2B**; Roh et al., 2002). PATJ connects and stabilizes apical and lateral components of tight junctions in human intestinal cells (Michel et al., 2005). In some cells, both MUPP1 and PATJ complexes co-exist, and MUPP1 regulates the cellular levels of the PALS1/PATJ polarity complex (Assémat et al., 2013). Co-immunoprecipitation studies showed that Mupp1 interacts in the mouse retina with Crb1 and Pals1, but not or less with Patj (van de Pavert et al., 2004). PATJ preferentially binds with PALS1 and partitioning defective-6 homolog (PAR6; **Figure 2B**; Adachi et al., 2009; Assémat et al., 2013). PAR6 is a key adaptor protein that interact with the ERLI PDZ domain of CRB in mammalian cells (Hurd et al., 2003; Lemmers et al., 2004). PAR6 leads to recruitment of PAR3, atypical protein kinase C (αPKC) and cell division control 42 (CDC42), known as the PAR complex (Joberty et al., 2000; Lin et al., 2000; Suzuki et al., 2001; Yamanaka et al., 2001; Hurd et al., 2003; Whitney et al., 2016; Pichaud, 2018). This PAR6-CDC42 complex is required for the apical-basal polarity and cell adhesion (Yamanaka et al., 2001).

Alternatively, the importance of a CRB-PALS1-EPB4.1L5 complex in mammals has been described (Laprise et al., 2006, 2009; Gosens et al., 2007). Co-expression and co-localization studies suggested that in several epithelial derived tissues Epb4.1l5 interact with at least one Crumbs homolog and with PALS1 (**Figure 2C**). In addition, in the adult retina, Epb4.1l5 showed substantial overlap at the outer limiting membrane (OLM) with CRB1 and PALS1 (Gosens et al., 2007). Overexpression of Epb4.1l5 in polarized MDCK cells affects tightness of cell junctions and results in disorganization of the tight junction markers ZO-1 and PATJ (Gosens et al., 2007). However, another group discovered, unlike in the zebrafish and *Drosophila* orthologs, that mouse Crumbs proteins are localized normally in absence of Epb4.1l5 (Lee et al., 2007). Additional research should be performed to define its precise molecular mechanism in mammalian cells.

The alternative isoform CRB3B contains a distinct carboxy terminal motif namely the CLPI motif, suggesting different binding partners in epithelial cells. CRB3 is widely expressed in epithelial cells. A *Crb3* KO mouse demonstrates extensive defects in epithelial morphogenesis, the mice die shortly after birth with cystic kidneys and lung proteinaceous debris throughout the lungs (Whiteman et al., 2014). Interestingly, these defects are also seen in Ezrin knockout mice, which is in line with the detected interaction between CRB3B and Ezrin in mice and mammalian cells (**Figure 2D**; Whiteman et al., 2014; Tilston-Lünel et al., 2016). This indicates that CRB3B is also crucial for epithelial morphogenesis and plays a role in linking the apical membrane to the underlying cytoskeleton (Whiteman et al., 2014; Gao et al., 2016; Tilston-Lünel et al., 2016). Therefore, the roles of the two CRB3 variants in the mouse lungs remain to be determined.

D*rosophila* Crb has also been found to inhibit the positive-feedback loop of phosphoinositide 3-kinase (PI-3K) and Rac1, thereby repressing the activation of Rac1 as well as PI-3K and maintaining proper apical domain and epithelial tissue integrity (**Figure 2E**; Chartier et al., 2011). This process could potentially be conserved in different species, however, more research in mammalian cells is required to support this hypothesis.

CRB Function in Cell Proliferation

In MGCs of *Drosophila* and *Xenopus,* yes-associated protein 1 (YAP) an important role in damaged retina (Hamon et al., 2017, 2019; Rueda et al., 2019). YAP is a core member of the Hippo pathway, which regulates several biological processes including cell proliferation, and survival (Yu et al., 2015). The intracellular domain of *Drosophila* Crb interacts with Expanded and thereby regulates the activity of Hippo pathway kinases (Yu and Guan, 2013; Yu et al., 2015). In mammalian lung epithelial and breast cancer cells, CRB3 expression also correlates with the Hippo pathway (Szymaniak et al., 2015; Mao et al., 2017). More specifically, CRB3 affects the Hippo pathway by interacting with Kibra and/or FRMD6 (FRMD6 is the homolog of *Drosophila* Expanded; **Figure 2F**). With low CRB3 expression levels, the Hippo-pathway is inactivated, YAP is not phosphorylated and can move to the nucleus where YAP target genes are expressed leading to increased cell proliferation and decreased apoptosis (Mao et al., 2017). Also in *Crb1*^{rd8} versus wild-type mouse retina several Hippo signaling related genes were differentially expressed (Hamon et al., 2017). In addition, CRB1 and CRB2 deletion also lead to YAP signaling dysregulation in developing murine retinas (Pellissier et al., 2013). These data suggest an essential role of the Hippo pathway in the control of cell proliferation.

CRB1 AND CRB2 IN RETINAL DISEASES

Mutations in the *CRB1* gene are associated with a wide spectrum of retinal dystrophies, such as retinitis pigmentosa (RP) and

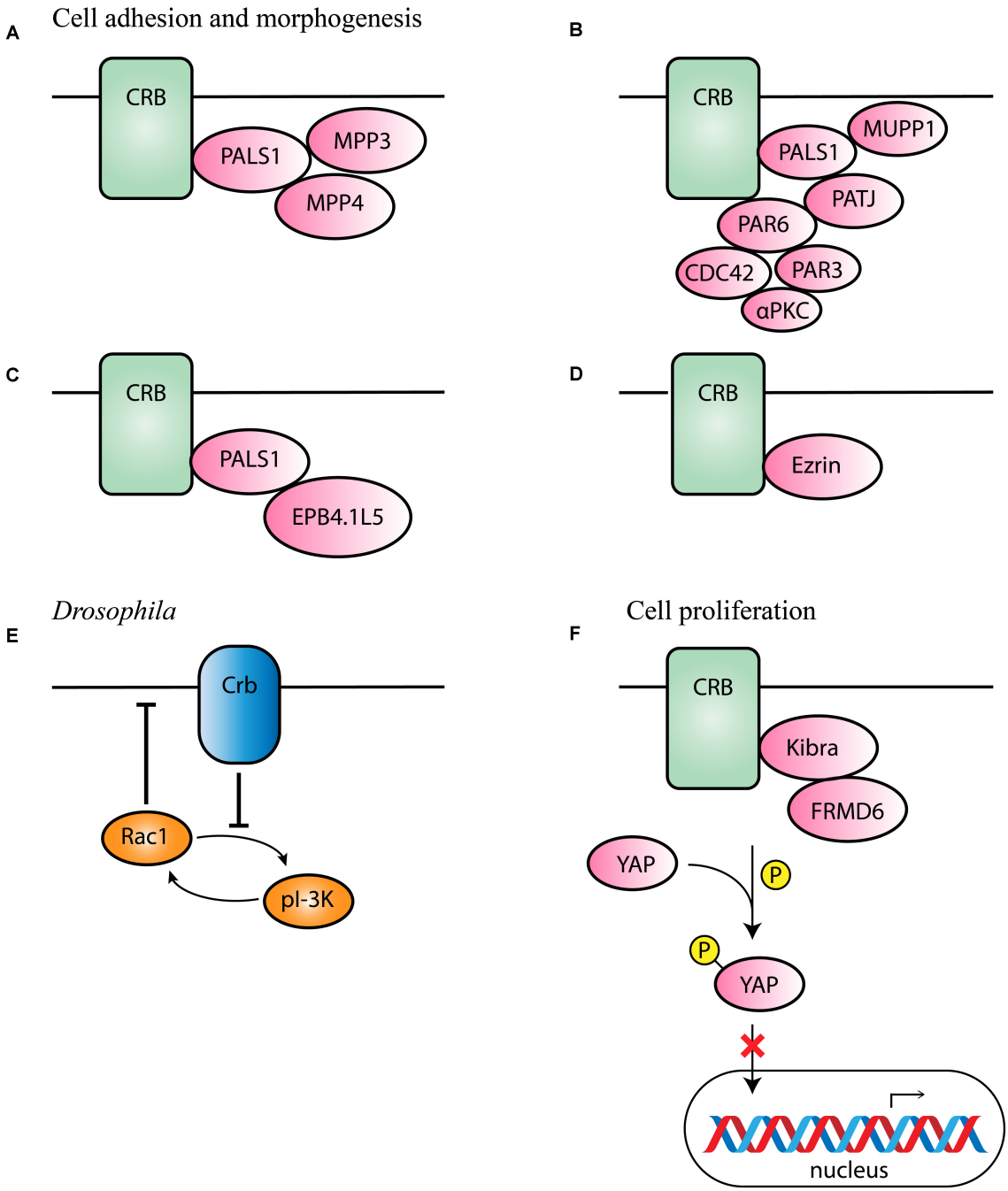

FIGURE 2 | Schematic representation of CRB interaction partners. **(A–D)** Proposed interaction partners and formed CRB complexes in mammals involved in cell adhesion and morphogenesis. **(E)** Proposed interaction partner in *Drosophila* suggested to be conserved among species. **(F)** Proposed interaction partners involved in cell proliferation.

Leber congenital amaurosis (LCA). RP is a clinically and genetically heterogeneous disease affecting more than 1.5 million people worldwide, where patients typically experience night blindness followed by progressive visual field loss ultimately leading to complete loss of vision in early or middle-life (Talib et al., 2017; Verbakel et al., 2018). The age at symptom onset for RP patients ranged from 0 to 47 years, with a median onset of 4 years (Talib et al., 2017). Approximately 3–9% of non-syndromic cases of autosomal recessive RP are caused by a mutation in the *CRB1* gene (Vallespin et al., 2007; Bujakowska et al., 2012; Corton et al., 2013). LCA is a more severe retinal dystrophy, causing serious visual impairment or blindness in newborns (Den Hollander et al., 2004). Mutations in the *CRB1* gene account for approximately 7–17% of all

LCA cases (Den Hollander et al., 2004; Vallespin et al., 2007; Bujakowska et al., 2012; Corton et al., 2013). There are more than 200 different mutations described along the *CRB1* gene resulting in retinal dystrophies without a clear genotype-phenotype correlation with RP or LCA, *CRB1* patients may display unique clinical features such as pigmented paravenous chorioretinal atrophy, macular atrophy alone, retinal degeneration associated with Coats-like exudative vasculopathy, para-arteriolar preservation of the RPE, or nanophthalmia (Henderson et al., 2011; Bujakowska et al., 2012; Corton et al., 2013). The clinical variability of disease onset and severity, even within a patient cohort with the same homozygous mutations, supports the hypothesis that the phenotype of patients with *CRB1* mutations is modulated by other factors (Mathijssen et al., 2017). So far, no treatment options exist for patients with mutations in the *CRB1* gene. To study *CRB1*-related retinal dystrophies for treatment options, several models have been used. Below, *CRB1*-related human- and animal-derived retinal models are described.

Until recently, no RP patients were described with mutations in the *CRB2* gene. However, Chen et al. (2019) discovered, using whole exome sequencing (WES), a homozygous *CRB2* p.R1249G mutation in a consanguineous Chinese family presenting RP. This mutation disturbs the stability of CRB2 protein and thereby induces RPE degeneration, impairs RPE phagocytosis, and accelerates RPE apoptosis. However, only a limited number of patients with this mutation are described, identification of *CRB2* mutations in more RP patients is warranted to better support its pathogenicity.

HUMAN-DERIVED RETINAL MODELS

The use of human-induced pluripotent stem cell (hiPSC) models for research is an emerging strategy to explore patient phenotypes *in vitro*. These techniques allow access to previously limited or inaccessible material and have been explored in many ophthalmic laboratories worldwide. A commonly used method is the differentiation of hiPSC into retinal organoids. Since the first one, numerous groups have adapted or created their own method to more efficiently generate well laminated retinal organoids (Meyer et al., 2011; Nakano et al., 2012; Zhong et al., 2014; Luo et al., 2018; Ovando-Roche et al., 2018). Nevertheless, a wide variability in differentiation efficiency across hiPSC lines is often reported (Capowski et al., 2019; Cora et al., 2019; Mellough et al., 2019; Chichagova et al., 2020). Chichagova et al. (2020) have shown that the ability of three different hiPSC lines to differentiate into retinal organoids in response to IGF1 or BMP4 activation was line- and method-dependent. Hallam et al. (2018) differentiated five hiPSC lines with a variability in efficiency, but by 5 months of differentiation all the retinal organoids were able to generate light responses and contained a well-formed ONL with PRCs containing inner segments, cilia, and outer-like segments. Attempts have been made to decrease this wide variability, Luo et al. (2018) described that the use of a Wnt signaling pathway antagonist, Dickkopf-related protein 1 (DKK-1), efficiently generated retinal organoids in all six hiPSC lines. Bulk RNA-sequencing profiling of retinal organoids demonstrated that the retinal differentiation *in vitro* recapitulated the *in vivo* retinogenesis in temporal expression of cell differentiation markers, retinal disease genes, and mRNA alternative splicing (Kim et al., 2019). These results make the retinal organoids, despite their high variability, of great interest in a wide range of applications including drug discovery, investigating the mechanism of retinal degeneration, developing cell-based therapeutic strategies and many more.

Defining the localization and onset of expression of the CRB complex members has been achieved in healthy hiPSC-derived retinal organoids. Several members of the CRB complex, CRB2, PALS1, PATJ, and MUPP1, were detected at the outer limiting membrane as early as differentiation day 28 (DD28), typical and clear puncta-like staining patterns for CRB1 were found only after DD120. All CRB complex members together with adherence junction markers, p120-catenin and N-cadherin, were still detectable in DD180 retinal organoids (Quinn et al., 2019a). The onset of CRB1 and CRB2 protein expression recapitulates those observed in the human fetal retina, with a clear onset of CRB2 expression before CRB1 expression (Quinn et al., 2019a).

Three *CRB1* patient hiPSC lines containing a homozygous missense mutation (c.3122T > C), or heterozygous missense mutations (c.2983G > T and c.1892A > G, or c.2843G > A and c.3122T > C) were successfully differentiated into retinal organoids and analyzed at DD180. Here, all three retinal layers were developed: retinal ganglion cell layer marked by Tuj1 positive dendrites, neuroblast layer marked by SOX9 positive retinal progenitor cells, and an outer nuclear layer marked by recoverin positive PRCs. However, frequently, there were ectopic recoverin positive cells found above the outer limiting membrane and all missense *CRB1* organoid lines developed small but frequent disruptions of localization of CRB complex members at the OLM that were not found in control lines (Quinn et al., 2019a). Data from these *CRB1* patient hiPSC retinal organoids suggest a retinal degeneration phenotype similar to that previously found in mice lacking CRB1, mice expressing the C249W CRB1 variant, or mouse retina lacking CRB2 (van de Pavert et al., 2004, 2007a; Alves et al., 2013). Another study shortly describes the successful differentiation of hiPSC carrying a compound heterozygous mutation in the *CRB1* gene (c.1892A > G and c.2548G > A) to retinal organoids. All three germ layers and expressed markers of retinal progenitor cells, including N-cadherin, rhodopsin, and PAX6, after 35 days of differentiation were present, but no phenotype was described in this paper (Zhang et al., 2018). To our knowledge, only these two papers have reported the generation of *CRB1* patient hiPSC-derived retinal organoids. The reproducible phenotype observed in these three *CRB1* patient lines (Quinn et al., 2019a) provides a good model for assessing potential gene therapy approaches.

Another frequently used method in the ophthalmic field is the differentiation of hiPSC into RPE monolayers. Efficient protocols for differentiating hiPSC into RPE monolayers using a mixture of growth factors have been established (Zahabi et al., 2012; Buchholz et al., 2013; Shutova et al., 2016). However, attempts are currently made to use non-biological products, such as small molecules, that would limit the risks of infection or immune rejection when transplanted. Maruotti et al. (2015) developed a protocol which uses chemotin (CTM) in combination with

a previously known neural inducer nicotinamide (NIC) to efficiently differentiate hiPSC into RPE monolayers. In three independent hiPSC lines, RPE differentiation was efficient, and key RPE markers such as microphthalmia-associated transcription factor (MITF), PMEL17, and tight junction protein zonula occludens 1 (ZO-1) were strongly expressed. When left longer in culture to mature, bestrophin 1 (BEST1) and RPE-specific protein of 65 kDa (RPE65) were also strongly expressed (Maruotti et al., 2015). Using a slightly adapted protocol, Smith et al. (2019) differentiated six more hiPSC lines into hiPSC-RPE monolayers, all six also expressed the key RPE markers ZO-1, BEST-1, and MITF. Another study revealed by RNA sequencing data that hiPSC-RPE grouped with fetal RPE samples, indicating that their gene expression was highly correlated and similar (Smith et al., 2019). In addition, Zahabi et al. (2012) provided proof-of-concept that multiple retinal-disease specific hiPSC lines, including two RP lines, can be differentiated into RPE monolayers. Altogether, this data illustrates the potential of hiPSC-RPE as a model system for retinal diseases with mutations in the RPE. Related to CRB, recent studies have shown that CRB2 but not CRB1 is expressed in the human RPE during the differentiation into retinal organoids (Quinn et al., 2019a). In addition, there are RP patients described with specific *CRB2* variations expressed in RPE cells (Chen et al., 2019). Therefore, the method of generating hiPSC-RPE could be used to explore treatment possibilities for patients with specific variations in *CRB2*.

CRB1-RELATED ANIMAL RETINAL DEGENERATION MODELS

Numerous research groups focus on animal models to gain, understand, and develop gene therapy strategies that potentially can be used to treat retinal degeneration of RP and LCA patients. Over the years there are multiple animal models developed mimicking the CRB1-related phenotype in patients. These models vary from mild to more severe, early- to late-onset, and MGC or photoreceptor specific phenotypes. Double retinal knock-outs of *CRB1* and *CRB2,* have helped to understand the contribution of the two CRB proteins to the retinal disease etiology, and explain the relatively mild phenotype observed in *Crb1* variant mouse models (Mehalow et al., 2003; van de Pavert et al., 2004, 2007a,b).

LCA-Like Mouse Models

Four mouse models showing a *CRB1* LCA-like phenotype have been reported: $Crb1^{KO}Crb2^{\Delta RPC}$ where both Crb1 and Crb2 are ablated in retinal progenitor cells (Pellissier et al., 2013), secondly the $Crb1^{KO}Crb2^{\Delta imPRC}$ where Crb1 is ablated in MGC and Crb2 is ablated in immature PRCs with remaining Crb2 levels in MGC and progenitor cells (Quinn et al., 2018), thirdly the $Crb1^{KO/WT}Crb2^{\Delta RPC}$ mouse model with reduced levels of Crb1 in MGC and ablation of Crb2 in retinal progenitor cells (Pellissier et al., 2013), and finally $Crb1^{KO}Crb2^{\Delta MGC}$ in which both Crb1 and Crb2 are ablated in MGC (Quinn et al., 2019b). All four models exhibit vision loss indicated by a reduced electroretinography (ERG) response. In addition, retinal degeneration was observed by outer limiting membrane disruptions, abnormal retinal lamination, intermingling of nuclei of the ONL and INL, and ectopic localization of retinal cells. These mouse models show an early onset phenotype with distinct severity indicated by the order mentioned above. In short, in the most severe mouse model, $Crb1^{KO}Crb2^{\Delta RPC}$, the phenotype onset was found as early as embryonal day 13 (E13) which was observed throughout the retina (Pellissier et al., 2013). Retinal degeneration in $Crb1^{KO}Crb2^{\Delta imPRC}$ was detected at E15 in the whole retina, but in adult mice the superior retina was more affected than the inferior retina (Quinn et al., 2018). Also in $Crb1^{KO/WT}Crb2^{\Delta RPC}$ mice retinal degeneration was detected at E15, but was mostly affecting the peripheral retina (Pellissier et al., 2013). Finally, the $Crb1^{KO}Crb2^{\Delta MGC}$ mice showed the first signs of degeneration at E17, where mostly the peripheral retina was affected. More subtle differences between these models are described and summarized before (Quinn et al., 2019b). These data show that all four *Crb1* mouse models mimic the LCA phenotype in patients and could therefore be used for future therapy development.

RP-Like Mouse Models

Twelve *CRB1* RP-like mouse models have been described so far, including (1) $Crb1^{KO/C249W}$ with a missense variation in the *Crb1* gene (van de Pavert et al., 2007a), (2) $Crb2^{\Delta MGC}$ where only Crb2 is ablated in MGC (Alves et al., 2014), (3) the $Crb1^{rd8}$ mice with a naturally occurring nonsense mutation in the *Crb1* gene (Mehalow et al., 2003), (4) the $Crb1^{KO}$ where the full length Crb1 protein is ablated from retinal radial glial progenitor cells, MGCs, and the rest of the body (van de Pavert et al., 2004), (5) the $Crb1^{del-B}$ were *Crb1-B* is abolished from photoreceptor and MGCs (Ray et al., 2020), (6) the $Crb1^{null}$ where a deletion of alternate exon 5a up to intron 7 disrupts all *Crb1* isoforms (Ray et al., 2020), (7) $Crb2^{\Delta rods}$ where Crb2 is ablated only in developed rod PRCs (Alves et al., 2019), (8) $Crb1^{KO}Crb2^{\Delta rods}$ where Crb1 is ablated in MGC and Crb2 in rod PRCs (Alves et al., 2019), (9) $Crb1^{KO}Crb2^{low-imPRC}$ with absence of Crb1 and reduced levels of Crb2 in immature photoreceptors (Quinn et al., 2018), (10) $Crb1^{KO}Crb2^{\Delta low-RPC}$ with absence of Crb1 and reduced levels of Crb2 in retinal progenitor cells (Pellissier et al., 2014b), (11) $Crb2^{\Delta RPC}$ where Crb2 is ablated in retinal progenitor cells (Alves et al., 2013), and finally, (12) $Crb2^{\Delta imPRC}$ with Crb2 ablation in immature PRCs (Alves et al., 2014). The different Cre mouse models show variations in mosaicism (mutant adjacent to wildtype cells), but eleven out of twelve *Crb* models show disruptions at the outer limiting membrane with rows or single photoreceptor nuclei protruding into the subretinal space or ingressing into the outer plexiform layer leading to a degenerative retinal phenotype (**Table 1**).

The $Crb1^{rd8}$ mice have a naturally occurring single base deletion in exon 9 of the *Crb1* gene causing a frame shift and premature stop codon, thereby truncating the transmembrane and cytoplasmic domain of Crb1. This results in a photoreceptor degeneration mainly observed in the inferior nasal quadrant of the eye, caused by retinal folds and pseudorosettes (Mehalow et al., 2003). In the $Crb1^{KO}$ mouse

TABLE 1 | Schematic overview retinitis pigmentosa (RP) mouse models.

	$Crb1^{KO/C249W}$	$Crb2^{\Delta MGC}$	$Crb1^{del-B}$	$Crb1^{rd8}$	$Crb1^{KO}$	$Crb1^{null}$	$Crb2^{\Delta Rods}$	$Crb1^{KO}$ $Crb2^{\Delta Rods}$	$Crb1^{KO}$ $Crb2^{low-imPRC}$	$Crb1^{KO}$ $Crb2^{low-RPC}$	$Crb2^{\Delta RPC}$	$Crb2^{\Delta imPRC}$
Severity	+	+	–	++	++	++	++	+++	+++	+++	++++	++++
CRB1-A ablation	MGC	–	–	Natural occurring mutation	MGC	MGC	–	MGC	MGC	MGC	–	–
CRB1-B ablation	–	–	PRC and MGC	Natural occurring mutation	–	PRC and MGC	–	–	–	–	–	–
CRB2 ablation	–	MGC	–	–	–	–	Rod PRC	Rod PRC	50% in immature PRC	50% in RPC	RPC	Immature PRC
Morphologic phenotype onset*	8M	1M	NA	1M	P14	3M	3M	1M	P10	P10	E18.5	E15.5
ERG differences*	No	No	NA	No	No	NA	Yes (9 M)	Yes (3 M)	Yes (3 M)	Yes (3 M)	Yes (1 M)	Yes (1 M)
Affected areas	NA	Mainly periphery	NA	Inferior nasal quadrant	Inferior temporal quadrant	Inferior retina	Superior retina	Superior retina	Inferior retina	Throughout retina	Throughout retina	Throughout retina
OLM disruptions	Yes, sporadic	Yes	No	Yes	Yes	Yes	Yes	Yes	Yes	Yes	Yes	Yes
PRC nuclei protrusions	Yes, sporadic	Yes	No	Yes	Yes	Yes	Yes	Yes	Yes	Yes	Yes	Yes

*MGC, Müller glial cells; OLM, outer limiting membrane; PRC, photoreceptor cell; RPC, retinal progenitor cell. * The phenotype onset and ERG differences can be marginal on the indicated ages; the severity of the phenotype increases over time.*

model the retinal lamination is predominantly maintained, and degeneration is found in the inferior temporal quadrant of the retina. Degeneration is indicated by single or groups of PRCs protruding into the subretinal space, rosette formation, and neovascularization. In 18M-old mice there was no loss of overall retinal function measured by electroretinography, suggesting that a major part of the retina was not affected by loss of Crb1 (van de Pavert et al., 2004, 2007b). Light exposure experiments reveal that light exposure doesn't initiate but rather enhances the retinal degeneration (van de Pavert et al., 2007b). The mild phenotype observed in these *Crb1* mouse models suggests that Crb2 protein may compensate the effect of CRB1 deletion.

In the $Crb1^{del-B}$ the alternative *Crb1-B* isoform is abolished from PRCs, while the $Crb1^{null}$ disrupts all potential *Crb1* isoforms (Ray et al., 2020). The $Crb1^{del-B}$ mouse do not show significant disruptions in the OLM, while the disruptions in the $Crb1^{null}$ mice were comparable with $Crb1^{rd8}$ (Ray et al., 2020). Although not mentioned by Ray et al. (2020), also the $Crb1^{KO}$ mice shows significant OLM disruptions strongly depending on genetic background as well as exposure to light (van de Pavert et al., 2004, 2007b). As the IrCaptureSeq suggested that *Crb1-B* is the most abundant transcript in mouse and human retina, a cross-breeding of $Crb1^{null}$ with $Crb1^{del-B}$ mice was performed to define the relevance of Crb1-B in the retina. This heterozygous $Crb1^{null/del-B}$ showed similar OLM disruptions with the homozygous $Crb1^{null}$ mouse (Ray et al., 2020). Similar OLM disruptions were thus found in $Crb1^{rd8}$, $Crb1^{null}$, $Crb1^{null/del-B}$, and $Crb1^{KO}$ mice. It is essential to perform retinal function measurements on the mouse models affecting *Crb1-B* to understand its function and to compare it with previously described *Crb1* mouse models. In addition, the most severe retinal phenotype so far derives from *Crb1* mice with concomitant loss of Crb2. Both $Crb2^{\Delta RPC}$ and $Crb2^{\Delta imPRC}$ show an early onset retinal degeneration at embryonic day 18.5 (E18.5) and E15.5, respectively, the difference is caused by the distinct expression pattern and timing of the Cre recombinase and morphological phenotypes result in differences in the scotopic and photopic ERG conditions already at 1 M of age (Alves et al., 2013, 2014). Interestingly, in contrast to $Crb2^{\Delta RPC}$ mice, the lamination of Müller glial, ganglion and amacrine cells were also misplaced in $Crb2^{\Delta imPRC}$ mice. These lamination defects were also observed in $Crb1^{KO/WT}Crb2^{\Delta RPC}$ mice (Pellissier et al., 2013).

Another mouse model, $Crb2^{\Delta rods}$, show a mild and late onset phenotype limited to the superior retina (Alves et al., 2019). In some 3 M and all 6 M old $Crb2^{\Delta rods}$ mice, disruptions of the outer limiting membrane, a thinned photoreceptor layer at the peripheral superior retina, and PRCs protruding into the subretinal space were observed. A reduction in ERG scotopic a-wave was observed in 9 M old mice, while no difference in optokinetic head tracking response (OKT) spatial frequency or contrast sensitivity was observed. Interestingly, while most PRCs were affected, all the remaining PRCs showed mature inner- and outer-segments. Remaining rods were functional and the cones showed normal morphology. This phenotype is enhanced by a concomitant loss of Crb1 in MGCs (Alves et al., 2019). These mice, $Crb1^{KO}Crb2^{\Delta rods}$, show a similar but enhanced phenotype

in comparison to $Crb2^{\Delta \text{rods}}$ mice. Here, a reduction in ERG scotopic a-wave was observed at 3 M and became more apparent at 6 M onward. In addition, a significant decrease in OKT contrast sensitivity was found from 3 M of age onward (Alves et al., 2019). The difference in phenotype onset between all these mouse models might be explained by the onset of Cre expression during retinogenesis and by cell-type specific ablation; ablation of Crb2 from a later time point resulted in a milder phenotype. Interestingly, when Crb2 is ablated in MGCs, $Crb2^{\Delta \text{MGC}}$, a very mild morphological phenotype with no functional consequences measured using ERG was observed (Alves et al., 2014), but ablation of both Crb1 and Crb2 from MGCs caused a severe LCA phenotype (Quinn et al., 2019b). This data suggests that Crb2 has a redundant function in MGCs, while in PRCs it is essential for proper retinal lamination and function.

Interestingly, the $Crb1^{\text{KO}}$ phenotype is located at the inferior temporal quadrant whereas the $Crb2^{\Delta \text{rods}}$ phenotype is mainly observed at the peripheral and central superior retina. These differences might be related to higher levels of Crb2 in the inferior retina while Crb1 is expressed at higher levels in the superior retina (Pellissier et al., 2014b). In addition, there might be modifying factors present which are enriched in either the superior or inferior retina causing the different phenotypes.

In addition to these mouse models, a rat with a spontaneous mutation in *Crb1* exon 6 was discovered mimicking human macular telangiectasia type 2 (Zhao et al., 2015). The autosomal recessive indel mutation causes an early onset phenotype with a strongly reduced ERG response in 3-week old rats. These rats showed a focal loss of retinal lamination, OLM disruptions, and PRC, MGC, and RPE alterations (Zhao et al., 2015). Differences between this and the *Crb1* mouse models could result from different types of mutations or from different genetic setups displayed by these different animal species.

GENE AUGMENTATION STRATEGIES FOR *CRB1* RETINAL DYSTROPHIES

There is an emerging interest in gene augmentation strategies for retinal dystrophies. Recently, gene therapy became available for young RP and LCA patients with biallelic mutations in the *RPE65* gene. Voretigene neparvovec-rzyl, or its commercial name: LUXTURNA$^{\text{TM}}$, uses the adeno-associated viral vector serotype 2 (AAV2) to deliver by subretinal injection a functional copy of the *RPE65* gene into the RPE cells. *RPE65* transgene expression results in the production and correct localization of RPE65 protein in RPE cells, thereby compensating for the loss of the protein and restoring the visual cycle in these patients (Maguire et al., 2019). Nowadays, there are numerous clinical studies ongoing which explore the use of AAV as a therapeutic vector for retinal diseases, such as RP, wet age-related macular dystrophy (AMD), LCA, and many more (Wang et al., 2019). However, so far, no treatment options are available for RP and LCA patients with mutations in the *CRB1* gene. Below, we will describe novel therapeutic tools which could be promising for *CRB1* retinal gene augmentation therapy in RP patients.

Currently, AAVs are the leading platform for gene delivery in the treatment of retinal dystrophies. AAVs are mainly investigated because of their low toxicity, their capability to transduce both dividing and non-dividing cells, they do not integrate into the host genome, and AAV capsid variants display distinct cell tropisms. A complete overview of basic AAV biology, AAV vectorology, and current therapeutic strategies and clinical progress was recently reviewed by Wang et al. (2019) and Buck and Wijnholds (2020). The major disadvantage of AAVs is their limited package capacity, bigger gene expression cassettes than 4.5 kb are not able to fit within a single AAV. Because of this, the development of AAV-mediated *CRB1* gene therapy is also challenging. Full-length cytomegalovirus (CMV) ubiquitous promoter and *CRB1* cDNA exceeds the AAV package limitation. However, using an engineered minimal CMV promoter and codon optimized *CRB1* cDNA allowed sufficient expression levels of full-length CRB1 protein in MGCs in mice (Pellissier et al., 2014a). Pre-clinical studies in mouse using this AAV-CMVmin-*hCRB1* have shown that expression of *CRB1* was deleterious in *CRB1* mouse models but not in wild-type mice (Pellissier et al., 2015). In addition, there are more potential *CRB1* transcript variants which could be targeted (Quinn et al., 2017). Interestingly, alternative strategies using the codon-optimized structural and functional family member *CRB2* to rescue *CRB1*-related retinopathies restored retinal function and structure in *Crb1* mouse models (Pellissier et al., 2015). In that study, improved photoreceptor layer morphology and ERG response was detected after *CRB2* delivery. The combination of AAV9 with a full-length CMV promoter was used to target both photoreceptor and MGCs, whereas no rescue was observed when either photoreceptor or MGCs were targeted with *CRB2* (Pellissier et al., 2015). In addition, several groups explored the possibility to overcome the limiting AAV package capacity by dual or triple-AAV approaches (Trapani et al., 2014; Carvalho et al., 2017; Maddalena et al., 2018) or by increasing the package capacity (Ding and Gradinaru, 2020). Yet, the studies performed so far have shown that the dual AAV approaches have lower expression levels compared to a single AAV vector (Trapani et al., 2014; Carvalho et al., 2017).

Several research groups focus on AAV-mediated gene delivery to define the tropism in hiPSC-derived retinal organoids and/or RPE. Out of four different AAV capsids packaged with the CAG promoter and GFP (AAV2, AAV2-7m8, AAV8, AAV9), Garita-Hernandez et al. (2020) showed with AAV2-7m8 infection at day 44 the most efficient transduction of the hiPSC-derived retinal and RPE organoids. Limited transduction of AAV9 was found (Garita-Hernandez et al., 2020). Another study showed, using AAV-CMV-*GFP* constructs, a more efficient retinal organoid transduction at DD220 especially in MGC with AAV5 or ShH10Y445F capsids in comparison with AAV9 (Quinn et al., 2019a). Recently, Lane et al. (2020) demonstrate efficient PRCs transduction in DD140 retinal organoids using an AAV5 packaged with the CAG promoter. Moreover, AAV5-mediated gene augmentation with human *RP2* was able to rescue the degeneration found in *RP2* KO retinal organoids by preventing ONL thinning

and restoring rhodopsin expression (Lane et al., 2020). Therefore, testing CRB1- or CRB2-expressing vectors in retinal organoids will aid in the discovery of *CRB* gene therapy treatment for *CRB1*-related retinal dystrophies in patients.

In addition, there are different non-viral mediated approaches for gene therapy. An example is the use of nanoparticles. Three representative nanoparticles, namely metal-based, polymer-based, and lipid-based nanoparticles, were recently reviewed describing their characteristics and recent application in ocular therapy (Wang et al., 2018). Shortly, the most extensive characterized nanoparticle is the polymer-based CK30-PEG nanoparticle, which contains plasmid DNA compacted with polyethylene glycol-substituted lysine 30-mers (Fink et al., 2006; Han et al., 2012). Theoretically, these approaches have an unlimited gene packaging capacity, which display a big advantage for large genes such as *CRB1*. These nanoparticles are also able to infect RPE and PRC, and can drive gene expression on a comparable scale and longevity than AAVs in mice (Cai et al., 2009; Han et al., 2012). CK30-PEG nanoparticles have a tolerable safety profile and is non-toxic in mouse and non-human primate eyes (Ding et al., 2009; Akelley et al., 2018). To our knowledge, there is no successful clinical study described using these nanoparticles so far. More research is required to define the clinical relevance of these nanoparticles in retinal gene therapy. Further pre-clinical research and clinical trials will aid in the discovery of new gene therapy approaches for *CRB1*-related retinal dystrophies in patients. A retrospective *CRB1* natural history study (NHS) has been published (Talib et al., 2017), and their prospective NHS with strategies for evaluation of the efficacy of novel clinical therapeutic interventions in the treatment of *CRB1*-retinal dystrophies will be reported in the end of 2020. Recently, a French biotech company called HORAMA signed an exclusive license agreement with Leiden University Medical Center targeting *CRB1* gene mutations to treat inherited retinal dystrophies. Based on current timelines, HORAMA expects initiating a Phase I/II clinical study with the drug candidate in 2023 (HORAMA, 2020).

CONCLUSION

In this review we have discussed (1) CRB protein function in mammalian cells, (2) recent advances and potential tools for *CRB1* human and animal retinal degeneration models, and (3) described therapeutic tools which potentially could be used for retinal gene augmentation therapy for RP and LCA patients with mutations in the *CRB1* gene.

AUTHOR CONTRIBUTIONS

NB, JW, and LP contributed to writing, reviewing, and editing the manuscript. NB wrote the original draft. All authors contributed to the article and approved the submitted version.

FUNDING

Funding was obtained from the Foundation Fighting Blindness (TA-GT-0715-0665-LUMC), The Netherlands Organisation for Health Research and Development (ZonMw grant 43200004), the Million Dollar Bike Ride Grant Program (MDBR-19-131-CRB1), and Stichting Blinden-Penning (Uitzicht 2014-1 to LP and JW). LP acknowledges the funding from the European Research Council (ERC) under the European Union's Horizon 2020 research and innovation program (grant agreement No. 851231).

REFERENCES

Adachi, M., Hamazaki, Y., Kobayashi, Y., Itoh, M., Tsukita, S., Furuse, M., et al. (2009). Similar and distinct properties of MUPP1 and Patj, two homologous PDZ domain-containing tight-junction proteins. *Mol. Cell. Biol.* 29, 2372–2389. doi: 10.1128/mcb.01505-08

Aguilar-Aragon, M., Fletcher, G., and Thompson, B. J. (2020). The cytoskeletal motor proteins Dynein and MyoV direct apical transport of crumbs. *Dev. Biol.* 459, 126–137. doi: 10.1016/j.ydbio.2019.12.009

Ahmed, S. M., and Macara, I. G. (2017). The Par3 polarity protein is an exocyst receptor essential for mammary cell survival. *Nat. Commun.* 8:14867. doi: 10.1038/ncomms14867

Akelley, R. A., Conley, S. M., Makkia, R., Watson, J. N., Han, Z., Cooper, M. J., et al. (2018). DNA nanoparticles are safe and nontoxic in non-human primate eyes. *Int. J. Nanomedicine* 13, 1361–1379. doi: 10.2147/IJN.S157000

Alves, C. H., Boon, N., Mulder, A. A., Koster, A. J., Jost, C. R., and Wijnholds, J. (2019). CRB2 loss in rod photoreceptors is associated with progressive loss of retinal contrast sensitivity. *Int. J. Mol. Sci.* 20:4069. doi: 10.3390/ijms20174069

Alves, C. H., Pellissier, L. P., Vos, R. M., Garrido, M. G., Sothilingam, V., Seide, C., et al. (2014). Targeted ablation of Crb2 in photoreceptor cells induces retinitis pigmentosa. *Hum. Mol. Genet.* 23, 3384–3401. doi: 10.1093/hmg/ddu048

Alves, C. H., Sanz sanz, A., Park, B., Pellissier, L. P., Tanimoto, N., Beck, S. C., et al. (2013). Loss of CRB2 in the mouse retina mimics human retinitis pigmentosa due to mutations in the CRB1 gene. *Hum. Mol. Genet.* 22, 35–50. doi: 10.1093/hmg/dds398

Assémat, E., Crost, E., Ponserre, M., Wijnholds, J., Le Bivic, A., and Massey-Harroche, D. (2013). The multi-PDZ domain protein-1 (MUPP-1) expression regulates cellular levels of the PALS-1/PATJ polarity complex. *Exp. Cell Res.* 319, 2514–2525. doi: 10.1016/j.yexcr.2013.07.011

Bazellières, E., Aksenova, V., Barthélémy-Requin, M., Massey-Harroche, D., and Le Bivic, A. (2018). Role of the Crumbs proteins in ciliogenesis, cell migration and actin organization. *Semin. Cell Dev. Biol.* 81, 13–20. doi: 10.1016/j.semcdb.2017.10.018

Buchholz, D. E., Pennington, B. O., Croze, R. H., Hinman, C. R., Coffey, P. J., and Clegg, D. O. (2013). Rapid and efficient directed differentiation of human pluripotent stem cells into retinal pigmented epithelium. *Stem Cells Transl. Med.* 2, 384–393. doi: 10.5966/sctm.2012-0163

Buck, T. M., and Wijnholds, J. (2020). Recombinant adeno-associated viral vectors (rAAV)-vector elements in ocular gene therapy clinical trials and transgene expression and bioactivity assays. *Int. J. Mol. Sci.* 21:4197. doi: 10.3390/ijms21124197

Bujakowska, K., Audo, I., Mohand-Säid, S., Lancelot, M. E., Antonio, A., Germain, A., et al. (2012). CRB1 mutations in inherited retinal dystrophies. *Hum. Mutat.* 33, 306–315. doi: 10.1002/humu.21653

Bulgakova, N. A., and Knust, E. (2009). The crumbs complex: from epithelial-cell polarity to retinal degeneration. *J. Cell Sci.* 122, 2587–2596. doi: 10.1242/jcs.023648

Cai, X., Nash, Z., Conley, S. M., Fliesler, S. J., Cooper, M. J., and Naash, M. I. (2009). A partial structural and functional rescue of a retinitis pigmentosa model with compacted DNA nanoparticles. *PLoS One* 4:e0005290. doi: 10.1371/journal.pone.0005290

Capowski, E. E., Samimi, K., Mayerl, S. J., Phillips, M. J., Pinilla, I., Howden, S. E., et al. (2019). Reproducibility and staging of 3D human retinal organoids across multiple pluripotent stem cell lines. *Development* 146:dev171686. doi: 10.1242/dev.171686

Carvalho, L. S., Turunen, H. T., Wassmer, S. J., Luna-Velez, M. V., Xiao, R., Bennett, J., et al. (2017). Evaluating efficiencies of dual AAV approaches for retinal targeting. *Front. Neurosci.* 11:503. doi: 10.3389/fnins.2017.00503

Chartier, F. J. M., Hardy, ÉJ. L., and Laprise, P. (2011). Crumbs controls epithelial integrity by inhibiting Rac1 and PI3K. *J. Cell Sci.* 124, 3393–3398. doi: 10.1242/jcs.092601

Chen, X., Jiang, C., Yang, D., Sun, R., Wang, M., Sun, H., et al. (2019). CRB2 mutation causes autosomal recessive retinitis pigmentosa. *Exp. Eye Res.* 180, 164–173. doi: 10.1016/j.exer.2018.12.018

Chichagova, V., Hilgen, G., Ghareeb, A., Georgiou, M., Carter, M., Sernagor, E., et al. (2020). Human iPSC differentiation to retinal organoids in response to IGF1 and BMP4 activation is line- and method-dependent. *Stem Cells* 38, 195–201. doi: 10.1002/stem.3116

Cora, V., Haderspeck, J., Antkowiak, L., Mattheus, U., Neckel, P. H., Mack, A. F., et al. (2019). A cleared view on retinal organoids. *Cells* 8:391. doi: 10.3390/cells8050391

Corton, M., Tatu, S. D., Avila-Fernandez, A., Vallespín, E., Tapias, I., Cantalapiedra, D., et al. (2013). High frequency of CRB1 mutations as cause of early-onset retinal dystrophies in the Spanish population. *Orphanet J. Rare Dis.* 8:20. doi: 10.1186/1750-1172-8-20

Den Hollander, A. I., Davis, J., Van Der Velde-Visser, S. D., Zonneveld, M. N., Pierrottet, C. O., Koenekoop, R. K., et al. (2004). CRB1 mutation spectrum in inherited retinal dystrophies. *Hum. Mutat.* 24, 355–369. doi: 10.1002/humu.20093

Den Hollander, A. I., Ten Brink, J. B., De Kok, Y. J. M., Van Soest, S., Van Den Born, L. I., Van Driel, M. A., et al. (1999). Mutations in a human homologue of *Drosophila* crumbs cause retinitis pigmentosa (RP12). *Nat. Genet.* 23, 217–221. doi: 10.1038/13848

Ding, X., and Gradinaru, V. (2020). "Structure-guided rational design of adeno-associated viral capsids with expanded sizes," in *Proceedings of the 23rd Annual Meeting of the American Society for Gene and Cell Therapy*, Milwaukee, WI.

Ding, X. Q., Quiambao, A. B., Fitzgerald, J. B., Cooper, M. J., Conley, S. M., and Naash, M. I. (2009). Ocular delivery of compacted DNA-nanoparticles does not elicit toxicity in the mouse retina. *PLoS One* 4:e0007410. doi: 10.1371/journal.pone.0007410

Dudok, J. J., Murtaza, M., Alves, H. C., Rashbass, P., and Wijnholds, J. (2016). Crumbs 2 prevents cortical abnormalities in mouse dorsal telencephalon. *Neurosci. Res.* 108, 12–23. doi: 10.1016/j.neures.2016.01.001

Dudok, J. J., Sanz, A. S., Lundvig, D. M. S., Sothilingam, V., Garrido, M. G., Klooster, J., et al. (2013). MPP3 regulates levels of PALS1 and adhesion between photoreceptors and Müller cells. *Glia* 61, 1629–1644. doi: 10.1002/glia.22545

Ebarasi, L., Ashraf, S., Bierzynska, A., Gee, H. Y., McCarthy, H. J., Lovric, S., et al. (2015). Defects of CRB2 cause steroid-resistant nephrotic syndrome. *Am. J. Hum. Genet.* 96, 153–161. doi: 10.1016/j.ajhg.2014.11.014

Fan, S., Fogg, V., Wang, Q., Chen, X. W., Liu, C. J., and Margolis, B. (2007). A novel Crumbs3 isoform regulates cell division and ciliogenesis via importin β interactions. *J. Cell Biol.* 178, 387–398. doi: 10.1083/jcb.200609096

Fink, T. L., Klepcyk, P. J., Oette, S. M., Gedeon, C. R., Hyatt, S. L., Kowalczyk, T. H., et al. (2006). Plasmid size up to 20 kbp does not limit effective in vivo lung gene transfer using compacted DNA nanoparticles. *Gene Ther.* 13, 1048–1051. doi: 10.1038/sj.gt.3302761

Gao, Y., Lui, W. Y., Lee, W. M., and Cheng, C. Y. (2016). Polarity protein Crumbs homolog-3 (CRB3) regulates ectoplasmic specialization dynamics through its action on F-actin organization in Sertoli cells. *Sci. Rep.* 6, 1–20. doi: 10.1038/srep28589

Garita-Hernandez, M., Routet, F., Guibbal, L., Khabou, H., Toualbi, L., Riancho, L., et al. (2020). AAV-mediated gene delivery to 3D retinal organoids derived from human induced pluripotent stem cells. *Int. J. Mol. Sci.* 21, 1–16. doi: 10.3390/ijms21030994

Gosens, I., Sessa, A., den Hollander, A. I., Letteboer, S. J. F., Belloni, V., Arends, M. L., et al. (2007). FERM protein EPB41L5 is a novel member of the mammalian CRB-MPP5 polarity complex. *Exp. Cell Res.* 313, 3959–3970. doi: 10.1016/j.yexcr.2007.08.025

Hallam, D., Hilgen, G., Dorgau, B., Zhu, L., Yu, M., Bojic, S., et al. (2018). Human-induced pluripotent stem cells generate light responsive retinal organoids with variable and nutrient-dependent efficiency. *Stem Cells* 36, 1535–1551. doi: 10.1002/stem.2883

Hamon, A., García-García, D., Ail, D., Bitard, J., Chesneau, A., Dalkara, D., et al. (2019). Linking YAP to müller glia quiescence exit in the degenerative retina. *Cell Rep.* 27, 1712.e6–1725.e6. doi: 10.1016/j.celrep.2019.04.045

Hamon, A., Masson, C., Bitard, J., Gieser, L., Roger, J. E., and Perron, M. (2017). Retinal degeneration triggers the activation of YAP/TEAD in reactive Müller cells. *Retin. Cell Biol.* 58, 1941–1953. doi: 10.1167/iovs.16-21366

Han, Z., Conley, S. M., Makkia, R., Guo, J., Cooper, M. J., and Naash, M. I. (2012). Comparative analysis of DNA nanoparticles and AAVs for ocular gene delivery. *PLoS One* 7:e0052189. doi: 10.1371/journal.pone.0052189

Henderson, R. H., Mackay, D. S., Li, Z., Moradi, P., Sergouniotis, P., Russell-Eggitt, I., et al. (2011). Phenotypic variability in patients with retinal dystrophies due to mutations in CRB1. *Br. J. Ophthalmol.* 95, 811–817. doi: 10.1136/bjo.2010.186882

HORAMA (2020). HORAMA Signs Exclusive License Agreement with Leiden University Medical Center Targeting CRB1 Gene Mutations to Treat Inherited Retinal Dystrophies. Available online at: https://www.horama.fr/horama-signs-exclusive-license-agreement-with-leiden-university-medical-center-targeting-crb1-gene-mutations-to-treat-inherited-retinal-dystrophies/ (accessed July 5, 2020).

Hu, Y., Wang, X., Hu, B., Mao, Y., Chen, Y., Yan, L., et al. (2019). Dissecting the transcriptome landscape of the human fetal neural retina and retinal pigment epithelium by single-cell RNA-seq analysis. *PLoS Biol.* 17:e3000365. doi: 10.1371/journal.pbio.3000365

Hurd, T. W., Gao, L., Roh, M. H., Macara, I. G., and Margolis, B. (2003). Direct interaction of two polarity complexes implicated in epthelial tight junction assembly. *Nat. Cell Biol.* 5, 137–142. doi: 10.1038/ncb923

Joberty, G., Petersen, C., Gao, L., and Macara, I. G. (2000). The cell-polarity protein Par6 links Par3 and atypical protein kinase C to Cdc42. *Nat. Cell Biol.* 2, 531–539. doi: 10.1038/35019573

Kantardzhieva, A., Alexeeva, S., Versteeg, I., and Wijnholds, J. (2006). MPP3 is recruited to the MPP5 protein scaffold at the retinal outer limiting membrane. *FEBS J.* 273, 1152–1165. doi: 10.1111/j.1742-4658.2006.05140.x

Kantardzhieva, A., Gosens, I., Alexeeva, S., Punte, I. M., Versteeg, I., Krieger, E., et al. (2005). MPP5 recruits MPP4 to the CRB1 complex in photoreceptors. *Investig. Ophthalmol. Vis. Sci.* 46, 2192–2201. doi: 10.1167/iovs.04-1417

Kim, S., Lowe, A., Dharmat, R., Lee, S., Owen, L. A., Wang, J., et al. (2019). Generation, transcriptome profiling, and functional validation of cone-rich human retinal organoids. *Proc. Natl. Acad. Sci. U.S.A.* 166, 10824–10833. doi: 10.1073/pnas.1901572116

Kraut, R. S., and Knust, E. (2019). Changes in endolysosomal organization define a pre-degenerative state in the crumbs mutant *Drosophila retina*. *PLoS One* 14:e0220220. doi: 10.1371/journal.pone.0220220

Lane, A., Jovanovic, K., Shortall, C., Ottaviani, D., Panes, A. B., Schwarz, N., et al. (2020). Modeling and rescue of RP2 retinitis pigmentosa using iPSC-derived retinal organoids. *Stem Cell Rep.* 15, 1–13. doi: 10.1016/j.stemcr.2020.05.007

Laprise, P., Beronja, S., Silva-gagliardi, N. F., Pellikka, M., Jensen, M., Mcglade, C. J., et al. (2006). The FERM protein yurt is a negative regulatory component of the crumbs complex that controls epithelial polarity and apical membrane size. *Dev. Cell* 11, 363–374. doi: 10.1016/j.devcel.2006.06.001

Laprise, P., Lau, K. M., Harris, K. P., Silva-Gagliardi, N. F., Paul, S. M., Beronja, S., et al. (2009). Yurt, Coracle, Neurexin IV and the Na+, K+-ATPase form a novel group of epithelial polarity proteins. *Nature* 459, 1141–1145. doi: 10.1038/nature08067

Lee, J. D., Silva-Gagliardi, N. F., Tepass, U., McGlade, C. J., and Anderson, K. V. (2007). The FERM protein Epb4.1l5 is required for organization of the neural plate and for the epithelial-mesenchymal transition at the primitive streak of the mouse embryo. *Development* 134, 2007–2016. doi: 10.1242/dev.000885

Lemmers, C., Michel, D., Lane-Guermonprez, L., Delgrossi, M.-H., Médina, E., Arsanto, J. P., et al. (2004). CRB3 binds directly to Par6 and regulates the morphogenesis of the tight junctions in mammalian epithelial cells. *Mol. Biol. Cell* 15, 1324–1333. doi: 10.1091/mbc.E03

Li, B. X., Satoh, A. K., and Ready, D. F. (2007). Myosin V, Rab11, and dRip11 direct apical secretion and cellular morphogenesis in developing *Drosophila* photoreceptors. *J. Cell Biol.* 177, 659–669. doi: 10.1083/jcb.200610157

Lin, D., Edwards, A. S., Fawcett, J. P., Mbamalu, G., Scott, J. D., and Pawson, T. (2000). A mammalian PAR-3-PAR-6 complex implicated in Cdc42/Rac1 and aPKC signalling and cell polarity. *Nat. Cell Biol.* 2, 540–547. doi: 10.1038/35019582

Luo, Z., Zhong, X., Li, K., Xie, B., Liu, Y., Ye, M., et al. (2018). An optimized system for effective derivation of three-dimensional retinal tissue via wnt signaling regulation. *Stem Cells* 36, 1709–1722. doi: 10.1002/stem.2890

Maddalena, A., Tornabene, P., Tiberi, P., Minopoli, R., Manfredi, A., Mutarelli, M., et al. (2018). Triple vectors expand AAV transfer capacity in the retina. *Mol. Ther.* 26, 524–541. doi: 10.1016/j.ymthe.2017.11.019

Maguire, A. M., Russell, S., Wellman, J. A., Chung, D. C., Yu, Z. F., Tillman, A., et al. (2019). Efficacy, safety, and durability of voretigene Neparvovec-rzyl in RPE65 mutation–associated inherited retinal dystrophy: results of phase 1 and 3 trials. *Ophthalmology* 126, 1273–1285. doi: 10.1016/j.ophtha.2019.06.017

Mao, X., Li, P., Wang, Y., Liang, Z., Liu, J., Li, J., et al. (2017). CRB3 regulates contact inhibition by activating the Hippo pathway in mammary epithelial cells. *Cell Death Dis.* 8:e2546. doi: 10.1038/cddis.2016.478

Margolis, B. (2018). The Crumbs3 polarity protein. *Cold Spring Harb. Perspect. Biol.* 10, 1–9. doi: 10.1101/cshperspect.a027961

Maruotti, J., Sripathi, S. R., Bharti, K., Fuller, J., Wahlin, K. J., Ranganathan, V., et al. (2015). Small-molecule-directed, efficient generation of retinal pigment epithelium from human pluripotent stem cells. *Proc. Natl. Acad. Sci. U.S.A.* 112, 10950–10955. doi: 10.1073/pnas.1422818112

Mathijssen, I. B., Florijn, R. J., Van Den Born, L. I., Zekveld-Vroon, R. C., Ten Brink, J. B., Plomp, A. S., et al. (2017). Long-term follow-up of patients with retinitis pigmentosa type 12 caused by CRB1 mutations: a severe phenotype with considerable interindividual variability. *Retina* 37, 161–172. doi: 10.1097/IAE.0000000000001127

Mehalow, A. K., Kameya, S., Smith, R. S., Hawes, N. L., Denegre, J. M., Young, J. A., et al. (2003). CRB1 is essential for external limiting membrane integrity and photoreceptor morphogenesis in the mammalian retina. *Hum. Mol. Genet.* 12, 2179–2189. doi: 10.1093/hmg/ddg232

Mellough, C. B., Collin, J., Queen, R., Hilgen, G., Dorgau, B., Zerti, D., et al. (2019). Systematic comparison of retinal organoid differentiation from human pluripotent stem cells reveals stage specific, cell line, and methodological differences. *Stem Cells Transl. Med.* 8, 694–706. doi: 10.1002/sctm.18-0267

Meyer, J. S., Howden, S. E., Wallace, K. A., Verhoeven, A. D., Wright, L. S., Capowski, E. E., et al. (2011). Optic vesicle-like structures derived from human pluripotent stem cells facilitate a customized approach to retinal disease treatment. *Stem Cells* 29, 1206–1218. doi: 10.1002/stem.674

Michel, D., Arsanto, J. P., Massey-Harroche, D., Béclin, C., Wijnholds, J., and Le Bivic, A. (2005). PATJ connects and stabilizes apical and lateral components of tight junctions in human intestinal cells. *J. Cell Sci.* 118, 4049–4057. doi: 10.1242/jcs.02528

Nakano, T., Ando, S., Takata, N., Kawada, M., Muguruma, K., Sekiguchi, K., et al. (2012). Self-formation of optic cups and storable stratified neural retina from human ESCs. *Cell Stem Cell* 10, 771–785. doi: 10.1016/j.stem.2012.05.009

Ovando-Roche, P., West, E. L., Branch, M. J., Sampson, R. D., Fernando, M., Munro, P., et al. (2018). Use of bioreactors for culturing human retinal organoids improves photoreceptor yields. *Stem Cell Res. Ther.* 9, 1–14. doi: 10.1186/s13287-018-0907-0

Park, B., Alves, C. H., Lundvig, D. M., Tanimoto, N., Beck, S. C., Huber, G., et al. (2011). PALS1 is essential for retinal pigment epithelium structure and neural retina stratification. *J. Neurosci.* 31, 17230–17241. doi: 10.1523/JNEUROSCI.4430-11.2011

Pellikka, M., Tanentzapf, G., Pinto, M., Smith, C., McGlade, C. J., Ready, D. F., et al. (2002). Crumbs, the *Drosophila* homologue of human CRB1/RP12, is essential for photoreceptor morphogenesis. *Nature* 416, 143–149. doi: 10.1038/nature721

Pellissier, L. P., Alves, C. H., Quinn, P. M., Vos, R. M., Tanimoto, N., Lundvig, D. M. S., et al. (2013). Targeted ablation of Crb1 and Crb2 in retinal progenitor cells mimics leber congenital amaurosis. *PLoS Genet.* 9:e1003976. doi: 10.1371/journal.pgen.1003976

Pellissier, L. P., Hoek, R. M., Vos, R. M., Aartsen, W. M., Klimczak, R. R., Hoyng, S. A., et al. (2014a). Specific tools for targeting and expression in Müller glial cells. *Mol. Ther. Methods Clin. Dev.* 1:14009. doi: 10.1038/mtm.2014.9

Pellissier, L. P., Lundvig, D. M. S., Tanimoto, N., Klooster, J., Vos, R. M., Richard, F., et al. (2014b). CRB2 acts as a modifying factor of CRB1-related retinal dystrophies in mice. *Hum. Mol. Genet.* 23, 3759–3771. doi: 10.1093/hmg/ddu089

Pellissier, L. P., Quinn, P. M., Henrique Alves, C., Vos, R. M., Klooster, J., Flannery, J. G., et al. (2015). Gene therapy into photoreceptors and Muller glial cells restores retinal structure and function in CRB1 retinitis pigmentosa mouse models. *Hum. Mol. Genet.* 24, 3104–3118. doi: 10.1093/hmg/ddv062

Pichaud, F. (2018). PAR-Complex and crumbs function during photoreceptor morphogenesis and retinal degeneration. *Front. Cell. Neurosci.* 12:90. doi: 10.3389/fncel.2018.00090

Pocha, S. M., Shevchenko, A., and Knust, E. (2011). Crumbs regulates rhodopsin transport by interacting with and stabilizing myosin V. *J. Cell Biol.* 195, 827–838. doi: 10.1083/jcb.201105144

Polgar, N., and Fogelgren, B. (2018). Regulation of cell polarity by exocyst-mediated traffickin. *Cold Spring Harb. Perspect. Biol.* 10:a031401. doi: 10.1101/cshperspect.a031401

Quinn, P. M., Alves, C. H., Klooster, J., and Wijnholds, J. (2018). CRB2 in immature photoreceptors determines the superior-inferior symmetry of the developing retina to maintain retinal structure and function. *Hum. Mol. Genet.* 27, 3137–3153. doi: 10.1093/hmg/ddy194

Quinn, P. M., Buck, T. M., Mulder, A. A., Ohonin, C., Alves, C. H., Vos, R. M., et al. (2019a). Human iPSC-derived retinas recapitulate the fetal CRB1 CRB2 Complex Formation And Demonstrate That Photoreceptors And Müller Glia Are Targets of AAV5. *Stem Cell Rep.* 12, 906–919. doi: 10.1016/j.stemcr.2019.03.002

Quinn, P. M., Mulder, A. A., Henrique Alves, C., Desrosiers, M., de Vries, S. I., Klooster, J., et al. (2019b). Loss of CRB2 in Müller glial cells modifies a CRB1-associated retinitis pigmentosa phenotype into a Leber congenital amaurosis phenotype. *Hum. Mol. Genet.* 28, 105–123. doi: 10.1093/hmg/ddy337

Quinn, P. M., Pellissier, L. P., and Wijnholds, J. (2017). The CRB1 complex: following the trail of crumbs to a feasible gene therapy strategy. *Front. Neurosci.* 11:175. doi: 10.3389/fnins.2017.00175

Ray, T. A., Cochran, K., Kozlowski, C., Wang, J., Alexander, G., Cady, M. A., et al. (2020). Comprehensive identification of mRNA isoforms reveals the diversity of neural cell-surface molecules with roles in retinal development and disease. *Nat. Commun.* 11:3328. doi: 10.1038/s41467-020-17009-7

Roh, M. H., Makarova, O., Liu, C. J., Shin, K., Lee, S., Laurinec, S., et al. (2002). The Maguk protein, Pals1, functions as an adapter, linking mammalian homologues of crumbs and discs lost. *J. Cell Biol.* 157, 161–172. doi: 10.1083/jcb.200109010

Rueda, E. M., Hall, B. M., Hill, M. C., Swinton, P. G., Tong, X., Martin, J. F., et al. (2019). The hippo pathway blocks mammalian retinal müller glial cell reprogramming. *Cell Rep.* 27, 1637.e6–1649.e6. doi: 10.1016/j.celrep.2019.04.047

Shutova, M. V., Surdina, A. V., Ischenko, D. S., Naumov, V. A., Bogomazova, A. N., Vassina, E. M., et al. (2016). An integrative analysis of reprogramming in human isogenic system identified a clone selection criterion. *Cell Cycle* 15, 986–997. doi: 10.1080/15384101.2016.1152425

Slavotinek, A., Kaylor, J., Pierce, H., Cahr, M., Deward, S. J., Schneidman-Duhovny, D., et al. (2015). CRB2 mutations produce a phenotype resembling congenital nephrosis, Finnish type, with cerebral ventriculomegaly and raised alpha-fetoprotein. *Am. J. Hum. Genet.* 96, 162–169. doi: 10.1016/j.ajhg.2014.11.013

Smith, E. N., D'Antonio-Chronowska, A., Greenwald, W. W., Borja, V., Aguiar, L. R., Pogue, R., et al. (2019). Human iPSC-derived retinal pigment epithelium: a model system for prioritizing and functionally characterizing causal variants at AMD risk loci. *Stem Cell Rep.* 12, 1342–1353. doi: 10.1016/j.stemcr.2019.04.012

Suzuki, A., Yamanaka, T., Hirose, T., Manabe, N., Mizuno, K., Shimizu, M., et al. (2001). Atypical protein kinase C is involved in the evolutionarily conserved PAR protein complex and plays a critical role in establishing epithelia-specific junctional structures. *J. Cell Biol.* 152, 1183–1196. doi: 10.1083/jcb.152.6.1183

Szymaniak, A. D., Mahoney, J. E., Cardoso, W. V., and Varelas, X. (2015). Crumbs3-mediated polarity directs airway epithelial cell fate through the hippo pathway effector yap. *Dev. Cell* 34, 283–296. doi: 10.1016/j.devcel.2015.06.020

Tait, C., Chinnaiya, K., Manning, E., Murtaza, M., Ashton, J.-P., Furley, N., et al. (2020). Crumbs2 mediates ventricular layer remodelling to form the spinal cord central canal. *PLoS Biol.* 18:e3000470. doi: 10.1371/journal.pbio.3000470

Talib, M., van Schooneveld, M. J., van Genderen, M. M., Wijnholds, J., Florijn, R. J., ten Brink, J. B., et al. (2017). Genotypic and phenotypic

characteristics of CRB1-associated retinal dystrophies: a long-term follow-up study. *Ophthalmology* 124, 884–895. doi: 10.1016/j.ophtha.2017.01.047

Tepass, U., Theres, C., and Knust, E. (1990). crumbs encodes an EGF-like protein expressed on apical membranes of *Drosophila* epithelial cells and required for organization of epithelia. *Cell* 61, 787–799. doi: 10.1016/0092-8674(90)90189-L

Tilston-Lünel, A. M., Haley, K. E., Schlecht, N. F., Wang, Y., Chatterton, A. L. D., Moleirinho, S., et al. (2016). Crumbs 3b promotes tight junctions in an ezrin-dependent manner in mammalian cells. *J. Mol. Cell Biol.* 8, 439–455. doi: 10.1093/jmcb/mjw020

Trapani, I., Colella, P., Sommella, A., Iodice, C., Cesi, G., de Simone, S., et al. (2014). Effective delivery of large genes to the retina by dual AAV vectors. *EMBO Mol. Med.* 6, 194–211. doi: 10.1002/emmm.201302948

Vallespin, E., Cantalapiedra, D., Riveiro-Alvarez, R., Wilke, R., Aguirre-Lamban, J., Avila-Fernandez, A., et al. (2007). Mutation screening of 299 Spanish families with retinal dystrophies by leber congenital amaurosis genotyping microarray. *Investig. Ophthalmol. Vis. Sci.* 48, 5653–5661. doi: 10.1167/iovs.07-0007

van de Pavert, S. A., Kantardzhieva, A., Malysheva, A., Meuleman, J., Versteeg, I., Levelt, C., et al. (2004). Crumbs homologue 1 is required for maintenance of photoreceptor cell polarization and adhesion during light exposure. *J. Cell Sci.* 117, 4169–4177. doi: 10.1242/jcs.01301

van de Pavert, S. A., Meuleman, J., Malysheva, A., Aartsen, W. M., Versteeg, I., Tonagel, F., et al. (2007a). A single amino acid substitution (Cys249Trp) in Crb1 causes retinal degeneration and deregulates expression of pituitary tumor transforming gene Pttg1. *J. Neurosci.* 27, 564–573. doi: 10.1523/JNEUROSCI.3496-06.2007

van de Pavert, S. A., Sanz sanz, A., Aartsen, W. M., Vos, R. M., Versteeg, I., Beck, S. C., et al. (2007b). Crb1 is a determinant of retinal apical muller glia cell features. *Glia* 55, 1486–1497. doi: 10.1002/glia

van Rossum, A. G. S. H., Aartsen, W. M., Meuleman, J., Klooster, J., Malysheva, A., Versteeg, I., et al. (2006). Pals1/Mpp5 is required for correct localization of Crb1 at the subapical region in polarized Müller glia cells. *Hum. Mol. Genet.* 15, 2659–2672. doi: 10.1093/hmg/ddl194

Verbakel, S. K., van Huet, R. A. C., Boon, C. J. F., den Hollander, A. I., Collin, R. W. J., Klaver, C. C. W., et al. (2018). Non-syndromic retinitis pigmentosa. *Prog. Retin. Eye Res.* 66, 157–186. doi: 10.1016/j.preteyeres.2018.03.005

Wang, D., Tai, P. W. L., and Gao, G. (2019). Adeno-associated virus vector as a platform for gene therapy delivery. *Nat. Rev. Drug Discov.* 18, 358–378. doi: 10.1038/s41573-019-0012-9

Wang, Y., Rajala, A., and Rajala, R. V. S. (2018). Nanoparticles as delivery vehicles for the treatment of retinal degenerative diseases. *Adv. Exp. Med. Biol.* 1074, 117–123. doi: 10.1007/978-3-319-75402-4_15

Whiteman, E. L., Fan, S., Harder, J. L., Walton, K. D., Liu, C.-J., Soofi, A., et al. (2014). Crumbs3 is essential for proper epithelial development and viability. *Mol. Cell. Biol.* 34, 43–56. doi: 10.1128/mcb.00999-13

Whitney, D. S., Peterson, F. C., Kittel, A. W., Egner, J. M., Prehoda, K. E., and Volkman, B. F. (2016). Crumbs binding to the Par-6 CRIB-PDZ module is regulated by Cdc42. *Biochemistry* 55, 1455–1461.

Yamanaka, T., Horikoshi, Y., Suzuki, A., Sugiyama, Y., Kitamura, K., Maniwa, R., et al. (2001). PAR-6 regulates aPKC activity in a novel way and mediates cell-cell contact-induces formation of the epithelial junctional complex. *Genes Cells* 6, 721–731. doi: 10.1046/j.1365-2443.2001.00453.x

Yu, F., and Guan, K. (2013). The Hippo pathway: regulators and regulations. *Genes Dev.* 27, 335–371. doi: 10.1101/gad.210773.112.a

Yu, F., Zhao, B., and Guan, K. (2015). Hippo pathway in organ size control, tissue homeostasis, and cancer. *Cell* 163, 811–828. doi: 10.1016/j.cell.2015.10.044

Zahabi, A., Shahbazi, E., Ahmadieh, H., Hassani, S. N., Totonchi, M., Taei, A., et al. (2012). A new efficient protocol for directed differentiation of retinal pigmented epithelial cells from normal and retinal disease induced pluripotent stem cells. *Stem Cells Dev.* 21, 2262–2272. doi: 10.1089/scd.2011.0599

Zhang, X., Zhang, D., Chen, S. C., Lamey, T., Thompson, J. A., McLaren, T., et al. (2018). Establishment of an induced pluripotent stem cell line from a retinitis pigmentosa patient with compound heterozygous CRB1 mutation. *Stem Cell Res.* 31, 147–151. doi: 10.1016/j.scr.2018.08.001

Zhao, M., Andrieu-Soler, C., Kowalczuk, L., Paz Cortés, M., Berdugo, M., Dernigoghossian, M., et al. (2015). A new CRB1 rat mutation links müller glial cells to retinal telangiectasia. *J. Neurosci.* 35, 6093–6106. doi: 10.1523/jneurosci.3412-14.2015

Zhong, X., Gutierrez, C., Xue, T., Hampton, C., Vergara, M. N., Cao, L. H., et al. (2014). Generation of three-dimensional retinal tissue with functional photoreceptors from human iPSCs. *Nat. Commun.* 5:4047. doi: 10.1038/ncomms5047

Conflict of Interest: The LUMC is the holder of patent number PCT/NL2014/050549, which describes the potential clinical use of *CRB2*; JW and LP are listed as co-inventors of this patent, and JW is an employee of the LUMC.

The remaining author declares that the research was conducted without any commercial or financial relationship that could be construed as a potential conflict of interest.

Copyright © 2020 Boon, Wijnholds and Pellissier. This is an open-access article distributed under the terms of the Creative Commons Attribution License (CC BY). The use, distribution or reproduction in other forums is permitted, provided the original author(s) and the copyright owner(s) are credited and that the original publication in this journal is cited, in accordance with accepted academic practice. No use, distribution or reproduction is permitted which does not comply with these terms.

frontiers in Neuroscience

REVIEW
published: 20 August 2020
doi: 10.3389/fnins.2020.00838

Novel Therapeutic Approaches for the Treatment of Retinal Degenerative Diseases: Focus on CRISPR/Cas-Based Gene Editing

*Carmen Gallego[1], Manuel A. F. V. Gonçalves[2] and Jan Wijnholds[1,3]**

[1] Department of Ophthalmology, Leiden University Medical Center, Leiden, Netherlands, [2] Department of Cell and Chemical Biology, Leiden University Medical Center, Leiden, Netherlands, [3] Netherlands Institute for Neuroscience, Royal Netherlands Academy of Arts and Sciences (KNAW), Amsterdam, Netherlands

Inherited retinal diseases encompass a highly heterogenous group of disorders caused by a wide range of genetic variants and with diverse clinical symptoms that converge in the common trait of retinal degeneration. Indeed, mutations in over 270 genes have been associated with some form of retinal degenerative phenotype. Given the immune privileged status of the eye, cell replacement and gene augmentation therapies have been envisioned. While some of these approaches, such as delivery of genes through recombinant adeno-associated viral vectors, have been successfully tested in clinical trials, not all patients will benefit from current advancements due to their underlying genotype or phenotypic traits. Gene editing arises as an alternative therapeutic strategy seeking to correct mutations at the endogenous locus and rescue normal gene expression. Hence, gene editing technologies can in principle be tailored for treating retinal degeneration. Here we provide an overview of the different gene editing strategies that are being developed to overcome the challenges imposed by the post-mitotic nature of retinal cell types. We further discuss their advantages and drawbacks as well as the hurdles for their implementation in treating retinal diseases, which include the broad range of mutations and, in some instances, the size of the affected genes. Although therapeutic gene editing is at an early stage of development, it has the potential of enriching the portfolio of personalized molecular medicines directed at treating genetic diseases.

Keywords: retinal degeneration, gene editing, CRISPR/Cas systems, adeno-associated viral vectors, adenoviral vectors

OPEN ACCESS

Edited by:
Nicolás Cuenca, University of Alicante, Spain

Reviewed by:
Shaomei Wang, Cedars-Sinai Medical Center, Los Angeles, United States
Elvir Becirovic, Ludwig Maximilian University of Munich, Germany

****Correspondence:***
Jan Wijnholds
J.Wijnholds@lumc.nl

Specialty section:
This article was submitted to Neurodegeneration, a section of the journal Frontiers in Neuroscience

Received: *10 June 2020*
Accepted: *20 July 2020*
Published: *20 August 2020*

Citation:
Gallego C, Gonçalves MAFV and Wijnholds J (2020) Novel Therapeutic Approaches for the Treatment of Retinal Degenerative Diseases: Focus on CRISPR/Cas-Based Gene Editing. Front. Neurosci. 14:838. doi: 10.3389/fnins.2020.00838

INTRODUCTION

Inherited retinal diseases (IRDs) constitute a heterogenous group of neurodegenerative conditions affecting the retina, a layered structure of neural origin at the back of the eye. Mutations associated with IRDs lead to retinal degeneration resulting in impaired vision and ultimately, irreversible and complete blindness (Berger et al., 2010). Clearly, this outcome negatively impacts patients' quality of life and currently, there are no specific treatments that halt the degenerative process

or, ideally, restore eyesight. Indeed, most treatments only delay the onset of symptoms or slow down the progressive retinal degeneration when applied at the early stages of the disease. Recently, the prevalence of autosomal recessive IRD variants has been analyzed and it is estimated that approximately 36% of the population carries at least one mutation that causes IRD (Hanany et al., 2020). This finding highlights the substantial global burden of blinding diseases and the imperative need for developing novel therapeutic strategies.

More than 270 genes have been identified as the cause of IRD with many disease-causing gene variants having been reported for each disorder.[1] These variants include deletions, insertions, missense and frameshifting mutations as well as mutations that create cryptic splice sites and exonization of non-coding sequences. Genes associated with IRDs are mostly involved in photoreceptor and retinal pigment epithelium biology, including the maintenance of the visual cycle. Consequently, defective or absent retinal gene products resulting from pathological mutations invariably lead to photoreceptor death and retinal degeneration. IRDs present also different hereditary patterns (i.e., autosomal dominant, autosomal recessive or X-linked) and, in the case of recessive inheritance, patients harbor homozygous or compound heterozygous mutations (Berger et al., 2010; Khan et al., 2019). Collectively, all these parameters help defining IRDs in clinical categories attending to the genetic defect, the type of inheritance and the affected cell type, complemented with information on symptoms onset age and disease progression. IRDs can be classified in rod-dominant dystrophies (e.g., retinitis pigmentosa), cone-dominant dystrophies and generalized photoreceptor diseases (e.g., Leber congenital amaurosis). In addition, there are non-syndromic and syndromic forms of IRDs, the latter being associated with other organ pathologies. However, there is an overlap in clinical diagnoses and genotype-phenotype correlations are often difficult to establish in IRDs (Berger et al., 2010; Khan et al., 2019). A specific IRD phenotype can be caused by mutations in many different genes, one paradigmatic example being retinitis pigmentosa, associated with mutations in 84 genes. Conversely, a specific gene can be associated with several IRD phenotypes depending on the underlying mutation(s) (Berger et al., 2010; Cremers et al., 2018). Moreover, a particular genetic mutation can cause diverse phenotypes in different individuals, suggesting a role for genetic modifiers, i.e., non-allelic genetic variants, in disease penetrance and progression, which might explain the heterogeneity of certain IRDs (Venturini et al., 2012; Meyer and Anderson, 2017; Li et al., 2020).

As currently there is no standardized therapy available for patients suffering from retinal degeneration, numerous studies are focused on developing new therapeutic approaches to halt or reverse retinal degeneration. These efforts face nonetheless major challenges. Firstly, the broad range of defective genes and mutations makes it difficult to develop a single general therapy applicable to several patient groups. Rather, therapies tend to target a specific genotype. Ideally, genetic therapies for IRDs should correct or complement as many gene mutations as possible to open up the perspective for treating large patient cohorts. For example, by targeting one or more exons found to be mutational hotspots for a particular gene. Secondly, various genes causing IRDs are large genes whose coding sequences cannot be packaged in viral vectors commonly used for gene augmentation therapies **(Table 1)**. A third challenge in the treatment of degenerative diseases, including those affecting the retina, is that the therapy needs to be applied when cells are still alive for them to be rescued from the degenerative process. Indeed, once the retina structure is compromised, and cells start dying, it is difficult to obtain any significant improvement regardless of the applied therapy. Thus, clinical research should also be focused on early diagnostics and close follow-up by the physician.

Current experimental strategies for treating retinal degeneration can be divided in genetic therapies (i.e., gene augmentation, involving the transfer of functional wild-type copies of defective genes; and gene editing, comprising the targeted chromosomal insertion of therapeutic genes or the direct *in situ* repair of defective endogenous genes) and cell therapies (i.e., cell transplantation). In addition, next to these approaches, neurotrophic and neuroprotective factors can be delivered or modulated to prevent or slow down photoreceptor degeneration. For instance, *in vitro* studies and *in vivo* experimental therapies are exploring the use of brain-derived neurotrophic factor (BDNF), ciliary neurotrophic factor (CNTF) and glial-derived neurotrophic factor (GDNF) as candidate auxiliary therapeutic agents (Sieving et al., 2006; Jung et al., 2013; Labrador-Velandia et al., 2019). However, the benefits of this type of approaches are

TABLE 1 | List of large-size genes associated with inherited retinal diseases.

Gene name	Accession number	CDS (bp)	Disease(s)
ABCA4	NM_000350.3	6822	Recessive Stargardt disease, macular dystrophy, recessive retinitis pigmentosa, recessive cone-rod dystrophy
CDH23	NM_022124.6	10065	Recessive Usher syndrome, type 1d
CEP290	NM_025114.4	7440	Recessive Leber congenital amaurosis
CRB1	NM_201253.3	4221	Recessive retinitis pigmentosa; recessive Leber congenital amaurosis
EYS	NM_001142800.2	9435	Recessive retinitis pigmentosa
GPR179	NM_001004334.4	7104	Recessive complete congenital stationary night blindness
MYO7A	NM_000260.4	6648	Recessive Usher syndrome, type 1b
PRPF8	NM_006445.4	7008	Dominant retinitis pigmentosa
RP1	NM_006269.2	6471	Dominant retinitis pigmentosa; recessive retinitis pigmentosa
USH2A	NM_206933.4	15609	Recessive Usher syndrome, type 2a; recessive retinitis pigmentosa

Representative list of genes associated with IRDs containing large coding sequences (CDS). Gene names are listed alphabetically, accession numbers and CDS sizes were retrieved from Ensembl (https://www.ensembl.org/). The disease descriptions were obtained from RetNet (https://sph.uth.edu/retnet/home.htm).

[1] https://sph.uth.edu/retnet/

still limited, with some clinical studies showing no improvements over the untreated eye (Birch et al., 2016). Furthermore, some promising therapies with small molecules are moving from *in vitro* studies to clinical trials. In the case of IRDs caused by an aberrant splicing process, antisense oligonucleotides can be used to avoid the recognition of cryptic splice sites and the inclusion of pseudoexons (Collin et al., 2012; Huang et al., 2017). For other retinal disorders (e.g., retinitis pigmentosa or Leber congenital amaurosis), a pharmacological approach targeting signaling pathways is being envisioned. For instance, inhibitory analogs of the second messenger cGMP, whose signaling is relevant for the light signal transduction cascade, can inhibit the activation of cGMP effectors preventing excessive photoreceptor cell death (Vighi et al., 2018; Tolone et al., 2019). Other therapies may target the visual cycle by, for instance, assuring adequate levels of 11-*cis*-retinal, after administering the synthetic *cis*-retinoid drug QLT019001, or reducing the accumulation of toxic by-products, after applying the visual cycle modulator Emixustat for the treatment of Stargardt disease (NCT03772665) (Sundaramurthi et al., 2019). Moreover, other IRD-associated mutations result in misfolded non-functional proteins that could be rescued using small-molecule drugs or pharmacological chaperones that assure protein stability by preventing protein aggregation, and thus, cell death associated with oxidative stress (Kosmaoglou et al., 2008; Wang et al., 2016; Trachsel-Moncho et al., 2018; Lévy et al., 2019). In cases in which the disease stage is too advanced and the photoreceptor cells are irreversibly lost, optogenetic tools might be exploited to enable other retinal cells to behave as surrogate photoreceptors by endowing them with light signal transduction capabilities (Simunovic et al., 2019). In this regard, optogenetic tools based on light-sensitive proteins are being investigated in different experimental settings, including (i) *in vitro* 3D retinal organoids differentiated from induced pluripotent stem cells (iPSCs); (ii) *ex vivo* post-mortem human retinas, (iii) *in vivo* late-stage retinal degeneration murine models to determine vision restoration upon transplantation of optogenetically modified photoreceptors and (iv) *in vivo* non-human primate models to assess the safety and efficiency of adeno-associated viral (AAV) vector delivery of optogenetic tools (Chaffiol et al., 2017; Garita-Hernandez et al., 2018, 2019; Kamar et al., 2020). Finally, it is noteworthy mentioning that, beyond these experimental settings, optogenetic tools are also starting to be applied in clinical trials (e.g., NCT03326336, for retinitis pigmentosa patients).

These candidate therapeutic solutions for treating the eye have been recently reviewed from different perspectives (see, e.g., Scholl et al., 2016; Dias et al., 2018; Sanjurjo-Soriano and Kalatzis, 2018; Vázquez-Domínguez et al., 2019). Here, we will focus on covering the equally fast-paced advances in the gene editing field, with an eye for its potential to the management and treatment of congenital ophthalmologic disorders. We start by briefly discussing "classic" gene augmentation approaches and their limitations and, thereafter, move forward by elaborating on key developments that gene editing techniques are currently undergoing. In the context of these genetic interventions, we also discuss the different vectors and delivery options to reach retinal cell types, including the potential of high-capacity adenoviral vectors (HC-AdVs) to deliver large therapeutic transgenes or gene editing tools to retinal cells.

GENETIC THERAPIES FOR TREATING IRDS: FROM GENE AUGMENTATION TO GENE EDITING

Genetic therapies consist of providing new genetic information into cells damaged by trauma, infectious agents or inherited diseases with the goal of attaining a stable therapeutic effect. Monogenic inherited disorders constitute an ideal target for genetic therapies involving either "classical" gene therapy based on gene addition or, more recently, therapeutic gene editing based on site-specific genome modifications. This stems from the fact that the disease-causing gene is known with its mechanistic function being often well understood. Gene therapy encompasses the delivery of "healthy" wild-type versions of mutant alleles; whereas gene editing entails the transfer of molecular tools (e.g., sequence-specific programmable nucleases) needed to inactivate or correct disease-causing mutant alleles (DiCarlo et al., 2018; Takahashi et al., 2018; Gordon et al., 2019).

Depending on the inheritance pattern of the disease, the therapeutic approach varies. Gene therapies involving gene addition or augmentation can be used for the complementation of homozygous recessive loss-of-function mutations through the delivery and expression of a "healthy" functioning copy of the affected gene. The delivery of the genetic material to the retina can be done in different ways and these will be discussed in the next section. Currently, AAV vectors are the predominant candidate therapeutic options for tackling ocular diseases with a gene therapy to treat Leber congenital amaurosis based on the delivery of *RPE65* by an AAV serotype 2 (AAV-2) vector having already been approved by the Food and Drug Administration (United States) and the European Medicines Agency (Russell et al., 2017). Long-term efficacy of AAV-based *RPE65* gene therapies appeared to be limited to 2 years after treatment (Wang et al., 2020), however, a recent follow-up report on therapeutic outcomes confirmed that 86% of patients receiving this approved *RPE65* gene therapy (named voretigene neparvovec) maintained improved visual function 4 years after the treatment (Drack et al., 2019). More results are warranted as the study includes a 15-year follow-up of patients (NCT00999609).

The small cargo capacity of AAV capsids (∼4.7 Kb) makes these viral vectors incompatible with the delivery of large transgenes. Various IRD-associated genes have coding sequences that exceed the maximum packaging capacity of AAV capsids (e.g., *ABCA4*, *CEP290*, and *USH2A*) (Arbabi et al., 2019; **Table 1**). Thus, other approaches are needed for treating IRDs caused by such genes. Gene editing, while offering the potential for correcting *in situ* endogenous mutated alleles, can also be applied to diseases caused by gain-of-function allelic mutations that exert dominance over wild-type alleles (e.g., mutations in *RHO* gene responsible for autosomal dominant retinitis pigmentosa). In these cases of dominant inheritance, gene editing tools can be designed for (i) the specific inactivation of mutant, disease-causing, alleles, (ii) restoring the endogenous allele or (iii)

inserting an exogenous "healthy" copy at a specific genomic position, e.g., at "safe harbor" locus "from where transgene overexpression can ensue".

Genome Editing: Advances in CRISPR/Cas-Based Gene Editing Systems for Non-dividing Cells

In this section, we focus on recent advancements in the conversion of clustered regularly interspaced short palindromic repeats (CRISPR)/CRISPR-associated Cas (CRISPR/Cas) nuclease systems into gene editing tools, in particular, for the precise insertion of genetic material in post-mitotic cells. CRISPR/Cas systems provide adaptive immunity in prokaryotes (Barrangou and Marraffini, 2014). In 2012, it was found that CRISPR-derived nucleases cleave DNA in an RNA-programmable manner involving initial protein-DNA and subsequent RNA-DNA interactions (Gasiunas et al., 2012; Jinek et al., 2012). On the basis of these seminal findings, the native CRISPR/Cas9 system from *Streptococcus pyogenes* was the first to be readily adapted into RNA-guided nucleases (RGNs) for genome engineering in mammalian cells and tissues (Cho et al., 2013; Cong et al., 2013; Jinek et al., 2013; Mali et al., 2013). It consists of an RNA-guided Cas9 enzyme with two separate endonuclease domains (i.e., HNH and RuvC). After Cas9 binding to a so-called protospacer adjacent motif (PAM), hybridization of the 5' end (spacer) of the single guide RNA (gRNA) to a typically 20-nt complementary sequence (protospacer) activates the nuclease domains leading to the cleavage of the target DNA sequence at both strands (Doudna and Charpentier, 2014). The gRNA consists of a fusion between two key components derived from the native CRISPR locus, i.e., the sequence-specific CRISPR RNA (crRNA) and the Cas9 scaffolding trans-activating crRNA (tracrRNA) (Doudna and Charpentier, 2014). There are different types of CRISPR endonucleases that vary in their PAM sequence and spacer length requirements as well as in their specificity and type of DNA cleavage products, i.e., blunt-ended or staggered double-stranded DNA breaks (DSBs). Currently, the most commonly used RGNs contain the Cas9 proteins from *Streptococcus pyogenes* (Doudna and Charpentier, 2014) or *Staphylococcus aureus* (Ran et al., 2015), whose PAMs read NGG or NNGRRT, respectively.

RGN complexes have been used in a great variety of organisms (e.g., zebrafish, insects and mammals). They offer flexibility and are much easier to construct and customize than previous gene editing tools such as transcription activator-like effector nucleases (TALENs) and zinc-finger nucleases (ZFNs) (see, e.g., Chandrasegaran and Carroll, 2016; Yanik et al., 2017). As with TALENs and ZFNs, RGNs can also present off-target activities that constitute a major drawback for their application in the clinic. Thus, variants of Cas nucleases have been engineered to limit these harmful off-target effects and hence improve the specificity while, for the most part, maintaining the efficiency of the corresponding RGNs (Nakade et al., 2017; Chen and Gonçalves, 2018). For example, high-specificity nuclease variants based on amino acid substitutions (Kleinstiver et al., 2016a; Slaymaker et al., 2016) or sequence- and strand-specific nucleases (nickases) that only produce a single-stranded cut in the DNA (Jinek et al., 2012; Cong et al., 2013; Mali et al., 2013).

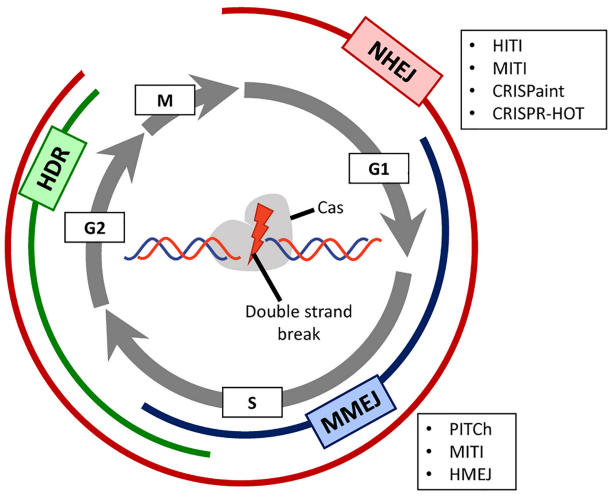

FIGURE 1 | Prevalence of DNA repair pathways during the different stages of the cell cycle. A Cas-containing RGN is directed to a target site in the genome consisting of a PAM and a sequence complementary to the spacer portion of the guide RNA. Depending on the RGN type, the produced double-stranded DNA breaks (DSBs) present either blunt or staggered ends. Depending on the phase of the cell cycle (displayed as gray circular arrows), different DNA repair mechanisms, each of which with their own set of factors, will be activated for repairing the site-specific DSB. Non-homologous end joining (NHEJ, in red) is active during the whole cell cycle except in mitosis, and homology-directed repair (HDR, in green) is mainly active during the S/G2 phases. Microhomology-mediated end joining (MMEJ, in blue) is an alternative NHEJ pathway mainly active during the G1/early S phases. This pathway shares some features with canonical NHEJ and HDR but uses a different molecular machinery and short homology sequences to repair the DNA break. In post-mitotic cells, the mostly error-free, HDR pathway is not active. For this reason, there are several innovative CRISPR/Cas-based strategies (boxed acronyms) that rely instead on NHEJ or MMEJ to allow for precise gene knock-in in non-dividing cells.

The catalytic activity of the Cas9 endonuclease produces a DSB in the target DNA region complementary to the gRNA spacer sequence. DSBs are detected by the DNA damage response and repaired by different DNA repair pathways whose selection is, to a great extent, dependent on the cell cycle phase (Ceccaldi et al., 2016; Yeh et al., 2019; **Figure 1**). The non-homologous end-joining (NHEJ) pathways (canonical and alternative) are active during most phases of the cell cycle and are generally considered more error-prone mechanisms than those underlying homology-directed DNA repair (HDR) pathway. In the process of end-to-end joining of chromosomal termini, NHEJ pathways can introduce small insertions and deletions (indels) especially in the presence of a programmable nuclease that re-cleaves accurately joined termini until an indel disrupts its target sequence. Usually, the activation of NHEJ pathways by programmable nucleases is a key strategy to generate target gene knock-outs upon the incorporation of frameshifting indels within coding sequences (Chandrasegaran and Carroll, 2016). The HDR pathway involving homologous recombination

comprises extensive DSB end-processing, single-strand DNA invasion, donor-templated DNA synthesis and Holliday junction resolution. This HDR pathway is only active during the S and late G2 phases of the cell cycle being hence restricted to dividing cells (Iyama and Wilson, 2013; **Figure 1**), and relies on exogenous donor DNA templates containing regions homologous to sequences surrounding the DSB. The HDR mechanism is harnessed to direct precise genome editing and generate specific targeted knock-ins whose lengths can vary from single base pairs to whole transgenes (Doudna and Charpentier, 2014; Chandrasegaran and Carroll, 2016; Chen and Gonçalves, 2018; Yeh et al., 2019). A third mechanism for DNA repair is microhomology-mediated end-joining (MMEJ) (McVey and Lee, 2008), which is a non-canonical NHEJ pathway that relies on microhomology regions (5–25 base pairs) surrounding the DSB. This DNA repair pathway is usually active in G1/early S phases (**Figure 1**).

There are several studies in the field of retinal degeneration that have explored the feasibility of applying CRISPR/Cas9-based gene editing tools *in vivo* to inactivate dominant alleles through the NHEJ pathway. A first proof-of-concept work, in which expression of the yellow fluorescent protein reporter was reduced in the retina of transgenic mice (Hung et al., 2016), paved the way for other researchers starting to investigate the potential of engineered CRISPR/Cas systems for disrupting or correcting gene variants associated with IRDs. For instance, Bakondi et al. (2016) achieved the disruption of a *Rho* allele harboring a dominant mutation in a rat model of retinitis pigmentosa. The strategy induced indels in the mutant allele but not in the wild-type allele and, in doing so, prevented retinal degeneration that subsequently led to improved visual function (Bakondi et al., 2016). In another study, a deletion of an intronic fragment of the murine *Cep290* gene, homologous to the human region that contains a deep intronic variant causing Leber congenital amaurosis type 10, was achieved in mouse retinas (Ruan et al., 2017). These studies used AAV vectors to deliver RGNs directly to mouse retinas and will be further discussed below.

Importantly, the transcriptional signatures of the DNA repair pathways in the retina have been recently characterized using transcriptomic analyses of *in vivo* and *in vitro* models (Pasquini et al., 2020). This study showed that photoreceptors, as post-mitotic cells, display low expression levels of HDR pathway components; whereas NHEJ and MMEJ pathway factors are expressed and active in these cells. Given that precise gene editing has generally relied on HDR, there are continuous efforts aimed at improving the efficiency of seamless DSB-mediated gene editing through the activation and recruitment of alternative DNA repair pathways that remain active in terminally differentiated cells, such as those that constitute the retina in mammals. Crucially, in the past few years, there has been a myriad of novel CRISPR/Cas-based strategies that allow for the precise insertion of genetic material at a specific genomic locus in non-dividing cells and, following from the above, these efforts are particularly relevant for the treatment of retinal disorders (Nami et al., 2018; Broeders et al., 2020). These new strategies are also dependent on the delivery of a donor template that is designed for the site-specific insertion of exogenous genetic material into the genome; yet the insertion process takes place independently of the homologous recombination mechanism. In the next paragraphs, we will describe these new approaches and how they can be exploited to target the retina (**Figure 2**).

Novel Strategies for Precise Gene Targeting in Non-dividing Cells

A homologous recombination-independent gene editing strategy is named Precise Integration into Target Chromosome (PITCh) and it was initially described as an alternative for the more laborious process of designing and incorporating extensive homology regions required in HDR donor templates. This method was designed to be used with both TALENs and RGNs and it depends on the engagement of the MMEJ pathway in that the programmable nuclease-induced DSBs at donor and target sequences create microhomology regions that allow for site-specific chromosomal integration of the transgene independently of long stretches of homology (**Figure 2**; Nakade et al., 2014; Sakuma et al., 2016). However, in these proof-of-principle experiments, in which an exogenous reporter cassette was inserted in the last exon of the human fibrillarin (*FBL*) gene, were only performed in cultures of transformed human embryonic kidney (HEK) 293 cells and no quantitative assessments were made (Nakade et al., 2014). Furthermore, as expected from the MMEJ pathway, indels were found at the junctions between the endogenous DNA and the integrated expression cassette, although the reading frame was not affected and the fluorescent reporter protein was expressed (Nakade et al., 2014).

Suzuki et al. (2016) designed an Homology-Independent Targeted Integration (HITI) strategy to direct the integration of a transgene through the RGN-induced activation of the NHEJ pathway. In this case, the designed donor DNA includes RGN target sites flanking the transgene, which are in the reverse orientation to that found in the genomic locus (**Figure 2**). Upon RGN-mediated cleavage of both genome and donor sequences, DNA ends are ligated by NHEJ. In instances in which the transgene is integrated in an inverted orientation, the gRNA target sites will be reconstructed, becoming available for further cleavage and excision from the genomic locus, giving another opportunity for correct integration. Once the transgene is inserted in the appropriate orientation, the gRNA target sites are disrupted, preventing further RGN cleavage and unwarranted donor DNA excision (Suzuki et al., 2016, 2018). The HITI process was applied *in vitro* in non-dividing cells, specifically in cultures of primary murine neurons and human embryonic stem cell-derived neurons, albeit the knock-in efficiency was low (i.e., 0.58% of absolute gene targeting efficiency in primary mouse neurons). Of note, the PITCh approach barely yielded knock-in events in cultured neurons (Suzuki et al., 2016). To increase the *in vivo* efficiency of HITI, the authors used AAV vectors to deliver RGNs and donor constructs rather than performing electroporation. By injecting AAVs in the visual cortex of the adult mouse brain, they reached an absolute knock-in efficiency of 3.5% compared to the 0.2% achieved by *in utero* electroporation. Suzuki and

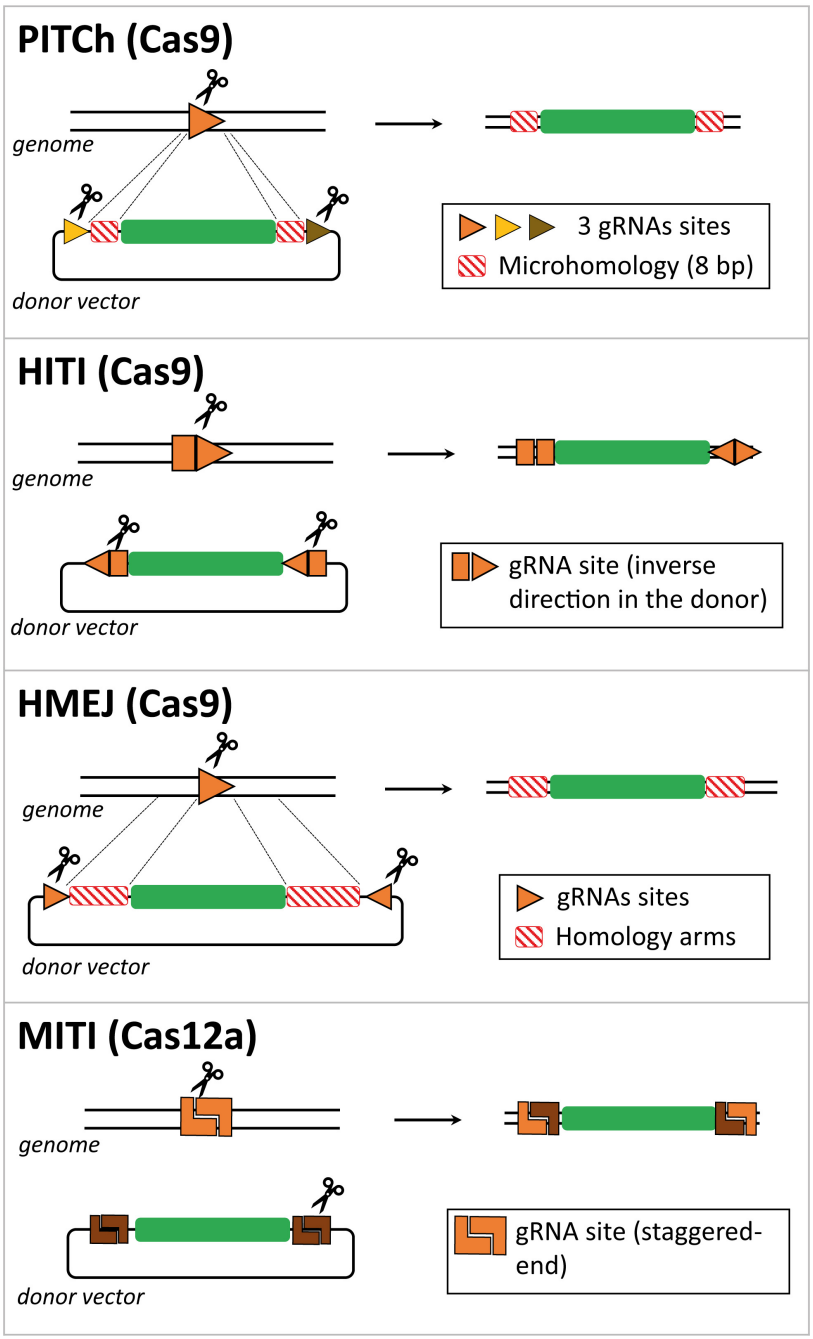

FIGURE 2 | Comparison between CRISPR/Cas-based strategies for targeted gene insertion in non-dividing cells. Schematic representation of several gene editing methodologies developed to direct targeted transgene integration in the genome independently of the HDR pathway, that is not active in non-dividing cells such as photoreceptors. The genomic locus and the donor DNA are cut by Cas effector proteins at gRNA target sites. Typically, the donor DNA contains two gRNA target sites to release the exogenous genetic information from the context of the delivery vector and aid its recombination with the target locus. These two gRNA target sites can have identical or dissimilar sequences and can be incorporated in a direct or inverted orientation. The Cas-induced DSB can generate microhomology regions between target and donor DNA, e.g., in the case of the PITCh and MITI methods. In the case of the HMEJ method, the lengths of the homology regions in the donor DNA are similar to those incorporated in HDR donors (i.e., ∼800 bp), yet they can be shortened to 24–48 bp.

colleagues also tested the AAV-HITI method in the Royal College of Surgeons rat model of retinitis pigmentosa, in which a deletion encompassing part of intron 1 and exon 2 sequences of the *Mertk* gene leads to dysfunctional retinal pigment epithelium and subsequent retinal degeneration. This data is highly relevant for the topic of this review, as the

successful integration of the full *Mertk* exon 2 sequence in the genome via the subretinal delivery of two AAV vectors, one containing the HITI donor construct and the other the RGN expression unit, significantly improved retinal degeneration and eye function (Suzuki et al., 2016). These promising results warrant additional preclinical studies aiming at treating retinitis pigmentosa and other retinal degeneration disorders, especially in models other than rodents which are more representative of human phenotypes. Furthermore, the use of AAV vectors is limited whenever gene editing interventions depend on the knocking-in of large genetic payloads and/or large RGN components, such as, *S. pyogenes* Cas9 and multiplexing gRNA pairs designed for targeted chromosomal deletions (Cong et al., 2013).

Another genome engineering method, dubbed Homology-Mediated End-Joining (HMEJ), was developed by Yao and colleagues, in which the donor DNA, similarly to HDR constructs, contains homology regions flanking the transgene. In the case of HMEJ donors, however, the homology regions are further flanked by gRNA target sites to allow for the excision of the transgenic sequences (Yao et al., 2017; **Figure 2**). Repair of the DSBs, induced at the genomic site and the donor DNA, can in principle be achieved via HDR or NHEJ repair pathways, although the authors did not investigate which DNA repair mechanisms underlie the HMEJ methodology. The performance of HMEJ-based gene editing in terms of targeted gene knock-in efficiencies varied depending on the experimental system. When comparing gene knock-in efficiencies, there were no differences between HMEJ- and HDR-based methods in mouse embryonic stem cells and in a murine neuroblastoma cell line (approximately 7% and 30% of absolute knock-in frequencies, respectively) (Yao et al., 2017). However, in the human HEK293T cell line and in murine primary neurons, HMEJ resulted in higher relative gene knock-in frequencies when compared to those resulting from the HDR-dependent strategy (approximately 2.6 to 4 fold increase) (Yao et al., 2017). The HMEJ approach was further tested to modify mouse embryos yielding, in this system, gene knock-in levels that were higher than those achieved by gene editing approaches based on the engagement of the NHEJ, HDR or MMEJ pathways. In addition, similarly to the study by Suzuki and colleagues (Suzuki et al., 2016), AAV vectors were used to deliver *S. pyogenes* RGNs and, in this case, HMEJ donor constructs to the visual cortex of the adult mouse brain. The authors reported an absolute gene knock-in efficiency of 5.3% (Yao et al., 2017). This innovative strategy holds therapeutic potential as it was also used for *in vivo* correction of an hereditary tyrosinemia disorder caused by mutations in the *Fah* gene, coding for fumarylacetoacetate hydrolase, that results in liver failure (Grompe et al., 1993; Yao et al., 2018). The HMEJ-based gene editing method successfully rescued *Fah* expression with hepatocyte proliferation being higher than that obtained with the MMEJ-based method (Yao et al., 2018). In another study, the HMEJ strategy was compared side-by-side with the HITI- and HDR-based gene editing methods in chicken DF-1 and primordial germ cells. The results from this work showed that HMEJ was the most efficient in mediating precise gene knock-in (Xie et al., 2019). A recent publication introduced another HMEJ-based approach (named GeneWeld) in which shorter homology segments of 24–48 base pairs were sufficient to drive precise reporter gene knock-in in zebrafish and mammalian cells using easily engineered donor DNA constructs in which the reporter transgene was flanked by universal gRNA target sequences (Wierson et al., 2020). Although more mechanistic insights are needed to understand how HMEJ operates, these studies expand nonetheless the range of donor DNA toolboxes and associated CRISPR/Cas-based gene editing strategies. To enrich the options to generate reporter cell lines and animal models, the CRISPaint system was developed to introduce reporter tags at the C-terminal coding portion of any gene of interest using a universal donor plasmid and the NHEJ pathway to repair the RGN-induced DSBs (Schmid-Burgk et al., 2016). More recently, this methodology was applied in human organoids, named CRISPR-HOT for homology-independent organoid transgenesis (Artegiani et al., 2020).

As previously mentioned, Cas9 proteins from the type II CRISPR systems of *S. pyogenes* and *S. aureus* are the most commonly used Cas effector proteins. Importantly, Cas orthologs have been identified in many other species of bacteria and have been further adapted for genome engineering of mammalian cells (Nakade et al., 2017; Chen and Gonçalves, 2018; Ishino et al., 2018). For instance, Cas12a from the type V CRISPR system of *Acidominococcus* sp., formerly known as Cpf1, is an RNA-guided endonuclease that differs from Cas9 in that it naturally has a single guide RNA with a strand polarity opposite to that of the composite single gRNA of Cas9 proteins formed by a fusion between crRNA and tracrRNA moieties. Other differences between RGNs based on Cas12a and Cas9 nucleases include the generation by the former of staggered ends instead of blunt ends and the recognition of T-rich instead of G-rich PAMs (Zetsche et al., 2015). It is also noteworthy mentioning that Cas12a RGNs present higher specificities than their Cas9 counterparts (Kleinstiver et al., 2016b). Moreover, similarly to Cas9, novel Cas12a variants have been engineered through mutagenesis screens to alter PAM preferences and hence enlarge the range of targetable sequences by the corresponding RGNs (Gao et al., 2017). Altogether, these features make Cas12a an appealing alternative for precise gene editing. Indeed, a recent study has reported an innovative Cas12a-based method named microhomology-dependent targeted integration (MITI) that permitted increased gene knock-in efficiency when compared to the Cas9-based HITI method (Li et al., 2019). This methodology is based on the generation of complementary sticky sequences between transgene and target site termini that assist in directing genomic DNA integration (**Figure 2**). This proof-of-concept study was only performed in cultured cell lines and requires further optimization to assure seamless transgene integration at the intended genomic loci. Indeed, the authors reported that approximately 30% of the integration events were not accurate at the 5' junction with the precision observed at the 3' junction being even less accurate (Li et al., 2019). These outcomes were partially improved by incorporating two different Cas12a gRNA cleavage sites flanking the transgene resulting in higher integration accuracy at the 3' junction,

although at the 5' junction, 36.6% of the integration events were still inaccurate. Notwithstanding the fact that MITI facilitates site-specific knock-ins, the use of several gRNAs complicates somewhat its application, including in the context of candidate genetic therapies. In this regard, a platform for Cas12a-based multiplexed genome editing, named SiT-Cas12a, has been developed based on a single transcript that encodes for Cas12a from *Acidominococcus* sp. and an array of crRNAs under the control of a single promoter (Campa et al., 2019). This strategy was used to target multiple sites in a gene, resulting in knock-out frequencies higher than those achieved by targeting a single site (37% versus 11% of gene knockouts in cell populations, respectively). This approach might further empower the capabilities of CRISPR/Cas techniques to investigate the underlying mechanisms of multifactorial diseases.

In conclusion, a plethora of innovative tools and strategies are being devised to improve the performance of CRISPR/Cas-based genomic manipulations and, as a result, increase the range and potential of therapeutic gene editing applications. These various reagents and methods are highly relevant for designing new candidate genetic therapies and, as a consequence, increasing the chances of advancing pre-clinical proof-of-concept studies into much-needed effective ophthalmologic treatments. The capacity for achieving targeted integration of transgenes in post-mitotic cells (e.g., photoreceptors), offered by several of the covered gene editing approaches, might also aid in providing mechanistic insights into retinal diseases and hence guide the development of genetic therapies for these conditions.

CONCERNS AND CHALLENGES FOR THE USE OF GENE EDITING IN THE TREATMENT OF RETINAL DISEASES

Before making the transition toward clinical applications, gene editing techniques must reach higher efficiency and safety profiles. These parameters are contingent upon the delivery and specificity of the necessary gene editing reagents as well as on their tight control once inside the cell (Yu and Wu, 2018). As described in the previous section, several innovative strategies have been developed that in principle might allow for precise gene insertion in post-mitotic cells such as those affected by congenital disorders of the retina. However, it is important to highlight that most techniques were developed and tested in *in vitro* systems with only a few of them having, so far, made the transition to *in vivo* genome editing testing in physiologically relevant animal models.

A major challenge concerns the need for efficient delivery of gene editing tools into the proper target cells *in vivo* and subsequently achieve gene modification in a sufficient number of cells for preventing or halting disease progression. The delivery to target cells can, to some extent, be controlled by the choice between subretinal or intravitreal injection. Undertaking multiple injections might increase the percentage of cells that uptake the genetic therapy. However, the evaluation of these parameters is limited to end-point functional readouts as taking retina biopsies from treated patients to quantify the percentage of modified cells is not feasible. Neither is tracking or selecting cells for *in vivo* assessment of the genetic therapy. In addition, a balance between increased efficacy and adverse side effects must be carefully established. One may argue that the risks associated with multiple injections (e.g., retina detachment or bleeding) are non-negligible. As for other neurodegenerative disorders, it is also crucial to determine the optimal time of intervention or therapeutic window. Early diagnostics and treatment undoubtedly generate better clinical outcomes. Further pre-clinical studies using animal models could shed some light into the genuine efficacy of genetic therapies at later stages of degeneration that resemble the advanced degenerative phenotype of some patient populations.

Moreover, continuous expression of RGNs raises safety issues because it can cause cytotoxicity or trigger immune responses due to their foreign, prokaryotic, origins. *In vitro* transcribed gRNAs can trigger innate immune responses and anti-Cas9 antibodies (against *S. pyogenes* and *S. aureus*) together with Cas9-specific T cells have been detected in the blood of healthy human donors (Crudele and Chamberlain, 2018; Kim et al., 2018; Charlesworth et al., 2019; Mehta and Merkel, 2020). Preexisting adaptive immunity, through cytotoxic T cells, might be responsible for the killing of cells expressing Cas9 antigens. The immune privileged status of the retina at early stages of degeneration and/or the administration of immunosuppression treatments might ameliorate or overcome these adverse reactions. Importantly, the safety, tolerability and efficacy of a CRISPR/Cas9-based therapy will be addressed in a recent, currently recruiting, Phase I/II clinical trial to treat patients with Leber congenital amaurosis type 10 (NCT03872479). In this study, patients will receive the EDIT-101 therapy, an AAV5 vector expressing Cas9 from *S. aureus* and two gRNAs that target and remove a deep intronic variant in the *CEP290* gene, aiming at restoring normal gene expression and ensuing functional rescue (Maeder et al., 2019). In addition, an ideal CRISPR/Cas-based genetic therapy should include a strategy to shut down the machinery once the editing process is over, to decrease the chances for off-target activities. For example, optogenetic-regulated switches could be an interesting approach to regulate transgene expression (Polesskaya et al., 2018). Indeed, viable strategies for spatiotemporal control of the CRISPR/Cas components should ideally be envisioned and tested before applying gene editing as a therapy for retinal degeneration.

Genome Editing Approaches Independent of Double-Stranded DNA Break Formation

Another safety issue arises directly from RGN-induced DSB formation in that DSBs are one of the most severe types of DNA lesions as they can lead to deleterious rearrangements in the genome, e.g., intra- and inter-chromosomal translocations. For this reason, nickases are becoming increasingly investigated for bringing about precise HDR-mediated seamless gene editing as single-stranded DNA breaks are intrinsically less disruptive to the genome when compared to DSBs (Chen et al., 2017, 2020; Nakajima et al., 2018; Hyodo et al., 2020).

Furthermore, in order to use CRISPR/Cas-based techniques for genetic therapies, a deep knowledge on how DNA repair pathways operate in retinal cell types is needed. For instance, favoring certain NHEJ pathways (e.g., MMEJ) might lead to an increase in mutagenic events. Pre-clinical studies should aim at carefully understanding which mechanisms are prevalently involved in the repair of RGN-induced DSBs resulting in transgene integration, while minimizing the generation of mutagenic indels at target and off-target sites. The further development of sensitive and unbiased genome-wide DSB detection methods should assist and complement the development of bioinformatic tools that can predict with higher confidence off-target events. Together these technologies should be instrumental for monitoring and validating the specificity of gene editing procedures.

Importantly, alternative CRISPR/Cas-based genome editing strategies that do not require DSB formation or donor DNA templates are being engineered and investigated (Komor et al., 2016; Nishida et al., 2016; Chen et al., 2017, 2020; Gaudelli et al., 2017; Nakajima et al., 2018; Anzalone et al., 2019; Hyodo et al., 2020). One of such alternative strategies is base editing. The basic principle of base editors consists of fusing a Cas9 nickase to a cytosine or adenine deaminase that induces single base pair changes (i.e., C > T or A > G transitions, respectively) within a so-called editing window located in the protospacer bound by the gRNA spacer (Komor et al., 2016; Gaudelli et al., 2017; Rees et al., 2017). The first base editors contained the cytosine deaminases APOBEC1 from rat (Komor et al., 2016) or PmCDA1 from sea lamprey (Nishida et al., 2016). Subsequently, base editors capable of inducing A > G transitions were obtained through directed evolution and selection of a bacterial transfer RNA adenosine deaminase that acts on DNA (Gaudelli et al., 2017). More recently, a dual base editor has been engineered by fusing a Cas9 nickase to both an adenine and cytosine deaminase base editors, allowing simultaneous substitutions in adenine and cytosine bases in the same target sequence (Grünewald et al., 2020). Although base editors can function in non-dividing cells, they have a limited performance in terms of the range of nucleotide conversions that they can implement. Indeed, base editors install neither transversions nor small insertions or deletions. Importantly, recently, prime editing has expanded the repertoire of DSB-free CRISPR/Cas-based systems for gene editing in that it permits installing all possible base-to-base conversions as well as small insertions and deletions (Anzalone et al., 2019). This new methodology is based on a nickase Cas9 fused to an engineered reverse transcriptase (RT). Cas9 is directed to the target sequence with a prime editing guide RNA (pegRNA) consisting of a 3' end-extended gRNA that acts as a primer for reverse transcription initiation. Upon site-specific nicking of the PAM-containing strand, the released single-stranded DNA hybridizes to a portion of the pegRNA (primer binding site) that provides for a free 3'-OH group for reverse transcription of the desired genetic modifications encoded in another portion of pegRNA (RT template). Ultimately, the synthesized complementary DNA (cDNA) becomes incorporated at the target site after a series of events presumably encompassing genomic DNA-cDNA hybridization and non-hybridizing DNA flap removal. The prime editor is a versatile tool in that it is independent of donor DNA templates and, as aforementioned, allows for the introduction of any base-pair substitution, small deletions (i.e., up to 80-bp) and small insertions, e.g., epitope tags (Anzalone et al., 2019). Interestingly, although the highest efficiencies of prime editing were observed in transformed HEK293T cells, the authors demonstrated that post-mitotic cells, in particular primary cortical murine neurons, can also undergo prime editing (Anzalone et al., 2019). Clearly, further research is warranted to improve the efficiency of prime editing, assess its genome-wide off-targets and its performance in *in vivo* applications. To this end, delivery systems capable of introducing the large prime editing and pegRNA components into primary cells will become instrumental.

IN VIVO DELIVERY OPTIONS FOR GENE EDITING TOOLS: FROM CLASSICAL AAV VECTORS TO THIRD-GENERATION ADV VECTORS?

There are several methods to deliver a gene therapy to the retina. In general, these can be divided into viral and non-viral categories. Viral vectors consist of non-replicating viruses that carry the therapeutic genetic material that is introduced into target cells through transduction. Viral vectors are often used for CRISPR/Cas-mediated *in vivo* gene editing, however, delivering gRNAs and Cas nucleases directly as ribonucleoprotein complexes offers the distinct advantage of limiting the exposure of cells to long-lasting RGN activity (Kim et al., 2017; Lino et al., 2018; Yu and Wu, 2018). Non-viral vectors include lipid-based carriers or liposomes with chemical modifications (Chu-Tan et al., 2020), different nanoparticle formulations (Himawan et al., 2019) or salt solutions that enhance cell penetrance (iTOP) (D'Astolfo et al., 2015). For instance, cationic lipids were used to deliver Cas9 and gRNA as a ribonucleoprotein to the mouse retina following subretinal injection (Kim et al., 2017). In addition, synthetic nanoparticles with reduced cytotoxicity have been developed and tested for the *in vivo* delivery of RGN complexes to murine retinal pigment epithelium (Chen et al., 2019). Each method has its own set of advantages and limitations with regard to the treatment of retinal diseases. In this section, we will briefly discuss the use of AAV vectors, which are currently the gold standard vehicles for targeting the retina. Subsequently, we will focus on the potential use of HC-AdVs, also known as "gutless" or third-generation adenoviral vectors, to circumvent some of the limitations of the AAV-based platform.

AAV vectors are the most widely used tools for delivering genetic material to retinal cell types owing to their low immunogenicity and high transduction efficiencies (Trapani, 2019). They can be tested for gene replacement or gene editing therapies. Once inside the target cell nucleus, AAV vector genomes stay, for the most part, as extrachromosomal episomes

that sustain long-term transgene expression in non-dividing cells. For recent reviews on the use of AAV vectors for gene therapy and on their optimization, including serotype selection and expression cassette design (e.g., promoter and transgene codon-optimization, see Wang et al., 2019; Li and Samulski, 2020). The tropism of the different AAV serotypes has been extensively characterized with regard to their capability to transduce different retinal cell types (e.g., photoreceptors, retinal pigment epithelium cells and Müller glial cells, amongst others). The different routes of AAV vector administration (e.g., intravitreal or subretinal) have equally been extensively characterized (e.g., Moore et al., 2018). Building upon these research efforts, AAV vectors are currently being tested in clinical trials for the treatment of several IRDs. These ongoing clinical developments have been recently summarized (i.e., Moore et al., 2018; Arbabi et al., 2019; Trapani, 2019; Vázquez-Domínguez et al., 2019).

As aforementioned, a major drawback of AAV vectors is their limited packaging capacity of ∼4.7 kb, that includes the two inverted terminal repeats. This limitation has been somewhat ameliorated with the development of so-called dual AAV vectors. The dual AAV vector strategy consists in splitting the sequence of a large transgene through two AAV vector genomes that, once inside the cell, can become concatemerized through recombination involving ITR sequences or shared homologous regions (McClements and Maclaren, 2017; Trapani, 2019). After this end-to-end recombination between the two AAV vector genomes, judiciously placed splice donor and splice acceptor motifs guarantee the assembly of full-length mRNA transcripts and ensuing expression of full-length gene products (McClements and Maclaren, 2017; Trapani, 2019). In the case of gene editing, different AAV vectors can be assembled for transferring expressing units encoding RGN components (i.e., Cas9 nucleases and gRNAs) or donor templates containing the exogenous DNA of interest (see, e.g., Chen and Gonçalves, 2016; Suzuki et al., 2016). However, the need for two or more AAV vectors increases the AAV product production burden, reduces the overall efficiency of the therapeutic approach and is expected to render regulatory approvals substantially more complex.

Still concerning the testing of AAV vectors for therapeutic gene editing, it is noteworthy mentioning recent data demonstrating prevalent integration of Cas9-encoding AAV DNA at RGN target sequences in animal models (Hanlon et al., 2019; Nelson et al., 2019). Thorough deep sequencing assays revealed that fragments of AAV ITRs, joined to full-length or truncated transgene sequences, were consistently found at RGN target sites in various mouse tissues, i.e., muscle, brain and cochlea (Hanlon et al., 2019). In addition to raising concerns linked to the chromosomal integration of RGN-coding sequences in transduced cells, these data extend previous and recent studies reporting that AAV vector DNA can become "captured" through homology-independent recombination processes at ZFN- and RGN-induced DSBs in the liver and eye, respectively, of mouse models (Anguela et al., 2013; Maeder et al., 2019). Collectively, these findings highlight the need to carefully monitor the accuracy of AAV-based gene editing procedures and stress the importance of expanding the range of gene editing vehicles, especially those that, similarly to AAV vectors, do not carry viral genes.

Albeit less often than AAV vectors, other viral vectors, such as lentiviral (LV) vectors and adenoviral (AdV) vectors, have also been tested for gene replacement in retinal degeneration. Gene therapy clinical trials using LV vectors have been initiated to deliver large transgenes encoding *ABCA4* and *MYO7A* (NCT01367444 and NCT01505062, respectively). However, the long-term outcome of these clinical trials is still pending. Prototypic AdV vectors based on the human adenovirus serotype 5 use the Coxsackie B and adenovirus receptor (CAR) to enter cells (Bergelson, 1997). This receptor is not detected in the outer segments of photoreceptors in mouse and human retina, while being detected in other retinal cells including retinal pigmented epithelium and Müller glial cells (Mallam et al., 2004). In this regard, ongoing research efforts are directed at modifying the tropism of AdV vectors by designing variants of the viral capsid or of the receptor-interacting fiber motifs (Gao et al., 2019; Tasca et al., 2020). Although still controversial, studies indicate that photoreceptor transduction in mouse retina can be achieved by deleting the RGD domain from the penton base capsomer of AdV serotype 5 (Mallam et al., 2004; Sweigard et al., 2010). In addition, AdV vector genomes are maintained as extrachromosomal elements in post-mitotic cells, offering the potential for stable and long-term transgene expression (Rauschhuber et al., 2012; Ricobaraza et al., 2020; Tasca et al., 2020). Moreover, when compared to free-ended viral and non-viral vector DNA, protein-capped AdV genomes have been shown to be refractory to chromosomal DNA integration in transduction experiments comprising the delivery of TALENs and RGNs (Holkers et al., 2014).

These findings on the amenability of AdV systems to tropism modifications and prevalent episomal nature, make investigating HC-AdV vector delivery of RGN machineries *in vitro* and *in vivo* appealing. In contrast to their first- and second-generation counterparts, these third-generation AdV vectors are devoid of all viral genes which expands their cargo capacity to 36 kb while reducing cytotoxicity and immune responses in transduced cells and animal models, respectively (Gonçalves and de Vries, 2006; Ricobaraza et al., 2020; Tasca et al., 2020). Their large cargo capacity has in fact permitted the delivery of all RGN components, including gRNA multiplexing formats, in single HC-AdV vector particles (Ehrke-Schulz et al., 2017; Brescia et al., 2020; Tasca et al., 2020). The capability of HC-AdV vectors to achieve long-term transgene expression *in vivo* has been demonstrated in the retina (Kreppel et al., 2002; Chen et al., 2008) and in other organs of small and large animal models (for a recent review, see Ricobaraza et al., 2020). Assessment of the potential of HC-AdV vectors for gene editing therapies is at early stages. For instance, HC-AdV-mediated delivery of high-specificity RGN pairs targeting a mutational hotspot in the dystrophin-encoding *DMD* gene, whose mutations underlie Duchenne muscular dystrophy, permitted restoring the *DMD* reading frame in muscle progenitor cells (Brescia et al., 2020). Upon triggering myogenic differentiation of the resulting *DMD*-edited

cell populations, shorter yet partially functional, dystrophin molecules (i.e., Becker-like dystrophins) were readily detected (Brescia et al., 2020). In another study, Xia and colleagues investigated the use of HC-AdV vectors for the treatment of cystic fibrosis, a monogenic disease caused by mutations in the *CFTR* gene. They reported the seamless integration of the *CFTR*-encoding transgene at a predefined genomic locus in airway epithelial cells (Xia et al., 2018). For a recent review on the application of AdV systems for gene editing purposes; see Tasca et al., 2020.

COMBINING GENE EDITING WITH CELL-BASED APPROACHES TO TREAT RETINAL DEGENERATION

In this last section, we discuss cell-based approaches for the treatment of retinal degeneration. As neurodegenerative conditions, IRDs lead to a progressive loss of functional cell populations that cannot be replenished due to a lack of progenitors. Cell therapies for treating IRDs, are still highly experimental. These cell therapies are based on the transplantation into the retina of photoreceptor progenitors or retinal pigmented epithelium derived from either embryonic stem cells (ESCs) (Lamba et al., 2009; Shirai et al., 2016; Da Cruz et al., 2018) or induced pluripotent stem cells (iPSCs) (Reichman et al., 2017; Gagliardi et al., 2018). Cell therapies can be broadly divided in allogeneic and autologous. The former relies on the transplantation of cells from a healthy donor with HLA matching alleles; the latter involves the transplantation of patient-own cells previously genetically corrected *ex vivo*. Hence, transplantation of genetically corrected autologous cells integrates genetic and cell-based therapies. A recent study showed the feasibility in combining *ex vivo* correction of isolated photoreceptors with their subsequent transplantation into the retina in a murine model of retinitis pigmentosa (Barnea-Cramer et al., 2020). Recipient mice harbored a homozygous null mutation in the rhodopsin gene (*Rho*) that was corrected in isolated photoreceptor precursor cells through gene replacement using minicircle DNA delivery (Barnea-Cramer et al., 2020). Subsequently, these photoreceptor precursors were transplanted into the retina of mutant mice where they expressed maturation markers (e.g., *Pde6b* coding for phosphodiesterase 6 beta) at 3 months post-transplantation and, importantly, formed synaptic networks within the host retina (Barnea-Cramer et al., 2020). In fact, with the exception of electro retinal function, visual function and behavioral light responses were improved in recipient mutant mice, as measured by optomotor responses, behavioral light avoidance and pupil light reflex (Barnea-Cramer et al., 2020). In an *in vitro* study, the most prevalent mutations in the *USH2A* gene, responsible for Usher syndrome, characterized by retinitis pigmentosa and hearing loss, were corrected in patient-derived iPSCs by using enhanced specificity Cas9 from *S. pyogenes* (Sanjurjo-Soriano et al., 2020). Using whole-exome sequencing, no off-target events were detected after RGN-mediated *USH2A* correction. Moreover, the gene-edited iPSC lines retained their pluripotency as demonstrated by the expression of pluripotency markers SOX2, NANOG and OCT3/4, as well the ability to differentiate into the three germ layers, i.e., ectoderm, mesoderm and endoderm (Sanjurjo-Soriano et al., 2020).

Although far from its implementation in clinical trials, these reports highlight the possibility to integrate gene and cell therapy concepts and hence broaden the range of therapeutic options to halt retinal degeneration. There are nonetheless safety and efficacy concerns related to the source and differentiation capabilities of the transplanted cells. Most preeminent among these concerns is whether uncontrolled proliferation of iPSC-derived cells can occur and whether the graft will properly integrate in the host retina as to provide for functional rescue of the pathologic phenotype. Finally, in addition to the aforementioned assessments of the specificity and accuracy of gene editing procedures, much more research is warranted to (i) assure good manufacturing practices during the generation of retinal progenitors and (ii) implement exhaustive quality control protocols that minimize contaminants in cell products that may otherwise trigger adverse reactions.

CONCLUSION

Many patients suffering from IRDs are still lacking therapeutic options that tackle the underlying cause of their blindness. There are many challenges on the path to the development of such therapies given the fact that, amongst the scientific and technological bottlenecks described herein, IRDs present considerable clinical and genotypic heterogeneity. In this review, we have presented some of the milestones and advances in gene editing strategies that are offering novel paths for treating IRDs. We have highlighted innovative gene editing concepts directed at achieving efficient and targeted chromosomal integration of therapeutic genes or precise *in situ* correction of genetic mutations in post-mitotic cells, such as those found in the retina. Therefore, it is plausible to consider that these novel gene editing strategies will start to be increasingly tested in *in vivo* models of retinal degeneration (e.g., mouse models) or in *in vitro* 3D human retinal organoids. Furthermore, although AAV vectors have demonstrated to be safe, well tolerated and efficient in delivering genetic material to the retina, they might not be the most suitable vehicle for transferring gene editing tools based on various CRISPR/Cas systems due to their limited packaging capacity and significant chromosomal integration potential. In conclusion, assisted by the implementation of delivery systems, future research avenues will undoubtedly focus on developing and optimizing gene editing components and procedures aiming at significantly improving the quality of life of patients afflicted by IRDs.

AUTHOR CONTRIBUTIONS

CG, MG, and JW performed the conceptualization and wrote, reviewed, and edited the manuscript. CG wrote the original draft.

JW acquired the funding. All authors contributed to the article and approved the submitted version.

FUNDING

Funding was obtained from Foundation Fighting Blindness (TA-GT-0715-0665-LUMC), the Dutch blindness funds (Uitzicht 2019-19): Rotterdamse Stichting Blindenbelangen, Stichting Oogfonds, Landelijke Stichting voor Blinden en Slechtzienden, and Stichting Blindenhulp.

ACKNOWLEDGMENTS

The authors thank their team members for valuable discussions and advice.

REFERENCES

Anguela, X. M., Sharma, R., Doyon, Y., Miller, J. C., Li, H., Haurigot, V., et al. (2013). Robust ZFN-mediated genome editing in adult hemophilic mice. *Blood* 122, 3283–3287. doi: 10.1182/blood-2013-04-497354

Anzalone, A. V., Randolph, P. B., Davis, J. R., Sousa, A. A., Koblan, L. W., Levy, J. M., et al. (2019). Search-and-replace genome editing without double-strand breaks or donor DNA. *Nature* 576, 149–157. doi: 10.1038/s41586-019-1711-4

Arbabi, A., Liu, A., and Ameri, H. (2019). Gene therapy for inherited retinal degeneration. *J. Ocul. Pharmacol. Ther.* 35, 79–97. doi: 10.1089/jop.2018.0087

Artegiani, B., Hendriks, D., Beumer, J., Kok, R., Zheng, X., Joore, I., et al. (2020). Fast and efficient generation of knock-in human organoids using homology-independent CRISPR–Cas9 precision genome editing. *Nat. Cell Biol.* 22, 321–331. doi: 10.1038/s41556-020-0472-5

Bakondi, B., Lv, W., Lu, B., Jones, M. K., Tsai, Y., Kim, K. J., et al. (2016). *In vivo* CRISPR/Cas9 gene editing corrects retinal dystrophy in the S334ter-3 rat model of autosomal dominant retinitis pigmentosa. *Mol. Ther.* 24, 556–563. doi: 10.1038/mt.2015.220

Barnea-Cramer, A. O., Singh, M., Fischer, D., De Silva, S., McClements, M. E., Barnard, A. R., et al. (2020). Repair of retinal degeneration following *ex vivo* minicircle DNA gene therapy and transplantation of corrected photoreceptor progenitors. *Mol. Ther.* 28, 830–844. doi: 10.1016/j.ymthe.2020.01.023

Barrangou, R., and Marraffini, L. A. (2014). CRISPR-cas systems: prokaryotes upgrade to adaptive immunity. *Mol. Cell* 54, 234–244. doi: 10.1016/j.molcel.2014.03.011

Bergelson, J. M. (1997). Isolation of a common receptor for Coxsackie B Viruses and Adenoviruses 2 and 5. *Science* 275, 1320–1323. doi: 10.1126/science.275.5304.1320

Berger, W., Kloeckener-Gruissem, B., and Neidhardt, J. (2010). The molecular basis of human retinal and vitreoretinal diseases. *Prog. Retin. Eye Res.* 29, 335–375. doi: 10.1016/j.preteyeres.2010.03.004

Birch, D. G., Bennett, L. D., Duncan, J. L., Weleber, R. G., and Pennesi, M. E. (2016). Long-term follow-up of patients with retinitis pigmentosa receiving intraocular ciliary neurotrophic factor implants. *Am. J. Ophthalmol.* 170, 10–14. doi: 10.1016/j.ajo.2016.07.013

Brescia, M., Janssen, J. M., Liu, J., and Gonçalves, M. A. F. V. (2020). High-capacity adenoviral vectors permit robust and versatile testing of DMD gene repair tools and strategies in human cells. *Cells* 9:869. doi: 10.3390/cells9040869

Broeders, M., Herrero-hernandez, P., Ernst, M. P. T., and Pijnappel, W. W. M. P. (2020). Sharpening the molecular scissors?: advances in gene-editing technology. *iScience* 23:100789. doi: 10.1016/j.isci.2019.100789

Campa, C. C., Weisbach, N. R., Santinha, A. J., Incarnato, D., and Platt, R. J. (2019). Multiplexed genome engineering by Cas12a and CRISPR arrays encoded on single transcripts. *Nat. Methods* 16, 887–893. doi: 10.1038/s41592-019-0508-6

Ceccaldi, R., Rondinelli, B., and D'Andrea, A. D. (2016). Repair pathway choices and consequences at the double-strand break. *Trends Cell Biol.* 26, 52–64. doi: 10.1016/j.tcb.2015.07.009

Chaffiol, A., Caplette, R., Jaillard, C., Brazhnikova, E., Desrosiers, M., Dubus, E., et al. (2017). A new promoter allows optogenetic vision restoration with enhanced sensitivity in macaque retina. *Mol. Ther.* 25, 2546–2560. doi: 10.1016/j.ymthe.2017.07.011

Chandrasegaran, S., and Carroll, D. (2016). Origins of programmable nucleases for genome engineering. *J. Mol. Biol.* 428, 963–989. doi: 10.1016/j.jmb.2015.10.014

Charlesworth, C. T., Deshpande, P. S., Dever, D. P., Camarena, J., Lemgart, V. T., Cromer, M. K., et al. (2019). Identification of preexisting adaptive immunity to Cas9 proteins in humans. *Nat. Med.* 25, 249–254. doi: 10.1038/s41591-018-0326-x

Chen, G., Abdeen, A. A., Wang, Y., Shahi, P. K., Robertson, S., Xie, R., et al. (2019). A biodegradable nanocapsule delivers a Cas9 ribonucleoprotein complex for *in vivo* genome editing. *Nat. Nanotechnol.* 14, 974–980. doi: 10.1038/s41565-019-0539-2

Chen, P., Hamilton, M., Thomas, C. A., Kroeger, K., Carrion, M., MacGill, R. S., et al. (2008). Persistent expression of PEDF in the eye using high-capacity adenovectors. *Mol. Ther.* 16, 1986–1994. doi: 10.1038/mt.2008.211

Chen, X., and Gonçalves, M. A. F. V. (2016). Engineered viruses as genome editing devices. *Mol. Ther.* 24, 447–457. doi: 10.1038/mt.2015.164

Chen, X., and Gonçalves, M. A. F. V. (2018). DNA, RNA, and protein tools for editing the genetic information in human cells. *iScience* 6, 247–263. doi: 10.1016/j.isci.2018.08.001

Chen, X., Janssen, J. M., Liu, J., Maggio, I., T'Jong, A. E. J., Mikkers, H. M. M., et al. (2017). In trans paired nicking triggers seamless genome editing without double-stranded DNA cutting. *Nat. Commun.* 8:657. doi: 10.1038/s41467-017-00687-1

Chen, X., Tasca, F., Wang, Q., Liu, J., Janssen, J. M., Brescia, M. D., et al. (2020). Expanding the editable genome and CRISPR-Cas9 versatility using DNA cutting-free gene targeting based on in trans paired nicking. *Nucleic Acids Res.* 48, 974–995. doi: 10.1093/nar/gkz1121

Cho, S. W., Kim, S., Kim, J. M., and Kim, J. S. (2013). Targeted genome engineering in human cells with the Cas9 RNA-guided endonuclease. *Nat. Biotechnol.* 31, 230–232. doi: 10.1038/nbt.2507

Chu-Tan, J. A., Fernando, N., Aggio-Bruce, R., Cioanca, A. V., Valter, K., Andronikou, N., et al. (2020). A method for gene knockdown in the retina using a lipid-based carrier. *Mol. Vis.* 26, 48–63.

Collin, R. W., Den Hollander, A. I., Der Velde-Visser, S. D. V., Bennicelli, J., Bennett, J., and Cremers, F. P. (2012). Antisense oligonucleotide (AON)-based therapy for leber congenital amaurosis caused by a frequent mutation in CEP290. *Mol. Ther. Nucleic Acids* 1:e14. doi: 10.1038/mtna.2012.3

Cong, L., Ran, F. A., Cox, D., Lin, S., Barretto, R., Habib, N., et al. (2013). Multiplex genome engineering using CRISPR/Cas systems. *Science* 339, 819–823. doi: 10.1126/science.1231143

Cremers, F., Boon, C., Bujakowska, K., and Zeitz, C. (2018). Special issue introduction: inherited retinal disease: novel candidate genes, genotype–phenotype correlations, and inheritance models. *Genes* 9:215. doi: 10.3390/genes9040215

Crudele, J. M., and Chamberlain, J. S. (2018). Cas9 immunity creates challenges for CRISPR gene editing therapies. *Nat. Commun.* 9:3497. doi: 10.1038/s41467-018-05843-9

Da Cruz, L., Fynes, K., Georgiadis, O., Kerby, J., Luo, Y. H., Ahmado, A., et al. (2018). Phase 1 clinical study of an embryonic stem cell-derived retinal pigment epithelium patch in age-related macular degeneration. *Nat. Biotechnol.* 36, 328–337. doi: 10.1038/nbt.4114

D'Astolfo, D. S., Pagliero, R. J., Pras, A., Karthaus, W. R., Clevers, H., Prasad, V., et al. (2015). Efficient intracellular delivery of native proteins. *Cell* 161, 674–690. doi: 10.1016/j.cell.2015.03.028

Dias, M. F., Joo, K., Kemp, J. A., Fialho, S. L., da Silva Cunha, A., Woo, S. J., et al. (2018). Molecular genetics and emerging therapies for retinitis pigmentosa: basic research and clinical perspectives. *Prog. Retin. Eye Res.* 63, 107–131. doi: 10.1016/j.preteyeres.2017.10.004

DiCarlo, J. E., Mahajan, V. B., and Tsang, S. H. (2018). Gene therapy and genome surgery in the retina. *J. Clin. Invest.* 128, 2177–2188. doi: 10.1172/JCI120429

Doudna, J. A., and Charpentier, E. (2014). The new frontier of genome engineering with CRISPR-Cas9. *Science* 346:1258096. doi: 10.1126/science.1258096

Drack, A. V., Bennett, J., Russell, S., High, K. A., Yu, Z., Tillman, A., et al. (2019). How long does gene therapy last? 4-year follow-up of phase 3 voretigene neparvovec trial in RPE65-associated LCA/inherited retinal disease. *J. Am. Assoc. Pediatr. Ophthalmol. Strabismus* 23:e7. doi: 10.1016/j.jaapos.2019.08.018

Ehrke-Schulz, E., Schiwon, M., Leitner, T., Dávid, S., Bergmann, T., Liu, J., et al. (2017). CRISPR/Cas9 delivery with one single adenoviral vector devoid of all viral genes. *Sci. Rep.* 7:17113. doi: 10.1038/s41598-017-17180-w

Gagliardi, G., Ben, M., Barek, K., Chaffiol, A., Slembrouck-Brec, A., Conart, J. B., et al. (2018). Characterization and transplantation of CD73-positive photoreceptors isolated from human iPSC-derived retinal organoids. *Stem Cell Rep.* 11, 665–680. doi: 10.1016/j.stemcr.2018.07.005

Gao, J., Mese, K., Bunz, O., and Ehrhardt, A. (2019). State-of-the-art human adenovirus vectorology for therapeutic approaches. *FEBS Lett.* 593, 3609–3622. doi: 10.1002/1873-3468.13691

Gao, L., Cox, D. B. T., Yan, W. X., Manteiga, J. C., Schneider, M. W., Yamano, T., et al. (2017). Engineered Cpf1 variants with altered PAM specificities. *Nat. Biotechnol.* 35, 789–792. doi: 10.1038/nbt.3900

Garita-Hernandez, M., Guibbal, L., Toualbi, L., Routet, F., Chaffiol, A., Winckler, C., et al. (2018). Optogenetic light sensors in human retinal organoids. *Front. Neurosci.* 12:789. doi: 10.3389/fnins.2018.00789

Garita-Hernandez, M., Lampič, M., Chaffiol, A., Guibbal, L., Routet, F., Santos-Ferreira, T., et al. (2019). Restoration of visual function by transplantation of optogenetically engineered photoreceptors. *Nat. Commun.* 10:4524. doi: 10.1038/s41467-019-12330-2

Gasiunas, G., Barrangou, R., Horvath, P., and Siksnys, V. (2012). Cas9-crRNA ribonucleoprotein complex mediates specific DNA cleavage for adaptive immunity in bacteria. *Proc. Natl. Acad. Sci. U.S.A.* 109, E2579–E2586. doi: 10.1073/pnas.1208507109

Gaudelli, N. M., Komor, A. C., Rees, H. A., Packer, M. S., Badran, A. H., Bryson, D. I., et al. (2017). Programmable base editing of AT to GC in genomic DNA without DNA cleavage. *Nature* 551, 464–471. doi: 10.1038/nature24644

Gonçalves, M. A. F. V., and de Vries, A. A. F. (2006). Adenovirus: from foe to friend. *Rev. Med. Virol.* 16, 167–186. doi: 10.1002/rmv.494

Gordon, K., Del Medico, A., Sander, I., Kumar, A., and Hamad, B. (2019). Gene therapies in ophthalmic disease. *Nat. Rev. Drug Discov.* 18, 415–416. doi: 10.1038/d41573-018-00016-1

Grompe, M., Al-Dhalimy, M., Finegold, M., Ou, C. N., Burlingame, T., Kennaway, N. G., et al. (1993). Loss of fumarylacetoacetate hydrolase is responsible for the neonatal hepatic dysfunction phenotype of lethal albino mice. *Genes Dev.* 7, 2298–2307. doi: 10.1101/gad.7.12a.2298

Grünewald, J., Zhou, R., Lareau, C. A., Garcia, S. P., Iyer, S., Miller, B. R., et al. (2020). A dual-deaminase CRISPR base editor enables concurrent adenine and cytosine editing. *Nat. Biotechnol.* 38, 861–864. doi: 10.1038/s41587-020-0535-y

Hanany, M., Rivolta, C., and Sharon, D. (2020). Worldwide carrier frequency and genetic prevalence of autosomal recessive inherited retinal diseases. *Proc. Natl. Acad. Sci. U.S.A.* 117, 2710–2716. doi: 10.1073/pnas.1913179117

Hanlon, K. S., Kleinstiver, B. P., Garcia, S. P., Zaborowski, M. P., Volak, A., Spirig, S. E., et al. (2019). High levels of AAV vector integration into CRISPR-induced DNA breaks. *Nat. Commun.* 10:4439. doi: 10.1038/s41467-019-12449-2

Himawan, E., Ekström, P., Buzgo, M., Gaillard, P., Stefánsson, E., Marigo, V., et al. (2019). Drug delivery to retinal photoreceptors. *Drug Discov. Today* 24, 1637–1643. doi: 10.1016/j.drudis.2019.03.004

Holkers, M., Maggio, I., Henriques, S. F. D., Janssen, J. M., Cathomen, T., and Gonçalves, M. A. F. V. (2014). Adenoviral vector DNA for accurate genome editing with engineered nucleases. *Nat. Methods* 11, 1051–1057. doi: 10.1038/nmeth.3075

Huang, D., Fletcher, S., Wilton, S. D., Palmer, N., McLenachan, S., Mackey, D. A., et al. (2017). Inherited retinal disease therapies targeting precursor messenger ribonucleic acid. *Vision* 1:22. doi: 10.3390/vision1030022

Hung, S. S. C., Chrysostomou, V., Li, F., Lim, J. K. H., Wang, J. H., Powell, J. E., et al. (2016). AAV-mediated CRISPR/Cas gene editing of retinal cells *in Vivo*. *Investig. Ophthalmol. Vis. Sci.* 57, 3470–3476. doi: 10.1167/iovs.16-19316

Hyodo, T., Rahman, M. L., Karnan, S., Ito, T., Toyoda, A., Ota, A., et al. (2020). Tandem paired nicking promotes precise genome editing with scarce interference by p53. *Cell Rep.* 30, 1195–1207.e7. doi: 10.1016/j.celrep.2019.12.064

Ishino, Y., Krupovic, M., and Forterre, P. (2018). History of CRISPR-Cas from encounter with a mysterious repeated sequence to genome editing technology. *J. Bacteriol.* 200:e00580-17. doi: 10.1128/JB.00580-17

Iyama, T., and Wilson, D. M. (2013). DNA repair mechanisms in dividing and non-dividing cells. *DNA Repair* 12, 620–636. doi: 10.1016/j.dnarep.2013.04.015

Jinek, M., Chylinski, K., Fonfara, I., Hauer, M., Doudna, J. A., and Charpentier, E. (2012). A programmable dual-RNA-guided DNA endonuclease in adaptive bacterial immunity. *Science* 337, 816–821. doi: 10.1126/science.1225829

Jinek, M., East, A., Cheng, A., Lin, S., Ma, E., and Doudna, J. (2013). RNA-programmed genome editing in human cells. *eLife* 2:e00471. doi: 10.7554/eLife.00471

Jung, G., Sun, J., Petrowitz, B., Riecken, K., Kruszewski, K., Jankowiak, W., et al. (2013). Genetically modified neural stem cells for a local and sustained delivery of neuroprotective factors to the dystrophic mouse retina. *Stem Cells Transl. Med.* 2, 1001–1010. doi: 10.5966/sctm.2013-0013

Kamar, S., Howlett, M. H. C., Klooster, J., de Graaff, W., Csikós, T., Rabelink, M. J. W. E., et al. (2020). Degenerated cones in cultured human retinas can successfully be optogenetically reactivated. *Int. J. Mol. Sci.* 21:522. doi: 10.3390/ijms21020522

Khan, M., Fadaie, Z., Cornelis, S. S., Cremers, F. P. M., and Roosing, S. (2019). "Identification and analysis of genes associated with inherited retinal diseases," in *Methods in Molecular Biology*, eds B. H. F. Weber, and T. Langmann (New York, NY: Humana Press Inc), 3–27. doi: 10.1007/978-1-4939-8669-9_1

Kim, K., Park, S. W., Kim, J. H., Lee, S. H., Kim, D., Koo, T., et al. (2017). Genome surgery using Cas9 ribonucleoproteins for the treatment of age-related macular degeneration. *Genome Res.* 27, 419–426. doi: 10.1101/gr.219089.116

Kim, S., Koo, T., Jee, H. G., Cho, H. Y., Lee, G., Lim, D. G., et al. (2018). CRISPR RNAs trigger innate immune responses in human cells. *Genome Res.* 28, 367–373. doi: 10.1101/gr.231936.117

Kleinstiver, B. P., Pattanayak, V., Prew, M. S., Tsai, S. Q., Nguyen, N. T., Zheng, Z., et al. (2016a). High-fidelity CRISPR-Cas9 nucleases with no detectable genome-wide off-target effects. *Nature* 529, 490–495. doi: 10.1038/nature16526

Kleinstiver, B. P., Tsai, S. Q., Prew, M. S., Nguyen, N. T., Welch, M. M., Lopez, J. M., et al. (2016b). Genome-wide specificities of CRISPR-Cas Cpf1 nucleases in human cells. *Nat. Biotechnol.* 34, 869–874. doi: 10.1038/nbt.3620

Komor, A. C., Kim, Y. B., Packer, M. S., Zuris, J. A., and Liu, D. R. (2016). Programmable editing of a target base in genomic DNA without double-stranded DNA cleavage. *Nature* 533, 420–424. doi: 10.1038/nature17946

Kosmaoglou, M., Schwarz, N., Bett, J. S., and Cheetham, M. E. (2008). Molecular chaperones and photoreceptor function. *Prog. Retin. Eye Res.* 27, 434–449. doi: 10.1016/j.preteyeres.2008.03.001

Kreppel, F., Luther, T. T., Semkova, I., Schraermeyer, U., and Kochanek, S. (2002). Long-term transgene expression in the RPE after gene transfer with a high-capacity adenoviral vector. *Investig. Ophthalmol. Vis. Sci.* 43, 1965–1970.

Labrador-Velandia, S., Alonso-Alonso, M. L., Di Lauro, S., García-Gutierrez, M. T., Srivastava, G. K., Pastor, J. C., et al. (2019). Mesenchymal stem cells provide paracrine neuroprotective resources that delay degeneration of co-cultured organotypic neuroretinal cultures. *Exp. Eye Res.* 185:107671. doi: 10.1016/j.exer.2019.05.011

Lamba, D. A., Gust, J., and Reh, T. A. (2009). Transplantation of human embryonic stem cell-derived photoreceptors restores some visual function in Crx-deficient mice. *Cell Stem Cell* 4, 73–79. doi: 10.1016/j.stem.2008.10.015

Lévy, E., El Banna, N., Baille, D., Heneman-Masurel, A., Truchet, S., Rezaei, H., et al. (2019). Causative links between protein aggregation and oxidative stress: A review. *Int. J. Mol. Sci.* 20:3896. doi: 10.3390/ijms20163896

Li, C., and Samulski, R. J. (2020). Engineering adeno-associated virus vectors for gene therapy. *Nat. Rev. Genet.* 21, 255–272. doi: 10.1038/s41576-019-0205-4

Li, P., Zhang, L., Li, Z., Xu, C., Du, X., and Wu, S. (2019). Cas12a mediates efficient and precise endogenous gene tagging via MITI: microhomology-dependent targeted integrations. *Cell. Mol. Life Sci.* doi: 10.1007/s00018-019-03396-8 [Epub ahead of print].

Li, S., Datta, S., Brabbit, E., Love, Z., Woytowicz, V., Flattery, K., et al. (2020). Nr2e3 is a genetic modifier that rescues retinal degeneration and promotes homeostasis in multiple models of retinitis pigmentosa. *Gene Ther.* doi: 10.1038/s41434-020-0134-z [Epub ahead of print].

Lino, C. A., Harper, J. C., Carney, J. P., and Timlin, J. A. (2018). Delivering CRISPR: a review of the challenges and approaches. *Drug Deliv.* 25, 1234–1257. doi: 10.1080/10717544.2018.1474964

Maeder, M. L., Stefanidakis, M., Wilson, C. J., Baral, R., Barrera, L. A., Bounoutas, G. S., et al. (2019). Development of a gene-editing approach to restore vision loss in Leber congenital amaurosis type 10. *Nat. Med.* 25, 229–233. doi: 10.1038/s41591-018-0327-9

Mali, P., Yang, L., Esvelt, K. M., Aach, J., Guell, M., DiCarlo, J. E., et al. (2013). RNA-guided human genome engineering via Cas9. *Science* 339, 823–826. doi: 10.1126/science.1232033

Mallam, J. N., Hurwitz, M. Y., Mahoney, T., Chévez-Barrios, P., and Hurwitz, R. L. (2004). Efficient gene transfer into retinal cells using adenoviral vectors: dependence on receptor expression. *Investig. Ophthalmol. Vis. Sci.* 45, 1680–1687. doi: 10.1167/iovs.03-0730

McClements, M. E., and Maclaren, R. E. (2017). Adeno-associated virus (AAV) dual vector strategies for gene therapy encoding large transgenes. *Yale J. Biol. Med.* 90, 611–623.

McVey, M., and Lee, S. E. (2008). MMEJ repair of double-strand breaks (director's cut): deleted sequences and alternative endings. *Trends Genet.* 24, 529–538. doi: 10.1016/j.tig.2008.08.007

Mehta, A., and Merkel, O. M. (2020). Immunogenicity of Cas9 Protein. *J. Pharm. Sci.* 109, 62–67. doi: 10.1016/j.xphs.2019.10.003

Meyer, K. J., and Anderson, M. G. (2017). Genetic modifiers as relevant biological variables of eye disorders. *Hum. Mol. Genet.* 26, R58–R67. doi: 10.1093/hmg/ddx180

Moore, N. A., Morral, N., Ciulla, T. A., and Bracha, P. (2018). Gene therapy for inherited retinal and optic nerve degenerations. *Expert Opin. Biol. Ther.* 18, 37–49. doi: 10.1080/14712598.2018.1389886

Nakade, S., Tsubota, T., Sakane, Y., Kume, S., Sakamoto, N., Obara, M., et al. (2014). Microhomology-mediated end-joining-dependent integration of donor DNA in cells and animals using TALENs and CRISPR/Cas9. *Nat. Commun.* 5:5560. doi: 10.1038/ncomms6560

Nakade, S., Yamamoto, T., and Sakuma, T. (2017). Cas9, Cpf1 and C2c1/2/3—What's next? *Bioengineered* 8, 265–273. doi: 10.1080/21655979.2017.1282018

Nakajima, K., Zhou, Y., Tomita, A., Hirade, Y., Gurumurthy, C. B., and Nakada, S. (2018). Precise and efficient nucleotide substitution near genomic nick via noncanonical homology-directed repair. *Genome Res.* 28, 223–230. doi: 10.1101/gr.226027.117

Nami, F., Basiri, M., Satarian, L., Curtiss, C., Baharvand, H., and Verfaillie, C. (2018). Strategies for *in vivo* genome editing in nondividing cells. *Trends Biotechnol.* 36, 770–786. doi: 10.1016/j.tibtech.2018.03.004

Nelson, C. E., Wu, Y., Gemberling, M. P., Oliver, M. L., Waller, M. A., Bohning, J. D., et al. (2019). Long-term evaluation of AAV-CRISPR genome editing for Duchenne muscular dystrophy. *Nat. Med.* 25, 427–432. doi: 10.1038/s41591-019-0344-3

Nishida, K., Arazoe, T., Yachie, N., Banno, S., Kakimoto, M., Tabata, M., et al. (2016). Targeted nucleotide editing using hybrid prokaryotic and vertebrate adaptive immune systems. *Science* 353:aaf8729. doi: 10.1126/science.aaf8729

Pasquini, G., Cora, V., Swiersy, A., Achberger, K., Antkowiak, L., Müller, B., et al. (2020). Using transcriptomic analysis to assess double-strand break repair activity: towards precise *in vivo* genome editing. *Int. J. Mol. Sci* 21:1380. doi: 10.3390/ijms21041380

Polesskaya, O., Baranova, A., Bui, S., Kondratev, N., Kananykhina, E., Nazarenko, O., et al. (2018). Optogenetic regulation of transcription. *BMC Neurosci.* 19:12. doi: 10.1186/s12868-018-0411-6

Ran, F. A., Cong, L., Yan, W. X., Scott, D. A., Gootenberg, J. S., Kriz, A. J., et al. (2015). *In vivo* genome editing using Staphylococcus aureus Cas9. *Nature* 520, 186–191. doi: 10.1038/nature14299

Rauschhuber, C., Noske, N., and Ehrhardt, A. (2012). New insights into stability of recombinant adenovirus vector genomes in mammalian cells. *Eur. J. Cell Biol.* 91, 2–9. doi: 10.1016/j.ejcb.2011.01.006

Rees, H. A., Komor, A. C., Yeh, W. H., Caetano-Lopes, J., Warman, M., Edge, A. S. B., et al. (2017). Improving the DNA specificity and applicability of base editing through protein engineering and protein delivery. *Nat. Commun.* 8:15790. doi: 10.1038/ncomms15790

Reichman, S., Slembrouck, A., Gagliardi, G., Chaffiol, A., Terray, A., Nanteau, C., et al. (2017). Generation of storable retinal organoids and retinal pigmented epithelium from adherent human iPS cells in xeno-free and feeder-free conditions. *Stem Cells* 35, 1176–1188. doi: 10.1002/stem.2586

Ricobaraza, A., Gonzalez-Aparicio, M., Mora-Jimenez, L., Lumbreras, S., and Hernandez-Alcoceba, R. (2020). High-capacity adenoviral vectors: expanding the scope of gene therapy. *Int. J. Mol. Sci.* 21:3643. doi: 10.3390/ijms21103643

Ruan, G. X., Barry, E., Yu, D., Lukason, M., Cheng, S. H., and Scaria, A. (2017). CRISPR/Cas9-mediated genome editing as a therapeutic approach for Leber Congenital Amaurosis 10. *Mol. Ther.* 25, 331–341. doi: 10.1016/j.ymthe.2016.12.006

Russell, S., Bennett, J., Wellman, J. A., Chung, D. C., Yu, Z. F., Tillman, A., et al. (2017). Efficacy and safety of voretigene neparvovec (AAV2-hRPE65v2) in patients with RPE65-mediated inherited retinal dystrophy: a randomised, controlled, open-label, phase 3 trial. *Lancet* 390, 849–860. doi: 10.1016/S0140-6736(17)31868-8

Sakuma, T., Nakade, S., Sakane, Y., Suzuki, K. I. T., and Yamamoto, T. (2016). MMEJ-Assisted gene knock-in using TALENs and CRISPR-Cas9 with the PITCh systems. *Nat. Protoc.* 11, 118–133. doi: 10.1038/nprot.2015.140

Sanjurjo-Soriano, C., Erkilic, N., Baux, D., Mamaeva, D., Hamel, C. P., Meunier, I., et al. (2020). Genome editing in patient iPSCs corrects the most prevalent *USH2A* mutations and reveals intriguing mutant mRNA expression profiles. *Mol. Ther. Methods Clin. Dev.* 17, 156–173. doi: 10.1016/j.omtm.2019.11.016

Sanjurjo-Soriano, C., and Kalatzis, V. (2018). Guiding lights in genome editing for inherited retinal disorders: implications for gene and cell therapy. *Neural Plast.* 2018:5056279. doi: 10.1155/2018/5056279

Schmid-Burgk, J. L., Höning, K., Ebert, T. S., and Hornung, V. (2016). CRISPaint allows modular base-specific gene tagging using a ligase-4-dependent mechanism. *Nat. Commun.* 7:12338. doi: 10.1038/ncomms12338

Scholl, H. P. N., Strauss, R. W., Singh, M. S., Dalkara, D., Roska, B., Picaud, S., et al. (2016). Emerging therapies for inherited retinal degeneration. *Sci. Transl. Med.* 8:368rv6. doi: 10.1126/scitranslmed.aaf2838

Shirai, H., Mandai, M., Matsushita, K., Kuwahara, A., Yonemura, S., Nakano, T., et al. (2016). Transplantation of human embryonic stem cell-derived retinal tissue in two primate models of retinal degeneration. *Proc. Natl. Acad. Sci. U.S.A.* 113, E81–E90. doi: 10.1073/pnas.1512590113

Sieving, P. A., Caruso, R. C., Tao, W., Coleman, H. R., Thompson, D. J. S., Fullmer, K. R., et al. (2006). Ciliary neurotrophic factor (CNTF) for human retinal degeneration: Phase I trial of CNTF delivered by encapsulated cell intraocular implants. *Proc. Natl. Acad. Sci. U.S.A.* 103, 3896–3901. doi: 10.1073/pnas.0600236103

Simunovic, M. P., Shen, W., Lin, J. Y., Protti, D. A., Lisowski, L., and Gillies, M. C. (2019). Optogenetic approaches to vision restoration. *Exp. Eye Res.* 178, 15–26. doi: 10.1016/j.exer.2018.09.003

Slaymaker, I. M., Gao, L., Zetsche, B., Scott, D. A., Yan, W. X., and Zhang, F. (2016). Rationally engineered Cas9 nucleases with improved specificity. *Science* 351, 84–88. doi: 10.1126/science.aad5227

Sundaramurthi, H., Moran, A., Perpetuini, A. C., Reynolds, A., and Kennedy, B. (2019). "Emerging drug therapies for inherited retinal dystrophies," in *Advances in Experimental Medicine and Biology*, eds C. Bowes Rickman, C. Grimm, R. Anderson, J. Ash, M. LaVail, and J. Hollyfield, (Cham: Springer) 263–267. doi: 10.1007/978-3-030-27378-1_43

Suzuki, K., and Izpisua Belmonte, J. C. (2018). *In vivo* genome editing via the HITI method as a tool for gene therapy. *J. Hum. Genet.* 63, 157–164. doi: 10.1038/s10038-017-0352-4

Suzuki, K., Tsunekawa, Y., Hernandez-Benitez, R., Wu, J., Zhu, J., Kim, E. J., et al. (2016). *In vivo* genome editing via CRISPR/Cas9 mediated homology-independent targeted integration. *Nature* 540, 144–149. doi: 10.1038/nature20565

Sweigard, J. H., Cashman, S. M., and Kumar-Singh, R. (2010). Adenovirus vectors targeting distinct cell types in the retina. *Investig. Ophthalmol. Vis. Sci.* 51, 2219–2228. doi: 10.1167/iovs.09-4367

Takahashi, V. K. L., Takiuti, J. T., Jauregui, R., Tsang, S. H., Takahashi, V. K. L., Takiuti, J. T., et al. (2018). Gene therapy in inherited retinal degenerative diseases, a review. *Ophthalmic Genet.* 39, 560–568. doi: 10.1080/13816810.2018.1495745

Tasca, F., Wang, Q., and Gonçalves, M. A. F. V. (2020). Adenoviral vectors meet gene editing: a rising partnership for the genomic engineering of human stem cells and their progeny. *Cells* 9:953. doi: 10.3390/cells9040953

Tolone, A., Belhadj, S., Rentsch, A., Schwede, F., and Paquet-Durand, F. (2019). The cGMP pathway and inherited photoreceptor degeneration: targets, compounds, and biomarkers. *Genes* 10:453. doi: 10.3390/genes10060453

Trachsel-Moncho, L., Benlloch-Navarro, S., Fernández-Carbonell, Á., Ramírez-Lamelas, D. T., Olivar, T., Silvestre, D., et al. (2018). Oxidative stress and autophagy-related changes during retinal degeneration and development. *Cell Death Dis*. 9:812. doi: 10.1038/s41419-018-0855-8

Trapani, I. (2019). Adeno-associated viral vectors as a tool for large gene delivery to the retina. *Genes* 10:287. doi: 10.3390/genes10040287

Vázquez-Domínguez, I., Garanto, A., and Collin, R. W. J. (2019). Molecular therapies for inherited retinal diseases—current standing, opportunities and challenges. *Genes* 10:654. doi: 10.3390/genes10090654

Venturini, G., Rose, A. M., Shah, A. Z., Bhattacharya, S. S., and Rivolta, C. (2012). CNOT3 is a modifier of PRPF31 mutations in retinitis pigmentosa with incomplete penetrance. *PLoS Genet.* 8:e1003040. doi: 10.1371/journal.pgen.1003040

Vighi, E., Trifunovic, D., Veiga-Crespo, P., Rentsch, A., Hoffmann, D., Sahaboglu, A., et al. (2018). Combination of cGMP analogue and drug delivery system provides functional protection in hereditary retinal degeneration. *Proc. Natl. Acad. Sci. U.S.A.* 115, E2997–E3006. doi: 10.1073/pnas.1718792115

Wang, D., Tai, P. W. L., and Gao, G. (2019). Adeno-associated virus vector as a platform for gene therapy delivery. *Nat. Rev. Drug Discov.* 18, 358–378. doi: 10.1038/s41573-019-0012-9

Wang, J., Saul, A., Roon, P., and Smith, S. B. (2016). Activation of the molecular chaperone, sigma 1 receptor, preserves cone function in a murine model of inherited retinal degeneration. *Proc. Natl. Acad. Sci. U.S.A.* 113, E3764–E3772. doi: 10.1073/pnas.1521749113

Wang, X., Yu, C., Tzekov, R. T., Zhu, Y., and Li, W. (2020). The effect of human gene therapy for RPE65-associated Leber's congenital amaurosis on visual function: a systematic review and meta-analysis. *Orphanet J. Rare Dis.* 15:49. doi: 10.1186/s13023-020-1304-1

Wierson, W. A., Welker, J. M., Almeida, M. P., Mann, C. M., Webster, D. A., Torrie, M. E., et al. (2020). Efficient targeted integration directed by short homology in zebrafish and mammalian cells. *eLife* 9:e53968. doi: 10.7554/eLife.53968

Xia, E., Duan, R., Shi, F., Seigel, K. E., Grasemann, H., and Hu, J. (2018). Overcoming the Undesirable CRISPR-Cas9 expression in gene correction. *Mol. Ther. Nucleic Acids* 13, 699–709. doi: 10.1016/j.omtn.2018.10.015

Xie, L., Sun, J., Mo, L., Xu, T., Shahzad, Q., Chen, D., et al. (2019). HMEJ-mediated efficient site-specific gene integration in chicken cells. *J. Biol. Eng.* 13:90. doi: 10.1186/s13036-019-0217-9

Yanik, M., Müller, B., Song, F., Gall, J., Wagner, F., Wende, W., et al. (2017). *In vivo* genome editing as a potential treatment strategy for inherited retinal dystrophies. *Prog. Retin. Eye Res.* 56, 1–18. doi: 10.1016/j.preteyeres.2016.09.001

Yao, X., Wang, X., Hu, X., Liu, Z., Liu, J., Zhou, H., et al. (2017). Homology-mediated end joining-based targeted integration using CRISPR/Cas9. *Cell Res.* 27, 801–814. doi: 10.1038/cr.2017.76

Yao, X., Wang, X., Liu, J., Shi, L., Huang, P., Yang, H., et al. (2018). CRISPR/Cas9-mediated targeted integration *in vivo* using a homology-mediated end joining-based strategy. *J. Vis. Exp.* 133:56844. doi: 10.3791/56844

Yeh, C. D., Richardson, C. D., and Corn, J. E. (2019). Advances in genome editing through control of DNA repair pathways. *Nat. Cell Biol.* 21, 1468–1478. doi: 10.1038/s41556-019-0425-z

Yu, W., and Wu, Z. (2018). *In vivo* applications of CRISPR-based genome editing in the retina. *Front. Cell Dev. Biol.* 6:53. doi: 10.3389/fcell.2018.00053

Zetsche, B., Gootenberg, J. S., Abudayyeh, O. O., Slaymaker, I. M., Makarova, K. S., Essletzbichler, P., et al. (2015). Cpf1 is a single RNA-guided endonuclease of a Class 2 CRISPR-Cas System. *Cell* 163, 759–771. doi: 10.1016/j.cell.2015.09.038

Conflict of Interest: The authors declare that the research was conducted in the absence of any commercial or financial relationships that could be construed as a potential conflict of interest.

Copyright © 2020 Gallego, Gonçalves and Wijnholds. This is an open-access article distributed under the terms of the Creative Commons Attribution License (CC BY). The use, distribution or reproduction in other forums is permitted, provided the original author(s) and the copyright owner(s) are credited and that the original publication in this journal is cited, in accordance with accepted academic practice. No use, distribution or reproduction is permitted which does not comply with these terms.

frontiers in Neuroscience

SYSTEMATIC REVIEW
published: 21 August 2020
doi: 10.3389/fnins.2020.00755

Cerebral Modifications and Visual Pathway Reorganization in Maculopathy: A Systematic Review

Raffaele Nuzzi, Laura Dallorto and Alessio Vitale*

Eye Clinic, Department of Surgical Sciences, University of Turin, Turin, Italy

Background: Macular degeneration (MD) is one of the most frequent causes of visual deficit, resulting in alterations affecting not only the retina but also the entire visual pathway up to the brain areas. This would seem related not just to signal deprivation but also to a compensatory neuronal reorganization, having significant implications in terms of potential rehabilitation of the patient and therapeutic perspectives.

Objective: This paper aimed to outline, by analyzing the existing literature, the current understanding of brain structural and functional changes detected with neuroimaging techniques in subjects affected by juvenile and age-related maculopathy.

Methods: Articles using various typologies of central nervous system (CNS) imaging in at least six patients affected by juvenile or age-related maculopathy were considered. A total of 142 were initially screened. Non-pertinent articles and duplicates were rejected. Finally, 19 articles, including 649 patients, were identified.

Results: In these sources, both structural and functional modifications were found in MD subjects' CNS. Changes in visual cortex gray matter volume were observed in both age-related MD (AMD) and juvenile MD (JMD); in particular, an involvement of not only its posterior part but also the anterior one suggests further causes besides an input-deprivation mechanism only. White matter degeneration was also found, more severe in JMD than in AMD. Moreover, functional analysis revealed differences in cortical activation patterns between MD and controls, suggesting neuronal circuit reorganization. Interestingly, attention and oculomotor training allowed better visual performances and correlated to a stronger cortical activation, even of the area normally receiving inputs from lesioned macula.

Conclusion: In MD, structural and functional changes in cerebral circuits and visual pathway can happen, involving both cerebral volume and activation patterns. These modifications, possibly due to neuronal plasticity (already observed and described for several brain areas), can allow patients to compensate for macular damage and gives therapeutic perspectives which could be achievable through an association between oculomotor training and biochemical stimulation of neuronal plasticity.

Keywords: maculopathy, age-related macular degeneration, juvenile macular degeneration, neurodegeneration, neuroplasticity, systematic review

OPEN ACCESS

Edited by:
Ayse Sahaboglu,
University of Tübingen, Germany

Reviewed by:
Antonio Gallo,
University of Campania Luigi Vanvitelli, Italy
Alessandro d'Ambrosio,
University of Campania Luigi Vanvitelli, Italy

****Correspondence:***
Raffaele Nuzzi
prof.nuzzi_raffaele@hotmail.it

Specialty section:
This article was submitted to Neurodegeneration, a section of the journal Frontiers in Neuroscience

Received: *18 April 2020*
Accepted: *26 June 2020*
Published: *21 August 2020*

Citation:
Nuzzi R, Dallorto L and Vitale A (2020) Cerebral Modifications and Visual Pathway Reorganization in Maculopathy: A Systematic Review. Front. Neurosci. 14:755. doi: 10.3389/fnins.2020.00755

INTRODUCTION

Rationale

Macular degeneration (MD) is one of the most common causes of visual deficit (Pascolini and Mariotti, 2012). In 2010, there were 32.4 million blind people and 191 million vision-impaired people, of which 2.1 and 6.0 million, respectively, were due to macular diseases (Jonas et al., 2014), and the number is expected to increase as a consequence of the increase in life expectancy (Wong et al., 2014). Prevalence of juvenile MD (JMD) is around 0.03% (Pi et al., 2012), but it implies higher clinical and socioeconomic consequences than age-related MD (AMD) (North et al., 2014).

Although AMD (Buschini et al., 2011) and JMD (Altschwager et al., 2017) have different pathogenesis, they share central visual loss due to photoreceptor cell death (Zarbin, 2004). The damage in visual function due to MD can be very debilitating for daily activities (Scilley et al., 2002; Knudtson et al., 2005) and thus has a significant social impact. It is remarkable how some patients, in order to overcome losing central visual acuity as the result of MD, develop eccentric vision using a different point in the more peripheral retina, the so-called "preferred retinal locus" (PRL) (Vingolo et al., 2007; Verdina et al., 2013). This kind of behavior may imply a certain degree of neural reorganization (Andrade et al., 2001) and could be used and strengthened through rehabilitative exercises to improve patients' quality of life. Moreover, new potential treatments such as pharmacological therapy, prosthesis implants, stem cell transplantation, and gene therapy could be developed on the basis of an existent potential neural plasticity or not (Gehrs et al., 2006; Bowes Rickman et al., 2013; Van Lookeren Campagne et al., 2014). The ability of the neural visual pathway to reorganize itself, even though adult cerebral plasticity remains elusive, has indeed already been highlighted in other studies (Nuzzi et al., 2017); moreover, a further evidence in favor of this possibility seems to come from studies conducted on animal models, as discussed below. It could also be assumed that some form of plastic reorganization might also happen in case of MD, through a modification of neuronal circuits. It is therefore interesting to look for evidences in the current literature regarding modifications that have occurred in the cerebral volume and cortical activation in patients suffering from these conditions: this review aims to summarize current findings in patients suffering from maculopathy in terms of structural and functional brain changes, detected with the modern techniques of neuroimaging, wondering whether such modifications may imply neuronal plasticity and whether this could have implications in current therapeutic practice.

Over the last two decades, different methods became available to investigate the central nervous system (CNS), both structurally and functionally. Functional magnetic resonance imaging (fMRI) is a neuroimaging procedure capable of detecting functional brain activities by analyzing changes in blood flow (Miki et al., 2001, 2002; Kollias, 2004). Structural brain characteristics could instead be studied using voxel-based morphometry (VBM) analysis which is computed on MRI and quantifies the gray and white matter volume (Ashburner and Friston, 2000). Moreover, surface-based morphometry (SBM), through T1-weighted morphometric analysis, can provide additional information about the brain structure (i.e., cortical thickness, curvature, and surface area) (Clarkson et al., 2011).

METHODS

In this research, we adhered to the Preferred Items for Systematic Reviews and Meta-Analyses (*PRISMA*) guidelines.

Search Strategy

We searched MEDLINE Daily and MEDLINE (Ovid), MEDLINE In-Process and Other Non-Indexed Citations, CENTRAL (which contains the Cochrane Eyes and Vision Group Trials Register), EMBASE (Ovid), Latin American and Caribbean Literature on Health Sciences (LILACS), CINAHL (EBSCO), Trip Database, and the National Institute for Health and Care Excellence (NICE).

We used the following search string: [("Functional magnetic resonance" OR "Functional magnetic resonance imaging" OR fMRI) OR (SBM OR "surface-based morphometry" OR "surface-based analysis") OR (VMB OR "Voxel based morphometry" OR "Voxel based analysis")] AND ["gray matter" OR "cerebr* OR cortex OR (visual AND (pathways OR cortex OR cortic* OR cerbr*)) AND (Maculopathy OR (Macular AND disease) OR (macula* AND dystrophy) OR "macular degeneration" AMD OR JMD OR (Juvenile AND macula*)].

These searches were supplemented by hand-searching the bibliographies of all the included studies. Gray literature was not considered due to excessive lack of essential information that usually affects this type of research. We did not use any data or language restrictions in the electronic searches. Articles published until March 2020 were included.

Study Design

Study typologies included in this review were randomized controlled trials (RCTs), clinical trials, non-randomized comparative studies, cohort studies, and case series (CS).

Exclusion criteria for eligibility were case report, case series with less than six patients, and absence of outcome data.

Participants and Interventions

We included studies on patients affected by AMD, both the exudative and the dry forms, and JMD. JMD includes a group of disease causing a loss of photoreceptor usually inherited starting early in childhood, such as Stargardt's disease (Tanna et al., 2017), Best vitelliform retinal dystrophy (Blodi and Stone, 1990), cone-rod dystrophy, and central areolar choroidal dystrophy (Xiao et al., 2010; Bondarenko et al., 2014; Molday, 2015; Palejwala et al., 2016; Hohman, 2017). Patient characteristics are reported in **Table 1**. The following techniques were used for investigating brain changes:

- fMRI
- VBM
- SBM

TABLE 1 | Demographic and clinical characteristics.

Author, year	*N* patients			Mean age (range)			Sex (M/F%)			Clinical characteristic	
	AMD	JMD	H	AMD	JMD	H	AMD	JMD	H	AMD	JMD
Baker et al., 2008	0	7	7	NS	NS	NS	NA	57/43	NS	NA	Bilateral large central bilateral scotoma (5 with no foveal function, 2 with foveal function)
Baseler et al., 2009*	8	8	12 (O 7 Y 5)	76 (70–90)	30 (19–49)	O (61–77) Y (18–37)	50/50	38/62	NS	Bilateral 1-year central scotoma with stable PRL	Stargardt's disease with bilateral 1-year central scotoma with stable PRL
Boucard et al., 2009	9	0	12	73 (61–85)	NA	66 (60–82)	78/22	NA	75/25	Bilateral scotoma >10° for minimum 3 years	NA
Haak et al., 2016*	0	8	12	NA	30 (19–49)	(18–41)	NA	38/62	NS	NA	Stargardt's disease with bilateral 1-year central scotoma with stable PRL
Hernowo et al., 2014*	24	34	55 (O 22 Y 33)	75.2 (52–91)	40.2 (12–66)	O 68 (61–83) Y 37 (13–60)	58/42	62/38	46/54	Binocular VF defect (mean scotoma 14°)	Binocular VF defect (mean scotoma 20°)
Lešták et al., 2013	10	0	9	74.7 (58–85)	NA	54.1 (45–65)	10/90	NA	78/22	Wet form of AMD with various degrees of bilateral impairment	NA
Little et al., 2008	6	0	12 (O 6 Y 6)	(55–83)	NA	O 25 (22–31) Y 73 (54–78)	50/50	NA	O 67/33 Y 50/50	Bilateral GA with eccentric PRL	NA
Liu et al., 2010	4	4	2	(70–90)	(30–50)	(70–90)	NA	NA	NA	More than 10 years AMD with stability of PRL for at least 5 years	More than 10 years Stargardt's disease
Olivo et al., 2015	0	18	23	NA	30.6 (15–54)	30.8 (18–60)	NA	67/33	65/35	NA	Clinical and molecular diagnosis of Stargardt's disease
Plank et al., 2011*	0	26	26	NA	42 (12–66)	43 (13–70)	NA	69/31	50/50	NA	Binocular central scotoma >10° and VA <0.2 decimal

(Continued)

TABLE 1 | Continued

Author, year	*N* patients			Mean age (range)			Sex (M/F%)			Clinical characteristic	
	AMD	JMD	H	AMD	JMD	H	AMD	JMD	H	AMD	JMD
Plank et al., 2013*	0	22	22	NA	41.5 (12–65)	42.4 (13–70)	NA	64/36	50/50	NA	Hereditary retinal dystrophies with binocular absolute central scotoma >10° and VA <0.2 decimal
Plank et al., 2014	8	5	12	66.8 (58–79)	59 (47–69)	62.1 (47–78)	50/50	80/20	33/67	Minimal duration of disease: 5 years, scotoma size: 10–25°	3 patients with cone-rod dystrophy and 2 patients with Stargardt's disease. Scotoma size: 10–15°
Plank et al., 2017*	0	19	19	NA	41.11 (13–65)	41.74 (13–70)	NA	58/42	53/47	NA	Hereditary retinal dystrophies with binocular absolute central scotoma >10° and VA <0.2 decimal
Prins et al., 2016*	24	34	55 (O 22 Y 33)	75.2 (52–91)	40.2 (12–66)	O 68 (61–83) Y 37 (13–60)	58/42	62/38	46/54	Binocular VF defect (mean scotoma 14°)	Binocular VF defect (mean scotoma 20°)
Rosengarth et al., 2013	9	0	7	72 (55–84)	NA	69 (51–83)	45/55	NA	29/71	Scotoma size >10°	NA
Schumacher et al., 2008	5	1	7	73.5 (63–82)	NA	75.2 (63–82)	67/33	NA	83/17	5 AMD + 1 JMD	NA
Szlyk and Little, 2009	6	0	12 (O 6 Y 6)	72 (55–83)	NA	O 73 (54–78) Y 25 (22–31)	50/50	NA	Y 50/50 O 67/33	Bilateral GA with eccentric PRL	NA
Whitson et al., 2015	7	0	32 (O 16 Y 16)	79.9 (69–91)	NA	O 68.3 (65–74) Y 23.5 (18–35)	14/86	NA	50/50	Long-standing bilateral AMD	–
Masuda et al., 2008	0	4	3	NA	37 (22–57)	(29–33)	NA	3/1	3/6	NA	2 cases of Stargardt's Disease and 2 cases of cone-rod dystrophy, with central-bilateral scotoma

**Baseler et al. (2011), Hernowo et al. (2014), Haak et al. (2016), and Prins et al. (2016) share the same patients, Plank et al. (2011, 2013, 2017) shared some of the patients median value of age. Y, young; O, old; NS, not specified; NA, not applicable; PRL, preferred retinal locus; VF, visual field; AMD, age-related macular dystrophy.*

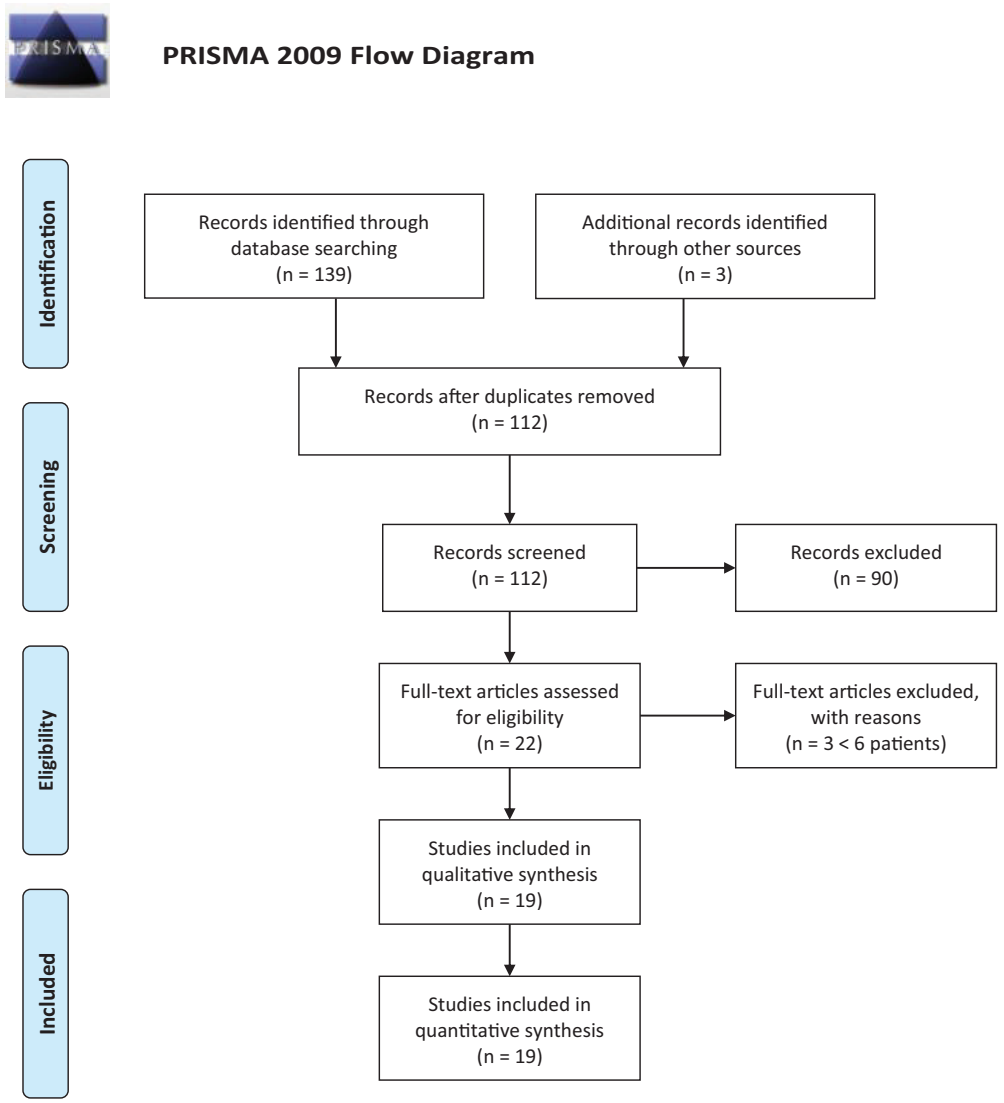

FIGURE 1 | PRISMA flow diagram.

Data Sources, Study Sections, and Data Extraction

The data were collected independently by two reviewers.

The research resulted in 142 articles (37 from *PubMed*; 39 from *EBSCO*; 52 from *Embase*; 11 from *Trip Database*; and 3 from free search). Thirty duplicate results were removed using the *EPPI* reviewer (by EPPI-Center, Social Science Research Unit, the Institute of Education, the University of London, United Kingdom). Screening of titles and abstracts was then carried out, and no pertinent articles were rejected: after this selection, 22 articles were assessed for eligibility. Three articles were later rejected due to exclusion criteria, with a final number of 19 articles.

Full texts of these articles were evaluated independently.

The entire process was carried out according to the PRISMA flow diagram: details on screening process are given in **Figure 1**.

Data Analysis

Analyzed parameters are listed below:

- VBM: gray and white matter volume.
- SBM: morphologic characteristic of the brain cortex such as thickness, curvature, and surface area.
- fMRI: blood oxygenation level-dependent (BOLD) evaluation. Changes in hemoglobin oxygenation in focal blood flow are used to detect neuronal activity fluctuation.

RESULTS

Study Characteristics

Five out of 19 (26%) studies examined brain changes in terms of structural parameters (one study used SBM and four used VBM).

The remaining 14 studies (74%) used fMRI to evaluate cortical response changes following MD.

All included studies were case series with a sample ranging from 6 to 58 patients; patient characteristics are reported in **Table 1**. Subjects showed high heterogeneity in mean age, disease duration, and disease stage.

Six studies (31.5%) included only AMD patients, seven studies included only JMD patients, and the remaining six studies included both AMD and JMD patients.

Outcomes of Structural Analysis (Table 2)

Four studies (Boucard et al., 2009; Plank et al., 2011; Hernowo et al., 2014; Olivo et al., 2015) investigated brain changes using VBM in 33 patients with AMD and 78 with JMD: two of them (Hernowo et al., 2014; Olivo et al., 2015) reported results on both gray and white matter, while the other two studies (Boucard et al., 2009; Plank et al., 2011) showed results on gray matter only.

Boucard et al. (2009) compared gray matter density in 9 AMD, 8 primary open angle glaucoma (POAG), and 12 healthy subjects. In particular, VBM was used to assess local changes in gray matter density in the whole brain and in specific volumes of interest (VOIs): 21-mm-diameter spheres in each hemisphere posterior and anterior to the calcarine cortex, corresponding to the foveal and the peripheral visual field projection zones, respectively. In the AMD subjects, gray matter density was reduced mainly in the posterior part; POAG patients showed instead a more anterior reduction in the occipital cortex. These data demonstrated a retinotopically gray matter damage caused by late-onset acquired visual field defect.

Plank et al. (2011) used VBM to analyze structural brain changes in 26 patients with central scotoma due to hereditary retinal dystrophies. Patients with JMD showed a significant reduction of gray matter volume in the posterior part of calcarine sulcus in both hemispheres. Gray matter density analysis produced results comparable to those about gray matter volume. Correlation analysis showed a negative correlation between scotoma size and gray matter volume in central VOI along the calcarine sulcus. Reading speed positively correlated to gray matter volume in the more anterior part of the calcarine sulcus in the left hemisphere, while eccentric fixation stability positively correlated with gray matter volume of a cluster in the right superior frontal gyrus.

Similar results came from Olivo et al. (2015) who used VBM to analyze gray and white matter volume in Stargardt's disease. A gray matter loss was demonstrated bilaterally in the occipital cortex and in the adjacent parietal lobe. Moreover, gray matter volume correlated inversely with retinal thickness in the left supramarginal gyrus: since, among other tasks, this part controls oculomotor mechanisms, it is possible to assume a compensatory role for this occurrence, in terms of adaptive oculomotor learning.

Hernowo et al. (2014) investigated changes in both white and gray matter of 24 AMD and 34 JMD patients: whole-brain analysis showed a reduction of gray and white matter located in the visual cortex and optic radiations. Volumetric reduction was demonstrated throughout all the retrobulbar afferent structures, with some differences: JMD patients showed a reduction all along the visual pathway; on the other hand, in AMD patients, only the lateral geniculate bodies and the optic radiations were affected. Also, volumetric reduction in JMD was greater than that in AMD, maybe because of the larger functional damage that JMD subjects had. Moreover, in the AMD group, volumetric reduction of white matter was also demonstrated in the frontal lobe, but it might be related to the different ages of AMD and JMD patients.

Only one study (Prins et al., 2016) analyzed cortical changes using SBM. This study was conducted on the same patients analyzed with VBM by Hernowo et al. (2014): volumetric changes, detected in MD patient's visual cortex using VBM, were further characterized by a more accurate representation of structural differences. The surface area in the anterior region of the visual cortex was found to be reduced. Another result was the more widespread structural damage in terms of cortical thinning and the greater reduction of surface area and volume in JMD than in AMD patients; this result could be, however, biased by the larger visual field defect and poorer visual acuity in JMD patients, resulting in greater visual deprivation. No structural changes outside the visual cortex were found, nor was there a significant correlation between disease duration and structural parameters.

Outcomes of Functional MRI (Table 3)

Fourteen studies used fMRI in order to investigate functional changes in brains of patients suffering from AMD or JMD.

Little et al. (2008), analyzed several region-of-interest (ROI) activation patterns during standardized eye movements (saccade and smooth pursuit) in patients suffering from AMD. ROIs included frontal and supplementary eye fields (FEFs and SMA/SEFs), prefrontal cortex (PFC), intraparietal sulci (IPS), and visual cortex areas (V1/V2/V3 and MT/V5). Results showed a marked reduction of activity in the visual cortex but an increased activity in FEFs, PFC, IPS, and SMA/SEFs, if compared with those of control subjects. Patients with AMD can try to overcome the impaired visual function using paracentral PRLs: the incongruence between gaze direction and visual input elaboration, normally closely associated, results mostly in difficult performance of oculomotor tasks, with a high impact on everyday activities such as reading; the attempt to overcome this incongruity, including through a learning path and involving other areas of visual control, can justify the detected pattern of activation.

Szlyk and Little (2009) studied cortical activation in patients suffering from AMD who learned to use a PRL to overcome central vision loss, during a visual task of three-letter and six-letter word recognition: if compared with controls, patients showed an increased brain activation in many areas such as the frontal eye fields, parietal lobules, and prefrontal cortex. As a possible explanation of these findings, it was assumed that not only the decreased sensory input but, rather, also the continuous research for the visual target required in a situation of central visual field deficit was causing an increased involvement of cognitive resources, among which attention has a great importance, justifying the higher activation of these superior cortical areas in these patients.

Plank et al. (2013) studied visual cortex activation (V1, V2, and V3) in JMD patients using fMRI, during retinotopic

mapping and visual tasks. Patients with an established PRL exhibited significantly higher activation in the primary visual cortex during the visual search task, especially when the target stimuli fell near the PRL. Compared with those with less stable fixation, patients with firm eccentric fixation at the PRL exhibited greater performance levels and higher brain activation. Plank et al. (2014) an fMRI study in 8 AMD, 5 JMD, and 12 controls from the same group showed that visual exercise [in this case, a texture discrimination task (TDT)] focused on PRL can enhance eccentric vision in patients with central vision loss. Both patients and control subjects exhibited a learning effect on the TDT, enhancing eccentric vision ability and so allowing better performances. This enhancement was also accompanied by an increased response in the PRL projection zone of the visual cortex.

Plank et al. (2017) used fMRI on JMD patients and controls to examine whether a visual stimulation of PRL would have caused a greater activation of the visual cortex in comparison with stimulating an equivalent peripheral area in the opposite hemifield (oppPRL). Retinal loci were stimulated using a flickering checkerboard and real-object pictures during fMRI measurement. Stimulation of PRL produced coactivation of the central representation area in the early visual cortex in patients, but not in controls. Moreover, especially in patients with highly stable eccentric fixation, it caused a stronger activation of the early visual cortex and also a response by higher visual areas beyond the retinotopic cortex. In addition, cortical response given by PRL was more intense than the one triggered by stimulating the oppPRL. Lastly, stimulation with everyday objects led to overall larger responses than those evoked by flickering checkerboards.

Rosengarth et al. (2013) observed changes in gray and white matter density due to fixation training in nine cases of AMD and seven controls. They also found a positive correlation between the increasing fixation stability and cortical response in the PRL projection zone. Structural changes were also found in the cerebellum of patients following oculomotor training: increments in gray and white matter density in the cerebellum might be the consequence of the learning effect achieved by performing visual tasks using eccentric viewing. Thus, this study showed how patients with AMD can actually benefit from specific oculomotor training procedures and how these improvements correspond to functional and structural changes in the CNS.

Lešťák et al. (2013) found that patients with a wet form of AMD showed, during retinal light stimulation, a lower fMRI activity of the visual cortex compared with the control group of healthy subjects. However, the dependence of the neurological activity on visual acuity was not statistically significant.

Liu et al. (2010) studied cortical activation in four cases of AMD, four cases of JMD, and two controls using fMRI. Six ROIs were chosen along the calcarine sulcus, extending from the posterior pole of the occipital cortex to the anterior part of the calcarine sulcus in each hemisphere. The results of this study demonstrated that a stimulation of PRL generated more extensive cortical activation than non-PRL, but no activation in the foveal cortical projection was detected. Both passive and active viewing of full-field stimuli left a silent zone at the posterior pole of the occipital cortex, even if smaller in case of active viewing during a visual task, especially in subjects suffering from JMD. Since activity in cortical areas corresponding to central scotoma projection is considered an evidence of functional reorganization, these results suggested a certain degree of remodeling in the early visual cortex in both JMD and AMD, even if not complete and apparently more prominent in JMD.

Baseler et al. (2011), studied 8 AMD cases, 8 JMD cases, and 12 control subjects with fMRI and structural MRI, recording cortical activity in early visual areas (V1–V3) of occipital pole during visual stimulation. All affected subjects had developed a stable PRL that allowed good eccentric fixation. Stimulation was based on passive viewing, without any active visual tasks requested. Their results ran contrary to the belief that the visual cortex could reorganize itself after retinal damage and input deprivation to respond to peripheral retinal stimulation: the cortical area corresponding to the lesion projection zone (LPZ) gave activity signals in the patient group in a different way than in the control group in whom a central scotoma was simulated. Furthermore, these findings were not dependent on the age at which the individuals acquired retinal lesions.

Moreover, areas with "ectopic" receptive fields were detected throughout the LPZ, equally representing the same regions of visual field in both patients and controls and questioning if the existence of ectopic receptive fields can continue to be considered as an evidence of remapping that occurred or, instead, a simple effect given by neuronal feedback and lateral connections.

It is worth noting that this study used a passive visual stimulation, and not a visual task, that has already been proven in others to be an important factor for the response of the LPZ in the early visual cortex (Masuda et al., 2008; Plank et al., 2013, 2014). Baseler hypothesized however, that these findings could be justified by the existence of feedback from the extrastriate cortex and/or the absence of feedforward signals from the visual cortex, rather than by a remapping that has occurred. He concluded there was no need to invoke remapping as an explanation of responses in V1 of individuals with MD.

Masuda et al. (2008) studied LPZ responses to different visual stimuli (checkerboards, drifting contrast patterns, scrambled, and intact faces) in four cases of Stargardt's disease and cone-rod dystrophy with central–bilateral scotoma and three controls, using fMRI. JMD subjects viewed a fixation point at the center of the stimulus using their PRL, while in controls, the fixation point fell in a retinal locus corresponding to patients' PRL. LPZ activation was indeed observed, but only as a consequence of stimulus-related tasks: any activity was recorded during passive viewing or visual tasks unrelated to stimulus. In control subjects, in which visual stimulus was presented only within the peripheral visual field, there was no response in the foveal projection zone in any condition. The study concluded that LPZ responses are not simply stimulus driven but rather are resulting from stimulus-related tasks: these findings may depend on new cortical pathways carrying task-dependent signals (neural reorganization) or the unmasking of preexisting task-dependent cortical signals that ordinarily are suppressed by the retinal visual input (no reorganization).

TABLE 2 | Outcomes of structural analysis.

Author, year	Methods	Parameter analyzed	Area analyzed	Outcomes	Principal results		Secondary results
					AMD	JMD	
Boucard et al., 2009	VBM	Gray matter density in AMD, POAG, controls	(1) Whole brain (2) VOI (21 mm diameter) at the occipital pole: posteriorly and anteriorly in the calcarine cortex, corresponding to foveal and peripheral visual field projection zone respectively	Differences compared to age-matched groups and to glaucoma group	(1) Gray matter density of occipital pole, especially around calcarine fissure, is reduced (primarily in the left hemisphere). (2) Gray matter density is more reduced in the posterior than in the anterior region, corresponding to the foveal projecton zone.	NA	POAG patients showed a more anterior reduction in the occipital cortex, corresponding to the peripheral visual field projection zone
Plank et al., 2011	VBM	Gray matter volume and density in patients with central scotoma due to hereditary retinal dystrophies	(1) Regional differences (2) 4 VOI along the calcarine sulcus. (4 VOIs of 5 mm radius from posterior to anterior)	Differences compared to age-matched groups	NA	(1) Significant reduction of gray matter volume around the calcarine sulcus of both hemispheres. (2) In both hemispheres VOI was more reduced in the posterior part of calcarine sulcus than anterior part. (3) Density analyses results was comparable to those founded in volume analyses.	(1) Scotoma size negatively correlated with GM volume in VOIs 2 and 3. (2) Reading speed positively correlated to GM volume of the more anterior VOI in the left hemisphere. (3) Fixation stability positively correlated with GM volume of a cluster in the right superior frontal gyrus.
Olivo et al., 2015	VBM	Gray and white matter volume in pz. Suffering from in Stargardt's disease	Regional differences	Differences compared to age-matched groups	NA	(1) Gray matter loss bilaterally in the occipital cortices (with a greater extension on the right one). (2) Smaller cluster of GM loss in the adjacent parietal lobe on the right one (within the precuneus).	Gray matter volume correlated directly with mean visual sensitivity in the right middle frontal and left calcarine gyri, and inversely with retinal thickness in the left supramarginal gyrus.

(Continued)

TABLE 2 | Continued

Author, year	Methods	Parameter analyzed	Area analyzed	Outcomes	Principal results		Secondary results
					AMD	JMD	
Hernowo et al., 2014*	VBM	Gray and white matter volume in AMD and JMD	(1) Whole brain (2) 5 ROI: PGCL (optic nerve, chiasm and optic tract), LGBs, GCRs, OCP, CCR (intracalcarine and supracalcarine cortices)	Differences compared to age-matched groups	(1) Reductions of gray and white matter located in the visual cortex and optic radiations; reduction of white matter in the frontal lobe. (2) Volume reduction throughout all visual pathway: GCR, OCP, CCR.	(1) Reductions of gray and white matter located in the visual cortex and optic radiations. (2) Volume reduction throughout all visual pathway: LGB, GCR, OCP.	(1) Reductions, specially of white matter, is more pronounced in the AMD group. (2) Volume of LGB, OCP, CCR reduces with age (3) No correlation between ROI volume and disease duration.
Prins et al., 2016*	SBM	Gray matter thickness, mean curvature, surface area and volume in AMD and JMD	(1) Whole brain (cortical thicknesses and mean curvature) (2) ROI: V1 and V2 areas, both divided in anterior and posterior	Differences compared to age-matched groups	(1) Whole brain: No differences. (2) ROI: thinner cortex in V2 anterior and V2 posterior. No differences in mean curvature, surface area size and gray matter volume.	(1) Whole brain: No differences. (2) ROI: thinner cortex in V1 posterior and V2 posterior, smaller surface area in V1 anterior, V1 posterior and V2 posterior and lower gray matter volume in V1 posterior, V2 anterior and V2 posterior. No differences in mean curvature.	No correlation between structural parameters in the ROIs or whole image and disease duration

*VOI, volume of interest; POAG, primary open angle glaucoma; ROI, region-of-interest; PGCL, pregeniculate structures; GCR, geniculocalcarine radiations; LGB, lateral geniculate body; OCP, the occipital pole; CCR, calcarine region; GM, gray matter; MS, mean sensitivity; CRT, central retinal thickness. *Hernowo et al. (2014) and Prins et al. (2016) share the same patients.*

TABLE 3 | Outcomes of functional analysis.

Author, year	Methods	Parameter analyzed	Outcomes	Principal results		Secondary results
				AMD	**JMD**	
Little et al., 2008	fMRI	ROI activation patterns during eye movements in AMD patients and controls. (ROI: FEFs, SMA/SEFs, IPS, IPS, V1, V2/V3, MT/V5, PFC)	To examine the cortical networks that underlie saccadic and pursuit eye movements in patients affected by AMD who use PRLs and to compared to old and young groups.	Decreased activation in visual cortex. Increased activation of FEFs, PFC, IPS, and SMA/SEFs	NA	–
Szlyk and Little, 2009	fMRI	ROI activation during 3-letters and 6-letters word recognition in AMD patients using PRLs vs controls (ROIs: left and right frontal eye fields; supplementary motor areas, superior parietal lobule, left and right inferior parietal lobule, primary visual cortices; secondary and tertiary visual cortex; fusiform gyrus; prefrontal cortex)	Existing activation differences compared to control	Patients showed increased brain activation in frontal eye fields, superior and inferior parietal lobules, and regions within the prefrontal cortex. Peak activation within these prefrontal regions was correlated with increased accuracy and decreased reaction times for the 3-letter task within the group of patients. Correlations between peak activity and behavioral performance were also found in both the right and left superior parietal lobules for the 3-letter task	NA	–
Plank et al., 2013	fMRI + structural MRI	Visual cortex activation (V1–V3 areas) in JMD patients vs controls during retinotopic mapping and visual tasks	Existing activation differences compared to control	NA	Patients with an established PRL had higher activation in early visual cortex during the visual search task, especially when the target stimuli fell in the vicinity of the PRL. Patients with stable eccentric fixation at the PRL exhibited greater performance levels and more brain activation compared with those with unstable eccentric fixation	–

(Continued)

TABLE 3 | Continued

Author, year	Methods	Parameter analyzed	Outcomes	Principal results		Secondary results
				AMD	**JMD**	
Plank et al., 2014	fMRI	Visual cortex activation (V1–V3 areas) in AMD and JMD patients, compared with controls, after training	Cortical activation changes after visual training at eccentric PRL to perform a challenging TDT	Both patients and control subjects exhibited a typical learning effect on the TDT. Training on the TDT enhances eccentric vision in patients with central vision loss, allowing better performances in the task. This enhancement is accompanied by an increased response in in the PRL projection zone of the visual cortex.		–
Plank et al., 2017	fMRI	Activation of visual cortex and other ROIs during stimulation of PRL and oppPRL with flickering check board or object pictures, in JMD. (ROIs: areas 17-18 Brodmann; lateral occipital complex, fusiform cortex, and inferior temporal grus)	Differences in cortical activation by stimulating PRL and oppPRL.	NA	(1) PRL stimulation, especially in patients with highly stable eccentric fixation, caused activation of early visual cortex and higher visual areas. (2) PRL stimulation caused higher activation than oppPRL (3) PRL stimulation produced coactivation of the central representation area in early visual cortex in patients, but not in controls.	Stimulation with everyday objects led to larger responses than flickering checkerboards
Rosengarth et al., 2013	fMRI	Cortical activation and Gray and White matter density changes after fixation training in AMD patients and controls	Existing differences before/after training, and in comparison to control	(1) Positive correlation between achieved fixation stability and cortical response in the PRL-projection zones. (2) Increments in Gray and White matter density in the cerebellum after training	NA	–
Lešták et al., 2013	fMRI	Visual cortex activation by retinal stimulation	Existing differences in cortical responses between AMD patients and controls	Lower fMRI activity of the visual cortex in wet form of AMD compared with the control group.	–	Dependence of fMRI activity on visual acuity was not statistically significant

(Continued)

TABLE 3 | Continued

Author, year	Methods	Parameter analyzed	Outcomes	Principal results		Secondary results
				AMD	**JMD**	
Liu et al., 2010	fMRI	Visual cortex activation by retinal stimulation (Six ROIs along the calcarine sulcus, from posterior pole of the occipital cortex to anterior part of the calcarine)	Existing differences in cortical activation generated by stimuli at PRL or non-PRL locations in AMD, JMD and controls.	(1) Small stimulus at the PRL generated more extensive cortical activation than at a non-PRL location, but no activation in the fovea cortical projection. (2) Both passive and active viewing of full-field stimuli left a silent zone at the posterior pole of the occipital cortex, even if smaller in case of active viewing during a visual task, especially in subject suffering from JMD Since activity in cortical areas corresponding to central scotoma projection is considered evidence for functional reorganization, these results suggested a certain degree of functional reorganization in early visual cortex in both JMD and AMD, even if not complete, and apparently more prominent in JMD.		–
Baseler et al., 2011	fMRI + structural MRI	Cortical response of calcarine sulcus (peripheral retina), occipital pole (fovea) and non-visual cortex after passive visual stimulation	To compare responses presented by AMD patients, JMD patients and controls. All patients using PRLs.	(1) No difference in response of lesion projection zone between patients and controls (simulating scotoma) (2) 'Ectopic' receptive fields areas were detected in lesion projection zone equally in both patients and controls Questioning if responses in V1 in patients with macular degeneration has to be explained by occurred remapping or as an effect given by neuronal feedback and lateral connections		Findings were not dependent on the age at which the individuals acquired retinal lesions
Masuda et al., 2008	fMRI	Visual cortex activation (V1 area, particularri LPZ)	To determine cortical response to different visual stimuli (checkerboards, drifting contrast patterns, scrambled, intact faces) directed toward PRL (in JMD) or a retinal location that corresponded to PRL (in controls)	NA	Significant responses were observed in the LPZ only when performing stimulus-related tasks. No significant cortical activation was recorded during passive viewing or visual tasks unrelated to stimulus In controls peripherap retinal stimulation did not produce response in foveal projection zone	–

(Continued)

TABLE 3 | Continued

Author, year	Methods	Parameter analyzed	Outcomes	Principal results		Secondary results
				AMD	**JMD**	
Baker et al., 2008	fMRI	Measure the magnitude of response in cortical regions corresponding to the representation of the fovea in occipital pole.	To compare the response to stimuli presented at the fovea and PRL in JMD and AMD (divided in foveal damage and fovea residual function) and control groups.	(1) MD with foveal damage: stimuli presented at the PRL elicited strong responses in the occipital pole while stimuli presented at the fovea elicited little or no response. (2) MD with fovea residual function: stimulation of the fovea produced weak activation of the occipital pole. Stimulation of PRL produced no activation. (3) Control participants: no activation of investigated areas for stimuli presented to peripheral retina (corresponding to the matched MD participant's PRL).		–
Whitson et al., 2015	fMRI	Activation of ROI involved in networks that support executive function, language and/or vision during a phonemic fluency test in AMD patients (ROIs: Left opercular portion of inferior frontal gyrus, left superior temporal gyrus, inferior parietal lobe, right superior parietal lobe, right supramarginal gyrus, right supplementary motor area, right precentral gyrus)	To examine the relationship between fMRI measures of rsFC (*Resting-state functional connectivity)*, across several preselected functional networks, and behavioral assessment of phonemic fluency (obtained prior to the scanning session) in individuals with AMD	AMD subjects phonemic fluency resulted inversely related to the existing connectivity among these areas: patients with stronger connections exhibited worse fluency. In controls there was no correlation between connectivity and fluency.	NA	–
Schumacher et al., 2008	fMRI	Activation of visual cortex (ROI: alcarine sulcus)	To measure brain activity in calcarine sulcus while visually stimulating PRL, non-PRL in AMD/JMD patients and corresponding retinal areas in controls	MD patients showed more brain activity in posterior calcarine sulcus (i.e., the foveal confluence) in response to visual stimulation of their PRL than in response to stimulation of other visual field sections (e.g., non-PRL), or corresponding retinal areas in age-matched controls		–
Haak et al., 2016	fMRI + connective modeling	BOLD responses and connective field modeling which estimates a voxel's population receptive field (pRF) toward estimating a voxel's connective field.	To determine whether the functional connectivity between the input-deprived portions of V1 and V2/3 is still retinotopically organized.	NA	Functional connectivity between the input-deprived portions of visual areas V1 and extrastriate cortex is still largely retinotopically organized in MD, although on average less than in controls.	–

FEFs, frontal eye fields; SMA/SEFs, supplementary eye fields; IPS, intraparietal sulci; V1, primary visual area; V2/V3, secondary and tertiary visual area; PRL, Preferred Retinal Locus; oppPRL, retinal area comparable to PRL but in the opposite hemifield; TDT, texture discrimination task; MT/V5, visual motion regions; PFC, prefrontal cortex; LPZ, Lesion Projection Zone.

Baker et al. (2008) conducted a study in which seven subjects affected by JMD or AMD and seven healthy controls viewed blocks of images, recording activation of the occipital cortex using fMRI. In two of the affected subjects, MD preserved foveal function, while the other ones used a PRL. Images were presented at either a foveal or a peripheral retinal location (PRL or a matched location in controls). After PRL stimulation, patients with foveal damage elicited strong responses of cortical regions corresponding to the foveal representation, while stimuli presented at the fovea evoked little or no response. On the other hand, subjects with still foveal residual function produced a response after its stimulation, even if weak, while stimulation of a corresponding PRL produced no activation of these areas. In controls, stimuli presented to the corresponding PRL retinal point did not produce any response in the analyzed areas; on the contrary, stimuli presented at the fovea produced a strong response. The conclusion was that large-scale reorganization of visual processing occurs only in the complete absence of functional foveal vision.

Whitson et al. (2015) examined the relationship between vision impairment caused by AMD and poor performance on phonemic fluency tests, using fMRI in seven subjects with long-standing bilateral AMD. In particular, activation of several ROIs was investigated: left opercular portion of inferior frontal gyrus (which includes Broca's area), left superior temporal gyrus (which includes part of Wernicke's area), inferior parietal lobe, right superior parietal lobe, right supramarginal gyrus, right supplementary motor area, and right precentral gyrus. All these areas are involved in networks that support executive function, language, and vision during a phonemic fluency test. In AMD subjects, phonemic fluency was inversely related to the existing connectivity among these areas, since patients with stronger connections exhibited worse fluency; meanwhile, in controls, there was no correlation between connectivity and fluency. So compared with controls, patients showed stronger connectivity within these areas, but these findings were not an unequivocal explanation: it was not clear if they simply reflected the increased cognitive effort required to support this kind of task in the context of non-specific age-related brain changes or, rather, some compensatory changes to support cortical elaboration in a setting of reduced vision.

Schumacher et al. (2008) evaluated calcarine sulcus activity during visual stimulation in AMD and JMD patients compared with controls using fMRI. Cortical response was recorded during stimulation of both PRL and non-PRL retinal areas in patients, and peripheral retinal loci in controls, by using a checkerboard pattern. Cortical activity of the posterior calcarine sulcus in response to visual stimulation of PRL was higher than that of non-PRL in patients and than that of PRL-corresponding regions in a group of age-matched controls, possibly implying that a large-scale cortical reorganization of visual processing occurred in response to MD.

Haak et al. (2016) studied 8 patients with Stargardt's disease and 12 healthy controls, using fMRI and connective field modeling, to establish whether connectivity between input-deprived portions of the primary visual cortex (V1) and early extrastriate areas (V2/V3) was still retinotopically organized. The study showed that functional connectivity between V1 and V2/V3 was still largely retinotopically organized, although less than that in controls, concluding that despite the prolonged lack of visual input due to MD, corticocortical connections of the primary visual cortex remained largely intact.

DISCUSSION

Hereditary and age-related macular dystrophies, diseases with great epidemiological and social weight, lead to a loss of photoreceptors in the macular area (Holz et al., 2004; Takahashi et al., 2016; Chirco et al., 2017), resulting in central visual field defect (Scullica and Falsini, 2001; Gehrs et al., 2006; Cassels et al., 2017) and implying an inadequate input from this part of the retina to the visual cortex. It has been largely debated whether this could lead to a change and to a reorganization of the retinotopic maps in the visual cortex, thanks to neuronal plasticity (Kitajima et al., 1997; Dreher et al., 2001; Sunness et al., 2004; Baker et al., 2005; Baseler et al., 2009; Dilks et al., 2009, 2014; Masuda et al., 2010; Chung, 2013; Barton and Brewer, 2015). Actually, the ability to adapt to lesions by a mechanism of neuronal plasticity has already been demonstrated in the CNS of both young subjects and, although to a lesser degree, adult subjects (Rosa et al., 2013). So there are reasons to question whether such an eventuality can also occur in cerebral visual areas. A clue in favor of such a thesis could come from studies conducted on animal models: experiments concerning reorganization of the primary visual cortex following retinal lesions has been performed by several authors.

Kaas et al. (1990) analyzed cortical modifications in adult cats after iatrogenic lesion of the central retinal area of one eye and enucleation of the other eye, recording single-neuron responses from the primary visual cortex: it was detected that neurons originally receiving inputs from the central retina became responsive to stimuli presented to intact peripheral retinal locations surrounding the destroyed area. This result can suggest a reorganization of the visual cortex: neurons in the deprived zone of the cortex acquired new receptive fields representing inputs originating from retinal locations around the margins of the lesion.

Similarly, Heinen and Skavenski (1991) described that in adult monkeys, after bilateral macular lesions, cortical neurons in foveal representation became responsive to visual stimuli presented to intact peripheral retina 2.5 months after lesions.

Again, Botelho et al. (2014) observed how monocular lesions in monkeys caused a significant reorganization of the topographic map in the visual area, both inside and outside the cortical LPZ, starting immediately after the retinal lesion. The short time frame observed in this case between macular lesion and cortical reorganization allowed us to assume the preexistence of intracortical connections in V1 unmasked by cortical deafferentation.

Lastly, mouse visual cortex structural modifications, represented by a rapid and lasting reduction in the number of cell spines of inhibitory neurons after removal of visual input, were described by Keck et al. (2011).

Analysis of Structural Results

All reviewed studies found cerebral structural changes in terms of reduced volume following MD, suggesting how a central scotoma, even if acquired later in life, can lead to transsynaptic degeneration. These modifications involved both gray and white matter, eventually all along the entire visual pathway from the optic nerve to the cortex. These results are consistent with the current knowledge that gives to the neuronal afferents not only a task of transmission of information but also a trophic effect toward target cells. A structural consequence is therefore undoubted, but with the volumetric analysis alone, it is difficult to understand if, along with a variation due to the ceased trophic effect by afferent innervation, there is also a variation related to a reshaping/reorganization. Some structural results are worthy of attention:

- Regarding visual cortex volume, a reduction in both anterior and posterior thickness was recorded in AMD as well as JMD patients. So, as central vision is represented in the posterior region of the visual cortex, not only could cortical damage be related to a degeneration due to retinotopic-specific deprivation, but further explanations of the anterior modifications could also be given by an effect of spontaneous oscillatory spike bursts that retinal ganglion cells were demonstrated to produce after retinal degenerations, as well as by a changed function that the more peripheral retina acquires in MD patients due to the selection of a new PRL to obtain an eccentric fixation (Prins et al., 2016).
- Moreover, in the comparison of the results between AMD and JMD groups, some differences emerged (Hernowo et al., 2014; Prins et al., 2016): in JMD, a more extensive damage was identified in terms of both involved structure amount (the whole optical pathway, from the optic nerve to the cortex, while only from lateral genicolate bodies in AMD) and volumetric reduction. In the two reference studies, however, this outcome was considered, rather than as a marker of reshaping, as the effect of JMD patients having more severe retinal alterations and greater visual deficits if compared to AMD patients.
- Potential structural indicators of remodeling that occurred come from Plank et al. (2011) and Boucard et al. (2009): an increased volume at the level of supramarginal gyrus, involved in oculomotor coordination, and a positive correlation between gray matter in right superior and middle frontal gyri and fixation stability were findings that could be the consequence of oculomotor learning in patients with central scotoma, forced to use their own peripheral visual field to obtain an eccentric fixation.

Analysis of Functional Results

Studies using functional imaging to analyze cortical activity in MD patients produced variable results, generating some controversy:

- All studies have shown changes in cortical activity; in particular, the visual cortex activation pattern was different and less intense if compared to healthy controls (Lešťák et al., 2013). It should be noted, however, that in addition to the expected changes in the occipital lobe, there was also an increase in activity of frontal brain areas (frontal eye fields, supplementary eye fields, prefrontal cortex, and intraparietal sulci), classically associated with attention (Little et al., 2008; Szlyk and Little, 2009): this suggests that an adaptation of the brain occurred, although not clearly indicative of remodeling. It can be assumed that, in patients trying to overcome the impaired visual function using paracentral PRL, the incongruence between gaze direction and visual input elaboration, normally closely associated, results in an increased activation of attentional networks as a compensatory behavior and, thus, that integrity of these cerebral areas is necessary for the use of PRL as a new main point of visual processing outside the diseased fovea.
- Oculomotor training, mainly aimed at the use of a PRL to obtain stability in eccentric fixation, has a positive effect on the performances obtained in the visual task (Plank et al., 2014). These effects are accompanied both by structural changes in the cerebellum (Rosengarth et al., 2013) and by interesting functional changes, where PRL stimulation generates a response of the LPZ, and greater fixation stability corresponds to a greater consequent activation (Plank et al., 2017).
- In multiple occasions, PRL stimulation was investigated: in patients using PRL for visual elaboration, its stimulation has proven to trigger a more extensive visual cortical activation than in patients not using it (Plank et al., 2013); in particular, stimulation of the PRL was able in some studies to activate that very cortical area normally receiving input from the lesioned macula (Baker et al., 2008; Masuda et al., 2008; Schumacher et al., 2008; Plank et al., 2017) but not in all of them (Liu et al., 2010). However, in another one, PRL stimulation did not give any significant difference in response to the control group in whom a central scotoma was simulated.
- Even attention was found to influence cortical activation in the LPZ. In some JMD patients (Masuda et al., 2008; Liu et al., 2010), this area was activated during visual tasks, in contrast with passive viewing stimulation. It is not certain whether this finding can simply be justified by the unmasking of preexisting feedback signals from higher visual areas and by the upregulation of existing synaptic connections or instead if it can be a signal of a large-scale reorganization that occurred. It should be noted that there is one study that did not detect the activation of LPZ by the PRL by using only passive visual stimuli, without visual task.
- The nature of the stimulus seems also to influence brain response (Plank et al., 2017): object pictures were found to elicit stronger responses of the central representation area in the visual cortex than did the flickering checkerboard, probably due to feedback projections from higher visual areas.
- Finally, against the hypothesis of remodeling, it was pointed out by Haak et al. (2016) that a retinotopic organization of

the visual cortex has proven to persist although long after the deafferentation generated by AMD, even if decreased in comparison to healthy controls.

Possible Causes of Cerebral Changes in MD Patients

Causes of cerebral changes in MD patients appear therefore to be multifarious and not completely understood. Retinal degeneration in MD subjects led to a reduction of neuronal volume along specific parts of the visual pathway: as already mentioned above, functional deprivation is presumably responsible for a part of the structural changes, as also suggested by animal experimental models (Vercelli and Cracco, 1994; Palanza et al., 2002), maybe by anterograde transsynaptic degeneration (Medeiros and Curcio, 2001; Kim et al., 2002). However, it is not clear yet whether this could be the only explanation; other reasons might be its weight and whether the CNS changes in volume and density could also be associated with a plastic remodeling, for example, as a consequence of oculomotor training. In the analysis of functional studies, it has been reported that there is a variation not only in occipital cortical activation, as could be expected, but interestingly also in other areas not immediately related with the visual elaboration, suggesting that, if not a remodeling, at least an adaptation to the new situation with the involvement of other cortical functions had occurred in order to compensate for the pathological condition, for example, to support a more complex activity of fixation. Oculomotor training has proven to be able both to improve the patient's performance and to cause functional and structural changes in the brain and cerebellum.

Extremely interesting was the analysis of cortical activity in relation to PRL: in patients able to use a PRL, its stimulation increased the occipital cortical activity and even caused the activation of LPZ, the cortical area normally activated by stimulation of the fovea being now damaged. This result strongly suggests the idea of a successful remodeling occurring in terms of receptive fields, but as rightly pointed out by some authors (Masuda et al., 2008), functional analysis does not allow us to discern whether this is related to a true neuronal plasticity or simply to preexisting conditions (feedback from extrastriate cortex, unmasking of preexisting task-dependent cortical signals that ordinarily are suppressed by the retinal visual input, and lateral connections). Even the results (Masuda et al., 2008) regarding how attention (visual task) affects the activation of visual cortex and LPZ do not clearly clarify whether such observations are related to a remodeling or an unmasking of preexisting synaptic connections.

It is, however, very important to emphasize as some results go in an opposite sense: Liu et al. (2010) and Baseler did not find any evidence of an increased activation of the visual cortex part normally receiving input from the lesioned retina, and Haak et al. (2016) showed that functional connectivity between V1 and V2–V3 was still largely retinotopically organized despite a prolonged lack of visual input due to MD. Is it therefore really possible that in an adult SNC a plastic remodeling can take place? Even though cerebral plasticity during childhood is a well-established phenomenon, adult plasticity remains actually elusive. The ability of the cerebral cortex to adapt to changes in visual experience and the mechanisms underlying this process are still highly debated (Wandell and Smirnakis, 2009). Nevertheless, many human studies have suggested that, during the life span, the visual cortex maintains the ability to structurally and functionally reorganize itself; two types of neuroplasticity are involved, although their borders are not well defined: structural and synaptic/functional plasticity. Structural plasticity refers to changes in axons, dendrites, and dendritic spines; synaptic plasticity refers to changes in synaptic activity (Rosa et al., 2013). Visual cortical plasticity was also proven in healthy subjects in the absence of visual loss as consequence of training (Berry and Nedivi, 2016).

We are therefore justified in assuming that cerebral remodeling, based on neuronal plasticity, could probably also take place in conditions of MD.

Limits

It has been impossible to standardize the results available in literature due to the low sample size of the existing studies and the variability of intersubject anatomy, demographic characteristics, cortical reconstruction, and ROI identification. The extension and severity of maculopathy, the duration of the disease, and the type of lesions were also heterogeneous.

Moreover, as regards the fMRI studies, there was also a great variability in the kind of stimuli used, and the use of the task-related fMRI is another potential source of variability, if compared for example to the resting-state fMRI.

Therapeutic Perspectives

Neuronal reorganization is undoubtedly useful in compensating for the deficit caused by MD and above all in being able to take full advantage of the rehabilitation possibilities, such as through oculomotor training aimed at using PRL, as described above. But would remodeling always be considered a positive occurrence? It is interesting to observe how the stability of visual neuronal organization may be beneficial: many of the most promising treatments aimed at restoring vision at a retinal level, such as antiangiogenic injections or more pioneering ones such as retinal prostheses, stem cell therapy, or even genetic therapy, rely on the assumption that cortical circuitry remains largely unchanged.

So such changes would first need to be reversed before the restored inputs could be normally processed. Structural changes also, especially in terms of volume reduction caused by the ceased trophic effect, could be a tough challenge, and we do not know at this time if it could be possible to bypass this obstacle or whether the visual brain would no longer be able to process retinal inputs appropriately.

That said, worthy of research is the possibility of stimulating neuronal plasticity to our advantage: perineuronal nets were found to control and contrast plasticity in the adult CNS (Sorg et al., 2016), as demonstrated by studies about neuronal axon regeneration. An eligible candidate to fight this effect seems to come from digestion of their glycosaminoglycan chains, thanks to the enzyme chondroitinase ABC (*ChABC*): interestingly, administration of ChABC after spinal cord injury

permits some axon regeneration and greatly increases plasticity, and when combined with appropriate rehabilitation, ChABC treatment can lead to a considerable restoration of function, even in patients with neurodegenerative diseases (Fawcett, 2015). Since rehabilitation attempts through exercises and oculomotor training (Rosengarth et al., 2013; Plank et al., 2014, 2017) can be a worthwhile option but can achieve results only if these structural and functional modifications in the visual system occur, we can imagine, as a possible future therapeutic perspective, a combination of specific oculomotor and visual training and pharmacological stimulation of neuroplasticity aimed at obtaining a percentage of improvement in both AMD and JMD patients (Kwok et al., 2008; Fawcett, 2009; Yang et al., 2015; de Winter et al., 2016; Restani and Caleo, 2016; Foscarin et al., 2017).

CONCLUSION

Through this systematic review, we highlighted how several brain modifications, both structural and functional ones, have been recorded in both AMD and JMD. Results were, however, heterogeneous and not always with unequivocal interpretations, not clearly demonstrating the existence of neuronal remodeling following macular damage, although it would seem that there exist more data in favor of this hypothesis than against it. It is quite possible that, after a retinal damage, both plastic remodeling and reorganization based on the unmasking of preexisting circuits may occur in these patients.

In subjects who have carried out ocular training exercises, for example, aimed at using a PRL as the new main area of light elaboration or obtaining stable eccentric fixation, the greatest cortical activities were recorded and achieved best performances in visual tasks. Although the possibility of a brain circuit remodeling would not be beneficial for all possible future therapeutic strategies, as it could hinder the correct processing of light signal once retinal function would be restored, it would support this kind of rehabilitation therapy which, as demonstrated, requires structural and functional modifications, as well as the involvement of upper cortical areas.

Further studies are therefore needed, preferably with greater sample size and more standardized in patient characteristics, disease entity, stimulus type, and analysis, in order to obtain more evidence of remodeling occurrence and how to use it in a therapeutic key, but we can imagine, as a possible future, a combination of specific oculomotor training and biochemical stimulation of neuroplasticity aimed at obtaining a percentage of improvement in both AMD and JMD patients.

AUTHOR CONTRIBUTIONS

All authors gave their substantial contribution to conception and design of the manuscript and to the acquisition and interpretation of data and materials. All authors gave their contribution in drafting the manuscript and in its critical revision for important intellectual content. All authors have approved the manuscript in its present form for publication. All authors agreed to be accountable for all aspects of the work in ensuring that questions related to the accuracy or integrity of any part of the work are appropriately investigated and resolved.

REFERENCES

Altschwager, P., Ambrosio, L., Swanson, E. A., Moskowitz, A., and Fulton, A. B. (2017). Juvenile macular degenerations. *Semin. Pediatr. Neurol.* 24, 104–109. doi: 10.1016/j.spen.2017.05.005

Andrade, M. A., Muro, E. M., and Morán, F. (2001). Simulation of plasticity in the adult visual cortex. *Biol. Cybern.* 84, 445–451. doi: 10.1007/PL00007988

Ashburner, J., and Friston, K. J. (2000). Voxel-based morphometry—the methods. *Neuroimage* 11, 805–821. doi: 10.1006/nimg.2000.0582

Baker, C. I., Dilks, D. D., Peli, E., and Kanwisher, N. (2008). Reorganization of visual processing in macular degeneration: replication and clues about the role of foveal loss. *Vis. Res.* 48, 1910–1919. doi: 10.1016/j.visres.2008.05.020

Baker, C. I., Peli, E., Knouf, N., and Kanwisher, N. G. (2005). Reorganization of visual processing in macular degeneration. *J. Neurosci.* 25, 614–618. doi: 10.1523/JNEUROSCI.3476-04.2005

Barton, B., and Brewer, A. A. (2015). fMRI of the rod scotoma elucidates cortical rod pathways and implications for lesion measurements. *Proc. Natl. Acad. Sci. U.S.A.* 112, 5201–5206. doi: 10.1073/pnas.1423673112

Baseler, H. A., Gouws, A., Haak, K. V., Racey, C., Crossland, M. D., Tufail, A., et al. (2011). Large-scale remapping of visual cortex is absent in adult humans with macular degeneration. *Nat. Neurosci.* 14, 649–655. doi: 10.1038/nn.2793

Baseler, H. A., Gouws, A., and Morland, A. B. (2009). The organization of the visual cortex in patients with scotomata resulting from lesions of the central retina. *Neuro Ophthalmol.* 33, 149–157. doi: 10.1080/01658100903050053

Berry, K. P., and Nedivi, E. (2016). Experience-dependent structural plasticity in the visual system. *Annu. Rev. Vis. Sci.* 2, 17–35. doi: 10.1146/annurev-vision-111815-114638

Blodi, C. F., and Stone, E. M. (1990). Best's vitelliform dystrophy. *Ophthalm. Paediatr. Genet.* 11, 49–59.

Bondarenko, M. T., Zhorzholadze, N. V., Sheremet, N. L., Ronzina, I. A., Galoian, N. S., Loginova, A. N., et al. (2014). Stargardt's disease and abiotrophy of franceschetti (fundus flavimaculatus): pathogenetic, clinical, and molecular genetic characteristics. *Vestn. Oftalmol.* 130, 72–76.

Botelho, E. P., Ceriatte, C., Soares, J. G. M., Gattass, R., and Fiorani, M. (2014). Quantification of early stages of cortical reorganization of the topographic map of V1 following retinal lesions in monkeys. *Cereb. Cortex* 24, 1–16. doi: 10.1093/cercor/bhs208

Boucard, C. C., Hernowo, A. T., Maguire, R. P., Jansonius, N. M., Roerdink, J. B. T. M., Hooymans, J. M. M., et al. (2009). Changes in cortical grey matter density associated with long-standing retinal visual field defects. *Brain* 132, 1898–1906. doi: 10.1093/brain/awp119

Bowes Rickman, C., Farsiu, S., Toth, C. A., and Klingeborn, M. (2013). *Dry Age-Related Macular Degeneration: Mechanisms, Therapeutic Targets, and Imaging*. Available online at: https://ai2-s2-pdfs.s3.amazonaws.com/be3d/a21d002e310e5e43f79f5d3f1b99fa289e57.pdf (accessed August 8, 2017).

Buschini, E., Piras, A., Nuzzi, R., and Vercelli, A. (2011). Age related macular degeneration and drusen: neuroinflammation in the retina. *Prog. Neurobiol.* 95, 14–25. doi: 10.1016/j.pneurobio.2011.05.011

Cassels, N. K., Wild, J. M., Margrain, T. H., Chong, V., and Acton, J. H. (2017). The use of microperimetry in assessing visual function in age-related macular degeneration. *Surv. Ophthalmol.* 63, 40–55. doi: 10.1016/j.survophthal.2017.05.007

Chirco, K. R., Sohn, E. H., Stone, E. M., Tucker, B. A., and Mullins, R. F. (2017). Structural and molecular changes in the aging choroid: implications for age-related macular degeneration. *Eye* 31, 10–25. doi: 10.1038/eye.2016.216

Chung, S. T. L. (2013). Cortical reorganization after long-term adaptation to retinal lesions in humans. *J. Neurosci.* 33, 18080–18086. doi: 10.1523/JNEUROSCI.2764-13.2013

Clarkson, M. J., Cardoso, M. J., Ridgway, G. R., Modat, M., Leung, K. K., Rohrer, J. D., et al. (2011). A comparison of voxel and surface based cortical thickness estimation methods. *Neuroimage* 57, 856–865. doi: 10.1016/j.neuroimage.2011.05.053

de Winter, F., Kwok, J. C. F., Fawcett, J. W., Vo, T. T., Carulli, D., and Verhaagen, J. (2016). The chemorepulsive protein semaphorin 3A and perineuronal net-mediated plasticity. *Neural Plast.* 2016, 1–14. doi: 10.1155/2016/3679545

Dilks, D. D., Baker, C. I., Peli, E., and Kanwisher, N. (2009). Reorganization of visual processing in macular degeneration is not specific to the & quot preferred retinal locus & quot. *J. Neurosci.* 29, 2768–2773. doi: 10.1523/JNEUROSCI.5258-08.2009

Dilks, D. D., Julian, J. B., Peli, E., and Kanwisher, N. (2014). Reorganization of visual processing in age-related macular degeneration depends on foveal loss. *Optom. Vis. Sci.* 91, e199–e206. doi: 10.1097/OPX.0000000000000325

Dreher, B., Burke, W., and Calford, M. B. (2001). Cortical plasticity revealed by circumscribed retinal lesions or artificial scotomas. *Prog. Brain Res.* 134, 217–246. doi: 10.1016/s0079-6123(01)34016-5

Fawcett, J. (2009). Molecular control of brain plasticity and repair. *Prog. Brain Res.* 175, 501–509. doi: 10.1016/S0079-6123(09)17534-9

Fawcett, J. W. (2015). The extracellular matrix in plasticity and regeneration after CNS injury and neurodegenerative disease. *Prog. Brain Res.* 218, 213–226. doi: 10.1016/bs.pbr.2015.02.001

Foscarin, S., Raha-Chowdhury, R., Fawcett, J. W., and Kwok, J. C. F. (2017). Brain ageing changes proteoglycan sulfation, rendering perineuronal nets more inhibitory. *Aging* 9, 1607–1622. doi: 10.18632/aging.101256

Gehrs, K. M., Anderson, D. H., Johnson, L. V., and Hageman, G. S. (2006). Age-related macular degeneration–emerging pathogenetic and therapeutic concepts. *Ann. Med.* 38, 450–471. doi: 10.1080/07853890600946724

Haak, K. V., Morland, A. B., Rubin, G. S., and Cornelissen, F. W. (2016). Preserved retinotopic brain connectivity in macular degeneration. *Ophthalm. Physiol. Opt.* 36, 335–343. doi: 10.1111/opo.12279

Heinen, S. J., and Skavenski, A. A. (1991). Recovery of visual responses in foveal V1 neurons following bilateral foveal lesions in adult monkey. *Exp. Brain Res.* 83, 670–674. doi: 10.1007/BF00229845

Hernowo, A. T., Prins, D., Baseler, H. A., Plank, T., Gouws, A. D., Hooymans, J. M. M., et al. (2014). Morphometric analyses of the visual pathways inmacular degeneration. *Cortex* 56, 99–110. doi: 10.1016/j.cortex.2013.01.003

Hohman, T. C. (2017). Hereditary retinal dystrophy. *Handb. Exper. Pharmacol.* 242, 337–367. doi: 10.1007/164_2016_91

Holz, F. G., Pauleikhoff, D., Klein, R., and Bird, A. C. (2004). Pathogenesis of lesions in late age-related macular disease. *Am. J. Ophthalmol.* 137, 504–510. doi: 10.1016/j.ajo.2003.11.026

Jonas, J. B., Bourne, R. R. A., White, R. A., Flaxman, S. R., Keeffe, J., Leasher, J., et al. (2014). Visual impairment and blindness due to macular diseases globally: a systematic review and meta-analysis. *Am. J. Ophthalmol.* 158, 808–815. doi: 10.1016/j.ajo.2014.06.012

Kaas, J. H., Krubitzer, L. A., Chino, Y. M., Langston, A. L., Polley, E. H., and Blair, N. (1990). Reorganization of retinotopic cortical maps in adult mammals after lesions of the retina. *Science* 248, 229–231. doi: 10.1126/science.2326637

Keck, T., Scheuss, V., Jacobsen, R. I., Wierenga, C. J., Eysel, U. T., Bonhoeffer, T., et al. (2011). Loss of sensory input causes rapid structural changes of inhibitory neurons in adult mouse visual cortex. *Neuron* 71, 869–882. doi: 10.1016/j.neuron.2011.06.034

Kim, S. Y., Sadda, S., Humayun, M. S., de Juan, E., Melia, B. M., and Green, W. R. (2002). Morphometric analysis of the macula in eyes with geographic atrophy due to age-related macular degeneration. *Retina* 22, 464–470. doi: 10.1097/00006982-200208000-00011

Kitajima, M., Korogi, Y., Hirai, T., Hamatake, S., Ikushima, I., Sugahara, T., et al. (1997). MR changes in the calcarine area resulting from retinal degeneration. *AJNR Am. J. Neuroradiol.* 18, 1291–1295.

Knudtson, M. D., Klein, B. E. K., Klein, R., Cruickshanks, K. J., and Lee, K. E. (2005). Age-related eye disease, quality of life, and functional activity. *Arch. Ophthalmol.* 123:807. doi: 10.1001/archopht.123.6.807

Kollias, S. S. (2004). Investigations of the human visual system using functional magnetic resonance imaging (FMRI). *Eur. J. Radiol.* 49, 64–75. doi: 10.1016/j.ejrad.2003.09.005

Kwok, J. C. F., Afshari, F., García-Alías, G., and Fawcett, J. W. (2008). Proteoglycans in the central nervous system: plasticity, regeneration and their stimulation with chondroitinase ABC. *Restor. Neurol. Neurosci.* 26, 131–145.

Lešťák, J., Tintìra, J., Karel, I., Svatá, Z., and Rozsíval, P. (2013). functional magnetic resonance imaging in patients with the wet form of age-related macular degeneration. *Neuro Ophthalmol.* 37, 192–197. doi: 10.3109/01658107.2013.819581

Little, D. M., Thulborn, K. R., and Szlyk, J. P. (2008). An fMRI study of saccadic and smooth-pursuit eye movement control in patients with age-related macular degeneration. *Investig. Opthalmol. Vis. Sci.* 49, 1728–1738. doi: 10.1167/iovs.07-0372

Liu, T., Cheung, S. H., Schuchard, R. A., Glielmi, C. B., Hu, X., He, S., et al. (2010). Incomplete cortical reorganization in macular degeneration. *Investig. Ophthalmol. Vis. Sci.* 51, 6826–6834. doi: 10.1167/iovs.09-4926

Masuda, Y., Dumoulin, S. O., Nakadomari, S., and Wandell, B. A. (2008). V1 projection zone signals in human macular degeneration depend on task, not stimulus. *Cereb. Cortex* 18, 2483–2493. doi: 10.1093/cercor/bhm256

Masuda, Y., Horiguchi, H., Dumoulin, S. O., Furuta, A., Miyauchi, S., Nakadomari, S., et al. (2010). Task-dependent V1 responses in human retinitis pigmentosa. *Investig. Opthalmol. Vis. Sci.* 51:5356. doi: 10.1167/iovs.09-4775

Medeiros, N. E., and Curcio, C. A. (2001). Preservation of ganglion cell layer neurons in age-related macular degeneration. *Investig. Opthalmol. Vis. Sci.* 42, 795–803.

Miki, A., Haselgrove, J. C., and Liu, G. T. (2002). Functional magnetic resonance imaging and its clinical utility in patients with visual disturbances. *Surv. Ophthalmol.* 47, 562–579. doi: 10.1016/S0039-6257(02)00356-9

Miki, A., Liu, G. T., Modestino, E. J., Liu, C. S., Bonhomme, G. R., Dobre, C. M., et al. (2001). Functional magnetic resonance imaging of the visual system. *Curr. Opin. Ophthalmol.* 12, 423–431.

Molday, R. S. (2015). Insights into the molecular properties of ABCA4 and its role in the visual cycle and stargardt disease. *Prog. Mol. Biol. Transl. Sci.* 134, 415–431. doi: 10.1016/bs.pmbts.2015.06.008

North, V., Gelman, R., and Tsang, S. H. (2014). Juvenile-onset macular degeneration and allied disorders. *Dev. Ophthalmol.* 53, 44–52. doi: 10.1159/000357293

Nuzzi, R., Buschini, E., Monteu, F., and Vercelli, A. (2017). Blindsight: the anatomical, and functional post-injury neural plasticity of the visual system. *J. Neurol. Neurosci.* 8:3. doi: 10.21767/2171-6625.1000191

Olivo, G., Melillo, P., Cocozza, S., D'Alterio, F. M., Prinster, A., Testa, F., et al. (2015). Cerebral involvement in stargardt's disease: a VBM and TBSS study. *Investig. Opthalmol. Vis. Sci.* 56, 7388–7397. doi: 10.1167/iovs.15-16899.7

Palanza, L., Nuzzi, R., Repici, M., and Vercelli, A. (2002). Ganglion cell apoptosis and increased number of NADPH-d-positive neurones in the rodent retina in an experimental model of glaucoma. *Acta Ophthalmol. Scand. Suppl.* 236, 47–48. doi: 10.1034/j.1600-0420.80.s236.27.x

Palejwala, N. V., Gale, M. J., Clark, R. F., Schlechter, C., Weleber, R. G., and Pennesi, M. E. (2016). Insight into autosomal dominant Stargardt-like macular dystrophy through multimodal diagnostic imaging. *Retina* 36, 119–130. doi: 10.1097/IAE.0000000000000659

Pascolini, D., and Mariotti, S. P. (2012). Global estimates of visual impairment: 2010. *Br. J. Ophthalmol.* 96, 614–618. doi: 10.1136/bjophthalmol-2011-300539

Pi, L.-H., Chen, L., Liu, Q., Ke, N., Fang, J., Zhang, S., et al. (2012). Prevalence of eye diseases and causes of visual impairment in school-aged children in Western China. *J. Epidemiol.* 22, 37–44. doi: 10.2188/jea.je20110063

Plank, T., Frolo, J., Brandl-ru, S., Renner, A. B., Jagle, H., and Greenlee, M. W. (2017). fMRI with central vision loss: effects of fixation locus and stimulus type. *Optom. Vis. Sci.* 94, 297–310. doi: 10.1097/OPX.0000000000001047

Plank, T., Frolo, J., Brandl-Rühle, S., Renner, A. B., Hufendiek, K., Helbig, H., et al. (2011). Gray matter alterations in visual cortex of patients with loss of central vision due to hereditary retinal dystrophies. *Neuroimage* 56, 1556–1565. doi: 10.1016/j.neuroimage.2011.02.055

Plank, T., Frolo, J., Farzana, F., Brandl-Rühle, S., Renner, A. B., and Greenlee, M. W. (2013). Neural correlates of visual search in patients with hereditary retinal dystrophies. *Hum. Brain Mapp.* 34, 2607–2623. doi: 10.1002/hbm.22088

Plank, T., Rosengarth, K., Schmalhofer, C., Goldhacker, M., Brandl-Rühle, S., and Greenlee, M. W. (2014). Perceptual learning in patients with macular degeneration. *Front. Psychol.* 5:1189. doi: 10.3389/fpsyg.2014.01189

Prins, D., Plank, T., Baseler, H. A., Gouws, A. D., Beer, A., Morland, A. B., et al. (2016). Surface-based analyses of anatomical properties of the visual cortex in macular degeneration. *PLoS One* 11:146684. doi: 10.1371/journal.pone.0146684

Restani, L., and Caleo, M. (2016). Reorganization of visual callosal connections following alterations of retinal input and brain damage. *Front. Syst. Neurosci.* 10:86. doi: 10.3389/fnsys.2016.00086

Rosa, A. M., Silva, M. F., Ferreira, S., Murta, J., and Castelo-Branco, M. (2013). Plasticity in the human visual cortex: an ophthalmology-based perspective. *Biomed. Res. Int.* 2013, 1–13. doi: 10.1155/2013/568354

Rosengarth, K., Keck, I., Brandl-Rühle, S., Frolo, J., Hufendiek, K., Greenlee, M. W., et al. (2013). Functional and structural brain modifications induced by oculomotor training in patients with age-related macular degeneration. *Front. Psychol.* 4:428. doi: 10.3389/fpsyg.2013.00428

Schumacher, E. H., Jacko, J. A., Primo, S. A., Main, K. L., Moloney, K. P., Kinzel, E. N., et al. (2008). Reorganization of visual processing is related to eccentric viewing in patients with macular degeneration. *Restor. Neurol. Neurosci.* 26, 391–402.

Scilley, K., Jackson, G. R., Cideciyan, A. V., Maguire, M. G., Jacobson, S. G., and Owsley, C. (2002). Early age-related maculopathy and self-reported visual difficulty in daily life2 2The authors have no commercial interests in any device or product mentioned in this article. *Ophthalmology* 109, 1235–1242. doi: 10.1016/S0161-6420(02)01060-6

Scullica, L., and Falsini, B. (2001). Diagnosis and classification of macular degenerations: an approach based on retinal function testing. *Doc. Ophthalmol.* 102, 237–250.

Sorg, B. A., Berretta, S., Blacktop, J. M., Fawcett, J. W., Kitagawa, H., Kwok, J. C. F., et al. (2016). Casting a wide net: role of perineuronal nets in neural plasticity. *J Neurosci* 36, 11459–11468. doi: 10.1523/JNEUROSCI.2351-16.2016

Sunness, J. S., Liu, T., and Yantis, S. (2004). Retinotopic mapping of the visual cortex using functional magnetic resonance imaging in a patient with central scotomas from atrophic macular degeneration. *Ophthalmology* 111, 1595–1598. doi: 10.1016/j.ophtha.2003.12.050

Szlyk, J. P., and Little, D. M. (2009). An fMRI study of word-level recognition and processing in patients with age-related macular degeneration. *Investig. Opthalmol. Vis. Sci.* 50, 4487–4495. doi: 10.1167/iovs.08-2258

Takahashi, A., Ooto, S., Yamashiro, K., Oishi, A., Tamura, H., Nakanishi, H., et al. (2016). Photoreceptor damage and reduction of retinal sensitivity surrounding geographic atrophy in age-related macular degeneration. *Am. J. Ophthalmol.* 168, 260–268. doi: 10.1016/j.ajo.2016.06.006

Tanna, P., Strauss, R. W., Fujinami, K., and Michaelides, M. (2017). Stargardt disease: clinical features, molecular genetics, animal models and therapeutic options. *Br. J. Ophthalmol.* 101, 25–30. doi: 10.1136/bjophthalmol-2016-308823

Van Lookeren Campagne, M., LeCouter, J., Yaspan, B. L., and Ye, W. (2014). Mechanisms of age-related macular degeneration and therapeutic opportunities. *J. Pathol.* 232, 151–164. doi: 10.1002/path.4266

Vercelli, A., and Cracco, C. M. (1994). Effects of eye enucleation on NADPH-diaphorase positive neurons in the superficial layers of the rat superior colliculus. *Brain Res. Dev. Brain Res.* 83, 85–98. doi: 10.1016/0165-3806(94)90182-1

Verdina, T., Giacomelli, G., Sodi, A., Pennino, M., Paggini, C., Murro, V., et al. (2013). Biofeedback rehabilitation of eccentric fixation in ?patients with Stargardt disease. *Eur. J. Ophthalmol.* 23, 723–731. doi: 10.5301/ejo.5000291

Vingolo, E. M., Cavarretta, S., Domanico, D., Parisi, F., and Malagola, R. (2007). Microperimetric Biofeedback in AMD Patients. *Appl. Psychophysiol. Biofeedback* 32, 185–189. doi: 10.1007/s10484-007-9038-6

Wandell, B. A., and Smirnakis, S. M. (2009). Plasticity and stability of visual field maps in adult primary visual cortex. *Nat. Rev. Neurosci.* 10, 873–884. doi: 10.1038/nrn2741

Whitson, H. E., Chou, Y. H., Potter, G. G., Diaz, M. T., Chen, N. K., Lad, E. M., et al. (2015). Phonemic fluency and brain connectivity in age-related macular degeneration: a pilot study. *Brain Connect.* 5, 126–135. doi: 10.1089/brain.2014.0277

Wong, W. L., Su, X., Li, X., Cheung, C. M. G., Klein, R., Cheng, C. Y., et al. (2014). Global prevalence of age-related macular degeneration and disease burden projection for 2020 and 2040: a systematic review and meta-analysis. *Lancet Glob. Heal.* 2, e106–e116. doi: 10.1016/S2214-109X(13)70145-1

Xiao, Q., Hartzell, H. C., and Yu, K. (2010). Bestrophins and retinopathies. *Pflügers Arch. Eur. J. Physiol.* 460, 559–569. doi: 10.1007/s00424-010-0821-5

Yang, S., Cacquevel, M., Saksida, L. M., Bussey, T. J., Schneider, B. L., Aebischer, P., et al. (2015). Perineuronal net digestion with chondroitinase restores memory in mice with tau pathology. *Exp. Neurol.* 265, 48–58. doi: 10.1016/j.expneurol.2014.11.013

Zarbin, M. A. (2004). Current concepts in the pathogenesis of age-related macular degeneration. *Arch. Ophthalmol.* 122, 598–614. doi: 10.1001/archopht.122.4.598

Conflict of Interest: The authors declare that the research was conducted in the absence of any commercial or financial relationships that could be construed as a potential conflict of interest.

Copyright © 2020 Nuzzi, Dallorto and Vitale. This is an open-access article distributed under the terms of the Creative Commons Attribution License (CC BY). The use, distribution or reproduction in other forums is permitted, provided the original author(s) and the copyright owner(s) are credited and that the original publication in this journal is cited, in accordance with accepted academic practice. No use, distribution or reproduction is permitted which does not comply with these terms.

frontiers in Neuroscience

MINI REVIEW
published: 24 September 2020
doi: 10.3389/fnins.2020.588234

Mutation-Independent Therapies for Retinal Diseases: Focus on Gene-Based Approaches

Sabrina Carrella[1,2], Alessia Indrieri[1,3], Brunella Franco[1,4] and Sandro Banfi[1,2]**

[1] Telethon Institute of Genetics and Medicine (TIGEM), Pozzuoli, Italy, [2] Medical Genetics, Department of Precision Medicine, University of Campania "Luigi Vanvitelli", Naples, Italy, [3] Institute for Genetic and Biomedical Research (IRGB), National Research Council (CNR), Milan, Italy, [4] Medical Genetics, Department of Translational Medical Sciences, University of Naples Federico II, Naples, Italy

Gene therapy is proving to be an effective approach to treat or prevent ocular diseases ensuring a targeted, stable, and regulated introduction of exogenous genetic material with therapeutic action. Retinal diseases can be broadly categorized into two groups, namely monogenic and complex (multifactorial) forms. The high genetic heterogeneity of monogenic forms represents a significant limitation to the application of gene-specific therapeutic strategies for a significant fraction of patients. Therefore, mutation-independent therapeutic strategies, acting on common pathways that underly retinal damage, are gaining interest as complementary/alternative approaches for retinal diseases. This review will provide an overview of mutation-independent strategies that rely on the modulation in the retina of key genes regulating such crucial degenerative pathways. In particular, we will describe how gene-based approaches explore the use of neurotrophic factors, microRNAs (miRNAs), genome editing and optogenetics in order to restore/prolong visual function in both outer and inner retinal diseases. We predict that the exploitation of gene delivery procedures applied to mutation/gene independent approaches may provide the answer to the unmet therapeutic need of a large fraction of patients with genetically heterogeneous and complex retinal diseases.

Keywords: retinal disease, mutation-independent, gene therapy, neuroprotection, microRNA, genome editing, optogenetics

OPEN ACCESS

Edited by:
Nicolás Cuenca, University of Alicante, Spain

Reviewed by:
Riccardo Carlo Natoli, Australian National University, Australia
Ilaria Piano, University of Pisa, Italy

****Correspondence:***
Sabrina Carrella
carrella@tigem.it
Sandro Banfi
banfi@tigem.it

Specialty section:
This article was submitted to Neurodegeneration, a section of the journal Frontiers in Neuroscience

Received: *28 July 2020*
Accepted: *02 September 2020*
Published: *24 September 2020*

Citation:
Carrella S, Indrieri A, Franco B and Banfi S (2020) Mutation-Independent Therapies for Retinal Diseases: Focus on Gene-Based Approaches. Front. Neurosci. 14:588234. doi: 10.3389/fnins.2020.588234

INTRODUCTION

The retina is the neuronal tissue in charge of visual function. It comprises five main neuronal types that form morphologically and functionally distinct circuits working, in parallel and in combination, to produce a complex visual output (Hoon et al., 2014; **Figure 1A**). The outer retina (OR) is composed of the Retinal Pigment Epithelium (RPE) and of photoreceptors. The RPE is a monolayer of pigmented cells that contribute to the visual cycle and provide metabolic support to photoreceptors. The latter, subdivided into rods and cones, are the neurons in charge to convert light energy into membrane potential changes in the phototransduction cascade. Rod and cone photoreceptors synapse with neurons of the inner retina (IR), namely bipolar cells, which in turn contact retinal ganglion cells (RGCs) and amacrine cells. The sole output neurons of the retina are RGCs, which project axons, forming the optic nerve, to higher visual centers in the brain (Hoon et al., 2014). Besides neurons, the retina contains a glial component, represented by Müller cells, astrocytes, and the microglia. Müller cells account for about 90% of the retinal glia and, together with astrocytes, provide neurotrophic, metabolic and mechanical support to neurons. Microglia

constitute the resident immune cell population in the retina and orchestrate neuroinflammatory response, recovery from injury and progression of disease (Rashid et al., 2019).

Most retinal diseases can be categorized into those involving death of photoreceptors in the OR, and those directly affecting neurons of the IR, usually RGCs. Retinal diseases affecting the OR are the most important causes of vision impairment in the working-age population and include: (a) inherited disorders, e.g., retinitis pigmentosa (RP), Leber congenital amaurosis, and macular dystrophies, which display high genetic heterogeneity with more than 250 causative genes[1] and (b) multifactorial conditions, e.g., AMD. Degeneration of RPE and/or photoreceptor cells are the common landmarks of these diseases, although the underlying molecular and cellular events are still poorly understood. Mitochondrial dysfunction, neuroinflammation and microglia activation, among others, have been shown to exacerbate disease progression (Ambati et al., 2013; Cuenca et al., 2014; Zhao et al., 2015; Lefevere et al., 2017). Schematically, the disease proceeds through three different stages (**Figures 1B–D**): (a) functional impairment, in which photoreceptors are intact but start to lose their functionality; (b) ongoing photoreceptors degeneration; (c) complete loss of photoreceptors. The choice of the appropriate therapy may depend on the specific timing of intervention (**Figures 1B–D**).

Inner retina diseases are mostly represented by optic neuropathies (ONs), that comprise a group of monogenic and complex disorders mainly affecting RGCs (Carelli et al., 2017). The mechanisms underlying RGC degeneration are still unknown, but axonal injury has been proposed as the earliest event that eventually leads to RGC death (Dratviman-Storobinsky et al., 2008). Among the possible mechanisms, mitochondrial dysfunction, has been correlated, directly or indirectly, to the majority of ONs, likely due to the particular vulnerability of RGCs to mitochondrial impairment (Carelli et al., 2017). A tight connection between ON and mitochondrial dysfunction has been extensively described (Gueven et al., 2017). Several mitochondrial diseases are associated with vision impairment. Among them, Leber Hereditary Optic Neuropathy (LHON) and Autosomal Dominant Optic Atrophy represent the most frequent genetic form of ONs (Carelli et al., 2004; Yu-Wai-Man et al., 2011). Interestingly, also the most common and multifactorial forms of ONs, such as glaucoma and diabetic retinopathy, show signs of mitochondrial dysfunction and share clinical similarities with mitochondrial ONs (Jarrett et al., 2008; Yu-Wai-Man et al., 2011; Chhetri and Gueven, 2016; Gueven et al., 2017). Despite the efforts employed, ONs are still only symptomatically treated. In this respect, mitochondria could represent the common denominator and hence a promising common therapeutic target (**Figure 2**).

Mutation-Independent Strategies Based on Gene-Therapy Approaches

Gene-based therapy consists in the delivery of exogenous genetic material in order to modulate the expression of specific genes to treat pathological conditions. This approach ensures a targeted, stable and spatially regulated modulation of gene expression, either through overexpression or silencing, with a final therapeutic outcome and was initially devised for gene-specific applications. Adeno-associated viruses (AAV) represent the vectors of choice for gene therapy in the retina, due to the limitation of lentiviruses and adenoviruses in transducing the mature retina. AAVs have an excellent safety profile (lack of pathogenicity and low immunogenicity) and provide long-lasting transgene expression (Colella and Auricchio, 2010; Trapani, 2019). Diseases caused by loss-of-function mutations can be treated by gene-replacement therapy. Indeed, the success of clinical trials and the recent approval of Luxturna (Ledford, 2017; Apte, 2018) are laying the bases for a more widespread use of gene replacement strategies for the treatment of retinal diseases. However, the extensive genetic heterogeneity of both OR and IR diseases poses a significant limitation to the development and application of gene-specific strategies to the majority of patients. Another problem is that AAV particles can package only up to about 4.7 kilobases of DNA, which represent a serious obstacle to the delivery of larger genes (Trapani, 2018, 2019). Moreover, gene replacement is not effective, by itself, in diseases caused by gain-of-function mutations, which primarily require silencing of mutant alleles. Finally, gene replacement therapies at present cannot be applied to complex multifactorial retinal diseases, including age-related macular degeneration (AMD), glaucoma, and diabetic retinopathy which are characterized by a polygenic, not fully elucidated, pathogenicity, with the contribution of environmental factors.

For the above-mentioned reasons, mutation-independent therapeutic strategies, represent valid alternatives and/or complementary approaches to gene-replacement strategies. They aim at minimizing and/or delaying cell loss in the diseased retina regardless of the primary genetic defect, targeting common dysregulated pathways that play a key effector role in retinal damage (e.g., oxidative stress, inflammation, neovascularization, pyroptosis, etc.).

It is becoming clear that gene-based strategies can considerably enhance the efficacy and safety of mutation-independent therapies for retinal diseases that, to date, are mainly based on the use of therapeutic active compounds. Indeed, their systemic administration may not be always efficient considering that many molecules cannot pass the blood–retinal barrier (Almasieh and Levin, 2017). Moreover, compounds intraocular administration can be deleterious because requires repeated local injections that may cause endophthalmitis and retinal detachment. In this respect, the exploitation of viral vector-mediated intraocular delivery is raising considerable interest for the devise of mutation-independent therapies because it ensures a more stable expression and efficacy of the therapeutic agent and usually requires a single administration, safeguarding patients' welfare. Finally, the appropriate combination of specific vector serotypes and cell type−specific promoters would limit transgene expression to the desired cells.

In this review, we will discuss the technical and conceptual reasons underlying the advantages of AAV delivery- and

[1] https://sph.uth.edu/retnet/disease.htm

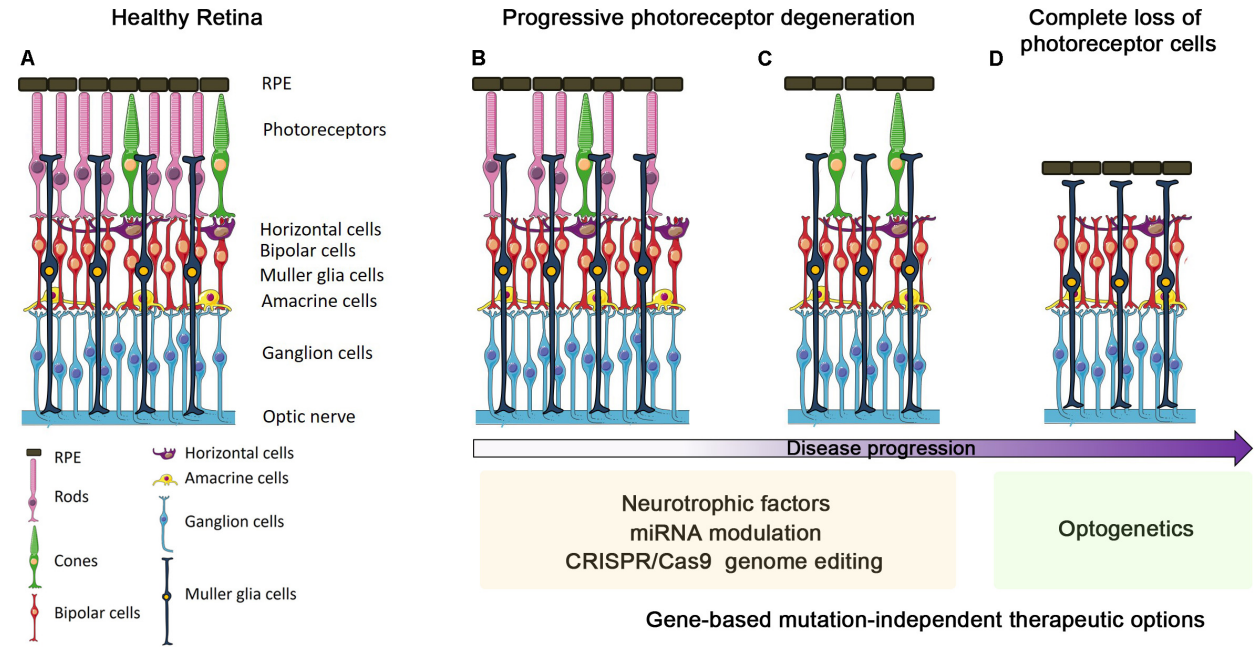

FIGURE 1 | Progression of outer retinal degenerative disease and gene-based mutation-independent therapy options. Schematic representation of either retinas in healthy conditions **(A)** or undergoing different stages of degeneration progression **(B–D)**. The ongoing photoreceptor degeneration **(B)** and before the progressive cone degeneration **(C)** stages can benefit from the use of neurotrophic factors, miRNA modulation and CRISPR/Cas9 genome editing. In the final stage, i.e., when all photoreceptors are lost **(D)**, optogenetics seems to be the only suitable gene-based mutation-independent therapy option.

more in general, of gene-based therapies applied to mutation-independent strategies for the treatment of OR and IR diseases and the most promising applications reported to date.

Neuroprotection Approaches

Neuroprotective strategies are the ideal mutation-independent approach to treat diseases with initial and/or ongoing photoreceptor degeneration (**Figures 1B,C**). However, the half-life of neurotrophic factors is in general short thus requiring frequent administrations to maintain appropriate therapeutic levels (Poduslo and Curran, 1996). On the contrary, AAV-mediated expression of neurotrophic factors can ensure stable transgene expression and therapeutic efficacy. Glial cell–derived neurotrophic factor, ciliary neurotrophic factor (CNTF), brain-derived neurotrophic factor (BDNF), basic fibroblast growth factor, and pigment epithelium–derived factor (PEDF) were shown to have beneficial effects in preventing photoreceptor death in several mouse models of retinal degeneration (Unsicker, 2013; Paulus and Campbell, 2016; Pardue and Allen, 2018). Numerous studies have suggested that CNTF and the activation of IL-6 signaling, also through overexpression of STAT3 (Jiang et al., 2014), are important in the response to retinal degeneration although treatment with CNTF has shown limited efficacy in RP patients (Birch et al., 2016).

Neurotrophic agents have also been tested in ONs (Boia et al., 2020; **Figure 2**). AAV-mediated delivery of Fibroblast growth factor-2, or delivery of the *BDNF* gene leads to significant increase in RGC survival and reduced RGC axons loss after optic nerve injury or induction of intraocular pressure (IOP) (Martin et al., 2003; Sapieha et al., 2006).

More recently, a single AAV vector expressing both BDNF and its receptor, the tropomyosin-related receptor kinase-B (TrkB), was tested *in vivo* in a model of optic nerve crush and in a model of high tension glaucoma (HTG) obtained by trabecular laser-induced IOP elevation (Osborne et al., 2018). This strategy promoted significant long-term RGCs survival and improved positive scotopic threshold responses (measuring RGCs activity) after optic nerve crush or laser-induced IOP elevation (Osborne et al., 2018).

Similarly, the effect of an AAV-mediated CNTF gene therapy was tested in different models of RGC degeneration, such as optic nerve crush and laser-induced HTG with promising results (Leaver et al., 2006; Pease et al., 2009). Interestingly, co-administration of CNTF and BDNF vectors did not improve RGC survival, possibly because this combination reduced the efficiency of AAV-CNTF compared to a single vector administration (Pease et al., 2009).

Conversely, combined overexpression of CNTF and Bcl-2, or CNTF and RhoA-shRNA were tested in models of optic nerve injury (Leaver et al., 2006; Cen et al., 2017). Inhibition of the Rho GTPase signaling pathway by RhoA downregulation led to enhancement of axon regrowth (Fujita and Yamashita, 2014). Interestingly, both strategies demonstrated additive effects on increased survival and axonal regeneration of RGCs highlighting the importance of a therapeutic approach enhancing simultaneously neuroprotection and regeneration in ON (Leaver et al., 2006; Cen et al., 2017).

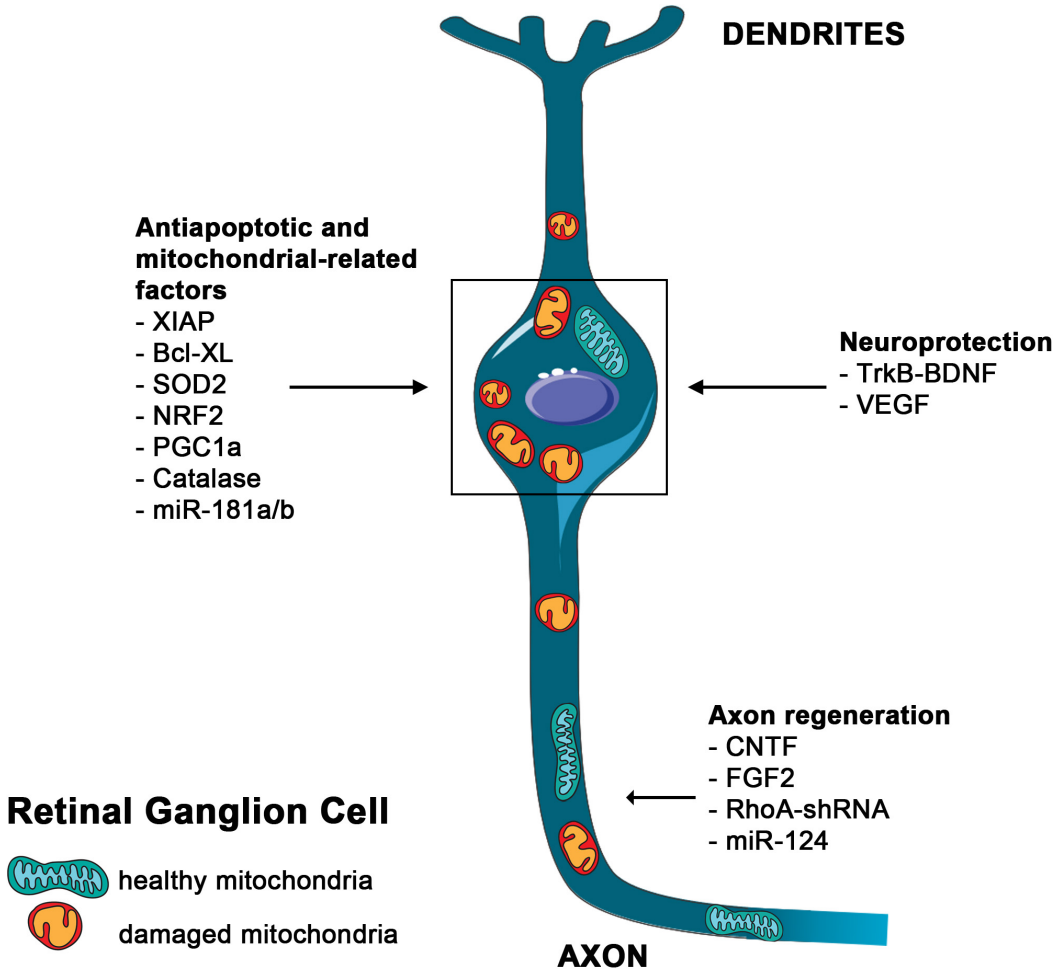

FIGURE 2 | Main mutation-independent therapies applicable to RGC neuroprotection. Schematic representation of an RGC. Damaged mitochondria are depicted in the soma and along the axon. Therapies aimed to block RGCs death and to induce axon regeneration are indicated.

Within neuroprotection, a special place is occupied by the rod-derived cone viability factor (RdCVF) whose discovery and characterization uncovered an entirely novel mechanism of neuroprotection. Most forms of RP are due to primary damage of rod cells, which is followed by a secondary loss of cones (**Figure 1C**; Sancho-Pelluz et al., 2008). RdCVF is a retina-specific trophic factor that induces cone survival and functional rescue in RP animal models (Leveillard et al., 2004; Yang et al., 2009) by modulating energy metabolism, accelerating glucose entry and enhancing aerobic glycolysis, thus holding good promises as an effective AAV-mediated mutation-independent therapy (Leveillard and Sahel, 2010; Ait-Ali et al., 2015; Byrne et al., 2015; Clerin et al., 2020).

Neurotrophic factors have also been tested in combination with other mutation-independent therapeutic agents. PEDF displays antiangiogenic and anti-inflammatory properties and was tested in combination with the microRNA-mediated inhibition of the vascular endothelial growth factor-A (VEGF-A) to prevent choroidal neovascularization in vasoproliferative retinal diseases, such as AMD. The dual-acting vector showed enhanced therapeutic efficacy with respect to the delivery of a single antiangiogenic factor (Askou et al., 2019).

Despite the known role of VEGF in neovascularization (Folk and Stone, 2010), it has been shown that VEGF treatment reduces apoptosis in models of glaucoma whereas anti-VEGF therapies exacerbate neuronal cell death (Boia et al., 2020). Engineered zinc finger proteins (ZFPs) that upregulate multiple forms of VEGF in their natural, endogenous, ratios were generated to avoid vascular permeability, edema, and inflammation due to VEGF overexpression. AAV-VEGF-ZFPs significantly increased RGCs survival after optic nerve transection or ophthalmic artery ligation without affecting retinal vasculature (D'Onofrio et al., 2011).

Within IR diseases, mutation-independent strategies acting on mitochondrial dysfunction, oxidative stress and mitochondrial-mediated cell death have been proposed to protect RGCs and restore visual function (**Figure 2**). Delivery of the caspase inhibitor BIRC4 (also known as XIAP), of the antiapoptotic member of the Bcl-2 protein family Bcl-X_L, and of the mitochondrial superoxide dismutase (SOD2), a ROS-detoxifying

enzyme, have been tested in *in vivo* models of RGC degeneration with promising results (McKinnon et al., 2002; Malik et al., 2005; Qi et al., 2007).

Interestingly, Xiong et al. (2015) created several AAV vectors to deliver antioxidant genes to the retina. These vectors encode the main mitochondrial ROS scavenger enzymes SOD2 and catalase, and the master transcription factors *NRF2* and *PGC1a*, which globally regulate antioxidant defense responses (St-Pierre et al., 2006). Moreover, PGC1a also regulates mitochondrial biogenesis and respiration (Wu et al., 1999). Notably, AAV-mediated delivery of *NRF2* was more effective than SOD2 and catalase in the protection of both photoreceptor and RGC degenerative models, while surprisingly, expression of PGC1a accelerated photoreceptor death (Xiong et al., 2015). These results suggested that the pleiotropic effect of *NRF2* may be broadly applicable to many ocular diseases characterized by oxidative damage.

MicroRNA-Based Approaches

Several microRNAs (miRNAs) have been associated with retinal development and function as well as with disease pathogenesis (Karali and Banfi, 2019). As an example, a dominant mutation in the mature sequence of miR-204 was linked to a form of RP associated with ocular coloboma (Conte et al., 2015). Recently, it was reported that AAV-mediated subretinal administration of miR-204 preserved retinal function in mouse models of inherited retinal diseases by slowing down photoreceptor degeneration and dampening microglia activation (Karali et al., 2020). MiR-204 represents a paradigmatic example of a promising mutation-independent approach due to miRNA capability to simultaneously modulate multiple molecular pathways involved in disease pathogenesis and progression.

MicroRNAs represent attractive therapeutic targets for complex retinal disorders as well. A growing number of miRNAs were found to be essential in normal and pathological retinal angiogenesis and were reported to be dysregulated in AMD (Wang et al., 2012; Berber et al., 2017; Askou et al., 2018). Indeed, modulations of miR-184, miR-21, miR-31, miR-150 or miR-23/27 were highlighted as a potential therapeutic approach for AMD (Shen et al., 2008; Sabatel et al., 2011; Zhou et al., 2011; Murad et al., 2014).

Due to their pleiotropic effect, miRNA-based therapeutic strategies have also been tested in ONs with promising results. The effect of miR-124 in axon growth of RGCs derived from Müller cells was tested both *in vitro* and *in vivo* in a model of HTG (He et al., 2018). Isolated rat Müller cells were dedifferentiated into retinal stem cells, induced to differentiate into RGCs and then transfected with miR-124 or anti-miR-124. Interestingly, miR-124 promoted axon growth of RGCs differentiated from retinal stem cells. In a rat HTG model, the extent of axon growth was the longest in the miR-124 group and the shortest in the anti-miR-124 group indicating that miR-124 has translational potential for gene therapy of glaucoma (He et al., 2018).

Finally, the potential therapeutic effect of miR-181a and b downregulation was tested in different models of LHON (Indrieri et al., 2019). The miR-181 family, composed of four members, is highly expressed in different regions of the CNS, including retina, where they regulate neurotrophic signaling, axon guidance, immunity and mitochondrial-related pathways (Indrieri et al., 2020). Genetic inactivation of miR-181a/b protects RGCs and ameliorates visual function in different *in vivo* LHON models strongly suggesting that these miRNAs may represent effective mutation-independent therapeutic targets for this disease (Indrieri et al., 2019).

The therapeutic potential of miRNAs for retinal diseases is also demonstrated by the promising results obtained using Extracellular Vesicles (EV). EV is the collective term for secreted vesicles (exosomes, microvesicles, and apoptotic bodies). They are considered signaling mediators between cells due to their capability of transporting and delivering proteins, mRNA, miRNA, and lipids. EV are gaining attraction as a candidate treatment for ocular diseases and have already been tested in many retinal damage models, such as glaucoma, retinal ischemia, autoimmune uveitis, and diabetic retinopathy, with promising results (Mead and Tomarev, 2020). Interestingly, it is becoming evident that the miRNA component of EV plays a relevant contribution to the protective action of EV. It was recently demonstrated that neural stem/progenitor cells (NPCs)-derived exosomes administration delayed photoreceptor degeneration and preserved visual function mainly through the action of a set of 17 miRNAs that suppressed microglial activation and inflammation in retinal degeneration rodent models (Bian et al., 2020).

CRISPR/Cas9 Approaches

Therapeutic genome editing is considered an ideal strategy for permanent correction of genetic defects and, since the advent of CRISPR (clustered regularly interspaced short palindromic repeats)/Cas9-mediated genome editing, these strategies are advancing rapidly (Cox et al., 2015). Therapeutic application of CRISPR/Cas9 has shown promising outcomes in animal models of retinal diseases (Benati et al., 2020). In particular, an AAV-CRISPR/Cas9 approach was recently used, in a mutation-independent manner, to inactivate VEGF-A and vascular endothelial growth factor receptor-2 in RPE cells, thus abrogating angiogenesis (Huang et al., 2017; Kim et al., 2017a,b). In three different mouse models of OR degeneration, an AAV-CRISPR/Cas9 was used to target the Neural retina-specific leucine zipper (*Nrl*) gene, which acts in concert with *Nr2e3* in determining rod fate. Loss of *Nrl* in rods causes them to acquire cone-like features. The preservation of cone function is a major therapeutic goal to preserve daylight and color vision and ameliorate RP patients' quality of life. CRISPR/Cas9-mediated *Nrl* loss showed an improvement of photoreceptors survival and function (Yu et al., 2017). Moreover, double CRISPR/Cas9-mediated targeted inactivation of *Nrl* and *Nr2e3* led to a much more significant rescue of photoreceptor degeneration and restoration of visual function over either single gene targeting (Zhu et al., 2017).

Optogenetic Approaches

When OR degeneration is at the end stage of disease progression and all photoreceptors are lost (**Figure 1D**), patients will have little chance to benefit from the previously described approaches

and the only mutation-independent strategy available based on gene-delivery is represented by optogenetic therapy. Compared to other therapeutic approaches available at this disease stage, i.e., retinal prostheses and stem cells (Dalkara et al., 2016), optogenetics has the advantage of using pre-existing retinal neural synapses. This approach relies on the creation of newly generated photosensors by transferring photosensitive genes to the residual retinal circuitry. Critical points are represented by the types of light sensors to be used and the retinal cells to target (i.e., RGCs, bipolar, and amacrine cells). The possibility of expressing photosensitive molecules in RGCs represents a promising strategy to treat the most advanced stages of disease, when the retinal circuitry is heavily compromised. Optogenetics mostly uses the light-sensitive proteins channelrhodopsin (ChRs), halorhodopsin (NpHR), and melanopsin (Busskamp et al., 2012; Dalkara et al., 2016; Klapper et al., 2016). ChRs2 and melanopsin expression in bipolar cells restored visual function in murine RP models (Lagali et al., 2008; Doroudchi et al., 2011; Mace et al., 2015), while NpHR could be especially helpful to reactivate the inhibitory modulation of RGCs through expression in bipolar cells (Zhang et al., 2007). Several pre-clinical trials have been conducted in murine, canine, and simian models. These trials include different type of optogenetic molecules expressed alone or in combination and present different targeted cell population (Simunovic et al., 2019). Currently, two Phase I/II clinical trial of optogenetics for vision restoration are registered and underway (NCT02556736) or in the patient recruiting status (NCT03326336).

CONCLUSION

Gene delivery approaches have an enormous application potential in retinal disorders not only for gene-specific therapeutic strategies (see the recent approval of the clinical use of the Luxturna drug) but also, for mutation-independent strategies. It is obvious that the use of gene-specific approaches is always the first choice of treatment for a genetic retinal disease, whenever possible. However, as discussed above, mutation-independent therapies constitute a valid alternative/complementary approach to overcome some of the main obstacles related to gene-specific ones, starting from the high genetic heterogeneity of these conditions. Gene-based approaches are predicted to considerably expand the successful application of mutation-independent therapies, for inherited and multifactorial forms of retinal disorders thanks to several advantages summarized as follows:

a) a more stable and long-term expression of the therapeutic gene/product, with significant advantages in safeguarding patients' welfare over approaches requiring repeated intraocular injections/administrations;
b) the possibility to better target, down to specific cell types, the administration of therapeutic products thus minimizing undesired effects, which is particularly relevant when a combined administration of multiple agents is required;
c) the possibility to apply mutation-independent therapies, e.g., those based on genome editing and optogenetics, for which a different delivery route is either less effective or even impossible.

Based on the above considerations, we believe that gene-based mutation-independent strategies will lead in the near future to the expansion of therapeutic avenues for retinal diseases.

AUTHOR CONTRIBUTIONS

SC and SB conceived the manuscript. SC and AI wrote the first draft of the manuscript. SB and BF edited the manuscript. All authors contributed to the article and approved the submitted version.

FUNDING

This study was kindly supported by the Foundation Fighting Blindness (grant TA-NMT-0619-0764-TIGEM to SB).

ACKNOWLEDGMENTS

We thank the Italian Telethon Foundation for continuous support and Dr. Ivana Trapani for discussion and critical reading of the manuscript.

REFERENCES

Ait-Ali, N., Fridlich, R., Millet-Puel, G., Clerin, E., Delalande, F., Jaillard, C., et al. (2015). Rod-derived cone viability factor promotes cone survival by stimulating aerobic glycolysis. *Cell* 161, 817–832. doi: 10.1016/j.cell.2015.03.023

Almasieh, M., and Levin, L. A. (2017). Neuroprotection in glaucoma: animal models and clinical trials. *Annu. Rev. Vis. Sci.* 3, 91–120. doi: 10.1146/annurev-vision-102016-061422

Ambati, J., Atkinson, J. P., and Gelfand, B. D. (2013). Immunology of age-related macular degeneration. *Nat. Rev. Immunol.* 13, 438–451.

Apte, R. S. (2018). Gene therapy for retinal degeneration. *Cell* 173:5. doi: 10.1016/j.cell.2018.03.021

Askou, A. L., Alsing, S., Benckendorff, J. N. E., Holmgaard, A., Mikkelsen, J. G., Aagaard, L., et al. (2019). Suppression of choroidal neovascularization by AAV-based dual-acting antiangiogenic gene therapy. *Mol. Ther. Nucleic Acids* 16, 38–50. doi: 10.1016/j.omtn.2019.01.012

Askou, A. L., Alsing, S., Holmgaard, A., Bek, T., and Corydon, T. J. (2018). Dissecting microRNA dysregulation in age-related macular degeneration: new targets for eye gene therapy. *Acta Ophthalmol.* 96, 9–23. doi: 10.1111/aos.13407

Benati, D., Patrizi, C., and Recchia, A. (2020). Gene editing prospects for treating inherited retinal diseases. *J. Med. Genet.* 57, 437–444. doi: 10.1136/jmedgenet-2019-106473

Berber, P., Grassmann, F., Kiel, C., and Weber, B. H. (2017). An eye on age-related macular degeneration: the role of MicroRNAs in disease pathology. *Mol. Diagn. Ther.* 21, 31–43. doi: 10.1007/s40291-016-0234-z

Bian, B., Zhao, C., He, X., Gong, Y., Ren, C., Ge, L., et al. (2020). Exosomes derived from neural progenitor cells preserve photoreceptors during retinal degeneration by inactivating microglia. *J. Extracell. Vesicles* 9:1748931. doi: 10.1080/20013078.2020.1748931

Birch, D. G., Bennett, L. D., Duncan, J. L., Weleber, R. G., and Pennesi, M. E. (2016). Long-term follow-up of patients with retinitis pigmentosa receiving

intraocular ciliary neurotrophic factor implants. *Am. J. Ophthalmol.* 170, 10–14. doi: 10.1016/j.ajo.2016.07.013

Boia, R., Ruzafa, N., Aires, I. D., Pereiro, X., Ambrosio, A. F., Vecino, E., et al. (2020). Neuroprotective strategies for retinal ganglion cell degeneration: current status and challenges ahead. *Int. J. Mol. Sci.* 21:2262. doi: 10.3390/ijms21072262

Busskamp, V., Picaud, S., Sahel, J. A., and Roska, B. (2012). Optogenetic therapy for retinitis pigmentosa. *Gene Ther.* 19, 169–175. doi: 10.1038/gt.2011.155

Byrne, L. C., Dalkara, D., Luna, G., Fisher, S. K., Clerin, E., Sahel, J. A., et al. (2015). Viral-mediated RdCVF and RdCVFL expression protects cone and rod photoreceptors in retinal degeneration. *J. Clin. Invest.* 125, 105–116. doi: 10.1172/jci65654

Carelli, V., La Morgia, C., Ross-Cisneros, F. N., and Sadun, A. A. (2017). Optic neuropathies: the tip of the neurodegeneration iceberg. *Hum. Mol. Genet.* 26, R139–R150.

Carelli, V., Ross-Cisneros, F. N., and Sadun, A. A. (2004). Mitochondrial dysfunction as a cause of optic neuropathies. *Prog. Retin. Eye Res.* 23, 53–89. doi: 10.1016/j.preteyeres.2003.10.003

Cen, L. P., Liang, J. J., Chen, J. H., Harvey, A. R., Ng, T. K., Zhang, M., et al. (2017). AAV-mediated transfer of RhoA shRNA and CNTF promotes retinal ganglion cell survival and axon regeneration. *Neuroscience* 343, 472–482. doi: 10.1016/j.neuroscience.2016.12.027

Chhetri, J., and Gueven, N. (2016). Targeting mitochondrial function to protect against vision loss. *Expert Opin. Ther. Targets* 20, 721–736. doi: 10.1517/14728222.2015.1134489

Clerin, E., Marussig, M., Sahel, J. A., and Leveillard, T. (2020). Metabolic and redox signaling of the nucleoredoxin-like-1 gene for the treatment of genetic retinal diseases. *Int. J. Mol. Sci.* 21:1625. doi: 10.3390/ijms21051625

Colella, P., and Auricchio, A. (2010). AAV-mediated gene supply for treatment of degenerative and neovascular retinal diseases. *Curr. Gene Ther.* 10, 371–380. doi: 10.2174/156652310793180670

Conte, I., Hadfield, K. D., Barbato, S., Carrella, S., Pizzo, M., Bhat, R. S., et al. (2015). MiR-204 is responsible for inherited retinal dystrophy associated with ocular coloboma. *Proc. Natl. Acad. Sci. U.S.A.* 112, E3236–E3245.

Cox, D. B., Platt, R. J., and Zhang, F. (2015). Therapeutic genome editing: prospects and challenges. *Nat. Med.* 21, 121–131. doi: 10.1038/nm.3793

Cuenca, N., Fernandez-Sanchez, L., Campello, L., Maneu, V., De La Villa, P., Lax, P., et al. (2014). Cellular responses following retinal injuries and therapeutic approaches for neurodegenerative diseases. *Prog. Retin. Eye Res.* 43, 17–75. doi: 10.1016/j.preteyeres.2014.07.001

Dalkara, D., Goureau, O., Marazova, K., and Sahel, J. A. (2016). Let there be light: gene and cell therapy for blindness. *Hum. Gene Ther.* 27, 134–147. doi: 10.1089/hum.2015.147

D'Onofrio, P. M., Thayapararajah, M., Lysko, M. D., Magharious, M., Spratt, S. K., Lee, G., et al. (2011). Gene therapy for traumatic central nervous system injury and stroke using an engineered zinc finger protein that upregulates VEGF-A. *J. Neurotrauma* 28, 1863–1879. doi: 10.1089/neu.2011.1896

Doroudchi, M. M., Greenberg, K. P., Liu, J., Silka, K. A., Boyden, E. S., Lockridge, J. A., et al. (2011). Virally delivered channelrhodopsin-2 safely and effectively restores visual function in multiple mouse models of blindness. *Mol. Ther.* 19, 1220–1229. doi: 10.1038/mt.2011.69

Dratviman-Storobinsky, O., Hasanreisoglu, M., Offen, D., Barhum, Y., Weinberger, D., and Goldenberg-Cohen, N. (2008). Progressive damage along the optic nerve following induction of crush injury or rodent anterior ischemic optic neuropathy in transgenic mice. *Mol. Vis.* 14, 2171–2179.

Folk, J. C., and Stone, E. M. (2010). Ranibizumab therapy for neovascular age-related macular degeneration. *N. Engl. J. Med.* 363, 1648–1655.

Fujita, Y., and Yamashita, T. (2014). Axon growth inhibition by RhoA/ROCK in the central nervous system. *Front. Neurosci.* 8:338. doi: 10.3389/fnins.2014.00338

Gueven, N., Nadikudi, M., Daniel, A., and Chhetri, J. (2017). Targeting mitochondrial function to treat optic neuropathy. *Mitochondrion* 36, 7–14. doi: 10.1016/j.mito.2016.07.013

He, Y., Li, H. B., Li, X., Zhou, Y., Xia, X. B., and Song, W. T. (2018). MiR-124 promotes the growth of retinal ganglion cells derived from muller cells. *Cell Physiol. Biochem.* 45, 973–983. doi: 10.1159/000487292

Hoon, M., Okawa, H., Della Santina, L., and Wong, R. O. (2014). Functional architecture of the retina: development and disease. *Prog. Retin. Eye Res.* 42, 44–84. doi: 10.1016/j.preteyeres.2014.06.003

Huang, X., Zhou, G., Wu, W., Duan, Y., Ma, G., Song, J., et al. (2017). Genome editing abrogates angiogenesis in vivo. *Nat. Commun.* 8:112.

Indrieri, A., Carrella, S., Carotenuto, P., Banfi, S., and Franco, B. (2020). The pervasive role of the miR-181 family in development, neurodegeneration, and cancer. *Int. J. Mol. Sci.* 21:2092. doi: 10.3390/ijms21062092

Indrieri, A., Carrella, S., Romano, A., Spaziano, A., Marrocco, E., Fernandez-Vizarra, E., et al. (2019). miR-181a/b downregulation exerts a protective action on mitochondrial disease models. *EMBO Mol. Med.* 11:e8734.

Jarrett, S. G., Lin, H., Godley, B. F., and Boulton, M. E. (2008). Mitochondrial DNA damage and its potential role in retinal degeneration. *Prog. Retin. Eye Res.* 27, 596–607. doi: 10.1016/j.preteyeres.2008.09.001

Jiang, K., Wright, K. L., Zhu, P., Szego, M. J., Bramall, A. N., Hauswirth, W. W., et al. (2014). STAT3 promotes survival of mutant photoreceptors in inherited photoreceptor degeneration models. *Proc. Natl. Acad. Sci. U.S.A.* 111, E5716–E5723.

Karali, M., and Banfi, S. (2019). Non-coding RNAs in retinal development and function. *Hum. Genet.* 138, 957–971. doi: 10.1007/s00439-018-1931-y

Karali, M., Guadagnino, I., Marrocco, E., De Cegli, R., Carissimo, A., Pizzo, M., et al. (2020). AAV-miR-204 protects from retinal degeneration by attenuation of microglia activation and photoreceptor cell death. *Mol. Ther. Nucleic Acids* 19, 144–156. doi: 10.1016/j.omtn.2019.11.005

Kim, E., Koo, T., Park, S. W., Kim, D., Kim, K., Cho, H. Y., et al. (2017a). In vivo genome editing with a small Cas9 orthologue derived from *Campylobacter jejuni*. *Nat. Commun.* 8:14500.

Kim, K., Park, S. W., Kim, J. H., Lee, S. H., Kim, D., Koo, T., et al. (2017b). Genome surgery using Cas9 ribonucleoproteins for the treatment of age-related macular degeneration. *Genome Res.* 27, 419–426. doi: 10.1101/gr.219089.116

Klapper, S. D., Swiersy, A., Bamberg, E., and Busskamp, V. (2016). Biophysical properties of optogenetic tools and their application for vision restoration approaches. *Front. Syst. Neurosci.* 10:74. doi: 10.3389/fnsys.2016.00074

Lagali, P. S., Balya, D., Awatramani, G. B., Munch, T. A., Kim, D. S., Busskamp, V., et al. (2008). Light-activated channels targeted to ON bipolar cells restore visual function in retinal degeneration. *Nat. Neurosci.* 11, 667–675. doi: 10.1038/nn.2117

Leaver, S. G., Cui, Q., Bernard, O., and Harvey, A. R. (2006). Cooperative effects of bcl-2 and AAV-mediated expression of CNTF on retinal ganglion cell survival and axonal regeneration in adult transgenic mice. *Eur. J. Neurosci.* 24, 3323–3332. doi: 10.1111/j.1460-9568.2006.05230.x

Ledford, H. (2017). FDA advisers back gene therapy for rare form of blindness. *Nature* 550:314. doi: 10.1038/nature.2017.22819

Lefevere, E., Toft-Kehler, A. K., Vohra, R., Kolko, M., Moons, L., and Van Hove, I. (2017). Mitochondrial dysfunction underlying outer retinal diseases. *Mitochondrion* 36, 66–76. doi: 10.1016/j.mito.2017.03.006

Leveillard, T., Mohand-Said, S., Lorentz, O., Hicks, D., Fintz, A. C., Clerin, E., et al. (2004). Identification and characterization of rod-derived cone viability factor. *Nat. Genet.* 36, 755–759. doi: 10.1038/ng1386

Leveillard, T., and Sahel, J. A. (2010). Rod-derived cone viability factor for treating blinding diseases: from clinic to redox signaling. *Sci. Transl. Med.* 2:26s16.

Mace, E., Caplette, R., Marre, O., Sengupta, A., Chaffiol, A., Barbe, P., et al. (2015). Targeting channelrhodopsin-2 to ON-bipolar cells with vitreally administered AAV Restores ON and OFF visual responses in blind mice. *Mol. Ther.* 23, 7–16. doi: 10.1038/mt.2014.154

Malik, J. M., Shevtsova, Z., Bahr, M., and Kugler, S. (2005). Long-term in vivo inhibition of CNS neurodegeneration by Bcl-XL gene transfer. *Mol. Ther.* 11, 373–381. doi: 10.1016/j.ymthe.2004.11.014

Martin, K. R., Quigley, H. A., Zack, D. J., Levkovitch-Verbin, H., Kielczewski, J., Valenta, D., et al. (2003). Gene therapy with brain-derived neurotrophic factor as a protection: retinal ganglion cells in a rat glaucoma model. *Invest. Ophthalmol. Vis. Sci.* 44, 4357–4365. doi: 10.1167/iovs.02-1332

McKinnon, S. J., Lehman, D. M., Tahzib, N. G., Ransom, N. L., Reitsamer, H. A., Liston, P., et al. (2002). Baculoviral IAP repeat-containing-4 protects optic nerve axons in a rat glaucoma model. *Mol. Ther.* 5, 780–787. doi: 10.1006/mthe.2002.0608

Mead, B., and Tomarev, S. (2020). Extracellular vesicle therapy for retinal diseases. *Prog. Retin. Eye Res.* 10:100849. doi: 10.1016/j.preteyeres.2020.100849

Murad, N., Kokkinaki, M., Gunawardena, N., Gunawan, M. S., Hathout, Y., Janczura, K. J., et al. (2014). miR-184 regulates ezrin, LAMP-1 expression, affects phagocytosis in human retinal pigment epithelium and is downregulated in

age-related macular degeneration. *FEBS J.* 281, 5251–5264. doi: 10.1111/febs.13066

Osborne, A., Khatib, T. Z., Songra, L., Barber, A. C., Hall, K., Kong, G. Y. X., et al. (2018). Neuroprotection of retinal ganglion cells by a novel gene therapy construct that achieves sustained enhancement of brain-derived neurotrophic factor/tropomyosin-related kinase receptor-B signaling. *Cell Death Dis.* 9:1007.

Pardue, M. T., and Allen, R. S. (2018). Neuroprotective strategies for retinal disease. *Prog. Retin. Eye Res.* 65, 50–76. doi: 10.1016/j.preteyeres.2018.02.002

Paulus, Y. M., and Campbell, J. P. (2016). Neuroprotection and retinal diseases. *Dev. Ophthalmol.* 55, 322–329.

Pease, M. E., Zack, D. J., Berlinicke, C., Bloom, K., Cone, F., Wang, Y., et al. (2009). Effect of CNTF on retinal ganglion cell survival in experimental glaucoma. *Invest. Ophthalmol. Vis. Sci.* 50, 2194–2200. doi: 10.1167/iovs.08-3013

Poduslo, J. F., and Curran, G. L. (1996). Permeability at the blood-brain and blood-nerve barriers of the neurotrophic factors: NGF, CNTF, NT-3, BDNF. *Brain Res. Mol. Brain Res.* 36, 280–286. doi: 10.1016/0169-328x(95)00250-v

Qi, X., Sun, L., Hauswirth, W. W., Lewin, A. S., and Guy, J. (2007). Use of mitochondrial antioxidant defenses for rescue of cells with a Leber hereditary optic neuropathy-causing mutation. *Arch. Ophthalmol.* 125, 268–272. doi: 10.1001/archopht.125.2.268

Rashid, K., Akhtar-Schaefer, I., and Langmann, T. (2019). Microglia in retinal degeneration. *Front. Immunol.* 10:1975. doi: 10.3389/fimmu.2019.01975

Sabatel, C., Malvaux, L., Bovy, N., Deroanne, C., Lambert, V., Gonzalez, M. L., et al. (2011). MicroRNA-21 exhibits antiangiogenic function by targeting RhoB expression in endothelial cells. *PLoS One* 6:e16979. doi: 10.1371/journal.pone.0016979

Sancho-Pelluz, J., Arango-Gonzalez, B., Kustermann, S., Romero, F. J., Van Veen, T., Zrenner, E., et al. (2008). Photoreceptor cell death mechanisms in inherited retinal degeneration. *Mol. Neurobiol.* 38, 253–269. doi: 10.1007/s12035-008-8045-9

Sapieha, P. S., Hauswirth, W. W., and Di Polo, A. (2006). Extracellular signal-regulated kinases 1/2 are required for adult retinal ganglion cell axon regeneration induced by fibroblast growth factor-2. *J. Neurosci. Res.* 83, 985–995. doi: 10.1002/jnr.20803

Shen, J., Yang, X., Xie, B., Chen, Y., Swaim, M., Hackett, S. F., et al. (2008). MicroRNAs regulate ocular neovascularization. *Mol. Ther.* 16, 1208–1216. doi: 10.1038/mt.2008.104

Simunovic, M. P., Shen, W., Lin, J. Y., Protti, D. A., Lisowski, L., and Gillies, M. C. (2019). Optogenetic approaches to vision restoration. *Exp. Eye Res.* 178, 15–26. doi: 10.1016/j.exer.2018.09.003

St-Pierre, J., Drori, S., Uldry, M., Silvaggi, J. M., Rhee, J., Jager, S., et al. (2006). Suppression of reactive oxygen species and neurodegeneration by the PGC-1 transcriptional coactivators. *Cell* 127, 397–408. doi: 10.1016/j.cell.2006.09.024

Trapani, I. (2018). Dual AAV vectors for stargardt disease. *Methods Mol. Biol.* 1715, 153–175. doi: 10.1007/978-1-4939-7522-8_11

Trapani, I. (2019). Adeno-associated viral vectors as a tool for large gene delivery to the retina. *Genes* 10:287. doi: 10.3390/genes10040287

Unsicker, K. (2013). Neurotrophic molecules in the treatment of neurodegenerative disease with focus on the retina: status and perspectives. *Cell Tissue Res.* 353, 205–218. doi: 10.1007/s00441-013-1585-y

Wang, S., Koster, K. M., He, Y., and Zhou, Q. (2012). miRNAs as potential therapeutic targets for age-related macular degeneration. *Future Med. Chem.* 4, 277–287. doi: 10.4155/fmc.11.176

Wu, Z., Puigserver, P., Andersson, U., Zhang, C., Adelmant, G., Mootha, V., et al. (1999). Mechanisms controlling mitochondrial biogenesis and respiration through the thermogenic coactivator PGC-1. *Cell* 98, 115–124. doi: 10.1016/s0092-8674(00)80611-x

Xiong, W., Maccoll Garfinkel, A. E., Li, Y., Benowitz, L. I., and Cepko, C. L. (2015). NRF2 promotes neuronal survival in neurodegeneration and acute nerve damage. *J. Clin. Invest.* 125, 1433–1445. doi: 10.1172/jci79735

Yang, Y., Mohand-Said, S., Danan, A., Simonutti, M., Fontaine, V., Clerin, E., et al. (2009). Functional cone rescue by RdCVF protein in a dominant model of retinitis pigmentosa. *Mol. Ther.* 17, 787–795. doi: 10.1038/mt.2009.28

Yu, W., Mookherjee, S., Chaitankar, V., Hiriyanna, S., Kim, J. W., Brooks, M., et al. (2017). Nrl knockdown by AAV-delivered CRISPR/Cas9 prevents retinal degeneration in mice. *Nat. Commun.* 8:14716.

Yu-Wai-Man, P., Griffiths, P. G., and Chinnery, P. F. (2011). Mitochondrial optic neuropathies - disease mechanisms and therapeutic strategies. *Prog. Retin. Eye Res.* 30, 81–114. doi: 10.1016/j.preteyeres.2010.11.002

Zhang, F., Wang, L. P., Brauner, M., Liewald, J. F., Kay, K., Watzke, N., et al. (2007). Multimodal fast optical interrogation of neural circuitry. *Nature* 446, 633–639. doi: 10.1038/nature05744

Zhao, L., Zabel, M. K., Wang, X., Ma, W., Shah, P., Fariss, R. N., et al. (2015). Microglial phagocytosis of living photoreceptors contributes to inherited retinal degeneration. *EMBO Mol. Med.* 7, 1179–1197. doi: 10.15252/emmm.201505298

Zhou, Q., Gallagher, R., Ufret-Vincenty, R., Li, X., Olson, E. N., and Wang, S. (2011). Regulation of angiogenesis and choroidal neovascularization by members of microRNA-23~27~24 clusters. *Proc. Natl. Acad. Sci. U.S.A.* 108, 8287–8292. doi: 10.1073/pnas.1105254108

Zhu, J., Ming, C., Fu, X., Duan, Y., Hoang, D. A., Rutgard, J., et al. (2017). Gene and mutation independent therapy via CRISPR-Cas9 mediated cellular reprogramming in rod photoreceptors. *Cell. Res.* 27, 830–833. doi: 10.1038/cr.2017.57

Conflict of Interest: The authors declare that the research was conducted in the absence of any commercial or financial relationships that could be construed as a potential conflict of interest.

Copyright © 2020 Carrella, Indrieri, Franco and Banfi. This is an open-access article distributed under the terms of the Creative Commons Attribution License (CC BY). The use, distribution or reproduction in other forums is permitted, provided the original author(s) and the copyright owner(s) are credited and that the original publication in this journal is cited, in accordance with accepted academic practice. No use, distribution or reproduction is permitted which does not comply with these terms.

frontiers in Neuroscience

REVIEW
published: 25 September 2020
doi: 10.3389/fnins.2020.566858

Amyotrophic Lateral Sclerosis: A Neurodegenerative Motor Neuron Disease With Ocular Involvement

Pilar Rojas[1,2†], Ana I. Ramírez[1,3,4†], José A. Fernández-Albarral[1], Inés López-Cuenca[1], Elena Salobrar-García[1,3,4], Manuel Cadena[2], Lorena Elvira-Hurtado[1], Juan J. Salazar[1,3,4], Rosa de Hoz[1,3,4] and José M. Ramírez[1,3,5]**

[1] Instituto de Investigaciones Oftalmológicas Ramón Castroviejo, Universidad Complutense de Madrid, Madrid, Spain, [2] Hospital General Universitario Gregorio Marañón, Instituto Oftálmico de Madrid, Madrid, Spain, [3] OFTARED, ISCIII, Madrid, Spain, [4] Departamento de Inmunología Oftalmología y ORL, Facultad de Óptica y Optometría, Universidad Complutense de Madrid, Madrid, Spain, [5] Departamento de Inmunología Oftalmología y ORL, Facultad de Medicina, Universidad Complutense de Madrid, Madrid, Spain

OPEN ACCESS

Edited by:
Nicolás Cuenca,
University of Alicante, Spain

Reviewed by:
Jose-Alberto Palma,
New York University, United States
Inigo Gabilondo,
Biocruces Bizkaia Health Research Institute, Spain

***Correspondence:**
Rosa de Hoz
rdehoz@med.ucm.es
José M. Ramírez
ramirezs@med.ucm.es

† These authors have contributed equally to this work

Specialty section:
This article was submitted to Neurodegeneration, a section of the journal Frontiers in Neuroscience

Received: 28 May 2020
Accepted: 24 August 2020
Published: 25 September 2020

Citation:
Rojas P, Ramírez AI, Fernández-Albarral JA, López-Cuenca I, Salobrar-García E, Cadena M, Elvira-Hurtado L, Salazar JJ, de Hoz R and Ramírez JM (2020) Amyotrophic Lateral Sclerosis: A Neurodegenerative Motor Neuron Disease With Ocular Involvement. Front. Neurosci. 14:566858. doi: 10.3389/fnins.2020.566858

Amyotrophic lateral sclerosis (ALS) is a neurodegenerative disease that causes degeneration of the lower and upper motor neurons and is the most prevalent motor neuron disease. This disease is characterized by muscle weakness, stiffness, and hyperreflexia. Patients survive for a short period from the onset of the disease. Most cases are sporadic, with only 10% of the cases being genetic. Many genes are now known to be involved in familial ALS cases, including some of the sporadic cases. It has also been observed that, in addition to genetic factors, there are numerous molecular mechanisms involved in these pathologies, such as excitotoxicity, mitochondrial disorders, alterations in axonal transport, oxidative stress, accumulation of misfolded proteins, and neuroinflammation. This pathology affects the motor neurons, the spinal cord, the cerebellum, and the brain, but recently, it has been shown that it also affects the visual system. This impact occurs not only at the level of the oculomotor system but also at the retinal level, which is why the retina is being proposed as a possible biomarker of this pathology. The current review discusses the main aspects mentioned above related to ALS, such as the main genes involved, the most important molecular mechanisms that affect this pathology, its ocular involvement, and the possible usefulness of the retina as a biomarker.

Keywords: ALS, motor neuron, neurodegenerative diseases, retina, optic nerve, eye, neuroinflammation, biomarker

INTRODUCTION: OVERVIEW OF AMYOTROPHIC LATERAL SCLEROSIS DISEASE

Motor neuron diseases (MNDs) have a high morbidity and mortality and cause a gradual deterioration of voluntary muscle function due to progressive neuronal damage (Rowland and Shneider, 2001; Turner et al., 2009; Yedavalli et al., 2018; Pinto et al., 2019). MND has a global incidence of one to three cases per 100,000, while its prevalence ranges from one to nine cases per 100,000. Within the group of these diseases, amyotrophic lateral sclerosis (ALS) is the most common, accounting for 80–90% of all MND cases (Román, 1996) and having an incidence per 100,000 people of 0.3–2.5 cases per year (Rowland and Shneider, 2001; Sathasivam, 2010;

Kiernan et al., 2011; Pratt et al., 2012). Of all ALS cases, 10% are familial (FALS) (Byrne et al., 2011) ranging from 2% to 15% depending on the population (Conwit, 2006). Overall, both the incidence (Haberlandt, 1959) and the prevalence (Williams et al., 1988) of this pathology can be variable depending on the region and ethnicity.

In ALS, a combination of the symptoms of both upper motor neurons (UMNs) and lower motor neurons (LMNs) occurs (Rowland and Shneider, 2001; Kiernan et al., 2011; Yedavalli et al., 2018). This condition involves muscle weakness and stiffness, overactive reflexes, and sometimes changes in emotions (Carra et al., 2012; Zarei et al., 2015; Yedavalli et al., 2018). ALS involves the swallowing, speech, and respiratory muscles (Carra et al., 2012; Zarei et al., 2015; Yedavalli et al., 2018). The disease usually begins in the extremities (spinal onset), although 25% of patients have a bulbar onset, which has a worse prognosis (Kiernan et al., 2011). ALS is a disease that is asymmetrical with respect to the onset and spread of UMN and LMN dysfunction and constitutes a heterogeneous disease, because not all forms behave in the same way, which makes its classification complex (Zhang et al., 2014).

Although ALS has only been considered a motor disease, neuroimaging tests have recently shown the involvement of non-motor areas such as cerebral global atrophy, decrease in gray matter density, and regional white matter alterations (Ellis et al., 2001; Abrahams et al., 2005; Kassubek et al., 2005; Ringholz et al., 2005; Mezzapesa et al., 2007; Zhang et al., 2014). The alteration of these areas leads to cognitive and behavioral changes (Abrahams et al., 2005; Mezzapesa et al., 2007). Cognitive impairment, mainly featuring executive dysfunction and mild memory loss during the course of the disease, has been found in 50% of ALS patients (Ringholz et al., 2005; Meier et al., 2010).

Mechanisms and Risk Factors Involved in the Pathogenesis of Motor Neuron Diseases

There are different risk factors involved in ALS (Yu et al., 2014; Zarei et al., 2015), which include smoking (Weisskopf et al., 2009; Wang et al., 2014), agricultural chemicals (Ward et al., 2014; Seals et al., 2017), heavy metals (Simons, 1986; Mcguire et al., 1997; Savolainen et al., 1998; Kamel et al., 2002), and low-frequency electromagnetic waves (Zhou et al., 2012). In addition, athletes (Chiò et al., 2004; Turner et al., 2012; Zarei et al., 2015) and hypermetabolic phenotype (Desport et al., 2001; Bouteloup et al., 2009; Vaisman et al., 2009; Dupuis et al., 2011; Ferri and Coccurello, 2017; Steyn et al., 2018; Pape and Grose, 2020) have a higher risk for ALS. A low body mass index can induce disease progression and reduced survival time (Jawaid et al., 2010; Park et al., 2015). Other factors that may affect ALS patients are hyperlipidemia (Palamiuc et al., 2015) and glutamate-rich and fat-rich diets (Iwasaki et al., 2005; Veldink et al., 2007; Morozova et al., 2008; Fitzgerald et al., 2014). However, progesterone and estrogen provide protection against ALS (Gargiulo Monachelli et al., 2011; De Jong et al., 2013; Pape and Grose, 2020).

Several molecular mechanisms can cause neurodegeneration in ALS (De Vos et al., 2000; Magrané and Manfredi, 2009; Shi et al., 2010; Forsberg et al., 2011; Zhu and Sheng, 2011; Donnelly et al., 2013; Jaiswal, 2014; Mitsumoto et al., 2014; Wang et al., 2014), and others can be considered secondary in the development of ALS (Vucic and Kiernan, 2007).

Glutamate Excitotoxicity

Glutamate has a neurotoxic effect when it accumulates at the synapses (Gazulla and Cavero-Nagore, 2006). In patients with ALS (both spinal cord and motor cortex involvement), and in the superoxide dismutase 1 (SOD1) transgenic mouse model, a decrease in glutamate receptors (GluRs) was found in astrocytes. This decrease induces extracellular glutamate accumulation, which causes overstimulation of GluRs and neuronal death via excitotoxicity (Lin et al., 1998; Trotti et al., 1999; Barbeito et al., 2004; Pratt et al., 2012). In ALS patients, a decrease in glutamate transporters is mainly due to an alteration in messenger RNA (Lin et al., 1998; Honig et al., 2000).

Structural and Functional Abnormalities of the Mitochondria

Mitochondrial function disturbances, such as fragmentation and aggregation, are frequently found in ALS patients (Vielhaber et al., 2000; Chung and Suh, 2002; Krasnianski et al., 2005; Echaniz-Laguna et al., 2006; Crugnola et al., 2010; Cozzolino and Carrì, 2012). Increased crests, swelling, and fragmentation have been observed in the mitochondria of the spinal motor neurons and proximal axons of skeletal muscle in ALS-related tissues (Chung and Suh, 2002; Echaniz-Laguna et al., 2002; Boillée et al., 2006a). The increase in the misfolded SOD1 enzyme in the mitochondria of the spinal cord of mice is considered to be the main cause of mitochondrial dysfunction. In addition, aggregates of the enzyme SOD1 may also interact with the apoptosis regulator protein Bcl-2, inducing an apoptotic cascade and contributing to the deterioration of neurons and neuromuscular degeneration (Boillée et al., 2006a).

Impaired Axonal Structure and Transport Defects

Axonal transport (retrograde and anterograde) is impaired in ALS patients and in mutant SOD1 mice, as evidenced by the accumulation of altered structures, such as mitochondria, neurofilaments, and autophagosomes, in the spinal motor neuron axons (Ikenaka et al., 2012; Zarei et al., 2015). Mutations in the dynein genes have been seen in models of ALS mice. Dyneins are responsible for the transport of mitochondria and autophagosomes, causing both to accumulate in the axon (Ikenaka et al., 2012). Autophagosomes are necessary for the elimination of altered mitochondria and dilated endoplasmic reticules, which accumulate in the axons of motor neurons and cause them to malfunction (Zarei et al., 2015). All of the above suggest that an alteration in axonal transport could be fundamental for the development of ALS.

Free Radical-Mediated Oxidative Stress

Increased free radical and oxidative damage has been found in biopsies from ALS patients, as well as in cerebrospinal fluid, serum, and urine samples (Simpson et al., 2004; Shin Hee and Lee Keun, 2013). This oxidative damage also affects RNA, which

has been shown in both human central nervous system (CNS) biopsies and in mouse ALS models of SOD1 (Chang et al., 2008). The enzyme SOD1 is an important anti-oxidant. The alterations in the redox reactions are one of the first theories of how mutations in SOD1 can cause cytotoxicity (Carrì et al., 2015). In addition, it has been observed in the motor cortex, using positron emission tomography (PET), that increased oxidative stress is related to the severity of the disease in ALS patients (Tsujikawa et al., 2015).

Protein Aggregates

It has been shown that in ALS, abnormal protein accumulations are produced that aid in the pathogenesis of the disease (Blokhuis et al., 2013). The ubiquitin–proteasome (UP) system, which repairs and removes proteins, plays an important role in ALS, with ubiquitin-reactive inclusions being characteristic of this pathology (Han-Xiang et al., 2011; Pratt et al., 2012). Among these, the inclusions of proteins TDP-43 and p62 are indicative of this pathology (Al-Sarraj et al., 2011; Williams et al., 2016). Some ALS patients present numerous inclusions positive for p62 but negative for TDP-43 in the hippocampus and cerebellum (Al-Sarraj et al., 2011). These p62-positive and TDP-43-negative inclusions have also been observed in other CNS areas including the retina (Brettchneider et al., 2013; Fawzi et al., 2014).

Neuroinflammation

Neuroinflammation occurs in many neurodegenerative diseases, such as Parkinson's, Alzheimer's, and ALS, resulting in the activation of astroglial and microglial cells (Ramírez et al., 2017). Specifically, in ALS, it has been observed that reactive glia (microglia and astrocytes) can influence the damage and subsequent death of motor neurons (Vargas and Johnson, 2010; Philips and Robberecht, 2011; Liao et al., 2012). In the ALS, the presence of mutant proteins (SOD1 and TDP-43), oxidative stress, mitochondrial damage, etc., produces continuous damage, which can trigger a chronic activation of glial cells and, therefore, a sustained inflammatory process that could exacerbate neuronal damage (Philips and Robberecht, 2011). It has been observed that the mutant SOD1 protein can have a toxic function on motor neurons only when the activated microglia is present through a mechanism involving a toll receptor (CD14-TLR) that causes an increase in free radicals (Zhao et al., 2010). Astrocyte activation (Vargas and Johnson, 2010), microglial activation (Alexianu et al., 2001), and lymphocyte appearance (Engelhardt et al., 1993) have been found in animal models of ALS (mutants of SOD1) (Alexianu et al., 2001; Boillée et al., 2006b) and in ALS patients (Kushner et al., 1991; Kawamata et al., 1992; Nagy et al., 1994; Schiffer et al., 1996; Turner et al., 2004). In both cases, the mutant SOD1 causes the microglia to increase the expression of pro-inflammatory cytokines, such as IL-1β and TNF-α (Weydt et al., 2004), and inflammatory mediators, such as cyclooxygenase 2 (COX-2) (Almer et al., 2001) and nitric oxide (NO). The NO released by the microglia could induce apoptosis in motor neurons through the activation of Fas via (Raoul et al., 2002).

Mutant protein TDP-43 can produce microglial activation through the surface receptor CD14, which stimulates the NF-κB and AP-1 pathways and the inflammasome. This can cause a neurotoxic cascade leading to motor neuron death (Zhao et al., 2015). In the ALS SOD1 model, the microglia isolated at the onset of the disease has an M2 or anti-inflammatory phenotype; however, the microglia isolated at the end of the disease has a neurotoxic M1 phenotype. This demonstrates a dual role of microglial cells during the disease process in this ALS model (Liao et al., 2012).

Astrogliosis has been observed in ALS models with mutations in *C9orf72*, *FUS*, *SOD1*, and *TARDBP* genes (Wong et al., 1995; Liu et al., 2016; Sharma et al., 2016). In the last model, the death of the motor neurons could be due, in part, to a loss of the function of the TDP-43 protein in the astrocytes (Yang et al., 2014). In ALS SOD1 models, astrocytes can release ATP, causing the activation of microglial cells via purinergic receptors (P2X7) (Gandelman et al., 2010). They can also release transforming growth factor-β1 (TGF-β1), which can induce microglial inactivation, thereby eliminating the possible beneficial effects of the microglia and, thus, accelerating the progression of the pathology (Endo et al., 2015). Moreover, the microglia in ALS can affect astrocytes by favoring the appearance of a neurotoxic subtype (Liddelow et al., 2017).

Considering all of the above, both the microglia and reactive astrocytes can affect neural function in ALS by playing an important role in the progression of the disease.

Genetics

Although most cases (90–95%) of ALS are sporadic (SALS) and not inherited, 10% of cases are of genetic origin (Byrne et al., 2011). Specific genetic locus mutations have been found to constitute the cases of FALS (Deivasigamani et al., 2014). The pattern of inheritance depends on the genes involved. Most cases are inherited in an autosomal dominant pattern (He et al., 2015). Men show more intense symptoms of the disease than women. There are many genes involved in the development of this disease. In FALS, mutations in the *C9orf72* gene represent 30–40% of cases, those in the *SOD1* gene make up 15–20%, those in the *FUS* and *TARDBP* genes each represent approximately 5% of cases, and the remaining genes that have been associated with FALS each represent a small proportion of cases (Pratt et al., 2012; Blokhuis et al., 2013). We next describe some of these genes.

C9orf72 Gene

This gene is located at the locus 9p21 of chromosome 9. It has been proposed that the *C9orf72* mutation can decrease the C9orf72 protein, thus causing less endocytosis, which is necessary for autophagy (Mathis et al., 2019). Moreover, the massive accumulation of the expanded hexanucleotide GGGGCC could be neurotoxic and sequester proteins that bind to RNA, thereby causing the disruption of the machinery that processes RNA (Mathis et al., 2019). This mutation could also lead to increased vulnerability to excitotoxicity due to increased calcium permeability mediated by AMPA type receptors (Selvaraj et al., 2018). The form of inheritance is autosomal dominant, although some carriers do not develop the disease, so it has an incomplete penetrance (Renton et al., 2011). This variant represents the most frequent cause of SALS (7%) and FALS (30–40%) (Majounie et al., 2012). The manifestations at the onset of the disease are typical of

ALS and have a bulbar onset. This variant is often associated with an earlier age of onset, a faster clinical course, and shorter survival (Schymick and Traynor, 2010).

FUS Gene

The *FUS* gene, located on the short arm of chromosome 16 (16p11.2), encodes a protein called sarcoma fusion protein (FUS) (Hübers et al., 2015; Scekic-Zahirovic et al., 2017). In ALS, mutations in the *FUS* gene have been observed, most of which can produce changes in amino acids in the region of the protein related to DNA binding and mRNA processing. These mutations may interfere with the importation of FUS into the cell nucleus, which will cause an accumulation of FUS in the cytoplasm. This has been observed particularly in the nerve cells that control muscle movement (Scekic-Zahirovic et al., 2017). This mutation occurs in 3–5% of FALS and in 1% of SALS cases (Deng et al., 2010; Mackenzie et al., 2010). In addition, patients with *FUS* mutations tend to develop the disease earlier and have a shorter life expectancy than those observed with mutations in other genes. Patients with ALS and *FUS* mutations may also develop frontotemporal dementia (FTD) (Kwiatkowski et al., 2009; Vance et al., 2009).

OPTN Gene

The optineurin gene (*OPTN*) is located on chromosome 10 and encodes a protein called optineurin, which is a multifunctional ubiquitin-binding phosphoprotein found in the cytoplasm. Changes of this protein can cause alterations in intracellular traffic and lead to inclusions in ALS. In addition, this protein is also involved in the signaling of the tumor necrosis factor α/NF-κB pathway (Zhu et al., 2007) and the mGluR (Ying et al., 2010). In 2010, Maruyama et al. (2010) and Schymick and Traynor (2010) found mutations in the *OPTN* gene in ALS patients. These mutations are present in 1.2% of patients with FALS (Del Bo et al., 2011). ALS patients with OPTN mutations presented typical spinal-onset disease (Weishaupt et al., 2013). Mutations in this gene were previously shown to be involved in primary open-angle glaucoma (Maruyama et al., 2010). This gene has also been linked to normotensional glaucoma in ALS patients (Weishaupt et al., 2013). In cells from patients with SALS and FALS, optineurin can be placed in inclusion bodies with TDP-43 (Maruyama et al., 2010), FUS (Ito et al., 2011), and SOD1 (Maruyama et al., 2010). Both retinal ganglion cells (RGCs) and motor neurons share common susceptibility factors (Weishaupt et al., 2013).

SOD1 Gene

The *SOD1* gene is located on the long arm of chromosome 21 (21q22.11). This gene encodes a cytosolic enzyme called copper zinc (Cu/Zn) SOD1 (Gatchel and Zoghbi, 2005; Valentine et al., 2005) that plays a very important role in the elimination of superoxide radicals, thereby protecting against free radicals (Azadmanesh and Borgstahl, 2018). Around 2.5–23% of patients with FALS and 0.44–7% of those with SALS have mutations in SOD1 (Andersen, 2006; Van Es et al., 2010). Most of the inherited forms of SOD1 gene mutations are dominant (Hayward et al., 1998; Marucci et al., 2007). Mutations in the SOD1 enzyme can induce configurational changes in the SOD1 protein leading to motor neuron toxicity (Mathis et al., 2019). ALS patients who present mutations in SOD1 show an earlier time of onset and a longer duration of disease. In addition, they usually do not present cognitive disorders, and their motor symptoms usually begin in the lower extremities (Mathis et al., 2019).

TARDBP Gene

The Tar DNA binding protein (*TARDBP*) gene is located on the short arm of chromosome 1 (1p36.22) and encodes the TDP-43 protein. More than 40 mutations have been identified in the *TARDBP* gene and result in 6.5% of FALS cases. The form of inheritance is dominant (Kühnlein et al., 2008; Van Deerlin et al., 2008) and represents 0–5% of SALS cases (Kühnlein et al., 2008; Rutherford et al., 2008; Sreedharan et al., 2008). Most of the mutations cause changes in the amino acids in the TDP-43 protein and affect the region of the protein involved in the processing of RNA (Neumann et al., 2006; Da Cruz and Cleveland, 2011). Cytoplasmic inclusions of ubiquitin-reactive hyperphosphorylated TDP-43 proteins have been found in tissues of patients with FTD (Arai et al., 2006; Neumann et al., 2006). These inclusions have also been seen in the glial tissue and neurons of patients with SALS (Maekawa et al., 2009). These inclusions can often be placed with p62 and ubiquitin but are not found in FALS with *FUS* mutation (Vance et al., 2009) or *SOD1* mutation (Mackenzie et al., 2007). Some patients with FALS and *TARDBP* mutation may also develop FTD (Arai et al., 2006; Neumann et al., 2006).

MATERIALS AND METHODS

A literature search was performed up to May 2020 using the "MESH" terms in PubMed with the following keywords and word combinations: "Amyotrophic Lateral Sclerosis," AND "Environmental Exposure," "Nerve Degeneration," "mitochondria," "oxidative stress," "Protein Aggregates," "Microglia," "Genetics," "Oculomotor Muscles," "Visual Pathways," "Evoked Potentials, Visual," "Contrast Sensitivity," "Visual Fields," "Visual Field Tests," "Visual Acuity," "Retina," OR "Optical Coherence Tomography." After filtering by author criteria (articles published in the last 10 years), English or Spanish language, and the condition that all address the relationship between ALS and visual pathway as the main subject, 196 articles were considered, and 304 articles did not satisfy the selection criteria (**Figure 1**).

Inclusion criteria: Articles were selected according to the following criteria: (i) articles focused on general features of ALS pathology, (ii) research that related the ALS with visual system alterations, (iii) retinal research developed in both ALS patients and animal experimental models of ALS, and (iv) articles based on human clinical trials with optical coherence tomography (OCT) analysis.

Exclusion criteria: Articles were excluded with the following characteristics: (i) research not carried out in mammalian experimental models of ALS and (ii) articles that did not have the sufficient outcomes associated with the objective of this review or did not meet the selection criteria of the authors.

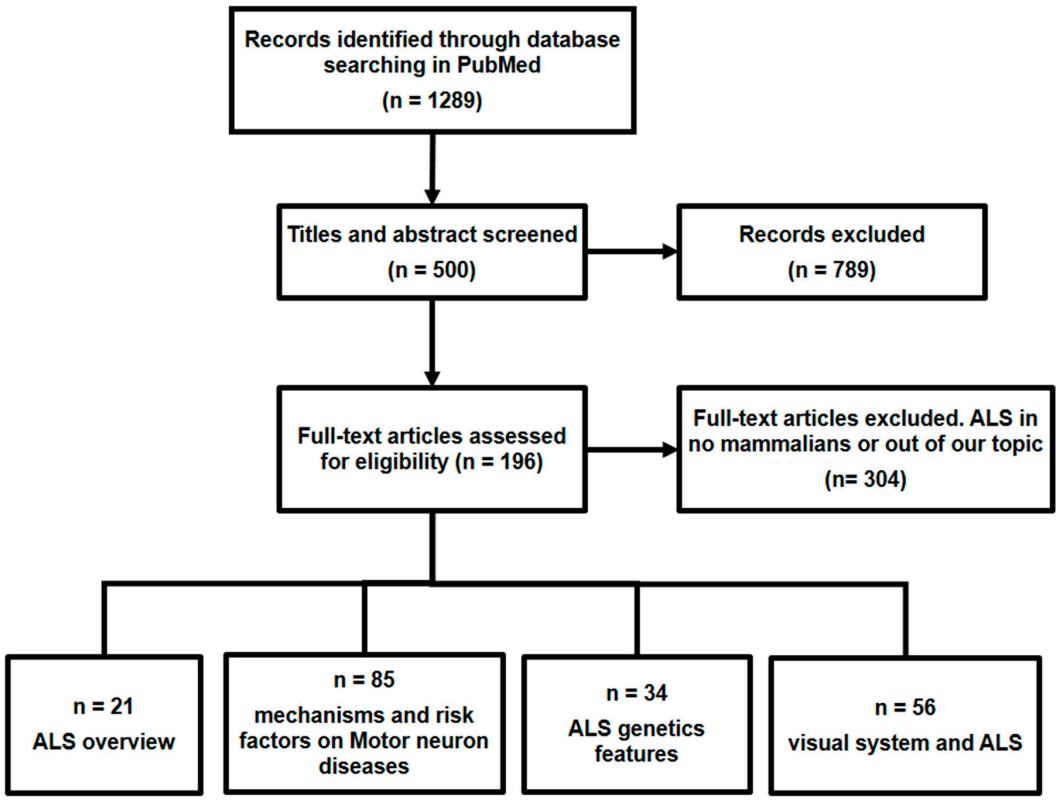

FIGURE 1 | Flow chart materials and methods.

AMYOTROPHIC LATERAL SCLEROSIS AND THE EYE

As discussed above, ALS affects not only motor neurons, the spinal cord, the cerebellum, and large areas of the brain but also the visual system, including the oculomotor and visual pathways. However, patients usually do not have visual complaints. For this reason, studies focusing on the visual pathway are not common. Most previous studies were related to the oculomotor function and the study of visual evoked potentials (VEPs) that analyze the visual pathway. However, some studies of ALS have subsequently emerged that are more related to visual function, using tests such as visual acuity, contrast sensitivity, and visual field (VF). In addition, the retina has now been described as a "window to the brain," and the changes that the brain suffers in neurodegenerative diseases can also appear in the retinal tissue (MacCormick et al., 2015). Changes in retinal tissue can be detected using OCT, which is a diagnostic technique widely used in ophthalmology and has recently been used for the analysis of retinal and optic nerve changes in neurodegenerative diseases such as ALS disease. This technique can help in the diagnosis and follow-up of these pathologies (Salobrar-García et al., 2015a,b, 2016).

The following is a description of the main alterations found in this visual system using the aforementioned techniques and tests (**Figure 2**).

Oculomotor Function Alterations

Amyotrophic lateral sclerosis is a condition that affects motor neurons and large areas of the brain, so ocular movements may be affected. Thus, numerous studies on oculomotor function have appeared since the 1980s and continue to appear today (**Table 1** and **Figure 2**). Although oculomotor function is generally retained in ALS patients, they may manifest various oculomotor dysfunctions both at a relative early stage and in advanced stages of the disease. These include (i) a worsening of saccadic and pursuit eye movements (Leveille et al., 1982; Cohen and Caroscio, 1983; Saito and Yamamoto, 1989; Gizzi et al., 1992; Marti-Fàbregas and Roig, 1993; Ohki et al., 1994; Abel et al., 1995; Shaunak et al., 1995; Okuda et al., 2009; Donaghy et al., 2010; Moss et al., 2012; Kang et al., 2018); (ii) a lack of suppression of the vestibulo-ocular reflex (Ohki et al., 1994); (iii) a significant increase in error rates (distraction) and latency in anti-saccadic movements (Shaunak et al., 1995; Donaghy et al., 2010) that may evoke saccadic paradigms, head shaking (Kang et al., 2018), and positional nystagmus of central origin (Saito and Yamamoto, 1989; Marti-Fàbregas and Roig, 1993; Ohki et al., 1994; Kang et al., 2018); (iv) gaze fixation instability (Saito and Yamamoto, 1989; Palmowski et al., 1995; Shaunak et al., 1995; Donaghy et al., 2009; Moss et al., 2012; Kang et al., 2018); (v) eyelid opening apraxia (Averbuch-Heller et al., 1998; Moss et al., 2012); and (vi) square wave jerks (Gizzi et al., 1992; Shaunak et al., 1995; Kang et al., 2018), which may reflect the incidence

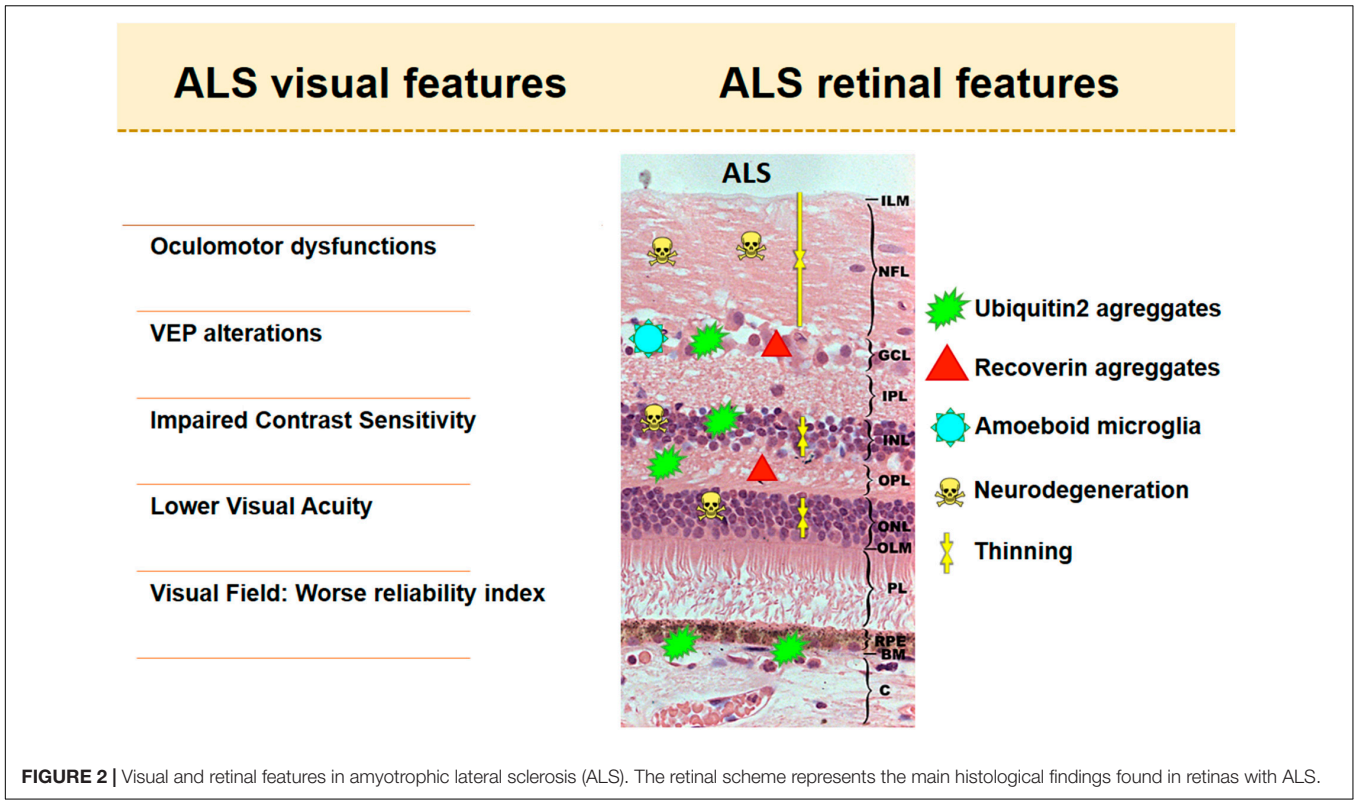

FIGURE 2 | Visual and retinal features in amyotrophic lateral sclerosis (ALS). The retinal scheme represents the main histological findings found in retinas with ALS.

TABLE 1 | Previous studies of extraocular movements in ALS patients.

Study and year of publication	Type of study	Number of ALS/control patients	Disease duration (months)	ALSFRS score	Alterations in ocular movements in ALS
Leveille et al., 1982	–	10/–	–	–	↓Saccadic pursuit, unidirectional saccadic pursuit, ↓saccadic velocities
Saito and Yamamoto, 1989	Observational	23/100	–	–	Slight limitations of upward only, upward and downward and upward and horizontal gaze, incomplete convergence, horizontal gaze nystagmus. ↑Amplitude ratio of saccade and ↑degree of ocular dysmetria
Marti-Fàbregas and Roig, 1993	Cross-sectional	13/16	29.09	–	↑Saccadic latencies and ↓smooth pursuit gain. Positive relationship between smooth pursuit saccadic intrusions and the bulbar clinical score and the rate of progression and a ↓optokinetic nystagmus maximal velocity in patients with pseudobulbar syndrome
Shaunak et al., 1995	Cross-sectional	17/11	24.5 (6–60)	–	↑Error rates (distractibility) and latency in the anti-saccade and remembered saccade paradigms. ↑Square–wave jerks. Gaze fixation instability
Donaghy et al., 2010	Cross-sectional	30 spinal and 14 bulbar/45	52	35 (18–47)	↓Reflexive saccades in bulbar-onset vs. to spinal-onset patients and controls. ↑Anti-saccade latency and ↑anti-saccade type 1 errors. ↓"Proportion of time spent in smooth pursuit" and ↓smooth pursuit "velocity gain"
Moss et al., 2012	Cross-sectional	63/37	43.2 ± 37.25 (7.2–204)	16 (6–46)	Gaze impersistence, voluntary upgaze restriction, eyelid opening apraxia, saccadic horizontal pursuits
Ohki et al., 1994	Observational	9/–	13 (3–49)	Early stages	↓Velocity of saccades. Abnormalities of smooth pursuit, optokinetic nystagmus, and visual poor suppression of vestibular ocular reflect
Proudfoot et al., 2016	Cross-sectional/ longitudinal	61/39	38.6 (31)	33.5 (6.5)	↓Executive and visual search tasks; normal basic saccadic function. ↓Anti-saccade performance, ↑error rate and latency
Kang et al., 2018	Retrospective/ observational	22 spinal cord/10 bulbar	Spinal 55.1 ± 9.5, bulbar 62.2 ± 11.1	–	Square wave jerks, saccadic dysmetria, abnormal cogwheeling smooth pursuits, head shaking, and positional nystagmus of central origin. ↑ Abnormal smooth pursuits and saccadic dysmetria

ALS, amyotrophic lateral sclerosis; ALSFRS, Amyotrophic Lateral Sclerosis Functional Rating Scale.

of secondary abnormalities, such as parkinsonism (Gizzi et al., 1992), and facilitate prefrontal dysfunction in these patients (Shaunak et al., 1995). In bulbar onset compared with spinal onset, saccadic dysmetria and abnormal cogwheeling smooth pursuits are increased, which suggests neurodegeneration in ALS involving more than motor neurons (dysfunction of vestibule cerebellar connections), especially in bulbar-onset disease (Kang et al., 2018). In a longitudinal study (Proudfoot et al., 2016), ALS patients, even those with normal saccadic function, were shown to have problems with executive and visual search tasks. These impairments were often more severe than expected in ALS patients. However, no significant progression was observed in the longitudinal study, nor were changes found in the connectivity of the R-FMRI network (Proudfoot et al., 2016). In the postmortem histopathological examination of ALS patients, cell loss was found in the substantia nigra and the rostral interstitial nucleus of the medial longitudinal fasciculus, suggesting that the early involvement of vertical saccades might correspond to a different clinical–pathological type (Averbuch-Heller et al., 1998). Therefore, as suggested by Sharma et al. (2011), changes in the oculomotor function of ALS patients could be promising biomarkers for the mechanical diagnosis, prognosis, and follow-up of ALS.

The extraocular muscles (EOMs) and their motor neurons are retained in ALS. However, from the onset of this disease, the muscles of the limbs show axon retraction at the neuromuscular junctions. Wnt is a preserved family of secreted signaling molecules that are primarily involved in the formation of neuromuscular junctions. This signaling pathway was analyzed both in ALS patients and in a SOD1G93A mouse model for its possible implications in the preservation of normal morphology and the function in EOMs in this disease (McLoon et al., 2014). The authors found differential patterns of expression for Wnt1 and Wnt3a isoforms in the EOMs for limb muscles, especially at the neuromuscular junction level. This suggests that in ALS patients, this signaling pathway is preserved in the EOMs and dysregulated in the muscles of the limbs that subsequently develop a pathology (McLoon et al., 2014).

Visual Pathway Alterations

The alteration of the visual pathway can be analyzed using VEPs, contrast sensitivity, and VF. Next, we describe the different alterations found in the visual pathway of each.

Visual Evoked Potentials

Few studies have analyzed the VEPs in ALS patients (**Table 2** and **Figure 2**). It was not until 1986 that alterations in VEPs were found in patients with ALS, with abnormal relative difference in latencies between each eye. In this study of 32 patients analyzed, only four had VEP abnormalities (increased latency time); however, these alterations were mild (Matheson et al., 1986). In other studies, while wave latency and amplitudes were within normal limits in all ALS patients (Ghezzi et al., 1989; Palma et al., 1993), somatosensory evoked potentials were abnormally delayed (N9–N13 and N13–N19 latencies), but no correlation was found among these abnormalities and the duration and severity of the disease (Ghezzi et al., 1989).

In addition, in ALS patients the P1 component was also found to be absent, and the P300 component was delayed and attenuated (Münte et al., 1998). In a study of six ALS patients, only one patient with a 9-month disease evolution had abnormal P100 bilateral extension VEPs and a significant interocular difference of P100. In addition, none of the patients presented alterations in their electroretinogram (González Díaz et al., 2004). Subsequently, electrophysiological studies of ALS patients showed new evidence of cortical participation involving visual areas, with alterations in the early sensory components of VEPs (Münte et al., 1998).

Contrast Sensitivity

While one study revealed impaired contrast sensitivity during an eye examination in two ALS patients with *C9orf72* mutation (Fawzi et al., 2014), another study concluded that this function is not affected in ALS patients (Volpe et al., 2015; **Table 2** and **Figure 2**).

Visual Acuity

Visual acuity in ALS patients is controversial. While a study found a lower visual acuity in ALS patients in both high-contrast and low-contrast (2.5% and 1.5%) visual acuity with Sloan charts (Moss et al., 2012), in others, the visual acuity exam revealed no differences in monocular high-contrast visual acuity (Volpe et al., 2015; Moss et al., 2016; Rojas et al., 2019) or low-contrast visual acuity (Moss et al., 2016).

Visual Field

Only two studies describe VF in early ALS spinal onset patients. With a decrease of mean sensitivity and an increase of the square of loss variance (Liu et al., 2018), ALS patients presented a worse reliability index (fixation losses, false positives, and negatives) due to motor difficulties. For this reason, the authors suggested that VF is not a suitable test to assess ALS patients (Rojas et al., 2019; **Table 2** and **Figure 2**).

Retinal Abnormalities in Amyotrophic Lateral Sclerosis

Retinal tissue can be analyzed using histological techniques on postmortem tissues or using the OCT technique mentioned above. This technique is an optical analog of ultrasonic imaging using low-coherence interferometry to produce cross-sectional images of the retina and allows *in vivo* observation of retinal tissue alterations (Bhende et al., 2018).

Retinal Histopathological Studies in Amyotrophic Lateral Sclerosis Patients and Amyotrophic Lateral Sclerosis Experimental Models of Mammals

Few studies have focused on the histopathology of retinal tissue in both ALS patients and animal models of mammals with this condition. Histopathological studies in ALS patients demonstrated intraretinal protein inclusions. The first histopathological analysis of the retinas of patients with ALS was performed in 2014 on a patient with the *C9orf72* mutation. In this study, the authors found p62-positive and pTDP43-negative intracytoplasmic perinuclear inclusions in

TABLE 2 | Psychophysics visual test studies in ALS patients.

Study and year of publication	Alterations in visual functions in ALS				
	VEP	**ERG**	**VA**	**VF**	**CS**
Matheson et al., 1986	Abnormal latencies between eyes	–	–	–	–
Ghezzi et al., 1989	WNL	–	–	–	–
Münte et al., 1998	P300 delayed and attenuated	P1 absent	–	–	–
González Díaz et al., 2004	P100 latency prolongation	WNL	–	–	–
Fawzi et al., 2014	–	–	–	–	↓CS
Volpe et al., 2015	–	–	No changes high contrast VA	–	No changes
Moss et al., 2016	–	–	↓High contrast and low contrast VA	–	–
Liu et al., 2018	–	–	–	MS↓ and ↑sLV	–
Rojas et al., 2019	–	–	No changes high contrast VA	↓ reliability index (↑fixation losses, ↑false positives and negatives)	–

ALS, amyotrophic lateral sclerosis; VEP, visual evoked potentials; ERG, electroretinogram; VA, visual acuity; VF, visual field; CS, contrast sensitivity; WNL, within normal limits; MS, mean sensibility; sLV, square of loss variance.

the inner nuclear layer (INL). These deposits were similar to those observed in the dentate gyrus of ALS patients with the *C9orf72* mutation. The p62-positive staining was colocalized for both the poly-(GA)n dipeptide repeat and ubiquitin in the retina, which is similar to the perinuclear inclusions located in the brains of patients with this mutation. The p62-positive inclusions found were likely located in specific cone bipolar cells and within the amacrine and horizontal cells, as they were also marked with GLT-1 and recoverin. The authors suggested that these deposits may be related to the affectation of contrast sensitivity (Fawzi et al., 2014). In addition, in other ALS patients with *C9orf72* mutations, specific p62 inclusions were observed in the retinal ganglion cell layer (GCL) in a far smaller proportion than in INL (94.9% in INL vs. 5.1% in GCL). Numerous positive ubiquitin2 + aggregates were also observed in a mutant *UBQLN2* transgenic mice experimental model, mainly in the INL, with fewer in the outer plexiform layer (OPL) and some in the GCL (Volpe et al., 2015). The accumulation of ubiquitin2 aggregates in the layers of the retina with more synapses is related to the accumulation of these aggregates in the dendritic spines of the hippocampus. The location of the aggregates at the synapses, and their spines, may be associated with the dementia observed in this experimental model of ALS. In addition, few ubiquitin2 positive aggregates were detected in the subretinal space of the retinal pigment epithelium, which sometimes elevated these levels in the same way as druses (Volpe et al., 2015). Furthermore, lipofuscin deposits sometimes related to subretinal drusen-like aggregates were found in progranulin-deficient FTD patients (Ward et al., 2017). Retinal thinning in these patients was detected by OCT before symptoms, suggesting that the eye is affected in progranulin-deficient FTD disease (Ward et al., 2014).

As noted previously, microglial and astroglial cell activation occurs in ALS. However, to our knowledge, there are only two works that analyzed the glial cells of the retina in relation to ALS. hSOD1 + vacuoles located in the dendrites of excitatory retinal neurons were observed in a mouse model of ALS SOD1 ($SOD1^{G93A}$), mainly in the inner plexiform layer (IPL) and rarely in the GCL and INL. However, there were no signs of activation of either the astroglia or the microglia of the retina compared with those of wild-type mice (Ringer et al., 2017). In contrast, microglial activation was demonstrated in a mouse model of ALS [devoid of ran-binding protein2 (Ranbp2)]. Ranbp2 is a protein involved in nucleo-cytoplasmic transport whose regulation is impaired in both SALS and FALS (Ferreira, 2019). In ALS mice without this protein (with respect to wild-type controls), there was an increase in the number of CD45 +, CD11b +, and F4/80 + microglial cells surrounding the RGCs, in addition to a notable increase in amoeboid forms. An increase of metalloproteinase 28, which is an immune regulator, was also observed in the RGCs, suggesting that Ranbp2 may be involved in the signaling between the microglia and the RGCs in the immune response of ALS disease (Cho et al., 2019; **Figure 2**).

Optical Coherence Tomography

Although the first study performed in 75 ALS patients with Cirrus OCT showed no changes in the peripapillary and macular areas (Roth et al., 2013), further studies have shown that there are changes in the retina of ALS patients (Ringelstein et al., 2014; Volpe et al., 2015; Hübers et al., 2016; Simonett et al., 2016; Mukherjee et al., 2017; Abdelhak et al., 2018; Liu et al., 2018; Rohani et al., 2018; Rojas et al., 2019; **Table 3**).

In the retina of ALS patients, high-resolution SD-OCT revealed reduction in the mean total macular thickness, in the peripapillary retinal nerve fiber layer (pRNFL), the INL (Ringelstein et al., 2014; Hübers et al., 2016), and the outer nuclear layer (ONL) (Abdelhak et al., 2018), suggesting neurodegeneration of the retina in ALS patients.

Volpe et al. studied whether clinical and histopathological findings were present in the eyes of ALS patients and explored their correlation with an animal model (ALS/dementia transgenic mice with dysfunctional ubiquilin2, UBQLN2P497H) (Volpe et al., 2015). Using SD-OCT, the authors observed that (i) in ALS patients compared with the controls, there was a decrease in total macular volume; (ii) 37.5% of ALS patients

TABLE 3 | OCT studies in ALS patients.

Study and year of publication	OCT device	Type of study	Number of ALS/control patients	Disease duration (months)	ALSFRS-R score	Alterations in visual functions	Differences ALS vs. control						Correlation OCT-ALSFRS-R
							Macula	GCC	pRNFL	mRNFL	ONL	INL	
Roth et al., 2013	Cirrus HD-OCT	Cross-sectional	76/54	42 ± 34 (7–166)	34 ± 7	–	–	No	No	No	No	No	No
Ringelstein et al., 2014	SD-OCT Spectralis	Cross-sectional	24/24	22.3 ± 22.57 (3–120)		–	–	No	↓	↓	No	↓	No
Hübers et al., 2016	SD-OCT Spectralis	Cross-sectional	71/20	12 (2–98)	40 (16–48)	–	–	No	↓	No	No	↓	–
Volpe et al., 2015	SD-OCT Spectralis	Cross-sectional	16/15	85.3 ± 110.79	–	= VA, color vision, and CS. Histopathology study	–	–	↓	↓		–	No. OCT inversely correlates with disease duration
Simonett et al., 2016	SD-OCT Spectralis	Cross-sectional	21/21	43.2 ± 43.4 (10–197)	28.1 ± 12.5	–	–	No	–	↓	No	No	No. (correlation FVC% and FEV1%)
Mukherjee et al., 2017	SD-OCT Spectralis	Cross-sectional	21/normative OCT database	–	30 ± 10	VA (Snellen)	–	–	↓Global and six sectors	–	–	–	No
Rohani et al., 2018	SD-OCT Topcon 3D	Cross-sectional	20	14.5 ± 11.3	33.1 ± 3.8	–	–	–	↓Mean, sup and nasal	–	–	–	Direct correlation
Liu et al., 2018	HD-OCT Cirrus 4000	Cross-sectional	51/126	18.46 ± 6.16 (6–72)	39.58 ± 10.41 (10–48)	VF: MS↓ and ↑sLV	No	No	↑Nasal quadrant	–	–	–	Macula direct correlation (temporal Q correlated with duration of the disease)
Abdelhak et al., 2018	SD-OCT Spectralis	Cross-sectional	34/20	12 (7–17)	–	Diameters of retinal vessels	–	No	No	–	↓	No	Retinal thickness inverse correlation
Rojas et al., 2019	HD-OCT Cirrus 4000	Prospective longitudinal	38/20	10.80 ± 5.5 (1–18)	Baseline 29.50 ± 14.89 Follow-up 35.6 ± 14.08 (some patients dead)	VA and VF	↑Temporal and ↑inferior. Follow-up: ↓ Inferior	No	↓Sup, ↓inf. ↓H3, H5, H6, H12 ↑H8	–	–	–	pRNFL inverse correlation

ALS, amyotrophic lateral sclerosis; GCC, ganglion cell complex; RNFL, retinal nerve fiber layer; pRNFL, peripapillary RNFL; mRNFL, macular RNFL; ONL, outer nuclear layer; INL, inner nuclear layer; VA, visual acuity; CS, contrast sensitivity; FVC%, Forced vital capacity% predicted; FEV1%, forced expiratory volume in 1 s% predicted; MS, mean sensibility; sLV, square of loss variance; ALSFRS, Amyotrophic Lateral Sclerosis Functional Rating Scale.

showed an average pRNFL below the first percentile, and temporal and papillomacular bundle were more affected; and (iii) in ALS patients, the total macular thickness and pRNFL thickness correlated inversely with the time of evolution of ALS (Volpe et al., 2015).

Recently, in a study performed in early ALS patients with spinal onset and without ocular diseases, a significant macular thickness increase was found in the temporal and inferior areas of the inner macular ring in comparison with that in a healthy control, suggesting that this retinal thickening in early ALS patients could be due a microglial activation in the neuroinflammatory process (Ringelstein et al., 2014; Rojas et al., 2019). In contrast, in another study in ALS patients, only the macular retinal nerve fiber layer (mRNFL) showed a significant thickness decrease by OCT, which correlated positively with pulmonary function tests (Simonett et al., 2016). However, neither total macular thickness nor macular thickness showed changes (Simonett et al., 2016).

Only one study exists that detected a thinning in the ONL (Abdelhak et al., 2018), suggesting a possible impact on the photoreceptors and linking this finding with this subclinical visual acuity impairment (Moss et al., 2012; Abdelhak et al., 2018). Using SD-OCT, this work analyzed the retinal vessels, finding that in ALS patients compared with the control, the outer wall thickness of the retinal vessels was higher than in the control group (Abdelhak et al., 2018). Similar microvascular alterations in the brain and spinal cord of ALS model mice were found to precede the degeneration of motor neurons (Zhong et al., 2008).

In ALS patients, an analysis of the relationship of clinical features and retinal changes using SD-OCT and diffusion tensor imaging (DTI) found no significant correlation between clinical features and retinal thickness; however, there was a direct correlation between retinal thickness and fractional anisotropy of the corticospinal tract (Hübers et al., 2016). On the basis of these observations, it was suggested that retinal changes could be related to damage of white matter in the corticospinal tract and may be a possible biomarker in ALS (Hübers et al., 2016).

Although several papers have demonstrated the pRNFL decrease in ALS patients without ocular pathology (Mukherjee et al., 2017; Rohani et al., 2018; Rojas et al., 2019), there is controversy about its correlation with ALSFRS-R values. While one study did not demonstrate a correlation between RNFL thickness and the ALSFRS-R score and their progression rates (Mukherjee et al., 2017), other authors found a correlation with some OCT parameters (Abdelhak et al., 2018; Liu et al., 2018; Rohani et al., 2018; Rojas et al., 2019; Salobrar-García et al., 2019). In a study of the pRNFL thickness in four quadrants, the average pRNFL thickness showed a significant positive correlation with the ALSFRS-R score (Rohani et al., 2018), and the pRNFL thickness in the inferior sector was negative (Rojas et al., 2019). When the analysis was more detailed, dividing the papilla into 12 hourly sectors, sectors H5 and H6 had a positive direct significant correlation, and H8 had an inverse significant correlation of pRNFL with the ALSFRS-R values (Rojas et al., 2019). In addition, the entire retinal thickness correlated negatively with the ALSFRS-R score (Abdelhak et al., 2018).

Follow-up OCT studies of ALS patients are very rare. In the only one performed of early ALS patients with spinal onset (basal patients) who were examined 6 months after the basal scan (follow-up patients), the SD-OCT follow-up analysis of ALS patients showed a significant macular thickness decrease in the inferior areas of the inner and outer macular ring and a significant pRNFL thickness decrease in the superior and inferior quadrants, compared with the baseline (Rojas et al., 2019).

Asymmetry is a typical hallmark of ALS, as mentioned above. In the left eye (LE) of ALS patients, after adjustment for multiplicity, there was a significant decrease in pRNFL thickness in the nasal quadrant compared with the corresponding quadrant thickness in the right eye (RE) (Rohani et al., 2018). In the follow-up study mentioned above (Rojas et al., 2019), there were significant interocular asymmetries in some areas between the LE, which were always thinner, and the RE were observed. In the baseline ALS group, in the LE, the inferior-nasal quadrant of the macular ganglion cell complex (GCC), and the H7 and H9 hourly-sectors of the pRNFL were significantly thinner than those in the RE, while in the follow-up ALS group, both the supero-nasal quadrant of macular GCC and the temporal quadrant, and the H8 and H9 hourly sectors of the pRNFL, were significantly thinner in the LE than those in the RE. Therefore, the asymmetric participation of the CNS in this disease is not exclusive to the motor system (Rohani et al., 2018).

Thinning of the inner retina was also observed by SD-OCT in other neurodegenerative diseases, including Alzheimer's disease and Parkinson's disease, in which both RNFL and GCL thinning were detected (Moreno-Ramos et al., 2013; Coppola et al., 2015; Salobrar-García et al., 2015b; Garcia-Martin et al., 2016). However, in FTD, OCT identified ONL thinning, specifically in the ellipsoid zone, and this thinning of the outer retina correlated with cognitive changes (Kim et al., 2017). Moreover, the relationship between ONL thinning and FTD was especially apparent in the subgroup of patients considered to have "likely tauopathy" based on their symptoms or their genetics (Kim et al., 2017).

The differences observed in retinal thickness measurements using OCT may be due to the following: (i) the different disease stages of ALS patients included in the studies; (ii) the heterogeneous nature of this pathology (Hübers et al., 2016); and (iii) the small number of participants in these studies, since most ALS patients do not manifest visual problems.

Many authors observed changes in retinal thickness, as shown in this section. Therefore, retinal changes constitute a biomarker of neurodegeneration and progression of ALS disease (Hübers et al., 2016; Rohani et al., 2018), and OCT analysis is a useful tool for the study of this pathology (Rojas et al., 2019).

CONCLUSION

In view of the above, changes in visual function are moderate in ALS. The main changes occur at the oculomotor level, but with no great affect. Functional tests such as VA, contrast sensitivity,

VF, and VEPs show mild alterations in ALS. However, the low rate of functional impairment does not mean that there are no structural changes in the visual pathway in ALS patients. New techniques such as OCT have made it possible to detect structural changes in the retina (due to retrograde or anterograde involvement), but which ultimately reflect changes in the visual pathway. These changes monitored with OCT could help to follow up this pathology. However, these studies are recent and are not homogeneous due to differences in the patients' degree of disease, time of evolution, age group, or ALS scores. In addition, differences in the OCT technology make it difficult to compare between the different studies. Thus, it is necessary to perform more studies to analyze the retinal changes that occur in ALS disease. In addition, there are also many unanswered questions, including when and where the changes in the retina first occur, which subgroups of patients exhibit retinal phenotypes, and whether these phenotypes change over time. Longer studies are needed to determine whether retinal thickness might be a useful way to measure disease progression and whether patients with different genetic mutations that cause ALS experience more severe retinal involvement.

We conclude that, in addition to CNS disorders, there are also peripheral neurological diseases that can affect the retina. We have shown that the retina has great sensitivity as a biomarker for susceptibility/risk in MND, despite the fact that the retinal changes do not produce clinical visual symptoms. Therefore, the use of OCT in ALS patients could be a recommended test within the diagnostic techniques of this pathology.

AUTHOR CONTRIBUTIONS

PR, AR, IL-C, ES-G, RH, and JR designed the concept and drafted the manuscript. JF-A, IL-C, ES-G, MC, LE-H, and JS collected the literature, analyzed the data, and edited the language in the manuscript. All authors contributed to the article and approved the submitted version.

FUNDING

This work was supported by the Ophthalmological Network OFTARED (*Enfermedades oculares: Prevención, detección precoz, tratamiento y rehabilitación de las patologías oculares*) (RD16/0008/0005), Institute of Health of Carlos III, Spanish Ministry of Economy and the European program FEDER and Network RETiBRAIN (*La retina un modelo para investigar Neuroprotección en patologías del Sistema Nervioso Central*) (RED2018-102499-T), Spanish Ministry of Science, Innovation and Universities. JF-A was currently supported by a Predoctoral Fellowship (FPU17/01023) from the Spanish Ministry of Science, Innovation and Universities. IL-C was currently supported by a Predoctoral Fellowship (CT42/18-CT43/18) from the Complutense University of Madrid.

REFERENCES

Abdelhak, A., Hübers, A., Böhm, K., Ludolph, A. C., Kassubek, J., and Pinkhardt, E. H. (2018). In vivo assessment of retinal vessel pathology in amyotrophic lateral sclerosis. *J. Neurol.* 265, 949–953.doi:10.1007/s00415-018-8787-x

Abel, L. A., Williams, I. M., Gibson, K. L., and Levi, L. (1995). Effects of stimulus velocity and acceleration on smooth pursuit in motor neuron disease. *J. Neurol.* 242, 419–424. doi: 10.1007/BF00873543

Abrahams, S., Goldstein, L. H., Suckling, J., Ng, V., Simmons, A., Chitnis, X., et al. (2005). Frontotemporal white matter changes in amyotrophic lateral sclerosis. *J. Neurol.* 252, 321–331. doi: 10.1007/s00415-005-0646-x

Alexianu, M. E., Kozovska, M., and Appel, S. H. (2001). Immune reactivity in a mouse model of familial ALS correlates with disease progression. *Neurology* 57, 1282–1289. doi: 10.1212/WNL.57.7.1282

Almer, G., Guégan, C., Teismann, P., Naini, A., Rosoklija, G., Hays, A. P., et al. (2001). Increased expression of the pro-inflammatory enzyme cyclooxygenase-2 in amyotrophic lateral sclerosis. *Ann. Neurol.* 49, 176–185. doi: 10.1002/1531-8249(20010201)49:2<176::aid-ana37>3.0.co;2-x

Al-Sarraj, S., King, A., Troakes, C., Smith, B., Maekawa, S., Bodi, I., et al. (2011). p62 positive, TDP-43 negative, neuronal cytoplasmic and intranuclear inclusions in the cerebellum and hippocampus define the pathology of C9orf72-linked FTLD and MND/ALS. *Acta Neuropathol.* 122, 691–702. doi: 10.1007/s00401-011-0911-2

Andersen, P. M. (2006). Amyotrophic lateral sclerosis associated with mutations in the CuZn superoxide dismutase gene. *Curr. Neurol. Neurosci. Rep.* 6, 37–46. doi: 10.1007/s11910-996-0008-9

Arai, T., Hasegawa, M., Akiyama, H., Ikeda, K., Nonaka, T., Mori, H., et al. (2006). TDP-43 is a component of ubiquitin-positive tau-negative inclusions in frontotemporal lobar degeneration and amyotrophic lateral sclerosis. *Biochem. Biophys. Res. Commun.* 351, 602–611. doi: 10.1016/j.bbrc.2006.10.093

Averbuch-Heller, L., Helmchen, C., Horn, A. K., Leigh, R. J., and Büttner-Ennerver, J. A. (1998). Slow vertical saccades in motor neuron disease: correlation of structure and function. *Ann. Neurol.* 44, 641–648. doi: 10.1002/ana.410440410

Azadmanesh, J., and Borgstahl, G. E. O. (2018). A review of the catalytic mechanism of human manganese superoxide dismutase. *Antioxidants* 7:25. doi: 10.3390/antiox7020025

Barbeito, L. H., Pehar, M., Cassina, P., Vargas, M. R., Peluffo, H., Viera, L., et al. (2004). A role for astrocytes in motor neuron loss in amyotrophic lateral sclerosis. *Brain Res. Rev.* 47, 263–274. doi: 10.1016/j.brainresrev.2004.05.003

Bhende, M., Shetty, S., Parthasarathy, M., and Ramya, S. (2018). Optical coherence tomography: a guide to interpretation of common macular diseases. *Indian J. Ophthalmol.* 66, 20–35. doi: 10.4103/ijo.ijo_902_17

Blokhuis, A. M., Groen, E. J., Koppers, M., van den Berg, L. H., and Pasterkamp, R. J. (2013). Protein aggregation in amyotrophic lateral sclerosis. *Acta Neuropathol.* 125, 777–794. doi: 10.1007/s00401-013-1125-6

Boillée, S., Vande Velde, C., and Cleveland, D. W. (2006a). ALS: a disease of motor neurons and their nonneuronal neighbors. *Neuron* 52, 39–59. doi: 10.1016/j.neuron.2006.09.018

Boillée, S., Yamanaka, K., Lobsiger, C. S., Copeland, N. G., Jenkins, N. A., Kassiotis, G., et al. (2006b). Onset and progression in inherited ALS determined by motor neurons and microglia. *Science* 312, 1389–1392. doi: 10.1126/science.1123511

Bouteloup, C., Desport, J.-C., Clavelou, P., Guy, N., Derumeaux-Burel, H., Ferrier, A., et al. (2009). Hypermetabolism in ALS patients: an early and persistent phenomenon. *J. Neurol.* 256, 1236–1242. doi: 10.1007/s00415-009-5100-z

Brettchneider, J., Del Tredici, K., Toledo, J. B., Robinson, J. L., Irwin, D. J., Grossman, M., et al. (2013). Stages of pTDP-43 pathology in amyotrophic lateral sclerosis. *Ann. Neurol.* 74, 20–38. doi: 10.1002/ana.23937.Stages

Byrne, S., Walsh, C., Lynch, C., Bede, P., Elamin, M., Kenna, K., et al. (2011). Rate of familial amyotrophic lateral sclerosis: a systematic review and meta-analysis. *J. Neurol. Neurosurg. Psychiatry* 82, 623–627. doi: 10.1136/jnnp.2010.224501

Carra, S., Crippa, V., Rusmini, P., Boncoraglio, A., Minoia, M., Giorgetti, E., et al. (2012). Alteration of protein folding and degradation in motor neuron

diseases: implications and protective functions of small heat shock proteins. *Prog. Neurobiol.* 97, 83–100. doi: 10.1016/j.pneurobio.2011.09.009

Carrì, M. T., Valle, C., Bozzo, F., and Cozzolino, M. (2015). Oxidative stress and mitochondrial damage: importance in non-SOD1 ALS. *Front. Cell. Neurosci.* 9:41. doi: 10.3389/fncel.2015.00041

Chang, Y., Kong, Q., Shan, X., Tian, G., Ilieva, H., Cleveland, D. W., et al. (2008). Messenger RNA oxidation occurs early in disease pathogenesis and promotes motor neuron degeneration in ALS. *PLoS One* 3:e2849. doi: 10.1371/journal.pone.0002849

Chiò, A., Gauthier, A., Montuschi, A., Calvo, A., Vito, D. N., Ghiglione, P., et al. (2004). A cross sectional study on determinants of quality of life in ALS. *J. Neurol. Neurosurg. Psychiatry* 75, 1597–1601. doi: 10.1136/jnnp.2003.033100

Cho, K., Yoon, D., Yu, M., Peachey, N. S., and Ferreira, P. A. (2019). Microglial activation in an amyotrophic lateral sclerosis-like model caused by Ranbp2 loss and nucleocytoplasmic transport impairment in retinal ganglion neurons. *Cell. Mol. Life Sci.* 76, 3407–3432. doi: 10.1007/s00018-019-03078-5

Chung, M. J., and Suh, Y.-L. (2002). Ultrastructural changes of mitochondria in the skeletal muscle of patients with amyotrophic lateral sclerosis. *Ultrastruct. Pathol.* 26, 3–7. doi: 10.1080/01913120252934260

Cohen, B., and Caroscio, J. (1983). Eye movements in amyotrophic lateral sclerosis. *J. Neural Transm. Suppl.* 19, 305–315.

Conwit, R. A. (2006). Preventing familial ALS: A clinical trial may be feasible but is an efficacy trial warranted? *J. Neurol. Sci.* 251, 1–2. doi: 10.1016/j.jns.2006.07.009

Coppola, G., Di Renzo, A., Ziccardi, L., Martelli, F., Fadda, A., Manni, G., et al. (2015). Optical coherence tomography in Alzheimer's disease: a meta-analysis. *PLoS One* 10:e0134750. doi: 10.1371/journal.pone.0134750

Cozzolino, M., and Carrì, M. T. (2012). Mitochondrial dysfunction in ALS. *Prog. Neurobiol.* 97, 54–66. doi: 10.1016/j.pneurobio.2011.06.003

Crugnola, V., Lamperti, C., Lucchini, V., Ronchi, D., Peverelli, L., Prelle, A., et al. (2010). Mitochondrial respiratory chain dysfunction in muscle from patients with amyotrophic lateral sclerosis. *Arch. Neurol.* 67, 849–854. doi: 10.1001/archneurol.2010.128

Da Cruz, S., and Cleveland, D. W. (2011). Understanding the role of TDP-43 and FUS/TLS in ALS and beyond. *Curr. Opin. Neurobiol.* 21, 904–919. doi: 10.1016/j.conb.2011.05.029

De Jong, S., Huisman, M., Sutedja, N., Van Der Kooi, A., De Visser, M., Schelhaas, J., et al. (2013). Endogenous female reproductive hormones and the risk of amyotrophic lateral sclerosis. *J. Neurol.* 260, 507–512. doi: 10.1007/s00415-012-6665-5

De Vos, K., Severin, F., Van Herreweghe, F., Vancompernolle, K., Goossens, V., Hyman, A., et al. (2000). Tumor necrosis factor induces hyperphosphorylation of kinesin light chain and inhibits kinesin-mediated transport of mitochondria. *J. Cell Biol.* 149, 1207–1214. doi: 10.1083/jcb.149.6.1207

Deivasigamani, S., Verma, H. K., Ueda, R., Ratnaparkhi, A., and Ratnaparkhi, G. S. (2014). A genetic screen identifies Tor as an interactor of VAPB in a Drosophila model of amyotrophic lateral sclerosis. *Biol. Open* 3, 1127–1138. doi: 10.1242/bio.201410066

Del, Bo, R., Tiloca, C., Pensato, V., Corrado, L., Ratti, A., et al. (2011). Novel optineurin mutations in patients with familial and sporadic amyotrophic lateral sclerosis. *J. Neurol. Neurosurg. Psychiatry* 82, 1239–1243. doi: 10.1136/jnnp.2011.242313

Deng, H. X., Zhai, H., Bigio, E. H., Yan, J., Fecto, F., Ajroud, K., et al. (2010). FUS-immunoreactive inclusions are a common feature in sporadic and non-SOD1 familial amyotrophic lateral sclerosis. *Ann. Neurol.* 67, 739–748. doi: 10.1002/ana.22051

Desport, J., Preux, P., Magy, L., Boirie, Y., Vallat, J., Beaufrère, B., et al. (2001). Factors correlated with hypermetabolism in patients with amyotrophic lateral sclerosis. *Am. J. Clin. Nutr.* 74, 328–334. doi: 10.1093/ajcn/74.3.328

Donaghy, C., Pinnock, R., Abrahams, S., Cardwell, C., Hardiman, O., Patterson, V., et al. (2009). Ocular fixation instabilities in motor neurone disease: AA marker of frontal lobe dysfunction? *J. Neurol.* 256, 420–426. doi: 10.1007/s00415-009-0109-x

Donaghy, C., Pinnock, R., Abrahams, S., Cardwell, C., Hardiman, O., Patterson, V., et al. (2010). Slow saccades in bulbar-onset motor neurone disease. *J. Neurol.* 257, 1134–1140. doi: 10.1007/s00415-010-5478-7

Donnelly, C. J., Zhang, P.-W., Pham, J. T., Heusler, A. R., Mistry, N. A., Vidensky, S., et al. (2013). RNA Toxicity from the ALS/FTD C9ORF72 expansion is mitigated by antisense intervention. *Neuron* 415–428. doi: 10.1016/j.neuron.2013.10.015

Dupuis, L., Pradat, P. F., Ludolph, A. C., and Loeffler, J. P. (2011). Energy metabolism in amyotrophic lateral sclerosis. *Lancet Neurol.* 10, 75–82. doi: 10.1016/S1474-4422(10)70224-6

Echaniz-Laguna, A., Zoll, J., Ponsot, E., N'guessan, B., Tranchant, C., Loeffler, J.-P., et al. (2006). Muscular mitochondrial function in amyotrophic lateral sclerosis is progressively altered as the disease develops: a temporal study in man. *Exp. Neurol.* 198, 25–30. doi: 10.1016/j.expneurol.2005.07.020

Echaniz-Laguna, A., Zoll, J., Ribera, F., Tranchant, C., Warter, J. M., Lonsdorfer, J., et al. (2002). Mitochondrial respiratory chain function in skeletal muscle of ALS patients. *Ann. Neurol.* 52, 623–627. doi: 10.1002/ana.10357

Ellis, C. M., Suckling, J., Amaro, E., Bullmore, E. T., Simmons, A., Williams, S. C., et al. (2001). Volumetric analysis reveals corticospinal tract degeneration and extramotor involvement in ALS. *Neurology* 57, 1571–1578. doi: 10.1212/wnl.57.9.1571

Endo, F., Komine, O., Fujimori-Tonou, N., Katsuno, M., Jin, S., Watanabe, S., et al. (2015). Astrocyte-Derived TGF-β1 accelerates disease progression in als mice by interfering with the neuroprotective functions of microglia and T Cells. *Cell Rep.* 11, 592–604. doi: 10.1016/j.celrep.2015.03.053

Engelhardt, J. I., Tajti, J., and Appel, S. H. (1993). Lymphocytic Infiltrates in the Spinal Cord in Amyotrophic Lateral Sclerosis. *Arch. Neurol.* 50, 30–36. doi: 10.1001/archneur.1993.00540010026013

Fawzi, A. A., Simonett, J. M., Purta, P., Moss, H. E., Lowry, J. L., Deng, H.-X., et al. (2014). Clinicopathologic report of ocular involvement in ALS patients with C9orf72 mutation. *Amyotroph. Lateral Scler. Frontotemporal Degener.* 15, 569–580. doi: 10.3109/21678421.2014.951941

Ferreira, P. A. (2019). The coming-of-age of nucleocytoplasmic transport in motor neuron disease and neurodegeneration. *Cell. Mol. Life Sci.* 76, 2247–2273. doi: 10.1007/s00018-019-03029-0

Ferri, A., and Coccurello, R. (2017). What is "Hyper" in the ALS Hypermetabolism? *Mediat. Inflamm.* 2017:7821672. doi: 10.1155/2017/7821672

Fitzgerald, K. C., O'Reilly, É. J., Falcone, G. J., McCullough, M. L., Park, Y., Kolonel, L. N., et al. (2014). Dietary ω-3 polyunsaturated fatty acid intake and risk for amyotrophic lateral sclerosis. *JAMA Neurol.* 71, 1102–1110. doi: 10.1001/jamaneurol.2014.1214

Forsberg, K., Andersen, P. M., Marklund, S. L., and Brännström, T. (2011). Glial nuclear aggregates of superoxide dismutase-1 are regularly present in patients with amyotrophic lateral sclerosis. *Acta Neuropathol.* 121, 623–634. doi: 10.1007/s00401-011-0805-3

Gandelman, M., Peluffo, H., Beckman, J. S., Cassina, P., and Barbeito, L. (2010). Extracellular ATP and the P2X7receptor in astrocyte-mediated motor neuron death: implications for amyotrophic lateral sclerosis. *J. Neuroinflammation* 7:33. doi: 10.1186/1742-2094-7-33

Garcia-Martin, E., Bambo, M. P., Marques, M. L., Satue, M., Otin, S., Larrosa, J. M., et al. (2016). Ganglion cell layer measurements correlate with disease severity in patients with Alzheimer's disease. *Acta Ophthalmol.* 94, e454–e459. doi: 10.1111/aos.12977

Gargiulo Monachelli, G., Meyer, M., Rodríguez, G. E., Garay, L. I., Sica, R. E. P., De Nicola, A. F., et al. (2011). Endogenous progesterone is associated to amyotrophic lateral sclerosis prognostic factors. *Acta Neurol. Scand.* 123, 60–67. doi: 10.1111/j.1600-0404.2010.01385.x

Gatchel, J. R., and Zoghbi, H. Y. (2005). Diseases of unstable repeat expansion: mechanisms and common principles. *Nat. Rev. Genet.* 6, 743–755. doi: 10.1038/nrg1691

Gazulla, J., and Cavero-Nagore, M. (2006). [Glutamate and Alzheimer's disease]. *Rev. Neurol.* 42, 427–432. doi: 10.33588/rn.4207.2005223

Ghezzi, A., Mazzalovo, E., Locatelli, C., Zibetti, A., Zaffaroni, M., and Montanini, R. (1989). Multimodality evoked potentials in amyotrophic lateral sclerosis. *Acta Neurol. Scand.* 79, 353–356. doi: 10.1111/j.1600-0404.1989.tb03799.x

Gizzi, M., DiRocco, A., Sivak, M., and Cohen, B. (1992). Ocular motor function in motor neuron disease. *Neurology* 42, 1037–1046. doi: 10.1212/wnl.42.5.1037

González Díaz, N., Barrios, E. E., Escamilla Chávez, C., and Escobar Rodríguez, D. A. (2004). Multimodal-evoked potentials in patients with amyotrophic lateral sclerosis. *Rev. Med. IMSS* 42, 477–486.

Haberlandt, W. (1959). Genetic aspects of amyotrophic lateral sclerosis and progressive bulbar paralysis. *Acta Genet. Med. Gemellol.* 8, 369–374. doi: 10.1017/s1120962300018801

Han-Xiang, D., Chen, W., Seong-Tshool, S., Boycott, K. M., Gorrie, G. H., Siddique, N., et al. (2011). Mutations in UBQLN2 cause dominant X-linked juvenile and adult-onset ALS and ALS/dementia. *Nature* 477, 211–215. doi: 10.1038/nature10353

Hayward, C., Brock, D. J., Minns, R. A., and Swingler, R. J. (1998). Homozygosity for Asn86Ser mutation in the CuZn-superoxide dismutase gene produces a severe clinical phenotype in a juvenile onset case of familial amyotrophic lateral sclerosis. *J. Med. Genet.* 35:174. doi: 10.1136/jmg.35.2.174

He, J., Mangelsdorf, M., Fan, D., Bartlett, P., and Brown, M. A. (2015). Amyotrophic lateral sclerosis genetic studies: from genome-wide association mapping to genome sequencing. *Neuroscientist* 21, 599–615. doi: 10.1177/1073858414555404

Honig, L. S., Chambliss, D. D., Bigio, E. H., Carroll, S. L., and Elliott, J. L. (2000). Glutamate transporter EAAT2 splice variants occur not only in ALS, but also in AD and controls. *Neurology* 55, 1082–1088. doi: 10.1212/WNL.55.8.1082

Hübers, A., Just, W., Rosenbohm, A., Müller, K., Marroquin, N., Goebel, I., et al. (2015). De novo FUS mutations are the most frequent genetic cause in early-onset German ALS patients. *Neurobiol. Aging* 36, 3117.e1–3117.e6. doi: 10.1016/j.neurobiolaging.2015.08.005

Hübers, A., Müller, H. P., Dreyhaupt, J., Böhm, K., Lauda, F., Tumani, H., et al. (2016). Retinal involvement in amyotrophic lateral sclerosis: a study with optical coherence tomography and diffusion tensor imaging. *J. Neural Transm.* 123, 281–287. doi: 10.1007/s00702-015-1483-4

Ikenaka, K., Katsuno, M., Kawai, K., Ishigaki, S., Tanaka, F., and Sobue, G. (2012). Disruption of axonal transport in motor neuron diseases. *Int. J. Mol. Sci.* 13, 1225–1238. doi: 10.3390/ijms13011225

Ito, H., Fujita, K., Nakamura, M., Wate, R., Kaneko, S., Sasaki, S., et al. (2011). Optineurin is co-localized with FUS in basophilic inclusions of ALS with FUS mutation and in basophilic inclusion body disease. *Acta Neuropathol.* 121, 555–557. doi: 10.1007/s00401-011-0809-z

Iwasaki, Y., Ikeda, K., and Kinoshita, M. (2005). Molecular and cellular mechanism of glutamate receptors in relation to amyotrophic lateral sclerosis. *Curr. Drug Targets CNS Neurol. Disord.* 1, 511–518. doi: 10.2174/1568007023339021

Jaiswal, M. K. (2014). Selective vulnerability of motoneuron and perturbed mitochondrial calcium homeostasis in amyotrophic lateral sclerosis: implications for motoneurons specific calcium dysregulation. *Mol. Cell. Ther.* 2, 2–15. doi: 10.1186/2052-8426-2-26

Jawaid, A., Murthy, S. B., Wilson, A. M., Qureshi, S. U., Amro, M. J., Wheaton, M., et al. (2010). A decrease in body mass index is associated with faster progression of motor symptoms and shorter survival in ALS. *Amyotroph. Lateral Scler.* 11, 542–548. doi: 10.3109/17482968.2010.482592

Kamel, F., Umbach, D. M., Munsat, T. L., Shefner, J. M., Hu, H., and Sandler, D. P. (2002). Lead exposure and amyotrophic lateral sclerosis. *Epidemiology* 13, 311–319. doi: 10.1097/00001648-200205000-00012

Kang, B.-H., Kim, J.-I., Lim, Y.-M., and Kim, K.-K. (2018). Abnormal oculomotor functions in amyotrophic lateral sclerosis. *J. Clin. Neurol.* 14:464. doi: 10.3988/jcn.2018.14.4.464

Kassubek, J., Unrath, A., Huppertz, H.-J., Lulé, D., Ethofer, T., Sperfeld, A.-D., et al. (2005). Global brain atrophy and corticospinal tract alterations in ALS, as investigated by voxel-based morphometry of 3-D MRI. *Amyotroph. Lateral Scler. Other Motor Neuron Disord.* 6, 213–220. doi: 10.1080/14660820510038538

Kawamata, T., Akiyama, H., Yamada, T., and McGeer, P. L. (1992). Immunologic reactions in amyotrophic lateral sclerosis brain and spinal cord tissue. *Am. J. Pathol.* 140, 691–707.

Kiernan, M. C., Vucic, S., Cheah, B. C., Turner, M. R., Eisen, A., Hardiman, O., et al. (2011). Amyotrophic lateral sclerosis. *Lancet* 377, 942–955. doi: 10.1016/S0140-6736(10)61156-7

Kim, B. J., Irwin, D. J., Song, D., Daniel, E., Leveque, J. D., Raquib, A. R., et al. (2017). Optical coherence tomography identifies outer retina thinning in frontotemporal degeneration. *Neurology* 89, 1604–1611. doi: 10.1212/WNL.0000000000004500

Krasnianski, A., Deschauer, M., Neudecker, S., Gellerich, F. N., Müller, T., Schoser, B. G., et al. (2005). Mitochondrial changes in skeletal muscle in amyotrophic lateral sclerosis and other neurogenic atrophies. *Brain* 128, 1870–1876. doi: 10.1093/brain/awh540

Kühnlein, P., Sperfeld, A.-D., Vanmassenhove, B., Van Deerlin, V., Lee, V. M.-Y., Trojanowski, J. Q., et al. (2008). Two German kindreds with familial amyotrophic lateral sclerosis due to TARDBP mutations. *Arch. Neurol.* 65, 1185–1189. doi: 10.1001/archneur.65.9.1185

Kushner, P. D., Stephenson, D. T., and Wright, S. (1991). Reactive astrogliosis is widespread in the subcortical white matter of amyotrophic lateral sclerosis brain. *J. Neuropathol. Exp. Neurol.* 50, 263–277. doi: 10.1097/00005072-199105000-00008

Kwiatkowski, T. J., Bosco, D. A., LeClerc, A. L., Tamrazian, E., Vanderburg, C. R., Russ, C., et al. (2009). Mutations in the FUS/TLS gene on chromosome 16 cause familial amyotrophic lateral sclerosis. *Science* 323, 1205–1208. doi: 10.1126/science.1166066

Leveille, A., Kiernan, J., Goodwin, J. A., and Antel, J. (1982). Eye movements in amyotrophic lateral sclerosis. *Arch. Neurol.* 39, 684–686. doi: 10.1001/archneur.1982.00510230010003

Liao, B., Zhao, W., Beers, D. R., Henkel, J. S., and Appel, S. H. (2012). Transformation from a neuroprotective to a neurotoxic microglial phenotype in a mouse model of ALS. *Exp. Neurol.* 237, 147–152. doi: 10.1016/j.expneurol.2012.06.011

Liddelow, S. A., Guttenplan, K. A., Clarke, L. E., Bennett, F. C., Bohlen, C. J., Schirmer, L., et al. (2017). Neurotoxic reactive astrocytes are induced by activated microglia. *Nature* 541, 481–487. doi: 10.1038/nature21029

Lin, C.-L. G., Bristol, L. A., Jin, L., Dykes-Hoberg, M., Crawford, T., Clawson, L., et al. (1998). Aberrant RNA processing in a neurodegenerative disease: the cause for absent EAAT2, a glutamate transporter, in Amyotrophic Lateral Sclerosis. *Neuron* 20, 589–602. doi: 10.1016/S0896-6273(00)80997-6

Liu, Y., Pattamatta, A., Zu, T., Reid, T., Bardhi, O., Borchelt, D. R., et al. (2016). C9orf72 BAC mouse model with motor deficits and neurodegenerative features of ALS/FTD. *Neuron* 90, 521–534. doi: 10.1016/j.neuron.2016.04.005

Liu, Z., Wang, H., Fan, D., and Wang, W. (2018). Comparison of optical coherence tomography findings and visual field changes in patients with primary open-angle glaucoma and amyotrophic lateral sclerosis. *J. Clin. Neurosci.* 48, 233–237. doi: 10.1016/j.jocn.2017.10.080

MacCormick, I. J., Czanner, G., and Faragher, B. (2015). Developing retinal biomarkers of neurological disease: an analytical perspective. *Biomark. Med.* 9, 691–701. doi: 10.2217/bmm.15.17

Mackenzie, I. R. A., Bigio, E. H., Ince, P. G., Geser, F., Neumann, M., Cairns, N. J., et al. (2007). Pathological TDP-43 distinguishes sporadic amyotrophic lateral sclerosis from amyotrophic lateral sclerosis with SOD1 mutations. *Ann. Neurol.* 61, 427–434. doi: 10.1002/ana.21147

Mackenzie, I. R. A., Rademakers, R., and Neumann, M. (2010). TDP-43 and FUS in amyotrophic lateral sclerosis and frontotemporal dementia. *Lancet Neurol.* 9, 995–1007. doi: 10.1016/S1474-4422(10)70195-2

Maekawa, S., Leigh, P. N., King, A., Jones, E., Steele, J. C., Bodi, I., et al. (2009). TDP-43 is consistently co-localized with ubiquitinated inclusions in sporadic and Guam amyotrophic lateral sclerosis but not in familial amyotrophic lateral sclerosis with and without SOD1 mutations. *Neuropathology* 29, 672–683. doi: 10.1111/j.1440-1789.2009.01029.x

Magrané, J., and Manfredi, G. (2009). Mitochondrial function, morphology, and axonal transport in amyotrophic lateral sclerosis. *Antioxid. Redox Signal.* 11, 1615–1626. doi: 10.1089/ars.2009.2604

Majounie, E., Renton, A. E., Mok, K., Dopper, E. G. P., Waite, A., Rollinson, S., et al. (2012). Frequency of the C9orf72 hexanucleotide repeat expansion in patients with amyotrophic lateral sclerosis and frontotemporal dementia: a cross-sectional study. *Lancet Neurol.* 11, 323–330.

Marti-Fàbregas, J., and Roig, C. (1993). Oculomotor abnormalities in motor neuron disease. *J. Neurol.* 240, 475–478. doi: 10.1007/BF00874116

Marucci, G., Morandi, L., Bartolomei, I., Salvi, F., Pession, A., Righi, A., et al. (2007). Amyotrophic lateral sclerosis with mutation of the Cu/Zn superoxide dismutase gene (SOD1) in a patient with Down syndrome. *Neuromuscul. Disord.* 17, 673–676. doi: 10.1016/j.nmd.2007.06.003

Maruyama, H., Morino, H., Ito, H., Izumi, Y., Kato, H., Watanabe, Y., et al. (2010). Mutations of optineurin in amyotrophic lateral sclerosis. *Nature* 465, 223–226. doi: 10.1038/nature08971

Matheson, J. K., Harrington, H. J., and Hallett, M. (1986). Abnormalities of multimodality evoked potentials in amyotrophic lateral sclerosis. *Arch. Neurol.* 43, 338–340. doi: 10.1001/archneur.1986.00520040026013

Mathis, S., Goizet, C., Soulages, A., Vallat, J. M., Masson, G., and Le. (2019). Genetics of amyotrophic lateral sclerosis: a review. *J. Neurol. Sci.* 399, 217–226. doi: 10.1016/j.jns.2019.02.030

Mcguire, V., Longstreth, W. T., Nelson, L. M., Koepsell, T. D., Checkoway, H., Morgan, M. S., et al. (1997). Occupational exposures and Amyotrophic Lateral Sclerosis a population-based case-control study. *Am. J. Epidemiol.* 145, 1076–1088. doi: 10.1093/oxfordjournals.aje.a009070

McLoon, L. K., Harandi, V. M., Brännström, T., Andersen, P. M., and Liu, J. X. (2014). Wnt and extraocular muscle sparing in amyotrophic lateral sclerosis. *Invest. Ophthalmol. Vis. Sci.* 55, 5482–5496. doi: 10.1167/iovs.14-14886

Meier, S. L., Charleston, A. J., and Tippett, L. J. (2010). Cognitive and behavioural deficits associated with the orbitomedial prefrontal cortex in amyotrophic lateral sclerosis. *Brain* 133, 3444–3457. doi: 10.1093/brain/awq254

Mezzapesa, D., Ceccarelli, A., Dicuonzo, F., Carella, A., Caro, M. F., De, et al. (2007). Whole-brain and regional brain atrophy in amyotrophic lateral sclerosis. *AJNR Am. J. Neuroradiol.* 28, 255–259.

Mitsumoto, H., Factor-Litvak, P., Andrews, H., Goetz, R. R., Andrews, L., Rabkin, J. G., et al. (2014). ALS Multicenter Cohort Study of Oxidative Stress (ALS COSMOS): the study methodology, recruitment, and baseline demographic and disease characteristics. *Amyotroph. Lateral Scler. Front. Degener.* 15, 192–203. doi: 10.3109/21678421.2013.864312

Moreno-Ramos, T., Benito-León, J., Villarejo, A., and Bermejo-Pareja, F. (2013). Retinal nerve fiber layer thinning in dementia associated with parkinson's disease, dementia with lewy bodies, and alzheimer's disease. *J. Alzheimers Dis.* 34, 659–664. doi: 10.3233/JAD-121975

Morozova, N., Weisskopf, M. G., McCullough, M. L., Munger, K. L., Calle, E. E., Thun, M. J., et al. (2008). Diet and amyotrophic lateral sclerosis. *Epidemiology* 19, 324–337. doi: 10.1097/EDE.0b013e3181632c5d

Moss, H. E., McCluskey, L., Elman, L., Hoskins, K., Talman, L., Grossman, M., et al. (2012). Cross-sectional evaluation of clinical neuro-ophthalmic abnormalities in an amyotrophic lateral sclerosis population1. Moss, H. E. et al. Cross-sectional evaluation of clinical neuro-ophthalmic abnormalities in an amyotrophic lateral sclerosis population. *J. Neurol. Sci.* 314, 97–101. doi: 10.1016/j.jns.2011.10.016

Moss, H. E., Samelson, M., Mohan, G., and Jiang, Q. L. (2016). High and low contrast visual acuity are not affected in amyotrophic lateral sclerosis. *PLoS One* 11:e0168714. doi: 10.1371/journal.pone.0168714

Mukherjee, N., McBurney-Lin, S., Kuo, A., Bedlack, R., and Tseng, H. (2017). Retinal thinning in amyotrophic lateral sclerosis patients without ophthalmic disease. *PLoS One* 12:e0185242. doi: 10.1371/journal.pone.0185242

Münte, T. F., Tröger, M. C., Nusser, I., Wieringa, B. M., Johannes, S., Matzke, M., et al. (1998). Alteration of early components of the visual evoked potential in amyotrophic lateral sclerosis. *J. Neurol.* 245, 206–210. doi: 10.1007/s004150050206

Nagy, D., Kato, T., and Kushner, P. D. (1994). Reactive astrocytes are widespread in the cortical gray matter of amyotrophic lateral sclerosis. *J. Neurosci. Res.* 38, 336–347. doi: 10.1002/jnr.490380312

Neumann, M., Sampathu, D. M., Kwong, L. K., Truax, A. C., Micsenyi, M. C., Chou, T. T., et al. (2006). Ubiquitinated TDP-43 in frontotemporal lobar degeneration and amyotrophic lateral sclerosis. *Science* 314, 130–133. doi: 10.1126/science.1134108

Ohki, M., Kanayama, R., Nakamura, T., Okuyama, T., Kimura, Y., and Koike, Y. (1994). Ocular abnormalities in amyotrophic lateral sclerosis. *Acta Otolaryngol.* 114, 138–142. doi: 10.3109/00016489409128318

Okuda, B., Yamamoto, T., Yamasaki, M., Maya, K., and Imai, T. (2009). Motor neuron disease with slow eye movements and vertical gaze palsy. *Acta Neurol. Scand.* 85, 71–76. doi: 10.1111/j.1600-0404.1992.tb03999.x

Palamiuc, L., Schlagowski, A., Ngo, S. T., Vernay, A., Dirrig-Grosch, S., Henriques, A., et al. (2015). A metabolic switch toward lipid use in glycolytic muscle is an early pathologic event in a mouse model of amyotrophic lateral sclerosis. *EMBO Mol. Med* 7, 526–546. doi: 10.15252/emmm.201404433

Palma, V., Guadagnino, M., Brescia Morra, V., and Nolfe, G. (1993). Multimodality evoked potentials in sporadic amyotrophic lateral sclerosis: a statistical approach. *Electromyogr. Clin. Neurophysiol.* 33, 167–171.

Palmowski, A., Jost, W. H., Osterhage, J., Prudlo, J., Käsmann, B., Schimrigk, K., et al. (1995). [Disorders of eye movement in amyotrophic lateral sclerosis–report of 2 patients]. *Klin. Monbl. Augenheilkd.* 206, 170–172. doi: 10.1055/s-2008-1035424

Pape, J. A., and Grose, J. H. (2020). The effects of diet and sex in amyotrophic lateral sclerosis. *Rev. Neurol.* 176, 301–315. doi: 10.1016/j.neurol.2019.09.008

Park, Y., Park, J., Kim, Y., Baek, H., and Kim, S. H. (2015). Association between nutritional status and disease severity using the amyotrophic lateral sclerosis (ALS) functional rating scale in ALS patients. *Nutrition* 31, 1362–1367. doi: 10.1016/j.nut.2015.05.025

Philips, T., and Robberecht, W. (2011). Neuroinflammation in amyotrophic lateral sclerosis: role of glial activation in motor neuron disease. *Lancet Neurol.* 10, 253–263. doi: 10.1016/S1474-4422(11)70015-1

Pinto, W. B. V. R., Debona, R., Nunes, P. P., Assis, A. C. D., Lopes, C. G., Bortholin, T., et al. (2019). Atypical motor neuron disease variants: still a diagnostic challenge in neurology. *Rev. Neurol.* 175, 221–232. doi: 10.1016/j.neurol.2018.04.016

Pratt, A. J., Getzoff, E. D., and Perry, J. J. P. (2012). Amyotrophic lateral sclerosis: update and new developments. *Degener. Neurol. Neuromuscul. Dis.* 2012, 1–14. doi: 10.2147/DNND.S19803

Proudfoot, M., Menke, R. A. L., Sharma, R., Berna, C. M., Hicks, S. L., Kennard, C., et al. (2016). Eye-tracking in amyotrophic lateral sclerosis: a longitudinal study of saccadic and cognitive tasks. *Amyotroph. Lateral Scler. Front. Degener.* 17, 101–111. doi: 10.3109/21678421.2015.1054292

Ramírez, A. I., de Hoz, R., Salobrar-García, E., Salazar, J. J., Rojas, B., Ajoy, D., et al. (2017). The role of microglia in retinal neurodegeneration: Alzheimer's disease, Parkinson, and glaucoma. *Front. Aging Neurosci.* 9:214. doi: 10.3389/fnagi.2017.00214

Raoul, C., Estévez, A. G., Nishimune, H., Cleveland, D. W., DeLapeyrière, O., Henderson, C. E., et al. (2002). Motoneuron death triggered by a specific pathway downstream of fas: potentiation by ALS-linked SOD1 mutations. *Neuron* 35, 1067–1083. doi: 10.1016/S0896-6273(02)00905-4

Renton, A. E., Majounie, E., Waite, A., Simón-Sánchez, J., Rollinson, S., Gibbs, J. R., et al. (2011). A hexanucleotide repeat expansion in C9ORF72 is the cause of chromosome 9p21-linked ALS-FTD. *Neuron* 72, 257–268. doi: 10.1016/j.neuron.2011.09.010

Ringelstein, M., Albrecht, P., Südmeyer, M., Harmel, J., Müller, A. K., Keser, N., et al. (2014). Subtle retinal pathology in amyotrophic lateral sclerosis. *Ann. Clin. Transl. Neurol.* 1, 290–297. doi: 10.1002/acn3.46

Ringer, C., Weihe, E., and Schütz, B. (2017). SOD1 G93A mutant mice develop a neuroinflammation-independent dendropathy in excitatory neuronal subsets of the olfactory bulb and retina. *J. Neuropathol. Exp. Neurol.* 76, 769–778. doi: 10.1093/jnen/nlx057

Ringholz, G. M., Appel, S. H., Bradshaw, M., Cooke, N. A., Mosnik, D. M., and Schulz, P. E. (2005). Prevalence and patterns of cognitive impairment in sporadic ALS. *Neurology* 65, 586–590. doi: 10.1212/01.wnl.0000172911.39167.b6

Rohani, M., Meysamie, A., Zamani, B., Sowlat, M. M., and Akhoundi, F. H. (2018). Reduced retinal nerve fiber layer (RNFL) thickness in ALS patients: a window to disease progression. *J. Neurol.* 265, 1557–1562. doi: 10.1007/s00415-018-8863-2

Rojas, P., Hoz, R., De, Ramírez, A. I., Ferreras, A., Salobrar-Garcia, E., et al. (2019). Changes in Retinal OCT and their correlations with neurological disability in early ALS patients, a follow-up study. *Brain Sci.* 9, 1–18. doi: 10.3390/brainsci9120337

Román, G. C. (1996). Neuroepidemiology of amyotrophic lateral sclerosis: clues to aetiology and pathogenesis. *J. Neurol. Neurosurg. Psychiatry* 61, 131–137. doi: 10.1136/jnnp.61.2.131

Roth, N. M., Saidha, S., Zimmermann, H., Brandt, A. U., Oberwahrenbrock, T., Maragakis, N. J., et al. (2013). Optical coherence tomography does not support optic nerve involvement in amyotrophic lateral sclerosis. *Eur. J. Neurol.* 20, 1170–1176. doi: 10.1111/ene.12146

Rowland, L. P., and Shneider, N. A. (2001). Amyotrophic lateral sclerosis. *N. Engl. J. Med.* 344, 1688–1700. doi: 10.1056/NEJM200105313442207

Rutherford, N. J., Zhang, Y. J., Baker, M., Gass, J. M., Finch, N. C. A., Xu, Y. F., et al. (2008). Novel mutations in TARDBP(TDP-43) in patients with familial amyotrophic lateral sclerosis. *PLoS Genet.* 4:e1000193. doi: 10.1371/journal.pgen.1000193

Saito, S., and Yamamoto, H. (1989). [Analysis of oculomotor disorders in motor neuron disease]. *Clin. Neurol.* 29, 969–975.

Salobrar-García, E., de Hoz, R., Ramírez, A. I., Salazar, J. J., Rojas, P., López-Cuenca, I., et al. (2019). "Ocular Exploration in the Diagnosis and Follow-Up of the Alzheimer's Dementia," in *Alzheimer's Disease [Internet]*, ed. T. Wisniewski (Brisbane: Codon Publications), 159–178. doi: 10.15586/alzheimersdisease.2019.ch10

Salobrar-García, E., de Hoz, R., Rojas, B., Ramirez, A. I., Salazar, J. J., Yubero, R., et al. (2015a). Ophthalmologic psychophysical tests support OCT findings in mild Alzheimer's disease. *J. Ophthalmol.* 2015:736949. doi: 10.1155/2015/736949

Salobrar-García, E., Hoyas, I., Leal, M., de Hoz, R., Rojas, B., Ramirez, A. I., et al. (2015b). Analysis of retinal peripapillary segmentation in early Alzheimer's disease patients. *Biomed Res. Int.* 2015:636548. doi: 10.1155/2015/636548

Salobrar-García, E., Ramírez, A. I., de Hoz, R., Rojas, P., Salazar, J. J., Rojas, B., et al. (2016). "The impact of the eye in dementia: the eye and its role in diagnosis and follow-up," in *Update on Dementia*, ed. D. Moretti (London: InTech), 379–426. doi: 10.5772/64490

Sathasivam, S. (2010). Motor neurone disease: clinical features, diagnosis, diagnostic pitfalls and prognostic markers. *Singapore Med. J.* 51, 367–372.

Savolainen, K. M., Loikkanen, J., Eerikäinen, S., and Naarala, J. (1998). Interactions of excitatory neurotransmitters and xenobiotics in excitotoxicity and oxidative stress: glutamate and lead. *Toxicol. Lett.* 10, 363–367. doi: 10.1016/S0378-4274(98)00233-1

Scekic-Zahirovic, J., Oussini, H., El, Mersmann, S., Drenner, K., Wagner, M., et al. (2017). Motor neuron intrinsic and extrinsic mechanisms contribute to the pathogenesis of FUS-associated amyotrophic lateral sclerosis. *Acta Neuropathol.* 133, 887–906. doi: 10.1007/s00401-017-1687-9

Schiffer, D., Cordera, S., Cavalla, P., and Migheli, A. (1996). Reactive astrogliosis of the spinal cord in amyotrophic lateral sclerosis. *J. Neurol. Sci.* 139, 27–33. doi: 10.1016/0022-510X(96)00073-1

Schymick, J. C., and Traynor, B. J. (2010). Expanding the genetics of amyotrophic lateral sclerosis and frontotemporal dementia. *Alzheimer Res. Ther.* 4:30. doi: 10.1186/alzrt133

Seals, R. M., Kioumourtzoglou, M. A., Gredal, O., Hansen, J., and Weisskopf, M. G. (2017). Occupational formaldehyde and amyotrophic lateral sclerosis. *Eur. J. Epidemiol.* 32, 893–899. doi: 10.1007/s10654-017-0249-8

Selvaraj, B. T., Livesey, M. R., Zhao, C., Gregory, J. M., James, O. T., Cleary, E. M., et al. (2018). C9ORF72 repeat expansion causes vulnerability of motor neurons to Ca2+-permeable AMPA receptor-mediated excitotoxicity. *Nat. Commun.* 9:347. doi: 10.1038/s41467-017-02729-0

Sharma, A., Lyashchenko, A. K., Lu, L., Nasrabady, S. E., Elmaleh, M., Mendelsohn, M., et al. (2016). ALS-associated mutant FUS induces selective motor neuron degeneration through toxic gain of function. *Nat. Commun.* 4:10465. doi: 10.1038/ncomms10465

Sharma, R., Hicks, S., Berna, C. M., Kennard, C., Talbot, K., and Turner, M. R. (2011). Oculomotor dysfunction in amyotrophic lateral sclerosis: a comprehensive review. *Arch. Neurol.* 68, 857–861. doi: 10.1001/archneurol.2011.130

Shaunak, S., Orrell, R. W., O'Sullivan, E., Hawken, M. B., Lane, R. J., Henderson, L., et al. (1995). Oculomotor function in amyotrophic lateral sclerosis: evidence for frontal impairment. *Ann. Neurol.* 38, 38–44. doi: 10.1002/ana.410380109

Shi, P., Ström, A.-L., Gal, J., and Zhu, H. (2010). Effects of ALS-related SOD1 mutants on dynein-and KIF5-mediated retrograde and anterograde axonal transport. *Biochim. Biophys. Acta* 1802, 707–716. doi: 10.1016/j.bbadis.2010.05.008

Shin Hee, J., and Lee Keun, J. (2013). "Multiple routes of motor neuron degeneration in ALS," in *Current Advances in Amyotrophic Lateral Sclerosis*, ed. A. Éstevez (London: InTech), 35–71. doi: 10.5772/56625

Simonett, J. M., Huang, R., Siddique, N., Farsiu, S., Siddique, T., Volpe, N. J., et al. (2016). Macular sub-layer thinning and association with pulmonary function tests in Amyotrophic Lateral Sclerosis. *Sci. Rep.* 6:29187. doi: 10.1038/srep29187

Simons, T. J. (1986). Cellular interactions between lead and calcium. *Br. Med. Bull.* 42, 431–434. doi: 10.1093/oxfordjournals.bmb.a072162

Simpson, E. P., Henry, Y. K., Henkel, J. S., Smith, R. G., and Appel, S. H. (2004). Increased lipid peroxidation in sera of ALS patients: a potential biomarker of disease burden. *Neurology* 62, 1758–1765. doi: 10.1212/WNL.62.10.1758

Sreedharan, J., Blair, I. P., Tripathi, V. B., Hu, X., Vance, C., Rogelj, B., et al. (2008). TDP-43 mutations in familial and sporadic amyotrophic lateral sclerosis. *Science* 319, 1668–1672. doi: 10.1126/science.1154584

Steyn, F. J., Ioannides, Z., van Eijk, R., Heggie, S., Thorpe, K., Ceslis, A., et al. (2018). Hypermetabolism in ALS is associated with greater functional decline and shorter survival Neurodegeneration. *J. Neurol. Neurosurg. Psychiatry* 89, 1016–1023. doi: 10.1136/jnnp-2017-317887

Trotti, D., Rolfs, A., Danbolt, N. C., Brown, R. H. Jr., and Hediger, M. A. (1999). SOD1 mutants linked to amyotrophic lateral sclerosis selectively inactivate a glial glutamate transporter. *Nat. Neurosci.* 2, 427–433. doi: 10.1038/8091

Tsujikawa, T., Kiyono, Y., Matsunaga, A., Ikawa, M., Nakamoto, Y., Mori, T., et al. (2015). Increased oxidative stress is related to disease severity in the ALS motor cortex: a PET study. *Neurology* 84, 2033–2039. doi: 10.1212/wnl.0000000000001588

Turner, M. R., Cagnin, A., Turkheimer, F. E., Miller, C. C. J., Shaw, C. E., Brooks, D. J., et al. (2004). Evidence of widespread cerebral microglial activation in amyotrophic lateral sclerosis: an [11C](R)-PK11195 positron emission tomography study. *Neurobiol. Dis.* 15, 601–609. doi: 10.1016/j.nbd.2003.12.012

Turner, M. R., Kiernan, M. C., Leigh, P. N., and Talbot, K. (2009). Biomarkers in amyotrophic lateral sclerosis. *Lancet Neurol.* 8, 94–109. doi: 10.1016/S1474-4422(08)70293-X

Turner, M. R., Wotton, C., Talbot, K., and Goldacre, M. J. (2012). Cardiovascular fitness as a risk factor for amyotrophic lateral sclerosis: indirect evidence from record linkage study. *J. Neurol. Neurosurg. Psychiatry* 83, 395–398. doi: 10.1136/jnnp-2011-301161

Vaisman, N., Lusaus, M., Nefussy, B., Niv, E., Comaneshter, D., Hallack, R., et al. (2009). Do patients with amyotrophic lateral sclerosis (ALS) have increased energy needs? *J. Neurol. Sci.* 279, 26–29. doi: 10.1016/j.jns.2008.12.027

Valentine, J. S., Doucette, P. A., and Zittin Potter, S. (2005). Copper-zinc superoxide dismutase and amyotrophic lateral sclerosis. *Annu. Rev. Biochem.* 74, 563–593. doi: 10.1146/annurev.biochem.72.121801.161647

Van Deerlin, V. M., Leverenz, J. B., Bekris, L. M., Bird, T. D., Yuan, W., Elman, L. B., et al. (2008). TARDBP mutations in amyotrophic lateral sclerosis with TDP-43 neuropathology: a genetic and histopathological analysis. *Lancet Neurol.* 7, 409–416. doi: 10.1016/S1474-4422(08)70071-1

Van Es, M. A., Dahlberg, C., Birve, A., Veldink, J. H., van den Berg, L. H., and Andersen, P. M. (2010). Large-scale SOD1 mutation screening provides evidence for genetic heterogeneity in amyotrophic lateral sclerosis. *J. Neurol. Neurosurg. Psychiatry* 81, 562–566. doi: 10.1136/jnnp.2009.181453

Vance, C., Rogelj, B., Hortobágyi, T., De Vos, K. J., Nishimura, A. L., Sreedharan, J., et al. (2009). Mutations in FUS, an RNA processing protein, cause familial amyotrophic lateral sclerosis type 6. *Science* 323, 1208–1211. doi: 10.1126/science.1165942

Vargas, M. R., and Johnson, J. A. (2010). Astrogliosis in amyotrophic lateral sclerosis: role and therapeutic potential of astrocytes. *Neurother. J. Am. Soc. Exp. Neurother.* 7, 471–481. doi: 10.2174/138161282366170622095802

Veldink, J. H., Kalmijn, S., Groeneveld, G. J., Wunderink, W., Koster, A., de Vries, J. H., et al. (2007). Intake of Polyunsaturated fatty acids and vitamin E reduce the risk of developing ALS. *J. Neurol. Neurosurg. Psychiatry* 78, 367–371. doi: 10.1136/jnnp.2005.083378

Vielhaber, S., Kunz, D., Winkler, K., Wiedemann, F. R., Kirches, E., Feistner, H., et al. (2000). Mitochondrial DNA abnormalities in skeletal muscle of patients with sporadic amyotrophic lateral sclerosis. *Brain* 123(Pt 7), 1339–1348. doi: 10.1093/brain/123.7.1339

Volpe, N. J., Simonett, J., Fawzi, A. A., and Siddique, T. (2015). Opthalmic manifestations of amyotrophic lateral sclerosis (an American Ophthalmological Society thesis). *Trans. Am. Ophthalmol. Soc.* 113, 1–15. doi: 10.3109/21678421.2013.838413

Vucic, S., and Kiernan, M. C. (2007). Abnormalities in cortical and peripheral excitability in flail arm variant amyotrophic lateral sclerosis. *J. Neurol. Neurosurg. Psychiatry* 78, 849–852. doi: 10.1136/jnnp.2006.105056

Wang, W., Zhang, F., Li, L., Tang, F., Siedlak, S. L., Fujioka, H., et al. (2014). MFN2 couples glutamate excitotoxicity and mitochondrial dysfunction in motor neurons. *J. Biol. Chem.* 290, 168–182. doi: 10.1074/jbc.M114.617167

Ward, M. E., Chen, R., Huang, H. Y., Ludwig, C., Telpoukhovskaia, M., Taubes, A., et al. (2017). Individuals with progranulin haploinsufficiency exhibit features of neuronal ceroid lipofuscinosis. *Sci. Transl. Med.* 9:eaah5642. doi: 10.1126/scitranslmed.aah5642

Ward, M. E., Taubes, A., Chen, R., Miller, B. L., Sephton, C. F., Gelfand, J. M., et al. (2014). Early retinal neurodegeneration and impaired Ran-mediated nuclear import of TDP-43 in progranulin-deficient FTLD. *J. Exp. Med.* 211, 1937–1945. doi: 10.1084/jem.20140214

Weishaupt, J. H., Waibel, S., Birve, A., Volk, A. E., Mayer, B., Meyer, T., et al. (2013). A novel optineurin truncating mutation and three glaucoma-associated missense variants in patients with familial amyotrophic lateral

sclerosis in Germany. *Neurobiol. Aging* 34, 1516.e9–1516.e15. doi: 10.1016/j.neurobiolaging.2012.09.007

Weisskopf, M. G., Morozova, N., O'Reilly, E. J., McCullough, M. L., Calle, E. E., Thun, M. J., et al. (2009). Prospective study of chemical exposures and amyotrophic lateral sclerosis. *J. Neurol. Neurosurg. Psychiatry* 80, 558–561. doi: 10.1136/jnnp.2008.156976

Weydt, P., Yuen, E. C., Ransom, B. R., and Möller, T. (2004). Increased cytotoxic potential of microglia from ALS-transgenic mice. *Glia* 48, 179–182. doi: 10.1002/glia.20062

Williams, D. B., Floate, D. A., and Leicester, J. (1988). Familial motor neuron disease: differing penetrance in large pedigrees. *J. Neurol. Sci.* 86, 215–230. doi: 10.1016/0022-510X(88)90100-1

Williams, K. L., Topp, S., Yang, S., Smith, B., Fifita, J. A., Warraich, S. T., et al. (2016). CCNF mutations in amyotrophic lateral sclerosis and frontotemporal dementia. *Nat. Commun.* 7:11253. doi: 10.1038/ncomms11253

Wong, P. C., Pardo, C. A., Borchelt, D. R., Lee, M. K., Copeland, N. G., Jenkins, N. A., et al. (1995). An adverse property of a familial ALS-linked SOD1 mutation causes motor neuron disease characterized by vacuolar degeneration of mitochondria. *Neuron* 14, 1105–1116. doi: 10.1016/0896-6273(95)90259-7

Yang, C., Wang, H., Qiao, T., Yang, B., Aliaga, L., Qiu, L., et al. (2014). Partial loss of TDP-43 function causes phenotypes of amyotrophic lateral sclerosis. *Proc. Natl. Acad. Sci. U.S.A.* 111, E1121–E1129. doi: 10.1073/pnas.1322641111

Yedavalli, V. S., Patil, A., and Shah, P. (2018). Amyotrophic lateral sclerosis and its mimics/variants: a comprehensive review. *J. Clin. Imaging Sci.* 8:53. doi: 10.4103/jcis.JCIS_40_18

Ying, H., Shen, X., Park, B., and Yue, B. Y. J. T. (2010). Posttranslational modifications, localization, and protein interactions of optineurin, the product of a glaucoma gene. *PLoS One* 5:e9168. doi: 10.1371/journal.pone.0009168

Yu, Y., Hayashi, S., Cai, X., Fang, C., Shi, W., Tsutsui, H., et al. (2014). Pu-erh tea extract induces the degradation of FET family proteins involved in the pathogenesis of amyotrophic lateral sclerosis. *Biomed Res. Int.* 2014:254680. doi: 10.1155/2014/254680

Zarei, S., Carr, K., Reiley, L., Diaz, K., Guerra, O., Altamirano, P. F., et al. (2015). A comprehensive review of amyotrophic lateral sclerosis. *Surg. Neurol. Int.* 6:171. doi: 10.4103/2152-7806.169561

Zhang, Q., Mao, C., Jin, J., Niu, C., Bai, L., Dang, J., et al. (2014). Side of limb-onset predicts laterality of gray matter loss in amyotrophic lateral sclerosis. *Biomed Res. Int.* 2014:473250. doi: 10.1155/2014/473250

Zhao, W., Beers, D. R., Bell, S., Wang, J., Wen, S., Baloh, R. H., et al. (2015). TDP-43 activates microglia through NF-κB and NLRP3 inflammasome. *Exp. Neurol.* 273, 24–35. doi: 10.1016/j.expneurol.2015.07.019

Zhao, W., Beers, D. R., Henkel, J. S., Zhang, W., Urushitani, M., Julien, J. P., et al. (2010). Extracellular mutant SOD1 induces microglial-mediated motoneuron injury. *Glia* 58, 231–243. doi: 10.1002/glia.20919

Zhong, Z., Deane, R., Ali, Z., Parisi, M., Shapovalov, Y., O'Banion, M. K., et al. (2008). ALS-causing SOD1 mutants generate vascular changes prior to motor neuron degeneration. *Nat. Neurosci.* 11, 420–422. doi: 10.1038/nn2073

Zhou, H., Chen, G., Chen, C., Yu, Y., and Xu, Z. (2012). Association between extremely low-frequency electromagnetic fields occupations and amyotrophic lateral sclerosis: a meta-analysis. *PLoS One* 7:e48354. doi: 10.1371/journal.pone.0048354

Zhu, G., Wu, C. J., Zhao, Y., and Ashwell, J. D. (2007). Optineurin Negatively Regulates TNFα- Induced NF-κB Activation by Competing with NEMO for Ubiquitinated RIP. *Curr. Biol.* 17, 1438–1443. doi: 10.1016/j.cub.2007.07.041

Zhu, Y.-B., and Sheng, Z.-H. (2011). Increased axonal mitochondrial mobility does not slow amyotrophic lateral sclerosis (ALS)-like disease in mutant SOD1 Mice. *J. Biol. Chem.* 286, 23432–23440. doi: 10.1074/jbc.M111.237818

Conflict of Interest: The authors declare that the research was conducted in the absence of any commercial or financial relationships that could be construed as a potential conflict of interest.

Copyright © 2020 Rojas, Ramírez, Fernández-Albarral, López-Cuenca, Salobrar-García, Cadena, Elvira-Hurtado, Salazar, de Hoz and Ramírez. This is an open-access article distributed under the terms of the Creative Commons Attribution License (CC BY). The use, distribution or reproduction in other forums is permitted, provided the original author(s) and the copyright owner(s) are credited and that the original publication in this journal is cited, in accordance with accepted academic practice. No use, distribution or reproduction is permitted which does not comply with these terms.

frontiers in Neuroscience

ORIGINAL RESEARCH
published: 06 October 2020
doi: 10.3389/fnins.2020.556700

Novel Porcine Retina Cultivation Techniques Provide Improved Photoreceptor Preservation

Natalie Wagner[1], Sabrina Reinehr[1], Maurice R. Gammel[1], Andrea Greulich[1], José Hurst[2], H. Burkhard Dick[1], Sven Schnichels[2†] and Stephanie C. Joachim[1†]*

[1] Experimental Eye Research Institute, University Eye Hospital, Ruhr-University Bochum, Bochum, Germany, [2] University Eye Hospital, Centre for Ophthalmology, Tübingen, Germany

OPEN ACCESS

Edited by:
Javier Sancho-Pelluz, Valencia Catholic University Saint Vincent Martyr, Spain

Reviewed by:
María Miranda, Universidad CEU Cardenal Herrera, Spain
Christine A. Curcio, University of Alabama at Birmingham, United States

***Correspondence:**
Stephanie C. Joachim
stephanie.joachim@rub.de

† These authors have contributed equally to this work and share senior authorship

Specialty section:
This article was submitted to Neurodegeneration, a section of the journal Frontiers in Neuroscience

Received: 28 April 2020
Accepted: 07 September 2020
Published: 06 October 2020

Citation:
Wagner N, Reinehr S, Gammel MR, Greulich A, Hurst J, Dick HB, Schnichels S and Joachim SC (2020) Novel Porcine Retina Cultivation Techniques Provide Improved Photoreceptor Preservation. Front. Neurosci. 14:556700. doi: 10.3389/fnins.2020.556700

Age-related macular degeneration (AMD) is the leading cause of blindness in industrialized countries among people over 60 years. It has multiple triggers and risk factors, but despite intense research efforts, its pathomechanisms are currently not completely understood. AMD pathogenesis is characterized by soft drusen in Bruch's membrane and involves the retinal pigment epithelium–Bruch's membrane-choroid complex and adjacent structures, like photoreceptors. This study explores the potential of novel cultivation techniques to preserve photoreceptors in retinal explants to gain better insights in AMD pathology. The porcine retina explants were cultured for 4 and 8 days using three different explantation techniques, namely, control (photoreceptors facing down, touching the filter), filter (photoreceptors facing up, turned sample using a filter), and tweezers (photoreceptors facing up, turned sample using tweezers). Optical coherence tomography revealed that the tweezers method had the best capacity to limit thinning of the retinal explants. Both novel methods displayed advantages in maintaining outer segment thickness. Additionally, immunofluorescence evaluation revealed a better preservation of opsin$^+$ cells and rhodopsin signal intensity in both novel methods, especially the tweezers method. Furthermore, RT-qPCR analysis demonstrated an upregulation of *OPSIN* and *RHODOPSIN* mRNA expression in tweezers samples at 8 days. Amacrine and bipolar cell numbers were not altered at day 4 of cultivation, while cultivation until 8 days led to reduced bipolar cell numbers. At 4 days, *CALRETININ* mRNA was upregulated in filter samples, but *protein kinase C alpha* expression was downregulated. Retinal ganglion cells were diminished in both novel techniques due to a direct physical contact with the insert. Remarkably, no difference in *TUBB3* mRNA expression was detected among the techniques. Nevertheless, both novel methods exhibited an improved retention of photoreceptor cells. In conclusion, the tweezers technique was the most promising one. Due to the high homology of the porcine to the human retina, it provides a reasonable alternative to *in vivo* rodent models. Consequently, an adapted coculture system based on the current findings may serve as an *ex vivo* model suitable to analyze AMD pathomechanisms and novel therapeutic approaches.

Keywords: age-related macular degeneration, porcine, photoreceptor, optical coherence tomography, organotypic retina culture, opsin, rhodopsin

INTRODUCTION

Vision loss is one of the most dreaded constraints together with cancer and Morbus Alzheimer (Scott et al., 2016). One of the leading causes of blindness in industrialized countries, among people over the age of 60, is age-related macular degeneration (AMD) (Klein et al., 1992, 2004; Nowak, 2006; Wong et al., 2014). The early form of AMD is characterized by the presence of lipid-rich deposits, e.g. drusen, and retinal pigment epithelium (RPE) hypopigmentation and hyperpigmentation (Curcio et al., 2013; Klettner et al., 2013). Drusen are located beneath the RPE and consist of many components, such as lipids, amyloid proteins, immune complexes, and complement proteins (Mullins et al., 2000; Crabb et al., 2002). The atrophic (dry) late form is characterized by areas of RPE and photoreceptor degeneration, so-called geographic atrophy. The exudative (wet) form has choroidal neovascularization, resulting in edema and photoreceptor degeneration (Ferris et al., 2013). Several risk factors, such as advanced age, genetic disposition, family history of AMD, race, smoking, obesity, or hypertension, are known to be involved in this multifactorial disease (Mares et al., 2011; Grassmann et al., 2015; Merle et al., 2019). In AMD, characteristic extracellular lipid-rich deposits between outer retinal cells are formed (Buitendijk et al., 2013). RPE cells accumulate lipofuscin, which is a remnant of retinoid metabolites from shed photoreceptor outer-segment membranes (Eldred et al., 1982). The precise role of lipofuscin in AMD is currently under investigation (Fritsche et al., 2014; Gambril et al., 2019; Bermond et al., 2020). Overall, the exact AMD pathogenesis is still not fully understood.

Appropriate *in vivo* models for this retinal disease are limited. In most animal models, the disease induced is acute and the animals are specially bred and killed for the experiment. There is a need for reliable, reproducible, and close-to-human *ex vivo* models, which could be an alternative to animal, especially rodent, models (Dithmar et al., 2000; Shah et al., 2015; Carver et al., 2017; Park et al., 2017; Tode et al., 2018). These rodent models are either based on laser-induced injuries to the RPE and Bruch's membrane or AMD-like defects, which are caused by genetic knockouts. Additionally, like most animals, rodents lack a macula (Huber et al., 2010). Moreover, they have different photoreceptor types. In particular, they only have two types of cones, while humans have three types enabling red light vision (Jacobs et al., 2001). The porcine eye resembles the human eye much closer in regard to anatomy and morphology. Hence, they are often used as *ex vivo* animal models in ophthalmologic research (Schnichels et al., 2020). Especially, the structure of the retinal layers is quite comparable to the human one due to similar development (Gu et al., 2007). However, porcine eyes do not have a macula with a fovea but a comparable central zone called visual streak (Chandler et al., 1999; Hendrickson and Hicks, 2002; Kiilgaard et al., 2007; Bertschinger et al., 2008). The broad horizontal visual streak is located in the tapetal region slightly superior and temporal to the optic nerve and contains the greatest density of photoreceptors and retinal ganglion cells (RGCs) (Maggs et al., 2008). For example, cones can be found in a density of about 15,000 to 40,000 cells/mm^2 (Nicoli et al., 2009), similar to the human macula (Bertschinger et al., 2008). Besides that, porcine eyes can be easily obtained from abattoirs, as a side product of the food industry. Hence, these animals are not solely bred and killed for research experiments.

Our study aimed to investigate a novel *ex vivo* porcine organ culture model where photoreceptors are well preserved. The analysis of photoreceptor degeneration processes is of crucial importance when composing an *ex vivo* AMD model. Our novel tweezers method provides a good preservation of photoreceptor outer segments; thus, it could be used in future studies as part of an *ex vivo* AMD model.

MATERIALS AND METHODS

Preparation and Cultivation of Porcine Neuroretina Explants

Porcine eyes were obtained from the local abattoir and immediately transported to the laboratory, while stored on ice. The eyes were processed within 3 h after animals were sacrificed. First, eyes were cleaned by removing excessive tissue with scissors and immersed in 70% ethanol. Subsequently, they were dissected with a scalpel under a laminar flow hood, and an incision in the cornea was made. Then, cornea, lens, and vitreous were discarded, and the eye cup was washed in sterile phosphate buffered saline (PBS) to eliminate vitreous body residues. To protect the photosensitive retina, the posterior eyeball was rinsed with medium (Neurobasal-A medium, Life Technologies, Carlsbad, CA, United States) supplemented with 0.8 mM L-glutamine (Life Technologies), 2% B27 (Life Technologies), 1% N2 (Life Technologies), and 2% penicillin/streptomycin (Sigma-Aldrich, St. Louis, MO, United States). A cloverleaf-like structure was generated to gain retinal explant from the visual streak. Next, three different techniques, named control, filter, and tweezers method, were performed to obtain retina explants using a dermal punch (Ø = 6 mm, Pmf medical AG, Cologne, Germany). In the control method, explants were obtained by punching out retinal samples. Then, the RPE was removed by washing retinal explants in Neurobasal-A medium. Finally, retinal samples were placed on a Millicell culture insert (Millipore, Burlington, VT, United States) with the ganglion cell layer (GCL) facing up (Kuehn et al., 2016, 2017; **Figure 1A**). The filter technique was adapted from Wang et al. (2011) (**Figure 1A**). Here, a punch was made through the retina, and then a sterile filter paper was carefully applied onto the stamped-out retina sample (Wang et al., 2011). Following, the explant was slowly lifted, the GCL attached to the filter, and placed in a six-well plate (Millipore). The third technique was also performed using a dermal punch. However, much more pressure was exerted to gain an explant from the neuroretina and the underlying structures including the sclera. Subsequently, the sample was lifted with tweezers and rotated 180 degrees. Afterward, the explant was placed on a

cell culture insert. After this step, the sclera and underlying structures, like choroid and RPE, were removed with tweezers, pinching the sclera, to leave the neuroretina explant on the insert (**Figure 1A**). To have an adequate uncultivated control, samples of the three different methods at day 0 were used as native controls. Finally, retinal samples were cultured in 1 ml medium at 37°C and 5% CO_2 for 4 and 8 days. The medium was completely replaced on days 0, 1, 2, and 3. At days 5 and 7, only 50% of the medium was exchanged. At days 4 and 8, the retinal samples were obtained for spectral domain optical coherence tomography (SD-OCT, n = 5/group), quantitative real-time PCR (RT-qPCR, n = 5/group), and histological or immunofluorescence (IF) analysis (n = 9–10/group; **Figure 1B**).

In total, four different groups were compared. Samples that were obtained at day 0 using control, filter, and tweezers technique comprised the native group (**Supplementary Figure S1**). The second group of retinas with GCL facing up was the control technique. The third group consisted of retinas extracted by the filter technique, photoreceptors facing up. The fourth group consisted of retinas obtained by the tweezers method, photoreceptors facing up.

Optical Coherence Tomography

The high-resolution OCT examination of porcine retina samples was performed with an SD-OCT (Spectralis, Heidelberg Engineering, Heidelberg, Germany). For the exploration of the explants, a customized mounting device was used (Schnichels et al., 2016). The holder was adapted to fit the 12-mm Ø cell culture inserts. The retina samples of all groups (n = 5/group) were investigated immediately after preparation at day 0 (= native) and after 4 and 8 days. Three 30°-line scans (ART:100) and an additional group scan, consisting of 20 frames, were performed. During the whole procedure, attention was paid to keep constant aseptic conditions and to prevent a dehydration of the explant. The retina thickness was evaluated according to established protocols (Schnichels et al., 2016; Klemm et al., 2019). To this end, the thickness was measured five times per picture *via* ImageJ (version 1.3u, National Institutes of Health, Bethesda, MD, United States). Three pictures per explant were taken, and a mean of 15 values was calculated per sample.

Preparation of Retinal Sections for (Immuno)Histology

In order to cut cross sections of the retina samples, they were fixed with 4% paraformaldehyde (PFA; Merck, Darmstadt, Germany) for 15 min. Afterwards, the explants were drained with 15% sucrose solution (Sigma-Aldrich) for 15 min and 30% sucrose solution for 30 min. Finally, the explants were embedded in NEG-50 Tissue Tek medium (Thermo Fisher Scientific, Waltham, MA, United States) and stored at −80°C. Subsequently, a microtome (Thermo Fisher Scientific) was used to prepare 10 µm cross sections. Three tissue sections were placed on a Histobond slide (Paul Marienfeld GmbH & Co., KG, Lauda-Königshofen, Germany) and air-dried at room temperature overnight. For histological analyses, all slides were fixed in ice-cold acetone for 10 min on the following day and stored at −80°C.

Hematoxylin and Eosin Staining and Immunofluorescence of Retinal Cross Sections

To evaluate morphologic changes, hematoxylin and eosin (H&E; Merck) stains were performed (Fischer et al., 2008). Thereby, nuclei are stained blue, whereas the cytoplasm and extracellular matrix appear pink. Two pictures of the central region of each cross section (six sections per sample) were taken *via* a microscope equipped with a CCD camera (Axio Imager M1, Zeiss, Oberkochen, Germany) at 200 × magnification. Afterward, the retinal thickness was measured with a measurement tool using Zen software (Zeiss). Per picture, the total thickness as well as the outer (OS) and inner segment (IS) thickness (= bacillary layer) was measured at three positions of the retina. For the total retinal thickness, the measurement tool was used to scale the distance between the GCL and the outer segments of the photoreceptor cells. To evaluate the bacillary layer (OS and IS), we measured the outermost layer of the retina from the outer nuclear layer to the outer segment of the photoreceptor cells. The average values of all three methods at 0 days were classified as the native group. The whole retina and bacillary layer thickness of the native group was defined as 100%.

To identify different cell types of the retina, specific primary antibodies (**Table 1**) were used for IF staining (Kuehn et al., 2016; Hurst et al., 2017). First, retinal sections were defrosted and dried at 37°C for at least 15 min. Then, they were rinsed in PBS (Biochrome, Schaffhausen, Switzerland) and blocked with antisera (goat or donkey) diluted in 0.1–0.2% Triton X-100 (Sigma-Aldrich) in PBS (PBST) and 1% bovine serum albumin. Thereafter, sections were incubated with primary antibodies (**Table 1**) containing antisera solution diluted in PBST at room temperature overnight. Next, the slides were incubated with secondary antibodies (**Table 1**), which were labeled with Alexa Fluor 488 or Alexa Fluor 555, at room temperature for 1 h. Subsequently, nuclei were counterstained with 4′,6-diamidino-2-phenylindole (DAPI; 0.01 µg/ml; Serva Electrophoresis, Heidelberg, Germany). Slides, where the primary antibody solution was omitted, served as negative controls. At the last step, all slides were covered in Shandon mount media (Thermo Fisher Scientific).

To evaluate the retinal IF pictures, four images per section were taken using an Axio Imager M1 or M2 microscope (Zeiss). For further evaluation, images were masked using Ant Renamer 2 software (version 2.10, Antoine Potten, Brussels, Belgium) and then cut in predefined sections (800 × 600 pixels) with Corel PaintShop Pro X8 (Corel, Corel Corporation, Ottawa, ON, Canada). Within those predefined windows, calretinin-, opsin-, protein kinase C alpha (PKCα)-, and RNA-binding protein with multiple splicing (RBPMS)-positive labeled cell bodies were counted using the ImageJ plugin "cell counter." For the signal intensity analysis of rhodopsin, ImageJ was used and all the images were transformed into gray scale. In the next step, the

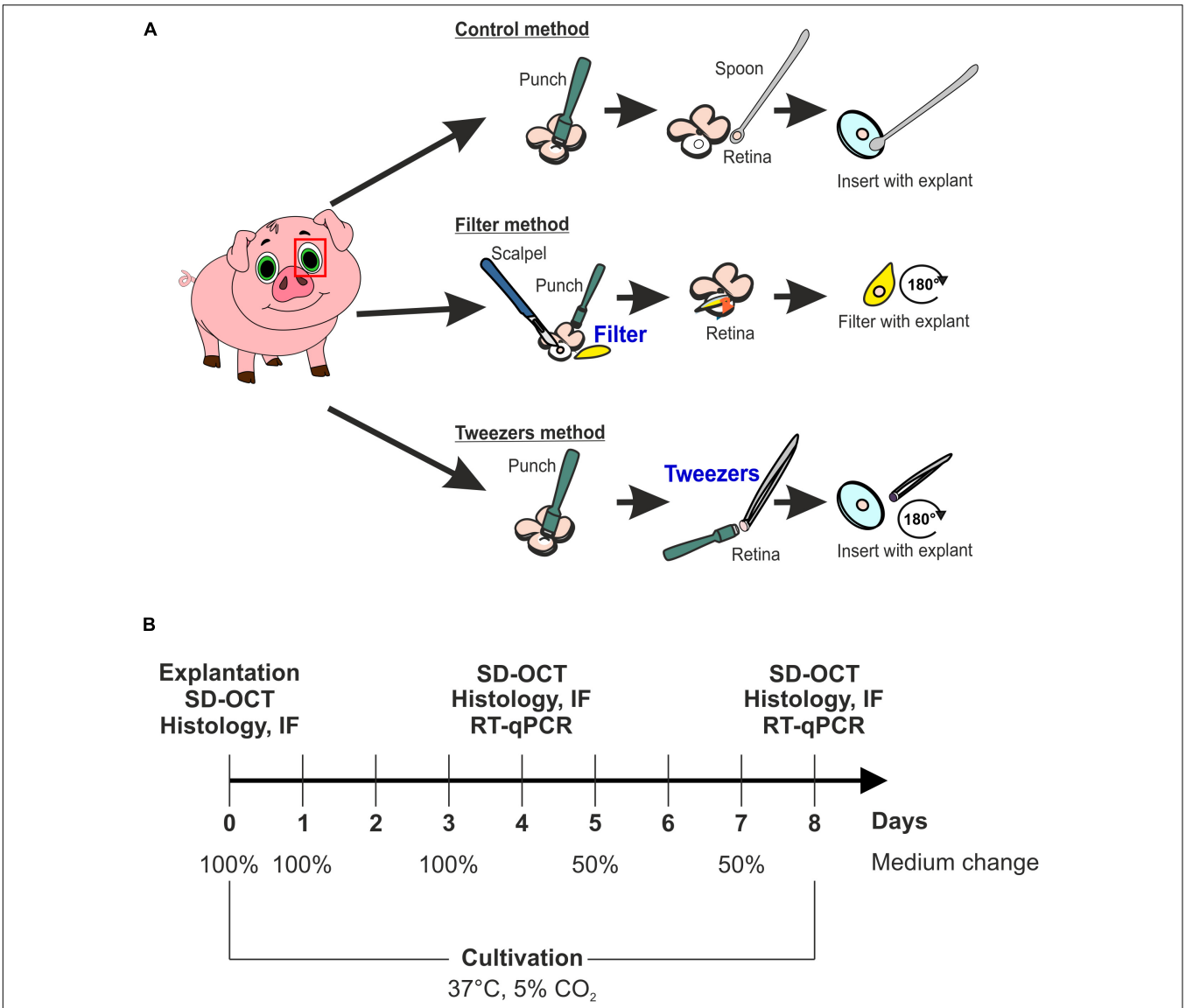

FIGURE 1 | Scheme of the used explant methods and study design. **(A)** Scheme of the three different explantation techniques, named control, filter, and tweezers method. The fourth group was a native one consisting of samples gained *via* the three different methods, which were analyzed at day 0. **(B)** Timeline of the study to investigate which explantation method best preserves the photoreceptor morphology *ex vivo*. Three techniques were compared during the cultivation periods of 4 and 8 days using spectral domain optical coherence tomography (SD-OCT), immunofluorescence (IF), and quantitative real-time PCR (RT-qPCR). Native samples were also included in the analysis.

TABLE 1 | List of primary and secondary antibodies used for immunofluorescence staining.

Primary antibodies			Secondary antibodies		
Antibody	**Company**	**Dilution**	**Antibody**	**Company**	**Dilution**
Anti-calretinin	Santa Cruz Biotechnology	1:100	Donkey anti-goat Alexa Fluor 488	Dianova	1:500
Anti-opsin	Merck Millipore	1:1,200	Donkey anti-rabbit Alexa Fluor 555	Invitrogen	1:500
Anti-PKCα	Santa Cruz Biotechnology	1:300	Goat anti-mouse Alexa Fluor 488	Invitrogen	1:500
Anti-RBPMS	Merck Millipore	1:400	Donkey anti-rabbit Alexa Fluor 555	Invitrogen	1:500
Anti-rhodopsin	Abcam	1:400	Goat anti-mouse Alexa Fluor 488	Invitrogen	1:500

PKCα, protein kinase C alpha; RBPMS, RNA-binding protein with multiple splicing.

background was subtracted (50 pixels) and a lower and upper threshold (lower: 11.55, upper: 82.39) was determined to quantify the rhodopsin signal intensity per section (Reinehr et al., 2016).

Quantitative Real-Time PCR

RNA isolation and cDNA synthesis of porcine retina explants were performed as described previously (Hurst et al., 2017) and according to the manufacturer's instructions with a MultiMACS cDNA Kit (Miltenyi Biotec, Bergisch Gladbach, Germany). For specific primer design, Primer3 software, based on the published GenBank sequence (GenBank: *sus scrofa* taxid:9823)[1], was used (**Table 2**). RT-qPCR was carried out (CfX 96 System, Bio-Rad Laboratories, Inc., Hercules, CA, United States) using the SYBR Green SsoAdvanced™ Universal SYBR® Mastermix (Bio-Rad Laboratories). In a reaction volume of 20 µl, 5 ng of cDNA were present. Final primer concentration was 2 µM, and samples were analyzed twice. The relative expression of the target genes in the novel groups filter and tweezers in comparison to the control group was calculated with REST© 2009 (Qiagen, Hilden, Germany) and expressed as the fold changes in gene expression. The expression levels of the target genes were normalized against the housekeeping genes *ACTB (β-ACTIN)* and *RPL4* (*ribosomal protein L4*) (Wang et al., 2014).

Statistical Analyses

The SD-OCT, histology, and IF results are presented as mean ± SEM, while RT-qPCR results are displayed as median ± quartile + minimum/maximum. A p-value < 0.05 was considered statistically significant. The level of significance was defined as $^{*}p < 0.05$, $^{**}p < 0.01$, and $^{***}p < 0.001$ when compared to the native group, $^{\#}p < 0.05$, $^{\#\#}p < 0.01$, and $^{\#\#\#}p < 0.001$ when compared to the control group, and $^{¥}p < 0.05$ and $^{¥¥}p < 0.01$ when compared to the filter group.

For the evaluation of SD-OCT, histology, and IF data, groups were compared by ANOVA, followed by Tukey *post hoc* test (Statistica; version 13.3; Dell Software, Round Rock, TX, United States). The CT values of the RT-qPCR analysis were evaluated with REST© 2009 software (Qiagen).

RESULTS

Preservation of Retinal Thickness in Tweezers Samples

The SD-OCT enabled an assessment of porcine retina samples during different time points. During all investigated points in time (zero = native, 4 and 8 days), a detailed observation of the layers was possible (**Figure 2A**). The filter paper/insert could be clearly identified above (native, control) or below (filter, tweezers) the explants *via* SD-OCT. The measurement of the retinal thickness revealed no changes in control samples compared to native ones at 4 days ($p = 0.11$; **Figure 2B**). In the filter group, a significantly decreased retina thickness could be noted compared to native samples ($p < 0.001$), while no differences were observed between tweezers and native retinas ($p = 0.60$). No differences were revealed when comparing filter ($p = 0.08$) and tweezers samples ($p = 0.66$) to the control group. A better preservation of the retinal thickness was observed in tweezers samples compared to filter retinas at 4 days ($p = 0.008$). At 8 days of cultivation, the retinal thickness in the control group did not differ from native retinas ($p = 0.08$). The retinal thickness in the filter group was significantly diminished compared to native samples ($p < 0.001$). The tweezers samples showed a similar thickness in comparison to native ones ($p = 0.52$). Both novel methods, filter ($p = 0.08$) and tweezers ($p = 0.66$), showed no differences in the retinal thickness compared to control samples. Eight days after cultivation, the retinal thickness in tweezers samples was significantly higher compared to filter retinas ($p = 0.008$).

Less Reduction in the Total and Photoreceptor Layer Thickness Using the Novel Methods

Hematoxylin and eosin-stained porcine retinas enabled to distinguish between nuclear and cytoplasmic structures, in particular measuring the thickness of the total retina from GCL to the outer photoreceptor segments. The bacillary layer measured spanning from the outer nuclear layer until the outer segment of the photoreceptors (**Figure 3A**).

When comparing retinas of the control group to native samples cultivated for 4 days, a significant reduction of the total retinal thickness was observed ($p = 0.005$; **Figure 3B**). Comparing filter ($p = 0.10$) and tweezers ($p = 0.99$) to the native samples, no significant differences were seen. When filter and control samples were compared, no differences were detected ($p = 0.70$). A significantly better preservation of the retinal thickness was noted in tweezers samples compared to the controls at 4 days ($p = 0.009$). Similar effects could be observed when the retinal explants were cultivated for 8 days. At this time point, there was a significant decrease in the retina thickness in the control group compared to native retinas ($p = 0.04$). Interestingly, a good preservation of the total retina thickness could be achieved by the filter ($p = 0.12$) and tweezers method ($p = 0.50$) when compared to native samples after 8 days of cultivation. Also, no changes were noted when comparing filter ($p = 0.96$) and tweezers retinas ($p = 0.54$) to controls.

Going into detail, by assessing only the bacillary layer thickness at 4 days (**Figure 3C**), a significant reduction was detected in controls compared to native samples ($p = 0.04$). Comparing filter ($p = 1.0$) and tweezers bacillary layer ($p = 0.17$) to native samples, no differences were noted. A better preservation of this layer was visible in filter retinas when compared to control samples ($p = 0.046$), while no differences were noted between tweezers and control samples ($p = 0.89$). After 8 days of cultivation, a significant reduction of the bacillary layer was also measurable in control compared to native samples ($p = 0.001$). On the other hand, a well-preserved bacillary layer was observed in filter ($p = 0.39$) and tweezers methods ($p = 0.22$) when compared to native samples. Filter ($p = 0.08$) and tweezers bacillary layer ($p = 0.18$) were similar to controls.

[1] http://www.bioinformatics.nl/cgi-bin/primer3plus/primer3plus.cgi/

TABLE 2 | List of quantitative real-time PCR (RT-qPCR) primer pairs used. *ACTB* and *RPL4* served as housekeeping genes.

Gene	Oligonucleotides 5′ → 3′	GenBank accession number	Amplicon size
ACTB for	ctcttccagccttccttc	XM_021086047.1	178
ACTB rev	gggcagtgatctctttct		
CALBINDIN 2 for	tgaacccaagctccaagagt	NM_001194980.2	176
CALBINDIN 2 rev	aaaaggtgaagatggcgttg		
OPSINM for	ggggagcatcttcacctaca	NM_001011506.1	244
OPSINM rev	gatgatggtctctgccaggt		
PKCα for	accgaacaacaaggaacgac	XM_021066740.1	163
PKCα rev	ctgagctccacgtttccttc		
RHODOPSIN for	tccaggtacatcccagaagg	NM_214221.1	151
RHODOPSIN rev	gctgcccatagcagaagaag		
RPL4 for	caagagtaactacaaccttc	XM_005659862.3	122
RLP4 rev	gaactctacgatgaatcttc		
TUBB3 for	cagatgttcgatgccaagaa	NM_001044612.1	164
TUBB3 rev	gggatccactccacgaagta		

for, forward; rev, reverse.

Better Survival of Rods and L-Cones With the Novel Methods

Porcine retinal cross sections of all three methods and corresponding native controls were stained with opsin to mark L-cones and with rhodopsin to label rods (**Figure 4A**). The native explants had an almost intact photoreceptor morphology and structure. L-cones were found organized in orderly rows, and rods appeared in organized laminar structures. No striking differences were observed in the organization of the L-cones, located in the outer photoreceptor segment, comparing native, filter, and tweezers samples after 4 days, while the opsin$^+$ and rhodopsin$^+$ cells in the control group looked different. In detail, the opsin$^+$ L-cone cells appeared more disorganized, and the rhodopsin$^+$ area seemed thinner, rather atrophic. Eight days after cultivation, the opsin$^+$ cells appeared to be more disorganized in all three techniques compared to native samples.

At 4 days, a loss of L-cones was noted in the control group compared to native samples ($p = 0.02$; **Figure 4B**). There was no significant loss of opsin$^+$ cones in retinas gained *via* filter ($p = 0.62$) and tweezers technique ($p = 0.97$) when compared to native samples. While no changes could be observed in filter retinas ($p = 0.41$), the number of opsin$^+$ cells was significantly higher in tweezers samples than in control ones at 4 days ($p = 0.04$). A severe loss of opsin$^+$ cells was discovered after 8 days of cultivation in control compared to native samples ($p < 0.001$). The number of L-cones was comparable in filter ($p = 0.62$) and tweezers samples ($p = 0.97$) compared to native ones. Significantly more opsin$^+$ cells were detected in the two novel methods (filter: $p < 0.001$; tweezers: $p < 0.001$) compared to control retinas.

No differences were identified when comparing the *OPSINM* mRNA expression in both novel methods to controls at 4 days (tweezers: 0.94-fold, $p = 0.9$; filter: 0.6-fold, $p = 0.3$; **Figure 4C**). Accordingly, no differences in *OPSINM* expression were seen when the filter method was compared to the controls at 8 days (0.5-fold, $p = 0.3$). Interestingly, an upregulation in *OPSINM* mRNA expression was demonstrated in tweezers samples compared to the controls at 8 days of cultivation (9.6-fold, $p = 0.002$).

Additionally, the signal intensity of rhodopsin was evaluated (**Figure 4A**). At 4 days, the signal intensity of control ($p < 0.001$) and filter retinas ($p = 0.013$) was significantly lower than in native samples (**Figure 4D**). Tweezers and native samples, on the other hand, showed nearly identical intensities ($p = 0.98$). The signal intensity of rhodopsin was significantly higher in tweezers ($p < 0.001$) and filter samples ($p = 0.047$) compared to the controls. When comparing both novel groups, the rhodopsin intensity was significantly higher in tweezers samples compared to filter retinas ($p = 0.04$). After 8 days in cultivation, a clearly diminished rhodopsin signal intensity was documented in all three groups compared to native samples (control: $p < 0.001$, filter: $p < 0.001$, tweezers: $p < 0.001$). No difference was observed when comparing filter ($p = 0.88$) and tweezers samples ($p = 0.07$) to control retinas.

RHODOPSIN mRNA expression was not altered in filter (1.1-fold, $p = 0.85$) and tweezers samples (0.5-fold, $p = 0.22$) compared to the controls at 4 days of cultivation (**Figure 4E**). *RHODOPSIN* mRNA expression in filter samples was not significantly altered at 8 days (1.3-fold, $p = 0.56$). However, we discovered a significant upregulation of *RHODOPSIN* mRNA expression in tweezers samples (2.6-fold, $p = 0.02$) in comparison to control samples.

Comparable Amacrine Cell Numbers but Loss of Bipolar Cells at 8 Days

Characteristic cell types of the inner nuclear layer are amacrine and bipolar cells, which were analyzed to investigate the integrity of the inner retina layer (**Figure 5A**). No difference in the number of calretinin$^+$ cells was detected in controls in comparison to native samples ($p = 0.93$; **Figure 5B**). Also, with the novel techniques, namely, filter ($p = 0.62$) and tweezers ($p = 1.00$), a similar cell number as in native samples was noted at 4 days of cultivation. The same was the case when comparing the filter ($p = 0.93$) and tweezers method ($p = 0.96$) to the controls. Furthermore, after 8 days of cultivation, a slightly lower number

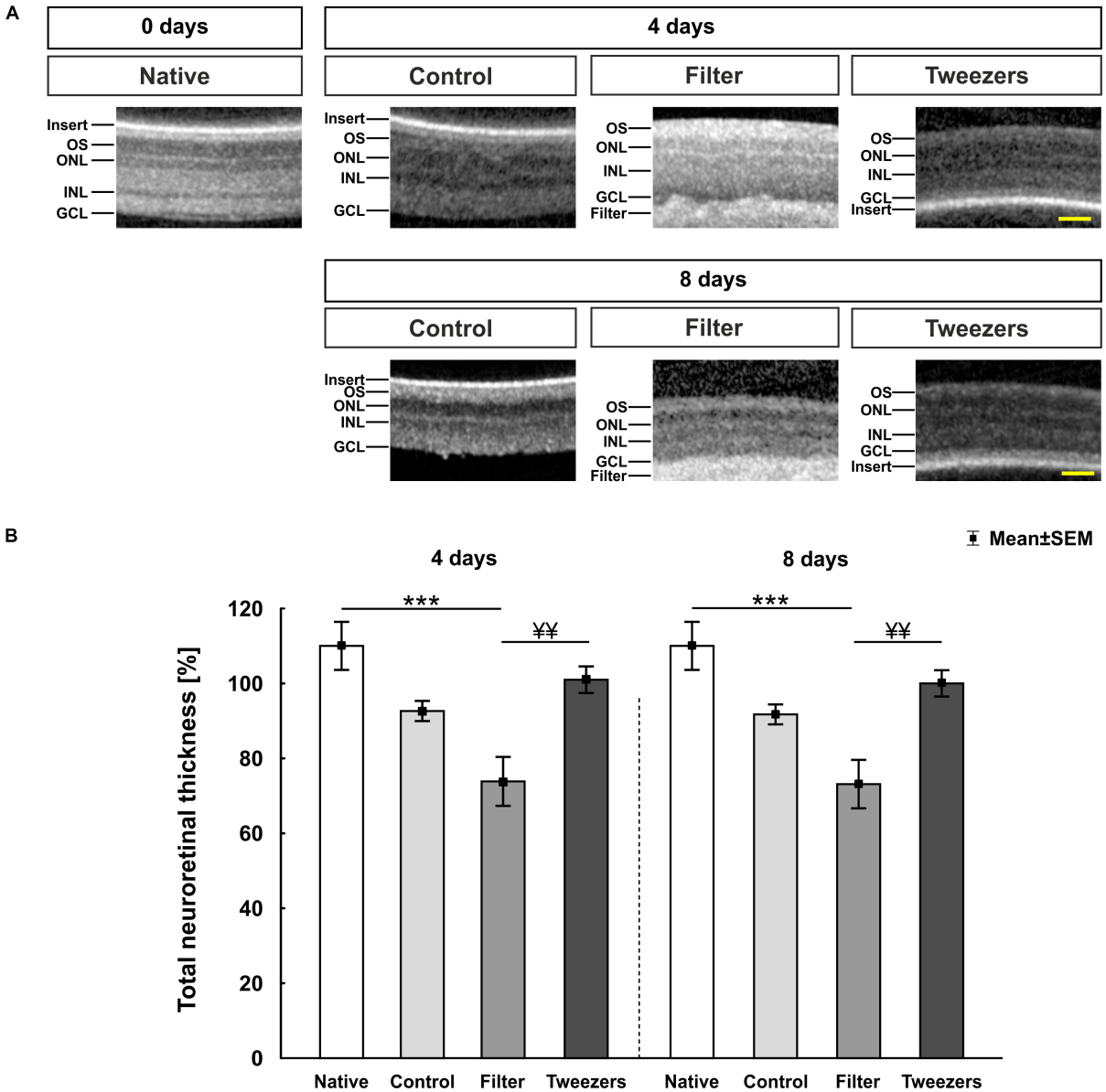

FIGURE 2 | Spectral Domain Optical Coherence Tomography (SD-OCT) analysis of porcine retinas. **(A)** Exemplary pictures of all measured time points and used techniques. Samples of all three explantation methods and the native group were investigated at 0 (= native), 4, and 8 days *via* SD-OCT. **(B)** At 4 days, no changes were noted in regard to the retinal thickness between control and native samples. A significantly thinner retinal thickness was revealed in filter ($p < 0.001$), but not in tweezers samples, compared to native retinas. No alterations were noted in filter and tweezers retinas compared to the controls. The filter group showed a significantly decreased retinal thickness compared to the tweezers group ($p = 0.008$). The retinal thickness of control and native samples was comparable at 8 days. While a significant thinning of the filter group was observed compared to native retinas ($p < 0.001$), no changes were noted between tweezers and native samples. Furthermore, the retinal thickness of the filter group was significantly diminished compared to tweezers samples ($p = 0.008$). OS, photoreceptor outer segments; ONL, outer nuclear layer; OPL, outer plexiform layer; INL, inner nuclear layer; IPL, inner plexiform layer; GCL, ganglion cell layer. Scale bars: 50 μm, values are mean ± SEM. $n = 5$/group. $^{***}p < 0.001$ vs. native group; $^{¥¥}p < 0.01$ vs. filter group.

of calretinin^{+} cells was observed in all three groups compared to the native situation; however, this cell loss was not significant (control: $p = 0.10$; filter: $p = 0.07$; tweezers: $p = 0.07$). In addition, no significant differences were detected between filter ($p = 1.00$) or tweezers samples ($p = 1.00$) and controls.

To quantify *CALRETININ* on the mRNA level, RT-qPCR analysis was performed (**Figure 5C**). An upregulation of relative *CALRETININ* mRNA expression was detected in filter retinas (2.1-fold, $p = 0.001$) in comparison to control samples at 4 days of cultivation. The expression in tweezers samples was similar to controls (0.1-fold, $p = 0.93$). Interestingly, at 8 days of cultivation, no difference was measured neither in the filter (0.4-fold, $p = 0.09$) nor in the tweezers group (0.7-fold, $p = 0.28$) in comparison to control retinas.

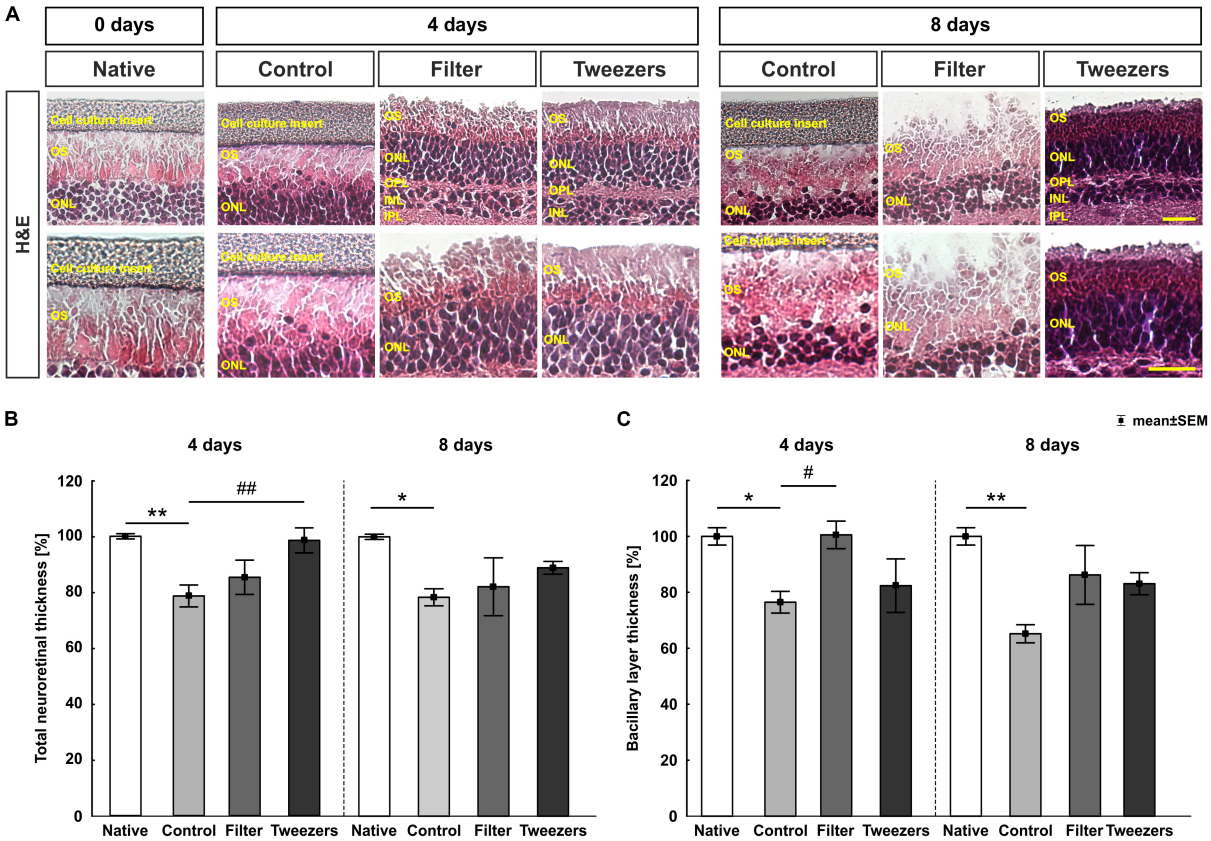

FIGURE 3 | Total and bacillary layer thickness measurement in stained retinas. **(A)** Representative images of H&E-stained retinas for all three explantation methods and the native group in 400 × (upper panel) and 630 × magnification (lower panel). **(B)** At 4 days, a significant reduction of the total retinal thickness in control compared to native samples ($p = 0.005$) was observed, while a preservation was detected in the novel techniques filter and tweezers when compared to native samples. Comparing tweezers to control samples, a significantly thicker retinal thickness was noted ($p = 0.009$), while a similar thickness was observed between filter and control retinas. Similar results were found at 8 days. A reduction of the total retinal thickness was revealed comparing control to native samples ($p = 0.04$). A conservation of the total retinal thickness was detected comparing filter and tweezers to native or control retinas. **(C)** A significant thinning of the bacillary layer was seen in the control group compared to native ($p = 0.04$) and filter samples ($p = 0.046$). However, a better-preserved bacillary layer was noted in the tweezers method compared to the native and control samples at 4 days. A reduction in the bacillary layer thickness was measured at day 8 comparing the control and native samples ($p = 0.001$). The novel methods filter and tweezers maintained the bacillary layer thickness better than did control retinas. OS, photoreceptor outer segments; ONL, outer nuclear layer; OPL, outer plexiform layer; INL, inner nuclear layer; IPL, inner plexiform layer. Scale bars: 20 μm, values are mean ± SEM. $n = 9$–10/group. $^{*}p < 0.05$ and $^{**}p < 0.01$ vs. native group; $^{\#}p < 0.05$ and $^{\#\#}p < 0.01$ vs. controls.

Bipolar cells in the inner nuclear layer were examined using PKCα labeling. When comparing control retinas to native samples, no difference in cell numbers was found ($p = 0.76$; **Figure 5D**). With both novel techniques, the amount of PKCα^{+} cells also remained nearly unchanged when compared to native (filter: $p = 0.98$; tweezers: $p = 0.65$) and control samples (filter: $p = 0.94$; tweezers: $p = 1.0$). Notably, the number of PKCα^{+} cells decreased significantly in all three groups at 8 days of cultivation compared to native samples (control: $p = 0.04$; filter: $p = 0.02$; tweezers: $p = 0.02$). In contrast, no alterations in PKCα^{+} cell counts were seen in filter ($p = 1.00$) and tweezers retinas ($p = 1.00$) compared to the controls.

The RT-qPCR examination of *PKCα* mRNA expression revealed no alteration in filter samples compared to the controls (1.7-fold, $p = 0.31$; **Figure 5E**). Likewise, retina samples cultivated for 4 days *via* the tweezers method showed no significant difference in the *PKCα* expression compared to control samples (0.8-fold, $p = 0.64$). A significant downregulation was also visible in *PKCα* mRNA expression of filter samples compared to the controls after 8 days of cultivation (0.3-fold, $p = 0.02$). In contrast, no alteration was detectable in the mRNA expression of *PKCα* in tweezers retinas compared to the controls (1.0-fold, $p = 0.99$).

Loss of Retinal Ganglion Cells in Novel Explant Methods

To evaluate the effects of the novel cultivation methods on RGCs, they were examined using an anti-RBPMS antibody (**Figure 6A**). No RGC loss was noted in retinas gained *via* the control technique compared to native samples at 4 days of cultivation ($p = 0.14$; **Figure 6B**). On the contrary, comparing the novel methods filter ($p < 0.001$) and tweezers ($p < 0.001$) to native retinas, a severe loss of RGCs was seen after 4 days of cultivation. A significantly decreased number of RGCs were observed in filter

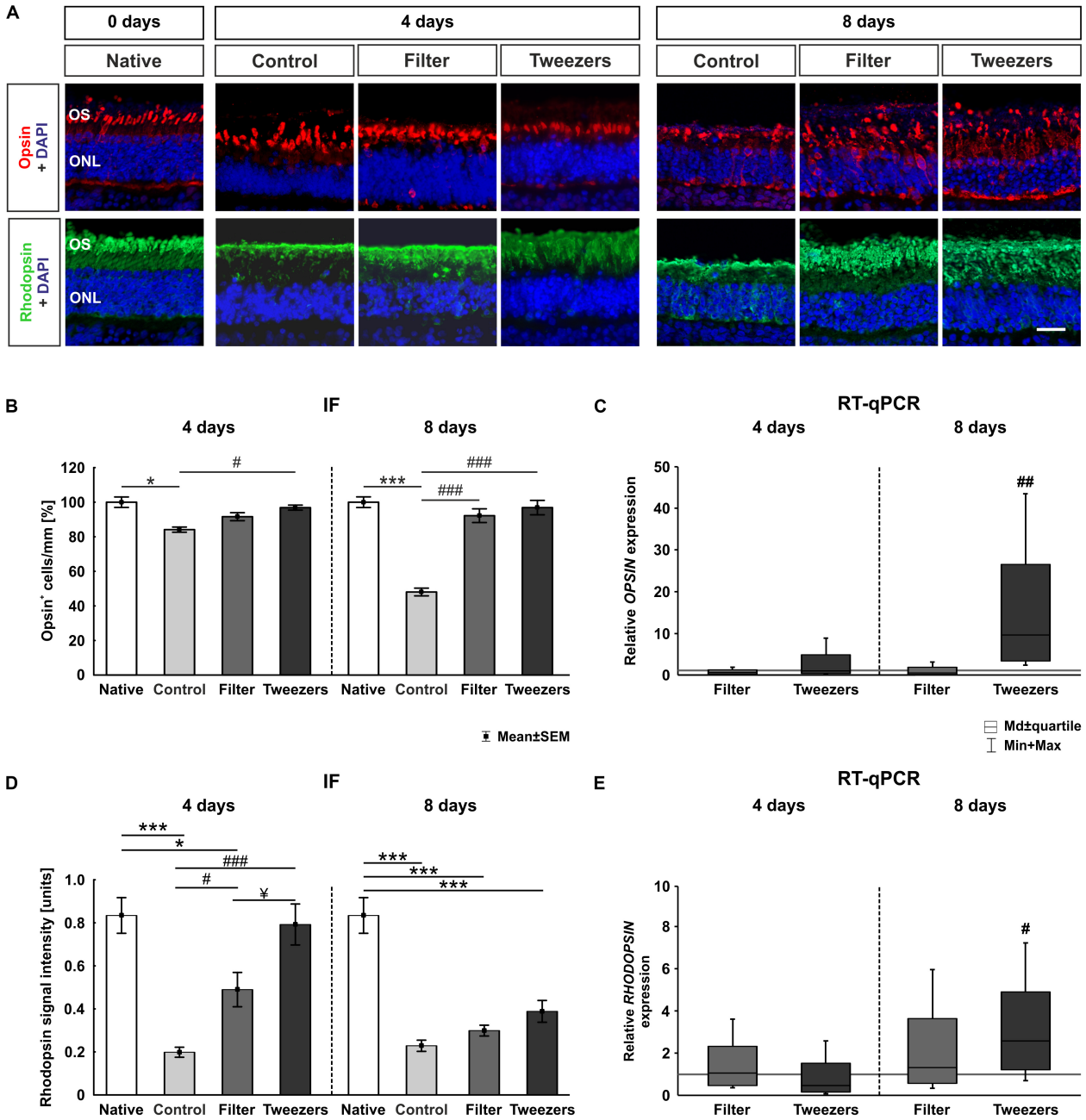

FIGURE 4 | Analysis of photoreceptors. **(A)** Exemplary immunofluorescence pictures of opsin (red) staining for L-cones and rhodopsin (green) staining for rods in photoreceptor outer segments. Nuclei were labeled with 4′,6-diamidino-2-phenylindole (DAPI) (blue). **(B)** Fewer opsin$^+$ cells were found in control compared to native retinas ($p = 0.02$). The filter and tweezers method showed, compared to native retinas, a better preservation over a cultivation period of 4 days. The number of opsin$^+$ cells was significantly higher in tweezers samples ($p = 0.04$) compared to the control ones, while no changes were noted between filter and control retinas. A severe loss of opsin$^+$ cells was discovered in the control compared to native samples after 8 days ($p < 0.001$). In the novel methods filter and tweezers, the number of opsin-labeled cells was comparable to native retinas. When comparing filter and tweezers samples (both: $p < 0.001$) to the controls, more opsin$^+$ cells could be detected. **(C)** *OPSIN* expression was not altered at 4 days. *OPSIN* mRNA expression in tweezers samples was significantly upregulated compared to control retinas at 8 days ($p = 0.002$). **(D)** The rhodopsin signal found in control ($p < 0.001$) and filter samples ($p = 0.01$) was significantly less intense at 4 days compared to that in native samples. A significantly higher signal intensity was documented in tweezers ($p < 0.001$) and filter retinas ($p = 0.047$) compared to the controls. Moreover, a higher rhodopsin signal intensity was observed in tweezers retinas compared to filter samples ($p = 0.04$) at 4 days. At 8 days of cultivation, all three methods showed a significantly diminished rhodopsin intensity compared to native samples (all: $p < 0.001$). **(E)** *RHODOPSIN* mRNA expression was not altered at 4 days. Quantitative real-time PCR (RT-qPCR) examination of *RHODOPSIN* demonstrated an upregulation in tweezers samples compared to control retinas at 8 days ($p = 0.02$). OS, photoreceptor outer segments; ONL, outer nuclear layer. Scale bar: 20 μm, values are mean ± SEM for immunofluorescence (IF) and median ± quartile + min/max for RT-qPCR. IF: $n = 9$–10/group; RT-qPCR: $n = 5$/group. $^*p < 0.05$ and $^{***}p < 0.001$ vs. native group; $^{\#}p < 0.05$, $^{\#\#}p < 0.01$, and $^{\#\#\#}p < 0.001$ vs. controls; $^{¥}p < 0.05$ vs. filter group.

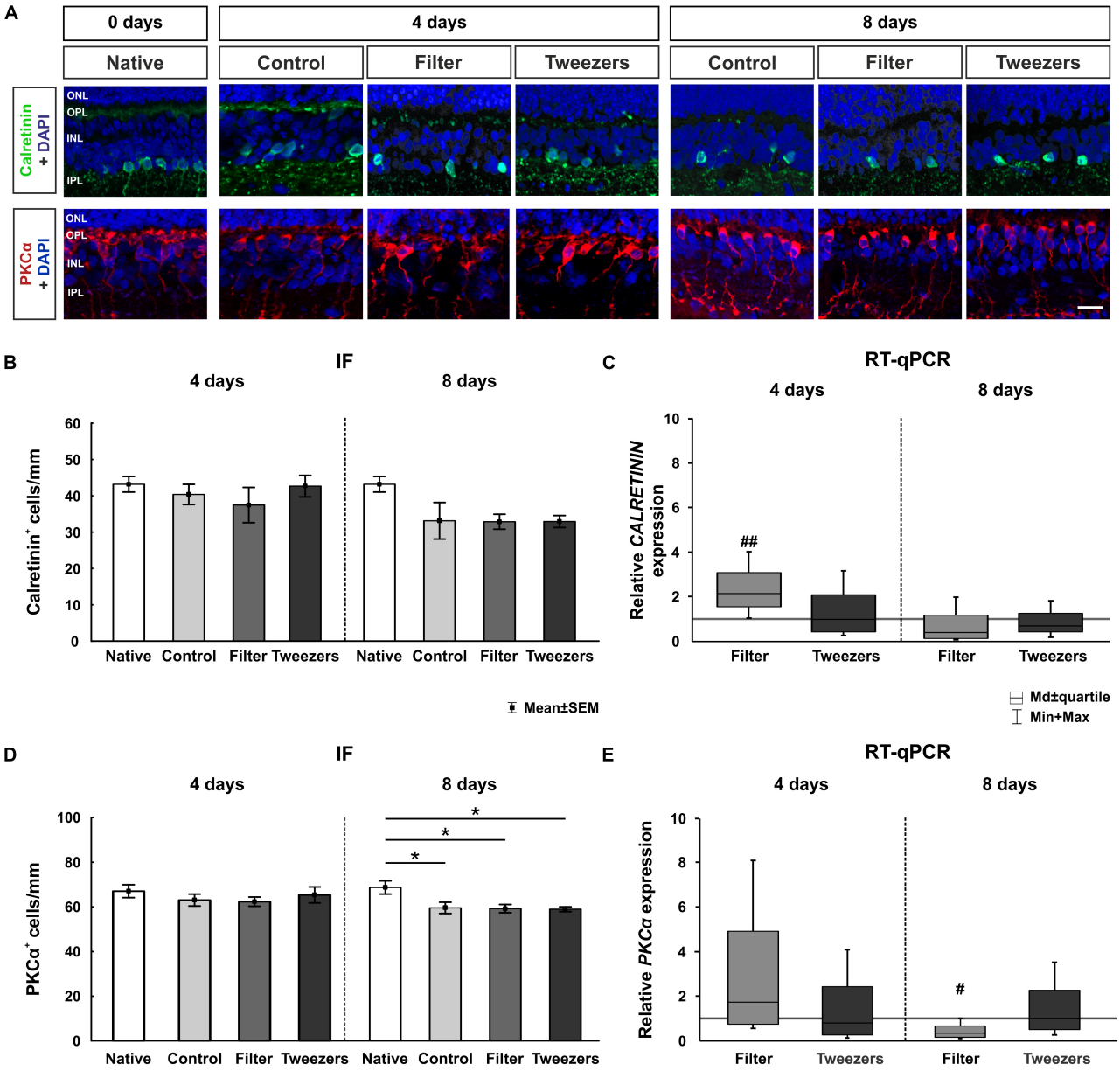

FIGURE 5 | Effect on cells in the inner nuclear layer. **(A)** Amacrine cells were labeled with calretinin (green) and bipolar cells with protein kinase C alpha (PKCα) (red). Cell nuclei were stained with 4′,6-diamidino-2-phenylindole (DAPI) (blue). **(B)** No differences were observed regarding the number of calretinin$^+$ cells between all groups at 4 and 8 days. **(C)** An upregulation of the relative *CALRETININ* mRNA expression was detected in filter retinas compared to control samples at 4 days ($p = 0.001$). No differences were noted at 8 days. **(D)** The number of bipolar cells was not altered in any group at 4 days. However, fewer PKCα$^+$ cells were discovered in control ($p = 0.04$), filter ($p = 0.02$), and tweezers retinas ($p = 0.02$) compared to those in native samples at 8 days. **(E)** A significant *PKCα* mRNA downregulation was observed in filter samples compared to control ones at 8 days ($p = 0.02$). ONL, outer nuclear layer; OPL, outer plexiform layer; INL, inner nuclear layer; IPL, inner plexiform layer. Scale bar: 20 μm, values are mean ± SEM for immunofluorescence (IF) and median ± quartile + min/max for quantitative real-time PCR (RT-qPCR). IF: $n = 9$–10/group; RT-qPCR: $n = 5$/group. $^*p < 0.05$ vs. native group; $^{\#}p < 0.05$ and $^{\#\#}p < 0.01$ vs. controls.

($p = 0.002$) and tweezers retinas ($p = 0.03$) compared to the controls. With the ongoing time of cultivation, the RGC loss progressed. At 8 days of cultivation, the number of RGCs was significantly lower in control retinas compared to native explants ($p < 0.001$). A severe decrease in RGC numbers was also noted in samples gained *via* filter ($p < 0.001$) and tweezers method ($p < 0.001$) compared to native retinas. With both novel methods, filter ($p = 0.16$) and tweezers ($p = 0.97$), the number of RGCs was comparable to control retinas at 8 days.

RT-qPCR was used to evaluate β-*III-Tubulin (TUBB3)* gene expression in retina samples of all groups, since this gene is enriched in RGCs (Soto et al., 2008; Jiang et al., 2015). The relative *TUBB3* mRNA expression was neither altered in filter (0.8-fold, $p = 0.43$) nor in tweezers retinas (0.9-fold, $p = 0.74$)

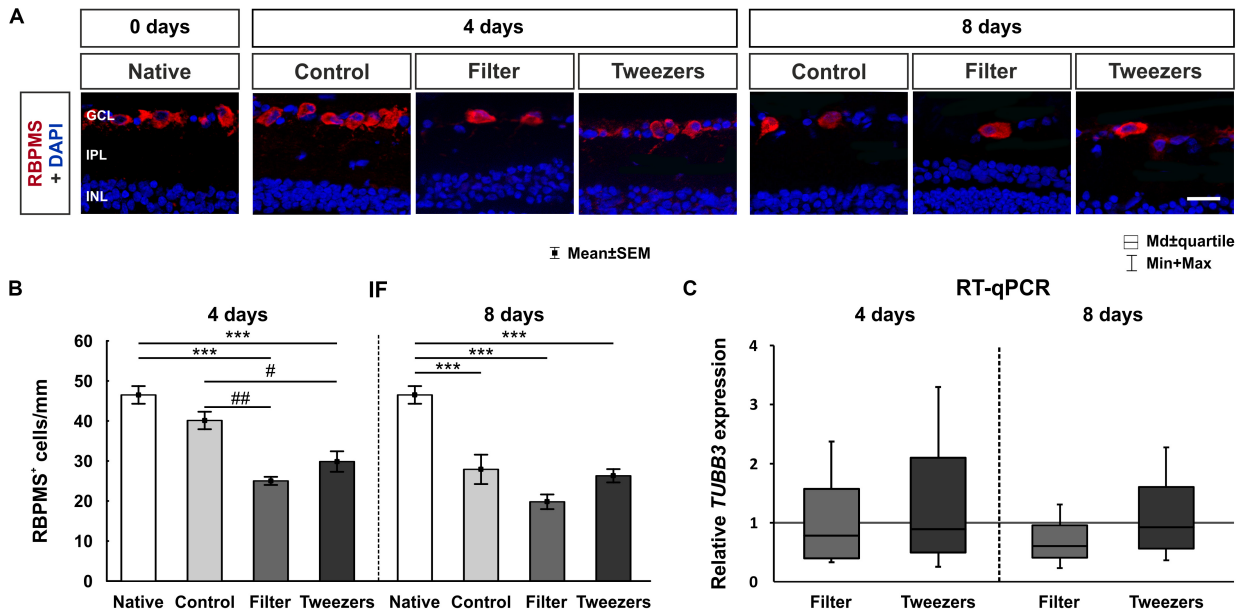

FIGURE 6 | Evaluation of retinal ganglion cells (RGCs). **(A)** RGCs were labeled with RNA-binding protein with multiple splicing (RBPMS) (red) and cell nuclei with 4′,6-diamidino-2-phenylindole (DAPI) (blue). **(B)** The amount of $RBPMS^+$ cells in control retinas was comparable to that in native ones. The number of RGCs was significantly reduced in both novel methods, filter ($p < 0.001$) and tweezers ($p < 0.001$), compared to the native method at 4 days. A significant loss of RGCs was noted in filter ($p = 0.002$) and tweezers samples ($p = 0.03$) compared to control ones. At 8 days, fewer RGCs were visible for all three groups control, filter, and tweezers compared to those in native samples (all: $p < 0.001$). **(C)** No differences in the *TUBB3* mRNA expression levels were detected between all groups at 4 and 8 days. GCL, ganglion cell layer; IPL, inner plexiform layer; INL, inner nuclear layer. Scale bar: 20 μm, values are mean ± SEM for immunofluorescence (IF) and median ± quartile + min/max for quantitative real-time PCR (RT-qPCR). IF: n = 9–10/group; RT-qPCR: n = 5/group. $^{***}p < 0.001$ vs. native group; $^{\#}p < 0.05$ and $^{\#\#}p < 0.01$ vs. controls.

compared to retinas gained *via* control technique after 4 days of cultivation (**Figure 6C**). In retinas of the filter technique, a trend toward a downregulation of *TUBB3* gene expression (0.6-fold, $p = 0.06$) was noted in comparison to control samples at 8 days. However, no changes in mRNA level were found for tweezers retinas (0.9-fold, $p = 0.78$).

DISCUSSION

AMD is a multifactorial disease and one of the major reasons for irreversible blindness. Although there are animal models and cell culture approaches available, there is a certain demand for organ culture models or organoids, mimicking the molecular mechanisms contributing to AMD. This need also applies to other retinal diseases, such as diabetic retinopathy or *retinitis pigmentosa*. Cell cultures have certain limitations, especially a good photoreceptor cell line does not really exist, and working with primary photoreceptor cells has certain obstacles (MacLeod et al., 1999; Romano and Hicks, 2007). Animal models often only mimic specific aspects of retinal disease, while retinal explant cultures provide a simplified system for investigating the retinal function and possible pathomechanisms of these diseases (Murali et al., 2019; Schnichels et al., 2019). Organ cultures still possess elementary structures of the organ, in this case the retina, allowing analysis of complex interactions, e.g., signaling pathways.

To this end, we evaluated new techniques for the preparation of porcine organotypic neuroretina explants, which should preserve the bacillary layer in a better fashion than previous protocols. The two novel methods, named tweezers and filter, resulted in a better conservation of the sensitive rod and L-cone cells than the control technique. The results demonstrated that *via* rotation of 180°, hence having the photoreceptor layer facing up during cultivation, the retinal morphology could be maintained much better. Therefore, this *ex vivo* model should mimic the *in vivo* situation.

Ex vivo cultivation of photoreceptor cells is complicated for several reasons. Many degenerative processes are directly initiated through the explantation of the neuroretina. The detachment of photoreceptor cells from the RPE is inducing rapid apoptotic processes (Cook et al., 1995). Hence, a sensitive method, with as little physical manipulation as possible, is mandatory for the preparation of adult neuroretina explants. Regarding these facts, our methods aimed to explant the retina using a "no touch" technique to minimize the harm to the retina as much as possible. The investigation of the total retina thickness revealed a better maintenance of retinas in the tweezers group compared to control and filter retinas over the cultivation time. Our study suggested that omitting direct physical contact using the two new techniques led to an improved preservation of rods and L-cones. This preservation of photoreceptors could not be noted in the control group, where these cells had direct contact to the insert. This led to a thinning of the whole retina. This

effect can be explained by looking closer at the morphology of rods and cones. Compared to other neuronal cell types of the retina, both photoreceptor cell types have a more elongated thin shape of the outer segment, resulting in easy breakage of the sensitive connection to the photoreceptor nuclei (Mustafi et al., 2009; Kawamura and Tachibanaki, 2012).

OCT is an interferometry and non-invasive technique that can be used to acquire cross-sectional tomographic pictures. This enables recording of dynamic changes in the course and progression of diseases. In AMD, the ultrastructure of drusen as well as geographic atrophy can be imaged and characterized (Khanifar et al., 2008; Yehoshua et al., 2010). The advantages of this method can also be applied in animal models or organ cultures. Therefore, in this study, the retinal explants were evaluated by SD-OCT as well as by histology (H&E staining). Interestingly, the results between both methods differed. For example, the filter samples appeared less preserved in SD-OCT than in the H&E staining. In contrast, the tweezers group had a significant thicker total retina *via* SD-OCT measurements, but not after H&E staining at 8 days. This could be explained by the fact that disruption of the retina can be generated during dissection, embedding, cutting, and staining for H&E (Dailey et al., 2017). Especially, processing the samples of the filter group could be worse through the attached filter. The use of the SD-OCT provides the ability to measure the same sample over time, while for H&E analyses, new samples are needed for every evaluation time point. In future studies, SD-OCT measurements could help to identify the development and progression of drusen in an AMD-like coculture system.

In general, a longer cultivation time makes a preservation of retina less likely, which applies to all neuronal cell types. In this aspect, cultivation time should be kept as short as possible but also adequately mimic the *in vivo* situation and give enough time for studies. Therefore, we were interested in adapting and improving the cultivation method of photoreceptor cells to extend the cultivation time and enabling us to analyze aging effects. The rhodopsin and opsin signals in tweezers samples in our study were comparable to those of the native samples at 8 days. Previous studies using mouse and porcine retinas revealed that photoreceptors become pyknotic after 3–4 days *in vitro* (Tansley, 1933; Ogilvie et al., 2000; Taylor et al., 2013a,b). However, Wang et al. (2011) demonstrated that the rotation and inner retina support conserved the photoreceptor layer for up to 7 days in culture. A loss of neuronal cells in an adult explant culture system is given through the limitations of an *ex vivo* culture, such as the detachment of supporting tissue, the missing RPE cells, and the lack of choroidal circulation. In contrast, our explants cultured using the novel techniques (filter and tweezers) displayed a significantly better photoreceptor survival than the control technique. The number of opsin$^+$ cells was, even after 8 days *ex vivo*, still comparable to the number of the native samples. Moreover, the rhodopsin signal intensity was well preserved in tweezers samples and comparable to native samples after 4 days of cultivation. Also, *OPSIN* and *RHODOPSIN* mRNA expression in the tweezers group was upregulated after 8 days of cultivation, which indicates a preserved photoreceptor cell health. However, the opsin$^+$ cells appeared more disorganized compared to native samples at this time point. This may influence the function of these cells. In future studies, electroretinography should be included to clarify this point.

To investigate the effects of the different methods on the inner retina, amacrine and bipolar cells were analyzed. Interestingly, the number of calretinin$^+$ cells was not altered in all groups. In contrast, an upregulation of *CALRETININ* mRNA was found in the filter group at 4 days. The used antibody against PKCα is specific for rod bipolar cells, which are representing only a part of the bipolar cells of the retina. The amount of PKCα$^+$ cells was stable in explants of all techniques at 4 days. However, at day 8, a significant loss of bipolar cells was visible in all three techniques compared to native controls. Thus, a progressive loss of PKCα$^+$ cells was detectable with ongoing cultivation. This result was supported by a significant downregulation of the *PKCα* mRNA expression in filter samples cultivated for 8 days. Consequently, our findings indicate that in neuroretina explant cultures, bipolar cells are probably more sensitive than amacrine cells. Amacrine cells represent a very diverse class of intrinsic interneurons in the inner retina, forming a network. Hence, they receive synaptic input from other amacrine cells as well as bipolar cells. They provide this input to further amacrine cells, bipolar cells, and RGCs (Wilson and Vaney, 2010). Bipolar cells interact directly with RGCs or indirectly through the amacrine cells (Fitzpatrick, 2015). Stained amacrine and bipolar cell types are located in the inner retina, but they are affected differently. Interestingly, Fernandez-Bueno et al. (2012) made the same observation when cultivating human retinas. They discovered a loss of bipolar cells and impairment of their axons with ongoing time of cultivation, while such a degenerating process was not documented for amacrine cells (Fernandez-Bueno et al., 2012). The loss of RGCs in our study was severe in filter and tweezers samples already at 4 days of cultivation and increased over time. These results confirm that direct contact with the membrane fosters cell damage. The RGCs are axotomized and hence deprived of their trophic support, resulting in apoptosis. The bipolar cells are connected to the RGCs, so an increased degeneration at 8 days of cultivation might indirectly also affect them.

The aim of this study was to find a suitable preparation technique that preserves photoreceptor cells in a porcine organ culture model. This was successfully achieved by introducing the tweezers and filter method. Both new methods led to a significantly improved morphology of photoreceptors, making them more comparable to the *in vivo* situation. Although both methods revealed just small differences in comparison, the tweezers method showed more preserved photoreceptor cells (protein and mRNA level) and a better morphology *via* SD-OCT. In addition, handling of the explants was much easier with the tweezers method, leading to a higher reproducibility. Consequently, this method seems to be more adequate for following coculture experiments of RPE and neuroretina. The improved photoreceptor cultivation should enable us to analyze the interaction of RPE and photoreceptor cells. Both structures and their interaction are essential in understanding the pathomechanisms underlying AMD. To

reproduce an AMD-like pathology, RPE and a functional barrier are needed to induce drusen. Pilgrim et al. (2017) already revealed that in a primary RPE cell culture system, sub-RPE deposits were formed. These deposits contained, for example, proteins, lipids, and hydroxyapatite, as seen in AMD patients (Pilgrim et al., 2017). These drusen-like deposits should also be implemented in future coculture models for AMD research.

In conclusion, this work provides two explant methods for organotypic porcine retina culture models focusing on photoreceptors. Both novel methods improve photoreceptor cultivation in contrast to the established control technique. Especially, the tweezers method facilitates the analysis of photoreceptor degeneration and can be further utilized to study different diseases, such as AMD, diabetic retinopathy, or *retinitis pigmentosa*. Furthermore, the tweezers method could be used in a coculture system of neuroretina and RPE cells, which would provide a promising and innovative technique to effectively reduce the number of animal experiments in retina research.

DATA AVAILABILITY STATEMENT

The raw data supporting the conclusions of this article will be made available by the authors, without undue reservation.

AUTHOR CONTRIBUTIONS

NW performed the experiments, analyzed the data, and wrote the manuscript. SR performed the experiments and revised the manuscript. MG, AG, and JH performed the experiments and analyzed the data. HD revised the manuscript. SJ and SS designed the study and revised the manuscript. All authors read and approved the final version of the manuscript.

FUNDING

This study was in part supported by PRO RETINA-Foundation for Prevention of Blindness and Novartis Pharma GmbH. We acknowledged the support by the DFG Open Access Publication Funds of the Ruhr-Universität Bochum.

SUPPLEMENTARY MATERIAL

The Supplementary Material for this article can be found online at: https://www.frontiersin.org/articles/10.3389/fnins.2020.556700/full#supplementary-material

Supplementary Figure 1 | Comparison of the three methods on day 0 *via* SD-OCT and H&E staining. **(A)** Exemplary SD-OCT pictures of all used techniques at day 0. **(B)** No difference in the total retina thickness was observed between all three techniques at day 0 (= native). The filter ($p = 1.00$) as well as the tweezers samples ($p = 0.76$) were comparable to the control ones. Furthermore, no alterations were noted between tweezers and filter native retinas ($p = 0.76$). **(C)** All samples were stained with H&E. No difference in the morphology or structure was noted in retinas from all three explantation techniques. **(D)** The statistical evaluation showed no difference in the total retinal thickness (all: $p > 0.05$). OS, photoreceptor outer segments; ONL, outer nuclear layer; OPL, outer plexiform layer; INL, inner nuclear layer; IPL, inner plexiform layer; GCL, ganglion cell layer. Scale bar: 50 μm, values are mean ± SEM. $n = 9$–10/group.

REFERENCES

Bermond, K., Wobbe, C., Tarau, I. S., Heintzmann, R., Hillenkamp, J., Curcio, C. A., et al. (2020). Autofluorescent granules of the human retinal pigment epithelium: phenotypes, intracellular distribution, and age-related topography. *Invest. Ophthalmol. Vis. Sci.* 61:35. doi: 10.1167/iovs.61.5.35

Bertschinger, D. R., Beknazar, E., Simonutti, M., Safran, A. B., Sahel, J. A., Rosolen, S. G., et al. (2008). A review of in vivo animal studies in retinal prosthesis research. *Graefes Arch. Clin. Exp. Ophthalmol.* 246, 1505–1517. doi: 10.1007/s00417-008-0891-7

Buitendijk, G. H. S., Rochtchina, E., Myers, C., Van Duijn, C. M., Lee, K. E., Klein, B. E. K., et al. (2013). Prediction of age-related macular degeneration in the general population: the Three Continent AMD Consortium. *Ophthalmology* 120, 2644–2655.

Carver, K. A., Lin, C. M., Bowes Rickman, C., and Yang, D. (2017). Lack of the P2X7 receptor protects against AMD-like defects and microparticle accumulation in a chronic oxidative stress-induced mouse model of AMD. *Biochem. Biophys. Res. Commun.* 482, 81–86. doi: 10.1016/j.bbrc.2016.10.140

Chandler, M. J., Smith, P. J., Samuelson, D. A., and Mackay, E. O. (1999). Photoreceptor density of the domestic pig retina. *Vet. Ophthalmol.* 2, 179–184. doi: 10.1046/j.1463-5224.1999.00077.x

Cook, B., Lewis, G. P., Fisher, S. K., and Adler, R. (1995). Apoptotic photoreceptor degeneration in experimental retinal detachment. *Invest. Ophthalmol. Vis. Sci.* 36, 990–996.

Crabb, J. W., Miyagi, M., Gu, X., Shadrach, K., West, K. A., Sakaguchi, H., et al. (2002). Drusen proteome analysis: an approach to the etiology of age-related macular degeneration. *Proc. Natl. Acad. Sci. U.S.A.* 99, 14682–14687.

Curcio, C. A., Messinger, J. D., Sloan, K. R., Mcgwin, G., Medeiros, N. E., and Spaide, R. F. (2013). Subretinal drusenoid deposits in non-neovascular age-related macular degeneration: morphology, prevalence, topography, and biogenesis model. *Retina* 33, 265–276. doi: 10.1097/iae.0b013e31827e25e0

Dailey, W. A., Drenser, K. A., Wong, S. C., Cheng, M., Vercellone, J., Roumayah, K. K., et al. (2017). Ocular coherence tomography image data of the retinal laminar structure in a mouse model of oxygen-induced retinopathy. *Data Brief* 15, 491–495. doi: 10.1016/j.dib.2017.09.075

Dithmar, S., Curcio, C. A., Le, N. A., Brown, S., and Grossniklaus, H. E. (2000). Ultrastructural changes in Bruch's membrane of apolipoprotein E-deficient mice. *Invest. Ophthalmol. Vis. Sci.* 41, 2035–2042.

Eldred, G. E., Miller, G. V., Stark, W. S., and Feeney-Burns, L. (1982). Lipofuscin: resolution of discrepant fluorescence data. *Science* 216, 757–759. doi: 10.1126/science.7079738

Fernandez-Bueno, I., Fernandez-Sanchez, L., Gayoso, M. J., Garcia-Gutierrez, M. T., Pastor, J. C., and Cuenca, N. (2012). Time course modifications in organotypic culture of human neuroretina. *Exp. Eye Res* 104, 26–38. doi: 10.1016/j.exer.2012.08.012

Ferris, F. L. I. I. I., Wilkinson, C. P., Bird, A., Chakravarthy, U., Chew, E., Csaky, K., et al. (2013). Clinical classification of age-related macular degeneration. *Ophthalmology* 120, 844–851.

Fischer, A. H., Jacobson, K. A., Rose, J., and Zeller, R. (2008). Hematoxylin and eosin staining of tissue and cell sections. *CSH Protoc* 2008:dbrot4986.

Fitzpatrick, D. (2015). *Implantable Electronic Medical Devices*. Amsterdam: Elsevier Ltd.

Fritsche, L. G., Fariss, R. N., Stambolian, D., Abecasis, G. R., Curcio, C. A., and Swaroop, A. (2014). Age-related macular degeneration: genetics and biology coming together. *Annu. Rev. Genomics Hum. Genet.* 15, 151–171.

Gambril, J. A., Sloan, K. R., Swain, T. A., Huisingh, C., Zarubina, A. V., Jeffrey, D., et al. (2019). Quantifying retinal pigment epithelium dysmorphia and

loss of histologic autofluorescence in age-related macular degeneration. *Invest. Ophthalmol. Vis. Sci.* 60, 2481–2493. doi: 10.1167/iovs.19-26949

Grassmann, F., Ach, T., Brandl, C., Heid, I. M., and Weber, B. H. F. (2015). What does genetics tell us about age-related macular degeneration? *Annu. Rev. Vis. Sci.* 1, 73–96. doi: 10.1146/annurev-vision-082114-035609

Gu, P., Harwood, L. J., Zhang, X., Wylie, M., Curry, W. J., and Cogliati, T. (2007). Isolation of retinal progenitor and stem cells from the porcine eye. *Mol. Vis.* 13, 1045–1057.

Hendrickson, A., and Hicks, D. (2002). Distribution and density of medium- and short-wavelength selective cones in the domestic pig retina. *Exp Eye Res.* 74, 435–444. doi: 10.1006/exer.2002.1181

Huber, G., Heynen, S., Imsand, C., Vom Hagen, F., Muehlfriedel, R., Tanimoto, N., et al. (2010). Novel rodent models for macular research. *PLoS One* 5:e13403. doi: 10.1371/journal.pone.0013403

Hurst, J., Kuehn, S., Jashari, A., Tsai, T., Bartz-Schmidt, K. U., Schnichels, S., et al. (2017). A novel porcine ex vivo retina culture model for oxidative stress induced by H(2)O(2). *Altern. Lab. Anim.* 45, 11–25. doi: 10.1177/026119291704500105

Jacobs, G. H., Fenwick, J. A., and Williams, G. A. (2001). Cone-based vision of rats for ultraviolet and visible lights. *J. Exp. Biol.* 204, 2439–2446.

Jiang, S. M., Zeng, L. P., Zeng, J. H., Tang, L., Chen, X. M., and Wei, X. (2015). beta-III-Tubulin: a reliable marker for retinal ganglion cell labeling in experimental models of glaucoma. *Int. J. Ophthalmol.* 8, 643–652.

Kawamura, S., and Tachibanaki, S. (2012). Explaining the functional differences of rods versus cones. *WIREs Membr. Transp. Signal.* 1, 675–683. doi: 10.1002/wmts.8

Khanifar, A. A., Koreishi, A. F., Izatt, J. A., and Toth, C. A. (2008). Drusen ultrastructure imaging with spectral domain optical coherence tomography in age-related macular degeneration. *Ophthalmology* 115, 1883–1890. doi: 10.1016/j.ophtha.2008.04.041

Kiilgaard, J. F., Prause, J. U., Prause, M., Scherfig, E., Nissen, M. H., and La Cour, M. (2007). Subretinal posterior pole injury induces selective proliferation of RPE cells in the periphery in in vivo studies in pigs. *Invest. Ophthalmol. Vis. Sci.* 48, 355–360. doi: 10.1167/iovs.05-1565

Klein, R., Klein, B. E., and Linton, K. L. (1992). Prevalence of age-related maculopathy. The Beaver Dam Eye Study. *Ophthalmology* 99, 933–943.

Klein, R., Peto, T., Bird, A., and Vannewkirk, M. R. (2004). The epidemiology of age-related macular degeneration. *Am. J. Ophthalmol.* 137, 486–495.

Klemm, P., Hurst, J., Blak, M., Herrmann, T., Melchinger, M., Bartz-Schmidt, K. U., et al. (2019). Hypothermia protects retinal ganglion cells against hypoxia-induced cell death in a retina organ culture model. *Clin. Exp. Ophthalmol.* 47, 1043–1054. doi: 10.1111/ceo.13565

Klettner, A., Kauppinen, A., Blasiak, J., Roider, J., Salminen, A., and Kaarniranta, K. (2013). Cellular and molecular mechanisms of age-related macular degeneration: from impaired autophagy to neovascularization. *Int. J. Biochem. Cell Biol.* 45, 1457–1467. doi: 10.1016/j.biocel.2013.04.013

Kuehn, S., Hurst, J., Jashari, A., Ahrens, K., Tsai, T., Wunderlich, I. M., et al. (2016). The novel induction of retinal ganglion cell apoptosis in porcine organ culture by NMDA - an opportunity for the replacement of animals in experiments. *Altern. Lab. Anim.* 44, 557–568. doi: 10.1177/026119291604400608

Kuehn, S., Hurst, J., Rensinghoff, F., Tsai, T., Grauthoff, S., Satgunarajah, Y., et al. (2017). Degenerative effects of cobalt-chloride treatment on neurons and microglia in a porcine retina organ culture model. *Exp. Eye Res.* 155, 107–120. doi: 10.1016/j.exer.2017.01.003

MacLeod, R. A., Dirks, W. G., Matsuo, Y., Kaufmann, M., Milch, H., and Drexler, H. G. (1999). Widespread intraspecies cross-contamination of human tumor cell lines arising at source. *Int. J. Cancer* 83, 555–563. doi: 10.1002/(sici)1097-0215(19991112)83:4<555::aid-ijc19>3.0.co;2-2

Maggs, D., Miller, P. E., and Ofri, R. (2008). *Slatter's Fundamentals of Veterinary Ophthalmology*. Philadelphia, PA: Saunders Elsevier.

Mares, J. A., Voland, R. P., Sondel, S. A., Millen, A. E., Larowe, T., Moeller, S. M., et al. (2011). Healthy lifestyles related to subsequent prevalence of age-related macular degeneration. *Arch. Ophthalmol.* 129, 470–480. doi: 10.1001/archophthalmol.2010.314

Merle, B. M. J., Colijn, J. M., Cougnard-Gregoire, A., De Koning-Backus, A. P. M., Delyfer, M. N., Kiefte-De Jong, J. C., et al. (2019). mediterranean diet and incidence of advanced age-related macular degeneration: the EYE-RISK Consortium. *Ophthalmology* 126, 381–390.

Mullins, R. F., Russell, S. R., Anderson, D. H., and Hageman, G. S. (2000). Drusen associated with aging and age-related macular degeneration contain proteins common to extracellular deposits associated with atherosclerosis, elastosis, amyloidosis, and dense deposit disease. *FASEB J.* 14, 835–846. doi: 10.1096/fasebj.14.7.835

Murali, A., Ramlogan-Steel, C. A., Andrzejewski, S., Steel, J. C., and Layton, C. J. (2019). Retinal explant culture: a platform to investigate human neuro-retina. *Clin. Exp. Ophthalmol.* 47, 274–285. doi: 10.1111/ceo.13434

Mustafi, D., Engel, A. H., and Palczewski, K. (2009). Structure of cone photoreceptors. *Prog. Retin. Eye Res.* 28, 289–302.

Nicoli, S., Ferrari, G., Quarta, M., Macaluso, C., Govoni, P., Dallatana, D., et al. (2009). Porcine sclera as a model of human sclera for in vitro transport experiments: histology. SEM, and comparative permeability. *Mol. Vis.* 15, 259–266.

Nowak, J. Z. (2006). Age-related macular degeneration (AMD): pathogenesis and therapy. *Pharmacol. Rep.* 58, 353–363.

Ogilvie, J. M., Speck, J. D., and Lett, J. M. (2000). Growth factors in combination, but not individually, rescue rd mouse photoreceptors in organ culture. *Exp. Neurol.* 161, 676–685. doi: 10.1006/exnr.1999.7291

Park, S. W., Im, S., Jun, H. O., Lee, K., Park, Y. J., Kim, J. H., et al. (2017). Dry age-related macular degeneration like pathology in aged 5XFAD mice: ultrastructure and microarray analysis. *Oncotarget* 8, 40006–40018. doi: 10.18632/oncotarget.16967

Pilgrim, M. G., Lengyel, I., Lanzirotti, A., Newville, M., Fearn, S., Emri, E., et al. (2017). Subretinal pigment epithelial deposition of drusen components including hydroxyapatite in a primary cell culture model. *Invest. Ophthalmol. Vis. Sci.* 58, 708–719. doi: 10.1167/iovs.16-21060

Reinehr, S., Reinhard, J., Gandej, M., Kuehn, S., Noristani, R., Faissner, A., et al. (2016). Simultaneous complement response via lectin pathway in retina and optic nerve in an experimental autoimmune glaucoma model. *Front. Cell Neurosci.* 10:140. doi: 10.3389/fncel.2016.00140

Romano, C., and Hicks, D. (2007). Adult retinal neuronal cell culture. *Prog. Retin. Eye Res.* 26, 379–397. doi: 10.1016/j.preteyeres.2007.03.001

Schnichels, S., Dorfi, T., Schultheiss, M., Arango-Gonzalez, B., Bartz-Schmidt, K. U., Januschowski, K., et al. (2016). Ex-vivo-examination of ultrastructural changes in organotypic retina culture using near-infrared imaging and optical coherence tomography. *Exp. Eye Res.* 147, 31–36. doi: 10.1016/j.exer.2016.04.011

Schnichels, S., Kiebler, T., Hurst, J., Maliha, A. M., Loscher, M., Dick, H. B., et al. (2019). Retinal organ cultures as alternative research models. *Altern. Lab Anim.* 47, 19–29. doi: 10.1177/0261192919840092

Schnichels, S., Paquet-Durand, F., Loscher, M., Tsai, T., Hurst, J., Joachim, S. C., et al. (2020). Retina in a dish: cell cultures, retinal explants and animal models for common diseases of the retina. *Prog. Retin. Eye Res.* 2020:100880. doi: 10.1016/j.preteyeres.2020.100880

Scott, A. W., Bressler, N. M., Ffolkes, S., Wittenborn, J. S., and Jorkasky, J. (2016). Public Attitudes About Eye and Vision Health. *JAMA Ophthalmol* 134, 1111–1118. doi: 10.1001/jamaophthalmol.2016.2627

Shah, R. S., Soetikno, B. T., Lajko, M., and Fawzi, A. A. (2015). A Mouse Model for Laser-induced Choroidal Neovascularization. *J. Vis. Exp.* 106: e53502.

Soto, I., Oglesby, E., Buckingham, B. P., Son, J. L., Roberson, E. D., Steele, M. R., et al. (2008). Retinal ganglion cells downregulate gene expression and lose their axons within the optic nerve head in a mouse glaucoma model. *J. Neurosci.* 28, 548–561. doi: 10.1523/jneurosci.3714-07.2008

Tansley, K. (1933). The formation of rosettes in the rat retina. *Br. J. Ophthalmol.* 17, 321–336. doi: 10.1136/bjo.17.6.321

Taylor, L., Arner, K., Engelsberg, K., and Ghosh, F. (2013a). Effects of glial cell line-derived neurotrophic factor on the cultured adult full-thickness porcine retina. *Curr. Eye Res.* 38, 503–515. doi: 10.3109/02713683.2013.763989

Taylor, L., Moran, D., Arner, K., Warrant, E., and Ghosh, F. (2013b). Stretch to see: lateral tension strongly determines cell survival in long-term cultures of adult porcine retina. *Invest. Ophthalmol. Vis. Sci.* 54, 1845–1856. doi: 10.1167/iovs.12-11420

Tode, J., Richert, E., Koinzer, S., Klettner, A., Von Der Burchard, C., Brinkmann, R., et al. (2018). Thermal stimulation of the retina reduces bruch's membrane

thickness in age related macular degeneration mouse models. *Transl. Vis. Sci. Technol.* 7:2. doi: 10.1167/tvst.7.3.2

Wang, J., Kolomeyer, A. M., Zarbin, M. A., and Townes-Anderson, E. (2011). Organotypic culture of full-thickness adult porcine retina. *J. Vis. Exp.* 49:2655.

Wang, J., Wang, Y., Wang, H., Hao, X., Wu, Y., and Guo, J. (2014). Selection of reference genes for gene expression studies in porcine whole blood and peripheral blood mononuclear cells under polyinosinic:polycytidylic acid stimulation. *Asian Austr. J. Anim. Sci.* 27, 471–478. doi: 10.5713/ajas.2013.13471

Wilson, M., and Vaney, D. I. (2010). *Amacrine Cells. In The Senses: A Comprehensive Reference*. Amsterdam: Elsevier Inc.

Wong, W. L., Su, X., Li, X., Cheung, C. M., Klein, R., Cheng, C. Y., et al. (2014). Global prevalence of age-related macular degeneration and disease burden projection for 2020 and 2040: a systematic review and meta-analysis. *Lancet Glob Health* 2, e106–e116.

Yehoshua, Z., Rosenfeld, P. J., Gregori, G., and Penha, F. (2010). Spectral domain optical coherence tomography imaging of dry age-related macular degeneration. *Ophthalmic Surg. Lasers Imaging* 41(Suppl.), S6–S14.

Conflict of Interest: The authors declare that the research was conducted in the absence of any commercial or financial relationships that could be construed as a potential conflict of interest.

Copyright © 2020 Wagner, Reinehr, Gammel, Greulich, Hurst, Dick, Schnichels and Joachim. This is an open-access article distributed under the terms of the Creative Commons Attribution License (CC BY). The use, distribution or reproduction in other forums is permitted, provided the original author(s) and the copyright owner(s) are credited and that the original publication in this journal is cited, in accordance with accepted academic practice. No use, distribution or reproduction is permitted which does not comply with these terms.

frontiers in Neuroscience

ORIGINAL RESEARCH
published: 03 November 2020
doi: 10.3389/fnins.2020.581579

Photoreceptor Degeneration in Pro23His Transgenic Rats (Line 3) Involves Autophagic and Necroptotic Mechanisms

Kiana Kakavand[1], Andrew I. Jobling[1], Ursula Greferath[1], Kirstan A. Vessey[1], Robb U. de Iongh[2†] and Erica L. Fletcher[1†]*

[1] Visual Neuroscience Laboratory, Department of Anatomy and Neuroscience, The University of Melbourne, Parkville, VIC, Australia, [2] Ocular Development Laboratory, Department Anatomy and Neuroscience, The University of Melbourne, Parkville, VIC, Australia

Photoreceptor death contributes to 50% of irreversible vision loss in the western world. Pro23His (P23H) transgenic albino rat strains are widely used models for the most common rhodopsin gene mutation associated with the autosomal dominant form of retinitis pigmentosa. However, the mechanism(s) by which photoreceptor death occurs are not well understood and were the principal aim of this study. We first used electroretinogram recording and optical coherence tomography to confirm the time course of functional and structural loss. Electroretinogram analyses revealed significantly decreased rod photoreceptor (a-wave), bipolar cell (b-wave) and amacrine cell responses (oscillatory potentials) from P30 onward. The cone-mediated b-wave was also decreased from P30. TUNEL analysis showed extensive cell death at P18, with continued labeling detected until P30. Focused gene expression arrays indicated activation of, apoptosis, autophagy and necroptosis in whole retina from P14-18. However, analysis of mitochondrial permeability changes ($\Delta\Psi$m) using JC-1 dye, combined with immunofluorescence markers for caspase-dependent (cleaved caspase-3) and caspase-independent (AIF) cell death pathways, indicated mitochondrial-mediated cell death was not a major contributor to photoreceptor death. By contrast, reverse-phase protein array data combined with RIPK3 and phospho-MLKL immunofluorescence indicated widespread necroptosis as the predominant mechanism of photoreceptor death. These findings highlight the complexity of mechanisms involved in photoreceptor death in the Pro23His rat model of degeneration and suggest therapies that target necroptosis should be considered for their potential to reduce photoreceptor death.

Keywords: apoptosis, autophagy, cell death, necroptosis, retinitis pigmentosa photoreceptor

OPEN ACCESS

Edited by:
Nicolás Cuenca, University of Alicante, Spain

Reviewed by:
Victoria Maneu, University of Alicante, Spain
Demetrios G. Vavvas, Harvard Medical School, United States

***Correspondence:**
Robb U. de Iongh
r.deiongh@unimelb.edu.au

†These authors share first authorship

Specialty section:
This article was submitted to Neurodegeneration, a section of the journal Frontiers in Neuroscience

Received: *09 July 2020*
Accepted: *02 October 2020*
Published: *03 November 2020*

Citation:
Kakavand K, Jobling AI, Greferath U, Vessey KA, de Iongh RU and Fletcher EL (2020) Photoreceptor Degeneration in Pro23His Transgenic Rats (Line 3) Involves Autophagic and Necroptotic Mechanisms. Front. Neurosci. 14:581579. doi: 10.3389/fnins.2020.581579

INTRODUCTION

Photoreceptor death causes approximately 50% of all cases of irreversible vision loss in the western world (Taylor et al., 2005). Retinitis pigmentosa (RP) is the most common form of inherited retinopathy, characterized by progressive loss of photoreceptors (rods and cones), which leads to severe visual impairment (Guadagni et al., 2015; Bravo-Gil et al., 2017). While approximately

96 different mutated genes have been identified in patients with RP (RetNet; November 2019)[1], mutations in rhodopsin (*RHO*) are the most common causes of RP, accounting for approximately 15% of all inherited human retinal degenerations (Chapple et al., 2001) and 30–40% of patients with the autosomal dominant form of the disease (Ferrari et al., 2011). More than 150 different mutations have been identified in *RHO*, but the most frequent is a single-base C-to-A transversion, resulting in substitution of proline for histidine in codon 23 (P23H), causing autosomal dominant RP (Dryja et al., 1990; Athanasiou et al., 2018). P23H-RHO is thought to cause improper folding at the N-terminal, the binding site of 11-*cis*-retinal, resulting in the formation of dysfunctional, oligomeric aggregates within the endoplasmic reticulum (ER) and Golgi (Chapple et al., 2001). Although not entirely clear, it is likely that the resultant recruitment of ER-resident chaperones and activation of ubiquitin/proteasome system (Chapple et al., 2001) becomes overwhelmed resulting in ER stress and activation of the unfolded protein response (UPR), which in turn leads to photoreceptor death (Chiang et al., 2012, 2015, 2016; Athanasiou et al., 2017). However, the precise mechanisms that lead to photoreceptor loss are not well understood.

Rat models carrying a transgene expressing the mouse rhodopsin gene (*Rho*) with a C-A substitution at codon 23 (P23H amino acid conversion) were first described in Steinberg et al. (1996). Three different lines have been developed and while many studies have focused predominantly on line 1 (Cuenca et al., 2004, 2014; Pennesi et al., 2008; Garcia-Ayuso et al., 2013; Orhan et al., 2015), various studies have shown that line 3 (P23H-3) shows an intermediate rate of degeneration compared to lines 1 (which is more rapid) and 2 (slow). While transgene expression begins at P5, morphological change is not detectable until after P30, with the ONL decreasing in thickness to ∼85% of wild-type by P30, 50% by P120-P200 and ∼40% by P260 (Lewin et al., 1998; Machida et al., 2000; Pennesi et al., 2008). This progressive decline is matched by similar declines in retinal function with the rod a-wave showing a decline of 74% between 4 and 29 weeks (Machida et al., 2000; LaVail et al., 2018), though the effects of the mutation on retinal function appear to be affected by pigmentation and also copy number of the transgene (Cuenca et al., 2014).

The mechanism(s) of photoreceptor death in the P23H-3 rat are not well understood and many pathways have been implicated including oxidative stress, inflammation, ER stress, caspase-dependent and/or–independent pathways of apoptosis, necroptosis and autophagy. Autophagy is an important pathway for turning over the organelles within a cell and is known to be a critical factor in photoreceptor homeostasis. Indeed, inhibition of autophagy is known to reduce photoreceptor loss in the P23H-3 mouse model of retinal degeneration (Yao et al., 2018). Necrosis, which is characterized by swelling of the cytoplasm and organelles, followed by cell membrane disruption and release of the cytosolic constituents into the surrounding extracellular space, is associated with inflammation. In some circumstances, the inflammatory cytokines release from cells mediates a form of "programmed" necrosis called necroptosis (Shan et al., 2018).

In this study, we describe in detail the early time course and cell death mechanisms that result in photoreceptor dysfunction and loss in P23H-3 rats aged from postnatal (P) days P18 to P90 (3 months). Twin-flash ERG showed evidence of rod and cone photoreceptor dysfunction from P30, whereas structural decreases in the ONL [optical coherence tomography (OCT) and histology] were not evident until P60, with changes more pronounced in central and mid-peripheral retina. The first evidence of cell death occurred at P18, with large numbers of TUNEL$^+$ cells detected in the ONL. However, analysis of mitochondrial permeability, caspase cleavage and apoptosis-inducing factor (AIF) localization suggest that neither caspase-dependent, nor independent apoptotic pathways are major contributors to photoreceptor cell death in the P23H-3 rat model. Expression profiling of the retina combined with protein analyses suggest that multiple pathways including apoptosis, autophagy and necroptosis are modulated in the P23H-3 retina, but that necroptosis is the over-riding mechanism by which photoreceptors die, consistent with another recent study (Viringipurampeer et al., 2019).

MATERIALS AND METHODS

Animals

All animal procedures were approved by the Animal Ethics Committees of the University of Melbourne (AEC# 1312958 and #1614030) and were carried out in accordance with the Association for Research in Vision and Ophthalmology (ARVO) statement for the Use of Animals in Ophthalmic and Vision Research. Initial breeding stock of P23H-3 transgenic rats (Steinberg et al., 1996) on the Sprague–Dawley (SD) background, were provided by A/Prof. Krisztina Valter-Kocsi (Australian National University). SD albino rats were obtained from Animal Resource Center (ARC) (Murdoch, WA, Australia). Homozygous male P23H-3 transgenic rats were mated with wild-type SD female rats to generate hemizygous P23H-3 rats for study. Both male and female rats were used. All rats were bred and housed at The University of Melbourne Medical Animal Facility (Parkville, VIC, Australia) on a 12-h light/dark cycle (luminance levels inside cages ranged from 13 to 58 Lux). Food and water were available *ad libitum*.

Retinal Function Using Electroretinography

We used the electroretinogram to measure retinal function of wild-type and P23H-3 rats ($n \geq 10$) at P18, P30, P60, and P90, as described previously (Jobling et al., 2013; Vessey et al., 2015; Von Eisenhart-Rothe et al., 2018). There are a number of different ways of using the electroretinogram to measure rod and cone mediated responses (Kremers and Tanimoto, 2018). We used a paired flash paradigm to assess rod and cone mediated responses; the first light stimulus elicits a mixed rod and cone mediated waveform, whereas the second light

[1]https://sph.uth.edu/retnet/

stimulus elicits a cone-only response. Briefly, dark-adapted (12 h) rats were anesthetized by intraperitoneal (IP) injection of ketamine (60 mg/kg, Provet, Melbourne, VIC, Australia) and xylazine (5 mg/kg, Provet) and 0.5% proparacaine hydrochloride (Alcaine; Alcon Laboratories, French's Forest, NSW, Australia) eye drops. The pupil was dilated using 1% Atropine sulfate (Alcon Laboratories) and 2.5% phenylephrine hydrochloride (Bausch & Lomb, Chatswood, NSW, Australia). The reference electrode was placed in the mouth and the recording electrode (Ag/AgCl) on the cornea. Twin 2.1 log cd.s/m^2 full-field flashes with 0.8-s inter-stimulus interval (ISI), from a Nikon SB900 camera flash (Nikon, Lidcombe, NSW, Australia), were used to evaluate the contribution of rod and cone photoreceptors in the ERG response (Lyubarsky and Pugh, 1996; Phipps et al., 2004). Responses were amplified (gain × 5,000; −3 dB at 1 Hz and 1 kHz) using a ML132 BioAmp amplifier (ADInstruments, Castle Hill, NSW, Australia) and digitized at 10 kHz over a 250-ms period (ML785 Powerlab/8sp amplifier; ADInstruments). The stimulus and recording of the ERG were coordinated by Scope software version 3.6.10 (ADInstruments). To isolate rod responses, the cone responses were subtracted from the initial mixed responses (Phipps et al., 2004; Weymouth and Vingrys, 2008; Jobling et al., 2013; Vessey et al., 2015). ERG component analysis was completed using previously published equations and techniques (Hood and Birch, 1996; Weymouth and Vingrys, 2008). The rod a-wave photoreceptor responses (rod a-wave) were isolated and analyzed using a modified PIII model, to derive the PIII amplitude (PIII Rmax in μV) and sensitivity ($m^2cd^{-1}s^{-3}$). The rod and cone post-photoreceptoral function (b-wave) was isolated and then fitted using an inverted γ function to generate the PII. From the PII fit, the amplitude of the PII response (PII amplitude in μV) and the time to peak (ms) were derived. For oscillatory potentials (OPs), summed amplitudes of OP 2, 3, and 4 were used. OP1 and OP5 of the rod OPs were excluded as they are often small and cannot be distinguished from system noise. For each animal, three individual measurements were represented as an average.

Measurement of Retinal Structure Using Optical Coherence Tomography

After completion of ERG recording, OCT and fundus images were captured on a Micron III rodent fundus camera using Micron III software (Phoenix Technology Group, Pleasanton, CA, United States) as described previously (Von Eisenhart-Rothe et al., 2018).

RNA Extraction and Quantitative Real-Time PCR

Rats, anesthetized by ketamine and xylazine (as above), were euthanized by intracardial injection of pentobarbitone (Lethabarb, Virbac Pty., Ltd., Milperra, NSW, Australia). Eyes were enucleated, anterior segments removed, and posterior eyecups from P14 and P18, P23H-3 and SD rats (n = 9 per group) were dissected in ice-cold M199 culture medium (Sigma-Aldrich) to separate retinae from RPE/choroid/sclera. Retinae were snap frozen in liquid nitrogen and total RNA was extracted using the RNeasy® Mini Kit (Qiagen, Chadstone, VIC, Australia) with on-column DNase-I digestion as per manufacturer's instructions. RNA quality and concentration were measured using an Agilent 2200 Tape Station (Agilent Technologies, Germany) and only samples with RIN >8 were used.

The rat cell death pathway finder RT^2 profiler PCR array (Cat#: PARN-212Z, Qiagen, Melbourne, VIC, Australia) was used to profile expression of 84 genes involved in programmed cell death pathways. Three pooled RNA samples (n = 3 retinae/sample) from P23H-3 and SD rats at each age (P14, P18) were assayed. Total RNA (400 ng) from each sample was reverse transcribed using the RT^2 First Strand cDNA Kit (Qiagen, Melbourne, VIC, Australia) according to manufacturer's instructions. Negative controls for genomic DNA contamination, lacking RT enzyme were included. The cDNA samples were mixed with RT^2 SYBR Green Master mix (Qiagen, Melbourne, VIC, Australia) and amplified in 384-well plates containing four replicates of 96 assays (84 different genes of interest, five control genes, one gDNA control, three RT controls and three positive PCR controls), using the Applied Biosystems ViiA 7 Real-Time PCR System at 95°C for 15 min, followed by 95°C for 15 s and 60°C for 1 min (40 cycles).

The quantitative PCR data were analyzed by the ΔΔCt method, using a commercial Excel template (Qiagen) with normalization to the average of five housekeeping genes and fold-change calculated as $2^{-\Delta\Delta Ct}$. While the pathways represented on the PCR array were known, we used the Ingenuity Pathway Analysis software (Qiagen) to predict whether these pathways were activated or inhibited using the Molecule Activity Predictor function.

Reverse-Phase Protein Arrays (RPPA)

Sprague–Dawley and P23H-3 retinae (n = 6/group), dissected in cold phosphate buffer saline (PBS) from eyes of P18 rats, were homogenized in 60 μl of CLB1 lysis buffer (Zeptosens, Bayer; 7M Urea, 2M thiourea, 4% CHAPS, 1% dithiothreitol, 4 mM spermidine, 2% Pharmalyte® with protease inhibitors added), samples were centrifuged at 7500 × g for 10 min in a benchtop centrifuge and the supernatant was transferred to a fresh tube for analysis by reverse phase protein arrays (RPPA) at the ACRF Translational RPPA platform at Peter MacCallum Cancer Centre (Parkville, VIC, Australia). After quantification of protein concentration by Bradford assay (Bio-Rad), samples were diluted serially using a Caliper ALH3000 liquid handling robot (Perkin Elmer), and spotted onto ZeptoChips (Zeptosens, Bayer, Witerswil, Switzerland) in duplicate using a Nano-Plotter-NP2.1 non-contact arrayer (GeSim, Radeberg, Germany). After incubating with pre-validated primary antibodies (1:500; See **Supplementary Table S2**) for 20 h, chips were washed and incubated with Alexa Fluor®-647 conjugated anti-rabbit IgG (#Z-25308; 1:1000; Thermo Fisher Scientific, Scoresby, VIC, Australia) for 4 h. Zeptosens instrument and software (version 3.1) were used to scan and calculate the relative fluorescence

intensities. All data were normalized to the background values obtained with secondary antibody only.

Immunofluorescence and TUNEL

Fresh eyecups from P14, P18, P30, and P60 P23H-3 and SD rats were isolated and dissected, as described above, to remove the anterior segments, prior to being fixed in different fixatives specific for immunofluorescence and TUNEL assays (**Supplementary Table S3**). Tissues were either fixed at room temperature in 4% paraformaldehyde in 0.1M phosphate buffer (PB; pH 7.4) for 30 min for frozen sections or in Davidson's fixative (8% paraformaldehyde, 31.5% ethanol, 2M acetic acid) for 4 h for paraffin embedding. In some cases, the eyecups were incubated for 30 min at RT in 10 nM MitoTracker Orange CMTMRos (M7510; Thermo Fisher Scientific) to label mitochondria, prior to paraformaldehyde fixation and freezing. For frozen sections, paraformaldehyde-fixed eyecups were cryoprotected in a series of graded concentrations of sucrose (10, 20, 30% in PB), embedded in Tissue-Tek O.C.T compound (Sakura Seiki, Tokyo, Japan) and frozen in isopentane cooled by liquid nitrogen as described previously (Von Eisenhart-Rothe et al., 2018). Mid-sagittal frozen sections (12 μm) were collected on poly-L-lysine coated glass slides (Polysine® Adhesion slides, Thermo Fisher Scientific) and kept at −20°C. Paraffin embedded, Davidson-fixed tissues were sectioned at 5 μm and mounted on poly-L-lysine coated glass slides.

Optimal immunofluorescence staining protocols varied, depending upon the antibody used (see **Supplementary Table S3** for details of fixation, antigen retrieval and antibody dilutions). After incubation of sections overnight at 4°C with primary antibodies in blocking solution (PB, supplemented with 3% normal goat serum, 1% w/v bovine serum albumin (BSA), 0.05% w/v sodium azide, 0.5% v/v Triton-X), reactivity was detected by incubation with the appropriate species Alexa Fluor 488/594-conjugated antibodies (1:500 Invitrogen) in phosphate buffer containing 1 μg/ml 4′,6-diamidino-2-phenylindole (DAPI) (Thermo Fisher Scientific) to label cell nuclei. Following washes in PB, sections were cover-slipped with fluorescence mounting medium (Dako) and imaged by confocal microscopy (Zeiss LSM510 Meta, Carl Zeiss, North Ryde, NSW, Australia).

To label dying cells, TUNEL assay (DeadEnd™ Fluorometric TUNEL System; Promega Corp., Alexandria, NSW, Australia) was performed on fixed-frozen sections as per manufacturer's instructions. Briefly, sections were washed in PBS, immersed in 0.2% Triton-X in PBS for 20 min and incubated in equilibration buffer (Promega, Alexandria, NSW, Australia) for 10 min prior to the rTdT reaction at 37°C for 1 h in the dark. Subsequently, sections were washed 15 min in 2× SSC and PBS (3 × 5 min) before a counter-stain with 1 μg/ml DAPI (Thermo Fisher Scientific) in PBS for 20 min. Sections were cover-slipped and imaged by confocal microscopy as described above.

To quantify photoreceptor death, TUNEL$^+$ cells in the ONL were counted in three mid-sagittal eye sections per animal (n > 5/group). Each half retina (from optic nerve to periphery) was divided into three segments (central, mid-peripheral and peripheral regions) and using ImageJ software the number of TUNEL$^+$ was expressed per millimeter of retinal length. Similarly, the mean thicknesses of the ONL, INL, and GCL were measured in each segment using Image J.

To label cone photoreceptors, frozen sections were incubated with FITC-conjugated peanut agglutinin (PNA) used at 1:500 (Vector Laboratories, Burlingame, CA, United States) in PBS. The number of PNA$^+$ cells were quantified across the whole retina.

Mitochondrial Permeability Assay

To analyze mitochondrial membrane potential changes ($\Delta\Psi m$) in the P23H-3 retina, the MitoProbe™ JC-1 Assay Kit (Thermo Fisher Scientific) was performed according to the manufacture's instruction with minor modifications. Briefly, retinae from P23H-3 and SD rats at P14 and P18 (n = 6 per group) were isolated as above, cut into small pieces using a scalpel and dissociated into single cells using the Papain Dissociation System (Worthington Biochemical Corporation, Lakewood, NJ, United States). Cells obtained from each sample were counted on a Countess™ automated cell counter (Thermo Fisher Scientific) and 1×10^6 cells from each sample were suspended in 1 mL warm PBS, containing 0.5 μM JC-1 dye and incubated 30 min at 37°C with 5% CO_2. A positive control sample was incubated with a mitochondrial depolarizing agent (0.5 mM CCCP) prior to JC-1 staining. After washing in warm PBS, cells were centrifuged at 300 × g for 5 min and resuspended in 200 μL PBS. Prior to analysis on a flow cytometer (BD FACS Aria III Cell Sorter), cells were stained with DAPI as an indicator of cell viability. Initial gating by forward-scatter (FSC) versus side-scatter (SSC) distinguished three distinct subpopulations: small dead cells, small live cells, and large live cells (**Supplementary Figure S3**), before analysis with 488 nm excitation and emission filters Alexa Fluor 488 dye (530 nm) and R-phycoerythrin (695 nm). Data were analyzed using FlowJo (V.10.4.2) software.

Based on previous studies, isolated photoreceptors are characteristically smaller than other retinal cells due to being terminally differentiated (Akimoto et al., 2006). To determine which populations of cells in our flow cytometry analysis were enriched for photoreceptors, we prepared single cell suspensions of retinal cells isolated from P16 P23H-3 rats (n = 2), stained with DAPI and separated as described above. RNA was extracted from isolated cell populations using the RNeasy Micro Kit (Qiagen, Hilden, Germany) and purity confirmed on an Agilent Tape Station as described above. cDNA library preparation and pre-amplification was performed using the Smart-seq2 protocol (Picelli et al., 2014) with 9 cycles of pre-amplification. Quantitative PCR analysis was performed using a Rotor gene 3000 PCR cycler (Qiagen, Hilden, Germany) using specific primers for rat *Rho* (Forward 3′-AGCAACAGGAGTCGGCTACC-5′; Reverse 3′-CCGAAGTTGGAGCCCTGGTG-5′), *Opn1mw*, (Fw 3′-GTCCAGACGTGTTCAGCG; Rev 3′-GACCATCACCACCACCAT-5′) *Opn1sw* (Fw 3′-CAGCCTTCATGGGATTTG; Rev 3′-GTGCGTGCTTGGAGTTGA) and *Hprt* (Fw 3′-CCTAAAAGACAGCGGCAAGTTGAA; Rev 3′-CCACAGGACTAGAACGTCTGCTAG). Relative expression was calculated using the $2^{-\Delta\Delta Ct}$ method.

Statistical Analysis

Analysis and curve fitting of the ERG data was carried out in Excel (Microsoft, Redmond, WA, United States). Statistical analysis and graphing were performed using Graph Pad Prism 7 (San Diego, CA, United States). All data are expressed as mean ± standard error of the mean (SEM). Two-way analyses of variance (ANOVA) were used to determine statistical difference among experimental groups where the two independent variables were genotype and age, followed by Tukey's *post hoc* tests for further pair-wise comparisons. Comparisons of fluorescence ratios from P23H-3 and SD flow-sorted cells were conducted using two-tailed, unpaired *t*-tests. *p*-values less than 0.05 were considered statistically significant and represented as $^{*}p < 0.05$, $^{**}p < 0.01$, $^{***}p < 0.001$, and $^{****}p < 0.0001$ in all graphs.

RESULTS

Structural and Functional Changes in the Retina Occur in the P23H-3 Rat From an Early Age

The central aim of this study was to examine the mechanisms by which photoreceptor death develops in the P23H-3 model of retinal degeneration. We first evaluated retinal function and structure using electroretinogram (ERG) recording and OCT. Fundus imaging showed no overt alterations in the retina or presence of distinct pathological features at P18, P30, P60 (**Figures 1A,B**) or P90. By contrast, OCT imaging (**Figures 1C,D**) clearly revealed reductions in total retinal thickness at P18, P60, and P90 (**Figure 1E**). Quantification of total retinal thickness showed a reduction at P18 (**Figure 1E**) that was attributed to significant thinning of the IPL and GCL (**Figures 1G,H**) but not the ONL (**Figure 1F**). In contrast, a redution in total retinal thickness at P60 and P90 was associated with a significant decreases in ONL thickness at these ages (**Figure 1F**).

Twin flash ERG was used to assess rod- and cone-mediated function in P23H-3 and SD rats from P18. Representative rod-mediated waveforms for the SD and P23H-3 rats are shown in **Figures 2A–D**. No apparent difference in response was observed at P18, whereas at P30, P60, and P90, the amplitudes of the responses in P23H-3 rats were reduced compared to age-matched SD rats. Quantification of rod a-wave amplitudes showed a developmental increase in the rod responses from P18 to P30 in SD control which was not evident in P23H-3 rats (**Figure 2E**). The developmental increase in photoreceptor response has been reported to coincide with the post-natal elongation of the outer segments after eye opening (Fulton et al., 1995). While both strains showed a progressive a-wave decrease with age ($p < 0.0001$), the photoreceptor responses in the P23H-3 retina were significantly reduced ($p < 0.0001$) compared to SD responses from P30 onward (**Figure 2E**).

The rod b-wave responses, representing rod bipolar cell activity, were significantly reduced ($p < 0.0001$) in P23H-3 compared to SD from P30 onward and both P23H-3 and SD b-waves exhibited an age-related decline in amplitude from P30 (**Figure 2F**). A similar pattern was observed in the summed OP amplitude (**Figure 2G**), a waveform that is thought to reflect amacrine cell function. Unlike the rod photoreceptor amplitudes, rod implicit times remained unaffected at all ages (**Supplementary Figure S1B**) while rod sensitivity was only significantly different at P18 (**Supplementary Figure S1A**). As the ERG response is serial in nature, it is possible that the inner retinal changes (b-wave and OP) reflect altered photoreceptoral response. To explore this, we compared the percentage changes in rod (a-wave) with change in rod post-photoreceptor (b-wave, and summed OP) responses (**Figure 2H**). Overall, the changes in rod a-wave and rod b-wave at P30 and P60 were similar, suggesting that loss of photoreceptor function is the predominant functional change occurring within the retina. However, at these ages the OP responses were reduced to a greater extent, suggesting that in the P23H-3 rat there is photoreceptoral loss, as well as inner retinal changes affecting amacrine cell function. Together, these data show that retinal dysfunction occurs from P30 in the P23H-3 rat, with a specific photoreceptor and amacrine deficit evident.

While cone photoreceptor function cannot be measured directly in rats, the cone-mediated post-photoreceptoral response (cone b-wave) indicated smaller cone ERG responses in P23H-3 from P30 compared to age-matched controls (**Figures 3A–D**). Quantification showed a developmental increase in cone responses from P18 to P30 in both SD and P23H-3 rats (**Figure 3E**). However, there were significant reductions in P23H-3 cone responses when compared to SD retinae at P30 and P60, but not at P90 (**Figure 3E**). The lack of difference at P90 may reflect the greater age-related decline in the SD cone response compared to P23H-3 and the difficulty in measuring the cone b-wave amplitudes. In contrast to the cone b-wave amplitudes, the cone b-wave implicit time (**Figure 3F**), OP amplitudes and timing remained unaffected in the P23H-3 retinae compared to the SD rats (**Figures 3G,H**). While these data show that cone photoreceptor responses are altered from P30 onward, counts of PNA^{+} cells at P30 showed no significant difference (**Supplementary Figure S2G**), suggesting changes are functional and not due to cell death.

Photoreceptor Degeneration Is Evident From P18 in P23H-3 Rats

TUNEL assays were used to identify the time-course of photoreceptor degeneration in P23H-3 rat retina. In contrast to SD retinae, abundant labeled cells were observed in the ONL of the P23H-3 retinae at P18 (**Figures 4A,B**). Quantification of $TUNEL^{+}$ cells showed that at P18 an average of ∼30 cells/mm were detected in the P23H-3 retina, which declined with age to approximately 8 cells/mm of retina at P30 and 1–2 cells/mm at P60 (**Figure 4C**). Similar to the OCT analyses (**Figures 1C–H**), measurement of ONL thickness in these sections showed progressive age-related decreases in ONL thickness from P18 to P60 in both SD and P23H-3 (**Figure 4E**) and at P60 the ONL was significantly thinner in P23H-3 than in SD rats. Further analyses across retinal eccentricity showed no significant differences in numbers of $TUNEL^{+}$ cells in control SD retinae across eccentricity at any age (**Figure 4D** and **Supplementary Figures S2A,B**). By contrast in P23H-3 rats,

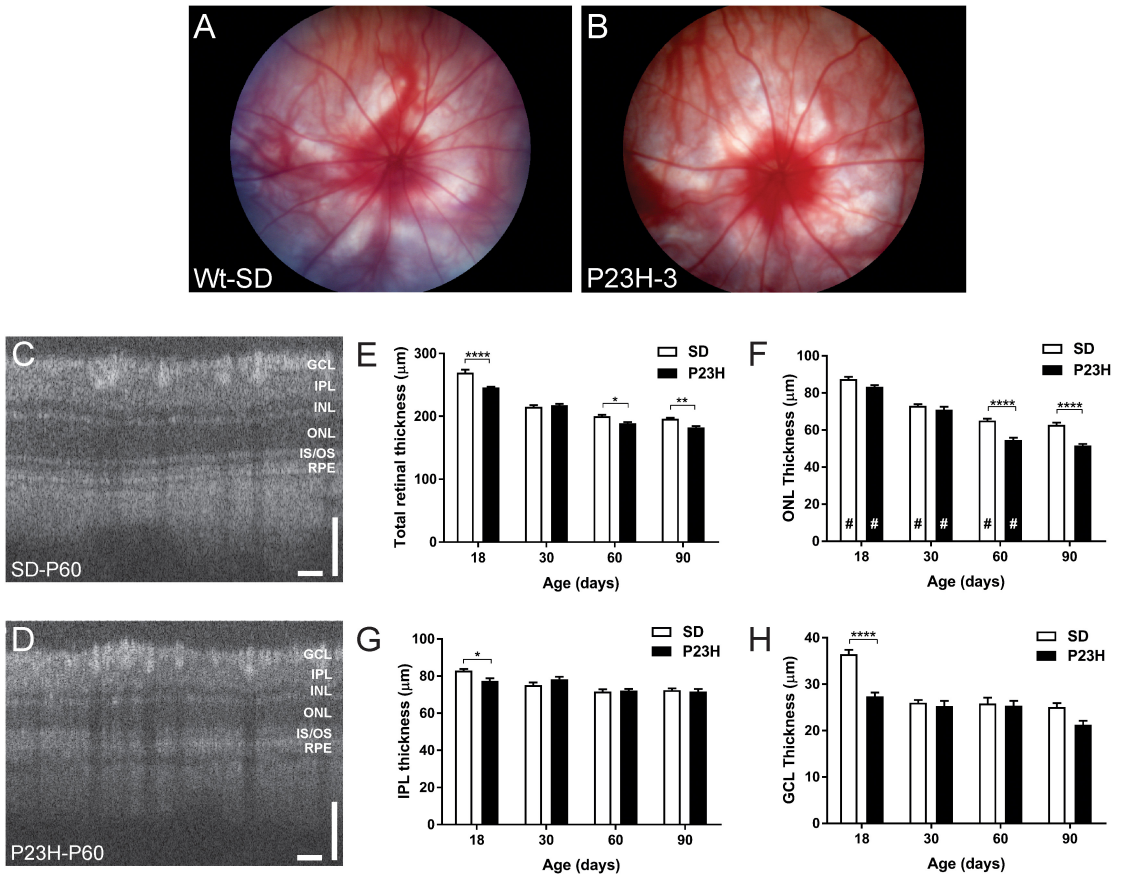

FIGURE 1 | Fundus and OCT imaging images of P23H-3 and SD rat retinae. Representative fundus images SD **(A)** and P23H-3 **(B)** rats at P60. No morphological differences were apparent in fundus scans of P23H-3 rats at any age, compared to age-matched SD rats. Representative OCT images of the central retina in SD **(C)** and P23H-3 **(D)** rats at P60. Segmentation analyses of OCT images showing mean thicknesses of total retina **(E)**, ONL **(F)**, IPL **(G)**, and GCL **(H)**. Total thicknesses of P23H-3 retinae were significantly thinner than SD at P18, P60, and P90 **(E)**. At P18 this was attributable to changes in the thickness of IPL **(G)** and GCL **(H)** but not the ONL **(F)**. Changes in the ONL were only detected at P60 and P90 **(F)**. All histograms indicate mean ± SEM, two-way ANOVA, Tukey's *post hoc* test, $^{*}p < 0.05$, $^{**}p < 0.001$, and $^{****}p < 0.0001$, $n \geq 8$ in each group. *: significant difference for genotype, #: significant difference for age. Abbreviations: ONL, outer nuclear layer; INL, inner nuclear layer; IPL, inner plexiform layer; GCL, ganglion cell layer. Scale bar **(C,D)** = 100 μm.

while there were no differences in TUNEL^{+} cells at P18 or P30 across eccentricity (**Supplementary Figures S2A,B**), at P60 mean number of TUNEL^{+} photoreceptor cells in the peripheral retina was significantly lower than in the central and mid-peripheral regions (**Figure 4D**). Consistent with this, there were significant reductions in ONL thickness in central and mid-peripheral, regions of the retina at P60, but not at P18 or P30 (**Figure 4F**). No significant differences in ONL thickness were detected in P18 or P30 retinae at any eccentricity (**Supplementary Figures S2C,D**). While there were significant age-related decreases in INL and GCL thickness with age, no differences were observed in INL or GCL thickness between WT and P23H3 retinae at P18, P30 or P60 (**Supplementary Figures S2E,F**).

Identification of Cell Death Pathways in the P23H-3 Rat

To investigate the mechanisms by which photoreceptors die in the P23H-3 retina, we analyzed gene expression changes in several cell death pathways using a commercial quantitative RT-PCR array system at P14 and P18. At P14, 13 of 84 genes on the PCR array showed significantly different levels of expression in P23H-3 compared to SD retinae (**Figure 5A** and **Supplementary Table S3**). The only down-regulated gene (−1.2 fold; $p = 0.047$) was the apoptotic effector, caspase-3. By contrast, three other genes implicated in the apoptotic pathways *Igf1r* (1.2 fold; $p = 0.007$), *Mcl1* (1.2 fold; $p = 0.044$), and *Tnfrsf11b* (1.7 fold; $p = 0.017$) were significantly up-regulated. Importantly, the master regulator of cell death, *Tp53* was also significantly up-regulated (1.4 fold; $p = 0.022$). The five genes that were broadly classified as being associated with necrosis (*Spata2*, *Mag*, *Hspbap1*, *Dpysl14*, and *Atp6v1g2*) were all up-regulated to similar levels (1.2 to 1.5-fold; $p < 0.05$). Similarly, three genes associated with autophagy (*App*, *Htt*, *Sqstm1*) were up-regulated (1.1 to 1.3-fold; $p < 0.05$).

At P18, 25 of 84 genes on the array showed significantly different levels of expression in P23H-3 compared to SD retinae

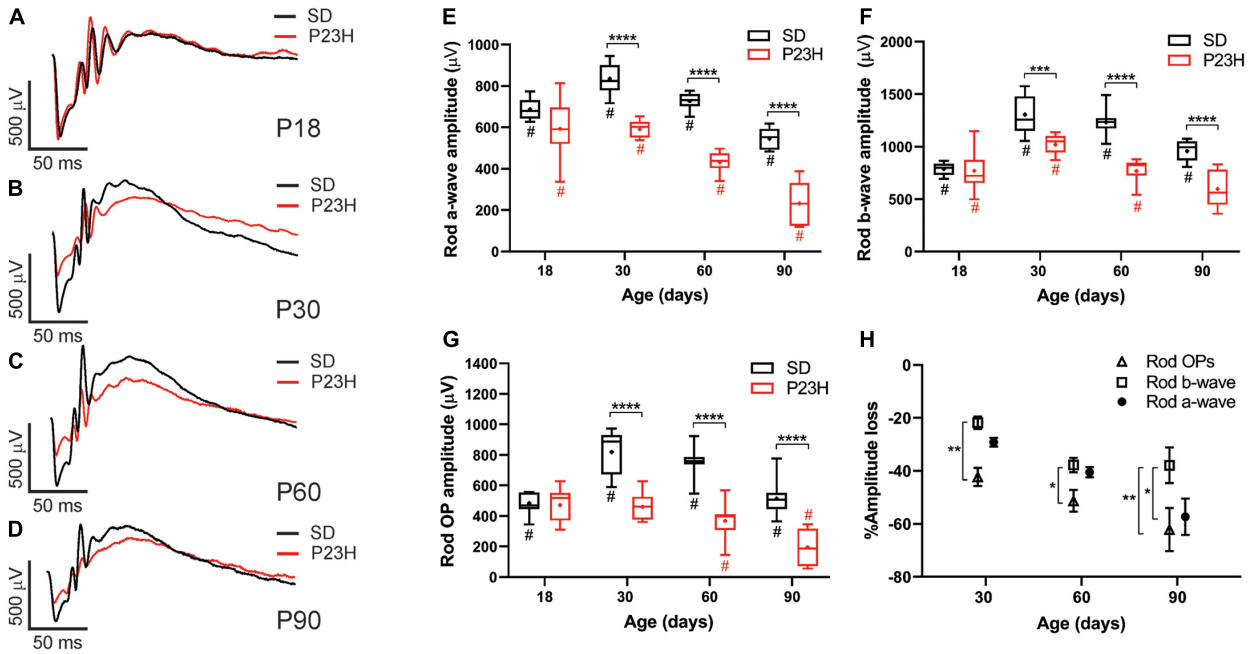

FIGURE 2 | Alterations in rod responses of P23H-3 rats with age. **(A–D)** Representative rod responses in SD and P23H-3 rats at P18 **(A)**, P30 **(B)**, P60 **(C)**, and P90 **(D)**. **(E–G)** Box and whisker plots of rod ERG responses showing change in rod a-wave amplitudes **(E)**, rod b-wave amplitudes **(F)**, and rod OP amplitudes **(G)**. Rod a-wave amplitudes were significantly reduced in the P23H-3 compared to the SD from P30 **(E)**. The rod b-wave amplitudes were significantly attenuated in the P23H-3 rats from P30 onward **(F)**. The rod a-wave (PIII) **(E)**, rod b-wave (PII) **(F)**, and summed rod OP **(G)** showed a progressive age-related reduction from P30 to P90 in both strains. All box and whisker plots show interquartile range (box), median (transverse line), mean (+) and 95% confidence intervals (error bars). **(H)** Relative percentage changes in rod a-wave, b-wave, and summed OP responses. At P30 and P60, the a-wave and b-wave responses were reduced in P23H-3 to a similar extent. However, the loss of summed OP amplitudes was significantly increased compared to those of b-wave. At P90, the extent of the b-wave loss was significantly less than a-wave and summed OP. Data were analyzed by two-way ANOVA with Tukey's *post hoc* test. $^{*}p < 0.05$, $^{**}p < 0.01$, $^{***}p < 0.001$, and $^{****}p < 0.0001$, $n \geq 8$ in each group. *, significant difference for genotype; #, significant difference for age.

(**Figure 5B** and **Supplementary Table S5**). Seven genes associated with the autophagy pathway (*Atg16l1*, *Atg3*, *Atg5*, *Becn1*, *Ctss*, *Mapk8*, *Sqstm1*) were significantly ($p < 0.05$) up-regulated at similarly low levels (1.2 to 1.5-fold). Of the twelve genes associated with the apoptotic pathway, six (*Fas*, *Bcl2a1*, *Bcl2l11*, *Birc3*, *Casp6*, *Tnfrsf10b*) were significantly down-regulated (−1.2 to −3.1-fold; $p < 0.05$) and seven (*Casp2*, *Casp9*, *Dffa*, *Gadd45a*, *Mcl1*, *Nol3*, *Xiap*) were significantly up-regulated (1.2 to 1.9-fold; $p < 0.05$). The largest expression changes were observed for two of the five differentially expressed necrosis genes (*Defb1*, *Galnt5*), which were significantly down-regulated −19.9 ($p = 0.001$) and −4.5-fold ($p = 0.033$), respectively. The other three necrosis-associated genes (*Dpysl4*, *Hspbap1*, *Tnfrsf4*) were significantly up-regulated 1.1 to 1.9-fold ($p < 0.05$).

The broad clustering of the dysregulated genes represented on the cell death array into the autophagy, apoptosis and necrosis cell death pathways, suggested that all three types of programmed cell death (**Figure 5**) are potentially modulated during P23H-mediated photoreceptor degeneration. To determine the activation states of the pathways, we conducted IPA analyses of this limited set of expression data using the Molecule Activity Predictor function in IPA. IPA predicted that the mitochondrial associated parts of the apoptotic pathway were inhibited at P14, but likely to be activated at P18 (**Supplementary Figure S4**). By contrast, the autophagy pathway appeared to be activated at both P14 and P18 (**Supplementary Figure S5**). While a canonical pathway for necrosis was not available in IPA, a network analyses incorporating key necroptosis genes, indicated that components of the necroptotic pathway, particularly RIPK1 and RIPK3 were predicted to become activated from P14 to P18 (**Supplementary Figure S6**).

To validate the mRNA analyses and to further discriminate which of these pathways were activated at P18, we conducted RPPA analyses on protein extracts from SD and P23H-3 retinae and immunofluorescence analyses on retinal sections at P18. Some genes showed significant changes at mRNA level (*Xiap*, *Mcl1*, *Bcl2l11*), which were not evident at the protein level due to these being below the threshold of detection (**Table 1**). Interestingly, while there appeared to be a significant increase in cleaved caspase-3, the levels were also below threshold for the antibody using this technique, suggesting that there was no large-scale induction of caspase-dependent apoptotic death pathways. While not all gene expression data could be validated by this technique, due to restricted antibody availability, the data indicated significantly reduced phosphorylation of AKT, which is an important regulator of apoptosis and autophagy (Heras-Sandoval et al., 2014), but also of necroptosis (Liu et al., 2014).

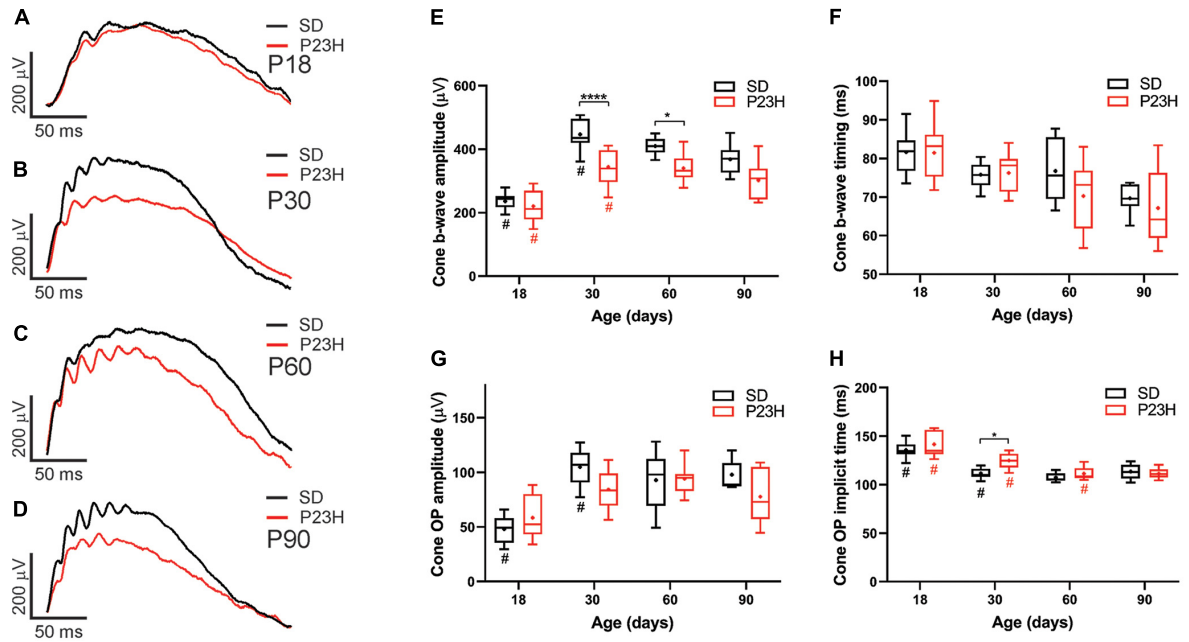

FIGURE 3 | Alterations in cone responses of P23H-3 rats with age. Representative modeled cone responses in SD and P23H-3 rats at P18 **(A)**, P30 **(B)**, P60 **(C)**, and P90 **(D)**. **(E–H)** Box and whisker plots of cone ERG responses in SD and P23H-3 rats showing change in cone b-wave amplitudes **(E)**, cone b-wave time-to peak **(F)**, cone OP amplitude amplitudes **(G)**, and cone OP implicit times **(H)**. Cone b-wave amplitudes were significantly lower in P23H-3 compared to age-matched SD controls at P30 and P60 **(E)**. The cone b-wave timing and summed OP amplitudes were not significantly affected in P23H-3 at any age examined **(F,G)**. OP implicit timing showed a significant increase in P23H-3 compared to SD only at P30 **(H)**. All box and whisker plots show interquartile range (box), median (transverse line), mean (+), and 95% confidence intervals (error bars). Data were analyzed by two-way ANOVA, Tukey's *post hoc* test, $^{*}p < 0.05$, and $^{****}p < 0.0001$, $n \geq 8$ in each group. *, significant difference for genotype; #, significant difference for age.

Photoreceptor Death in P23H-3 Does Not Involve Mitochondrial-Mediated Pathways

To investigate the involvement of mitochondrial-mediated cell death in photoreceptor degeneration in P23H-3, we utilized a flow cytometric JC-1 assay to investigate the mitochondrial membrane potential ($\Delta\psi m$) in P23H-3 and SD retinae at P14 and P18 (Reers et al., 1995; Salvioli et al., 1998). The JC-1 assay is based on a shift in emission fluorescence from red to green wavelengths if the mitochondrial membrane is depolarized. The gating strategy (**Supplementary Figure S3**) allowed us to distinguish three different cell populations based on cell size and cell viability (**Figure 6A**).

Overall, similar proportions of cells were isolated for each population in each group (**Figures 6A,E,I**). While previous studies, using a *Nrl-GFP* transgene in mice had indicated that rod photoreceptors are the smallest cells isolated by flow cytometry (Akimoto et al., 2006), our quantitative PCR analyses of the cell populations we isolated, indicated that only dead small cells were enriched for rod photoreceptors compared to the other populations, therefore we also analyzed this cell population. The positive control cells, involving treatment of cells with carbonyl cyanide m-chlorophenyl hydrazone (CCCP), clearly showed a marked shift from red to green fluorescence (**Figures 6B–D**), indicating drug-induced mitochondrial membrane depolarization. No such fluorescence shift was detected in small live (**Figure 6K**) or large live cell (**Figure 6L**) populations of the P23H-3 retinal cells, compared to SD control retinal cells (**Figures 6G,H**). In the small dead cell populations, there appeared to be an increase in the number of small cells with higher levels of green fluorescence (compare arrowheads, **Figures 6F,J**). Quantification of the ratio of red:green fluorescence intensity for all three cell populations (**Figures 6M–O**) showed that only small dead cells were significantly different ($p < 0.0001$, two-tailed unpaired *t*-test) in P23H-3 compared to SD retinae (**Figure 6M**). To determine if this feature was unique to P18 retinae, we repeated the analysis at P14 and obtained similar data (**Supplementary Figure S4**).

Overall, the flow cytometry data indicated that in small or large live cells, isolated from the P23H-3 retina, there was no evidence of significant changes in mitochondrial permeability. However, greater numbers of small dead cells, isolated from the P23H-3 retina had disrupted mitochondrial permeability. Quantitative PCR analyses of P23H-3 retinae at P16 showed that this population of cells was enriched for rod photoreceptors by approximately 1.6- to 1.8-fold (**Supplementary Table S1**). These data suggested that dying or dead photoreceptors were undergoing or had undergone increased mitochondrial permeability. Alternatively, this population of cells may arise as an artifactual effect of the isolation protocol or represent dead cells (including photoreceptors) at the time of collection and isolation. Thus, this could be an artifactual apparent increase

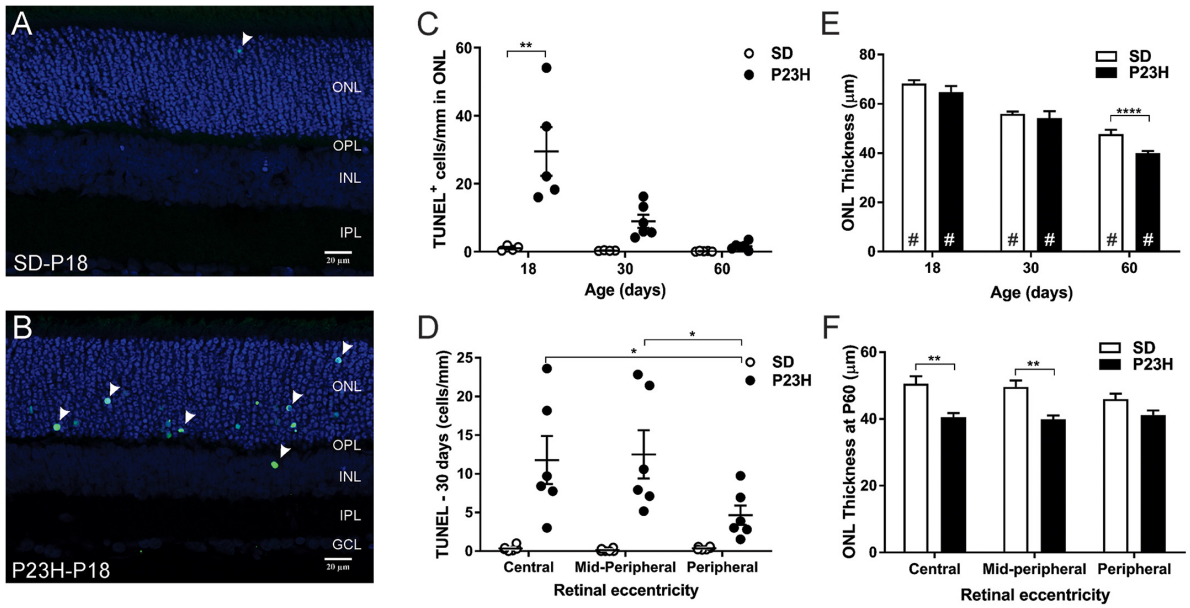

FIGURE 4 | Photoreceptor cell death in P23H-3 rats with age. TUNEL (green) and nuclei (blue) staining in SD **(A)** and P23H-3 **(B)** retina at P18 **(A,B)**. TUNEL positive cells (arrowheads) were detected predominantly in ONL of P23H-3 retinae across all ages but were rarely detected in the ONL of SD retinae. **(C)** Quantification of total retinal TUNEL$^+$ cells at each age revealed significantly increased numbers of TUNEL$^+$ cells in P23H-3 retina at P18, but not at P30 or P60. **(D)** Significant differences in the number of TUNEL$^+$ cells across retinal eccentricity were detected in the P23H-3 retina at P30 with greater photoreceptor death in central and mid-peripheral than in peripheral regions of retina. **(E)** Quantification of mean ONL thickness showed significant decreases with age (#), with P23H-3 ONL significantly thinner than SD at P60, but not at P18 or P30. **(F)** Across central to peripheral eccentricity at P60 there were significant decreases in ONL in the central and mid-peripheral, but not peripheral regions. Data are expressed as means ± SEM, Two-way ANOVA, Tukey's *post hoc* test, $^*p < 0.05$, $^{**}p < 0.001$, and $^{****}p < 0.0001$, $n \geq 5$ in each group. *: significant difference for genotype, $^{\#}$: significant difference for age. Abbreviations: ONL, outer nuclear layer; INL, inner nuclear layer. Scale bar = 20 μm.

in mitochondrial permeability as a consequence and not a cause of cell death. To further investigate the involvement of mitochondrial-mediated cell death mechanism, we conducted immunostaining for cleaved caspase-3 and nuclear AIF at P18. Only occasional photoreceptor cells in the ONL of P23H-3 were positive for either cleaved caspase-3 or AIF at P18 (**Figures 7A,B**, respectively). Similarly, only occasional stained cells were detected in the SD retinae (not shown). These observations, combined with the flow cytometric JC-1 assay, suggest that classical caspase-mediated apoptosis (either extrinsic or intrinsic) or caspase-independent apoptosis via AIF translocation to the nucleus are not major contributors to photoreceptor death in the P23H-3 retina. Consistent with this, expression and activation of proteins associated with apoptosis were poorly detectable (BCL-2, XIAP, MCL1, BIM, TP53, cleaved CASP3) or did not show significant changes (IGFR1, BCL-XL, BAX, CASP3) in retinal extracts by RPPA analysis (**Table 1**).

Evidence for Increased Autophagy During Photoreceptor Cell Death in P23H-3 Retina

The PCR array data indicated moderate increases in autophagy-related proteins in P23H-3 retinae at both P14 and P18. The involvement of autophagy in photoreceptor death was examined by immunofluorescence of BECN1 and ATG5. The staining for BECN1 (compare **Figures 8A,B**) and ATG5 (compare **Figures 8C,D**) were relatively diffuse in the SD inner segments but appeared brighter and more distinct in the inner segments of the P23H-3 photoreceptors and the OPL. As translocation of BECN1 to mitochondria is associated with autophagosome formation and mitophagy (Gelmetti et al., 2017), we co-labeled sections with cytochrome oxidase (CO) and found increased association of BECN1 with mitochondrial CO in the proximal region of the inner segments (insets **Figures 8A,B**). Similar results were obtained when ATG5 was co-localized with MitoTracker (inset **Figure 8D**). The increased association of BECN1 and ATG5 with mitochondria suggests increased mitophagy in the inner segments of the P23H-3 retina. Consistent with this, there appeared to be moderately increased phagosome formation as detected by immunofluorescence with an antibody to LC3B (**Figures 8E,F** insets).

Widespread Necroptosis Is a Major Contributor to P23H-3 Photoreceptor Cell Death

From P14 to P18, the most dramatic changes in gene expression occurred in genes associated with necrosis (**Figure 5**) and combined with the altered activation of AKT, shown by RPPA, suggesting the induction of necroptosis. To investigate the possibility of programmed necrosis (necroptosis) being involved in photoreceptor cell death, we examined the localization of the kinase, RIPK3, and the phosphorylated

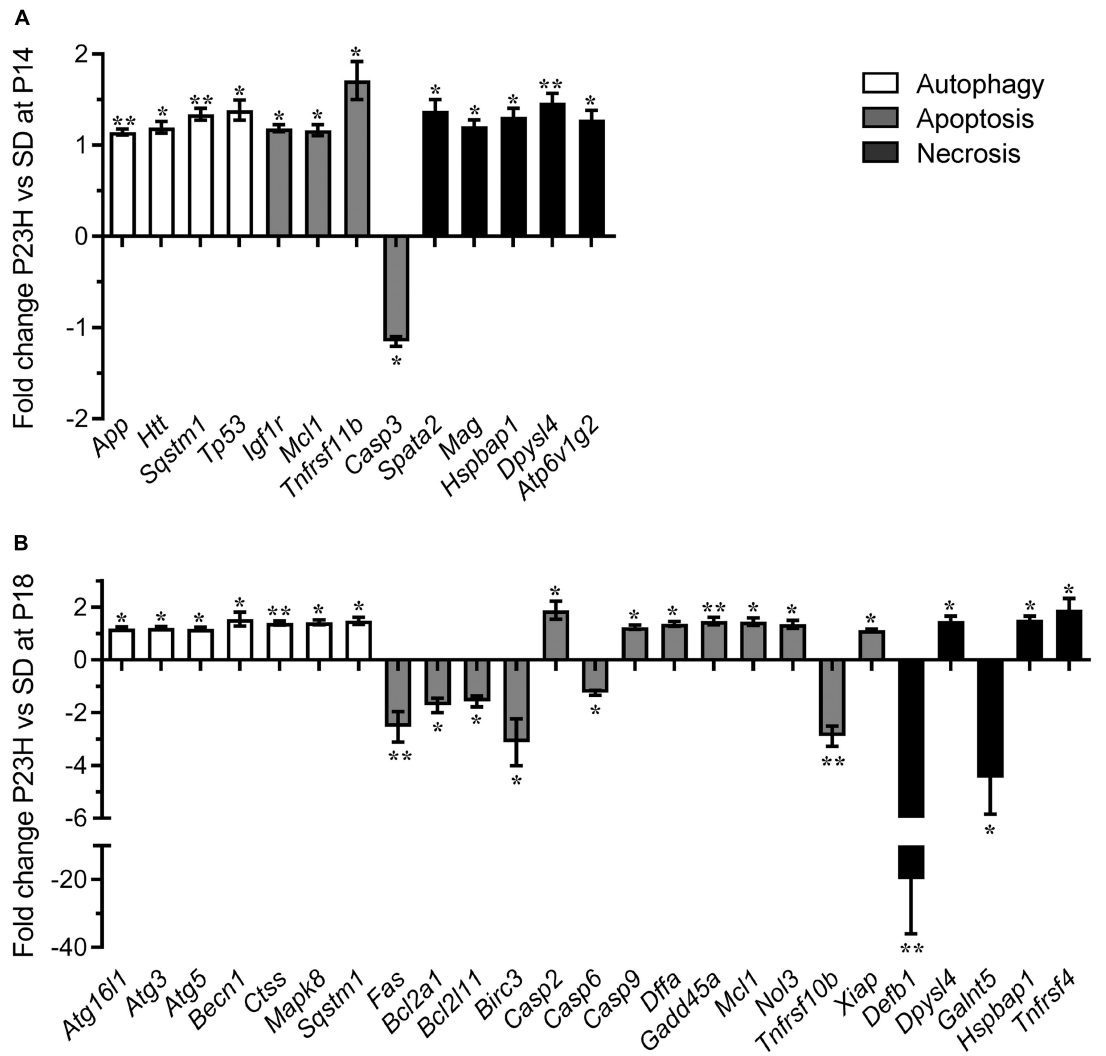

FIGURE 5 | Dysregulation of programmed cell death-related genes in P23H-3 retinae. Changes in programmed cell death related genes (fold regulation) in P23H-3 compared to age-matched SD rats at P14 **(A)** and P18 **(B)**. Genes are clustered according to involvement in autophagy, apoptosis or necrosis pathways as defined by Qiagen. Data presented as mean ± SEM, Student's *t*-test, $^{*}p < 0.05$, $^{**}p < 0.01$.

form of its target, MLKL. While there appeared to be no difference in the expression of RIPK3 in the inner segments of P23H-3 retinae (**Figure 9B**) compared to the SD control retinae (**Figure 9A**), expression of phospho-MLKL was markedly increased in the inner and outer segments of the P23H-3 retinae (**Figure 9D**) compared to wild-type SD retinae (**Figure 9C**). These data suggest that at P18, when photoreceptors are actively dying, the necroptosis pathway is highly activated.

DISCUSSION

The present study provides a detailed and comprehensive phenotypic analysis of retinal structure and function in the P23H-3 rat model of inherited retinal degeneration and highlights the complexity of mechanisms involved in photoreceptor death. Notably, mechanisms associated with necroptosis are particularly important for rod photoreceptor death.

P23H-3 Rats Show a Progressive Decline in Retinal Function From P30

In wild-type SD rats there was a clear developmental profile for rod ERG responses as reported previously (Fulton et al., 1995; Gibson et al., 2013; Nadal-Nicolas et al., 2018), with significant increases in amplitudes of a- and b-waves and OP from P18 to P30 with subsequent decreases in amplitudes at P60 and P90. A similar developmental pattern of ERG responses was seen for the cone b-wave response, which was significantly increased at P30 from P18 in SD normal rats, with a subsequent decline at P60. The functional increases from P18 to P30 likely reflect the postnatal development of the photoreceptors, including elongation of outer segments, increased expression of

TABLE 1 | Comparison of mRNA and protein expression of genes involved in cell death pathways in P18 retinae.

PCR Array				Reverse Phase Protein Array			
Array Pathway*	**Symbol**	**FC**	***p*-value**	**Protein**	**FR**	***p*-value**	**Comment**
Anti-apoptotic	*Igf1r*	−1.036	0.618	IGF1R	0.872	0.281	
Anti-apoptotic/Autophagy	*Akt1*	−1.017	0.790	AKT1-3 protein	0.973	0.787	
				AKT_P Thr308	0.804	0.039	
				AKT_P S473	0.561	0.042	
Autophagy	*Pten*	1.205	0.058	PTEN	0.909	0.247	
Autophagy	*Mapk8/Jnk2*	1.205	0.058	JNK2	0.875	0.210	At or below threshold
				JNK1/JNK2/JNK3	0.953	0.803	At or below threshold
Anti-apoptotic; Autophagy	*Bcl2*	−1.061	0.747	BCL-2	1.254	0.143	Below detection threshold
Anti-apoptotic	*Xiap*	1.122	0.037	XIAP	0.910	0.538	Below detection threshold
Pro- and Anti-apoptotic, Autophagy	*Bcl2l1/BclxL*	1.425	0.127	BCL-XL	1.030	0.639	
Anti-apoptotic	*Mcl1*	1.445	0.013	MCL1	1.932	0.223	Below detection threshold
Autophagy	*Rps6kb1*	1.291	0.321	RPS6KB1	1.375	0.134	Below detection threshold
Pro-apoptotic	*Bcl2l11/Bim*	−1.581	0.020	BIM	1.206	0.476	Below detection threshold
Pro-apoptotic	*Tp53*	−1.363	0.053	TP53	1.080	0.294	
				TP53_P S15	3.170	0.061	Below detection threshold
Pro-apoptotic; Autophagy	*Bax*	−1.054	0.690	BAX	1.358	0.085	
Pro-apoptotic; Autophagy	*Casp3*	1.188	0.061	CASP3	0.898	0.270	
				CASP3_Cleaved Asp175	1.828	0.022	Below detection threshold
Pro-apoptotic	*Casp7*	−1.079	0.881	CASP7_Cleaved Asp198	1.475	0.064	At or below threshold
Necrosis	*Parp1*	−1.136	0.573	PARP	0.972	0.852	

*Significant p-values are highlighted in gray.Abbreviations: *, as supplied by Qiagen; FC, fold-change; FR, fold-regulation.*

opsins (Fulton et al., 1995; Chrysostomou et al., 2009; Gibson et al., 2013) as well as continued functional and morphological modifications of synaptic connections of downstream circuits (Tian, 2004, 2008). By contrast, P23H-3 rats showed significantly attenuated amplitudes of rod photoreceptor (a-wave) and post-receptoral responses (b-wave and OP) as early as P30. At P60, the amplitude of the rod a-wave, b-wave and OP decreased by 60, 40, and 62%, respectively and are similar to the reductions in rod a-wave b-wave amplitudes reported previously (Machida et al., 2000; Chrysostomou et al., 2009; LaVail et al., 2018). However, the normal developmental functional overlay raises the question of whether these reductions in ERG components after P30 are due to impairment of the normal functional maturation of the retina and/or the underlying P23H-induced cell loss.

Comparison of the mean percentage loss of rod a-wave, b-wave and OP amplitudes from P30-P90 showed that while the percentage decline in the summed OP was significantly greater than the percentage decline in the a-wave, the rate of decline over the 3 months was similar to that of the declines in the a-wave, suggesting amacrine cell function declines in parallel with the rod photoreceptors. However, the percentage decline in the b-wave plateaued at P90, suggesting that Müller/bipolar cell function is somewhat preserved at this stage.

Our analysis of cone post-photoreceptoral responses indicated that P23H-3 animals had significantly lower cone b-wave amplitudes compared to SD controls at P30 and P60, while the cone, OP amplitudes remained relatively unaffected. This suggests that cone dysfunction occurs from an early stage of disease – earlier than has been previously reported (Machida et al., 2000; Chrysostomou et al., 2009). While previous studies showed significantly lower numbers of L/M-cones in P23H-1 homozygous albino rat retinae when compared to SD rats from P30 to P180 (Garcia-Ayuso et al., 2013), we did not find any significant differences in total cone numbers detected by PNA in the P23H-3 retina at P30 (**Supplementary Figure S2G**). Overall, these data suggest that in the P23H-3 strain, cone dysfunction, but not cone death, occurs from P30 or even earlier. However, it should be noted that the analyses in this study were conducted on albino P23H-3 rats and that the timing of retinal functional and morphological changes are different when this mutation is present on a pigmented strain background (Cuenca et al., 2014; Lowe et al., 2019). Indeed, it has been proposed that the lack of pigmentation possibly affects cone function more than rod function over time (Cuenca et al., 2014).

Structural Changes and Patterns of Cell Loss Follow Functional Losses

While fundus imaging in these albino rats failed to reveal overt characteristics of RP (due to lack of pigmentation), both OCT and histological analyses demonstrated significant, progressive thinning of ONL in P23H-3 rats from P60 onward, reaching 22% reduction at P90. These observations are consistent with previous studies indicating similar progression of retinal thinning, with 15% loss of photoreceptors by P30, 50% by P203 (Machida et al., 2000) and 68% by P230 (Chrysostomou et al., 2009). While our OCT measurements did not show significant changes in the photoreceptor inner/outer segments, histological studies have

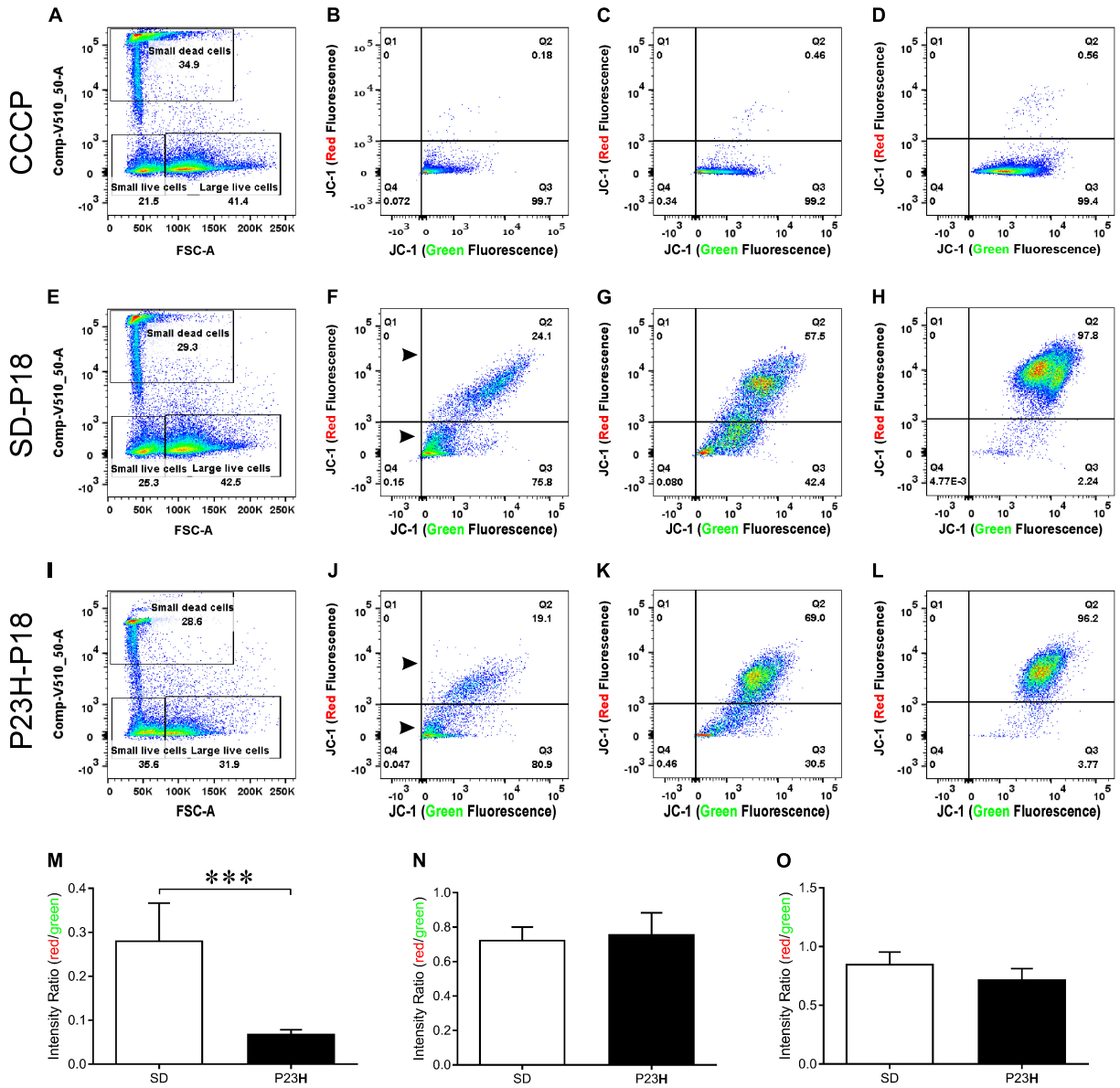

FIGURE 6 | Mitochondrial membrane potential ($\Delta\psi m$) in P23H-3 and SD retinal cells at P18. Cell gating strategy for the analysis of retinal cells with different mitochondrial membrane potentials **(A,E,I)** was based on cell size and DAPI fluorescence. Three distinct subpopulations of cells were detected in all samples: small dead cells **(B,F,J)**, small live cells **(C,G,K)**, and large live cells **(D,H,L)**. Representative plots for each of the three populations of cells show levels of polarized (red fluorescence) and depolarized (green fluorescence) mitochondria due to the JC1 dye, in CCCP-treated **(B–D)**, SD **(F–H)**, and P23H-3 **(J–L)** retinal cells. While no major fluorescence shifts could be detected for small live and large live cells between SD and P23H-3 samples, there appeared to be a slight shift from red- green for the small dead cells (Arrowheads; **F,J**). Quantification of red:green fluorescence intensity ratio in the three cell populations from P23H-3 and SD samples showed that small dead **(M)**, but not small live **(N)** or large live cells **(O)**, had a significant drop in red:green fluorescence intensity ratio ($p < 0.0001$; two-tailed unpaired *t*-test) in the P23H-3 retinae. Data presented as mean ± SEM, Student's *t*-test, $^{***}p < 0.001$, $n = 6$ in each group.

detected shortened OS from P30 to P203 (Machida et al., 2000), suggesting that OCT resolution may not be sufficient to detect subtle structural changes in rat eyes.

Our TUNEL assays show prolific photoreceptor cell death by P18 that gradually subsides from P30 to P90. Consistent with previous studies, these results suggest that retinal degeneration is biphasic, with a rapid initial phase, with a peak occurring at approximately P17-P20 (Lee et al., 2003; Yu et al., 2004; Kaur et al., 2011; Zhu et al., 2013), followed by a slower phase up to P60. In particular, the early phase of photoreceptor degeneration overlaps with naturally occurring morphogenetic death of photoreceptors during retinal maturation and is a critical period when photoreceptors are susceptible to oxygen levels (Maslim et al., 1997). As a result, cells may be even more susceptible to stress-induced damage by *Rho* mutations during this period (Lee et al., 2003).

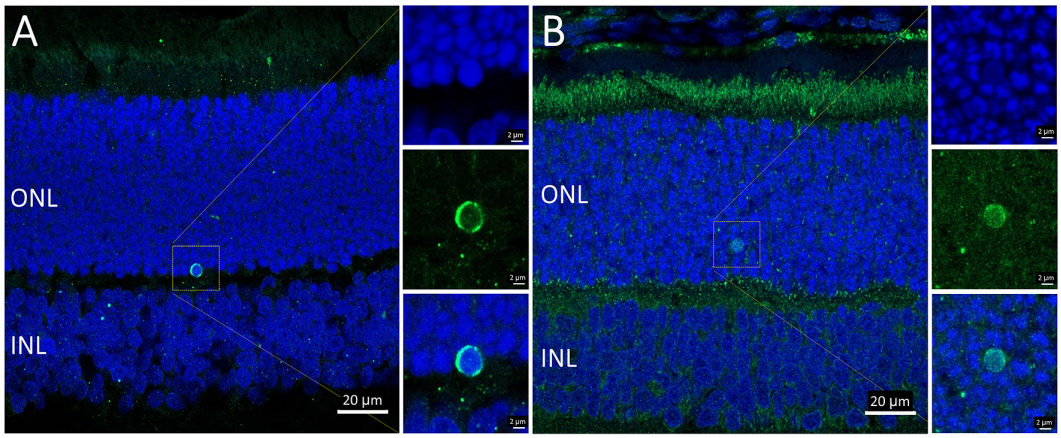

FIGURE 7 | Activated caspase-3 and AIF staining in P23H-3 retinae at P18. Confocal images of P18 retinal sections labeled with anti-cleaved caspase-3 (**A**, green) and AIF (**B**, green), showing only occasional cells were labeled. AIF is clearly detectable in the numerous mitochondria in the photoreceptor inner segments and also in the retinal pigmented epithelium and outer plexiform layer. Each of the labeled cells is shown at higher magnification in the three insets showing fluorescence due to DAPI (blue), the antibody (green) and the merged image. Abbreviations: ONL, outer nuclear layer; INL, inner nuclear layer. Scale bar = 20 µm **(A,B)**; 2 µm (insets).

Quantification of ONL thickness across retinal eccentricity indicated that by P60 there was significantly greater loss of ONL cells in the central and mid-peripheral regions. Consistent with this, TUNEL analyses showed greater numbers of TUNEL^{+} cells in these regions at P30. This is consistent with a recent study reporting higher rate of retinal degeneration in the superior than inferior hemisphere of P23-3 strains from P90 onward and that the loss of photoreceptors proceeds in a central-peripheral gradient (LaVail et al., 2018). By contrast Machida et al. (2000), using resin-embedded sections, found no significant differences in ONL cell counts in superior and inferior hemispheres of P23H-3 retinae from 4 to 29 weeks of age (Machida et al., 2000). While the reasons for this discrepancy in the P23H-3 rat retina are not clear, in human patients with P23H mutations, degeneration usually initiates in the mid peripheral retina and progresses gradually to the macula and more peripheral regions, with loss of rod photoreceptors in the far periphery occurring at relatively advanced stages (Heckenlively et al., 1991; Stone et al., 1991).

Multiple Death Pathways Are Modulated During Photoreceptor Death

While early studies, based on TUNEL assays, suggested photoreceptor cell death was via an apoptotic mechanism (Chang et al., 1993), TUNEL also labels DNA fragments generated by non-apoptotic mechanisms of cell death, such as necrosis (Grasl-Kraupp et al., 1995). Subsequently, various different mechanisms of cell death have been proposed to mediate photoreceptor cell death in the degenerating retinae of various animal models for RP. These include intrinsic and stress-induced, caspase-dependent apoptosis (Jomary et al., 2001), as well as activation of calpains and AIF-dependent photoreceptor cell death, also known as "parthenatos" (Paquet-Durand et al., 2010; Kaur et al., 2011; Comitato et al., 2016). It has been shown that the mutant P23H protein undergoes abnormal folding and its accumulation leads to ER stress and the UPR (Lin et al., 2007). Components of the three UPR response pathways are elevated at P15 (Kroeger et al., 2012), P30 (Lin et al., 2007; Gorbatyuk et al., 2010), and at P60 (Kroeger et al., 2012), correlating with the onset of receptor death, functional loss and structural decrements, respectively. While short term activation of UPR facilitates degradation of accumulated unfolded proteins via the proteasome or by autophagy, prolonged UPR can lead to activation of apoptosis or, as more recent evidence suggests, necroptosis (Iurlaro and Munoz-Pinedo, 2016; Wang et al., 2018). Thus, UPR can be an early protective response or, if sustained, a mechanism that contributes to photoreceptor death.

To gain further insight into molecular pathways downstream of this UPR that potentially mediate P23H-RHO related photoreceptor death, we used quantitative RT-PCR arrays, focused on genes that are involved in major cell death pathways (apoptosis, autophagy, and necrosis), to survey expression changes at P14 and P18. Pathway analysis of the expression data indicated that while both autophagy and necroptosis are activated at both P14 and P18, activation of the intrinsic apoptotic pathway was predicted to occur only at P18.

Photoreceptor Death Does Not Involve Apoptosis or Parthenatos

Overall, the mildly dysregulated expression changes at P14 are suggestive of mechanisms that suppress apoptosis, but promote cell survival, autophagy and necroptotic pathways. For example, *Tnfrsf11b*, a TNF superfamily receptor involved in bone regulation, has been detected in vitreous, retina and RPE (Ehlken et al., 2015) and can inhibit apoptosis mediated via the P38 MAPK stress pathway (Holen et al., 2005). Similarly, *Mcl1* is a member of the Bcl2 family of anti-apoptotic proteins and the longest form of its three alternatively spliced variants enhances cell survival (Morciano et al., 2016). Finally, *Igfr1*, is commonly considered as anti-apoptotic and through its binding of insulin and IGF1 can potentially rescue retinal neurons from cell death

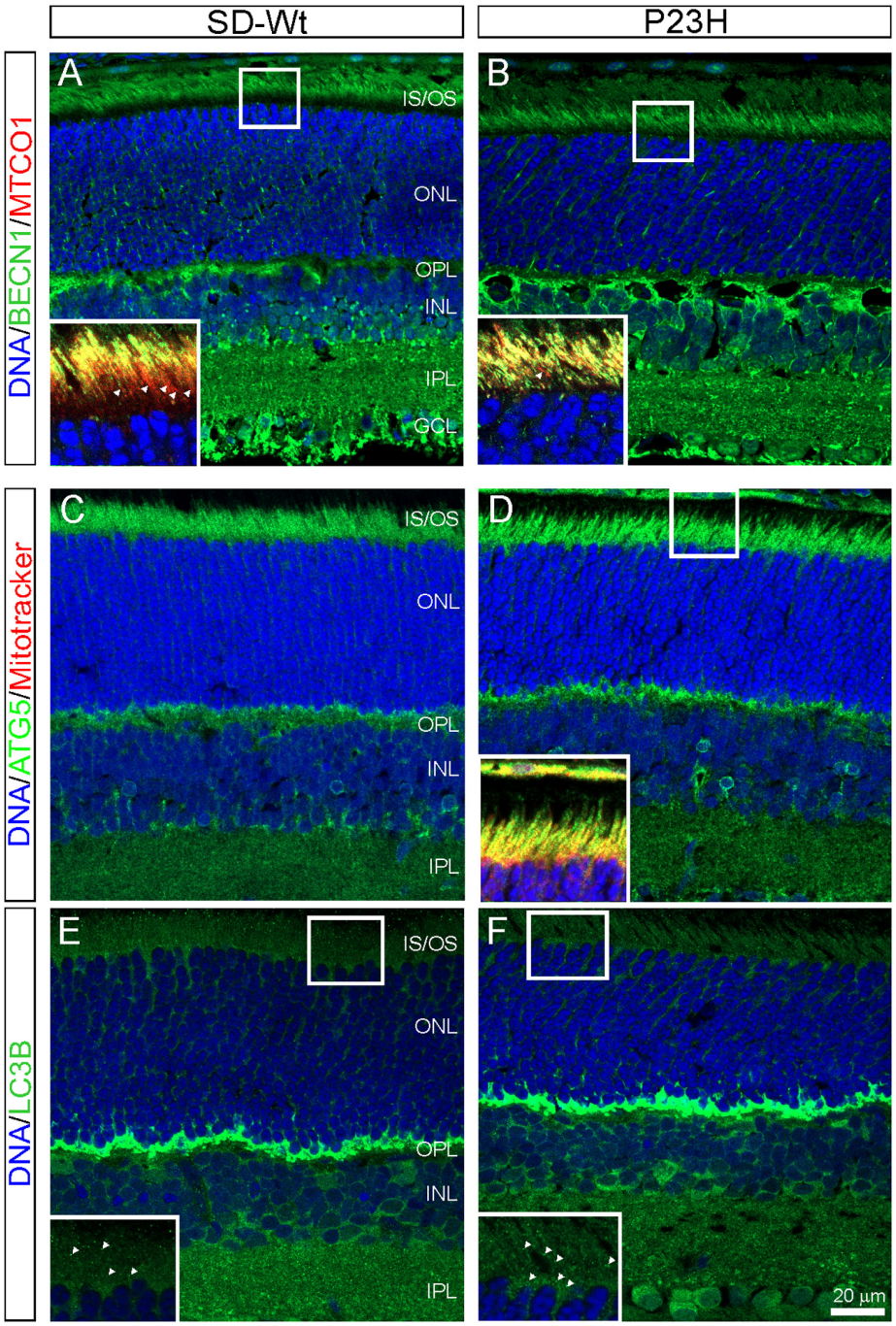

FIGURE 8 | Autophagy markers (BECN1, ATG5, LC3B) in P23H-3 retinae at P18. Confocal images of P18 retinal sections labeled with BECN1 (**A,B**, green) and cytochrome oxidase (MTCO1; insets **A,B**, red), ATG5 (**C,D**, green) and MitoTracker (inset, **D**) and LC3B (**E,F**, green) in wild-type SD **(A,C,E)** and P23H-3 **(B,D,F)** retinae. Staining for BECN1 **(B)** and ATG5 **(D)** appeared to be mildly increased and more distinct in the P23H-3 retina. The yellow colored co-labeling with cytochrome oxidase (insets **A,B**, red) or MitoTracker (inset, **D**, red) indicates increased association of BECN1 and ATG5 with mitochondria in P23H inner segments. Labeling of phagosomes (arrowheads) in the inner segments with LC3B appeared to be increased in the P23H-3 **(F)** compared to SD retina **(E)**. All sections were counter-stained with DAPI (blue) to label cell nuclei. Abbreviations: GCL, ganglion cell layer; INL: inner nuclear layer; IPL, inner plexiform layer; IS/OS, inner/outer segments; ONL, outer nuclear layer; OPL, outer plexiform layer. Scale bar: **(A–F)**, 20 μm; insets, 10 μm.

by activating PI3K/AKT/mTOR cell survival pathway (Seigel et al., 2000; Barber et al., 2001; Punzo et al., 2009), which in turn can modulate autophagy and necroptosis.

Similarly, the expression patterns of apoptotic pathway genes at P18 suggest contrasting regulatory effects on pathway activity. The dysregulation of some genes (e.g., *Bcl2l11*, *Fas*,

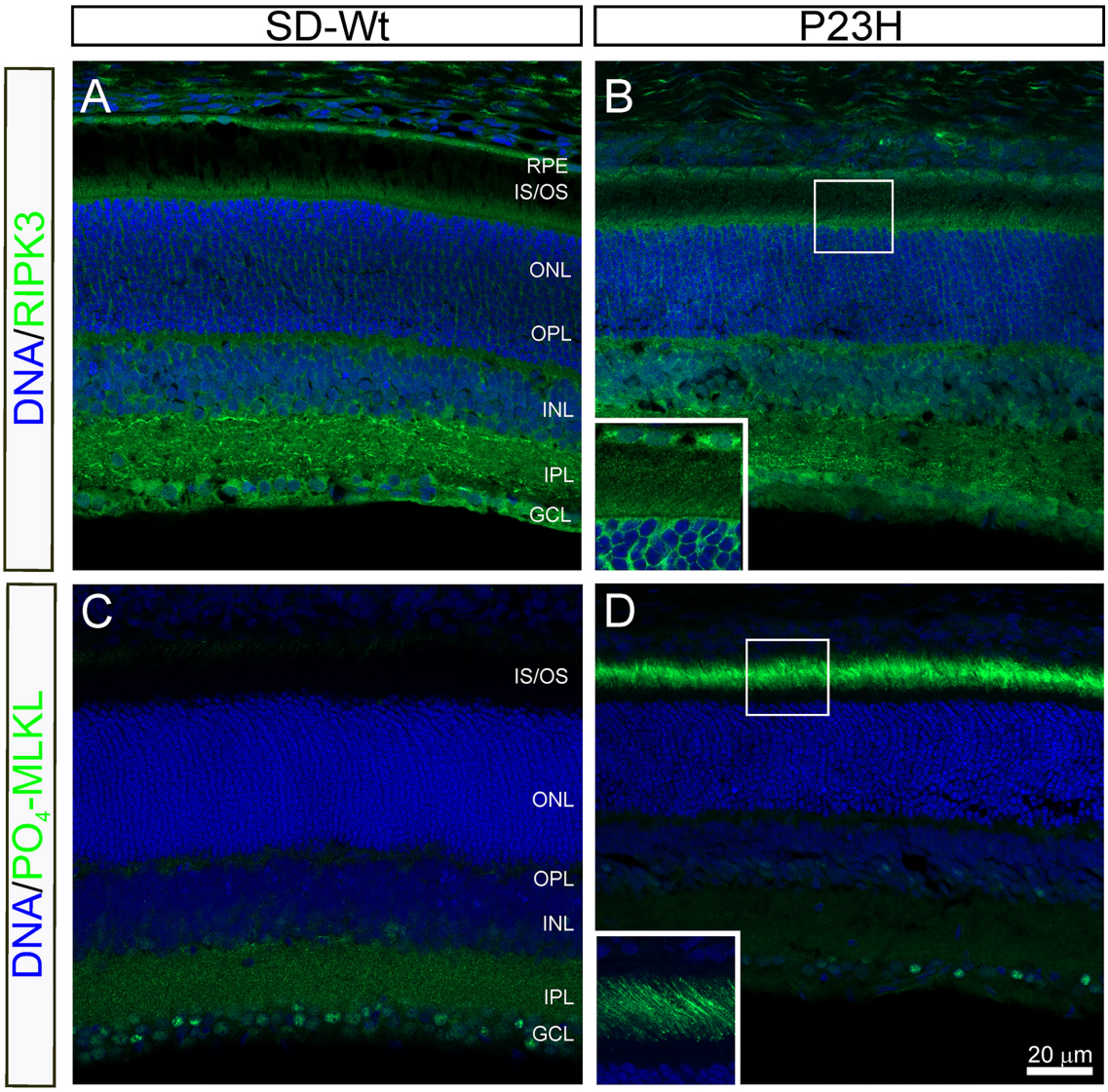

FIGURE 9 | RIPK3 and phospho-MLKL staining in P23H-3 retinae at P18. Confocal images of P18 retinal sections labeled with RIPK3 (**A,B** green) and phosphorylated (S345)-MLKL (**C,D** green) antibodies. No differences were noted in localization of the RIPK3 kinase in the wild-type SD **(A)** compared to P23H-3 **(B)** retina, with weak but specific staining observed in the inner segments of the photoreceptors (inset, **B**) as well as in the OPL, INL, IPL, and GCL. By contrast, there was a marked difference in the expression of phosphorylated MLKL, with dramatic induction in the outer segments of the P23H-3 retina **(D)**, which was completely absent in the wild-type SD retina **(C)**. The inset in panel **(D)**, shows the distinct localization in the outer segments. Abbreviations: GCL, ganglion cell layer; INL: inner nuclear layer; IPL, inner plexiform layer; IS/OS, inner/outer segments; ONL, outer nuclear layer; OPL, outer plexiform layer; RPE, retinal pigmented epithelium. Scale bar = 20 μm.

Casp6, *Gadd45a*, *Mcl1*, *Nol3*, *Tnfrsf10b*, *Xiap*) potentially inhibit apoptosis whereas dysregulation of others (e.g., *Birc3*, *Bcl2a1*, *Casp2*, *Casp9*, *Dffa*, *Gadd45a*) potentially promote apoptosis. In addition, the dysregulation of other apoptotic genes is suggestive of links to necroptosis (via CASP2 interaction with RIPK1 complexes) and to autophagy (via MCL1 phosphorylation by GSK3beta/BECN1) (Bouchier-Hayes and Green, 2012).

Consistent with these expression findings of variable activation of intrinsic apoptosis, our JC-1 dye in flow cytometry assays of mitochondrial permeability at P14 and P18, demonstrated very little evidence for changes in mitochondrial permeability at P14 and P18 in live cells collected from P23H-3 retinae. It is unclear if the significant changes in mitochondrial permeability in small dead cells reflects a greater susceptibility of P23H-3 retinal cells to undergo apoptotic cell death due to the dissociation procedure, or if more dead cells are present in these retinae than the wild-type at the time of collection. However, consistent with these mitochondrial permeability data, immunolabelling for cleaved caspase-3 as a marker for intrinsic/extrinsic apoptosis and nuclear AIF for non-caspase mediated parthenatos showed only sparse reactivity in the ONL of P23H-3 retinae at P18. Similar findings of negligible

caspase-3 activity have been reported in the P23H-1 strain at P15 (Kaur et al., 2011; Arango-Gonzalez et al., 2014). Nor is there evidence for caspase-9 activity, cytochrome-C leakage or abundant nuclear translocation of cleaved AIF in P23H-1 rats (Kaur et al., 2011; Sizova et al., 2014). Overall, these studies indicate that cell death mechanisms, acting via altered mitochondrial permeability via either caspase-dependent or caspase-independent parthenatos pathways, are not major contributors to cell death induced by P23H RHO.

Increased Autophagy During Photoreceptor Death in P23H-3 Retina

The upregulation of several genes associated with autophagy (*App*, *Htt*, *Sqstm1*, and *Tp53*) at P14 can be interpreted as both cytoprotective and potentially increasing autophagy. For instance, while pathological processing of amyloid precursor protein (APP) to amyloid β in Alzheimer's disease has been implicated in disrupting autophagy via the BECN1 complex (Salminen et al., 2013), the normal non-amyloidogenic processing of APP has been associated with neuroprotection in the retina (Cimdins et al., 2019).

Similarly, at P18 there is marked dysregulation of genes that are core components of the autophagy machinery (*Atg16l1*, *Atg3*, *Atg5*, and *Becn1*) (Suzuki et al., 2017) and also *Sqstm1*, which is a key mediator in marking and directing cellular components to the autophagy machinery (Lamark et al., 2017). These data are consistent with a previous study showing dynamic expression profiles of autophagy-related genes in P23H-3 retinae at P21 (Sizova et al., 2014). Moreover, autophagy and lysosomal proteins have been shown to colocalize with mutant P23H protein (Kaushal, 2006). In our experiments, ATG5 and BECN1 showed increased co-localization with mitochondria in the inner segments of the mutant photoreceptors, suggesting that there is increased mitophagy. Indeed, localization of BECN 1 at mitochondrial membranes has been shown to promote tethering of ER and mitochondria to initiate autophagosome formation (Gelmetti et al., 2017).

Overall, the upregulation of these autophagy-promoting genes is consistent with the notion that ER stress, induced by accumulating misfolded P23H rhodopsin protein, induces an autophagic response in mice carrying the P23H mutation (Song et al., 2018; Yao et al., 2018). However, somewhat surprisingly inhibition of autophagy increases photoreceptor survival, whereas increasing autophagy promotes retinal degeneration, suggesting that autophagy actually contributes to PR cell death (Yao et al., 2018). Thus, while autophagy may help to clear ER-resident misfolded proteins, it likely comes at the cost of increased autophagy-mediated loss of the ER and mitochondria with consequent photoreceptor cell death.

Necroptosis Is a Major Contributor to Photoreceptor Death in P23H-3 Retina

Various genes that were up-regulated at P14 and P18 suggest that there was activation of necroptosis in the P23H-3 retina. The well-known tumor suppressor, *p53* (TP53), has been associated with not only caspase-dependent and caspase-independent pathways of apoptosis, but also with non-apoptotic mechanisms of cell death, including programmed necrosis (necroptosis) (Nikoletopoulou et al., 2013; Ranjan and Iwakuma, 2016). The coincident up-regulated expression of *Dpysl4*, a direct target of P53 transcriptional activity and calpain cleavage activity (Kimura et al., 2011), suggests that, in the retina at P14, P53 may upregulate a calpain-mediated necrotic cell death pathway. Further evidence for upregulation of necrosis comes from the increased expression of genes that have been implicated in programmed necrotic cell death (*Mag*, *Spata2*, *Hspbap1*, and *Atp6v1g2*). In particular, upregulation of *Spata2*, which modulates TNFα signaling, can promote TNFα-mediated necroptosis and inhibit the apoptotic pathway (Schlicher et al., 2017). Indeed, inhibition of apoptosis is a common contributing trigger for induction of necroptosis (Morris et al., 2018). Similarly, at P18, dysregulation of *Casp2* can potentially activate necroptosis via interaction with RIPK1 complexes (Bouchier-Hayes and Green, 2012).

It has been suggested previously that necroptotic-mediated signaling is an important driver of rod photoreceptor cell death in the P23H-3 model, whereas NLRP3 inflammasome activation is the mechanism for subsequent cone cell death Viringipurampeer et al., 2019. Viringipurampeer et al. (2019) demonstrated increased expression of RIPK3 in P23H-3 rats by western blot at P21, P45 and P120 and its co-localization with ID4 a rhodopsin marker. Moreover, long-term injections of a combination of inhibitors for RIPK1, PARP and calpain with an anti-oxidant/inflammatory inhibitor ameliorated ONL cell/outer segment loss and provided some protective effect on cone flicker amplitudes (Viringipurampeer et al., 2019). While our study did not demonstrate any detectable change in RIPK3 expression or localization in the P23H-3 photoreceptor outer segments, we did demonstrate dramatically increased localization in the outer segments of phosphorylated MLKL, which is the substrate for the active RIPK1/RIPK3 complex and, in its phosphorylated form, a key effector of necroptosis (Shan et al., 2018).

CONCLUSION

In conclusion, we have shown that in P23H-3 rats various cell death pathways are modulated from P14 to P18, with distinct activation of autophagy and necroptosis but limited activation of caspase-dependent or caspase-independent (parthenatos) pathways. The induction of MLKL phosphorylation at P18 provides definitive evidence for large-scale activation of necroptosis as the principal cause of photoreceptor death in the P23H-3 retina. This cell death manifests as a functional decline in rod photoreceptor, bipolar and amacrine cell responses from P30 and morphologically as ONL cell losses from P60, which progresses from central to peripheral regions of the retina. In addition, we have documented an earlier onset of cone photoreceptor functional decline from P30 than described previously. Together with other studies, these data suggest that retinal degenerations may activate multiple cell death pathways (Lohr et al., 2006; Comitato et al., 2016; Viringipurampeer et al., 2016, 2019) and that therapies aimed at ameliorating

photoreceptor death may need to target multiple cell death pathways as well as potential sequelae, such as inflammation, gliosis and microglial activation that can contribute subsequently to photoreceptor degeneration.

DATA AVAILABILITY STATEMENT

All datasets presented in this study are included in the article/**Supplementary Material.**

ETHICS STATEMENT

The animal studies were reviewed and approved (AEC#1312958 and #1614030) by the Animal Ethics Committee of the University of Melbourne.

AUTHOR CONTRIBUTIONS

EF, AJ, and RI: conceptualization and supervision. KK, UG, EF, KV, and AJ: methodology. RI: software (IPA). KK and RI: validation, writing – original draft preparation, and visualization. KK, UG, AJ, and RI: investigation. EF: resources, project administration, and funding acquisition. KK, AJ, EF, and RI: data curation. All authors contributed to formal analysis and writing – review and editing.

FUNDING

This research was funded by grants from the National Health and Medical Research Council (APP#1138253 to EF, KV and APP1061418 to EF, AJ).

ACKNOWLEDGMENTS

We thank A/Prof. Kaylene J. Simpson and Arthi M. Macpherson from the Victorian Centre for Functional Genomics and the ACRF Translational RPPA platform at Peter MacCallum Cancer Centre for generating the RPPA data. We acknowledge the assistance and services provided by the Biological Optical Microscopy Platform (BOMP) and the Melbourne Brain Centre Flow Cytometry Platform at the University of Melbourne.

SUPPLEMENTARY MATERIAL

The Supplementary Material for this article can be found online at: https://www.frontiersin.org/articles/10.3389/fnins.2020.581579/full#supplementary-material

Supplementary Figure 1 | Measures of rod sensitivity, rod implicit time and OP implicit times by ERG in P23H-3 rats.

Supplementary Figure 2 | Photoreceptor cell death and ONL morphometry in P23H-3 retina at different eccentricities and ages.

Supplementary Figure 3 | Gating strategy for distinguishing different retinal cell populations, based on size and viability at time of isolation.

Supplementary Figure 4 | Ingenuity pathway modeling of apoptosis gene expression data.

Supplementary Figure 5 | Ingenuity pathway modeling of autophagy gene expression data.

Supplementary Figure 6 | Ingenuity pathway modeling of necrosis gene expression data.

Supplementary Figure 7 | Mitochondrial membrane potential ($\Delta\psi m$) in P23H-3 and SD retinal cells at P14.

Supplementary Table 1 | Quantitative PCR analyses of flow cytometry separated cell populations.

Supplementary Table 2 | Antibodies and fixation conditions used in immunofluorescence.

Supplementary Table 3 | Antibodies used in reverse-phase protein arrays (RPPA).

Supplementary Table 4 | Quantitative RT-PCR array data for cell death genes expressed in SD and P23H-3 rat retinae at P14.

Supplementary Table 5 | Quantitative RT-PCR array data for cell death genes expressed SD and P23H-3 rat retinae at P18.

REFERENCES

Akimoto, M., Cheng, H., Zhu, D., Brzezinski, J. A., Khanna, R., Filippova, E., et al. (2006). Targeting of GFP to newborn rods by Nrl promoter and temporal expression profiling of flow-sorted photoreceptors. *Proc. Natl. Acad. Sci. U.S.A.* 103, 3890–3895. doi: 10.1073/pnas.0508214103

Arango-Gonzalez, B., Trifunovic, D., Sahaboglu, A., Kranz, K., Michalakis, S., Farinelli, P., et al. (2014). Identification of a common non-apoptotic cell death mechanism in hereditary retinal degeneration. *PLoS One* 9:e112142. doi: 10.1371/journal.pone.0112142

Athanasiou, D., Aguila, M., Bellingham, J., Kanuga, N., Adamson, P., and Cheetham, M. E. (2017). The role of the ER stress-response protein PERK in rhodopsin retinitis pigmentosa. *Hum. Mol. Genet.* 26, 4896–4905. doi: 10.1093/hmg/ddx370

Athanasiou, D., Aguila, M., Bellingham, J., Li, W., McCulley, C., Reeves, P. J., et al. (2018). The molecular and cellular basis of rhodopsin retinitis pigmentosa reveals potential strategies for therapy. *Prog. Retin. Eye Res.* 62, 1–23. doi: 10.1016/j.preteyeres.2017.10.002

Barber, A. J., Nakamura, M., Wolpert, E. B., Reiter, C. E., Seigel, G. M., Antonetti, D. A., et al. (2001). Insulin rescues retinal neurons from apoptosis by a phosphatidylinositol 3-kinase/Akt-mediated mechanism that reduces the activation of caspase-3. *J. Biol. Chem.* 276, 32814–32821. doi: 10.1074/jbc.M104738200

Bouchier-Hayes, L., and Green, D. R. (2012). Caspase-2: the orphan caspase. *Cell Death Different.* 19, 51–57. doi: 10.1038/cdd.2011.157

Bravo-Gil, N., Gonzalez-Del Pozo, M., Martin-Sanchez, M., Mendez-Vidal, C., Rodriguez-de la Rua, E., Borrego, S., et al. (2017). Unravelling the genetic basis of simplex Retinitis Pigmentosa cases. *Sci. Rep.* 7:41937. doi: 10.1038/srep41937

Chang, G. Q., Hao, Y., and Wong, F. (1993). Apoptosis: final common pathway of photoreceptor death in rd, rds, and rhodopsin mutant mice. *Neuron* 11, 595–605. doi: 10.1016/0896-6273(93)90072-y

Chapple, J. P., Grayson, C., Hardcastle, A. J., Saliba, R. S., van der Spuy, J., and Cheetham, M. E. (2001). Unfolding retinal dystrophies: a role for molecular chaperones? *Trends Mol. Med.* 7, 414–421.

Chiang, W. C., Hiramatsu, N., Messah, C., Kroeger, H., and Lin, J. H. (2012). Selective activation of ATF6 and PERK endoplasmic reticulum stress signaling

pathways prevent mutant rhodopsin accumulation. *Investigat. Ophthalmol. Vis. Sci.* 53, 7159–7166. doi: 10.1167/iovs.12-10222

Chiang, W. C., Joseph, V., Yasumura, D., Matthes, M. T., Lewin, A. S., Gorbatyuk, M. S., et al. (2016). Ablation of chop transiently enhances photoreceptor survival but does not prevent retinal degeneration in transgenic mice expressing human P23H rhodopsin. *Adv. Exp. Med. Biol.* 854, 185–191. doi: 10.1007/978-3-319-17121-0_25

Chiang, W. C., Kroeger, H., Sakami, S., Messah, C., Yasumura, D., Matthes, M. T., et al. (2015). Robust endoplasmic reticulum-associated degradation of rhodopsin precedes retinal degeneration. *Mol. Neurobiol.* 52, 679–695. doi: 10.1007/s12035-014-8881-8

Chrysostomou, V., Stone, J., and Valter, K. (2009). Life history of cones in the rhodopsin-mutant P23H-3 rat: evidence of long-term survival. *Investigat. Ophthalmol. Vis. Sci.* 50, 2407–2416. doi: 10.1167/iovs.08-3003

Cimdins, K., Waugh, H. S., Chrysostomou, V., Lopez, S. M. I. G., Johannsen, V. A., Cook, M. J., et al. (2019). Amyloid precursor protein mediates neuronal protection from rotenone toxicity. *Mol. Neurobiol.* 19:7. doi: 10.1007/s12035-018-1460-7

Comitato, A., Di Salvo, M. T., Turchiano, G., Montanari, M., Sakami, S., Palczewski, K., et al. (2016). Dominant and recessive mutations in rhodopsin activate different cell death pathways. *Hum. Mol. Genet.* 25, 2801–2812. doi: 10.1093/hmg/ddw137

Cuenca, N., Fernandez-Sanchez, L., Sauve, Y., Segura, F. J., Martinez-Navarrete, G., Tamarit, J. M., et al. (2014). Correlation between SD-OCT, immunocytochemistry and functional findings in an animal model of retinal degeneration. *Front. Neuroanat.* 8:151. doi: 10.3389/fnana.2014.00151

Cuenca, N., Pinilla, I., Sauve, Y., Lu, B., Wang, S., and Lund, R. D. (2004). Regressive and reactive changes in the connectivity patterns of rod and cone pathways of P23H transgenic rat retina. *Neuroscience* 127, 301–317. doi: 10.1016/j.neuroscience.2004.04.042

Dryja, T. P., McGee, T. L., Reichel, E., Hahn, L. B., Cowley, G. S., Yandell, D. W., et al. (1990). A point mutation of the rhodopsin gene in one form of retinitis pigmentosa. *Nature* 343, 364–366. doi: 10.1038/343364a0

Ehlken, C., Grundel, B., Michels, D., Junker, B., Stahl, A., Schlunck, G., et al. (2015). Increased expression of angiogenic and inflammatory proteins in the vitreous of patients with ischemic central retinal vein occlusion. *PLoS One* 10:e0126859. doi: 10.1371/journal.pone.0126859

Ferrari, S., Di Iorio, E., Barbaro, V., Ponzin, D., Sorrentino, F. S., and Parmeggiani, F. (2011). Retinitis pigmentosa: genes and disease mechanisms. *Curr. Genom.* 12, 238–249. doi: 10.2174/138920211795860107

Fulton, A. B., Hansen, R. M., and Findl, O. (1995). The development of the rod photoresponse from dark-adapted rats. *Investigat. Ophthalmol. Vis. Sci.* 36, 1038–1045.

Garcia-Ayuso, D., Ortin-Martinez, A., Jimenez-Lopez, M., Galindo-Romero, C., Cuenca, N., Pinilla, I., et al. (2013). Changes in the photoreceptor mosaic of P23H-1 rats during retinal degeneration: implications for rod-cone dependent survival. *Investigat. Ophthalmol. Vis. Sci.* 54, 5888–5900. doi: 10.1167/iovs.13-12643

Gelmetti, V., De Rosa, P., Torosantucci, L., Marini, E. S., Romagnoli, A., Di Rienzo, M., et al. (2017). PINK1 and BECN1 relocalize at mitochondria-associated membranes during mitophagy and promote ER-mitochondria tethering and autophagosome formation. *Autophagy* 13, 654–669. doi: 10.1080/15548627.2016.1277309

Gibson, R., Fletcher, E. L., Vingrys, A. J., Zhu, Y., Vessey, K. A., and Kalloniatis, M. (2013). Functional and neurochemical development in the normal and degenerating mouse retina. *J. Comparat. Neurol.* 521, 1251–1267. doi: 10.1002/cne.23284

Gorbatyuk, M. S., Knox, T., LaVail, M. M., Gorbatyuk, O. S., Noorwez, S. M., Hauswirth, W. W., et al. (2010). Restoration of visual function in P23H rhodopsin transgenic rats by gene delivery of BiP/Grp78. *Proc. Natl. Acad. Sci. U.S.A.* 107, 5961–5966. doi: 10.1073/pnas.0911991107

Grasl-Kraupp, B., Ruttkay-Nedecky, B., Koudelka, H., Bukowska, K., Bursch, W., and Schulte-Hermann, R. (1995). In situ detection of fragmented DNA (TUNEL assay) fails to discriminate among apoptosis, necrosis, and autolytic cell death: a cautionary note. *Hepatology (Baltimore Md)* 21, 1465–1468. doi: 10.1002/hep.1840210534

Guadagni, V., Novelli, E., Piano, I., Gargini, C., and Strettoi, E. (2015). Pharmacological approaches to retinitis pigmentosa: a laboratory perspective. *Prog. Retin. Eye Res.* 48, 62–81. doi: 10.1016/j.preteyeres.2015.06.005

Heckenlively, J. R., Rodriguez, J. A., and Daiger, S. P. (1991). Autosomal dominant sectoral retinitis pigmentosa. Two families with transversion mutation in codon 23 of rhodopsin. *Arch. Ophthalmol. (Chicago Ill 1960)* 109, 84–91. doi: 10.1001/archopht.1991.01080010086038

Heras-Sandoval, D., Perez-Rojas, J. M., Hernandez-Damian, J., and Pedraza-Chaverri, J. (2014). The role of PI3K/AKT/mTOR pathway in the modulation of autophagy and the clearance of protein aggregates in neurodegeneration. *Cell. Signal.* 26, 2694–2701. doi: 10.1016/j.cellsig.2014.08.019

Holen, I., Cross, S. S., Neville-Webbe, H. L., Cross, N. A., Balasubramanian, S. P., Croucher, P. I., et al. (2005). Osteoprotegerin (OPG) expression by breast cancer cells in vitro and breast tumours in vivo–a role in tumour cell survival? *Breast Cancer Res. Treat.* 92, 207–215. doi: 10.1007/s10549-005-2419-8

Hood, D. C., and Birch, D. G. (1996). Assessing abnormal rod photoreceptor activity with the a-wave of the electroretinogram: applications and methods. *Docum. Ophthalmol. Adv. Ophthalmol.* 92, 253–267.

Iurlaro, R., and Munoz-Pinedo, C. (2016). Cell death induced by endoplasmic reticulum stress. *FEBS J.* 283, 2640–2652. doi: 10.1111/febs.13598

Jobling, A. I., Vessey, K. A., Waugh, M., Mills, S. A., and Fletcher, E. L. A. (2013). naturally occurring mouse model of achromatopsia: characterization of the mutation in cone transducin and subsequent retinal phenotype. *Investigat. Ophthalmol. Vis. Sci.* 54, 3350–3359. doi: 10.1167/iovs.13-11831

Jomary, C., Neal, M. J., and Jones, S. E. (2001). Characterization of cell death pathways in murine retinal neurodegeneration implicates cytochrome c release, caspase activation, and bid cleavage. *Mol. Cell. Neurosci.* 18, 335–346. doi: 10.1006/mcne.2001.1036

Kaur, J., Mencl, S., Sahaboglu, A., Farinelli, P., van Veen, T., Zrenner, E., et al. (2011). Calpain and PARP activation during photoreceptor cell death in P23H and S334ter rhodopsin mutant rats. *PLoS One* 6:e22181. doi: 10.1371/journal.pone.0022181

Kaushal, S. (2006). Effect of rapamycin on the fate of P23H opsin associated with retinitis pigmentosa (an American Ophthalmological Society thesis). *Transact. Am. Ophthalmol. Soc.* 104, 517–529.

Kimura, J., Kudoh, T., Miki, Y., and Yoshida, K. (2011). Identification of dihydropyrimidinase-related protein 4 as a novel target of the p53 tumor suppressor in the apoptotic response to DNA damage. *Int. J. Cancer* 128, 1524–1531. doi: 10.1002/ijc.25475

Kremers, J., and Tanimoto, N. (2018). Measuring retinal function in the mouse. *Methods Mol. Biol. (Clifton N. J.)* 1753, 27–40. doi: 10.1007/978-1-4939-7720-8_2

Kroeger, H., Messah, C., Ahern, K., Gee, J., Joseph, V., Matthes, M. T., et al. (2012). Induction of endoplasmic reticulum stress genes, BiP and chop, in genetic and environmental models of retinal degeneration. *Investigat. Ophthalmol. Vis. Sci.* 53, 7590–7599. doi: 10.1167/iovs.12-10221

Lamark, T., Svenning, S., and Johansen, T. (2017). Regulation of selective autophagy: the p62/SQSTM1 paradigm. *Essays Biochem.* 61, 609–624. doi: 10.1042/ebc20170035

LaVail, M. M., Nishikawa, S., Steinberg, R. H., Naash, M. I., Duncan, J. L., Trautmann, N., et al. (2018). Phenotypic characterization of P23H and S334ter rhodopsin transgenic rat models of inherited retinal degeneration. *Exp. Eye Res.* 167, 56–90. doi: 10.1016/j.exer.2017.10.023

Lee, D., Geller, S., Walsh, N., Valter, K., Yasumura, D., Matthes, M., et al. (2003). Photoreceptor degeneration in Pro23His and S334ter transgenic rats. *Adv. Exp. Med. Biol.* 533, 297–302.

Lewin, A. S., Drenser, K. A., Hauswirth, W. W., Nishikawa, S., Yasumura, D., Flannery, J. G., et al. (1998). Ribozyme rescue of photoreceptor cells in a transgenic rat model of autosomal dominant retinitis pigmentosa. *Nat. Med.* 4, 967–971.

Lin, J. H., Li, H., Yasumura, D., Cohen, H. R., Zhang, C., Panning, B., et al. (2007). IRE1 signaling affects cell fate during the unfolded protein response. *Science (New York N. Y.)* 318, 944–949. doi: 10.1126/science.1146361

Liu, Q., Qiu, J., Liang, M., Golinski, J., van Leyen, K., Jung, J. E., et al. (2014). Akt and mTOR mediate programmed necrosis in neurons. *Cell Death Dis.* 5:e1084. doi: 10.1038/cddis.2014.69

Lohr, H. R., Kuntchithapautham, K., Sharma, A. K., and Rohrer, B. (2006). Multiple, parallel cellular suicide mechanisms participate in photoreceptor cell death. *Exp. Eye Res.* 83, 380–389. doi: 10.1016/j.exer.2006.01.014

Lowe, R. J., Daniello, K. M., Duncan, J. L., Yang, H., Yasumura, D., Matthes, M. T., et al. (2019). Influence of eye pigmentation on retinal degeneration in P23H and S334ter mutant rhodopsin transgenic rats. *Exp. Eye Res.* 187:107755. doi: 10.1016/j.exer.2019.107755

Lyubarsky, A. L., and Pugh, E. N. Jr. (1996). Recovery phase of the murine rod photoresponse reconstructed from electroretinographic recordings. *J. Neurosci.* 16, 563–571.

Machida, S., Kondo, M., Jamison, J. A., Khan, N. W., Kononen, L. T., Sugawara, T., et al. (2000). P23H rhodopsin transgenic rat: correlation of retinal function with histopathology. *Investigat. Ophthalmol. Vis. Sci.* 41, 3200–3209.

Maslim, J., Valter, K., Egensperger, R., Hollander, H., and Stone, J. (1997). Tissue oxygen during a critical developmental period controls the death and survival of photoreceptors. *Investigat. Ophthalmol. Vis. Sci.* 38, 1667–1677.

Morciano, G., Giorgi, C., Balestra, D., Marchi, S., Perrone, D., Pinotti, M., et al. (2016). Mcl-1 involvement in mitochondrial dynamics is associated with apoptotic cell death. *Mol. Biol. Cell* 27, 20–34. doi: 10.1091/mbc.E15-01-0028

Morris, G., Walker, A. J., Berk, M., Maes, M., and Puri, B. K. (2018). Cell death pathways: a novel therapeutic approach for neuroscientists. *Mol. Neurobiol.* 55, 5767–5786. doi: 10.1007/s12035-017-0793-y

Nadal-Nicolas, F. M., Vidal-Sanz, M., and Agudo-Barriuso, M. (2018). The aging rat retina: from function to anatomy. *Neurobiol. Aging* 61, 146–168. doi: 10.1016/j.neurobiolaging.2017.09.021

Nikoletopoulou, V., Markaki, M., Palikaras, K., and Tavernarakis, N. (2013). Crosstalk between apoptosis, necrosis and autophagy. *Biochim. Biophys. Acta* 1833, 3448–3459. doi: 10.1016/j.bbamcr.2013.06.001

Orhan, E., Dalkara, D., Neuille, M., Lechauve, C., Michiels, C., Picaud, S., et al. (2015). Genotypic and phenotypic characterization of P23H line 1 rat model. *PLoS One* 10:e0127319. doi: 10.1371/journal.pone.0127319

Paquet-Durand, F., Sanges, D., McCall, J., Silva, J., van Veen, T., Marigo, V., et al. (2010). Photoreceptor rescue and toxicity induced by different calpain inhibitors. *J. Neurochem.* 115, 930–940. doi: 10.1111/j.1471-4159.2010.06983.x

Pennesi, M. E., Nishikawa, S., Matthes, M. T., Yasumura, D., and LaVail, M. M. (2008). The relationship of photoreceptor degeneration to retinal vascular development and loss in mutant rhodopsin transgenic and RCS rats. *Exp. Eye Res.* 87, 561–570. doi: 10.1016/j.exer.2008.09.004

Phipps, J. A., Fletcher, E. L., and Vingrys, A. J. (2004). Paired-flash identification of rod and cone dysfunction in the diabetic rat. *Investigat. Ophthalmol. Vis. Sci.* 45, 4592–4600. doi: 10.1167/iovs.04-0842

Picelli, S., Faridani, O. R., Bjorklund, A. K., Winberg, G., Sagasser, S., and Sandberg, R. (2014). Full-length RNA-seq from single cells using Smart-seq2. *Nat. Protoc.* 9, 171–181. doi: 10.1038/nprot.2014.006

Punzo, C., Kornacker, K., and Cepko, C. L. (2009). Stimulation of the insulin/mTOR pathway delays cone death in a mouse model of retinitis pigmentosa. *Nat. Neurosci.* 12, 44–52. doi: 10.1038/nn.2234

Ranjan, A., and Iwakuma, T. (2016). Non-canonical cell death induced by p53. *Int. J. Mol. Sci.* 17:68. doi: 10.3390/ijms17122068

Reers, M., Smiley, S. T., Mottola-Hartshorn, C., Chen, A., Lin, M., and Chen, L. B. (1995). Mitochondrial membrane potential monitored by JC-1 dye. *Methods Enzymol.* 260, 406–417.

Salminen, A., Kaarniranta, K., Kauppinen, A., Ojala, J., Haapasalo, A., Soininen, H., et al. (2013). Impaired autophagy and APP processing in Alzheimer's disease: the potential role of Beclin 1 interactome. *Prog. Neurobiol.* 106-107, 33–54. doi: 10.1016/j.pneurobio.2013.06.002

Salvioli, S., Maseroli, R., Pazienza, T. L., Bobyleva, V., and Cossarizza, A. (1998). Use of flow cytometry as a tool to study mitochondrial membrane potential in isolated, living hepatocytes. *Biochem. Biokhim.* 63, 235–238.

Schlicher, L., Brauns-Schubert, P., Schubert, F., and Maurer, U. (2017). SPATA2: more than a missing link. *Cell Death Different.* 24, 1142–1147. doi: 10.1038/cdd.2017.26

Seigel, G. M., Chiu, L., and Paxhia, A. (2000). Inhibition of neuroretinal cell death by insulin-like growth factor-1 and its analogs. *Mol. Vis.* 6, 157–163.

Shan, B., Pan, H., Najafov, A., and Yuan, J. (2018). Necroptosis in development and diseases. *Genes Dev.* 32, 327–340. doi: 10.1101/gad.312561.118

Sizova, O. S., Shinde, V. M., Lenox, A. R., and Gorbatyuk, M. S. (2014). Modulation of cellular signaling pathways in P23H rhodopsin photoreceptors. *Cell. Signal.* 26, 665–672. doi: 10.1016/j.cellsig.2013.12.008

Song, S., Tan, J., Miao, Y., and Zhang, Q. (2018). Crosstalk of ER stress-mediated autophagy and ER-phagy: involvement of UPR and the core autophagy machinery. *J. Cell. Physiol.* 233, 3867–3874. doi: 10.1002/jcp.26137

Steinberg, R. H., Flannery, J. G., Naash, M., Oh, P., Matthes, M. T., Yasumura, D., et al. (1996). Transgenic rat models of inherited retinal degeneration caused by mutant opsin genes. *Investigat. Ophthalmol. Vis. Sci.* 37:S698.

Stone, E. M., Kimura, A. E., Nichols, B. E., Khadivi, P., Fishman, G. A., and Sheffield, V. C. (1991). Regional distribution of retinal degeneration in patients with the proline to histidine mutation in codon 23 of the rhodopsin gene. *Ophthalmology* 98, 1806–1813. doi: 10.1016/s0161-6420(91)32046-3

Suzuki, H., Osawa, T., Fujioka, Y., and Noda, N. N. (2017). Structural biology of the core autophagy machinery. *Curr. Opin. Struct. Biol.* 43, 10–17. doi: 10.1016/j.sbi.2016.09.010

Taylor, H. R., Keeffe, J. E., Vu, H. T., Wang, J. J., Rochtchina, E., Pezzullo, M. L., et al. (2005). Vision loss in Australia. *Med. J. Austr.* 182, 565–568.

Tian, N. (2004). Visual experience and maturation of retinal synaptic pathways. *Vis. Res.* 44, 3307–3316. doi: 10.1016/j.visres.2004.07.041

Tian, N. (2008). Synaptic activity, visual experience and the maturation of retinal synaptic circuitry. *J. Physiol.* 586, 4347–4355. doi: 10.1113/jphysiol.2008.159202

Vessey, K. A., Waugh, M., Jobling, A. I., Phipps, J. A., Ho, T., Trogrlic, L., et al. (2015). Assessment of retinal function and morphology in aging Ccl2 knockout mice. *Investigat. Ophthalmol. Vis. Sci.* 56, 1238–1252. doi: 10.1167/iovs.14-15334

Viringipurampeer, I. A., Gregory-Evans, C. Y., Metcalfe, A. L., Bashar, E., Moritz, O. L., and Gregory-Evans, K. (2019). Cell death pathways in mutant rhodopsin rat models identifies genotype-specific targets controlling retinal degeneration. *Mol. Neurobiol.* 19:8. doi: 10.1007/s12035-018-1192-8

Viringipurampeer, I. A., Metcalfe, A. L., Bashar, A. E., Sivak, O., Yanai, A., Mohammadi, Z., et al. (2016). NLRP3 inflammasome activation drives bystander cone photoreceptor cell death in a P23H rhodopsin model of retinal degeneration. *Hum. Mol. Genet.* 25, 1501–1516. doi: 10.1093/hmg/ddw029

Von Eisenhart-Rothe, P., Grubman, A., Greferath, U., Fothergill, L. J., Jobling, A. I., Phipps, J. A., et al. (2018). Failure of autophagy-lysosomal pathways in rod photoreceptors causes the early retinal degeneration phenotype observed in cln6nclf mice. *Investigat. Ophthalmol. Vis. Sci.* 59, 5082–5097. doi: 10.1167/iovs.18-24757

Wang, M., Law, M. E., Castellano, R. K., and Law, B. K. (2018). The unfolded protein response as a target for anticancer therapeutics. *Critic. Rev. Oncol. Hematol.* 127, 66–79. doi: 10.1016/j.critrevonc.2018.05.003

Weymouth, A. E., and Vingrys, A. J. (2008). Rodent electroretinography: methods for extraction and interpretation of rod and cone responses. *Prog. Ret. Eye Res.* 27, 1–44. doi: 10.1016/j.preteyeres.2007.09.003

Yao, J., Qiu, Y., Frontera, E., Jia, L., Khan, N. W., Klionsky, D. J., et al. (2018). Inhibiting autophagy reduces retinal degeneration caused by protein misfolding. *Autophagy* 14, 1226–1238. doi: 10.1080/15548627.2018.1463121

Yu, D. Y., Cringle, S., Valter, K., Walsh, N., Lee, D., and Stone, J. (2004). Photoreceptor death, trophic factor expression, retinal oxygen status, and photoreceptor function in the P23H rat. *Investigat. Ophthalmol. Vis. Sci.* 45, 2013–2019. doi: 10.1167/iovs.03-0845

Zhu, Y., Misra, S., Nivison-Smith, L., Acosta, M. L., Fletcher, E. L., and Kalloniatis, M. (2013). Mapping cation entry in photoreceptors and inner retinal neurons during early degeneration in the P23H-3 rat retina. *Vis. Neurosci.* 30, 65–75. doi: 10.1017/s0952523813000047

Conflict of Interest: The authors declare that the research was conducted in the absence of any commercial or financial relationships that could be construed as a potential conflict of interest.

Copyright © 2020 Kakavand, Jobling, Greferath, Vessey, de Iongh and Fletcher. This is an open-access article distributed under the terms of the Creative Commons Attribution License (CC BY). The use, distribution or reproduction in other forums is permitted, provided the original author(s) and the copyright owner(s) are credited and that the original publication in this journal is cited, in accordance with accepted academic practice. No use, distribution or reproduction is permitted which does not comply with these terms.

frontiers in Neuroscience

REVIEW
published: 11 November 2020
doi: 10.3389/fnins.2020.570909

Optogenetic Gene Therapy for the Degenerate Retina: Recent Advances

Michelle E. McClements[1], Federica Staurenghi[1], Robert E. MacLaren[1,2] and Jasmina Cehajic-Kapetanovic[1,2]*

[1] Nuffield Laboratory Ophthalmology, Department of Clinical Neurosciences, NIHR Oxford Biomedical Research Centre, University of Oxford, Oxford, United Kingdom, [2] Oxford Eye Hospital, Oxford University Hospitals NHS Foundation Trust, Oxford, United Kingdom

The degeneration of light-detecting rod and cone photoreceptors in the human retina leads to severe visual impairment and ultimately legal blindness in millions of people worldwide. Multiple therapeutic options at different stages of degeneration are being explored but the majority of ongoing clinical trials involve adeno-associated viral (AAV) vector-based gene supplementation strategies for select forms of inherited retinal disease. Over 300 genes are associated with inherited retinal degenerations and only a small proportion of these will be suitable for gene replacement therapy. However, while the origins of disease may vary, there are considerable similarities in the physiological changes that occur in the retina. When early therapeutic intervention is not possible and patients suffer loss of photoreceptor cells but maintain remaining layers of cells in the neural retina, there is an opportunity for a universal gene therapy approach that can be applied regardless of the genetic origin of disease. Optogenetic therapy offers such a strategy by aiming to restore vision though the provision of light-sensitive molecules to surviving cell types of the retina that enable light perception through the residual neurons. Here we review the recent progress in attempts to restore visual function to the degenerate retina using optogenetic therapy. We focus on multiple pre-clinical models used in optogenetic strategies, discuss their strengths and limitations, and highlight considerations including vector and transgene designs that have advanced the field into two ongoing clinical trials.

Keywords: optogenetics, gene therapy, AAV, retinal degeneration, opsins

OPEN ACCESS

Edited by:
Jacqueline Reinhard, Ruhr-University, Germany

Reviewed by:
Jose R. Hombrebueno, University of Birmingham, United Kingdom
Ilaria Piano, University of Pisa, Italy

****Correspondence:***
Michelle E. McClements
enquiries@eye.ox.ac.uk

Specialty section:
This article was submitted to Neurodegeneration, a section of the journal Frontiers in Neuroscience

Received: *09 June 2020*
Accepted: *23 October 2020*
Published: *11 November 2020*

Citation:
McClements ME, Staurenghi F, MacLaren RE and Cehajic-Kapetanovic J (2020) Optogenetic Gene Therapy for the Degenerate Retina: Recent Advances. Front. Neurosci. 14:570909. doi: 10.3389/fnins.2020.570909

INTRODUCTION

Optogenetics is a method that allows optical control of neural circuitry by ectopic expression of light-sensitive tools in target cells (Deisseroth et al., 2006). It offers a unique opportunity to treat inherited retinal degenerations of varied genetic origins with a universal therapeutic strategy. In a degenerate retina that has lost the light-sensitive photoreceptor cells, optogenetic therapy is a promising approach that combines neurobiology and genetic engineering techniques to provide light-mediated control over the cell physiology in surviving retinal cells that are normally insensitive to light. In a pioneering study, adeno-associated viral (AAV) vector-based delivery of a transgene encoding light-sensitive protein, channelrhodopsin (ChR2), was shown to be targeted to surviving cells of the retina, whereby its ectopic expression in cellular membranes converted the

cells into artificial photoreceptors (Bi et al., 2006; Sahel and Roska, 2013). However, this landmark study highlighted several important challenges that needed to be addressed before optogenetics could be considered for human studies. The light levels needed for activation of the ChR2 sensor were very high and not encountered under normal light conditions. Thus, stimulation via external artificial light source would be necessary for this strategy to work as human therapy, but such high radiation levels are potentially toxic to the retina. In addition, being a microbial opsin, questions regarding safety and immune responses if used in humans needed to be answered. The strategy was also shown to have limited expression of the transgene in in the inner retina of a murine model of retinal degeneration and questions were raised about its translational potential when used in larger animal models and indeed human retina.

In this review we consider the multiple areas of research that have enabled development of optogenetic strategies for the treatment of inherited retinal degeneration, including vector design, transgene and opsin selection across various models of disease. Combined, the work reviewed highlight the great progress achieved in the field to date, which has led to two ongoing clinical trials with further upcoming human trials trials likely in the near future.

INHERITED RETINAL DISEASE AND THE DEGENERATE RETINA

Inherited retinal degeneration can result from different mutations in more than 300 genes (RetNet: https://sph.uth.edu/retnet/) and is the leading cause of blindness in the working age population, affecting approximately 1 in 3,000 people world-wide (Sohocki et al., 2001). Clinical trials have shown encouraging success in recent years and have primarily focused on AAV vector gene supplementation strategies for particular forms of inherited retinal disease (Bainbridge et al., 2015; Russell et al., 2017; Xue et al., 2018; Cehajic-Kapetanovic et al., 2020b). However, such therapies are suitable for only a small subset of people suffering from inherited retinal disease. Many of the identified genetic causes have very low prevalence, which makes it unfeasible to develop gene-specific treatments for all forms and yet, regardless of the differences in genetic origin, the progression of disease occurs similarly in many patients. The process of retinal degeneration in the condition retinitis pigmentosa typically involves loss of rod photoreceptor cells followed by loss of cone photoreceptor cells with subsequent migration of retinal pigment epithelium into the inner retina (**Figure 1**). A healthy retina is highly structured and enables complex interactions between multiple cell types. When there is significant loss of photoreceptor cells, which form the outer retinal layer, cells of the inner retina continue to survive but over time can undergo remodeling. This refers to a change in the normal structure of the remaining retinal layers and includes synaptic rewiring, retraction of bipolar cell dendrites and changes to protein expression patterns and trafficking (Marc et al., 2003; Puthussery et al., 2009). Despite this, residual cells have been shown to maintain key molecular signatures and morphology, suggesting the surviving retina is a receptive environment for ectopic optogene expression (Jones et al., 2003).

The pattern of retinal degeneration is common across cases of retinitis pigmentosa regardless of the genetic origin and the strategy of optogenetic therapy therefore holds great potential as a universal treatment approach. It aims to target the surviving cell populations of the retina, which remain largely functional despite the structural changes that occur (Jones et al., 2016; Pfeiffer et al., 2020) and convert them to become light-sensitive through the provision of a light-sensitive opsin protein. The disease state of a given patient will determine the cell types that would most benefit from being targeted. For example, loss of rod photoreceptors occurs before cone photoreceptor cells, which can continue to survive for some time despite changes to their structure (Milam et al., 1998; Banin et al., 1999). In this scenario, encouraging light sensitivity in these residual cell types may prove beneficial. However, it may be the case that such cells are too few in number or too diseased to function following gene therapy and therefore the secondary layer of neurons, the bipolar cells, might prove a better target. In a healthy retina, the bipolar cells transfer the light signals received from photoreceptor cells to amacrine and retinal ganglion cells (**Figure 1**). Targeting these secondary neurons may therefore provide more opportunity for visual processing via the interconnected pathways than targeting the inner most cells of the retinal ganglion layer. Finally, in some instances of severe degeneration and retina remodeling, the retinal ganglion cells may be the desired cell targets. Hence there is justification for targeting different cell types of the degenerate retina for optogenetic therapy, which will be discussed further within this review.

RELEVANT MODELS FOR OPTOGENETIC THERAPY

Developing optogenetic therapies requires pre-clinical testing in relevant *in vivo* and *ex vivo* models of inherited retinal disease (**Table 1**). The selection of model when investigating optogenetic therapies is critical to understanding their translational potential and may impact the degree of therapeutic efficacy observed. The efficacy of a particular optogenetic sensor may thus depend on the level of expression achieved in the target cell, which in turn can depend on the study model used. For example, studies with AAV-based reporter vectors indicate that cellular transduction profiles can vary depending on the mouse model used (Charbel Issa et al., 2013; van Wyk et al., 2017). Specifically, there are differences in transduction profiles achieved in healthy, wild-type retinas compared to disease models (Kolstad et al., 2010) or those with compromised barriers (Vacca et al., 2013). In addition, the stages of the disease in humans are mimicked in various animal models, both naturally occurring and transgenic in origin, and whilst preliminary data are often achieved in *rd1* mice for testing in eyes that reflect a late-stage degenerate retina, subsequent efficacy and long-term approaches may be better suited in a variety of models with different genetic origins and rates of disease. This would provide an indication on the potential and scope of optogenetic strategies, which are hoped to have universal application across

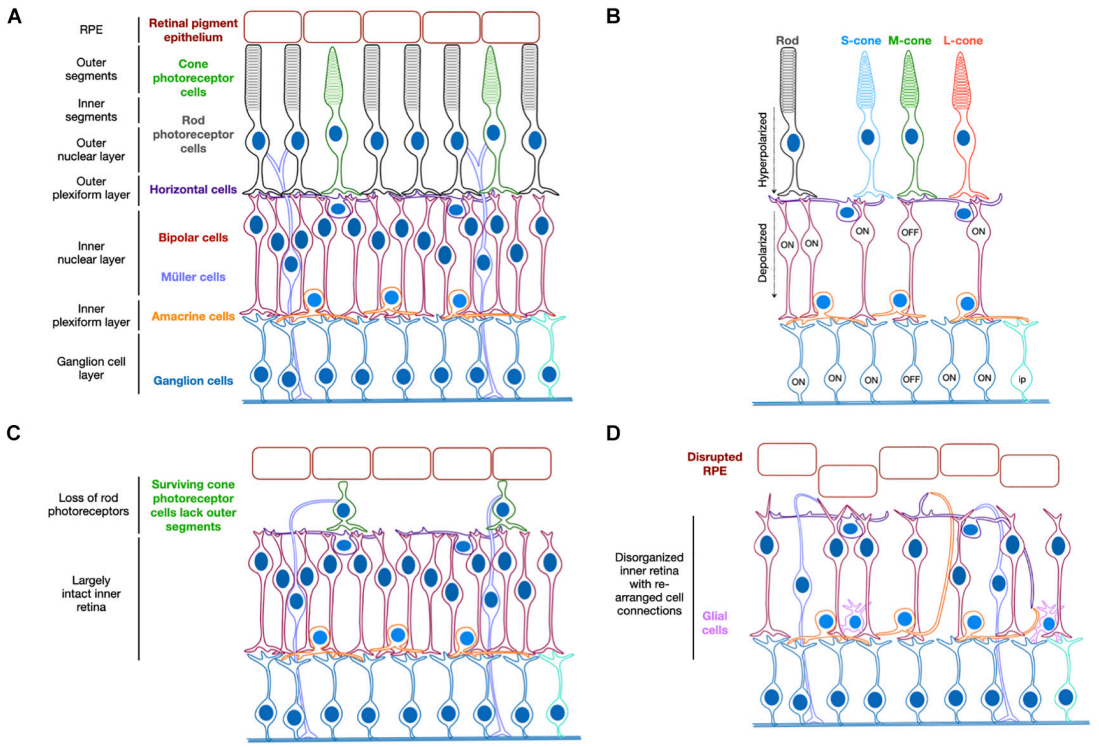

FIGURE 1 | Schematic representation of the organized structure of a healthy retina **(A)**. Light activation of opsins triggers photoreceptor hyperpolarization, which causes depolarization of ON-bipolar cells with cone OFF-bipolar cells in the same receptive field hyperpolarized. The ON-ganglion cells are subsequently activated and the OFF-ganglion cells inhibited **(B)**. Degeneration begins by loss of rod photoreceptor cells and loss of outer segments on residual cone photoreceptor cells **(C)** followed by further cell loss and structural rearrangements in later stages of disease **(D)**. S/M/L-cone = cone photoreceptor cells containing short, medium or long wavelength-sensitive opsins. Ip = intrinsically photosensitive ganglion cell.

patients with different causative mutations. The progression of retinal disease changes the global structure and function of the retina but at a cellular level, the genetic origin will impact the function of a given cell type. It may be that expanded testing across different mouse models, and indeed larger animal models, will confirm the promise of optogenetic strategies or provide evidence of preferred optogene selection for particular groups of patients. Current studies tend to be limited to testing in a single model when the scope of the field could be expanded by testing across multiple models. Different genes mean different mechanisms for disease and though the principle of optogenetics is to act as a universal approach, it needs to be confirmed that this is feasible.

COMMONLY USED MURINE MODELS OF INHERITED RETINAL DEGENERATION

The most historic model of inherited retinal disease is the naturally occurring *rd1* (Farber et al., 1994). Resulting from a mutation in the photoreceptor-specific gene *Pde6b*, this model is well characterized and displays a fast rate of degeneration in which most rod photoreceptor cells are lost by post-natal day 18 while the inner neural retinal structure is maintained with subsequent functional and morphological changes occurring over time (Strettoi et al., 2002). This rate of change is not equivalent to human disease, yet it is the most commonly used model for pre-clinical testing of optogenetic therapies. This is largely due to the fact that in a short time frame the mouse displays a retina lacking photoreceptor cells and that structurally reflects the later stages of human disease. The drawback of this rapid loss of photoreceptor cells is that it makes the *rd1* model less appropriate for testing optogenetic strategies aiming to rescue function from residual cone photoreceptor cells. Whereas cone photoreceptor cells can survive for many years following the loss of rod photoreceptor cells in human presentations of inherited retinal disease (Milam et al., 1998; Banin et al., 1999) and are therefore a potential target of optogenetic therapy, testing such an approach in *rd1* mice may be of limited use as they maintain only a single row of cone cells at 3 weeks of age. Although despite this, AAV targeting of residual cone photoreceptors with cone-specific promoters has been achieved with reporter EYFP expression observed in *rd1* mice up to 8 months of age (Busskamp et al., 2010). While residual cone photoreceptors were observed to survive in the *rd1* model, the opportunity for effective optogenetic intervention of cone photoreceptors may be greater in a slower model of degeneration. The health and function of cones in *rd1* mice may be compromised due to the early absence of rods, slower models of retinal degeneration should suffer less from these issues and

TABLE 1 | Summary of models that can be used in the pre-clinical assessment of optogenetic gene therapies.

Model	Gene	Structural changes (P = postnatal day)	Functional changes	Strengths/Limitations	Model references	Optogenetic related studies
Murine models						
Naturally occurring						
Wild-type	*e.g., C57BL/6*	Normal.	Normal.	Small ocular size with similar retinal structure and function compared to the primate retina but differing in size and inner limiting membrane thickness.	Shupe et al. (2006), Mohan et al. (2012)	Multiple studies (see main text).
Rd1	*Pde6b* Y347*	Rod photoreceptor degeneration begins at P8–P10 with complete loss by P21. Cone degeneration begins around P35 with continual loss up to P50, at which point a single row remains for up to 8 months of age.	Complete loss of scotopic ERG by P21 with loss of photopic ERG by P50.	Early onset, severe degeneration providing a model of late stage human retinal degeneration. Good for proof-of-principle assessments and for strategies aimed at end-stage disease. Offers a limited window of intervention for approaches that might be applied at earlier stages of disease and targeting residual cone photoreceptor cells.	Pittler et al. (1993), Farber et al. (1994), Hackam et al. (2004)	Multiple studies (see main text).
Rd2/rds	*Prph2* Large intron insertion leading to absence of protein	Photoreceptors lack outer segments at P7 and slow degeneration begins at P14 with complete loss of periphery at 9 months and central retina at 12 months.	ERG responses reduced but detectable with continual age-related decline and abolished by 12 months of age.	Slow, progressive rate of degeneration reflective of PRPH2 retinitis pigmentosa in humans, useful for optogenetic therapy safety and efficacy assessments in early stage retinal degeneration.	Reuter and Sanyal (1984), Jansen and Sanyal (1984), Travis and Hepler (1993), Ma et al. (1995)	Not to date.
Rd6	*Mfrp* Deletion of splice donor site and exon skipping	Subretinal deposits appear around P50. Photoreceptor degeneration occurs progressively with age with significant thinning at 7 months of age and complete loss at 24 months.	Abnormal rod and cone ERG responses are detected from P28 and show slow degeneration over time with absence of responses by P490.	Slow degeneration with limited changes to retinal structure and function with both rod and cones similarly affected. Long-term assessment of optogenetic therapy applied at an early stage of disease would require extensive aging to determine efficacy over time.	Hawes et al. (2000), Kameya et al. (2002)	Not to date.
Rd7	*Nr2e3* Deletion of exons 4 and 5	Rosette formation of the outer nuclear layer begins by P13 but these resolve over time and are not present at 16 months of age. Outer nuclear layer and outer segments show reduced thickness compared to controls.	Rod and cone responses are normal at P30 and 5 months of age. Responses reduce to ∼50% compared to controls at 16 months of age.	Slow progressive photoreceptor degeneration with unusual early structural phenotype and aged mice showing only mild retinal degeneration.	Akhmedov et al. (2000)	Not to date.
Rd8	*Crb1* c.3481delC	Shortened inner and outer segments by P14. Subretinal spots appear that represent retinal disorganization and dysplasia apparent at P35.	ERG responses are attenuated compared to controls but not significantly so and are stable up to 12 months of age at which point progressive loss in function occurs.	Unusual structural changes, including to the inner layer, not reflective of a traditional retinitis pigmentosa phenotype and with limited functional defects.	Chang et al. (2002), Mehalow et al. (2003), Aleman et al. (2011)	Not to date.
Rd9	*Rpgr* 32bp duplication in ORF15	Normal structure up to 8 weeks of age with detectable differences in outer retinal thickness up to 12 months of age.	Normal rod and cone responses at 1 month of age with gradual age-related decline, responses detectable at 24 months of age.	Slow degeneration with limited changes to retinal function. The rate of degeneration is likely too slow to be appropriate for optogenetic strategies and is not characteristic of human late stage retinal degeneration.	Thompson et al. (2012)	Not to date.

(Continued)

TABLE 1 | Continued

Model	Gene	Structural changes (P = postnatal day)	Functional changes	Strengths/Limitations	Model references	Optogenetic related studies
Rd10	*Pde6b* R560C	Rod photoreceptor degeneration begins at P18 with complete loss by P35 with subsequent cone loss. By P45 only a single layer of cone cells remain.	Reduced but measurable scotopic ERG and good photopic ERG at P14-P28 with complete loss by P60.	With an early onset but mild rate of degeneration this model is more reflective of human disease and useful for long-term assessment of safety and efficacy.	Chang et al. (2002), Gargini et al. (2007)	Doroudchi et al. (2011), van Wyk et al. (2017)
Rd12	*Rpe65* c.130C > T	Normal appearance up to P40 with outer nuclear layer structure maintained to 3 months of age, at which point clear loss of outer segments occurs plus deposits in the RPE.	Rod ERG response significantly reduced by P21 and barely detectable at 8 months of age whilst cone responses are maintained.	Slow rate of structural changes yet early onset functional changes. This model offers the potential to target residual cones in a retina reflecting earlier stages of disease. The causative gene is important in RPE function and causes LCA therefore offers a different model in which to test optogenetic therapy.	Pang et al. (2005)	Not to date.
Rd16	*Cep290* Deletion of exons 35–39	Reduced outer nuclear layer thickness at P19 with only a single layer of cone cells by P45.	Reduced rod and cone functions at P18 with absent signals by P30.	Early onset with a rate of degeneration that falls between *rd1* and *rd10*, this offers the benefits of a good window of opportunity for intervention plus reduced aging requirements for assessments of efficacy.	Chang et al. (2006)	Doroudchi et al. (2011)
(Nyx^{nob})	*Nyx* 85bp deletion	Model of congenital stationary night blindness with a non-degenerate retina.	Normal a-wave but absent b-wave.	Of limited use for optogenetic studies due to abnormal bipolar cell function.	Pardue et al. (1998), Gregg et al. (2003)	Scalabrino et al. (2015)
Transgenic						
$Cpfl1/Rho^{-/-}$	Cone photoreceptor function loss 1/rhodopsin double-knockout	Normal outer nuclear layer thickness at 3 weeks with ONL degenerating to one row of cell bodies by 10 to 12 weeks.	Loss of scotopic and photopic responses by week 12.	Good model reflecting retinitis pigmentosa through loss of photoreceptor cells whilst maintaining the inner retina and providing a good window for intervention.	Santos-Ferreira et al. (2016)	Santos-Ferreira et al. (2016)
$Opn4^{-/-}$, $Gnat1^{-/-}$, $Cnga3^{-/-}$	*Opn4, Gnat, Cnga3* triple-knockout (TKO)	Normal retinal structure is maintained but functional loss occurs.	Response to flash ERG is achieved, considered to be due to stimulated rod opsin.	Mice lack optomotor responses and pupillary constriction to light yet maintain photoreceptor cells. This is an unusual model that displays abnormal function but not degeneration.	Hattar et al. (2003), Allen et al. (2010)	Lu et al. (2020)
$Rho^{-/-}$	*Rho* Knockout	Normal outer nuclear layer thickness but an absence of outer segments at P24. Thinning begins at P30 and by P90 only a single row of cone cells remain with no outer segments.	Reduced rod responses by P24. Cone ERG maintained to P47 after which degeneration occurs.	Retinal degeneration with cone cell survival and function allowing for a big window of intervention with optogenetic therapy.	Humphries et al. (1997), Toda et al. (1999), Hassall et al. (2020)	Not to date.
$Nrl^{-/-}$	*Nrl* Knockout	Absence of rods from birth with abnormal outer nuclear layer structure at P35. Surviving cones display reduced outer segment thickness and irregular outer nuclear layer stacking.	Absence of rod ERG function by P35. Cone responses enhanced.	Unusual structural changes to the outer nuclear layer and despite cone cell survival, the phenotype is not characteristic of typical retinitis pigmentosa.	Mears et al. (2001), Daniele et al. (2005)	Not to date.
P23H/+	*Rho* Knock-in of human P23H	Reduced outer nuclear layer thickness due to loss of rods at P63 with further loss to only 2–4 rows of nuclei at P112. Cone nuclei counts equivalent to age-matched control mice.	Scotopic ERG strongly reduced at P41 and barely detectable by P170. Photopic responses normal up to P40, mildly reduced at P70 and severely reduced by P170.	Slow, progressive degeneration, reflective of human RHO P23H retinitis pigmentosa and useful for assessment of safety and efficacy of optogenetic therapy in early stage retinal degeneration.	Sakami et al. (2011)	Not to date.
$Dp71^{-/-}$	Knockout of the Duchenne muscular dystrophy small protein Dp71	Blood-retinal barrier permeability.	Slightly reduced ERG a-wave compared to WTs.	Of limited use for optogenetic strategies but useful comparisons for vector transduction studies in the presence of altered barriers.	Dalloz et al. (2003)	Vacca et al. (2013)

(Continued)

TABLE 1 | Continued

Model	Gene	Structural changes (P = postnatal day)	Functional changes	Strengths/Limitations	Model references	Optogenetic related studies
Large animal models						
Canine	e.g., Briard dog with a naturally occurring 4bp deletion in Rpe65	Progressive loss of photoreceptors over many years.	Reduced ERG.	Useful as a naturally occurring larger model of retinal degeneration.	Narfström et al. (1989), Wrigstad et al. (1992)	Ameline et al. (2017)
Non-human primates	Marmoset, Macaque	Normal.	Normal.	Useful for *in vivo* assessment of safety of optogenetic strategies with post-mortem evaluation of efficacy in the presence of pharmacological blockade of native photoreception.	Picaud et al. (2019)	Ivanova et al. (2010), Dalkara et al. (2013), Sengupta et al. (2016), Chaffiol et al. (2017), McGregor et al. (2020)
Human-based organoids and explants						
Human-derived organoids	Can be derived from iPSCs of normal controls or patients with inherited retinal disease.	Absence of outer segments when derived from normal controls.	Able to generate light-sensitive responses.	Being human-derived is advantageous to confirm efficacy of vectors in human cells but these take time to develop and convert from iPSCs (up to 200 days) and to then achieve evidence of transduction (up to 50 days), but functional outputs are possible.	Zhong et al. (2014), Reichman et al. (2017), Chichagova et al. (2019)	Gonzalez-Cordero et al. (2017), Khabou et al. (2018), Garita-Hernandez et al. (2020), Lane et al. (2020)
Human retinal explants		May be damage or scarred depending on the donor origin.		Restricted to donor availability, which may be of limited sample quality. Difficult to achieve any functional or quantitative output.	Orlans et al. (2018)	De Silva et al. (2016), van Wyk et al. (2017), Khabou et al. (2018)

The asterisk indicates a premature stop codon/termination of the protein occurs. Broadly, the assessments include optimizations of vector and transgene biology and their transduction efficiency in target retinal cells, functional assessments of optogenetic molecules, as well as general safety of optogenetic gene therapy. These considerations will in turn determine the choice of a study model, or indeed assessments across multiple models within or across species.

therefore better reflect the degenerative status of the neural retina in human patients.

The *rd10* mouse offers an alternative slower model of retinal degeneration but also results from a mutation in *Pde6b*, although in this case it is a missense mutation that enables partial activity of Pde6b (Gargini et al., 2007). Though less commonly used than the *rd1* model, optogenetic strategies have been tested in *rd10* mice (Doroudchi et al., 2011; van Wyk et al., 2017). Whilst this model presents an early onset of retinal changes, the severity of disease is reduced compared to *rd1* and the rate of progression slower, providing greater opportunity for optogenetic intervention and long-term assessment. Other models of retinal degeneration offer similar opportunities, such as the naturally occurring *rd12*, *rd16* and the transgenic models $Rho^{-/-}$, $Rho^{P23H/+}$, and $Cpfl1/Rho^{-/-}$. Consideration of the structural and functional features of retinal degeneration and the equivalent stage of human disease are important when assessing optogenetic therapy success. Another factor for consideration in pre-clinical testing in models of retinal degeneration is that one argument for use of optogenetic therapy is that the same vector may be applied to patients with various genetic origins of disease. To this end, initial testing may be best achieved in the *rd1* model with subsequent assessments performed in slower models of disease. Presentation of efficacy across different models of retinal disease would provide the strongest evidence of optogenetic success. **Table 1** includes various models used in optogenetic studies to date and other potential models that could be explored in future studies.

LARGE ANIMAL MODELS

While murine models are commonly used in pre-clinical testing, large animal models such as pigs, dogs and non-human primates, have become increasingly necessary to investigate the safety and efficacy of potential optogenetic therapies prior to use in human trials. There are several important differences in ocular anatomy and physiology that make larger animal models more advantageous (**Figure 2**). First, the ocular size in a larger model enables investigations of intraocular vector delivery and development of surgical delivery techniques that would not be possible in the much smaller murine eye. In addition, the dimensions of the canine and non-human primate eyes enable intravitreal vector delivery that would have a comparable dilution effect to the pediatric human eye. Importantly, larger animals and specifically the primate retina has a thicker inner limiting membrane, a physical barrier separating the vitreous from the neural retina. In addition, canine and primate immune responses are likely to differ from murine models. These critical inter-species differences need to be taken into consideration when developing optogenetic vectors with ability to penetrate retinal cells from the vitreous.

In contrast to non-human primates, there are naturally occurring canine models of retinal degeneration, where progressive retinal atrophy secondary to mutations in, for example, *RPE65*, *XLPRA1* or *PDE6*β genes, displays great phenotypic similarities with equivalent retinal degeneration in humans (Beltran, 2009). On the other hand, the macula is

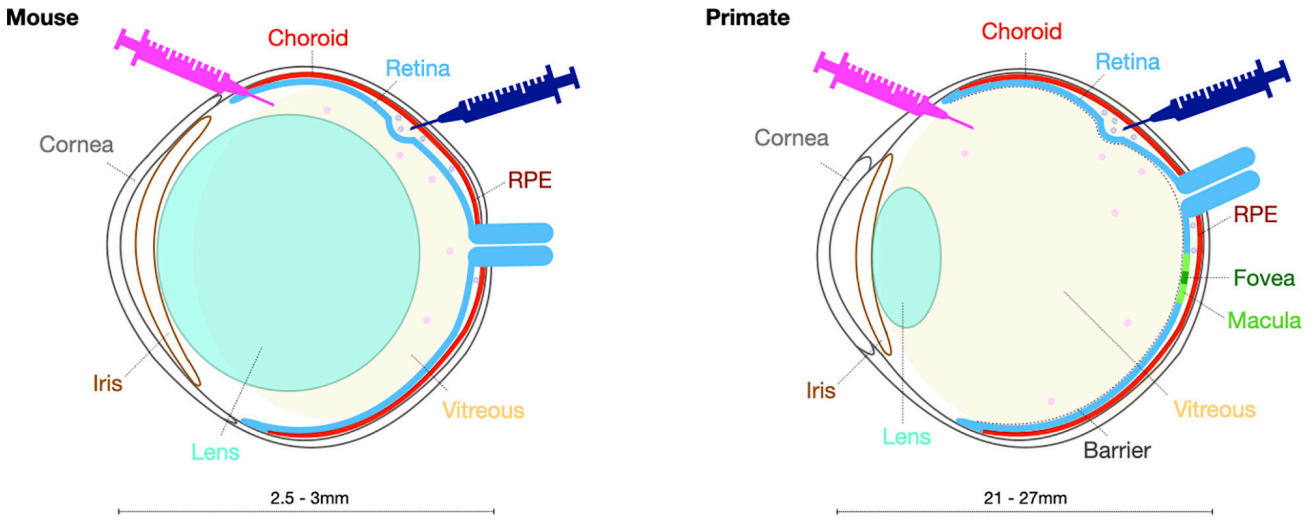

FIGURE 2 | Schematic presentation highlighting key structural differences in the mouse and primate eye to be taken into account when selecting the surgical delivery method.

only present in primates and has different cellular composition and anatomical arrangement, especially at the cone rich fovea where retinal ganglion cells and bipolar cells are displaced laterally. Canines nevertheless possess "area centralis" a central region of the retina with an increased density of cone photoreceptors. These important differences need to be considered when developing treatments for retinal degenerations that involve the macula, both in terms of cellular transduction profiles and functional assessments of ectopically expressed optogenetic molecules.

Several pre-clinical optogenetic studies have used canine and non-human primate models to assess the safety and expression profile of optogenetic vectors (Ivanova et al., 2010; Sengupta et al., 2016; Ameline et al., 2017) as well as the function and characteristics of optogenetic tools in terms of their ability to restore vision (Chaffiol et al., 2017; McGregor et al., 2020). Compared to murine models, limited *in vivo* (Ivanova et al., 2010; Chaffiol et al., 2017; McGregor et al., 2020) and *ex-vivo* (Sengupta et al., 2016) transduction of retinal ganglion cells was demonstrated in marmoset and macaque retinae, respectively, following delivery of AAV encoding microbial opsin-based sensors, with intra-ocular inflammatory responses observed in treated eyes (Chaffiol et al., 2017). In addition, despite long-term expression, similar findings of limited expression were observed in a canine model following treatment with a microbial and a human opsin (Ameline et al., 2017). Even the "state-of-the art" AAV vectors evolved for improved transduction in murine models (as will be discussed later in the review), demonstrate expression that is limited to a central para-foveal ring of retinal ganglion cells in a macaque retina following intraocular application (Dalkara et al., 2013). These results thus highlight the importance of testing optogenetic systems in primate models with outcomes most likely to mimic those of human subjects. However, these primate retinae are wild-type healthy retinae and not affected by retinal degeneration and remodeling that are likely to influence type of cell transduced and level of transgene expression within the cell. Additionally, healthy non-human primate retinae with a full set of photoreceptors make any functional electrophysiological or behavioral assessments of optogenetic therapies very challenging, although *in vitro* electrophysiology evaluation is achievable following pharmacological blockade of native photoreception (Chaffiol et al., 2017).

HUMAN-DERIVED RETINAL ORGANOIDS

Use of model organisms serve several purposes and the benefits of *in vivo* testing are many, particularly in the field of optogenetics where assessment of visual function and processing can be achieved. However, it is important to consider the benefits of other models in pre-clinical testing. In recent years, protocols for generating retinal organoids from human iPSCs have been developed, which enable formation of cultured structures derived from human cells that reflect the cell types and organization of a neural retina (Zhong et al., 2014; Reichman et al., 2017; Quinn et al., 2018). These retinal organoids provide an incredibly useful tool not only for optogenetic therapy pre-clinical testing but also in general for the field of retinal gene therapy. As described above, not all animal models replicate effectively human disease states therefore testing of gene therapy vectors can be challenging. For example, the $Rp2^{-/-}$ mouse model poorly replicates human retinal disease caused by absence of RP2 function. Generation of retinal organoids from patient-derived samples was recently described and these proved a useful *in vitro* model for assessing *RP2* gene therapy rescue (Lane et al., 2020). For optogenetic strategies, retinal organoids also provide an interesting model for pre-clinical testing. Whilst they do not perfectly replicate the neural retina, distinctive layers of different cell types have been

shown across different research groups using similar protocols (Zhong et al., 2014; Reichman et al., 2017; Quinn et al., 2018; Chichagova et al., 2019). A consistent feature across all protocols appears to be a lack of photoreceptor outer segment structures, but this does not pose a problem for testing of optogenetic vectors as indeed it mimics the absence of such structures in retinitis pigmentosa.

The initial challenge of testing any gene therapy strategy is to achieve transduction of the desired cell types. Vector tropisms and photoreceptor-specific promoters have been tested in retinal organoids (Gonzalez-Cordero et al., 2017; Garita-Hernandez et al., 2020). Current data suggest a large number of AAV capsid serotypes offer relatively poor transduction efficiencies (2–20%), including AAV2, ShH10, AAV5, AAV8, AAV8 Y733F, and AAV9 with the most encouraging variant appearing to be AAV2(7m8), achieving up to 60% transduction efficiency (Gonzalez-Cordero et al., 2017; Khabou et al., 2018; Garita-Hernandez et al., 2020). Differentiation of retinal organoids is a long process and can take up to 140 days with vector application possible during early stages of the differentiation process (Garita-Hernandez et al., 2020) or at the later stages of differentiation (Lane et al., 2020). The extensive protocols and long experimental time frames required for retinal organoid differentiation and the subsequent transduction reflect the inhibitory aspects of using these for pre-clinical testing, but the benefits of testing in human-derived samples may outweigh such issues.

A successful optogenetic strategy will depend on achieving opsin localization in the membrane of the targeted cell type whilst avoiding build-up inside the cell. It has been indicated that while delivery and expression of a variety of different microbial opsins can be achieved in retinal organoids, not all localized well to the membrane with endoplasmic reticulum accumulation and unfolded protein responses mechanisms observed (Garita-Hernandez et al., 2020). For the opsin variants that trafficked well to the membrane of targeted photoreceptor cells, functional activation was achieved. In addition, any mutagenic changes within protein structures aimed to improve functional properties of optogenetic molecules (e.g., making them more light sensitive) may have deleterious effect on protein trafficking and expression within cell membrane. In general, human cone opsin mutations can lead to accumulation within the cells and an absence of functional response (McClements et al., 2013) and rhodopsin mutations may impair folding and trafficking and lead to cell death (Athanasiou et al., 2017). While pre-clinical testing of optogenetic strategies in retinal organoids is still a relatively new technique, the data achieved so far indicate it offers an exciting addition to the development and assessment of such therapies.

HUMAN RETINAL EXPLANTS

A final model for consideration when conducting pre-clinical testing involves the use of human retinal explants. These can be obtained and cultured post-mortem (van Wyk et al., 2017; Khabou et al., 2018) or following an emergency retinectomy (De Silva et al., 2016) and may be derived from human or non-human primates (Hickey et al., 2017). Whilst useful as a screening tool to observe successful transduction of human cells, the health of such explants can be problematic and maintaining survival in culture long enough to observe successful transduction can be an issue. Additionally, the cell types that can be transduced in human retinal explants appear to be limited with no detectable expression observed in ON-bipolar cells, most likely due to downregulation of bipolar cell specific gene expression in the explant system (van Wyk et al., 2017). With human retinal explants unlikely to provide any quantitative or functional outputs following gene therapy treatment, retinal organoids may provide a more appropriate model for *in vitro* testing of optogenetic vectors.

CELL-SPECIFIC TARGETING IN THE DEGENERATE RETINA

Vector Considerations

While optogenetic strategies are not intended to be restricted by the original genetic cause of degeneration, the stage of disease will influence the type of suitable vector and hence key features of vector design. To be successful, optogenetic therapy requires expression of a light-sensitive opsin molecule in the membranes of the surviving cells of the retina and achieving this relies on efficient delivery and expression of an optogenetic transgene to target cells. AAV vectors have been the primary vector of choice over the past decade and several AAV vectors have now been used in numerous clinical trials for a wide variety of retinal diseases (Bainbridge et al., 2015; Russell et al., 2017; Xue et al., 2018; Cehajic-Kapetanovic et al., 2020b), the majority being single gene diseases. Indeed, the first approved human AAV gene therapy (Luxturna) is for the treatment of an inherited retinal disease, Leber congenital amaurosis. While systemic delivery of AAV vectors has proved more challenging and recently resulted in the tragic deaths of trial participants (Wilson and Flotte, 2020), their use in the eye has been shown to cause minimal adverse events in clinical trials (Nuzbrokh et al., 2020). While lentiviral vectors can struggle to achieve good transduction efficiency and with transgene expression typically only observed around the site of injection (Balaggan and Ali, 2012; Puppo et al., 2014), AAV delivery can achieve transduction patterns exceeding the area of the bleb (Boye et al., 2016; Yiu et al., 2020). AAV vectors also offer flexibility on the delivery route used, namely intravitreal or subretinal (**Figures 2**, **3**).

Currently, the main limitations of AAV vector use for treating inherited retinal disease appear to be their packaging capacity and ability to favor transduction of particular cell types. For optogenetic transgenes, the packaging capacity is not likely to be an issue as opsin coding sequences are relatively small compared to genes used in gene supplementation strategies, such as *RPGR* (Fischer et al., 2017). However, AAV vectors for optogenetic strategies have benefited in recent years from development of engineered capsid variants. While unnecessary for current clinical trials targeting photoreceptors or cells of the retinal pigment epithelium, for which AAV8 and AAV2 variants have proven effective (Xue et al., 2018; Cehajic-Kapetanovic et al., 2020b), the requirement of

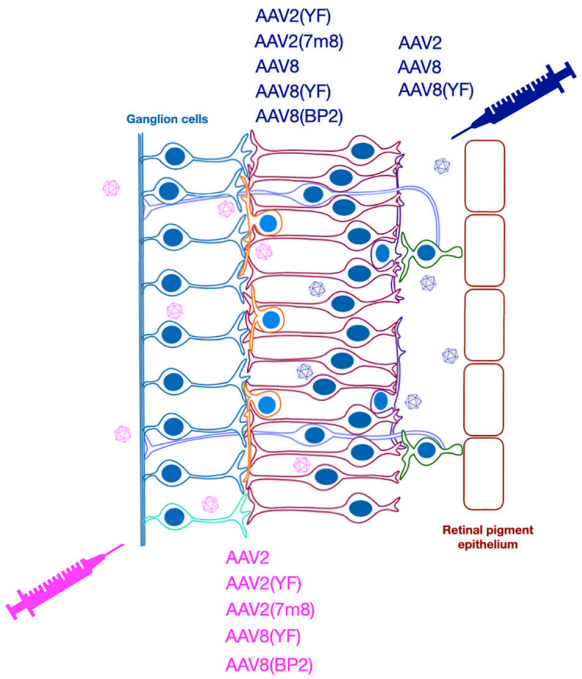

FIGURE 3 | Optogenetic strategies have used subretinal or intravitreal injection to deliver various AAV vectors for expression of different opsins.

optogenetic therapies to target residual cone photoreceptors, inner retinal layers and the outer ganglion cell layer has required investigation of new capsid variants. As previously discussed, cone photoreceptor cells can survive for many years after the loss of the rod photoreceptor cells and despite the loss of outer segments, and therefore light sensitivity (Milam et al., 1998; Banin et al., 1999), they are nevertheless considered an optogenetic target. Historically, efficient transduction in cones has proven difficult relative to rod photoreceptors (Mussolino et al., 2011; Boye et al., 2012) but recent studies with new capsid variants have increased potency (Khabou et al., 2018). Successful reporter transgene expression was shown in the cone photoreceptors of *rd10* mice as well as retinal organoids, human post-mortem explants and in non-human primates (Khabou et al., 2018). However, despite the improvements in cone photoreceptor targeting abilities for pre-clinical testing, these cell types will not be appropriate targets for all cases of late stage retinitis pigmentosa. Although the cones may survive, targeting a cell of compromised health and structure may not provide the best long-term option and indeed in some patients, they may not maintain enough surviving cones for optogenetic therapy of these cells to be worthwhile. Delivery of optogenetic transgenes to residual cone photoreceptors in *rd1* mice enabled restoration of visual function (Busskamp et al., 2010) and while this is encouraging, it should be considered that the pattern of cone density in mice is different to humans. In humans, cone photoreceptors are enriched in the macula region and reduce in density outwardly from this point, therefore targeting such cells will make use only of a small central region of the retina.

Optogenetic strategies that target the inner layer of the retina or ganglion cell layer have potential to enable a broader area of induced photosensitivity. Achieving efficient transduction of the inner retinal layers has largely relied on engineered and novel AAV capsid serotypes as opposed to wild type forms that have struggled to transduce the inner retina (Charbel Issa et al., 2013). Increased tropism and transduction success of the retinal layers has been achieved by mutation of multiple surface tyrosine (Y) residues to phenylalanine (F). While single residue Y to F changes do not effectively enable inner retinal targeting (De Silva et al., 2016), multiple residue mutations in AAV2(2–4YF) have shown more success in both in wild type mice (Petrs-Silva et al., 2011) and mice with retinal degeneration (Gaub et al., 2015). Furthermore, a directed evolution approach has created the AAV2(7m8) variant featuring a seven amino acid insertion in capsid protein VP1 (Dalkara et al., 2013). The AAV2(4YF) and AAV2(7m8) variants provided similar transduction profiles when directly compared following subretinal and intravitreal injection in the *rd1* mouse and included transduction of the inner retina (Hickey et al., 2017). However, expression in bipolar cells was not robust, indicating that while successful, further improvements in transduction may be required.

A particularly promising AAV capsid option for optogenetic approaches targeting the inner retina is the AAV8(BP2) variant. This was created by directed selection of a library of AAV8 capsid mutants focused on a variable region of nine amino acids, considered important for receptor attachment and transduction (Cronin et al., 2014). This AAV8(BP2) capsid provided good transduction of ON-bipolar cells, including limited expression in non-diseased human retinal explants with a strong pan-neuronal CMV promoter. This was the first demonstration of robust bipolar cell transduction from an AAV vector but transduction in a wild type mouse does not necessarily translate to degenerate retina or indeed non-human primate and human retina. Further confirmation of human bipolar cell transduction was provided in a later study using human retinal explants that also showed targeting of cone ON-bipolar cells by a reporter AAV8(BP2) vector (van Wyk et al., 2017). This study showed comparable human bipolar cell expression patterns were achieved from both AAV8(BP2) and AAV2(7m8) vectors and also performed similarly in the degenerate 11-week-old *rd10* mice. Such developments in capsids have advanced the potential of optogenetic strategies by enabling transduction in bipolar cells.

Transduction of the innermost layer of the retina, the retinal ganglion cells has been readily achieved in mouse models following intravitreal injection (Yin et al., 2011; Smith and Chauhan, 2018). Wild type AAV capsid transduction appears limited to the retinal ganglion cells unless applying an additional adjunctive (Cehajic-Kapetanovic et al., 2011, 2018) whereas modified AAV capsids penetrate further following intravitreal injection into the inner retina (Kay et al., 2013; Hickey et al., 2017; van Wyk et al., 2017).

Transgene Considerations

While the first hurdle in any gene therapy strategy is getting the AAV to enter the desired cell type, transgene design can influence the success of subsequent expression. In addition to

being difficult to target with AAV, cone photoreceptor cells have also proved difficult in the development of efficient cell-specific promoters (Li et al., 2008) but the development of a 1.7kb version of the human red/green cone opsin promoter, known as PR1.7, was shown to achieve robust and selective expression in cone photoreceptor cells (Ye et al., 2016; Khabou et al., 2018). Utilizing the AAV2(7m8) capsid and an intravitreal injection route, the latter research group found the PR1.7 promoter to be more specific than the mouse cone arrestin (mCAR) promoter, which resulted in expression in both rod and cone photoreceptor cells. Cell-specific promoters are often considered to pose a risk in gene therapy strategies in case of changes in gene expression profiles in degenerating cells. This may be particularly concerning for optogenetic strategies targeting residual cone photoreceptor cells, which have a changing profile of expression, function and morphology over time (Hassall et al., 2020). Despite these concerns, successful expression from the PR1.7 promoter was observed 2 months post-injection in *rd10* mice though how this might translate to humans should be approached with caution.

Following loss of photoreceptors in the degenerating retina, the secondary neurons of the retina, the horizontal and the bipolar cells are considered as the next best option for optogenetic approaches. Transducing the distal retinal circuitry has greater chance of preserving upstream retinal processing, and the ON-bipolar cell-specific expression is thought to be particularly important in achieving this. In a normal retina, the bipolar cells transfer the light signals received from photoreceptor cells to amacrine and retinal ganglion cells (**Figure 1**). Morphological comparisons have determined there to be just one rod-bipolar cell type but multiple cone-bipolar cell types (Wässle et al., 2009) and these fall into two broad functional categories of ON (rod and cone) and OFF (cone only) (Nelson and Connaughton, 2007). The ON-bipolar cells are depolarized by light-stimulated photoreceptor cells whilst OFF-bipolar cells are hyperpolarized in the same receptive field. Selective expression of opsins in ON-bipolar cells is considered important to avoid interfering with the complex interconnected signaling pathways of the remaining neural retina. Making both ON- and OFF-bipolar cells respond to light in the same way could result in ambiguous signals, although cortical plasticity could play a role in filtering out the noise, as seen with subretinal implants (Cehajic-Kapetanovic et al., 2020a). A combination of effective AAV transduction and promoter for selective expression of opsins in ON-bipolar cells are therefore highly desirable features of optogenetic therapies.

To date, *4xGrm6-SV40* is the most studied promoter for optogenetic strategies aiming to achieve opsin expression in ON-bipolar cells. The metabotropic glutamate receptor type 6 (mGluR6) receptor was found to be associated with ON-bipolar cell activity (Nakajima et al., 1993; Nomura et al., 1994). A critical 200bp enhancer region in the mouse *Grm6* gene that encodes mGluR6 was subsequently paired with the SV40 promoter to achieve ON-bipolar cell specific expression of a reporter gene (Kim et al., 2008). This has since been used with success by other research groups in their optogenetic approaches (Lagali et al., 2008; Doroudchi et al., 2011; Cehajic-Kapetanovic et al., 2015; Macé et al., 2015). A comparison of multiple copies of the *Grm6* enhancer identified that including four copies prior to the SV40 promoter improved reporter gene expression (Cronin et al., 2014). Whilst this promoter has been shown to primarily enable transgene expression in ON-bipolar cells, expression has been identified in other cell types (van Wyk et al., 2015, 2017). The expression profile of an optogenetic transgene with fluorescent reporter revealed predominant expression in amacrine cells and a lack of ON-bipolar cell targeting in *rd1* mice. In wild type mice, amacrine cells were also the most targeted cell type when using the AAV2(7m8) yet when the AAV8(BP2) capsid was used, multiple cell types revealed reporter transgene expression, including ON-bipolar cells. Interestingly, a similar expression profile was then observed in *rd10* mice yet not in *rd1* mice, even when injected at earlier age. This highlights the consideration raised earlier regarding the need to use multiple models of retinal degeneration when assessing a given optogenetic therapy. Furthermore, the difference in expression profile from a given promoter varies between mouse models and is to an extent dependent on other vector selections, such as the capsid.

Use of an extended *mGluR6* promoter containing additional intronic sequence enabled enhanced reporter gene expression in ON-bipolar cells in mice and non-human primates (Lu et al., 2016). However, this promoter variant is considerably longer than the commonly used variant and therefore potentially less desirable as this can be limiting to transgene design. Transgenes for AAV vectors cannot exceed the packaging capacity of AAV, which is typically ∼4.8 kb. The majority of opsin coding sequences are relatively small (∼2 kb) enabling room for a larger promoter. However, other transgene elements may be desirable to enhance expression, such as inclusion of a WPRE (Patrício et al., 2017) or fluorescent marker to create a fusion protein. Additional membrane trafficking signals may also be required (discussed later within opsin considerations). Therefore, the larger *mGluR6* promoter may not prove to be a limiting factor in its future use in optogenetic transgenes but it will be dependent on other factors of transgene design that may prove critical for a given optogenetic strategy.

A mini-promoter named Ple155 (derived from the *PCP2* gene) has also been shown to provide ON-bipolar cell expression in wild-type mice (De Leeuw et al., 2014) and was used to restore vision in a mouse model ($Nyx^{-/-}$) of congenital stationary night blindness and non-degenerated retina (Scalabrino et al., 2015). Whilst the $Nyx^{-/-}$ mouse model is not of relevance to optogenetic strategies, *NYX* is a bipolar cell-specific gene and is therefore of interest in its use as an alternative ON-bipolar specific promoter. Interestingly, ON-bipolar cell specific expression was achieved only when using the Ple155 promoter in combination with an AAV2 (and not AAV8) vector and only in very young mice (at P2 and not at P30) with undifferentiated bipolar cells. It therefore remains to be seen whether the Ple155 promoter offers any advantage in ON-bipolar cell targeting over the *4xGrm6-SV40* in degenerate retina and whether ON-bipolar cell transduction can be achieved with either promoter in non-human primate or indeed in human retina.

Targeting of bipolar cells may be preferable in the earlier stages of retinal degeneration but in later stages of disease, these cells can become disordered and also degenerate (Pfeiffer et al., 2020).

These changes include alterations in the neural connections made between cell types of the neural retina structure but also their morphology and general structural layout, **Figure 1**. Not all patients will present in clinics at the earlier stages of disease, therefore some optogenetic approaches aim to target the retinal ganglion cells, which remain most resistant to degeneration retaining their physiological properties and laminar location in the retina. In mouse models, this is achieved relatively easily with multiple AAV serotypes by intravitreal injection and gene expression can be restricted using the synapsin-1 promoter (*Syn1*) (Sengupta et al., 2016) or the neurofilament heavy polypeptide promoter (*Nefh*) (Hanlon et al., 2017). Given the preference for transduction of ganglion cells when using the intravitreal injection route, ubiquitous promoters have also been used with success (Bi et al., 2006; Bin Lin et al., 2008; Zhang et al., 2009; Liu et al., 2016). However, the risks of introducing light-sensitive responses to more than one cell type are currently unknown and may interfere with the interconnectivity of the complex neural circuits of the retina.

OPSINS FOR OPTOGENETIC THERAPY

The opsins used for optogenetic approaches include both microbial and vertebrate varieties (**Figure 4**). These have different characteristics and vary in many ways including their sensitivity to light, recovery rates and in the type of response they elicit (Simon et al., 2020). Opsins are transmembrane proteins that absorb light and in the case of vertebrate opsins, they are G-protein coupled receptors whose activation leads to cGMP-gated cation channels closing and a subsequent hyperpolarization of the photoreceptor cell (**Figure 4**). In contrast, microbial opsins are light-activated ion channels rather than G-protein coupled receptors that can cause depolarization or hyperpolarization depending on the nature of the ion channel. It is for this reason that the microbial opsins have proven popular for optogenetic strategies as they can directly influence the cell polarization in response to light without the need for other G-protein cascade elements. This may prove important in successfully converting cells that were not intended to be light sensitive.

Opsin selection requires consideration of various factors related to opsin function, including the conductance rate and ion selectivity. For example, microbial opsins exhibit differences in their conductance of cations or anions and in the rate of ion influx achieved upon light activation. Considerations of opsin kinetics are also important as the timing of a channel opening and closing to enable ion influx will influence the extent of a response. Opsins differ in the intensity of the light required to induce a response and the peak wavelength of light they respond to (**Figure 4**). The intensity of light necessary to induce stimulation is of particular safety importance as the retina can be damaged by certain light intensities and wavelengths (Youssef et al., 2011). Natural light provides a general exposure range of 10^{-4} to 10^{5} lux and safety thresholds for humans have been defined (The European Parliament and the Council of the European Union, 2006; ICNIRP, 2013; van Norren and Vos, 2015) therefore an optogenetic therapy would need to be successful within these limits. The position of the opsin is also critical in order to be optimally exposed to the light source and in a great enough proportion to achieve an appropriate response without inducing membrane instability or overexpression. Finally, opsins can suffer desensitization, in which they become less responsive to light after repeated stimulation and therefore require recovery time prior to their next light-activation. This is also referred to as bleaching and opsins vary in the extent to which they suffer and recover from this process, for example, rhodopsin of the rod photoreceptors is particularly susceptible and suffers reduced phototransduction capacity following exposure to bright light (Pepperberg, 2003). These features are all important considerations and will be referred to throughout the following discussion of opsin candidates for optogenetic therapeutic approaches.

MICROBIAL OPSINS

The first microbial opsin identified for use as an optogenetic tool was channelrhodopsin-2 (ChR2) (Boyden et al., 2005), which causes entry of cations into the cell resulting in depolarization. It has been the most commonly used microbial opsin to date and is induced by blue light (470 nm). It was used in the first pre-clinical optogenetic strategy for rescuing visual function to the *rd1* mouse (Bi et al., 2006) and a subsequent humanized version (containing an H143R mutation) fused to GFP has been stably expressed using the *Grm6-SV40* promoter in *rd1* mice following subretinal

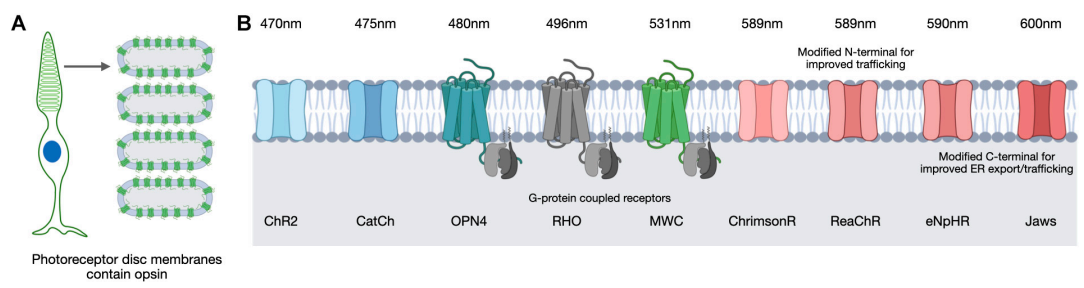

FIGURE 4 | In the human retina, light-sensitive opsins for vision are located in the photoreceptor cells on the membranes of specialized discs **(A)**. Optogenetic strategies use multiple opsin variants of microbial and vertebrate origin that are sensitive to different peak wavelengths **(B)**. Images created using BioRender.com.

injection (Doroudchi et al., 2011) and intravitreal injection (Macé et al., 2015). In the latter approach, both ON and OFF visual responses were detected at 4–10 weeks post-injection, indicating its potential for optogenetic therapy.

An engineered variant of ChR2 carrying an L132C mutation was developed and named CatCh as it is a calcium translocating channelrhodopsin and has nearly six-fold enhanced Ca^{2+} permeability relative to ChR2, which improved its sensitivity to light and kinetics (Kleinlogel et al., 2011). An optogenetic transgene containing an EGFP fusion of this protein was expressed in ON-bipolar cells in *rd1* mice and incurred light-induced ganglion cell responses 4 weeks post-injection (Cronin et al., 2014). A red-light activated depolarizing ChR (ReaChR) was generated with a peak spectral sensitivity of 590nm and this ReaChR included an *N*-terminal sequence to aid membrane trafficking (Lin et al., 2013). When expressed specifically in retinal ganglion cells using the *SYN1* promoter following AAV2 intravitreal delivery in *rd1* mice, visual and behavioral responses to light were observed at light intensities within safety thresholds (Sengupta et al., 2016). An algal-derived variant similar to ReaChR is ChrimsonR (Klapoetke et al., 2014). Comparisons of ReaChR and ChrimsonR localization and function in human retinal organoids revealed better trafficking of ReaChR to the cell membrane than ChrimsonR but both provided detectable responses to light stimulation (Garita-Hernandez et al., 2018). Despite the reduced trafficking efficiency, ChrimsonR did not accumulate excessively in the cell organelles or co-localize with markers of endoplasmic reticulum retention or the unfolded protein response.

Other microbial opsins being used for optogenetic strategies are light-activated hyperpolarizing chloride pumps, of which halorhodopsin (NpHR) was the first to be reported and is sensitive to yellow light (Zhang et al., 2007). Hyperpolarizing opsins are of particular interest in optogenetic strategies targeting surviving cone photoreceptor cells, which as described above, can continue to exist in a dormant state in the degenerate retina despite loss of cone-mediated light responses (Lin et al., 2009; Busskamp et al., 2010). NpHR has a peak wavelength sensitivity of 589 nm and light activation leads to hyperpolarization of the cell, mimicking the native response of a photoreceptor cell. However, this protein was found to accumulate and form unwanted aggregates when expressed at high levels (Gradinaru et al., 2007) so an enhanced version, eNpHR, was created (Gradinaru et al., 2008). The addition of an *N*-terminal signal peptide and a *C*-terminal endoplasmic reticulum export signal improved the membrane localization of this hyperpolarizing opsin. AAV delivery of eNpHR using photoreceptor-specific promoters achieved electrophysiological responses to light in *rd1* mice equivalent to those in wild type mice (Busskamp et al., 2010). Further improvements to eNpHR were made by way of additional trafficking signals to provide variant eNpHR 3.0 (Gradinaru et al., 2010).

Despite the addition of these signals, testing *in vitro* did not reveal membrane localization, however, testing in human retinal organoids did achieve membrane localization and subsequent light responses (Garita-Hernandez et al., 2018). However, despite the addition of export and localization signals, these comparisons in human retinal organoids indicated the hyperpolarizing opsin Jaws showed better membrane localization relative to eNpHR 3.0. Jaws is an engineered chloride pump cruxhalorhodopsin that is red-shifted by 14 nm relative to the eNpHR variants and therefore has a peak sensitivity of 600 nm (Chuong et al., 2014). AAV delivery in *rd1* mice of a Jaws transgene driven by the mCAR promoter achieved expression 4 weeks post-injection and achieved spike responses from isolated ON- and OFF-retinal ganglion cells following light stimulation at 600 nm (Chuong et al., 2014). It was also observed that responses could be achieved from 550 nm (green) and 470 nm (blue) wavelengths and that Jaws provided more retinal ganglion cell spiking than eNpHR over a broader light spectrum, which suggest Jaws may be more suitable for use in human optogenetic therapy.

The eNpHR 2.0 variant has been used in combination with a human rhodopsin promoter to achieve expression in rod photoreceptors of wild type mice, which were then harvested and the eNpHR 2.0-expressing rod photoreceptor cells subsequently isolated and injected into *Cpfl1/Rho*$^{-/-}$ female mice (Garita-Hernandez et al., 2019). Responses to 580 nm light were achieved as were spike recordings of ON- and OFF-retinal ganglion cells, indicating connections were made between the transplanted cells and the surviving secondary neurons of the host retina. Encouragingly, light intensities within the safe limits defined for the human eye successfully stimulated responses and light avoidance behavior in treated mice was also observed. This same study also induced Jaws expression from the mCAR promoter in human iPSC-derived cone photoreceptor cells, which were then injected into *Cpfl1/Rho*$^{-/-}$ and *rd1* mice. Robust photocurrents were achieved, which peaked when stimulated with a wavelength of 575 nm. As for eNpHR stimulation, responses were achieved from light intensities below safety thresholds and both ON- and OFF-retinal ganglion cell responses were achieved. Jaws has also been shown to have good membrane localization in cone photoreceptor cells of non-human primates following delivery of an AAV9(7m8) vector with the PR1.7 promoter (Khabou et al., 2018). These studies highlight the potential for both eNpHR and, in particular, Jaws to be used in future human clinical trials for optogenetic stimulation of residual cone cells.

VERTEBRATE OPSINS

Despite the encouraging data from studies using microbial opsins use of a native human opsin may be more desirable as it poses less risk of immune reaction. Both human and mouse retinal cells produce five main opsin variants that respond to different wavelengths of light: rhodopsin, expressed by rod photoreceptor cells (RHO); short-wave cone opsin (SWC), medium-wave cone opsin (MWC), and long-wave cone opsin (LWC), expressed by cone photoreceptor cells; and finally, melanopsin (OPN4). This latter opsin is not essential for vision but instead is an important sensor for the circadian clock and is expressed by a sub-population of intrinsically photosensitive

retinal ganglion cells (ipRGCs). One of the first optogenetic studies to use a native opsin for pre-clinical testing in *rd1* mice boosted the melanopsin expression with rescue of basic visual functions (Bin Lin et al., 2008). Subsequently, human melanopsin expression in cells of the inner retina of *rd1* mice has also been achieved (Bin Lin et al., 2008; Liu et al., 2016; De Silva et al., 2017). These studies reported greater light sensitivity compared to the microbial opsins with rescue of visual responses achieved up to 12 months post-injection (De Silva et al., 2017). A further study created a chimera of mouse melanopsin and the mGluR6 receptor, Opto-mGluR6, under the control of the *Grm6-SV40* promoter in order to test the melanopsin kinetics in ON-bipolar cells in a transgenic mouse model (van Wyk et al., 2015). Encouragingly, transduction of only a small fraction of ON-bipolar cells (∼12%) using AAV2(4YF) vector delivery, was sufficient to induce light responses in retinal ganglion cells.

Success in restoring responses to light in the degenerate retina with human opsins have also been achieved with ectopic expression of native rod opsin, rhodopsin. Intravitreal delivery of AAV2 achieved human rhodopsin expression in ON-bipolar cells of *rd1* mice and improved visual and behavioral responses 8–12 weeks post-injection including resolution of flicker, coarse spatial patterns and elements of natural scene (Cehajic-Kapetanovic et al., 2015; Eleftheriou et al., 2017). Encouraging data were also achieved with the same transgene in *rd1* mice but using an AAV2(4YF) vector (Gaub et al., 2015). The responses of rhodopsin-treated mice were compared to those treated with an identical vector delivering humanized ChR2, and rhodopsin was found to offer greater and more sensitive responses than ChR2. The same study group recently expressed vertebrate MWC in the retinal ganglion cells of *rd1* mice (Berry et al., 2019) with behavioral tests showing signs of functional rescue. The speed and sensitivity of response to light of MWC was improved compared to rhodopsin function in ganglion cells, but it remains to be seen how the function of cone photopigments compares to rhodopsin kinetics in ON-bipolar cells. Ultimately, human trials are needed to determine how these ectopically expressed human opsins compare to visual function achieved by native rod and cone opsins in photoreceptor cells.

DISCUSSION

The pre-clinical work to date demonstrates that optogenetic strategies are able to restore vision to the degenerate retina using a multitude of transgene and vector combinations. Development of new capsid varieties has greatly aided transduction success of the inner retina and improved cell-specific expression profiles. Progress has been made in understanding visual and behavioral responses following delivery of a wide variety of opsins in various cell types of the surviving retina in animal models. The major barrier to translation of many of these optogenetic therapies has been the lack of evidence of efficient optogene expression in healthy non-human primate, or indeed degenerate human retina, using the available tools.

None-the-less, both ChR2 and ChrimsonR are currently being tested in Phase I/IIa clinical trials. The NCT02556736 trial describes delivering ChR2 primarily to retinal ganglion cells using AAV2 intravitreal injection in patients with advanced retinitis pigmentosa. This trial was initiated by Retrosense Therapeutics (now part of Allergan) and is an open-label, dose escalation study that began recruiting in 2015 but to date, no data have been released. A more recent trial initiated by GenSight Biologics in 2017 (NCT03326336) also involves intravitreal delivery but of an AAV2(7m8) vector aiming to express the ChrimsonR-tdTomato fusion protein. This PIONEER trial by GenSight is not only of interest because it is the first to use the capsid variant AAV2(7m8) for expression of ChrimsonR-tdTomato, but also because it combines the gene therapy with a specialized wearable visual stimulation device. Given the considerations discussed earlier in this review regarding the microbial opsins, the selection of ChrimsonR instead of ChR2 offers a safer and potentially more sensitive opsin than the first trial using ChR2. The inclusion of tdTomato is intriguing as this is a fluorescent marker used to confirm transgene expression and provides no functional benefit. Typically, such markers are used for pre-clinical studies and are then removed prior to use in human clinical trials. In this particular study design, the confirmation of ChrimsonR expression by detection of tdTomato enables researchers to be confident successful transduction has occurred and that the visual stimulation device can subsequently be used. This is an interesting step forward in gene therapy transgene design for human clinical trials and it may be that such implementation of fluorescent reporters may be used more often in the future. However, caution should always be applied in expressing proteins in human cells if they are not necessarily required to achieve a therapeutic outcome. This year, press releases of preliminary clinical trial safety data have also been provided, suggesting good tolerance of the vector so far (gensight-biologics.com). However, it remains to be seen what the long-term effects of expressing an algal-derived protein on the membranes of retinal cells are and whether these may be detected by the immune system and therefore lead to an undesired immune response against the transgene product. It is clear though that the current dose-escalation study is a vital step forward in providing such treatments to individuals with severe retinal degeneration and limited light perception.

Given the limited light sensitivity of current microbial opsins, the need for an additional device and the potential for immune responses triggered by foreign proteins, it could be that future therapies with human opsins provide a better opportunity for success. It is worth noting that Acucela Inc (now Kubota Vision) are currently developing human rhodopsin optogenetic therapy as are Applied Genetic Technologies Corporation (AGTC) in collaboration with Bionic Sight but the details of the latter treatment are currently unavailable.

In summary, studies to date indicate optogenetic therapies show great therapeutic potential for restoring vision in patients with advanced inherited retinal disease and more human trials are necessary as the next major step in advancing the field. It remains to be seen how the human visual system, affected

by degeneration and remodeling, responds to optogenetic stimulation at the level of retinal photoreception and by means of cortical plasticity for improved and meaningful visual perception.

AUTHOR CONTRIBUTIONS

MM drafted, edited, and created figures for the manuscript. FS reviewed and edited the manuscript. RM provided funding and critical review of the manuscript. JC-K initiated the manuscript and provided critical review. All authors contributed to the article and approved the submitted version.

FUNDING

This work was funded by the NIHR Oxford Biomedical Research Centre.

REFERENCES

Akhmedov, N. B., Piriev, N. I., Chang, B., Rapoport, A. L., Hawes, N. L., Nishina, P. M., et al. (2000). A deletion in a photoreceptor-specific nuclear receptor mRNA causes retinal degeneration in the rd7 mouse. *Proc. Natl. Acad. Sci. U.S.A.* 97, 5551–5556. doi: 10.1073/pnas.97.10.5551

Aleman, T. S., Cideciyan, A. V., Aguirre, G. K., Huang, W. C., Mullins, C. L., Roman, A. J., et al. (2011). Human CRB1-associated retinal degeneration: comparison with the rd8 Crb1-mutant mouse model. *Invest. Ophthalmol. Vis. Sci.* 52, 6898–6910. doi: 10.1167/iovs.11-7701

Allen, A. E., Cameron, M. A., Brown, T. M., Vugler, A. A., and Lucas, R. J. (2010). Visual responses in mice lacking critical components of all known retinal phototransduction cascades. *PLoS One* 5:e15063. doi: 10.1371/journal.pone.0015063

Ameline, B., Tshilenge, K.-T., Weber, M., Biget, M., Libeau, L., Caplette, R., et al. (2017). Long-term expression of melanopsin and channelrhodopsin causes no gross alterations in the dystrophic dog retina. *Gene Ther.* 24, 735–741. doi: 10.1038/gt.2017.63

Athanasiou, D., Aguila, M., Bellingham, J., Li, W., McCulley, C., Reeves, P. J., et al. (2017). The molecular and cellular basis of rhodopsin retinitis pigmentosa reveals potential strategies for therapy. *Prog. Retinal Eye Res.* 17, 1–84. doi: 10.1016/j.preteyeres.2017.10.002

Bainbridge, J. W. B., Mehat, M. S., Sundaram, V., Robbie, S. J., Barker, S. E., Ripamonti, C., et al. (2015). Long-term effect of gene therapy on leber's congenital amaurosis. *Engl. J. Med.* 372, 1887–1897. doi: 10.1056/NEJMoa1414221

Balaggan, K. S., and Ali, R. R. (2012). Ocular gene delivery using lentiviral vectors. *Gene Ther.* 19, 145–153. doi: 10.1038/gt.2011.153

Banin, E., Cideciyan, A. V., Aleman, T. S., Petters, R. M., Wong, F., Milam, A. H., et al. (1999). Retinal rod photoreceptor-specific gene mutation perturbs cone pathway development. *Neuron* 23, 549–557. doi: 10.1016/s0896-6273(00)80807-7

Beltran, W. A. (2009). The use of canine models of inherited retinal degeneration to test novel therapeutic approaches. *Vet. Ophthalmol.* 12, 192–204. doi: 10.1111/j.1463-5224.2009.00694.x

Berry, M. H., Holt, A., Salari, A., Veit, J., Visel, M., Levitz, J., et al. (2019). Restoration of high-sensitivity and adapting vision with a cone opsin. *Nat. Commun.* 10, 1–12. doi: 10.1038/s41467-019-09124-x

Bi, A., Cui, J., Ma, Y.-P., Olshevskaya, E., Pu, M., Dizhoor, A. M., et al. (2006). Ectopic expression of a microbial-type rhodopsin restores visual responses in mice with photoreceptor degeneration. *Neuron* 50, 23–33. doi: 10.1016/j.neuron.2006.02.026

Bin Lin, Koizumi, A., Tanaka, N., Panda, S., and Masland, R. H. (2008). Restoration of visual function in retinal degeneration mice by ectopic expression of melanopsin. *Proc. Natl. Acad. Sci. U.S.A.* 105, 16009–16014. doi: 10.1073/pnas.0806114105

Boyden, E. S., Zhang, F., Bamberg, E., Nagel, G., and Deisseroth, K. (2005). Millisecond-timescale, genetically targeted optical control of neural activity. *Nat. Neurosci.* 8, 1263–1268. doi: 10.1038/nn1525

Boye, S. E., Alexander, J. J., Boye, S. L., Witherspoon, C. D., Sandefer, K., Conlon, T., et al. (2012). The human rhodopsin kinase promoter in an AAV5 vector confers rod and cone specific expression in the primate retina. *Hum. Gene Ther.* 23, 1101–1115. doi: 10.1089/hum.2012.125

Boye, S. E., Alexander, J. J., Witherspoon, C. D., Boye, S. L., Peterson, J. J., Clark, M. E., et al. (2016). Highly efficient delivery of adeno-associated viral vectors to the primate retina. *Hum. Gene Ther.* 27, 580–597. doi: 10.1089/hum.2016.085

Busskamp, V., Duebel, J., Balya, D., Fradot, M., Viney, T. J., Siegert, S., et al. (2010). Genetic reactivation of cone photoreceptors restores visual responses in retinitis pigmentosa. *Science* 329, 413–417. doi: 10.1126/science.1190897

Cehajic-Kapetanovic, J., Eleftheriou, C., Allen, A. E., Milosavljevic, N., Pienarr, A., Bedford, R., et al. (2015). Restoration of vision with ectopic expression of human rod opsin. *Curr. Biol.* 25, 2111–2122. doi: 10.1016/j.cub.2015.07.029

Cehajic-Kapetanovic, J., Le Goff, M. M., Allen, A., Lucas, R. J., and Bishop, P. N. (2011). Glycosidic enzymes enhance retinal transduction following intravitreal delivery of AAV2. *Mol. Vis.* 17, 1771–1783.

Cehajic-Kapetanovic, J., Milosavljevic, N., Bedford, R. A., Lucas, R. J., and Bishop, P. N. (2018). Efficacy and safety of glycosidic enzymes for improved gene delivery to the retina following intravitreal injection in mice. *Mol. Ther. Methods Clin. Dev.* 9, 192–202. doi: 10.1016/j.omtm.2017.12.002

Cehajic-Kapetanovic, J., Troelenberg, N., Edwards, T. L., Xue, K., Ramsden, J. D., Stett, A., et al. (2020a). Highest reported visual acuity after electronic retinal implantation. *Acta Ophthalmol.* 43, 1–5. doi: 10.1111/aos.14443

Cehajic-Kapetanovic, J., Xue, K., La Camara De, C. M.-F., Nanda, A., Davies, A., Wood, L. J., et al. (2020b). Initial results from a first-in-human gene therapy trial on X-linked retinitis pigmentosa caused by mutations in RPGR. *Nat. Med.* 26, 354–359. doi: 10.1038/s41591-020-0763-1

Chaffiol, A., Caplette, R., Jaillard, C., Brazhnikova, E., Desrosiers, M., Dubus, E., et al. (2017). A new promoter allows optogenetic vision restoration with enhanced sensitivity in macaque retina. *Mol. Ther.* 25, 2546–2560. doi: 10.1016/j.ymthe.2017.07.011

Chang, B., Hawes, N. L., Hurd, R. E., Davisson, M. T., Nusinowitz, S., and Heckenlively, J. R. (2002). Retinal degeneration mutants in the mouse. *Vision Res.* 42, 517–525. doi: 10.1016/S0042-6989(01)00146-8

Chang, B., Khanna, H., Hawes, N., Jimeno, D., Shirley, H., Lillo, C., et al. (2006). In-frame deletion in a novel centrosomal/ciliary protein CEP290/NPHP6 perturbs its interaction with RPGR and results in early-onset retinal degeneration in the rd16 mouse | Human Molecular Genetics | Oxford Academic. *Hum. Mol. Genet.* 15:107. doi: 10.1093/hmg/ddl107

Charbel Issa, P., De Silva, S. R., Lipinski, D. M., Singh, M. S., Mouravlev, A., You, Q., et al. (2013). Assessment of tropism and effectiveness of new primate-derived hybrid recombinant AAV serotypes in the mouse and primate retina. *PLoS One* 8:e60361. doi: 10.1371/journal.pone.0060361

Chichagova, V., Dorgau, B., Felemban, M., Georgiou, M., Armstrong, L., and Lako, M. (2019). Differentiation of retinal organoids from human pluripotent stem cells. *Curr. Protoc. Stem Cell Biol.* 50, 4975–4911. doi: 10.1002/cpsc.95

Chuong, A. S., Miri, M. L., Busskamp, V., Matthews, G. A. C., Acker, L. C., Sørensen, A. T., et al. (2014). Noninvasive optical inhibition with a red-shifted microbial rhodopsin. *Nat. Neurosci.* 17, 1123–1129. doi: 10.1038/nn.3752

Cronin, T., Vandenberghe, L. H., Hantz, P., Juttner, J., Reimann, A., Kacsó, A.-E., et al. (2014). Efficient transduction and optogenetic stimulation of retinal bipolar cells by a synthetic adeno-associated virus capsid and promoter. *EMBO Mol. Med.* 6, 1175–1190. doi: 10.15252/emmm.201404077

Dalkara, D., Byrne, L. C., Klimczak, R. R., Visel, M., Yin, L., Merigan, W. H., et al. (2013). In vivo–directed evolution of a new adeno-associated virus for therapeutic outer retinal gene delivery from the vitreous. *Sci. Transl. Med.* 5:189ra76. doi: 10.1126/scitranslmed.3005708

Dalloz, C., Sarig, R., Fort, P., Yaffe, D., Bordais, A., Pannicke, T., et al. (2003). Targeted inactivation of dystrophin gene product Dp71: phenotypic impact

in mouse retina | Human Molecular Genetics | Oxford Academic. *Hum. Mol. Genet.* 12, 1543–1554. doi: 10.1093/hmg/ddg170

Daniele, L. L., Lillo, C., Lyubarsky, A. L., Nikonov, S. S., Philp, N., Mears, A. J., et al. (2005). Cone-like morphological, molecular, and electrophysiological features of the photoreceptors of the Nrl knockout mouse. *Invest Ophthalmol. Vis. Sci.* 46, 2156–2167. doi: 10.1167/iovs.04-1427

De Leeuw, C. N., Dyka, F. M., Boye, S. L., Zhou, M., Chou, A. Y., Borretta, L., et al. (2014). Targeted CNS delivery using human MiniPromoters and demonstrated compatibility with adeno-associated viral vectors. *Mol. Ther. Methods Clin. Dev.* 1, 1–15. doi: 10.1038/mtm.2013.5

De Silva, S. R., Barnard, A. R., Hughes, S., Tam, S. K. E., Martin, C., Singh, M. S., et al. (2017). Long-term restoration of visual function in end-stage retinal degeneration using subretinal human melanopsin gene therapy. *Proc. Natl. Acad. Sci. U.S.A.* 114, 11211–11216. doi: 10.1073/pnas.1701589114

De Silva, S. R., Issa, P. C., Singh, M. S., Lipinski, D. M., Barnea-Cramer, A. O., Walker, N. J., et al. (2016). Single residue AAV capsid mutation improves transduction of photoreceptors in the Abca4(-/-) mouse and bipolar cells in the rd1 mouse and human retina ex-vivo. *Gene Ther.* 23, 767–774. doi: 10.1038/gt.2016.54

Deisseroth, K., Feng, G., Majewska, A. K., Miesenböck, G., Ting, A., and Schnitzer, M. J. (2006). Next-generation optical technologies for illuminating genetically targeted brain circuits. *J. Neurosci.* 26, 10380–10386. doi: 10.1523/JNEUROSCI.3863-06.2006

Doroudchi, M. M., Greenberg, K. P., Liu, J., Silka, K. A., Boyden, E. S., Lockridge, J. A., et al. (2011). Virally delivered channelrhodopsin-2 safely and effectively restores visual function in multiple mouse models of blindness. *Mol. Ther.* 19, 1220–1229. doi: 10.1038/mt.2011.69

Eleftheriou, C. G., Cehajic-Kapetanovic, J., Martial, F. P., Milosavljevic, N., Bedford, R. A., and Lucas, R. J. (2017). Meclofenamic acid improves the signal to noise ratio for visual responses produced by ectopic expression of human rod opsin. *Mol. Vis.* 23, 334–345.

Farber, D. B., Flannery, J. G., and Rickman, C. B. (1994). The rd mouse story: Seventy years of research on an animal model of inherited retinal degeneration. *Prog. Retinal Res.* 13, 31–64. doi: 10.1016/1350-9462(94)90004-3

Fischer, M. D., McClements, M. E., Martinez-Fernandez de la Camara, C., Bellingrath, J.-S., Dauletbekov, D., Ramsden, S. C., et al. (2017). Codon-optimized RPGR improves stability and efficacy of AAV8 Gene therapy in two mouse models of X-linked retinitis pigmentosa. *Mol. Ther.* 25, 1854–1865. doi: 10.1016/j.ymthe.2017.05.005

Gargini, C., Terzibasi, E., Mazzoni, F., and Strettoi, E. (2007). Retinal organization in the retinal degeneration 10 (rd10) mutant mouse: a morphological and ERG study. *J. Comp. Neurol.* 500, 222–238. doi: 10.1002/cne.21144

Garita-Hernandez, M., Guibbal, L., Toualbi, L., Routet, F., Chaffiol, A., Winckler, C., et al. (2018). Optogenetic Light sensors in human retinal organoids. *Front. Neurosci.* 12:232. doi: 10.3389/fnins.2018.00789

Garita-Hernandez, M., Lampič, M., Chaffiol, A., Guibbal, L., Routet, F., Santos-Ferreira, T., et al. (2019). Restoration of visual function by transplantation of optogenetically engineered photoreceptors. *Nat. Commun.* 10, 1–13. doi: 10.1038/s41467-019-12330-2

Garita-Hernandez, M., Routet, F., Guibbal, L., Khabou, H., Toualbi, L., Riancho, L., et al. (2020). AAV-mediated gene delivery to 3D retinal organoids derived from human induced pluripotent stem cells. *Int. J. Mol. Sci.* 20:994. doi: 10.3390/ijms21030994

Gaub, B. M., Berry, M. H., Holt, A. E., Isacoff, E. Y., and Flannery, J. G. (2015). Optogenetic vision restoration using rhodopsin for enhanced sensitivity. *Mol. Ther.* 23, 1562–1571. doi: 10.1038/mt.2015.121

Gonzalez-Cordero, A., Goh, D., Kruczek, K., Naeem, A., Fernando, M., Kleine Holthaus, S.-M., et al. (2017). Assessment of AAV Vector tropisms for mouse and human pluripotent stem cell–derived RPE and photoreceptor cells. *Hum. Gene Ther.* 2018:27. doi: 10.1089/hum.2018.027

Gradinaru, V., Thompson, K. R., and Deisseroth, K. (2008). eNpHR: a Natronomonas halorhodopsin enhanced for optogenetic applications. *Brain Cell Biol.* 36, 129–139. doi: 10.1007/s11068-008-9027-6.pdf

Gradinaru, V., Thompson, K. R., Zhang, F., Mogri, M., Kay, K., Schneider, M. B., et al. (2007). Targeting and readout strategies for fast optical neural control in vitro and In Vivo. *J. Neurosci.* 27, 14231–14238. doi: 10.1523/JNEUROSCI.3578-07.2007

Gradinaru, V., Zhang, F., Ramakrishnan, C., Mattis, J., Prakash, R., Diester, I., et al. (2010). Molecular and cellular approaches for diversifying and extending optogenetics. *Cell* 141, 154–165. doi: 10.1016/j.cell.2010.02.037

Gregg, R. G., Mukhopadhyay, S., Candille, S. I., Ball, S. L., Pardue, M. T., McCall, M. A., et al. (2003). Identification of the gene and the mutation responsible for the mouse nob phenotype. *Invest Ophthalmol. Vis. Sci.* 44, 378–384. doi: 10.1167/iovs.02-0501

Hackam, A. S., Strom, R., Liu, D., Qian, J., Wang, C., Otteson, D., et al. (2004). Identification of gene expression changes associated with the progression of retinal degeneration in the rd1 mouse. *Invest. Ophthalmol. Vis. Sci.* 45, 2929–2942. doi: 10.1167/iovs.03-1184

Hanlon, K. S., Chadderton, N., Palfi, A., Blanco-Fernandez, A., Humphries, P., Kenna, P. F., et al. (2017). A Novel retinal ganglion cell promoter for utility in AAV vectors. *Front. Neurosci.* 11:521. doi: 10.3389/fnins.2017.00521

Hassall, M. M., McClements, M. E., Barnard, A. R., Patrício, M. I., Aslam, S. A., and MacLaren, R. E. (2020). Analysis of early cone dysfunction in an in vivo model of rod-cone dystrophy. *Int. J. Mol. Sci.* 20, 6055–6017. doi: 10.3390/ijms21176055

Hattar, S., Lucas, R. J., Mrosovsky, N., Thompson, S., Douglas, R. H., Hankins, M. W., et al. (2003). Melanopsin and rod–cone photoreceptive systems account for all major accessory visual functions in mice. *Nature* 424, 75–81. doi: 10.1038/nature01761

Hawes, N. L., Chang, B., Hageman, G. S., Nusinowitz, S., Nishina, P. M., Schneider, B. S., et al. (2000). Retinal degeneration 6 (rd6): a new mouse model for human retinitis punctata albescens. *Invest. Ophthalmol. Vis. Sci.* 41, 3149–3157.

Hickey, D. G., Edwards, T. L., Barnard, A. R., Singh, M. S., De Silva, S. R., McClements, M. E., et al. (2017). Tropism of engineered and evolved recombinant AAV serotypes in the rd1 mouse and ex vivo primate retina. *Gene Ther.* 24, 787–800. doi: 10.1038/gt.2017.85

Humphries, M. M., Rancourt, D., Farrar, G. J., Kenna, P., Hazel, M., Bush, R. A., et al. (1997). Retinopathy induced in mice by targeted disruption of the rhodopsin gene. *Nat. Genet.* 15, 216–219. doi: 10.1038/ng0297-216

ICNIRP (2013). ICNIRP guidelines on limits of exposure to incoherent visible and infrared radiation. *Health Phys.* 13, 74–96.

Ivanova, E., Hwang, G.-S., Pan, Z.-H., and Troilo, D. (2010). Evaluation of AAV-mediated expression of Chop2-GFP in the marmoset retina. *Invest Ophthalmol. Vis. Sci.* 51, 5288–5296. doi: 10.1167/iovs.10-5389

Jansen, H. G., and Sanyal, S. (1984). Development and degeneration of retina inrds mutant mice: electron microscopy. *J. Comp. Neurol.* 224, 71–84. doi: 10.1002/cne.902240107

Jones, B. W., Pfeiffer, R. L., Ferrell, W. D., Watt, C. B., Marmor, M., and Marc, R. E. (2016). Retinal remodeling in human retinitis pigmentosa. *Exp. Eye Res.* 150, 149–165. doi: 10.1016/j.exer.2016.03.018

Jones, B. W., Watt, C. B., Frederick, J. M., Baehr, W., Chen, C.-K., Levine, E. M., et al. (2003). Retinal remodeling triggered by photoreceptor degenerations. *J. Comp. Neurol.* 464, 1–16. doi: 10.1002/cne.10703

Kameya, S., Hawes, N. L., Chang, B., Heckenlively, J. R., Naggert, J. K., and Nishina, P. M. (2002). Mfrp, a gene encoding a frizzled related protein, is mutated in the mouse retinal degeneration 6. *Hum. Mol. Genet.* 11, 1879–1886. doi: 10.1093/hmg/11.16.1879

Kay, C. N., Ryals, R. C., Aslanidi, G. V., Min, S.-H., Ruan, Q., Sun, J., et al. (2013). Targeting photoreceptors via intravitreal delivery using novel, capsid-mutated AAV vectors. *PLoS One* 8:e62097. doi: 10.1371/journal.pone.0062097

Khabou, H., Garita-Hernandez, M., Chaffiol, A., Reichman, S., Jaillard, C., Brazhnikova, E., et al. (2018). Noninvasive gene delivery to foveal cones for vision restoration. *JCI Insight* 3:D358. doi: 10.1172/jci.insight.96029

Kim, D. S., Matsuda, T., and Cepko, C. L. (2008). A core paired-type and POU homeodomain-containing transcription factor program drives retinal bipolar cell gene expression. *J. Neurosci.* 28, 7748–7764. doi: 10.1523/JNEUROSCI.0397-08.2008

Klapoetke, N. C., Murata, Y., Kim, S. S., Pulver, S. R., Birdsey-Benson, A., Cho, Y. K., et al. (2014). Independent optical excitation of distinct neural populations. *Nat. Methods* 11, 338–346. doi: 10.1038/nmeth.2836

Kleinlogel, S., Feldbauer, K., Dempski, R. E., Fotis, H., Wood, P. G., Bamann, C., et al. (2011). Ultra light-sensitive and fast neuronal activation with the Ca 2+ -permeable channelrhodopsin CatCh. *Nat. Neurosci.* 14, 513–518. doi: 10.1038/nn.2776

Kolstad, K. D., Dalkara, D., Guerin, K., Visel, M., Hoffmann, N., Schaffer, D. V., et al. (2010). Changes in adeno-associated virus-mediated gene delivery in retinal degeneration. *Hum. Gene Ther.* 21, 571–578. doi: 10.1089/hum.2009.194

Lagali, P. S., Balya, D., Awatramani, G. B., Münch, T. A., Kim, D. S., Busskamp, V., et al. (2008). Light-activated channels targeted to ON bipolar cells restore visual function in retinal degeneration. *Nat. Neurosci.* 11, 667–675. doi: 10.1038/nn.2117

Lane, A., Jovanovic, K., Shortall, C., Ottaviani, D., Brugulat Panes, A., Schwarz, N., et al. (2020). Modeling and Rescue of RP2 retinitis pigmentosa using iPSC-derived retinal organoids. *Stem. Cell Rep.* 15, 67–79. doi: 10.1016/j.stemcr.2020.05.007

Li, Q., Timmers, A. M., Guy, J., Pang, J., and Hauswirth, W. W. (2008). Cone-specific expression using a human red opsin promoter in recombinant AAV. *Vision Res.* 48, 332–338. doi: 10.1016/j.visres.2007.07.026

Lin, B., Masland, R. H., and Strettoi, E. (2009). Remodeling of cone photoreceptor cells after rod degeneration in rd mice. *Exp. Eye Res.* 88, 589–599. doi: 10.1016/j.exer.2008.11.022

Lin, J. Y., Knutsen, P. M., Muller, A., Kleinfeld, D., and Tsien, R. Y. (2013). ReaChR: a red-shifted variant of channelrhodopsin enables deep transcranial optogenetic excitation. *Nat. Neurosci.* 16, 1499–1508. doi: 10.1038/nn.3502

Liu, M.-M., Dai, J.-M., Liu, W.-Y., Zhao, C.-J., Lin, B., and Yin, Z.-Q. (2016). Human melanopsin-AAV2/8 transfection to retina transiently restores visual function in rd1 mice. *Int. J. Ophthalmol.* 9, 655–661. doi: 10.18240/ijo.2016.05.03

Lu, Q., Ganjawala, T. H., Ivanova, E., Cheng, J. G., Troilo, D., and Pan, Z.-H. (2016). AAV-mediated transduction and targeting of retinal bipolar cells with improved mGluR6 promoters in rodents and primates. *Gene Ther.* 23, 680–689. doi: 10.1038/gt.2016.42

Lu, Q., Ganjawala, T. H., Krstevski, A., Abrams, G. W., and Pan, Z.-H. (2020). Comparison of AAV-Mediated optogenetic vision restoration between retinal ganglion cell expression and ON bipolar cell targeting. *Mol. Ther. Methods Clin. Dev.* 18, 15–23. doi: 10.1016/j.omtm.2020.05.009

Ma, J., Norton, J. C., Allen, A. C., Burns, J. B., Hasel, K. W., Burns, J. L., et al. (1995). Retinal degeneration slow (rds) in mouse results from simple insertion of a t haplotype-specific element into protein-coding exon II. *Genomics* 28, 212–219. doi: 10.1006/geno.1995.1133

Macé, E., Caplette, R., Marre, O., Sengupta, A., Chaffiol, A., Barbe, P., et al. (2015). Targeting channelrhodopsin-2 to ON-bipolar cells with vitreally administered AAV restores ON and OFF visual responses in blind mice. *Mol. Ther.* 23, 7–16. doi: 10.1038/mt.2014.154

Marc, R. E., Jones, B. W., Watt, C. B., and Strettoi, E. (2003). Neural remodeling in retinal degeneration. *Prog. Retinal Eye Res.* 22, 607–655. doi: 10.1016/S1350-9462(03)00039-9

McClements, M., Davies, W. I. L., Michaelides, M., Young, T., Neitz, M., MacLaren, R. E., et al. (2013). Variations in opsin coding sequences cause x-linked cone dysfunction syndrome with myopia and dichromacy. *Invest Ophthalmol. Vis. Sci.* 54, 1361–1369. doi: 10.1167/iovs.12-11156

McGregor, J. E., Godat, T., Dhakal, K. R., Parkins, K., Strazzeri, J. M., Bateman, B. A., et al. (2020). Optogenetic restoration of retinal ganglion cell activity in the living primate. *Nat. Commun.* 11, 1–9. doi: 10.1038/s41467-020-15317-6

Mears, A. J., Kondo, M., Swain, P. K., Takada, Y., Bush, R. A., Saunders, T. L., et al. (2001). Nrl is required for rod photoreceptor development. *Nat. Genet.* 29, 447–452. doi: 10.1038/ng774

Mehalow, A. K., Kameya, S., Smith, R. S., Hawes, N. L., Denegre, J. M., Young, J. A., et al. (2003). CRB1 is essential for external limiting membrane integrity and photoreceptor morphogenesis in the mammalian retina. *Hum. Mol. Genet.* 12, 2179–2189. doi: 10.1093/hmg/ddg232

Milam, A. H., Li, Z. Y., and Fariss, R. N. (1998). Histopathology of the human retina in retinitis pigmentosa. *Prog. Retinal Eye Res.* 17, 175–205.

Mohan, K., Harper, M. M., Kecova, H., Ye, E. A., Lazic, T., Sakaguchi, D. S., et al. (2012). Characterization of structure and function of the mouse retina using pattern electroretinography, pupil light reflex, and optical coherence tomography. *Vet. Ophthalmol.* 15, 94–104. doi: 10.1111/j.1463-5224.2012.01034.x

Mussolino, C., Corte, Della, M., Rossi, S., Viola, F., Di Vicino, U., et al. (2011). AAV-mediated photoreceptor transduction of the pig cone-enriched retina. *Gene Ther.* 18, 637–645. doi: 10.1038/gt.2011.3

Nakajima, Y., Iwakabe, H., Akazawa, C., Nawa, H., Shigemoto, R., Mizuno, N., et al. (1993). Molecular characterization of a novel retinal metabotropic glutamate receptor mGluR6 with a high agonist selectivity for L-2-amino-4-phosphonobutyrate. *J. Biol. Chem.* 268, 11868–11873.

Narfström, K., Wrigstad, A., and Nilsson, S. E. (1989). The Briard dog: a new animal model of congenital stationary night blindness. *Br. J. Ophthalmol.* 73, 750–756. doi: 10.1136/bjo.73.9.750

Nelson, R., and Connaughton, V. (2007). "Bipolar Cell pathways in the vertebrate retina," in *The Organization of the Retina and Visual System Webvision: The Organization of the Retina and Visual System*, eds E. Fernandez, and R. Nelson (Salt Lake City, UT: University of Utah Health Sciences Center), 1–48.

Nomura, A., Shigemoto, R., Nakamura, Y., Okamoto, N., Mizuno, N., and Nakanishi, S. (1994). Developmentally regulated postsynaptic localization of a metabotropic glutamate receptor in rat rod bipolar cells. *Cell* 77, 361–369. doi: 10.1016/0092-8674(94)90151-1

Nuzbrokh, Y., Kassotis, A. S., Ragi, S. D., Jauregui, R., and Tsang, S. H. (2020). Treatment-emergent adverse events in gene therapy trials for inherited retinal diseases: a narrative review. *Ophthalmol. Ther.* 20, 1–16. doi: 10.1007/s40123-020-00287-1

Orlans, H. O., Edwards, T. L., De Silva, S. R., Patrício, M. I., and MacLaren, R. E. (2018). *Human Retinal Explant Culture for Ex Vivo Validation of AAV Gene Therapy: Retinal Gene Therapy*. New York, NY: Humana Press, 289–303. doi: 10.1007/978-1-4939-7522-8_21

Pang, J., Chang, B., Hawes, N. L., Hurd, R. E., Davisson, M. T., Li, J., et al. (2005). Retinal degeneration 12 (rd12): a new, spontaneously arising mouse model for human Leber congenital amaurosis (LCA). *Mol. Vis.* 11, 152–162.

Pardue, M. T., McCall, M. A., LaVail, M. M., Gregg, R. G., and Peachey, N. S. (1998). A naturally occurring mouse model of X-linked congenital stationary night blindness. *Invest. Ophthalmol. Vis. Sci.* 39, 2443–2449.

Patrício, M. I., Barnard, A. R., Orlans, H. O., McClements, M. E., and MacLaren, R. E. (2017). Inclusion of the woodchuck hepatitis virus posttranscriptional regulatory element enhances AAV2-driven transduction of mouse and human retina. *Mol. Ther. Nucleic Acids* 6, 198–208. doi: 10.1016/j.omtn.2016.12.006

Pepperberg, D. R. (2003). Bleaching desensitization: background and current challenges. *Vision Res.* 43, 3011–3019. doi: 10.1016/S0042-6989(03)00484-X

Petrs-Silva, H., Dinculescu, A., Li, Q., Deng, W.-T., Pang, J.-J., Min, S.-H., et al. (2011). Novel properties of tyrosine-mutant AAV2 vectors in the mouse retina. *Mol. Ther.* 19, 293–301. doi: 10.1038/mt.2010.234

Pfeiffer, R. L., Marc, R. E., and Jones, B. W. (2020). Persistent remodeling and neurodegeneration in late-stage retinal degeneration. *Prog. Retinal Eye Res.* 74:100771. doi: 10.1016/j.preteyeres.2019.07.004

Picaud, S., Dalkara, D., Marazova, K., Goureau, O., Roska, B., and Sahel, J.-A. (2019). The primate model for understanding and restoring vision. *Proc. Natl. Acad. Sci. U.S.A.* 116, 26280–26287. doi: 10.1073/pnas.1902292116

Pittler, S. J., Keeler, C. E., Sidman, R. L., and Baehr, W. (1993). PCR analysis of DNA from 70-year-old sections of rodless retina demonstrates identity with the mouse rd defect. *Proc. Natl. Acad. Sci. U.S.A.* 90, 9616–9619. doi: 10.1073/pnas.90.20.9616

Puppo, A., Cesi, G., Marrocco, E., Piccolo, P., Jacca, S., Shayakhmetov, D. M., et al. (2014). Retinal transduction profiles by high-capacity viral vectors. *Gene Ther.* 21, 855–865. doi: 10.1038/gt.2014.57

Puthussery, T., Primo, J. G., Pandey, S., Duvoisin, R. M., and Taylor, W. R. (2009). Differential loss and preservation of glutamate receptor function in bipolar cells in the rd10 mouse model of retinitis pigmentosa. *Eur. J. Neurosci.* 29, 1533–1542. doi: 10.1111/j.1460-9568.2009.06728.x

Quinn, P. M., Buck, T. M., Ohonin, C., Mikkers, H. M. M., and Wijnholds, J. (2018). *Production of iPS-Derived Human Retinal Organoids for Use in Transgene Expression Assays: Retinal Gene Therapy* Methods and Protocols. New York, NY: Humana Press, 261–273. doi: 10.1007/978-1-4939-7522-8_19

Reichman, S., Slembrouck, A., Gagliardi, G., Chaffiol, A., Terray, A., Nanteau, C., et al. (2017). Generation of storable retinal organoids and retinal pigmented epithelium from adherent human iPS cells in xeno-free and feeder-free conditions. *Stem Cells* 35, 1176–1188. doi: 10.1002/stem.2586

Reuter, J. H., and Sanyal, S. (1984). Development and degeneration of retina in rds mutant mice: The electroretinogram. *Neurosci. Lett.* 48, 231–237. doi: 10.1016/0304-3940(84)90024-7

Russell, S., Bennett, J., Wellman, J. A., Chung, D. C., Yu, Z.-F., Tillman, A., et al. (2017). Efficacy and safety of voretigene neparvovec (AAV2-hRPE65v2)

in patients with RPE65-mediated inherited retinal dystrophy: a randomised, controlled, open-label, phase 3 trial. *Lancet* 390, 849–860. doi: 10.1016/S0140-6736(17)31868-8

Sahel, J.-A., and Roska, B. (2013). Gene therapy for blindness. *Annu. Rev. Neurosci.* 36, 467–488. doi: 10.1146/annurev-neuro-062012-170304

Sakami, S., Maeda, T., Bereta, G., Okano, K., Golczak, M., Sumaroka, A., et al. (2011). Probing mechanisms of photoreceptor degeneration in a new mouse model of the common form of autosomal dominant retinitis pigmentosa due to P23H opsin mutations. *J. Biol. Chem.* 286, 10551–10567. doi: 10.1074/jbc.M110.209759

Santos-Ferreira, T., Voelkner, M., Borsch, O., Haas, J., Cimalla, P., Vasudevan, P., et al. (2016). Stem cell-derived photoreceptor transplants differentially integrate into mouse models of cone-rod dystrophy. *Invest. Ophthalmol. Vis. Sci.* 57, 3509–3520. doi: 10.1167/iovs.16-19087

Scalabrino, M. L., Boye, S. L., Fransen, K. M. H., Noel, J. M., Dyka, F. M., Min, S.-H., et al. (2015). Intravitreal delivery of a novel AAV vector targets ON bipolar cells and restores visual function in a mouse model of complete congenital stationary night blindness. *Hum. Mol. Genet.* 24, 6229–6239. doi: 10.1093/hmg/ddv341

Sengupta, A., Chaffiol, A., Macé, E., Caplette, R., Desrosiers, M., Lampič, M., et al. (2016). Red-shifted channelrhodopsin stimulation restores light responses in blind mice, macaque retina, and human retina. *EMBO Mol. Med.* 8, 1248–1264. doi: 10.15252/emmm.201505699

Shupe, J. M., Kristan, D. M., Austad, S. N., and Stenkamp, D. L. (2006). The Eye of the laboratory mouse remains anatomically adapted for natural conditions. *BBE* 67, 39–52. doi: 10.1159/000088857

Simon, C.-J., Sahel, J.-A., Duebel, J., and Herlitze, S. (2020). Opsins for vision restoration. *Biochem. Biophys. Res. Commun.* 20, 1–6. doi: 10.1016/j.bbrc.2019.12.117

Smith, C. A., and Chauhan, B. C. (2018). In vivo imaging of adeno-associated viral vector labelled retinal ganglion cells. *Sci. Rep.* 8, 1–11. doi: 10.1038/s41598-018-19969-9

Sohocki, M. M., Daiger, S. P., Bowne, S. J., Rodriquez, J. A., Northrup, H., Heckenlively, J. R., et al. (2001). Prevalence of mutations causing retinitis pigmentosa and other inherited retinopathies. *Hum. Mutat.* 17, 42–51. doi: 10.1002/1098-1004200117:1<42::AID-HUMU5<3.0.CO;2-K

Strettoi, E., Porciatti, V., Falsini, B., Pignatelli, V., and Rossi, C. (2002). Morphological and functional abnormalities in the inner retina of the rd/rd mouse. *J. Neurosci.* 22, 5492–5504. doi: 10.1523/jneurosci.22-13-05492.2002

The European Parliament and the Council of the European Union (2006). European parliament and council of the european union. directive 2006/25/EC on artificial optical radiation. *Off. J. Eur.Union* 6, 38–59.

Thompson, D. A., Khan, N. W., Othman, M. I., Chang, B., Jia, L., Grahek, G., et al. (2012). Rd9 is a naturally occurring mouse model of a common form of retinitis pigmentosa caused by mutations in RPGR-ORF15. *PLoS One* 7:e35865. doi: 10.1371/journal.pone.0035865

Toda, K., Bush, R. A., Humphries, P., and Sieving, P. A. (1999). The electroretinogram of the rhodopsin knockout mouse. *Vis. Neurosci.* 16, 391–398. doi: 10.1017/S0952523899162187

Travis, G. H., and Hepler, J. E. (1993). A medley of retinal dystrophies. *Nat. Genet.* 3, 191–192. doi: 10.1038/ng0393-191

Vacca, O., Darche, M., Schaffer, D. V., Flannery, J. G., Sahel, J.-A., Rendon, A., et al. (2013). AAV-mediated gene delivery in Dp71-null mouse model with compromised barriers. *Glia* 62, 468–476. doi: 10.1002/glia.22617

van Norren, D., and Vos, J. J. (2015). Light damage to the retina: an historical approach. *Eye (Lond.)* 30, 169–172. doi: 10.1038/eye.2015.218

van Wyk, M., Hulliger, E. C., Girod, L., Ebneter, A., and Kleinlogel, S. (2017). Present molecular limitations of ON-bipolar cell targeted gene therapy. *Front. Neurosci.* 11:11372. doi: 10.3389/fnins.2017.00161

van Wyk, M., Pielecka-Fortuna, J., Löwel, S., and Kleinlogel, S. (2015). Restoring the ON switch in blind retinas: opto-mGluR6, a next-generation, cell-tailored optogenetic tool. *PLoS Biol.* 13:e1002143. doi: 10.1371/journal.pbio.1002143

Wässle, H., Puller, C., Müller, F., and Haverkamp, S. (2009). Cone contacts, mosaics, and territories of bipolar cells in the mouse retina. *J. Neurosci.* 29, 106–117. doi: 10.1523/JNEUROSCI.4442-08.2009

Wilson, J. M., and Flotte, T. R. (2020). Moving forward after two deaths in a gene therapy trial of myotubular myopathy. *Hum. Gene Ther.* 2020:182. doi: 10.1089/hum.2020.182

Wrigstad, A., Nilsson, S. E. G., and Narfström, K. (1992). Ultrastructural changes of the retina and the retinal pigment epithelium in briard dogs with hereditary congenital night blindness and partial day blindness. *Exp. Eye Res.* 55, 805–818. doi: 10.1016/0014-4835(92)90007-F

Xue, K., Jolly, J. K., Barnard, A. R., Rudenko, A., Salvetti, A. P., Patrício, M. I., et al. (2018). Beneficial effects on vision in patients undergoing retinal gene therapy for choroideremia. *Nat. Med.* 24, 1507–1512. doi: 10.1038/s41591-018-0185-5

Ye, G.-J., Budzynski, E., Sonnentag, P., Nork, T. M., Sheibani, N., Gurel, Z., et al. (2016). Cone-specific promoters for gene therapy of achromatopsia and other retinal diseases. *Hum. Gene Ther.* 27, 72–82. doi: 10.1089/hum.2015.130

Yin, L., Greenberg, K., Hunter, J. J., Dalkara, D., Kolstad, K. D., Masella, B. D., et al. (2011). Intravitreal injection of AAV2 transduces macaque inner retina. *Invest. Ophthalmol. Vis. Sci.* 52, 2775–2783. doi: 10.1167/iovs.10-6250

Yiu, G., Chung, S. H., Mollhoff, I. N., Nguyen, U. T., Thomasy, S. M., Yoo, J., et al. (2020). Suprachoroidal and Subretinal Injections of AAV Using transscleral microneedles for retinal gene delivery in nonhuman primates. *Mol. Ther. Methods Clin. Dev.* 16, 179–191. doi: 10.1016/j.omtm.2020.01.002

Youssef, P. N., Sheibani, N., and Albert, D. M. (2011). Retinal light toxicity. *Eye (Lond.)* 25, 1–14. doi: 10.1038/eye.2010.149

Zhang, F., Wang, L.-P., Brauner, M., Liewald, J. F., Kay, K., Watzke, N., et al. (2007). Multimodal fast optical interrogation of neural circuitry. *Nature* 446, 633–639. doi: 10.1038/nature05744

Zhang, Y., Ivanova, E., Bi, A., and Pan, Z.-H. (2009). Ectopic expression of multiple microbial rhodopsins restores ON and OFF light responses in retinas with photoreceptor degeneration. *J. Neurosci.* 29, 9186–9196. doi: 10.1523/JNEUROSCI.0184-09.2009

Zhong, X., Gutierrez, C., Xue, T., Hampton, C., Vergara, M. N., Cao, L.-H., et al. (2014). Generation of three-dimensional retinal tissue with functional photoreceptors from human iPSCs. *Nat. Commun.* 5, 1–14. doi: 10.1038/ncomms5047

Conflict of Interest: The authors declare that the research was conducted in the absence of any commercial or financial relationships that could be construed as a potential conflict of interest.

Copyright © 2020 McClements, Staurenghi, MacLaren and Cehajic-Kapetanovic. This is an open-access article distributed under the terms of the Creative Commons Attribution License (CC BY). The use, distribution or reproduction in other forums is permitted, provided the original author(s) and the copyright owner(s) are credited and that the original publication in this journal is cited, in accordance with accepted academic practice. No use, distribution or reproduction is permitted which does not comply with these terms.

frontiers in Neuroscience

MINI REVIEW
published: 25 November 2020
doi: 10.3389/fnins.2020.583392

Organ Cultures for Retinal Diseases

*José Hurst[1], Agnes Fietz[1], Teresa Tsai[2], Stephanie C. Joachim[2] and Sven Schnichels[1]**

[1] Center for Ophthalmology, University Eye Hospital, University of Tübingen, Tübingen, Germany, [2] Experimental Eye Research Institute, University Eye Hospital, Ruhr-University Bochum, Bochum, Germany

The successful development of novel therapies is closely linked with understanding the underlying pathomechanisms of a disease. To do so, model systems that reflect human diseases and allow for the evaluation of new therapeutic approaches are needed. Yet, preclinical animal studies often have limited success in predicting human physiology, pathology, and therapeutic responses. Moreover, animal testing is facing increasing ethical and bureaucratic hurdles, while human cell cultures are limited in their ability to represent *in vivo* situations due to the lack of the tissue microenvironment, which may alter cellular responses. To overcome these struggles, organ cultures, especially those of complex organs such as the retina, can be used to study physiological reactions to substances or stressors. Human and animal organ cultures are now well established and recognized. This mini-review discusses how retinal organ cultures can be used to preserve tissue architecture more realistically and therefore better represent disease-related changes. It also shows how molecular biological, biochemical, and histological techniques can be combined to investigate how anatomical localization may alter cellular responses. Examples for the use of retinal organ cultures, including models to study age-related macular degeneration (AMD), *retinitis pigmentosa* (RP), central artery occlusion (CRAO), and glaucoma are presented, and their advantages and disadvantages are discussed. We conclude that organ cultures significantly improve our understanding of complex retinal diseases and may advance treatment testing without the need for animal testing.

Keywords: *ex vivo*, retinal organ culture, age-related macular degeneration, glaucoma, retinitis pigmentosa, central artery occlusion

OPEN ACCESS

Edited by:
Miguel Flores-Bellver, University of Colorado Anschutz Medical Campus, United States

Reviewed by:
Thomas Vincent Johnson, Johns Hopkins University, United States
Natalia Vergara, University of Colorado, United States

***Correspondence:**
Sven Schnichels
sven.schnichels@med.uni-tuebingen.de

Specialty section:
This article was submitted to Neurodegeneration, a section of the journal Frontiers in Neuroscience

Received: *14 July 2020*
Accepted: *13 October 2020*
Published: *25 November 2020*

Citation:
Hurst J, Fietz A, Tsai T, Joachim SC and Schnichels S (2020) Organ Cultures for Retinal Diseases. Front. Neurosci. 14:583392. doi: 10.3389/fnins.2020.583392

INTRODUCTION

Cell cultures have become indispensable in translational research. Many preclinical evaluations, like toxicity testing or drug screening, are still based on standardized cell lines. Usually, these assays are simple, inexpensive, reproducible, and allow a fast and efficient screening for cell proliferation, metabolism, viability, and apoptosis (Schnichels et al., 2012a, 2013; Hurst et al., 2017b). Cell cultures are the method of choice to observe the reaction of a specific cell type. Already 20 years ago, it was published that at least 15–20% of all immortalized cell lines used in research are contaminated or wrongly categorized, resulting in non-transferable data (MacLeod et al., 1999). Moreover, immortalized cells react to stimuli differently than primary cells (MacLeod et al., 1999), and for several cell types, no corresponding cell lines are available. For example, primary photoreceptor cells are very difficult to cultivate under *in vitro* conditions and degenerate rapidly after dissociation from the retina (Fontaine et al., 1998; Romano and Hicks, 2007). The same applies to retinal ganglion cells (RGCs). The only existing RGC line is the presumably rat-derived RGC-5 cell line, which was mainly used for glaucoma research. Over the years, the literature has

increasingly described altered properties of these cells, showing a reduced expression of specific neural and ganglion cell markers (Harper et al., 2009; Van Bergen et al., 2009; Ganapathy et al., 2010; Wood et al., 2010). In the meantime, early contamination with a murine cell line was assumed (Krishnamoorthy et al., 2013). Until today, the origin of the RGC-5 cell line could not be verified, and researchers are strongly advised to avoid using it (Clark et al., 2013; Krishnamoorthy et al., 2013; Sippl and Tamm, 2014).

In general, cell cultures do not mimic the tissue homeostasis, physiology, and interactions that occur between different cell types within a tissue *in vivo*; thus, *in vitro* models can never completely replace *in vivo* ones. However, *in vivo* experiments also have their disadvantages: They are rather expensive and time-consuming. Even after long-term and well-performed research, not a single treatment option for sporadic neurodegenerative diseases has proven its value in registration-sized clinical trials (Li et al., 2018; Murali et al., 2019).

In response to these gaps and struggles, organ cultures are gaining ground, including organoids generated from stem cells, tissue parts taken from organs, and construction of new 3D structures with different cell types, containing cell lines, primary or stem cells depending on the respective research approach (Aizawa and Shoichet, 2012; Hunt et al., 2017). The big advantage of organ cultures is that elementary structures of the organ are modeled, allowing investigations of complex interactions.

This especially holds for ophthalmology, where *ex vivo* models of the cornea and retina are common research tools with the additional positive effect of reducing the number of animals used in research and, most importantly, replacing the need for certain *in vivo* procedures (Schnichels et al., 2019).

ORGAN CULTURES: ADVANTAGES AND CHALLENGES

Nowadays, numerous retinal organ models from different mammalian species are well established. However, compared to the cultivation of cornea models, retinal organ cultures are more difficult to maintain, mainly due to the different cell types involved, which are generally more complex to cultivate. Especially designed growth medium, containing growth factors for neurons, supports cell survival. Co-cultivation with retinal pigment epithelium (RPE) cells improves tissue structure, cellular organization, and preservation of photoreceptors (Di Lauro et al., 2016; Schnichels et al., 2020). Zhao and Barnstable (Zhao and Barnstable, 1996) pointed out that retinoic acid but not basic fibroblast growth factor (bFGF) promotes rod photoreceptor differentiation, whereas bFGF endorses RGC differentiation in *ex vivo* rat retinae. B-27 and N2 are the most commonly used supplements in retinal explant culture; although they were reported to be useful in rat retinal culture, the same benefit is not necessarily valid for human retinal explants (Osborne et al., 2016; Li et al., 2018; Murali et al., 2019).

To establish a functional retinal model, several challenges need to be overcome. A major problem is the limited viability of most retinal organ culture systems due to axotomy or lack of blood flow and biomechanical tissue support leading to metabolic disorders and cell death (Åkerström et al., 2017; Schnichels et al., 2019). This mainly affects RGCs, but also other cell types such as macroglia, displaying gliosis (Tanihara et al., 1997; Wurm et al., 2011; Joachim et al., 2012; Hurst et al., 2017a) and reducing the time frame for experiments with these cultures.

Likewise, depending on the assay, small effects of individual cell types are lost in the total reaction or very heterogeneous results are obtained. Biological diversity might be an issue; heterogeneity and variability between samples also occur. This can be reduced if retinae from genetically identical laboratory animals, such as mice or rats, of the same age and sex are used. Likewise, an altered expression profile may occur due to the preparation, cultivation, or medium composition (Roark et al., 1992; Fernandez-Bueno et al., 2012; Schnichels et al., 2019). This deviation from the *in vivo* situation should always be taken into account when results from an *ex vivo* approach are interpreted.

Due to their matching anatomical and physiological structures, human retinal organ cultures represent the ideal model system. *Ex vivo* human cultures can be cultivated up to 6 weeks, as demonstrated by Engelsberg et al. (Engelsberg et al., 2008) on human fetal retinal explants. Osborne et al. (Osborne et al., 2016) showed that neither donor age nor postmortem time significantly affects the initial expression levels of RGC markers and that donor retinae are suitable as a long-term model for RGC degeneration. Nevertheless, the availability of human organs is extremely low and severe ethical issues arise when using fetal eyes. One solution is the use of organoids produced from stem cells or even from patient cells, which mimic retinal structure and composition, but they also have their disadvantages (Eiraku et al., 2011). Therefore, the aim is to establish retinal organ cultures from species reflecting human morphology and physiology very closely.

The most commonly used animals in ophthalmologic research, rodent, dog, cow, and pig retinae do not have a macula but instead possess a region called *area centralis*. Furthermore, instead of three different cone types as humans, lower mammals only have two types (Peichl, 2005; Murali et al., 2019). As a result of these anatomical differences, the development of some diseases is different.

Nevertheless, the use of porcine or bovine retinae has several advantages. During research studies on RGCs, porcine retinal explants have been shown to remain viable for 8 days (Kuehn et al., 2016, 2017; Hurst et al., 2017a). Not to mention the fact that no laboratory animals have to be bred and killed. Those animals have larger eyes, so several explants can be obtained from a single eye, leading to more reliable data. The anatomy and vascularization of porcine eye cultures resemble those of the human eye (Guduric-Fuchs et al., 2009).

Taken together, advantages of *ex vivo* organ cultures are multiple: numbers of laboratory animals can be reduced, the experiments are less cost intensive, larger sample quantities can be generated, and there is better standardization of the experiment. In addition, the application of possible therapeutics is easier than that *in vivo* (Schnichels et al., 2019) and different retinal cell types can be studied under the same condition (Hurst et al., 2017a).

EXPERIMENTAL METHODS ON ORGAN CULTURES

The further development of certain techniques contributes to the development of more useful organ cultures for ophthalmologic research. For example, new methods for the introduction of DNA/vectors/plasmids are available or under development, which overcome the problem of uneven penetration or cellular uptake, as well as vector transcription in, e.g., neuronal cells (Marwick and Hardingham, 2017; Jüttner et al., 2019). Besides using viral vectors for tissue transfection, this includes magnetofection on *ex vivo* organ cultures (Yang et al., 2008; Soto-Sanchez et al., 2015; Jüttner et al., 2019). In order to regulate the expression of the vectors, new promoters were invented, which can be read in the retina under non-mitotic conditions (Dalkara et al., 2013, 2016).

There are numerous bioassays to investigate cell metabolism, cell death, or proliferation. Many of these assays can also be performed on retinal tissue, such as the measurement of reactive oxygen species (ROS) production from hypoxia-stressed retinal explants (Maliha et al., 2019; Sasaki et al., 2019; **Figure 1**).

Furthermore, more sophisticated techniques like single-cell Western blot or single-cell PCR allow the analysis of individual cells in tissues (Hughes et al., 2014). Using non-linear optical microscopy, in particular confocal Raman microscopy or two-photon-excited fluorescence microscopy, limitations can be overcome, providing depth penetration up to 1 mm without destroying the tissue (Helmchen and Denk, 2005; Sharma et al., 2016; Gomes da Costa et al., 2019). In addition to the common laboratory methods, specialized methods from neurobiology and ophthalmology can be applied to retinal organ cultures (**Figure 1**).

Optical Coherence Tomography

Optical coherence tomography (OCT) is a well-established diagnostic imaging technique that allows both qualitative (morphology) and quantitative (thickness) analyses of the retinal architecture (Fujimoto et al., 1998). OCT examination of the retina is used to diagnose retinal diseases and measure therapeutic effects. Since OCT has become available, correlations between anatomy on OCT and visual function have been investigated in a number of retinal diseases (Keane et al., 2008). Using a specially developed holder, OCT examinations can be performed *ex vivo* on retinal organ cultures (Schnichels et al., 2016). On the one hand, OCT is a good alternative if you do not have access to confocal or multiphoton microscopy; on the other hand, OCT measurements allow the comparison of experimental data with patient data, can be repeated several times, and are a simple and fast method that does not require fixation of the retina.

Electroretinograms

Electroretinograms (ERGs) record the electrical responses of various retinal cell types, including photoreceptors and inner retinal cells (bipolar and amacrine cells). ERG recordings in isolated retinae are highly standardized in different species like human, bovine, or retinal tissue deriving from rodents (Kuchler et al., 1956; Albanna et al., 2009; Hurst et al., 2018). In contrast to *in vivo* experiments, *ex vivo* retinae are not affected by the depth of anesthesia and electrode placement (Homma et al., 2009). ERG is used in the clinic to diagnose various retinal diseases such as RP, choroideremia, or achromatopsia. It serves as a sensitive pharmacological tool to test effects of applied substances on photoreceptors and neurons that contribute to the generation of the a- and b-wave (Januschowski et al., 2014a,b). Luke et al. (2009) investigated the effects of ranibizumab (Lucentis) on retinal function in *ex vivo* bovine retinae. Ranibizumab blocks vascular endothelial growth factor (VEGF), the major factor in age-related macular degeneration (AMD) progress. Ranibizumab therapy could induce retinal dysfunction; however, no reduction of the a- or b-wave in the ERG was observed (Luke et al., 2009).

Microelectrode Array Recording

Microelectrode array (MEA) recording is the method of choice to measure electrical activity in cell and tissue preparations. MEAs were developed on cell cultures and are now used *ex vivo* in tissue for pharmacological studies and *in vivo* as implantable devices in brain pacemakers or cochlear implants (Obien et al., 2014). They consist of a multitude of microscopic electrodes on the surface of a glass plate on which the cells are cultivated. The electrodes enable electrical stimulation and simultaneous measurement of electrical activity of ganglion cells. This allows for accurate mapping of RGCs in neuronal tissue and to use the gained information for disease models (Baden et al., 2016; Zeck, 2018; Ran et al., 2020). In addition, MEAs are also ideal biosensors for measuring acute and chronic effects of drugs and toxins (Rosolen et al., 2008; Tao et al., 2020).

DISEASE MODELS AND THERAPY TESTS ON RETINAL ORGAN CULTURES

Regrettably, for certain retinal disorders like AMD, glaucoma, RP, diabetic retinopathy, or CRAO, relevant *in vivo* models are missing or are imperfect for studying underlying pathophysiology. However, there is a high number of retinal organ cultures of different species with which a spectrum of disease simulations can be performed. These models are used to visualize the cellular basis of retinal pathogenesis to elucidate the role of specific genes and proteins in normal and disease processes and to test therapies without the use of laboratory animals. For example, Huang et al. (2017) explored new methods such as injection by ultrasound for retinal drug delivery. Intravitreal injection is the most common route of administration, and the vitreous body and the inner limiting membrane are the main obstacles to efficient administration. For this experiment, bovine retina with vitreous was cultured to preserve the membranes and simulate the hindrances (Huang et al., 2017). In the following, some published models are presented to get an impression of the potential of retinal organ cultures.

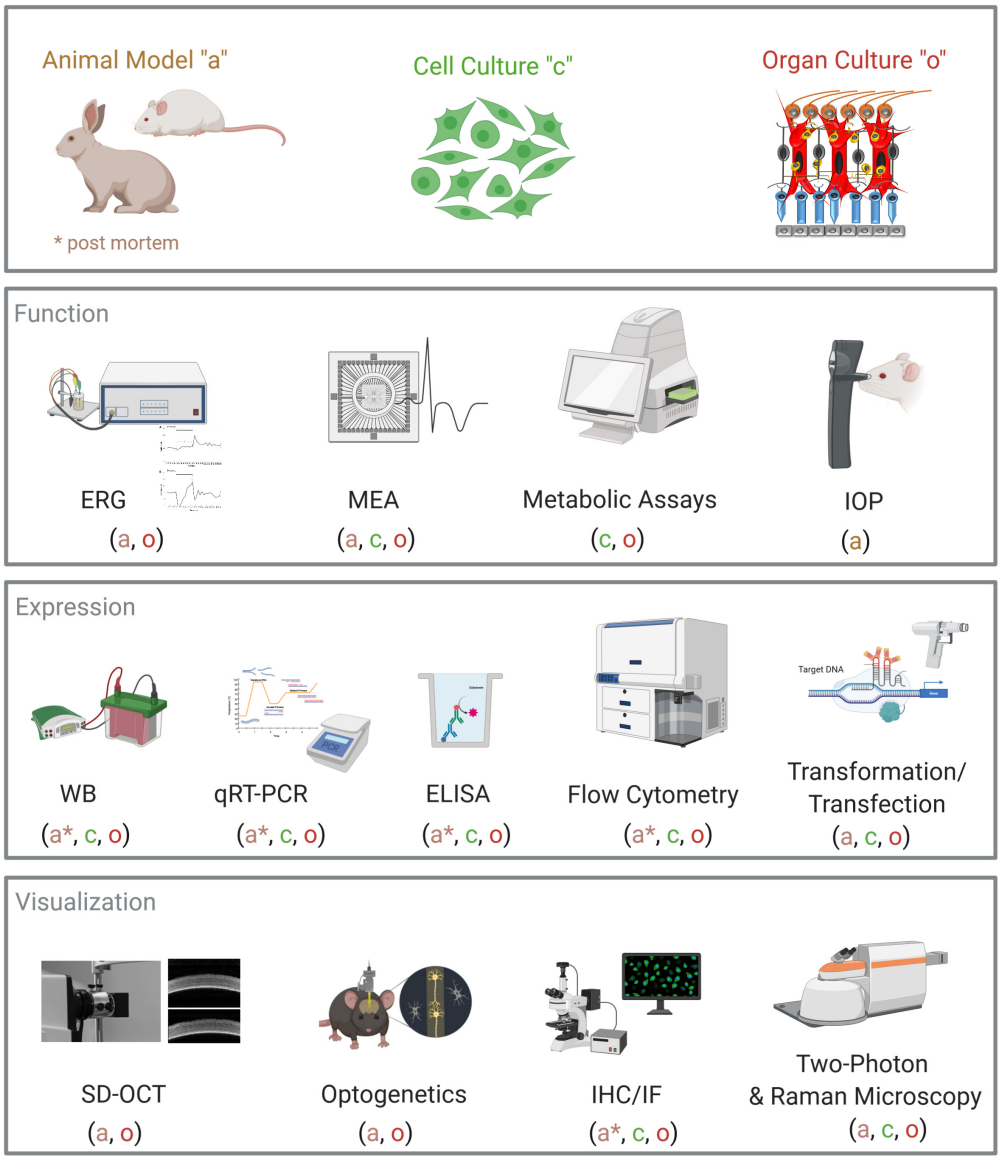

FIGURE 1 | Overview of analytical methods for retinal organ cultures. Common laboratory and diagnostic methods are displayed. For each method, it is noted if it can be performed on animal models (a), on cell cultures (c), or on organ cultures (o). Abbreviations: ERG, electroretinogram; MEA, microelectrode array; IOP, intraocular pressure; WB, Western blot; qRT-PCR, quantitative real-time PCR; ELISA, enzyme-linked immunosorbent assay; SD-OCT, spectral domain optical coherence tomography; IHC, immunohistochemistry; IF, immunofluorescence. Created with BioRender.com.

Age-Related Macular Degeneration

AMD represents a complex and heterogeneous disease that affects the macula, with both genetic and environmental factors playing a role (Bhutto and Lutty, 2012). AMD can be divided into the dry, non-exudative form with cellular debris (drusen) accumulating between the Bruch's membrane and the RPE layer, leading to an undersupply and atrophy of RPE cells, and a wet, exudative form with growing blood vessels behind the retina causing hemorrhaging. Appropriate *in vivo* models for this multifactorial eye disease are limited. Various animal models were created in mice, rats, or rabbits and resembled some of the histological features of AMD, but none of these models summarizes all of the conditions of human AMD (Zeiss, 2010; Pennesi et al., 2012b; Armento et al., 2020). Most models rely on damages like laser-induced injuries to the RPE and Bruch's membrane or transgenic animals displaying AMD-like defects (Shah et al., 2015; Carver et al., 2017; Park et al., 2017; Tode et al., 2018). Furthermore, severe differences in immune response between humans and rodents make research of diseases that have a high inflammatory component challenging (Mestas and Hughes, 2004). The absence of a macula in these animals makes it even more difficult. Therefore, it can be concluded that all these models give only simplified information on the pathogenesis of this complex disease, as reviewed in detail in Schnichels et al. (2020). Due to

the lack of suitable *ex vivo* models for AMD, so far, most studies on primary RPE cultures have been performed (Schnichels et al., 2020).

In contrast to commonly used retinal explants, which consist only of the detached retina, co-cultivation of primary RPE cells, human ARPE-19, or hTERT-RPE1 cells with neuroretina explanate is particularly important to create a functioning model for studying AMD pathogenesis (Armento et al., 2020; Wagner et al., 2020). Retinal explant cultures with RPE can be maintained *in vitro* for several weeks under entirely controlled conditions (Söderpalm et al., 1994). Choroid/RPE cultures are another important organ model in this research field and were used to study AMD-related molecular pathways. Klettner et al. (2013) demonstrated in RPE/choroid cultures that VEGF can be regulated independently by p38 and NFκB.

Glaucoma

Glaucoma is defined by a loss of RGCs and optic nerve degeneration, leading to visual field defects. Since an elevated intraocular pressure (IOP) is the main risk factor, many glaucoma (animal) models rely on increased IOP or optic nerve damage (Bouhenni et al., 2012; Ishikawa et al., 2015; McMonnies, 2017). Glaucoma research mainly depends on rat and mouse models due to improved methods of inducing and evaluating glaucoma damage and the availability of genetic tools in rodents (Pang and Clark, 2020). In most of these models, the IOP is surgically increased by laser-induced damage or microbead injection (Zhang et al., 2017; Calkins et al., 2018; de Hoz et al., 2018). Other glaucoma models are optic nerve crush or axotomy (Schnichels et al., 2012b; Donahue et al., 2019). Although acute optic nerve damage models are often not suitable to mimic chronic glaucoma, they are useful to evaluate RGC pathogenesis and neuroregeneration (Nadal-Nicolás et al., 2017). Consequently, several retinal *ex vivo* models are based on physically or chemically induced damage of RGCs. Although even the axotomy leads to RGC injury, chemical treatment with hydrogen peroxide (H_2O_2) or cobalt chloride ($CoCl_2$) may additionally induce oxidative stress or hypoxia-like processes in retinal cells (del Olmo-Aguado et al., 2013; Kuehn et al., 2017; Maliha et al., 2019). Incubation with H_2O_2 led to severe degeneration of RGCs with persistent apoptosis. Furthermore, a strong microglial response was observed, which was demonstrated by an increased expression of corresponding markers heat shock protein (HSP)70, inducible nitric oxide synthase (iNOS), and interleukin (IL)-1β (Hurst et al., 2017a). $CoCl_2$ application on porcine retinal cultures resulted in a loss of RGCs as well as amacrine and bipolar cells. Interestingly, $CoCl_2$ inhibited not only the number but also the activity of microglial cells (Kuehn et al., 2017). An effect of macroglia was not observed under any substance (Hurst et al., 2017a; Kuehn et al., 2017). Using these models, it was possible to perform therapy tests in which the neuroprotective effect of hypothermia and of the iNOS inhibitor 1400W on the different retinal cells was tested. It was found that both therapies provide improved RGC survival (Hurst et al., 2019, 2020; Maliha et al., 2019).

Retinitis Pigmentosa

RP is a genetically determined multifactorial disease that leads to dystrophy of the photoreceptors (Hamel, 2006). Many animal models of (natural and transgenic) RP are available like rd1- and rd10 mice or S334-ter line rats and have led to a better understanding of the pathology of the disease and the development of therapeutic strategies (Pennesi et al., 2012a; Seiler et al., 2014). In case of the rd1 mice, a nonsense mutation in exon 7 of the Pde6b gene leads to the degeneration of rod photoreceptor within the first 3 weeks (Chang and Min, 2011). Therefore, the possible culture time for organ explants is perfect to investigate degenerative processes. Retinal postnatal day 2 (P2) explants from wild-type mice, as well as from rd1-mice (P2), can be cultivated for up to 4 weeks and follow the same developmental time course as that in *in vivo* littermates (Ogilvie et al., 1999). The cultured retinae follow the same developmental time course as that *in vivo* and provide the degeneration environment needed to study several factors and therapeutic treatments. A great advantage of these *ex vivo* cultures is that therapeutic treatments can be easily applied, whereas injection into the small eyes of young mice is challenging. Further, organ cultures enable a constant and controlled treatment for the wished duration (Ogilvie et al., 1999; Sahaboglu et al., 2010).

Central Retinal Occlusion

CRAO is an acute, painless sudden occlusion of the central retinal artery, which first leads to ischemia and then vision loss (Graefe, 1859). The molecular mechanisms and reactions following retinal ischemia are complex, which makes the pathophysiological assessment very difficult (Osborne et al., 2004). Different models were developed for ischemia by either placing the organ cultures in a hypoxia chamber or by chemically inducing ischemia or neurodegeneration by adding glutamate. In the hypoxia *ex vivo* models, the retina is placed in culture, with the retina lying on a lower insert, i.e., the outer retina is supplied with oxygen and nutrients by the underlying medium. Hypoxia therefore mainly affects the inner retina. Thus, these *ex vivo* models are comparable to the *in vivo* situation where the outer retina is still nourished while the inner retina lacks oxygen, glucose, and other nutrients. These models were also used to test possible therapies as hypothermia, which represents an already established therapy in neurology (Schultheiss et al., 2016; Klemm et al., 2019). Hypothermia treatment on retinae under hypoxic stress prevented the death of RGCs and attenuated the gliosis response (Klemm et al., 2019). Testing this rather simple therapy *in vivo* would have been much more difficult or even impossible.

DISCUSSION

The culture system most similar to *in vivo* conditions is the retinal explant culture, which conserves the complex connections of neuronal and other functionally important non-neuronal cells of the retina. The presence of several cell types allows the study of *in vivo* dynamics of cell–cell interaction, immune responses, and degeneration pathways. Retinal explant models provide insights into retinal pathologies and can be used for therapy testing

(Li et al., 2018; Cheng et al., 2019; Schnichels et al., 2020). However, their use in AMD research is still limited.

Yet, depending on the species used for organ culture, it needs to be assessed whether the results are at all transferable to the human situation. This transferability is not always possible for some organ cultures of rodents, but for organ cultures of higher mammals, it is quite realistic due to the high homology (Neitz and Neitz, 2001; Peichl, 2005; Volland et al., 2015; Murali et al., 2019; Schnichels et al., 2019). Further efforts to improve current *ex vivo* culture techniques should aim to produce models to fill this gap.

In summary, promising models are already developed, but a continuous further modification and refinement of these models are necessary to reflect the complexity of the retina more precisely.

AUTHOR CONTRIBUTIONS

JH, AF, and SS wrote and revised the manuscript. SJ and TT revised the manuscript. All authors read and approved the final version of the manuscript.

FUNDING

JH acknowledges funding from the Tübinger Athene-Programm für Nachwuchs-Wissenschaftlerinnen and the Forschungsorientierte Gleichstellungsförderung. SS acknowledges funding from the Fortüne Program of the Medical Faculty Tübingen (2543-1-0).

REFERENCES

Aizawa, Y., and Shoichet, M. S. (2012). The role of endothelial cells in the retinal stem and progenitor cell niche within a 3D engineered hydrogel matrix. *Biomaterials* 33, 5198–5205. doi: 10.1016/j.biomaterials.2012.03.062

Åkerström, B., Cederlund, M., Bergwik, J., Manouchehrian, O., Arnér, K., Taylor, I. H., et al. (2017). The role of mitochondria, oxidative stress, and the radical-binding protein A1M in cultured porcine retina. *Curr. Eye Res.* 42, 948–961. doi: 10.1080/02713683.2016.1254247

Albanna, W., Banat, M., Albanna, N., Alnawaiseh, M., Siapich, S. A., Igelmund, P., et al. (2009). Longer lasting electroretinographic recordings from the isolated and superfused murine retina. *Graefes Arch. Clin. Exp. Ophthalmol.* 247, 1339–1352. doi: 10.1007/s00417-009-1119-1

Armento, A., Honisch, S., Panagiotakopoulou, V., Sonntag, I., Jacob, A., Bolz, S., et al. (2020). Loss of complement factor H impairs antioxidant capacity and energy metabolism of human RPE cells. *Sci. Rep.* 10:10320. doi: 10.1038/s41598-020-67292-z

Baden, T., Berens, P., Franke, K., Roman Roson, M., Bethge, M., and Euler, T. (2016). The functional diversity of retinal ganglion cells in the mouse. *Nature* 529, 345–350. doi: 10.1038/nature16468

Bhutto, I., and Lutty, G. (2012). Understanding age-related macular degeneration (AMD): relationships between the photoreceptor/retinal pigment epithelium/Bruch's membrane/choriocapillaris complex. *Mol. Aspects Med.* 33, 295–317. doi: 10.1016/j.mam.2012.04.005

Bouhenni, R. A., Dunmire, J., Sewell, A., and Edward, D. P. (2012). Animal models of glaucoma. *J. Biomed. Biotechnol.* 2012:692609.

Calkins, D. J., Lambert, W. S., Formichella, C. R., McLaughlin, W. M., and Sappington, R. M. (2018). The microbead occlusion model of ocular hypertension in mice. *Methods Mol. Biol.* 1695, 23–39. doi: 10.1007/978-1-4939-7407-8_3

Carver, K. A., Lin, C. M., Bowes Rickman, C., and Yang, D. (2017). Lack of the P2X7 receptor protects against AMD-like defects and microparticle accumulation in a chronic oxidative stress-induced mouse model of AMD. *Biochem. Biophys. Res. Commun.* 482, 81–86. doi: 10.1016/j.bbrc.2016.10.140

Chang, K. T., and Min, K. T. (2011). Progress in molecular biology and translational science. Animal models of human disease. Preface. *Prog. Mol. Biol. Transl. Sci.* 100:xv. doi: 10.1016/b978-0-12-384878-9.00021-2

Cheng, Z., Yao, W., Zheng, J., Ding, W., Wang, Y., Zhang, T., et al. (2019). A derivative of betulinic acid protects human retinal pigment epithelial (RPE) cells from cobalt chloride-induced acute hypoxic stress. *Exp. Eye Res.* 180, 92–101. doi: 10.1016/j.exer.2018.12.011

Clark, A., Tamm, E. R., Al-Ubaidi, M. R., and Hollyfield, J. G. (2013). On the use of immortalized ocular cell lines in vision research: the unfortunate story of RGC-5. *Exp. Eye Res.* 116:433. doi: 10.1016/j.exer.2013.08.002

Dalkara, D., Byrne, L. C., Klimczak, R. R., Visel, M., Yin, L., Merigan, W. H., et al. (2013). In vivo-directed evolution of a new adeno-associated virus for therapeutic outer retinal gene delivery from the vitreous. *Sci. Transl. Med.* 5:189ra76. doi: 10.1126/scitranslmed.3005708

Dalkara, D., Goureau, O., Marazova, K., and Sahel, J. A. (2016). Let there be light: gene and cell therapy for blindness. *Hum. Gene Ther.* 27, 134–147. doi: 10.1089/hum.2015.147

de Hoz, R., Ramirez, A. I., Gonzalez-Martin, R., Ajoy, D., Rojas, B., Salobrar-Garcia, E., et al. (2018). Bilateral early activation of retinal microglial cells in a mouse model of unilateral laser-induced experimental ocular hypertension. *Exp. Eye Res.* 171, 12–29. doi: 10.1016/j.exer.2018.03.006

del Olmo-Aguado, S., Nunez-Alvarez, C., Ji, D., Manso, A. G., and Osborne, N. N. (2013). RTP801 immunoreactivity in retinal ganglion cells and its down-regulation in cultured cells protect them from light and cobalt chloride. *Brain Res. Bull.* 98, 132–144. doi: 10.1016/j.brainresbull.2013.08.002

Di Lauro, S., Rodriguez-Crespo, D., Gayoso, M. J., Garcia-Gutierrez, M. T., Pastor, J. C., Srivastava, G. K., et al. (2016). A novel coculture model of porcine central neuroretina explants and retinal pigment epithelium cells. *Mol. Vis.* 22, 243–253.

Donahue, R. J., Maes, M. E., Grosser, J. A., and Nickells, R. W. (2019). BAX-depleted retinal ganglion cells survive and become quiescent following optic nerve damage. *Mol. Neurobiol.* 57, 1070–1084. doi: 10.1007/s12035-019-01783-7

Eiraku, M., Takata, N., Ishibashi, H., Kawada, M., Sakakura, E., Okuda, S., et al. (2011). Self-organizing optic-cup morphogenesis in three-dimensional culture. *Nature* 472, 51–56. doi: 10.1038/nature09941

Engelsberg, K., Ehinger, B., and Ghosh, F. (2008). Early development of retinal subtypes in long-term cultures of human embryonic retina. *Curr. Eye Res.* 33, 185–191. doi: 10.1080/02713680701843784

Fernandez-Bueno, I., Fernandez-Sanchez, L., Gayoso, M. J., Garcia-Gutierrez, M. T., Pastor, J. C., and Cuenca, N. (2012). Time course modifications in organotypic culture of human neuroretina. *Exp. Eye Res.* 104, 26–38. doi: 10.1016/j.exer.2012.08.012

Fontaine, V., Kinkl, N., Sahel, J., Dreyfus, H., and Hicks, D. (1998). Survival of purified rat photoreceptors *in vitro* is stimulated directly by fibroblast growth factor-2. *J. Neurosci.* 18, 9662–9672. doi: 10.1523/jneurosci.18-23-09662.1998

Fujimoto, J. G., Bouma, B., Tearney, G. J., Boppart, S. A., Pitris, C., Southern, J. F., et al. (1998). New technology for high-speed and high-resolution optical coherence tomography. *Ann. N. Y. Acad. Sci.* 838, 95–107.

Ganapathy, P. S., Dun, Y., Ha, Y., Duplantier, J., Allen, J. B., Farooq, A., et al. (2010). Sensitivity of staurosporine-induced differentiated RGC-5 cells to homocysteine. *Curr. Eye Res.* 35, 80–90. doi: 10.3109/02713680903421194

Gomes da Costa, S., Richter, A., Schmidt, U., Breuninger, S., and Hollricher, O. (2019). Confocal Raman microscopy in life sciences. *Morphologie* 103, 11–16. doi: 10.1016/j.morpho.2018.12.003

Graefe, A. (1859). Ueber embolie der arteria centralis retinae als ursache plotzlicher erblindung. *Albrecht Von Graefes Arch. Ophthalmol.* 5, 136–157. doi: 10.1007/bf02720764

Guduric-Fuchs, J., Ringland, L. J., Gu, P., Dellett, M., Archer, D. B., and Cogliati, T. (2009). Immunohistochemical study of pig retinal development. *Mol. Vis.* 15, 1915–1928.

Hamel, C. (2006). Retinitis pigmentosa. *Orphanet J. Rare Dis.* 1:40.

Harper, M. M., Adamson, L., Blits, B., Bunge, M. B., Grozdanic, S. D., and Sakaguchi, D. S. (2009). Brain-derived neurotrophic factor released from engineered mesenchymal stem cells attenuates glutamate-and hydrogen peroxide-mediated death of staurosporine-differentiated RGC-5 cells. *Exp. Eye Res.* 89, 538–548. doi: 10.1016/j.exer.2009.05.013

Helmchen, F., and Denk, W. (2005). Deep tissue two-photon microscopy. *Nat. Methods* 2, 932–940. doi: 10.1038/nmeth818

Homma, K., Osakada, F., Hirami, Y., Jin, Z. B., Mandai, M., and Takahashi, M. (2009). Detection of localized retinal malfunction in retinal degeneration model using a multielectrode array system. *J. Neurosci. Res.* 87, 2175–2182. doi: 10.1002/jnr.22024

Huang, D., Chen, Y. S., Thakur, S. S., and Rupenthal, I. D. (2017). Ultrasound-mediated nanoparticle delivery across *ex vivo* bovine retina after intravitreal injection. *Eur. J. Pharm. Biopharm.* 119, 125–136. doi: 10.1016/j.ejpb.2017.06.009

Hughes, A. J., Spelke, D. P., Xu, Z., Kang, C. C., Schaffer, D. V., and Herr, A. E. (2014). Single-cell western blotting. *Nat. Methods* 11, 749–755.

Hunt, N. C., Hallam, D., Karimi, A., Mellough, C. B., Chen, J., Steel, D. H. W., et al. (2017). 3D culture of human pluripotent stem cells in RGD-alginate hydrogel improves retinal tissue development. *Acta Biomater.* 49, 329–343. doi: 10.1016/j.actbio.2016.11.016

Hurst, J., Kuehn, S., Jashari, A., Tsai, T., Bartz-Schmidt, K. U., Schnichels, S., et al. (2017a). A novel porcine ex vivo retina culture model for oxidative stress induced by H(2)O(2). *Altern. Lab. Anim.* 45, 11–25. doi: 10.1177/026119291704500105

Hurst, J., Maliha, A., Kuehn, S., Herms, F., Schnichels, S., and Joachim, S. C. (2019). iNOS-inhibitor treatment leads to cell rescue in a porcine retina organ culture model. *Invest. Ophthalmol. Vis. Sci.* 60:4873.

Hurst, J., Mueller-Buehl, A. M., Hofmann, L., Kuehn, S., Herms, F., Schnichels, S., et al. (2020). iNOS-inhibitor driven neuroprotection in a porcine retina organ culture model. *J. Cell. Mol. Med.* 24, 4312–4323. doi: 10.1111/jcmm.15091

Hurst, J., Schnichels, S., Spitzer, M. S., Bartz-Schmidt, K. U., Farecki, M. L., Szurman, P., et al. (2017b). Negative effects of acid violet-17 and MBB dual in vitro on different ocular cell lines. *Curr. Eye Res.* 42, 1209–1214. doi: 10.1080/02713683.2017.1285942

Hurst, J., Vitkute, M., Hofmann, K., Muller, S., Loscher, M., Bartz-Schmidt, K. U., et al. (2018). Comparison of different cell culture media in the model of the isolated and superfused bovine retina: investigating the limits of more physiological perfusion solutions. *Curr. Eye Res.* 43, 232–243. doi: 10.1080/02713683.2017.1387668

Ishikawa, M., Yoshitomi, T., Zorumski, C. F., and Izumi, Y. (2015). Experimentally induced mammalian models of glaucoma. *Biomed. Res. Int.* 2015: 281214.

Januschowski, K., Mueller, S., Dollinger, R., Schnichels, S., Hofmann, J., Spitzer, M. S., et al. (2014a). Investigating retinal toxicity of tempol in a model of isolated and perfused bovine retina. *Graefes Arch. Clin. Exp. Ophthalmol.* 252, 935–941. doi: 10.1007/s00417-014-2632-4

Januschowski, K., Schnichels, S., Hagemann, U., Koch, V., Hofmann, J., Spitzer, M. S., et al. (2014b). Electrophysiological toxicity testing of VEGF Trap-Eye in an isolated perfused vertebrate retina organ culture model. *Acta Ophthalmol.* 92, e305–e311.

Joachim, S. C., Gramlich, O. W., Laspas, P., Schmid, H., Beck, S., von Pein, H. D., et al. (2012). Retinal ganglion cell loss is accompanied by antibody depositions and increased levels of microglia after immunization with retinal antigens. *PLoS One* 7:e40616. doi: 10.1371/journal.pone.0040616

Jüttner, J., Szabo, A., Gross-Scherf, B., Morikawa, R. K., Rompani, S. B., Hantz, P., et al. (2019). Targeting neuronal and glial cell types with synthetic promoter AAVs in mice, non-human primates and humans. *Nat. Neurosci.* 22, 1345–1356. doi: 10.1038/s41593-019-0431-2

Keane, P. A., Liakopoulos, S., Chang, K. T., Wang, M., Dustin, L., Walsh, A. C., et al. (2008). Relationship between optical coherence tomography retinal parameters and visual acuity in neovascular age-related macular degeneration. *Ophthalmology* 115, 2206–2214. doi: 10.1016/j.ophtha.2008.08.016

Klemm, P., Hurst, J., Dias Blak, M., Herrmann, T., Melchinger, M., Bartz-Schmidt, K. U., et al. (2019). Hypothermia protects retinal ganglion cells against hypoxia-induced cell death in a retina organ culture model. *Clin. Exp. Ophthalmol.* 47, 1043–1054. doi: 10.1111/ceo.13565

Klettner, A., Westhues, D., Lassen, J., Bartsch, S., and Roider, J. (2013). Regulation of constitutive vascular endothelial growth factor secretion in retinal pigment epithelium/choroid organ cultures: p38, nuclear factor κB, and the vascular endothelial growth factor receptor-2/phosphatidylinositol 3 kinase pathway. *Mol. Vis.* 19, 281–291.

Krishnamoorthy, R. R., Clark, A. F., Daudt, D., Vishwanatha, J. K., and Yorio, T. (2013). A forensic path to RGC-5 cell line identification: lessons learned. *Invest. Ophthalmol. Vis. Sci.* 54, 5712–5719. doi: 10.1167/iovs.13-12085

Kuchler, G., Pilz, A., and Sickel, W. (1956). [Adaptation and photostimulability of isolated frog eyes in electroretinography]. *Pflugers Arch. Gesamte Physiol. Menschen Tiere* 263, 577–588.

Kuehn, S., Hurst, J., Jashari, A., Ahrens, K., Tsai, T., Wunderlich, I. M., et al. (2016). The novel induction of retinal ganglion cell apoptosis in porcine organ culture by NMDA – an opportunity for the replacement of animals in experiments. *Altern. Lab. Anim.* 44, 557–568. doi: 10.1177/026119291604400608

Kuehn, S., Hurst, J., Rensinghoff, F., Tsai, T., Grauthoff, S., Satgunarajah, Y., et al. (2017). Degenerative effects of cobalt-chloride treatment on neurons and microglia in a porcine retina organ culture model. *Exp. Eye Res.* 155, 107–120. doi: 10.1016/j.exer.2017.01.003

Li, Y., Zhang, Y., Qi, S., and Su, G. (2018). Retinal organotypic culture – a candidate for research on retinas. *Tissue Cell* 51, 1–7. doi: 10.1016/j.tice.2018.01.005

Luke, M., Januschowski, K., Luke, J., Peters, S., Wirtz, N., Yoruk, E., et al. (2009). The effects of ranibizumab (Lucentis) on retinal function in isolated perfused vertebrate retina. *Br. J. Ophthalmol.* 93, 1396–1400. doi: 10.1136/bjo.2009.157511

MacLeod, R. A., Dirks, W. G., Matsuo, Y., Kaufmann, M., Milch, H., and Drexler, H. G. (1999). Widespread intraspecies cross-contamination of human tumor cell lines arising at source. *Int. J. Cancer* 83, 555–563. doi: 10.1002/(sici)1097-0215(19991112)83:4<555::aid-ijc19>3.0.co;2-2

Maliha, A. M., Kuehn, S., Hurst, J., Herms, F., Fehr, M., Bartz-Schmidt, K. U., et al. (2019). Diminished apoptosis in hypoxic porcine retina explant cultures through hypothermia. *Sci. Rep.* 9:4898.

Marwick, K. F. M., and Hardingham, G. E. (2017). Transfection in primary cultured neuronal cells. *Methods Mol. Biol.* 1677, 137–144. doi: 10.1007/978-1-4939-7321-7_6

McMonnies, C. W. (2017). Glaucoma history and risk factors. *J. Optom.* 10, 71–78.

Mestas, J., and Hughes, C. C. (2004). Of mice and not men: differences between mouse and human immunology. *J. Immunol.* 172, 2731–2738. doi: 10.4049/jimmunol.172.5.2731

Murali, A., Ramlogan-Steel, C. A., Andrzejewski, S., Steel, J. C., and Layton, C. J. (2019). Retinal explant culture: a platform to investigate human neuro-retina. *Clin. Exp. Ophthalmol.* 47, 274–285. doi: 10.1111/ceo.13434

Nadal-Nicolás, F. M., Jiménez-López, M., Salinas-Navarro, M., Sobrado-Calvo, P., Vidal-Sanz, M., and Agudo-Barriuso, M. (2017). Microglial dynamics after axotomy-induced retinal ganglion cell death. *J. Neuroinflamm.* 14:218.

Neitz, M., and Neitz, J. (2001). The uncommon retina of the common house mouse. *Trends Neurosci.* 24, 248–250. doi: 10.1016/s0166-2236(00)01773-2

Obien, M. E., Deligkaris, K., Bullmann, T., Bakkum, D. J., and Frey, U. (2014). Revealing neuronal function through microelectrode array recordings. *Front. Neurosci.* 8:423. doi: 10.3389/fnins.2014.00423

Ogilvie, J. M., Speck, J. D., Lett, J. M., and Fleming, T. T. (1999). A reliable method for organ culture of neonatal mouse retina with long-term survival. *J. Neurosci. Methods* 87, 57–65. doi: 10.1016/s0165-0270(98)00157-5

Osborne, A., Hopes, M., Wright, P., Broadway, D. C., and Sanderson, J. (2016). Human organotypic retinal cultures (HORCs) as a chronic experimental model for investigation of retinal ganglion cell degeneration. *Exp. Eye Res.* 143, 28–38. doi: 10.1016/j.exer.2015.09.012

Osborne, N. N., Casson, R. J., Wood, J. P., Chidlow, G., Graham, M., and Melena, J. (2004). Retinal ischemia: mechanisms of damage and potential therapeutic strategies. *Prog. Retin. Eye Res.* 23, 91–147. doi: 10.1016/j.preteyeres.2003.12.001

Pang, I. H., and Clark, A. F. (2020). Inducible rodent models of glaucoma. *Prog. Retin. Eye Res.* 75:100799. doi: 10.1016/j.preteyeres.2019.100799

Park, S. W., Im, S., Jun, H. O., Lee, K., Park, Y. J., Kim, J. H., et al. (2017). Dry age-related macular degeneration like pathology in aged 5XFAD mice: ultrastructure and microarray analysis. *Oncotarget* 8, 40006–40018. doi: 10.18632/oncotarget.16967

Peichl, L. (2005). Diversity of mammalian photoreceptor properties: adaptations to habitat and lifestyle? *Anat. Rec. A Discov. Mol. Cell. Evol. Biol.* 287, 1001–1012. doi: 10.1002/ar.a.20262

Pennesi, M. E., Michaels, K. V., Magee, S. S., Maricle, A., Davin, S. P., Garg, A. K., et al. (2012a). Long-term characterization of retinal degeneration in rd1 and rd10 mice using spectral domain optical coherence tomography. *Invest. Ophthalmol. Vis. Sci.* 53, 4644–4656. doi: 10.1167/iovs.12-9611

Pennesi, M. E., Neuringer, M., and Courtney, R. J. (2012b). Animal models of age related macular degeneration. *Mol. Aspects Med.* 33, 487–509.

Ran, Y., Huang, Z., Baden, T., Schubert, T., Baayen, H., Berens, P., et al. (2020). Type-specific dendritic integration in mouse retinal ganglion cells. *Nat. Commun.* 11:2101.

Roark, E. F., Paradies, N. E., Lagunowich, L. A., and Grunwald, G. B. (1992). Evidence for endogenous proteases, mRNA level and insulin as multiple mechanisms of N-cadherin down-regulation during retinal development. *Development* 114, 973–984.

Romano, C., and Hicks, D. (2007). Adult retinal neuronal cell culture. *Prog. Retin. Eye Res.* 26, 379–397. doi: 10.1016/j.preteyeres.2007.03.001

Rosolen, S. G., Kolomiets, B., Varela, O., and Picaud, S. (2008). Retinal electrophysiology for toxicology studies: applications and limits of ERG in animals and ex vivo recordings. *Exp. Toxicol. Pathol.* 60, 17–32. doi: 10.1016/j.etp.2007.11.012

Sahaboglu, A., Tanimoto, N., Kaur, J., Sancho-Pelluz, J., Huber, G., Fahl, E., et al. (2010). PARP1 gene knock-out increases resistance to retinal degeneration without affecting retinal function. *PLoS One* 5:e15495. doi: 10.1371/journal.pone.0015495

Sasaki, T., Tamaki, J., Nishizawa, K., Kojima, T., Tanaka, R., Moriya, R., et al. (2019). Evaluation of cell viability and metabolic activity of a 3D cultured human epidermal model using a dynamic autoradiographic technique with a PET radiopharmaceutical. *Sci. Rep.* 9:10685.

Schnichels, S., Schultheiss, M., Hofmann, J., Szurman, P., Bartz-Schmidt, K. U., and Spitzer, M. S. (2012a). Trichostatin A induces cell death at the concentration recommended to differentiate the RGC-5 cell line. *Neurochem. Int.* 60, 581–591. doi: 10.1016/j.neuint.2012.02.017

Schnichels, S., Heiduschka, P., and Julien, S. (2012b). RGMA and neogenin protein expression are influenced by lens injury following optic nerve crush in the rat retina. *Graefes Arch. Clin. Exp. Ophthalmol.* 250, 39–50. doi: 10.1007/s00417-011-1791-9

Schnichels, S., Hagemann, U., Januschowski, K., Hofmann, J., Bartz-Schmidt, K. U., Szurman, P., et al. (2013). Comparative toxicity and proliferation testing of aflibercept, bevacizumab and ranibizumab on different ocular cells. *Br. J. Ophthalmol.* 97, 917–923. doi: 10.1136/bjophthalmol-2013-303130

Schnichels, S., Dorfi, T., Schultheiss, M., Arango-Gonzalez, B., Bartz-Schmidt, K. U., Januschowski, K., et al. (2016). Ex-vivo-examination of ultrastructural changes in organotypic retina culture using near-infrared imaging and optical coherence tomography. *Exp. Eye Res.* 147, 31–36. doi: 10.1016/j.exer.2016.04.011

Schnichels, S., Kiebler, T., Hurst, J., Maliha, A. M., Loscher, M., Dick, H. B., et al. (2019). Retinal organ cultures as alternative research models. *Altern. Lab. Anim.* 47, 19–29. doi: 10.1177/0261192919840092

Schnichels, S., Paquet-Durand, F., Loscher, M., Tsai, T., Hurst, J., Joachim, S. C., et al. (2020). Retina in a dish: cell cultures, retinal explants and animal models for common diseases of the retina. *Prog. Retin. Eye Res.* 100880. doi: 10.1016/j.preteyeres.2020.100880

Schultheiss, M., Schnichels, S., Hermann, T., Hurst, J., Feldkaemper, M., Arango-Gonzalez, B., et al. (2016). Hypothermia protects and prolongs the tolerance time of retinal ganglion cells against ischemia. *PLoS One* 11:e0148616. doi: 10.1371/journal.pone.0148616

Seiler, M. J., Aramant, R. B., Jones, M. K., Ferguson, D. L., Bryda, E. C., and Keirstead, H. S. (2014). A new immunodeficient pigmented retinal degenerate rat strain to study transplantation of human cells without immunosuppression. *Graefes Arch. Clin. Exp. Ophthalmol.* 252, 1079–1092. doi: 10.1007/s00417-014-2638-y

Shah, R. S., Soetikno, B. T., Lajko, M., and Fawzi, A. A. (2015). A mouse model for laser-induced choroidal neovascularization. *J. Vis. Exp.* 106:e53502.

Sharma, R., Schwarz, C., Williams, D. R., Palczewska, G., Palczewski, K., and Hunter, J. J. (2016). In vivo two-photon fluorescence kinetics of primate rods and cones. *Invest. Ophthalmol. Vis. Sci.* 57, 647–657. doi: 10.1167/iovs.15-17946

Sippl, C., and Tamm, E. R. (2014). What is the nature of the RGC-5 cell line? *Adv. Exp. Med. Biol.* 801, 145–154. doi: 10.1007/978-1-4614-3209-8_19

Söderpalm, A., Szél, A., Caff, A. R., and van Veen, T. (1994). Selective development of one cone photoreceptor type in retinal organ culture. *Invest. Ophthalmol. Vis. Sci.* 35, 3910–3921.

Soto-Sanchez, C., Martinez-Navarrete, G., Humphreys, L., Puras, G., Zarate, J., Pedraz, J. L., et al. (2015). Enduring high-efficiency in vivo transfection of neurons with non-viral magnetoparticles in the rat visual cortex for optogenetic applications. *Nanomedicine* 11, 835–843. doi: 10.1016/j.nano.2015.01.012

Tanihara, H., Hangai, M., Sawaguchi, S., Abe, H., Kageyama, M., Nakazawa, F., et al. (1997). Up-regulation of glial fibrillary acidic protein in the retina of primate eyes with experimental glaucoma. *Arch. Ophthalmol.* 115, 752–756. doi: 10.1001/archopht.1997.01100150754011

Tao, Y., Zhu, Q., Wang, L., Zha, X., Teng, D., and Xu, L. (2020). Adeno-associated virus (AAV)-mediated neuroprotective effects on the degenerative retina: the therapeutic potential of erythropoietin. *Fundam. Clin. Pharmacol.* 34, 131–147. doi: 10.1111/fcp.12494

Tode, J., Richert, E., Koinzer, S., Klettner, A., von der Burchard, C., Brinkmann, R., et al. (2018). Thermal stimulation of the retina reduces Bruch's membrane thickness in age related macular degeneration mouse models. *Transl. Vis. Sci. Technol.* 7:2. doi: 10.1167/tvst.7.3.2

Van Bergen, N. J., Wood, J. P., Chidlow, G., Trounce, I. A., Casson, R. J., Ju, W. K., et al. (2009). Recharacterization of the RGC-5 retinal ganglion cell line. *Invest. Ophthalmol. Vis. Sci.* 50, 4267–4272. doi: 10.1167/iovs.09-3484

Volland, S., Esteve-Rudd, J., Hoo, J., Yee, C., and Williams, D. S. (2015). A comparison of some organizational characteristics of the mouse central retina and the human macula. *PLoS One* 10:e0125631. doi: 10.1371/journal.pone.0125631

Wagner, N., Reinehr, S., Gammel, M. R., Greulich, A., Hurst, J., Dick, H. B., et al. (2020). Novel porcine retina cultivation techniques provide improved photoreceptor preservation. *Front. Cell. Neurosci.* 14:556700. doi: 10.3389/fnins.2020.556700

Wood, J. P., Chidlow, G., Tran, T., Crowston, J. G., and Casson, R. J. (2010). A comparison of differentiation protocols for RGC-5 cells. *Invest. Ophthalmol. Vis. Sci.* 51, 3774–3783. doi: 10.1167/iovs.09-4305

Wurm, A., Iandiev, I., Uhlmann, S., Wiedemann, P., Reichenbach, A., Bringmann, A., et al. (2011). Effects of ischemia-reperfusion on physiological properties of Muller glial cells in the porcine retina. *Invest. Ophthalmol. Vis. Sci.* 52, 3360–3367. doi: 10.1167/iovs.10-6901

Yang, S. Y., Sun, J. S., Liu, C. H., Tsuang, Y. H., Chen, L. T., Hong, C. Y., et al. (2008). Ex vivo magnetofection with magnetic nanoparticles: a novel platform for nonviral tissue engineering. *Artif. Organs* 32, 195–204. doi: 10.1111/j.1525-1594.2007.00526.x

Zeck, G. (2018). Investigation of the functional retinal output using microelectrode arrays. *Methods Mol. Biol.* 1695, 81–88. doi: 10.1007/978-1-4939-7407-8_8

Zeiss, C. J. (2010). Animals as models of age-related macular degeneration: an imperfect measure of the truth. *Vet. Pathol.* 47, 396–413. doi: 10.1177/0300985809359598

Zhang, L., Li, G., Shi, M., Liu, H. H., Ge, S., Ou, Y., et al. (2017). Establishment and characterization of an acute model of ocular hypertension by laser-induced occlusion of episcleral veins. *Invest. Ophthalmol. Vis. Sci.* 58, 3879–3886. doi: 10.1167/iovs.16-20807

Zhao, S., and Barnstable, C. J. (1996). Differential effects of bFGF on development of the rat retina. *Brain Res.* 723, 169–176. doi: 10.1016/0006-8993(96)00237-5

Conflict of Interest: The authors declare that the research was conducted in the absence of any commercial or financial relationships that could be construed as a potential conflict of interest.

Copyright © 2020 Hurst, Fietz, Tsai, Joachim and Schnichels. This is an open-access article distributed under the terms of the Creative Commons Attribution License (CC BY). The use, distribution or reproduction in other forums is permitted, provided the original author(s) and the copyright owner(s) are credited and that the original publication in this journal is cited, in accordance with accepted academic practice. No use, distribution or reproduction is permitted which does not comply with these terms.

frontiers in Neuroscience

GENERAL COMMENTARY
published: 23 July 2021
doi: 10.3389/fnins.2021.714094

Commentary: Organ Cultures for Retinal Diseases

*Stephen R. Mut† and Maribel Vazquez**

Department of Biomedical Engineering, Rutgers, The State University of New Jersey, New Brunswick, NJ, United States

Keywords: microfluidics, vision loss, *in vitro*, stem cells, regeneration

A Commentary on

Organ Cultures for Retinal Diseases
by Hurst, J., Fietz, A., Tsai, T., Joachim, S. C., and Schnichels, S. (2020). Front. Neurosci. 14:583392. doi: 10.3389/fnins.2020.583392

The review by Hurst et al. (2020) is a comprehensive article published within this journal about the use of organotypic culture systems as models to study retinal diseases. The article noted that use of microfluidic technologies, such as microelectrode arrays (MEAs), can be significant in measuring cellular activity within organ culture systems (Hurst et al., 2020). An additional emerging area for microfluidics is their integration with explants to enrich transplantation strategies used to treat retinal degenerative diseases.

Progressive vision loss in adults is escalating worldwide, as the incidence of macular degeneration and diabetic retinopathy are expected to exceed 300 million and 642 million, respectively, by 2040 (Mitchell et al., 2018; Simo-Servat et al., 2019). The retina consists of a varied network of neurons that synapse with one another across three nuclear layers. Damage to any one type of neuron within this intricate network propagates dysfunction to result in progressive vision loss.

Contemporary cell replacement therapies offer exciting promise to restore vision by replacing damaged neurons with transplanted stem cells. Numerous platforms have been developed to elucidate the cellular mechanisms able to promote stem cell integration within mature retinal hosts (Wu et al., 2018). However, ongoing projects have produced mixed results, including low stem cell survival and the inability of stem cells to differentiate and/or position themselves appropriately within the retinal network (Gokoffski et al., 2019). A variety of *in vitro* and organotypic platforms have been developed to examine native stem cell behaviors within microscale environments (reviewed in Greene et al., 2019). Surprisingly, few of these projects have incorporated microfluidic technologies to model cues from damaged adult retina, such as fields of injury cytokines and degraded cellular matrixes (reviewed in Vazquez, 2020), that differ significantly from stem cell environments. A current thrust is to bridge microfluidic technologies with explanted retina to develop hybrid, quantitative models to examine stem cell behaviors within adult, organotypic cultures.

Initial hybrid models (**Figure 1**) cultured retinal explants within micro-scale transwell systems to measure long-term viability (Rettinger and Wang, 2018), while newer models integrated

OPEN ACCESS

Edited by:
Miguel Flores-Bellver, University of Colorado Anschutz Medical Campus, United States

Reviewed by:
Natalia Martínez-Gil, University of Alicante, Spain
María Miranda, Universidad CEU Cardenal Herrera, Spain

***Correspondence:**
Maribel Vazquez
maribel.vazquez@rutgers.edu

†ORCID:
Stephen R. Mut
orcid.org/0000-0002-1535-8342

Specialty section:
This article was submitted to Neurodegeneration, a section of the journal Frontiers in Neuroscience

Received: *24 May 2021*
Accepted: *15 June 2021*
Published: *23 July 2021*

Citation:
Mut SR and Vazquez M (2021) Commentary: Organ Cultures for Retinal Diseases. Front. Neurosci. 15:714094. doi: 10.3389/fnins.2021.714094

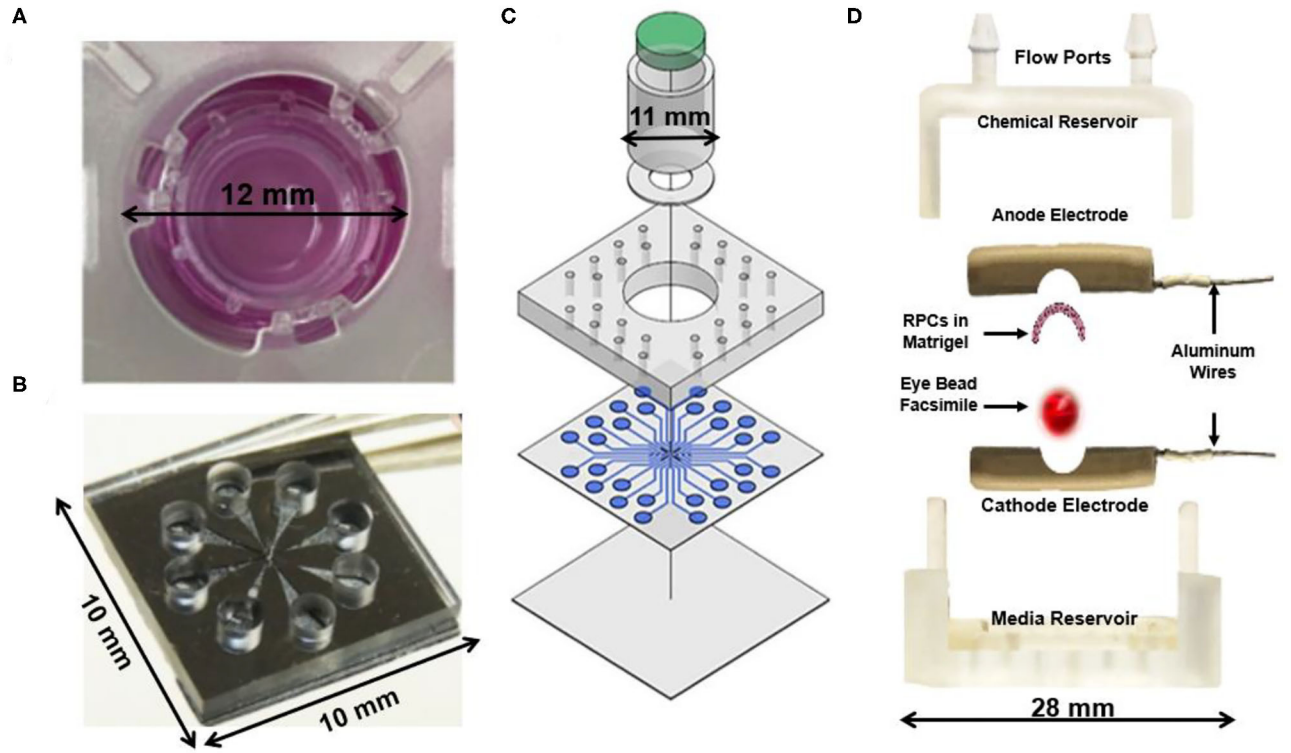

FIGURE 1 | Current hybrid explant systems for studying the retina. **(A)** An *ex vivo* chamber for a porcine retina explant capable of maintaining tissue viability for 1–2 weeks to enable long-term investigation of the *ex vivo* retina (Rettinger and Wang, 2018). **(B)** A glutamate perfusion system to stimulate retinal neurons with neurotransmitters to augment the phototransduction process that occurs within the body (Rountree et al., 2017). **(C)** Retina on a chip microfluidic perfusion assay system for point access delivery of therapeutics to specific parts of the rat retina (Dodson et al., 2015). **(D)** *Ex Vivo* Eye Facsimile (EVES) hybrid explant system designed for delivery of electrical and chemical stimulation to a whole-enucleated eye explant from mouse (Vazquez et al., 2020).

microfluidic perfusion systems for controlled delivery of neurotransmitters and therapeutics (Dodson et al., 2015; Rountree et al., 2017). Most recently, our group developed a hybrid system called the Ex Vivo Eye Facsimile System (EVES) to examine how extrinsic factors, such as chemical and electrical gradients, can promote appropriate stem cell positioning within retinal hosts (Mishra et al., 2019; Vazquez et al., 2020). Our system consists of a 3D environment that can be rapidly prototyped to meet the geometric constraints of enucleated eyes derived from a variety of animal models. Our preliminary EVES studies illustrated that combined electrochemical fields increased the numbers of motile stem cells and the distances migrated within rodent eye facsimiles. The integration of microfluidics with organotypic retinal cultures will therefore produce a new generation of quantitative platforms that enable newfound applications of external fields to enrich stem cell replacement strategies.

AUTHOR CONTRIBUTIONS

SM developed and wrote the manuscript. MV wrote and provided edits to the manuscript. All authors approved the final manuscript version for publication.

FUNDING

This work was supported by the US National Science Foundation (NSF CBET 180441) and the US National Institutes of Health (NEI 1R21 EY031439-01).

REFERENCES

Dodson, K. H., Echevarria, F. D., Li, D., Sappington, R. M., and Edd, J. F. (2015). Retina-on-a-chip: a microfluidic platform for point access signaling studies. *Biomed. Microdevices* 17:114. doi: 10.1007/s10544-015-0019-x

Gokoffski, K. K., Jia, X., Shvarts, D., Xia, G., and Zhao, M. (2019). Physiologic electrical fields direct retinal ganglion cell axon growth *in vitro*. *Invest. Ophthalmol. Vis. Sci.* 60, 3659–3668. doi: 10.1167/iovs.18-25118

Greene, W. A., Kaini, R. R., and Wang, H. C. (2019). Utility of induced pluripotent stem cell-derived retinal pigment epithelium for an *in vitro*

model of proliferative vitreoretinopathy. *Adv. Exp. Med. Biol.* 1186, 33–53. doi: 10.1007/978-3-030-28471-8_2

Hurst, J., Fietz, A., Tsai, T., Joachim, S. C., and Schnichels, S. (2020). Organ cultures for retinal diseases. *Front. Neurosci.* 14:583392. doi: 10.3389/fnins.2020.583392

Mishra, S., Pena, J. S., Redenti, S., and Vazquez, M. (2019). A novel electro-chemotactic approach to impact the directional migration of transplantable retinal progenitor cells. *Exp. Eye Res.* 185:107688. doi: 10.1016/j.exer.2019.06.002

Mitchell, P., Liew, G., Gopinath, B., and Wong, T. Y. (2018). Age-related macular degeneration. *Lancet* 392, 1147–1159. doi: 10.1016/S0140-6736(18)31550-2

Rettinger, C. L., and Wang, H. C. (2018). Quantitative assessment of retina explant viability in a porcine *ex vivo* neuroretina model. *J. Ocul. Pharmacol. Ther.* 34, 521–530. doi: 10.1089/jop.2018.0021

Rountree, C. M., Raghunathan, A., Troy, J. B., and Saggere, L. (2017). Prototype chemical synapse chip for spatially patterned neurotransmitter stimulation of the retina *ex vivo*. *Microsyst. Nanoeng.* 3:17052. doi: 10.1038/micronano.2017.52

Simo-Servat, O., Hernandez, C., and Simo, R. (2019). Diabetic retinopathy in the context of patients with diabetes. *Ophthalmic Res.* 62, 211–217. doi: 10.1159/000499541

Vazquez, M. (2020). Microfluidic and microscale assays to examine regenerative strategies in the neuro retina. *Micromachines* 11:1089. doi: 10.3390/mi11121089

Vazquez, M., Pena, J. S., and Mut, S. (2020). An *Ex Vivo* Eye Facsimile System, (EVES) to evaluate transplantation strategies for cell replacement therapy. *Investig. Ophthalmol. Vis. Sci.* 61:795. Available online at: https://iovs.arvojournals.org/article.aspx?articleid=2769637

Wu, S., Chang, K. C., Nahmou, M., and Goldberg, J. L. (2018). Induced pluripotent stem cells promote retinal ganglion cell survival after transplant. *Invest. Ophthalmol. Vis. Sci.* 59, 1571–1576. doi: 10.1167/iovs.17-23648

Conflict of Interest: The authors declare that the research was conducted in the absence of any commercial or financial relationships that could be construed as a potential conflict of interest.

Publisher's Note: All claims expressed in this article are solely those of the authors and do not necessarily represent those of their affiliated organizations, or those of the publisher, the editors and the reviewers. Any product that may be evaluated in this article, or claim that may be made by its manufacturer, is not guaranteed or endorsed by the publisher.

Copyright © 2021 Mut and Vazquez. This is an open-access article distributed under the terms of the Creative Commons Attribution License (CC BY). The use, distribution or reproduction in other forums is permitted, provided the original author(s) and the copyright owner(s) are credited and that the original publication in this journal is cited, in accordance with accepted academic practice. No use, distribution or reproduction is permitted which does not comply with these terms.

frontiers in Neuroscience

ORIGINAL RESEARCH
published: 26 November 2020
doi: 10.3389/fnins.2020.571479

Optimized OPA1 Isoforms 1 and 7 Provide Therapeutic Benefit in Models of Mitochondrial Dysfunction

Daniel M. Maloney[1], Naomi Chadderton[1], Sophia Millington-Ward[1], Arpad Palfi[1], Ciara Shortall[1], James J. O'Byrne[2,3], Lorraine Cassidy[4], David Keegan[3], Peter Humphries[1], Paul Kenna[1,4] and Gwyneth Jane Farrar[1]*

[1] The School of Genetics & Microbiology, Trinity College Dublin, Dublin, Ireland, [2] National Centre for Inherited Metabolic Disorders, The Mater Misericordiae University Hospital, Dublin, Ireland, [3] Clinical Genetics Centre for Ophthalmology, The Mater Misericordiae University Hospital, Dublin, Ireland, [4] The Research Foundation, Royal Victoria Eye and Ear Hospital, Dublin, Ireland

Optic Atrophy 1 (OPA1) is a mitochondrially targeted GTPase that plays a pivotal role in mitochondrial health, with mutations causing severe mitochondrial dysfunction and typically associated with Dominant Optic Atrophy (DOA), a progressive blinding disease involving retinal ganglion cell loss and optic nerve damage. In the current study, we investigate the use of codon-optimized versions of OPA1 isoform 1 and 7 as potential therapeutic interventions in a range of *in vitro* and *in vivo* models of mitochondrial dysfunction. We demonstrate that both isoforms perform equally well in ameliorating mitochondrial dysfunction in OPA1 knockout mouse embryonic fibroblast cells but that OPA1 expression levels require tight regulation for optimal benefit. Of note, we demonstrate for the first time that both OPA1 isoform 1 and 7 can be used independently to protect spatial visual function in a murine model of retinal ganglion cell degeneration caused by mitochondrial dysfunction, as well as providing benefit to mitochondrial bioenergetics in DOA patient derived fibroblast cells. These results highlight the potential value of OPA1-based gene therapy interventions.

Keywords: optic atrophy 1, dominant optic atrophy, mitochondria, gene therapy, optic neuropathy, AAV, bioenergetics, retinal ganglion cells

OPEN ACCESS

Edited by:
Jacqueline Reinhard, Ruhr-University, Germany

Reviewed by:
Pascale Belenguer, Université de Toulouse, France
Derek Narendra, National Institutes of Health (NIH), United States

****Correspondence:***
Daniel M. Maloney
dmmalone@tcd.ie

Specialty section:
This article was submitted to Neurodegeneration, a section of the journal Frontiers in Neuroscience

Received: *10 June 2020*
Accepted: *30 October 2020*
Published: *26 November 2020*

Citation:
Maloney DM, Chadderton N, Millington-Ward S, Palfi A, Shortall C, O'Byrne JJ, Cassidy L, Keegan D, Humphries P, Kenna P and Farrar GJ (2020) Optimized OPA1 Isoforms 1 and 7 Provide Therapeutic Benefit in Models of Mitochondrial Dysfunction. Front. Neurosci. 14:571479. doi: 10.3389/fnins.2020.571479

INTRODUCTION

Optic Atrophy 1 (OPA1) is a mitochondrially targeted GTPase that plays a pivotal role in mitochondrial health, with mutations causing severe mitochondrial dysfunction. The OPA1 protein possesses a mitochondrial targeting sequence and localizes to the inner mitochondrial membrane (IMM), where it promotes fusion of the IMM by interaction with cardiolipin on the opposing section of IMM (Ban et al., 2017; Lee and Yoon, 2018). OPA1 is sufficient for IMM fusion but in order to successfully form tubular mitochondrial networks OPA1 works in conjunction with two other GTPases, Mitofusin 1 and 2 (*MFN1* and *MFN2*), which mediate outer mitochondrial membrane fusion (Song et al., 2009). The process of mitochondrial fusion is counter-balanced by mitochondrial fission mediated by a fourth GTPase, dynamin 1-like protein (*DNM1L*) (Smirnova et al., 1998; Macdonald et al., 2016). Independent of its role in mitochondrial fusion, OPA1 has also been shown to be anti-apoptotic as OPA1 disassembly mediates the release of cytochrome c

from the mitochondria (Yamaguchi et al., 2008), potentially due to the role OPA1 plays in regulating cristae junctions (Frezza et al., 2006). Furthermore OPA1 protein is needed for the correct maintenance of the mitochondrial genome (Chen et al., 2010), as well as playing a role in the organization of the mitochondrial supercomplexes (Cogliati et al., 2013; Lee et al., 2017). Recently OPA1 has been implicated in regulating DNA methylation in human neuronal development (Caglayan et al., 2020) and also in the spatial arrangement of the mitochondria in adjacent photoreceptor cells (Meschede et al., 2020).

The *OPA1* gene consists of 31 exons, which produce 8 mRNA isoforms that differ due to the alternate splicing of exons 4, 4b, and 5b (Delettre et al., 2001). Once located to the mitochondrial IMM, full length OPA1 protein (l-form) can be proteolytically cleaved by either OMA1 or YME1L at sites on exon 5 or 5b, respectively (Song et al., 2007; Ehses et al., 2009). These l and s-forms have been shown to play distinct physiological roles. Expression of any of the eight isoforms was sufficient to restore mtDNA levels, reorganize mitochondrial cristae, and boost the function of the electron transport chain in OPA1 knock out cells. However, the presence of both l and s-forms of OPA1 are needed to fully restore wild-type mitochondrial physiology (Del Dotto et al., 2017). OPA1 mRNA isoforms show a tissue specific expression pattern but to date human retinal tissue has not been directly examined for OPA1 isoform expression (Olichon et al., 2007; Akepati et al., 2008).

Dominant Optic Atrophy (DOA) is an inherited blinding disease that primarily targets the retinal ganglion cells (RGC). DOA has an estimated prevalence of between 1–10,000 and 1–30,000, making it one of the most common optic neuropathies (Yu-Wai-Man et al., 2010; Lenaers et al., 2012). DOA typically manifests in the first or second decade of life, with progressive bilateral visual loss with central scotomas, decreased thickness of the retinal nerve fiber layer (RNFL) and optic nerve damage (Chun and Rizzo, 2017). Around 20% of DOA patients show a multi-system disorder characterized by hearing loss, ataxia, myopathy, late onset cardio myopathy and peripheral neuropathy called DOA plus (Skidd et al., 2013). Mutations in *OPA1* are commonly associated with DOA, with around 65–90% of cases due to mutations in the *OPA1* gene and around 370 variants in *OPA1* associated with the disease (Delettre et al., 2000; Del Dotto et al., 2018a). DOA patient derived fibroblasts have previously been shown to suffer significant levels of mitochondrial dysfunction showing decreased mitochondrial oxygen consumption rates, decreased ATP levels, fragmented mitochondria, mtDNA depletion and dysfunctional mitophagy, but the exact phenotypic manifestation depends on the particular mutation (Belenguer and Pellegrini, 2013; Vidoni et al., 2013; Liao et al., 2017).

Significant research has been undertaken highlighting the potential use of OPA1 as a therapeutic entity, both as a therapeutic for DOA and other mitochondrial associated diseases, as well as other more general apoptotic insults. A mouse model constitutively expressing OPA1 showed increased mitochondrial supercomplex formation, as well as protection from reperfusion ischemia damage and mitigation of the deleterious effects of the *Ndufs4*$^{-/-}$ and *Cox15* mouse models (Cogliati et al., 2013; Civiletto et al., 2015; Varanita et al., 2015). The use of l-form OPA1 has been shown to alleviate acute ischemic stroke injury in rat brain, preventing neuronal cell loss (Lai et al., 2020).

AAV delivered OPA1 isoform 1 showed significant protection of RGCs in a mouse model heterozygous for a pathogenic *Opa1* mutation (Opa1 delTTAG/ +), but did not show a significant increase in visual acuity (Sarzi et al., 2018). In addition, it is notable that AAV delivered OPA1 has also been shown to be beneficial in a laser induced model of glaucoma in rats, where it provided protection of RGCs (Hu et al., 2018) and in a chemical model of ocular mitochondrial uncoupling (Sun et al., 2016b).

In this study we have explored the potential of two codon optimized *OPA1* isoforms, 1 and 7, to rescue mitochondrial dysfunction in a range of *in vitro* and *in vivo* models, including DOA patient derived fibroblasts and a rotenone induced mouse model of ocular complex 1 deficiency (Zhang et al., 2002). Rotenone irreversibly inhibits Complex 1 leading to significant RGC loss, RNFL thinning and a progressive decrease in visual acuity, thus phenotypically resembling optic neuropathies such as DOA, and Leber Hereditary Optic Neuropathy. Notably, AAV-mediated intravitreal delivery resulted in significant protection of visual function in rotenone treated animals. Furthermore, DOA patient derived fibroblasts treated with the same AAVs showed a significant improvement in mitochondrial bioenergetics.

MATERIALS AND METHODS

RNAseq Data Analysis

RNAseq data of healthy human retina was uploaded by (Li et al., 2014) and accessed through the NCBI Gene Expression Omnibus (GEO; Accession: GSE94437, mean age = 74). All 16 retinal samples were used, 8 macular retinal samples and 8 peripheral retinal samples. 26 healthy human Dorsolateral prefrontal cortex samples were acquired from GSE80655 (Ramaker et al., 2017, mean age = 48). 19 healthy human skeletal muscle samples were acquired from GSE129643 (Ubaida-Mohien et al., 2019, mean age = 56). All samples were from Caucasian donors.

Sequence data were analyzed using Kallisto Quant (Bray et al., 2016) on the Galaxy platform (usegalaxy.org, Afgan et al., 2018) to generate RNA isoform abundance tables.

Expression Construct Synthesis and Cloning

The OPA1 isoform 1 and isoform 7 cDNA sequences were obtained from NCBI (OPA1 isoform 1 Accession: CCDS43186.1; OPA1 isoform 7 Accession: CCDS33917). The coding sequences were both codon optimized (GeneArt, Thermo Fisher Scientific, United States) and a 6x HIS tag appended before the stop codon. A minimal rabbit β-globin poly(A) signal (Levitt et al., 1989) and flanking restriction enzyme sites, to aid subsequent cloning, were also added. The resulting sequences were synthesized by IDT (United States) and cloned into the pCMV-MCS expression plasmid (GenBank Accession: AF369966.1) using appropriate restriction enzymes (New England Biolabs, United States) as per the manufacturers protocol.

Cell Culture

OPA1$^{-/-}$ mouse embryonic fibroblast (MEF) cells, developed by the Chan lab (Chen et al., 2003; ATCC, CRL-2995) and NIH-3T3 cells (ECACC; 9301524) were routinely cultured in either glucose medium [DMEM GlutaMax (Thermo Fisher Scientific, United States; 61965-026) which contains 25 mM Glucose supplemented with 10% FBS (Merck; F7524) and 1 mM Sodium Pyruvate (Thermo Fisher Scientific, United States; 11360.039)] or Galactose medium (DMEM (Thermo Fisher Scientific, United States; A1443001) supplemented with 10 mM Galactose (Merck; G5388), 10% FBS, 1 mM Sodium Pyruvate and 2 mM L-Glutamine (Thermo Fisher Scientific, United States; 25030081).

Primary Cell Lines

Patient derived primary fibroblasts were isolated from biopsies obtained with prior informed consent from patients with genetically confirmed and clinically diagnosed DOA associated visual dysfunction. DOA 1 (46 y/o, Female) has a heterozygous 53del10 deletion and DOA 2 (49 y/o, Female) and DOA 3 (18 y/o, Female) have heterozygous 1334G > A mutations. DOA 3 has primarily an eye phenotype at 18 years while DOA 2 has developed a more severe phenotype at age 49 years including optic atrophy, bilateral ptosis, progressive external ophthalmoplegia, ataxia and peripheral sensory neuropathy without cardiac involvement.

Control fibroblast cell lines were from individuals with no history of visual or mitochondrial dysfunction. Control 1 was derived from a female aged 32, control 2 was derived from a male aged 35 and control 3 was from a female aged 40.

Plasmid Transient Transfection

Cells were transiently transfected using Lipofectamine 2000 (Thermo Fisher Scientific, United States; 11668019) as per the manufacturer's protocol, with adjustments to account for differences in plasmid size to ensure equal plasmid copy numbers between groups. All cells were transfected 24 h after seeding when cells were at ∼70% confluency. Assays were performed 48 h post transfection.

Cell Culture Histology

After appropriate treatments, culture medium was removed and cells were washed with PBS. Cells were fixed with 4% paraformaldehyde (pfa) for 20 min at room temperature. Cells were washed three times with PBS, before being blocked (5% Donkey Serum and 0.3% triton in PBS) at room temperature (RT) for 2 h. Primary antibody staining was carried out in blocking solution using Anti-6xHIS (1:500; Abcam; ab9108), at 4°C overnight. Secondary staining was carried out in blocking solution using Alexa Fluor 488 Anti-Rabbit (1:400; Jackson ImmunoResearch; 711-545-152) for 2 h at RT. Nuclei were stained with DAPI 1:50,000 in PBS for 10 min at RT.

Stable Cell Line Generation

The OPA1 isoform 1 and 7 cDNAs were cloned into pcDNA3.1 (+) (Thermo Fisher) and transfected into OPA1$^{-/-}$ MEF cells as above. Successfully transfected cells were then selected for with 200 μg/ml G418 (Santa-Cruz Biotechnology, Inc., United States). After 2 weeks of selection cells were serially diluted and seeded at ∼1 cell per well in a 96 well plate, in the presence of G418. Wells containing a single cell were identified and split into 24 then 6 well plates before being assessed for OPA1 isoform 1 and 7 construct RNA and protein expression. Positive cell lines were then maintained under routine cell culture conditions, with the addition of G418. As a control, a stable OPA1$^{-/-}$ MEF cell line was also generated using an empty pcDNA3.1 (+) plasmid.

Mitotracker Staining of Mitochondria and Morphological Analysis

Mitotracker CMTM Orange (M7510, Thermo Fisher Scientific) was used as per the manufacturers protocol. Briefly, a stock solution of Mitotracker was reconstituted to 1 mM with DMSO. The stock solution was then diluted to a working concentration of 100–500 nM in pre-warmed complete medium. Medium was removed from cells and 1 ml of Mitotracker staining solution added. Cells were incubated at 37°C with 5% CO_2 for 30 min. Cells were then washed once in complete media or were fixed and stained as previously described.

For analysis of mitochondrial morphology 10 random fields of view (FOV) were taken of three separate wells for each cell type after Mitotracker staining using an Olympus IX83 inverted motorized microscope. Images were analyzed blind and scored by eye for any cells that demonstrated any tubular branching mitochondria and were reported as a proportion of all cells per FOV.

Cell Growth Analysis

Cells were seeded in a 6 well plate at 1×10^6 cells per well with either glucose or galactose medium. 48 h later cells were trypsinised and cell number was determined using trypan-blue exclusion on a Luna Cell Counter (Logos Biosystems). Trypsinised cells were then reseeded at 1×10^6 and the process was repeated for a total of 192 h.

Seahorse Mitochondrial Metabolism Assays

The Seahorse XFe96 extracellular flux analyser (Agilent) was used to assay a number of mitochondrial metabolic parameters. For the Mitochondrial Stress Test of OPA1$^{-/-}$ MEFs and stable cell lines, cells were seeded 24 h prior to the assay in Seahorse Biosciences 96 well plates at 2.5×10^4 cells per well in 80 μl of complete glucose or galactose DMEM. One hour prior to the assay, culture media was substituted for Seahorse XF DMEM medium, pH7.4 (Agilent; 103575-100), supplemented with 1 mM Sodium Pyruvate, 2 mM L-Glutamine and either 25 mM Glucose or 10 mM Galactose, and placed in a non-CO_2 37°C incubator. The Mitochondrial Stress Test was performed by the sequential addition of 1 μM Oligomycin, 1 μM FCCP, and 0.5 μM Rotenone and Antimycin A.

The above protocol was modified for use with primary fibroblasts. Cells were seeded 72 h prior to the assay at 5×10^3

cells per well in complete glucose or galactose DMEM. 24 h later media was replaced with 50 μl 2% FBS DMEM GlutaMAX (containing glucose or galactose and 1 mM Sodium Pyruvate) as cells were transduced with AAV at various multiplicities of infection (MOIs). After a further 12 h an equal volume of 18% FBS DMEM was added. The Mitochondrial Stress Test was performed 48 h after AAV transduction as described above, but with 2.25 μM FCCP instead.

The ATP Rate Assay was carried out as per the manufacturers protocol (Agilent; 103592-100) using 2.5×10^4 OPA1$^{-/-}$ MEF or stable cells per well. Briefly, cells were sequentially treated with 1.5 μM Oligomycin then 0.5 μM Rotenone and Antimycin A. Rates were calculated using the ATP Rate Assay plug-in for the Wave software package.

Data from Seahorse runs were normalized either to cell count or using the Bradford method of protein quantification as per the manufacturers protocol (Thermo Fisher Scientific; Cat. No. 23246)

Mitochondrial Fusion Assay

Mitochondrial fusion assay was adapted from Karbowski et al. (2014). Briefly, 5×10^5 cells were seeded into a 35 mm μ-Dish (iBidi; 81156) 72 h prior to the assay. 24 h later cells were transfected with a mito-PAGFP plasmid (Richard Youle; Addgene plasmid #23348; Karbowski et al., 2004) and a mito-dsRED plasmid (Michael Davidson; Addgene plasmid # 55838). The presence of mito-dsRED allows transfected cells to be identified. The analysis was performed on a Leica SP8 gated STED confocal microscope where cell dishes were placed in the incubated stage and given 10 min to equilibrate to temperature. Five mito-dsRED positive FOV were then identified, and their stage co-ordinates marked. Z-stack limits were then set for each of the target cells. The five FOV are imaged as $T = -1$. A 2.5 μm × 2.5 μm region of interest (ROI) was then demarcated on an area rich in mitochondria in each cell. The microscope was then set to illuminate only the ROI (background set to 0%) with the UV lamp, with lamp power set to 40%. Sequentially, all cells were then illuminated with the UV lamp in the predefined ROI. Cells were imaged immediately as T0. Cells were imaged further every 15 min for a total of 45 min.

Analysis of the images was completed using Leica Application Suite X. Two 2.5 μm × 2.5 μm ROIs were taken for each cell at each timepoint, one measuring the fluorescent intensity of the area that received UV illumination, and a second ROI elsewhere in the cell that did not receive any illumination. The intensity levels for the green channel (PA-GFP) were recorded. The green value in the unilluminated ROI for a given cell was used to normalize the intensity levels of the cell to other cells, accounting for fluctuations in protein expression between cells. The overall level of fission and fusion was expressed as the percentage of green signal that remained in the UV illuminated ROI after 45 min ($T = 45$), when compared to $T = 1$.

Peredox Assay for NADH Level

The change in NADH level in cells was estimated using the Peredox fluorescent protein as outlined in Hung et al. (2011). Briefly, cells were seeded in 8 well chamber slides suitable for confocal imaging. Twenty four hours later cells were transfected with the pcDNA3.1-Peredox-mCherry plasmid [Gary Yellen (Addgene plasmid # 32383)]. 48 h later cells were imaged with a Carl Zeiss LSM 710 confocal microscope using the heated stage at 37°C and 5% CO_2. Random FOV were selected and cells were imaged using the red and green channels using consistent imaging settings. Image analysis was carried out using ZEN blue edition software by Carl Zeiss AG. An ROI was drawn in each cell and the intensity of green and red signals recorded. The green signal, corresponding to NADH level, was then normalized to the red signal, corresponding to Peredox protein level.

Western Blotting

Protein was extracted from cells after washing with ice-cold PBS using RIPA buffer supplemented with cOmplete mini Protease inhibitor cocktail (Roche; 11836153001). Crude lysates were incubated on ice for 30 min with occasional vortexing before centrifugation at 14,000G at 4°C for 30 min. Supernatants were then aliquoted for protein quantification via the Bradford method and stored at −80°C.

Extracted protein was separated by 4–12% SDS-PAGE gel electrophoresis and semi-dry transferred to PVDF membranes (Merck; IPVH00010). Membranes were blocked in 5% non-fat milk at room temperature for 1 h before overnight incubation with primary antibody in blocking solution [Anti-6xHIS (1:1,000; Abcam; ab9108), OPA1 (1:500; Abcam; ab90857) or β-actin (1:5,000; Abcam; ab8227)]. Blots were incubated with Anti-Rabbit Peroxidase secondary antibody (1:10,000; Sigma; A9169) followed by exposure using an enhanced chemiluminescence (ECL) kit (Thermo Fisher Scientific; 32209 or Advansta; K-12045-D20) before imaging with the C-DiGit Blot Scanner (Li-Cor) or being developed in a darkroom. Densitometry analysis was carried out using the Fiji distribution of Image J (Schindelin et al., 2012).

Real-Time RT-PCR

RNA was extracted from cells using an RNeasy kit (Qiagen; 74104). OPA1 and codon optimized OPA1 (huOPA1) mRNA expression levels were assayed via real-time RT-PCR using a StepOnePlus system (Applied Biosystems) with QuantiTect SYBR Green RT-PCR kit (Qiagen; 204245). Cells from 4 virally treated wells were pooled and all samples were run in triplicate. Primers were designed to target all 8 endogenous OPA1 mRNA isoforms (All isoforms OPA1: F 5′-AGTAGAGGTTGCTTGG GAGAC-3′ and R 5′-TGTCATCATGCTCTTTCCCT-3′) and a separate pair were designed to target both optimized OPA1 iso 1 and 7 (optOPA1: F 5′- TACCCCAGACTGAGAGAGCT-3′ and R 5′- ACTTGGCTCAGGGAGATCAC-3′). β-actin levels were used as an endogenous control (β-actin: F 5′-TCA CCCACACTGTGCCCATCTACGA-3′ and R 5′-CAGCG GAACCGCTCATTGCCAATGG-3′). To obtain copy numbers of both endogenous OPA1 and optimized OPA1 transgene, a standard curve was generated from a plasmid of known copy number containing fragments of both wild type OPA1 and codon optimized OPA1 versions.

AAV production

AAV2/2-OPA1 iso 1, AAV2/2-OPA1 iso 7 and AAV2/2-CAG EGFP were prepared by the Farrar group at TCD (Lane et al., 2020). The two OPA1 cDNAs were cloned into pAAV-MCS (accession no. AF396260.1; Agilent Technologies, Inc., United States).

Recombinant AAV2/2 viruses were generated by helper virus free, triple transfection based on the method described by (Xiao et al., 1998). Human embryonic kidney cells (accession number CRL-1573; ATCC, United States) were transfected with pAAV-MCS plasmids containing OPA1 iso 1 or 7, pRep2/Cap2 and pHelper (Agilent Technologies, Inc., United States) at a ratio of 1:1:2, using polyethylenimine, as previously described (O'Reilly et al., 2007). 72 h post-transfection, AAV particles were purified from the clarified lysate by cesium gradient centrifugation. AAV containing fractions were dialyzed against PBS supplemented with Pluronic F68 (0.001%; Bennicelli et al., 2008). Genomic titers (viral genomes/ml; vg/ml) were determined by quantitative real-time PCR (Rohr et al., 2002).

Intravitreal Injections

All animal work was performed in accordance with the European Union (Protection of Animals used for Scientific Purposes) Regulations 2012 (S.I. no. 543 of 2012) and the Association for Research in Vision and Ophthalmology (ARVO) statement for the use of animals. Adult wild type 129 S2/SvHsd mice (Harlan UK Ltd., Oxfordshire, United Kingdom) were maintained in a specific pathogen free (SPF) facility. Adult mice were anaesthetized by intraperitoneal injection of medetomidine and ketamine (0.5 mg and 57 mg/kg body weight, respectively). Pupils were dilated with 1% tropicamide and 2.5% phenylephrine. Using topical anaesthesia (Amethocaine), a small puncture was made in the sclera. A 32 gauge blunt-ended microneedle attached to a 10 μl Hamilton syringe was inserted through the puncture, and 3 μl AAV2/2-OPA1-iso 1 or AAV2/2-OPA1-iso 7 (1×10^9 vector genomes) plus 1×10^8 AAV2/2 CAG-EGFP was slowly, over a 2-min period, administered into the vitreous of both eyes. Following intravitreal injection, an anaesthetic reversing agent (Atipamezole Hydrochloride, 1.33 mg/kg body weight) was delivered by intraperitoneal injection. Body temperature was maintained using a homeothermic heating device. 3 weeks later, 0.6 μl of 1.5 mM rotenone in DMSO was administered by the same method of intravitreal injection to one eye. Animals were sacrificed by CO_2 asphyxiation.

The sex breakdown of each group were as follows: OPA1 iso 7 ± rotenone: 5F + 5M, Wt ± rotenone (OPA1 iso 7 cohort): 5F + 2M, Opa1 ± rotenone: 4F + 3M and Wt ± rotenone (OPA1 iso 1 cohort): 3F + 5M.

Photopic Negative Response (PhNR)

Two weeks post rotenone the cohort of mice underwent assessment of the cone electroretinogram (ERG) Photopic Negative Response (PhNR). Detection was enhanced with an orange filter. The PhNR, the first negative deflection following the cone b wave response, was evaluated under photopic conditions using a Roland Consult RetiScan ERG RetiPort electrophysiology unit. Mice were anaesthetized as described above. PhNR responses were recorded simultaneously from both eyes by means of goldwire electrodes (Roland Consulting, Brandenburg-Wiesbaden, Germany). Standardized flashes of light were presented in a Ganzfeld bowl. Cone-isolated responses were recorded to the maximal intensity flash (−25 dB maximal intensity where maximal flash intensity was 3 candelas/m^2/s). Following accepted convention, the initial positive deflection was termed N1, the subsequent negative deflection P1 and the next positive deflection N2. The PhNR was calculated as the negative difference between N1 and P1. The recording was only deemed successful if this was indeed negative and the trace did not deflect above N2 for the remainder of the recording.

Optokinetic Response (OKR)

One week post PhNR assessment (3 weeks post rotenone injection), mice underwent optokinetic analysis as previously described (Chadderton et al., 2013). OKR spatial frequency thresholds were measured blind using a virtual optokinetic system (VOS, OptoMotry, Cerebral Mechanics, Lethbridge, Alberta, Canada; Prusky et al., 2004). Briefly, a virtual-reality chamber was created with four 17-inch computer monitors facing inwards and the unrestrained mouse was placed on a platform in the center. A video camera, situated above the animal, provided real-time video feedback. The experimenter centered the virtual drum on the mouse's head and judged whether the mouse made slow tracking movements with its head and neck. OptoMotry measures the threshold of the mouse's optokinetic tracking response to moving gratings. The visual capabilities of each eye can be measured simply by changing the direction of rotation as only rotation in the temporal-to-nasal direction evokes a tracking response (Douglas et al., 2005). The spatial frequency threshold, the point at which the mouse no longer tracked, was obtained by incrementally increasing the spatial frequency of the grating at 100% contrast. A staircase procedure was used in which the step size was halved after each reversal, and terminated when the step size became smaller than the hardware resolution (∼0.003 cyc/deg, 0.2% contrast). One staircase was presented for each direction of rotation to measure each eye separately, with the two staircases being interspersed. OKRs for each mouse were measured 3–4 times on separate days, averaged and SD values calculated.

Retinal Ganglion Cell counts

Mice were sacrificed 3 days after OKR assessment and eyes were enucleated and fixed in 4% paraformaldehyde in PBS overnight. Eyes were washed in PBS, then the retinas were removed from the eyecups and immediately processed for immunocytochemistry. Immunocytochemistry was performed as described previously (Palfi et al., 2016). Whole retinas were incubated with primary antibodies for RBPMS (ABN1376, Millipore, 1:200; Rodriguez et al., 2014) overnight for 3 days at 4°C. Retinas were then washed in PBS and incubated with secondary antibodies conjugated with Alexa-Fluor-488, Cy3 (Jackson ImmunoResearch Laboratories; 1:400) for 2 days and nuclei counterstained with DAPI. Samples were covered using Hydromount (National Diagnostics). Fluorescent microscopy

was carried out utilizing an Olympus IX83 inverted motorized microscope (cellSens v1.9 software) equipped with a SpectraX LED light source (Lumencor) and an Orca-Flash4.0 LT PLUS/sCMOS camera (Hamamatsu). Samples were imaged using a 10x plan fluorite objective utilizing enhanced focal imaging (EFI) with typically 5–8 Z-slices. Lateral frames were stitched together and analyzed in cellSens. Automated cell staining area was calculated utilizing 2D deconvolution, manual threshold and object size filter in cellSense; the same settings/operations were applied to all images.

Data Handling and Statistics

Data handling was performed in either RStudio [RStudio Team (2015), RStudio: Integrated Development for R. RStudio, Inc., Boston, MA[1])] or Microsoft Excel 2016. Graphs were created using either ggplot2 (Wickham, 2016) or Microsoft Excel. All statistical analysis was carried out in R. Unless otherwise stated, Kruskal-Wallis testing with pairwise Wilcoxon signed rank test *post hoc* and Bonferroni-Holm correction was used, with $p < 0.05$ considered statistically significant. Data are reported ± SD unless otherwise stated.

RESULTS

Retinal OPA1 Isoforms

The human *OPA1* gene has been identified as having a number of isoforms which have been shown to be expressed at differing levels across tissue types (Olichon et al., 2007) which are generated by alternative splicing of exons 4, 4b, and 5b (**Figure 1A**). Initial proteomic work has identified OPA1 isoform 1 as the primary isoform present in mouse tissue (Akepati et al., 2008). However, to the best of our knowledge the OPA1 isoform expression profile in the healthy human retinal tissue has not been investigated. In order to address this, we analyzed publicly available RNAseq data from retinal tissue from the macular retina and peripheral retina of 8 healthy post-mortem retinae (Li et al., 2014; Gene Expression Omnibus, Accession: GSE94437), as well as 26 brain tissue samples from the Dorsolateral prefrontal cortex (Ramaker et al., 2017; GSE80655) and 25 skeletal muscle samples (Ubaida-Mohien et al., 2019; GSE129643) from healthy individuals. **Figure 1C** shows that RNA levels of OPA1 are broadly similar across the three tissues analyzed. **Figure 1D** shows the transcripts per million data for the 8 protein coding isoforms of OPA1 identified in the Ensembl database (Yates et al., 2020; ENSG00000198836) in the 8 macular and 8 peripheral retinal samples. OPA1 isoforms 1 and 7 are the most highly expressed in these retinal samples, but differences between macular and peripheral retinal samples were present.

To investigate the relationship between mitochondrial remodeling proteins further, the relative expression of *DNM1L*, *MFN1, MFN2,* and *OPA1* was compared (**Figure 1E**), demonstrating that the RNA transcripts for *DNM1L*, *MFN2,* and *OPA1* are all expressed at similar levels in retinal cells, whereas *MFN1* levels are substantially lower than the others. To investigate any relationship between transcript expression levels, correlation coefficients were calculated between each pair of transcripts, and with *ACTB* as a control (**Table 1**). There is a significant positive correlation between transcript levels of *MFN2*, *DNM1L* and *OPA1* (Pearson's correlation coefficient, Bonferroni Correction $p < 0.01$, $n = 16$), all showing around $r \approx 0.8$ correlation coefficient. However, there is no significant correlation between *ACTB* transcript levels and those of the mitochondrial remodeling proteins. **Figures 1F,G** shows representative scatter plots demonstrating the correlation between *OPA1* and *DNM1L* transcript levels as well as *OPA1* and *ACTB* levels. All comparisons can be seen in **Table 1**.

As OPA1 isoforms 1 and 7 were shown to be the most highly expressed in retinal tissue, in line with previous studies of non-ocular human tissues (Olichon et al., 2007), these two isoforms were tested for utility as a therapeutic intervention. Two expression cassettes were constructed for this purpose (**Figure 1B**). The amino acid sequences of OPA1 isoform 1 and isoform 7, henceforth referred to as OPA1 iso 1 and OPA1 iso 7, respectively, were unaltered except for the addition of a 6x HIS tag immediately 5′ of the stop codon. The cDNAs were codon optimized for human codon usage bias in order to maximize potential levels of expression.

Ectopic Expression of OPA1 iso 1 and OPA1 iso 7 Can Restore Mitochondrial Function

To demonstrate that the optimization process does not perturb mitochondrial localization of the OPA1 iso 1 or OPA1 iso 7 proteins, HEK 293 cells were transiently transfected separately with the two isoforms. When co-stained with an anti-6xHIS tag antibody and Mitotracker orange there was a clear overlap of the two signals, indicating the OPA1 isoforms were successfully targeted to the mitochondria (data not shown).

To investigate if optimized OPA1 iso 1 and OPA1 iso 7 can independently restore mitochondrial morphology, OPA1 knockout MEF ($OPA1^{-/-}$) cells were utilized. These $OPA1^{-/-}$ cells show a characteristic punctate, fragmented mitochondrial network (**Figure 2A**). In contrast, representative cells transfected with either OPA1 iso 1 or 7 (**Figures 2B,C**, respectively) show tubular mitochondrial networks indicating restoration of mitochondrial fusion in these cells.

During the morphological analysis of the mitochondrial network of these cells it was noted that a number of cells displayed high levels of HIS-tagged OPA1 fluorescence, indicating high levels of OPA1 protein, but also showed a distinctive punctate mitochondrial network morphology, with consistent levels of mitotracker staining (**Figures 2D,E**, here showing representative OPA1 iso 1 transiently transfected cells). To further examine if this phenomenon was due to OPA1 overexpression 15 fields of view (FOV) were imaged over 3 separate transfections and the morphology of cells were manually scored as being rescued or showing a punctate mitochondrial network distinct from unrescued cells, in cells displaying measurable levels of HIS-tagged OPA1 fluorescence. **Figure 3F** shows the distribution of the HIS fluorescence varies significantly depending on the

[1]http://www.rstudio.com/

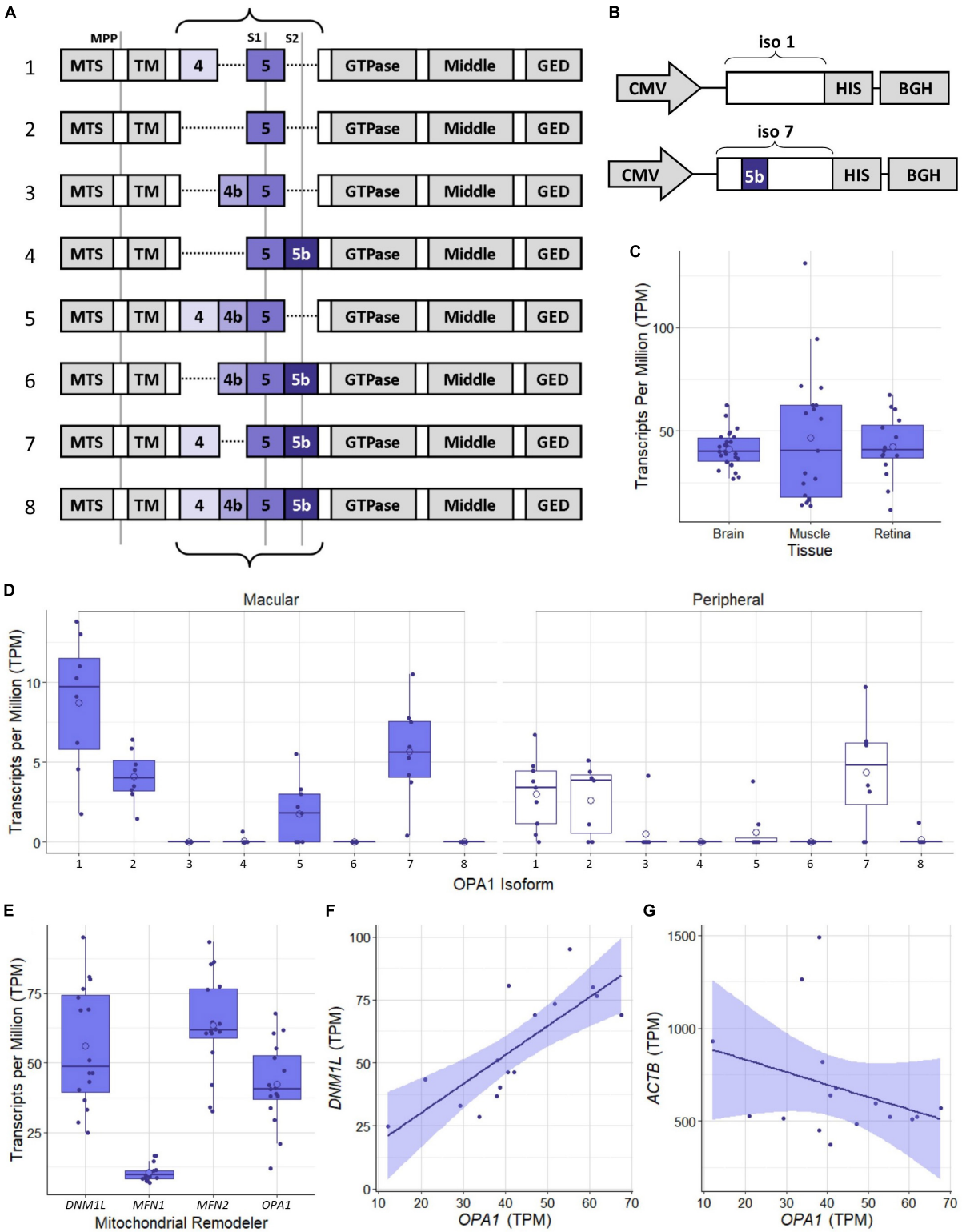

FIGURE 1 | Schematic representation of OPA1 RNA isoforms and RNAseq analysis of healthy human tissue. **(A)** The 8 primary protein coding mRNA variants of OPA1 in humans. The curly braces indicate the area that undergoes alternate splicing of exons 4, 4b, and 5b. Gray lines indicate protease cleavage sites, MPP = matrix processing peptidases, S1 = OMA1 and S2 = YME1L. Gray blocks outside of the curly braces indicate functional domains; MTS, Mitochondrial Targeting Sequence; TM, Transmembrane domain; GED, GTPase effector domain. **(B)** Schematics of optimized OPA1 isoform 1 or 7 expression cassettes. CMV,

(Continued)

FIGURE 1 | Continued
Cytomegalovirus promoter; HIS, 6x HIS tag; BGH, Bovine Growth Hormone polyadenylation signal. Note that only exon 5b differs between them. **(C)** Comparison of *OPA1* transcript levels in Transcripts Per Million (TPM) in healthy dorsolateral prefrontal cortex brain tissue ($n = 26$ samples), skeletal muscle tissue ($n = 19$) and retinal tissue ($n = 16$). The open circle on each boxplot represents the mean. **(D)** Expression levels of the 8 protein coding isoforms of *OPA1* as identified in the ensemble database (ENSG00000198836) measured in TPM. $n = 8$ macular samples and $n = 8$ peripheral samples. **(E)** RNA transcript expression levels in TPM of 4 significant mitochondrial remodeling proteins Drp1 (*DNM1L*), Mitofusin 1 and 2 (*MFN1* and *2*) and *OPA1*. $n = 16$ (macular and peripheral) samples. **(F,G)** Are representative scatter plots of the correlation between mitochondrial remodeler RNA transcripts, with *ACTB* as a control. *OPA1* transcript expression is compared to either *DNM1L* or *ACTB* transcript levels, measured in TPM. *DNM1L* and *OPA1* transcript levels show a significant positive correlation ($r = 0.79$, Pearson's Correlation Coefficient, $n = 16$, $p < 0.05$), whereas *ACTB* and *OPA1* transcript levels show no significant correlation ($r = –0.32$, Pearson's Correlation Coefficient, $n = 16$, $p > 0.05$). Shaded region represents 95% confidence interval, BH correction for multiple testing.

mitochondrial phenotype displayed by the cell for both OPA1 iso 1 and OPA1 iso 7 transiently expressing cells ($n = > 50$ cells for each morphology, $p < 0.001$ for both isoforms).

To investigate if this phenotype was due to OPA1$^{-/-}$ cells having a specific sensitivity to OPA1 iso 1 and 7 mediated over-expression, NIH-3T3 MEF cells were transiently transfected with OPA1 iso 1 or 7. **Figure 2G** shows representative MEF cells labeled with Mitotracker orange, with **Figure 2H** showing a heat map of HIS-tagged OPA1 iso 7 protein fluorescence demonstrating that mitochondrial morphology is altered with increasing levels of OPA1 iso 7 protein. OPA1 iso 1 expressing cells also demonstrated this overexpression phenotype in NIH-3T3 cells.

OPA1 Isoform 1 and 7 Expression Leads to Bioenergetic Rescue of OPA1 Cells

To modulate expression levels of OPA1 isoform 1 and 7, cell lines were generated from OPA1$^{-/-}$ MEF cells to stably express the optimized OPA1 isoforms, termed pcOPA1 iso 1 and 7, given the varied mitochondrial morphological phenotype observed in the transiently transfected cells. As a control, a pcOPA1$^{-/-}$ cell line was created using an empty pcDNA3.1 plasmid.

Densitometry of Western blot analysis of the stable cell lines (**Figure 3A** and **Supplementary Figure 1**) showed that pcOPA1 iso 1 restored 105.8% (± 16.4%, $p > 0.05$, $n = 3$ replicates) of NIH-3T3 OPA1 protein levels whereas pcOPA1 iso 7 cells restored 61.8% (± 5.5%, $p < 0.05$, $n = 3$) of endogenous NIH-3T3 OPA1 protein levels, showing a substantial increase but still significantly lower than wild-type levels. The overlaid dot plot shows protein extracted from cells sampled at three different time points (●: $T = 0$, ▲: $T = 7$, ■: $T = 14$ days).

TABLE 1 | Pearson's correlation coefficient of the RNA transcript levels of four known mitochondrial remodeler proteins with β-actin as a control from RNAseq of human retinal punches (Li et al., 2014).

	OPA1	*MFN1*	*MFN2*	*DNM1L*	ACTB
OPA1		*n.s.*	***	**	n.s.
MFN1	0.33		*n.s.*	*n.s.*	n.s.
MFN2	0.85	0.2		**	n.s.
DNM1L	0.79	0.6	0.79		n.s.
ACTB	–0.32	–0.14	–0.51	–0.37	

*Numbers below the purple diagonal represent Pearson's r, with significance values above the orange diagonal with Bonferroni-Holm correction. (n = 16 samples, macular and peripheral). **p < 0.01 and ***p < 0.001.*

The stable pcOPA1 iso 1 and 7 cell lines demonstrated a significant improvement in mitochondrial network morphology. These cells, grown in galactose to force the cells to utilize mitochondrial respiration, showed a significant increase in the number of cells whose mitochondria showed morphological rescue (**Figure 3B**). To examine if this morphological rescue allowed dynamic remodeling of the mitochondrial networks a mitochondrial fusion assay was performed. This assay monitors the rate of dispersal of PA-GFP signal selectively illuminated in a portion of a cell's mitochondria; the quicker the rate of dispersal, the higher the rate of fusion in the mitochondria. This assay demonstrated a significant restoration in the ability of pcOPA1 iso 1 and 7 cells to diffuse the PA-GFP signal compared to pcOPA1$^{-/-}$ cells, with an average PA-GFP signal of 30.2% ± 10.9% and 25.7% ± 6.3% remaining in pcOPA1 iso 1 and 7 cells, respectively, at T = 45, compared to 68.6% ± 7.8% in pcOPA1$^{-/-}$ cells (**Figure 3C**, $n = 10$ ROI from 5 FOV, $p < 0.05$). This indicates enhanced mitochondrial fusion mediated by expression of either OPA1 isoform.

To investigate if the stable expression of the two optimized OPA1 isoforms can provide metabolic benefit compared to pcOPA1$^{-/-}$ cells, a number of biochemical assays were performed. Stably expressing cells were passaged for an extended period of time in either 10 mM galactose media or 25 mM glucose media, the former to force cells to utilize mitochondrial respiration in preference to glycolysis. All cell lines performed equally when grown in glucose media for 192 h (**Figure 3D**). Conversely pcOPA1 iso 1 and 7 cells survived significantly better when grown in galactose media (**Figure 3E**), with pcOPA1$^{-/-}$ cells showing a significant decrease in cell number after 96 h ($3.37 \times 10^6 \pm 2 \times 10^5$ pcOPA1 iso 1 and $3.07 \times 10^6 \pm 1.7 \times 10^5$ pcOPA1 iso 7 vs. $1.23 \times 10^6 \pm 3.1 \times 10^5$ pcOPA1$^{-/-}$ cells, $n = 3$ replicates, $p < 0.01$), indicating improved ability to utilize mitochondrial respiration in pcOPA1 iso 1 and 7 cells.

In addition, the oxygen consumption rate (OCR) of these cells was measured (**Figure 3F**). Notably when pcOPA1 iso 1 and 7 cells are compared to pcOPA$^{-/-}$ cells in either glucose or galactose growth conditions, pcOPA1 iso 1 and 7 cells demonstrate a far greater ability to modulate their mitochondrial respiration. Both pcOPA1 iso 1 and 7 cells outperform pcOPA1$^{-/-}$ cells when grown in glucose (basal OCR in glu: pcOPA1$^{-/-}$ 38.9 ± 0.84 pmol/min vs. pcOPA1 iso 1 49.7 ± 0.86 pmol/min and pcOPA1 iso 7 53.62 ± 1.5 pmol/min, normalized to cell count, $n = 8$ replicates, $p < 0.01$, **Figure 3E**). If each cell line is compared when grown in either galactose (gal) or glucose (glu) media, pcOPA1 iso 1 and 7 cells

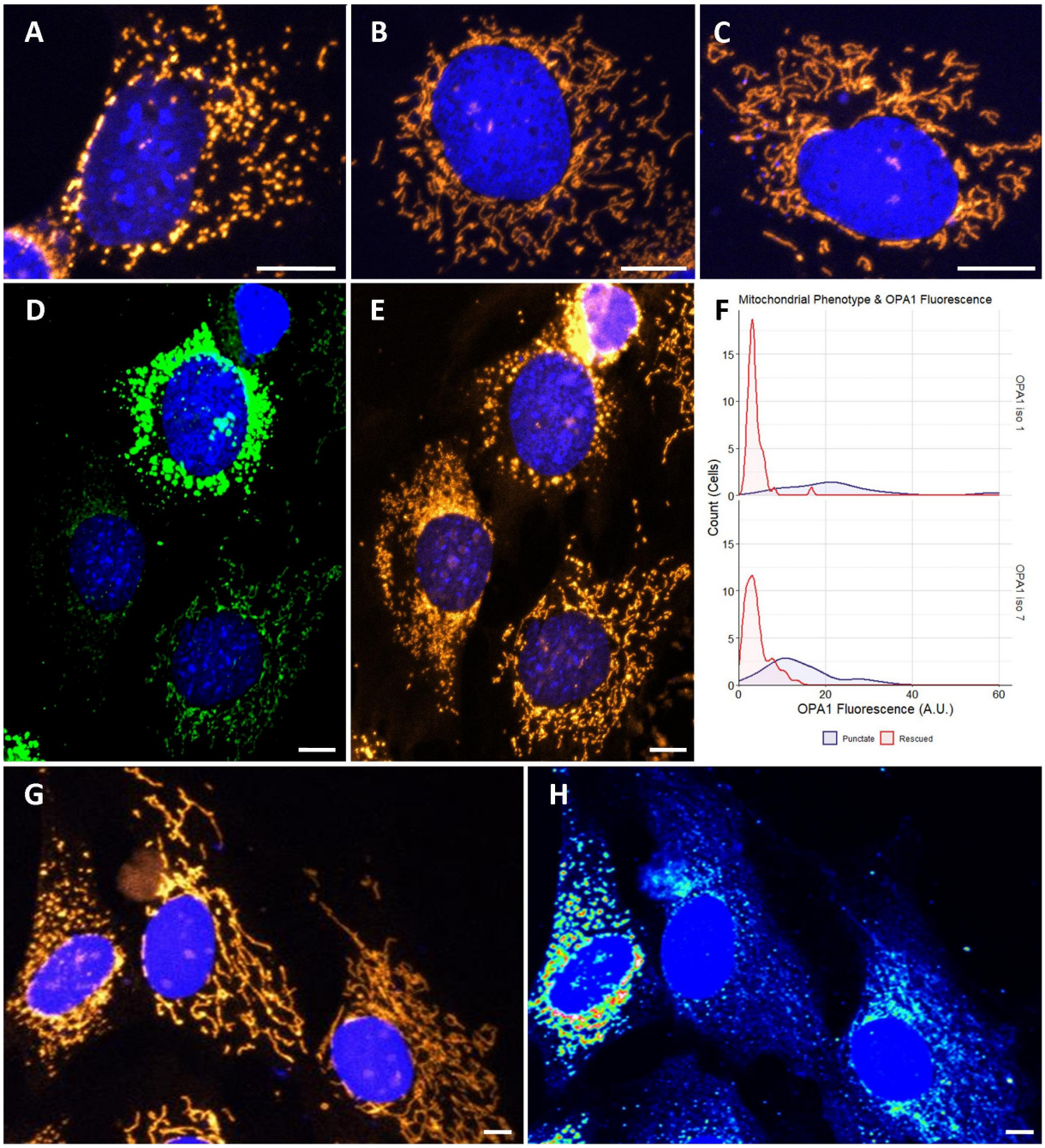

FIGURE 2 | Cytological analysis of OPA1 iso 1 and 7 transient expression. **(A–C)** Show the mitochondrial network of representative OPA1$^{-/-}$ cells, or transiently transfected OPA1$^{-/-}$ with either OPA1 iso 1 or 7 plasmid, respectively. **(D)** A representative image of cells showing widely varying levels of HIS-tagged OPA1 expression. **(E)** Shows that these cells also exhibit distinct mitochondrial phenotypes. **(F)** Cells were grouped by mitochondrial phenotype, demonstrating either punctate (purple) or rescued (red) mitochondria, and the OPA1 fluorescence levels were measured. Only cells that exhibited measurable OPA1 fluorescence were included for this analysis. The two mitochondrial phenotypes demonstrate significantly distinct distributions of OPA1 fluorescence ($n > 50$ cells for each group from 15 FOV over 3 separate transfections, $p < 0.0001$, Wilcoxon rank sum test). **(G,H)** Representative wild type NIH-3T3 MEF cells transfected with OPA1 iso 7. Mitotracker staining in **(G)** demonstrates the gross morphology differences observed with **(H)** showing a heat map of HIS-tagged OPA1 iso 7 protein signal in these cells. This morphological change in the mitochondrial network is seen with OPA1 iso 1 transfection also. Red scale bar = 10 μm.

also showed a marked increase in both basal OCR and Spare Respiratory Capacity (SRC) (**Figure 3G**; basal OCR: pcOPA1$^{-/-}$ glu 38.9 ± 0.84 pmol/min vs. gal 41 ± 0.57 pmol/min ($p > 0.05$), pcOPA1 iso 1 glu 49.7 ± 0.86 pmol/min vs. gal 70.2 ± 1.7 pmol/min ($p < 0.001$), pcOPA1 iso 7 glu 53.62 ± 1.5 pmol/min vs. gal 67.7 ± 2 pmol/min ($p < 0.001$); SRC (% of

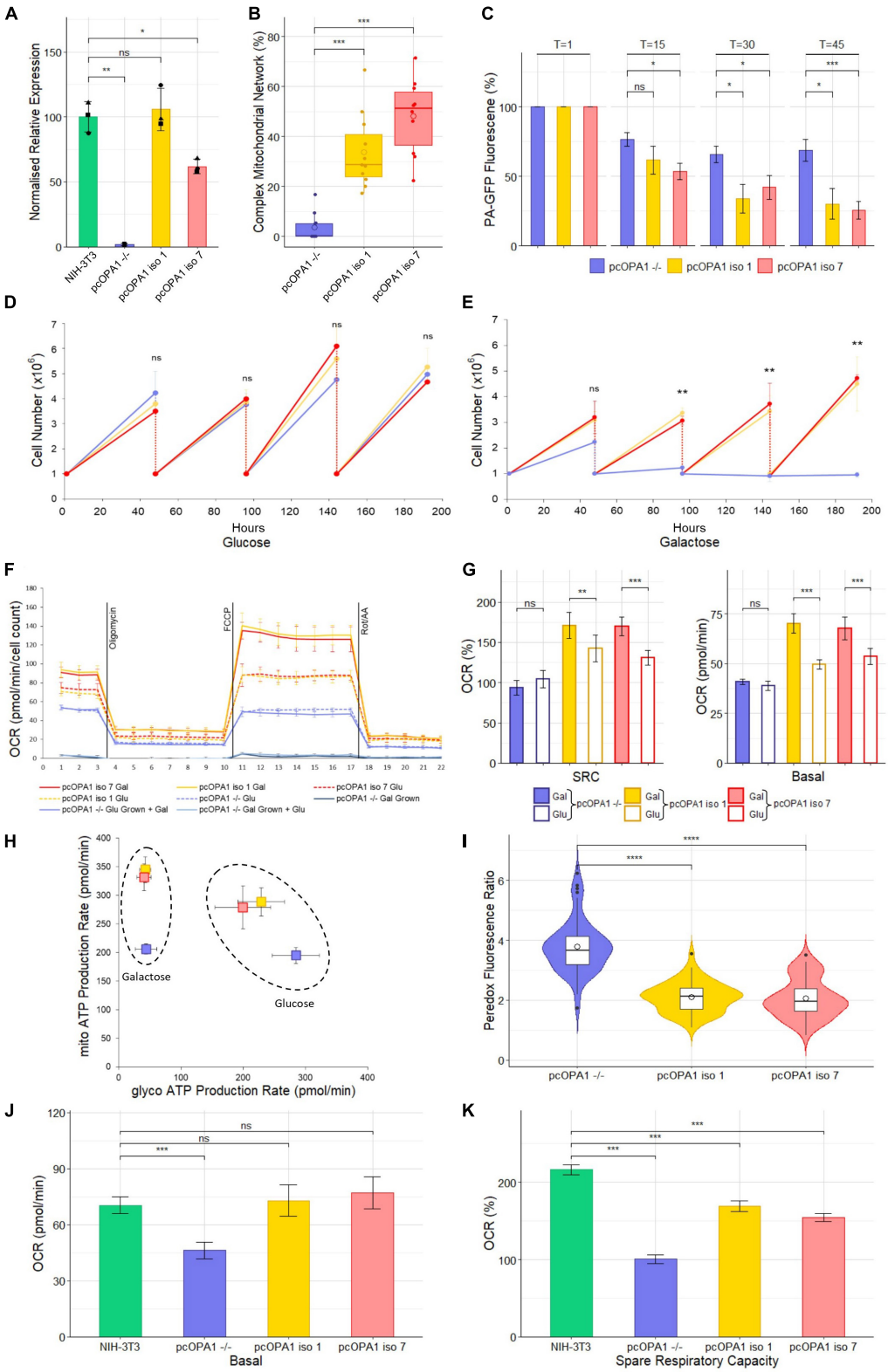

FIGURE 3 | Biochemical analysis of pcOPA1 iso 1 (yellow) and pcOPA1 iso 7 (red) stable cells compared to pcOPA1$^{-/-}$ (purple) stable cells and wild type NIH-3T3 MEFs (green). **(A)** Western blot densitometry analysis of pcOPA1 iso 1, iso 7, and –/– stable cell lines relative to NIH-3T3 cells. Values have been normalized to β-actin. The ●, ▲, and ■ symbols represent samples taken 1, 7, and 14 days apart, demonstrating little variation in protein expression levels over time. ($n = 3$

(Continued)

FIGURE 3 | Continued
replicates of each cell type and $n = 4$ technical replicates, error bars ± SD). **(B)** Morphological analysis of mitotracker stained mitochondria showing proportion of cells that showed evidence of complex mitochondrial structure ($n = 10$ random FOV across 3 independent trials). **(C)** Mitochondrial Fission Analysis. PA-GFP fluorescence as a percentage of T = 1 measured at 15, 30, and 45 min post illumination ($n = 10$ cells from 5 FOV, error bars ± SE) Rescued cells show a significant improvement in the rate of mitochondrial fusion compared to pcOPA1$^{-/-}$ cells. **(D,E)** show growth curves of each stable cell line with either glucose or galactose as their primary energy source ($n = 3$ independent trials). **(F)** Seahorse XFe96 Mitochondrial Stress Test of the stable cell lines under different growth conditions. Solid lines represent cells grown in 10 mM galactose, hatched lines represent cells grown in 25 mM glucose media for 48 h prior to the experiment ($n = 8$ replicates each group, normalized to cell count, error bars ± SD). **(G)** Shows the basal OCR and SRC as a% of basal OCR from F), ($n = 8$ replicates each group, normalized to cell count, error bars ± SE) Taken together **(F,G)** demonstrate that pcOPA1 iso 1 and 7 cells glucose showed an increase in both basal and SRC when compared to pcOPA1$^{-/-}$ cells grown in glucose. Furthermore, when pcOPA1 iso 1 or 7 cells were grown in galactose they outperform pcOPA1 iso 1 and 7 cells grown in glucose, suggesting improved ability to remodel mitochondria to meet metabolic demands. **(H)** The ATP Rate Assay demonstrates that pcOPA1 iso 1 and 7 cells can utilize their mitochondria more when forced to do so in galactose media, and favor mitochondrial ATP production more even when grown in glucose. ($n = 8$ replicates, error bars ± SD). **(I)** Peredox analysis suggest a significant decrease in cytosolic NADH levels in glucose grown pcOPA1 iso 1 and 7 cells suggesting less reliance on glycolysis for ATP production. ($n = 60$ cells across 3 separate transfections). **(J,K)** Seahorse XFe96 data for pcOPA1 iso 1 and 7 and control compared to wild type NIH-3T3 MEF cells. Both pcOPA1 isoform expressing cells show basal OCR rescue to wild type levels, but do not fully restore SRC. ($n = 8$ replicates per group, normalized to cell count, error bars ± SD). All statistical comparisons are Kruskal-Wallis with *post hoc* pairwise Wilcoxon rank sum test with BH correction, $^{*}p < 0.05$, $^{**}p < 0.01$, $^{***}p < 0.001$, $^{****}p < 0.0001$

basal OCR): pcOPA1$^{-/-}$ glu 93.6% ± 3.8% vs. gal 104% ± 3.7% ($p > 0.05$), pcOPA1 iso 1 glu 142.4% ± 6.2% vs. gal 170.6% ± 5.7% ($p < 0.01$), pcOPA1 iso 7 glu 130.7% ± 3.5% vs. gal 169.7% ± 4.1% ($p < 0.001$), normalized to cell count, $n = 8$ replicates). This suggests a much improved ability of pcOPA1 iso 1 and 7 cells to alter their metabolism to meet environmental constraints compared to pcOPA$^{-/-}$ cells. Furthermore, when pcOPA1$^{-/-}$ cells were grown in galactose prior to the Seahorse analysis they demonstrated extremely low OCRs (basal OCR: galactose grown pcOPA1$^{-/-}$ 3.8 ± 0.65 pmol/min) which could not be rescued by providing the cells with glucose during the assay (basal OCR: glucose grown 3.4 ± 0.57 pmol/min).

To examine the reliance of pcOPA1 cells on glycolysis vs. mitochondrial respiration for ATP production, an ATP rate assay was undertaken. When grown in galactose pcOPA1 iso 1 and 7 cells showed an increase in ATP production from mitochondrial processes compared to pcOPA1$^{-/-}$ cells indicating rescued mitochondrial function (**Figure 3H**, mito-ATP production in galactose: pcOPA1$^{-/-}$206 ± 8.8 pmol/min, pcOPA1 iso 1 345.1 ± 22.5 pmol/min, pcOPA1 iso 7 331.6 ± 23.5 pmol/min). Interestingly this ability to use mitochondria for ATP generation is still favored by pcOPA1 iso 1 and 7 cells when grown in glucose media, with an increase in mitochondrial ATP production (mito-ATP production glucose: pcOPA1$^{-/-}$ 195 ± 13 pmol/min, pcOPA1 iso 1 279.1 ± 37.6 pmol/min, pcOPA1 iso 7 288.7 ± 24.7 pmol/min) and a corresponding decrease in glycolytic ATP production (glycol-ATP production glucose: pcOPA1$^{-/-}$ 284.7 ± 37.8 pmol/min, pcOPA1 iso 1 199.7 ± 44.7 pmol/min, pcOPA1 iso 7 229.1 ± 37.4 pmol/min).

To confirm this reduction in reliance of glycolysis in pcOPA1 iso 1 and 7 cells, the Peredox fluorescent protein assay was employed (Hung et al., 2011). Peredox protein increases its fluorescence in response to cytosolic NADH levels, with higher levels of cytosolic NADH being indicative of increased levels of glycolysis. pcOPA1 iso 1 and 7 cells grown in glucose show significantly lower levels of Peredox NADH mediated fluorescence (pcOPA1$^{-/-}$ 3.8 ± 0.9 vs. pcOPA1 iso 1 2.1 ± 0.5 and pcOPA1 iso 7 2.1 ± 0.6 normalized fluorescence ratio, $n = 55$ cells observations across 3 separate transfections, $p < 0.0001$), suggesting these cells have a decreased reliance on glycolysis for ATP production compared to pcOPA1$^{-/-}$ cells (**Figure 3I**).

The mitochondrial activity of pcOPA1 iso 1 and 7 was compared to wild-type (wt) MEF levels grown in galactose media. Notably, rescued cells had no statistical difference in basal OCR when normalized to cell count (**Figure 3J**; Basal OCR: NIH-3T3 70.3 ± 4.4 pmol/min, pcOPA1 iso 1 72.8 ± 8.3 pmol/min, pcOPA1 iso 7 77.1 ± 8.5 pmol/min, normalized to cell count, $n = 8$ replicates, $p > 0.05$) although all three showed a significant improvement compared to pcOPA1$^{-/-}$ cells (Basal OCR: pcOPA1$^{-/-}$ 46.2 ± 4.6 pmol/min, $n = 8$ replicates, $p < 0.001$). However, there was a significant difference in the spare respiratory capacity (SRC) of rescued cells compared to wt MEF cells (**Figure 3K**; SRC as% of baseline: NIH-3T3 216.4% ± 6.5%, pcOPA1 iso 1 168.9% ± 7.1%, pcOPA1 iso 7 154.5% ± 5%, pcOPA1$^{-/-}$ 100.8% ± 5.4%).

AAV delivered OPA1 iso 1 and OPA1 iso 7 Show Benefit in a Mouse Model of Retinal Mitochondrial Dysfunction

Previously our lab has utilized an established rotenone model of complex I deficiency which phenotypically resembles optic neuropathies such as DOA and Leber Hereditary Optic Neuropathy due to significant RGC loss leading to RNFL thinning and a progressive decrease in visual acuity (Zhang et al., 2002; Chadderton et al., 2013).

To investigate the utility of OPA1 iso 1 and OPA1 iso 7 as therapeutic entities, recombinant AAV vectors were produced and evaluated in the rotenone induced mouse model of mitochondrial dysfunction. The AAV2/2 serotype was chosen for the study due to its ability to transduce RGCs efficiently (Dudus et al., 1999; Chadderton et al., 2013). Adult 129 S2/SvHsd mice were intravitreally injected with 1×10^9 vg of AAV2/2-OPA1 iso 1 or AAV2/2-OPA1 iso 7 followed by injection of the complex I inhibitor rotenone 3 weeks later. After 2 weeks mice were analyzed for visual function (**Figure 4**). As AAV2/2-OPA1 iso 1 and AAV2/2-OPA1 iso 7 were injected at different times, each is considered with its respective cohort of controls independently.

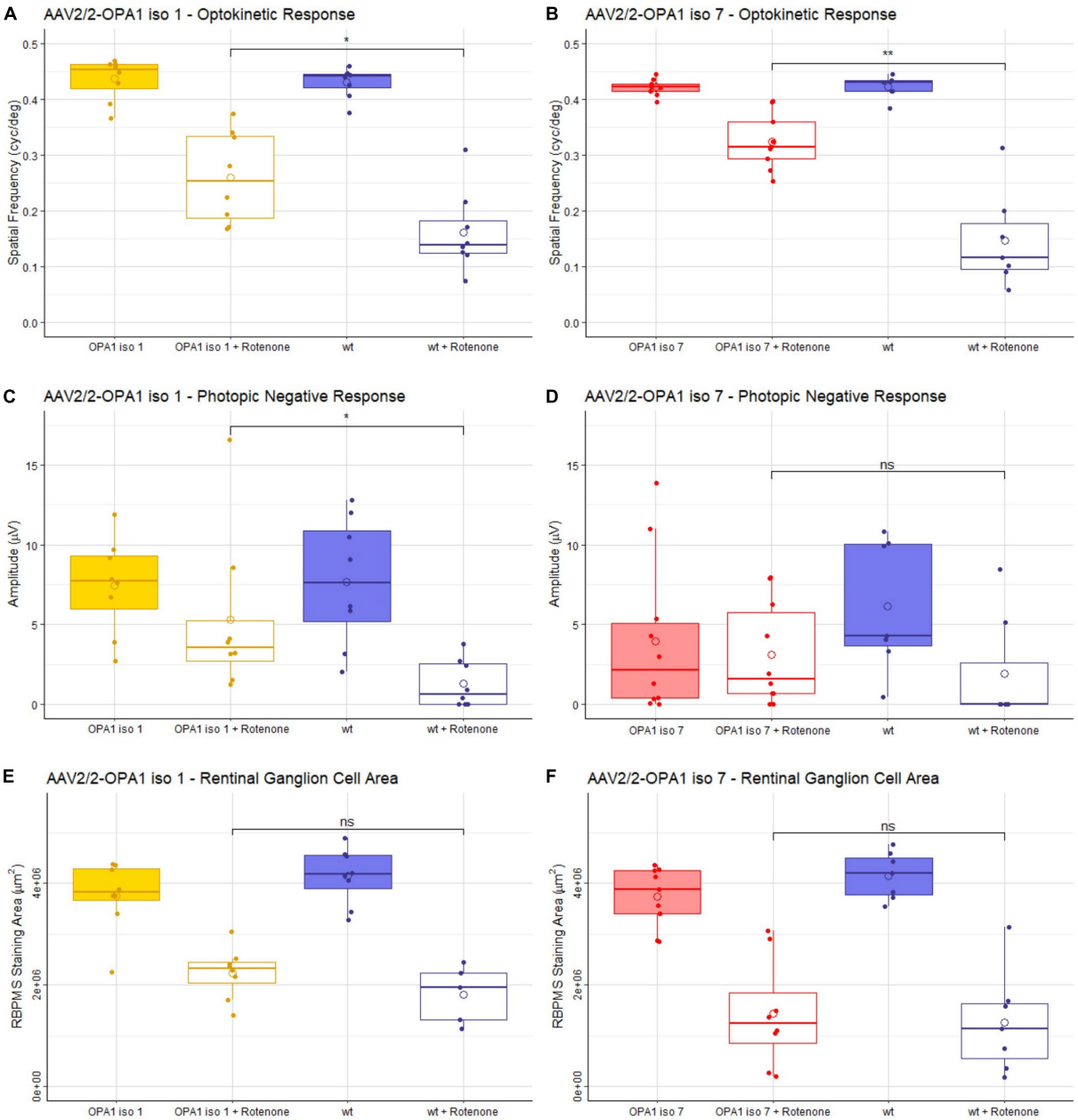

FIGURE 4 | Analysis of AAV2/2-OPA1 iso 1 and AAV2/2-OPA1 iso 7 treatment in a rotenone induced model of optic neuropathy. Adult 129 S2/SvHsd mice were intravitreally injected in both eyes with 1×10^9 vg of either AAV-OPA1 iso 1 or AAV-OPA1 iso 7 and 1×10^8 vg of AAV-CBA-EGFP, 3 weeks post AAV delivery 0.6 μl 1.5 mM rotenone was administered intravitreally. **(A,B)** optokinetic response, maximum spatial frequency (cyc/deg), measured 3 weeks post-rotenone administration. Rotenone treated wt animals in both cohorts show a significant decrease in OKR which is significantly improved by AAV2/2-OPA1 iso 1 or 7 treatment ($p < 0.05$ and $p < 0.01$, respectively). **(C,D)** Show the photopic negative response (PhNR) measured 2 weeks post-rotenone. AAV2/2-OPA1 iso 1 treated animals administered with rotenone show significant protection of PhNR amplitudes compared to wt animals given rotenone ($p < 0.05$), however, AAV2/2-OPA1 iso 7 treated eyes administered with rotenone only showed a modest trend toward protection ($p \approx 0.2$). **(E,F)** Show the area of RBPMS staining (μm^2) as a measure of RGC cell survival. Neither treatment showed statistically significant benefit in RGC area, however, AAV2/2-OPA1 iso 1 should a modest trend toward protection ($p \approx 0.2$). Open circle = mean, OPA1 iso 1 and 7 ± rotenone; $n = 7$; wt ± rotenone, $n = 8$ (OPA1 iso 1 cohort) and wt ± rotenone, $n = 10$ (OPA1 iso 7 cohort) pairwise Wilcoxon rank sum test with BH correction (*$p < 0.05$, **$p < 0.01$).

The optokinetic response (OKR) is a measure of the visual tracking response elicited by a moving pattern. This pattern can be altered to test the maximum spatial frequency the mouse can observe, measured in cycles/degree. The higher the spatial frequency the better the visual acuity. Critically, mice treated with either AAV2/2-OPA1 iso 1 or AAV2/2-OPA1 iso 7 showed no decrease in OKR when compared to uninjected age matched 129 S2/SvHsd mice [hereon referred to as wild-type (wt)] with a mean

of 0.43 ± 0.03 cyc/deg for wt compared to 0.43 ± 0.04 cyc/deg AAV2/2-OPA1 iso 1 treated animals (**Figure 4A**, $n = 7$, $p > 0.05$) and 0.42 ± 0.02 cyc/deg wt compared to 0.42 ± 0.01 cyc/deg AAV2/2-OPA1 iso 7 treated animals (**Figure 4B**, $n = 7$, $p > 0.05$). Injection of rotenone significantly decreased the OKR of wt mice compared to untreated wt eyes (wt + rotenone OPA1 iso 1 cohort: 0.15 ± 0.09 cyc/deg, $n = 8$, $p < 0.01$; OPA1 iso 7 cohort: 0.16 ± 0.07cyc/deg, $n = 7$, $p < 0.001$). There was significant protection of spatial visual function when eyes were treated with either AAV vector prior to rotenone insult with AAV2/2-OPA1 iso 1 showing an OKR of 0.26 ± 0.08 cyc/deg ($n = 7$, $p < 0.05$ compared to wt + rotenone) and AAV2/2-OPA1 iso 7 showing an OKR of 0.32 ± 0.05 cyc/deg ($n = 7$, $p < 0.01$ compared to wt + rotenone). AAV treatment with AAV2/2-OPA1 iso 1 or AAV2/2-OPA1 iso 7 demonstrated maintenance of 60.5 ± 19% and 76.9 ± 11.9% of the OKR, respectively, compared to their wt controls, with rotenone treated eyes demonstrating 37.6± 17.7% and 34.9± 20.4% of the OKR in the OPA1 iso 1 and 7 groups, respectively. This represents a large proportion of protection, although the OKR was still significantly lower than wt controls.

The photopic negative response (PhNR) of treated animals was interrogated. PhNRs are an electroretinogram (ERG) measurement obtained under dark-adapted conditions as a measure of inner retinal electrical activity and are used as a selective measure of RGC activity (**Figures 4C,D**). AAV2/2-OPA1 iso 1 (7.4 ± 3 μV) and AAV2/2-OPA1 iso 7 (3.9 ± 4.9 μV) treated animals show no statistical decrease in PhNR compared to untreated wt eyes (iso 1 cohort: 7.7 ± 4 μV, iso 7 cohort: 6.1 ± 4.1 μV), however there is a clear trend toward decreased PhNR in AAV2/2-OPA1 iso 7 treated eyes. Both groups showed a significant decrease in PhNR amplitudes in eyes injected with rotenone when compared to untreated wt eyes (wt + rotenone OPA1 iso 1 cohort: 1.28 ± 1.5 μV, $n = 8$, $p < 0.01$; OPA1 iso 7 cohort: 1.9 ± 3.5 μV, $n = 10$, $p < 0.05$). Notably, AAV2/2-OPA1 iso 1 treated eyes show a significant benefit in PhNR when insulted with rotenone compared to wt eyes (AAV2/2-OPA1 iso 1 + rotenone: 5.3 ± 5.1 μV, $n = 7$, $p < 0.05$) In comparison AAV2/2-OPA1 iso 7 treated eyes showed a modest trend toward benefit (AAV2/2-OPA1 iso 7 + rotenone: 3.1 ± 3.2 μV, $n = 7$, $p \approx 0.2$) but displayed more variability within the treated group. As AAV2/2-OPA1 iso 1 treated eyes (without rotenone insult) maintained 96% of the PhNR amplitude of wt animals and AAV2/2-OPA1 iso 7 treated only maintained 64% of wt PhNR it suggests there may have been a modest detrimental effect of AAV2/2-OPA1 iso 7 treatment at this dose.

Whole mounts of the experimental retinae stained for RBPMS, a marker for RGCs, were analyzed to assess if AAV2/2-OPA1 iso 1 and AAV2/2-OPA1 iso 7 retinae showed increased protection of RGCs, by measuring the total area of RBPMS positive staining (**Figures 4E,F** and **Supplementary Figure 2** shows representative wholemount images). Treatment with either AAV-OPA1 construct did not lead to significant changes in RGC area when compared to untreated wt retinae (AAV2/2-OPA1 iso 1: $3.75 \pm 0.69\ mm^2$ ($n = 7$) vs. wt $4.14 \pm 0.55\ mm^2$ ($n = 8$), $p > 0.05$; AAV2/2-OPA1 iso 7: $3.73 \pm 0.59\ mm^2$ ($n = 7$) vs. wt $4.15 \pm 0.46\ mm^2$ ($n = 10$), $p > 0.05$). Treatment of wt eyes with rotenone led to significant loss of RGCs (wt + rotenone OPA1 iso 1 cohort: $1.81 \pm 0.57\ mm^2$, $n = 10$, $p < 0.01$; wt + rotenone OPA1 iso 7 cohort: $1.26 \pm 1\ mm^2$, $n = 8$, $p < 0.001$) which neither AAV2/2-OPA1 iso 1 ($2.23 \pm 0.5\ mm^2$, $n = 7$, $p \approx 0.2$) nor AAV2/2-OPA1 iso 7 ($1.43 \pm 1\ mm^2$, $n = 7$, $p > 0.05$) treatment was able to protect from, however AAV2/2-OPA1 showed a modest trend toward RGC protection.

AAV Treatment Shows Benefit in Primary DOA Patient Derived Fibroblasts

To investigate if AAV mediated delivery of OPA1 iso 1 or 7 could improve mitochondrial function in a DOA model, patient derived fibroblasts were generated from 3 DOA patients. DOA 1 (46 y/o, Female) is heterozygous for 53del10 deletion and DOA 2 (49 y/o, Female) and DOA 3 (18 y/o, Female) represent two generations from the same family and are heterozygous for the 1334G > A mutation which leads to an R445H substitution. To act as controls 3 age matched control fibroblast cell lines were used. These donors showed no indication of either mitochondrial or ocular deficits. **Figure 5A** shows endogenous OPA1 mRNA levels as well as Western blot densitometry analysis of OPA1 protein normalized to β-actin levels in each of the 6 cell lines ($n = 4$ technical replicates, see **Supplementary Figure 3** for representative blot). Although mRNA levels remain similar between DOA patients and controls, all three patient cell lines appear to show a deficit of OPA1 protein compared to the control lines, with DOA 1 (53del10) showing the largest decrease. To test the feasibility of AAV2/2-OPA1 mediated therapy all three patient cell lines were treated with 1×10^5 MOI of either AAV2/2-OPA1 iso 1 or 7 before levels of OPA1 mRNA and protein were assessed (**Figure 5B**). Densitometry was performed on total OPA1 protein normalized to β-actin protein levels and for statistical analysis all DOA samples treated with a given virus were combined. **Figure 5B** shows there is a significant increase of total OPA1 protein in cells treated with OPA1 iso 1 virus, but this did not quite reach significance with OPA1 iso 7 treated cells.

These fibroblasts were treated with multiple MOI doses of AAV2/2-OPA1 iso 1 and 7 ranging from 5×10^4 to 2×10^5 in 5-fold increments and were subjected to Seahorse analysis of OCR as a dosing study to test if any functional benefit could be observed. **Figures 5C,D** shows the basal OCR and Spare Respiratory Capacity of these cells normalized to protein content. The basal OCR of these cells remains largely unaltered by AAV treatment apart from DOA 1 cells treated with AAV2/2-OPA1 iso 7 at an MOI of 2.5×10^4 (**Figure 5C**, 38.5 ± 2.6 pmol/min/mg protein, Dunnett's test, $n = 3$ replicates, $p < 0.05$).

When examining the SRC of treated DOA patient cells (**Figure 5D**, only AAV2/2-OPA1 iso 7 treated cells showed significant benefit when compared to untreated, with AAV2/2-OPA1 iso 1 having no significant positive or negative affect in our study. DOA 1 showed maximal benefit to SRC when treated with the highest dose of 2×10^5 MOI (53.3 ± 4.6 pmol/min/mg protein, Dunnett's test, $n = 3$ replicates, $p < 0.05$). DOA 2 showed significant improvement of their SRC at 1×10^5 MOI (40.8 ± 3.4 pmol/min/mg protein, Dunnett's test, $n = 3$ replicates, $p < 0.05$). Of note, DOA 3 showed benefit at two separate MOIs, 2.5×10^4 and 1×10^5 (81.8 ± 3.9 pmol/min/mg protein and

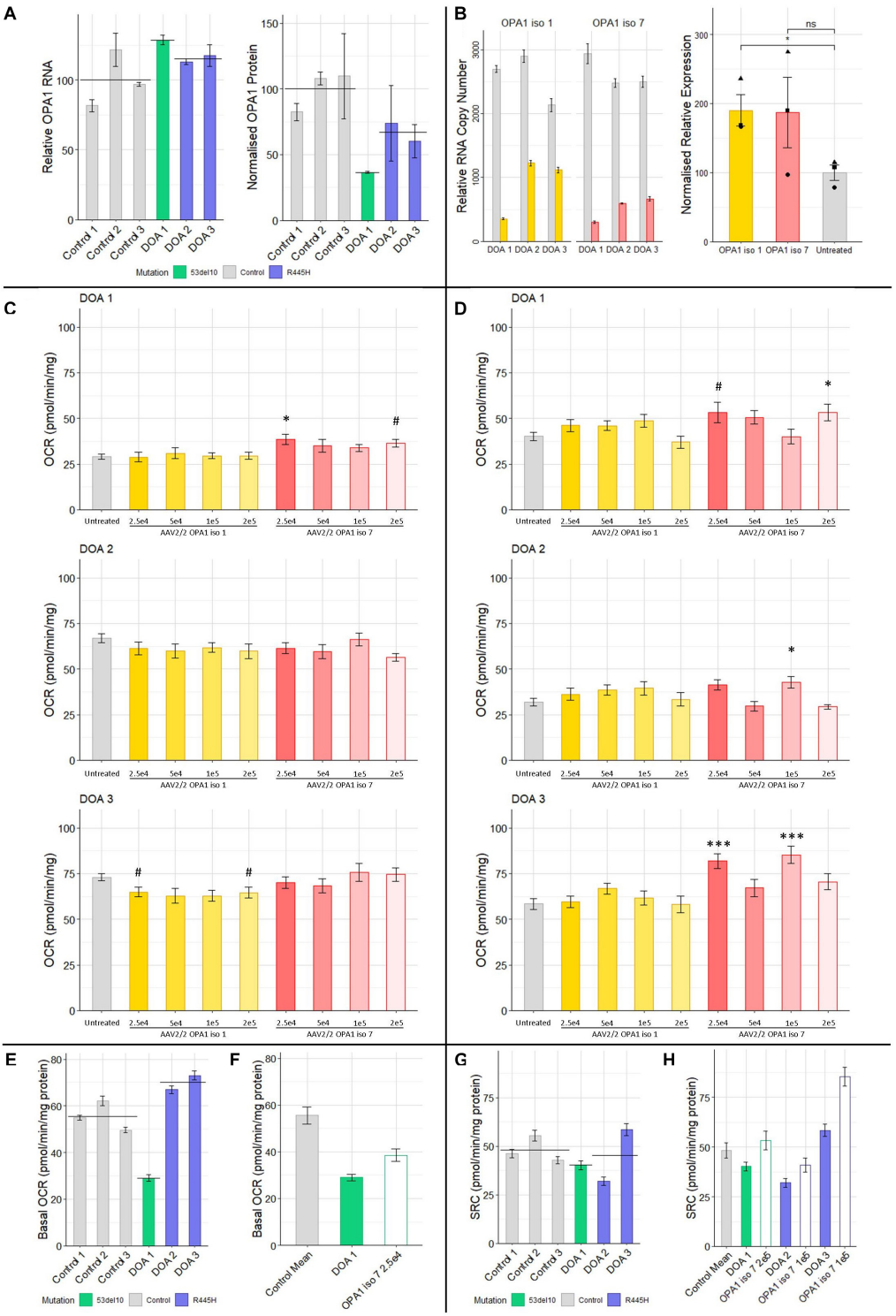

FIGURE 5 | (A) Protein and RNA analysis of 3 DOA fibroblast lines (het 53del10: green and het R445H: purple) and 3 control fibroblast lines (gray). RNA ($n = 4$ technical replicates) and protein ($n = 4$ technical replicates) levels are relative to the mean of control samples. **(B)** RNA and protein analysis from patient cells treated with 1×10^5 MOI of AAV-OPA1 iso 1 or 7. RNA samples are relative copy numbers for each construct ($n = 4$ technical replicates) and compare endogenous RNA from all OPA1 isoforms (gray) and transduced OPA1 iso 1 (yellow) or 7 (red) RNA. Densitometry analysis of transduced cells is normalized to the untreated mean for all 3 patient cell lines and shows the mean of all three cell lines for a given treatment ($n = 3$ replicates per cell line, ●, ▲, and ■ represent DOA 1, 2, and 3, respectively). **(C)** Basal OCR and **(D)** SRC analysis of three DOA patient derived fibroblast lines, DOA 1 (het 53del10) DOA 2 (het R445H) and DOA 3 (het R445H),

(Continued)

FIGURE 5 | Continued
grown in galactose either untreated (gray) or treated with four MOIs of either AAV2/2-OPA1 iso 1 (yellow shades) or AAV2/2-OPA1 iso 7 (red shades) 48 h prior to analysis (Seahorse XFe96). OCR was normalized to protein content. SRC was measured as the difference between basal and maximal OCR after removal of non-mitochondrial OCR. ($n = 3$ replicates, Dunnett's Test vs. Untreated). **(E)** Comparison of the basal OCR of 3 control fibroblast cell lines with the 3 patient cell lines untreated, color coded by mutation ($n = 3$ replicates). **(F)** Comparison of the mean control basal OCR and the only dose found to significantly alter basal OCR from C), 2.5×10^4 MOI AAV-OPA1 iso 7 in DOA 1 cells. **(G)** SRC of control cell lines compared to DOA cell lines, color coded by mutation ($n = 3$ replicates). **(H)** Comparison of the mean SRC of the 3 control lines with untreated DOA SRC values and the viral doses that achieved the largest increase in SRC for each from **(D)** [outlined bars ($n = 3$ replicates)]. $^{\#}p < 0.1$, $^{*}p < 0.05$, $^{***}p < 0.001$, error bars ± SE.

85.3 ± 4.6 pmol/mg/protein respectively, Dunnett's test, $n = 3$ replicates, $p < 0.001$) but not with the MOI in between of 5×10^4.

Figure 5E shows the basal OCR of the 6 different fibroblast lines, color coded by genotype (gray: controls, green: 53del10, purple: R445H, and black bar indicates the group mean). There is a large deficit in basal OCR in DOA 1 cells harboring 53del10. Intriguingly there appears to be an increase in the basal OCR of the R445H cell lines, DOA 2 and 3 which show 120.5 and 131.5% of control cell basal oxygen consumption respectively. To further demonstrate the beneficial effect observed with AAV2/2-OPA1 iso 7 treatment, **Figure 5F** shows a comparison between the average basal OCR of the three control lines compared to that of DOA 1 cells, as well as the DOA 1 cells treated with 2.5×10^4 AAV2/2-OPA1 iso 7. Before treatment DOA 1 showed 52.2% of the basal OCR of the control cells, with AAV treatment increasing this to 69.4%.

Figure 5G shows the SRC of control cells compared to the DOA cell lines. Both DOA 1 and DOA 2 show a reduction in SRC when compared to control cell lines, however DOA 3 shows high levels of SRC. When comparing the level of increase in SRC AAV-OPA1 treatment mediates (**Figure 5H**), DOA 1 increases from 83.3 to 120.6% of control levels, DOA 2 increases from 66.3 to 84.7% of control levels and DOA 3 increases from 121.2 to 177% of control levels.

DISCUSSION

The current study provides clear support for the value of OPA1 based gene therapies for DOA and potentially more broadly for other ocular disorders involving mitochondrial dysfunction. These results suggest that OPA1 isoforms 1 and 7 are the prevalent isoforms expressed in healthy retinal tissue and that both isoforms can be used as potential therapeutic modalities, but consideration needs to be given to ensure appropriate dosing of OPA1 protein. Notably, codon optimized versions of OPA1 isoform 1 and 7 were generated and both isoforms were shown to modulate mitochondrial bioenergetics in cell models of OPA1 dysfunction and protect spatial visual function and PhNR responses in a chemically induced mouse model displaying many of the morphological and functional phenotypes of optic neuropathy, although the OPA1 based therapy only provided a trend toward protection of RGCs. Of note, we demonstrated for the first time that AAV-OPA1 therapeutic interventions can alter mitochondrial bioenergetics in DOA patient derived fibroblast cells, with both OPA1 isoforms evaluated demonstrating the ability to significantly alter mitochondrial bioenergetics by increasing mitochondrial SRC. Taken together, these data underscore the potential utility of OPA1 based gene therapy.

Initial analysis of the OPA1 isoforms expressed in healthy human retinal tissue (Li et al., 2014), representing the first time human retinal tissue has been directly assessed, corroborated with previous studies showing isoforms 1 and 7 to be most prevalently expressed in human tissue in general. It is worth noting that isoform 5 was previously identified as the most highly expressed in human brain tissue (Olichon et al., 2007). In the data analyzed here this was not the case but intriguingly there was a difference in isoform 5 expression levels when comparing the peripheral and macular retinal samples. This difference could be due to the different cellular composition across the human retina, with differences in rod and cone photoreceptor density and cells such as RGCs becoming less prevalent toward the retinal periphery (Drasdo et al., 2007). RNAseq data stratified by cell type would help illuminate the exact isoform distribution in RGCs, however previous analysis of OPA1 isoforms in rat RGCs suggested there was no significant difference in isoform expression patterns between RGCs and the retina at large (Kamei et al., 2005).

The correlation observed between RNA transcript levels involved in mitochondrial fission and fusion suggests that relative expression levels of mitochondrial remodelers may be important to balance mitochondrial network morphology. It is plausible that the increased OPA1 expression provided by transient expression of either OPA1 isoform tested here led to an aggregated mitochondrial network frequently observed due to shifting the balance of fission and fusion. This phenotype has previously been suggested to be due to a compensatory increase in mitochondrial fission (Misaka et al., 2002; Cipolat et al., 2004). Our study highlights the necessity to regulate expression levels of OPA1 tightly in order to provide the maximal benefit to the recipient cell.

Once appropriate levels of OPA1 protein can be achieved there is clear potential for benefit to mitochondrial outputs, as demonstrated by analysis of OPA1 isoform 1 and 7 $OPA1^{-/-}$ MEF stable cell lines. Codon optimization of OPA1 isoform 1 and 7 did not perturb their function as $OPA1^{-/-}$ MEF cells stably expressing either isoform could use mitochondria for ATP production significantly better than $OPA1^{-/-}$ cells, and moreover, OCR under normal physiological conditions could be restored to wild type levels. In terms of their bioenergetic profiles, the two isoforms provide similar levels of functional rescue using these assays. However, pcOPA1 iso 7 cells do show an increased rescue of mitochondrial network morphology (**Figure 3A**).

Importantly, this study represents the first demonstration that AAV-OPA1 based gene therapy can maintain visual function, evaluated here by OKR. However, just a trend to a corresponding protection of RGCs was obtained. There appears to be a disparity between the two isoforms tested in ability to protect against rotenone insult, with OPA1 iso 1 also demonstrating protection of the PhNR response in treated animals—although a trend toward PhNR protection can also be seen in OPA1 isoform 7 treated animals. One could hypothesize that the disparity between OKR protection compared to PhNR may be due to preferential protection of subsets of RGCs involved in movement, allowing visual function to be preserved whilst there is still a significant reduction in overall RGC activity. It is also noteworthy that AAV-OPA1 iso 7 treatment appears to have had a more dramatic effect on the PhNR response in these animals in the absence of rotenone when compared to AAV-OPA1 iso 1 treatment alone. This is also interesting given that there was no reduction in RGC area between OPA1 iso 7 treated and untreated animals, suggesting cell survival and functionality may be separable. In this study, at equal doses, the two isoforms do not provide equal levels of protection.

Previous AAV-OPA1 based therapeutic studies have shown some protection of RGCs (Sun et al., 2016b; Hu et al., 2018; Sarzi et al., 2018). While this was not recapitulated in our study, there is a trend toward increased RGC number in the rotenone treated AAV-OPA1 isoform 1 cohort compared to wild type mice treated with rotenone. The data suggest that despite levels of RGC loss being similar in all rotenone treated groups, the function of the remaining RGCs is enhanced by both of the OPA1 isoforms, allowing for maintenance of a significant level of visual function. Further work is needed to examine potential dosage levels of each isoform to establish whether both functional and histological benefits can be achieved.

The rotenone model presented here is not directly analogous to a DOA animal model as the insult is acute rather than a prolonged retinal degeneration. Although the model does recapitulate the preferential RGC dysfunction, the mechanism of rotenone induced degeneration is different from that seen in DOA, namely the inhibition of complex I of the electron transport chain vs. OPA1 haploinsufficiency (Alavi et al., 2007; Davies et al., 2007). As such the data here show that OPA1 based gene therapy potentially has a wider applicability as a therapeutic agent for mitochondrial disorders outside of its potential utility in DOA.

The analysis of DOA patient derived fibroblasts underscores the differing effects different viral doses of AAV-OPA1 isoforms can enact and also highlights the range of effects different OPA1 mutations can have on mitochondrial function. Previous analysis of fibroblasts derived from DOA patients with the OPA1 R445H have also found an increase basal OCR over that of control cells, with the hypothesis proposed that basal OCR is increased in these cells as a compensatory mechanism (exact age at time of all biopsies unclear; mean age 23 for 3 patients, $n = 5$; Amati-Bonneau et al., 2005). Furthermore, the FCCP mediated, maximal respiration and spare respiratory capacity of a fibroblast line with the R445H mutation has previously been shown to be significantly increased compared to control fibroblasts, but no increase in basal OCR was observed (age 30; Kane et al., 2017). However this situation is not so clear cut as R445H has also been found to be one of the most deleterious mutations in patient derived fibroblasts, with cells exhibiting lower, but not significantly so, basal and maximal respiration compared to controls (mean age: 38; $n = 2$; Del Dotto et al., 2018b). It is possible that age is a modulating factor for the phenotypic variation observed with the R445H mutation, as mitochondria have long been associated with age related dysfunction (Jarrett et al., 2010; Sun et al., 2016a; Elfawy and Das, 2019). The two patients with the R445H mutations in this study have a mean age of 33.5, with both displaying higher basal OCR than controls. Age could also potentially explain why the SRC of DOA 2 (49 years) is lower compared to DOA 3 (18 years), and indeed why the SRC of DOA 3 is the highest of all cells assayed in this study. Further work is needed to fully elucidate the underlying biochemical effect of the R445H mutation. It is positive that AAV delivered OPA1 isoform 7 significantly increased the SRC in both DOA 2 and DOA 3 cells, which would in theory allow cells to better modulate their metabolism to meet fluctuating energy demands. In this study, efficacy was related to the viral dose delivered. The youngest patient, DOA 3 (∼30 years younger than the others) demonstrated the highest untreated SRC and the largest level of benefit with two doses of virus, potentially suggesting a higher level of plasticity in mitochondrial dynamics.

Currently no other studies have examined the 53del10 deletion, but our data suggests it leads to haploinsufficiency via a decrease in OPA1 protein levels coupled with a decrease in basal OCR and SRC below that of control fibroblasts. Here we have shown that AAV delivered OPA1 isoform 7 can significantly improve both the basal OCR and SRC of these cells, albeit at different doses.

The increase in SRC is promising for potential DOA therapeutics as previous studies have shown patient derived cells to have OCR deficiencies (Amati-Bonneau et al., 2005; Belenguer and Pellegrini, 2013; Vidoni et al., 2013; Kane et al., 2017; Liao et al., 2017; Del Dotto et al., 2018b). Clearly SRC is part of a broader range of mitochondrial roles that are affected by mutations in OPA1, with some debate as to whether mitochondrial dysfunction or the deficiency in mitochondrial network regulation is the main component in DOA related RGC loss (Del Dotto et al., 2018a), but this study highlights the potential utility of AAV delivered OPA1 isoforms to modulate mitochondrial bioenergetics in patient derived cells.

It is unclear why OPA1 isoform 7 outperformed isoform 1 in DOA patient cells and is in contrast to the greater benefit found with OPA1 isoform 1 in the rotenone model shown here, but this could potentially be due to differing physiological roles performed by the two isoforms, although previous work examining the functions of different isoforms has found limited difference between isoforms 1 and 7 (Del Dotto et al., 2017). It seems plausible that with an altered dose that OPA1 isoform 7 could prove as effective as isoform 1 in the animal model and likewise OPA1 isoform 1 could show similar levels of benefit in patient cells.

The current study supports the view that finely regulated dosage appears to be crucial to provide functional benefit when

utilizing OPA1 based therapies, and therefore it may be of great benefit to employ the endogenous *OPA1* promoter for such therapies, however, currently the endogenous *OPA1* promoter remains poorly defined. If of a suitable size, incorporating the endogenous promoter into an AAV-OPA1 expression cassette, or employing genome editing strategies, thereby utilizing the endogenous promoter *in situ*, could potentially much improve ability of the construct to provide appropriate OPA1 protein dosage.

Critically, the study provides clear evidence of rescue of spatial visual function *in vivo* of an AAV-OPA1 based gene therapy and represents a step forward in the use of OPA1 isoforms as therapeutic interventions for DOA and potentially for other optic neuropathies more broadly as seen in the rotenone induced mouse model. Intriguingly, this further adds to the evidence that the neuro protective properties of OPA1 may potentially be utilized in a wide array of scenarios. However, the study also underscores that if OPA1 based therapeutics are to be fully efficacious then careful regulation of dosage needs to be achieved.

DATA AVAILABILITY STATEMENT

The raw data supporting the conclusions of this article will be made available by the authors, without undue reservation, to any qualified researcher.

ETHICS STATEMENT

The animal study was reviewed and approved by the animal research ethics committee, in Trinity College Dublin. Ref. no. 140514. Ethics approval for patient cells obtained from Royal Victoria Eye and Ear Hospital. Ref. no. RF024/17.

AUTHOR CONTRIBUTIONS

DM: experimental design, experimentation, figures, writing, editing. NC and SM-W: experimental design, experimentation, writing, editing. AP, CS, and, PK: experimental design, experimentation. JO'B, LC, and DK: experimentation. PH: experimental design. GF: experimental design, writing, editing, funding. All authors contributed to the article and approved the submitted version.

FUNDING

This research was supported by Science Foundation Ireland (16/IA/4452), Fighting Blindness Ireland - Health Research Charities Ireland (MRCG-2012-4 and MRCG-2016-14) and Health Research Board of Ireland (HRA-POR-2015-1140).

ACKNOWLEDGMENTS

We would like to thank Dr. Stephanie James for their help in organizing the patient biopsies. We would also like to thank Trinity College Comparative Medicine Unit for animal husbandry. We would also like to extend our gratitude to Fighting Blindness Ireland, Health Research Charities Ireland and the patients and their families for their continued support.

SUPPLEMENTARY MATERIAL

The Supplementary Material for this article can be found online at: https://www.frontiersin.org/articles/10.3389/fnins.2020.571479/full#supplementary-material

REFERENCES

Afgan, E., Baker, D., Batut, B., Van Den Beek, M., Bouvier, D., Ech, M., et al. (2018). The Galaxy platform for accessible, reproducible and collaborative biomedical analyses: 2018 update. *Nucleic Acids Res.* 46, W537–W544. doi: 10.1093/nar/gky379

Akepati, V. R., Müller, E.-C., Otto, A., Strauss, H. M., Portwich, M., and Alexander, C. (2008). Characterization of OPA1 isoforms isolated from mouse tissues. *J. Neurochem.* 106, 372–383. doi: 10.1111/j.1471-4159.2008.05401.x

Alavi, M. V., Bette, S., Schimpf, S., Schuettauf, F., Schraermeyer, U., Wehrl, H. F., et al. (2007). A splice site mutation in the murine Opa1 gene features pathology of autosomal dominant optic atrophy. *Brain* 130, 1029–1042. doi: 10.1093/brain/awm005

Amati-Bonneau, P., Guichet, A., Olichon, A., Chevrollier, A., Viala, F., Miot, S., et al. (2005). OPA1 R445H mutation in optic atrophy associated with sensorineural deafness. *Ann. Neurol.* 58, 958–963. doi: 10.1002/ana.20681

Ban, T., Ishihara, T., Kohno, H., Saita, S., Ichimura, A., Maenaka, K., et al. (2017). Molecular basis of selective mitochondrial fusion by heterotypic action between OPA1 and cardiolipin. *Nat. Cell Biol.* 19, 856–863. doi: 10.1038/ncb3560

Belenguer, P., and Pellegrini, L. (2013). The dynamin GTPase OPA1: more than mitochondria? *Biochim. Biophys. Acta Mol. Cell Res.* 1833, 176–183. doi: 10.1016/j.bbamcr.2012.08.004

Bennicelli, J., Wright, J. F., Komaromy, A., Jacobs, J. B., Hauck, B., Zelenaia, O., et al. (2008). Reversal of blindness in animal models of leber congenital amaurosis using optimized AAV2-mediated gene transfer. *Mol. Ther.* 16, 458–465. doi: 10.1038/sj.mt.6300389

Bray, N. L., Pimentel, H., Melsted, P., and Pachter, L. (2016). Near-optimal probabilistic RNA-seq quantification. *Nat. Biotechnol.* 34, 525–527. doi: 10.1038/nbt.3519

Caglayan, S., Hashim, A., Cieslar-Pobuda, A., Jensen, V., Behringer, S., Talug, B., et al. (2020). Optic atrophy 1 controls human neuronal development by preventing aberrant nuclear DNA methylation. *iScience* 23:101154. doi: 10.1016/j.isci.2020.101154

Chadderton, N., Palfi, A., Millington-Ward, S., Gobbo, O., Overlack, N., Carrigan, M., et al. (2013). Intravitreal delivery of AAV-NDI1 provides functional benefit in a murine model of Leber hereditary optic neuropathy. *Eur. J. Hum. Genet.* 21, 62–68. doi: 10.1038/ejhg.2012.112

Chen, H., Detmer, S. A., Ewald, A. J., Griffin, E. E., Fraser, S. E., and Chan, D. C. (2003). Mitofusins Mfn1 and Mfn2 coordinately regulate mitochondrial fusion and are essential for embryonic development. *J. Cell Biol.* 160, 189–200. doi: 10.1083/jcb.200211046

Chen, H., Vermulst, M., Wang, Y. E., Chomyn, A., Prolla, T. A., McCaffery, J. M., et al. (2010). Mitochondrial fusion is required for mtDNA stability in skeletal muscle and tolerance of mtDNA mutations. *Cell* 141, 280–289. doi: 10.1016/j.cell.2010.02.026

Chun, B. Y., and Rizzo, J. F. (2017). Dominant optic atrophy and Leber's hereditary optic neuropathy: update on clinical features and current therapeutic approaches. *Semin. Pediatr. Neurol.* 24, 129–134. doi: 10.1016/J.SPEN.2017.06.001

Cipolat, S., Martins de Brito, O., Dal Zilio, B., and Scorrano, L. (2004). OPA1 requires mitofusin 1 to promote mitochondrial fusion. *Proc. Natl. Acad. Sci. U.S.A.* 101, 15927–15932. doi: 10.1073/pnas.0407043101

Civiletto, G., Varanita, T., Cerutti, R., Gorletta, T., Barbaro, S., Marchet, S., et al. (2015). Opa1 overexpression ameliorates the phenotype of two mitochondrial disease mouse models. *Cell Metab.* 21, 845–854. doi: 10.1016/j.cmet.2015.04.016

Cogliati, S., Frezza, C., Soriano, M. E., Varanita, T., Quintana-Cabrera, R., Corrado, M., et al. (2013). Mitochondrial cristae shape determines respiratory chain supercomplexes assembly and respiratory efficiency. *Cell* 155, 160–171. doi: 10.1016/J.CELL.2013.08.032

Davies, V. J., Hollins, A. J., Piechota, M. J., Yip, W., Davies, J. R., White, K. E., et al. (2007). Opa1 deficiency in a mouse model of autosomal dominant optic atrophy impairs mitochondrial morphology, optic nerve structure and visual function. *Hum. Mol. Genet.* 16, 1307–1318. doi: 10.1093/hmg/ddm079

Del Dotto, V., Fogazza, M., Lenaers, G., Rugolo, M., Carelli, V., and Zanna, C. (2018a). OPA1: how much do we know to approach therapy? *Pharmacol. Res.* 131, 199–210. doi: 10.1016/J.PHRS.2018.02.018

Del Dotto, V., Fogazza, M., Musiani, F., Maresca, A., Aleo, S. J., Caporali, L., et al. (2018b). Deciphering OPA1 mutations pathogenicity by combined analysis of human, mouse and yeast cell models. *Biochim. Biophys. Acta Mol. Basis Dis.* 1864, 3496–3514. doi: 10.1016/J.BBADIS.2018.08.004

Del Dotto, V., Mishra, P., Vidoni, S., Fogazza, M., Maresca, A., Caporali, L., et al. (2017). OPA1 isoforms in the hierarchical organization of mitochondrial functions. *Cell Rep.* 19, 2557–2571. doi: 10.1016/j.celrep.2017.05.073

Delettre, C., Griffoin, J. M., Kaplan, J., Dollfus, H., Lorenz, B., Faivre, L., et al. (2001). Mutation spectrum and splicing variants in the OPA1 gene. *Hum. Genet.* 109, 584–591. doi: 10.1007/s00439-001-0633-y

Delettre, C., Lenaers, G., Griffoin, J. M., Gigarel, N., Lorenzo, C., Belenguer, P., et al. (2000). Nuclear gene OPA1, encoding a mitochondrial dynamin-related protein, is mutated in dominant optic atrophy. *Nat. Genet.* 26, 207–210. doi: 10.1038/79936

Douglas, R. M., Alam, N. M., Silver, B. D., Mcgill, T. J., Tschetter, W. W., and Prusky, G. T. (2005). Independent visual threshold measurements in the two eyes of freely moving rats and mice using a virtual-reality optokinetic system. *Vis. Neurosci.* 22, 677–684. doi: 10.1017/S0952523805225166

Drasdo, N., Millican, C. L., Katholi, C. R., and Curcio, C. A. (2007). The length of Henle fibers in the human retina and a model of ganglion receptive field density in the visual field. *Vis. Res.* 47, 2901–2911. doi: 10.1016/j.visres.2007.01.007

Dudus, L., Anand, V., Acland, G. M., Chen, S. J., Wilson, J. M., Fisher, K. J., et al. (1999). Persistent transgene product in retina, optic nerve and brain after intraocular injection of rAAV. *Vis. Res.* 39, 2545–2553. doi: 10.1016/S0042-6989(98)00308-3

Ehses, S., Raschke, I., Mancuso, G., Bernacchia, A., Geimer, S., Tondera, D., et al. (2009). Regulation of OPA1 processing and mitochondrial fusion by m-AAA protease isoenzymes and OMA1. *J. Cell Biol.* 187, 1023–1036. doi: 10.1083/jcb.200906084

Elfawy, H. A., and Das, B. (2019). Crosstalk between mitochondrial dysfunction, oxidative stress, and age related neurodegenerative disease: etiologies and therapeutic strategies. *Life Sci.* 218, 165–184. doi: 10.1016/j.lfs.2018.12.029

Frezza, C., Cipolat, S., Martins de Brito, O., Micaroni, M., Beznoussenko, G. V., Rudka, T., et al. (2006). OPA1 controls apoptotic cristae remodeling independently from mitochondrial fusion. *Cell* 126, 177–189. doi: 10.1016/J.CELL.2006.06.025

Hu, X., Dai, Y., Zhang, R., Shang, K., and Sun, X. (2018). Overexpression of optic atrophy type 1 protects retinal ganglion cells and upregulates parkin expression in experimental glaucoma. *Front. Mol. Neurosci.* 11:350. doi: 10.3389/fnmol.2018.00350

Hung, Y. P., Albeck, J. G., Tantama, M., and Yellen, G. (2011). Imaging cytosolic NADH-NAD+ redox state with a genetically encoded fluorescent biosensor. *Cell Metab.* 14, 545–554. doi: 10.1016/J.CMET.2011.08.012

Jarrett, S. G., Lewin, A. S., and Boulton, M. E. (2010). The importance of mitochondria in age-related and inherited eye disorders. *Ophthalm. Res.* 44, 179–190. doi: 10.1159/000316480

Kamei, S., Chen-Kuo-Chang, M., Cazevieille, C., Lenaers, G., Olichon, A., Bélenguer, P., et al. (2005). Expression of the Opa1 mitochondrial protein in retinal ganglion cells: its downregulation causes aggregation of the mitochondrial network. *Investig. Ophthalmol. Vis. Sci.* 46, 4288–4294. doi: 10.1167/iovs.03-1407

Kane, M. S., Alban, J., Desquiret-Dumas, V., Gueguen, N., Ishak, L., Ferre, M., et al. (2017). Autophagy controls the pathogenicity of *OPA1* mutations in dominant optic atrophy. *J. Cell. Mol. Med.* 21, 2284–2297. doi: 10.1111/jcmm.13149

Karbowski, M., Arnoult, D., Chen, H., Chan, D. C., Smith, C. L., and Youle, R. J. (2004). Quantitation of mitochondrial dynamics by photolabeling of individual organelles shows that mitochondrial fusion is blocked during the Bax activation phase of apoptosis. *J. Cell Biol.* 164, 493–499. doi: 10.1083/jcb.200309082

Karbowski, M., Cleland, M. M., and Roelofs, B. A. (2014). Photoactivatable green fluorescent protein-based visualization and quantification of mitochondrial fusion and mitochondrial network complexity in living cells. *Methods Enzymol.* 547, 57–73. doi: 10.1016/B978-0-12-801415-8.00004-7

Lai, Y., Lin, P., Chen, M., Zhang, Y., Chen, J., Zheng, M., et al. (2020). Restoration of L-OPA1 alleviates acute ischemic stroke injury in rats via inhibiting neuronal apoptosis and preserving mitochondrial function. *Redox Biol.* 34:101503. doi: 10.1016/j.redox.2020.101503

Lane, A., Jovanovic, K., Shortall, C., Ottaviani, D., Panes, A. B., Schwarz, N., et al. (2020). Modeling and rescue of RP2 retinitis pigmentosa using iPSC-derived retinal organoids. *Stem Cell Rep.* 15, 67–79. doi: 10.1016/j.stemcr.2020.05.007

Lee, H., Smith, S. B., and Yoon, Y. (2017). The short variant of the mitochondrial dynamin OPA1 maintains mitochondrial energetics and cristae structure. *J. Biol. Chem.* 292, 7115–7130. doi: 10.1074/jbc.M116.762567

Lee, H., and Yoon, Y. (2018). Mitochondrial membrane dynamics—functional positioning of OPA1. *Antioxidants* 7:186. doi: 10.3390/antiox7120186

Lenaers, G., Hamel, C., Delettre, C., Amati-Bonneau, P., Procaccio, V., Bonneau, D., et al. (2012). Dominant optic atrophy. *Orphanet. J. Rare Dis.* 7:46. doi: 10.1186/1750-1172-7-46

Levitt, N., Briggs, D., Gil, A., and Proudfoot, N. J. (1989). Definition of an efficient synthetic poly (A) site. *Genes Dev.* 3, 1019–1025. doi: 10.1101/gad.3.7.1019

Li, M., Jia, C., Kazmierkiewicz, K. L., Bowman, A. S., Tian, L., Liu, Y., et al. (2014). Comprehensive analysis of gene expression in human retina and supporting tissues. *Hum. Mol. Genet.* 23, 4001–4014. doi: 10.1093/hmg/ddu114

Liao, C., Ashley, N., Diot, A., Morten, K., Phadwal, K., Williams, A., et al. (2017). Dysregulated mitophagy and mitochondrial organization in optic atrophy due to OPA1 mutations. *Neurology* 88, 131–142. doi: 10.1212/WNL.0000000000003491

Macdonald, P. J., Francy, C. A., Stepanyants, N., Lehman, L., Baglio, A., Mears, J. A., et al. (2016). Distinct splice variants of dynamin-related protein 1 differentially utilize mitochondrial fission factor as an effector of cooperative GTPase activity. *J. Biol. Chem.* 291, 493–507. doi: 10.1074/jbc.M115.680181

Meschede, I. P., Ovenden, N. C., Seabra, M. C., Futter, C. E., Votruba, M., Cheetham, M. E., et al. (2020). Symmetric arrangement of mitochondria:plasma membrane contacts between adjacent photoreceptor cells regulated by Opa1. *Proc. Natl. Acad. Sci. U.S.A.* 117, 15684–15693. doi: 10.1073/pnas.2000304117

Misaka, T., Miyashita, T., and Kubo, Y. (2002). Primary structure of a dynamin-related mouse mitochondrial GTPase and its distribution in brain, subcellular localization, and effect on mitochondrial morphology. *J. Biol. Chem.* 277, 15834–15842. doi: 10.1074/jbc.M109260200

Olichon, A., ElAchouri, G., Baricault, L., Delettre, C., Belenguer, P., and Lenaers, G. (2007). OPA1 alternate splicing uncouples an evolutionary conserved function in mitochondrial fusion from a vertebrate restricted function in apoptosis. *Cell Death Differ.* 14, 682–692. doi: 10.1038/sj.cdd.4402048

O'Reilly, M., Palfi, A., Chadderton, N., Millington-Ward, S., Ader, M., Cronin, T., et al. (2007). RNA interference-mediated suppression and replacement of human rhodopsin in vivo. *Am. J. Hum. Genet.* 81, 127–135. doi: 10.1086/519025

Palfi, A., Hokamp, K., Hauck, S. M., Vencken, S., Millington-Ward, S., Chadderton, N., et al. (2016). MicroRNA regulatory circuits in a mouse model of inherited retinal degeneration. *Sci. Rep.* 6, 1–14. doi: 10.1038/srep31431

Prusky, G. T., Alam, N. M., Beekman, S., and Douglas, R. M. (2004). Rapid quantification of adult and developing mouse spatial vision using a virtual optomotor system. *Investig. Ophthalmol. Vis. Sci.* 45, 4611–4616. doi: 10.1167/iovs.04-0541

Ramaker, R. C., Bowling, K. M., Lasseigne, B. N., Hagenauer, M. H., Hardigan, A. A., Davis, N. S., et al. (2017). Post-mortem molecular profiling of three psychiatric disorders. *Genome Med.* 9:72. doi: 10.1186/s13073-017-0458-5

Rodriguez, A. R., de Sevilla Müller, L. P., and Brecha, N. C. (2014). The RNA binding protein RBPMS is a selective marker of ganglion cells in the mammalian retina. *J. Comp. Neurol.* 522, 1411–1443. doi: 10.1002/cne.23521

Rohr, U. P., Wulf, M. A., Stahn, S., Steidl, U., Haas, R., and Kronenwett, R. (2002). Fast and reliable titration of recombinant adeno-associated virus type-2 using quantitative real-time PCR. *J. Virol. Methods* 106, 81–88. doi: 10.1016/S0166-0934(02)00138-6

Sarzi, E., Seveno, M., Piro-Mégy, C., Elzière, L., Quilès, M., Péquignot, M., et al. (2018). OPA1 gene therapy prevents retinal ganglion cell loss in a dominant optic atrophy mouse model. *Sci. Rep.* 8:2468. doi: 10.1038/s41598-018-20838-8

Schindelin, J., Arganda-Carreras, I., Frise, E., Kaynig, V., Longair, M., Pietzsch, T., et al. (2012). Fiji: an open-source platform for biological-image analysis. *Nat. Methods* 9, 676–682. doi: 10.1038/nmeth.2019

Skidd, P. M., Lessell, S., and Cestari, D. M. (2013). Autosomal dominant hereditary optic neuropathy (ADOA): a review of the genetics and clinical manifestations of ADOA and ADOA+. *Semin. Ophthalmol.* 28, 422–426. doi: 10.3109/08820538.2013.825296

Smirnova, E., Shurland, D. L., Ryazantsev, S. N., and van der Bliek, A. M. (1998). A human dynamin-related protein controls the distribution of mitochondria. *J. Cell Biol.* 143, 351–358. doi: 10.1083/jcb.143.2.351

Song, Z., Chen, H., Fiket, M., Alexander, C., and Chan, D. C. (2007). OPA1 processing controls mitochondrial fusion and is regulated by mRNA splicing, membrane potential, and Yme1L. *J. Cell Biol.* 178, 749–755. doi: 10.1083/jcb.200704110

Song, Z., Ghochani, M., McCaffery, J. M., Frey, T. G., and Chan, D. C. (2009). Mitofusins and OPA1 mediate sequential steps in mitochondrial membrane fusion. *Mol. Biol. Cell* 20, 3525–3532. doi: 10.1091/mbc.e09-03-0252

Sun, N., Youle, R. J., and Finkel, T. (2016a). The mitochondrial basis of aging. *Mol. Cell* 61, 654–666. doi: 10.1016/j.molcel.2016.01.028

Sun, Y., Xue, W., Song, Z., Huang, K., and Zheng, L. (2016b). Restoration of Opa1-long isoform inhibits retinal injury-induced neurodegeneration. *J. Mol. Med.* 94, 335–346. doi: 10.1007/s00109-015-1359-y

Ubaida-Mohien, C., Lyashkov, A., Gonzalez-Freire, M., Tharakan, R., Shardell, M., Moaddel, R., et al. (2019). Discovery proteomics in aging human skeletal muscle finds change in spliceosome, immunity, proteostasis and mitochondria. *eLife* 8:e49874. doi: 10.7554/eLife.49874

Varanita, T., Soriano, M. E., Romanello, V., Zaglia, T., Quintana-Cabrera, R., Semenzato, M., et al. (2015). The Opa1-dependent mitochondrial cristae remodeling pathway controls atrophic, apoptotic, and ischemic tissue damage. *Cell Metab.* 21, 834–844. doi: 10.1016/J.CMET.2015.05.007

Vidoni, S., Zanna, C., Rugolo, M., Sarzi, E., and Lenaers, G. (2013). Why mitochondria must fuse to maintain their genome integrity. *Antioxid. Redox Signal.* 19, 379–388. doi: 10.1089/ars.2012.4800

Wickham, H. (2016). *ggplot2 Elegant Graphics for Data Analysis (Use R!)*. Berlin: Springer.

Xiao, X., Li, J., and Samulski, R. J. (1998). Production of high-titer recombinant adeno-associated virus vectors in the absence of helper adenovirus. *J. Virol.* 72, 2224–2232. doi: 10.1128/jvi.72.3.2224-2232.1998

Yamaguchi, R., Lartigue, L., Perkins, G., Scott, R. T., Dixit, A., Kushnareva, Y., et al. (2008). Opa1-mediated cristae opening is Bax/Bak and BH3 dependent, required for *Apoptosis*, and independent of Bak oligomerization. *Mol. Cell* 31, 557–569. doi: 10.1016/j.molcel.2008.07.010

Yates, A. D., Achuthan, P., Akanni, W., Allen, J., Allen, J., Alvarez-Jarreta, J., et al. (2020). Ensembl 2020. *Nucleic Acids Res.* 48, D682–D688. doi: 10.1093/nar/gkz966

Yu-Wai-Man, P., Griffiths, P. G., Burke, A., Sellar, P. W., Clarke, M. P., Gnanaraj, L., et al. (2010). The prevalence and natural history of dominant optic atrophy due to OPA1 mutations. *Ophthalmology* 117, 1538–1546.e1. doi: 10.1016/j.ophtha.2009.12.038

Zhang, X., Jones, D., and Gonzalez-Lima, F. (2002). Mouse model of optic neuropathy caused by mitochondrial complex I dysfunction. *Neurosci. Lett.* 326, 97–100. doi: 10.1016/S0304-3940(02)00327-0

Conflict of Interest: The authors declare that the research was conducted in the absence of any commercial or financial relationships that could be construed as a potential conflict of interest.

Copyright © 2020 Maloney, Chadderton, Millington-Ward, Palfi, Shortall, O'Byrne, Cassidy, Keegan, Humphries, Kenna and Farrar. This is an open-access article distributed under the terms of the Creative Commons Attribution License (CC BY). The use, distribution or reproduction in other forums is permitted, provided the original author(s) and the copyright owner(s) are credited and that the original publication in this journal is cited, in accordance with accepted academic practice. No use, distribution or reproduction is permitted which does not comply with these terms.

frontiers in Neuroscience

ORIGINAL RESEARCH
published: 26 November 2020
doi: 10.3389/fnins.2020.571293

An *in vitro* Model of Human Retinal Detachment Reveals Successive Death Pathway Activations

*Jelena Potic[1,2,3], Martial Mbefo[1], Adeline Berger[1], Michael Nicolas[1], Dana Wanner[1], Corinne Kostic[1], Alexandre Matet[1,4], Francine Behar-Cohen[1,5], Alexandre Moulin[1] and Yvan Arsenijevic[1]**

[1] Department of Ophthalmology, University of Lausanne, Jules-Gonin Eye Hospital, Fondation Asile des Aveugles, Lausanne, Switzerland, [2] Clinic for Eye Diseases, Clinical Center of Serbia, Belgrade, Serbia, [3] Department of Ophthalmology, Faculty of Medicine, University of Belgrade, Belgrade, Serbia, [4] Department of Ophthalmology, Institut Curie, Université de Paris, Paris, France, [5] INSERM U 1138, Centre de Recherches des Cordeliers, Université Paris Descartes, Université Pierre et Marie Curie, Paris, France

OPEN ACCESS

Edited by:
Miguel Flores-Bellver, University of Colorado Anschutz Medical Campus, United States

Reviewed by:
Dragana Trifunovic, University of Tübingen, Germany
Demetrios G. Vavvas, Harvard Medical School, United States
Valeria Marigo, University of Modena and Reggio Emilia, Italy

***Correspondence:**
Yvan Arsenijevic
yvan.arsenijevic@fa2.ch

Specialty section:
This article was submitted to Neurodegeneration, a section of the journal Frontiers in Neuroscience

Received: *10 June 2020*
Accepted: *29 October 2020*
Published: *26 November 2020*

Citation:
Potic J, Mbefo M, Berger A, Nicolas M, Wanner D, Kostic C, Matet A, Behar-Cohen F, Moulin A and Arsenijevic Y (2020) An in vitro Model of Human Retinal Detachment Reveals Successive Death Pathway Activations. Front. Neurosci. 14:571293. doi: 10.3389/fnins.2020.571293

Purpose: was to create an *in vitro* model of human retinal detachment (RD) to study the mechanisms of photoreceptor death.

Methods: Human retinas were obtained through eye globe donations for research purposes and cultivated as explants. Cell death was investigated in retinas with (control) and without retinal pigment epithelium (RPE) cells to mimic RD. Tissues were studied at different time points and immunohistological analyses for TUNEL, Cleaved caspase3, AIF, CDK4 and the epigenetic mark H3K27me3 were performed. Human and monkey eye globes with retinal detachment served as controls.

Results: The number of TUNEL-positive cells, compared between 1 and 7 days, increased with time in both retinas with RPE (from 1.2 ± 0.46 to 8 ± 0.89, $n = 4$) and without RPE (from 2.6 ± 0.73 to 16.3 ± 1.27, $p < 0.014$). In the group without RPE, cell death peaked at day 3 ($p = 0.014$) and was high until day 7. Almost no Cleaved-Caspase3 signal was observed, whereas a transient augmentation at day 3 of AIF-positive cells was observed to be about 10-fold in comparison to the control group ($n = 2$). Few CDK4-positive cells were found in both groups, but significantly more in the RD group at day 7 (1.8 ± 0.24 vs. 4.7 ± 0.58, $p = 0.014$). The H3K27me3 mark increased by 7-fold after 5 days in the RD group ($p = 0.014$) and slightly decreased at day 7 and was also observed to be markedly increased in human and monkey detached retina samples.

Conclusion: AIF expression coincides with the first peak of cell death, whereas the H3K27me3 mark increases during the cell death plateau, suggesting that photoreceptor death is induced by different successive pathways after RD. This *in vitro* model should permit the identification of neuroprotective drugs with clinical relevance.

Keywords: human retina, *in vitro* model, retinal detachment, photoreceptor death, cell death pathways

INTRODUCTION

Retinal detachment (RD) is one of the most common causes of photoreceptor cell death worldwide (Subramanian and Topping, 2004). Photoreceptor cells die when they are physically separated from the underlying retinal pigment epithelium (RPE) and choroidal vessels, which provide metabolic support to the outer layers of the retina. Although various pathological changes occur in detached retinas (Anderson et al., 1981; Lewis et al., 1994; Jablonski et al., 2000), studies on experimental models have shown that photoreceptor cell death is immediately induced, as early as 12 h after the RD event, and peaks after 2 or 3 days (Cook et al., 1995; Hisatomi et al., 2001; Arroyo et al., 2005). This indicates that an early intervention could potentially preserve the photoreceptors, but delayed care may lead to photoreceptor loss and visual acuity deterioration as consequences. Photoreceptor degeneration processes are currently not fully understood. In rodent models of RD, apoptotic and cell death factors such as apoptosis inducing factor (AIF) and RIPK3 were detected 3 days post detachment (Hisatomi et al., 2001, 2002; Trichonas et al., 2010). The contribution of the apoptotic pathway to photoreceptor death was clearly demonstrated in rodent models of RD by the anti-apoptotic intraperitoneal injection treatment of Bcl-X-TAT fusion protein, which markedly decreased photoreceptor death, 3 days post detachment (Hisatomi et al., 2008). AIF release and Caspase-9 activation were observed in RD human retinas (Hisatomi et al., 2008), but the use of anti-apoptotic factors such as Z-VAD in rodent models of RD did not significantly reduced photoreceptor death (Murakami et al., 2013), suggesting that other pathways are also activated during the cell death process.

Photoreceptor cell death also occurs during the disease course of other retinal disorders such as retinitis pigmentosa (RP), age-related macular degeneration (AMD), and after light-damage of the retina (Wenzel et al., 2005; Ambati and Fowler, 2012; Sahaboglu et al., 2013). Although the causes and clinical characteristics of each retinal disorder differ, accumulating evidence suggests that some molecular pathways leading to photoreceptor cell death appear to be shared by these diseases at least in part (Sancho-Pelluz et al., 2008; Murakami et al., 2013; Zencak et al., 2013). As example, cell cycle proteins play a key role in neurons committed to cell death in several neurodegenerative diseases (Herrup and Yang, 2007) including inherited retinal dystrophies as well as acute retinal injury by light (Al-Ubaidi et al., 1992; Vincent et al., 1996; Yang et al., 2001; Nguyen et al., 2003; Höglinger et al., 2007; Zencak et al., 2013), where post-mitotic neurons start to express nuclear cyclin-dependent kinase 4 (CDK4), usually implicated in the re-entry into the cell cycle. The *in vitro* CDK4 inhibition in retina explants of a mouse model of RP induced by roscovitine evidenced the role of this kinase in the cell death process (Zencak et al., 2013). Loss-of-function studies revealed that downstream and upstream molecular actors, E2F1 and BMI1, respectively, contribute also to cell death induction, BMI1 having the most important role.

Interestingly, and in accordance with the potential action of BMI1, epigenetic modifications recently appeared to play a role during retinal degeneration – such as DNA methylation (Wahlin et al., 2013; Farinelli et al., 2014) and histone modifications (Corso-Díaz et al., 2018; Zheng et al., 2018). An interference with DNA methylation using a DNMT (DNA methyltransferases) inhibitor *in vitro* in retinal explants showed a neuroprotective action on photoreceptor survival during the degenerating process (Farinelli et al., 2014). The authors also demonstrated an increase in DNA methylation in dying photoreceptors in several RP animal models analyzed, suggesting DNA hypermethylation as a common denominator in the photoreceptor degeneration pathway. Their findings thus propose a complex relation between DNA methylation and retinal degeneration, which may include both protective actions and disease-driving elements (Farinelli et al., 2014). A similar observation was postulated with the appearance of the H3K27me3 mark, which presents a small increase during the degenerative process in the *Rd1* retina, a mouse model of retinitis pigmentosa (Zheng et al., 2018), but the cell type expressing this mark was not determined.

In this study, we investigated human retinas *in vitro,* in order to have a better comprehension of the cell death mechanisms that may occur in patients affected by RD. Our work aims to reveal whether apoptosis, cell cycle reentry and epigenetic modifications are also involved in an *in vitro* model of human RD.

MATERIALS AND METHODS

Biological Samples

Retina tissues from human eye globes were obtained following procedures conformed to the tenets of the Declaration of Helsinki for biomedical research involving human subjects and according to the ethical approval (protocol No 340-15) and Swiss law. Human globes received from the Lausanne Eye Bank had been assessed as unsuitable for cornea transplantation. The overall health of the donor before death was considered and tissue from donors with previous history or treatment that might damage the retina was rejected.

We also used sections of *Macaca fascicularis* eye globes obtained for a previous experiment we performed for a gene therapy study, including controls injected with vehicle (TSSM) in which a retinal detachment was observed (for the animal origin and experimentation authorization, please refer to Matet et al., 2017).

Protocol for Preparing Human Retinal Explants

Following the donor cornea retrieval, the posterior segment was recovered; the vitreous was removed, then the sclera and retina were cut in a flower shape with four cuts. Next the retina was detached from the RPE, choroid and sclera, in order to obtain the *in vitro* model of RD. For the control samples, to maintain the RPE, Proteinase-K incubation during 20 min was performed as previously described in Zencak et al., 2013. The peripheral retina was dissected into small pieces of a minimum of about 5 mm × 5 mm. Retinal explants were placed on Millipore membrane inserts (Millicell Cell Culture Plate Inserts, Merck Millipore, Merck, Darmstadt, Germany), which were then placed

in a 6 well plate (Nalgene Nunc, Rochester, NY, United States), with 1.5 mL of medium in each well. The R16 medium was first used, but we observed little cell death in this condition. The medium used contained: 1% B27, 1% FBS, 1% P/S, 97% DMEM/F12. The explants were maintained at 37°C, 5% CO2, and the medium was changed every 48 h. During this protocol, fixation was performed 1, 3, 5 and 7 days after dissection using 4% paraformaldehyde for 120 min. The explants were cryopreserved in 30% sucrose, then mounted using Yazulla [water solution containing 22.5% of egg albumin (Applichem) and 2.3% gelatin (Merck)] and subsequently frozen at −20°C.

Retinal Explant Cultures

In order to mimic retinal detachment, the retinal explant of each donor sample was held in the medium without RPE, and with RPE for the control group [as previously described for mouse retina explants (Zencak et al., 2013)]. The presence of RPE was ascertained by a regular pigmented epithelium with normal nuclei. No choroid or sclera was present in the samples analyzed in this work. Indeed, we observed that the presence of the choroid provoked marked cell death (data not shown).

Four retinal explants fulfilled the inclusion criteria (n = 4). All 4 explants were negative for known retinal diseases. Each biological sample was divided in two groups: RD group (without RPE) n = 4, and control group (with RPE) n = 4, and served for all the time points analyzed.

Immunohistochemistry

Immunohistochemical analysis was performed according to standard protocols (see below), on a series of 14 μm-thick cryosections. Antibodies against Cleaved-Caspase-3, apoptosis-inducing factor (AIF), Cyclin-dependent-kinase 4 (CDK4), BCL2 Associated X, Apoptosis regulator (BAX), Receptor Interacting Serine/Threonine Kinase 3 (RIPK3) and the H3K27me3 antigens were used (**Table 1**). Slides were incubated 1h with the blocking solution containing 10% Normal Goat Serum (NGS) and 0.3% TritonX-100, followed by overnight incubation with the primary antibody diluted in blocking solution, and then washed 3 times with PBS. Appropriate fluorescent secondary antibody was incubated for 1h at room temperature (**Table 1**). Nuclei were counter-stained with 4,6-diamidino-2-phenylindole (DAPI). When comparison of fluorescence was made between groups (for instance in **Figure 3**), pictures were taken with the same acquisition time for a specific labeling (in this figure, H3K27me3: 900 ms, AIF, 700 ms and DAPI: 25 ms).

H3K27me3 and AIF Labelings

An antigen retrieval treatment was performed prior to antibody incubation. The cryosections, in a 10 mM citrate buffer at pH 6.0, were first heated in a microwave oven 5 min at 696 W and then cooled down for 30 min at room temperature (RT).

H3K27me3 fluorescence intensity (**Supplementary Figure S2**) was quantified using Fiji (ImageJ). The images were cropped to select only the ONL, then the same intensity threshold was applied to all the pictures, and the mean intensity was automatically measured in the area above threshold. Some nuclei in the RD proximity picture were saturated, leading to an underestimation of the mean intensity on this picture.

TABLE 1 | List of primary and secondary antibodies for immunochemistry.

	Species	Source	Working dilution/ incubation time
Primary antibody			
M/L Opsin	Rabbit	Chemicon	1/2000 ON
Cdk4	Rabbit	Santa Cruz, SC-601	1/100 ON
H3K27me3	Rabbit	Merck Millipore #07-449	1/200 ON
Cleaved Caspase-3	Rabbit	Cell Signaling Technology #9661	1/250 ON
AIF	Rabbit	Abcam #ab32516	1/250 ON
BAX	Rabbit	Cell Signaling	1/200 ON
RIPK3	Mouse	Labforce	1/50 ON
Secondary antibody			
Alexa Fluor 633 Goat anti-Rabbit IgG	**Goat**	Invitrogen A21072	1/2000, 1 h, RT
Biotinylated anti-rabbit IgG (H+L)	**Goat**	Vector BA1000	1/200

ON = overnight, RT = room temperature.

CDK4 Labeling

To amplify CDK4 signal, a DAB staining was performed with a previous anti-peroxidase agent (0.3% H_2O_2 for 5 min at RT). After primary antibody incubation, biotinylated goat anti-rabbit antibody was added for 1h and then the ABC substrate for 30 min. DAB revelation lasted 2 min at RT.

Active Caspase-3 Staining

The Cleaved-Caspase-3 staining (Cell Signaling Technology #9661, **Table 1**) was performed according to standard protocol, with one hour blocking with 5% NGS.

TUNEL Staining

To visualize dying cells on sections, a TUNEL assay kit conjugated with TMR (Terminal deoxynucleotidyl Transferase Biotin-dUTP Nick End Labeling) was performed following instructions (Roche Diagnostics, Basel, Switzerland). Negative controls consisted of omitting the terminal deoxynucleotidyl transferase enzyme from the labeling, and gave no staining at all. Cells with a homogenous nucleus staining the size of the whole nucleus, or a little shrunk, or with a circle staining (corresponding probably to the euchromatin), were taken into account as previously described in Sahaboglu et al., 2013.

Statistical Analysis

Positive cells were counted in the most central retina sections. All measurements were taken by Olympus BX6 fluorescein microscopy. The quantification of positive cells was performed on the pictures from 10 different slices for each sample. Because after 3 days *in vitro*, the shape of the retinal tissue can change, we always considered (1) areas which were well layered and where no confusion could be made between ONL and INL cells, and (2) homogeneous areas in a full 40x field. All the data are expressed as mean plus or minus the standard error of the mean (SEM).

Data were analyzed using the Mann-Whitney *U*-test and the *p*-value given.

RESULTS

Number of Photoreceptor Layers

In all explants, the number of photoreceptor layers was quite stable in both groups and at different time points **(Table 2** and **Figure 2C**). Some heterogeneity exists within the same tissue sample, but each group contained retina with similar numbers of photoreceptor rows (**Figure 2**). We checked the presence of cones and found M/L-OPSIN-positive cells from 1 to 7 days of the culture period (data not shown). With time, many cells had M/L-OPSIN mislocalization suggesting a degenerative process. However, we did not investigate the rate of the cone degeneration because of the heterogeneity of the samples received, which were often from the retinal periphery region.

TUNEL Staining; Cell Death Marker

TUNEL-positive cells were present from the beginning of the experiment at a low level in the control group despite the different postmortem delays (12, 14, 23, and 24 h) and the dissection procedure of the tissue. The number of TUNEL-positive cells significantly and markedly increased after 3 days *in vitro* (DIV) and remained elevated until 7 DIV. An increase of more than 10-fold of TUNEL-positive cells was observed at 3 DIV between the RD and the control groups ($p = 0.014$) (**Table 2** and **Figures 1A,D**). Interestingly, this augmentation of cell death coincides with what has been described for rhegmatogenous RD *in vivo* (Hisatomi et al., 2001; Arroyo et al., 2005). A significant 38% increase of TUNEL-positive cells continued to occur between 3 DIV and 7 DIV (**Table 2** and **Figures 1A,D**). We then investigated the presence of potential actors of the cell death process. Note that the TUNEL-positive cells also appeared in the INL (**Figure 1A** and **Table 2**), and their number is increased at all time points, by the absence of the RPE.

Neither the Canonical Apoptotic Pathway, nor Necrosis Is Activated in the Human RD Group

Cleaved-Caspase-3 is a final effector of apoptosis (Slee et al., 2001; Kim et al., 2002; Zacks et al., 2003; Murakami et al., 2013) and was chosen to reveal the extent of apoptotic events in the retina with and without RPE. Surprisingly, very rare positive cells in the ONL were present in both groups and no peaks of apoptosis were identified (data not shown). In the INL, an average of 0.6 positive cell per 40× field was observed in explants without RPE at 3 DIV ($n = 1$), none at 5 DIV ($n = 1$), and 0.3 at 7 DIV ($n = 2$). BAX was not found in the ONL of any explant at any time point. A few BAX-positive cells were observed in the INL: none at 1 DIV in both groups and an average of 0.9 positive cell per field was present at 7 DIV in explants with RPE, and none in explants without RPE ($n = 3$). RIPK3, a marker of necrosis, was also absent from the ONL of both groups. Only some cells in the retinal ganglion layer were observed after 7 days *in vitro* without RPE (**Supplementary Figure S1**). RIPK3 was also absent from the INL of explants with and without RPE at 1 and 7 DIV ($n = 1$). However, the technique sensitivity may have revealed only cells with highly expressed antigens and thus may underestimate the total number of positive cells.

Apoptosis-Inducing Factor (AIF) Staining

Apoptosis-Inducing Factor is normally localized in mitochondria membranes. During cell death, AIF is released and translocated to the nucleus (Susin et al., 1999; Hisatomi et al., 2001, 2008). AIF can be released from mitochondria either in a caspase-dependent or caspase-independent way (Sanges and Marigo, 2006) and can mediate caspase-independent cell death (Sanges and Marigo, 2006). We observed that AIF was present in

TABLE 2 | Temporal expression of cell death markers during the culture of human retina explants with and without RPE.

	Treatment	1 Div		3 Div		5 Div		7 Div	
		Average *n* = 4	*p*	Average *n* = 4	*p*	Average *n* = 4	*p*	Average *n* = 4	*p*
PR rows	−RPE	8.3	*0.76*	7.8	*0.88*	7.0	*0.61*	8.1	*0.77*
	+RPE	7.5		7.2		6.4		7.7	
CDK4	−RPE	1.95	*0.02*	3.70	*0.03*	3.36	*0.1*	4.70	*0.014*
	+RPE	0.00		1.62		1.70		1.75	
H3K27me3	−RPE	1.73	*0.24*	2.67	*0.61*	11.95	*0.014*	10.09	*0.014*
	+RPE	1.63		2.72		2.92		3.93	
TUNEL ONL	−RPE	2.63	*0.04*	11.83	*0.014*	11.03	*0.04*	16.30	*0.014*
	+RPE	1.16		1.36		4.36		7.98	
TUNEL INL*	−RPE	3.9	/	9.6	/	11.7	/	8.7	/
	+RPE	4.1		6.5		4.3#		3.3	
AIF*	−RPE	0.7	/	5.7	/	0.3	/	0	/
	+RPE	0.2		0.6		0		0	

** : n = 2, # : n = 1, PR = photoreceptors.*

Note the transient expression of AIF as previously documented and the delayed appearance of the H3K27me3 mark. The peak of TUNEL-positive cells in the ONL rises at 3 DIV and remains elevated until 7 DIV at least.

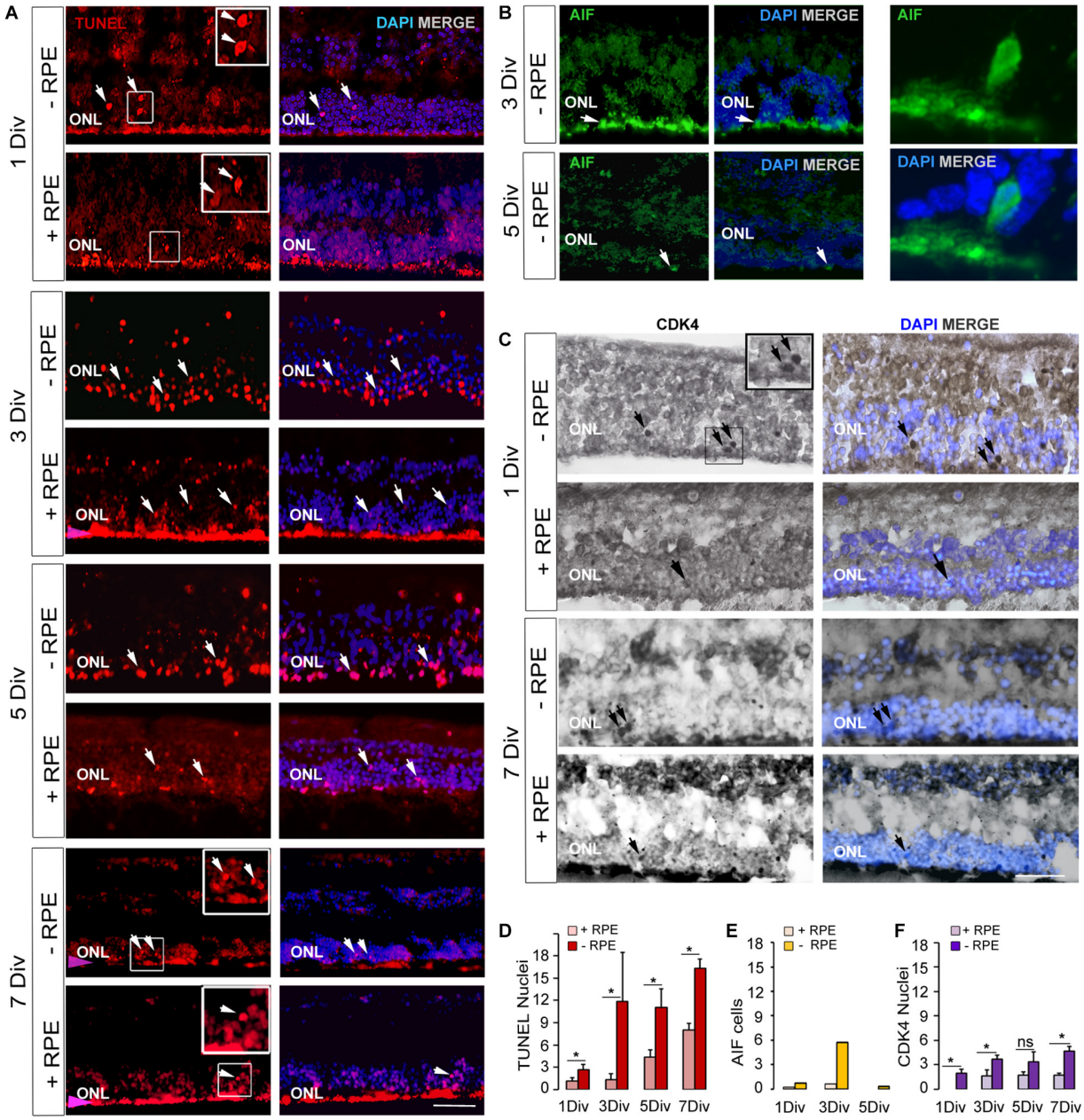

FIGURE 1 | Expression of cell death markers on human retinal explants, an *in vitro* model of retinal detachment. **(A,D)** TUNEL-positive cells imaging (arrows) and counting at 1 DIV, 3 DIV, 5 DIV, 7 DIV in RD group (-RPE) and control group (+RPE). The presence of RPE produced an artifact red fluorescent background (pink arrow). **(B,E)** Imaging and counting of AIF-positive cells, which are present at 3 DIV in RD group (-RPE), but are rare at 5 DIV (arrow). A representative AIF-positive cell is shown at high magnification. **(C,F)** CDK4 positive cells imaging (arrows) and counting in RD group (-RPE) and control group (+RPE), at 1 DIV and 7 DIV. DIV: Days *in vitro*, ONL: outer nuclear layer, RPE: retinal pigment epithelium. Calibration bar: 20 μm.

cell nuclei in the ONL at 1 DIV and with a marked peak at 3 DIV in the RD group. AIF-positive cells augmented when TUNEL-positive cells increased at 3 DIV (**Table 2** and **Figures 1B,E**). The increase was about 10-fold in comparison to the control group (n = 2). At 5 DIV and 7 DIV there were almost no visible AIF-positive cells. No AIF-positive cells were detected in the INL at any time point in explants with RPE (n = 1) or without RPE (n = 3).

The Cell Cycle Marker CDK4 Is Moderately Expressed During the Degenerative Process in Absence of RPE

No CDK4 was observed in the photoreceptor nuclei of the control group after 1 DIV and only very few cells expressed this protein between 3 and 7 DIV. In the RD group, CDK4-positive cells were present starting at 1 DIV (**Table 2** and **Figures 1C,F**); their

number moderately increased afterwards and remained stable between 3 and 7 DIV. Comparison between the two groups showed statistical difference at each time-point, except for 5 DIV (**Table 2** and **Figure 1F**). Note that the numbers of CDK4-positive cells are much lower in comparison to TUNEL-positive ones (**Table 2**).

Epigenetic Modifications of the H3K27me3 Mark Occur at the Late Stage of the Degenerative Process

Recent works described epigenetic modifications during the course of retinal degeneration (Wahlin et al., 2013; Corso-Díaz et al., 2018) with a small increase of the H3K27me3 mark level in retina extract (Zheng et al., 2018). As we also observed that epigenetic modifications occur at the histone level in some rodent models of retinitis pigmentosa (unpublished data), we investigated the H3K27me3 mark known to regulate gene repression (Wahlin et al., 2013). In the control group, the number of H3K27me3-positive cells in the ONL remained low until 5 DIV and showed a slight elevation at 7 DIV, whereas an important increase of this mark was observed at 5 DIV in the RD group and stayed elevated at 7 DIV, although partially reduced (**Table 2** and **Figures 2A,B**). Note that the elevated number of H3K27me3-positive cells appears after the peak of TUNEL-positive cells at 3 DIV.

The H3K27me3 Mark Is Present in Photoreceptors of Detached Retina

Seizing the opportunity to obtain sections from 4 eye globes containing a uveal melanoma resulting in retinal detachment, we investigated the distribution of the H3K27me3 mark in these retinas. In the attached region close to the center of the retina, the H3K27me3 was present in photoreceptors and homogenously distributed. In the area where the detachment was the most noticeable (mid-periphery, at the opposite side of the optic nerve) and where the retina was thinner, many photoreceptors expressed high level of H3K27me3. To ensure that such difference in the mark presence was not due to retinal area or thickness, we also looked at the periphery where the retina was of the same size and not detached by the tumor. We observed a discrete H3K27me3 labeling as described for the non-detached central part. The **Figure 3** presents two representative cases out of four with the same pattern. The intensity of the H3K27me3 fluorescence signal was quantified in the ONL shown in the **Supplementary Figure S2** and provides the following results: no RD fluorescence mean intensity = 107.8; RD mean intensity = 146.1 and no RD periphery mean intensity = 108.5. Interestingly, more TUNEL-positive cells were observed in the thin retina area close to the tumor, where the H3K27me3 level was high (**Supplementary Figure S3**). Two samples showed several dying cells in the ONL and, remarkably, the upper INL also contained TUNEL-positive cells (5 and 8 TUNEL-positive cells per slice in INL in each positive sample in the detached area).

No AIF labeling in the nucleus of ONL cells was detected (**Figure 3**). Unfortunately, we were no longer able to check the expression of CDK4 in these samples, due to human-CDK4 antibody issues (Santa Cruz antibody production discontinued). However, we used previous material from monkeys (*Macaca fascicularis* eyes). We performed subretinal injections with TSSM (vehicle) as a control group for a

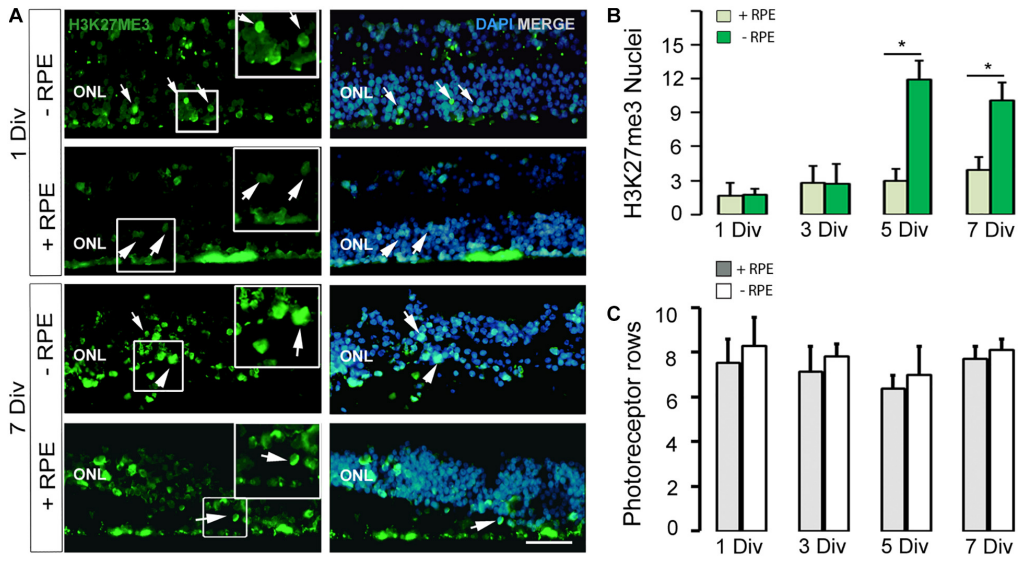

FIGURE 2 | (A,B) Imaging and counting of H3K27me3-positive cells at 1 DIV and 7 DIV, in the human *in vitro* model of RD (-RPE) and control (+RPE). Note the marked increased number of H3K27me3-positive cells at 5 DIV **(B)** and 7 DIV in the RD group (-RPE). **(C)** The number of photoreceptor rows is stable all along the culture system in the two groups (RD model +RPE and control -RPE). DIV: Days *in vitro*, ONL: outer nuclear layer, RPE: retinal pigment epithelium. Calibration bar: 20 μm.

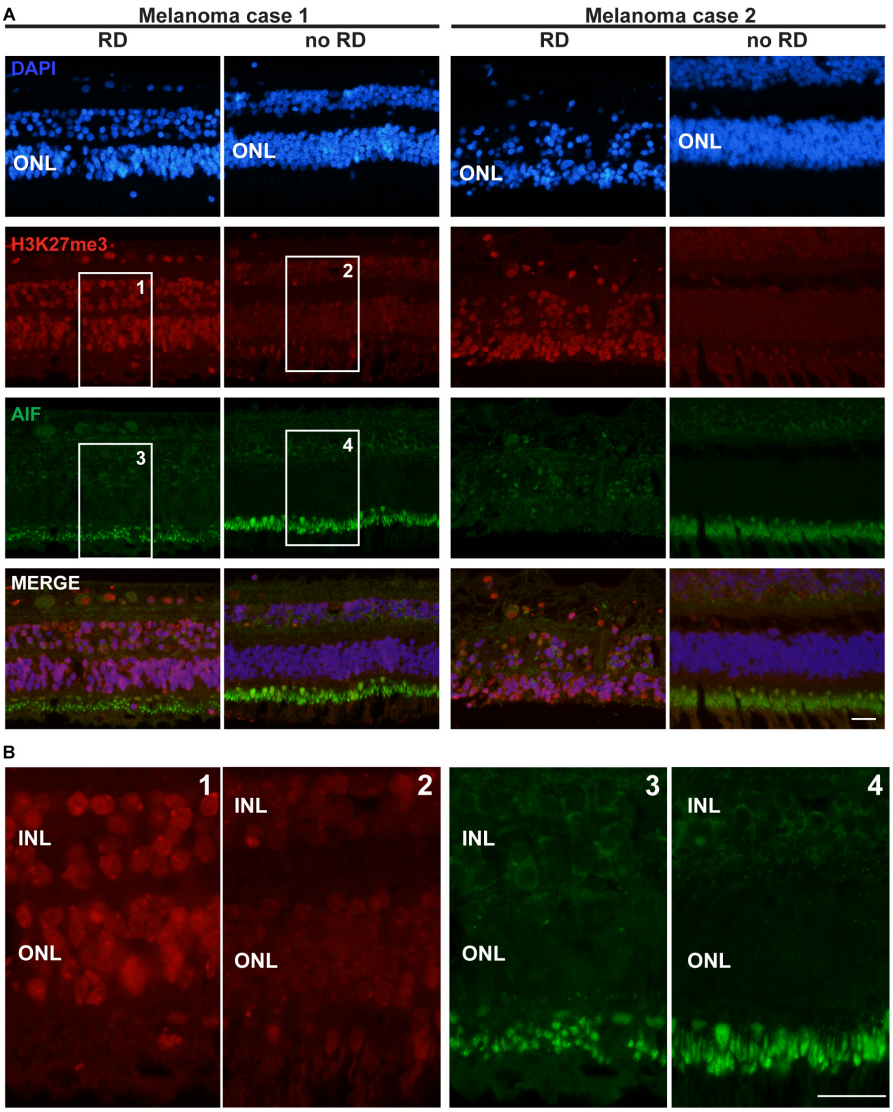

FIGURE 3 | H3K27me3 mark distribution in a retina of two patients with retinal detachment (RD) due to tumor growth. **(A)** The first row of pictures showing the retina nuclei evidenced by DAPI staining indicates that in the retinal detachment (RD) area, the cell density is weaker in the ONL and this layer is thinner for patient 2 compared to the control area. The H3K27me3 staining shows a markedly stronger level in the RD area (see also magnification in Panel **B**) in comparison to the intact area. AIF labeling is absent in all ONL samples, but highly present in the inner segments of rods and cones (better shown in panel **B**). A light expression is also present around some nuclei of INL cells. The fourth row presents the merged labeling of the three previous stainings. **(B)** High magnification of the insets presented for H3K27me3 and AIF labeling in panel **(A)**. Note the altered size of the inner segments in the detachment area as suggested by the AIF labeling (probably present in the mitochondria of this organelle). RD: Retinal detachment, ONL: outer nuclear layer, INL: inner nuclear layer. Calibration bar: 25 μm.

gene therapy study and to complete the present work we evaluated whether the retina detachment, which led to some very local tissue thinning, was correlated to CDK4 expression and the presence of the H3K27me3 mark. The CDK4 labeling was made previously and we added labeling for H3K27me3. The detached area displayed a higher level of H3K27me3 marks after 90 days in comparison to the non-detached area. Some very rare CDK4-positive cells were observed (**Supplementary Figure S4**). The ONL size cannot be compared, because the samples are not from the same regions.

DISCUSSION

The present data open new perspectives to test *in vitro* different drugs to block a specific cell death pathway, at several time points of the degenerative process, in order to optimize cell survival. This work reveals the presence of various potential actors of cell death and the comprehension of their mechanisms is still necessary to correctly propose a protective approach for the injured photoreceptors.

A clear demonstration of apoptosis as a major form of photoreceptor cell death after RD was made by Cook and

colleagues in a cat model of RD (Gavrieli et al., 1992; Cook et al., 1995). They showed that photoreceptor cells in the detached retina exhibit strong TUNEL reactivity as well as pyknotic morphological changes. Moreover, they demonstrated that the photoreceptor cell death after RD occurs within an earlier period than previously recognized: TUNEL-positive cells are detected as early as 1–3 days after RD, followed by a decline in their number over the next few weeks. This early activation of cell death, has been confirmed in other animal models of RD with rhegmatogenous RD (Hisatomi et al., 2001; Arroyo et al., 2005).

In our *in vitro* model of human RD, we noticed the peak of TUNEL-positive cells at 3 days *in vitro* (DIV), with a plateau until 7 DIV (latest time-point), thus underlining the need for urgent surgery in patients affected by retinal detachment. Surprisingly, a post-mortem delay inferior to 24 h (12, 14, 23, and 24 h) had little effect on photoreceptor death, probably because a minimal metabolism is maintained between the RPE and the photoreceptors. We also noticed cell death in the INL, mostly in the absence of the RPE. A similar observation, but with fewer TUNEL-positive cells, was made in two eye globes (out of four) where the retinal detachment occurred after tumor growth. The tumor may have compromised the retina vessel blood flow in those cases. These data suggest that the culture conditions recapitulate some features of the *in vivo* retinal detachment, but the environment does not contain immune cells and factors that may be secreted after prolonged retina detachment. In addition, the lack of blood flow may also influence the rate of photoreceptor death.

Several works revealed in animal models that Caspase-3 is activated during some forms of retinal degeneration (Wenzel et al., 2005; Sancho-Pelluz et al., 2008; Trichonas et al., 2010; Murakami et al., 2013). We thus investigated the course of Cleaved-Caspase-3 activation in our *in vitro* model. Surprisingly in both groups, only few cells were positive for this enzyme suggesting alternative pathways conducting the sensory cells to death.

However, the AIF expression pattern resembles that described after retinal detachment in rodents as well as in human samples (Hisatomi et al., 2008). Interestingly, the peak of AIF parallels the first elevated raise of dying photoreceptors suggesting a role of AIF in this early degenerative process. The appearance of AIF is only transitory whereas the cell death process is still continuing, implying that other actors are involved in this process. Nonetheless, these results suggest that the first wave of degenerating photoreceptors requires appropriate and specific drugs to block AIF action in order to enhance the survival of the retina. They also support previous studies in rodents showing that inhibitors of the HIV protease, nelfinavir and ritonavir, can act as anti-cell death factors, impeding, in the photoreceptors, the translocation of AIF into the nucleus, and suggest that such mechanisms may also be involved in the RD in human retina (Hisatomi et al., 2008).

We also investigated whether a factor involved in the necrosis process, RIPK3, was expressed during the retinal degeneration phase. No positive cells were observed in the ONL, but some appeared in the GCL at a late stage of the culture without RPE, suggesting that retinal detachment does not stimulate necrosis in photoreceptors. A similar observation was made in the retinas detached due to melanoma tumors.

Concerning the potential factors that may be responsible for the continuation of cell death, we investigated whether proteins of the cell cycle were re-expressed as observed in several models of retinal degeneration (Vincent et al., 1996; Yang et al., 2001; Nguyen et al., 2003; Höglinger et al., 2007). We previously identified that CDK4 is reactivated in various rodent models of inherited retinal dystrophies as well as during light damage (Zencak et al., 2013) and plays a role in the execution phase of photoreceptor death (Zencak et al., 2013). In control explants, a low number of CDK4-positive photoreceptors was present in all time points examined starting at 3 DIV. In the RD group, CDK4 was significantly more expressed in all time points, but the kinetics of CDK4 appearance did not correlate or precede the peak of cell death observed at 3 DIV. Moreover, the number of CDK4-positive cells was much lower than the number of TUNEL-positive cells. This observation differs from those obtained in rodent models of retinal dystrophies (Zencak et al., 2013). These results suggest that CDK4 is probably not involved in the first peak of cell death at 3 DIV and may little account for the continuation of photoreceptor degeneration at later time points. In this situation, we cannot exclude that some microglia may also express CDK4.

We found that the H3K27me3 mark showed a massive increase at 5 DIV in the RD group, in contrast with the control group where the level was very low. Epigenetic modifications have been poorly documented so far in retinal diseases, nonetheless interesting changes in DNA methylation were observed in retinas of different mouse models of retinal degeneration. DNA methylation is generally associated with repression of transcription (Jones and Liang, 2009) and was recently observed to be increased in dying photoreceptors (Farinelli et al., 2014). The TUNEL assay for dying cells co-labeled the 5mC-positive cells (anti-5-methylcytosine antibody was used to analyze photoreceptor DNA methylation *in situ*) to a great extent, suggesting an intimate connection between increased DNA methylation and the degeneration of the photoreceptors (Chang et al., 2002; Kaur et al., 2011; Sahaboglu et al., 2013; Farinelli et al., 2014). DNA methylation was found to be most prominent during the final stages of cell death (Farinelli et al., 2014). However, it cannot be excluded that hypermethylation of specific genes may be starting far earlier (Farinelli et al., 2014). Our positive results for the H3K27me3 mark well correlate with DNA methylation in photoreceptors. Indeed, EZH2, the enzyme that methylates H3 on lysine 27, recruits the DNA-methyl transferase (DNMT) necessary for DNA methylation (Viré et al., 2006) suggesting that EZH2 first initiates epigenetic changes which are then reinforced by DNMTs. EZH2 belongs to the Polycomb repressive complex-2 (PRC2) and interestingly, BMI1, a protein of PRC1 often acting after PRC2, was identified to be crucial during photoreceptor death (Zencak et al., 2013). H3K27me3 staining may thus be more relevant to identify genes involved in the process of cell death.

However, in the present study, the highest peak of H3K27me3-positive cells is expressed at 5 DIV, suggesting that the first wave of photoreceptor death is independent of EZH2 activity and that the continuation of the degeneration may be related to EZH2. Supporting this hypothesis the anti-apoptotic agent

Z-VAD reduced the number of TUNEL-positive cells in a rat model of RD, but not photoreceptor loss (Murakami et al., 2013), suggesting other death mechanisms. The histological analysis of retinal detachment due to tumor growth showing high level of H3K27me3 supports also a potential role for EZH2 in photoreceptor death, in pathophysiological conditions *in situ*. Interestingly, a higher expression of H3K27me3 was also found in the photoreceptor layer of a monkey retina, 90 days after detachment, suggesting that this injury induced a long term change of the cell homeostasis, the consequence being enigmatic at this stage although rare CDK4-positive cells were observed. This *in vitro* work needs to be confirmed by future studies with specific inhibitors to prevent photoreceptor death at different injury stages. This should reveal whether the medication to slow down photoreceptor degeneration has to be adapted to each stage of the degenerative process. Such studies were not possible yet due to the low number of samples obtained each year.

These data also support the clinical observations highlighting the importance to take in charge the patient to perform RD surgery within the first 3 days, in order to optimize for the best functional recovery. In view of our and other previously published results, successive death pathways are activated after retinal detachment, necessitating adapted therapies for each disease stage to protect the retina.

CONCLUSION

This study demonstrates the relevance of human retina explant cultures to model retinal detachment. Furthermore our results suggest that the cell death due to retinal detachment is controlled by different features including AIF during the early photoreceptor death wave, whereas epigenetic modifications, controlled by the H3K27me3 mark, may account for the late phase of the degenerative process. Further studies need to identify which gene expressions are affected by such modifications and if drugs inhibiting these pathways may have a protective action on photoreceptors during RD.

DATA AVAILABILITY STATEMENT

The raw data supporting the conclusion of this article will be made available by the authors, without undue reservation.

ETHICS STATEMENT

The studies involving human participants were reviewed and approved by Commission cantonale d'éthique de la recherche sur l'être humain (CER-VD) protocol No 340-15. Written informed consent for participation was not required for this study in accordance with the national legislation and the institutional requirements.

AUTHOR CONTRIBUTIONS

YA designed the experiments, performed the analyses and wrote the manuscript. MM, DW, and AM participated to the experiments and analyses. JP performed the experiments and wrote the manuscript. AB performed experiments and the analyses and contributed to the manuscript writting. CK and AM performed experiments and critically revised the manuscript. FB-C performed experiments and managed the human tissue access and the biobank and wrote the manuscript. All authors contributed to the article and approved the submitted version.

FUNDING

We would like to thank the support of the Fondation Provisu and the Swiss National Foundation (#31003A_169492), Fondation Asile des aveugles and the University of Lausanne. The content of this manuscript has been published in part as part of the thesis of Jelena Potic "Characterization of the mechanisms of photoreceptor degeneration during retinal detachment; the evaluation of post-operative anatomical and functional recovery. University of Belgrade, School of Medicine, Belgrade 2018."

SUPPLEMENTARY MATERIAL

The Supplementary Material for this article can be found online at: https://www.frontiersin.org/articles/10.3389/fnins.2020.571293/full#supplementary-material

Supplementary Figure 1 | BAX and RIPK3 expression in human retina explants with and without RPE. BAX expression was very rarely observed in both groups. An example of BAX labeling is presented for the 1 DIV time point **(upper left panel)**. RIPK3 expression was observed in the retinal ganglion cell layer of retina cultivated without RPE at 7 DIV without RPE **(lower right panel)**. DIV: Days *in vitro*, ONL: outer nuclear layer. Calibration bar: 25 μm.

Supplementary Figure 2 | H3K27me3 mark labeling in a retina of one patient (case 3) with retinal detachment (RD) due to tumor growth, whose intensity has been quantified (see body text). The left and right columns show the homogeneous presence of the H3K27me3 mark in all retinal layers. The central column shows a markedly higher expression of the H3K27me3 mark in the ONL in the RD area. Note that also some cells in the INL are well positive. The DAPI staining also appears brighter, probably due to chromatin condensation induced by the H3K27me3 mark. RD: Retinal detachment, ONL: outer nuclear layer, INL: inner nuclear layer, GCL: ganglion cell layer. Calibration bar: 25 μm.

Supplementary Figure 3 | TUNEL-positive cells are present in the detached retina area of the patient case 1. TUNEL-positive cells (red) were detected in the detached retina area above the melanoma (upper right picture) and not in the attached region (upper left picture). The corresponding nucleus stainings (DAPI, blue) are presented below. The merged pictures reveal that the great majority of the TUNEL-positive cells are present in the ONL. The stars show two red spots in the INL corresponding to two red blood cells (autofluorescence and no DAPI staining). RD: Retinal detachment, ONL: outer nuclear layer. Calibration bar: 25 μm.

Supplementary Figure 4 | H3K27me3 mark is present in ONL cells long time after retinal detachment. No detection of the H3K27me3 mark is visible in the non-detached retina, whereas 90 days after RD, the detached retina presents punctuated labeling of the mark. The second and third rows of pictures present the retina nucleus (DAPI staining) and the merged pictures. Note the reduced number of photoreceptor in the RD group. The last panels show a regular expression of CDK4 in the INL (probably in the Muller cells nuclei), whereas the ONL is devoid of its expression. Rare CDK4-positive cells were detected in the ONL of detached retina. RD: Retinal detachment, ONL: outer nuclear layer. Calibration bar: 50 μm.

REFERENCES

Al-Ubaidi, M. R., Hollyfield, J. G., Overbeek, P. A., and Baehr, W. (1992). Photoreceptor degeneration induced by the expression of simian virus 40 large tumor antigen in the retina of transgenic mice. *Proc. Natl. Acad. Sci. U.S.A.* 89, 1194–1198. doi: 10.1073/pnas.89.4.1194

Ambati, J., and Fowler, B. J. (2012). Mechanisms of age-related macular degeneration. *Neuron* 75, 26–39.

Anderson, D. H., Stern, W. H., Fisher, S. K., Erickson, P. A., and Borgula, G. A. (1981). The onset of pigment epithelial proliferation after retinal detachment. *Invest. Ophthalmol. Vis. Sci.* 21, 10–16.

Arroyo, J. G., Yang, L., Bula, D., and Chen, D. F. (2005). Photoreceptor apoptosis in human retinal detachment. *Am. J. Ophthalmol.* 139, 605–610. doi: 10.1016/j.ajo.2004.11.046

Chang, B., Hawes, N. L., Hurd, R. E., Davisson, M. T., Nusinowitz, S., and Heckenlively, J. R. (2002). Retinal degeneration mutants in the mouse. *Vis. Res.* 42, 517–525. doi: 10.1016/s0042-6989(01)00146-8

Cook, B., Lewis, G. P., Fisher, S. K., and Adler, R. (1995). Apoptotic photoreceptor degeneration in experimental retinal detachment. *Invest. Ophthalmol. Vis. Sci.* 36, 990–996.

Corso-Díaz, X., Jaeger, C., Chaitankar, V., and Swaroop, A. (2018). Epigenetic control of gene regulation during development and disease: a view from the retina. *Prog. Retin. Eye Res.* 65, 1–27. doi: 10.1016/j.preteyeres.2018.03.002

Farinelli, P., Perera, A., Arango-Gonzalez, B., Trifunovic, D., Wagner, M., Carell, T., et al. (2014). DNA methylation and differential gene regulation in photoreceptor cell death. *Cell Death Dis.* 5, e1558. doi: 10.1038/cddis.2014.512

Gavrieli, Y., Sherman, Y., and Ben-Sasson, S. A. (1992). Identification of programmed cell death in situ via specific labelling of nuclear DNA fragmentation. *J. Cell Biol.* 119, 493–501. doi: 10.1083/jcb.119.3.493

Herrup, K., and Yang, Y. (2007). Cell cycle regulation in the postmitotic neuron: oxymoron or new biology? *Nat. Rev. Neurosci.* 8, 368–378. doi: 10.1038/nrn2124

Hisatomi, T., Nakazawa, T., Noda, K., Almulki, L., Miyahara, S., Nakao, S., et al. (2008). HIV protease inhibitors provide neuroprotection through inhibition of mitochondrial apoptosis in mice. *J. Clin. Invest.* 118, 2025–2038.

Hisatomi, T., Sakamoto, T., Goto, Y., Yamanaka, I., Oshima, Y., Hata, Y., et al. (2002). Critical role of photoreceptor apoptosis in functional damage after retinal detachment. *Curr. Eye Res.* 24, 161–172. doi: 10.1076/ceyr.24.3.161.8305

Hisatomi, T., Sakamoto, T., Murata, T., Yamanaka, I., Oshima, Y., Hata, Y., et al. (2001). Relocalization of apoptosis-inducing factor in photoreceptor apoptosis induced by retinal detachment in vivo. *Am. J. Pathol.* 158, 1271–1278. doi: 10.1016/s0002-9440(10)64078-3

Höglinger, G. U., Breunig, J. J., Depboylu, C., Rouaux, C., Michel, P. P., Alvarez-Fischer, D., et al. (2007). The pRb/E2F cell-cycle pathway mediates cell death in Parkinson's disease. *Proc. Natl. Acad. Sci. U.S.A.* 104, 3585–3590. doi: 10.1073/pnas.0611671104

Jablonski, M. M., Tombran-Tink, J., Mrazek, D. A., and Iannaccone, A. (2000). Pigment epithelium-derived factor supports normal development of photoreceptor neurons and opsin expression after retinal pigment epithelium removal. *J. Neurosci.* 20, 7149–7157. doi: 10.1523/jneurosci.20-19-07149.2000

Jones, P. A., and Liang, G. (2009). Rethinking how DNA methylation patterns are maintained. *Nat. Rev. Genet.* 10, 805–811. doi: 10.1038/nrg2651

Kaur, J., Mencl, S., Sahaboglu, A., Farinelli, P., van Veen, T., Zrenner, E., et al. (2011). Calpain and PARP activation during photoreceptor cell death in P23H and S334ter rhodopsin mutant rats. *PLoS One* 6:e22181. doi: 10.1371/journal.pone.0022181

Kim, D. H., Kim, J. A., Choi, J. S., and Joo, C. K. (2002). Activation of caspase-3 during degeneration of the outer nuclear layer in the rd mouse retina. *Ophthalm. Res.* 34, 150–157. doi: 10.1159/000063659

Lewis, G. P., Guérin, C. J., Anderson, D. H., Matsumoto, B., and Fisher, S. K. (1994). Rapid changes in the expression of glial cell proteins caused by experimental retinal detachment. *Am. J. Ophthalmol.* 118, 368–376. doi: 10.1016/s0002-9394(14)72962-9

Matet, A., Kostic, C., Bemelmans, A. P., Moulin, A., Rosolen, S. G., Martin, S., et al. (2017). Evaluation of tolerance to lentiviral LV-RPE65 gene therapy vector after subretinal delivery in non-human primates. *Transl. Res.* 188, 40–57.e4.

Murakami, Y., Notomi, S., Hisatomi, T., Nakazawa, T., Ishibashi, T., Miller, J. W., et al. (2013). Photoreceptor cell death and rescue in retinal detachment and degenerations. *Prog. Retin. Eye Res.* 37, 114–140. doi: 10.1016/j.preteyeres.2013.08.001

Nguyen, M. D., Boudreau, M., Kriz, J., Couillard-Després, S., Kaplan, D. R., and Julien, J. P. (2003). Cell cycle regulators in the neuronal death pathway of amyotrophic lateral sclerosis caused by mutant superoxide dismutase 1. *J. Neurosci.* 23, 2131–2140. doi: 10.1523/jneurosci.23-06-02131.2003

Sahaboglu, A., Paquet-Durand, O., Dietter, J., Dengler, K., Bernhard-Kurz, S., Ekström, P. A. R., et al. (2013). Retinitis pigmentosa: rapid neurodegeneration is governed by slow cell death mechanisms. *Cell Death Dis.* 4:e488. doi: 10.1038/cddis.2013.12

Sancho-Pelluz, J., Arango-Gonzalez, B., Kustermann, S., Romero, F. J., van Veen, T., Zrenner, E., et al. (2008). Photoreceptor cell death mechanisms in inherited retinal degeneration. *Mol. Neurobiol.* 38, 253–269.

Sanges, D., and Marigo, V. (2006). Cross-talk between two apoptotic pathways activated by endoplasmic reticulum stress: differential contribution of caspase-12 and AIF. *Apoptosis* 11, 1629–1641. doi: 10.1007/s10495-006-9006-2

Slee, E. A., Adrain, C., and Martin, S. J. (2001). Executioner caspase-3, -6, and -7 perform distinct, non-redundant roles during the demolition phase of apoptosis. *J. Biol. Chem.* 276, 7320–7326. doi: 10.1074/jbc.m008363200

Subramanian, M. L., and Topping, T. M. (2004). Controversies in the management of primary retinal detachments. *Int. Ophthalmol. Clin.* 44, 103–114. doi: 10.1097/00004397-200404440-00009

Susin, S. A., Lorenzo, H. K., Zamzami, N., Marzo, I., Snow, B. E., Brothers, G. M., et al. (1999). Molecular characterization of mitochondrial apoptosis-inducing factor. *Nature* 397, 441–446.

Trichonas, G., Murakami, Y., Thanos, A., Morizane, Y., Kayama, M., Debouck, C. M., et al. (2010). Receptor interacting protein kinases mediate retinal detachment-induced photoreceptor necrosis and compensate for inhibition of apoptosis. *Proc. Natl. Acad. Sci. U.S.A.* 107, 21695–21700. doi: 10.1073/pnas.1009179107

Vincent, I., Rosado, M., and Davies, P. (1996). Mitotic mechanisms in Alzheimer's disease? *J. Cell Biol.* 132, 413–426.

Viré, E., Brenner, C., Deplus, R., Blanchon, L., Fraga, M., Didelot, C., et al. (2006). The Polycomb group protein EZH2 directly controls DNA methylation. *Nature* 439, 871–874. doi: 10.1038/nature04431

Wahlin, K. J., Enke, R. A., Fuller, J. A., Kalesnykas, G., Zack, D. J., and Merbs, S. L. (2013). Epigenetics and cell death: DNA hypermethylation in programmed retinal cell death. *PLoS One* 8:e79140. doi: 10.1371/journal.pone.0079140

Wenzel, A., Grimm, C., Samardzija, M., and Remé, C. E. (2005). Molecular mechanisms of light-induced photoreceptor apoptosis and neuroprotection for retinal degeneration. *Prog. Retin. Eye Res.* 24, 275–306. doi: 10.1016/j.preteyeres.2004.08.002

Yang, Y., Geldmacher, D. S., and Herrup, K. (2001). DNA replication precedes neuronal cell death in Alzheimer's disease. *J. Neurosci.* 21, 2661–2668. doi: 10.1523/jneurosci.21-08-02661.2001

Zacks, D. N., Hänninen, V., Pantcheva, M., Ezra, E., Grosskreutz, C., and Miller, J. W. (2003). Caspase activation in an experimental model of retinal detachment. *Invest. Ophthalmol. Vis. Sci.* 44, 1262–1267. doi: 10.1167/iovs.02-0492

Zencak, D., Schouwey, K., Chen, D., Ekström, P., Tanger, E., Bremner, R., et al. (2013). Retinal degeneration depends on Bmi1 function and reactivation of cell cycle proteins. *Proc. Natl. Acad. Sci. U.S.A.* 110, E593–E601.

Zheng, S., Xiao, L., Liu, Y., Wang, Y., Cheng, L., Zhang, J., et al. (2018). DZNep inhibits H3K27me3 deposition and delays retinal degeneration in the rd1 mice. *Cell Death Dis.* 9:310.

Conflict of Interest: The authors declare that part of the research was included in a patent (WO2020/011607A1) and could be construed as a potential conflict of interest.

The authors declare that the research was conducted in the absence of any commercial or financial relationships that could be construed as a potential conflict of interest.

Copyright © 2020 Potic, Mbefo, Berger, Nicolas, Wanner, Kostic, Matet, Behar-Cohen, Moulin and Arsenijevic. This is an open-access article distributed under the terms of the Creative Commons Attribution License (CC BY). The use, distribution or reproduction in other forums is permitted, provided the original author(s) and the copyright owner(s) are credited and that the original publication in this journal is cited, in accordance with accepted academic practice. No use, distribution or reproduction is permitted which does not comply with these terms.

frontiers in Neuroscience

MINI REVIEW
published: 18 December 2020
doi: 10.3389/fnins.2020.618019

Degeneration-Dependent Retinal Remodeling: Looking for the Molecular Trigger

*Michael Telias[1], Scott Nawy[1] and Richard H. Kramer[1,2]**

[1] Department of Molecular and Cell Biology, University of California, Berkeley, CA, United States, [2] Helen Wills Neuroscience Institute, University of California, Berkeley, CA, United States

Vision impairment and blindness in humans are most frequently caused by the degeneration and loss of photoreceptor cells in the outer retina, as is the case for age-related macular degeneration, retinitis pigmentosa, retinal detachment and many other diseases. While inner retinal neurons survive degeneration, they undergo fundamental pathophysiological changes, collectively known as "remodeling." Inner retinal remodeling downstream to photoreceptor death occurs across mammalian retinas from mice to humans, independently of the cause of degeneration. It results in pervasive spontaneous hyperactivity and membrane hyperpermeability in retinal ganglion cells, which funnel all retinal signals to the brain. Remodeling reduces light detection in vision-impaired patients and precludes meaningful vision restoration in blind individuals. In this review, we summarize current hypotheses proposed to explain remodeling and their potential medical significance highlighting the important role played by retinoic acid and its receptor.

Keywords: retinal degeneration, retinal remodeling, synaptic plasticity, retinoic acid, retinal ganglion cell, retinitis pigmentosa, age-related macular degeneration

OPEN ACCESS

Edited by:
Ayse Sahaboglu,
University of Tübingen, Germany

Reviewed by:
Ilaria Piano,
University of Pisa, Italy
Nataliya G. Kolosova,
Institute of Cytology and Genetics, Russian Academy of Sciences, Russia

***Correspondence:**
Richard H. Kramer
rhkramer@berkeley.edu

Specialty section:
This article was submitted to Neurodegeneration, a section of the journal Frontiers in Neuroscience

Received: *16 October 2020*
Accepted: *27 November 2020*
Published: *18 December 2020*

Citation:
Telias M, Nawy S and Kramer RH (2020) Degeneration-Dependent Retinal Remodeling: Looking for the Molecular Trigger. Front. Neurosci. 14:618019. doi: 10.3389/fnins.2020.618019

INTRODUCTION

The retina is a multilayered sensory organ located in the back of the eye, in the inner side of the eyecup, behind the lens (Kolb, 1995). It is divided into two main compartments: the outer retina, populated by photoreceptors (rods and cones), and the inner retina, populated by neural and glial cells, including horizontal cells, bipolar cells, amacrine cells, retinal ganglion cells (RGCs), astrocytes and microglia. Large retinal-specific cells, known as Müller glia, span radially across the outer and inner retinal regions. Light stimulation of photoreceptors initiates a chain of electrochemical responses which are transmitted and modulated by retinal interneurons (i.e., horizontal, bipolar, and amacrine cells), finally converging on RGCs. RGCs reside in the ganglion cell layer (GCL), the inner-most layer of the retina, and their axons form the optic nerve, which leaves the retina and enters the brain, synapsing at the lateral geniculate nucleus on both hemispheres. From there, visual information is finally sent into the primary visual cortex area (V1) located in the occipital lobe. The basic retina-to-brain pathway of visual information is shared by virtually all known mammals as well as other animals with anatomical parallels.

In humans, most cases of vision loss are due to photoreceptor degeneration. Photoreceptor cell death can be the result of many different types of diseases and disorders,

including inherited monogenic retinitis pigmentosa (RP, incidence ∼1:4000) (Verbakel et al., 2018), idiopathic age-related macular degeneration (AMD, ∼200 million patients worldwide) (Wong et al., 2014), retinal detachment (Kreissig, 2016), and environmental injuries (Athanasiou et al., 2013).

In RP rods die before cones, night-vision is lost early-on, and the visual field increasingly shrinks from the periphery to the center, until all photoreceptors die. The process can take years to decades in humans and weeks to months in different animal models (Collin et al., 2020; Winkler et al., 2020). Many different mutations in several different genes can cause RP. If the mutation is characterized early on, gene-therapy mediated delivery of the corrected gene can prevent or reduce photoreceptor death (Miraldi Utz et al., 2018; Takahashi et al., 2018). However, in most cases, treatment is unfeasible, and only a handful of successful clinical trials have been approved and conducted so far. Therefore, RP still remains an orphan disease with no routine treatment that can slow down photoreceptor loss or improve residual vision before complete blindness. Transgenic mice and rats with single-gene mutations, for example in Rhodopsin or Pde6b, reliably recapitulate the features of the disease in humans, with progressive vision loss ending in total absence of photoreceptors and light responses (Nakazawa et al., 2019). In addition, there are also important RP models in large mammalians, including dogs, cats, sheep, horses, pigs and non-human primates (Winkler et al., 2020).

As opposed to RP, AMD is much more frequent and caused by a still unknown etiology, even though specific risk factors have been identified (Hageman et al., 2008). Cones degenerate in the macula, where their density is the highest, at the point of sharpest vision in the human retina. High-acuity vision is damaged, and the central visual field is affected much more than the periphery. An initial phase of this disease, called dry-AMD, is characterized mainly by the death of photoreceptor cells. It, is followed by wet-AMD, characterized by expanding deterioration of the retinal tissue, including neovascularization and the formation of drusen deposits. Neovascularization is driven primarily by an increase in vascular-endothelial growth factor (VEGF). Most available anti-AMD treatments are designed to reduce or slow-down neovascularization, using monoclonal antibodies against VEGF or its receptor (Gil-Martinez et al., 2020). However, there is currently no treatment that can prevent or stop the death of photoreceptors, let alone reverse it. The macula is a sub-compartment of the retina which, in mammalians, exists only in primates. Therefore, available animal models used for AMD research, from rodents to pigs and rhesus monkeys, can recapitulate only some aspects of the disease (Zeiss, 2010; Pennesi et al., 2012).

DOWNSTREAM EFFECTS OF PHOTORECEPTOR DEGENERATION

The progressive death of photoreceptors in the outer retina sends ripple effects to the much less numerous inner retinal neurons, including most critically the RGCs, which funnel all visual information out of the retina. In response to the progressive death of photoreceptors, there are a number of both structural and functional changes in inner retinal neurons and RGCs. These pathophysiological changes, observed in the surviving inner retina cells, are collectively known as remodeling (Jones et al., 2012, 2016a), and have been described in human AMD (Jones et al., 2016c) and human RP (Jones et al., 2016b). Structural changes in the surviving areas include *de novo* neuritogenesis and dendritic reorganization, cell migration and layer disruption, and the formation of a thick inner limiting membrane by reactive Müller glia cells (Iandiev et al., 2006; Lin et al., 2012a; Pfeiffer et al., 2020). Functional abnormalities across outer and inner retinal circuits include changes in synaptic transmission and electrical coupling among similar and different neuronal subtypes, as well as persistent spontaneous oscillations and retinal waves (Marc et al., 2007; Lin et al., 2012b; Euler and Schubert, 2015). RGCs develop intrinsic spontaneous hyperactivity and cell membrane hyperpermeability (Tochitsky et al., 2016; Telias et al., 2019; Denlinger et al., 2020).

These structural and functional abnormalities observed during remodeling do not happen in unison across the degenerating retina. Changes such as neuronal hyperactivity and enhanced membrane hyperpermeability can be observed as soon as days or weeks upon degeneration onset in mice and rat models of RP and AMD (Tochitsky et al., 2016; Telias et al., 2019; Denlinger et al., 2020), while structural changes and the disruption of cell layers happen only upon prolonged degeneration of many weeks to months (Garcia-Ayuso et al., 2019; Pfeiffer et al., 2020). Collectively, functional remodeling results in a "noisy" retina, obscuring remaining light-responses and reducing signal fidelity in treatments aimed at restoring vision (Barrett et al., 2015; Stasheff, 2018).

RETINOIC ACID-DEPENDENT SIGNALING IS ESSENTIAL FOR REMODELING

Every day, rod and cone cells can synthesize millions of copies of opsin proteins and there are hundreds of millions of rods and cones in the mouse retina (Kolb, 2005; Goldberg et al., 2016). To react to light, each individual opsin molecule binds to retinaldehyde (specifically, *11-cis-retinal*), the universal chromophore (Daruwalla et al., 2018). Retinaldehyde in mammals is synthesized by dehydrogenation of vitamin A (retinol), a reaction carried out by retinol dehydrogenase (RDH) in RPE cells, rods, cones and Müller glia cells. In humans suffering from malnutrition, vitamin A deficiency results in night blindness and photoreceptor cell damage and subsequent degeneration (Wiseman et al., 2017). Retinaldehyde is oxidized into retinoic acid (RA) by retinaldehyde dehydrogenase (RALDH), an enzyme that is expressed across retinal cells (Luo et al., 2006; Harper et al., 2015). Binding of RA to its nuclear receptor ($RAR_{\alpha/\beta/\gamma}$) releases it from co-repressor (CoR), allowing it to form a heterodimeric complex with retinoid orphan receptors ($RXR_{\alpha/\beta/\gamma}$) that can bind DNA and act as a transcriptional activator and enhancer.

An early *ex vivo* study of retinal bipolar cells, testing the hypothesis that RA is the trigger behind remodeling, was conducted using light-induced retinal degeneration in albino mice (Lin et al., 2012a). The effects of remodeling were assessed by measuring neuritogenesis in bipolar cells. *De novo* neuritogenesis and an increase in neurite length shown in degenerated retinas, were recapitulated when RA-signaling was enhanced. Conversely, they were prevented when RA-signal was pharmacologically or genetically blocked. Interestingly, manipulation of RXR had a stronger effect on remodeling than similar manipulations of RA synthesis and RAR activity. Retinal degeneration was associated with increased translation of glutamate receptor 2 (GluA2) and β-Ca^{2+}/calmodulin-dependent protein kinase II (βCaMKII) in the inner retina, where all three RXR isoforms directly bind βCaMKII during remodeling. This might suggest a form of homeostatic plasticity in response to increased excitation. However, the molecular mechanism downstream to this interaction, and how it is part of neuritogenesis, or any other aspect of remodeling, was not elucidated. Furthermore, in a model of light-induced retinal damage, neuritogenesis is observed as soon as a few days after insult, while in most transgenic mouse and rat models of RP, these changes occur during late stages of remodeling, but hyperactivity can be detected very early-on. Thus, although morphological reorganization of dendrites in the inner plexiform layer might have important consequences to signal processing and synaptic plasticity, it is not likely to be the source of persistent retinal hyperactivity and sustained spontaneous electrical oscillations, but rather its result.

Our studies have demonstrated that RA/RAR-signaling is necessary and sufficient to explain two critical and early aspects of remodeling in RGCs: hyperactivity and hyperpermeability (Tochitsky et al., 2016; Telias et al., 2019; Denlinger et al., 2020). Using mouse models for fast and slow RP (rd1 and rd10, respectively), we found that photoreceptor degeneration is directly associated with a P2X-dependent increase in RGCs membrane permeability. This increase in permeability, termed hyperpermeability, was measured by *ex vivo* incubation of retinas with nuclear dyes that can pass through the P2X receptor pore ("Yo-Pro") but are otherwise unable to enter cells. In wildtype retinas only ∼5% of all GCL cells (excluding vascular pericytes) loaded Yo-Pro, while ∼30% of cells did so in rd retinas. Loading was always prevented by pre-incubation with the P2X receptor antagonist TNP-ATP, and it could not be potentiated by adding the P2X receptor agonist Bz-ATP in neither type of retina. Hyperpermeability could be induced in healthy retinas when intravitreally injected with all-*trans* RA and was reduced in rd retinas upon intraocular injection of RALDH blockers or RAR antagonists. In wildtype mice, overexpression of a constitutively active form of RARα that is never repressed by CoR and does not require activation by RA, resulted in increased membrane permeability in almost every transduced RGCs. Furthermore, delivery of a dominant-negative form of RARα to rd mice prevented Yo-Pro permeability in RGCs. Therefore, we found RAR activation to be necessary and sufficient to induce P2X-dependent membrane hyperpermeability, in an ATP-independent manner.

Blockade of RAR activation in the inner retina of rd mice, using small-molecule inhibitors, resulted in reduced spontaneous hyperactivity 3–7 days later (Telias et al., 2019). Ablation of endogenous RAR activation by viral transduction of rd RGCs with dominant-negative RARα for 1–2 months, also resulted in decreased hyperactivity. Both treatments reduced the average frequency firing of RGCs by ∼50%, from 6–8 Hz to 2–4 Hz. Overall, activity levels in all cases were not affected by acute pharmacological blockade of synaptic input, suggesting that RGCs are the intrinsic and main source of hyperactivity during degeneration, as well as RA's main cellular target. Given the way retinaldehyde and RA are transported between cells and shuttled from the cytoplasm to the nucleus (Maden, 2002), it might be the case that the source of RA to RGCs are Müller glial cells which take up retinaldehyde from the outer retina and re-distribute it throughout the inner retina, including the RGCs, where sustained RAR activation causes persistent post-synaptic hyperactivity (**Figure 1**).

Whatever mechanism delivers RA to RGCs, the resulting remodeling is stereotypical and found in RGCs of mice and rat models of RP (Tochitsky et al., 2016; Telias et al., 2019), as well as in a rat model of AMD (Denlinger et al., 2020). In RP mice, degeneration-dependent spontaneous hyperactivity obscures remaining light responses, and blocking RAR activation *in vivo* improves light sensitivity and visual perception (Telias et al., 2019). In AMD rats, RAR-dependent hyperpermeability in RGCs allows region-specific visual restoration using photoswitches (Denlinger et al., 2020). Since the P2X7 promoter does not include RARE sequences, it is unlikely that RAR directly drives an increase in P2X7 expression. Thus, factors that mediate the interaction between RAR-dependent transcription and P2X receptors, and whether the same factors are in charge for both hyperpermeability and hyperactivity, remain to be determined. Still, blocking RALDH, RA, or RAR is a promising and available prospective to augment residual vision in patients with slow retinal degeneration, and boost visual restoration in completely blind patients, by increasing the signal-to-noise ratio in RGCs.

SYNAPTIC REMODELING AND HYPERACTIVITY IN RETINAL DEGENERATION

The question of whether photoreceptor degeneration alters the circuitry in the outer and inner retina is critical for vision restoration. If the circuits remain unaltered, or any alterations to them are compensated for by a homeostatic counter-mechanism, then vision restoration technologies in humans, such as prosthetic devices, can be expected to achieve high acuity. Early studies on retinal remodeling showed that the surviving retina does not remain intact (i.e., spontaneous hyperactivity), and that these pathophysiological changes could be attributed to abnormal synaptic plasticity, including cell- and layer-specific alterations to the expression of metabotropic and ionotropic glutamate receptors in bipolar cells, amacrine cells and RGCs of degenerating retinas (Marc et al., 2003, 2007; Stasheff, 2008). Yet, other studies make the argument that the structure and

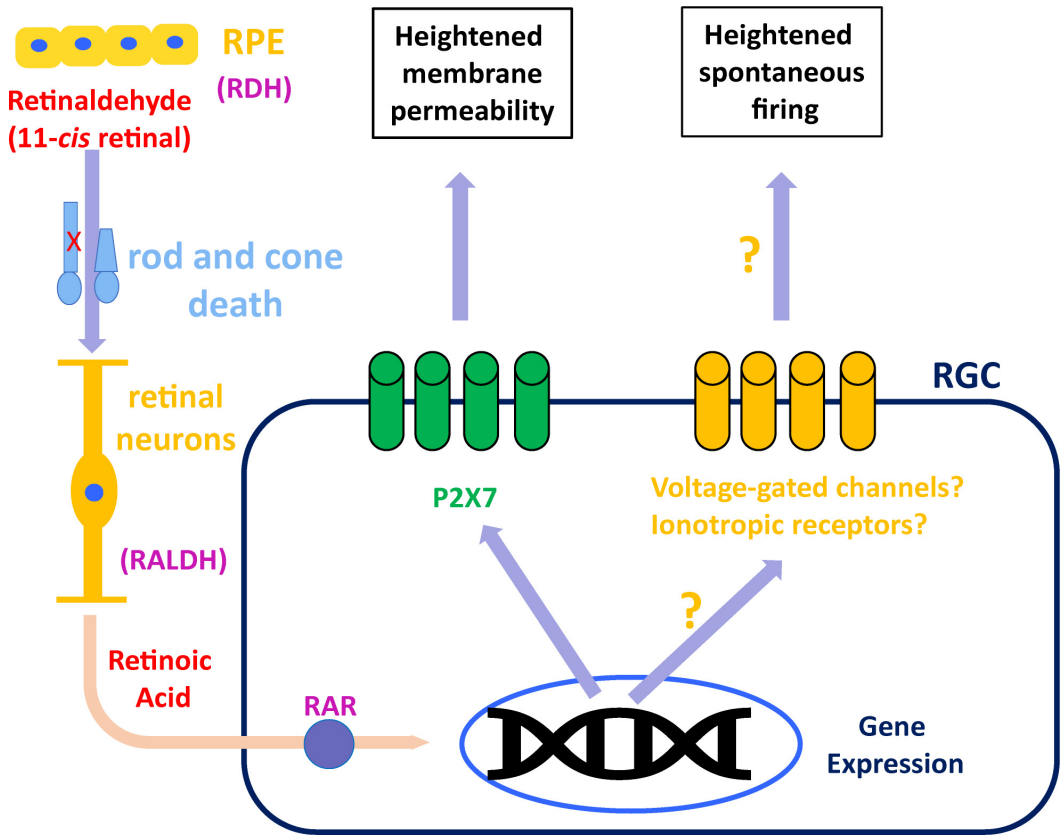

FIGURE 1 | Suggested model for RAR-dependent remodeling. Retinaldehyde is synthesized in the outer retina by retinol dehydrogenase (RDH) in rods, cones and retinal pigmented epithelium (RPE). Excess retinaldehyde as the result of photoreceptor death is converted by retinaldehyde dehydrogenase (RALDH) into retinoic acid, probably in different retinal neurons and eventually transported to retinal ganglion cells (RGCs). In RGCs, retinoic acid binds its receptor (RAR), initiating transcriptional activation, which leads to increased P2X7 expression, making it hyperpermeable. Another, still unknown mechanism, results in RAR-dependent hyperactivity, probably via overexpression or activation of voltage-gated ion channels or ionotropic receptors for neurotransmitters.

function of the circuitries that converge on RGCs remain largely unchanged by photoreceptor degeneration (Margolis et al., 2008; Mazzoni et al., 2008).

A change in synaptic input can be indirectly measured by assessing the expression of synaptic proteins and neurotransmitter-associated receptors and enzymes, in inner retinal neurons in correlation with photoreceptor degeneration. When mice were subjected to light-induced retinal damage, photoreceptor death was associated with an increase in the expression and trafficking of ionotropic glutamate receptors (GluR2) in the outer plexiform layer 7 days later, but this increase subsides after 30 days (Lin et al., 2012b). Immunohistochemistry analysis of synaptic markers (i.e., RIBEYE and gephyrin) in WT vs. rd1 retinas, shows a decrease in excitatory input on ON-RGCs and an increase in GABAergic input onto OFF-RGCs in correlation with degeneration, but the distribution of the synaptic connections across the dendritic trees of RGCs remained unchanged by degeneration and the differences between WT and rd1 are relatively modest (Saha et al., 2016).

Photoreceptors are continuously releasing glutamate onto counterpart bipolar cells, and light reduces glutamate release at the ribbon synapse. As photoreceptors die, they lose their outer segments and therefore their reactivity to photons, leading to an expected loss of light-dependent changes in glutamate release in the outer retina, affecting bipolar cells as degeneration progresses. This sustained abnormal excitation of bipolar cells by dying photoreceptors would be expected to induce different downstream effects onto different types of amacrine cells and RGCs, depending on the ON or OFF sign of the second synapse. Indeed, studies into degeneration-dependent hyperactivity have shown that two separate oscillatory networks exist (Euler and Schubert, 2015). The oscillatory network in the outer retina, composed by dying cones, rod bipolar cells and horizontal cells, oscillates at a frequency of up to ∼3 Hz (Haq et al., 2014). These oscillations, the study claims, arise from retrograde release of GABA from horizontal cells back onto cones. The oscillatory network of the inner retina is composed by AII amacrine cells and cone bipolar cells, and oscillates at ∼10 Hz (Borowska et al., 2011; Trenholm et al., 2012). These inner retinal oscillations seem to be an important component of the spontaneous hyperactivation induced by photoreceptor death and were shown to be insensitive to blockers of voltage-gated Ca^{2+}-channels and enhanced by blockers of hyperpolarization-activated currents (I_h). They seem to originate from the activation of voltage-gated Na^{+}-channels

expressed in AII amacrine cells and spread to ON-bipolar cells through gap junctions. In particular, the role of gap junctions in mediating these oscillations has been confirmed in several studies (Ivanova et al., 2016). This is functionally meaningful, as in visually impaired rd mice *ex vivo* treatment with gap junction blockers reduces hyperactivity and improves light responses (Toychiev et al., 2013; Barrett et al., 2015).

However, these studies do not identify the trigger mechanism behind these plastic events in inner retinal neurons, and how these cells are able to "sense" the death of photoreceptors in the outer retinal compartment. While these hypotheses might explain many of the electrophysiological abnormalities associated with pathological hyperactivity, it is still insufficient to explain other aspects of remodeling, such as membrane hyperpermeability, *de novo* neuritogenesis and layer disruption. For specific synaptic proteins to increase or decrease their expression in specific cell types, a complex feedback signaling network must exist, ultimately triggering aberrant gene expression. Yet, these signaling networks and their "core" gene-expression event remains absent from studies into synaptic remodeling. Furthermore, in both mice and rats with retinal degeneration, blockade of all synaptic input onto RGCs is not sufficient to significantly reduce degeneration-dependent hyperactivity (Sekirnjak et al., 2009; Tochitsky et al., 2016; Telias et al., 2019; Denlinger et al., 2020). Most importantly, whatever functional and synaptic changes might be affecting different cell types across the outer and inner retina during degeneration, the structural constrains of the retina itself compel research to focus on the net effect of remodeling on RGCs, as all information leaving the retina must transit through them. While many studies show pathological or homeostatic plasticity taking place in bipolar and other cells, evidence from RGCs suggesting a significant pre-synaptic mechanism driving their hyperactivity is still missing at large. From this we conclude that, in order to reduce hyperactivity and boost residual light responses and visual restoration techniques, efforts must be put into understanding the mechanisms behind intrinsic pathophysiological changes caused by degeneration in RGCs.

SUMMARY AND CONCLUSIONS

Finding the molecular mechanism behind pathophysiological remodeling is essential to block degeneration-dependent hyperactivity. During retinal degeneration, a process that can take decades in humans, remnant light responses are obscured by hyperactivity. Blocking or reducing hyperactivity unmasks light responses, opening a therapeutic window to enhance vision in patients suffering from RP, AMD and other photoreceptor degeneration diseases. In patients that are completely blind, restoration of vision might be possible through photo-pharmacology (Tochitsky et al., 2018), optogenetics (Baker and Flannery, 2018) or prosthetic devices (Mirochnik and Pezaris, 2019). However, low signal-to-noise ratio will result in poor visual restoration, regardless of the method employed. In the best-case scenario, the dead outer retina would be repopulated by implantation of photoreceptors differentiated from stem cells (Llonch et al., 2018). Yet, even in such a case, remodeling might persist, as its long-lasting effects and their reversibility are still largely unknown. Therefore, understanding the source of hyperactivity becomes critical.

As photoreceptors die, their necrotic outer disks and bodies release their content into the extracellular matrix. Since photoreceptors greatly outnumber the rest of the cells in the retina (∼70% of the cells in a mouse retina), their slow degeneration provides a sustained source of bioactive molecules that can percolate the inner retina, crossing cell and layer membranes. Among these, purines and retinoids have been proposed as candidates (Aplin et al., 2016; Telias et al., 2019). In parallel, loss of photoreceptors deprives bipolar cells of glutamate, triggering consequent pathological homeostatic mechanisms (Haq et al., 2014). All of these might contribute to the many aspects of remodeling, and most importantly to the pervasive hyperactivity that develops in the inner retina in general and in RGCs in particular.

AUTHOR CONTRIBUTIONS

MT, SN, and RK wrote and revised the manuscript. RK provided funding. All authors contributed to the article and approved the submitted version.

FUNDING

This work was supported by grants from the National Eye Institute (R01EY024334, R24EY023937, and P30EY003176).

REFERENCES

Aplin, F. P., Vessey, K. A., Luu, C. D., Guymer, R. H., Shepherd, R. K., and Fletcher, E. L. (2016). Retinal changes in an ATP-induced model of retinal degeneration. *Front. Neuroanat.* 10:46. doi: 10.3389/fnana.2016.00046

Athanasiou, D., Aguila, M., Bevilacqua, D., Novoselov, S. S., Parfitt, D. A., Cheetham, M. E. et al. (2013). The cell stress machinery and retinal degeneration. *FEBS Lett.* 587, 2008–2017. doi: 10.1016/j.febslet.2013.05.020

Baker, C. K., and Flannery, J. G. (2018). Innovative optogenetic strategies for vision restoration. *Front. Cell Neurosci.* 12:316. doi: 10.3389/fncel.2018.00316

Barrett, J. M., Degenaar, P., and Sernagor, E. (2015). Blockade of pathological retinal ganglion cell hyperactivity improves optogenetically evoked light responses in rd1 mice. *Front. Cell Neurosci.* 9:330. doi: 10.3389/fncel.2015.00330

Borowska, J., Trenholm, S., and Awatramani, G. B. (2011). An intrinsic neural oscillator in the degenerating mouse retina. *J. Neurosci.* 31, 5000–5012. doi: 10.1523/jneurosci.5800-10.2011

Collin, G. B., Gogna, N., Chang, B., Damkham, N., Pinkney, J., Hyde, L. F., et al. (2020). Mouse Models of Inherited Retinal Degeneration with Photoreceptor Cell Loss. *Cells* 9:931. doi: 10.3390/cells9040931

Daruwalla, A., Choi, E. H., Palczewski, K., and Kiser, P. D. (2018). Structural biology of 11-cis-retinaldehyde production in the classical visual cycle. *Biochem. J.* 475, 3171–3188. doi: 10.1042/bcj20180193

Denlinger, B., Helft, Z., Telias, M., Lorach, H., Palanker, D., and Kramer, R. H. (2020). Local photoreceptor degeneration causes local pathophysiological remodeling of retinal neurons. *JCI Insight* 5:e132114.

Euler, T., and Schubert, T. (2015). Multiple independent oscillatory networks in the degenerating retina. *Front. Cell Neurosci.* 9:444. doi: 10.3389/fncel.2015.00444

Garcia-Ayuso, D., Di Pierdomenico, J., Vidal-Sanz, M., and Villegas-Perez, M. P. (2019). Retinal ganglion cell death as a late remodeling effect of photoreceptor degeneration. *Int. J. Mol. Sci.* 20:4649. doi: 10.3390/ijms20184649

Gil-Martinez, M., Santos-Ramos, P., Fernandez-Rodriguez, M., Abraldes, M. J., Rodriguez-Cid, M. J., Santiago-Varela, M., et al. (2020). Pharmacological advances in the treatment of age-related macular degeneration. *Curr. Med. Chem.* 27, 583–598.

Goldberg, A. F., Moritz, O. L., and Williams, D. S. (2016). Molecular basis for photoreceptor outer segment architecture. *Prog. Retin. Eye Res.* 55, 52–81. doi: 10.1016/j.preteyeres.2016.05.003

Hageman, G. S., Gehrs, K., Johnson, L. V., and Anderson, D. (2008). "Age-Related Macular Degeneration (AMD)," in *Webvision: The Organization of the Retina and Visual System*, eds H. Kolb, E. Fernandez, and R. Nelson (Salt Lake City: University of Utah Health Sciences Center).

Haq, W., Arango-Gonzalez, B., Zrenner, E., Euler, T., and Schubert, T. (2014). Synaptic remodeling generates synchronous oscillations in the degenerated outer mouse retina. *Front. Neural. Circuits* 8:108. doi: 10.3389/fncir.2014.00108

Harper, A. R., Wiechmann, A. F., Moiseyev, G., Ma, J. X., and Summers, J. A. (2015). Identification of active retinaldehyde dehydrogenase isoforms in the postnatal human eye. *PLoS One* 10:e0122008. doi: 10.1371/journal.pone.0122008

Iandiev, I., Uckermann, O., Pannicke, T., Wurm, A., Tenckhoff, S., Pietsch, U. C., et al. (2006). Glial cell reactivity in a porcine model of retinal detachment. *Invest. Ophthalmol. Vis. Sci.* 47, 2161–2171. doi: 10.1167/iovs.05-0595

Ivanova, E., Yee, C. W., Baldoni, R. Jr., and Sagdullaev, B. T. (2016). Aberrant activity in retinal degeneration impairs central visual processing and relies on Cx36-containing gap junctions. *Exp. Eye Res.* 150, 81–89. doi: 10.1016/j.exer.2015.05.013

Jones, B. W., Kondo, M., Terasaki, H., Lin, Y., Mccall, M., and Marc, R. E. (2012). Retinal remodeling. *Jpn. J. Ophthalmol.* 56, 289–306.

Jones, B. W., Marc, R. E., and Pfeiffer, R. L. (2016a). "Retinal Degeneration, Remodeling and Plasticity," in *Webvision: The Organization of the Retina and Visual System*, eds H. Kolb, E. Fernandez, and R. Nelson (Salt Lake City: University of Utah Health Sciences Center).

Jones, B. W., Pfeiffer, R. L., Ferrell, W. D., Watt, C. B., Marmor, M., and Marc, R. E. (2016b). Retinal remodeling in human retinitis pigmentosa. *Exp. Eye Res.* 150, 149–165. doi: 10.1016/j.exer.2016.03.018

Jones, B. W., Pfeiffer, R. L., Ferrell, W. D., Watt, C. B., Tucker, J., and Marc, R. E. (2016c). Retinal remodeling and metabolic alterations in human AMD. *Front. Cell Neurosci.* 10:103. doi: 10.3389/fncel.2016.00103

Kolb, H. (1995). "Simple Anatomy of the Retina," in *Webvision: The Organization of the Retina and Visual System*, eds H. Kolb, E. Fernandez, and R. Nelson (Salt Lake City: University of Utah Health Sciences Center).

Kolb, H. (2005). "Photoreceptors," in *Webvision: The Organization of the Retina and Visual System*, eds H. Kolb, E. Fernandez, and R. Nelson (Salt Lake City: University of Utah Health Sciences Center).

Kreissig, I. (2016). Primary retinal detachment: a review of the development of techniques for repair in the past 80 years. *Taiwan J. Ophthalmol.* 6, 161–169. doi: 10.1016/j.tjo.2016.04.006

Lin, Y., Jones, B. W., Liu, A., Tucker, J. F., Rapp, K., Luo, L., et al. (2012a). Retinoid receptors trigger neuritogenesis in retinal degenerations. *FASEB J.* 26, 81–92. doi: 10.1096/fj.11-192914

Lin, Y., Jones, B. W., Liu, A., Vazquez-Chona, F. R., Lauritzen, J. S., Ferrell, W. D., et al. (2012b). Rapid glutamate receptor 2 trafficking during retinal degeneration. *Mol. Neurodegener.* 7:7. doi: 10.1186/1750-1326-7-7

Llonch, S., Carido, M., and Ader, M. (2018). Organoid technology for retinal repair. *Dev. Biol.* 433, 132–143. doi: 10.1016/j.ydbio.2017.09.028

Luo, T., Sakai, Y., Wagner, E., and Drager, U. C. (2006). Retinoids, eye development, and maturation of visual function. *J. Neurobiol.* 66, 677–686. doi: 10.1002/neu.20239

Maden, M. (2002). Retinoid signalling in the development of the central nervous system. *Nat. Rev. Neurosci.* 3, 843–853. doi: 10.1038/nrn963

Marc, R. E., Jones, B. W., Anderson, J. R., Kinard, K., Marshak, D. W., Wilson, J. H., et al. (2007). Neural reprogramming in retinal degeneration. *Invest. Ophthalmol. Vis. Sci.* 48, 3364–3371.

Marc, R. E., Jones, B. W., Watt, C. B., and Strettoi, E. (2003). Neural remodeling in retinal degeneration. *Prog. Retin. Eye Res.* 22, 607–655. doi: 10.1016/s1350-9462(03)00039-9

Margolis, D. J., Newkirk, G., Euler, T., and Detwiler, P. B. (2008). Functional stability of retinal ganglion cells after degeneration-induced changes in synaptic input. *J. Neurosci.* 28, 6526–6536. doi: 10.1523/jneurosci.1533-08.2008

Mazzoni, F., Novelli, E., and Strettoi, E. (2008). Retinal ganglion cells survive and maintain normal dendritic morphology in a mouse model of inherited photoreceptor degeneration. *J. Neurosci.* 28, 14282–14292. doi: 10.1523/jneurosci.4968-08.2008

Miraldi Utz, V., Coussa, R. G., Antaki, F., and Traboulsi, E. I. (2018). Gene therapy for RPE65-related retinal disease. *Ophthalmic Genet.* 39, 671–677. doi: 10.1080/13816810.2018.1533027

Mirochnik, R. M., and Pezaris, J. S. (2019). Contemporary approaches to visual prostheses. *Mil. Med. Res.* 6:19.

Nakazawa, M., Hara, A., and Ishiguro, S. I. (2019). Optical coherence tomography of animal models of retinitis pigmentosa: from animal studies to clinical applications. *Biomed. Res. Int.* 2019:8276140.

Pennesi, M. E., Neuringer, M., and Courtney, R. J. (2012). Animal models of age related macular degeneration. *Mol. Aspects Med.* 33, 487–509.

Pfeiffer, R. L., Marc, R. E., and Jones, B. W. (2020). Persistent remodeling and neurodegeneration in late-stage retinal degeneration. *Prog. Retin. Eye Res.* 74:100771. doi: 10.1016/j.preteyeres.2019.07.004

Saha, S., Greferath, U., Vessey, K. A., Grayden, D. B., Burkitt, A. N., and Fletcher, E. L. (2016). Changes in ganglion cells during retinal degeneration. *Neuroscience* 329, 1–11. doi: 10.1016/j.neuroscience.2016.04.032

Sekirnjak, C., Hulse, C., Jepson, L. H., Hottowy, P., Sher, A., Dabrowski, W., et al. (2009). Loss of responses to visual but not electrical stimulation in ganglion cells of rats with severe photoreceptor degeneration. *J. Neurophysiol.* 102, 3260–3269. doi: 10.1152/jn.00663.2009

Stasheff, S. F. (2008). Emergence of sustained spontaneous hyperactivity and temporary preservation of OFF responses in ganglion cells of the retinal degeneration (rd1) mouse. *J. Neurophysiol.* 99, 1408–1421. doi: 10.1152/jn.00144.2007

Stasheff, S. F. (2018). Clinical impact of spontaneous hyperactivity in degenerating retinas: significance for diagnosis, symptoms, and treatment. *Front. Cell Neurosci.* 12:298. doi: 10.3389/fncel.2018.00298

Takahashi, V. K. L., Takiuti, J. T., Jauregui, R., and Tsang, S. H. (2018). Gene therapy in inherited retinal degenerative diseases, a review. *Ophthalmic Genet.* 39, 560–568. doi: 10.1080/13816810.2018.1495745

Telias, M., Denlinger, B., Helft, Z., Thornton, C., Beckwith-Cohen, B., and Kramer, R. H. (2019). Retinoic acid induces hyperactivity, and blocking its receptor unmasks light responses and augments vision in retinal degeneration. *Neuron* 102:e575.

Tochitsky, I., Helft, Z., Meseguer, V., Fletcher, R. B., Vessey, K. A., Telias, M., et al. (2016). How azobenzene photoswitches restore visual responses to the blind retina. *Neuron* 92, 100–113. doi: 10.1016/j.neuron.2016.08.038

Tochitsky, I., Kienzler, M. A., Isacoff, E., and Kramer, R. H. (2018). Restoring vision to the blind with chemical photoswitches. *Chem. Rev.* 118, 10748–10773. doi: 10.1021/acs.chemrev.7b00723

Toychiev, A. H., Ivanova, E., Yee, C. W., and Sagdullaev, B. T. (2013). Block of gap junctions eliminates aberrant activity and restores light responses during retinal degeneration. *J. Neurosci.* 33, 13972–13977. doi: 10.1523/jneurosci.2399-13.2013

Trenholm, S., Borowska, J., Zhang, J., Hoggarth, A., Johnson, K., Barnes, S., et al. (2012). Intrinsic oscillatory activity arising within the electrically coupled AII amacrine-ON cone bipolar cell network is driven by voltage-gated Na+ channels. *J. Physiol.* 590, 2501–2517. doi: 10.1113/jphysiol.2011.225060

Verbakel, S. K., Van Huet, R. A. C., Boon, C. J. F., Den Hollander, A. I., Collin, R. W. J., Klaver, C. C. W., et al. (2018). Non-syndromic retinitis pigmentosa. *Prog. Retin. Eye Res.* 66, 157–186.

Winkler, P. A., Occelli, L. M., and Petersen-Jones, S. M. (2020). Large animal models of inherited retinal degenerations: a review. *Cells* 9:889.

Wiseman, E. M., Bar-El Dadon, S., and Reifen, R. (2017). The vicious cycle of vitamin a deficiency: a review. *Crit. Rev. Food Sci. Nutr.* 57, 3703–3714. doi: 10.1080/10408398.2016.1160362

Wong, W. L., Su, X., Li, X., Cheung, C. M., Klein, R., Cheng, C. Y., et al. (2014). Global prevalence of age-related macular degeneration and disease burden projection for 2020 and 2040: a systematic review and meta-analysis. *Lancet Glob. Health* 2, e106–e116.

Zeiss, C. J. (2010). Animals as models of age-related macular degeneration: an imperfect measure of the truth. *Vet. Pathol.* 47, 396–413. doi: 10.1177/0300985809359598

Conflict of Interest: The authors declare that the research was conducted in the absence of any commercial or financial relationships that could be construed as a potential conflict of interest.

Copyright © 2020 Telias, Nawy and Kramer. This is an open-access article distributed under the terms of the Creative Commons Attribution License (CC BY). The use, distribution or reproduction in other forums is permitted, provided the original author(s) and the copyright owner(s) are credited and that the original publication in this journal is cited, in accordance with accepted academic practice. No use, distribution or reproduction is permitted which does not comply with these terms.

frontiers in Neuroscience

REVIEW
published: 17 March 2021
doi: 10.3389/fnins.2021.652215

Gene Therapy to the Retina and the Cochlea

Ryan Crane[1], Shannon M. Conley[2,3†], Muayyad R. Al-Ubaidi[1,4,5†] and Muna I. Naash[1,4,5*†]*

[1] Department of Biomedical Engineering, University of Houston, Houston, TX, United States, [2] Department of Cell Biology, University of Oklahoma Health Sciences Center, Oklahoma City, OK, United States, [3] Oklahoma Center for Neurosciences, University of Oklahoma Health Sciences Center, Oklahoma City, OK, United States, [4] College of Optometry, University of Houston, Houston, TX, United States, [5] Depatment of Biology and Biochemistry, University of Houston, Houston, TX, United States

OPEN ACCESS

Edited by:
Jacqueline Reinhard, Ruhr-University, Germany

Reviewed by:
Elvir Becirovic, Ludwig Maximilian University of Munich, Germany
Erica Lucy Fletcher, The University of Melbourne, Australia

****Correspondence:***
Muayyad R. Al-Ubaidi
malubaid@central.uh.edu
Muna I. Naash
mnaash@central.uh.edu

†ORCID:
Shannon M. Conley
orcid.org/0000-0002-7550-3898
Muayyad R. Al-Ubaidi
orcid.org/0000-0002-4914-350X
Muna I. Naash
orcid.org/0000-0002-6534-5144

Specialty section:
This article was submitted to Neurodegeneration, a section of the journal Frontiers in Neuroscience

Received: *11 January 2021*
Accepted: *22 February 2021*
Published: *17 March 2021*

Citation:
Crane R, Conley SM, Al-Ubaidi MR and Naash MI (2021) Gene Therapy to the Retina and the Cochlea. Front. Neurosci. 15:652215. doi: 10.3389/fnins.2021.652215

Vision and hearing disorders comprise the most common sensory disorders found in people. Many forms of vision and hearing loss are inherited and current treatments only provide patients with temporary or partial relief. As a result, developing genetic therapies for any of the several hundred known causative genes underlying inherited retinal and cochlear disorders has been of great interest. Recent exciting advances in gene therapy have shown promise for the clinical treatment of inherited retinal diseases, and while clinical gene therapies for cochlear disease are not yet available, research in the last several years has resulted in significant advancement in preclinical development for gene delivery to the cochlea. Furthermore, the development of somatic targeted genome editing using CRISPR/Cas9 has brought new possibilities for the treatment of dominant or gain-of-function disease. Here we discuss the current state of gene therapy for inherited diseases of the retina and cochlea with an eye toward areas that still need additional development.

Keywords: retina, cochlea, gene therapy, nanoparticles, animal models

INTRODUCTION

Over 2.2 billion people worldwide experience vision impairment or irreversible vision loss[1], and over 466 million people worldwide experience serious hearing loss[2], making these the most prevalent sensory impairments. Many forms of vision and hearing loss are inherited and current treatments only provide patients with temporary or incomplete relief. Because many inherited sensory defects have identified disease genes, developing effective genetic therapies has been a primary research goal for several decades. Recent exciting advances in gene therapy have shown promise for the treatment of inherited retinal and cochlear diseases, both in the area of gene replacement and in the area of targeted genome editing (e.g., CRISPR/Cas9) to correct underlying

[1] https://www.who.int/en/news-room/fact-sheets/detail/blindness-and-visual-impairment

[2] https://www.who.int/en/news-room/fact-sheets/detail/deafness-and-hearing-loss

genetic defects. However, there are still substantial limitations hampering widespread clinical use of genetic therapies in the retina and cochlea, including issues of distribution and uptake of the vectors by the target cells, a limited window of opportunity for treatment in degenerative disorders, attenuation of gene expression after a period of time, and efficiency/off-target concerns with novel genome editing strategies.

Inherited Diseases of the Retina

The retina is the transparent, light-sensitive tissue at the back of the eye (**Figure 1A**) responsible for capturing light and converting it to an electrical signal to be delivered to the visual cortex in the brain where conception of vision occurs. The retina has evolved into a multi-cellular laminated structure, within which the different cells are organized and interconnected to maximize the efficiency and resolution of light perception (**Figure 1B**). The primary cells involved in the detection of light are the retinal rod and cone photoreceptors. Rods are necessary for low-light or "night" vision while cones perform bright-light color vision perception. The leading causes of irreversible vision loss are age-related eye diseases including age-related macular degeneration, diabetic retinopathy, glaucoma, and cataract[3] (reviewed in Haddad et al., 2006; Simo-Servat et al., 2013; Singh and Tyagi, 2018). While these highly prevalent retinal diseases are not monogenic, they do often have a genetic component that contributes to disease in combination with environmental or other factors. In addition, inherited retinal dystrophies/diseases (IRDs) affect roughly 1 in 1380 individuals with an estimated 36% of the population as healthy carriers of one or more IRD causing mutations (Hanany et al., 2020). Combined, this underscores the need for the development of genetic therapies targeting the retina.

IRDs are a group of retinal dystrophies caused by mutations in over 271 different known genes (with many still unknown), that can target various cells within the retina. Virtually all inheritance patterns are represented in IRD genes including autosomal dominant, autosomal recessive, X-linked, digenic, polygenic, and even mitochondrial disorders. IRD genes expressed in photoreceptors can lead to various macular degenerations/dystrophies and retinitis pigmentosa (RP) and are involved in ocular development, phototransduction, cellular metabolism, and in the development and maintenance of photoreceptor structure. Mutations in retinal pigment epithelium (RPE) genes include those involved in retinoid recycling, cellular metabolism, and cellular homeostasis and can lead to macular dystrophies as well as Leber's Congenital Amaurosis (LCA). Mutations in retinal ganglion cell IRD genes are largely associated with mitochondrial function, but also include regulators of intracellular transport and transcription, and can lead to optic atrophy. A summary of known IRD genes can be found at: https://sph.uth.edu/retnet/sum-dis.htm.

Depending on the gene, the onset of disease varies from birth to adulthood. Photoreceptor dystrophies are the most common within the retina and can be classified by the primary affected cell type and whether central or peripheral vision is lost first. RP and rod-cone dystrophies typically affect rods first, while macular dystrophies/degenerations and cone-rod dystrophies often affect cones first (Rattner et al., 1999). However, it is worth noting that in many cases of macular dystrophy, where macular cones are the first cells targeted, the causative gene is expressed in the adjacent RPE, with vision loss arising due to secondary cone damage. Patients with RP and rod-cone dystrophies often initially present with night-blindness which is followed by gradual peripheral vison loss (Ferrari et al., 2011). As the patients' visual fields gradually shrink over time, irreversible vision loss eventually ensues (Ferrari et al., 2011). Individuals with cone-rod dystrophies have a rapid loss of central vision early in their life, which is followed by gradual peripheral vison loss (Morimura et al., 1998; Fukui et al., 2002; Klevering et al., 2004).

Current treatment options to correct the more mild symptoms of vision loss include corrective lenses or contacts and more permanent laser correction surgery. In more severe cases where progressive vision loss occurs due to retinal degeneration, a more invasive approach is necessary. These advanced therapeutic options are all still in development or in early clinical use and include gene therapy, gene editing, reprogramming, cell therapy, optogenetic therapies, and retinal prostheses. The time at which these therapies are useful varies greatly. For maximum efficacy, gene therapy needs to be delivered in the early stage of disease to prevent further degeneration. In contrast, other options have a wider therapeutic window, but have had less success thus far, both in development and in clinical use (Maeda et al., 2019; Wood et al., 2019).

Inherited Diseases of the Cochlea

The inner ear is a small, fluid-filled compartment (**Figure 1C**) encased in the temporal bone and located at the base of the skull. The acoustic energy from sound is converted to an electrical impulse that the brain perceives as hearing through a multi-step process. Sound waves hit the tympanic membrane (eardrum) which vibrates the attached ossicular chain (three small ear bones). This vibration is transmitted to the fluid in the cochlea and basilar membrane (**Figure 1D**), and resulting fluid waves are sensed by the hair cells in the organ of Corti through mechanotransduction. The specialized sensory hair cells in the cochlea comprise a single layer of inner hair cells (IHCs) responsible for converting the mechanical signal into an electrochemical one, and three layers of outer hair cells (OHCs) involved in modulating and amplifying auditory signals. Mechanical deflection of stereocilia on the surface hair cells results in depolarization, and subsequent signal transmission to the auditory cortex (Rubel and Fritzsch, 2002). The differentiation of sound frequencies is facilitated by the length of the cochlea and the stiffness of the basilar membrane (Manoussaki et al., 2006).

Sensorineural hearing loss (SNHL), defined as the presence of a deafness-causing etiology in the cochlea or auditory nerve, accounts for more than 90% of hearing loss in adult patients. Approximately 50–60% of all cases of congenital deafness are directly linked to genetic factors, with higher numbers in developed countries (Marazita et al., 1993; Smith et al., 2005). Currently there are 49 identified genes known to be responsible

[3]https://www.cdc.gov/visionhealth/basics/ced/index.html

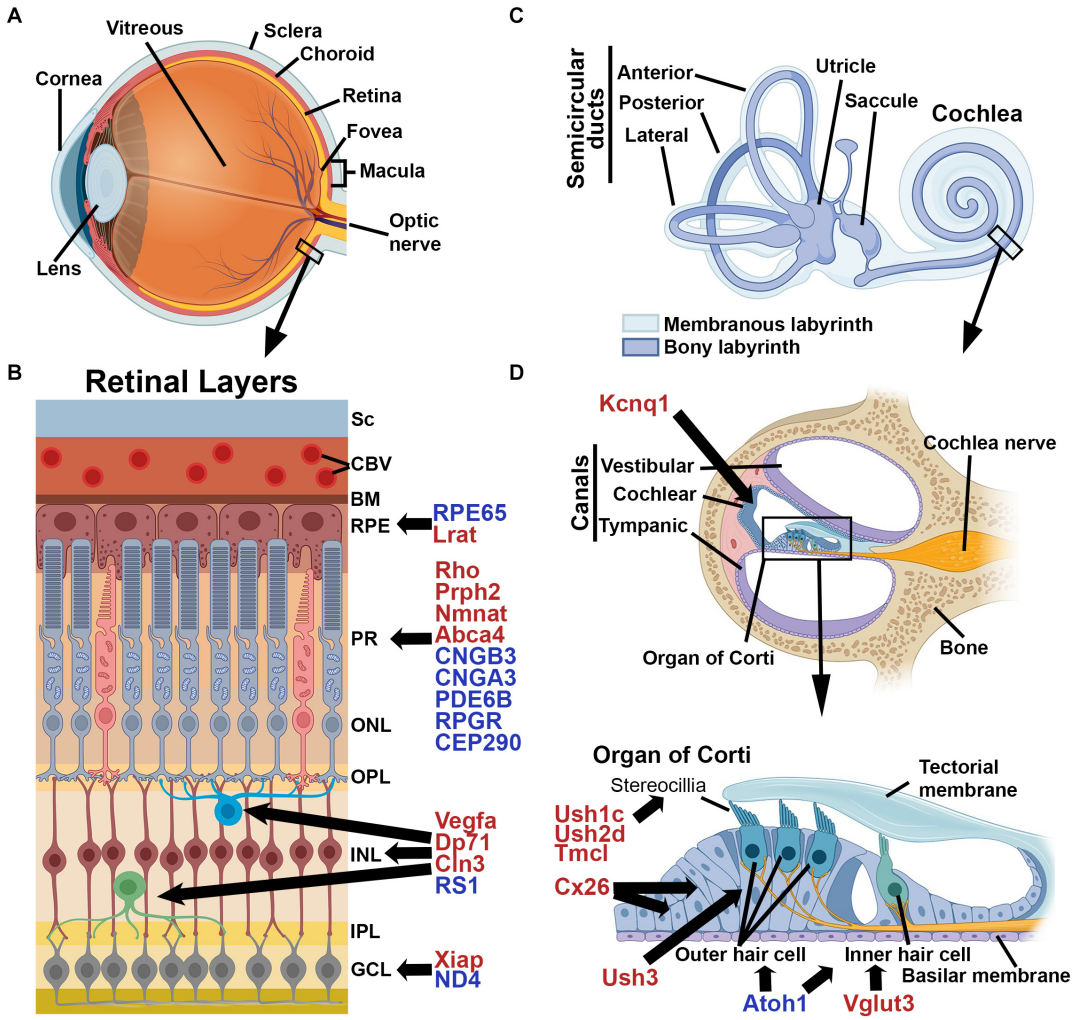

FIGURE 1 | Schematic Illustrations of the Cochlea and Retina. **(A)** The structure of the eye, **(B)** layers of the retina (Sc, sclera; CBV, choroidal blood vessel; BM, Bruch's membrane; RPE, retinal pigment epithelium; PR, photoreceptors; ONL, outer nuclear layer; OPL, outer plexiform layer; INL, inner nuclear layer; IPL, inner plexiform layer; GCL, ganglion cell layer) and **(C)** The structure of the inner ear, **(D)** cross-section of the cochlea and a close-up of the Organ of Corti. Shown are selected genes which are associated with disease in humans. Genes marked in red represent a selection of those that have been evaluated successfully in animal models while those in blue have been evaluated in human clinical trials. Images were created with BioRender.com.

for autosomal dominant non-syndromic hearing loss, 76 autosomal recessive genes, and 5 X-linked genes[4] and (Duman and Tekin, 2012; Yuan et al., 2020) with many more remaining to be mapped. These genes play a role in a variety of processes including hair bundle development/function, hair cell adhesion, synaptic transmission, cochlear ion homeostasis, cellular homeostasis/energy generation, and regulation of the extracellular matrix (reviewed in Dror and Avraham, 2010; Stamatiou and Stankovic, 2013; Zhang W. J. et al., 2018). As in the retina, disease onset can vary from birth to late adolescence. The pattern and progression of symptoms in patients help identify what mutation(s) may be involved and determine whether interventions, genetic or otherwise, may be beneficial.

Current treatment options focus on amplifying sound through hearing aids or electrical stimulation of auditory neurons via cochlear implants for individuals with severe deafness. Cochlear implants are currently the most successful sensory prosthetics available, allowing deaf individuals to understand speech (Wilson and Dorman, 2008; Roche and Hansen, 2015). However, their effectiveness is limited to quiet spaces and suffers from poorly detailed sensory perception (Muller and Barr-Gillespie, 2015; Roche and Hansen, 2015; Weiss et al., 2016). In addition, while highly beneficial, cochlear implants merely treat the symptoms of hearing loss without addressing the underlying cause, so cochlear gene therapy has been an exciting therapeutic goal.

Syndromic Sensory Inherited Diseases

In addition to inherited disease genes affecting a single tissue (e.g., the retina or the cochlea), there are a large variety of disease genes

[4]https://hereditaryhearingloss.org/

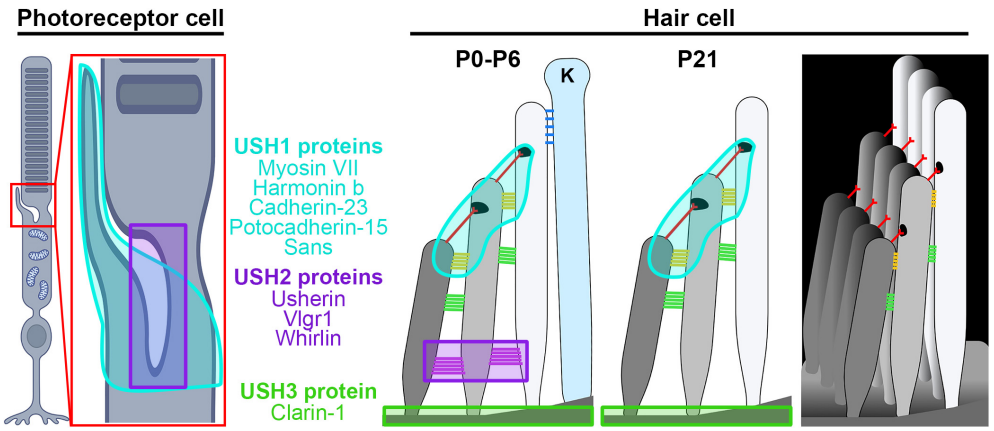

FIGURE 2 | Site of Usher proteins in the retina and the cochlea. Shown are illustrations of the photoreceptor and hair cell highlighting the regions affected by different Usher syndrome genes. Ush1 genes/locations are shown in cyan, Ush2 genes/locations in purple, and Ush 3 genes in lime green. Hair cell legend structures: ankle links (purple), lateral links (green), contact region (gold), tip link (red), kinocilium links (blue), kinocilium (K). Images were created with BioRender.com.

that are syndromic, affecting multiple tissues. Structural parallels in photoreceptors and cochlear hair cells mean that there are also a large number of disease genes that cause dual syndromic deafness and blindness. These genes often induce photoreceptor degeneration rather than optic atrophy and are frequently classed under the larger umbrella of ciliopathies. The most common form of dual deafness and irreversible vision loss involves the many genes associated with Usher syndrome (El-Amraoui and Petit, 2014; Mathur and Yang, 2015, 2019). Usher syndrome is clinically broken down into three types, Ush1, Ush2, and Ush3, due to the severity of hearing and vision loss, presence or absence of vestibular problems, and the age of onset for the symptoms (Millan et al., 2011). Patients with Ush1 are born with severe hearing loss, have abnormal vestibular systems, and progressive vision loss due to RP beginning during childhood. Individuals with Ush2 are born with mild to severe hearing loss and have progressive vision loss starting during adolescence. People with Ush3 develop hearing loss during adulthood and vision loss during adolescence and develop vestibular abnormalities. The types are further subdivided due to the underlying genetic cause. The proteins associated with each type are localized into similar regions in the retina and cochlea (**Figure 2**) and often associate or interact with one another, thus mutations in several genes can lead to similar patient phenotypes.

Other disease genes with multiple affected areas include many of the retinal disease genes that cause optic atrophy such as *MECR* and *ACO2* which are also associated with cerebellar defects and ataxias (Heimer et al., 1993; Sharkia et al., 2019). In other cases, these disorders also have a deafness component, for example in the case of *TIMM8A*, which is associated with deafness-dystonia-optic neuropathy syndrome (Tranebjaerg, 1993). However, these syndromic disorders are very complex, and in some cases, different mutations in the same gene lead to isolated optic atrophy or ataxias, such as the case of *AFG3L2* (Di Bella et al., 2010; Colavito et al., 2017). Some syndromic forms of vision loss such as Batten disease affect the brain and bipolar cells, the inner retinal neurons responsible for conveying signals from photoreceptors to ganglion cells (Kleine Holthaus et al., 2020). These various syndromic diseases highlight molecular similarities in various sensory disorders, and suggest that examining sensory disorders from a broader, non-organ-specific perspective may be beneficial.

Commonalities Between the Retina and the Cochlea

Favorable Biological Characteristics

One problem with systemic delivery or delivery to systemic organs besides rapid clearance/excretion of the vector is potential activation of the immune system. In contrast, both the eye and the ear represent accessible local delivery sites that are fairly protected from the systemic immune system. This permits a prolonged half-life for delivered material and reduces the chance of a systemic immune response or off-target effects in other parts of the body.

The inside of the eye, including the retina, is isolated from the systemic circulation by the blood-retinal barrier and the blood-aqueous barrier, maintained by tight junctions between retinal pigment epithelial cells; between vascular endothelial cells in the ciliary processes, Schlemm's canal inner wall endothelial cells and the iris vasculature; and between the cells in the non-pigmented ciliary epithelium (Campbell and Humphries, 2012; Coca-Prados, 2014). Thanks to these barriers, the eye has a limited immune system with only local immune and inflammatory responses present to maintain homeostasis, allowing the retina to be immune-privileged (Zhou and Caspi, 2010; Cunha-Vaz et al., 2011). Likewise, the cochlea is also isolated and surrounded by bone with even less access to the rest of the body. The endothelial cells lining the cochlear blood vessels form the blood-labyrinth barrier (BLB) or blood-cochlea barrier (BCB), which is comparable to the blood-brain barrier (BBB) in its ability to tightly regulate the exchange of macromolecules and ions between the blood system and the inner ear. The BLB maintains the homeostasis of the inner ear and isolates it from

any pathogens found in the blood, allowing the inner ear to also maintain relative immune-privilege (Salt and Hirose, 2018).

Another benefit of genetic therapies for both the retina and cochlea is the need to deliver only small amounts of therapeutic agents, which is due to the ability to deposit material directly to or in very close proximity to the target cells, allowing for greater chance of uptake by the desired cells with limited loss due to systemic distribution.

In addition, the majority of the cells in both the retina and cochlea are post-mitotic and fully differentiated. This provides both opportunities and challenges for gene delivery. One substantial advantage is that the lack of cell division permits evaluation of changes in gene expression over time (for example due to vector loss or epigenetic changes) without concern about dilution of non-integrated vectors by cell division. Similarly, non-integrated vectors are not lost over time due to cell proliferation. In contrast, post-mitotic cells can be harder to transfect and target than dividing ones, making it more difficult to achieve cellular uptake of therapeutic vector. In addition, the non-proliferating nature of retinal and cochlear sensory cells means that in general once lost, cells are gone forever. Though research effort has been focused on combatting this by the use of stem cells or by regenerating cochlear hair cells, in general the degenerative nature of disease when post-mitotic cells are affected means the therapeutic window is narrow, as treatments delivered after too many cells have died will not be effective.

Testing and Development Benefits

From a therapeutic development standpoint, the bilateral nature of the retina and cochlea is also beneficial. Treating only one eye or cochlea allows the contralateral eye/cochlea to serve as an internal control for analysis, since the treatment rarely escapes the treated eye/cochlea. However, leakage from one ear to the other after scala tympani injections has been reported (Lalwani et al., 2002b), so restriction of therapeutic agents to a single eye or retina should be confirmed prior to interpreting resultant functional data.

Another benefit of developing and testing gene therapies in the retina and cochlea is that there are a variety of ways to perform non-invasive functional testing to assess therapeutic efficacy in both animal models and humans. The non-invasive nature of these tools also enables measurements to be performed longitudinally, essential for efficiently evaluating the duration of therapeutic effects. *In vivo* imaging in the retina includes spectral-domain optical coherence tomography (OCT) and fundus imaging/angiography to assess distribution of tagged genetic vectors and retinal structure. Non-invasive functional testing in the retina include electroretinography (ERG) to measure retinal neuronal responses, as well as optokinetic tracking (OKT) to measure visual acuity (Cai et al., 2010; Koirala et al., 2013). *In vivo* cochlear functional testing includes assessments of auditory brainstem responses (ABR) and distortion product otoacoustic emissions (DPOAE) to evaluate inner ear function. Imaging modalities can be used in parallel, including computed tomography (CT) and magnetic resonance imaging (MRI) to evaluate cochlear structure (Razek and Huang, 2012; Al-Rawy et al., 2017).

THE USE OF ANIMAL MODELS TO STUDY RETINAL AND COCHLEAR INHERITED DISEASES

Preclinical gene therapy studies are an essential component of therapeutic development. They are used to assess safety and efficacy, but are also used to assess a variety of other parameters that can have a huge influence on outcomes. These can include (1) optimizing vector content, including promoter/enhance choice, gene sequence, inclusion of intronic and untranslated region (UTR) sequences, etc.; (2) evaluating methods to prevent gene silencing, such as elimination of CpG islands, the inclusion of insulators, etc.; (3) testing methods to promote or prevent genomic integration, such as the inclusion of transposases or S/MARs; (4) evaluating vector packaging, including the use or development of various viral compaction methods, engineering novel viral serotypes to enhance tissue tropism, engineering novel non-viral vectors; (5) assessing delivery methods; (6) assessing cellular uptake and targeting of vectors, including vector/particle optimizations to enhance cellular uptake; and (7) evaluating gene expression levels, knockdown efficiency, or duration of expression. The length of this list highlights how much development and testing often occurs before genetic therapies can even be evaluated for their ability to elicit functional improvement in the target disease.

Animal studies are necessary to fully understand the effects of gene therapy in a true organ microenvironment and to investigate the toxicities involved in long-term studies. The majority of preclinical retinal and cochlear studies have used rodents as preferred animal models. Mice have well characterized genomes, with genetic, biological, and behavioral characteristics similar to humans, and their genomes can be easily manipulated which is a boon for studies of inherited diseases. Guinea pigs have also been used for evaluation of auditory dysfunction as they are susceptible to noise induced hearing loss, making them a commonly used model for optimizing gene delivery approaches and to assess the efficacy of gene-based treatments not targeted to a specific disease gene (for example delivery of growth factors for general neuroprotection) (Chen et al., 2018; Pinyon et al., 2019; Lafond et al., 2020). Final preclinical studies for both safety and efficacy use larger animal models, including pigs, dogs, and non-human primates, as these animals may better mimic the anatomy or immune system of human structures or because they offer further evidence of efficacy, for example in the RPE65 dog model (Kelley et al., 2018; Maddalena et al., 2018; Ding et al., 2019; Gyorgy et al., 2019; Gardiner et al., 2020; Ivanchenko et al., 2020).

Retinal Animal Models

There is an extensive body of literature using mouse models for retinal gene therapy (for example, there are over 1,700 PubMed hits for "mouse retinal gene therapy") and for the study of IRD disease mechanisms (e.g., Sakamoto et al., 2009; Sakami et al., 2014; Chakraborty et al., 2020; Genc et al., 2020). However, there are some differences between the mouse and human eye that make evaluation in larger animals prudent.

First, in contrast to the human retina which is developed at birth, the cells of the mouse retina are not fully produced prenatally. While the first wave of retinogenesis begins during embryonic stages (E11–E18), including horizontal cells, cone photoreceptors, some amacrine cells, and retinal ganglion cells, the second wave of retinogenesis takes place postnatally (P0–P7) with the rod photoreceptors, bipolar interneurons, and Müller glial cells (Cepko et al., 1996; Heavner and Pevny, 2012). Thus studies showing effective gene therapy after early postnatal treatment in mice may not translate well to humans. There are also structural differences in addition to the obvious size difference, most notably the larger relative size of the lens and the lack of a macula in mice. The flatter lens in human eyes (compared to mice) means that the relative intravitreal volume is quite different, critical for designing and evaluating dosing strategies. Also important is the lack of a macula in the mouse eye. The macula is both very fragile and the primary site of pathology for many IRDs, so the lack of a macula in the mouse can make it challenging to test therapies that need to target the macula or adjacent areas. In addition to lacking a macula, the rod:cone ratio in mice is much higher than in humans, making studies on cone-specific macular dystrophies more challenging (Volland et al., 2015). In spite of this, many successful preclinical studies (further discussed below) have used mice to assess gene therapies in models of cone or macular dystrophies, however, modeling the physical constraints of the macula is challenging in rodents. Testing gene therapies in non-human primates allows for a better approximation of how results will translate clinically, especially with regards to vector delivery, uptake, and gene expression (Yiu et al., 2020). Non-human primates also have a macula, which is advantageous for developing treatments for both IRDs and other macula-targeted disease such as age-related macular degeneration (Picaud et al., 2019). However, there are several limitations to using non-human primate models, including cost, ethical concerns, and perhaps most importantly, the lack of models for IRDs. One rare early exception to the lack of non-human primate genetic models was a squirrel monkey model in which trichromatic vision was restored to animals lacking the L-opsin gene by the delivery of an adeno associated virus (AAV) 2/5 vector (Mancuso et al., 2009). However, in general, functional efficacy of IRD treatments has not been evaluated in non-human primates due to the historical lack of genetic flexibility.

Slowly however, there are signs that this lack of genetic primate models may be changing due to the genome-editing capabilities of CRISPR-based genome editing strategies. Germline knockout models in non-human primates have been established (Niu et al., 2014), but the long life-span and singleton birth pattern make germline models in non-human primates practically prohibitive. More recently however, a somatic, macular knockout model of *CNGB3*-associated achromatopsia has been generated in monkeys using AAV9-mediated delivery of a CRISPR/Cas9-based construct (Lin et al., 2020). Similarly, somatic, AAV5-mediated delivery of a CRISPR/Cas9 *GUCY2D* knockdown construct was used to generate a macaque model of cone-rod dystrophy (McCullough et al., 2019). While still in the early stages, these innovative genome editing tools may pave the way for expanded use of large animal models.

Cochlear Animal Models

Mice are also widely used as genetic models for hearing loss. Mouse models of hearing loss have been created using a variety of genetic approaches, ranging from traditional knockouts to modern gene-edited germline models (see for example Charizopoulou et al., 2011; Michel et al., 2017; Schrauwen et al., 2018; Zhang H. et al., 2018). The major difference between the mouse and human auditory system is the timeline of development. Mice are naturally born deaf and don't begin to hear until ∼P14, as the final development of the organ of Corti occurs early postnatally. This is a practical disadvantage for gene therapy for congenital deafness, firstly because delivery in rodent models during the early postnatal period—while likely to be successful—would be difficult to mimic clinically since the corresponding human developmental stage occurs *in utero*. Secondly, it has been proposed that in many cases of congenital deafness the cellular and molecular disease process has already started *in utero*, making effective postnatal interventions all the more difficult to achieve. While mice are widely used in genetic studies, guinea pigs are more notably used in cochlear studies involving cochlear implants due to easier and more reproducible surgical access to the inner ear compared to other rodent models (Wysocki, 2005; DeMason et al., 2012; Mistry et al., 2014) and their susceptibility to noise-induced hearing loss. The guinea pig also has a hearing range which is more conducive to human hearing comparisons, compared to other small rodent species (Heffner and Heffner, 2007).

In addition to developmental differences, there are also anatomical differences between the mouse and human ear that are relevant to the evaluation of gene therapies. The human cochlea and labyrinth are approximately 20-fold larger than rodents and 3 to 4-fold larger than monkeys (Ren et al., 2019). Studies have found that inner ear volumes correlated with animal body mass across different species while looking at mice, rhesus monkeys, and humans (Ekdale, 2013; Dai et al., 2017) suggesting that the larger size of primates might enable them to serve as intermediate models for translation of rodent findings into humans. In addition to inner ear volume differences, there are also anatomical differences between the human and mouse ear that have implications for gene/drug delivery. Intratympanic delivery is a common way to deliver drugs destined for the inner ear in patients and rodent models, and it is thought that drugs have some permeability through the otic capsule (the bony structure surrounding the cochlea) in addition to through the round window membrane. However, the human otic capsule is significantly thicker than that in mouse and guinea pig, so human drug/therapeutic delivery throughout the length of the cochlea may not be well-modeled by rodent studies (Mikulec et al., 2009).

Assessments of audiovestibular function after saline injection into the oval or round window in non-human primates showed no evidence of toxicity as assessed by auditory function, histology, or behavior suggesting that drugs and

therapies can be delivered to the primate ear (Dai et al., 2017). Consistent with this observation, primate models have been used to evaluate genetic therapies; for example, transmastoid injection in the round window of AAV9 carrying a GFP reporter achieved >90% transduction of both inner and outer hair cells in one of their test animals but no clear transduction of hair cells in the other (Gyorgy et al., 2019). In addition, as with the retina, the lack of genetic models for hearing loss in primates has also prevented their widespread use for testing of therapeutic efficacy, and as yet, no CRISPR/Cas9 non-human primate models of SNHL have been reported.

DELIVERY METHODS FOR GENE THERAPY

Delivery of Genes to the Retina

Delivery of genetic therapies to the retina typically involves subretinal, intravitreal, or suprachoroidal injection of material, with variations on the site of entry (**Figure 3A**). Subretinal injections deliver material between the photoreceptors and the RPE. This is the most widely used method for therapies targeting photoreceptors or RPE since material is in close proximity to most target cells. However, the method is invasive, causing retinal detachment at the site of injection, and has greater potential for complications during the procedure. Intravitreal injections avoid these issues by delivering into the vitreous cavity of the eye. This procedure is in routine clinical practice for the delivery of anti-angiogenesis agents to treat neovascularization associated with diseases such as age-related macular degeneration (Todorich et al., 2014). However, material delivered intravitreally typically has poor penetration into the outer retina (Farjo et al., 2006; Dias et al., 2019), due both to the content of the vitreous itself as well as to the inner limiting membrane which forms a physical barrier between the retina and the vitreous. Identifying ways to improve delivery of genetic material to the outer retina after intravitreal delivery has been a critical research goal in the past several years. Many methods have been tried, including making genetic modifications to AAV capsids (Petrs-Silva et al., 2009; Dalkara et al., 2013), including agents to digest or disrupt the inner limiting membrane (Dalkara et al., 2009; Cehajic-Kapetanovic et al., 2011), application of electrical currents (Song et al., 2019, Song C. et al., 2020), and the inclusion of adjuvants such as tyrosine kinase inhibitors or proteasome inhibitors (Dias et al., 2019). Modification of viral capsids led to almost complete transduction of the outer retina after intravitreal injection in the mouse retina, but did not achieve this milestone in larger animal models such as dog and non-human primate (Mowat et al., 2014; Boyd et al., 2016; Ramachandran et al., 2017). This highlights an area where testing in larger animals is essential due to the relative (and absolute) difference in vitreous volume and inner limiting membrane thickness between mice and other larger animals (Matsumoto et al., 1984; Puk et al., 2006; Dalkara et al., 2009). Consistent with this, many intravitreal optimization studies are now being done in large animals, including sheep and non-human primates (Ross et al., 2020; Song H. et al., 2020), and overall this field has made significant advancements. While all of the above-mentioned studies were designed to optimize delivery of AAV-based gene therapies to the outer retina, researchers are also experimenting with ways to enhance non-viral gene delivery to the outer retina after intravitreal delivery. For example, various agents, such as chloroquine and hyaluronic acid, have been incorporated into non-viral delivery complexes in order to enhance uptake, but thus far they have met with limited success (Devoldere et al., 2019; Mashal et al., 2019).

More recently, suprachoroidal injection has gained prominence for gene delivery to the outer retina. In this method, material is delivered between the choroid and the sclera (**Figure 3A**), a region largely accessible only in larger animals. It is further complicated by the need for advanced imaging techniques, such as OCT, to visualize and inject through the use of novel microneedles (Patel et al., 2011; Kim et al., 2014; Yiu et al., 2014; Willoughby et al., 2018). The most notable advantage of this approach is the potential ability to reach the outer retina without performing a disruptive subretinal injection, and many groups are exploring this new avenue. Recently, a phase 3 clinical trial using suprachoroidal injection to deliver triamcinolone for the treatment of uveitis with macular edema reported no serious adverse events related to the treatment and positive efficacy outcomes, paving the way for future clinical use of this delivery method (Yeh et al., 2020). Various groups are testing the use of this method for retinal gene therapy with AAVs in a variety of animal models including rats, pigs, and non-human primates with generally promising results (Touchard et al., 2012; Ding et al., 2019; Yiu et al., 2020). Some groups have also been testing suprachoroidal delivery with non-viral methods, but few full published results are available yet (Kansara et al., 2020). The suprachoroidal approach has great promise for less invasive delivery to the retina, but there are concerns about penetrating through multiple layers of tissue (from the choroid through the RPE into the retina) and about initiating immune responses. One alternative approach that has been shown to induce better retinal transduction with attenuated immune responses in non-human primates is transscleral microneedle-based subretinal delivery (Yiu et al., 2020), which may be another delivery method for further exploration.

Delivery of Genes to the Cochlea

As the cochlea is encased in bone (**Figure 1C**), the delivery of material to the right location without creating significant damage that may lead to further hearing loss is a major challenge. Largely because of this delivery challenge, the field of cochlear gene therapy has been slower to develop than retinal gene therapy. Yet in the last few years, preclinical studies targeting the cochlea have rapidly increased in number, as tools and methodologies have improved. Modes of delivery for the cochlea involve cochleostomy in the lateral wall of the cochlear basal turn, canalostomy in the semicircular canal or injections through the round window, scala media, or posterior semicircular canal (**Figure 3B**). Cochleostomy, in which a hole is drilled in the basal cochlea into the endolymphatic space and material is thereby injected directly into the scala media, has been shown

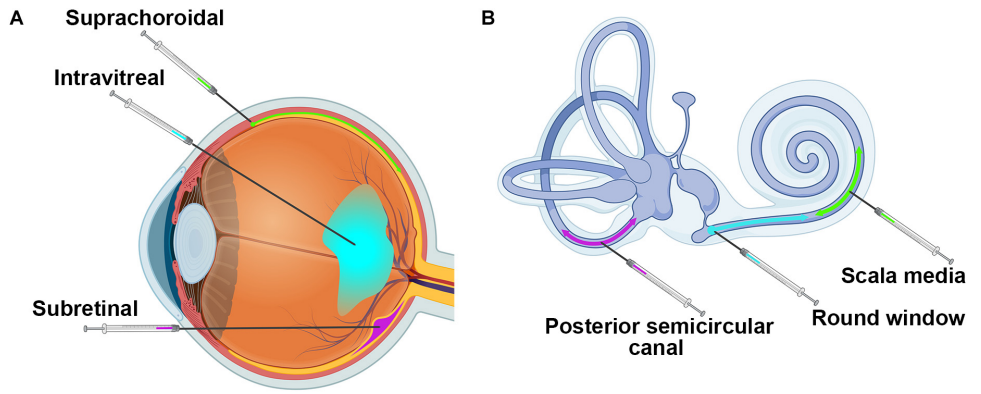

FIGURE 3 | Injection sites into the retina and the cochlea. Shown are **(A)** the three major injection sites for delivery to the retina and **(B)** the three main injection locations for the cochlea. Images were created with BioRender.com.

to be reasonably efficient in generating AAV-mediated gene expression in the inner ear (Shibata et al., 2009; Yoshimura et al., 2018). However, the procedure has been shown to have higher potential to induce hearing loss than round window membrane injection (Chien et al., 2015; Delmaghani and El-Amraoui, 2020). Round window membrane injections have been successfully used in early postnatal mice (Akil et al., 2012; Askew et al., 2015; Landegger et al., 2017; Pan et al., 2017), and very recent studies have shown this method to be effective in adult non-human primates (Gyorgy et al., 2019; Ivanchenko et al., 2020). Others have shown reporter gene or therapeutic gene expression in the murine inner ear after *in utero* injection of AAV2 into the otocyst (Miwa et al., 2013; Hu C. J. et al., 2020), potentially important given the very early onset of many forms of congenital deafness. Canalostomy involves injection in the posterior semicircular canal, and has been shown to efficiently transduce inner and outer hair cells after treatment of adult mice and is reported to have less chance of leading to damage (Suzuki et al., 2017). Canalostomy can also be combined with round window membrane injection to further improve inner ear transduction in adult mice (Yoshimura et al., 2018). While much remains to be refined in the area of cochlear gene delivery, recent successes using non-human primate models support an optimistic view for the future of human cochlear gene delivery.

GENE THERAPY IN THE RETINA AND COCHLEA

Preclinical Gene Therapy in the Retina

The earliest proof-of-principle studies for retinal gene therapy took place in the early 1990s and involved gene supplementation via transgenesis in spontaneously occurring IRD models (Lem et al., 1992; Travis et al., 1992). While paving the way for several decades of further development, even these early studies highlighted one of the most challenging, and as yet incompletely resolved, issues in retinal (and cochlear) gene therapy: levels of expression. For both recessive IRD genes as well as autosomal dominant genes associated with haploinsufficiency, generating enough expression to mediate full rescue remains problematic (Ali et al., 2000; Cai et al., 2009). Shortly after these initial transgenesis studies, efforts were made to use adenovirus to transduce the retina (Bennett et al., 1994; Li et al., 1994), but safety concerns and lack of efficiency led to a shift to the use of AAV (Ali et al., 1996). More recently, lentivirus has been used for retinal gene therapy, especially for targeting neovascularization, but lentiviruses have thus far been fairly ineffective at targeting photoreceptors (Kalesnykas et al., 2017; Becker et al., 2018; Holmgaard et al., 2019). In the intervening 25 years, AAV-mediated retinal gene therapy had been used in a vast number of different preclinical IRD models, including those targeting photoreceptors (e.g., *Rho*, *Prph2*, *Nmnat*, *Abca4*, *Cngb3, Rpgr),* retinal ganglion cells (e.g., *Xiap),* Müller cells (e.g., *Vegfa, Dp71),* bipolar cells, (*Cln3),* and the RPE, (e.g., *Rpe65, Lrat*) (Ali et al., 2000; Batten et al., 2005; Mookherjee et al., 2015; Georgiadis et al., 2016; Becker et al., 2018; Zhang et al., 2019; Barboni et al., 2020; Greenwald et al., 2020; Kleine Holthaus et al., 2020; McClements et al., 2020; Wassmer et al., 2020; **Figure 1B**). Notable successes with these models led to testing in larger animal models, in particularly RPE65 and RPGR dog studies providing further support for the efficacy of AAVs (Bainbridge et al., 2015; Beltran et al., 2015; Gardiner et al., 2020; Song C. et al., 2020).

Much recent work in the field of retinal gene therapy with AAVs has focused on evolving viral capsids to improve transduction efficiency and refine the type of cells that can be targeted. This has been successful in the mouse, where novel engineered viral capsids have been shown to be much more efficient that parent viruses (Dalkara et al., 2013; Khabou et al., 2016; Frederick et al., 2020). Because viral tropsims can also be species specific, recent work on directed evolution of AAV capsids has used the non-human primate model (Byrne et al., 2020). This approach involves injection with libraries generated with *cap* gene variants, harvesting the retina, performing PCR to enrich *cap* gene variants present (i.e., that transduced cells) and reformulating virus. This selection process is repeated several times with additional

steps included in subsequent rounds to increase diversity in *cap* genes. The exciting end result was the identification of novel AAV variants capable of efficiently transducing non-human primate cones after intravitreal injection, a key therapeutic goal that had not been achieved previously (Byrne et al., 2020).

While AAV-mediated therapies have been remarkably successful, there have been some concerns. Though largely considered safe, some studies have shown that the AAV vector is able to move from the eye to other areas of the body, from both intravitreal (Dudus et al., 1999; Han et al., 2012) and subretinal injection (Weber et al., 2003). Along with potential systemic distribution and immunogenicity, another challenge with AAV is its loading capacity. Standard AAVs can only accommodate genes which are <5 kbp (Wu et al., 2010), smaller than many IRD genes such as *USH2A* and *ABCA4*. There have been advancements in AAVs which increase capacity to 10 kbp, through dual AAV vectors. Dual AAV vectors split the load into two fragments which are then co-delivered and recombine in the target cell though either homologous recombination or trans-splicing strategies (Xu et al., 2004; Ghosh et al., 2011; Trapani et al., 2014). Though initially the efficiency of this approach was limited, additional novel strategies to overcome size limitations are being studied including the use of oversized AAV, trans-splicing dual AAV, overlapping dual AAV, and hybrid dual AAV (reviewed in Trapani, 2019). However, as a result of these potential limitations, for many years there has been interest in the development of non-viral gene delivery methods.

Though many different non-viral formulations have been successfully used to transfect cells, fewer have been successful *in vivo*. One of the most successful has been polylysine DNA nanoparticles complexed with polyethylene glycol. These nanoparticles are non-immunogenic, and have the capacity to compact up to 20 kbp of DNA (Fink et al., 2006). Importantly, they have demonstrated robust transfection, sustained for up to 15 months, in both photoreceptors and the RPE in the mouse retina (Farjo et al., 2006; Han et al., 2012; Koirala et al., 2013). This translated into improved functional outcomes in *Prph2*, *Rho, Abca4,* and *Rpe65*-associated IRD models (Cai et al., 2009, 2010; Koirala et al., 2013; Han et al., 2014, 2015). Other non-viral retinal gene therapy formulations have also recently been shown to promote improvement in murine IRD models. For example, solid lipid nanoparticles carrying the human *RS1* gene have been shown to mediate structural improvement in the mouse *Rs1h* knockout model of X-linked juvenile retinoschisis (Apaolaza et al., 2015, 2016). Another lipid-based system has also recently shown promising results. The ECO-lipid ((1-aminoethyl) iminobis[N-(oleicylcysteinyl-1-amino-ethyl) propionamide]) based system incorporates a pH sensitive endosomal escape mechanism to help promote release and preservation of DNA after uptake by cells. This system is multifunctional and can be conjugated to other compounds to facilitate targeted cell uptake. It has recently been used to deliver plasmid DNA and mediate improvements in the *Rpe65* and *Abca4* IRD models (Sun et al., 2017, 2020).

The vast majority of IRD model recue studies have involved gene supplementation to treat loss-of-function or haploinsufficiency-associated mutations. However, many IRD gene mutations are gain-of-function or dominant-negative alleles and for many years researchers have recognized the need for more complex therapies capable of knocking down mutant genes while also supplementing with the correct allele. This approach has been tested in a dog model of adRP; a mutation-independent shRNA targeting rhodopsin was paired with an RNAi-resistant human *RHO* cDNA (in AAV), and shown to promote long-term protection of retinal structure and function (Cideciyan et al., 2018). Proof-of-principle studies using RNAi-based approaches to knock down mutant transcripts have also been evaluated in mice for the treatment IRD associated with *Prph2*, *Impdh1* (RP10), *Guca1a* (cone-rod dystrophy), and *Pde6b* (RP) with varying levels of success (Tam et al., 2008; Tosi et al., 2011; Petrs-Silva et al., 2012; Jiang et al., 2013).

More recently, CRISPR/Cas9 based genome-editing approaches have gained popularity in preclinical studies to correct dominant IRD mutations. These approaches hold great promise for somatic gene editing, and various approaches have been tried. Perhaps the most obvious strategy is correcting IRD mutations using homology directed or micro-homology repair-based approaches. This has been tried in an RPGR model carrying a Cas9 transgene. AAV2/8 was used to deliver an RPGR-targeted gRNA and a region of homologous DNA carrying the corrected sequence (Hu S. et al., 2020). This study reported sequence correction in a large percentage of cells but the benefits were only apparent after ∼6 months, likely due to the overall inefficiency of homology directed repair. In addition, a challenge with homology-based repair approaches is the small carrying capacity of AAV. Designing a construct for delivery of Cas9, a homologous DNA segment for repair, and the gRNA can be challenging. To overcome this challenge, other groups have used two separate AAVs, one carrying the Cas9 and one carrying the gRNA and homologous region. This approach was used to target *Rpe65*, and reported homology-directed repair efficiencies in excess of 1%. Though this seems low, it was sufficient to mediate functional improvement. Other groups have taken advantage of an alternative repair pathway called micro-homology-mediated end joining, where a much shorter (∼20 bp) homologous region is supplied, and the whole expression cassette (Cas9, gRNAs, and homology region) fit into a single AAV. A study using this approach to target a *Gnat1* model reported improvement in light-sensitivity and visual acuity (Nishiguchi et al., 2020). An alternative approach for gain-of-function mutations is to target the mutant allele for knockout rather than correcting the mutation. While genes associated with haploinsufficiency may require concurrent gene supplementation, this approach has the benefit of relying on more efficient non-homologous end joining mechanisms rather than on the less efficient homology-based repair mechanisms. It has been tried with success in both rat and mouse models of rhodopsin-associated IRD (Bakondi et al., 2016; Giannelli et al., 2018; Patrizi et al., 2021). In addition to using CRISPR/Cas9 for gene editing, there are several

alternative approaches that utilize a dead (d)Cas9/gRNA to target a transcriptional regulator to the appropriate place in the genome. A recent exciting study used this approach to target the VPR transcriptional activator (dCas9-VPR) to the M-opsin gene (*Opn1mw*) with an *Opn1mw*-specific gRNA where it activates gene transcription (Bohm et al., 2020). When dCas9-VPR/*Opn1mw*-gRNA under the control of the rhodopsin promoter was delivered to the *Rho*$^{\pm}$ retina, researchers observed expression of M-opsin in rods, and importantly, improvements in scotopic vision and retinal structure. Genome editing in the mouse retina has also been attempted for *Pde6b*-associated RP (using electroporation), *Cep290*-associated LCA (further discussed below), and *Gucy2d*-associated cone-rod dystrophy (Ruan et al., 2017; McCullough et al., 2019; Vagni et al., 2019). Somatic genome-editing, and non-genome editing CRISPR-based therapeutic strategies are likely to become increasingly prevalent, particularly as tools to block chronic Cas9 activity, suppress immune responses, and increase the efficiency of homology directed repair are developed (reviewed in Nakamura et al., 2021).

The earliest clinical retinal gene therapy trials used AAV2 based vectors to deliver *RPE65* for the treatment of LCA (Bainbridge et al., 2008; Cideciyan et al., 2008; Maguire et al., 2008), with groups reporting varying degrees of improvement and persistence of effect. In initial phase I/II clinical trial using the AAV2/2 vector carrying *RPE65* cDNA with an RPE65 promotor, investigators observed improved visual function for 3 years (Bainbridge et al., 2008, 2015). Another group using rAAV2 carrying *h*RPE65 driven by the ubiquitous, chicken β-actin (CBA), promotor found no significant side-effects after 12 months but reported no significant improvement in vision (Hauswirth et al., 2008; Cideciyan et al., 2009). A follow-up done 6 years later saw progressive vision loss, reduced retinal sensitivity, and thinning of the photoreceptor outer nuclear layer (Jacobson et al., 2015). The third initial trial was conducted by Spark Therapeutics Inc. (Philadelphia, PA) using AAV2-hRPE65v2 with a CBA promotor (at three different doses) and reported sustained improvement after 2 years regardless of the dosage, with the greatest improvement in the younger children (Maguire et al., 2008, 2009). A few years later Spark Therapeutics Inc. released its results from a phase 3 clinical trial data using Luxturna^{TM} (voretigene neparvovec, AAV2-hRPE65v2) in patients with vision loss associated with RPE65. Bilateral subretinal injections of the highest dose tested in the prior trial found improved vision with no adverse effects or immune response after 1 year (Russell et al., 2017). This is the first phase 3 clinical trial to report significant gene therapy efficacy for IRD, and after submission to the FDA, Luxturna was approved for use and is now in clinical practice.

Since then, several other clinical trials for retinal gene therapy have been undertaken (**Figure 1B**). Recently promising results from a PhaseI/II trial for *CNGA3*-associated achromatopsia were published showing that the AAV vector was well-tolerated and initial measures of efficacy were promising, including improvement in visual acuity, contrast sensitivity, and cone function [NCT02610582 (Fischer et al., 2020)]. Many other retinal gene therapy clinical trials are currently ongoing or recruiting, targeting *RPGR* and *PDE6B*-associated RP, *CNGA3* and *CNGB3*-associated achromatopsia, *RPE65*-associated LCA, *RS1*-associated x-linked retinoschisis, and *ND4*-associated optic neuropathy[5]. All of these studies utilize an AAV-based delivery method, and thus far non-viral retinal gene therapy has not yet progressed to clinical testing. Excitingly, the first retinal gene therapy trial to use CRISPR/Cas9-based genome editing has recently started recruiting (NCT03872479). The trial, which targets *CEP290*-associated LCA is not only a milestone in retinal gene therapy, but also represents the first time CRISPR-based treatments will be delivered directly into the body in any trial, and results are eagerly anticipated. This study uses an AAV5 vector to deliver Cas9 and *CEP290* specific gRNAs and was effective in both a humanized *CEP290* mouse model and in a non-human primate model (Fischer et al., 2020).

Cochlear Gene Therapy

As in the retina, the earliest cochlear gene therapy took the form of proof-of-principle studies utilizing transgenic overexpression to rescue hearing in mutant models with hearing loss (Fujiyoshi et al., 1994; Ahmad et al., 2007). By the late 1990s, researchers were exploring ways to deliver AAVs and adenoviruses to the middle and inner ear often using the guinea pig model described above (Lalwani et al., 1996, 1998; Mondain et al., 1998). Subsequently, an extensive number of functional studies were undertaken to genetically deliver antioxidants or neurotrophic factors to the ear for the treatment or prevention of noise- and pharmaceutical-induced auditory toxicity, rather than for inherited cochlear diseases (e.g., Bowers et al., 2002; Lalwani et al., 2002a; Kawamoto et al., 2003b, 2004; Liu et al., 2008). However, neither of these approaches targets or corrects the underlying genetic defect in the case of inherited forms of hearing loss. Excitingly, in 2012 a model of congenital deafness was rescued by delivery of a gene therapy vector. This landmark study used an AAV1 vector delivered by either round window membrane injection or cochleostomy to generate Vglut3 expression in a *Vglut3* knockout mouse model of hereditary deafness. This study demonstrated almost complete rescue of ABR recordings for over one year (69 weeks was the longest time evaluated) after delivery at P10-12 (Akil et al., 2012). Subsequently, antisense oligonucleotides were used to correct splicing in an Usher syndrome mouse model (*Ush1c*) leading to functional improvements in low-frequency hearing (Lentz et al., 2013; Ponnath et al., 2018; Wang et al., 2020). Since then, some AAV-mediated functional and/or structural rescue has been reported in multiple inherited models of deafness, including those associated with mutations in the gap junction gene connexin 26, the potassium channel subunit *Kcnq1*, the stereocilia gene whirlin, the antioxidant gene *Msr3b*, the usher 1C gene harmonin, the usher 3 gene clarin, the gene *Slc26a4*, and the ion channel *Tmc1*, among others (Yu et al., 2014; Chang et al., 2015; Iizuka et al., 2015; Chien et al., 2016; Kim et al., 2016; Pan et al., 2017; Dulon et al., 2018; Nist-Lund et al., 2019; Lan et al., 2020; **Figure 1D**).

[5]https://clinicaltrials.gov/

Delivery of therapeutics to neonatal mice allows for therapeutic intervention before the organ of Corti develops fully, thus allowing for administration before early postnatal degeneration has begun, and this approach has been taken by several groups (Landegger et al., 2017; Pan et al., 2017). For example, AAV-mediated expression of *Ush1g*, a submembrane scaffold protein necessary for morphogenesis of the sensory stereocilia in cochlear hair cells, was delivered into *Sans* null mutant ($Ush1g^{-/-}$) mice at P2.5 and found to preserve hair cell function near wild-type levels (Emptoz et al., 2017). Critically, studies such as this one demonstrate that cochlear AAV-mediated gene delivery can generate protein that folds, transports, and functions properly, and that early delivery prior to full development can prevent hair cell degeneration.

Delivering AAV to older/adult mice (compared to neonates) results in a drop in efficiency and duration of expression. For example, AAV-mediated delivery of *Vglut3* led to better and longer lasting recovery after neonatal delivery (P1-3) than later delivery (P10) (Akil et al., 2012), although good results were reported for P10-12 delivery as well. A more recent investigation using a modified AAV2 vector to deliver harmonin at either P0-1 or P10-12 found improvement in the function and structure of the P0-1 treated mice with no treatment effects in those treated at P10-12 (Pan et al., 2017). However, other recent studies have achieved good gene expression in hair cells without damaging the organ of Corti after delivery in adult animals, with delivery at either 6 or 10 weeks of age (Suzuki et al., 2017; Tao et al., 2018; Yoshimura et al., 2018). Although gene expression was lower in most cases than with neonatal delivery, it is encouraging that post-development delivery for cochlear therapy is becoming more effective.

As in the retina, there has been great interest in designing optimized AAVs for cochlear delivery. This includes several new synthetic AAVs such as Anc80L65, which has shown very high efficiency in transducing both inner and outer hair cells after injections at 7 weeks of age through the posterior semicircular canal (Suzuki et al., 2017; Hu C. J. et al., 2020). As in the retina, the limited capacity of AAV (<5 kbp) is a significant limitation. This is particularly problematic since many cochlear disease genes, such as those associated with Usher syndrome, are too large to be delivered by AAV. As a result, the dual-AAV strategy, in which one AAV carried the 5′ end of the gene (in this case the congenital deafness gene otoferlin), while the second AAV carried the 3′ end has also been evaluated in the cochlea. Although this requires recombination of the two cDNAs after delivery, researchers reported stable otoferlin gene expression and improvement in hearing after dual-AAV delivery, suggesting it may be a useful therapeutic approach (Akil et al., 2019).

A number of non-viral gene therapy strategies have also been tested in the cochlea. One of the earliest was a study in which cationic liposomes were microinjected into the guinea pig cochlea, and short-term reporter gene expression was observed in the organ of Corti (Wareing et al., 1999). Lipid core nanocapsules have been evaluated for their ability to penetrate through the round window membrane for subsequent material delivery (Zou et al., 2008). Polyethyleneimine (PEI)/DNA complexes and quaternized chitosan coupled Na-carboxymethyl-beta-cyclodextrin complexes have also been tested for their ability to generate reporter gene expression, but overall transfection efficiency still has room for improvement (Tan et al., 2008; Ren et al., 2010).

CRISPR/Cas9 and somatic genome editing strategies have also begun to be applied to the cochlea. One major potential benefit of this approach is that if the endogenous gene error can be corrected in enough cells, the challenge of generating sufficient levels of expression from an exogenous transgene is circumvented. While some groups are working on optimizing individual steps in the path to effective *in vivo* cochlear genome editing (Tang et al., 2016; Kang et al., 2020; Zhao et al., 2020), other groups have directly applied genome editing technology to models of inherited deafness. Gao et al. used cochleostomy to deliver a cationic liposome formulation containing a Cas9-gRNA ribonucleoprotein (RNP) complex targeting a mutant *Tmc1* allele to the scala media at P0-2. They reported improved preservation of hair cells at 8 weeks post-injection and improved ABR thresholds at 4 weeks post-injection compared to uninjected controls (Gao et al., 2018). These exciting preliminary studies demonstrate the potential for future application to somatic genome editing for cochlear diseases.

In spite of rapid advancements in preclinical testing of cochlear gene therapies since 2012, this strategy has not made the jump to widespread clinical testing. Only one gene therapy Phase I/II safety and tolerability clinical trial for severe hearing loss has been completed (NCT02132130). The study involved intralabyrinthine delivery of recombinant adenovirus carrying the Hath1/Atoh1 transcription factor (**Figure 1D**). This transcription factor has been widely evaluated in preclinical studies to promote hair cell regeneration, however few data are available about the trial and its findings have not yet been reported, although as of September 2020, the study is listed as "completed" and results are eagerly awaited (Crowson et al., 2017).

ROLE OF TIME OF DELIVERY AND DURATION OF EFFECT ON THE OUTCOMES

While progress is being made for both retinal and cochlear gene therapy, it is necessary to remember one of the key limiting factors of gene therapy for inherited dystrophies: time. Due to the nature of degenerative hereditary diseases, unless intervention is applied early, the optimal therapeutic window will be missed. In many cases patients may not even know they have a genetic disorder until symptoms are severe enough to see their physician, at which point, the progression of the disease is often far enough along that affected cells are dead or dying. This is particularly challenging in the case of degenerations that affect neuronal cells, since there is, as yet, no effective way to regenerate or replace lost neurons (although this is a goal of the stem cell transplantation field). To a certain degree, this is an area where cochlear gene therapy is ahead of retinal gene therapy. There have been extensive preclinical studies focused

on regeneration of hair cells in deafened mice (largely in non-genetic models) by delivery of the transcription factor Math1 (also known as Hath1/Atoh1) (Kawamoto et al., 2003a; Shou et al., 2003; Baker et al., 2009; Kraft et al., 2013), and several of these studies have produced promising results. However, while cochlear regeneration of hair cells may be more within reach than photoreceptor regeneration, the earlier onset of many forms of congenital deafness (compared to inherited irreversible vision loss) counteracts some of this benefit. In studies with mice, this issue can be partially overcome by the fact that the sensory organs of the eye and ear are not fully developed at birth, and thus therapy can be administered very early in the course of the pathology. However, this advantage is lost in the transition to human patients. Individuals with an early developmental disorder would need to have therapy administered while still in the womb, which introduces additional challenges to the already complex nature of cochlear gene delivery. Regardless of the time-of-onset, early detection and intervention in patients is key to effective treatment. Clinical support for this idea comes from early reports from the LCA retinal gene therapy trials. RPE65-associated LCA is an early onset disease (in contrast to many inherited retinal diseases), and in the initial phase 1 clinical trial the greatest improvement was observed in the younger children (Maguire et al., 2008, 2009). The need for intervention early in the disease process also highlights the need for treatments and delivery strategies that do not themselves result in vision or hearing loss. Both subretinal injection and cochlear delivery methods have the potential to impair function (Wang et al., 2013), so optimizing delivery approaches should remain a key research goal.

In addition to delivery at the appropriate time in the course of the disease pathology, an additional concern is the potential need for repeat dosing. The ideal gene therapy would be effective long-term after delivery of a single dose. However, generating and maintaining sufficient levels of gene expression remains a challenge. Improving duration of expression at levels high enough to maintain functional rescue is essential (Adijanto and Naash, 2015; Hardee et al., 2017; Goswami et al., 2019; Patil et al., 2019; Wang et al., 2019).

In the case of the retina, the current measures of therapeutic longevity come from the early LCA trials, where results have been variable. Some groups reported functional visual improvement up to 3 years despite cell degeneration still taking place (Cideciyan et al., 2013; Testa et al., 2013), while other groups reported that the improvement in vision diminished in patients after 3 years (Bainbridge et al., 2015; Jacobson et al., 2015). In other cases, it has been reported that the beneficial effects are more durable, persisting at the 4 year follow-up (Maguire et al., 2019) however, different trials have used different outcome measures to assess improvement. The mechanism underlying limited duration of effects is unclear, however it has been suggested that the virally-expressed RPE65 levels declined over time to below the levels necessary to remain therapeutically relevant (Bainbridge et al., 2015). It is also possible that loss of non-transduced RPE cells led to such severe stress in the retina that the transduced RPE cells were insufficient to prevent the eventual photoreceptor degeneration. Clearly, these findings highlight both the promise and vast room for continued technical and scientific advancement needed for clinical application of retinal and cochlear gene therapy.

FUTURE PERSPECTIVES

Both the eye and cochlea are organs which have favorable anatomy for gene therapy with small sizes that can be easily treated with small doses of therapeutics, a contralateral control and easy non-invasive analytical techniques. They are also sites of many different forms of inherited hearing loss and irreversible vision loss caused by several hundred known genes, and thus they are prime targets for novel therapies. The monogenic nature of most inherited diseases of the eye and ear make gene therapy an attractive method to potentially correct causative genetic defects and cure disease, rather than just treating symptoms. There are various limitations and challenges still to face including (1) the limited number of patients carrying any given mutation, although allele-independent approaches are being developed, (2) limited carrying capacity of common viral-delivery methods, (3) the rapid progression of degeneration in some pathologies, (4) limited distribution and longevity of gene expression after single-dose treatments, (5) difficulty transfecting/transducing post-mitotic cells, and (6) the need for delivery methods that are less invasive. Yet all these areas are being actively studied, and outcomes with genetic therapies are likely to keep improving. Another area that has seen rapid progress in the last decade is genetic diagnosis. The accessibility and accuracy of genetic testing in the past few years has improved drastically (Shearer et al., 2011; Lin et al., 2012; Furutani and Shimamura, 2017; Men et al., 2017; Furutani et al., 2019). As genetic testing and screening improve, the ability to identify causative pathogenic alleles and potential at-risk individuals increases. Earlier screening and diagnosis are essential to earlier intervention.

The commonalities between the eye and the ear, coupled with the numerous syndromic genetic disorders with both an auditory and visual component mean that coordination between the fields is likely to be beneficial. Collaboration and resource sharing between groups studying both the retina and the cochlea may help advance the development of clinically relevant therapies for both vision and hearing loss, and lead to significantly improved quality of life in patients.

AUTHOR CONTRIBUTIONS

RC wrote initial draft and created the figures. SMC, MRA, and MIN were editors of final draft. All authors contributed to the article and approved the submitted version.

FUNDING

This study was supported by the grants from the National Institutes of Health (R01 EY018656, R01 EY10609, and R01 EY026499 to MIN and MRA and P20 GM125528 to SMC).

REFERENCES

Adijanto, J., and Naash, M. I. (2015). Nanoparticle-based technologies for retinal gene therapy. *Eur. J. Pharmaceut. Biopharmaceut.* 95, 353–367. doi: 10.1016/j.ejpb.2014.12.028

Ahmad, S., Tang, W., Chang, Q., Qu, Y., Hibshman, J., Li, Y., et al. (2007). Restoration of connexin26 protein level in the cochlea completely rescues hearing in a mouse model of human connexin30-linked deafness. *Proc. Natl. Acad. Sci. U.S.A.* 104, 1337–1341. doi: 10.1073/pnas.0606855104

Akil, O., Dyka, F., Calvet, C., Emptoz, A., Lahlou, G., Nouaille, S., et al. (2019). Dual AAV-mediated gene therapy restores hearing in a DFNB9 mouse model. *Proc. Natl. Acad. Sci. U.S.A.* 116, 4496–4501. doi: 10.1073/pnas.1817537116

Akil, O., Seal, R. P., Burke, K., Wang, C., Alemi, A., During, M., et al. (2012). Restoration of hearing in the VGLUT3 knockout mouse using virally mediated gene therapy. *Neuron* 75, 283–293. doi: 10.1016/j.neuron.2012.05.019

Al-Rawy, A. S., al-Shatouri, M., El Tabbakh, M., and Gad, A. A. (2017). Systematic approach by computed tomography and magnetic resonance imaging in cochlear implantation candidates in Suez Canal University Hospital. *Egypt. J. Radiol. Nucl. Med.* 48, 877–884. doi: 10.1016/j.ejrnm.2017.08.005

Ali, R. R., Reichel, M. B., Thrasher, A. J., Levinsky, R. J., Kinnon, C., Kanuga, N., et al. (1996). Gene transfer into the mouse retina mediated by an adeno-associated viral vector. *Hum. Mol. Genet.* 5, 591–594. doi: 10.1093/hmg/5.5.591

Ali, R. R., Sarra, G. M., Stephens, C., Alwis, M. D., Bainbridge, J. W., Munro, P. M., et al. (2000). Restoration of photoreceptor ultrastructure and function in retinal degeneration slow mice by gene therapy. *Nat. Genet.* 25, 306–310. doi: 10.1038/77068

Apaolaza, P. S., Del Pozo-Rodriguez, A., Solinis, M. A., Rodriguez, J. M., Friedrich, U., Torrecilla, J., et al. (2016). Structural recovery of the retina in a retinoschisin-deficient mouse after gene replacement therapy by solid lipid nanoparticles. *Biomaterials* 90, 40–49. doi: 10.1016/j.biomaterials.2016.03.004

Apaolaza, P. S., Del Pozo-Rodriguez, A., Torrecilla, J., Rodriguez-Gascon, A., Rodriguez, J. M., Friedrich, U., et al. (2015). Solid lipid nanoparticle-based vectors intended for the treatment of X-linked juvenile retinoschisis by gene therapy: in vivo approaches in Rs1h-deficient mouse model. *J. Control Release* 217, 273–283. doi: 10.1016/j.jconrel.2015.09.033

Askew, C., Rochat, C., Pan, B., Asai, Y., Ahmed, H., Child, E., et al. (2015). Tmc gene therapy restores auditory function in deaf mice. *Sci. Transl. Med.* 7:295ra108. doi: 10.1126/scitranslmed.aab1996

Bainbridge, J. W. B., Mehat, M. S., Sundaram, V., Robbie, S. J., Barker, S. E., Ripamonti, C., et al. (2015). Long-term effect of gene therapy on Leber's congenital amaurosis. *N. Engl. J. Med.* 372, 1887–1897. doi: 10.1056/NEJMoa1414221

Bainbridge, J. W. B., Smith, A. J., Barker, S. S., Robbie, S., Henderson, R., Balaggan, K., et al. (2008). Effect of gene therapy on visual function in Leber's congenital amaurosis. *N. Engl. J. Med.* 358, 2231–2239. doi: 10.1056/NEJMoa0802268

Baker, K., Brough, D. E., and Staecker, H. (2009). Repair of the vestibular system via adenovector delivery of Atoh1: a potential treatment for balance disorders. *Adv. Otorhinolaryngol.* 66, 52–63. doi: 10.1159/000218207

Bakondi, B., Lv, W., Lu, B., Jones, M. K., Tsai, Y., Kim, K. J., et al. (2016). In vivo CRISPR/Cas9 gene editing corrects retinal dystrophy in the S334ter-3 rat model of autosomal dominant retinitis pigmentosa. *Mol. Ther.* 24, 556–563. doi: 10.1038/mt.2015.220

Barboni, M. T. S., Vaillend, C., Joachimsthaler, A., Liber, A. M. P., Khabou, H., Roux, M. J., et al. (2020). Rescue of defective electroretinographic responses in Dp71-null mice with AAV-mediated reexpression of Dp71. *Invest. Ophthalmol. Vis. Sci.* 61:11. doi: 10.1167/iovs.61.2.11

Batten, M. L., Imanishi, Y., Tu, D. C., Doan, T., Zhu, L., Pang, J., et al. (2005). Pharmacological and rAAV gene therapy rescue of visual functions in a blind mouse model of Leber congenital amaurosis. *PLoS Med.* 2:e333. doi: 10.1371/journal.pmed.0020333

Becker, S., Wang, H., Simmons, A. B., Suwanmanee, T., Stoddard, G. J., Kafri, T., et al. (2018). Targeted knockdown of overexpressed VEGFA or VEGF164 in muller cells maintains retinal function by triggering different signaling mechanisms. *Sci. Rep.* 8:2003. doi: 10.1038/s41598-018-20278-4

Beltran, W. A., Cideciyan, A. V., Iwabe, S., Swider, M., Kosyk, M. S., McDaid, K., et al. (2015). Successful arrest of photoreceptor and vision loss expands the therapeutic window of retinal gene therapy to later stages of disease. *Proc. Natl. Acad. Sci. U.S.A.* 112, E5844–E5853. doi: 10.1073/pnas.1509914112

Bennett, J., Wilson, J., Sun, D., Forbes, B., and Maguire, A. (1994). Adenovirus vector-mediated in vivo gene transfer into adult murine retina. *Invest. Ophthalmol. Vis. Sci.* 35, 2535–2542.

Bohm, S., Splith, V., Riedmayr, L. M., Rotzer, R. D., Gasparoni, G., Nordstrom, K. J. V., et al. (2020). A gene therapy for inherited blindness using dCas9-VPR-mediated transcriptional activation. *Sci. Adv.* 6:eaba5614. doi: 10.1126/sciadv.aba5614

Bowers, W. J., Chen, X., Guo, H., Frisina, D. R., Federoff, H. J., and Frisina, R. D. (2002). Neurotrophin-3 transduction attenuates cisplatin spiral ganglion neuron ototoxicity in the cochlea. *Mol. Ther.* 6, 12–18. doi: 10.1006/mthe.2002.0627

Boyd, R. F., Sledge, D. G., Boye, S. L., Boye, S. E., Hauswirth, W. W., Komaromy, A. M., et al. (2016). Photoreceptor-targeted gene delivery using intravitreally administered AAV vectors in dogs. *Gene Ther.* 23, 223–230. doi: 10.1038/gt.2015.96

Byrne, L. C., Day, T. P., Visel, M., Strazzeri, J. A., Fortuny, C., Dalkara, D., et al. (2020). In vivo-directed evolution of adeno-associated virus in the primate retina. *JCI Insight* 5:e135112. doi: 10.1172/jci.insight.135112

Cai, X., Conley, S. M., Nash, Z., Fliesler, S. J., Cooper, M. J., and Naash, M. I. (2010). Gene delivery to mitotic and postmitotic photoreceptors via compacted DNA nanoparticles results in improved phenotype in a mouse model of retinitis pigmentosa. *FASEB J.* 24, 1178–1191. doi: 10.1096/fj.09-139147

Cai, X., Nash, Z., Conley, S. M., Fliesler, S. J., Cooper, M. J., and Naash, M. I. (2009). A partial structural and functional rescue of a retinitis pigmentosa model with compacted DNA nanoparticles. *PLoS One* 4:e5290. doi: 10.1371/journal.pone.0005290

Campbell, M., and Humphries, P. (2012). The blood-retina barrier: tight junctions and barrier modulation. *Adv. Exp. Med. Biol.* 763, 70–84.

Cehajic-Kapetanovic, J., Le Goff, M. M., Allen, A., Lucas, R. J., and Bishop, P. N. (2011). Glycosidic enzymes enhance retinal transduction following intravitreal delivery of AAV2. *Mol. Vis.* 17, 1771–1783.

Cepko, C. L., Austin, C. P., Yang, X. J., and Alexiades, M. (1996). Cell fate determination in the vertebrate retina. *Proc. Natl. Acad. Sci. U.S.A.* 93, 589–595. doi: 10.1073/pnas.93.2.589

Chakraborty, D., Strayve, D. G., Makia, M. S., Conley, S. M., Kakahel, M., Al-Ubaidi, M. R., et al. (2020). Novel molecular mechanisms for Prph2-associated pattern dystrophy. *FASEB J.* 34, 1211–1230. doi: 10.1096/fj.201901888R

Chang, Q., Wang, J., Li, Q., Kim, Y., Zhou, B., Wang, Y., et al. (2015). Virally mediated Kcnq1 gene replacement therapy in the immature scala media restores hearing in a mouse model of human Jervell and Lange-Nielsen deafness syndrome. *EMBO Mol. Med.* 7, 1077–1086. doi: 10.15252/emmm.201404929

Charizopoulou, N., Lelli, A., Schraders, M., Ray, K., Hildebrand, M. S., Ramesh, A., et al. (2011). Gipc3 mutations associated with audiogenic seizures and sensorineural hearing loss in mouse and human. *Nat. Commun.* 2:201. doi: 10.1038/ncomms1200

Chen, H., Xing, Y., Xia, L., Chen, Z., Yin, S., and Wang, J. (2018). AAV-mediated NT-3 overexpression protects cochleae against noise-induced synaptopathy. *Gene Ther.* 25, 251–259. doi: 10.1038/s41434-018-0012-0

Chien, W. W., Isgrig, K., Roy, S., Belyantseva, I. A., Drummond, M. C., May, L. A., et al. (2016). Gene therapy restores hair cell stereocilia morphology in inner ears of deaf Whirler mice. *Mol. Ther.* 24, 17–25. doi: 10.1038/mt.2015.150

Chien, W. W., McDougald, D. S., Roy, S., Fitzgerald, T. S., and Cunningham, L. L. (2015). Cochlear gene transfer mediated by adeno-associated virus: comparison of two surgical approaches. *Laryngoscope* 125, 2557–2564. doi: 10.1002/lary.25317

Cideciyan, A. V., Aleman, T. S., Boye, S. L., Schwartz, S. B., Kaushal, S., Roman, A. J., et al. (2008). Human gene therapy for RPE65 isomerase deficiency activates the retinoid cycle of vision but with slow rod kinetics. *Proc. Natl. Acad. Sci. U.S.A.* 105, 15112–15117. doi: 10.1073/pnas.0807027105

Cideciyan, A. V., Hauswirth, W. W., Aleman, T. S., Kaushal, S., Schwartz, S. B., Boye, S. L., et al. (2009). Human RPE65 gene therapy for Leber congenital amaurosis: persistence of early visual improvements and safety at 1 year. *Hum. Gene Ther.* 20, 999–1004. doi: 10.1089/hum.2009.086

Cideciyan, A. V., Jacobson, S. G., Beltran, W. A., Sumaroka, A., Swider, M., Iwabe, S., et al. (2013). Human retinal gene therapy for Leber congenital amaurosis

shows advancing retinal degeneration despite enduring visual improvement. *Proc. Natl. Acad. Sci. U.S.A.* 110, E517–E525. doi: 10.1073/pnas.1218933110

Cideciyan, A. V., Sudharsan, R., Dufour, V. L., Massengill, M. T., Iwabe, S., Swider, M., et al. (2018). Mutation-independent rhodopsin gene therapy by knockdown and replacement with a single AAV vector. *Proc. Natl. Acad. Sci. U.S.A.* 115, E8547–E8556. doi: 10.1073/pnas.1805055115

Coca-Prados, M. (2014). The blood-aqueous barrier in health and disease. *J. Glaucoma* 23(8 Suppl. 1), S36–S38. doi: 10.1097/IJG.0000000000000107

Colavito, D., Maritan, V., Suppiej, A., Del Giudice, E., Mazzarolo, M., Miotto, S., et al. (2017). Non-syndromic isolated dominant optic atrophy caused by the p.R468C mutation in the AFG3 like matrix AAA peptidase subunit 2 gene. *Biomed. Rep.* 7, 451–454. doi: 10.3892/br.2017.987

Crowson, M. G., Hertzano, R., and Tucci, D. L. (2017). Emerging therapies for sensorineural hearing loss. *Otol. Neurotol.* 38, 792–803. doi: 10.1097/MAO.0000000000001427

Cunha-Vaz, J., Bernardes, R., and Lobo, C. (2011). Blood-retinal barrier. *Eur. J. Ophthalmol.* 21, S3–S9. doi: 10.5301/Ejo.2010.6049

Dai, C. K., Lehar, M., Sun, D. Q., Swarthout, L., Carey, J. P., MacLachlan, T., et al. (2017). Rhesus cochlear and vestibular functions are preserved after inner ear injection of saline volume sufficient for gene therapy delivery. *Jaro J. Assoc. Res. Otolaryngol.* 18, 601–617. doi: 10.1007/s10162-017-0628-6

Dalkara, D., Byrne, L. C., Klimczak, R. R., Visel, M., Yin, L., Merigan, W. H., et al. (2013). In vivo-directed evolution of a new adeno-associated virus for therapeutic outer retinal gene delivery from the vitreous. *Sci. Transl. Med.* 5:189ra76. doi: 10.1126/scitranslmed.3005708

Dalkara, D., Kolstad, K. D., Caporale, N., Visel, M., Klimczak, R. R., Schaffer, D. V., et al. (2009). Inner limiting membrane barriers to AAV-mediated retinal transduction from the vitreous. *Mol. Ther.* 17, 2096–2102. doi: 10.1038/mt.2009.181

Delmaghani, S., and El-Amraoui, A. (2020). Inner ear gene therapies take off: current promises and future challenges. *J. Clin. Med.* 9:2309. doi: 10.3390/jcm9072309

DeMason, C., Choudhury, B., Ahmad, F., Fitzpatrick, D. C., Wang, J., Buchman, C. A., et al. (2012). Electrophysiological properties of cochlear implantation in the gerbil using a flexible array. *Ear Hear.* 33, 534–542. doi: 10.1097/AUD.0b013e3182498c28

Devoldere, J., Wels, M., Peynshaert, K., Dewitte, H., De Smedt, S. C., and Remaut, K. (2019). The obstacle course to the inner retina: hyaluronic acid-coated lipoplexes cross the vitreous but fail to overcome the inner limiting membrane. *Eur. J. Pharm. Biopharm.* 141, 161–171. doi: 10.1016/j.ejpb.2019.05.023

Di Bella, D., Lazzaro, F., Brusco, A., Plumari, M., Battaglia, G., Pastore, A., et al. (2010). Mutations in the mitochondrial protease gene AFG3L2 cause dominant hereditary ataxia SCA28. *Nat. Genet.* 42, 313–321. doi: 10.1038/ng.544

Dias, M. S., Araujo, V. G., Vasconcelos, T., Li, Q., Hauswirth, W. W., Linden, R., et al. (2019). Retina transduction by rAAV2 after intravitreal injection: comparison between mouse and rat. *Gene Ther.* 26, 479–490. doi: 10.1038/s41434-019-0100-9

Ding, K., Shen, J., Hafiz, Z., Hackett, S. F., Silva, R. L. E., Khan, M., et al. (2019). AAV8-vectored suprachoroidal gene transfer produces widespread ocular transgene expression. *J. Clin. Invest.* 129, 4901–4911. doi: 10.1172/JCI129085

Dror, A. A., and Avraham, K. B. (2010). Hearing impairment: a panoply of genes and functions. *Neuron* 68, 293–308. doi: 10.1016/j.neuron.2010.10.011

Dudus, L., Anand, V., Acland, G. M., Chen, S. J., Wilson, J. M., Fisher, K. J., et al. (1999). Persistent transgene product in retina, optic nerve and brain after intraocular injection of rAAV. *Vis. Res.* 39, 2545–2553. doi: 10.1016/s0042-6989(98)00308-3

Dulon, D., Papal, S., Patni, P., Cortese, M., Vincent, P. F., Tertrais, M., et al. (2018). Clarin-1 gene transfer rescues auditory synaptopathy in model of Usher syndrome. *J. Clin. Invest.* 128, 3382–3401. doi: 10.1172/JCI94351

Duman, D., and Tekin, M. (2012). Autosomal recessive nonsyndromic deafness genes: a review. *Front. Biosci. Landmark* 17:2213–2236. doi: 10.2741/4046

Ekdale, E. G. (2013). Comparative anatomy of the bony labyrinth (Inner Ear) of placental mammals. *PLoS One* 8:e66624. doi: 10.1371/journal.pone.0066624

El-Amraoui, A., and Petit, C. (2014). The retinal phenotype of Usher syndrome: pathophysiological insights from animal models. *C. R. Biol.* 337, 167–177. doi: 10.1016/j.crvi.2013.12.004

Emptoz, A., Michel, V., Lelli, A., Akil, O., de Monvel, J. B., Lahlou, G., et al. (2017). Local gene therapy durably restores vestibular function in a mouse model of Usher syndrome type 1G. *Proc. Natl. Acad. Sci. U.S.A.* 114, 9695–9700. doi: 10.1073/pnas.1708894114

Farjo, R., Skaggs, J., Quiambao, A. B., Cooper, M. J., and Naash, M. I. (2006). Efficient non-viral ocular gene transfer with compacted DNA nanoparticles. *PLoS One* 1:e38. doi: 10.1371/journal.pone.0000038

Ferrari, S., Di Iorio, E., Barbaro, V., Ponzin, D., Sorrentino, F. S., and Parmeggiani, F. (2011). Retinitis pigmentosa: genes and disease mechanisms. *Curr. Genomics* 12, 238–249. doi: 10.2174/138920211795860107

Fink, T. L., Klepcyk, P. J., Oette, S. M., Gedeon, C. R., Hyatt, S. L., Kowalczyk, T. H., et al. (2006). Plasmid size up to 20 kbp does not limit effective in vivo lung gene transfer using compacted DNA nanoparticles. *Gene Ther.* 13, 1048–1051. doi: 10.1038/sj.gt.3302761

Fischer, M. D., Michalakis, S., Wilhelm, B., Zobor, D., Muehlfriedel, R., Kohl, S., et al. (2020). Safety and vision outcomes of subretinal gene therapy targeting cone photoreceptors in achromatopsia: a nonrandomized controlled trial. *Jama Ophthalmol.* 138, 643–651. doi: 10.1001/jamaophthalmol.2020.1032

Frederick, A., Sullivan, J., Liu, L., Adamowicz, M., Lukason, M., Raymer, J., et al. (2020). Engineered capsids for efficient gene delivery to the retina and cornea. *Hum. Gene Ther.* 31, 756–774. doi: 10.1089/hum.2020.070

Fujiyoshi, T., Hood, L., and Yoo, T. J. (1994). Restoration of brain stem auditory-evoked potentials by gene transfer in shiverer mice. *Ann. Otolrhinollaryngol.* 103, 449–456. doi: 10.1177/000348949410300606

Fukui, T., Yamamoto, S., Nakano, K., Tsujikawa, M., Morimura, H., Nishida, K., et al. (2002). ABCA4 gene mutations in Japanese patients with Stargardt disease and retinitis pigmentosa. *Invest. Ophthalmol. Vis. Sci.* 43, 2819–2824.

Furutani, E., Newburger, P. E., and Shimamura, A. (2019). Neutropenia in the age of genetic testing: advances and challenges. *Am. J. Hematol.* 94, 384–393. doi: 10.1002/ajh.25374

Furutani, E., and Shimamura, A. (2017). Germline genetic predisposition to hematologic malignancy. *J. Clin. Oncol.* 35, 1018–1028. doi: 10.1200/Jco.2016.70.8644

Gao, X., Tao, Y., Lamas, V., Huang, M., Yeh, W. H., Pan, B., et al. (2018). Treatment of autosomal dominant hearing loss by in vivo delivery of genome editing agents. *Nature* 553, 217–221. doi: 10.1038/nature25164

Gardiner, K. L., Cideciyan, A. V., Swider, M., Dufour, V. L., Sumaroka, A., Komaromy, A. M., et al. (2020). Long-term structural outcomes of late-stage RPE65 gene therapy. *Mol. Ther.* 28, 266–278. doi: 10.1016/j.ymthe.2019.08.013

Genc, A. M., Makia, M. S., Sinha, T., Conley, S. M., Al-Ubaidi, M. R., and Naash, M. I. (2020). Elimination of a retinal riboflavin binding protein exacerbates degeneration in a model of cone-rod dystrophy. *Invest. Ophthalmol. Vis. Sci.* 61:17. doi: 10.1167/iovs.61.6.17

Georgiadis, A., Duran, Y., Ribeiro, J., Abelleira-Hervas, L., Robbie, S. J., Sunkel-Laing, B., et al. (2016). Development of an optimized AAV2/5 gene therapy vector for Leber congenital amaurosis owing to defects in RPE65. *Gene Ther.* 23, 857–862. doi: 10.1038/gt.2016.66

Ghosh, A., Yue, Y. P., and Duan, D. S. (2011). Efficient transgene reconstitution with hybrid dual AAV vectors carrying the minimized bridging sequences. *Hum. Gene Ther.* 22, 77–83. doi: 10.1089/hum.2010.122

Giannelli, S. G., Luoni, M., Castoldi, V., Massimino, L., Cabassi, T., Angeloni, D., et al. (2018). Cas9/sgRNA selective targeting of the P23H Rhodopsin mutant allele for treating retinitis pigmentosa by intravitreal AAV9.PHP.B-based delivery. *Hum. Mol. Genet.* 27, 761–779. doi: 10.1093/hmg/ddx438

Goswami, R., Subramanian, G., Silayeva, L., Newkirk, I., Doctor, D., Chawla, K., et al. (2019). Gene therapy leaves a vicious cycle. *Front. Oncol.* 9:297. doi: 10.3389/fonc.2019.00297

Greenwald, S. H., Brown, E. E., Scandura, M. J., Hennessey, E., Farmer, R., Pawlyk, B. S., et al. (2020). Gene therapy preserves retinal structure and function in a mouse model of NMNAT1-associated retinal degeneration. *Mol. Ther. Methods Clin. Dev.* 18, 582–594. doi: 10.1016/j.omtm.2020.07.003

Gyorgy, B., Meijer, E. J., Ivanchenko, M. V., Tenneson, K., Emond, F., Hanlon, K. S., et al. (2019). Gene transfer with AAV9-PHP.B rescues hearing in a mouse model of usher syndrome 3A and transduces hair cells in a non-human primate. *Mol. Ther. Methods Clin. Dev.* 13, 1–13. doi: 10.1016/j.omtm.2018.11.003

Haddad, S., Chen, C. A., Santangelo, S. L., and Seddon, J. M. (2006). The genetics of age-related macular degeneration: a review of progress to date. *Surv. Ophthalmol.* 51, 316–363. doi: 10.1016/j.survophthal.2006.05.001

Han, Z., Banworth, M. J., Makkia, R., Conley, S. M., Al-Ubaidi, M. R., Cooper, M. J., et al. (2015). Genomic DNA nanoparticles rescue rhodopsin-associated retinitis pigmentosa phenotype. *FASEB J.* 29, 2535–2544. doi: 10.1096/fj.15-270363

Han, Z., Conley, S. M., Makkia, R., Guo, J., Cooper, M. J., and Naash, M. I. (2012). Comparative analysis of DNA nanoparticles and AAVs for ocular gene delivery. *PLoS One* 7:e52189. doi: 10.1371/journal.pone.0052189

Han, Z., Conley, S. M., and Naash, M. I. (2014). Gene therapy for Stargardt disease associated with ABCA4 gene. *Adv. Exp. Med. Biol.* 801, 719–724. doi: 10.1007/978-1-4614-3209-8_90

Hanany, M., Rivolta, C., and Sharon, D. (2020). Worldwide carrier frequency and genetic prevalence of autosomal recessive inherited retinal diseases. *Proc. Natl. Acad. Sci. U.S.A.* 117, 2710–2716. doi: 10.1073/pnas.1913179117

Hardee, C. L., Arevalo-Soliz, L. M., Hornstein, B. D., and Zechiedrich, L. (2017). Advances in non-viral DNA vectors for gene therapy. *Genes* 8:65. doi: 10.3390/genes8020065

Hauswirth, W. W., Aleman, T. S., Kaushal, S., Cideciyan, A. V., Schwartz, S. B., Wang, L. L., et al. (2008). Treatment of Leber congenital amaurosis due to RPE65 mutations by ocular subretinal injection of adeno-associated virus gene vector: short-term results of a Phase I Trial. *Hum. Gene Ther.* 19, 979–990. doi: 10.1089/hum.2008.107

Heavner, W., and Pevny, L. (2012). Eye development and retinogenesis. *Cold Spring Harb. Perspect. Biol.* 4:a008391. doi: 10.1101/cshperspect.a008391

Heffner, H. E., and Heffner, R. S. (2007). Hearing ranges of laboratory animals. *J. Am. Assoc. Lab. Anim. Sci.* 46, 20–22.

Heimer, G., Gregited byory, A., Hogarth, P., Hayflick, S., Ben Zeev, B., Stephens, K., et al. (1993). "MECR-Related Neurologic Disorder," in *GeneReviews((R))*, eds M. P. Adam, H. H. Ardinger, R. A. Pagon, S. E. Wallace, and L. J. H. Bean (Seattle, WA: University of Washington).

Holmgaard, A., Alsing, S., Askou, A. L., and Corydon, T. J. (2019). CRISPR gene therapy of the eye: targeted knockout of vegfa in mouse retina by lentiviral delivery. *Methods Mol. Biol.* 1961, 307–328. doi: 10.1007/978-1-4939-9170-9_19

Hu, C. J., Lu, Y. C., Tsai, Y. H., Cheng, H. Y., Takeda, H., Huang, C. Y., et al. (2020). Efficient in utero gene transfer to the mammalian inner ears by the synthetic adeno-associated viral vector Anc80L65. *Mol. Ther. Methods Clin. Dev.* 18, 493–500. doi: 10.1016/j.omtm.2020.06.019

Hu, S., Du, J., Chen, N., Jia, R., Zhang, J., Liu, X., et al. (2020). In Vivo CRISPR/Cas9-mediated genome editing mitigates photoreceptor degeneration in a mouse model of X-Linked retinitis pigmentosa. *Invest. Ophthalmol. Vis. Sci.* 61:31. doi: 10.1167/iovs.61.4.31

Iizuka, T., Kamiya, K., Gotoh, S., Sugitani, Y., Suzuki, M., Noda, T., et al. (2015). Perinatal Gjb2 gene transfer rescues hearing in a mouse model of hereditary deafness. *Hum. Mol. Genet.* 24, 3651–3661. doi: 10.1093/hmg/ddv109

Ivanchenko, M. V., Hanlon, K. S., Devine, M. K., Tenneson, K., Emond, F., Lafond, J. F., et al. (2020). Preclinical testing of AAV9-PHP.B for transgene expression in the non-human primate cochlea. *Hear. Res.* 394:107930. doi: 10.1016/j.heares.2020.107930

Jacobson, S. G., Cideciyan, A. V., Roman, A. J., Sumaroka, A., Schwartz, S. B., Heon, E., et al. (2015). Improvement and decline in vision with gene therapy in childhood blindness. *N. Engl. J. Med.* 372, 1920–1926. doi: 10.1056/NEJMoa1412965

Jiang, L., Li, T. Z., Boye, S. E., Hauswirth, W. W., Frederick, J. M., and Baehr, W. (2013). RNAi-mediated gene suppression in a GCAP1(L151F) cone-rod dystrophy mouse model. *PLoS One* 8:e57676. doi: 10.1371/journal.pone.0057676

Kalesnykas, G., Kokki, E., Alasaarela, L., Lesch, H. P., Tuulos, T., Kinnunen, K., et al. (2017). Comparative study of adeno-associated virus, adenovirus, bacu lovirus and lentivirus vectors for gene therapy of the eyes. *Curr. Gene Ther.* 17, 235–247. doi: 10.2174/1566523217666171003170348

Kang, W., Zhao, X., Sun, Z., Dong, T., Jin, C., Tong, L., et al. (2020). Adeno-associated virus vector enables safe and efficient Cas9 activation in neonatal and adult Cas9 knockin murine cochleae. *Gene Ther.* 27, 392–405. doi: 10.1038/s41434-020-0124-1

Kansara, V., Muya, L., Wan, C. R., and Ciulla, T. A. (2020). Suprachoroidal delivery of viral and nonviral gene therapy for retinal diseases. *J. Ocul. Pharmacol. Ther.* 36, 384–392. doi: 10.1089/jop.2019.0126

Kawamoto, K., Ishimoto, S., Minoda, R., Brough, D. E., and Raphael, Y. (2003a). Math1 gene transfer generates new cochlear hair cells in mature guinea pigs in vivo. *J. Neurosci.* 23, 4395–4400.

Kawamoto, K., Sha, S. H., Minoda, R., Izumikawa, M., Kuriyama, H., Schacht, J., et al. (2004). Antioxidant gene therapy can protect hearing and hair cells from ototoxicity. *Mol. Ther.* 9, 173–181. doi: 10.1016/j.ymthe.2003.11.020

Kawamoto, K., Yagi, M., Stover, T., Kanzaki, S., and Raphael, Y. (2003b). Hearing and hair cells are protected by adenoviral gene therapy with TGF-beta1 and GDNF. *Mol. Ther.* 7, 484–492. doi: 10.1016/s1525-0016(03)00058-3

Kelley, R. A., Conley, S. M., Makkia, R., Watson, J. N., Han, Z., Cooper, M. J., et al. (2018). DNA nanoparticles are safe and nontoxic in non-human primate eyes. *Int. J. Nanomed.* 13, 1361–1379. doi: 10.2147/IJN.S157000

Khabou, H., Desrosiers, M., Winckler, C., Fouquet, S., Auregan, G., Bemelmans, A. P., et al. (2016). Insight into the mechanisms of enhanced retinal transduction by the engineered AAV2 capsid variant -7m8. *Biotechnol. Bioeng.* 113, 2712–2724. doi: 10.1002/bit.26031

Kim, M. A., Cho, H. J., Bae, S. H., Lee, B., Oh, S. K., Kwon, T. J., et al. (2016). Methionine sulfoxide reductase B3-targeted in utero gene therapy rescues hearing function in a mouse model of congenital sensorineural hearing loss. *Antioxid. Redox Signal.* 24, 590–602. doi: 10.1089/ars.2015.6442

Kim, Y. C., Edelhauser, H. F., and Prausnitz, M. R. (2014). Targeted delivery of antiglaucoma drugs to the supraciliary space using microneedles. *Invest. Ophthalmol. Vis. Sci.* 55, 7387–7397. doi: 10.1167/iovs.14-14651

Kleine Holthaus, S. M., Aristorena, M., Maswood, R., Semenyuk, O., Hoke, J., Hare, A., et al. (2020). Gene therapy targeting the inner retina rescues the retinal phenotype in a mouse model of CLN3 batten disease. *Hum. Gene Ther.* 31, 709–718. doi: 10.1089/hum.2020.038

Klevering, B. J., Maugeri, A., Wagner, A., Go, S. L., Vink, C., Cremers, F. P. M., et al. (2004). Three families displaying the combination of Stargardt's disease with cone-rod dystrophy or retinitis pigmentosa. *Ophthalmology* 111, 546–553. doi: 10.1016/j.ophtha.2003.06.010

Koirala, A., Conley, S. M., Makkia, R., Liu, Z., Cooper, M. J., Sparrow, J. R., et al. (2013). Persistence of non-viral vector mediated RPE65 expression: case for viability as a gene transfer therapy for RPE-based diseases. *J. Control Release* 172, 745–752. doi: 10.1016/j.jconrel.2013.08.299

Kraft, S., Hsu, C., Brough, D. E., and Staecker, H. (2013). Atoh1 induces auditory hair cell recovery in mice after ototoxic injury. *Laryngoscope* 123, 992–999. doi: 10.1002/lary.22171

Lafond, J. F., Tenneson, K., Emond, F., Foucault, C., Vogel, S., and Boubekeur, H. (2020). Evaluation of a model of long-term middle ear catheterization for repeat infusion administration and cochlear hair cell injury in guinea pigs. *Toxicol. Pathol.* 48, 586–592. doi: 10.1177/0192623320916635

Lalwani, A. K., Han, J. J., Castelein, C. M., Carvalho, G. J., and Mhatre, A. N. (2002a). In vitro and in vivo assessment of the ability of adeno-associated virus-brain-derived neurotrophic factor to enhance spiral ganglion cell survival following ototoxic insult. *Laryngoscope* 112(8 Pt 1), 1325–1334. doi: 10.1097/00005537-200208000-00001

Lalwani, A. K., Jero, J., and Mhatre, A. N. (2002b). Current issues in cochlear gene transfer. *Audiol. Neuro Otol.* 7, 146–151. doi: 10.1159/000058300

Lalwani, A. K., Walsh, B. J., Reilly, P. G., Muzyczka, N., and Mhatre, A. N. (1996). Development of in vivo gene therapy for hearing disorders: introduction of adeno-associated virus into the cochlea of the guinea pig. *Gene Ther.* 3, 588–592.

Lalwani, A., Walsh, B., Reilly, P., Carvalho, G., Zolotukhin, S., Muzyczka, N., et al. (1998). Long-term in vivo cochlear transgene expression mediated by recombinant adeno-associated virus. *Gene Ther.* 5, 277–281. doi: 10.1038/sj.gt.3300573

Lan, Y. Y., Tao, Y., Wang, Y. F., Ke, J. Z., Yang, Q. X., Liu, X. Y., et al. (2020). Recent development of AAV-based gene therapies for inner ear disorders. *Gene Ther.* 27, 329–337. doi: 10.1038/s41434-020-0155-7

Landegger, L. D., Pan, B., Askew, C., Wassmer, S. J., Gluck, S. D., Galvin, A., et al. (2017). A synthetic AAV vector enables safe and efficient gene transfer to the mammalian inner ear. *Nat. Biotechnol.* 35, 280–284. doi: 10.1038/nbt.3781

Lem, J., Flannery, J. G., Li, T., Applebury, M. L., Farber, D. B., and Simon, M. I. (1992). Retinal degeneration is rescued in transgenic rd mice by expression of the cGMP phosphodiesterase beta subunit. *Proc. Natl. Acad. Sci. U.S.A.* 89, 4422–4426. doi: 10.1073/pnas.89.10.4422

Lentz, J. J., Jodelka, F. M., Hinrich, A. J., McCaffrey, K. E., Farris, H. E., Spalitta, M. J., et al. (2013). Rescue of hearing and vestibular function by antisense oligonucleotides in a mouse model of human deafness. *Nat. Med.* 19, 345–350. doi: 10.1038/nm.3106

Li, T., Adamian, M., Roof, D. J., Berson, E. L., Dryja, T. P., Roessler, B. J., et al. (1994). In vivo transfer of a reporter gene to the retina mediated by an adenoviral vector. *Invest. Ophthalmol. Vis. Sci.* 35, 2543–2549.

Lin, Q., Lv, J. N., Wu, K. C., Zhang, C. J., Liu, Q., and Jin, Z. B. (2020). Generation of nonhuman primate model of cone dysfunction through in situ AAV-Mediated CNGB3 ablation. *Mol. Ther. Methods Clin. Dev.* 18, 869–879. doi: 10.1016/j.omtm.2020.08.007

Lin, X., Tang, W. X., Ahmad, S., Lu, J. Q., Colby, C. C., Zhu, J., et al. (2012). Applications of targeted gene capture and next-generation sequencing technologies in studies of human deafness and other genetic disabilities. *Hear. Res.* 288, 67–76. doi: 10.1016/j.heares.2012.01.004

Liu, Y., Okada, T., Shimazaki, K., Sheykholeslami, K., Nomoto, T., Muramatsu, S. I., et al. (2008). Protection against aminoglycoside-induced ototoxicity by regulated AAV vector-mediated GDNF gene transfer into the cochlea. *Mol. Ther.* 16, 474–480. doi: 10.1038/sj.mt.6300379

Maddalena, A., Tornabene, P., Tiberi, P., Minopoli, R., Manfredi, A., Mutarelli, M., et al. (2018). Triple vectors expand AAV transfer capacity in the retina. *Mol. Ther.* 26, 524–541. doi: 10.1016/j.ymthe.2017.11.019

Maeda, A., Mandai, M., and Takahashi, M. (2019). Gene and induced pluripotent stem cell therapy for retinal diseases. *Annu. Rev. Genomics Hum. Genet.* 20, 201–216. doi: 10.1146/annurev-genom-083118-015043

Maguire, A. M., High, K. A., Auricchio, A., Wright, J. F., Pierce, E. A., Testa, F., et al. (2009). Age-dependent effects of RPE65 gene therapy for Leber's congenital amaurosis: a phase 1 dose-escalation trial. *Lancet* 374, 1597–1605. doi: 10.1016/S0140-6736(09)61836-5

Maguire, A. M., Russell, S., Wellman, J. A., Chung, D. C., Yu, Z. F., Tillman, A., et al. (2019). Efficacy, safety, and durability of voretigene neparvovec-rzyl in RPE65 mutation-associated inherited retinal dystrophy: results of phase 1 and 3 trials. *Ophthalmology* 126, 1273–1285. doi: 10.1016/j.ophtha.2019.06.017

Maguire, A. M., Simonelli, F., Pierce, E. A., Pugh, E. N., Mingozzi, F., Bennicelli, J., et al. (2008). Safety and efficacy of gene transfer for Leber's congenital amaurosis. *N. Engl. J. Med.* 358, 2240–2248. doi: 10.1056/NEJMoa0802315

Mancuso, K., Hauswirth, W. W., Li, Q., Connor, T. B., Kuchenbecker, J. A., Mauck, M. C., et al. (2009). Gene therapy for red-green colour blindness in adult primates. *Nature* 461, 784–787. doi: 10.1038/nature08401

Manoussaki, D., Dimitriadis, E. K., and Chadwick, R. S. (2006). Cochlea's graded curvature effect on low frequency waves. *Phys. Rev. Lett.* 96:088701. doi: 10.1103/PhysRevLett.96.088701

Marazita, M. L., Ploughman, L. M., Rawlings, B., Remington, E., Arnos, K. S., and Nance, W. E. (1993). Genetic epidemiological studies of early-onset deafness in the U.S. school-age population. *Am. J. Med. Genet.* 46, 486–491. doi: 10.1002/ajmg.1320460504

Mashal, M., Attia, N., Martinez-Navarrete, G., Soto-Sanchez, C., Fernandez, E., Grijalvo, S., et al. (2019). Gene delivery to the rat retina by non-viral vectors based on chloroquine-containing cationic niosomes. *J. Control Release* 304, 181–190. doi: 10.1016/j.jconrel.2019.05.010

Mathur, P. D., and Yang, J. (2019). Usher syndrome and non-syndromic deafness: functions of different whirlin isoforms in the cochlea, vestibular organs, and retina. *Hear. Res.* 375, 14–24. doi: 10.1016/j.heares.2019.02.007

Mathur, P., and Yang, J. (2015). Usher syndrome: hearing loss, retinal degeneration and associated abnormalities. *Biochim. Biophys. Acta* 1852, 406–420. doi: 10.1016/j.bbadis.2014.11.020

Matsumoto, B., Blanks, J. C., and Ryan, S. J. (1984). Topographic variations in the rabbit and primate internal limiting membrane. *Invest. Ophthalmol. Vis. Sci.* 25, 71–82.

McClements, M. E., Barnard, A. R., Charbel Issa, P., and MacLaren, R. E. (2020). Assessment of AAV dual vector safety in theAbca4 (-/-) mouse model of stargardt disease. *Transl. Vis. Sci. Technol.* 9:20. doi: 10.1167/tvst.9.7.20

McCullough, K. T., Boye, S. L., Fajardo, D., Calabro, K., Peterson, J. J., Strang, C. E., et al. (2019). Somatic gene editing of GUCY2D by AAV-CRISPR/Cas9 alters retinal structure and function in mouse and macaque. *Hum. Gene Ther.* 30, 571–589. doi: 10.1089/hum.2018.193

Men, C. J., Bujakowska, K. M., Comander, J., Place, E., Bedoukian, E. C., Zhu, X. S., et al. (2017). The importance of genetic testing as demonstrated by two cases of CACNA1F-associated retinal generation misdiagnosed as LCA. *Mol. Vis.* 23, 695–706.

Michel, V., Booth, K. T., Patni, P., Cortese, M., Azaiez, H., Bahloul, A., et al. (2017). CIB2, defective in isolated deafness, is key for auditory hair cell mechanotransduction and survival. *Embo Mol. Med.* 9, 1711–1731. doi: 10.15252/emmm.201708087

Mikulec, A. A., Plontke, S. K., Hartsock, J. J., and Salt, A. N. (2009). Entry of substances into perilymph through the bone of the otic capsule after intratympanic applications in guinea pigs: implications for local drug delivery in humans. *Otol. Neurotol.* 30, 131–138. doi: 10.1097/mao.0b013e318191bff8

Millan, J. M., Aller, E., Jaijo, T., Blanco-Kelly, F., Gimenez-Pardo, A., and Ayuso, C. (2011). An update on the genetics of usher syndrome. *J. Ophthalmol.* 2011:417217. doi: 10.1155/2011/417217

Mistry, N., Nolan, L. S., Saeed, S. R., Forge, A., and Taylor, R. R. (2014). Cochlear implantation in the mouse via the round window: effects of array insertion. *Hear. Res.* 312, 81–90. doi: 10.1016/j.heares.2014.03.005

Miwa, T., Minoda, R., Ise, M., Yamada, T., and Yumoto, E. (2013). Mouse otocyst transuterine gene transfer restores hearing in mice with connexin 30 deletion-associated hearing loss. *Mol. Ther.* 21, 1142–1150. doi: 10.1038/mt.2013.62

Mondain, M., Restituito, S., Vincenti, V., Gardiner, Q., Uziel, A., Delabre, A., et al. (1998). Adenovirus-mediated in vivo gene transfer in guinea pig middle ear mucosa. *Hum. Gene Ther.* 9, 1217–1221. doi: 10.1089/hum.1998.9.8-1217

Mookherjee, S., Hiriyanna, S., Kaneshiro, K., Li, L., Li, Y., Li, W., et al. (2015). Long-term rescue of cone photoreceptor degeneration in retinitis pigmentosa 2 (RP2)-knockout mice by gene replacement therapy. *Hum. Mol. Genet.* 24, 6446–6458. doi: 10.1093/hmg/ddv354

Morimura, H., Fishman, G. A., Grover, S. A., Fulton, A. B., Berson, E. L., and Dryja, T. P. (1998). Mutations in the RPE65 gene in patients with autosomal recessive retinitis pigmentosa or leber congenital amaurosis. *Proc. Natl. Acad. Sci. U.S.A.* 95, 3088–3093. doi: 10.1073/pnas.95.6.3088

Mowat, F. M., Gornik, K. R., Dinculescu, A., Boye, S. L., Hauswirth, W. W., Petersen-Jones, S. M., et al. (2014). Tyrosine capsid-mutant AAV vectors for gene delivery to the canine retina from a subretinal or intravitreal approach. *Gene Ther.* 21, 96–105. doi: 10.1038/gt.2013.64

Muller, U., and Barr-Gillespie, P. G. (2015). New treatment options for hearing loss. *Nat. Rev. Drug Discov.* 14, 346–U84. doi: 10.1038/nrd4533

Nakamura, M., Gao, Y., Dominguez, A. A., and Qi, L. S. (2021). CRISPR technologies for precise epigenome editing. *Nat. Cell Biol.* 23, 11–22. doi: 10.1038/s41556-020-00620-7

Nishiguchi, K. M., Fujita, K., Miya, F., Katayama, S., and Nakazawa, T. (2020). Single AAV-mediated mutation replacement genome editing in limited number of photoreceptors restores vision in mice. *Nat. Commun.* 11:482. doi: 10.1038/s41467-019-14181-3

Nist-Lund, C. A., Pan, B., Patterson, A., Asai, Y., Chen, T., Zhou, W., et al. (2019). Improved TMC1 gene therapy restores hearing and balance in mice with genetic inner ear disorders. *Nat. Commun.* 10:236. doi: 10.1038/s41467-018-08264-w

Niu, Y., Shen, B., Cui, Y., Chen, Y., Wang, J., Wang, L., et al. (2014). Generation of gene-modified cynomolgus monkey via Cas9/RNA-mediated gene targeting in one-cell embryos. *Cell* 156, 836–843. doi: 10.1016/j.cell.2014.01.027

Pan, B., Askew, C., Galvin, A., Heman-Ackah, S., Asai, Y., Indzhykulian, A. A., et al. (2017). Gene therapy restores auditory and vestibular function in a mouse model of Usher syndrome type 1c. *Nat. Biotechnol.* 35, 264–272. doi: 10.1038/nbt.3801

Patel, S. R., Lin, A. S. P., Edelhauser, H. F., and Prausnitz, M. R. (2011). Suprachoroidal drug delivery to the back of the eye using hollow microneedles. *Pharmaceut. Res.* 28, 166–176. doi: 10.1007/s11095-010-0271-y

Patil, S., Gao, Y. G., Lin, X., Li, Y., Dang, K., Tian, Y., et al. (2019). The development of functional non-viral vectors for gene delivery. *Int. J. Mol. Sci.* 20:5491. doi: 10.3390/ijms20215491

Patrizi, C., Llado, M., Benati, D., Iodice, C., Marrocco, E., Guarascio, R., et al. (2021). Allele-specific editing ameliorates dominant retinitis pigmentosa in a transgenic mouse model. *Am. J. Hum. Genet.* 108, 295–308. doi: 10.1016/j.ajhg.2021.01.006

Petrs-Silva, H., Dinculescu, A., Li, Q., Min, S. H., Chiodo, V., Pang, J. J., et al. (2009). High-efficiency transduction of the mouse retina by tyrosine-mutant AAV serotype vectors. *Mol. Ther.* 17, 463–471. doi: 10.1038/mt.2008.269

Petrs-Silva, H., Yasumura, D., Matthes, M. T., LaVail, M. M., Lewin, A. S., and Hauswirth, W. W. (2012). Suppression of rds expression by siRNA and gene replacement strategies for gene therapy using rAAV vector. *Adv. Exp. Med. Biol.* 723, 215–223. doi: 10.1007/978-1-4614-0631-0_29

Picaud, S., Dalkara, D., Marazova, K., Goureau, O., Roska, B., and Sahel, J. A. (2019). The primate model for understanding and restoring vision. *Proc. Natl. Acad. Sci. U.S.A.* 116, 26280–26287. doi: 10.1073/pnas.1902292116

Pinyon, J. L., von Jonquieres, G., Crawford, E. N., Duxbury, M., Al Abed, A., Lovell, N. H., et al. (2019). Neurotrophin gene augmentation by electrotransfer to improve cochlear implant hearing outcomes. *Hear. Res.* 380, 137–149. doi: 10.1016/j.heares.2019.06.002

Ponnath, A., Depreux, F. F., Jodelka, F. M., Rigo, F., Farris, H. E., Hastings, M. L., et al. (2018). Rescue of outer hair cells with antisense oligonucleotides in usher mice is dependent on age of treatment. *J. Assoc. Res. Otolaryngol.* 19, 1–16. doi: 10.1007/s10162-017-0640-x

Puk, O., Dalke, C., Favor, J., de Angelis, M. H., and Graw, J. (2006). Variations of eye size parameters among different strains of mice. *Mamm. Genome* 17, 851–857. doi: 10.1007/s00335-006-0019-5

Ramachandran, P. S., Lee, V., Wei, Z., Song, J. Y., Casal, G., Cronin, T., et al. (2017). Evaluation of dose and safety of AAV7m8 and AAV8BP2 in the non-human primate retina. *Hum. Gene Ther.* 28, 154–167. doi: 10.1089/hum.2016.111

Rattner, A., Sun, H., and Nathans, J. (1999). Molecular genetics of human retinal disease. *Annu. Rev. Genet.* 33, 89–131. doi: 10.1146/annurev.genet.33.1.89

Razek, A. A., and Huang, B. Y. (2012). Lesions of the petrous apex: classification and findings at CT and MR imaging. *Radiographics* 32, 151–173. doi: 10.1148/rg.321105758

Ren, L. L., Wu, Y., Han, D., Zhao, L. D., Sun, Q. M., Guo, W. W., et al. (2010). Math1 gene transfer based on the delivery system of quaternized chitosan/Na-carboxymethyl-beta-cyclodextrin nanoparticles. *J. Nanosci. Nanotechnol.* 10, 7262–7265. doi: 10.1166/jnn.2010.2822

Ren, Y., Landegger, L. D., and Stankovic, K. M. (2019). Gene therapy for human sensorineural hearing loss. *Front. Cell. Neurosci.* 13:323. doi: 10.3389/fncel.2019.00323

Roche, J. P., and Hansen, M. R. (2015). On the horizon cochlear implant technology. *Otolaryngol. Clin. N. Am.* 48, 1097–1116. doi: 10.1016/j.otc.2015.07.009

Ross, M., Obolensky, A., Averbukh, E., Ezra-Elia, R., Yamin, E., Honig, H., et al. (2020). Evaluation of photoreceptor transduction efficacy of capsid-modified adeno-associated viral vectors following intravitreal and subretinal delivery in sheep. *Hum. Gene Ther.* 31, 719–729. doi: 10.1089/hum.2020.023

Ruan, G. X., Barry, E., Yu, D., Lukason, M., Cheng, S. H., and Scaria, A. (2017). CRISPR/Cas9-mediated genome editing as a therapeutic approach for Leber congenital amaurosis 10. *Mol. Ther.* 25, 331–341. doi: 10.1016/j.ymthe.2016.12.006

Rubel, E. W., and Fritzsch, B. (2002). Auditory system development: primary auditory neurons and their targets. *Annu. Rev. Neurosci.* 25, 51–101. doi: 10.1146/annurev.neuro.25.112701.142849

Russell, S., Bennett, J., Wellman, J. A., Chung, D. C., Yu, Z. F., Tillman, A., et al. (2017). Efficacy and safety of voretigene neparvovec (AAV2-hRPE65v2) in patients with RPE65-mediated inherited retinal dystrophy: a randomised, controlled, open-label, phase 3 trial. *Lancet* 390, 849–860. doi: 10.1016/S0140-6736(17)31868-8

Sakami, S., Kolesnikov, A. V., Kefalov, V. J., and Palczewski, K. (2014). P23H opsin knock-in mice reveal a novel step in retinal rod disc morphogenesis. *Hum. Mol. Genet.* 23, 1723–1741. doi: 10.1093/hmg/ddt561

Sakamoto, K., McCluskey, M., Wensel, T. G., Naggert, J. K., and Nishina, P. M. (2009). New mouse models for recessive retinitis pigmentosa caused by mutations in the Pde6a gene. *Hum. Mol. Genet.* 18, 178–192. doi: 10.1093/hmg/ddn327

Salt, A. N., and Hirose, K. (2018). Communication pathways to and from the inner ear and their contributions to drug delivery. *Hear. Res.* 362, 25–37. doi: 10.1016/j.heares.2017.12.010

Schrauwen, I., Chakchouk, I., Acharya, A., Liaqat, K., Nickerson, D. A., Bamshad, M. J., et al. (2018). Novel digenic inheritance of PCDH15 and USH1G underlies profound non-syndromic hearing impairment. *BMC Med. Genet.* 19:122. doi: 10.1186/s12881-018-0618-5

Sharkia, R., Wierenga, K. J., Kessel, A., Azem, A., Bertini, E., Carrozzo, R., et al. (2019). Clinical, radiological, and genetic characteristics of 16 patients with ACO2 gene defects: delineation of an emerging neurometabolic syndrome. *J. Inherit. Metab. Dis.* 42, 264–275. doi: 10.1002/jimd.12022

Shearer, A. E., Hildebrand, M. S., Sloan, C. M., and Smith, R. J. H. (2011). Deafness in the genomics era. *Hear. Res.* 282, 1–9. doi: 10.1016/j.heares.2011.10.001

Shibata, S. B., Di Pasquale, G., Cortez, S. R., Chiorini, J. A., and Raphael, Y. (2009). Gene transfer using bovine adeno-associated virus in the guinea pig cochlea. *Gene Ther.* 16, 990–997. doi: 10.1038/gt.2009.57

Shou, J., Zheng, J. L., and Gao, W. Q. (2003). Robust generation of new hair cells in the mature mammalian inner ear by adenoviral expression of Hath1. *Mol. Cell. Neurosci.* 23, 169–179. doi: 10.1016/s1044-7431(03)00066-6

Simo-Servat, O., Hernandez, C., and Simo, R. (2013). Genetics in diabetic retinopathy: current concepts and new insights. *Curr. Genomics* 14, 289–299. doi: 10.2174/13892029113149990008

Singh, M., and Tyagi, S. C. (2018). Genes and genetics in eye diseases: a genomic medicine approach for investigating hereditary and inflammatory ocular disorders. *Int. J. Ophthalmol.* 11, 117–134. doi: 10.18240/ijo.2018.01.20

Smith, R. J. H., Bale, J. F., and White, K. R. (2005). Sensorineural hearing loss in children. *Lancet* 365, 879–890. doi: 10.1016/S0140-6736(05)71047-3

Song, C., Dufour, V. L., Cideciyan, A. V., Ye, G. J., Swider, M., Newmark, J. A., et al. (2020). Dose range finding studies with two RPGR transgenes in a canine model of X-Linked retinitis pigmentosa treated with subretinal gene therapy. *Hum. Gene Ther.* 31, 743–755. doi: 10.1089/hum.2019.337

Song, H., Bush, R. A., Zeng, Y., Qian, H., Wu, Z., and Sieving, P. A. (2019). Trans-ocular electric current in vivo enhances AAV-mediated retinal gene transduction after intravitreal vector administration. *Mol. Ther. Methods Clin. Dev.* 13, 77–85. doi: 10.1016/j.omtm.2018.12.006

Song, H., Zeng, Y., Sardar Pasha, S. P. B., Bush, R. A., Vijayasarathy, C., Qian, H., et al. (2020). Trans-ocular electric current in vivo enhances AAV-mediated retinal transduction in large animal eye after intravitreal vector administration. *Transl. Vis. Sci. Technol.* 9:28. doi: 10.1167/tvst.9.7.28

Stamatiou, G. A., and Stankovic, K. M. (2013). A comprehensive network and pathway analysis of human deafness genes. *Otol. Neurotol.* 34, 961–970. doi: 10.1097/MAO.0b013e3182898272

Sun, D., Sahu, B., Gao, S., Schur, R. M., Vaidya, A. M., Maeda, A., et al. (2017). Targeted multifunctional lipid ECO plasmid DNA nanoparticles as efficient non-viral gene therapy for Leber's congenital amaurosis. *Mol. Ther. Nucleic Acids* 7, 42–52. doi: 10.1016/j.omtn.2017.02.005

Sun, D., Schur, R. M., Sears, A. E., Gao, S. Q., Vaidya, A., Sun, W., et al. (2020). Non-viral gene therapy for stargardt disease with ECO/pRHO-ABCA4 self-assembled nanoparticles. *Mol. Ther.* 28, 293–303. doi: 10.1016/j.ymthe.2019.09.010

Suzuki, J., Hashimoto, K., Xiao, R., Vandenberghe, L. H., and Liberman, M. C. (2017). Cochlear gene therapy with ancestral AAV in adult mice: complete transduction of inner hair cells without cochlear dysfunction. *Sci. Rep.* 7:45524. doi: 10.1038/srep45524

Tam, L. C., Kiang, A. S., Kennan, A., Kenna, P. F., Chadderton, N., Ader, M., et al. (2008). Therapeutic benefit derived from RNAi-mediated ablation of IMPDH1 transcripts in a murine model of autosomal dominant retinitis pigmentosa (RP10). *Hum. Mol. Genet.* 17, 2084–2100. doi: 10.1093/hmg/ddn107

Tan, B. T., Foong, K. H., Lee, M. M., and Ruan, R. (2008). Polyethylenimine-mediated cochlear gene transfer in guinea pigs. *Arch. Otolaryngol. Head Neck Surg.* 134, 884–891. doi: 10.1001/archotol.134.8.884

Tang, Z. H., Chen, J. R., Zheng, J., Shi, H. S., Ding, J., Qian, X. D., et al. (2016). Genetic correction of induced pluripotent stem cells from a deaf patient with MYO7A mutation results in morphologic and functional recovery of the derived hair cell-like cells. *Stem Cells Transl. Med.* 5, 561–571. doi: 10.5966/sctm.2015-0252

Tao, Y., Huang, M. Q., Shu, Y. L., Ruprecht, A., Wang, H. Y., Tang, Y., et al. (2018). Delivery of adeno-associated virus vectors in adult mammalian inner-ear cell subtypes without auditory dysfunction. *Hum. Gene Ther.* 29, 492–506. doi: 10.1089/hum.2017.120

Testa, F., Maguire, A. M., Rossi, S., Pierce, E. A., Melillo, P., Marshall, K., et al. (2013). Three-year follow-up after unilateral subretinal delivery of adeno-associated virus in patients with Leber congenital amaurosis type 2. *Ophthalmology* 120, 1283–1291. doi: 10.1016/j.ophtha.2012.11.048

Todorich, B., Yiu, G., and Hahn, P. (2014). Current and investigational pharmacotherapeutic approaches for modulating retinal angiogenesis. *Exp. Rev. Clin. Pharmacol.* 7, 375–391. doi: 10.1586/17512433.2014.890047

Tosi, J., Sancho-Pelluz, J., Davis, R. J., Hsu, C. W., Wolpert, K. V., Sengillo, J. D., et al. (2011). Lentivirus-mediated expression of cDNA and shRNA slows degeneration in retinitis pigmentosa. *Exp. Biol. Med.* 236, 1211–1217. doi: 10.1258/ebm.2011.011053

Touchard, E., Berdugo, M., Bigey, P., El Sanharawi, M., Savoldelli, M., Naud, M. C., et al. (2012). Suprachoroidal electrotransfer: a nonviral gene delivery method to transfect the choroid and the retina without detaching the retina. *Mol. Ther.* 20, 1559–1570. doi: 10.1038/mt.2011.304

Tranebjaerg, L. (1993). "Deafness-dystonia-optic neuronopathy syndrome," in *GeneReviews*, eds M. P. Adam, H. H. Ardinger, R. A. Pagon, S. E. Wallace, L. J. H. Bean, K. Stephens, et al. (Seattle, WA:University of Washington).

Trapani, I. (2019). Adeno-associated viral vectors as a tool for large gene delivery to the retina. *Genes* 10:287. doi: 10.3390/genes10040287

Trapani, I., Colella, P., Sommella, A., Iodice, C., Cesi, G., de Simone, S., et al. (2014). Effective delivery of large genes to the retina by dual AAV vectors. *Hum. Gene Ther.* 25, A33–A33.

Travis, G. H., Groshan, K. R., Lloyd, M., and Bok, D. (1992). Complete rescue of photoreceptor dysplasia and degeneration in transgenic retinal degeneration slow (rds) mice. *Neuron* 9, 113–119. doi: 10.1016/0896-6273(92)90226-4

Vagni, P., Perlini, L. E., Chenais, N. A. L., Marchetti, T., Parrini, M., Contestabile, A., et al. (2019). Gene editing preserves visual functions in a mouse model of retinal degeneration. *Front. Neurosci.* 13:945. doi: 10.3389/fnins.2019.00945

Volland, S., Esteve-Rudd, J., Hoo, J., Yee, C., and Williams, D. S. (2015). A comparison of some organizational characteristics of the mouse central retina and the human macula. *PLoS One* 10:e0125631. doi: 10.1371/journal.pone.0125631

Wang, D., Tai, P. W. L., and Gao, G. P. (2019). Adeno-associated virus vector as a platform for gene therapy delivery. *Nat. Rev. Drug Discov.* 18, 358–378. doi: 10.1038/s41573-019-0012-9

Wang, L., Kempton, J. B., Jiang, H., Jodelka, F. M., Brigande, A. M., Dumont, R. A., et al. (2020). Fetal antisense oligonucleotide therapy for congenital deafness and vestibular dysfunction. *Nucleic Acids Res.* 48, 5065–5080. doi: 10.1093/nar/gkaa194

Wang, Y. F., Sun, Y., Chang, Q., Ahmad, S., Zhou, B. F., Kim, Y. J., et al. (2013). Early postnatal virus inoculation into the scala media achieved extensive expression of exogenous green fluorescent protein in the inner ear and preserved auditory brainstem response thresholds. *J. Gene Med.* 15, 123–133. doi: 10.1002/jgm.2701

Wareing, M., Mhatre, A. N., Pettis, R., Han, J. J., Haut, T., Pfister, M. H., et al. (1999). Cationic liposome mediated transgene expression in the guinea pig cochlea. *Hear. Res.* 128, 61–69. doi: 10.1016/s0378-5955(98)00196-8

Wassmer, S. J., De Repentigny, Y., Sheppard, D., Lagali, P. S., Fang, L., Coupland, S. G., et al. (2020). XIAP protects retinal ganglion cells in the mutant ND4 mouse model of leber hereditary optic neuropathy. *Invest. Ophthalmol. Vis. Sci.* 61:49. doi: 10.1167/iovs.61.8.49

Weber, M., Rabinowitz, J., Provost, N., Conrath, H., Folliot, S., Briot, D., et al. (2003). Recombinant adeno-associated virus serotype 4 mediates unique and exclusive long-term transduction of retinal pigmented epithelium in rat, dog, and nonhuman primate after subretinal delivery. *Mol. Ther.* 7, 774–781. doi: 10.1016/s1525-0016(03)00098-4

Weiss, R. S., Voss, A., and Hemmert, W. (2016). Optogenetic stimulation of the cochlea-A review of mechanisms, measurements, and first models. *Netw. Comput. Neural Syst.* 27, 212–236. doi: 10.1080/0954898x.2016.1224944

Willoughby, A., Vuong, V., Cunefare, D., Farsiu, S., Noronha, G., Danis, R. P., et al. (2018). Choroidal changes after suprachoroidal injection of CLS-TA, triamcinolone acetonide injectable suspension, in eyes with macular edema secondary to retinal vein occlusion. *Invest. Ophthalmol. Vis. Sci.* 59:5969.

Wilson, B. S., and Dorman, M. F. (2008). Cochlear implants: a remarkable past and a brilliant future. *Hear. Res.* 242, 3–21. doi: 10.1016/j.heares.2008.06.005

Wood, E. H., Tang, P. H., De la Huerta, I., Korot, E., Muscat, S., Palanker, D. A., et al. (2019). Stem cell therapies, gene-based therapies, optogenetics, and retinal prosthetics: current state and implications for the future. *Retina* 39, 820–835. doi: 10.1097/IAE.0000000000002449

Wu, Z. J., Yang, H. Y., and Colosi, P. (2010). Effect of genome size on AAV vector packaging. *Mol. Ther.* 18, 80–86. doi: 10.1038/mt.2009.255

Wysocki, J. (2005). Topographical anatomy of the guinea pig temporal bone. *Hear. Res.* 199, 103–110. doi: 10.1016/j.heares.2004.08.008

Xu, Z. P., Yue, Y. P., Lai, Y., Ye, C. Y., Qiu, J. M., Pintel, D. J., et al. (2004). Trans-splicing adeno-associated viral vector-mediated gene therapy is limited by the accumulation of spliced mRNA but not by dual vector coinfection efficiency. *Hum. Gene Ther.* 15, 896–905. doi: 10.1089/hum.2004.15.896

Yeh, S., Khurana, R. N., Shah, M., Henry, C. R., Wang, R. C., Kissner, J. M., et al. (2020). Efficacy and safety of suprachoroidal CLS-TA for macular edema secondary to noninfectious uveitis: phase 3 randomized trial. *Ophthalmology* 127, 948–955. doi: 10.1016/j.ophtha.2020.01.006

Yiu, G., Chung, S. H., Mollhoff, I. N., Nguyen, U. T., Thomasy, S. M., Yoo, J., et al. (2020). Suprachoroidal and subretinal injections of AAV using transscleral microneedles for retinal gene delivery in nonhuman primates. *Mol. Ther. Methods Clin. Dev.* 16, 179–191. doi: 10.1016/j.omtm.2020.01.002

Yiu, G., Pecen, P., Sarin, N., Chiu, S. J., Farsiu, S., Mruthyunjaya, P., et al. (2014). Characterization of the choroid-scleral junction and suprachoroidal layer in healthy individuals on enhanced-depth imaging optical coherence tomography. *JAMA Ophthalmol.* 132, 174–181. doi: 10.1001/jamaophthalmol.2013.7288

Yoshimura, H., Shibata, S. B., Ranum, P. T., and Smith, R. J. H. (2018). Enhanced viral-mediated cochlear gene delivery in adult mice by combining canal fenestration with round window membrane inoculation. *Sci. Rep.* 8:2980. doi: 10.1038/s41598-018-21233-z

Yu, Q., Wang, Y., Chang, Q., Wang, J., Gong, S., Li, H., et al. (2014). Virally expressed connexin26 restores gap junction function in the cochlea of conditional Gjb2 knockout mice. *Gene Ther.* 21, 71–80. doi: 10.1038/gt.2013.59

Yuan, Y. Y., Li, Q., Su, Y., Lin, Q. F., Gao, X., Liu, H. K., et al. (2020). Comprehensive genetic testing of Chinese SNHL patients and variants interpretation using ACMG guidelines and ethnically matched normal controls. *Eur. J. Hum. Genet.* 28, 231–243. doi: 10.1038/s41431-019-0510-6

Zhang, H., Pan, H., Zhou, C., Wei, Y., Ying, W., Li, S., et al. (2018). Simultaneous zygotic inactivation of multiple genes in mouse through CRISPR/Cas9-mediated base editing. *Development* 145:dev168906. doi: 10.1242/dev.168906

Zhang, W. J., Kim, S. M., Wang, W. W., Cai, C. Y., Feng, Y., Kong, W. J., et al. (2018). Cochlear gene therapy for sensorineural hearing loss: current status and major remaining hurdles for translational success. *Front. Mol. Neurosci.* 11:221. doi: 10.3389/fnmol.2018.00221

Zhang, Y., Wang, S., Xu, M., Pang, J., Yuan, Z., and Zhao, C. (2019). AAV-mediated human CNGB3 restores cone function in an all-cone mouse model of CNGB3 achromatopsia. *J. Biomed. Res.* 34, 114–121. doi: 10.7555/JBR.33.20190056

Zhao, X., Jin, C., Dong, T., Sun, Z., Zheng, X., Feng, B., et al. (2020). Characterization of promoters for adeno-associated virus mediated efficient Cas9 activation in adult Cas9 knock-in murine cochleae. *Hear. Res.* 394:107999. doi: 10.1016/j.heares.2020.107999

Zhou, R., and Caspi, R. R. (2010). Ocular immune privilege. *F1000 Biol. Rep.* 2:3. doi: 10.3410/B2-3

Zou, J., Saulnier, P., Perrier, T., Zhang, Y., Manninen, T., Toppila, E., et al. (2008). Distribution of lipid nanocapsules in different cochlear cell populations after round window membrane permeation. *J. Biomed. Mater. Res. B Appl. Biomater.* 87, 10–18. doi: 10.1002/jbm.b.31058

Conflict of Interest: The authors declare that the research was conducted in the absence of any commercial or financial relationships that could be construed as a potential conflict of interest.

Copyright © 2021 Crane, Conley, Al-Ubaidi and Naash. This is an open-access article distributed under the terms of the Creative Commons Attribution License (CC BY). The use, distribution or reproduction in other forums is permitted, provided the original author(s) and the copyright owner(s) are credited and that the original publication in this journal is cited, in accordance with accepted academic practice. No use, distribution or reproduction is permitted which does not comply with these terms.

frontiers in Neuroscience

REVIEW
published: 20 April 2021
doi: 10.3389/fnins.2021.668857

Functional 3-Dimensional Retinal Organoids: *Technological Progress* and Existing Challenges

Meimanat Fathi[1,2], *Cody T. Ross*[3] *and Zohreh Hosseinzadeh*[2]*

[1] *Department of Cell Techniques and Applied Stem Cell Biology, Faculty of Medicine, Center for Biotechnology and Biomedicine (BBZ), University of Leipzig, Leipzig, Germany,* [2] *Physiology and Pathophysiology of the Retina Group, Department of Molecular and Cellular Mechanisms of Neurodegeneration, Paul Flechsig Institute of Brain Research, University of Leipzig, Leipzig, Germany,* [3] *Department of Human Behavior, Ecology and Culture, Max Planck Institute for Evolutionary Anthropology, Leipzig, Germany*

Stem cell scientists have developed methods for the self-formation of artificial organs, often referred to as organoids. Organoids can be used as model systems for research in multiple biological disciplines. Yoshiki Sasai's innovation for deriving mammalian retinal tissue from *in vitro* stem cells has had a large impact on the study of the biology of vision. New developments in retinal organoid technology provide avenues for *in vitro* models of human retinal diseases, studies of pathological mechanisms, and development of therapies for retinal degeneration, including electronic retinal implants and gene therapy. Moreover, these innovations have played key roles in establishing models for large-scale drug screening, studying the stages of retinal development, and providing a human model for personalized therapeutic approaches, like cell transplants to replace degenerated retinal cells. Here, we first discuss the importance of human retinal organoids to the biomedical sciences. Then, we review various functional features of retinal organoids that have been developed. Finally, we highlight the current limitations of retinal organoid technologies.

Keywords: organoids, retina, functionality, visual cycle, ON/OFF pathways

OPEN ACCESS

Edited by:
Miguel Flores-Bellver, University of Colorado Anschutz Medical Campus, United States

Reviewed by:
Magdalene J. Seiler, University of California, Irvine, United States
Ilaria Piano, University of Pisa, Italy

***Correspondence:**
Zohreh Hosseinzadeh
Zohreh.Hosseinzadeh@medizin.uni-leipzig.de;
zohoseinzadeh@gmail.com

Specialty section:
This article was submitted to Neurodegeneration, a section of the journal Frontiers in Neuroscience

Received: *17 February 2021*
Accepted: *24 March 2021*
Published: *20 April 2021*

Citation:
Fathi M, Ross CT and Hosseinzadeh Z (2021) Functional 3-Dimensional Retinal Organoids: Technological Progress and Existing Challenges. Front. Neurosci. 15:668857. doi: 10.3389/fnins.2021.668857

INTRODUCTION

The retina is a thin (~0.25 mm) layer of neurons in the back of the eyeball—it is a part of the central nervous system that grows inside of the eye during development. In the nineteenth century, Santiago Ramon y Cajal, father of the neuron theory of the nervous system, introduced the first comprehensive morphology of neural cell types, including the cells of the retina, in a number of vertebrate species (Lerma and De Carlos, 2014). Since then, many studies have investigated different aspects of this complex system and its development through ontogeny. We now know that the retina is composed of several layers, with different cell types consisting of horizontal, bipolar (BCs), amacrine, and ganglion cells (GCs), as well as photoreceptors (PRs), and three types of glial cells, including microglia, astrocytes, and Müller glial cells (Bringmann et al., 2006). However, many features of vertebrate retinal function and development are still unknown, making it difficult to recapitulate the retina *in vitro* using stem cells.

Organoids derived from induced pluripotent stem cells (iPSCs), or embryonic stem cells (ESCs), have been used by researchers to create *in vitro* tissues that mimic their natural counterparts,

advancing medical research in the 1980s and beyond (Shannon et al., 1987). More recently, new methodological advances for culturing tissues have opened up new possibilities for basic research on various human organs—e.g., the brain (Qian et al., 2019), intestine (Sprangers et al., 2020), kidney (Taguchi et al., 2014), prostate (Gao et al., 2014), and retina (Zhong et al., 2014; Cowan et al., 2020). Scientists have successfully developed retinal organoids that closely resemble many aspects of the real retina using human and mouse stem cells. Lab-grown retinal organoids are composed of several types of cells organized in a physiologically and morphologically complex manner (Eiraku et al., 2011). A retina-specific synapse, referred to as the ribbon synapse, is formed in such organoids (Castro et al., 2019). These organoids also show physiological responses to light stimuli to some degree (Zhong et al., 2014; Wahlin et al., 2017). As such, retinal organoids can be used as a basic model for investigating various therapies or treatments. For example, retinal organoids can be used to study retinal degeneration, human retinal implants, optogenetics and gene therapies, drug screening and toxicity, and the stages of retinal development. Therefore, they provide a human model for personalized therapeutic approaches and can be used in transplants of a patient's degenerated retinal cells (see the summary of potential applications of retinal organoids in **Figure 1**). Despite recent progress in retinal organoid technology, our knowledge is still in its infancy, and organoids have not recapitulated all developmental stages of the natural retina.

In this review, we discuss some real-world problems illustrating the necessity of speeding up the development of retinal organoid technology for medical research. We then highlight the key functional aspects of retinal organoids—e.g., visual cycles, synaptogenesis, and retinal pathways—and the physiological recovery of the retina after retinal cell or organoid transplantation. Finally, we discuss current constraints regarding, and unanswered questions about, retinal organoids.

THE NECESSITY OF IMPROVING RETINAL ORGANOID MODELS

According to the World Health Organization [WHO] (2019), more than one billion people globally have a vision impairment that could have been prevented or is yet to be addressed. According to eye health data and statistics, the number of people with the most common eye diseases will double by 2050 (Varma et al., 2016). In order to better understand retinal diseases, and develop treatments for them, a proper retinal model is critically needed.

Donated post-mortem retinal tissues, especially those affected by retinal disorders, are suitable *in vitro* testbeds for investigating underlying pathophysiology mechanisms. The quality of data obtained from the molecular biology, the imaging, and the visual function of a post-mortem retina depends on rapid isolation and a regular oxygen supply (Pannicke et al., 2005; Cowan et al., 2020). Gene expression can change rapidly post-mortem in a tissue-specific manner (Ferreira et al., 2018). Post-mortem transplantation of eye components depends on the persistence of tissue; for example, 36% of corneal transplants using post-mortem tissues with death-to-preservation times of more than 6 h failed (Mohamed et al., 2016). There are several constraints on using donated post-mortem retinal tissues, including organ availability and its pathological state, as well as the ethical requirements of the state and institution where the procedure is conducted.

The 2-dimensional (2D) culture of immortalized retinal cell lines is a resource for study of retinal pathologies and drug testing. 2D culture of different retinal cell lines is needed for studying different retinal diseases. For example, human retinal pigment epithelium (RPE) cell lines can be used to study age-related macular degeneration (AMD) (Kozlowski, 2015), and MIO-M1 human Müller glial cell lines can be used to study diabetic retinopathy or retinal degeneration (Yong et al., 2010). Moreover, the 2D culture of reprogrammed iPSCs-derived retinal cells (Lamba et al., 2006) has been established for the study of multiple conditions—e.g., disease modeling, drug testing and discovery, and cell replacement therapies (O'Hara-Wright and Gonzalez-Cordero, 2020). Nevertheless, 2D retinal culture may not emulate important naturalistic aspects of native retinal cells *in vivo*, and also fails to entirely recapitulate the morphology and functional physiology of the human retina.

Animal models are another widespread tool that can be used to study retinal diseases and develop treatments—e.g., through genetic or interventional modifications (Volobueva et al., 2019). The retinal tissue of non-human species can mimic aspects of retinal diseases found in humans. For example, rd10 mice carrying a spontaneous mutation of the phosphodiesterase gene in rod cells are a model of autosomal recessive retinitis pigmentosa, which leads to rod degeneration in humans (Gargini et al., 2007). Animal models assist researchers in understanding diseases and their prevention, diagnosis, and treatment, in cases where human research would be impractical or ethically prohibited. Although our understanding of retinal pathophysiology has been improved by animal models, there are considerable drawbacks in extrapolating the findings of rodents to humans. For example, the absence of the macula and photopigmentation in rodents, differences in color vision—e.g., dichromatism in rodents (Szatko et al., 2020) vs. trichromatism in humans—and differences in tissue structure, size, refractive properties, and the nature of the retinal vascular system (Achberger et al., 2019b; Castro et al., 2019). A key solution for overcoming the aforementioned limitations would be to generate 3-dimensional (3D) functional retinal tissues *in vitro*.

RETINAL ORGANOID FUNCTIONALITY

The Visual Cycle in Retinal Organoids

Retinal pigment epithelium (RPE) plays a critical role in photoreceptor survival and functionality, as well as modulation of the visual cycle—the conversion of an incoming photon into an electrical signal (Wright et al., 2015). Thus, in order to generate functional retinal organoids, it is important to integrate components of the visual cycle, including RPE. RPE is composed of polarized cells within the basal and apical membranes. On

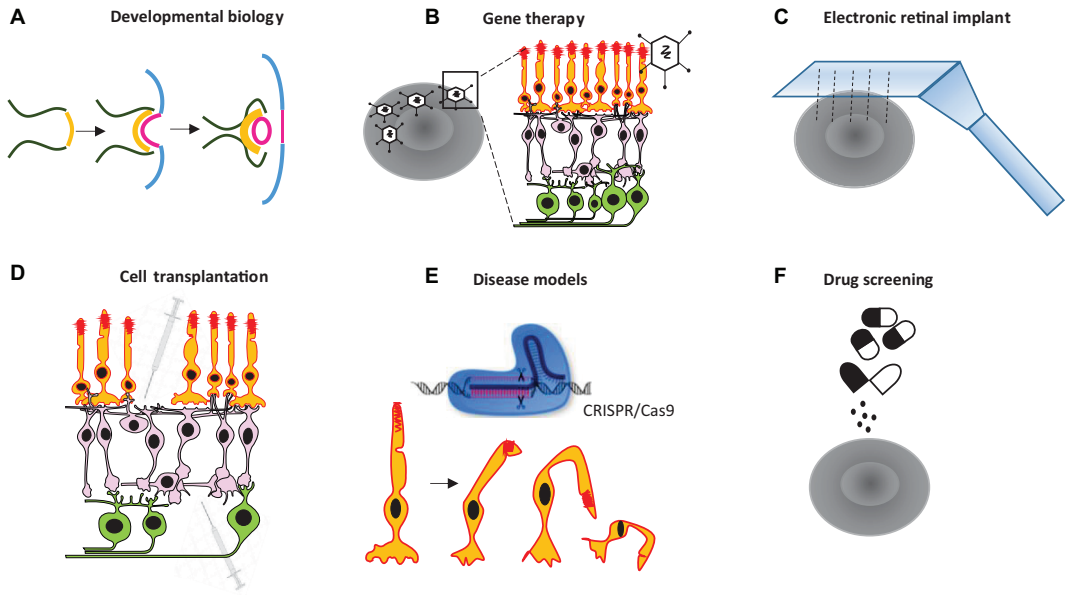

FIGURE 1 | Some potential applications for retinal organoid technology. Retinal organoids can be used to **(A)** study the development of the retina, **(B)** investigate various therapeutical approaches, including gene therapy for retinal disorders, **(C)** test electronic chip implants, **(D)** facilitate cell transplantation, **(E)** test human retinal disease models, and **(F)** conduct drug screening.

the apical side, RPE connects with PRs through a network of microvilli, which allows exchange of materials between PRs and RPE (Kang et al., 2009; Sahu and Maeda, 2018). RPE supports PRs by providing nutrients, removing waste products, releasing growth factors, and regulating the length of PRs by phagocytosis. Most importantly, the RPE plays a fundamental role in retinol cycling by recycling 11-cis retinal from all-trans isomers for the next visual cycle (Ramsden et al., 2013; Tsin et al., 2018; Choi et al., 2020). The expression of RPE markers includes MERTK (a phagocytosis marker) and BEST1 (a basal marker), as well as RPE65, LRAT, and CRALBP (which are visual cycle markers). Each of these markers has been identified *in vitro* in RPE differentiated from iPSCs (Chichagova et al., 2018).

RPE spheroids isolated from hiPSC-derived retinal organoids are able to reach maturation. Such a state of cellular, molecular, and physiological maturity is indicated by a number of features, including repigmentation, marker expression, and phagocytosis (Liu et al., 2018). Co-culturing retinal organoids with hiPSC-derived RPE elevates the differentiation of retinal progenitors derived from human iPSCs (Akhtar et al., 2019), suggesting that RPE promotes retinal differentiation. In the presence of 9-cis retinal, rod differentiation is accelerated in organoid cultures with proper rhodopsin expression at day 120, indicating visual cycle control between RPE and PRs as an essential part of retinal development (Kaya et al., 2019). Maturation of PRs is promoted in the presence of retinoic acid (the pleiotropic all-trans-retinol form) (Zerti et al., 2020). To date, the co-culturing of RPE with supplementary components, like 9-cis retinal, is the only available method for activating the visual cycle (to some degree) in retinal organoids. We discuss this further in the section: "Current limitations of retinal organoid technology."

The Maturation of Retinal Pathways

Visual inputs to the retina are encoded by distinct visual pathways in parallel for transmission to the brain via ganglion cells (GC). In mice, there are approximately 15–20 channels (pathways) based on GC dendritic morphologies (Coombs et al., 2006; Volgyi et al., 2009) and 30 functional output channels based on calcium imaging recordings (Baden et al., 2016). ON and OFF channels, which are responsible for the fundamental functional features of the visual system, can be recorded by electrophysiology techniques (Popova, 2014). ON pathways (ON cells) are activated by light increments, whereas OFF pathways (OFF cells) are activated by light decrements. The characterization of ON and OFF pathways is one of the main goals in retinal organoid engineering.

Single cell patch clamp recording lets us identify hyperpolarization and depolarization of mature PRs in retinal organoids, responding to light and darkness, respectively. Zhong et al. (2014) reported, by means of the patch clamp technique, that 2 out of 13 randomly chosen PRs responded to a light stimulus in hiPSC-derived retinal organoids at weeks 25–27. The authors inferred that the low number of responsive PRs could be due to the low levels of rhodopsin and downstream phototransduction steps that may still be under maturation (Zhong et al., 2014). Cones targeted by patch clamp recording reveal the presence of hyperpolarization-activated cyclic nucleotide-gated (HCN) channels, the fundamental key of phototransduction in PRs (Kim et al., 2019).

Using a microelectrode array (MEA), one can record the action potential of GCs in order to identify network-mediated retinal pathways. The response of GCs in retinal organoids

to light stimulus has been recorded at day 150 by MEA. These responses, however, were too indolent to document clear matched spikes to light pulses (Hallam et al., 2018). Such an event might be comparable with spontaneous waves of activity sweeping across the neonatal vertebrate retina before eye-opening (Maccione et al., 2014). Puffing 8-br-cGMP, a secondary messenger of the phototransduction cascade, binding to the gates of Na^+ -permeable channels, depolarizes PRs, thus mimicking dark current. In the presence of 8-br-cGMP puff in organoid cultures, MEA recording suggests that GCs with decreased spiking activity are ON, whereas GCs with increased firing rate are OFF (Hallam et al., 2018). The decellularized extracellular matrix-derived peptides from the neural retina (decel NR) and RPE conditions of retinal organoid cultures promote the light-driven responses of ON RGCs of organoids recorded by MEA (Dorgau et al., 2019). Very recently, Cowan et al. (2020) reported the transmission of light responses through the cascade of PRs to BCs and GCs in organoids by using live two-photon laser imaging; however, the percentage of the responsive cells was low (Cowan et al., 2020). To some extent, the ON and OFF retinal pathways of organoids have been characterized, but such responses are still far from replicating the spike activities of ON and OFF pathways *in vivo*. We discuss this further in the section: "Current limitations of retinal organoid technology."

Synaptogenesis in Retinal Organoids

The retina processes different visual features in parallel—e.g., brightness, darkness, color, contrast, and motion (Wassle, 2004). For the processing of visual signals, synapses with different kinetics in signal transmission are needed. Indeed, the retina possesses a range of synapses, including chemical, fast electrical, and ribbon synapses.

The somas of retinal neurons are located in the three nuclear layers of the retina, which are separated by a minimum of two synaptic layers. Synapses transmit the signals at the tonic rate of transmitter release and in a graded fashion. Two ribbon synapses exist in the retina: PRs transmit their signals in the outer plexiform layer (OPL), and BCs send signals in the inner plexiform layer (IPL). The ribbon is poised for fast transmitter release, and is ideal for reporting the rapid onset of stimuli (tom Dieck and Brandstatter, 2006; Lagnado and Schmitz, 2015; Okawa et al., 2019). The generation of such synaptic ribbon has been reported during retinal organoid development (Cowan et al., 2020; Sridhar et al., 2020). In human retinal organoids, PR ribbon synapses with vesicles and close contact with BCs and HCs have been observed (Cowan et al., 2020). Presynaptic ribbon markers (RIBEYE and SYNTAXIN3) contain vesicles, close to dense bars, in the synaptic endfeet of the OPL-like region (Gonzalez-Cordero et al., 2017). Moreover, the interconnection between PR axons and BC dendrites forming the retinal-specific ribbon synapses in retinal organoids has been observed using the passive clearing technique (Cora et al., 2019). Ribbon synapses at BCs in the IPL of retinal organoids have not yet been identified. To our knowledge, ribbon synapses at rods and cones of retinal organoids have not been distinguished either.

VISUAL FUNCTION AND CELL TRANSPLANTATION

Visual Function After Cell Transplantation

Cell transplantation is a novel therapeutic strategy to restore visual responses that have been lost to retinal degeneration or disease—for example, inherited retinitis pigmentosa or AMD (West et al., 2009; Stern et al., 2018). Stem-cell-derived retinal organoids and RPE organoid therapy have great therapeutic potential for treating such degenerative diseases. In this section, we focus on visual function after transplanting organoids and RPE sheets or cells isolated from them.

Photoreceptor Transplantation

Transplanted purified human cones isolated from retinal organoids (combining 2D/3D methods) have been incorporated within $Nrl^{-/-}$ mouse retinas with defective S- and M-cone opsins (Gonzalez-Cordero et al., 2017). Subretinally transplanted 3D hESC-derived retinal organoid sheets (day 30–65) in rho S334ter-3 rats have differentiated, integrated, and produced functional PRs, resulting in visual function and active synapses in the recipients' eyes (McLelland et al., 2018). Jaws-positive PRs (with red-shifted cruxhalorhodopsin) isolated from retinal organoids and subretinally transplanted into blind hosts (mice) can become integrated into the host retina and ON- and OFF pathway responses (Garita-Hernandez et al., 2019).

Cell transplantation may lead to natural interactions among donor and host cells, and transmit cytoplasmic materials. Numerous observations indicate that functional recovery of the host retina might be achieved by transferring cytoplasmic material from transplanted PRs to remaining host PRs (Santos-Ferreira et al., 2016; Chichagova et al., 2018; Gagliardi et al., 2018). Nevertheless, cell transplantation could lead to natural interaction of donor and host cells, as well as transmission of cytoplasmic materials. Transplanting hESC-derived retinal organoids into the retinas of immunodeficient RCS nude rats has been shown to improve visual function; transplanted cells migrate and integrate synaptic connectivity with the host cells during the transfer of cytoplasmic material (Lin et al., 2020).

RPE Transplantation

The transplantation of hESCs-derived RPE cells in patients with AMD has shown promising outcomes in clinical trials (phase I/II)—such outcomes include increases in vision-related quality-of-life and improvements in best-corrected visual acuity (but only in some patients) (Schwartz et al., 2015). Later, Takahashi's group reported that hiPSC-derived RPE sheets transplanted into human retinas with AMD remained intact and showed good retinal integrity, unchanging visual acuity, and no immune rejection (Mandai et al., 2017).

Cell transplantation entails several challenges: obtaining high-quality transplantable cells in sufficient quantities, achieving integration and function of transplanted cells (Gonzalez-Cordero

et al., 2017), and minimizing the risk of cancerogenesis (Singh et al., 2018). Finding specific markers of retinal cells for purification may provide a solution that improves the efficiency of obtaining cells. For example, Gagliardi et al. (2018) has developed the CD73 + PRs MACS method to purify and sort a pool of PRs from hiPSC-derived retinal organoids for transplanting into a host retina (Gagliardi et al., 2018). The other shortcomings remain to be resolved.

CURRENT LIMITATIONS OF RETINAL ORGANOID TECHNOLOGY

Although the field of retinal organoid technology has seen significant progress in recent years, the construction of highly complex mammalian retinas *in vitro* is still beyond the reach of our current tools. It is still not possible to generate retinal organoids that have the same biochemical and physiological characteristics as mature *in vivo* retinas. In order to create such organoids, future technology must integrate several additional features, including smooth muscle cells, vasculature, and immune cells like microglia. Additionally, researchers must ensure proper cell orientation and wiring within retinal neurons, and correct RPE orientation for the maturation of the visual cycle and mature ON and OFF pathways, as we discuss in more detail below (see **Figure 2**, and Achberger et al., 2019a; Kruczek and Swaroop, 2020; Singh and Nasonkin, 2020).

Vasculature

One of the major challenges in producing 3D organoids is the maintenance of long-term cell viability, which strongly depends on access to nutrients and oxygen (Ozbolat, 2015). The current inability to supply such nutrients has been attributed to the lack of endogenous, engineered vasculature or nutrient channels in the organ (Laschke and Menger, 2012). Without vasculature, the size of an organoid is limited to the diffusional limit of oxygen (Radisic et al., 2006). This problem may be resolved by applying new technological approaches—for example, optimization of scaffold porosity (Chen et al., 2019), inclusion of bioreactor (Ovando-Roche et al., 2018), incorporation of oxygen delivery mechanisms (Li et al., 2012), retina-on-a-chip (Achberger et al., 2019b), 3D bioprinting of vascularized tissues (Richards et al., 2017), and co-culture with mesodermal progenitor cells (Worsdorfer et al., 2019) are areas of current research.

Microglia

Microglial cells are primary resident immune cells that interact with Müller glial cells in the retina. Microglial cells are important for the natural development of a retina because they regulate neuronal survival and synaptic pruning (Li et al., 2012). Microglial cells and other retinal cells in organoids do not arise under the same differentiation conditions, due to differences in their lineages. Microglial cells come from the hematopoietic lineage that colonizes brain tissue during embryonic development (Cunningham et al., 2013). It is suspected that the existence of microglia within the retina may be key to successful retinal development (Li et al., 2019).

RPE

In retinal organoid cultures, mature and functional RPE around PRs is missing. RPE is a retinal cell type that is essential for retinal development. An ablation of RPE in mouse retina at embryonic day E10–11 leads to disruption of the retinal layers and eye growth. This deficiency does not affect retinogenesis at embryonic day E11.5–12.5; however, it disrupts the laminar structure and vitreous production (Raymond and Jackson, 1995; Fuhrmann et al., 2014). Indeed, RPE plays a vital role in the protection and survival of PRs (German et al., 2008). This is confirmed by the fact that the differentiation of PRs has been improved by co-culturing the retinal organoid with RPE (Akhtar et al., 2019). RPE maintains the physiology of the outer retina—for example, by enacting phagocytosis of shed PR outer segments, running the visual cycle, and secreting neurotrophic and vasculotrophic growth factors that promote vascularization (Sparrow et al., 2010; Achberger et al., 2019b). Therefore, the interaction between the retina and RPE is critical, not only during retinal organoid development, but also for visual function in a mature retina.

Degeneration and Loss of Orientation

Another major limitation in producing 3D retinal organoids is degeneration and the loss of orientation through development. The maturation of human retinal organoids *in vitro* proceeds at about the same rate as human retinal development *in vivo* (Nakano et al., 2012; Zhong et al., 2014; Wahlin et al., 2017). This long developmental process leads to the degeneration of the organoid. Such degeneration is generally caused by a lack of nutrition or poor passive diffusion, mainly in the inner layers. Therefore, the inner cells disappear before the PRs reach a fully mature stage in the organoid (Reichman et al., 2014). In contrast to the natural cup shape of the retina *in vivo*, retinal organoids have a spherical form. This shape may be caused by a tendency of suspended cells to form into spheroids with an equal distribution of surrounding cellular layers (Forgacs et al., 1998; Ajduk and Zernicka-Goetz, 2016). Lacking orientation, surrounding tissue and extracellular matrix prevent a proper polarized tissue development (Takano et al., 2015), which is necessary for optic-cup development and peripheral-central specialization.

Synaptogenesis

Retinal synapses are organized in the inner and outer plexiform layers in an orderly fashion. This structure can efficiently process visual signals—for example, through horizontal and vertical synaptic pathways (Wassle, 2004). Immunostaining and electron microscopy have shown ribbon synapse expression in retinal organoids, which in turn may conduct signals from the PRs to the BCs (Wahlin et al., 2017). However, there is a lack of sophisticated traits in the outer plexiform synapses (Haverkamp et al., 2000) within horizontal cells, PRs, and BCs in retinal organoids. Currently, ribbon synapses between BCs, amacrine cells, and GCs have not been detected in retinal organoids. This finding could be due to the disappearance of the inner layer, including the GCs after a certain time period in the

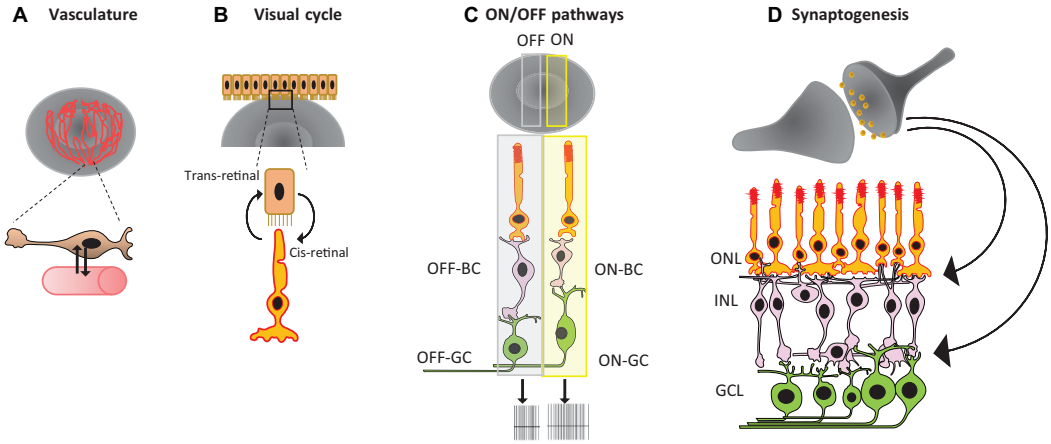

FIGURE 2 | Summary of major challenges in retinal organoid technology: **(A)** lack of vasculature, **(B)** RPE orientation for the visual cycle, **(C)** mature ON and OFF pathways, and **(D)** proper cell orientation and synaptogenesis.

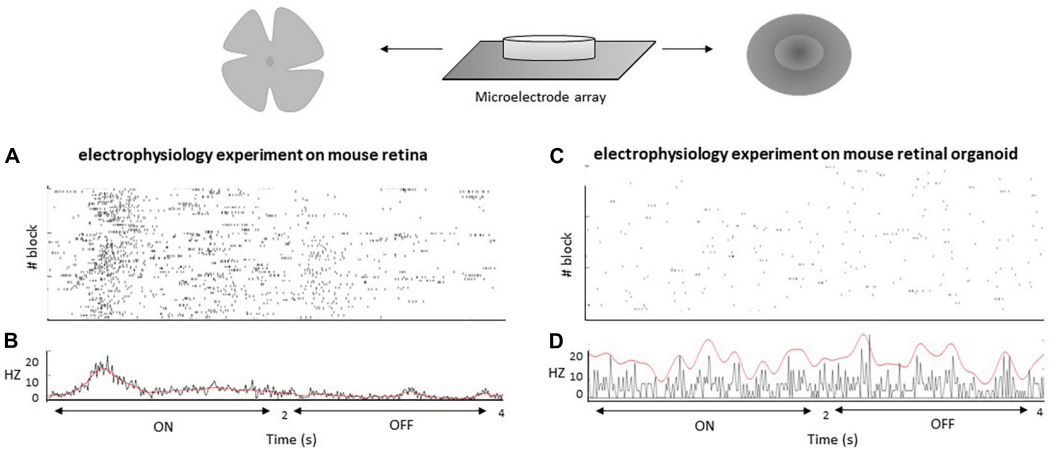

FIGURE 3 | MEA recordings from mouse retina at day P1 **(A)** and mouse retinal organoid at day 22 **(C)**. Frames **(A,C)** provide rastergrams of all responses for cells to visual stimulation blocks with a stimulus of 2 s ON and 2 s OFF that was cycled 25 times per block (3 blocks). Frames **(B,D)** provide peristimulus time histograms for all responses.

organoid culture process—e.g., before maturation of the PRs (Reichman et al., 2014; Zhong et al., 2014). Because BCs arise late in development (Cepko, 2014), GCs may have already disappeared. Moreover, rod and cone ribbon synapses have not been discovered in retinal organoids. Nevertheless, niches like IGF-1 for wiring between retinal cells may influence the formation of synapses in the inner layer of retinal organoids (Mellough et al., 2015).

Retinal Pathways

A fundamental functional feature of the retina is its ability to discriminate between different light stimuli in a way that is recordable by electrophysiology. This ability results from the fact that the retina is composed of different cell types with complex connectivity. However, comparing *in vitro* retinal organoids to *in vivo* retinal tissue, researchers have found that retinal organoids are far less morphologically and functionally sophisticated in terms of their synapses, connectivity, and cell subtype varieties (Masland, 2012). Even in long-term cultures, retinal organoids are incapable of generating and maintaining the three clearly separated nuclear layers found in *in vivo* retinas (Dorgau et al., 2019). Because of this fact, retinal organoids generally lack the complex arrangement of rods and cones found in natural retinas, as well as the connections from rods and cones to interneurons and GC types—e.g., ON and OFF pathways, direction-selective pathways, etc. (Baden et al., 2016; Behrens et al., 2016). Retinal organoids are not only unable to completely respond to light stimuli, but they are also characterized by a lack of retinal pathways, particularly ON and OFF pathways (Dorgau et al., 2019). Immature outer segments of PRs, as initial components of photocascades, might be one of the reasons (Castro et al., 2019). Using MEA as a method to measure retinal pathways, researchers have shown

that GCs in organoids are responsive to light stimuli; however, these responses are indolent and can be hard to separate from background noise and spontaneous spikes (Hallam et al., 2018). This behavior is similar to spontaneous activities of the retina during embryonic time (Maccione et al., 2014). However, light responses are clearly detectable at the same age in mice (Ford et al., 2012). New protocols for generating retinal organoids have partially improved responses to light, as measured by MEA recordings (Dorgau et al., 2019); however, such recordings are not comparable with clear light responses *in vivo*. Using calcium imaging with a two-photon laser microscope, only 16.7% of cells in the outer nuclear layer and 12.0% of cells in the inner nuclear layer of retinal organoids are light-mediated responsive (Cowan et al., 2020), reflecting immature retinal pathways. It appears that retinal organoids vary to some extent in their structure and functionality, a fact that might emanate from various properties of iPSCs lines (Castro et al., 2019). Hosseinzadeh and Fathi (2021) recorded ON and OFF light responses in mouse retinal organoids at day 22 and mouse retinas at postnatal day 1 (P1) via MEA. Mice retinal organoids have not shown any clear responses to light modulation (ON and OFF pathways), while mouse retinas have responded to such stimuli (see **Figure 3**). However, mouse retinal organoids have responded to electrical stimulus pulses. In addition, retinal organoids have generated spontaneous action potentials, as shown in **Figure 3**. Overall, retinal organoids mimic the earlier fetal stage concerning electrical activities, with some signs of light responses, but a lack of the clear character of two main retinal pathways, a shortcoming waiting to be resolved. Solutions for this shortcoming are likely to be closely related to synaptogenesis and establishment of electrical retinal pathways.

CONCLUSION

It is an exciting time to generate 3D organs *in vitro*. Technological advances have made much possible; however, several challenges remain to be resolved. ESCs- and iPSCs-derived cell subtypes play a promising role in the generation of retinal organoids, and have clinical implications, especially in personalized medicine. Overall, hiPSCs-derived retinal organoids are an advanced tool for overcoming current and future hurdles. Moreover, retinal organoids can provide us with the data needed to advance various fields of research—for example, models of retinal development and models of retinal pathology. Moreover, they can be used as cell sources for transplants and drug screening. However, recapitulation of human retinal development is currently only a dream. Retinal organoids face many constraints; in particular, visual responses are constrained by physiological pathways. Such challenges have stimulated scientists to advance technologies that may one day generate fully functional retinal organoids. Despite all of these limitations, 3D retinal organoids have already offered unprecedented opportunities to understand some of the mechanisms of retinal development, and have shed light on the pathomechanisms of retinal diseases and cell transplantation. We are close to reaching a technological tipping point where 3D retinal organoids will be able to fully address important questions.

AUTHOR CONTRIBUTIONS

MF and ZH reviewed the literature, and drafted and edited the manuscript. CR corrected and edited the manuscript. All authors approved the final version of the manuscript.

FUNDING

This work was supported by the Deutsche Forschungsgemeinschaft (HO 6221/1-1) to ZH, Tistou and Charlotte Kerstan Stiftung (D.30.21190) to ZH, Sächsische Aufbaubank (SAB), and EuProNet Förderung 100504761 to ZH.

REFERENCES

Achberger, K., Haderspeck, J. C., Kleger, A., and Liebau, S. (2019a). Stem cell-based retina models. *Adv. Drug Deliv. Rev.* 140, 33–50. doi: 10.1016/j.addr.2018.05.005

Achberger, K., Probst, C., Haderspeck, J., Bolz, S., Rogal, J., Chuchuy, J., et al. (2019b). Merging organoid and organ-on-a-chip technology to generate complex multi-layer tissue models in a human retina-on-a-chip platform. *ELife* 8:e46188.

Ajduk, A., and Zernicka-Goetz, M. (2016). Polarity and cell division orientation in the cleavage embryo: from worm to human. *Mol. Hum. Reprod.* 22, 691–703. doi: 10.1093/molehr/gav068

Akhtar, T., Xie, H., Khan, M. I., Zhao, H., Bao, J., Zhang, M., et al. (2019). Accelerated photoreceptor differentiation of hiPSC-derived retinal organoids by contact co-culture with retinal pigment epithelium. *Stem Cell Res.* 39, 101491. doi: 10.1016/j.scr.2019.101491

Baden, T., Berens, P., Franke, K., Roman Roson, M., Bethge, M., and Euler, T. (2016). The functional diversity of retinal ganglion cells in the mouse. *Nature* 529, 345–350. doi: 10.1038/nature16468

Behrens, C., Schubert, T., Haverkamp, S., Euler, T., and Berens, P. (2016). Connectivity map of bipolar cells and photoreceptors in the mouse retina. *Elife* 5:e20041.

Bringmann, A., Pannicke, T., Grosche, J., Francke, M., Wiedemann, P., Skatchkov, S. N., et al. (2006). Muller cells in the healthy and diseased retina. *Prog. Retin. Eye Res.* 25, 397–424. doi: 10.1016/j.preteyeres.2006.05.003

Castro, A., Rodríguez Jimenez, F. J., Jendelova, P., and Erceg, S. (2019). Deciphering retinal diseases through the generation of three dimensional stem cell−derived organoids: concise review. *Stem Cell* 37, 1496–1504. doi: 10.1002/stem.3089

Cepko, C. (2014). Intrinsically different retinal progenitor cells produce specific types of progeny. *Nat. Rev. Neurosci.* 15, 615–627. doi: 10.1038/nrn3767

Chen, T. C., She, P. Y., Chen, D. F., Lu, J. H., Yang, C. H., Huang, D. S., et al. (2019). Polybenzyl glutamate biocompatible scaffold promotes the efficiency of retinal differentiation toward retinal ganglion cell lineage from human-induced pluripotent stem cells. *Int. J. Mol. Sci.* 20:178. doi: 10.3390/ijms20010178

Chichagova, V., Hallam, D., Collin, J., Zerti, D., Dorgau, B., Felemban, M., et al. (2018). Cellular regeneration strategies for macular degeneration: past, present and future. *Eye (Lond.)* 32, 946–971. doi: 10.1038/s41433-018-0061-z

Choi, E. H., Daruwalla, A., Suh, S., Leinonen, H., and Palczewski, K. (2020). Retinoids in the visual cycle: role of the retinal G protein-coupled receptor. *J. Lipid Res.* 62:100040. doi: 10.1194/jlr.tr120000850

Coombs, J., van der List, D., Wang, G. Y., and Chalupa, L. M. (2006). Morphological properties of mouse retinal ganglion cells. *Neuroscience* 140, 123–136. doi: 10.1016/j.neuroscience.2006.02.079

Cora, V., Haderspeck, J., Antkowiak, L., Mattheus, U., Neckel, P. H., Mack, A. F., et al. (2019). A cleared view on retinal organoids. *Cells* 8:391. doi: 10.3390/cells8050391

Cowan, C. S., Renner, M., De Gennaro, M., Gross-Scherf, B., Goldblum, D., Hou, Y., et al. (2020). Cell types of the human retina and its organoids at single-cell resolution. *Cell* 182, 1623–1640.e34.

Cunningham, C. L., Martinez-Cerdeno, V., and Noctor, S. C. (2013). Microglia regulate the number of neural precursor cells in the developing cerebral cortex. *J. Neurosci.* 33, 4216–4233. doi: 10.1523/jneurosci.3441-12.2013

Dorgau, B., Felemban, M., Hilgen, G., Kiening, M., Zerti, D., Hunt, N. C., et al. (2019). Decellularised extracellular matrix-derived peptides from neural retina and retinal pigment epithelium enhance the expression of synaptic markers and light responsiveness of human pluripotent stem cell derived retinal organoids. *Biomaterials* 199, 63–75. doi: 10.1016/j.biomaterials.2019.01.028

Eiraku, M., Takata, N., Ishibashi, H., Kawada, M., Sakakura, E., Okuda, S., et al. (2011). Self-organizing optic-cup morphogenesis in three-dimensional culture. *Nature* 472, 51–56. doi: 10.1038/nature09941

Ferreira, P. G., Muñoz-Aguirre, M., Reverter, F., Sá Godinho, C. P., Sousa, A., Amadoz, A., et al. (2018). The effects of death and post-mortem cold ischemia on human tissue transcriptomes. *Nat. Commun.* 9:490.

Ford, K. J., Felix, A. L., and Feller, M. B. (2012). Cellular mechanisms underlying spatiotemporal features of cholinergic retinal waves. *J. Neurosci.* 32, 850–863. doi: 10.1523/jneurosci.5309-12.2012

Forgacs, G., Foty, R. A., Shafrir, Y., and Steinberg, M. S. (1998). Viscoelastic properties of living embryonic tissues: a quantitative study. *Biophys. J.* 74, 2227–2234. doi: 10.1016/s0006-3495(98)77932-9

Fuhrmann, S., Zou, C., and Levine, E. M. (2014). Retinal pigment epithelium development, plasticity, and tissue homeostasis. *Exp. Eye Res.* 123, 141–150. doi: 10.1016/j.exer.2013.09.003

Gagliardi, G., Ben, M., Barek, K., Chaffiol, A., Slembrouck-Brec, A., Conart, J. B., et al. (2018). Characterization and transplantation of CD73-positive photoreceptors isolated from human iPSC-derived retinal organoids. *Stem Cell Rep.* 11, 665–680. doi: 10.1016/j.stemcr.2018.07.005

Gao, D., Vela, I., Sboner, A., Iaquinta, P. J., Karthaus, W. R., Gopalan, A., et al. (2014). Organoid cultures derived from patients with advanced prostate cancer. *Cell* 159, 176–187.

Gargini, C., Terzibasi, E., Mazzoni, F., and Strettoi, E. (2007). Retinal organization in the retinal degeneration 10 (rd10) mutant mouse: a morphological and ERG study. *J. Comp. Neurol.* 500, 222–238. doi: 10.1002/cne.21144

Garita-Hernandez, M., Lampič, M., Chaffiol, A., Guibbal, L., Routet, F., Santos-Ferreira, T., et al. (2019). Restoration of visual function by transplantation of optogenetically engineered photoreceptors. *Nat. Commun.* 10:4524.

German, O. L., Buzzi, E., Rotstein, N. P., Rodriguez-Boulan, E., and Politi, L. E. (2008). Retinal pigment epithelial cells promote spatial reorganization and differentiation of retina photoreceptors. *J. Neurosci. Res.* 86, 3503–3514. doi: 10.1002/jnr.21813

Gonzalez-Cordero, A., Kruczek, K., Naeem, A., Fernando, M., Kloc, M., Ribeiro, J., et al. (2017). Recapitulation of human retinal development from human pluripotent stem cells generates transplantable populations of cone photoreceptors. *Stem Cell Rep.* 9, 820–837. doi: 10.1016/j.stemcr.2017.07.022

Hallam, D., Hilgen, G., Dorgau, B., Zhu, L., Yu, M., Bojic, S., et al. (2018). Human-induced pluripotent stem cells generate light responsive retinal organoids with variable and nutrient-dependent efficiency. *Stem Cells* 36, 1535–1551. doi: 10.1002/stem.2883

Haverkamp, S., Grunert, U., and Wassle, H. (2000). The cone pedicle, a complex synapse in the retina. *Neuron* 27, 85–95. doi: 10.1016/s0896-6273(00)00011-8

Hosseinzadeh, Z., and Fathi, M. (2021). *Characterization of ON and OFF Pathways in Mouse Retinal Organoids. OSF Supplementary Data File*. Frankfurt: OSF Storage, doi: 10.17605/OSF.IO/MZSG2

Kang, K. H., Lemke, G., and Kim, J. W. (2009). The PI3K-PTEN tug-of-war, oxidative stress and retinal degeneration. *Trends Mol. Med.* 15, 191–198. doi: 10.1016/j.molmed.2009.03.005

Kaya, K. D., Chen, H. Y., Brooks, M. J., Kelley, R. A., Shimada, H., Nagashima, K., et al. (2019). Transcriptome-based molecular staging of human stem cell-derived retinal organoids uncovers accelerated photoreceptor differentiation by 9-cis retinal. *Mol. Vis.* 25, 663–678.

Kim, S., Lowe, A., Dharmat, R., Lee, S., Owen, L. A., Wang, J., et al. (2019). Generation, transcriptome profiling, and functional validation of cone-rich human retinal organoids. *Proc. Natl. Acad. Sci. U.S.A.* 116, 10824–10833. doi: 10.1073/pnas.1901572116

Kozlowski, M. R. (2015). The ARPE-19 cell line: mortality status and utility in macular degeneration research. *Curr. Eye Res.* 40, 501–509. doi: 10.3109/02713683.2014.935440

Kruczek, K., and Swaroop, A. (2020). Pluripotent stem cell-derived retinal organoids for disease modeling and development of therapies. *Stem Cells* 38, 1206–1215.

Lagnado, L., and Schmitz, F. (2015). Ribbon synapses and visual processing in the retina. *Annu. Rev. Vis. Sci.* 1, 235–262. doi: 10.1146/annurev-vision-082114-035709

Lamba, D. A., Karl, M. O., Ware, C. B., and Reh, T. A. (2006). Efficient generation of retinal progenitor cells from human embryonic stem cells. *Proc. Natl. Acad. Sci. U.S.A.* 103, 12769–12774.

Laschke, M. W., and Menger, M. D. (2012). Vascularization in tissue engineering: angiogenesis versus inosculation. *Eur. Surg. Res.* 48, 85–92. doi: 10.1159/000336876

Lerma, J., and De Carlos, J. A. (2014). Epilog: cajal's unique and legitimated school. *Front. Neuroanat.* 8:58. doi: 10.3389/fnana.2014.00058

Li, F., Jiang, D., and Samuel, M. A. (2019). Microglia in the developing retina. *Neural Dev.* 14:12.

Li, Z., Guo, X., and Guan, J. (2012). An oxygen release system to augment cardiac progenitor cell survival and differentiation under hypoxic condition. *Biomaterials* 33, 5914–5923. doi: 10.1016/j.biomaterials.2012.05.012

Lin, B., McLelland, B. T., Aramant, R. B., Thomas, B. B., Nistor, G., Keirstead, H. S., et al. (2020). Retina organoid transplants develop photoreceptors and improve visual function in RCS Rats with RPE dysfunction. *Invest. Ophthalmol. Vis. Sci.* 61:34. doi: 10.1167/iovs.61.11.34

Liu, S., Xie, B., Song, X., Zheng, D., He, L., Li, G., et al. (2018). Self-formation of RPE spheroids facilitates enrichment and expansion of hiPSC-derived RPE generated on retinal organoid induction platform. *Invest. Ophthalmol. Vis. Sci.* 59, 5659–5669. doi: 10.1167/iovs.17-23613

Maccione, A., Hennig, M. H., Gandolfo, M., Muthmann, O., van Coppenhagen, J., Eglen, S. J., et al. (2014). Following the ontogeny of retinal waves: pan-retinal recordings of population dynamics in the neonatal mouse. *J. Physiol.* 592, 1545–1563. doi: 10.1113/jphysiol.2013.262840

Mandai, M., Watanabe, A., Kurimoto, Y., Hirami, Y., Morinaga, C., Daimon, T., et al. (2017). Autologous induced stem-cell-derived retinal cells for macular degeneration. *N. Engl. J. Med.* 376, 1038–1046.

Masland, R. H. (2012). The neuronal organization of the retina. *Neuron* 76, 266–280. doi: 10.1016/j.neuron.2012.10.002

McLelland, B. T., Lin, B., Mathur, A., Aramant, R. B., Thomas, B. B., Nistor, G., et al. (2018). Transplanted hESC-derived retina organoid sheets differentiate, integrate, and improve visual function in retinal degenerate rats. *Invest. Ophthalmol. Vis. Sci.* 59, 2586–2603. doi: 10.1167/iovs.17-23646

Mellough, C. B., Collin, J., Khazim, M., White, K., Sernagor, E., Steel, D. H., et al. (2015). IGF-1 Signaling plays an important role in the formation of three-dimensional laminated neural retina and other ocular structures from human embryonic stem cells. *Stem Cells* 33, 2416–2430. doi: 10.1002/stem.2023

Mohamed, A., Chaurasia, S., and Garg, P. (2016). Outcome of transplanted donor corneas with more than 6 h of death-to-preservation time. *Indian J. Ophthalmol.* 64, 635–638. doi: 10.4103/0301-4738.194338

Nakano, T., Ando, S., Takata, N., Kawada, M., Muguruma, K., Sekiguchi, K., et al. (2012). Self-formation of optic cups and storable stratified neural retina from human ESCs. *Cell Stem Cell* 10, 771–785. doi: 10.1016/j.stem.2012.05.009

O'Hara-Wright, M., and Gonzalez-Cordero, A. (2020). Retinal organoids: a window into human retinal development. *Development* 147:dev189746. doi: 10.1242/dev.189746

Okawa, H., Yu, W. Q., Matti, U., Schwarz, K., Odermatt, B., Zhong, H., et al. (2019). Dynamic assembly of ribbon synapses and circuit maintenance in a vertebrate sensory system. *Nat. Commun.* 10:2167.

Ovando-Roche, P., West, E. L., Branch, M. J., Sampson, R. D., Fernando, M., Munro, P., et al. (2018). Use of bioreactors for culturing human retinal organoids improves photoreceptor yields. *Stem Cell Res. Ther.* 9:156.

Ozbolat, I. T. (2015). Bioprinting scale-up tissue and organ constructs for transplantation. *Trends Biotechnol.* 33, 395–400. doi: 10.1016/j.tibtech.2015.04.005

Pannicke, T., Biedermann, B., Uckermann, O., Weick, M., Bringmann, A., Wolf, S., et al. (2005). Physiological properties of retinal Muller glial cells from the cynomolgus monkey, Macaca fascicularis–a comparison to human Muller cells. *Vision Res.* 45, 1781–1791. doi: 10.1016/j.visres.2005.01.016

Popova, E. (2014). ON-OFF interactions in the retina: role of glycine and GABA. *Curr. Neuropharmacol.* 12, 509–526. doi: 10.2174/1570159x13999150122165018

Qian, X., Song, H., and Ming, G. L. (2019). Brain organoids: advances, applications and challenges. *Development* 146:dev166074. doi: 10.1242/dev.166074

Radisic, M., Malda, J., Epping, E., Geng, W., Langer, R., and Vunjak-Novakovic, G. (2006). Oxygen gradients correlate with cell density and cell viability in engineered cardiac tissue. *Biotechnol. Bioeng.* 93, 332–343. doi: 10.1002/bit.20722

Ramsden, C. M., Powner, M. B., Carr, A. J., Smart, M. J., da Cruz, L., and Coffey, P. J. (2013). Stem cells in retinal regeneration: past, present and future. *Development* 140, 2576–2585.

Raymond, S. M., and Jackson, I. J. (1995). The retinal pigmented epithelium is required for development and maintenance of the mouse neural retina. *Curr. Biol.* 5, 1286–1295. doi: 10.1016/s0960-9822(95)00255-7

Reichman, S., Terray, A., Slembrouck, A., Nanteau, C., Orieux, G., Habeler, W., et al. (2014). From confluent human iPS cells to self-forming neural retina and retinal pigmented epithelium. *Proc. Natl. Acad. Sci. U.S.A.* 111, 8518–8523. doi: 10.1073/pnas.1324212111

Richards, D., Jia, J., Yost, M., Markwald, R., and Mei, Y. (2017). 3D bioprinting for vascularized tissue fabrication. *Ann. Biomed. Eng.* 45, 132–147. doi: 10.1007/s10439-016-1653-z

Sahu, B., and Maeda, A. (2018). RPE visual cycle and biochemical phenotypes of mutant mouse models. *Methods Mol. Biol.* 1753, 89–102. doi: 10.1007/978-1-4939-7720-8_6

Santos-Ferreira, T., Llonch, S., Borsch, O., Postel, K., Haas, J., and Ader, M. (2016). Retinal transplantation of photoreceptors results in donor-host cytoplasmic exchange. *Nat. Commun.* 7:13028.

Schwartz, S. D., Regillo, C. D., Lam, B. L., Eliott, D., Rosenfeld, P. J., Gregori, N. Z., et al. (2015). Human embryonic stem cell-derived retinal pigment epithelium in patients with age-related macular degeneration and Stargardt's macular dystrophy: follow-up of two open-label phase 1/2 studies. *Lancet* 385, 509–516. doi: 10.1016/s0140-6736(14)61376-3

Shannon, J. M., Mason, R. J., and Jennings, S. D. (1987). Functional differentiation of alveolar type II epithelial cells in vitro: effects of cell shape, cell-matrix interactions and cell-cell interactions. *Biochim. Biophys. Acta* 931, 143–156. doi: 10.1016/0167-4889(87)90200-x

Singh, R., Cuzzani, O., Binette, F., Sternberg, H., West, M. D., and Nasonkin, I. O. (2018). Pluripotent stem cells for retinal tissue engineering: current status and future prospects. *Stem Cell Rev. Rep.* 14, 463–483. doi: 10.1007/s12015-018-9802-4

Singh, R. K., and Nasonkin, I. O. (2020). Limitations and promise of retinal tissue from human pluripotent stem cells for developing therapies of blindness. *Front. Cell. Neurosci.* 14:179. doi: 10.3389/fncel.2020.00179

Sparrow, J. R., Hicks, D., and Hamel, C. P. (2010). The retinal pigment epithelium in health and disease. *Curr. Mol. Med.* 10, 802–823.

Sprangers, J., Zaalberg, I. C., and Maurice, M. M. (2020). Organoid-based modeling of intestinal development, regeneration, and repair. *Cell Death Differ.* 8, 95–107. doi: 10.1038/s41418-020-00665-z

Sridhar, A., Hoshino, A., Finkbeiner, C. R., Chitsazan, A., Dai, L., Haugan, A. K., et al. (2020). Single-cell transcriptomic comparison of human fetal retina, hPSC-derived retinal organoids, and long-term retinal cultures. *Cell Rep.* 30, 1644–1659.e4.

Stern, J. H., Tian, Y., Funderburgh, J., Pellegrini, G., Zhang, K., Goldberg, J. L., et al. (2018). Regenerating eye tissues to preserve and restore vision. *Cell Stem Cell* 22, 834–849. doi: 10.1016/j.stem.2018.05.013

Szatko, K. P., Korympidou, M. M., Ran, Y., Berens, P., Dalkara, D., Schubert, T., et al. (2020). Neural circuits in the mouse retina support color vision in the upper visual field. *Nat. Commun.* 11:3481.

Taguchi, A., Kaku, Y., Ohmori, T., Sharmin, S., Ogawa, M., Sasaki, H., et al. (2014). Redefining the in vivo origin of metanephric nephron progenitors enables generation of complex kidney structures from pluripotent stem cells. *Cell Stem Cell* 14, 53–67. doi: 10.1016/j.stem.2013.11.010

Takano, T., Xu, C., Funahashi, Y., Namba, T., and Kaibuchi, K. (2015). Neuronal polarization. *Development* 142, 2088–2093.

tom Dieck, S., and Brandstatter, J. H. (2006). Ribbon synapses of the retina. *Cell Tissue Res.* 326, 339–346. doi: 10.1007/s00441-006-0234-0

Tsin, A., Betts-Obregon, B., and Grigsby, J. (2018). Visual cycle proteins: structure, function, and roles in human retinal disease. *J. Biol. Chem.* 293, 13016–13021. doi: 10.1074/jbc.aw118.003228

Varma, R., Vajaranant, T. S., Burkemper, B., Wu, S., Torres, M., Hsu, C., et al. (2016). Visual impairment and blindness in adults in the United States: demographic and geographic variations from 2015 to 2050. *JAMA Ophthalmol.* 134, 802–809. doi: 10.1001/jamaophthalmol.2016.1284

Volgyi, B., Chheda, S., and Bloomfield, S. A. (2009). Tracer coupling patterns of the ganglion cell subtypes in the mouse retina. *J. Comp. Neurol.* 512, 664–687. doi: 10.1002/cne.21912

Volobueva, A. S., Orekhov, A. N., and Deykin, A. V. (2019). An update on the tools for creating transgenic animal models of human diseases – focus on atherosclerosis. *Braz. J. Med. Biol. Res.* 52:e8108.

Wahlin, K. J., Maruotti, J. A., Sripathi, S. R., Ball, J., Angueyra, J. M., Kim, C., et al. (2017). Photoreceptor outer segment-like structures in long-term 3D retinas from human pluripotent stem cells. *Sci. Rep.* 7:766.

Wassle, H. (2004). Parallel processing in the mammalian retina. *Nat. Rev. Neurosci.* 5, 747–757. doi: 10.1038/nrn1497

West, E. L., Pearson, R. A., MacLaren, R. E., Sowden, J. C., and Ali, R. R. (2009). Cell transplantation strategies for retinal repair. *Prog. Brain Res.* 175, 3–21. doi: 10.1016/s0079-6123(09)17501-5

World Health Organization [WHO] (2019). *World Report on Vision Executive Summary*. Available online at: https://www.who.int/docs/default-source/documents/publications/world-report-on-vision-accessible-executive-summary.pdf?sfvrsn=d159ec9f_2 (accessed March 24, 2021).

Worsdorfer, P., Dalda, N., Kern, A., Kruger, S., Wagner, N., Kwok, C. K., et al. (2019). Generation of complex human organoid models including vascular networks by incorporation of mesodermal progenitor cells. *Sci. Rep.* 9:15663.

Wright, C. B., Redmond, T. M., and Nickerson, J. M. (2015). A history of the classical visual cycle. *Prog. Mol. Biol. Transl. Sci.* 134, 433–448. doi: 10.1016/bs.pmbts.2015.06.009

Yong, P. H., Zong, H., Medina, R. J., Limb, G. A., Uchida, K., Stitt, A. W., et al. (2010). Evidence supporting a role for N-(3-formyl-3,4-dehydropiperidino)lysine accumulation in Muller glia dysfunction and death in diabetic retinopathy. *Mol. Vis.* 16, 2524–2538.

Zerti, D., Dorgau, B., Felemban, M., Ghareeb, A. E., Yu, M., Ding, Y., et al. (2020). Developing a simple method to enhance the generation of cone and rod photoreceptors in pluripotent stem cell-derived retinal organoids. *Stem Cells* 38, 45–51. doi: 10.1002/stem.3082

Zhong, X., Gutierrez, C., Xue, T., Hampton, C., Vergara, M. N., Cao, L. H., et al. (2014). Generation of three-dimensional retinal tissue with functional photoreceptors from human iPSCs. *Nat. Commun.* 5:4047.

Conflict of Interest: The authors declare that the research was conducted in the absence of any commercial or financial relationships that could be construed as a potential conflict of interest.

Copyright © 2021 Fathi, Ross and Hosseinzadeh. This is an open-access article distributed under the terms of the Creative Commons Attribution License (CC BY). The use, distribution or reproduction in other forums is permitted, provided the original author(s) and the copyright owner(s) are credited and that the original publication in this journal is cited, in accordance with accepted academic practice. No use, distribution or reproduction is permitted which does not comply with these terms.

frontiers in Neuroscience

ORIGINAL RESEARCH
published: 29 April 2021
doi: 10.3389/fnins.2021.636969

Mutant PRPF8 Causes Widespread Splicing Changes in Spliceosome Components in Retinitis Pigmentosa Patient iPSC-Derived RPE Cells

*Ángeles Arzalluz-Luque[1], Jose Luis Cabrera[2], Heli Skottman[3], Alberto Benguria[2], Arantxa Bolinches-Amorós[4,5], Nicolás Cuenca[6], Vincenzo Lupo[7,8], Ana Dopazo[2], Sonia Tarazona[1], Bárbara Delás[9], Miguel Carballo[9], Beatriz Pascual[9], Imma Hernan[9], Slaven Erceg[4,5,8,10] and Dunja Lukovic[8,11]**

[1] Department of Applied Statistics, Operations Research and Quality, Universitat Politècnica de València, València, Spain, [2] Genomics Unit, Centro Nacional de Investigaciones Cardiovasculares (CNIC). Madrid, Spain, [3] Faculty of Medicine and Health Technology, Tampere University, Tampere, Finland, [4] Stem Cells Therapies in Neurodegenerative Diseases Lab, Research Center Principe Felipe, Valencia, Spain, [5] National Stem Cell Bank-Valencia Node, Research Center Principe Felipe, Valencia, Spain, [6] Department of Physiology, Genetics and Microbiology, University of Alicante, Alicante, Spain, [7] Unit of Genetics and Genomics of Neuromuscular and Neurodegenerative Disorders, Centro de Investigación Príncipe Felipe (CIPF), Valencia, Spain, [8] Rare Diseases Joint Units, IIS La Fe-CIPF, Valencia, Spain, [9] Unitat de Genética Molecular, Hospital de Terrassa, Terrassa, Spain, [10] Department of Neuroregeneration, Institute of Experimental Medicine, Czech Academy of Sciences, Prague, Czechia, [11] Retinal Degeneration Lab, Research Centre Principe Felipe, Valencia, Spain

OPEN ACCESS

Edited by:
David Pozo,
University of Seville, Spain

Reviewed by:
Linda Lako,
Newcastle University, United Kingdom
Zi-Bing Jin,
Capital Medical University, China

***Correspondence:**
Dunja Lukovic
dlukovic@cipf.es

Specialty section:
This article was submitted to Neurodegeneration, a section of the journal Frontiers in Neuroscience

Received: *02 December 2020*
Accepted: *25 February 2021*
Published: *29 April 2021*

Citation:
Arzalluz-Luque Á, Cabrera JL, Skottman H, Benguria A, Bolinches-Amorós A, Cuenca N, Lupo V, Dopazo A, Tarazona S, Delás B, Carballo M, Pascual B, Hernan I, Erceg S and Lukovic D (2021) Mutant PRPF8 Causes Widespread Splicing Changes in Spliceosome Components in Retinitis Pigmentosa Patient iPSC-Derived RPE Cells. Front. Neurosci. 15:636969. doi: 10.3389/fnins.2021.636969

Retinitis pigmentosa (RP) is a rare, progressive disease that affects photoreceptors and retinal pigment epithelial (RPE) cells with blindness as a final outcome. Despite high medical and social impact, there is currently no therapeutic options to slow down the progression of or cure the disease. The development of effective therapies was largely hindered by high genetic heterogeneity, inaccessible disease tissue, and unfaithful model organisms. The fact that components of ubiquitously expressed splicing factors lead to the retina-specific disease is an additional intriguing question. Herein, we sought to correlate the retinal cell-type-specific disease phenotype with the splicing profile shown by a patient with autosomal recessive RP, caused by a mutation in pre-mRNA splicing factor 8 (PRPF8). In order to get insight into the role of PRPF8 in homeostasis and disease, we capitalize on the ability to generate patient-specific RPE cells and reveal differentially expressed genes unique to RPE cells. We found that spliceosomal complex and ribosomal functions are crucial in determining cell-type specificity through differential expression and alternative splicing (AS) and that PRPF8 mutation causes global changes in splice site selection and exon inclusion that particularly affect genes involved in these cellular functions. This finding corroborates the hypothesis that retinal tissue identity is conferred by a specific splicing program and identifies retinal AS events as a framework toward the design of novel therapeutic opportunities.

Keywords: iPSC, RPE, RNA-Seq, retinitis pigmentosa, pre-mRNA splicing, alternative splicing, PRPF8

INTRODUCTION

Retinitis pigmentosa (RP), the most common form of hereditary retinal dystrophies, is a progressive blinding disease that currently lacks effective therapies (Hartong et al., 2006). Typically, light-sensing photoreceptors and the underlying retinal pigment epithelium (RPE), responsible for photoreceptor homeostasis, are the primary degenerated cells. RP is highly genetically heterogeneous with over 80 disease-causing genes identified to date[1]. Mutations in splicing proteins are described to account altogether as a second most common cause of autosomal dominant RP (adRP) (Sullivan et al., 2006).

Splicing reaction is a process of excision of non-coding intervening sequences, introns, and exon ligations resulting in coding capacity diversification of a limited number of expressed genes with > 90% of 20,000 human protein-coding genes producing multiple mRNA isoforms. This stepwise reaction is performed by spliceosome, a multisubunit ribonucleoprotein complex with the core components uridine-rich small non-coding nuclear RNAs (snRNAs, U1, U2, U4, U5, and U6) and associated proteins that assemble on pre-mRNA to catalyze the excision of introns (Wahl et al., 2009). Mutations in seven genes coding for pre-mRNA processing factors known as PRPFs (PRPF8, PRPF31, PRPF3, PRPF4, and PRPF6), SNRNP200, and PAP-1 have been described to cause adRP (Sullivan et al., 2006).

While these genes are expressed ubiquitously in all tissues and are highly conserved among eukaryotes, it remains unclear why mutations thereof exhibit exclusively retinal phenotype. It has been proposed that *PRPF* mutations might cause global splicing dysregulation and affects only retina because of retinal enhanced splicing activity (Tanackovic et al., 2011). Alternatively, a retina-specific splicing code could confer tissue-specific transcripts that are altered by mutations in splicing factors and therefore cause the disease.

PRPF8 is a 220-kDa, evolutionary highly conserved protein described to play a central role in spliceosomal catalytic activity (Grainger and Beggs, 2005; Galej et al., 2013). Mutations in the C-terminal tail have been described to cause adRP (RP13, OMIM600059) (McKie et al., 2001) while mutations in the N-terminal part have recently been found in glaucoma patients. Mutations in PRPF8, unlike PRPF31, show in the majority of cases complete penetrance, with marked disease progression, exhibiting moderate phenotype with residual vision up to their fifth decade or severe clinical phenotypes initiating in the first decade of life (Martinez-Gimeno et al., 2003; Maubaret et al., 2011; Escher et al., 2018). The degree of severity is proposed to be related to the type of mutation (Escher et al., 2018). Mouse models, *Prpf8*-H2309P with knocked-in missense mutation, showed only mild phenotype in RPE ultrastructure only at 2 years of age, without any loss of ERG signal (Graziotto et al., 2011). Therefore, these animal models are insufficient and human models that recapitulate the clinical phenotype are required to decipher the mechanism of disease.

Native human retina is a largely inaccessible tissue that cannot provide enough research material. Moreover, it is non-expandable due to its postmitotic state. The generation of induced pluripotent stem cells (iPSCs) from accessible tissue like patient's skin, and coaxing them toward retinal tissue, offers an unprecedented opportunity to study the disease and also find new therapies. Moreover, the advantage of the iPSC-based models is that they recapitulate the disease-causing mutation and patient's genetic complexity, essential for complex and late-onset diseases. The iPSCs can be directed toward both photoreceptors and RPE cells, capturing their morphology and function (Hirami et al., 2009; Reichman et al., 2014; Zhong et al., 2014) and have been used successfully in disease modeling (Lukovic et al., 2015, 2020; Shimada et al., 2017; Buskin et al., 2018). The identification of primary affected cell type in RP is hampered due to strong interplay between photoreceptor and RPE cells; namely, mutations of genes expressed in RPE lead to secondary photoreceptor degeneration; conversely, mutations in genes expressed in photoreceptors induce collateral RPE disruptions. This task is additionally obscured in PRPF-caused RP owing to their ubiquitous nature. Recent studies support RPE as likely primary affected cell type by PRPF mutations. Mouse models *Prpf3*-T49M, *Prpf8*-H2309P and *Prpf31*$^{+/-}$ showed moderate ultrastructural alterations including loss of basal infoldings, accumulation of amorphous deposits beneath the RPE and presence of vacuoles while neural retina remained intact (Graziotto et al., 2011). These morphological alterations observed in old mice are preceded by functional disruption in phagocytosis of photoreceptor outer segments (POS) and altered adhesion between RPE microvilli and photoreceptors 10 days upon birth (Farkas et al., 2014). Finally, in PRPF31-RP patient-derived photoreceptors and RPE, both cell types were altered, however; iPSC-RPE were most severely affected with ultrastructural and functional abnormalities. Furthermore, this study showed that spliceosome global dysregulation underlies disrupted RPE polarity, trans-epithelial resistance, phagocytosis, primary cilia length, and incidence in human and mouse genetic background (Buskin et al., 2018). The aforementioned studies prompted us to study PRPF8 pathomechanism in a cell-autonomous manner in patient-derived RPE cells.

Herein, we have generated RPE cells from reprogrammed dermal skin fibroblasts derived from a patient diagnosed with adRP and bearing a pathogenic mutation in *PRPF8* (NM_006445:c.6974_6994del) (Lukovic et al., 2017) in a heterozygous state (from here on: *Patient-RPE*) and patient's non-affected tissue, i.e., fibroblasts (from here on: *Patient-fibroblasts*). An unrelated, non-affected individual was used as control (from here on: *Control-RPE* and *Control-fibroblasts*). We generated RNA sequencing (RNA-Seq) data for three independent experimental replicates per sample and performed a whole-transcriptome analysis where healthy control samples were compared to mutation-bearing cells, in order to depict retinal-specific transcriptional signature caused by the mutation.

MATERIALS AND METHODS

Human Subjects

Research procedures followed the principles of the Declaration of Helsinki. The study was approved by the Research Ethical Committee of the Hospital of Terrassa and Valencian Ethics

[1]http://www.sph.uth.tmc.edu/retnet

Committee CAEC (Comité Etico Autonomico de Estudios Clínicos), Valencia, Spain. Both subjects provided written informed consent after the nature of the study procedures had been fully explained.

adRP Patient's Clinical Phenotype

The patient reported a history of nyctalopia starting from the first decade of life. At the age of 20 the best-corrected visual acuity (BCVA) was 20/40 in the right eye and 20/30 in the left eye. Anterior segment examination showed minimal posterior subcapsular cataract in the right eye, being normal in the left eye. Fundus examination showed the typical RP changes, consisting in optic disk pallor, retinal vessel attenuation, and extensive bone spicule-like pigmentation extending from the vascular arcades toward the periphery. No abnormalities at the macula were detected. Humphrey visual field examination showed a severe visual field loss, with 10° central preserved and a peripheral remnant in the left eye. Electroretinography was abolished at that time.

At the age of 47, lens surgery had been performed in the right eye, so that BCVA was 20/40. In the right eye, she presented a moderate subcapsular cataract, being the BCVA 20/70. Fundus examination showed the typical RP changes. Spectral domain optical coherence tomography showed a complete absence of outer retinal bands corresponding to photoreceptors. Macular edema or epiretinal membrane was not detected in any moment of evolution.

Cell Line Derivation and Differentiation

Fibroblast Cell Culture

Cryopreserved fibroblast cell lines derived from skin biopsies from the female RP patient (Patient-fibroblasts) and a healthy (BCVA40/40) man (Control-fibroblasts) were thawed and cultured in DMEM (10% FBS, 2 mM GlutaMAX, 50 U/ml penicillin and 50 mg/ml streptomycin) at 37°C under 5% CO_2. Fibroblasts at passages 6–8 were used in this study. Samples were collected in triplicates, from independent cell cultures. Authentication of the fibroblast cell lines by microsatellite STR markers was performed to confirm the identity to the iPSC lines.

iPSC Cell Culture and Differentiation Toward RPE

Two iPSC lines were employed in this study (**Supplementary Table 4**). The iPSC line derived from the patient, clinically diagnosed with RP and molecularly genotyped previously, by reprogramming dermal fibroblasts using a non-integrative Sendai virus (Lukovic et al., 2017) has been employed. As control cell line, iPSC Ctrl1-FiPS4F1 (Spanish National Stem Cell Bank) obtained from a healthy individual by the same reprogramming strategy (Sendai virus, Cytotune, Thermo Fisher) was used. Both cell lines were induced to differentiate toward RPE following the previously published protocol (Lukovic et al., 2015; Hongisto et al., 2017). Briefly, the iPSCs were cultured in hESC medium (KO DMEM, KSR 20%, GlutaMAX 2 mM, non-essential amino acids 0.1 mM, β-mercaptoethanol 0.23 mM, basic FGF 10 ng/ml, and penicillin/streptomycin) on irradiated (45 Gy) human feeder cells (ATCC CRL2429) at 37°C under 5% CO_2. When the colonies reached confluency, they were lifted and cultured in suspension in the absence of bFGF until the dark patches appeared. The dark patches were excised, trypsinized, and plated on collagen type IV/LN-521 coated plastic cell culture dishes where they acquired the RPE morphology within 4–8 weeks. RPE-like cells were passed through a 70-μm cell strainer in order to reach a homogeneous, highly pigmented RPE-like monolayer with characteristic uniform polygonal cell morphology. The differentiation experiments were performed in triplicates for both genotypes (*Patient-RPE* and *Control-RPE*). The samples were collected from each differentiation experiment ($n = 3$) and RNA extraction was performed.

Immunocytochemistry

Cells were fixed with 4% paraformaldehyde (PFA), washed twice in PBS, and placed in blocking solution (3% normal goat or donkey serum and 0.5% Triton-X 100 in PBS) for 1 h at room temperature. Cells were then incubated overnight at 4°C with one of the following primary antibodies: anti-PRPF8 (1: 200, Santa Cruz sc55534, Abcam ab79237), rabbit anti-CRALBP (1:250, Abcam), rabbit anti-ZO1 (1:50, Invitrogen), and mouse anti-Na/K-ATPase (1:100, Santa Cruz). The following day, cells were washed three to five times in PBS and incubated with an appropriate secondary antibody (1:500, Invitrogen). After secondary antibody incubation, nuclei were stained with 4′,6-diamidino-2-phenylindole, dihydrochloride (DAPI) (Life Technologies, #D1306) and washed three times in PBS. The coverslips were mounted using Vectashield Mounting Medium (Vector Lab, Burlingame, CA, United States) and imaged on Leica confocal microscope SP8.

POS Phagocytosis Assay

Bovine rod POS were obtained from InVision BioResources (WA, United States) and labeled with FITC. Phagocytosis assay was performed as described previously (Lukovic et al., 2015). Briefly, iPSC-RPE cells were incubated with POS for 2 h/37°C, washed with PBS, and fixed by 4% PFA. After permeabilization by 0.1% Triton-X, phalloidin staining was performed and the samples were mounted with Vectashield mounting media. The samples were visualized by Leica confocal microscope SP8 using HCX PL APO lambda blue 63X/1.4 OIL objective. The quantification of POS particles was performed by imaging random fields from three different experiments in each condition. Five images were taken from each experiment. The relative intensity of internal POS labeling was quantified using Image J, and the pairwise comparison was performed using Student's t test. Results are expressed as the mean ± SD. Values of $p < 0.05$ were considered statistically significant.

Western Blot

Fibroblast cells were lysed in RIPA buffer (R0278 Sigma) containing a protease inhibitor cocktail (Roche), and total protein was quantified using a Bradford Reagent protein assay (B6916 Sigma-Aldrich). Protein lysates were denatured by 1X SDS Sample Buffer. The resulting samples were incubated at 95°C for 5 min. Protein samples (100 μg) were then separated on TGX Stain-FreeTM Gels (Bio-Rad) and electroblotted onto a

PVDF membrane (Trans-Blot® TurboTM Transfer Pack/Bio-Rad). Membranes were incubated in blocking buffer (5% non-fat dried milk diluted in TBS + 0.1% Tween) for 1 h at room temperature, washed three times in TBS + 0.1% Tween for 5 min, and incubated with primary antibody (PRPF8 Abcam ab79237) at 1:500 dilution in blocking buffer overnight at 4°C. Thereafter, blots were washed three times in TBS + 0.1% Tween and incubated with secondary HRP-conjugated antibody in blocking buffer for 45 min at RT. Blots were washed another five times and protein bands were visualized using SuperSignal West Pico PLUS (Thermo Scientific) on X-ray films. β-ACTIN (monoclonal, 1:4,000,000, Sigma-Aldrich A3854) was used as a loading control. HiMark Prestained Protein Standard (LC5699, Thermo) was used as a molecular weight standard.

Transmission Electron Microscopy

RPE cells were fixed in 4% PFA and 2% glutaraldehyde in 0.1 M sodium phosphate buffer (pH 7.2–7.4) for 2 h, washed with the same buffer, and then postfixed in 1% OsO4 in PB. After gradual dehydration in ethanol series, the pieces were embedded in EPON 812. Semithin and ultrathin sections were obtained in an ultramicrotome (Leica Ultracut R, Leica Microsystem). After staining with lead citrate and uranil acetate, ultrathin sections were examined in a JEM-1400 Plus electron microscope (JEOL GmbH, München, Germany).

RNA-Seq Library Preparation and Sequencing

High-quality total RNA (RIN > 7) from three independent experimental replicates of Patient-RPE, Control-RPE, Patient-fibroblasts, and Control-fibroblasts was extracted by RNeasy mini kit (Qiagen, Germany) and quantified by Agilent 2100 Bioanalyser. Total RNA (200 ng) was used to generate barcoded RNA-Seq libraries using the NEBNext Ultra RNA Library preparation kit (New England Biolabs). First, poly A + RNA was purified using poly-T oligo-attached magnetic beads followed by fragmentation and first and second cDNA strand synthesis. Next, cDNA ends were repaired and adenylated. The NEBNext adaptor was then ligated, followed by uracil excision from the adaptor and PCR amplification. The size of the libraries was checked using the Agilent 2100 Bioanalyzer and the concentration was determined using the Qubit® fluorometer (Life Technologies). Libraries were sequenced on a HiSeq2500 (Illumina) to generate 60-base (sequencing batch 1) or 50-base (sequencing batch 2) single-end reads, to a mean depth of 100M reads/sample for one replicate for each condition (sequencing batch 1) and a mean depth of 20M reads/sample for the other two replicates (sequencing batch 2). FastQ files for each sample were obtained using CASAVA v1.8 software (Illumina).

RNA-Seq Analysis

Read Mapping, Quantification and QC

Quality control assessments for raw RNA-Seq reads were performed using fastqc (version 11.5)[2]. TruSeq Illumina adapters (3′ adapters, sequence: AGATCGGAAG AGCACACGTCTGAACTCAGTCA) were removed using cutadapat (version 2.5, option –discard-trimmed activated, detected 2–5% reads with adapters) (Anders et al., 2015). Then, the STAR aligner (version 2.7.3a, median 89.3% reads mapped) was used for mapping the reads to the human genome (GRCh38.p7) using the ENSEMBL transcriptome (release 87) (Yates et al., 2020). Gene-level counts were obtained using HTSeq (Anders et al., 2015) (htseq-count, version 0.11.0, median 79.5% of reads assigned to genes). Mapping QC was performed using Qualimap (version 2.1.2) and MultiQC (version 1.7) (Ewels et al., 2016).

Gene-level counts were normalized using Trimmed Mean of M Values (TMM) (Robinson and Oshlack, 2010). RNA-Seq QC was performed using NOISeq (version 2.30.0) (Tarazona et al., 2015), removing features with mean expression < 1 Count per Million (CPM) across all samples. Batch effects between sequencing batches were then corrected using the ARSyN method (implemented in NOISeq) (Nueda et al., 2012). Principal Component Analysis (PCA) was performed using the prcomp() function included in the stats R package (version 3.6.3).

Differential Expression and Functional Enrichment Analysis

Differential expression (DE) analysis was performed using NOISeqBio (Tarazona et al., 2015). Four contrasts were performed to obtain DE genes (p value <0.05—equivalent to NOISeq probability > 0.95—and log2FC ≥ 1) between all meaningful pairs of clinical conditions and cell types: (A) two within-cell type contrasts to compare clinical conditions for the same cell type, i.e., Control-Fibroblasts vs. Patient-Fibroblasts and Control-RPE vs. Patient-RPE; and (B) two within-condition contrasts to detect differences between cell types for the same clinical condition, i.e., Control-Fibroblasts vs. Control-RPE and Patient-Fibroblasts vs. Patient-RPE.

To better interpret the DE results, we used the information in the control and fibroblast contrasts to filter the results of the patient and RPE contrasts, respectively. In particular, in the within-cell type contrasts, DE genes found in the Control-Fibroblasts vs. Patient-Fibroblasts that were common to the Control-RPE vs. Patient-RPE were removed from the latter list (**Supplementary Table 1**). Since fibroblasts present no disease phenotype, any differences in expression between fibroblasts from both clinical conditions is expected to arise from technical effects and non-phenotype-related biological effects and is considered to be a source of interference for correct interpretation. In case of the within-condition contrasts, we considered only unique DE genes detected in the control (Control-fibroblasts vs. Control-RPE) and patient (Patient-fibroblasts vs. Patient-RPE) contrasts and removed common DE genes from both. In this manner, we address differences in expression related to encoding of the healthy RPE phenotype that are lost in the disease (DE in control contrast, and not DE in patient contrast) as well as expression changes that arise due to the RP disease and were not present when comparing healthy cells (DE in patient contrast, and not DE in control contrast).

[2]http://www.bioinformatics.babraham.ac.uk/projects/fastqc/

Functional Enrichment analysis of these sets of DE genes was performed for Gene Ontology (GO) annotations [retrieved using the biomaRt (Durinck et al., 2005) R package version 2.42.1, GO database accessed December 2019 (Ashburner et al., 2000; Carbon et al., 2019)] using Fisher's Exact Test and Benjamini–Hochberg's multiple-testing correction method (significance threshold: adj p value <0.05).

Alternative Splicing Event Analysis and Functional Enrichment of Alternatively Spliced Genes

Alternative splicing (AS) event analysis was performed for the same four contrasts as in DE analysis using SUPPA2 (version 2.3) (Lareau and Brenner, 2015). The RefSeq human transcriptome (RefSeq release 96) (O'Leary et al., 2016) was used to define splicing events via the generateEvents function in SUPPA2. We then mapped sequencing reads to the human genome (GRCh38.p13) using STAR [ref STAR] (version 2.7.3a) and the same RefSeq transcriptome and obtained isoform-level expression estimates using RSEM (version 1.3.0) (Yates et al., 2020). Transcripts per Million (TPM) values were then used to obtain a Percentage Spliced In (PSI) value per splicing event using the psiPerEvent function (SUPPA2). Next, differential splicing analysis was performed using the diffSplice function (SUPPA2) to obtain the PSI difference (dPSI) and p value for the splicing change in the four contrasts of interest.

In order to obtain alternatively spliced genes for each contrast, we performed several filtering steps. For the within-cell type contrasts, events with a significant splicing change (p value <0.05) in both the fibroblast (Control-Fibroblasts vs. Patient-Fibroblasts) and RPE (Control-RPE vs. Patient-RPE) contrasts were removed from the latter to preserve only splicing differences related to the disease retinal phenotype (**Supplementary Table 2**). In the case of the within-condition contrasts, we removed common alternatively spliced events from the significant events obtained in each of the two contrasts, i.e., Control-fibroblasts vs. Control-RPE and Patient-fibroblast vs. Patient-RPE. Hence, significant events unique to the control were considered to be associated to splicing differences encoding the healthy phenotype that are then lost in the patient, while unique patient events were interpreted as arising as a result of the disease and the PRPF8 mutation. In this, case, however, we also considered common significant events changing the sign of dPSI between contrasts.

Functional enrichment analysis of differentially spliced genes was performed as described in the previous section. As our list of splicing-related genes, we performed a text-mining search of GO terms containing the words "mRNA", "pre-mRNA", "splicing", "spliceosome", "spliceosomal", and "rRNA" (total GOs: 106) and selected all genes annotated for at least one of these GOs (total genes: 987). A complete list of all considered GO terms is provided in **Supplementary File 9**. We note that some false-positive AS-related GOs may arise from this type of search; however, it is designed to be as comprehensive as possible in order to provide interesting candidates for the RP disease. Annotations are subsequently manually checked, and only truly AS-related genes are discussed and considered in the manuscript.

RESULTS

Patient-Specific iPSC-RPE Cells Reveal Normal Cellular Phenotype

We previously identified an adRP patient with the heterozygous mutation in *PRPF8* (NM_006445:c.6974-6994del, p.Val2325_Glu2331del) (Martinez-Gimeno et al., 2003) (**Supplementary Figure 1**). This mutation affects the C-terminal region of the PRPF8 within a region required for interaction with EFTUD2 and SNRNP200 (Pena et al., 2007). This 21-base pair deletion results in Val2325 to Glu2331 amino acid deletion at the C-terminal segment (**Supplementary Figure 1**) leading to the loss of a polar contact between the N atom of Lys592 in SNRNP200 and the O atom from Leu2333 in PRPF8 (**Supplementary Figure 2**).

The iPSCs were derived from the patient and differentiated toward RPE cells according to the previously described procedure (**Figure 1A**; Hongisto et al., 2017). As a control, a healthy subject's iPSCs were differentiated toward RPE. The obtained RPE cells exhibited typical native RPE traits including the formation of a cellular monolayer with a polygonal shape and pigmented cells and showed expression of RPE markers such as cellular retinaldehyde-binding protein (CRALBP), sodium/potassium-dependent ATPase (Na^+/K^+ ATPase) with predominantly apical distribution, and zonula-occludens-1 (ZO-1), a tight-junction marker, with typical apico-lateral distribution (**Figure 1B**). PRPF8 exhibited typical nuclear punctate distribution in control and patient's RPE, with the antibody that recognizes the N- and C-terminal end without any significant difference between two genotypes. The defective protein is 2,328 amino acids long compared to the wild-type, 2,335-amino-acid-long protein. This difference in size could not be detected by Western blot using the antibody raised against the N-terminus (**Figure 1D**) or the one recognizing the C-terminal amino acids (2,036–2,335) (data not shown). The identity of the iPSC-derived RPE cells was validated using RNA-Seq data, i.e., by DE analysis of several RPE trait markers (BEST1, MERTK, MITF, RLBP1, and RPE65) (Strunnikova et al., 2010) between fibroblasts and RPE cells in each condition (control and patient). Indeed, all these markers are upregulated in the RPE cells in comparison to fibroblasts, with comparable intensity in both control and disease cells (**Supplementary Figure 3**).

To further confirm the identity of RPE cells, ultrastructural analyses were performed and characteristic polarized RPE morphology was detected in Patient-RPE (**Figure 1E**) and Control-RPE (data not shown). The polarized organization of cuboidal cells typical of RPE was observed with basally positioned nuclei and apically distributed microvilli (**Figure 1E**, left panel). Melanosomes represented with black round and oval shapes were present in the apical portion of the cells while ellipsoidal mitochondria were seen below the nuclei, largely displaced toward the basal-lateral part of the cells, the natural position for these organelles *in vivo*. Intercellular junctional complexes are

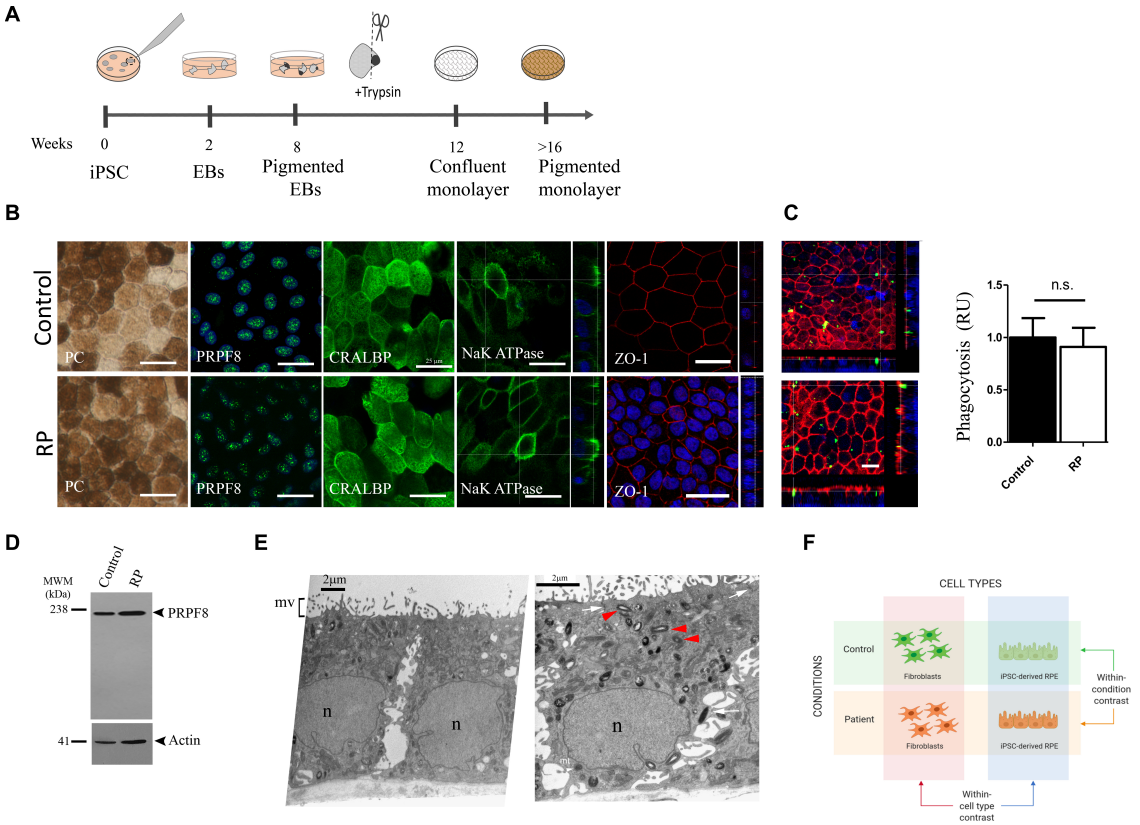

FIGURE 1 | Generation of iPSC-RPE cells from patient and control. **(A)** Schematic of iPSC differentiation toward RPE. **(B)** Characterization of iPSC-RPE. Bright-field images of iPSC-RPE monolayers. Immunocytochemistry to PRPF8 and characteristic RPE markers CRALBP, Na^+/K^+-ATPase (Na/K), and ZO-1. Vertical simulation sections for $Na^{+/}K^+$ ATPase show mainly apical distribution and ZO-1 showing typical apical lateral junction distribution. **(C)** POS phagocytosis assay: FITC-labeled POS (green); F-actin is stained by phalloidin (red) to visualize cell morphology and internalization of POS and quantitative analyses of ingested POS. **(D)** Western blot analysis of PRPF8. **(E)** Transmission electron microscopy of patient iPSC-RPE. Left panel: cuboid polarized RPE cell organized in monolayer with basally located nucleus (n) and apically distributed microvilli (mv). Right panel: RPE cells show melanin granules (red arrowheads) apically from the nucleus, intercellular junctional complexes that include the tight junctions, adherens junctions (arrows), and membrane interdigitations (arrowheads), and basally positioned nucleus (n). **(F)** Contrasts analyzed by RNA-Seq. Created with BioRender (https://biorender.com/). Data are expressed as means ± SD, *n* = 3 assays from two differentiation experiments; Student's *t* test, n.s., non-significant. Scale bar 25 µm where not indicated.

visible in appropriately aligned sections of RPE (**Figure 1E**, right panel). Again, the patient's RPE showed the main hallmarks of native RPE without any morphological differences compared to healthy individual control. Furthermore, we assessed the ability of iPSC-RPE to phagocytose POS, mimicking a daily rhythmic binding and internalization of POS tips by RPE cells essential for vision. The ability of patient and control iPSC-RPE was compared by quantifying the FITC-labeled POS fluorescence inside the cells. The results indicate that the disease and control iPSC-RPE ingested the photoreceptor membranes similarly (**Figure 1C**).

Functional Analysis of Gene Expression Differences Between Patient and Control Cells

In order to assess the transcriptional changes associated with disease, four pairwise comparisons between samples were performed in order to obtain DE genes between each relevant pair of conditions (**Figure 1F** and **Supplementary Files 1–4**). **Supplementary Table 1** summarizes the number of DE genes between each pair of conditions. Within-condition contrasts (RPE vs. fibroblasts for either patient or control samples) were performed to reveal differences related to the cell type identity, while the within-cell type contrasts (i.e., comparing patient vs. control for the same cell type) had the potential to unravel differences associated with the disease and the PRPF8 mutation. PCA of the different sample types (**Supplementary Figure 4**) indicated that cell-type differences (RPE vs. fibroblasts) explained the highest variance across samples (∼50%, PC1), followed by expression changes between the clinical conditions (∼13%, PC2). Nevertheless, the expression profile between healthy and disease RPE cells presented more differences than that of fibroblasts, as expected given that the PRPF8 mutation presents a phenotype only in the retina.

For the within-cell type contrasts (**Supplementary Files 1, 2**), DE analysis of Patient-RPE vs. Control-RPE was performed [False Discovery Rate (FDR)-adjusted *p* value <0.05], subsequently filtering genes that were also DE

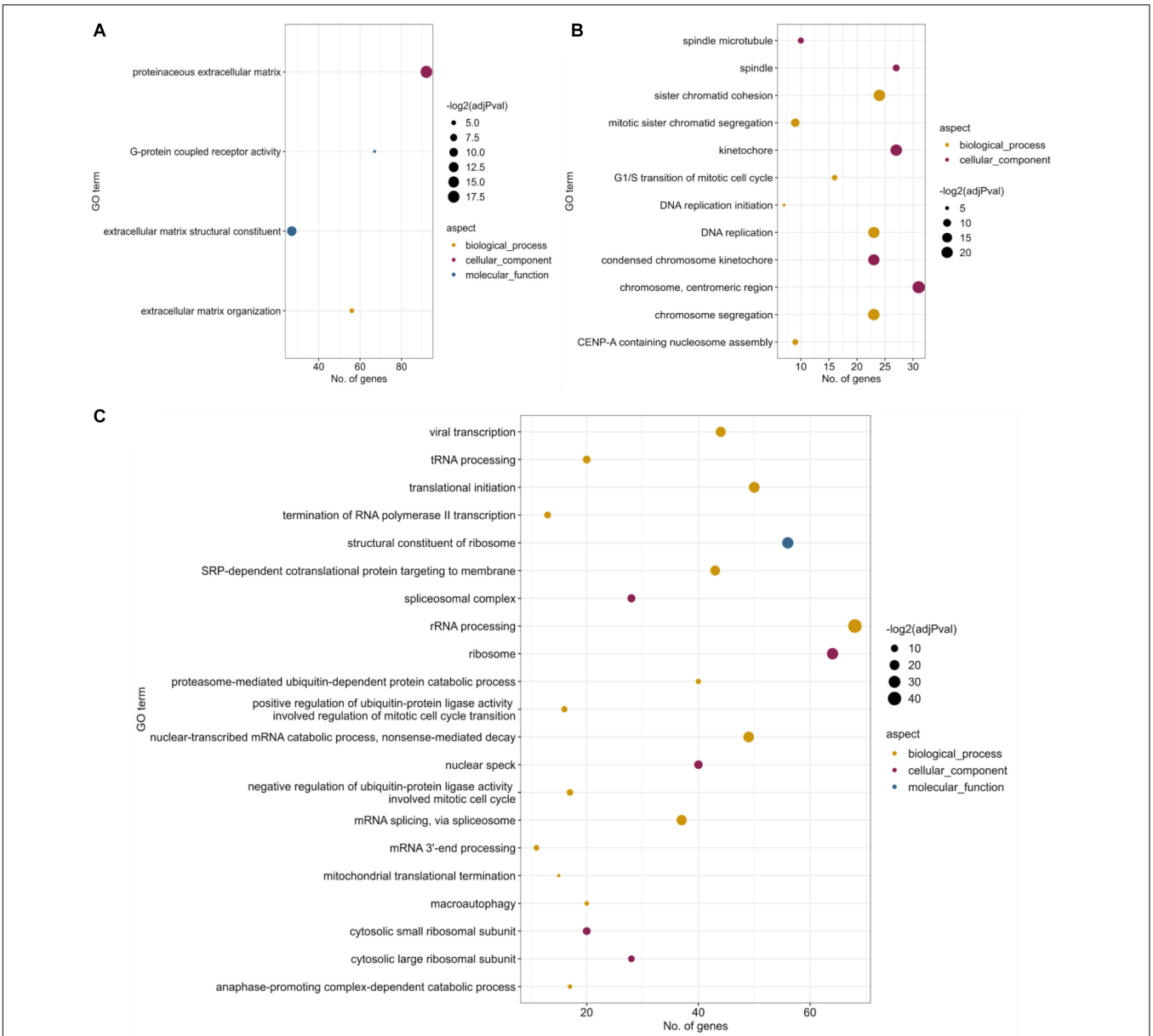

FIGURE 2 | Functional enrichment results for differential gene expression. Significantly enriched (FDR < 0.05) Gene Ontology terms for **(A)** Patient-RPE vs. Control-RPE contrast, filtering genes that are DE between patient and control fibroblasts. **(B)** Patient-RPE vs. Patient-fibroblasts, filtering genes that are DE in the control contrast, and **(C)** Control-RPE vs. Control-fibroblasts, filtering genes that are DE in the disease contrast. Dot size indicates significance of the Fisher's Exact Test [–log(adj *p* value)], *x*-axis position indicates the number of DE genes that are annotated for each significant GO term, and dot color indicates the GO aspect under which the term is annotated.

in Patient-fibroblasts vs. Control-fibroblasts (see *Materials and Methods*). We considered this set of DE genes (4,644, **Supplementary Table 1**) to be RPE-specific and therefore to encode a relevant part of the transcriptional signature of the disease. Functional enrichment analysis of this set of genes identified significantly enriched (Fisher's Exact test, FDR < 0.05) GO terms, namely, *G-protein coupled receptor activity* [GO:0004930, 67 genes, 45 (67%) upregulated in patient] and several extracellular matrix-related terms [GO:0005578, GO:0005201, GO:0030198; 92 genes in total, 70 (76%) upregulated in patient] (**Figure 2A**). This suggests a coordinated increase in expression for these genes in the disease condition. However, some of these genes are depleted in the patient condition and could also contribute to create an imbalance of these functions in the RP disease. Interestingly, none of the 67 genes annotated as G-protein-coupled receptor activity genes were differentially spliced in any of the comparisons performed (see the next section). Therefore, expression dysregulation without splicing alterations could be considered a secondary effect of the PRPF8 mutation. Among 92 genes annotated under an extracellular-matrix-related term, some show a splicing change in the within-cell-type contrasts, namely, *COL5A1*,

FN1, *LAMA2*, *VEGFA*, and *HAPLN3*. All except *HAPLN3* show differential splicing for at least one event in all contrasts, suggesting a possible direct impact of the mutated splicing factor.

Regarding the two within-condition contrasts (Control-RPE vs. Control-fibroblasts and Patient-RPE vs. Patient-fibroblasts, **Supplementary Files 3, 4**), we filtered common DE genes to obtain transcriptional signatures of RPE cell-type identity, i.e., healthy and disease RPE phenotypes. We observed 4,903 unique DE genes ($p < 0.05$) for the control comparison (**Supplementary Table 1**), which represent differences in expression between RPE and fibroblasts required for encoding healthy cell-type identity and presumably lost due to the disease mutation. For the disease condition, 1,838 unique DE genes were identified ($p < 0.05$, **Supplementary Table 1**), probably related to the development of the disease in RPE cells. The majority of common DE genes (7,491) present a similar change in expression between both cell types, supporting the robustness of the transcriptional differences between RPE and fibroblasts (**Supplementary Figure 4**).

Functional enrichment analysis of DE genes unique to the patient contrast (Patient-RPE vs. Patient-fibroblasts) identified significant enrichment (Fisher's Exact test, FDR < 0.05) of a broad set of biological functions related to cell division and the cytoskeletal elements participating in mitosis, including *spindle* (GO:0005819), *chromosome segregation* (GO:0007059), and *kinetochore* (GO:0000776) (**Figure 2B**). The functional enrichment analysis for DE genes unique to the control contrast (Control-RPE vs. Control-fibroblasts) included a much wider range of significantly overrepresented (Fisher's Exact Test, FDR < 0.05) biological processes, including mitosis-related GOs, but also terms associated to splicing (*spliceosomal complex,* GO:0005681; *mRNA splicing via spliceosome,* GO:0000398; *mRNA 3′-end processing,* GO:0031124; *nonsense-mediated decay,* GO:0000184) and ribosome structure and translation (*ribosomal subunits,* GO:0022625 and GO:0022627*; rRNA processing,* GO:0006364*; translational initiation,* GO:0006413 *SRP-dependent cotranslational targeting of membrane,* GO:0006614) (**Figure 2C**). Ribosome/translation-related terms included 76 genes, of which 69 (91%) were upregulated in Control-RPE. This coordinated upregulation does not appear in the case of the patient contrast, suggesting depletion of ribosomal functionality in Patient-RPE when compared with fibroblasts of the same clinical condition. Meanwhile, AS-related terms included a total of 45 genes, 26 (58%) of which were downregulated in Control-RPE, showing a relative balance of up-/downregulation of AS genes. In the patient contrast, no coordinated DE or significant overrepresentation was observed and pinpoints to the dysregulatory effect of the PRPF8 mutation on splicing machinery components, which have been shown to undergo widespread regulation by post-transcriptional mechanisms (Lareau et al., 2007; Ni et al., 2007; Han et al., 2010; Anko et al., 2012; Lareau and Brenner, 2015).

AS Signature of Healthy and Disease RPE Cells

In order to shed light on the mutant PRPF8 pathomechanism, we analyzed splicing patterns in the different cell types and clinical conditions and we evaluated the difference in Percentage Spliced In (dPSI, see section "Materials and Methods") for each of the four contrasts (**Figure 1D** and **Supplementary Files 5–8**), considering the following splicing event categories: alternative 3′ and 5′ site (A3/A5), alternative first (AF) and alternative last (AL) exon, mutually exclusive (MX) exons, retained intron (RI), and skipped exon (SE) (Trincado et al., 2018).

For the within-cell-type comparisons (**Supplementary Files 5, 6**), we observed a higher number of splicing events with significant differences (p value <0.05) when comparing RPE cells from different clinical conditions than in the case of fibroblasts (**Supplementary Figure 5**), which we attributed to the high complexity of splicing in RPE (Strunnikova et al., 2010; Farkas et al., 2013) and the fact that fibroblasts show no disease phenotype as a result of the PRPF8 mutation. After removing common significant events from the RPE contrast (**Supplementary Table 2**), we used dPSI values to check the direction in the splicing change, i.e., the clinical condition in which event inclusion is promoted for RPE cells (**Figure 3**). A strong tendency toward inclusion of RI events can be observed in Control-RPE in comparison with Patient-RPE, as well as promoted inclusion of A3 and A5 sites, while there were no global direction change patterns in AF, AL, or SE events.

We next performed a functional enrichment analysis of genes with at least one significant AS event, removing events common between the fibroblast and RPE contrasts as previously described for the DE analysis (see section "Materials and Methods"). Functional analysis of events unique to the RPE contrast showed no significantly overrepresented terms (FDR < 0.05). Hence, we ranked GO terms by their frequency of annotation in alternatively spliced genes to gain functional insight into the splicing patterns of the disease. The most frequently annotated GO terms were *RNA polymerase II DNA binding* (GO:0000977), including several alternatively spliced zinc finger genes (*ZNF154*, *ZNF211*, *ZNF419*, and *ZNF691*), as well as *ribosome* (GO:0005840) and *structural constituent of ribosome* (GO:0003735), which included some genes also annotated for mitochondrial translation, i.e., Mitochondrial Ribosome Protein genes from the Large subunit (MRPL genes). In addition, several splicing-related terms were among the most frequently annotated (**Figure 4**), namely, *spliceosomal complex* (GO:0005681) and *catalytic step 2 spliceosome* (GO:0071013). Genes under these annotations included *PRPF4*, *PRPF8*, and *PRPF31*, known to be involved in RP (Sullivan et al., 2006; Chen et al., 2014), as well as *SRSF1*, *HRNPA2B1*, and *SRRM2* (**Figure 5**). This suggests a high level of functional dependence between different spliceosome components that have been shown to cause RP and seems to further indicate that PRPF8 malfunction may propagate to other spliceosome components to generate the disease phenotype. In fact, *SRRM2* and *SRSF1* are also DE in the RPE contrast (downregulated in patient). Therefore, the PRPF8 mutation could have a dual role in altering both the expression and the splicing of other spliceosomal genes and, potentially, their function. Ultimately, we hypothesize that the RP disease would be caused by the cumulative effect of these alterations in the splicing machinery.

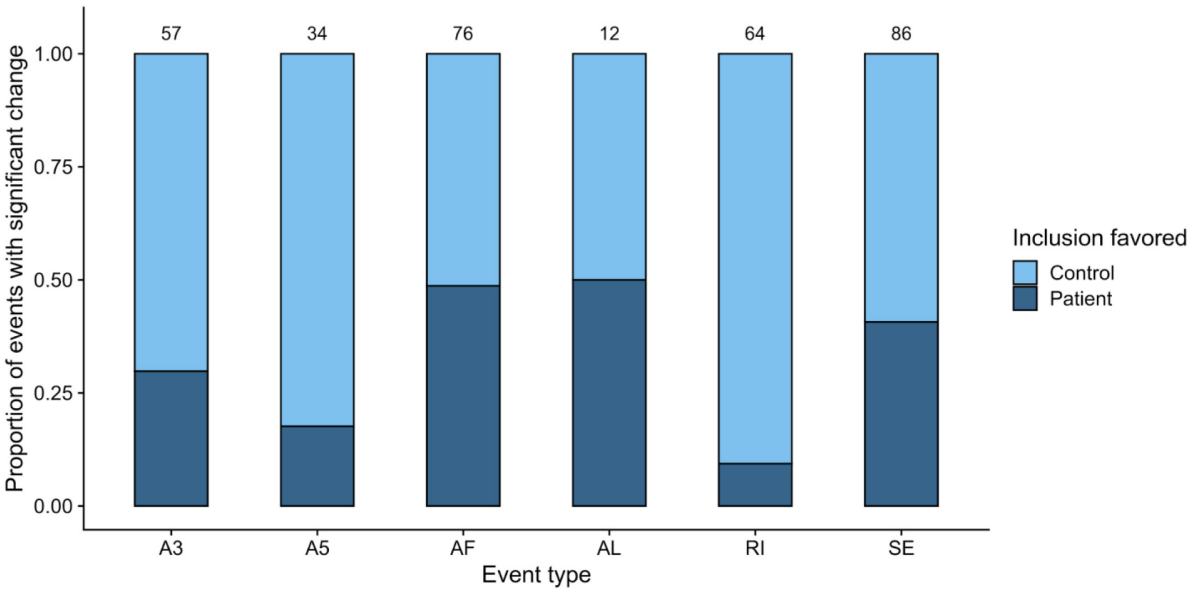

FIGURE 3 | Summary of alternatively spliced events (p value <0.05) in the RPE contrast. Only events unique to the Control-RPE vs. Patient-RPE contrast are shown. The proportion of events for which inclusion is favored in each clinical condition is indicated by the bar area. The number of events for each category is shown in the label above the bar. Event types: A3, Alternative 3′ site; A5, Alternative 5′ site; AF, Alternative First exon; AL, Alternative Last exon; MX, Mutually Exclusive Exons; RI, Retained Intron; SE, Skipped Exon.

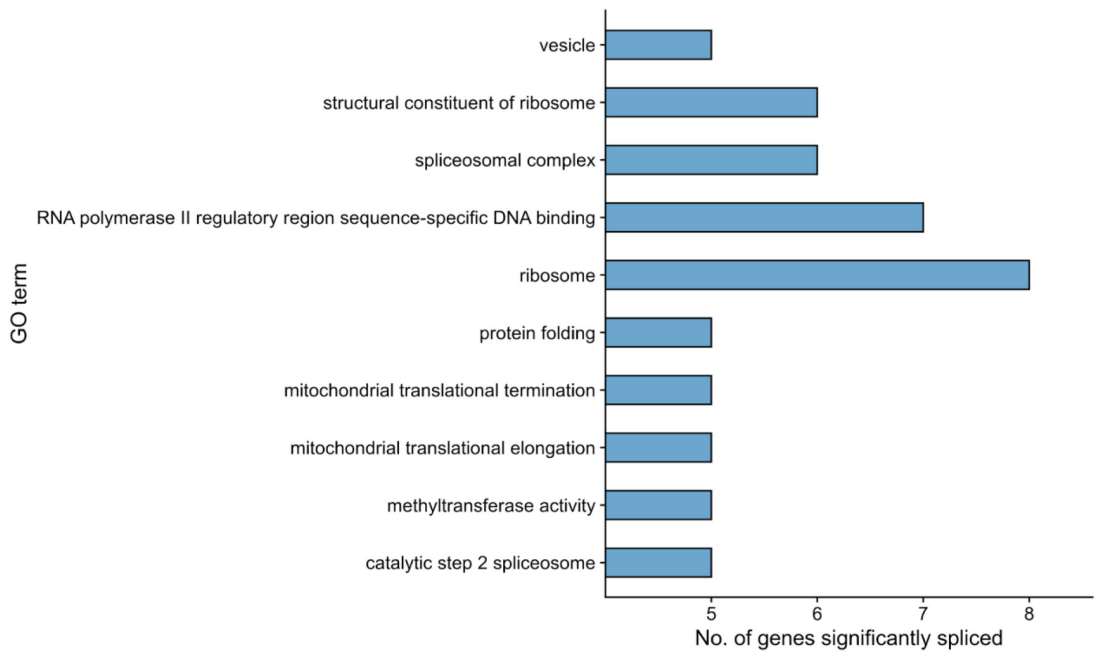

FIGURE 4 | Functional enrichment results for differentially spliced genes in the RPE contrast (Control-RPE vs. Patient-RPE, only unique events). The top-10 most frequently annotated GO terms are shown in the y-axis. The number of genes belonging to each GO term is indicated by bar height (x-axis).

In order to better understand the mechanism by which the PRPF8 mutation caused mis-splicing in splicing-related and non-splicing related genes, we analyzed the relationship between gene expression and splicing for each type of event (**Supplementary Figures 6–9**). Regarding RI events, we observed increased intron retention in Control-RPE that seemed to be decoupled from transcriptional regulation (**Supplementary Figure 6**), since intron retention does not appear to be related to a pattern of gene downregulation in the control condition. Nevertheless, *SRSF1* and *PRPF4B*, the latter involved in AS, contradicted this

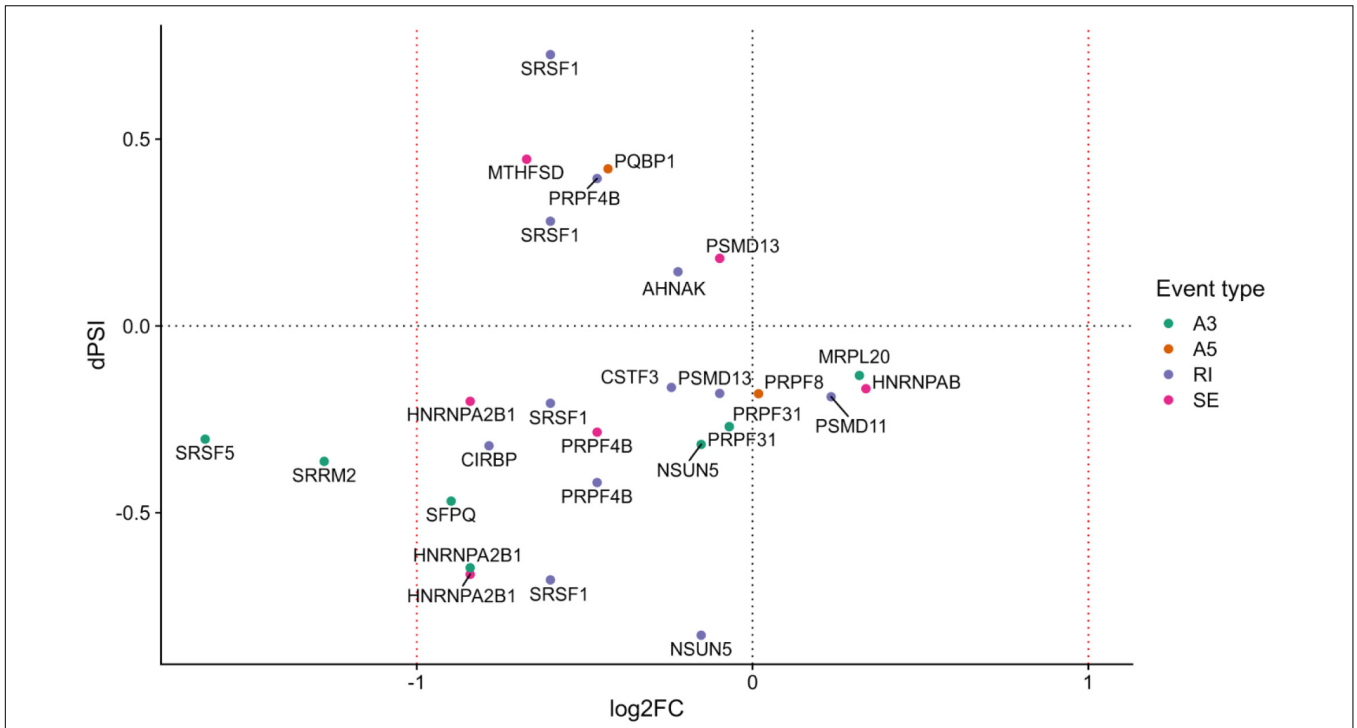

FIGURE 5 | Splicing-related genes with at least one differentially spliced event (p value <0.05) in the Control-RPE vs. Patient-RPE contrast (only genes unique to the RPE contrast are considered). Each event is colored by type (A3, alternative 3′ site; A5, alternative 5′ site; RI, retained intron; SE, skipped exon). dPSI is shown in the y-axis (dPSI < 0: event inclusion favored in control, bottom panel; dPSI > 0: event inclusion favored in patient, upper panel). log2(Fold Change) is shown in the x-axis (FC < 0: gene downregulated in patient, left panel; FC > 0: gene upregulated in patient, right panel).

pattern and showed highly included IR events in Patient-RPE, together with a decrease in expression in this clinical condition. This deviation from the general pattern for *SRSF1* and *PRPF4B* agrees with previous reports of increased intron retention in RP (Martinez-Contreras et al., 2007) as well as with its established role in decreasing expression levels of transcripts (Braunschweig et al., 2014) and may suggest a direct role for *PRPF8* in the splicing of these two genes, which generates an imbalance in coding vs. non-coding isoforms when the mutation is present.

In the case of SE events, we observed a similar number of patient and control-favored inclusion of alternative exons (**Supplementary Figure 7**). However, there seems to be a global tendency toward downregulation in patient for this group of genes. Importantly, this category of events includes alternatively spliced HNRNP genes (*HRNPA2B1, HNRNPDL, HNRNPAB*), which are known to participate in splicing control (Martinez-Contreras et al., 2007) as well as the RNA-binding protein MTHFSD, whose deregulation has been previously linked to disease (MacNair et al., 2016).

Regarding A5 and A3 sites, we observed very different behavior as a response to the mutation in PRPF8. While few A5 sites showed a significant splicing change (**Supplementary Figure 8**), with inclusion of the alternative portion of the exon being favored neither in patient nor in control, our analyses revealed a strong tendency toward A3 site inclusion in the Control-RPE (**Supplementary Figure 9**). Patient-RPE therefore showed more frequent usage of the A3 sites within these exons, while healthy cells (Control-RPE) tend to use the site that generates a longer exon. These results suggest an interaction between PRPF8 and the 3′ splice site. In addition, these splicing changes do not seem to be related to a DE pattern when comparing patient and control RPE cells (**Supplementary Figure 9**). Therefore, this PRPF8-mediated global A3 event inclusion, potentially caused by the mutation, would solely be associated to post-transcriptional regulation, in contrast to SE and IR results. AS-related genes showing this pattern included previously discussed *SRSF5, PRPF31, HRNPA2B1*, and *SRRM2,* as well as splicing factor *SFPQ* and RNA methyl-transferase *NSUN5* (**Supplementary Figure 9**).

AS Signature Encoding Healthy and Disease Cell-Type Identities of RPE Cells

Aiming to understand the contribution of AS to RPE cell identity, we analyzed within-condition changes in AS events (**Supplementary Files 7, 8**). We presumed significant AS events and AS genes unique to the control contrast (Control-fibroblasts vs. Control-RPE) to be key determinants of healthy RPE cells that are no longer present in the patient contrast. Meanwhile, unique significant AS events and genes in the patient contrast (Patient-fibroblasts vs. Patient-RPE) constitute splicing alterations that arise due to the disease. This analysis revealed an overall decrease in the number of significant events (p value <0.05) in the patient contrast (**Supplementary Figure 10**), which could

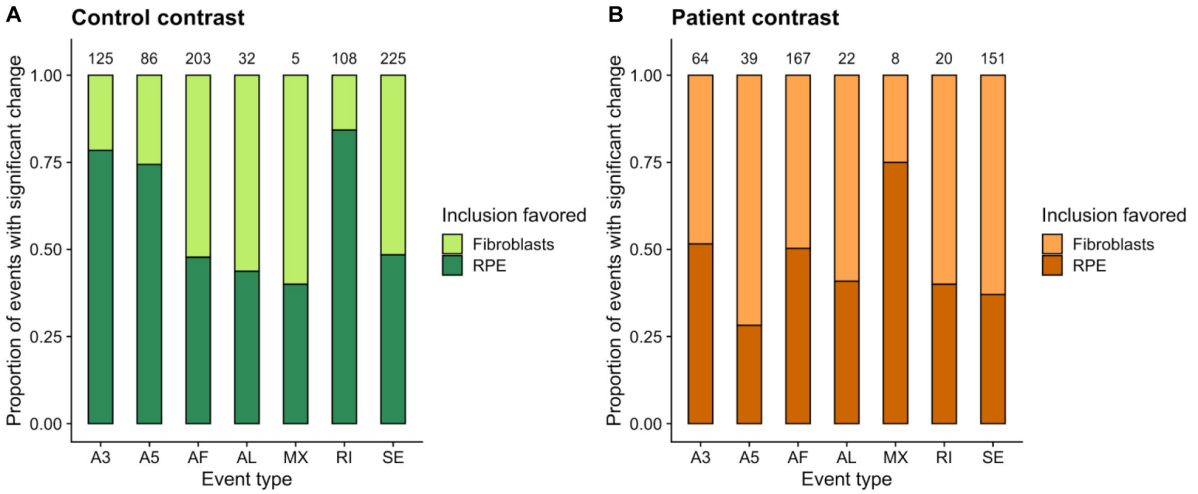

FIGURE 6 | Summary of unique alternatively spliced events (p value <0.05) detected in the control **(A**, Control-fibroblasts vs. Control-RPE**)** and patient **(B**, Patient-fibroblasts vs. Patient-RPE**)** contrasts. The proportion of events for which inclusion is favored in each clinical condition is indicated by bar area. The number of events for each category is shown in the label above the bar. Event types: A3, Alternative 3′ site; A5, Alternative 5′ site; AF, Alternative First exon; AL, Alternative Last exon; MX, Mutually Exclusive Exons; RI, Retained Intron; SE, Skipped Exon.

be attributed to a depletion in spliceosomal function caused by PRPF8 mutation.

We next used the dPSI values to look at event inclusion/exclusion patterns between cell types in each clinical condition (**Figure 6**). Regarding AF and AL events, there were no trends in either clinical condition, or high variation in the number of events with a significant splicing change between control (**Figure 6A**) and patient (**Figure 6B**). Interestingly, events in the rest of the categories showed preferential inclusion in one cell type in at least one of the clinical conditions or a drastic change in the number of significant AS events. AF and AL events are generated due to alternative start/end sites for transcription and therefore correspond to transcriptional regulation mechanisms, which further supports the hypothesis that the PRPF8 mutation has its effect via the alteration of post-transcriptional regulation, i.e., splicing. In the case of RI, while intron inclusion was favored in fibroblasts for most RI events in the patient contrast (which matches the decrease in RI detected for Patient-RPE in the within-cell type contrasts), the control contrast revealed a higher degree of intron retention in RPE. Of note, the number of significant RI events was much higher in the control contrast (108) in comparison to patient (20), suggesting the existence of an intron retention program that could be important for the determination of the healthy RPE phenotype. A3 and A5 events also tended to be less included in RPE in the patient contrast in comparison to the control, which revealed coordinated usage of exon alternative sites in Patient-RPE, as could be observed for A3 sites in the RPE contrast. Ultimately, this suggests a change in the way that PRPF8 interacts with both the 3′ and 5′ splice sites in the RP disease. Functional enrichment analysis of unique AS genes showed no significantly overrepresented GO terms (FDR < 0.05) in either contrast. We therefore looked at the frequencies of GO term annotations for these genes (**Figure 7**). Interestingly, genes whose splicing status encodes the healthy RPE phenotype (control contrast) are frequently annotated for *spliceosomal complex* (GO:0005681, 9 genes) and *rRNA processing* (GO:0006364, 9 genes), two functional terms that appear linked to the PRPF8 mutation and RP throughout this study. These findings are in line with our hypothesis regarding the existence of a healthy splicing signature, involving spliceosome and ribosomal genes, that is required to maintain correct retinal function and is disrupted via splicing defects initiated with defective PRPF8. Another cell function that was shown to be enriched in genes DE in the control contrast (**Figure 2**), *regulation of cell proliferation* (GO:0042127, eight genes), was the only common GO term among the most frequent annotations.

Finally, we studied the events that change in each within-condition contrast for the genes annotated under these three GO terms (**Supplementary Figures 11–15**). Regarding *rRNA processing* genes (**Supplementary Figure 11**), we observed variable trends regarding the cell type in which inclusion of the AS events is favored. While *PLXNB3*, *CFAP410*, and *RHOJ* presented SE events that showed inclusion in fibroblasts, a similar event in *MKLN1* was included in RPE. Regarding event categories, although several genes showed differentially spliced AF exons, we did not observe a pattern among significant event types for rRNA processing genes. However, FN1 and RASA1 present A3 and A5 sites, respectively, showing inclusion in RPE, matching the previously described trend (**Figure 6**). For spliceosome genes (**Supplementary Figure 12**), however, we noticed that most significant events were IR, A3 and A5 sites, while very few events within these three categories were observed in rRNA processing genes (**Supplementary Figure 11**). The abundance of A3 and A5 events changing among splicing-related genes could further support our hypothesis that WT PRPF8 is involved in spliceosomal binding to the splice sites. Indeed, all A3 and A5 sites showed inclusion in RPE

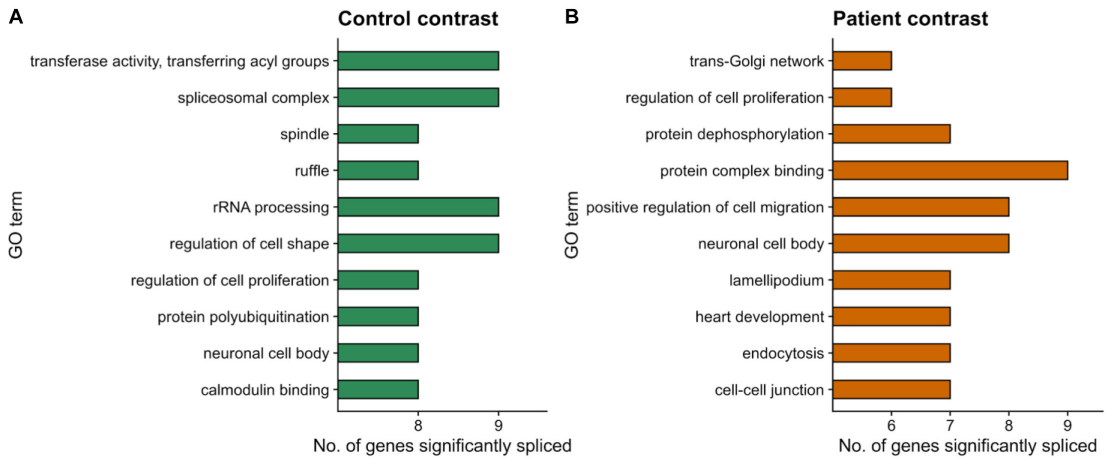

FIGURE 7 | Functional enrichment results for differentially spliced genes (p value <0.05) in the within-condition contrasts. **(A)** Control-fibroblasts vs. Control-RPE. **(B)** Patient-fibroblasts vs. Patient-RPE. Only events unique to each contrast are considered. The top-10 most frequently annotated GO terms are shown in the y-axis. The number of genes belonging to each GO term is indicated by bar height (x-axis).

(**Supplementary Figure 12**) and therefore selection of the splice sites that generated longer exons. This splicing change is lost in the patient contrast, suggesting a lack of control over this process in the disease for these set of spliceosomal genes, which include helicase *DHX37*, ribosomal components *RPL15* and *RPL31*, and several ribosome maturation factors and rRNA processing proteins. The exact role of splice site selection in the RP disease, however, requires further validation and is beyond the scope of this study.

Genes annotated for *regulation of cell proliferation* were the only functional group that was frequently annotated among AS genes in both clinical conditions, although the sets of genes in each contrast are different, with the exception of *NF2*. In the case of this gene group, most splicing changes occurred in SE and AF events, except for an A5 event detected in the control contrast (*STAT6*) and an A3 event in patient (*ITSN1*). We consider these, together with genes presenting SE events (control: *CNN2*, *IL4R*, *PKD2*, and *PIAS1*; patient: *MYH10, PALLD*, and *WASF2*), to be genes subject to strong post-transcriptional regulation and therefore candidates for future evaluation of the impact of these splicing changes on RPE function. Finally, among the 371 common events (significant in both contrasts), we found 14 events that presented different dPSI sign in the patient and control comparisons (**Supplementary Figure 15**), i.e., alternatively spliced events with different direction of change depending on the clinical phenotype. In addition to transcriptionally controlled AF exons, common events consisted mainly of SE that presented preferential inclusion in RPE in the control contrast (*MRPS31, MTX1, SHLD2P3*, and *HNRNPDL*), while the exon becomes excluded in RPE in the patient contrast. This set of genes included *HNRNPDL*, associated with pre-mRNA processing. A similar trend is observed for A3 events in the *CYB5D1* and *TPM2* genes, as well as for an RI event in the SNORD locus (C/D box Small Nucleolar RNAs).

In summary, after performing within-condition contrasts, we have observed a pattern of event inclusion in the control contrast that is lost in patient, when not completely reversed, as is the case of common genes. This mainly affects SE, A3, and A5 events for genes involved in splicing, rRNA processing, and proliferation. The role that the skipped exons or exon fragments play in the gene's functionality is to be defined; however, our analyses suggest that the PRPF8 mutation creates this event exclusion pattern. We believe that these changes could alter the splicing signature required for healthy RPE identity and that they may be a consequence of AS dysregulation in the RP disease. Ultimately, this list of alternatively spliced events and genes should constitute a valuable resource for further validation in order to find candidates that can explain the PRPF8-mediated RP pathomechanism.

DISCUSSION

Despite huge progress in the identification of genetic causes of the disease, the pathomechanism behind RP is largely unknown. While animal models have proven useful in many cases, albeit in the case of splicing factor-induced RP, they remain insufficient as the disease phenotype is poorly manifested. Moreover, the wide mutational landscape of splicing factor-caused RP is time- and cost-consuming to capture in animal models. In addition, studying disease-causing variants in genetic backgrounds that are demonstrably permissive of the disease is highly desirable in the case of splicing factor-induced RP due to high clinical diversity.

We set out to explore the transcriptional landscape of patient non-affected and affected cells in order to elucidate the unique role of PRPF8 in its target cells, namely, RPE cells vs. non-retinal tissue. The use of iPSCs that can be differentiated toward any human tissue leverages the lack of access to native retinal tissue.

After differentiation to RPE, patient and control cells were indistinguishable upon assessment of morphological, immunoreactive markers. We did not observe basal deposits or infoldings as described in the mouse model

(Graziotto et al., 2011). PRPF8 immunofluorescence was equivalent in both genotypes, likely as a result of mutant protein escape from nonsense-mediated decay due to the short C-terminal amino acid sequence loss. Additionally, after assessing POS phagocytosis capacity, we found that patient and control cells behave indistinctly. The difference with the *Prpf8*$^{H2309P/H2309P}$ mice, which showed reduced phagocytosis, possibly lies in the homozygous state of the causative mutation in the rodent model. The lack of morphological or protein marker expression differences between control and RP genotypes probably reflects the late-onset disease phenotype that emerges as a result of additional cumulative molecular events. It has been previously described that modeling late-onset diseases requires additional cellular insults, since reprogramming leads to erasure of age markers in the original fibroblasts (Horvath, 2013; Miller et al., 2013). Similar results were reported by Foltz et al. with PRPF8 (c.6901C > T, p.P2301S) mutant, who describe iPSC-RPE with similar apicobasal polarity and phagocytosis rate between the patient and gene-corrected isogenic line (Foltz et al., 2018). The rationale behind using the conventional differentiation paradigm toward disease-specific cell type in this work is that mutations in ubiquitously present splicing factors involved in a fundamental cellular process such as splicing is expected to capture early cell-type-specific events prior to overt morphological or functional degeneration.

We then examined mRNA expression and splicing patterns in patient and control fibroblasts and iPSC-derived RPE cells in order to decipher the tissue-specific pathomechanism of the disease. Differential expression analyses between control and patient RPE cell types identified G-protein coupled receptor (GPCR) activity genes and extracellular matrix-related genes, some of the latter also showing changes in AS. GPCRs, the largest family of membrane proteins, act through ligand binding and are responsible for a wide variety of physiological roles. Extracellular matrix proteins are known to play a crucial role in supporting RPE cells *in vivo* and in vitro (Sorkio et al., 2014). RPE synthesizes components of extracellular matrix proteins of Bruch's membrane and interphotoreceptor matrix, both of which are essential for RPE integrity and function. We hypothesize that these genes could be directly involved in the disease mechanism and constitute good candidates for further validation.

Within-condition differential expression analysis (fibroblasts vs. RPE cells in healthy and disease condition) identified a set of common DE genes associated with mitosis-related processes and components. Importantly, control contrast-unique DE genes showed significant enrichment of splicing and ribosome structure and translation terms, while this signature was completely lost in the patient contrast. This suggests that splicing and ribosome-related processes could be important for cellular identity specification and that their expression dynamics is disrupted in PRPF8-caused RP. In this study, we propose two hypothesis that could explain this mechanism. First, the alterations in the expression of splicing-associated elements could propagate to ribosomal components and translation regulators that may require intervention of the spliceosome for their normal expression. Alternatively, RPE cells may display translational control mechanisms for sustaining RPE properties.

Out of 90% AS genes in humans showing AS, it is estimated that 30% have tissue-specific isoforms (Xu et al., 2002). We set out to identify RPE-specific AS patterns and assess whether these tissue-specific splicing events were affected by the disease. To globally profile AS, we analyzed five modes of splicing events, all of which allow for a single gene to encode multiple protein variants that can have different functional properties. Among the within-cell-type contrasts, a higher number of significant splicing changes were detected when analyzing AS events in RPE cells in comparison to fibroblasts, consistent with the higher functional complexity of RPE cells and the primary effect of the PRPF8 mutation on these cells. Retained introns, as well as alternative 3′ and 5′ sites, showed favored inclusion in Control-RPE compared to Patient-RPE. Intron retention is classically considered as a result of mis-splicing and regarded as a mechanism of suppression of inappropriate transcripts presumably destined for nonsense-mediated decay (Braunschweig et al., 2014). However, emerging studies have demonstrated that introns are actively retained in mature mRNA and may have specific roles in normal physiology (Wong et al., 2016; Adusumalli et al., 2019). Some of the most significantly differentially included intron retention events belonged to genes annotated for splicing and ribosome-related GO terms. These included splicing factors such as PRPF4, PRPF8, and PRPF31, all of which are known to cause RP. Of note, SRSF1 and PRPF4B were highly included in patient-RPE and also downregulated in this condition.

For alternative first and last exons, which are equivalent to Alternative Transcription Start and End Sites, inclusion was not globally favored in any of the conditions. This is not surprising, given that transcription start and end site choice is driven by the transcriptional machinery, instead of by the spliceosome, which operates after transcription is initiated, either post-transcriptionally or simultaneously to transcription (Herzel et al., 2017). The lack of global direction changes could indicate that the disease phenotype is caused by the PRPF8 mutation and that it directly involves splicing rather than transcriptional alterations. Ultimately, usage of AL or AF sites could be stochastic or a functional consequence of splicing alterations in certain proteins, but hardly the root of the disease.

In sum, we identified 27 splicing-related genes, including PRPF8, with at least one differentially spliced event between Control-RPE and Patient-RPE. This result opens interesting possibilities regarding the role of PRPF8 as a splicing factor, regarding both autoregulation of AS of its own pre-mRNA and that of 26 additional splicing factors. In the context of the RP disease, PRPF8 may act as a master AS regulator in RPE cells, targeting a broad set of splicing-involved genes, leading to the propagation of defective PRPF8 function to the rest of the splicing machinery via splicing dysregulation. Similar results have already been described in literature, where the core splicing proteins were found to regulate RNA processing and RNA-binding factors (Saltzman et al., 2011). We hypothesize that these are suitable candidate genes and events to be further validated as RP disease markers and are key to explain how PRPF8-initiated splicing defects propagate to the entire splicing machinery.

Within-condition contrasts showed a higher number of significant AS changes in control over disease cells, similar to

the DE results, indicating a depletion of spliceosomal function by PRPF8 mutation. For instance, there were 108 significantly changing intron retention events in the control vs. 20 in the disease contrast. In addition, functional enrichment results for control contrast AS genes identified splicing and ribosome-related functions within the top 10 most frequently annotated GO terms. These within-condition AS results corroborate splicing machinery disruption hypothesis as a potential mechanism for PRPF8-induced RP. Meanwhile, the only common term between control and disease cell types was regulation of cell proliferation, although different genes were identified as AS in each condition's contrast. This finding is in line with previous reports where PRPF8 was found to affect mitotic cell cycle and RNA splicing GO terms after its depletion by siRNA (Wickramasinghe et al., 2015). After removing genes common to both contrasts, we identified sets of AS-related genes in the control but not in the patient contrast, which were involved in spliceosome machinery, ribosomal structure, and translation, according to GO annotations. The loss of these splicing patterns when comparing disease cells is an additional evidence of the propagation of alterations in the expression and splicing of spliceosomal components to ribosomal proteins and translation regulators, which may require intervention of the spliceosome for their normal expression. Alternatively, and in line with the second proposed hypothesis, RPE cells may display unique human translational control mechanisms for sustaining RPE properties, which are disrupted due to the pathomechanism of mutant PRPF8. However, either of these hypotheses would require further experimental validation.

AS has been previously described to be affected in the PRPF8-depleted condition by siRNA in established cell lines (Tanackovic et al., 2011). Although these conditions do not capture the physiological cell environment and co-expression of the wild-type protein, the data support the role of splicing defects in PRPF8 pathomechanism. Similarly, in a comprehensive PRPF31 study using iPSC-derived RPE cells, differential exon usage was found to affect splicing process itself (Buskin et al., 2018). Moreover, AS GO term analysis of mouse *Prpf31*$^{+/-}$ retina and RPE were enriched for genes involved in mRNA processing. The iPSC-RPE from the PRPF31-affected patients exhibited a range of cellular defects, including loss of apico-basal polarity, altered pigment epithelium-derived factor (PEDF), and basal vascular endothelial growth factor (VEGF) secretion, barrier function, phagocytosis, and primary cilia deficiencies. These data are supportive of disrupted AS as a trigger of splicing deficiencies underlying specific biological processes. The observed splicing differences in our iPSC-RPE bearing a mutant PRPF8 copy points to a common primary pathogenic event. The fact that we did not observe morphological and functional disruptions in studied cells can be attributed to a unique PRPF8 mechanism. Another possibility is that our iPSC-RPE were insufficiently matured, which delayed the concomitant cellular events. In that regard, efforts for quantitative quality control to assess maturity instead of image-based analyses are emerging (Plaza Reyes et al., 2020). Parallel studies with both genetic backgrounds are warranted in order to delineate the specific roles of each PRPF gene.

Of note, our study is limited by the small sample sizes in our experimental design. Therefore, further studies involving a larger number of patients would be required to confirm the findings described herein. It is also imperative to determine if different mutations of PRPF8 have a similar impact on the transcriptional profile. As an additional shortcoming, we are aware that the poly(A)-selected RNA profiling described here precludes the involvement of other biologically relevant RNA species, such as microRNAs or long non-coding RNAs, which may also play a role in PRPF8-induced RP (Zhang et al., 2014).

The development of therapies for autosomal dominant retinal diseases with gain-of-function mutations involve strategies to inhibit expression of mutant protein and reduce the ratio of malfunctioned to wild-type protein. Along these lines, DNA oligonucleotides complementary to the pathogenic mRNA (Murray et al., 2015) or gene editing by CRISPR/Cas system targeting mutant allele (Bakondi et al., 2016) were described. These patients would also benefit from gene-independent replacement therapies such as heterologous stem cell replacement or combined genetic and stem cell approach using autologous cells. Importantly, exploring therapies for highly conserved proteins such as PRPF8 can harness the large progeny and short lifespan of lower organisms that allows high-throughput drug or genetic screening (Kukhtar et al., 2020). In view of our findings, the mutated PRPF8 allele-specific therapeutics would be the most effective approach. This, strategy, however, would be efficient if applied very early in the disease before other affected splicing proteins compromise the main cellular functions.

DATA AVAILABILITY STATEMENT

The datasets presented in this study can be found in online repositories. The names of the repository/repositories and accession number(s) can be found below: NCBI, GEO GSE165322.

ETHICS STATEMENT

The studies involving human participants were reviewed and approved by CAEC Valencia. The patients/participants provided their written informed consent to participate in this study.

AUTHOR CONTRIBUTIONS

ÁA-L: designed analysis pipeline, performed data analysis, interpreted results, and wrote the manuscript. HS: iPSC expansion and RPE production. AB-A: performed experiments and data analyses. VL: mutation analyses and interpretation. NC: TEM analyses. BD: clinical data. IH, BP, and MC: provided patient's biopsy. JC, AB, and AD: library preparation and initial data analyses. SE: financial support. DL: overall concept and design, performed the experiments, manuscript writing, and financial support. All authors reviewed the manuscript.

FUNDING

This work was supported by Institute of Health Carlos III/ERDF (European Regional Development Fund), Spain [PI16/00409 (DL), PI20/01119 (DL), CP18/00033 (DL), PI15/00227 (MC), CPII16/00037 (SE), and PI18-00286 (SE)], Platform for Proteomics, Genotyping and Cell Lines; PRB3 of ISCIII (PT17/0019/0024); National Science Foundation GACR 18-04393S and the project "Centre of Reconstructive Neuroscience", registration number CZ.02.1.01/0.0./0.0/15_003/0000419PI15/00227; Spanish Ministry of Economy and Competitiveness grant BES-2016-076994 (ÁA-L); and Academy of Finland (HS).

ACKNOWLEDGMENTS

We are thankful to the patient and healthy individuals for generously donating skin biopsies and Mrs. Outi Melin and Hanna Pekkanen with help of RPE differentiations.

SUPPLEMENTARY MATERIAL

The Supplementary Material for this article can be found online at: https://www.frontiersin.org/articles/10.3389/fnins.2021.636969/full#supplementary-material

REFERENCES

Adusumalli, S., Ngian, Z. K., Lin, W. Q., Benoukraf, T., and Ong, C. T. (2019). Increased intron retention is a post-transcriptional signature associated with progressive aging and Alzheimer's disease. *Aging Cell* 18:e12928. doi: 10.1111/acel.12928

Anders, S., Pyl, P. T., and Huber, W. (2015). HTSeq–a Python framework to work with high-throughput sequencing data. *Bioinformatics* 31, 166–169. doi: 10.1093/bioinformatics/btu638

Anko, M. L., Muller-McNicoll, M., Brandl, H., Curk, T., Gorup, C., Henry, I., et al. (2012). The RNA-binding landscapes of two SR proteins reveal unique functions and binding to diverse RNA classes. *Genome Biol.* 13:R17.

Ashburner, M., Ball, C. A., Blake, J. A., Botstein, D., Butler, H., Cherry, J. M., et al. (2000). Gene ontology: tool for the unification of biology. *Nat. Genet.* 25, 25–29.

Bakondi, B., Lv, W., Lu, B., Jones, M. K., Tsai, Y., Kim, K. J., et al. (2016). In vivo CRISPR/Cas9 gene editing corrects retinal dystrophy in the S334ter-3 rat model of autosomal dominant retinitis pigmentosa. *Mol. Ther.* 24, 556–563. doi: 10.1038/mt.2015.220

Braunschweig, U., Barbosa-Morais, N. L., Pan, Q., Nachman, E. N., Alipanahi, B., Gonatopoulos-Pournatzis, T., et al. (2014). Widespread intron retention in mammals functionally tunes transcriptomes. *Genome Res.* 24, 1774–1786. doi: 10.1101/gr.177790.114

Buskin, A., Zhu, L., Chichagova, V., Basu, B., Mozaffari-Jovin, S., Dolan, D., et al. (2018). Disrupted alternative splicing for genes implicated in splicing and ciliogenesis causes PRPF31 retinitis pigmentosa. *Nat. Communi.* 9:4234.

Carbon, S., Douglass, E., Dunn, N., Good, B., Harris, N. L., Lewis, S. E., et al. (2019). The gene ontology resource: 20 years and still GOing strong. *Nucleic Acids Res.* 47, D330–D338. doi: 10.1093/nar/gky1055

Chen, X., Liu, Y., Sheng, X., Tam, P. O., Zhao, K., Rong, W., et al. (2014). PRPF4 mutations cause autosomal dominant retinitis pigmentosa. *Hum. Mol. Genet.* 23, 2926–2939. doi: 10.1093/hmg/ddu005

Durinck, S., Moreau, Y., Kasprzyk, A., Davis, S., De Moor, B., Brazma, A., et al. (2005). BioMart and Bioconductor: a powerful link between biological databases and microarray data analysis. *Bioinformatics* 21, 3439–3440. doi: 10.1093/bioinformatics/bti525

Escher, P., Passarin, O., Munier, F. L., Tran, V. H., and Vaclavik, V. (2018). Variability in clinical phenotypes of PRPF8-linked autosomal dominant retinitis pigmentosa correlates with differential PRPF8/SNRNP200 interactions. *Ophthalmic Genet.* 39, 80–86. doi: 10.1080/13816810.2017.1393825

Ewels, P., Magnusson, M., Lundin, S., and Kaller, M. (2016). MultiQC: summarize analysis results for multiple tools and samples in a single report. *Bioinformatics* 32, 3047–3048. doi: 10.1093/bioinformatics/btw354

Farkas, M. H., Grant, G. R., White, J. A., Sousa, M. E., Consugar, M. B., and Pierce, E. A. (2013). Transcriptome analyses of the human retina identify unprecedented transcript diversity and 3.5 Mb of novel transcribed sequence via significant alternative splicing and novel genes. *BMC Genomics* 14:486. doi: 10.1186/1471-2164-14-486

Farkas, M. H., Lew, D. S., Sousa, M. E., Bujakowska, K., Chatagnon, J., Bhattacharya, S. S., et al. (2014). Mutations in pre-mRNA processing factors 3, 8, and 31 cause dysfunction of the retinal pigment epithelium. *Am. J. Pathol.* 184, 2641–2652. doi: 10.1016/j.ajpath.2014.06.026

Foltz, L. P., Howden, S. E., Thomson, J. A., and Clegg, D. O. (2018). Functional assessment of patient-derived retinal pigment epithelial cells edited by CRISPR/Cas9. *Int. J. Mol. Sci.* 19:4127. doi: 10.3390/ijms19124127

Galej, W. P., Oubridge, C., Newman, A. J., and Nagai, K. (2013). Crystal structure of Prp8 reveals active site cavity of the spliceosome. *Nature* 493, 638–643. doi: 10.1038/nature11843

Grainger, R. J., and Beggs, J. D. (2005). Prp8 protein: at the heart of the spliceosome. *RNA* 11, 533–557. doi: 10.1261/rna.2220705

Graziotto, J. J., Farkas, M. H., Bujakowska, K., Deramaudt, B. M., Zhang, Q., Nandrot, E. F., et al. (2011). Three gene-targeted mouse models of RNA splicing factor RP show late-onset RPE and retinal degeneration. *Invest. Ophthalmol. Vis. Sci.* 52, 190–198. doi: 10.1167/iovs.10-5194

Han, S. P., Kassahn, K. S., Skarshewski, A., Ragan, M. A., Rothnagel, J. A., and Smith, R. (2010). Functional implications of the emergence of alternative splicing in hnRNP A/B transcripts. *RNA* 16, 1760–1768. doi: 10.1261/rna.2142810

Hartong, D. T., Berson, E. L., and Dryja, T. P. (2006). Retinitis pigmentosa. *Lancet* 368, 1795–1809.

Herzel, L., Ottoz, D. S. M., Alpert, T., and Neugebauer, K. M. (2017). Splicing and transcription touch base: co-transcriptional spliceosome assembly and function. *Nat. Rev. Mol. Cell Biol.* 18, 637–650. doi: 10.1038/nrm.2017.63

Hirami, Y., Osakada, F., Takahashi, K., Okita, K., Yamanaka, S., Ikeda, H., et al. (2009). Generation of retinal cells from mouse and human induced pluripotent stem cells. *Neurosci. Lett.* 458, 126–131. doi: 10.1016/j.neulet.2009.04.035

Hongisto, H., Ilmarinen, T., Vattulainen, M., Mikhailova, A., and Skottman, H. (2017). Xeno- and feeder-free differentiation of human pluripotent stem cells to two distinct ocular epithelial cell types using simple modifications of one method. *Stem Cell Res. Ther.* 8:291.

Horvath, S. (2013). DNA methylation age of human tissues and cell types. *Genome Biol.* 14:R115.

Kukhtar, D., Rubio-Pena, K., Serrat, X., and Ceron, J. (2020). Mimicking of splicing-related retinitis pigmentosa mutations in *C. elegans* allow drug screens and identification of disease modifiers. *Hum. Mol. Genet.* 29, 756–765. doi: 10.1093/hmg/ddz315

Lareau, L. F., and Brenner, S. E. (2015). Regulation of splicing factors by alternative splicing and NMD is conserved between kingdoms yet evolutionarily flexible. *Mol. Biol. Evol.* 32, 1072–1079. doi: 10.1093/molbev/msv002

Lareau, L. F., Inada, M., Green, R. E., Wengrod, J. C., and Brenner, S. E. (2007). Unproductive splicing of SR genes associated with highly conserved and ultraconserved DNA elements. *Nature* 446, 926–929. doi: 10.1038/nature05676

Lukovic, D., Artero Castro, A., Delgado, A. B., Bernal Mde, L., Luna Pelaez, N., Diez Lloret, A., et al. (2015). Human iPSC derived disease model of MERTK-associated retinitis pigmentosa. *Sci. Rep.* 5:12910.

Lukovic, D., Artero Castro, A., Kaya, K. D., Munezero, D., Gieser, L., Davo-Martinez, C., et al. (2020). Retinal organoids derived from hiPSCs of an AIPL1-LCA patient maintain cytoarchitecture despite reduced levels of mutant AIPL1. *Sci. Rep.* 10:5426.

Lukovic, D., Bolinches-Amoros, A., Artero-Castro, A., Pascual, B., Carballo, M., Hernan, I., et al. (2017). Generation of a human iPSC line from a patient with retinitis pigmentosa caused by mutation in PRPF8 gene. *Stem Cell Res.* 21, 23–25. doi: 10.1016/j.scr.2017.03.007

MacNair, L., Xiao, S., Miletic, D., Ghani, M., Julien, J. P., Keith, J., et al. (2016). MTHFSD and DDX58 are novel RNA-binding proteins abnormally regulated in amyotrophic lateral sclerosis. *Brain* 139, 86–100. doi: 10.1093/brain/awv308

Martinez-Contreras, R., Cloutier, P., Shkreta, L., Fisette, J. F., Revil, T., and Chabot, B. (2007). hnRNP proteins and splicing control. *Adv. Exp. Med. Biol.* 623, 123–147. doi: 10.1007/978-0-387-77374-2_8

Martinez-Gimeno, M., Gamundi, M. J., Hernan, I., Maseras, M., Milla, E., Ayuso, C., et al. (2003). Mutations in the pre-mRNA splicing-factor genes PRPF3, PRPF8, and PRPF31 in Spanish families with autosomal dominant retinitis pigmentosa. *Invest. Ophthalmol. Vis. Sci.* 44, 2171–2177. doi: 10.1167/iovs.02-0871

Maubaret, C. G., Vaclavik, V., Mukhopadhyay, R., Waseem, N. H., Churchill, A., Holder, G. E., et al. (2011). Autosomal dominant retinitis pigmentosa with intrafamilial variability and incomplete penetrance in two families carrying mutations in PRPF8. *Invest. Ophthalmol. Vis. Sci.* 52, 9304–9309. doi: 10.1167/iovs.11-8372

McKie, A. B., McHale, J. C., Keen, T. J., Tarttelin, E. E., Goliath, R., van Lith-Verhoeven, J. J., et al. (2001). Mutations in the pre-mRNA splicing factor gene PRPC8 in autosomal dominant retinitis pigmentosa (RP13). *Hum. Mol. Genet.* 10, 1555–1562. doi: 10.1093/hmg/10.15.1555

Miller, J. D., Ganat, Y. M., Kishinevsky, S., Bowman, R. L., Liu, B., Tu, E. Y., et al. (2013). Human iPSC-based modeling of late-onset disease via progerin-induced aging. *Cell Stem Cell* 13, 691–705. doi: 10.1016/j.stem.2013.11.006

Murray, S. F., Jazayeri, A., Matthes, M. T., Yasumura, D., Yang, H., Peralta, R., et al. (2015). Allele-specific inhibition of rhodopsin with an antisense oligonucleotide slows photoreceptor cell degeneration. *Invest. Ophthalmol. Vis. Sci.* 56, 6362–6375. doi: 10.1167/iovs.15-16400

Ni, J. Z., Grate, L., Donohue, J. P., Preston, C., Nobida, N., O'Brien, G., et al. (2007). Ultraconserved elements are associated with homeostatic control of splicing regulators by alternative splicing and nonsense-mediated decay. *Genes Dev.* 21, 708–718. doi: 10.1101/gad.1525507

Nueda, M. J., Ferrer, A., and Conesa, A. (2012). ARSyN: a method for the identification and removal of systematic noise in multifactorial time course microarray experiments. *Biostatistics* 13, 553–566. doi: 10.1093/biostatistics/kxr042

O'Leary, N. A., Wright, M. W., Brister, J. R., Ciufo, S., Haddad, D., McVeigh, R., et al. (2016). Reference sequence (RefSeq) database at NCBI: current status, taxonomic expansion, and functional annotation. *Nucleic Acids Res.* 44, D733–D745.

Pena, V., Liu, S., Bujnicki, J. M., Luhrmann, R., and Wahl, M. C. (2007). Structure of a multipartite protein-protein interaction domain in splicing factor prp8 and its link to retinitis pigmentosa. *Mol. Cell* 25, 615–624. doi: 10.1016/j.molcel.2007.01.023

Plaza Reyes, A., Petrus-Reurer, S., Padrell Sanchez, S., Kumar, P., Douagi, I., Bartuma, H., et al. (2020). Identification of cell surface markers and establishment of monolayer differentiation to retinal pigment epithelial cells. *Nat. Commun.* 11:1609.

Reichman, S., Terray, A., Slembrouck, A., Nanteau, C., Orieux, G., Habeler, W., et al. (2014). From confluent human iPS cells to self-forming neural retina and retinal pigmented epithelium. *Proc. Natl. Acad. Sci. U.S.A.* 111, 8518–8523. doi: 10.1073/pnas.1324212111

Robinson, M. D., and Oshlack, A. (2010). A scaling normalization method for differential expression analysis of RNA-seq data. *Genome Biol.* 11:R25.

Saltzman, A. L., Pan, Q., and Blencowe, B. J. (2011). Regulation of alternative splicing by the core spliceosomal machinery. *Genes Dev.* 25, 373–384. doi: 10.1101/gad.2004811

Shimada, H., Lu, Q., Insinna-Kettenhofen, C., Nagashima, K., English, M. A., Semler, E. M., et al. (2017). In vitro modeling using ciliopathy-patient-derived cells reveals distinct cilia dysfunctions caused by CEP290 mutations. *Cell Rep.* 20, 384–396. doi: 10.1016/j.celrep.2017.06.045

Sorkio, A., Hongisto, H., Kaarniranta, K., Uusitalo, H., Juuti-Uusitalo, K., and Skottman, H. (2014). Structure and barrier properties of human embryonic stem cell-derived retinal pigment epithelial cells are affected by extracellular matrix protein coating. *Tissue Eng. Part A* 20, 622–634.

Strunnikova, N. V., Maminishkis, A., Barb, J. J., Wang, F., Zhi, C., Sergeev, Y., et al. (2010). Transcriptome analysis and molecular signature of human retinal pigment epithelium. *Hum. Mol. Genet.* 19, 2468–2486. doi: 10.1093/hmg/ddq129

Sullivan, L. S., Bowne, S. J., Birch, D. G., Hughbanks-Wheaton, D., Heckenlively, J. R., Lewis, R. A., et al. (2006). Prevalence of disease-causing mutations in families with autosomal dominant retinitis pigmentosa: a screen of known genes in 200 families. *Invest. Ophthalmol. Vis. Sci.* 47, 3052–3064. doi: 10.1167/iovs.05-1443

Tanackovic, G., Ransijn, A., Thibault, P., Abou Elela, S., Klinck, R., Berson, E. L., et al. (2011). PRPF mutations are associated with generalized defects in spliceosome formation and pre-mRNA splicing in patients with retinitis pigmentosa. *Hum. Mol. Genet.* 20, 2116–2130. doi: 10.1093/hmg/ddr094

Tarazona, S., Furio-Tari, P., Turra, D., Pietro, A. D., Nueda, M. J., Ferrer, A., et al. (2015). Data quality aware analysis of differential expression in RNA-seq with NOISeq R/Bioc package. *Nucleic Acids Res.* 43:e140.

Trincado, J. L., Entizne, J. C., Hysenaj, G., Singh, B., Skalic, M., Elliott, D. J., et al. (2018). SUPPA2: fast, accurate, and uncertainty-aware differential splicing analysis across multiple conditions. *Genome Biol.* 19:40.

Wahl, M. C., Will, C. L., and Luhrmann, R. (2009). The spliceosome: design principles of a dynamic RNP machine. *Cell* 136, 701–718. doi: 10.1016/j.cell.2009.02.009

Wickramasinghe, V. O., Gonzalez-Porta, M., Perera, D., Bartolozzi, A. R., Sibley, C. R., Hallegger, M., et al. (2015). Regulation of constitutive and alternative mRNA splicing across the human transcriptome by PRPF8 is determined by 5' splice site strength. *Genome Biol.* 16:201.

Wong, J. J., Au, A. Y., Ritchie, W., and Rasko, J. E. (2016). Intron retention in mRNA: No longer nonsense: Known and putative roles of intron retention in normal and disease biology. *BioEssays* 38, 41–49. doi: 10.1002/bies.201500117

Xu, Q., Modrek, B., and Lee, C. (2002). Genome-wide detection of tissue-specific alternative splicing in the human transcriptome. *Nucleic Acids Res.* 30, 3754–3766. doi: 10.1093/nar/gkf492

Yates, A. D., Achuthan, P., Akanni, W., Allen, J., Alvarez-Jarreta, J., Amode, M. R., et al. (2020). Ensembl 2020. *Nucleic Acids Res.* 48, D682–D688.

Zhang, X. O., Yin, Q. F., Wang, H. B., Zhang, Y., Chen, T., Zheng, P., et al. (2014). Species-specific alternative splicing leads to unique expression of sno-lncRNAs. *BMC Genomics* 15:287. doi: 10.1186/1471-2164-15-287

Zhong, X., Gutierrez, C., Xue, T., Hampton, C., Vergara, M. N., Cao, L. H., et al. (2014). Generation of three-dimensional retinal tissue with functional photoreceptors from human iPSCs. *Nat. Commun.* 5:4047.

Conflict of Interest: The authors declare that the research was conducted in the absence of any commercial or financial relationships that could be construed as a potential conflict of interest.

Copyright © 2021 Arzalluz-Luque, Cabrera, Skottman, Benguria, Bolinches-Amorós, Cuenca, Lupo, Dopazo, Tarazona, Delás, Carballo, Pascual, Hernan, Erceg and Lukovic. This is an open-access article distributed under the terms of the Creative Commons Attribution License (CC BY). The use, distribution or reproduction in other forums is permitted, provided the original author(s) and the copyright owner(s) are credited and that the original publication in this journal is cited, in accordance with accepted academic practice. No use, distribution or reproduction is permitted which does not comply with these terms.

frontiers in Immunology

REVIEW
published: 12 May 2021
doi: 10.3389/fimmu.2021.621007

Immunologic Rejection of Transplanted Retinal Pigmented Epithelium: Mechanisms and Strategies for Prevention

Carson C. Petrash[1,2*], *Alan G. Palestine*[2*] *and M. Valeria Canto-Soler*[1,3*]

[1] CellSight Ocular Stem Cell and Regeneration Research Program, Department of Ophthalmology, Sue Anschutz-Rodgers Eye Center, University of Colorado School of Medicine, Aurora, CO, United States, [2] Department of Ophthalmology, University of Colorado Anschutz Medical Campus, Aurora, CO, United States, [3] Charles C. Gates Center for Regenerative Medicine, University of Colorado School of Medicine, Anschutz Medical Campus, Aurora, CO, United States

OPEN ACCESS

Edited by:
Javier Sancho-Pelluz,
Catholic University of Valencia San Vicente Mártir, Spain

Reviewed by:
Slaven Erceg,
Principe Felipe Research Center (CIPF), Spain
Kathryn Pepple,
University of Washington, United States

***Correspondence:**
Carson C. Petrash
carson.petrash@cuanschutz.edu
Alan G. Palestine
alan.palestine@cuanschutz.edu
M. Valeria Canto-Soler
valeria.canto-soler@cuanschutz.edu

Specialty section:
This article was submitted to Alloimmunity and Transplantation, a section of the journal Frontiers in Immunology

Received: 17 November 2020
Accepted: 28 April 2021
Published: 12 May 2021

Citation:
Petrash CC, Palestine AG and Canto-Soler MV (2021) Immunologic Rejection of Transplanted Retinal Pigmented Epithelium: Mechanisms and Strategies for Prevention. Front. Immunol. 12:621007. doi: 10.3389/fimmu.2021.621007

Replacement of dysfunctional retinal pigmented epithelium (RPE) with grafts derived from stem cells has the potential to improve vision for patients with retinal disorders. In fact, the potential is such that a great number of groups are attempting to realize this therapy through individual strategies with a variety of stem cell products, hosts, immunomodulatory regimen, and techniques to assess the success of their design. Comparing the findings of different investigators is complicated by a number of factors. The immune response varies greatly between xenogeneic and allogeneic transplantation. A unique immunologic environment is created in the subretinal space, the target of RPE grafts. Both functional assessment and imaging techniques used to evaluate transplants are susceptible to erroneous conclusions. Lastly, the pharmacologic regimens used in RPE transplant trials are as numerous and variable as the trials themselves, making it difficult to determine useful results. This review will discuss the causes of these complicating factors, digest the strategies and results from clinical and preclinical studies, and suggest places for improvement in the design of future transplants and investigations.

Keywords: retinal pigment epithelium (RPE), induced pluripotent stem cells (IPSC), age-related macular degeneration (AMD), transplant rejection, immune rejection, transplant acceptance, retinitis pigmentosa, immunosuppression

INTRODUCTION

Retinal diseases with degeneration or dystrophy of photoreceptors are visually devastating and there are no current therapies to regenerate retinal tissue. In age-related macular degeneration (AMD) and some forms of inherited retinal diseases (IRDs) such as Best Disease and MERTK-associated Retinitis Pigmentosa (RP), the primary dysfunction affects the retinal pigmented epithelium (RPE) (1–3). Adjacent to the neuroretina, the RPE is responsible for supporting the metabolism of light-sensing photoreceptors, regenerating 11-cis-retinol for the visual cycle, forming the outer blood-retinal barrier, and reducing light scatter (4). Degeneration of RPE leads to secondary loss of photoreceptors and subsequent permanent loss of vision (2, 3). The latest research seeks to treat these degenerative conditions by transplanting healthy RPE at early stages of disease.

Sources of RPE for transplantation have evolved through the years. Pioneering investigations studied primary cultures of RPE (5); however, more recent investigations have used RPE derived from stem cells due to the capacity for unlimited self-renewal and greater possibility of selecting for desired characteristics (6). Stem cell sources of RPE include RPE stem cells (RPESC) found in the adult native tissue (7), embryonic stem cells (ESCs), and induced pluripotent stem cells (iPSCs) (6). This review will primarily focus on studies involving transplantation of RPE derived from ESCs and particularly iPSCs as they have the greatest potential as graft tissue. Autologous transplant iPSC-RPE is currently under clinical trial [(8, 9), and ClinicalTrials.gov # NCT04339764]. Due to genetic variability, instability, and potential tumorigenicity of iPSCs, validation of an autologous cell line is a long and costly process that will be challenging to scale for treatment of the millions of potential recipients (10). Alternative approaches and preclinical investigations involve xenogeneic or allogeneic sources and carry heightened risk of immunologic rejection (11).

The eye as a whole represents a unique immunologic environment. The "immune privilege" of the eye is not what it was once hoped; nonetheless, features of the subretinal space (SRS) create a relatively safe target for transplantation of iPSCs (12). In addition, both stem cells and RPE are attributed with anti-inflammatory properties that enhance compatibility (13, 14). Nevertheless, stem cell derived RPE is susceptible to immune rejection from days to months following transplantation (15–17). Effector mechanisms of acute (i.e., after days) and chronic (weeks to months) are interrelated but distinct (18). For this broad problem of immune rejection, a one-fits-all solution is unlikely and multiple strategies for prevention are necessary.

The mere determination of rejection of an RPE graft is controversial. Subretinal biopsy for histologic confirmation is implausible, and the small volume of grafted tissue may be insufficient to produce systemic manifestations. Researchers instead rely on longitudinal functional tests and imaging techniques. Recent investigations are revealing that these surrogate markers are susceptible to confounding results (15, 19–21). No prior authors have comprehensively reviewed the common signs or alternative phenomena that can masquerade as immunologic rejection or lack thereof. Beyond determining rejection of RPE transplants, very little is known regarding how it may be prevented. To the best of our knowledge this is the first review to specifically compare immunomodulatory regimen and results and attempt to identify trends. Furthermore, new directions will be discussed, and specific strategies proposed to prevent rejection of RPE transplants in future trials.

SECTION I: TRANSPLANT IMMUNOLOGY

Rejection of solid transplants can result from any of a series of actions of the innate, nonspecific and the acquired, antigen-specific immune systems (22). Innate immunity includes cellular elements: macrophages, neutrophils, natural killer cells, and resident lymphocytes which can cause acute rejection within the first week (16). These cells also express pattern-recognition receptors (PRRs) such as toll-like receptors (TRLs) which allow them to recognize damage-associated molecular patterns (DAMPs) released as a result of tissue damage, including graft surgery or early rejection (23). Binding of the PRRs to DAMPs activates immune cells and potentiates inflammation, including expression of antigen presenting cells (APCs) and CD4 T-cells. T-cells in particular orchestrate the acquired cellular and humoral immune cascade to reinforce the innate response, generating an expansion in both CD8 "cytotoxic" T-cells and antibody-producing B-cells. These responses by lymphocytes cause chronic rejection of transplants beyond the first week (18).

Early work in solid organ transplants demonstrated that T-cells are necessary and sufficient for allograft rejection (24–26). Subsequently, immunosuppressive regimen were developed that target T-cell activation at three steps: signal 1) binding by APCs, signal 2) costimulatory molecules and ligands, or signal 3) the trigger for cell proliferation (27). Most common agents include tacrolimus and cyclosporine: calcineurin inhibitors that prevent signal 1. Antimetabolites such as mycophenolate mofetil (MMF) target signal 3. Likewise for RPE transplant studies, the most frequently used drug is tacrolimus. Glucocorticoids including prednisone, dexamethasone, and triamcinolone are prescribed as well, which have broad effects on T-cells by reducing expression of MHC II (signal 1), increasing percentage of regulatory T-cells, and inducing T-cell apoptosis (signal 3) (28–30). Despite these measures to modulate acquired immunity, RPE grafts routinely exhibit signs of rejection weeks to months after transplantation, and histology recovered from these eyes confirms a predominance of lymphocytic infiltrate (15, 17, 20, 31–35). Evidently there is room for improvement in understanding the immunologic response to subretinal RPE grafts.

In solid organ transplants, infiltration of mononuclear phagocytes (MNP) is a prominent feature of rejection (36). MNPs include bone marrow derived macrophages (BMM) and tissue resident macrophages (TRMs). Greater number of BMM correlates with worse clinical outcomes (37, 38) and depletion of BMM improves allograft function (39). BMM represent the majority of macrophages in rejected solid organ transplants (40). Similarly, MNPs form a large component of the cellular infiltrate of rejected RPE grafts (15–17, 20, 32, 33, 35). This is especially true when rejection of RPE occurs within the first week, prior to the development of acquired immunity (15, 16). Transplant immunologists have increasingly looked at MNPs to gain a better understanding of allograft rejection (26).

Compared to BMM which infiltrate inflamed tissue, TRM are critical to healthy tissue homeostasis. Microglia are the TRM of the central nervous system and retina and perform functions including phagocytosis of waste and regulation of vascular and neural growth (41, 42). In non-diseased retina, microglia are located in the inner and outer plexiform layers but are absent in the SRS (4). In IRD (43) and light-induced degeneration models (44), microglia were the dominant MNP lineage in the SRS, while BMM were largely limited to the neuroparenchyma. We speculate that this may underscore the relative importance of microglia in the immune response to transplanted RPE compared to other solid organ transplants given that recipients may have a pre-existing or predisposition to

microglial infiltrate. Furthermore, the avascularity of the graft and SRS represents an additional barrier to BMM infiltration of RPE grafts compared to solid organ transplants. Nonetheless, both microglia and BMM are likely to play important roles given their prevalence in inflammatory infiltrate around rejected RPE (15–17, 20, 32, 33, 35).

As the resident immune cells the graft site, TRM may direct the initial response to transplanted grafts (16, 26, 45, 46). Depicted in **Figure 1**, *in vitro* studies have demonstrated that DAMPs released as a result of transplantation surgery bind to TLRs and cause IFNγ driven proliferation of M1 microglia, which release TNFα, IL-1β, IL-6, nitric oxide, and reactive oxygen species to propagate inflammation and neural damage (48, 49). If the inciting trauma resolves, IL-4 induces proliferation of the M2 phenotype of microglia. M2 microglia produce anti-inflammatory TGFβ, IL-10, IL-13, Ccl2 (50–53), neurogenic oncomodulin (OCM), insulin-like growth factor (IGF)-1, and vascular endothelial growth factor (VEGF), returning the retina to healthy state (54, 55). However, if the original injury persists, the inflammatory M1 phenotype causes progressive tissue damage (41). To corroborate this *in vitro* evidence, *in vivo* studies have indicated that allograft transplantation without immune suppression is associated with persistent M1-type BMM, while macrophages rapidly convert to M2-phenotype with adequate immune suppression (26, 46, 56). In summary, we hypothesize that surgical trauma causes proliferation of destructive M1 microglia that contribute to acute rejection, and dysregulation of the M1 phenotype leads to macrophage infiltrate surrounding chronically rejected RPE grafts.

Due to anti-inflammatory and neuroprotective properties of M2 phenotype microglia, we speculate that supporting the transition from M1 to M2 may be an effective strategy to reduce immune rejection and improve retinal function. As shown in **Figure 1**, there are many potential therapies that stimulate the expression of M2 microglia, including mesencephalic astrocyte-derived neurotrophic factor (MANF) (41, 57), growth factors IGF-1 and NGF (58, 59), minocycline (60, 61), translocator protein (TSPO) (62), norgestrel (63, 64), and IFN-β (65). With the exception of minocycline, none of these therapies have been adopted in RPE transplant studies (66). Glucocorticoids have been included in RPE transplant trials and are known to reduce production of inflammatory cytokines IL-1 and TNFα and inhibit macrophage phagocytic function; however, the relative role of these pro-M2 functions compared to the effects of macrophages on T-cells and acquired immunity

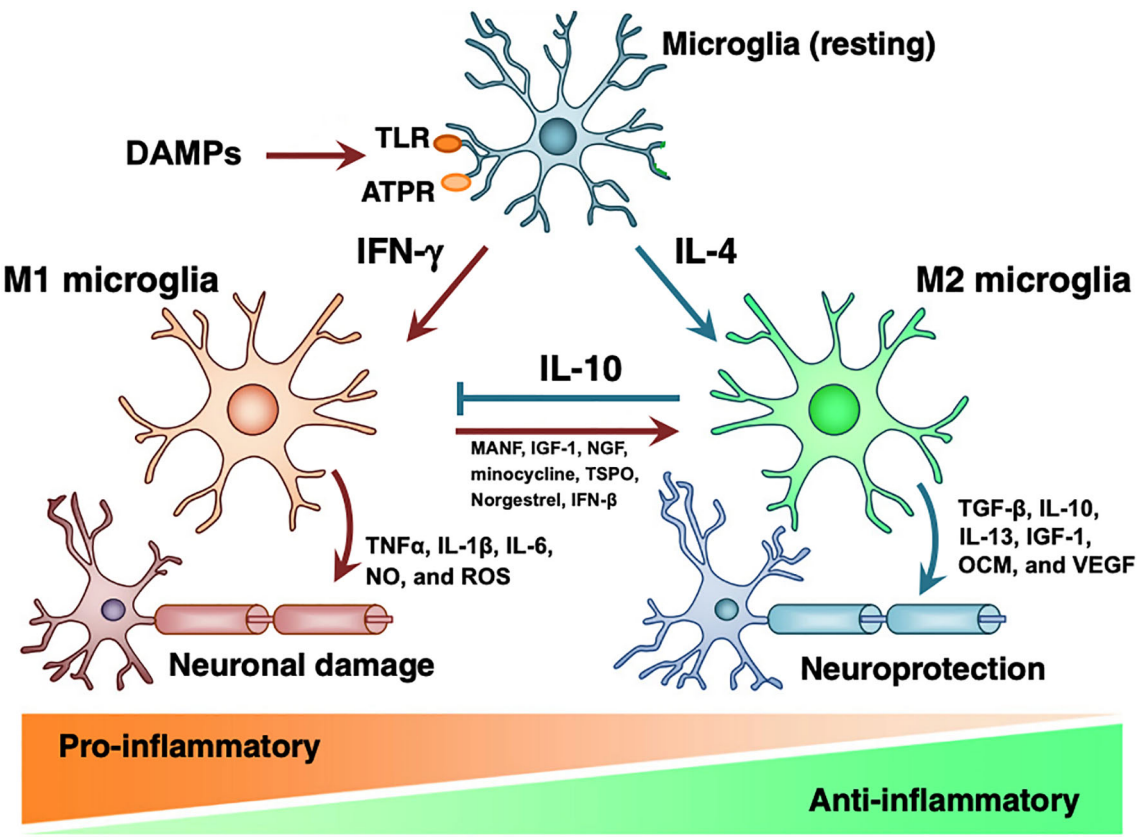

FIGURE 1 | Microglial M1 and M2 phenotypes. DAMPs act on PRRs on resting microglia to induce formation of M1 or M2 microglia. M1 microglia induce pro-inflammatory state and tissue damage by releasing TNFα, IL-1β, IL-6, nitric oxide, and ROS. M2 microglia have tissue-protective effects *via* TGF-β, IL-10, IL-13, IGF-1, OCM, and VEGF. While IL-10 inhibits M1 microglia, introduction of MANF, IGF-1, minocycline, TSPO, norgestrel, and IFN-βB induce transition to M2 phenotype. Modified from Nakagawa 2015 with notes from Kramer 2019, Elsevier license 4858840650798 (41, 47).

is undetermined (67–69). Therefore, specifically targeting microglial phenotype represents largely untested waters with potential benefits for both reducing immunologic rejection and improving the health of transplanted neurons.

Clinical and preclinical investigations to date have focused on inhibition of acquired immunity to prevent rejection; however, given the 1) variable chronicity of rejection, 2) prevalence of microglial/macrophage infiltrate on histology of rejected transplants, and 3) established immune physiology of the retina, we propose that is important to consider specifically targeting M2 macrophage phenotype. This strategy should be investigated first in pre-clinical studies. The primary effectors of rejection may depend on the level of transplantation. Due to the greater phylogenetic difference, xenografts may be more readily recognized by innate immune system and susceptible to acute rejection. Allografts that avoid innate recognition may have to evade the acquired immune system or else succumb to chronic rejection. Differences in strain (e.g., Yucatan pig versus P23H minipig) or immunophenotypes (e.g., MHC antigens) may also determine the chronicity and effectors of rejection. However, given that macrophages and T-cells secrete cytokines that affect one another's phenotype, i.e. M1 versus M2 macrophage or Th_1/Th_2 versus regulatory T-cells, we hypothesize that both T-cell inhibitors and M2 promoters offer immunologic benefits throughout the postsurgical period.

Two further strategies of transplant immunology warrant a mention. First, grafts composed of tissue constructs have demonstrated greater success than cellular suspensions, as demonstrated by the success of pancreas compared to islet cell transplants (70). Furthermore, there is evidence that hESC-RPE transplants may survive longer as a monolayer (71) and many current trials have adopted this strategy (66, 72, 73) and [ClinicalTrials.gov # NCT04339764]. Nonetheless, this is still up for debate (74) and even recent trials have delivered RPE cell suspensions (15, 35). Drawing conclusions regarding the ideal form of delivery is also complicated by the variable scaffolds on which RPE monolayers are implanted, and the possibility that they create a barrier to diffusion of metabolites from the choroidal vasculature. Secondly, long-term survival of solid organ transplants can be achieved without immune suppression through the infusion of hematopoietic stem cells (HSCs) at the time of transplantation. Transfused HSCs engraft within the thymus and bone marrow of the recipient and cause production of host blood T- and B-cells that are tolerant of graft antigens. While this effect has been demonstrated in both animal and human recipients of solid organs, its potential has not been tested with respect to RPE grafts (75).

SECTION II: SUB-RETINAL IMMUNE RESPONSE AND PRIVILEGE

The eye is unique among tissues in that its function is dependent on the optical clarity of its media: cornea, aqueous, lens, and vitreous. To prevent excessive inflammatory changes, the eye has physiologic systems that are distinct from the systemic immune system. In 1905 these mechanisms allowed the first successful corneal transplant before the advent of immunomodulatory medications, leading to the concept of "immunologic privilege". However, privilege of the SRS has been over-stated in the past: even allografts transplanted with immunomodulation are susceptible to rejection. Nonetheless, it is worthwhile to consider the mechanisms of immune privilege in order to design interventions. The physiology of immune privilege is extensive and only few features will be defined here, organized into three groups as detailed by Caspi et al., 2006: separation, local inhibition, and systemic regulation (76).

Immune Separation

Separation refers to the physical blood-retinal barrier (BRB) that prevents systemic immune cells and large molecules from passing into ocular tissues. The barrier is primarily created by intercellular tight junctions. An outer barrier is formed between cells of the retinal pigmented epithelium (RPE), while an inner barrier is formed between endothelial cells of the inner retinal vasculature. In addition to trauma, the BRB can be weakened by inflammation and neovascularization (77).

Surgical approaches for graft placement are transscleral or transretinal. While the transscleral approach violates the outer BRB, transretinal placement requires vitrectomy, retinotomy, and endolaser: all procedures associated with production of DAMPs and inflammation, thus stimulating proliferation of M1 microglia and subsequent tissue damage (78). Therefore, it is yet undetermined whether a transscleral or transretinal approach is immunologically preferable. However, subjects with retinal disease may be predisposed to rejection due to inflammation associated with their primary disorder (e.g., AMD or RP) or prior intraocular surgeries (79).

Based on what we know regarding immune separation, measures may be hypothesized to minimize rejection in the SRS. First, ideal study subjects should have no intraocular inflammation or neovascularization (77). Retinal diseases with degenerative or dystrophic RPE may increase risk as well. Secondly, the implant should be placed far from the retinotomy or Bruch's membranotomy to minimize M1 microglia in the location of the graft (41). Lastly, it is worth emphasizing that tissue trauma should be minimized (41, 77).

Local Inhibition

Disruption of the BRB leads to influx of reactive cells from the systemic circulation, and thus local inhibition of the invading cells and inflammatory mediators is necessary to prevent the escalation of inflammation. Native RPE has a primary role in this anti-inflammatory "effector blockade" (76). Cytokines produced by RPE include TGFβ, IL-11, and IFNβ (80). In addition to enhancing the M2 microglial phenotype, TGFβ is responsible for inhibiting the action of inflammatory T-cells and promoting development of regulatory T-cells (81, 82). IL-11 has cytoprotective and anti-inflammatory functions (83). IFNβ inhibits expression of cellular adhesion molecules and chemokines sICAM-1 and CXCL9, which attract T-cells and NK cells to sites of inflammation (80). With regards to membrane-bound receptors, Fas ligand (FasL) and PDL1 are

highly-expressed on RPE and responsible for inducing apoptosis of invading T-cells or converting them to regulatory T-cells (81, 84). CD46 on RPE prevents the activation of the complement cascade (76).

Paradoxically, RPE also has pro-inflammatory behavior. The most significant of these mechanisms is its role as an antigen presenting cell (APC) with MHC-II, a feature shared only by specific immune cells (85). This introduces the paradox that it may be beneficial to transplant atop RPE atrophy, despite the lack of an outer BRB, due to potentially reduced antigen presentation. No study has addressed this question. RPE has a vital role in the local control of inflammation in the SRS and targeting expression of MHC-II, TGFβ, or any of the local immune inhibitory factors of RPE may affect survival of grafted RPE (33).

Systemic Regulation

In states of trauma or inflammation, immune cells are able to pass the physical barriers and evade the local inhibitory mechanisms to access the SRS and subsequently re-enter systemic circulation. In the non-privileged immune response, APCs take antigens from the site of inflammation to local lymph nodes or the spleen where they activate delayed-hypersensitivity (DH) T-lymphocytes, potentiating the inflammatory response. The eye has mechanisms to regulate this reaction as well. Similar to the well-studied anterior chamber-associated immune deviation (ACAID), $CD11b^{+}$ microglia in the retina induce the development of regulatory T-cells in the spleen, which dampens the response of DH T-cells (86, 87). Despite years of study, ACAID has never been utilized for therapeutic effect. The physiology of ACAID suggests that it may be possible to stimulate regulatory T-cells and inhibit rejection by priming the host with graft antigens, similar to how HSCs engraft to induce tolerance to solid organ transplants. This remains an area for future study.

The relative role of immune separation, local inhibition, and systemic regulation in preventing rejection of transplanted RPE in the SRS is undetermined. Furthermore, the strategies that we propose for preserving immune separation are also unproven and alone insufficient to prevent rejection. However, understanding the immune mechanisms in the SRS will assist researchers in designing investigations and strategies, and our recommendations are compatible with further interventions that, together, may improve success of future trials.

SECTION III: EVALUATING REJECTION AND LACK OF REJECTION

Most organ transplants can be considered to not have been rejected by the host if the graft is performing its physiologic function: for example, a kidney producing urine, liver metabolizing toxins, or a lung exchanging gases. This is more difficult to define in the retina. For one, animal subjects are not able to comply with standard tests for visual function such as acuity or field tests. While human patients are able to complete these tests, results may be confounded by some degree of photoreceptor functional rescue induced by growth factors released as a byproduct of retinal detachment or other elements of the surgical procedure (88, 89). Therefore, improved acuity, fields, or even electrophysiologic response may be due to surgically induced cellular repair processes rather than function of transplanted cells. Secondly, there are no clear systemic parameters that indicate rejection of a retinal transplant. Elevated inflammatory cells in the blood can indicate rejection of a solid organ; however, stem cell RPE grafts may undergo a slow functional deterioration or rejection without manifest signs of inflammatory reaction (15, 21), perhaps due to the anti-inflammatory properties of the RPE graft or immune privilege mechanisms of the SRS (19).

In contrast to these challenges, retinal transplants have advantage of visibility with ophthalmoscopy. Studies from autologous transplants are perhaps the best resource to demonstrate the appearance of RPE grafts in the absence of rejection. As shown in **Figure 2**, a flat, expanding, pigmented monolayer is observed after transplantation of autologous iPSC-RPE (8, 9). In allogeneic clinical trials, Mehat 2018 found dose-dependent hyperpigmentation at the site of transplantation, and this study along with Schwartz 2016 observed a predilection for hyperpigmentation in areas of prior retinal atrophy, possibly representing migration of donor cells (21, 90, 91). While it may be true that successfully transplanted RPE would have this morphology, pigmented cells can also represent macrophages that have phagocytosed rejected or apoptotic RPE or host RPE that proliferates in response to the transplant surgery (92, 93). Mehat 2018 noted that their findings would also be consistent with subretinal spread of released pigment (21, 90). On the other hand, the lack of obvious pigmentation does not mean that transplanted RPE has been rejected, as RPE may have variable pigmentation (21, 94, 95). Schwartz 2016 found no correlation between pigmentation and changes in visual function (21). Nonetheless, serial fundus photographs may manifest changes when RPE is rejected (20). Clumping of pigment or pigment-laden cells has been reported and suggested as a sign of rejection, as seen in **Figure 3** (32, 35, 73). The appearance of the grafted tissue is a valuable parameter when determining the immunologic success of RPE transplantation, but it must be considered that appropriate morphology and pigmentation is not sufficient.

Along with direct visualization techniques, the retina allows imaging with techniques such as optical coherence tomography (OCT), fluorescein angiogram (FA), and fundus autofluorescence (AF). OCT enables cross-sectional visualization of neuroretina layers, transplanted tissues, and changes such as edema or retinal detachment. Images demonstrating both normal morphology and representative changes associated with rejection are seen in **Figure 3** and compiled in **Table 1**. Features that suggest lack of rejection include: 1) the presence of transplanted cells as a homogenous monolayer or hyperreflective outer retinal band (21, 35, 66, 72, 73), and 2) improved retinal morphology including formation of an external limiting membrane and outer nuclear layer thickness of greater than 20 um (34, 72). However, the presence of a hyper-reflective outer retinal band may persist following cellular rejection (15), and improved morphology may also result from

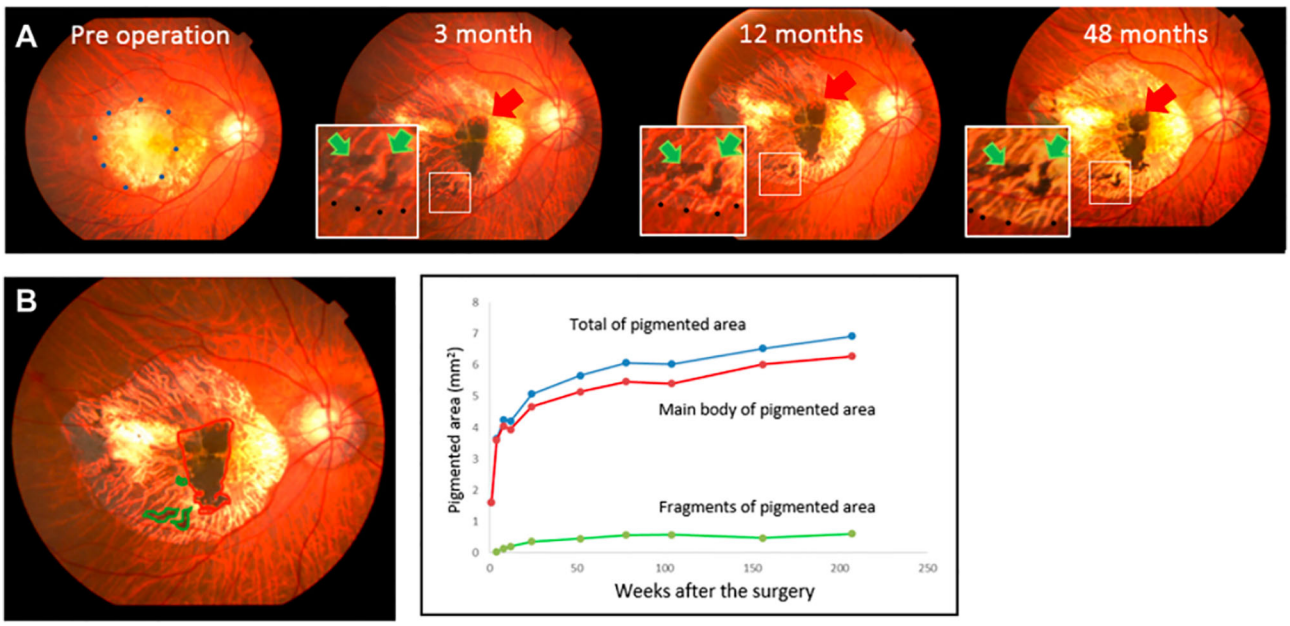

FIGURE 2 | Photographic fundus images over four years following transplant of sheet of autologous iPSC-RPE. **(A)** Red arrows point to the main graft while green arrows indicate islands of graft cells. **(B)** The graft area, identified by the presence of pigmentation, was calculated using ImageJ. Areas of the main graft and islands of grafted cells were plotted over 4 years. Expansion of pigmented area is exhibited in relatively homogenous distribution without clumping or signs of inflammation. Reprinted from Takagi 2019, license number 4867110135570.

surgically-induced changes (88). On the other hand, features that indicate rejection include: 1) signs of inflammation such as cystoid macular edema (CME), choroidal thickening, hazy vitreous, 2) deposition of subretinal material, 3) neuroretina atrophy, and 4) disintegration or clumping of transplanted cells (34, 35, 66, 72, 73). Nevertheless, it must be considered that rejection may occur without manifest signs of inflammation (15, 19), and inflammation or retinal atrophy can occur due to primary ophthalmic disease or the surgery alone in the absence of rejection.

Fluorescein angiography (FA) is used to reveal abnormal vasculature or changes in RPE. When used to assess RPE grafts, signs that indicate rejection are leakage of dye around grafts, CME, and optic disc edema, as seen in **Figure 3** (33). Leakage around grafts can be associated with surgical trauma to vasculature or Bruch's membrane or to the primary disease of the host: for example, central serous chorioretinopathy, which would increase likelihood of subsequent rejection. Again, since rejection may occur in the absence of inflammation (15, 19), destruction of the graft may occur without leakage or CME. Del Priore 2003 demonstrated no difference in serial FAs between immunocompetent and immunomodulated hosts despite the greater speed of rejection in the former (20).

Fundus autofluorescence (AF) is often used in RPE transplant studies to visualize lipofuscin and RPE pigments. Da Cruz 2018 reported a double-thickness of autofluorescence where host RPE overlapped native RPE, followed by uneven autofluorescence attributed to phagocytosis of RPE cells by immune cells (73). While AF cannot differentiate between host and transplanted RPE, a similar technique, green fluorescent protein (GFP), can make this distinction and is frequently applied to basic research. GFP is used to determine the survival percentage of transplanted RPE or follow their rejection by the loss of fluorescence over time (15, 31, 32, 66). Unfortunately, *in vivo* immunogenicity of GFP may cause cytotoxicity over time, meaning that transplanted GFP-positive RPE would be more susceptible to rejection (96).

Two recent studies proposed an alternative to visual techniques by correlating systemic donor specific antibody (DSA) with rejection of transplanted RPE (17, 35). The importance of DSA is well known in other areas of transplant medicine (97–99), and as described in Section I of this review, may have even more importance in rejection of subretinal RPE grafts. Sugita 2017 demonstrated reactivity of peripheral blood mononuclear cells (PBMCs, i.e. lymphocytes and monocytes) correlated with rejection of grafted RPE after eight weeks (17). Another serology with undetermined potential in RPE transplants: cell free DNA has been used to follow rejection of renal transplants (100). In the field of RPE transplantation where defining rejection or compatibility depends substantially on qualitative assessments, these objective measures should be considered for further applications.

There is no way to conclusively determine rejection or compatibility of transplanted RPE without histologic analysis, which can realistically only offer an endpoint. Functional tests are confounded by rescue of native photoreceptors. Fundoscopy is essential, but the presence of pigmentation has various causes. OCT, FA, and AF all provide important diagnostic clues, but rejection can occur in the absence of post-operative changes and inflammation can be due to ophthalmic disease or surgery. Furthermore, with functional tests and imaging it is not

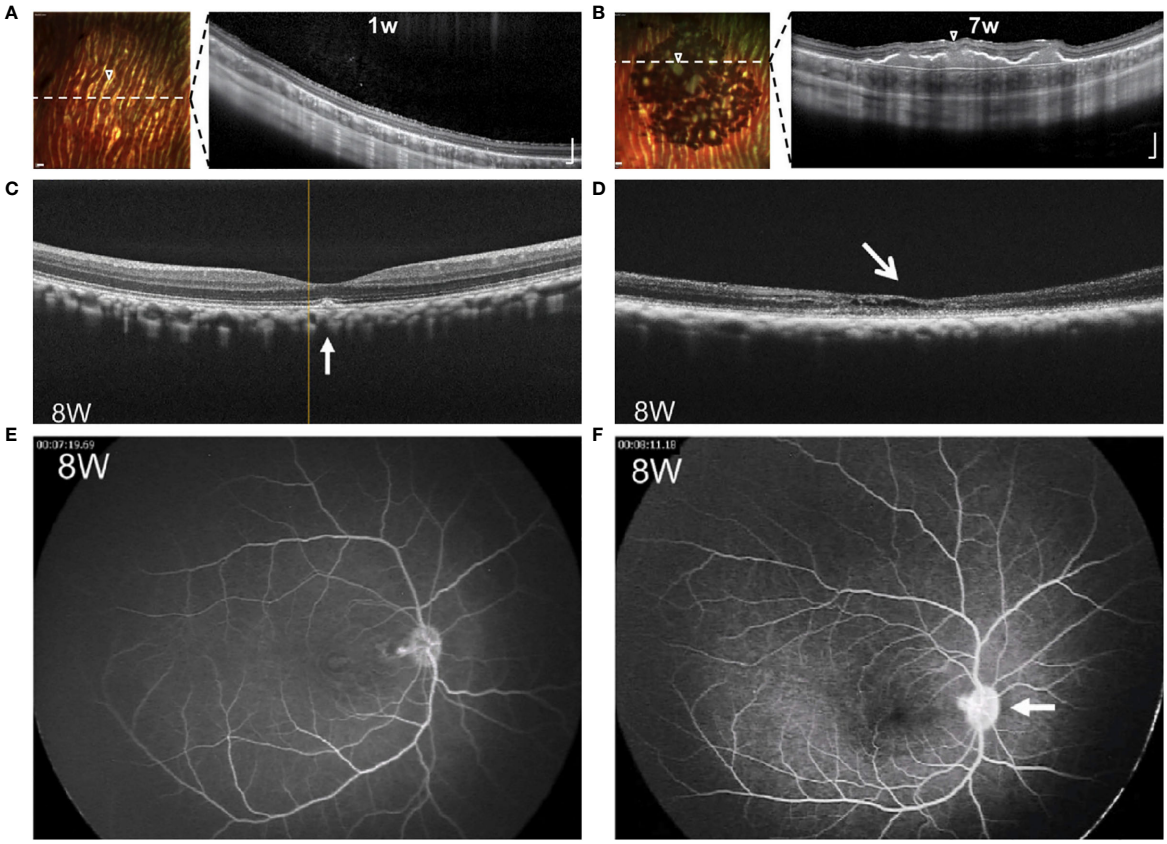

FIGURE 3 | Comparative images of RPE grafts with and without rejection. **(A, B)** Multicolor-confocal scanning laser ophthalmoscopy and corresponding OCT following subretinal injection of RPE cell suspension. Homogenous monolayer leads to clumping of pigment over 1-7 weeks. Dashed line indicates plane of corresponding OCT, where subretinal mass is seen along with choroidal thickening under the graft site. Modified from Petrus-Reurer 2020 (35). **(C, D)** OCT eight weeks following transplant of RPE suspension. Compared to non-rejected transplant **(C)**, retina with rejected graft **(D)** shows atrophy of the neuroretina with intraretinal and subretinal fluid. **(E, F)** FA eight weeks following transplant of RPE suspension. Compared to non-rejected transplant **(E)**, retina with the rejected transplant **(F)** shows leakage of the optic disc. Modified from Sugita 2016 (33).

TABLE 1 | Comparison of visual signs of rejected versus non-rejected transplanted RPE.

	Rejection	No Rejection
Fundoscopy	Clumping of pigment Optic nerve head hyperemia	Expanding, flat, pigmented layer
OCT	Inflammation: CME, choroidal thickening, vitreous haze Subretinal deposits Neuroretina atrophy Disintegration or clumping of transplant material	Hyperreflective monolayer Healthy neuroretina morphology: -Intact external limiting membrane -Outer nuclear layer > 20 um
FA	Optic nerve head leakage Leakage around graft	Absence of leakage around graft or optic nerve head
AF	Uneven autofluorescence Loss of autofluorescence over time	Double thickness of autofluorescence (transplanted over host RPE)

possible to differentiate immunologic rejection from cellular degeneration due to non-immunologic mechanisms. Serologic analysis of DSA, PBMCs, and GFP may offer objective evidence of rejection or survival but are infrequently used. For the time being, we must closely follow the trends that may yield more conclusive evidence of transplant function and survival in the host retina.

SECTION IV: PREVENTING REJECTION OF RPE GRAFTS

The literature demonstrates three strategies to prevent immune rejection of RPE grafts: 1) immunodeficient host models, 2) pharmacologic immune modulation, and 3) reducing the immunogenicity of the graft. Each of these strategies has

particular applications. Immunodeficient hosts are ideal for demonstrating functional potential of transplants and tumorigenicity of stem cell transplants in the absence of immune rejection. Without additional immune modulation, xenogeneic ESC-derived RPE survived for at least 240 days in the NIH III mouse, deficient in T-, B-, and NK cells (95), while ESC- and iPSC-derived RPE grafts have survived up to 12 months in the athymic nude rat (66, 71, 101). No studies of RPE-grafts have been performed in immunodeficient large mammals such as non-human primates or pigs, possibly related to a deficiency of these models or poor translation to clinical medicine.

Except in the cases of autologous or MHC-matched grafts, every study that has demonstrated evidence of temporary survival of RPE transplants in immunocompetent hosts has applied pharmacologic immune modulation. With respect to xenogeneic studies, Del Priore 2003 demonstrated "triple systemic" therapy with prednisone, cyclosporine, and azathioprine (anti-inflammatory antibiotic) to increase the survival of grafted RPE at four weeks (20). Similar results were obtained when the host was exposed to local cyclosporine alone, as a weekly intravitreal injection or slow-release capsule (31). Graft survival was prolonged to 100 days when cyclosporine was administered from pre-op day two until day 100 along with dexamethasone for two weeks (94). However, grafts survived less than four weeks in a similar study with a higher concentration and duration of dexamethasone (102), which may suggest the greater role of systemic cyclosporine compared to systemic steroids in preventing rejection. Local administration of steroid demonstrated a benefit with intravitreal triamcinolone administered at the end of the surgery and improved survival after four weeks compared to hosts that received daily intramuscular dexamethasone (102). This effect was repeated by a subsequent study, with the additional finding that intravitreal tacrolimus improved the morphology of RPE on OCT (34). Typically used as antibiotics, doxycycline and minocycline have been used for suppression of microglia of the innate immune system (61, 103) and were associated with 70% survival of grafted RPE after 10 weeks when administered with prednisone, tacrolimus, and sirolimus. Given coadministration with steroid and T-cell inhibitors, it is not possible to determine their specific effects from these studies.

Regarding allogeneic transplants, preclinical trials were performed with iPSC-RPE in pigs and macaques: the former with no immune modulation and the latter with subconjunctival and topical dexamethasone. Both investigations demonstrated histologic evidence of robust rejection in the period between postoperative day four and three weeks, reinforcing the need for appropriate immunomodulatory regimen in allogeneic iPSC trials (15, 32). The best evidence regarding local steroids comes from Sugita 2017, where a regimen of intravitreal triamcinolone at the time of surgery and sub-tenon triamcinolone at four weeks post-op prevented development of DSA, reactive PBMCs, and inflammatory infiltrate at six months compared to a control monkey without immunomodulation. In fact, these results were similar to an MHC-matched subject (17).

The remainder of allogeneic trials in the literature pertain to humans and subsequently lack histologic confirmation of rejection or compatibility. Four clinical trials administered tacrolimus with or without mycophenolate mofetil (MMF), an antimetabolite with favorable side effect profile (21, 72, 90, 93). Dosing of both tacrolimus and MMF started one week prior to surgery and continued for up to 13 weeks before withdrawal; however, MMF takes several months to become fully effective, so this may represent underutilization of the effect of this drug. A fourth clinical trial used perioperative prednisone with an intraocular steroid implant (73). If proven to prevent rejection in further studies, this could be an option for geriatric patients in whom systemic immune modulation may increase risk of complicating infection. All of these clinical trials demonstrated evidence of survival of the transplant past the cessation of pharmacologic immunomodulation but lack histologic confirmation.

Reducing the immunogenicity of an RPE graft is a primary objective of both preclinical and clinical trials. In immunologic terms, the ideal graft is autologous, or composed of tissue from the host. iPSC technology is currently used to create autologous RPE grafts derived from adult cells for clinical trials in Japan and the US [(8, 9, 104) and ClinicalTrials.gov # NCT04339764]. When transplanted into a human host without immunomodulation, an autologous iPSC-RPE graft survived for over one year and was associated with preserved neuroretina structure (8, 9). Despite these apparent successes, there are many barriers to widespread clinical application of autologous iPSC lines. High genetic variability and instability increases the risk of immunogenicity and tumorigenic potential in iPSCs (10). Properly verifying a new iPSC cell line may require 12-15 months and approximately $800,000 (105, 106). Perhaps a more viable option in the future, autologous-iPSC lines are not currently available for the majority of researchers or patients.

In lieu of autologous transplants, many authors have proposed banking of high-quality iPSC-RPE lines that can be matched for allogeneic transplants to patients (10). Banks of 10, 55, 80, and 150 donor iPSCs could match over 40% of genotypes in Korea, 80% in Japan, 50% in California, and 93% in the UK, respectively (41, 107–110). As evidence for this approach, when MHC-matched macaque-iPSC-RPE was transplanted in the SRS of allogeneic hosts, grafts survived without immune suppressants for 6 months and were associated with no development of DSA, reactive PBMCs, or infiltration of inflammatory cells compared to MHC-mismatched controls (33). A potential alternative studied by Petrus-Reurer 2020 is MHC-II knock-out hESC-RPE, which delayed the infiltration of inflammatory cells and production of DSA compared to controls with wild-type hESC-RPE (35). Knockout of β2-microglobulin and MHC-I were also studied, and reduced activation of NK cells compared to controls (111, 112). Notably, expression of MHC-II by RPE is also reduced by culture under xeno-free conditions, emphasizing the use of these methods to decrease rejection as well as comply with clinical requirements (34, 35). Significantly, donor RPE cannot present antigen to human hosts; however, modifying donor cells to be less immunogenic is compatible with the design of iPSC-RPE cell banks to increase the number of patients who may match to a limited number of cell lines.

In addition to the cellular components of a graft, the immunogenicity of the transplant vehicle is an important

consideration. Biodegradable scaffolds offer the potential benefit of reducing a chronic foreign body reaction but have potential disadvantages as well. Poly(lactic-co-glycolic acid) (PLGA) degrades into components lactic and glycolic acid, which are potentially toxic, but did not produce signs of inflammation on OCT 5 weeks after delivery (66). Fibrin is biochemically inert, but the mechanically suitable fibrin scaffold is approximately 200 μm thick, raising concerns regarding the ability of nutrients and waste to diffuse to and from the choriocapillaris (113). Nonetheless, when implanted in the SRS of pigs, the overlying neuroretina appeared to be healthy when the scaffold degraded after eight weeks.

Non degradable scaffolds include parylene, polyester, and polyethylene terephthalate (PET). Parylene increased survival of RPE transplants relative to cells delivered as a suspension (72, 114). Implantation of an acellular polyester membrane into the SRS was associated with a foreign body reaction with chronic inflammatory infiltrate; however, the presence of RPE on the membrane reduced this response (73). Following implantation of a PET acellular membrane, microscopy demonstrated an additional cellular layer between the host RPE and the PET membrane, attributed to reactive migration of host RPE or infiltration of macrophages (34). Immunologic consequences of these delivery materials are likely to be relatively more significant as advancements are made in autologous or universal RPE cell banks.

DISCUSSION

For years limited to basic science research, stem cells therapy for patients with retinal disease is currently in clinical trials. However, while treatments are seemingly close at hand, the mere survival of grafts is still a controversial determination. To reach millions of patients with retinal degenerations and dystrophies, it is of vital importance to correctly interpret these initial trials. Afterall, transplanted cells have no chance of improving vision if they cannot survive the host's immune reaction.

Investigations in the immunology of solid organ transplants have much to teach us regarding the reaction to RPE grafts. The innate and acquired immune systems cooperate but reject foreign cells by different mechanisms. Studies of RPE transplants have primarily focused on rejection effected by lymphocytes and attempted to prevent this with T-cell inhibitors and steroids. Here we have presented a case based on chronology, histology, and physiology that rejection by microglia and macrophages of the innate immune system should be regarded with increased appreciation. Furthermore, preclinical studies have demonstrated specific interventions that alter the microglial phenotype and should be considered for future trials.

While immune privilege of the eye is not the holy grail it was once hoped to be, understanding the physiology suggests mechanisms to minimize immune recognition. Implantation distant from the retinotomy is most likely to enhance immune separation. Alterations to RPE such as increasing expression of TGFβ or reducing MHC-II will support the effector blockade. An ACAID-type mechanism may allow for priming of host with graft antigens similar to engraftment.

Without available histology, investigators may make educated guesses regarding the health of grafted cells through fundoscopy, OCT, FA, and AF. Expansion of a flat pigmented layer and a healthy appearing neuroretina are good signs, while inflammation, subretinal deposition of material, and disintegration of the transplant all indicate pending or past rejection. However, all of these findings are potentially confounded by physiologic reactions to surgical trauma and inflammation. Measures such as systemic DSA, PBMC reactivity, or GFP fluorescence offer objective and quantifiable evidence of rejection and should be utilized in future investigations.

There are a variety of strategies to prevent immune rejection of transplanted RPE. Immunodeficient hosts are a good option for preclinical research. Xenographic studies of RPE transplants have employed some combination of T-cell inhibitors with steroidal anti-inflammatories. There is evidence that systemic T-cell inhibitors may be more important than systemic steroids for prevention of rejection, but local steroids offer a clear benefit. Allogeneic studies have used systemic tacrolimus and MMF with apparent success as well as intraocular steroids. Studies in basic research suggest that promoting transition of M1 to M2 microglia has potential benefits to both the graft and overlying retina, but this strategy is untested at the level of translational research. For future transplants in clinical patients, matching of banked cells will reduce immunogenicity of the graft. It is likely that researchers and clinicians who employ a combination of these strategies, tailored to their specific graft and host, will have the greatest chance of avoiding immunologic rejection.

AUTHOR CONTRIBUTIONS

CP for reviewing the literature in the field and compiling the manuscript. AP for lending his expertise regarding the immune physiology of the retina and potential strategies for evading rejection. VC-S for contributing her expertise in the field of stem cell transplantation. All authors contributed to the article and approved the submitted version.

FUNDING

Gates Grubstake Award (GGF012-18-01), Gates Frontiers Fund, The Solich Fund, CellSight Development Fund, and an unrestricted Research Award from Research to Prevent Blindness to the Department of Ophthalmology, University of Colorado.

ACKNOWLEDGMENTS

Researchers at the *CellSight* laboratory at the University of Colorado for their expertise in this field and assistance to these authors.

REFERENCES

1. Sparrow JR, Hicks D, Hamel CP. The Retinal Pigment Epithelium in Health and Disease. *Curr Mol Med* (2010) 10:802–23. doi: 10.2174/156652410793937813
2. Bird A. Role of Retinal Pigment Epithelium in Age-Related Macular Disease: A Systematic Review. *Br J Ophthalmol* (2020) 1–6. doi: 10.1136/bjophthalmol-2020-317447
3. Georgiou M, Fujinami K, Michaelides M. Inherited Retinal Diseases: Therapeutics, Clinical Trials and End Points-a Review. *Clin Exp Ophthalmol* (2021) 49:270–88. doi: 10.1111/ceo.13917
4. Strauss O. The Retinal Pigment Epithelium in Visual Function. *Physiol Rev* (2005) 85:845–81. doi: 10.1152/physrev.00021.2004
5. Gouras P, Flood MT, Kjedbye H, Bilek MK, Eggers H. Transplantation of Cultured Human Retinal Epithelium to Bruch's Membrane of the Owl Monkey's Eye. *Curr Eye Res* (1985) 4:253–65. doi: 10.3109/02713688509000857
6. Canto-Soler V, Flores-Bellver M, Vergara MN. Stem Cell Sources and Their Potential for the Treatment of Retinal Degenerations. *Invest Ophthalmol Vis Sci 57* (2016) 57:ORSFd1–9. doi: 10.1167/iovs.16-19127
7. Salero E, Blenkinsop TA, Corneo B, Harris A, Rabin D, Stern JH, et al. Adult Human RPE can be Activated Into a Multipotent Stem Cell That Produces Mesenchymal Derivatives. *Cell Stem Cell* (2012) 10:88–95. doi: 10.1016/j.stem.2011.11.018
8. Mandai M, Kurimoto Y, Takahashi M. Autologous Induced Stem-Cell-Derived Retinal Cells for Macular Degeneration. *N Engl J Med* (2017) 377:792–3. doi: 10.1056/NEJMc1706274
9. Takagi S, Mandai M, Gocho K, Hirami Y, Yamamoto M, Fujihara M, et al. Evaluation of Transplanted Autologous Induced Pluripotent Stem Cell-Derived Retinal Pigment Epithelium in Exudative Age-Related Macular Degeneration. *Ophthalmol Retina* (2019) 3:850–9. doi: 10.1016/j.oret.2019.04.021
10. Huang CY, Liu CL, Ting CY, Chiu YT, Cheng YC, Nicholson MW, et al. Human iPSC Banking: Barriers and Opportunities. *J BioMed Sci* (2019) 26:87. doi: 10.1186/s12929-019-0578-x
11. Khalpey Z, Koch CA, Platt JL. Xenograft Transplantation. *Anesthesiol Clin North Am* (2004) 22:871–85. doi: 10.1016/j.atc.2004.05.005
12. Zhou R, Caspi RR. Ocular Immune Privilege. *F1000 Biol Rep 2* (2010) 2:1–3. doi: 10.3410/B2-3
13. Drukker M, Katchman H, Katz G, Even-Tov Friedman S, Shezen E, Hornstein E, et al. Human Embryonic Stem Cells and Their Differentiated Derivatives are Less Susceptible to Immune Rejection Than Adult Cells. *Stem Cells* (2006) 24:221–9. doi: 10.1634/stemcells.2005-0188
14. Li L, Baroja ML, Majumdar A, Chadwick K, Rouleau A, Gallacher L, et al. Human Embryonic Stem Cells Possess Immune-Privileged Properties. *Stem Cells* (2004) 22:448–56. doi: 10.1634/stemcells.22-4-448
15. McGill TJ, Stoddard J, Renner LM, Messaoudi I, Bharti K, Mitalipov S, et al. Allogeneic Ipsc-Derived RPE Cell Graft Failure Following Transplantation Into the Subretinal Space in Nonhuman Primates. *Invest Ophthalmol Vis Sci* (2018) 59:1374–83. doi: 10.1167/iovs.17-22467
16. Kennelly KP, Holmes TM, Wallace DM, O'Farrelly C, Keegan DJ. Early Subretinal Allograft Rejection is Characterized by Innate Immune Activity. *Cell Transplant* (2017) 26:983–1000. doi: 10.3727/096368917X694697
17. Sugita S, Makabe K, Fujii S, Iwasaki Y, Kamao H, Shiina T, et al. Detection of Retinal Pigment Epithelium-Specific Antibody in Ipsc-Derived Retinal Pigment Epithelium Transplantation Models. *Stem Cell Rep* (2017) 9:1501–15. doi: 10.1016/j.stemcr.2017.10.003
18. Cozzi E, Colpo A, De Silvestro G. The Mechanisms of Rejection in Solid Organ Transplantation. *Transfus Apher Sci* (2017) 56:498–505. doi: 10.1016/j.transci.2017.07.005
19. Grisanti S, Szurman P, Jordan J, Kociok N, Bartz-Schmidt KU, Heimann K. Xenotransplantation of Retinal Pigment Epithelial Cells Into RCS Rats. *Jpn J Ophthalmol* (2002) 46:36–44. doi: 10.1016/S0021-5155(01)00464-6
20. Del Priore LV, Ishida O, Johnson EW, Sheng Y, Jacoby DB, Geng L, et al. Triple Immune Suppression Increases Short-Term Survival of Porcine Fetal Retinal Pigment Epithelium Xenografts. *Invest Ophthalmol Vis Sci* (2003) 44:4044–53. doi: 10.1167/iovs.02-1175
21. Schwartz SD, Tan G, Hosseini H, Nagiel A. Subretinal Transplantation of Embryonic Stem Cell-Derived Retinal Pigment Epithelium for the Treatment of Macular Degeneration: An Assessment At 4 Years. *Invest Ophthalmol Vis Sci 57* (2016) 57:ORSFc1–9. doi: 10.1167/iovs.15-18681
22. Gosset C, Lefaucheur C, Glotz D. New Insights in Antibody-Mediated Rejection. *Curr Opin Nephrol Hypertens* (2014) 23:597–604. doi: 10.1097/MNH.0000000000000069
23. Takeuchi O, Akira S. Pattern Recognition Receptors and Inflammation. *Cell* (2010) 140:805–20. doi: 10.1016/j.cell.2010.01.022
24. Hall BM, Dorsch S, Roser B. The Cellular Basis of Allograft Rejection In Vivo. I. The Cellular Requirements for First-Set Rejection of Heart Grafts. *J Exp Med* (1978) 148:878–89. doi: 10.1084/jem.148.4.878
25. Bradley JA, Sarawar SR, Porteous C, Wood PJ, Card S, Ager A, et al. Allograft Rejection in CD4+ T Cell-Reconstituted Athymic Nude Rats–the Nonessential Role of Host-Derived CD8+ Cells. *Transplantation* (1992) 53:477–82. doi: 10.1097/00007890-199202010-00040
26. Ordikhani F, Pothula V, Sanchez-Tarjuelo R, Jordan S, Ochando J. Macrophages in Organ Transplantation. *Front Immunol* (2020) 11:582939. doi: 10.3389/fimmu.2020.582939
27. Halloran PF. Immunosuppressive Drugs for Kidney Transplantation. *N Engl J Med* (2004) 351:2715–29. doi: 10.1056/NEJMra033540
28. Mathian A, Jouenne R, Chader D, Cohen-Aubart F, Haroche J, Fadlallah J, et al. Regulatory T Cell Responses to High-Dose Methylprednisolone in Active Systemic Lupus Erythematosus. *PloS One* (2015) 10:e0143689. doi: 10.1371/journal.pone.0143689
29. Paliogianni F, Ahuja SS, Balow JP, Balow JE, Boumpas DT. Novel Mechanism for Inhibition of Human T Cells by Glucocorticoids. Glucocorticoids Inhibit Signal Transduction Through IL-2 Receptor. *J Immunol* (1993) 151:4081–9.
30. Lanza L, Scudeletti M, Puppo F, Bosco O, Peirano L, Filaci G, et al. Prednisone Increases Apoptosis in In Vitro Activated Human Peripheral Blood T Lymphocytes. *Clin Exp Immunol* (1996) 103:482–90. doi: 10.1111/j.1365-2249.1996.tb08306.x
31. Lai CC, Gouras P, Doi K, Tsang SH, Goff SP, Ashton P. Local Immunosuppression Prolongs Survival of RPE Xenografts Labeled by Retroviral Gene Transfer. *Invest Ophthalmol Vis Sci* (2000) 41:3134–41.
32. Sohn EH, Jiao C, Kaalberg E, Cranston C, Mullins RF, Stone EM, et al. Allogenic Ipsc-Derived RPE Cell Transplants Induce Immune Response in Pigs: A Pilot Study. *Sci Rep* (2015) 5:11791. doi: 10.1038/srep11791
33. Sugita S, Iwasaki Y, Makabe K, Kamao H, Mandai M, Shiina T, et al. Successful Transplantation of Retinal Pigment Epithelial Cells From MHC Homozygote iPSCs in MHC-Matched Models. *Stem Cell Rep* (2016) 7:635–48. doi: 10.1016/j.stemcr.2016.08.010
34. Ilmarinen T, Thieltges F, Hongisto H, Juuti-Uusitalo K, Koistinen A, Kaarniranta K, et al. Survival and Functionality of Xeno-Free Human Embryonic Stem Cell-Derived Retinal Pigment Epithelial Cells on Polyester Substrate After Transplantation in Rabbits. *Acta Ophthalmol* (2019) 97:e688–99. doi: 10.1111/aos.14004
35. Petrus-Reurer S, Winblad N, Kumar P, Gorchs L, Chrobok M, Wagner AK, et al. Generation of Retinal Pigment Epithelial Cells Derived From Human Embryonic Stem Cells Lacking Human Leukocyte Antigen Class I and II. *Stem Cell Rep* (2020) 14:648–62. doi: 10.1016/j.stemcr.2020.02.006
36. Poulter LW, Bradley NJ, Turk JL. The Role of Macrophages in Skin Allograft Rejection. I. Histochemical Studies During First-Set Rejection. *Transplantation* (1971) 12:40–4. doi: 10.1097/00007890-197107000-00006
37. Tinckam KJ, Djurdjev O, Magil AB. Glomerular Monocytes Predict Worse Outcomes After Acute Renal Allograft Rejection Independent of C4d Status. *Kidney Int* (2005) 68:1866–74. doi: 10.1111/j.1523-1755.2005.00606.x
38. Hoshinaga K, Mohanakumar T, Goldman MH, Wolfgang TC, Szentpetery S, Lee HM, et al. Clinical Significance of in Situ Detection of T Lymphocyte Subsets and Monocyte/Macrophage Lineages in Heart Allografts. *Transplantation* (1984) 38:634–7. doi: 10.1097/00007890-198412000-00017
39. Ma FY, Woodman N, Mulley WR, Kanellis J, Nikolic-Paterson DJ. Macrophages Contribute to Cellular But Not Humoral Mechanisms of Acute Rejection in Rat Renal Allografts. *Transplantation* (2013) 96:949–57. doi: 10.1097/TP.0b013e3182a4befa
40. Pallett LJ, Burton AR, Amin OE, Rodriguez-Tajes S, Patel AA, Zakeri N, et al. Longevity and Replenishment of Human Liver-Resident Memory T Cells and Mononuclear Phagocytes. *J Exp Med* (2020) 217:1–11. doi: 10.1084/jem.20200050

41. Kramer J, Chirco KR, Lamba DA. Immunological Considerations for Retinal Stem Cell Therapy. *Adv Exp Med Biol* (2019) 1186:99–119. doi: 10.1007/978-3-030-28471-8_4
42. Yu C, Roubeix C, Sennlaub F, Saban DR. Microglia Versus Monocytes: Distinct Roles in Degenerative Diseases of the Retina. *Trends Neurosci* (2020) 43:433–49. doi: 10.1016/j.tins.2020.03.012
43. Sakami S, Maeda T, Bereta G, Okano K, Golczak M, Sumaroka A, et al. Probing Mechanisms of Photoreceptor Degeneration in a New Mouse Model of the Common Form of Autosomal Dominant Retinitis Pigmentosa Due to P23H Opsin Mutations. *J Biol Chem* (2011) 286:10551–67. doi: 10.1074/jbc.M110.209759
44. Noell WK, Walker VS, Kang BS, Berman S. Retinal Damage by Light in Rats. *Invest Ophthalmol* (1966) 5:450–73.
45. Sugita S, Mandai M, Kamao H, Takahashi M. Immunological Aspects of RPE Cell Transplantation. *Prog Retin Eye Res* (2021), 100950. doi: 10.1016/j.preteyeres.2021.100950
46. Conde P, Rodriguez M, van der Touw W, Jimenez A, Burns M, Miller J, et al. Dc-Sign(+) Macrophages Control the Induction of Transplantation Tolerance. . *Immun* (2015) 42:1143–58. doi: 10.1016/j.immuni.2015.05.009
47. Nakagawa Y, Chiba K. Diversity and Plasticity of Microglial Cells in Psychiatric and Neurological Disorders. *Pharmacol Ther* (2015) 154:21–35. doi: 10.1016/j.pharmthera.2015.06.010
48. Karlstetter M, Scholz R, Rutar M, Wong WT, Provis JM, Langmann T. Retinal Microglia: Just Bystander or Target for Therapy? *Prog Retin Eye Res* (2015) 45:30–57. doi: 10.1016/j.preteyeres.2014.11.004
49. Cuenca N, Fernandez-Sanchez L, Campello L, Maneu V, De la Villa P, Lax P, et al. Cellular Responses Following Retinal Injuries and Therapeutic Approaches for Neurodegenerative Diseases. *Prog Retin Eye Res* (2014) 43:17–75. doi: 10.1016/j.preteyeres.2014.07.001
50. Gordon S, Martinez FO. Alternative Activation of Macrophages: Mechanism and Functions. *Immunity* (2010) 32:593–604. doi: 10.1016/j.immuni.2010.05.007
51. Martinez FO, Helming L, Gordon S. Alternative Activation of Macrophages: An Immunologic Functional Perspective. *Annu Rev Immunol* (2009) 27:451–83. doi: 10.1146/annurev.immunol.021908.132532
52. Martinez FO, Gordon S. The M1 and M2 Paradigm of Macrophage Activation: Time for Reassessment. *F1000Prime Rep* (2014) 6:13. doi: 10.12703/P6-13
53. Sennlaub F, Auvynet C, Calippe B, Lavalette S, Poupel L, Hu SJ, et al. CCR2 (+) Monocytes Infiltrate Atrophic Lesions in Age-Related Macular Disease and Mediate Photoreceptor Degeneration in Experimental Subretinal Inflammation in Cx3cr1 Deficient Mice. *EMBO Mol Med* (2013) 5:1775–93. doi: 10.1002/emmm.201302692
54. Yin Y, Henzl MT, Lorber B, Nakazawa T, Thomas TT, Jiang F, et al. Oncomodulin is a Macrophage-Derived Signal for Axon Regeneration in Retinal Ganglion Cells. *Nat Neurosci* (2006) 9:843–52. doi: 10.1038/nn1701
55. Suh HS, Zhao ML, Derico L, Choi N, Lee SC. Insulin-Like Growth Factor 1 and 2 (IGF1, IGF2) Expression in Human Microglia: Differential Regulation by Inflammatory Mediators. *J Neuroinflamm* (2013) 10:37. doi: 10.1186/1742-2094-10-37
56. Garcia MR, Ledgerwood L, Yang Y, Xu J, Lal G, Burrell B, et al. Monocytic Suppressive Cells Mediate Cardiovascular Transplantation Tolerance in Mice. *J Clin Invest* (2010) 120:2486–96. doi: 10.1172/JCI41628
57. Neves J, Zhu J, Sousa-Victor P, Konjikusic M, Riley R, Chew S, et al. Immune Modulation by MANF Promotes Tissue Repair and Regenerative Success in the Retina. *Science* (2016) 353:aaf3646. doi: 10.1126/science.aaf3646
58. Calabrese F, Rossetti AC, Racagni G, Gass P, Riva MA, Molteni R. Brain-Derived Neurotrophic Factor: A Bridge Between Inflammation and Neuroplasticity. *Front Cell Neurosci* (2014) 8:430. doi: 10.3389/fncel.2014.00430
59. Prencipe G, Minnone G, Strippoli R, De Pasquale L, Petrini S, Caiello I, et al. Nerve Growth Factor Downregulates Inflammatory Response in Human Monocytes Through Trka. *J Immunol* (2014) 192:3345–54. doi: 10.4049/jimmunol.1300825
60. Yoon SY, Patel D, Dougherty PM. Minocycline Blocks Lipopolysaccharide Induced Hyperalgesia by Suppression of Microglia But Not Astrocytes. *Neuroscience* (2012) 221:214–24. doi: 10.1016/j.neuroscience.2012.06.024
61. Scholz R, Sobotka M, Caramoy A, Stempfl T, Moehle C, Langmann T. Minocycline Counter-Regulates Pro-Inflammatory Microglia Responses in the Retina and Protects From Degeneration. *J Neuroinflamm* (2015) 12:209. doi: 10.1186/s12974-015-0431-4
62. Scholz R, Caramoy A, Bhuckory MB, Rashid K, Chen M, Xu H, et al. Targeting Translocator Protein (18 kDa) (TSPO) Dampens Pro-Inflammatory Microglia Reactivity in the Retina and Protects From Degeneration. *J Neuroinflamm* (2015) 12:201. doi: 10.1186/s12974-015-0422-5
63. Jackson AC, Roche SL, Byrne AM, Ruiz-Lopez AM, Cotter TG. Progesterone Receptor Signalling in Retinal Photoreceptor Neuroprotection. *J Neurochem* (2016) 136:63–77. doi: 10.1111/jnc.13388
64. Roche SL, Wyse-Jackson AC, Gomez-Vicente V, Lax P, Ruiz-Lopez AM, Byrne AM, et al. Progesterone Attenuates Microglial-Driven Retinal Degeneration and Stimulates Protective Fractalkine-CX3CR1 Signaling. *PloS One* (2016) 11:e0165197. doi: 10.1371/journal.pone.0165197
65. Luckoff A, Caramoy A, Scholz R, Prinz M, Kalinke U, Langmann T. Interferon-Beta Signaling in Retinal Mononuclear Phagocytes Attenuates Pathological Neovascularization. *EMBO Mol Med* (2016) 8:670–8. doi: 10.15252/emmm.201505994
66. Sharma R, Khristov V, Rising A, Jha BS, Dejene R, Hotaling N, et al. Clinical-Grade Stem Cell-Derived Retinal Pigment Epithelium Patch Rescues Retinal Degeneration in Rodents and Pigs. *Sci Transl Med* (2019) 11:304–15. doi: 10.1126/scitranslmed.aat5580
67. Fauci AS, Dale DC, Balow JE. Glucocorticosteroid Therapy: Mechanisms of Action and Clinical Considerations. *Ann Intern Med* (1976) 84:304–15. doi: 10.7326/0003-4819-84-3-304
68. Boumpas DT, Chrousos GP, Wilder RL, Cupps TR, Balow JE. Glucocorticoid Therapy for Immune-Mediated Diseases: Basic and Clinical Correlates. *Ann Intern Med* (1993) 119:1198–208. doi: 10.7326/0003-4819-119-12-199312150-00007
69. Rinehart JJ, Sagone AL, Balcerzak SP, Ackerman GA, LoBuglio AF. Effects of Corticosteroid Therapy on Human Monocyte Function. *N Engl J Med* (1975) 292:236–41. doi: 10.1056/NEJM197501302920504
70. Moassesfar S, Masharani U, Frassetto LA, Szot GL, Tavakol M, Stock PG, et al. A Comparative Analysis of the Safety, Efficacy, and Cost of Islet Versus Pancreas Transplantation in Nonuremic Patients With Type 1 Diabetes. *Am J Transplant* (2016) 16:518–26. doi: 10.1111/ajt.13536
71. Diniz B, Thomas P, Thomas B, Ribeiro R, Hu Y, Brant R, et al. Subretinal Implantation of Retinal Pigment Epithelial Cells Derived From Human Embryonic Stem Cells: Improved Survival When Implanted as a Monolayer. *Invest Ophthalmol Vis Sci* (2013) 54:5087–96. doi: 10.1167/iovs.12-11239
72. Kashani AH, Lebkowski JS, Rahhal FM, Avery RL, Salehi-Had H, Dang W, et al. A Bioengineered Retinal Pigment Epithelial Monolayer for Advanced, Dry Age-Related Macular Degeneration. *Sci Transl Med* (2018) 10:328–37. doi: 10.1126/scitranslmed.aao4097
73. da Cruz L, Fynes K, Georgiadis O, Kerby J, Luo YH, Ahmado A, et al. Phase 1 Clinical Study of an Embryonic Stem Cell-Derived Retinal Pigment Epithelium Patch in Age-Related Macular Degeneration. *Nat Biotechnol* (2018) 36:328–37. doi: 10.1038/nbt.4114
74. Falkner-Radler CI, Krebs I, Glittenberg C, Povazay B, Drexler W, Graf A, et al. Human Retinal Pigment Epithelium (RPE) Transplantation: Outcome After Autologous RPE-choroid Sheet and RPE Cell-Suspension in a Randomised Clinical Study. *Br J Ophthalmol* (2011) 95:370–5. doi: 10.1136/bjo.2009.176305
75. Elahimehr R, Scheinok AT, McKay DB. Hematopoietic Stem Cells and Solid Organ Transplantation. *Transplant Rev (Orlando)* (2016) 30:227–34. doi: 10.1016/j.trre.2016.07.005
76. Caspi RR. Ocular Autoimmunity: The Price of Privilege? *Immunol Rev* (2006) 213:23–35. doi: 10.1111/j.1600-065X.2006.00439.x
77. Williams KA, Coster DJ. The Immunobiology of Corneal Transplantation. *Transplantation* (2007) 84:806–13. doi: 10.1097/01.tp.0000285489.91595.13
78. de Nie KF, Crama N, Tilanus MA, Klevering BJ, Boon CJ. Pars Plana Vitrectomy for Disturbing Primary Vitreous Floaters: Clinical Outcome and Patient Satisfaction. *Graefes Arch Clin Exp Ophthalmol* (2013) 251:1373–82. doi: 10.1007/s00417-012-2205-3
79. Mylonas G, Sacu S, Deak G, Dunavoelgyi R, Buehl W, Georgopoulos M, et al. Macular Edema Following Cataract Surgery in Eyes With Previous 23-Gauge Vitrectomy and Peeling of the Internal Limiting Membrane. *Am J Ophthalmol* (2013) 155:253–259 e2. doi: 10.1016/j.ajo.2012.07.013
80. Detrick B, Hooks JJ. Immune Regulation in the Retina. *Immunol Res* (2010) 47:153–61. doi: 10.1007/s12026-009-8146-1

81. Sugita S. Role of Ocular Pigment Epithelial Cells in Immune Privilege. *Arch Immunol Ther Exp (Warsz)* (2009) 57:263–8. doi: 10.1007/s00005-009-0030-0
82. Granstein RD, Staszewski R, Knisely TL, Zeira E, Nazareno R, Latina M, et al. Aqueous Humor Contains Transforming Growth Factor-Beta and a Small (Less Than 3500 Daltons) Inhibitor of Thymocyte Proliferation. *J Immunol* (1990) 144:3021–7. doi: 10.4049/jimmunol.0900622
83. Gurfein BT, Zhang Y, Lopez CB, Argaw AT, Zameer A, Moran TM, et al. Il-11 Regulates Autoimmune Demyelination. *J Immunol* (2009) 183:4229–40. doi: 10.4049/jimmunol.0900622
84. Ferguson TA, Griffith TS. A Vision of Cell Death: Fas Ligand and Immune Privilege 10 Years Later. *Immunol Rev* (2006) 213:228–38. doi: 10.1111/j.1600-065X.2006.00430.x
85. Liversidge JM, Sewell HF, Forrester JV. Human Retinal Pigment Epithelial Cells Differentially Express MHC Class II (Hla, DP, DR and DQ) Antigens in Response to In Vitro Stimulation With Lymphokine or Purified IFN-Gamma. *Clin Exp Immunol* (1988) 73:489–94.
86. Kaplan HJ, Stevens TR. A Reconsideration of Immunological Privilege Within the Anterior Chamber of the Eye. *Transplantation* (1975) 19:203–9. doi: 10.1097/00007890-197504000-00005
87. Lin HH, Faunce DE, Stacey M, Terajewicz A, Nakamura T, Zhang-Hoover J, et al. The Macrophage F4/80 Receptor is Required for the Induction of Antigen-Specific Efferent Regulatory T Cells in Peripheral Tolerance. *J Exp Med* (2005) 201:1615–25. doi: 10.1084/jem.20042307
88. Silverman MS, Hughes SE. Photoreceptor Rescue in the RCS Rat Without Pigment Epithelium Transplantation. *Curr Eye Res* (1990) 9:183–91. doi: 10.3109/02713689008995205
89. Leschey KH, Hackett SF, Singer JH, Campochiaro PA. Growth Factor Responsiveness of Human Retinal Pigment Epithelial Cells. *Invest Ophthalmol Vis Sci* (1990) 31:839–46. doi: 10.1016/j.ophtha.2018.04.037
90. Mehat MS, Sundaram V, Ripamonti C, Robson AG, Smith AJ, Borooah S, et al. Transplantation of Human Embryonic Stem Cell-Derived Retinal Pigment Epithelial Cells in Macular Degeneration. *Ophthalmology* (2018) 125:1765–75. doi: 10.1016/j.ophtha.2018.04.037
91. Schwartz SD, Regillo CD, Lam BL, Eliott D, Rosenfeld PJ, Gregori NZ, et al. Human Embryonic Stem Cell-Derived Retinal Pigment Epithelium in Patients With Age-Related Macular Degeneration and Stargardt's Macular Dystrophy: Follow-Up of Two Open-Label Phase 1/2 Studies. *Lancet* (2015) 385:509–16. doi: 10.1016/S0140-6736(14)61376-3
92. Anderson DH, Stern WH, Fisher SK, Erickson PA, Borgula GA. The Onset of Pigment Epithelial Proliferation After Retinal Detachment. *Invest Ophthalmol Vis Sci* (1981) 21:10–6. doi: 10.1016/j.stemcr.2015.04.005
93. Song WK, Park KM, Kim HJ, Lee JH, Choi J, Chong SY, et al. Treatment of Macular Degeneration Using Embryonic Stem Cell-Derived Retinal Pigment Epithelium: Preliminary Results in Asian Patients. *Stem Cell Rep* (2015) 4:860–72. doi: 10.1016/j.stemcr.2015.04.005
94. Lund RD, Wang S, Klimanskaya I, Holmes T, Ramos-Kelsey R, Lu B, et al. Human Embryonic Stem Cell-Derived Cells Rescue Visual Function in Dystrophic RCS Rats. *Cloning Stem Cells* (2006) 8:189–99. doi: 10.1089/clo.2006.8.189
95. Lu B, Malcuit C, Wang S, Girman S, Francis P, Lemieux L, et al. Long-Term Safety and Function of RPE From Human Embryonic Stem Cells in Preclinical Models of Macular Degeneration. *Stem Cells* (2009) 27:2126–35. doi: 10.1002/stem.149
96. Ansari AM, Ahmed AK, Matsangos AE, Lay F, Born LJ, Marti G, et al. Cellular GFP Toxicity and Immunogenicity: Potential Confounders in in Vivo Cell Tracking Experiments. *Stem Cell Rev Rep* (2016) 12:553–9. doi: 10.1007/s12015-016-9670-8
97. Yang CW. Importance and What to Watch Out for De Novo Donor Specific Anti-HLA Antibodies After Kidney Transplantation. *J Korean Med Sci* (2018) 33:e228. doi: 10.3346/jkms.2018.33.e228
98. Platt JL, Cascalho M. Donor Specific Antibodies After Transplantation. *Pediatr Transplant* (2011) 15:686–90. doi: 10.1111/j.1399-3046.2010.01436.x
99. Su JA, Baxter-Lowe LA, Kantor PF, Szmuszkovicz JR, Menteer J. The Clinical Impact of Donor-Specific Antibodies on Antibody-Mediated Rejection and Long-Term Prognosis After Heart Transplantation. *Curr Opin Organ Transplant* (2019) 24:245–51. doi: 10.1097/MOT.0000000000000636
100. Knight SR, Thorne A, Lo Faro ML. Donor-Specific Cell-free DNA as a Biomarker in Solid Organ Transplantation. A Systematic Review. *Transplantation* (2019) 103:273–83. doi: 10.1097/TP.0000000000002482
101. Ben M'Barek K, Habeler W, Plancheron A, Jarraya M, Regent F, Terray A, et al. Human ESC-derived Retinal Epithelial Cell Sheets Potentiate Rescue of Photoreceptor Cell Loss in Rats With Retinal Degeneration. *Sci Transl Med* (2017) 9:64–77. doi: 10.1126/scitranslmed.aai7471
102. Stanzel BV, Liu Z, Somboonthanakij S, Wongsawad W, Brinken R, Eter N, et al. Human RPE Stem Cells Grown Into Polarized RPE Monolayers on a Polyester Matrix are Maintained After Grafting Into Rabbit Subretinal Space. *Stem Cell Rep* (2014) 2:64–77. doi: 10.1016/j.stemcr.2013.11.005
103. Santa-Cecilia FV, Socias B, Ouidja MO, Sepulveda-Diaz JE, Acuna L, Silva RL, et al. Doxycycline Suppresses Microglial Activation by Inhibiting the P38 MAPK and NF-kB Signaling Pathways. *Neurotox Res* (2016) 29:447–59. doi: 10.1007/s12640-015-9592-2
104. Kamao H, Mandai M, Okamoto S, Sakai N, Suga A, Sugita S, et al. Characterization of Human Induced Pluripotent Stem Cell-Derived Retinal Pigment Epithelium Cell Sheets Aiming for Clinical Application. *Stem Cell Rep* (2014) 2:205–18. doi: 10.1016/j.stemcr.2013.12.007
105. Jacquet L, Stephenson E, Collins R, Patel H, Trussler J, Al-Bedaery R, et al. Strategy for the Creation of Clinical Grade hESC Line Banks That HLA-match a Target Population. *EMBO Mol Med* (2013) 5:10–7. doi: 10.1002/emmm.201201973
106. Bravery CA. Do Human Leukocyte Antigen-Typed Cellular Therapeutics Based on Induced Pluripotent Stem Cells Make Commercial Sense? *Stem Cells Dev* (2015) 24:1–10. doi: 10.1089/scd.2014.0136
107. Turner M, Leslie S, Martin NG, Peschanski M, Rao M, Taylor CJ, et al. Toward the Development of a Global Induced Pluripotent Stem Cell Library. *Cell Stem Cell* (2013) 13:382–4. doi: 10.1016/j.stem.2013.08.003
108. Nakajima F, Tokunaga K, Nakatsuji N. Human Leukocyte Antigen Matching Estimations in a Hypothetical Bank of Human Embryonic Stem Cell Lines in the Japanese Population for Use in Cell Transplantation Therapy. *Stem Cells* (2007) 25:983–5. doi: 10.1634/stemcells.2006-0566
109. Pappas DJ, Gourraud PA, Le Gall C, Laurent J, Trounson A, DeWitt N, et al. Proceedings: Human Leukocyte Antigen Haplo-Homozygous Induced Pluripotent Stem Cell Haplobank Modeled After the California Population: Evaluating Matching in a Multiethnic and Admixed Population. *Stem Cells Transl Med* (2015) 4:413–8. doi: 10.5966/sctm.2015-0052
110. Lee S, Huh JY, Turner DM, Lee S, Robinson J, Stein JE, et al. Repurposing the Cord Blood Bank for Haplobanking of HLA-Homozygous iPSCs and Their Usefulness to Multiple Populations. *Stem Cells* (2018) 36:1552–66. doi: 10.1002/stem.2865
111. Riolobos L, Hirata RK, Turtle CJ, Wang PR, Gornalusse GG, Zavajlevski M, et al. HLA Engineering of Human Pluripotent Stem Cells. *Mol Ther* (2013) 21:1232–41. doi: 10.1038/mt.2013.59
112. Gornalusse GG, Hirata RK, Funk SE, Riolobos L, Lopes VS, Manske G, et al. Hla-E-expressing Pluripotent Stem Cells Escape Allogeneic Responses and Lysis by NK Cells. *Nat Biotechnol* (2017) 35:765–72. doi: 10.1038/nbt.3860
113. Gandhi JK, Mano F, Iezzi RJr., LoBue SA, Holman BH, Fautsch MP, et al. Fibrin Hydrogels are Safe, Degradable Scaffolds for Sub-Retinal Implantation. *PloS One* (2020) 15:e0227641. doi: 10.1371/journal.pone.0227641
114. Thomas BB, Zhu D, Zhang L, Thomas PB, Hu Y, Nazari H, et al. Survival and Functionality of Hesc-Derived Retinal Pigment Epithelium Cells Cultured as a Monolayer on Polymer Substrates Transplanted in RCS Rats. *Invest Ophthalmol Vis Sci* (2016) 57:2877–87. doi: 10.1167/iovs.16-19238

Conflict of Interest: The authors declare that the research was conducted in the absence of any commercial or financial relationships that could be construed as a potential conflict of interest.

Copyright © 2021 Petrash, Palestine and Canto-Soler. This is an open-access article distributed under the terms of the Creative Commons Attribution License (CC BY). The use, distribution or reproduction in other forums is permitted, provided the original author(s) and the copyright owner(s) are credited and that the original publication in this journal is cited, in accordance with accepted academic practice. No use, distribution or reproduction is permitted which does not comply with these terms.

frontiers in Neuroscience

ORIGINAL RESEARCH
published: 20 May 2021
doi: 10.3389/fnins.2021.642176

Knock-Out of Tenascin-C Ameliorates Ischemia-Induced Rod-Photoreceptor Degeneration and Retinal Dysfunction

*Susanne Wiemann[1], Aisha Yousf[1], Stephanie C. Joachim[2], Carolin Peters[1], Ana M. Mueller-Buehl[2], Natalie Wagner[2] and Jacqueline Reinhard[1]**

[1] Department of Cell Morphology and Molecular Neurobiology, Faculty of Biology and Biotechnology, Ruhr-University Bochum, Bochum, Germany, [2] Experimental Eye Research Institute, University Eye Hospital, Ruhr-University Bochum, Bochum, Germany

OPEN ACCESS

Edited by:
Denise M. Inman,
University of North Texas Health Science Center, United States

Reviewed by:
Neal Peachey,
Case Western Reserve University, United States
Jeannie Chen,
University of Southern California, United States

***Correspondence:**
Jacqueline Reinhard
jacqueline.reinhard@rub.de

Specialty section:
This article was submitted to Neurodegeneration, a section of the journal Frontiers in Neuroscience

Received: 15 December 2020
Accepted: 14 April 2021
Published: 20 May 2021

Citation:
Wiemann S, Yousf A, Joachim SC, Peters C, Mueller-Buehl AM, Wagner N and Reinhard J (2021) Knock-Out of Tenascin-C Ameliorates Ischemia-Induced Rod-Photoreceptor Degeneration and Retinal Dysfunction. Front. Neurosci. 15:642176. doi: 10.3389/fnins.2021.642176

Retinal ischemia is a common pathomechanism in various eye diseases. Recently, evidence accumulated suggesting that the extracellular matrix (ECM) glycoprotein tenascin-C (Tnc) plays a key role in ischemic degeneration. However, the possible functional role of Tnc in retinal ischemia is not yet known. The aim of our study was to explore retinal function and rod-bipolar/photoreceptor cell degeneration in wild type (WT) and *Tnc* knock-out (KO) mice after ischemia/reperfusion (I/R) injury. Therefore, I/R was induced by increasing intraocular pressure in the right eye of wild type (WT I/R) and *Tnc* KO (KO I/R) mice. The left eye served as untreated control (WT CO and KO CO). Scotopic electroretinogram (ERG) recordings were performed to examine rod-bipolar and rod-photoreceptor cell function. Changes of Tnc, rod-bipolar cells, photoreceptors, retinal structure and apoptotic and synaptic alterations were analyzed by immunohistochemistry, Hematoxylin and Eosin staining, Western blot, and quantitative real time PCR. We found increased Tnc protein levels 3 days after ischemia, while Tnc immunoreactivity decreased after 7 days. *Tnc* mRNA expression was comparable in the ischemic retina. ERG measurements after 7 days showed lower a-/b-wave amplitudes in both ischemic groups. Nevertheless, the amplitudes in the KO I/R group were higher than in the WT I/R group. We observed retinal thinning in WT I/R mice after 3 and 7 days. Although compared to the KO CO group, retinal thinning was not observed in the KO I/R group until 7 days. The number of PKCα^+ rod-bipolar cells, recoverin$^+$ photoreceptor staining and *Prkca* and *Rcvrn* expression were comparable in all groups. However, reduced rhodopsin protein as well as *Rho* and *Gnat1* mRNA expression levels of rod-photoreceptors were found in the WT I/R, but not in the KO I/R retina. Additionally, a lower number of activated caspase 3$^+$ cells was observed in the KO I/R group. Finally, both ischemic groups displayed enhanced vesicular glutamate transporter 1 (vGlut1) levels. Collectively, KO mice showed diminished

rod-photoreceptor degeneration and retinal dysfunction after I/R. Elevated vGlut1 levels after ischemia could be related to an impaired glutamatergic photoreceptor-bipolar cell signaling and excitotoxicity. Our study provides novel evidence that Tnc reinforces ischemic retinal degeneration, possibly by synaptic remodeling.

Keywords: electroretinography, extracellular matrix, ischemia/reperfusion, retina, rod-bipolar cells, rod-photoreceptor cells, synapses, tenascin-C

INTRODUCTION

Retinal ischemia contributes to the pathophysiology of numerous eye disorders, such as vascular occlusions (e.g., central retinal vein/artery occlusion), acute glaucoma, and diabetic retinopathy (Osborne et al., 2004; Hayreh, 2005; Campochiaro, 2015). In the retina, ischemia develops as a result of capillary blockage and results in non-perfusion of this region. Just a few hours after ischemia, both inflammation and apoptosis occur. The mentioned diseases result in visual disturbances and possible blindness for these patients. A better understanding of the underlying pathomechanisms involved in retinal ischemia is therefore crucial for the development of novel diagnostic and therapy strategies to prevent vision loss.

Rodents represent useful *in vivo* systems to study the molecular mechanisms of ischemic neurodegeneration. Here, the ischemia/reperfusion (I/R) model represents a suitable experimental approach (Hartsock et al., 2016; Schultz et al., 2016; Joachim et al., 2017; Reinhard et al., 2017a; Renner et al., 2017; Palmhof et al., 2019). In the I/R model, retinal ischemia is induced by intraocular pressure (IOP) elevation for a definite period of time. Due to the induced high IOP, retinal blood vessels are compressed, which in turn leads to a loss or restriction of blood supply. The ischemic phase is followed by a natural reperfusion phase in which blood circulation is restored. This leads to further progressive damage of the retina through oxidative stress. Several studies indicate that ischemic neurodegeneration in the retina of different animal models is characterized by a loss of functional activity and loss of various neuronal subtypes (Kaur et al., 2008; Belforte et al., 2011; Joachim et al., 2012; Minhas et al., 2012; Schmid et al., 2014). I/R injury leads to the death of various retinal neurons, since they are sensitive to hypoxic stress (Kaur et al., 2008; Xu et al., 2015; Hu et al., 2016; Schultz et al., 2016; Palmhof et al., 2019).

There is increasing evidence that neurodegenerative processes are accompanied by an extensive remodeling of extracellular matrix (ECM) components (Roll et al., 2012; Roll and Faissner, 2014, 2019). The ECM forms a dynamic meshwork of macromolecules, termed matrisome, which is synthesized and secreted by the tissue-embedded cells themselves. Beside structural importance, the ECM regulates fundamental cellular processes such as adhesion, differentiation, migration, proliferation and survival. ECM components include fibrillary proteins, proteoglycans and glycoproteins. Especially, glycoproteins represent important receptor-, adhesion-, and adapter-molecules, which influence extra- as well as intracellular signaling pathways. Particularly, ECM molecules in the retina create a cellular environment that inhibits neuronal regeneration (Silver, 1994; Reinhard et al., 2015; Pearson et al., 2020). Nevertheless, the functional role of the ECM during ischemic processes and their impact on retinal neurodegeneration is not well known yet.

In the present study, we specifically focused on the functional importance of the ECM glycoprotein tenascin-C (Tnc) in retinal ischemia. During early retinogenesis, Tnc is first detectable at embryonic day 13 in post-mitotic cells of the inner neuroblastic layer (Klausmeyer et al., 2007). At this early stage, the knockout (KO) of *Tnc* led to a transient increase of post-mitotic neurons as well as an altered de-differentiation behavior of Müller glia *in vitro* (Besser et al., 2012). In the chicken retina, Tnc was reported to be expressed by horizontal, amacrine and displaced amacrine cells and in close association with the outer plexiform layer (OPL) and inner plexiform layer (IPL) (Bartsch et al., 1995; D'Alessandri et al., 1995). In the mouse retina, Tnc was also observed in colocalization with synaptophysin-immunoreactive synaptic sites of the plexiform layers (Reinhard et al., 2015). Additionally, optic nerve astrocytes can be a source of Tnc (Bartsch et al., 1992; Reinhard et al., 2015).

In the central nervous system (CNS), Tnc is a major functional constituent of the glial scar and has a harmful influence on neuronal cells after injury (Brodkey et al., 1995; Steindler et al., 1995; Kwok et al., 2011; Roll and Faissner, 2019). Interestingly, Tnc exhibits a low, if any expression in healthy tissue, while it is prominently upregulated following injury or in tumors (Faissner et al., 2017). Previously, evidence accumulated suggesting that Tnc is a key player in ischemic degeneration. In this regard, Tnc was previously described as crucial player in cerebral, hepatic as well as myocardial ischemia (Lu et al., 2003; Taki et al., 2010, 2015; Kuriyama et al., 2011).

Recently, we observed that Tnc and several interacting ECM molecules are dysregulated in a rat I/R model (Reinhard et al., 2017a,b). Tnc levels were reported to be increased in the optic nerve head of an ocular hypertension model (Johnson E. C. et al., 2007). Elevated Tnc expression could also be observed

Abbreviations: BSA: bovine serum albumin; CNS: central nervous system; CtBP2: C-terminal binding protein 2; ECM: extracellular matrix; ERG: electroretinogram; GCL: ganglion cell layer; *Gnat1*: *guanine nucleotide binding protein, alpha transducin 1*; H&E: Hematoxylin and Eosin; *Hprt*: *hypoxanthine guanine phosphoribosyl transferase*; INL: inner nuclear layer; IOP: intraocular pressure; IPL: inner plexiform layer; IS: inner segment; KO: knock-out; KO CO: non-ischemic control *Tnc* knock-out group; KO I/R: ischemic *Tnc* knock-out group; LTCC: L-type voltage-gated calcium channel; NFL: nerve fiber layer; ONL: outer nuclear layer; OPL: outer plexiform layer; OS: outer segment; PBS: phosphate-buffered saline; PFA: paraformaldehyde; PKCα/*Prkca*: protein kinase alpha C; RT: room temperature; RT-qPCR: quantitative real time PCR; SEM: standard error mean; TBS: Tris-buffered saline; Tnc: tenascin-C; vGlut1: vesicular glutamate transporter 1; WT: wild type; WT CO: non-ischemic control wild type group; WT I/R: ischemic wild type group.

in the optic nerve head of patients with primary open-angle glaucoma (Pena et al., 1999). In a previous study, we also verified an upregulation of Tnc, and its interaction partner the chondroitin sulfate proteoglycan phosphacan in an experimental autoimmune and an IOP-dependent glaucoma mouse model (Reinehr et al., 2016; Reinhard et al., 2021). Immunized *Tnc* KO mice exhibit a reduced retinal ganglion cell loss and an enhanced anti-inflammatory cytokine expression (Wiemann et al., 2020), suggesting that *Tnc* deficiency provides various neuroprotective effects. However, the functional relevance of Tnc in retinal ischemia is poorly understood.

The goal of the present study was to comparatively explore retinal function, rod-bipolar/photoreceptor cell degeneration and synaptic alterations in WT and *Tnc* KO mice after I/R injury. Interestingly, we observed a diminished rod-photoreceptor degeneration and an improved retinal function in *Tnc* KO mice after ischemia. Additionally, we found increased vesicular glutamate transporter 1 (vGlut1) protein levels in both ischemic groups, which could be related to an impaired glutamatergic photoreceptor-bipolar cell signaling and excitotoxicity. Thus, the present study provides first evidence that Tnc accelerates ischemic rod-photoreceptor damage, maybe by modulating synaptic sites.

MATERIALS AND METHODS

Mice

For all experiments, 6-week-old 129/Sv (129S2/SvPasCrl; background mouse strain) wild type (WT) and *Tnc* KO mice (Forsberg et al., 1996) of both genders were used. WT and *Tnc* KO mice were generated by the breeding of homozygous *Tnc* KO and WT mice, respectively. WT and *Tnc* KO breedings were derived from heterozygous breedings. Mouse colonies were maintained at the animal facility of the Faculty of Biology and Biotechnology, Ruhr-University Bochum (Bochum, Germany). Mice were housed under equal environmentally controlled lighting conditions (12 h light-dark cycle) with free access to chow and water.

Genotyping

Genomic DNA was isolated from tail biopsies using the DirectPCR® Lysis Reagent (Viagen Biotech Inc., Los Angeles, CA, United States). For genotyping, PCR analyses were performed using Taq DNA polymerase (Sigma-Aldrich St. Louis, MO, United States). The following primer pairs were used to amplify $Tnc^{+/+}$ (WT) and $Tnc^{-/-}$ (KO) alleles: Forward 5′-CTGCCAGGCATCTTTCTAGC-3′, reverse 5′-TTCTGCAGGTTGGAGGCAAC-3′ and neo forward 5′-CTGCTCTTTACTGAAGGCTC-3′ as described by Talts et al. (1999).

Retinal Ischemia/Reperfusion

Before inducing retinal I/R, mice were anesthetized with a mixture of Medetomidine (500 μg/kg; Dorbene vet® 1 mg/ml, Zoetis Deutschland GmbH, Berlin, Germany), Midazolam (5 mg/kg; Midazolam-hameln® 1 mg/ml, hameln pharma plus GmbH, Hameln, Germany), and Fentanyl (50 μg/kg; Fentadon® 50 μg/ml, Albrecht GmbH/Dechra Veterinary Products Deutschland GmbH, Aulendorf, Germany) by intraperitoneal injection. The cornea of the right eye of each animal was topically anesthetized with Oxybuprocaine hydrochloride (Novesine Stulln® 4 mg/ml, Stulln pharma, Stulln, Germany) and the pupil was dilated with Tropicamide (Mydriaticum Stulln® 5 mg/ml, Pharma Stulln, Stulln, Germany). A 27-gauge needle (Terumo Europe, Leuven, Belgium), which was connected by a flexible tube (B. Braun Intrafix SafeSet, Wolfram Droh GmbH, Mainz, Germany) to an NaCl reservoir (Isotonic saline solution 0.9% Ecoflac Plus, B. Braun Melsungen AG, Melsungen, Germany) was carefully inserted into the anterior chamber of the eye. By raising the saline reservoir, IOP was increased above a systolic blood pressure of 90 mmHg for 45 min. Ischemia was confirmed by blanching of the retina detected via an ophthalmoscope (Mini 3000, Heine Optotechnik, Herrsching, Germany). After removing of the needle, reperfusion of the retinal vasculature was observed by examining the fundus and the returning blood flow using an ophthalmoscope. Then, anesthesia was stopped by the subcutaneous application of Atipamezole (2.5 mg/kg; Alzane® 5 mg/ml, Zoetis Deutschland GmbH, Berlin, Germany), Flumazenil (0.5 mg/kg; FLUMAzenil® 0.1 mg/ml, B. Braun, Melsungen AG, Melsungen, Germany) and Naloxone (1200 μg/kg; Naloxon-hameln® 0.4 mg/ml, hameln pharma plus GmbH, Hameln, Germany) cocktail. Non-ischemic left eyes served as controls. To avoid drying, control eyes were treated with a Dexpanthenol solution (Bepanthen® Augen- und Nasensalbe 5 mg/g, Bayer Vital GmbH, Leverkusen, Germany). Ischemic eyes were treated with an Ofloxacin solution (Floxal® 3 mg/ml, Bausch & Lomb GmbH, Heidelberg, Germany) and Corneregel® (50 mg/g, Bausch & Lomb GmbH, Heidelberg, Germany). For pain therapy, metamizole (200 mg/kg) was administrated orally to drinking water for 4 days after ischemia. Eyes were inspected daily. Animals with signs of inflammation or cataract were excluded from the study. Animals were sacrificed by cervical dislocation at 3 and 7 days after I/R and retinae were explanted for immunohistochemistry, Western blot analyses and quantitative real time PCR (RT-qPCR).

Electroretinogram Recordings

Scotopic full-field flash electroretinogram (ERG) recordings (HMsERG system, OcuScience, Henderson, NV, United States) were performed 7 days after I/R (n = 5/group) as described previously (Schmid et al., 2014; Reinhard et al., 2019). In brief, mice were dark-adapted overnight before performing ERG recordings under dim red light. Mice were anesthetized by an intraperitoneal injection of a ketamine/xylazine mixture (120/16 mg/kg). Eyes were treated with Oxybuprocaine hydrochloride eye drops (Novesine Stulln® 4 mg/ml, Stulln pharma, Stulln, Germany) and the pupil was dilated with Tropicamide (Mydriaticum Stulln® 5 mg/ml, Pharma Stulln, Stulln, Germany). Two reference electrodes were inserted subcutaneously behind the right and left ear and the ground electrode was placed in the base of the tail. Methocel (Omni Vision, Puchheim, Germany) was applied to the cornea and a contact lens with a silver-tread recording electrode (OcuScience,

Henderson, NV, United States) was placed on the center of the cornea. Scotopic flash ERGs were recorded in non-ischemic control WT (WT CO) and KO (KO CO) as well as in ischemic WT (WT I/R) and KO (KO I/R) mice at 1.0, 3.0, 10.0, and 25.0 cd*s/m^2. From 1.0 to 3.0 cd*s/m^2, 4 flashes were averaged with an interstimulus interval of 10 s, while at 10.0 and 25.0 cd*s/m^2 1 flash was measured. ERG responses were amplified, digitized, and analyzed using the ERGView 4.380R software (OcuScience) (Liu Y. et al., 2014). Before evaluating the a- and b-waves amplitudes, a 150 Hz low-pass filter was applied. In brief, a-waves were measured from the pre-stimulus baseline up to the a-wave, whereas b-waves were measured from the a-wave to the b-wave peak.

Hematoxylin and Eosin Staining

At 3 and 7 days post-I/R, eyes were enucleated, fixed in 4% paraformaldehyde (PFA), dehydrated in 30% sucrose, and embedded in Tissue Freezing Medium® (Leica, Buffalo Grove, IL, United States) for cross-sectioning (16 μm) with a cryostat (CM3050 S, Leica Mikrosysteme, Wetzlar, Germany). Hematoxylin and Eosin (H&E) staining of retinal sections was performed in accordance with the manufacturer's protocol (Rapid Chrome H&E Frozen Section Staining Kit, Thermo Scientific). For thickness measurements, 2 central retinal sections per animal (n = 5/group) were analyzed. Brightfield images were captured with the Axio Zoom V16 (Carl Zeiss Microscopy, Jena, Germany) in central and mid-peripheral areas of each retinal section at a 200× magnification. Per image, measurements at 2 positions were performed using the Zeiss ZEN software (Carl Zeiss Microscopy). For total retinal thickness measurements, the distance from the basal ganglion cell layer (GCL) to the apical part of the outer nuclear layer (ONL) was measured. Additionally, we measured the thickness of the ONL and OPL alone and together (ONL + OPL). For layer measurements, the thickness of the WT CO group was set to 100%.

Immunohistochemistry and Microscopy

For the preparation of retinal cross-sections, eyes were enucleated after 3 and 7 days and fixed in 4% PFA for 1 day (n = 5/group). After dehydration in sucrose (30%), eyes were embedded in Tissue Freezing Medium® (Leica, Buffalo Grove, IL, United States). Retinal cross-sections (16 μm) were cut using a cryostat (CM3050 S, Leica Mikrosysteme, Wetzlar, Germany) and transferred onto Superfrost plus object slides (Menzel-Gläser, Braunschweig, Germany). Next, cross-sections were incubated in blocking solution [1% bovine serum albumin (BSA); Sigma-Aldrich; 3% goat serum, Dianova, Hamburg, Germany; 0.5% Triton^{TM}-X-100, Sigma-Aldrich in 1 × phosphate-buffered saline (1 × PBS)] for 1 h at room temperature (RT). Then, the primary antibodies were diluted in blocking solution and incubated on sections overnight at RT (**Table 1**). Afterward, retinal cross-sections were washed in 1 × PBS and incubated for 2 h with species-specific secondary antibodies (Jackson Immuno Research Labs, Germany; **Table 1**) in blocking solution without Triton^{TM}-X-100. Cell nuclei were counterstained using TO-PRO-3 (1:400; Thermo Fisher Scientific), which was diluted in secondary antibody solution.

Sections treated with secondary antibody only served as negative controls. Finally, sections were covered in Immu-Mount (Thermo Fisher Scientific) and stored at 4°C.

Immunostained retinal cross-sections were analyzed by confocal laser-scanning microscopy (LSM 510 META; Zeiss, Göttingen, Germany). For staining analyses, 2 central retinal sections per animal and 4 images per retina (2 mid-peripheral and two central) at a 400× magnification were captured. Laser lines and emission filters were adjusted using the Zeiss ZEN black software. Individual images were cropped with Coral Paint Shop Pro X8 (Coral Corporation, Gardena, CA, United States) and ImageJ software (ImageJ 1.51w, National Institutes of Health; Bethesda, MD, United States) was used to perform masked evaluation of the staining signal area (**Supplementary Figure 1**). Hence, images were converted into 32-bit gray scale. The background was subtracted, and lower and upper threshold values were determined for each image (**Supplementary Table 1**). Afterward, the percentage of the area fraction was measured by an ImageJ macro using antibodies directed against recoverin, rhodopsin and Tnc (Reinehr et al., 2018; Wiemann et al., 2020). Protein kinase alpha C (PKCα) cells were counted manually in a defined area of 225 × 225 μm using the cell counter tool of ImageJ. For these analyses, the staining area and the number of immunoreactive cells of the WT CO group was set to 100%. Activated caspase 3 immunoreactive cells were counted in the ONL of whole retinal sections.

Western Blot

Western blot analyses were performed according to a previously described protocol (Reinhard et al., 2017a). Ischemic and control retinae of both genotypes (n = 4/group) were homogenized in 80 μl lysis buffer containing 60 mM n-octyl-β-D-glucopyranoside, 50 mM sodium acetate, 50 mM Tris chloride, pH 8.0 and a protease inhibitor cocktail (Sigma-Aldrich) for 1 h on ice. After centrifugation at 14.000 × g at 4°C for 30 min, protein concentration in the supernatant was determined with the bicinchoninic acid assay (BCA) Protein Assay Kit (Pierce, Thermo Fisher Scientific) according to manufacturer's instructions. 4 × SDS buffer was added to each protein sample (15–20 μg) and denaturized for 5 min at 94°C. Following separation by SDS-PAGE using 4–12% polyacrylamide gels, proteins were transferred to a polyvinylidene difluoride (PVDF) membrane (Roth, Karlsruhe, Germany) via Western blotting. Next, membranes were blocked in TBST (5% w/v milk powder in Tris-buffered saline (TBS) and 0.05% Tween 20) at RT for 1 h. Primary antibodies (**Table 2**) were diluted in blocking solution and membranes were incubated in the solution at 4°C overnight. Membranes were washed in TBST and incubated with horseradish peroxidase (HRP) conjugated secondary antibodies (**Table 2**) in blocking solution at RT for 2 h. Non-bound antibody was washed off with TBST and finally in TBS. ECL substrate solutions were mixed 1:1 (Bio-Rad Laboratories GmbH, München, Germany) and applied to the membranes for 5 min. Immunoreactivity of proteins was recorded with a MicroChemi Chemiluminescence Reader (Biostep, Burkhardtsdorf, Germany). Protein band intensity was measured using ImageJ software and normalized to the internal

TABLE 1 | Primary and secondary antibodies used for immunohistochemistry.

Primary antibody	Dilution	Source/reference	RRID	Secondary antibody	Dilution	Source	RRID
Activated caspase 3	1:200	Sigma Aldrich	AB476884	Alexa Fluor 488-conjugated goat anti-rabbit	1:250	Jackson Immuno Research Labs	AB_2338049
Calbindin D-28k	1:500	Swant	AB_10000347	Alexa Fluor 488-conjugated goat anti-mouse	1:250	Jackson Immuno Research Labs	AB_2338844
GFAP	1:300	Sigma Aldrich	AB_477010	Alexa Fluor 488-conjugated goat anti-mouse	1:250	Jackson Immuno Research Labs	AB_2338844
PKCα	1:500	Santa Cruz	AB_628142	Alexa Fluor 488-conjugated goat anti-mouse	1:250	Jackson Immuno Research Labs	AB_2338844
Recoverin	1:600	Millipore	AB_2253622	Alexa Fluor 488-conjugated goat anti-rabbit	1:250	Jackson Immuno Research Labs	AB_2338049
Rhodopsin	1:600	Abcam	AB_304874	Cy3-conjugated goat anti-mouse	1:250	Jackson Immuno Research Labs	AB_2338686
Tnc (KAF12)	1:250	Wiemann et al., 2020	–	Cy3-conjugated goat anti-rabbit	1:250	Jackson Immuno Research Labs	AB_2338003

Cy2 = Cyanine; Cy3 = Indocarbocyanine; RRID = Research Resource Identification number.

TABLE 2 | Primary and secondary antibodies used for Western blot analyses.

Primary antibody	Dilution	Source/reference	RRID	Molecular weight (kDa)	Secondary antibody	Dilution	Source	RRID
α-Tubulin	1:10.000	Sigma Aldrich	AB_477593	∼50	Peroxidase-conjugated goat anti-mouse	1:10.000	Jackson Immuno Research Labs	AB_2338505
Actin	1:5.000	BD Biosciences	AB_399901	42	Peroxidase-conjugated goat anti-mouse	1:10.000	Jackson Immuno Research Labs	AB_2338505
CtBP2	1:2.000	BD Biosciences	AB_399431	48	Peroxidase-conjugated goat anti-mouse	1:10.000	Jackson Immuno Research Labs	AB_2338505
PKCα	1:500	Santa Cruz	AB_628142	80	Peroxidase-conjugated goat anti-mouse	1:10.000	Jackson Immuno Research Labs	AB_2338505
Recoverin	1:1.000	Millipore	AB_2253622	23	Peroxidase-conjugated goat anti-rabbit	1:10.000	Jackson Immuno Research Labs	AB_2307391
Rhodopsin	1:10.000	Abcam	AB_304874	40	Peroxidase-conjugated goat anti-mouse	1:10.000	Jackson Immuno Research Labs	AB_2338505
Tnc (KAF12)	1:5.000–1:10.000	Wiemann et al., 2020	–	∼250 and >250 kDa	Peroxidase-conjugated goat anti-rabbit	1:10.000	Jackson Immuno Research Labs	AB_2307391
vGlut1	1:2000	Sigma Aldrich	AB_261840	60	Peroxidase-conjugated goat anti-rabbit	1:10.000	Jackson Immuno Research Labs	AB_2307391

kDa = kilo Dalton; RRID = Research Resource Identification number.

reference proteins actin and α-tubulin (**Table 2**). The normalized values of the Western blot results were presented in arbitrary units (a.u.). Tnc protein was immunoaffinity-purified from postnatal mouse brains using the monoclonal Tnc antibodies J1/tn1 (clone number 576, rat, IgG), J1/tn2 (clone number 578, rat, IgG_{2a}), and J1/tn4 (clone number 633, rat, IgG_{2a}) as previously described (Faissner and Kruse, 1990; Husmann et al., 1992) (**Supplementary Figure 2**).

RNA Isolation, cDNA Synthesis and RT-qPCR Analysis

Retinae were explanted at 3 and 7 days after I/R and stored at −80°C (n = 4–5/group). RNA was extracted according to the manufacturer's instructions using the Gene Elute Mammalian Total RNA Miniprep Kit (Sigma-Aldrich, St. Louise, MO, United States). RNA quality and quantity were analyzed using a BioSpectrometer® (Eppendorf, Hamburg, Germany). Via reverse transcription with random hexamer primers, 1 μg RNA was used for cDNA synthesis (Thermo Fisher Scientific). Forward and reverse primer was designed using the Universal ProbeLibrary Assay Design Center software (Roche Molecular Systems; **Table 3**). For each primer set efficiencies were determined by a dilution series of 5, 25, and 125 ng cDNA. RT-qPCR analyses were performed with SYBR Green I in a Light Cycler 96® (Roche Applied Science, Mannheim, Germany) as described previously (Reinhard et al., 2019). Expression was normalized against the constantly expressed housekeeping gene *hypoxanthine guanine phosphoribosyl transferase* (*Hprt*).

Statistical Analysis

Pairwise analyses of Tnc protein levels in two groups (WT CO vs. WT I/R) were carried out with the Student t-test (Statistica software, V13.3; StatSoft Europe, Hamburg, Germany).

For a multiple comparison of all four groups (WT CO, WT I/R, KO CO, and KO I/R), ERG data, histological stainings and

TABLE 3 | List of primer pairs used for RT-qPCR analyses.

Primer	Sequence	Product size (base pairs)	Primer efficiency	GenBank accession number
*Cacna1f*_forward	TGTGTGCAGATGGTCCTTATATCT	78	0.685	NM_019582
*Cacna1f*_reverse	CTGGGCTCTGGGGTTGTAT			
*Gnat1*_forward	GAGGATGCTGAGAAGGATGC	106	0.806	NM_008140
*Gnat1*_reverse	CGTCCTGGTGGATAATCTTCA			
*Hprt*_forward	TGATAGATCCATTCCTATGACTGTAGA	126	0.931	NM_013556 XM_356404
*Hprt*_reverse	AAGACATTCTTTCCAGTTAAAGTTGAG			
*Prkca*_forward	CAAGGGATGAAATGTGACACC	96	0.980	NM_011101.3
*Prkca*_reverse	CCTCTTCTCTGTGTGATCCATTC			
*Rcvrn*_forward	CAATGGGACCATCAGCAAA	71	0.836	NM_009038.2
*Rcvrn*_reverse	CCTCAGGCTTGATCATTTTGA			
*Rho*_forward	ACCTGGATCATGGCGTTG	70	0.934	NM_145383.1
Rho_reverse	TGCCCTCAGGGATGTACC			
Tnc_forward	CAGGGATAGACTGCTCTGAGG	90	1.0	NM_001369211–14
Tnc_reverse	CATTGTCCCATGCCAGATTT			

Western blots were analyzed using a two-way ANOVA followed by Tukey's *post hoc* test.

A pairwise fixed reallocation and randomization test (REST software, Relative expression software tool 2009; QIAGEN GmbH, Hilden, Germany) was used to analyze RT-qPCR data.

RESULTS

Early Induction of Tnc Following Retinal Ischemia

It is not known whether Tnc is dysregulated in the retina of our I/R mouse model. Therefore, we analyzed the Tnc expression pattern in non-ischemic and ischemic WT retinae after 3 and 7 days (**Figure 1**). Immunohistochemistry of retinal cross-sections revealed an obvious Tnc immunoreactivity in the OPL and IPL as well as in close association with cells of the inner nuclear layer (INL) and nerve fiber layer (NFL) (**Figures 1A–D**). At 3 days after ischemia, we found a significant increase of the Tnc^+ staining area ($p < 0.01$; **Figure 1E**). Conversely, a decreased Tnc^+ staining area was noted in ischemic WT retinae at 7 days ($p = 0.02$; **Figure 1E**).

In order to analyze the expression pattern of Tnc after ischemia, we performed coimmunostaining (**Supplementary Figure 3**). Here, anti-calbindin was used as a specific marker for horizontal and amacrine cells, while anti-glial fibrillary acidic protein (GFAP) was used to label astrocytes. Calbindin- and Tnc-double-positive horizontal cells were observed in the most apical part of the INL. Tnc immunoreactivity in the basal part of the INL was also found in close association with $calbindin^+$ amacrine cells. In addition, we revealed a colocalization of $GFAP^+$ astrocytes and Tnc in the NFL, indicating that the mentioned cells are a source of Tnc expression in the retina.

To consolidate the dysregulation of Tnc after ischemia, we verified Tnc protein levels by Western blot analyses. For Tnc, two distinct bands were observed at ∼250 and >250 kDa (**Figures 1F,J** and **Supplementary Figure 2**). At 3 days, densiometric measurements of the total Tnc protein showed comparable levels in WT CO and WT I/R retinae ($p = 0.13$; **Figure 1G**). Interestingly, a significant upregulation of the larger Tnc isoforms was found in the WT I/R compared to the WT CO group ($p = 0.03$; **Figure 1H**). Unaltered protein levels were observed for shorter Tnc isoforms in both groups ($p = 0.15$; **Figure 1I**). At 7 days, total Tnc protein levels were unaltered ($p = 0.36$; **Figure 1K**). Also, protein levels of larger Tnc isoforms were comparable in control and ischemic WT retinae ($p = 0.63$; **Figure 1L**). Relative quantification showed a slight, but not statistically significant, decrease of shorter Tnc isoforms after I/R compared to the control condition ($p = 0.09$; **Figure 1M**).

Finally, we examined *Tnc* mRNA levels using RT-qPCR at both points in time. However, compared to the non-ischemic condition, *Tnc* mRNA expression was similar at 3 ($p = 0.78$) and 7 days ($p = 0.58$) after ischemia (**Figure 1N** and **Supplementary Table 2**).

Collectively, our temporal analyses of Tnc induction revealed a very early raise followed by a decrease of the Tnc protein level after ischemic damage, while *Tnc* mRNA expression was unaltered. Accordingly, our results indicate that the upregulation of Tnc is a very early event during retinal ischemic damage.

Improvement of Retinal Functionality in *Tnc* KO Mice After I/R

To examine possible functional deficits in control and ischemic WT and *Tnc* KO retinae, scotopic ERG-recordings were conducted at 7 days post-I/R (**Figures 2A–C** and **Supplementary Table 3**). In all experimental groups, increased a- and b-wave amplitudes were observed with rising light flash stimuli. Rod-photoreceptor cell and rod-bipolar cell responses were evaluated by a- and b-wave amplitude measurements, respectively.

Compared to the WT CO group, significantly reduced a-wave ($p < 0.05$) and b-wave ($p < 0.01$) amplitudes were recorded in the WT I/R condition. Also, the KO I/R group showed significantly reduced a-wave responses at lower light stimuli in comparison to the KO CO group ($p < 0.05$ from 1 to 3 cd^*s/m^2). However, although the amplitudes of the a-wave were comparable in both

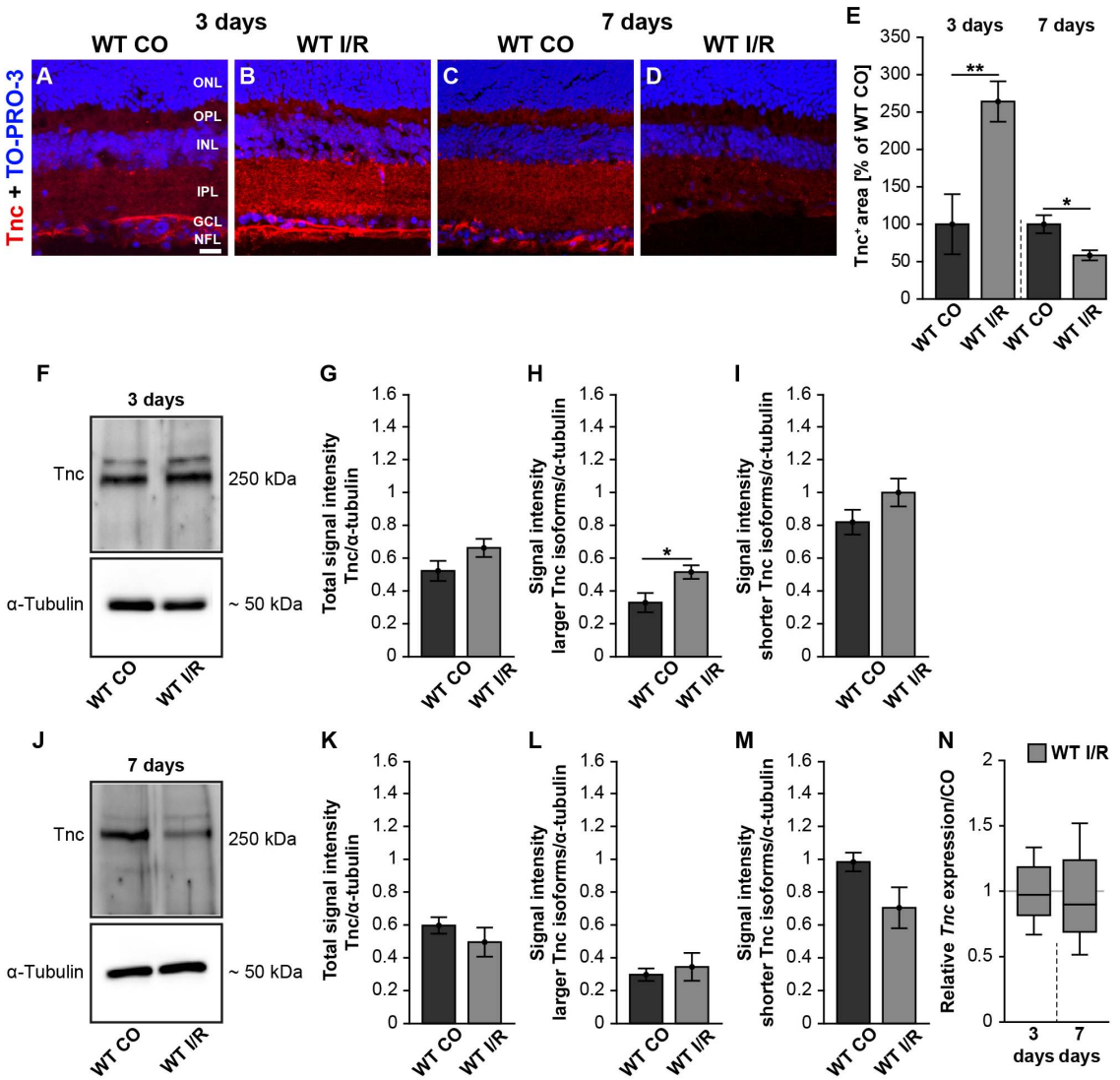

FIGURE 1 | Early induction of Tnc in the ischemic WT retina. **(A–D)** Images of Tnc stained retinal cross-sections from control and ischemic WT groups at 3 and 7 days. Immunohistochemistry revealed a Tnc signal in the IPL and OPL as well as in the NFL (red). Cell nuclei were counterstained with TO-PRO-3 (blue). **(E)** Tnc^+ staining area was significantly increased at 3 days, indicating an early induction of Tnc after ischemic injury. However, a significantly reduced Tnc staining could be demonstrated at 7 days. The WT CO group was set to 100%. **(F–I)** Consistently, relative protein quantification showed a significant upregulation of larger Tnc isoforms at 3 days after I/R. **(J–M)** Comparable Tnc protein levels were observed after 7 days. **(N)** No differences of the *Tnc* mRNA expression were noted at both points in time after ischemia. Data were analyzed via Student *t*-test and presented as mean ± standard error mean (SEM) in panels **(E,G–I,K–M)**. For RT-qPCR, groups were compared using the pairwise fixed reallocation and randomization test in panel **(N)**. These data are shown as median ± quartile ± minimum/maximum. $^*p < 0.05$; $^{**}p < 0.01$. $n = 4–5$/group. Scale bar = 20 μm. ONL: outer nuclear layer, OPL: outer plexiform layer, INL: inner nuclear layer, IPL: inner plexiform layer, GCL: ganglion cell layer, NFL: nerve fiber layer.

ischemic groups ($p > 0.05$), higher amplitudes were observed in the KO I/R group.

The KO I/R and KO CO groups showed similar b-wave amplitudes ($p \geq 0.05$). Compared to the KO I/R group, the WT I/R group exhibited significantly reduced b-wave responses ($p < 0.05$ from 3 to 25 cd^*s/m^2).

In summary, although the KO I/R group was less affected, impaired a-wave responses were observed in both genotypes after ischemia. Even though, in relation to the WT group, the KO group showed an impaired, but much better b-wave functionality following ischemia. Collectively, our results suggest that the loss of Tnc acts neuroprotective after I/R on a functional level.

Early Preservation of Retinal Integrity in the KO I/R Retina

In a further step, the structural integrity of the retina should be analyzed in WT and KO mice after ischemia. Thus, retinal cross-sections of all groups were stained with H&E (**Figures 3A–H**). Then, the thickness of the total retina, the ONL and OPL

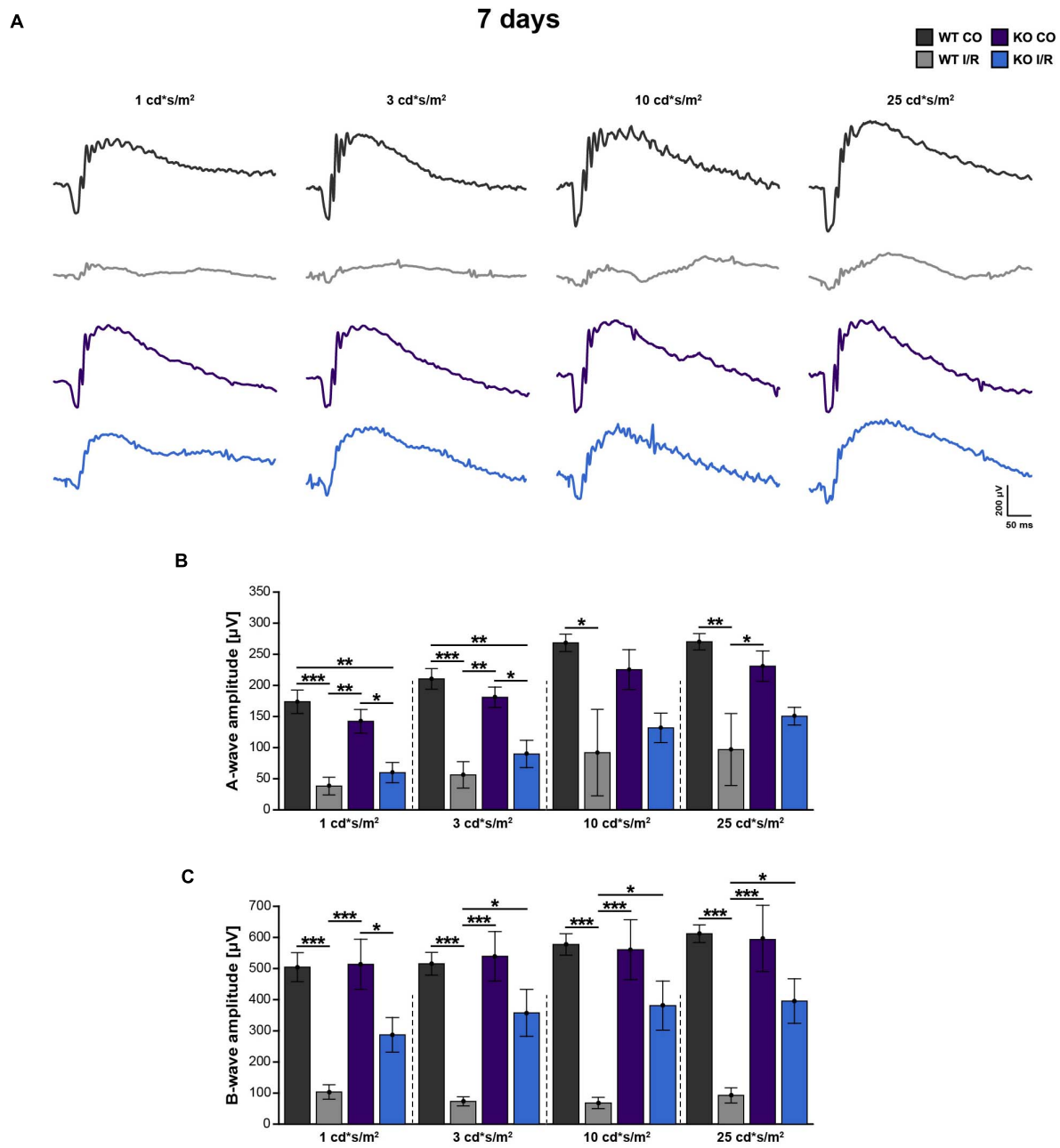

FIGURE 2 | Improvement of retinal function in ischemic *Tnc* KO mice. **(A–C)** Retinal function was analyzed in the control WT (WT CO) and *Tnc* KO (KO CO) groups as well as in the ischemic WT (WT I/R) and *Tnc* KO groups (KO I/R) at 7 days after I/R. **(A)** Exemplary ERG waveforms for all groups at the flash luminances of 1, 3, 10, and 25 cd*s/m^2 are shown. **(B,C)** The flash luminance (cd*s/m^2) and the a- or b-wave amplitude size (µV) are indicated in the graphs. Significant lower a- and b-wave amplitudes were found in both genotypes after I/R. However, the KO I/R group showed significantly reduced a-wave amplitudes only at lower flash luminances in comparison to the control KO group. Interestingly, in the KO I/R group, b-wave amplitudes from 3 to 25 cd*s/m^2 were significantly higher in comparison to the WT I/R group. *$p < 0.05$, **$p < 0.01$, ***$p < 0.001$. $n = 5$/group. Groups were analyzed using two-way ANOVA followed by Tukey's *post hoc* test. Data are shown as mean ± SEM. cd: candela; µV: micro volt; m: minutes; s: seconds.

together as well as the ONL and the OPL separately were measured. At 3 days, the non-ischemic control retinae were well defined and overall retinal thickness was comparable in both genotypes (WT CO vs. KO CO, $p = 0.23$; **Figure 3I**). Conversely, compared to the WT CO group, total retinal thickness, ONL + OPL thickness as well as OPL thickness were significantly reduced in the WT I/R group (WT CO vs. WT I/R, total: $p = 0.02$; ONL + OPL: $p = 0.03$; OPL: $p = 0.01$), while no differences were found in the ONL ($p > 0.11$). Interestingly, no significant reduction in the layer thickness was observed in the

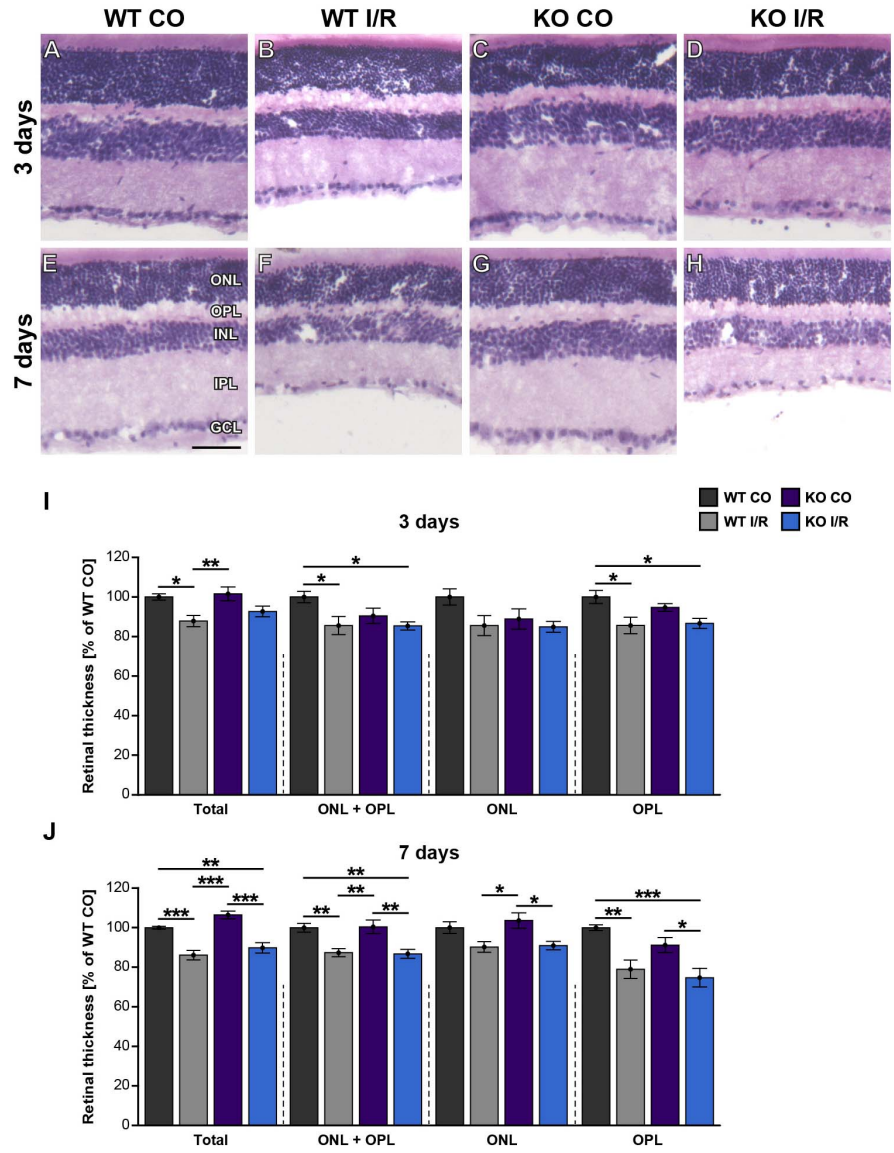

FIGURE 3 | Maintenance of early retinal integrity in *Tnc* KO mice. **(A–H)** Cross-sections of control and ischemic WT and KO retinae were stained with H&E at 3 and 7 days post-I/R. **(I)** At 3 days, a significant reduction of the total, ONL and OPL as well as OPL retinal thickness was noted in the WT I/R group compared to the WT CO group. However, overall outer retinal thickness was comparable in the KO I/R and KO CO group, suggesting an improved structural retinal integrity in the KO early after ischemia. **(J)** At 7 days, a comparable, progressive decline in the outer retinal thickness was observed in both ischemic groups. Groups were analyzed using two-way ANOVA followed by Tukey's *post hoc* test. Data are displayed as mean ± SEM in panels **(I,J)**. The WT CO group was set to 100%. $^{*}p < 0.05$, $^{**}p < 0.01$, $^{***}p < 0.01$. $n = 5$/group. Scale bar = 50 μm. ONL: outer nuclear layer, OPL: outer plexiform layer, INL: inner nuclear layer, IPL: inner plexiform layer, GCL: ganglion cell layer.

KO I/R group compared to the KO CO group (KO CO vs. KO I/R, $p = 0.13$). Although ONL + OPL ($p = 0.03$) as well as OPL thickness ($p = 0.02$) was reduced in the KO I/R compared to the WT CO state.

At 7 days, the thickness of retinae from WT CO and KO CO animals was quite similar (WT CO vs. KO CO, $p > 0.05$; **Figure 3J**). Overall, retinal thickness of both ischemic groups was reduced compared to the control groups (WT CO vs. WT I/R, total: $p < 0.001$; ONL + OPL: $p = 0.008$; ONL: $p = 0.13$; OPL: $p = 0.006$ and KO CO vs. KO I/R, total: $p < 0.001$; ONL + OPL: $p = 0.004$; ONL: $p = 0.03$; OPL: $p = 0.03$). In comparison to the WT CO group, the KO I/R group showed a significant total ($p = 0.008$), ONL and OPL ($p = 0.005$) and OPL ($p < 0.001$) layer reduction. Also, total ($p < 0.001$), ONL + OPL ($p = 0.006$) as well as the OPL ($p = 0.02$) was significantly thinner in the WT I/R compared to the KO CO condition. Similar retinal layer thicknesses were measured in both ischemic conditions ($p = 0.14$).

Collectively, we observed a reduced retinal thickness in the WT group at 3 and 7 days after ischemia. Strikingly, retinal

thickness was not affected in the KO group at 3 days post-I/R. *Tnc* deficient mice showed a reduced retinal thickness only at 7 days after ischemia. These data point to a delayed retinal degeneration and early maintenance of retinal integrity in the *Tnc* KO. In addition, our data indicate that the structural integrity of the OPL is in particular severely impaired after retinal ischemia, while the integrity of the ONL is less affected at both examined time points.

Bipolar Cells Are Not Affected by Ischemia in WT and *Tnc* KO Mice

In order to analyze whether rod-bipolar cells are affected in both genotypes after ischemic injury, we performed PKCα immunostainings. However, the number of PKCα$^+$ cells in control and ischemic retinae of both genotypes was similar at 3 days (WT CO vs. WT I/R, $p = 0.99$; KO CO vs. KO I/R, $p = 0.79$; **Figures 4A–D,I**) as well as at 7 days post-I/R (WT CO vs. WT I/R, $p = 0.72$; KO CO vs. KO I/R, $p = 0.18$; **Figures 4E–H,J**).

In line with these results, total PKCα protein levels, investigated by Western blotting at 7 days, were equivalent in all groups (WT CO vs. WT I/R, $p = 0.99$; KO CO vs. KO I/R, $p = 0.90$; **Figures 4K,L**).

RT-qPCR results showed no differences in the *Prkca* mRNA-expression between both control groups (WT CO vs. KO CO, $p = 0.78$; **Figure 4M** and **Supplementary Table 2**) at 3 days post-I/R. *Prkca* mRNA level in WT CO and KO CO animals resembled the expression level in the WT I/R (WT CO vs. WT I/R, $p = 0.18$) and the KO I/R group (KO CO vs. KO I/R, $p = 0.20$; **Figure 4N**). A similar *Prkca* expression was found in both ischemic groups (WT I/R vs. KO I/R, $p = 0.91$; **Figure 4O**). Also, at 7 days, RT-qPCR results verified no changes in the *Prkca* mRNA expression between the control and the ischemic groups (WT CO vs. KO CO, $p = 0.32$, **Figure 4M**; WT CO vs. WT I/R, $p = 0.35$, KO CO vs. KO I/R, $p = 0.86$; **Figure 4N** and WT I/R vs. KO I/R, $p = 0.60$; **Figure 4O**).

In conclusion, no differences regarding the rod-bipolar cell integrity were observed in WT and *Tnc* KO retinae after I/R. Therefore, we verified a preservation of the PKCα$^+$ rod-bipolar cell population in both genotypes following ischemic injury.

Less Vulnerability of Rod-Photoreceptors in Ischemic KO Mice

Next, we analyzed photoreceptor cells by recoverin staining, which was localized in the ONL as well as in the inner and outer photoreceptor segments (**Figures 5A–H**). The recoverin$^+$ staining area was comparable in both WT groups (WT CO vs. WT I/R, $p = 0.99$) as well as in the KO condition (KO CO vs. KO I/R, $p = 0.94$; **Figure 5I**) at 3 days after ischemia. An unaltered recoverin$^+$ staining area was also found in non-ischemic and ischemic WT and KO retinae at 7 days (WT CO vs. WT I/R, $p = 0.17$ and KO CO vs. KO I/R, $p = 0.99$; **Figure 5J**).

Furthermore, recoverin (23 kDa) was quantified via Western blot analyses (**Figure 5K**). The statistical evaluation revealed equal protein levels in WT as well as KO mice (WT CO vs. WT I/R, $p = 0.99$ and KO CO vs. KO I/R, $p = 1.0$; **Figure 5L**).

We also determined the expression levels of *recoverin* (*Rcvrn*) in control and ischemic WT and KO retinae at both points in time (**Figures 5M–O** and **Supplementary Table 2**). Non-ischemic eyes exhibited equal *Rcvrn* mRNA levels at both points in time (3 days: WT CO vs. KO CO, $p = 0.64$; 7 days: WT CO vs. KO CO, $p = 0.67$; **Figure 5M**). The RT-qPCR results also offered comparable expression levels between the non-ischemic control and ischemic WT groups (3 days: WT CO vs. WT I/R, $p = 0.07$; 7 days: WT CO vs. WT I/R, $p = 0.52$) as well as KO groups (3 days: KO CO vs. KO I/R, $p = 0.62$; 7 days: KO CO vs. KO I/R, $p = 0.84$; **Figure 5N**). Additionally, we observed a similar *Rcvrn* expression between the genotypes 3 days (WT I/R vs. KO I/R; $p = 0.32$) and at 7 days post-ischemia (WT I/R vs. KO I/R, $p = 0.57$; **Figure 5O**).

Our scotopic ERG recordings revealed significantly reduced a-wave amplitudes after ischemia. Since these reduced responses derived from the rod-photoreceptors, this cell type should be investigated more closely. Hence, rhodopsin$^+$ stained area was measured in control and ischemic WT and KO retinae at 3 (**Figures 6A–D,I**) and 7 days after I/R (**Figures 6E–H,J**). Our results indicated a comparable rhodopsin$^+$ staining area at 3 days after ischemia in both genotypes compared to the corresponding control groups (WT CO vs. WT I/R, $p = 0.49$ and KO CO vs. KO I/R, $p = 0.95$; **Figure 6I**). Remarkably, the statistical evaluation of both ischemic groups verified a significantly diminished rhodopsin$^+$ staining area in the WT I/R compared to the KO I/R group ($p = 0.048$). Also, an equal rhodopsin staining was found in both control groups at 7 days after I/R ($p = 0.72$; **Figure 6J**). However, the statistical analyses verified a significant lower rhodopsin immunoreactivity in ischemic WT retinae (WT CO vs. WT I/R, $p = 0.04$). In the KO condition no alterations were detectable at this point in time (KO CO vs. KO I/R, $p = 0.98$).

In addition, rhodopsin protein levels were determined via Western blot analyses at 7 days after ischemia. Therefore, we measured the band intensity of rhodopsin at ∼40 kDa (**Figure 6K**). We observed significantly reduced rhodopsin protein levels in WT I/R compared to both non-ischemic genotypes (WT I/R vs. WT CO, $p = 0.012$ and vs. KO CO, $p = 0.008$; **Figure 6L**). In a direct comparison of both ischemic groups, we noted a significant decrease of rhodopsin in the WT condition ($p < 0.001$). No differences were observed between the KO CO and the KO I/R groups ($p = 0.32$) as well as between the WT CO and KO CO groups ($p = 0.94$).

Finally, we analyzed the *rhodopsin* (*Rho*) expression via RT-qPCR at 3 and 7 days post-ischemia (**Figures 6M–O**). No changes in the *Rho* expression were found between non-ischemic WT and KO retinae at either point in time (3 days: WT CO vs. KO CO, $p = 0.58$; 7 days: WT CO vs. KO CO, $p = 0.54$; **Figure 6M** and **Supplementary Table 2**). A significant decrease of *Rho* mRNA levels was determined in WT I/R compared to WT CO at 3 days (WT CO vs. WT I/R, $p = 0.04$) as well as at 7 days after ischemia (WT CO vs. WT I/R, $p = 0.01$; **Figure 6N**). No significant alterations were seen between control and ischemic KO retinae (3 days: KO CO vs. KO I/R, $p = 0.15$; 7 days: KO CO vs. KO I/R, $p = 0.14$; **Figure 6N**). In a direct comparison of the two ischemic groups,

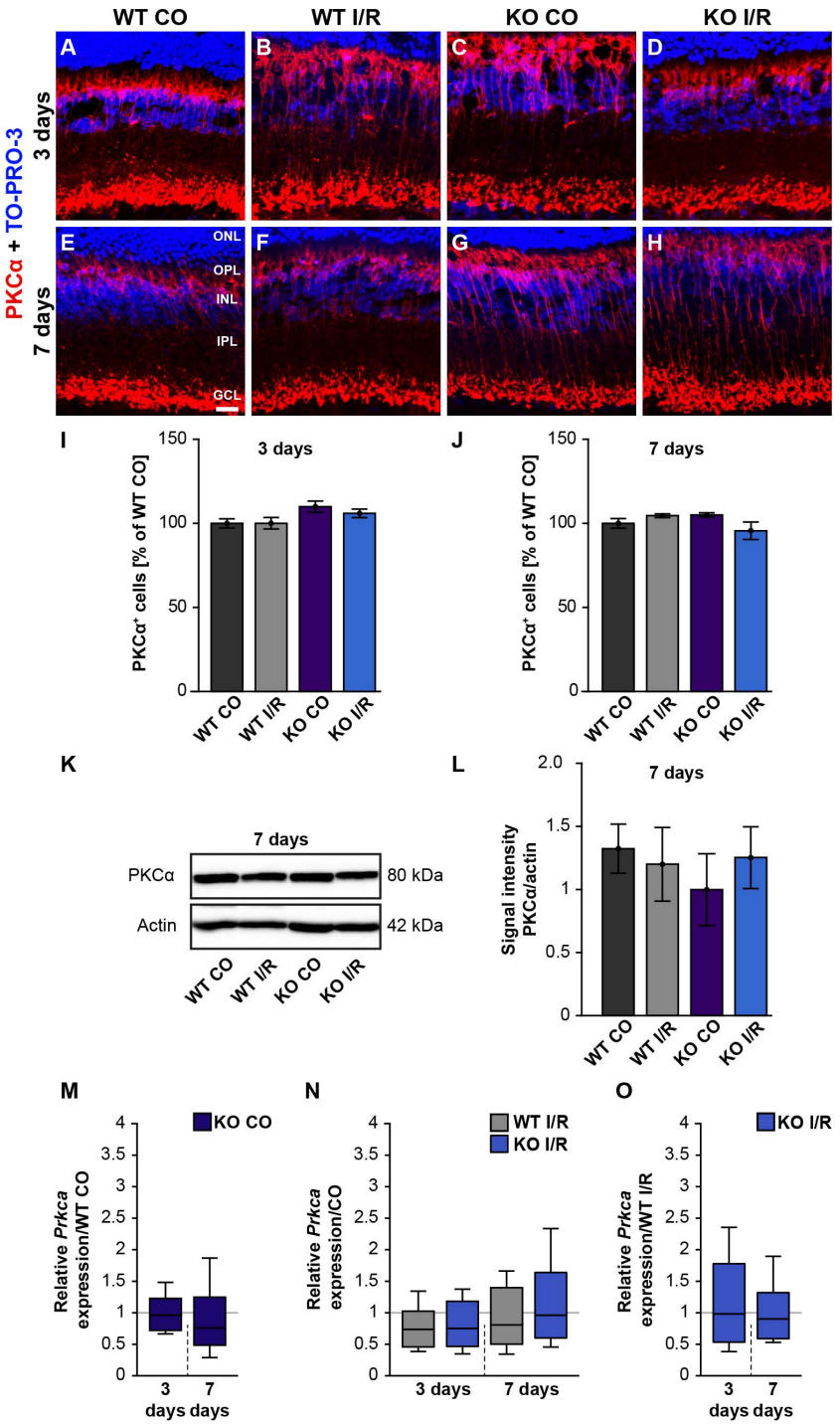

FIGURE 4 | Rod-bipolar cells are not affected early ischemia. **(A–H)** Anti-PKCα was used to label rod-bipolar cells (red) 3 and 7 days post-I/R. TO-PRO-3 (blue) was used as nuclear counterstain. **(I,J)** Countings of PKCα$^+$ cells demonstrated no changes between control and ischemic WT and KO retinae 3 and 7 days post-I/R. The WT CO group was set to 100%. **(K,L)** In line with the immunohistochemical results, comparable protein levels of PKCα were detected via Western blot in all four groups 7 days post-I/R. **(M–O)** RT-qPCR analyses showed an unaltered *Prkca* mRNA expression level in all groups at both points in time after ischemia. Groups were evaluated using two-way ANOVA followed by Tukey's *post hoc* test. Data are indicated as mean ± SEM in panels **(I,J,L)**. For RT-qPCR results, groups were analyzed using the pairwise fixed reallocation and randomization test. Data are shown as median ± quartile ± minimum/maximum in panels **(M–O)**. $p > 0.05$. n = 4–5/group. Scale bar = 20 μm. ONL: outer nuclear layer; OPL: outer plexiform layer; INL: inner nuclear layer; IPL: inner plexiform layer, GCL: ganglion cell layer.

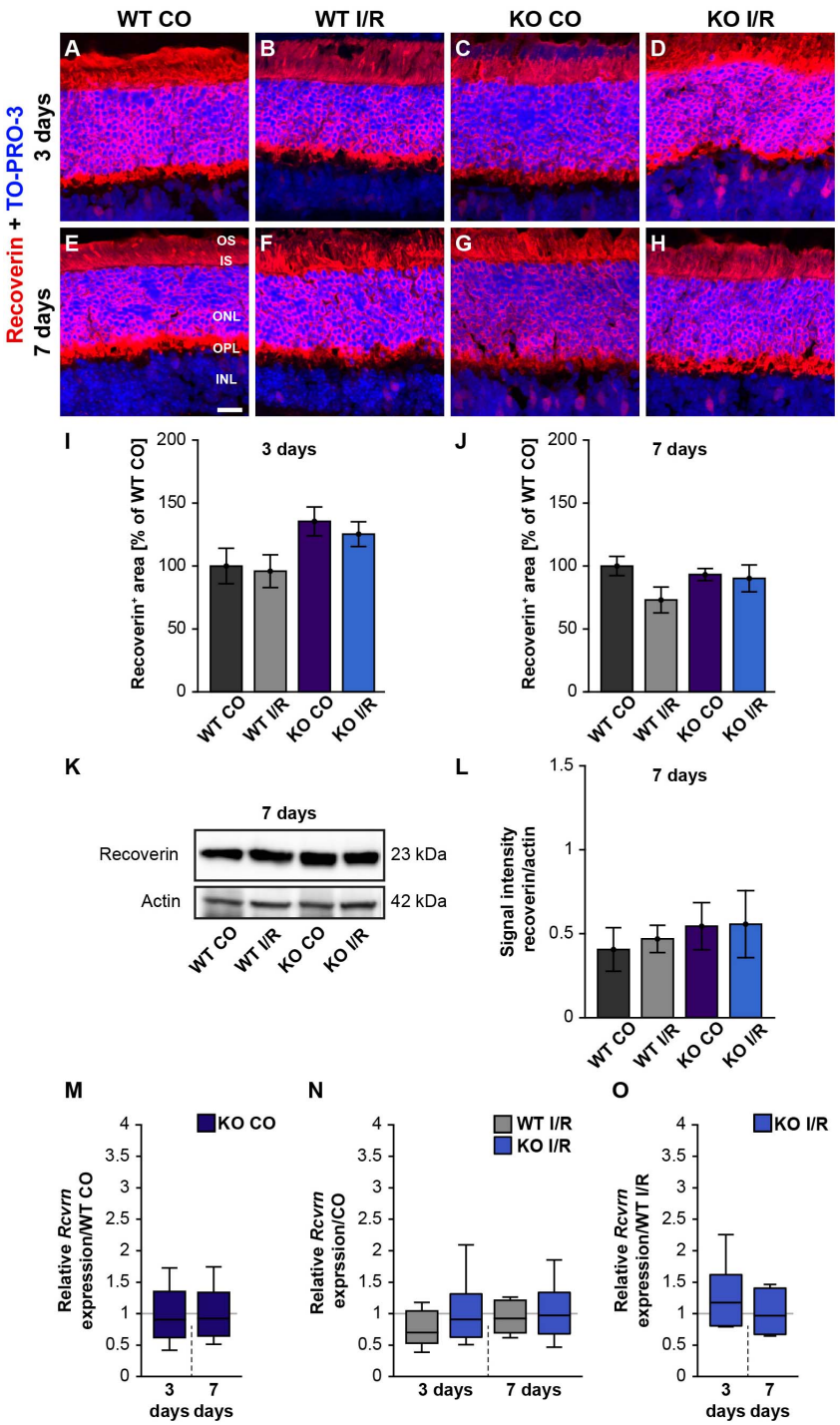

FIGURE 5 | Unaltered recoverin levels in WT and KO mice after ischemia. **(A–H)** Photoreceptors cells were marked with an antibody against recoverin (red) and cell nuclei were labeled with TO-PRO-3 (blue) at 3 and 7 days post-I/R. **(I,J)** Recoverin^{+} staining area was similar in the control and ischemic WT and KO groups at both analyzed points in time. The WT CO group was set to 100%. **(K)** Exemplary Western blots of recoverin at 7 days post-I/R. **(L)** No changes in the recoverin band intensity were observed in both genotypes. **(M)** A comparable *Rcvrn* expression was seen in the non-ischemic WT and KO groups at 3 as well as 7 days post-I/R. **(N)** An equal mRNA level of *Rcvrn* was detected in the ischemic groups when compared to the corresponding control groups. **(O)** In comparison to the WT I/R group, we also observed an unaltered *Rcvrn* expression in the KO I/R group. Groups were analyzed using two-way ANOVA followed by Tukey's *post hoc* test. Data are shown as mean ± SEM in panels **(I,J,L)**. For RT-qPCR analyses, groups were compared using the pairwise fixed reallocation and randomization test. Data are shown as median ± quartile ± minimum/maximum in panels **(M–O)**. $p > 0.05$. n = 4–5/group. Scale bar = 20 μm. OS: outer segments; IS: inner segments; ONL: outer nuclear layer; OPL: outer plexiform layer; INL: inner nuclear layer.

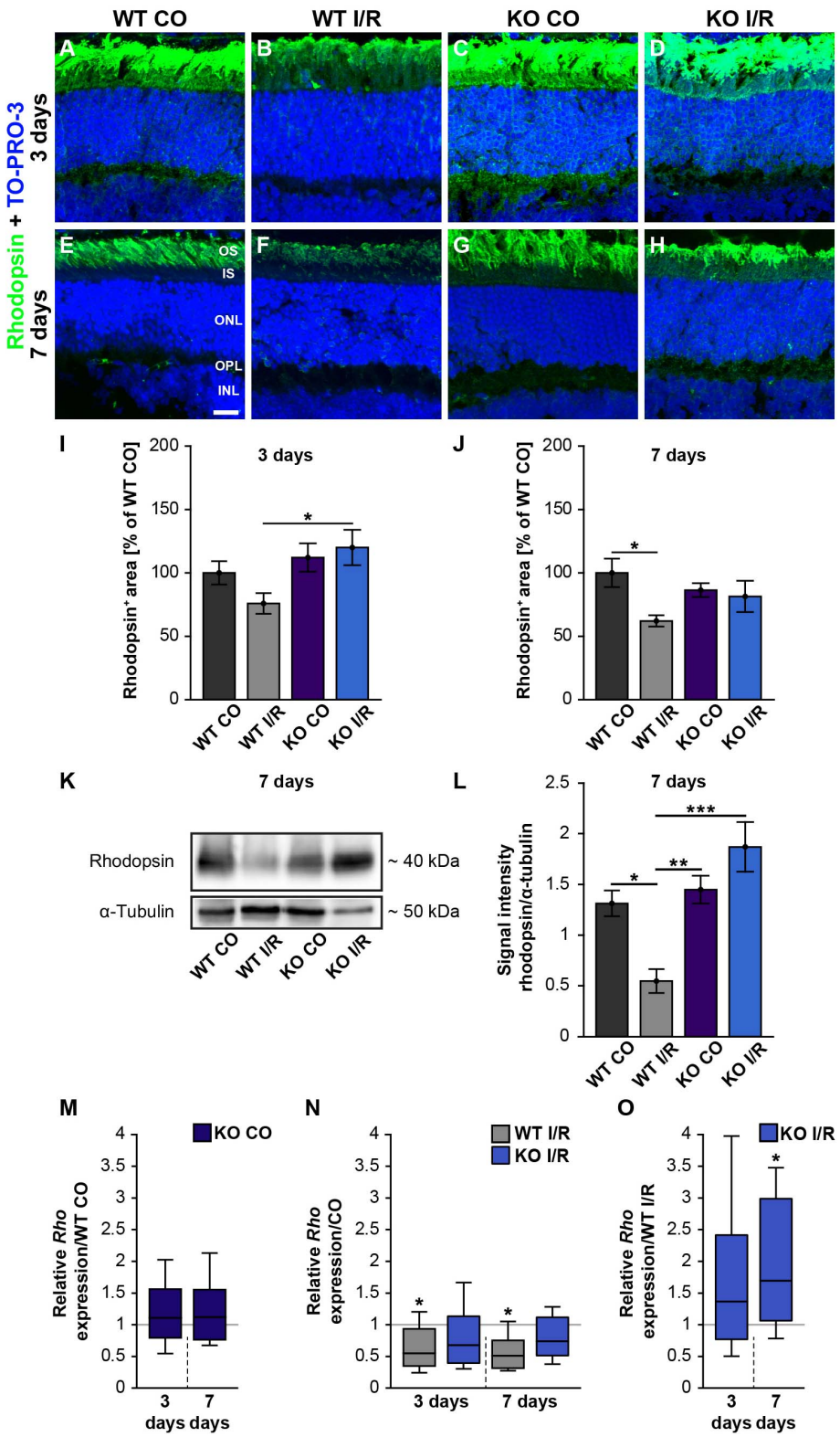

FIGURE 6 | Preservation of rod-photoreceptor cells in the ischemic *Tnc* KO retina. **(A–H)** Rod-photoreceptors were labeled with rhodopsin (green) in control and ischemic WT and KO retinae 3 and 7 days after I/R. TO-PRO-3 (blue) was used as nuclear counterstain. **(I)** At 3 days, a significantly decreased rhodopsin staining area was only noted in the ischemic WT group, but not in the ischemic KO group. Moreover, the rhodopsin staining was significantly increased in the KO I/R group

(Continued)

FIGURE 6 | Continued
when compared to the WT I/R group. **(J)** At 7 days post-I/R, we detected a significant reduction of the rhodopsin-stained area in the WT I/R compared to the WT CO group. However, the KO I/R group showed a comparable rhodopsin staining as the KO CO group. **(K)** Analyses of rhodopsin via Western blot. **(L)** Quantification of band intensity revealed reduced protein levels in the WT I/R group when compared to the other groups at 7 days post-I/R. **(M)** No difference in the *Rho* expression was noted in the KO CO group compared to the WT CO group at both points in time. **(N)** A significant downregulation of the *Rho* mRNA level was seen in the WT I/R group in comparison to the WT CO group at 3 and 7 days post-I/R. **(O)** Interestingly, an upregulation of *Rho* was observed in the KO group compared to the WT group at 7 days post-I/R. Statistics were done with a two-way ANOVA followed by Tukey's *post hoc* test. Data were presented as mean ± SEM in panels **(I,J,L)**. For RT-qPCR results, groups were compared using the pairwise fixed reallocation and randomization test. Data are shown as median ± quartile ± minimum/maximum in panels **(M–O)**. $^{*}p < 0.05$, $^{**}p < 0.01$; $^{***}p < 0.001$. n = 4–5/group. **(I,J)** The WT CO group was set to 100%. Scale bar = 20 μm. OS: outer segments; IS: inner segments; ONL: outer nuclear layer; OPL: outer plexiform layer; INL: inner nuclear layer.

a slightly enhanced *Rho* expression was found in the *Tnc* KO group at day 3 after ischemia (WT I/R vs. KO I/R, $p = 0.33$; **Figure 5O**). Interestingly, at 7 days, the *Rho* level was significantly enhanced in the ischemic KO condition (WT I/R vs. KO I/R, $p = 0.049$).

In order to further validate rod-photoreceptor degeneration, we analyzed the mRNA expression of another rod-photoreceptor marker, namely *rod transducin* [guanine nucleotide binding protein, alpha transducing 1 (*Gnat1*), **Supplementary Table 2** and **Supplementary Figures 4A–C**]. Our analyses showed significantly reduced *Gnat1* expression levels in the WT I/R compared to the WT CO group at 7 days post-I/R (WT CO vs. WT I/R, $p = 0.03$; **Supplementary Figure 4B**). However, in line with the previous findings, no significant changes were observed in the KO CO compared to the KO I/R group or in the other groups ($p = 0.66$; **Supplementary Figures 4A–C**).

To follow the degeneration of photoreceptors more closely, apoptotic cells were labeled with an antibody directed against activated caspase 3 (**Supplementary Figures 5A–E**). In comparison to the CO groups, we found a significantly higher number of activated caspase 3^{+} cells in the ONL of both ischemic groups (WT CO vs. WT I/R, $p < 0.001$; KO CO vs. KO I/R, $p < 0.001$). However, a reduced number of apoptotic cells was noted in the ischemic KO compared to the ischemic WT group (WT I/R vs. KO I/R, $p = 0.006$).

In sum, our analyses revealed rod-photoreceptors damage after retinal ischemia. However, compared to the KO retina, a more pronounced damage was observed in the WT retina, indicating a better rod-photoreceptor outcome in the ischemic *Tnc* KO retina. These results suggest that the loss of Tnc not only partially preserves the function of rod-photoreceptors, but also improves their survival.

Retinal Ischemia Impacts Glutamatergic Signaling

Due to our findings of the impaired structural integrity of the OPL after ischemia and the OPL-associated expression of Tnc, we next focused on possible synaptic changes in the WT and KO retina. Previously, it was described that L-type voltage-gated calcium channels (LTCCs)-dependent synaptic plasticity is impaired in the hippocampus of Tnc deficient mice (Evers et al., 2002). Cav1.4 is a major LTCC at the pre-synaptic terminals of photoreceptors. It is crucial for the release of neurotransmitters (Strom et al., 1998) as well as for the formation of ribbon synapses, which constitute important contact points between rod-photoreceptors and bipolar cells (Liu X. et al., 2013). Additionally, Laird et al. (2019) noted that Cav1.4 expression is necessary for synaptic terminal development of rod-photoreceptors. Based on these reports and the initial results of our study, we hypothesized that ischemia and Tnc loss affect photoreceptor ribbon synapses. Therefore, we examined the mRNA expression of the *Cacna1f* gene, encoding the α1F calcium channel subunit of Cav1.4 (Morgans et al., 2005), in control and ischemic WT and KO retinae by RT-qPCR analyses (**Figures 7A–C** and **Supplementary Table 2**). Our investigations revealed no notable change in the *Cacna1f* expression level between both control groups (WT CO vs. KO CO, $p = 0.84$; **Figure 7A**). No alterations were observed between the ischemic and control groups (WT CO vs. WT I/R, $p = 0.72$; KO CO vs. KO I/R, $p = 0.84$; **Figure 7B**). Also, a comparable mRNA level of *Cacna1f* was found in both ischemic groups (WT I/R vs. KO I/R, $p = 0.99$). Additionally, we analyzed protein levels of the synaptic ribbon component ribeye [C-terminal binding protein 2 (CtBP2)] (Schmitz et al., 2000) by Western blot analyses (**Figures 7D,E**). CtBP2 levels were equivalent in both control groups (WT CO vs. KO CO, $p = 0.99$) as well as in both ischemic groups (WT I/R vs. KO I/R, $p = 0.99$; **Figure 7E**). Also, the comparison of the control and ischemic groups (WT CO vs. WT I/R, $p = 0.86$; KO CO vs. KO I/R, $p = 0.60$; **Figure 7E**) revealed very similar CtBP2 protein levels.

Photoreceptors and bipolar cells transfer visual information via the release of excitatory glutamate at ribbon synapses (Brandstatter and Hack, 2001; tom Dieck and Brandstatter, 2006). Previous studies could demonstrate that the vGlut1 is associated with pre-synaptic terminals of photoreceptor and bipolar cells and required for their signaling (Johnson et al., 2003; Sherry et al., 2003; Johnson J. et al., 2007). Interestingly, in comparison to the respected control groups, we noted significantly increased vGlut1 protein levels in both ischemic groups (WT CO vs. WT I/R, $p = 0.01$; KO CO vs. KO I/R, $p = 0.001$; **Figures 7F,G**). Although vGlut1 protein levels were comparable in the WT I/R and KO I/R group (WT I/R vs. KO I/R, $p = 0.98$).

In sum, these results suggest that glutamatergic signaling is impaired after retinal ischemia but not different in the retina of WT and KO mice.

DISCUSSION

In the present study, we used a KO mouse I/R model to analyze the functional importance of the ECM component Tnc

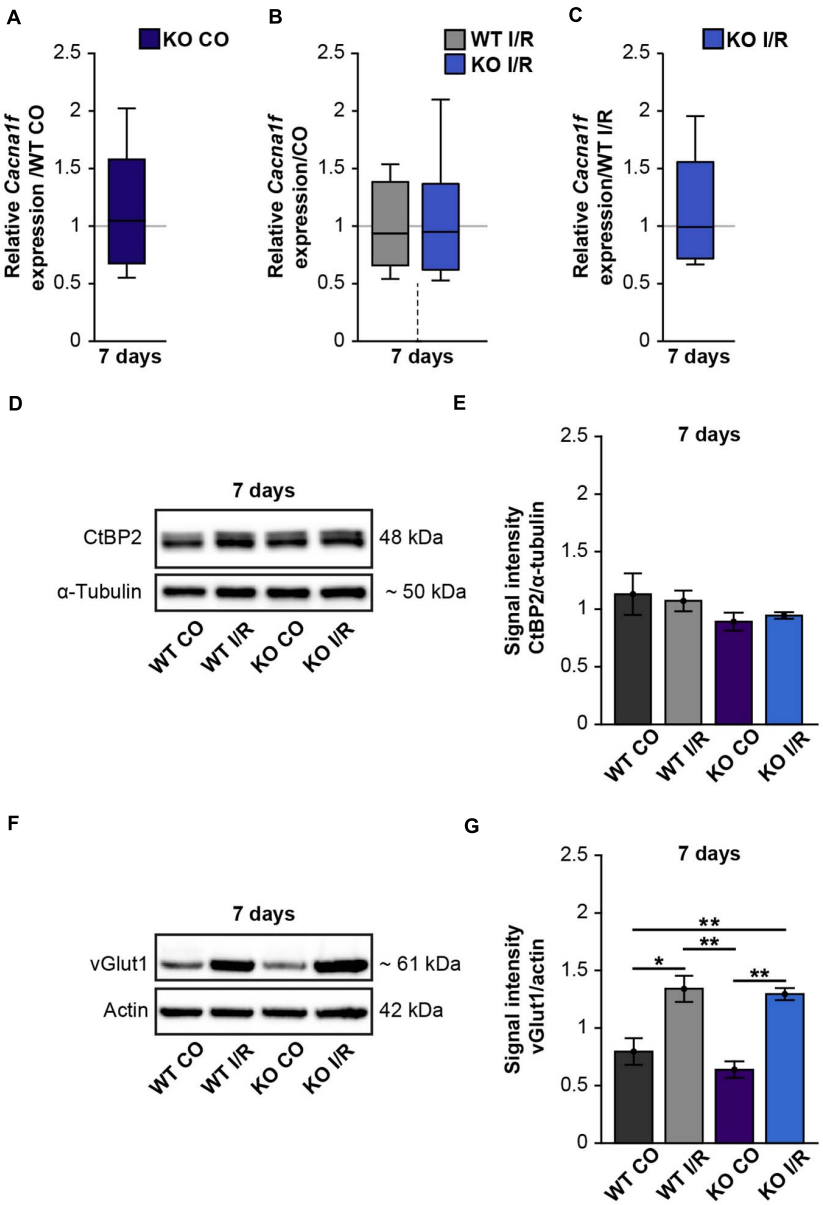

FIGURE 7 | Enhanced protein levels of the pre-synaptic marker vGlut1 after retinal ischemia. **(A–C)** RT-qPCR analyses of the synaptic marker *Cacna1f* at 7 days after ischemia. **(A)** Equivalent mRNA expression levels were observed for *Cacnaf1* in the KO CO compared to the WT CO group. **(B)** Similar levels of *Cacnaf1* were measured in the WT I/R compared to the WT CO group as well as in the KO I/R compared to the KO CO group. **(C)** *Cacnaf1* mRNA expression levels were also found to be comparable in both ischemic groups. **(D)** Representative Western blots of CtBP2/ribeye at 7 days post-I/R. **(E)** Quantification of the band intensity revealed similar CtBP2 protein levels in the retina of all groups. **(F)** Exemplary Western blots of vGlut1 at 7 days post-I/R. **(G)** Quantification of the band intensity showed significantly elevated vGlut1 protein levels in the retina of both ischemic groups. For Western blot analyses, groups were analyzed using two-way ANOVA followed by Tukey's *post hoc* test. These data are displayed as mean ± SEM in panels **(E,G)**. For RT-qPCR analyses, groups were analyzed using the pairwise fixed reallocation and randomization test and data in panels **(A–C)** are shown as median ± quartile ± minimum/maximum. $^{*}p < 0.05$; $^{**}p < 0.01$. n = 3–4/group.

in retinal neurodegeneration. Previously, Tnc dysregulation has been described not only after cerebral, but also hepatic and myocardial ischemic degeneration (Lu et al., 2003; Taki et al., 2010, 2015; Kuriyama et al., 2011). However, the role of Tnc in retinal ischemia is not yet understood.

Regarding the expression pattern, we found that extracellular Tnc associates with horizontal and amacrine cells and observed a synaptic layer-associated immunoreactivity in the OPL and IPL, even after ischemia. Additionally, we identified Tnc and GFAP co-expressing astrocytes in the ischemic retina, indicating that also reactive astrocytes are a cellular source of this ECM component. These observations are consistent with previous reports on the Tnc expression pattern in the healthy chick and mouse

retina (Bartsch et al., 1995; D'Alessandri et al., 1995; Reinhard et al., 2015).

We noted an increased Tnc immunoreactivity 3 days after I/R, but interestingly there was a significant reduction after 7 days. Via Western blot analyses, we were able to determine a specific increase of larger Tnc isoforms (>250 kDa). However, we could not detect any significant differences regarding Tnc protein levels 7 days post-I/R, indicating that protein levels drop back to a baseline level shortly after injury. Enhanced Tnc levels were reported in subarachnoid hemorrhage (Shiba et al., 2014; Suzuki et al., 2020), ischemic brain injury (Manrique-Castano et al., 2020) and acute cortical laser lesion (Roll et al., 2012). In the lesioned brain, an increase of relative *Tnc* expression could only be detected for a short time, while enhanced protein levels were found 3 and 7 days post-lesion, suggesting that high Tnc protein levels exceeded the brief upregulation seen on mRNA level (Roll et al., 2020). Furthermore, a temporally Tnc regulation was observed under retinal degenerative conditions. A significant increase of Tnc immunoreactivity was found in an experimental autoimmune glaucoma model at 7 and 14 days, whereas no differences were observed at a later point in time (Reinehr et al., 2016). In an IOP-dependent glaucoma model, however, we recently observed increased Tnc levels a few weeks after IOP elevation (Reinhard et al., 2021), which suggests that Tnc expression depends not only on the time, but also on the type of retinal damage. In an I/R rat model, we detected diminished levels of Tnc at 21 days post-ischemia. In this model, the loss of Tnc expressing amacrine and horizontal cells as a result of progressive ischemic damage could explain the Tnc dysregulation (Reinhard et al., 2017a). This might also correspond to our findings of a decreased Tnc immunoreactivity at 7 days after ischemia.

Based on our findings regarding equal mRNA and time-dependent altered protein levels, we propose that Tnc dysregulation under ischemic conditions takes place on translational or post-translation level. Our Western blot analyses indicate increased levels of larger Tnc isoforms after ischemia. *Vice versa* shorter isoforms were found unaltered. So far, 28 Tnc isoforms have been identified in the CNS (Joester and Faissner, 1999; von Holst et al., 2007). Previous findings revealed that the shorter Tnc variants are preferentially expressed in the healthy CNS, while larger forms dominate after cortical lesion. Here, a strong upregulation of the alternative spliced fibronectin III domains B and D was described 2–4 days post-lesion (Dobbertin et al., 2010). In a future perspective, it would be therefore interesting to perform comprehensive mRNA as well as protein analyses on specific Tnc isoforms, in particular after ischemic damage.

The main focus of our study was to comparatively explore retinal function and rod-bipolar/photoreceptor cell degeneration in WT and *Tnc* KO mice after ischemic insult. Previous studies already described that the functional restriction increased over time in ischemia rat models with an ischemia duration between 30 and 90 min (Jehle et al., 2008; Schmid et al., 2014; Palmhof et al., 2019). However, Zhao et al. (2013) could show that a moderate ischemia of only 17 min does not affect photoreceptors. To investigate functional deficits in the retina of our model, we performed ERG recordings 7 days post-ischemia. Here, mice underwent 45 min of I/R. Under scotopic conditions, a-wave amplitudes were significantly reduced after ischemia, indicating a diminished rod-photoreceptor response in both genotypes. Although not statistically significant, we observed a trend toward increased a-wave amplitudes in the ischemic KO compared to the WT group. This protective effect was even more pronounced in regard to the b-wave amplitudes, which display the response of rod-bipolar cells. In accordance with our results, it is well documented that the b-wave in particular is very sensitive to ischemic retinal injury (Osborne et al., 2004). We observed a significant b-wave amplitude decrease for all light flash luminances in the ischemic WT group compared to both non-ischemic control groups. Remarkably, a better outcome of the b-wave responses was observed after I/R in KO mice compared to the control groups. The ischemia-induced decrease was statistically significant in the WT compared to the KO. Overall, our analyses revealed that retinal function was clearly more affected in the presence of Tnc. Therefore, we suggest that the absence of Tnc may have a protective effect on rod-photoreceptors and rod-bipolar cells after ischemic damage in the retina. Reduced a-wave amplitudes indicate an impairment of rod-mediated photoreceptor function post-I/R.

In our study, we found unaltered recoverin levels, but a time-dependent decrease of rhodopsin mRNA and protein levels in the WT I/R group. As previously described, KO of rhodopsin abolished rod-driven electrophysical activity (Xiao et al., 2019). Moreover, a connection between altered rhodopsin levels and neurodegenerative processes as well as the use of rhodopsin as a potential early biomarker have been reviewed previously by Lenahan et al. (2020). In contrast, although *Rho* mRNA levels were also observed significantly lower, an unaltered rhodopsin immunoreactivity was found in ischemic rat models (Zhao et al., 2013; Palmhof et al., 2019). This indicates that the degeneration of rod-photoreceptor cells severely depends on the experimental conditions. However, our results demonstrate that the loss of Tnc prevents rhodopsin/*Rho* as well as *Gnat1* downregulation in rod-photoreceptor cells. This result is also reflected by the better a-wave amplitude outcome and a lower number of apoptotic cells in the ONL of ischemic *Tnc* KO mice. Our ERG recordings also revealed a significant reduction of b-wave amplitudes, indicating that rod-bipolar cells could also be affected after ischemia. However, we observed no change in the number of PKCα^+ rod-bipolar cells. This is in line with results of a previous study, which revealed no rod-bipolar cell loss after retinal ischemia in rats (Palmhof et al., 2019). Based on these overall findings, we propose that rod-bipolar cells are more robust against retinal ischemia on a structural level than rod-photoreceptors, but not on a functional level.

We also investigated the retinal structure by measuring layer thickness. Here, we found that the OPL was particularly diminished even 3 days post-I/R. It is well known that ischemia-induced damage is associated with a disorganization as well

as time-dependent thinning of retinal layers (Palmhof et al., 2019). We observed retinal thinning in WT I/R mice after 3 and 7 days. Although compared to the KO CO group, retinal thinning was not observed in the KO I/R group until 7 days. Therefore, our H&E stainings point to a time-delayed damage of the retinal layers in *Tnc* KO mice after I/R. Only a moderate thinning of the ONL was observed at 7 days after I/R. However, based on the increased number of apoptotic cells that we observed in the ONL, we expect a more progressive thinning at later points in time. As stated, we noted a thinning of the OPL. Thus, we speculate that this thinning could be caused by synaptic remodeling, which might precede the ONL thinning.

Tenascin-C has been reported to be implicated in synapse development and synaptic plasticity (Evers et al., 2002; Heikkinen et al., 2014; Gottschling et al., 2019). Based on these reports and due to our finding of reduced a- and b-wave amplitudes and severe reduction of the OPL after ischemia, we also examined the signal transfer from photoreceptors to bipolar cells by analyzing the expression of various synaptic proteins. Our analyses of *Cacna1f* and CtBP2 revealed comparable mRNA/protein levels in the WT and KO control and ischemic groups. Thus, these findings suggest that neither ischemia nor the loss of Tnc has a huge influence on photoreceptor/bipolar cell ribbon synapses. However, in this regard, immunohistochemical as well as ultrastructural analyses of ribbon synapses after ischemia and Tnc loss are necessary to explore a possible impact.

In our study, we observed a significant upregulation of vGlut1 protein levels in the ischemic WT and KO retinae. Since vGlut1 is predominantly expressed in the pre-synaptic terminals of photoreceptor and bipolar cells and important for signaling transmission (Johnson et al., 2003; Sherry et al., 2003; Johnson J. et al., 2007), elevated vGlut1 levels after ischemia strongly suggest an impaired glutamatergic photoreceptor-bipolar cell signaling. In retinal ischemia, abnormalities in the glutamate metabolism, including a dysregulation of various glutamate transporters, have been previously described (Bringmann et al., 2013; Ishikawa, 2013). However, *vGlut1* expression level alterations were not reported in a mouse model of central retinal artery occlusion and retinal ischemia 1 day after damage induction (Michalski et al., 2013). This discrepancy could again probably be explained by the examined time points as well as experimental conditions of the ischemic insult. VGlut1 plays an important role in packaging excitatory glutamate for synaptic release. Therefore, elevated vGlut1 levels could also be associated with glutamate excitotoxicity and apoptosis, which we also observed in our I/R model. Increased vGlut1 protein levels may also play a neuroprotective role, as a controlled excitatory glutamate storage is crucial to avoid neurotoxicity and to provide a normal signaling transfer from e.g., photoreceptors to bipolar cells (Yang, 2004; Omote et al., 2011; Liu K. et al., 2013). Additionally, elevated vGlut1 levels may point to plasticity by means of neuronal circuits reconstruction after ischemic insult (Kim et al., 2005). Previously, analyses of *vGlut1* KO mice could show that vGlut1 is required for synaptic signaling from photoreceptors to retinal output neurons but not for intrinsic visual functions (Johnson J. et al., 2007). ERG recordings in *vGlut1* KO mice revealed that no photoreceptor-driven visual signals are transmitted to ON bipolar cells. Thus, an overall imbalance of vGlut1 levels could also explain the impaired a- and b-wave amplitudes that we observed after ischemia. Importantly, we did not find any significant differences between ischemic WT and KO mice, which might indicate that the increase of vGlut1 is rather related to the ischemic damage than the Tnc deficiency.

CONCLUSION

Our results revealed an early, but short-term, upregulation of Tnc in the ischemic retina. Most importantly, our data indicate that ischemic *Tnc* KO mice have a better outcome in regard to retinal functionality and integrity as well as survival of rod-photoreceptor cells. Furthermore, increased vGlut1 levels after ischemia could point to an impaired glutamatergic photoreceptor-bipolar cell signaling and excitotoxicity. In summary, our findings suggest that the induction of the ECM glycoprotein Tnc contributes to ischemia-induced degenerative processes in the retina, possibly also by remodeling of synaptic sites. A better understanding of ECM remodeling and synaptic changes associated with retinal ischemia could be useful for the development of novel neuroprotective strategies.

DATA AVAILABILITY STATEMENT

The original contributions presented in the study are included in the article/**Supplementary Material**, further inquiries can be directed to the corresponding author/s.

ETHICS STATEMENT

Animal experiments adhered to the "Association for Research and Vision and Ophthalmology (ARVO)" Statement for the Use of Animals in Ophthalmic and Vision Research. All animal care and experimental procedures were conducted in accordance with the EU animal welfare protection laws and regulations and were approved by the Ethics Committee of the state North Rhine-Westphalia, Germany (AZ 81-02.04.2018.A194). The study was supervised by the animal welfare commissioner of the Ruhr-University Bochum.

AUTHOR CONTRIBUTIONS

SW and JR wrote the manuscript. SW, AY, CP, AM-B, NW, and JR performed the experiments. SW, AY, CP, AM-B, and JR analyzed the data. SJ revised the manuscript. JR designed the study. All authors read and approved the final manuscript.

FUNDING

This research was funded by MERCUR (An-2017-0029 to JR). SW was supported by the Konrad Adenauer Foundation (200520593).

ACKNOWLEDGMENTS

The authors would like to thank Andreas Faissner for expert comments during the project phase. We thank Stephanie Chun, Anja Coenen, Sebastian Hildebrandt, Sabine Kindermann, Franziska Mennes, and Marion Voelzkow for excellent technical assistance. We acknowledge support of the DFG Open Access Publication Funds of the Ruhr-University Bochum.

SUPPLEMENTARY MATERIAL

The Supplementary Material for this article can be found online at: https://www.frontiersin.org/articles/10.3389/fnins.2021.642176/full#supplementary-material

REFERENCES

Bartsch, S., Husmann, K., Schachner, M., and Bartsch, U. (1995). The extracellular matrix molecule tenascin: expression in the developing chick retinotectal system and substrate properties for retinal ganglion cell neurites in vitro. *Eur. J. Neurosci.* 7, 907–916. doi: 10.1111/j.1460-9568.1995.tb01078.x

Bartsch, U., Bartsch, S., Dorries, U., and Schachner, M. (1992). Immunohistological Localization of Tenascin in the Developing and Lesioned Adult Mouse Optic Nerve. *Eur. J. Neurosci.* 4, 338–352. doi: 10.1111/j.1460-9568.1992.tb00881.x

Belforte, N., Sande, P. H., De Zavalia, N., Fernandez, D. C., Silberman, D. M., Chianelli, M. S., et al. (2011). Ischemic tolerance protects the rat retina from glaucomatous damage. *PLoS One* 6:e23763. doi: 10.1371/journal.pone.0023763

Besser, M., Jagatheaswaran, M., Reinhard, J., Schaffelke, P., and Faissner, A. (2012). Tenascin C regulates proliferation and differentiation processes during embryonic retinogenesis and modulates the de-differentiation capacity of Muller glia by influencing growth factor responsiveness and the extracellular matrix compartment. *Dev. Biol.* 369, 163–176. doi: 10.1016/j.ydbio.2012.05.020

Brandstatter, J. H., and Hack, I. (2001). Localization of glutamate receptors at a complex synapse. The mammalian photoreceptor synapse. *Cell Tissue Res.* 303, 1–14. doi: 10.1007/s004410000304

Bringmann, A., Grosche, A., Pannicke, T., and Reichenbach, A. (2013). GABA and Glutamate Uptake and Metabolism in Retinal Glial (Muller) Cells. *Front. Endocrinol.* 4:48. doi: 10.3389/fendo.2013.00048

Brodkey, J. A., Laywell, E. D., O'brien, T. F., Faissner, A., Stefansson, K., Dorries, H. U., et al. (1995). Focal brain injury and upregulation of a developmentally regulated extracellular matrix protein. *J. Neurosurg.* 82, 106–112. doi: 10.3171/jns.1995.82.1.0106

Campochiaro, P. A. (2015). Molecular pathogenesis of retinal and choroidal vascular diseases. *Prog. Retin. Eye Res.* 49, 67–81. doi: 10.1016/j.preteyeres.2015.06.002

D'Alessandri, L., Ranscht, B., Winterhalter, K. H., and Vaughan, L. (1995). Contactin/F11 and tenascin-C co-expression in the chick retina correlates with formation of the synaptic plexiform layers. *Curr. Eye Res.* 14, 911–926. doi: 10.3109/02713689508995131

Dobbertin, A., Czvitkovich, S., Theocharidis, U., Garwood, J., Andrews, M. R., Properzi, F., et al. (2010). Analysis of combinatorial variability reveals selective accumulation of the fibronectin type III domains B and D of tenascin-C in injured brain. *Exp. Neurol.* 225, 60–73. doi: 10.1016/j.expneurol.2010.04.019

Evers, M. R., Salmen, B., Bukalo, O., Rollenhagen, A., Bosl, M. R., Morellini, F., et al. (2002). Impairment of L-type Ca2+ channel-dependent forms of hippocampal synaptic plasticity in mice deficient in the extracellular matrix glycoprotein tenascin-C. *J. Neurosci.* 22, 7177–7194. doi: 10.1523/jneurosci.22-16-07177.2002

Faissner, A., and Kruse, J. (1990). J1/tenascin is a repulsive substrate for central nervous system neurons. *Neuron* 5, 627–637. doi: 10.1016/0896-6273(90)90217-4

Faissner, A., Roll, L., and Theocharidis, U. (2017). Tenascin-C in the matrisome of neural stem and progenitor cells. *Mol. Cell Neurosci.* 81, 22–31. doi: 10.1016/j.mcn.2016.11.003

Forsberg, E., Hirsch, E., Frohlich, L., Meyer, M., Ekblom, P., Aszodi, A., et al. (1996). Skin wounds and severed nerves heal normally in mice lacking tenascin-C. *Proc. Natl. Acad. Sci. U. S. A.* 93, 6594–6599. doi: 10.1073/pnas.93.13.6594

Gottschling, C., Wegrzyn, D., Denecke, B., and Faissner, A. (2019). Elimination of the four extracellular matrix molecules tenascin-C, tenascin-R, brevican and neurocan alters the ratio of excitatory and inhibitory synapses. *Sci. Rep.* 9:13939.

Hartsock, M. J., Cho, H., Wu, L., Chen, W. J., Gong, J., and Duh, E. J. (2016). A Mouse Model of Retinal Ischemia-Reperfusion Injury Through Elevation of Intraocular Pressure. *J. Vis. Exp.* 113:54065.

Hayreh, S. S. (2005). Prevalent misconceptions about acute retinal vascular occlusive disorders. *Prog. Retin. Eye Res.* 24, 493–519. doi: 10.1016/j.preteyeres.2004.12.001

Heikkinen, A., Pihlajaniemi, T., Faissner, A., and Yuzaki, M. (2014). Neural ECM and synaptogenesis. *Prog. Brain Res.* 214, 29–51. doi: 10.1016/b978-0-444-63486-3.00002-5

Hu, T., You, Q., Chen, D., Tong, J., Shang, L., Luo, J., et al. (2016). Inhibiting Matrix Metalloproteinase 3 Ameliorates Neuronal Loss in the Ganglion Cell Layer of Rats in Retinal Ischemia/Reperfusion. *Neurochem. Res.* 41, 1107–1118. doi: 10.1007/s11064-015-1800-1

Husmann, K., Faissner, A., and Schachner, M. (1992). Tenascin promotes cerebellar granule cell migration and neurite outgrowth by different domains in the fibronectin type III repeats. *J. Cell Biol.* 116, 1475–1486. doi: 10.1083/jcb.116.6.1475

Ishikawa, M. (2013). Abnormalities in glutamate metabolism and excitotoxicity in the retinal diseases. *Scientifica* 2013:528940.

Jehle, T., Wingert, K., Dimitriu, C., Meschede, W., Lasseck, J., Bach, M., et al. (2008). Quantification of ischemic damage in the rat retina: a comparative study using evoked potentials, electroretinography, and histology. *Invest. Ophthalmol. Vis. Sci.* 49, 1056–1064. doi: 10.1167/iovs.07-1050

Joachim, S. C., Jehle, T., Boehm, N., Gramlich, O. W., Lagreze, W. A., Pfeiffer, N., et al. (2012). Effect of ischemia duration on autoantibody response in rats undergoing retinal ischemia-reperfusion. *Ophthalmic Res.* 48, 67–74. doi: 10.1159/000335965

Joachim, S. C., Renner, M., Reinhard, J., Theiss, C., May, C., Lohmann, S., et al. (2017). Protective effects on the retina after ranibizumab treatment in an ischemia model. *PLoS One* 12:e0182407. doi: 10.1371/journal.pone.0182407

Joester, A., and Faissner, A. (1999). Evidence for combinatorial variability of tenascin-C isoforms and developmental regulation in the mouse central nervous system. *J. Biol. Chem.* 274, 17144–17151. doi: 10.1074/jbc.274.24.17144

Johnson, E. C., Jia, L., Cepurna, W. O., Doser, T. A., and Morrison, J. C. (2007). Global changes in optic nerve head gene expression after exposure to elevated intraocular pressure in a rat glaucoma model. *Invest. Ophthalmol. Vis. Sci.* 48, 3161–3177. doi: 10.1167/iovs.06-1282

Johnson, J., Fremeau, R. T. Jr., Duncan, J. L., Renteria, R. C., Yang, H., Hua, Z., et al. (2007). Vesicular glutamate transporter 1 is required for photoreceptor synaptic signaling but not for intrinsic visual functions. *J. Neurosci.* 27, 7245–7255. doi: 10.1523/jneurosci.0815-07.2007

Johnson, J., Tian, N., Caywood, M. S., Reimer, R. J., Edwards, R. H., and Copenhagen, D. R. (2003). Vesicular neurotransmitter transporter expression in developing postnatal rodent retina: GABA and glycine precede glutamate. *J. Neurosci.* 23, 518–529. doi: 10.1523/jneurosci.23-02-00518.2003

Kaur, C., Foulds, W. S., and Ling, E. A. (2008). Hypoxia-ischemia and retinal ganglion cell damage. *Clin. Ophthalmol.* 2, 879–889. doi: 10.2147/opth.s3361

Kim, D. S., Kwak, S. E., Kim, J. E., Won, M. H., Choi, H. C., Song, H. K., et al. (2005). Bilateral enhancement of excitation via up-regulation of vesicular glutamate transporter subtype 1, not subtype 2, immunoreactivity in the unilateral hypoxic epilepsy model. Brain Res. 1055, 122–130. doi: 10.1016/j.brainres.2005.06.081

Klausmeyer, A., Garwood, J., and Faissner, A. (2007). Differential expression of phosphacan/RPTPbeta isoforms in the developing mouse visual system. *J. Comp. Neurol.* 504, 659–679. doi: 10.1002/cne.21479

Kuriyama, N., Duarte, S., Hamada, T., Busuttil, R. W., and Coito, A. J. (2011). Tenascin-C: a novel mediator of hepatic ischemia and reperfusion injury. *Hepatology* 54, 2125–2136. doi: 10.1002/hep.24639

Kwok, J. C., Dick, G., Wang, D., and Fawcett, J. W. (2011). Extracellular matrix and perineuronal nets in CNS repair. *Dev. Neurobiol.* 71, 1073–1089. doi: 10.1002/dneu.20974

Laird, J. G., Gardner, S. H., Kopel, A. J., Kerov, V., Lee, A., and Baker, S. A. (2019). Rescue of Rod Synapses by Induction of Cav Alpha 1F in the Mature Cav1.4 Knock-Out Mouse Retina. *Invest. Ophthalmol. Vis. Sci.* 60, 3150–3161. doi: 10.1167/iovs.19-27226

Lenahan, C., Sanghavi, R., Huang, L., and Zhang, J. H. (2020). Rhodopsin: a Potential Biomarker for Neurodegenerative Diseases. *Front. Neurosci.* 14:326. doi: 10.3389/fnins.2020.00326

Liu, K., Wang, Y., Yin, Z., Weng, C., and Zeng, Y. (2013). Changes in glutamate homeostasis cause retinal degeneration in Royal College of Surgeons rats. *Int. J. Mol. Med.* 31, 1075–1080. doi: 10.3892/ijmm.2013.1297

Liu, X., Kerov, V., Haeseleer, F., Majumder, A., Artemyev, N., Baker, S. A., et al. (2013). Dysregulation of Ca(v)1.4 channels disrupts the maturation of photoreceptor synaptic ribbons in congenital stationary night blindness type 2. *Channels* 7, 514–523. doi: 10.4161/chan.26376

Liu, Y., McDowell, C. M., Zhang, Z., Tebow, H. E., Wordinger, R. J., and Clark, A. F. (2014). Monitoring retinal morphologic and functional changes in mice following optic nerve crush. *Invest. Ophthalmol. Vis. Sci.* 55, 3766–3774. doi: 10.1167/iovs.14-13895

Lu, A., Tang, Y., Ran, R., Clark, J. F., Aronow, B. J., and Sharp, F. R. (2003). Genomics of the periinfarction cortex after focal cerebral ischemia. *J. Cereb. Blood Flow Metab.* 23, 786–810. doi: 10.1097/01.wcb.0000062340.80057.06

Manrique-Castano, D., Dzyubenko, E., Borbor, M., Vasileiadou, P., Kleinschnitz, C., Roll, L., et al. (2020). Tenascin-C preserves microglia surveillance and restricts leukocyte and, more specifically, T cell infiltration of the ischemic brain. *Brain Behav. Immun.* 91, 639–648. doi: 10.1016/j.bbi.2020.10.016

Michalski, D., Hartig, W., Krugel, K., Edwards, R. H., Boddener, M., Bohme, L., et al. (2013). Region-specific expression of vesicular glutamate and GABA transporters under various ischaemic conditions in mouse forebrain and retina. *Neuroscience* 231, 328–344. doi: 10.1016/j.neuroscience.2012.11.046

Minhas, G., Morishita, R., and Anand, A. (2012). Preclinical models to investigate retinal ischemia: advances and drawbacks. *Front. Neurol.* 3:75. doi: 10.3389/fneur.2012.00075

Morgans, C. W., Bayley, P. R., Oesch, N. W., Ren, G., Akileswaran, L., and Taylor, W. R. (2005). Photoreceptor calcium channels: insights from night blindness. *Vis. Neurosci.* 22, 561–568. doi: 10.1017/s0952523805225038

Omote, H., Miyaji, T., Juge, N., and Moriyama, Y. (2011). Vesicular neurotransmitter transporter: bioenergetics and regulation of glutamate transport. *Biochemistry* 50, 5558–5565. doi: 10.1021/bi200567k

Osborne, N. N., Casson, R. J., Wood, J. P., Chidlow, G., Graham, M., and Melena, J. (2004). Retinal ischemia: mechanisms of damage and potential therapeutic strategies. *Prog. Retin. Eye Res.* 23, 91–147. doi: 10.1016/j.preteyeres.2003.12.001

Palmhof, M., Frank, V., Rappard, P., Kortenhorn, E., Demuth, J., Biert, N., et al. (2019). From Ganglion Cell to Photoreceptor Layer: timeline of Deterioration in a Rat Ischemia/Reperfusion Model. *Front. Cell Neurosci.* 13:174. doi: 10.3389/fncel.2019.00174

Pearson, C. S., Solano, A. G., Tilve, S. M., Mencio, C. P., Martin, K. R., and Geller, H. M. (2020). Spatiotemporal distribution of chondroitin sulfate proteoglycans after optic nerve injury in rodents. *Exp. Eye Res.* 190:107859. doi: 10.1016/j.exer.2019.107859

Pena, J. D., Varela, H. J., Ricard, C. S., and Hernandez, M. R. (1999). Enhanced tenascin expression associated with reactive astrocytes in human optic nerve heads with primary open angle glaucoma. *Exp. Eye Res.* 68, 29–40. doi: 10.1006/exer.1998.0577

Reinehr, S., Kuehn, S., Casola, C., Koch, D., Stute, G., Grotegut, P., et al. (2018). HSP27 immunization reinforces AII amacrine cell and synapse damage induced by S100 in an autoimmune glaucoma model. *Cell Tissue Res.* 371, 237–249. doi: 10.1007/s00441-017-2710-0

Reinehr, S., Reinhard, J., Wiemann, S., Stute, G., Kuehn, S., Woestmann, J., et al. (2016). Early remodelling of the extracellular matrix proteins tenascin-C and phosphacan in retina and optic nerve of an experimental autoimmune glaucoma model. *J. Cell Mol. Med.* 20, 2122–2137. doi: 10.1111/jcmm.12909

Reinhard, J., Joachim, S. C., and Faissner, A. (2015). Extracellular matrix remodeling during retinal development. *Exp. Eye Res.* 133, 132–140. doi: 10.1016/j.exer.2014.07.001

Reinhard, J., Renner, M., Wiemann, S., Shakoor, D. A., Stute, G., Dick, H. B., et al. (2017a). Ischemic injury leads to extracellular matrix alterations in retina and optic nerve. *Sci. Rep.* 7:43470.

Reinhard, J., Roll, L., and Faissner, A. (2017b). Tenascins in Retinal and Optic Nerve Neurodegeneration. *Front. Integr. Neurosci.* 11:30. doi: 10.3389/fnint.2017.00030

Reinhard, J., Wiemann, S., Hildebrandt, S., and Faissner, A. (2021). Extracellular Matrix Remodeling in the Retina and Optic Nerve of a Novel Glaucoma Mouse Model. *Biology* 10:169. doi: 10.3390/biology10030169

Reinhard, J., Wiemann, S., Joachim, S. C., Palmhof, M., Woestmann, J., Denecke, B., et al. (2019). Heterozygous Meg2 Ablation Causes Intraocular Pressure Elevation and Progressive Glaucomatous Neurodegeneration. *Mol. Neurobiol.* 56, 4322–4345. doi: 10.1007/s12035-018-1376-2

Renner, M., Stute, G., Alzureiqi, M., Reinhard, J., Wiemann, S., Schmid, H., et al. (2017). Optic Nerve Degeneration after Retinal Ischemia/Reperfusion in a Rodent Model. *Front. Cell Neurosci.* 11:254. doi: 10.3389/fncel.2017.00254

Roll, L., Eysel, U. T., and Faissner, A. (2020). Laser Lesion in the Mouse Visual Cortex Induces a Stem Cell Niche-Like Extracellular Matrix, Produced by Immature Astrocytes. *Front. Cell Neurosci.* 14:102. doi: 10.3389/fncel.2020.00102

Roll, L., and Faissner, A. (2014). Influence of the extracellular matrix on endogenous and transplanted stem cells after brain damage. *Front. Cell Neurosci.* 8:219. doi: 10.3389/fncel.2014.00219

Roll, L., and Faissner, A. (2019). Tenascins in CNS lesions. *Semin. Cell Dev. Biol.* 89, 118–124. doi: 10.1016/j.semcdb.2018.09.012

Roll, L., Mittmann, T., Eysel, U. T., and Faissner, A. (2012). The laser lesion of the mouse visual cortex as a model to study neural extracellular matrix remodeling during degeneration, regeneration and plasticity of the CNS. *Cell Tissue Res.* 349, 133–145. doi: 10.1007/s00441-011-1313-4

Schmid, H., Renner, M., Dick, H. B., and Joachim, S. C. (2014). Loss of inner retinal neurons after retinal ischemia in rats. *Invest. Ophthalmol. Vis. Sci.* 55, 2777–2787. doi: 10.1167/iovs.13-13372

Schmitz, F., Konigstorfer, A., and Sudhof, T. C. (2000). RIBEYE, a component of synaptic ribbons: a protein's journey through evolution provides insight into synaptic ribbon function. *Neuron* 28, 857–872. doi: 10.1016/s0896-6273(00)00159-8

Schultz, R., Witte, O. W., and Schmeer, C. (2016). Increased Frataxin Levels Protect Retinal Ganglion Cells After Acute Ischemia/Reperfusion in the Mouse Retina In Vivo. *Invest. Ophthalmol. Vis. Sci.* 57, 4115–4124. doi: 10.1167/iovs.16-19260

Sherry, D. M., Wang, M. M., Bates, J., and Frishman, L. J. (2003). Expression of vesicular glutamate transporter 1 in the mouse retina reveals temporal ordering in development of rod vs. cone and ON vs. OFF circuits. *J. Comp. Neurol.* 465, 480–498. doi: 10.1002/cne.10838

Shiba, M., Fujimoto, M., Imanaka-Yoshida, K., Yoshida, T., Taki, W., and Suzuki, H. (2014). Tenascin-C causes neuronal apoptosis after subarachnoid hemorrhage in rats. *Transl. Stroke Res.* 5, 238–247. doi: 10.1007/s12975-014-0333-2

Silver, J. (1994). Inhibitory molecules in development and regeneration. *J. Neurol.* 242, S22–S24.

Steindler, D. A., Settles, D., Erickson, H. P., Laywell, E. D., Yoshiki, A., Faissner, A., et al. (1995). Tenascin knockout mice: barrels, boundary molecules, and glial scars. *J. Neurosci.* 15, 1971–1983. doi: 10.1523/jneurosci.15-03-01971.1995

Strom, T. M., Nyakatura, G., Apfelstedt-Sylla, E., Hellebrand, H., Lorenz, B., Weber, B. H. F., et al. (1998). An L-type calcium-channel gene mutated in incomplete

X-linked congenital stationary night blindness. *Nat. Genet.* 19, 260–263. doi: 10.1038/940

Suzuki, H., Fujimoto, M., Kawakita, F., Liu, L., Nakatsuka, Y., Nakano, F., et al. (2020). Tenascin-C in brain injuries and edema after subarachnoid hemorrhage: findings from basic and clinical studies. *J. Neurosci. Res.* 98, 42–56. doi: 10.1002/jnr.24330

Taki, J., Inaki, A., Wakabayashi, H., Imanaka-Yoshida, K., Ogawa, K., Hiroe, M., et al. (2010). Dynamic expression of tenascin-C after myocardial ischemia and reperfusion: assessment by 125I-anti-tenascin-C antibody imaging. *J. Nucl. Med.* 51, 1116–1122. doi: 10.2967/jnumed.109.071340

Taki, J., Inaki, A., Wakabayashi, H., Matsunari, I., Imanaka-Yoshida, K., Ogawa, K., et al. (2015). Effect of postconditioning on dynamic expression of tenascin-C and left ventricular remodeling after myocardial ischemia and reperfusion. *EJNMMI Res.* 5:21.

Talts, J. F., Wirl, G., Dictor, M., Muller, W. J., and Fassler, R. (1999). Tenascin-C modulates tumor stroma and monocyte/macrophage recruitment but not tumor growth or metastasis in a mouse strain with spontaneous mammary cancer. *J. Cell Sci.* 112, 1855–1864.

tom Dieck, S., and Brandstatter, J. H. (2006). Ribbon synapses of the retina. *Cell Tissue Res.* 326, 339–346. doi: 10.1007/s00441-006-0234-0

von Holst, A., Egbers, U., Prochiantz, A., and Faissner, A. (2007). Neural stem/progenitor cells express 20 tenascin C isoforms that are differentially regulated by Pax6. *J. Biol. Chem.* 282, 9172–9181. doi: 10.1074/jbc.m608067200

Wiemann, S., Reinhard, J., Reinehr, S., Cibir, Z., Joachim, S. C., and Faissner, A. (2020). Loss of the Extracellular Matrix Molecule Tenascin-C Leads to Absence of Reactive Gliosis and Promotes Anti-inflammatory Cytokine Expression in an Autoimmune Glaucoma Mouse Model. *Front. Immunol.* 11:566279. doi: 10.3389/fimmu.2020.566279

Xiao, J., Adil, M. Y., Chang, K., Yu, Z., Yang, L., Utheim, T. P., et al. (2019). Visual Contrast Sensitivity Correlates to the Retinal Degeneration in Rhodopsin Knockout Mice. *Invest. Ophthalmol. Vis. Sci.* 60, 4196–4204. doi: 10.1167/iovs.19-26966

Xu, Z., Cho, H., Hartsock, M. J., Mitchell, K. L., Gong, J., Wu, L., et al. (2015). Neuroprotective role of Nrf2 for retinal ganglion cells in ischemia-reperfusion. *J. Neurochem.* 133, 233–241. doi: 10.1111/jnc.13064

Yang, X. L. (2004). Characterization of receptors for glutamate and GABA in retinal neurons. *Prog. Neurobiol.* 73, 127–150. doi: 10.1016/j.pneurobio.2004.04.002

Zhao, Y., Yu, B., Xiang, Y. H., Han, X. J., Xu, Y., So, K. F., et al. (2013). Changes in retinal morphology, electroretinogram and visual behavior after transient global ischemia in adult rats. *PLoS One* 8:e65555. doi: 10.1371/journal.pone.0065555

Conflict of Interest: The authors declare that the research was conducted in the absence of any commercial or financial relationships that could be construed as a potential conflict of interest.

Copyright © 2021 Wiemann, Yousf, Joachim, Peters, Mueller-Buehl, Wagner and Reinhard. This is an open-access article distributed under the terms of the Creative Commons Attribution License (CC BY). The use, distribution or reproduction in other forums is permitted, provided the original author(s) and the copyright owner(s) are credited and that the original publication in this journal is cited, in accordance with accepted academic practice. No use, distribution or reproduction is permitted which does not comply with these terms.

frontiers in Neuroscience

ORIGINAL RESEARCH
published: 26 January 2022
doi: 10.3389/fnins.2022.831392

Effects of Hydrostatic Pressure on Electrical Retinal Activity in a Multielectrode Array-Based *ex vivo* Glaucoma Acute Model

*Claudia Ingensiep, Kim Schaffrath, Peter Walter and Sandra Johnen**

Department of Ophthalmology, University Hospital RWTH Aachen, Aachen, Germany

Glaucoma is a heterogeneous eye disease causing atrophy of the optic nerve head (ONH). The optic nerve is formed by the axons of the retinal ganglion cells (RGCs) that transmit visual input to the brain. The progressive RGC loss during glaucoma leads to irreversible vision loss. An elevated intraocular pressure (IOP) is described as main risk factor in glaucoma. In this study, a multielectrode array (MEA)-based *ex vivo* glaucoma acute model was established and the effects of hydrostatic pressure (10, 30, 60, and 90 mmHg) on the functionality and survival of adult male and female wild-type mouse (C57BL/6) retinae were investigated. Spontaneous activity, response rate to electrical and light stimulation, and bursting behavior of RGCs was analyzed prior, during, and after pressure stress. No pressure related effects on spontaneous firing and on the response rate of the RGCs were observed. Even a high pressure level (90 mmHg for 2 h) did not disturb the RGC functionality. However, the cells' bursting behavior significantly changed under 90 mmHg. The number of spikes in bursts doubled during pressure application and stayed on a high level after pressure stress. Addition of the amino sulfonic acid taurine (1 mM) showed a counteracting effect. OFF ganglion cells did not reveal an increase in bursts under pressure stress. Live/dead staining after pressure application showed no significant changes in RGC survival. The findings of our *ex vivo* model suggest that RGCs are tolerant toward high, short-time pressure stress.

Keywords: retina, RGC, pressure, glaucoma, MEA, taurine

OPEN ACCESS

Edited by:
Javier Sancho-Pelluz, Catholic University of Valencia San Vicente Mártir, Spain

Reviewed by:
Raghu R. Krishnamoorthy, University of North Texas Health Science Center, United States
Biju B. Thomas, University of Southern California, United States

****Correspondence:***
Sandra Johnen
sjohnen@ukaachen.de

Specialty section:
This article was submitted to Neurodegeneration, a section of the journal Frontiers in Neuroscience

Received: *08 December 2021*
Accepted: *04 January 2022*
Published: *26 January 2022*

Citation:
Ingensiep C, Schaffrath K, Walter P and Johnen S (2022) Effects of Hydrostatic Pressure on Electrical Retinal Activity in a Multielectrode Array-Based ex vivo Glaucoma Acute Model. Front. Neurosci. 16:831392. doi: 10.3389/fnins.2022.831392

INTRODUCTION

Glaucoma is the second leading cause of blindness worldwide (Quigley, 1996; Quigley and Broman, 2006; Tham et al., 2014). It describes a heterogeneous disorder. Excavation (cupping) of the optic nerve head (ONH) and progressive loss of retinal ganglion cell (RGC) axons are characteristic for glaucoma disease. RGC loss causes corresponding visual field defects (Leske et al., 2003; Inatani et al., 2008) which in most cases is a painless process starting in the peripheral vision of the patient's eye. Therefore, glaucoma often remains unnoticed in early stages. The pathogenesis is divided into mechanical (pressure related) and vascular (perfusion related) damage of the optic nerve. However, the main risk factor in glaucoma is an increased intraocular pressure (IOP). IOP mainly depends on the production and outflow of aqueous humor. Aqueous humor is secreted by the epithelium of the ciliary body into the posterior chamber. It subsequently enters the anterior chamber *via* the

pupil by moving down an osmotic gradient. The trabecular meshwork forms the main outflow pathway (90%), next to the uveoscleral outflow (10%). Blockage of the outflow by ongoing humor production results in an increased IOP. Lowering the IOP by medical treatment in the form of eye drops, laser treatment or surgical treatment is considered the standard therapy.

Intraocular pressure in healthy human eyes is very individual, but usually ranges between 10 and 21 mmHg (Leske et al., 1997). Glaucoma patients often suffer from chronically increased IOP > 21 mmHg. During a glaucomatous attack, the IOP can even raise to > 60 mmHg. A glaucomatous attack is one of the most severe emergencies in ophthalmology. Patients suffer from a strong headache, nausea, and reduced and blurred vision in combination with a red eye. Nevertheless, increased IOP is not an obligatory characteristic of glaucoma. Some patients with normal tension glaucoma suffer from ONH atrophy at normal eye pressure, whereas other patients show an increased IOP without morphological damage.

Next to its mechanical load on the tissue, elevated IOP especially disturbs the blood flow in the eye (Howard and Sawyer, 1975). Direct compression of retinal blood vessels due to high IOP causes reduced blood flow when the ocular perfusion pressure is beyond its autoregulation capacity. The vascular stress results in a lack of oxygen (hypoxia). Due to their high metabolic activity, RGCs react sensitively to hypoxic stress. Therefore, hypoxic conditions lead to RGC activity loss and cell death (Winkler, 1981; Osborne et al., 2004).

To differentiate between the effects the stressors hypoxia and pressure have on the retina in glaucomatic disease, analyses under defined hypoxic conditions and defined pressure conditions are necessary.

The effect of hypoxic stress on the functionality and survival of RGCs has been demonstrated in our previous work (Ingensiep et al., 2021) as well as in multiple other studies (Gross et al., 1999; Kergoat et al., 2006; Janaky et al., 2007; Tan et al., 2011). RGCs transit into a stress mode, even after short-time hypoxia, where no spontaneous electrical activity and no response to electrical or light stimuli can be recorded. This effect is conditionally reversible; however, the survival rate of RGCs under hypoxic stress is very low.

In this study, the effect of pressure stress on RGCs was analyzed. We established a multielectrode array (MEA)-based *ex vivo* pressure model to analyze the retinal electrical activity prior, during, and after hydrostatic pressure application.

We also analyzed the effect of 2-aminoethanesulfonic acid (taurine) on RGC functionality and the survival rate of retinal cells during pressure stress. Taurine is a free amino sulfonic acid which is very abundant in mammalian tissue and especially highly concentrated in the retina (Macaione et al., 1974). It is involved in multiple physiological processes and proven to have neuromodulating and neuroprotective effects (Froger et al., 2012). Taurine is structurally similar to γ-aminobutyric acid (GABA) and has the ability to inhibit the excitatory effect of glutamate by binding to GABA receptors and therefore prevents excitotoxicity (Louzada et al., 2004). It is highly antioxidant, regulates osmotic pressure in cells, and affects the homeostasis of intracellular ion concentrations (El-Sherbeny et al., 2004). Taurine plays a crucial regulatory role in intracellular (cytoplasmic and intra-mitochondrial) calcium (Ca^{2+}) transport by stimulating ATP-dependent Ca^{2+} uptake at low Ca^{2+} concentration [Ca^{2+}] and lowering the uptake at high [Ca^{2+}] (Pasantes-Morales and Ordonez, 1982; El Idrissi, 2008). This mechanism also affects Ca^{2+}-dependent mitochondrial pores (mPTPs). Apoptosis-induced factors, such as cytochrome c, use these pores to get into the cytosol. Therefore, mitochondria-mediated apoptosis can be prevented by taurine.

MATERIALS AND METHODS

Animals

Male and female C57BL/6J wild-type (wt) mice aged 12–20 weeks from Janvier (Le Genest-Saint-Isle, France) were kept under controlled light conditions (12:12 h light/dark cycle), at a room temperature of 21–23°C, and a humidity of 35–65% at the Institute of Laboratory Animal Science (Faculty of Medicine, RWTH Aachen University). Water and food were available *ad libitum* and cages were cleaned once a week. For sacrifice, mice were deeply anesthetized with isoflurane (AbbVie, Wiesbaden, Germany) and killed by decapitation. All experiments were performed after approval was obtained by the regulatory authorities and in accordance with the ARVO statement for the Use of Animals in Ophthalmic and Vision Research and the German Law for the Protection of Animals.

Medium

Ames' medium (Sigma-Aldrich, St. Louis, MO, United States) (Ames and Nesbett, 1981) was dissolved in water, bubbled with 100% CO_2 for 30 min at room temperature (RT), and supplemented with sodium bicarbonate. The medium was adjusted to a pH of 7.4–7.5 with sodium hydroxide and continuously bubbled with carbogen gas (95% O_2, 5% CO_2). Taurine was dissolved in Ames' medium to a concentration of 1 mM (Chen et al., 2009; Froger et al., 2012). NMDA receptor antagonist DL-2-Amino-5-phosphonopentanoic acid (DL-AP5, 50 μM) and AMPA/kainate receptor antagonist 6-cyano-7-nitroquinoxaline-2,3-dione (CNQX, 20 μM) were freshly prepared and added to the Ames' medium in order to block RGC glutamate receptor input (Biswas et al., 2014).

Retina Preparation

Retina preparation was performed as previously described (Ingensiep et al., 2021). Briefly, both eyes of an animal were enucleated directly after sacrifice and put into freshly carbogenated Ames' medium. The left eye was pierced at the limbus with a 27 G cannula and cut radially half open. It was kept separately in freshly carbogenated Ames' medium as backup for later use if the MEA experiment with the right eye failed. The right eye was opened at the limbus with an encircling cut. The anterior segment and lens were removed and the retina was carefully detached from the eye cup and separated by a cut through the optic nerve. The vitreous body was carefully removed completely using forceps. The retina was cut into a square shape and mounted on a nitrocellulose frame with RGCs facing up.

The frame was placed onto the electrode field of the MEA with RGCs facing down.

Multielectrode Array Setup

The MEA2100 system from Multi Channel Systems (Reutlingen, Germany) was used to perform electrophysiological recordings (chapter Multielectrode Array Recordings) of murine retinae. It comprised a head stage with an integrated preamplifier, which was used for recording as well as for stimulation, and an interface board that served as digital/analog converter transmitting data in real time. A MEA was placed in the head stage that was connected to the interface board, which was connected to a personal computer (PC). The setup was placed on an air-suspended table (Ametek, Berwyn, PA, United States) in a faraday cage (Ametek) to minimize noise caused by vibrations and electronic devices.

60MEA200/30iR-Ti-pr-T type MEAs (Multi Channel Systems) were used. The MEAs possess 60 titanium nitride (TiN) electrodes arranged in a square field of 8 × 8 electrodes with the four electrodes at the corners being spared out and one electrode serving as reference, resulting in 59 electrodes for recording and stimulation. The electrodes were 30 μm in diameter and positioned with a distance of 200 μm to each other. All MEAs had a plastic ring around the electrode field with an inner diameter of 26 mm and a thread on the inside. Before every experiment, MEAs were hydrophilized with oxygen plasma for 2 min at 0.5 mbar in a plasma cleaner (Diener Electronic, Ebhausen, Germany).

Pressure Stress

Hydrostatic pressure was applied to the retina by adding a custom-made pressure lid to the MEA setup. The lid was designed and fabricated in the in-house scientific workshop (*Wissenschaftliche Werkstatt*, University Hospital RWTH Aachen). It was screwed onto the inner thread of the ring of the MEA, forming a leak-proof chamber. The lid was connected to a gravitation based VC^3 perfusion system (ALA Scientific Instruments, Farmingdale, NY, United States) that provided the retina with freshly carbogenated medium during the experiments (inflow). The outflow was regulated by a flow control yielding a perfusion rate of 3 ml/min. The pressure inside the chamber was directly dependent on the height of the medium tube of the perfusion system. By raising the fluid column, the hydrostatic pressure inside the chamber increased. In order to keep the fluid column level during perfusion, an additional medium reservoir was installed on top of the medium tube, filling it with the same perfusion rate.

Access points in the lid for O_2-, pH-, and pressure sensors enabled monitoring of the experimental conditions inside the chamber during MEA recordings. Oxygen concentration [O_2] was measured by the OxyMicro sensor and recorded *via* OxyMicro software (World Precision Instruments, Sarasota, FL, United States). The pH was monitored by the pHOptica micro sensor and recorded *via* pHOptica software (World Precision Instruments). One measurement per minute was taken for [O_2] and pH, respectively. Pressure was continuously measured by an Xtrans pressure transducer (Codan, Lensahn, Germany) and displayed by a connected IntelliVue MP30 Anesthesia patient monitor (Philips, Hamburg, Germany). The aim pressure ± 1 mmHg was tolerated.

Figures 1A,B show a schematic diagram of the experimental setup and a picture of the pressure lid. Representative examples for pressure, [O_2], and pH over time are shown in **Figure 1C**. Examples of the RGC firing behavior under different pressure levels are shown in **Figure 1D**. The spontaneous electrical activity of RGCs as well as their responses to given stimuli (electrical and light) persisted under pressure and could be recorded throughout the experiment (pre, pressure, post). The control pressure was set to 10 mmHg according to the normal eye pressure of mice (Kim et al., 2007; Lei et al., 2011). Pressure levels of 30, 60, and 90 mmHg were tested to simulate an increased intraocular pressure. 30 mmHg (Choi et al., 2015) were chosen as moderate pressure increase since a commonly investigated mild pressure level of 20 mmHg (Aihara et al., 2014; Pang et al., 2015) did not reveal any effects on the RGC firing behavior. 60 mmHg (Bui et al., 2005; Osborne et al., 2015) were chosen as high pressure increase that can occur during glaucomatous attacks. 90 mmHg (Aihara et al., 2014; Osborne et al., 2015) were investigated to emphasize the slight effects that were measured under 60 mmHg. In order to rule out an effect of the pressure lid itself, two additional controls were performed: a control without any pressure application (0 mmHg) and a control using the conventional MEA setup without any lid (open MEA).

Every experiment started with a lead time of 30 min under control conditions (10 mmHg) (**Figure 1C**) to allow the retina to recover from the preparation stress and let electrical activity reach a steady state. After the lead time, recordings were started. If spontaneous RGC firing was detected on less than ten of the overall 59 recording channels after lead time, the retina was rejected. After additional 30 min under control conditions (pre-phase), the test pressure was applied for 2 h (pressure-phase). A recovery time of 2 h at 10 mmHg completed the experimental timeline (post-phase).

Multielectrode Array Recordings

The electrical activity of the RGCs was displayed and recorded with Multi Channel Experimenter software (Multi Channel Systems) at a sample rate of 25,000 Hz. Raw data was filtered with a second order Butterworth high pass filter with a cutoff at 200 Hz (filter 1) and a second order Butterworth low pass filter with a cutoff at 2,000 Hz (filter 2). A spike detector used the band pass filtered data from filter 1 and 2 to identify action potentials at a threshold of −20 μV. If necessary, noise channels had to be excluded from spike detection. Measurements of 60 s each were performed, recording either the spontaneous firing of the cells or their response to stimulation.

Electrical Stimulation

For each experiment, two different stimulation electrodes were chosen and used in sequence. During a stimulation recording, only one electrode stimulated the retina. A biphasic current pulse (± 80 μA, 500 μs per phase) with the cathodic phase preceding the anodic phase was used. Five pulses with an interstimulus interval (ISI) of 10 s were given per recording. Electrical stimulation was used to roughly investigate the

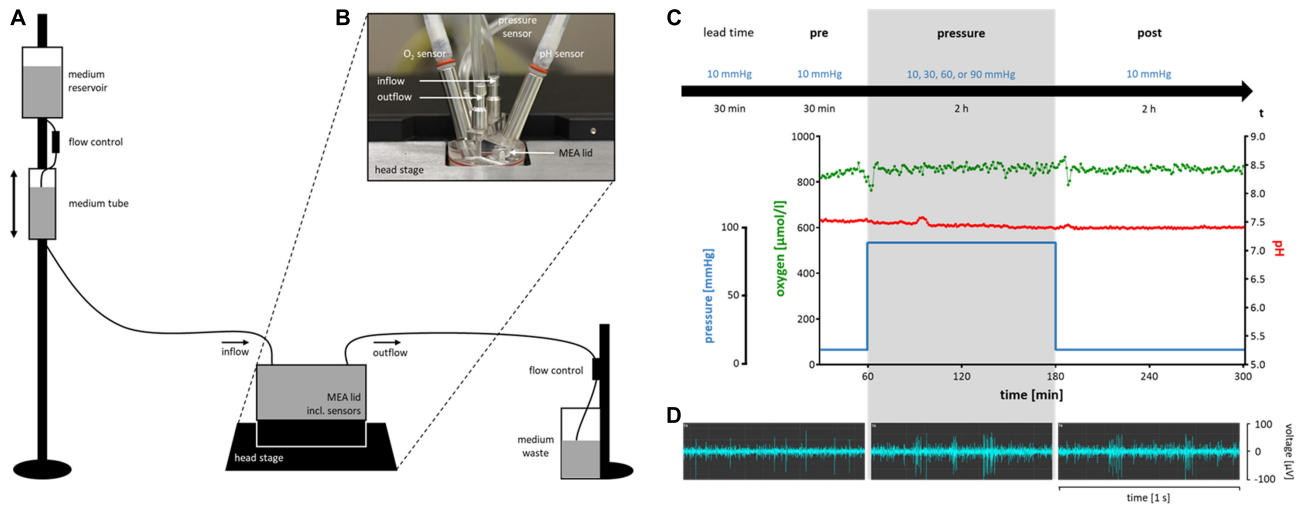

FIGURE 1 | Schematic diagram of the experimental setup of the pressure model and timeline with representative experimental conditions and RGC activity. **(A)** A simplified sketch of the experimental setup for the pressure model (not to scale). **(B)** The MEA lid on top of a MEA. The five integrated access points for in-, and outflow of the perfusion system, and for pressure, O_2, and pH sensors are shown. **(C)** The experimental timeline including a lead time of 30 min at 10 mmHg, the pre-phase of 30 min at 10 mmHg, the pressure-phase of 2 h at either 10 (control), 30, 60 or 90 mmHg, and the post-phase/recovery time of 2 h at 10 mmHg. Below the timeline, representative examples of pressure level, oxygen concentration, and pH of an experiment with 90 mmHg are shown. Note that during changes in the pressure level, $[O_2]$ and pH remain stable. **(D)** Representative examples of the electrical spontaneous RGC activity of a wt mouse retina in the pre-, pressure-, and post-phase of an experiment with 90 mmHg.

RGC functionality. For a more refined analysis, light as the physiological stimulus of the retina was used.

Light Stimulation

For experiments with light stimulation, mice were dark adapted for 1 h before sacrifice. Preparation and the experiment itself were performed in the dark under dim red light. The LED stimulator MEA2100-opto-stim and Stimulus generator STG4002-1.6A-opto (Multi Channel Systems) were added to the MEA setup. A neutral white 4100K LED (Quadica Developments Inc., AB, Canada) was positioned underneath the MEA, illuminating the retina from the ganglion cell layer (GCL). The LED was programmed with Multi Channel Stimulus ll software and stimulation time points were detected and recorded with Multi Channel Experimenter. Full-field light pulses (1 s, 10 s ISI) were generated five times per recording. The LED was run with 500 mA, resulting in a luminous flux of 160 lm.

Live/Dead Staining

To investigate the number of dead cells in different retinal layers after pressure stress, retinae were live/dead double stained with fluorescein diacetate (FDA) (Merck, Darmstadt, Germany) and propidium iodide (PI) (ICN Biomedicals, Costa Mesa, CA, United States). FDA enters the cellular membrane of living cells and is metabolized by esterases, resulting in green fluorescent somata. PI can only penetrate the disrupted membrane of dead cells and binds to DNA, resulting in red fluorescent nuclei. Three different groups, 10 mmHg (control), 90 mmHg, and 90 mmHg + taurine, were investigated. The pressure application was performed according to the setup and timeline of the MEA experiments excluding lead time and post pressure phase. However, some changes had to be done to ensure that the retinae could be removed from the pressure chamber after an experiment without causing any damage to the tissue. MEAs were not hydrophilized in advance and retinae were placed on the electrode field with the nitrocellulose frame facing down and RGCs facing up to prevent the tissue from sticking to the MEA. A metal ring with a nylon mesh was placed on top of the retinae, preventing the tissue from swimming freely inside the chamber. For staining experiments, both retinae of an animal were treated simultaneously. After pressure treatment, each retina was added to 600 µl of staining solution [20 µl FDA (5 mg/ml), 20 µl PI (1 mg/ml) in 1.2 ml Ames' medium] in a 24-well plate (Eppendorf, Hamburg, Germany). The well plate was put into a metal box and placed onto an orbital shaker (Heidolph Instruments, Schwabach, Germany). The dyes were applied for 5 min at 60 rpm to ensure that the tissue was completely saturated by the solution. Subsequently, the tissue was washed three times for 5 min in freshly carbogenated Ames' medium. To prevent bleaching and an increasing number of dead cells due to the acetone in the FDA solution, all steps were performed quickly, protected from light, and immediately before imaging. For positive PI controls, retinae suffered hypoxic stress for 4 h and were afterward stained using the same protocol.

Two-Photon Laser Scanning Microscopy

The live/dead double stained retinae were analyzed *via* two-photon laser scanning microscopy (TPLSM) as described earlier (Ingensiep et al., 2021). Imaging was done with a two-photon microscope (Olympus Fluoview FV1000 MPE, Olympus Corporation, Tokyo, Japan) attached to a pulsed

Ti:Sapphire laser (MaiTai DeepSee, SpectraPhysics, Santa Clara, CA, United States). A 25x NA 1.05 water dipping objective was used. Representative regions in the superior, inferior, nasal or temporal retina beyond the ONH and in between the main blood vessel branches were chosen and laser intensity was adjusted. Two stacks of subsequent images (xy-frames, 1,024 pixel × 1024 pixel) over depth (z, ∼150 μm) with a z-step of 1 μm were recorded for each retina.

Data Analysis

Multielectrode Array Recordings

Since one MEA electrode could detect the electrical activity of not only one, but several cells, spike sorting was mandatory to investigate the firing behavior on single cell level. Offline Sorter software version 4 (Plexon Inc., Dallas, TX, United States) was used to perform spike sorting *via* a principal component analysis (PCA). Spikes were clustered according to their characteristic waveforms and marked as units with one unit representing one cell.

Data was further processed with NeuroExplorer software version 5 (Nex Technologies, Colorado Springs, CO, United States). Firing frequency, response rate, spike amplitude, and bursting behavior were analyzed and exported into Excel by operating NeuroExplorer with a custom-written Python script.

The response rate for electrical stimulation was analyzed for cells on the eight recording channels surrounding the stimulation electrode. It was defined as the coefficient of the number of spikes 3 s before the stimulus and 0.5 s after the stimulus. For full-field light stimulation, the response rate was calculated for cells on all recording channels. The spike rate around the start (onset) and stop (offset) of the light pulse was investigated. The number of spikes 1 s before and 0.5 s after stimulus onset and offset, respectively, were analyzed and the coefficient was calculated. According to their response rate, RGCs were roughly categorized into ON, ON-OFF, and OFF cells. If the response rate to the onset was ≥ 1.5 and the response rate to the offset < 1.5, the cell was categorized as ON. If the response rate to the onset as well as to the offset was ≥ 1.5, the cell was categorized as ON-OFF. If the response rate to the onset was < 1.5 and the response rate to the offset ≥ 1.5, the cell was categorized as OFF. If both response rates were < 1.5, the cell remained uncategorized.

A burst analysis identified spikes in bursts with interval algorithm parameters of a 0.01 s maximal interval to start a burst, a 0.03 s maximal interval to end a burst, a 0.02 s minimal interval between bursts, a 0.01 s minimal duration of a burst, and a minimal number of three spikes within a burst.

Live/Dead Staining

Image analysis was performed in Imaris software version 9 (Bitplane, Oxford Instruments plc., Abingdon, United Kingdom). The recorded image stacks were 3D rendered and divided into three regions of interest (ROIs): GCL, inner nuclear layer (INL), and outer nuclear layer (ONL). The number of dead cells (red channel) was automatically counted for every ROI using the *Spot* function of the software. Virtual sections of the image stacks in x, y, and z direction were made for each group (10 mmHg, 90 mmHg, 90 mmHg + taurine).

Experimental Design and Statistical Analyses

For MEA recordings, a number of five animals per group was chosen. MEA experiments with addition of glutamate receptor antagonists were performed with three animals. Each group contained both male and female mice. 14 retinae of seven animals had to be rejected for not meeting the experimental criteria, resulting in an overall number of 50 mice (21 male, 29 female) used for MEA recordings.

Twelve retinae of three male and three female mice were used for the staining experiments, resulting in eight image stacks per group.

Design of graphs and statistical analyses were performed using GraphPad Prism version 7 (GraphPad Software Inc., San Diego, CA, United States). A p-value < 0.05 was considered significant. In figures, different significance levels are represented by asterisks: $^{*}p < 0.05$, $^{**}p < 0.01$, $^{***}p < 0.001$, $^{****}p < 0.0001$. Outliers were identified *via* robust regression and outlier removal (ROUT) with a ROUT coefficient (Q) of $Q = 0.1\%$. Mean values presented in graphs with identified outliers refer to the mean of the cleaned data. Mean values presented in the text include all data and are presented as mean ± standard deviation (SD).

RESULTS

Multielectrode Array Recordings

The spontaneous RGC firing frequency on single cell level after spike sorting was analyzed and plotted for each of the experimental phases pre, pressure, and post (**Figure 2**). For control experiments, the same temporal phases were investigated; however, no pressure change was applied (**Figure 2A**). In the control group without pressure lid (open MEA), the mean firing frequency decreased by 23% from 11.36 ± 12.08 Hz (pre) to 8.76 ± 10.78 Hz (pressure) and increased by 23% to 10.80 ± 11.78 Hz during the post-phase. In the 0 mmHg control group, the mean firing frequency of the RGCs decreased by 27% from 8.00 ± 11.13 Hz (pre) to 5.81 ± 10.03 Hz (pressure) and by 43% to 3.32 ± 4.66 Hz (post). In the control group with a pressure level of 10 mmHg, the mean firing frequency decreased by 43% from 7.13 ± 9.71 Hz (pre) to 4.08 ± 3.97 Hz (pressure) and by 8% to 3.75 ± 4.25 Hz (post). With an increased pressure of 30 mmHg, the mean firing frequency decreased by 21% from 10.90 ± 12.61 Hz to 8.59 ± 10.84 Hz and further decreased by 21% to 6.79 ± 9.74 Hz during the post-phase (**Figure 2B**). Under a pressure of 60 mmHg, the mean firing frequency decreased by 40% from 11.66 ± 11.39 Hz to 7.02 ± 6.75 Hz and further decreased by 9% to 6.42 ± 8.22 Hz. Under an increased pressure of 90 mmHg, the mean RGC firing frequency was not significantly different between the pre- (6.86 ± 7.56 Hz) and pressure-phase (7.21 ± 10.26 Hz), but decreased during the post-phase by 26% to 5.30 ± 8.44 Hz.

Spontaneous firing frequency was not affected by taurine. As in the corresponding MEA experiments with 90 mmHg without taurine, the spontaneous firing frequency decreased over time by 34% (pre: 9.56 ± 13.78 Hz, pressure: 9.56 ± 11.42 Hz,

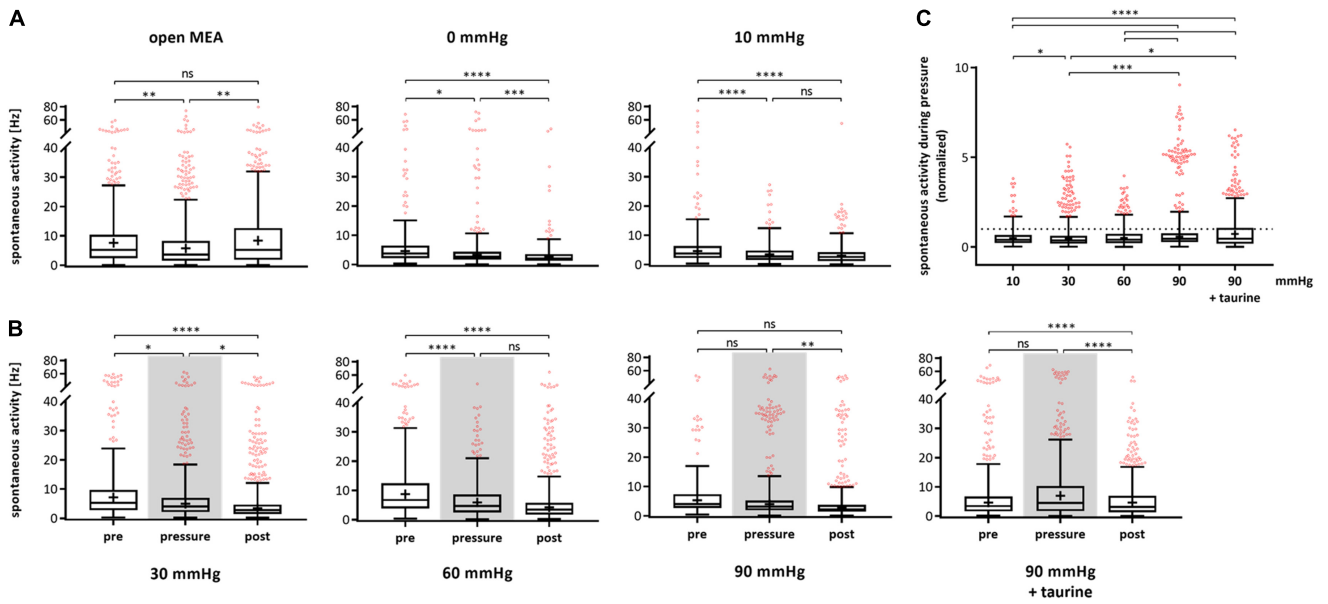

FIGURE 2 | Spontaneous activity of RGCs under different pressure levels. The spontaneous firing frequency [Hz] of RGCs before (pre), during (pressure), and after (post) pressure stress is shown. **(A)** The results of the control experiments without pressure lid (open MEA), 0 mmHg, and 10 mmHg are presented. **(B)** The results of the test groups with 30, 60, 90 mmHg, and 90 mmHg + taurine (1 mM) are presented. **(C)** Summary of the normalized spontaneous RGC activity during pressure is shown. The activity before pressure (pre) was set to 1. Data are presented as box and whisker (min to max) plots. Outliers calculated by ROUT ($Q = 0.1\%$) are shown as red circles. Mean values of the cleaned data are shown as + . Significant values are indicated by asterisks. Non-significant values are labeled with ns in panels **(A,B)** and not labeled in panel **(C)**. One-way ANOVA with *post hoc* Tukey's test was performed with GraphPad Prism Software version 7. **(A)** $F(2, 1447) = 6.965$, $p = 0.0010$; $F(2, 847) = 18.03$, $p < 0.0001$; $F(2, 939) = 24.55$, $p < 0.0001$; **(B)** $F(2, 1370) = 14.95$, $p < 0.0001$; $F(2, 1495) = 42.19$, $p < 0.0001$; $F(2, 1432) = 6.752$, $p = 0.0012$; $F(2, 1550) = 18$, $p < 0.0001$; **(C)** $F(4, 2467) = 20.54$, $p < 0.0001$. $n_{retinae}$ = 5/group, n_{cells} = 152–430/group, $n_{recordings}$ = 16/experiment.

post: 6.34 ± 7.47 Hz). **Figure 2C** sums up the spontaneous RGC activity during pressure stress and compares the different pressure levels. The normalized firing frequency is shown with the frequency during the respective pre-phase being set to 1. The mean RGC firing frequency under 10 mmHg was 57% of the initial frequency. Under 30 mmHg, the frequency was 79%, under 60 mmHg 60%, and under 90 mmHg 105%. However, no pressure dependent effect on the spontaneous activity of the RGCs was found. With the addition of taurine, the frequency was 100% under 90 mmHg.

The unsorted MEA data, representing RGC activity on recording channel/electrode level, showed an increase in spontaneous firing under 90 mmHg pressure. The spontaneous activity increased by 82% from 9.68 ± 15.10 Hz (pre) to 17.58 ± 23.60 Hz (pressure) and by 11% to 19.43 ± 31.18 Hz (post) (data not shown).

The RGC response to electrical stimulation (± 80 μA, 500 μs per phase) on single cell level after spike sorting was analyzed and plotted for each experimental phase (**Figure 3**). **Figure 3A** shows the response rates for the control experiments. The open MEA control revealed no significant changes in the RGC response rate (pre-phase: 19.00 ± 63.61, pressure-phase: 21.77 ± 80.06, post-phase: 20.79 ± 61.51). In the 0 mmHg control, the RGC response rate changed by 41% from 8.92 ± 19.04 to 12.59 ± 33.07 and by 26% to 9.26 ± 9.08. The 10 mmHg control revealed an increase by 56% from 8.44 ± 20.58 to 13.12 ± 24.00 and by 8% 12.10 ± 26.60. **Figure 3B** shows the results of the test groups. The mean RGC response rate in the 30 mmHg group increased by 228% from pre- (2.89 ± 4.53) to pressure- (9.49 ± 26.64) and by 2% to post-phase (9.71 ± 17.57). Under 60 mmHg, the response rate increased by 44% from 2.74 ± 3.08 to 3.94 ± 8.31 and further increased by 106% to 8.10 ± 17.30. Under 90 mmHg, the RGC response rate also increased by 50% from 3.47 ± 3.37 to 5.22 ± 8.01, and by 115% to 11.21 ± 19.03 after pressure stress. With addition of taurine, the response rate after electrical stimulation strongly increased by 237% during pressure and remained at a high level after pressure stress (pre: 12.77 ± 22.47, pressure: 43.12 ± 108.70, post: 42.43 ± 112.90).

Figure 3C shows a summary of the normalized response rate during pressure stress for each pressure level with the initial response rate before pressure stress being set to 1. The RGC response rate to electrical stimulation was 156% under 10 mmHg, 328% under 30 mmHg, 144% under 60 mmHg, 150% under 90 mmHg, and 337% under 90 mmHg with the addition of taurine. Overall, we observed big standard deviations throughout all groups and phases revealing a high variance of the RGC response to electrical stimulation in general. However, no significant pressure dependent effect on the RGC response was found.

During experiments with highly increased pressure of 60 and 90 mmHg, salves of spikes (bursts) fired by the RGCs were observed. A burst analysis was performed and the RGC bursting behavior on single cell level after spike sorting was analyzed and plotted for each experimental phase (**Figure 4**). The percentage

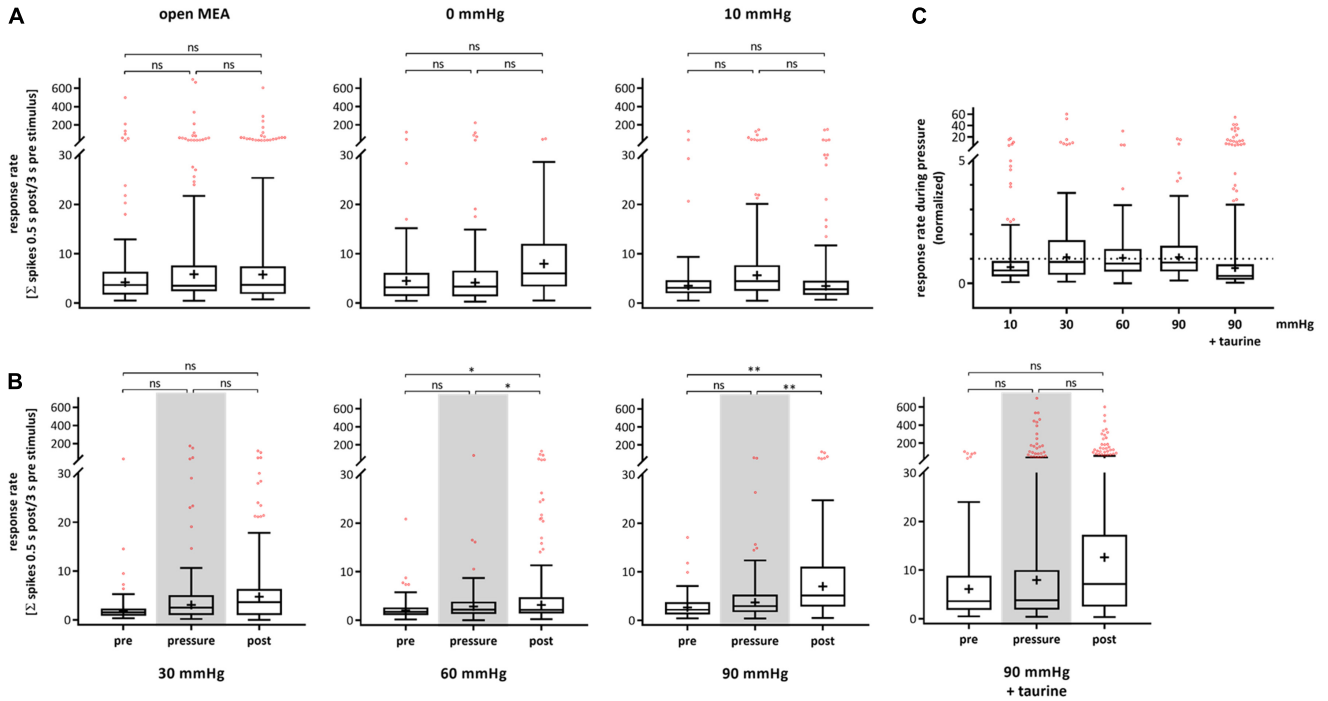

FIGURE 3 | Response rate of RGCs after electrical stimulation under different pressure levels. The RGC response to electrical stimulation (± 80 μA, 500 μs per phase) before (pre), during (pressure), and after (post) pressure stress is shown. The response rate was defined by the coefficient of the number of spikes 0.5 s after stimulation and 3 s before stimulation. **(A)** The results of the control experiments without pressure lid (open MEA), 0 mmHg, and 10 mmHg are presented. **(B)** The results of the test groups with 30, 60, 90 mmHg, and 90 mmHg + taurine (1 mM) are presented. **(C)** Summary of the normalized RGC response rate during pressure is shown. The response rate before pressure (pre) was set to 1. Data are presented as box and whisker (min to max) plots. Outliers calculated by ROUT (Q = 0.1%) are shown as red circles. Mean values of the cleaned data are shown as + . Significant values are indicated by asterisks. Not significant values are labeled with ns in panels **(A,B)** and not labeled in panel **(C)**. One-way ANOVA with *post hoc* Tukey's test was performed with GraphPad Prism Software version 7. **(A)** $F(2, 387) = 0.0403$, $p = 0.9605$; $F(2, 160) = 0.4285$, $p = 0.6522$; $F(2, 187) = 0.5299$, $p = 0.5896$; **(B)** $F(2, 224) = 2.654$, $p = 0.0726$; $F(2, 278) = 4.854$, $p = 0.0085$; $F(2, 240) = 2.257$, $p = 0.1069$; $F(2, 482) = 2.155$, $p = 0.1170$; **(C)** $F(4, 531) = 2.206$, $p = 0.0671$. $n_{retinae}$ = 5/group, n_{cells} = 47–118/group, $n_{recordings}$ = 19/experiment.

of spikes in bursts in relation to all the spikes fired by an RGC are shown. The control without pressure lid (open MEA) showed a slight increase of spikes fired in bursts (pre: 17.38 ± 22.83%, pressure: 22.37 ± 22.53%, post: 21.14 ± 20.63). In the 0 mmHg control group, the incidence of bursts did not significantly change (pre: 15.91 ± 22.00%, pressure: 16.92 ± 20.49%, post: 16.88 ± 19.25%). In the 10 mmHg control group, the incidence of bursts slightly increased over time (pre: 12.11 ± 19.33%, pressure: 17.14 ± 20.57%, post: 17.77 ± 20.05%) (**Figure 4A**). Under a pressure level of 30 mmHg, the incidence of bursts increased by 55% from 12.46 ± 18.75% to 19.37 ± 18.52% (**Figure 4B**) and persisted after lowering the pressure (20.53 ± 19.59%). Under 60 mmHg, the incidence of bursts increased by 39% from 11.02 ± 16.19% to 15.35 ± 18.13%; after pressure, the mean incidence of bursts was 13.98 ± 16.53%. Under 90 mmHg, the incidence of bursts increased by 108% from 9.90 ± 15.58% to 20.60 ± 20.42% and remained at a high level during the post-phase (21.21 ± 20.18%). Bursting behavior of the RGCs under pressure in the presence of taurine were different to the results under 90 mmHg without taurine: instead of an increase under pressure stress, the incidence of bursts decreased by 16% during, and by 20% after application of 90 mmHg (pre: 17.81 ± 23.97%, pressure: 15.03 ± 21.90%, post: 12.09 ± 18.93%). The addition of taurine significantly counteracted the effect of high pressure on the RGC bursting behavior.

Figure 4C shows a summary of the normalized spikes-in-bursts rate during pressure stress for each pressure level with the initial number before pressure stress being set to 1. The number of spikes in bursts was 140% under 10 mmHg, 155% under 30 mmHg, 139% under 60 mmHg, 208% under 90 mmHg, and 84% under 90 mmHg in addition of taurine (**Figure 4C**). Comparison of the number of spikes in bursts between the different pressure levels revealed a significantly higher incidence of bursts under 90 mmHg: more bursts occurred and the number of bursts stayed at a high level even after the pressure was reduced back to control conditions.

Multielectrode array experiments with dark adapted retinae were performed under dim red light and the effect of high pressure stress (90 mmHg) on RGC activity was analyzed. The spontaneous firing frequency did not change significantly from pre- (11.64 ± 12.77 Hz) to pressure-phase (11.10 ± 13.06 Hz), but decreased after pressure stress by 25% (8.38 ± 12.62 Hz) (**Figure 5A**). The incidence of bursts also increased under pressure by 37% and stayed at a high level throughout the post-phase (pre: 16.38 ± 19.22%, pressure: 22.38 ± 21.99%, post: 22.67 ± 21.26%) (**Figure 5B**).

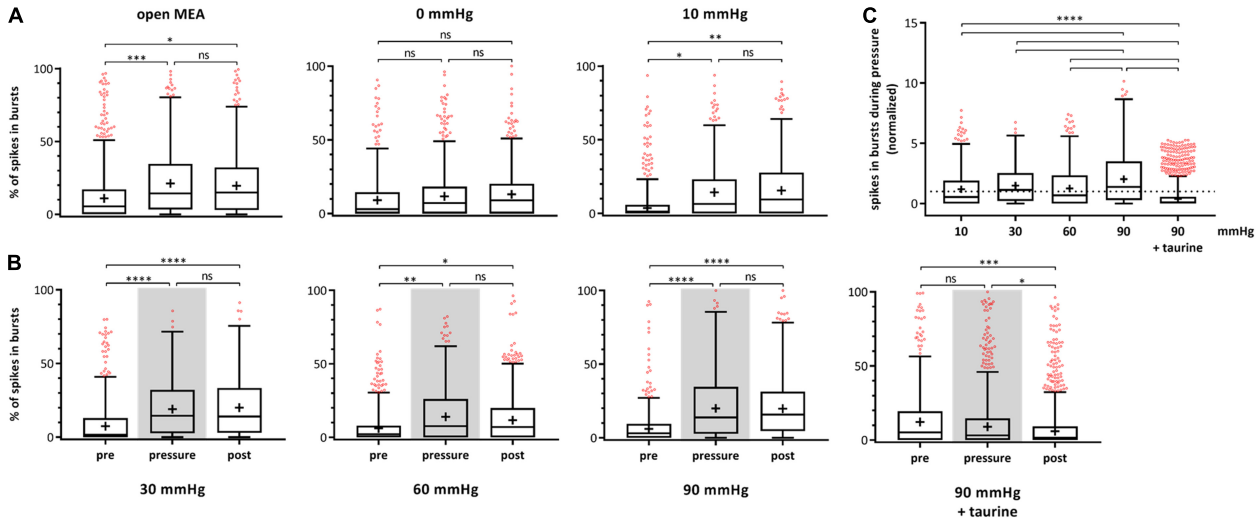

FIGURE 4 | Bursting behavior of RGCs under different pressure levels. The number of RGC spikes in bursts [%] before (pre), during (pressure), and after (post) pressure stress is shown. **(A)** The results of the control experiments without pressure lid (open MEA), 0 mmHg, and 10 mmHg, are presented. **(B)** The results of the test groups with 30, 60, 90 mmHg, and 90 mmHg + taurine (1 mM) are presented. **(C)** Summary of the normalized number of spikes in bursts during pressure is shown. The number of spikes in bursts before pressure (pre) was set to 1. Data are presented as box and whisker (min to max) plots. Outliers calculated by ROUT (Q = 0.1%) are shown as red circles. Mean values of the cleaned data are shown as + . Significant values are indicated by asterisks. Not significant values are labeled with ns in panels **(A,B)** and not labeled in panel **(C)**. One-way ANOVA with *post hoc* Tukey's test was performed with GraphPad Prism Software version 7. **(A)** $F(2, 1946) = 7.173$, $p = 0.0008$; $F(2, 847) = 0.1714$, $p = 0.8425$; $F(2, 939) = 5.471$, $p = 0.0043$; **(B)** $F(2, 1370) = 18.86$, $p < 0.0001$; $F(2, 1495) = 6.209$, $p = 0.0021$; $F(2, 1432) = 34.8$, $p < 0.0001$; $F(2, 1551) = 8.43$, $p = 0.0002$; **(C)** $F(4, 2885) = 57.32$, $p < 0.0001$. $n_{retinae}$ = 5/group, n_{cells} = 152–430/group, $n_{recordings}$ = 16/experiment.

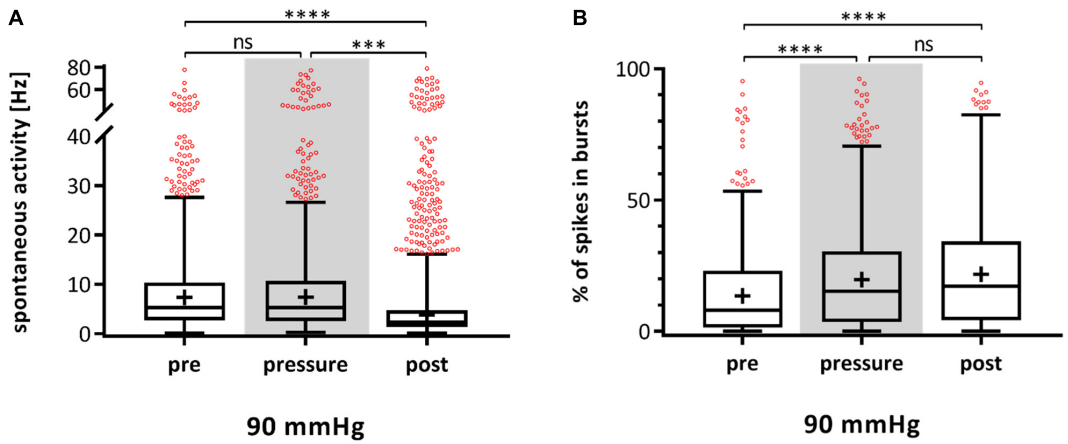

FIGURE 5 | Spontaneous activity and bursting behavior of RGCs in dark adapted retinae under 90 mmHg. The spontaneous firing frequency [Hz] **(A)** and the number of RGC spikes in bursts [%] **(B)** before (pre), during (pressure), and after (post) pressure stress of 90 mmHg is shown. The MEA experiments were carried out with dark adapted retinae under dim red light. Data are presented as box and whisker (min to max) plots. Outliers calculated by ROUT (Q = 0.1%) are shown as red circles. Mean values of the cleaned data are shown as + . Significant values are indicated by asterisks. Not significant values are labeled with ns. One-way ANOVA with *post hoc* Tukey's test was performed with GraphPad Prism Software version 7. **(A)** $F(2, 1922) = 12.79$, $p < 0.0001$; **(B)** $F(2, 1922) = 14.5$, $p < 0.0001$. $n_{retinae}$ = 5, n_{cells} = 262, $n_{recordings}$ = 90 **(A)**, 70 **(B)**.

According to their light response, the recorded RGCs were roughly sorted into three categories: ON, ON-OFF, and OFF. Characteristic examples of spike trains during light stimulation for the three categories are shown in **Figure 6A**. However, the different RGC types were not distributed equally. Excluding the uncategorized responses (18%), the vast majority of RGC light responses were categorized as ON with 80.25% (**Figure 6B**). ON-OFF and OFF responses were identified in equal parts (9.88% ON-OFF, 9.88% OFF). The ON cells revealed a significant increase in bursts of 47% during increased pressure and the incidence stayed at a high level after pressure stress (pre: 15.48 ± 15.04%, pressure: 22.78 ± 17.47%, post: 22.10 ± 16.60%) (**Figure 6C**). ON-OFF cells also showed an increase in bursts during and after pressure stress (pre: 4.53 ± 4.92%, pressure:

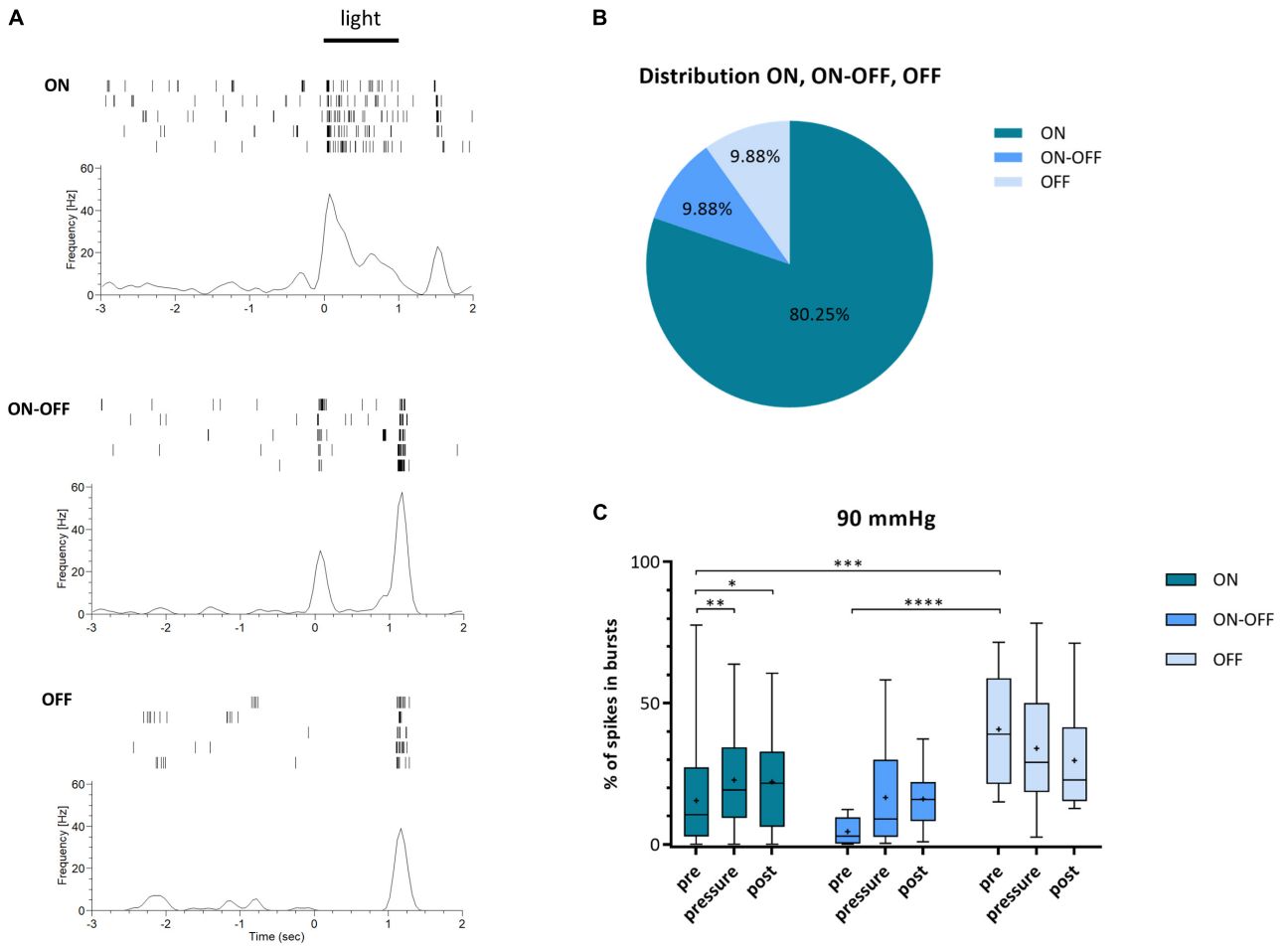

FIGURE 6 | Classification of RGCs into ON, ON-OFF, and OFF cells and their type specific bursting behavior under 90 mmHg. RGCs were categorized according to their response to light stimulation into the three categories ON, ON-OFF, and OFF. **(A)** Characteristic examples of ON-, ON-OFF-, and OFF responses of RGCs after light stimulation (full-field, 1 s, 160 lm) are shown. **(B)** The distribution of the three RGC categories ON (dark blue), ON-OFF (blue), and OFF (light blue) is presented. Uncategorized cells are not included. **(C)** The number of spikes in bursts [%] before (pre), during (pressure), and after (post) pressure stress of 90 mmHg for ON (dark blue), ON-OFF (blue), and OFF (light blue) RGCs is shown. Data are presented as box and whisker (min to max) plot. Mean values are shown as + . Significant values are indicated by asterisks. Two-way ANOVA with *post hoc* Tukey's test was performed with GraphPad Prism Software version 7. **(C)** $F(4, 156) = 2.12$, $p = 0.0809$. $n_{retinae} = 5$, $n_{cells} = 83$.

16.55 ± 20.18%, post: 16.08 ± 11.00%). Overall, the number of spikes in bursts increased by 265% under pressure. OFF cells, however, did not show an increase in bursts during and after pressure stress: under 90 mmHg, the number of spikes in bursts slightly decreased by 17% from 40.75 ± 20.58% (pre) to 33.96 ± 23.73% (pressure) and further to 29.66 ± 19.76% (post).

To investigate the origin of bursts during increased pressure, MEA experiments with 90 mmHg in addition of the glutamate receptor blockers DL-AP5 and CNQX were performed. The blockage of the glutamatergic input resulted in lesser fluctuations in the local field potentials (LFPs) and lead to a flat baseline (data not shown). The incidence of bursts during pre-, pressure-, and post-phase is presented in **Figure 7**. Under 90 mmHg, the number of spikes in bursts significantly increased by 51% from 13.24 ± 21.59% (pre) to 19.94 ± 24.95% (pressure) and stayed at a high level after pressure (post: 18.43 ± 24.93%).

Live/Dead Staining

Retinae were live/dead double stained to investigate the survival rate of the cells under pressure stress. The PI staining was successful throughout the tissue. FDA, however, mainly stained the blood vessels, nerve fiber layer (NFL), and only single cells (**Figures 8A,B**). Therefore, the number of dead cells could not be normalized to the number of living cells; instead, it was related to the mean number of dead cells of PI positive controls (**Figure 8C**). Here, a total number of 1,775.75 ± 180.00 cells for GCL, 4,925.00 ± 491.00 for INL, and 1,716.25 ± 1,003.00 for ONL was determined. Compared to literature values (Jeon et al., 1998), PI staining in the positive controls achieved an efficiency of 87%.

In the GCL, the number of dead cells changed from 1.23 ± 1.46% in the control group to 1.70 ± 1.52% under 90 mmHg and 3.24 ± 2.49% under 90 mmHg + taurine

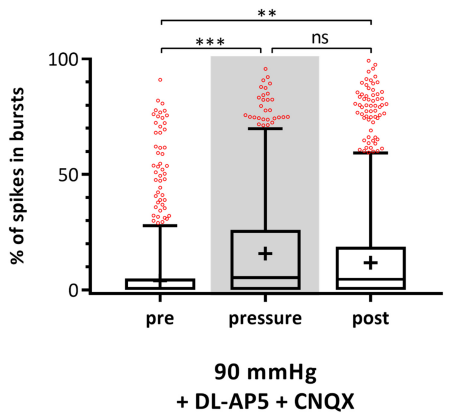

FIGURE 7 | Effect of glutamate receptor blockers on RGC bursting behavior under 90 mmHg. The number of spikes in bursts [%] before (pre), during (pressure), and after (post) pressure stress of 90 mmHg in addition of the glutamate receptor blockers DL-AP5 and CNQX is shown. Data are presented as box and whisker (min to max) plots. Outliers calculated by ROUT ($Q = 0.1\%$) are shown as red circles. Mean values of the cleaned data are shown as + . Significant values are indicated by asterisks. Not significant values are labeled with ns. One-way ANOVA with *post hoc* Tukey's test was performed with GraphPad Prism Software version 7. $F(2, 1365) = 6.814$, $p = 0.0011$. $n_{retinae} = 3$, $n_{cells} = 229$, $n_{recordings} = 48$.

(**Figure 8D**). In the INL, the number of dead cells was 0.55 ± 0.81% under 10 mmHg (control), 0.36 ± 0.47% under 90 mmHg, and 1.61 ± 1.65% under 90 mmHg + taurine. In the ONL, the number of dead cells changed from 0.41 ± 0.17% to 0.71 ± 0.36% under 90 mmHg and 0.52 ± 0.59% under 90 mmHg + taurine.

DISCUSSION

The retinal *ex vivo* pressure model established here serves as a glaucoma acute model for short-time increased IOP. The electrical RGC activity could be continuously measured before, during, and after pressure stress. Furthermore, the effect of taurine (1 mM) on the firing behavior was investigated. The experimental setup enabled a variation of hydrostatic pressure inside the chamber without influencing oxygen concentration or pH of the medium.

In all three experimental phases (pre, pressure, and post) the spontaneous activity as well as the response to given stimuli persisted. There was no pressure dependent effect on the firing frequency, nor on the response rate. There were changes over time; however, these changes occurred in all groups, so that they were rather time dependent than pressure related. The retinal functionality remained even under a highly increased pressure of 90 mmHg applied for 2 h. The unsorted MEA data (channel level) revealed an increase in RGC activity under pressure stress, whereas the sorted data (cell level) showed no increase in the RGCs' firing frequency. The increase in recorded activity at channel level was most likely a physical effect. Due to the increased hydrostatic pressure, the retina was pressed against the MEA electrodes so that the contact between tissue and electrodes improved and more cells could be recorded. This assumption was also supported by a slight increase in the spike amplitudes under pressure that subsided after lowering the pressure during the post-phase (data not shown). In general, RGC firing behavior was very diverse causing a high variability of the MEA recording results in all the groups including the controls. Therefore, many outliers have been identified and the gain of significant results was made more difficult. For example, spontaneous firing frequency decreased significantly in the 30 mmHg and the 60 mmHg group, but not significantly in the 90 mmHg group. However, the tendency was the same in all three groups.

Other studies presented impairment of retinal functionality in the form of changes in a- and b-waves in electroretinogram (ERG) recordings: pressure elevation was achieved by cannulation of rat eyes (Bui et al., 2005) or the microbead injection method in mouse eyes (Frankfort et al., 2013). The effect of increased pressure by microbead occlusion in mice was also analyzed using MEA recordings: after 3–7 weeks of mild increased IOP (15–24 mmHg), a slight light sensitivity loss was found (Pang et al., 2015) and after 2 weeks (+ 3 mmHg), decreased spontaneous RGC activity, altered interspike interval variance, and impaired contrast sensitivity were detected (Tao et al., 2019). Della Santina et al. (2013) showed that functional changes in RGCs preceded alterations in structure after IOP elevation (15 or 30 days) in microbead-injected mouse eyes. Ou et al. (2016) used MEA recordings to investigate αRGCs after transient laser-induced ocular hypertension (14 days) in CD-1 mice and found a decline in spontaneous activity in αOFF-transient RGCs. Although retinal ischemia is unlikely after photocoagulation, an effect on the ocular perfusion pressure cannot be ruled out completely. Furthermore, αRGCs only account for about four percent of murine RGCs (Sanes and Masland, 2015). These results do not contradict the findings of our study, but encourage further investigation of the susceptibility of different RGC types to pressure stress. Sabharwal et al. (2017) discovered a reduction of the receptive field after 6–7 weeks by whole-cell voltage clamp recordings. However, except for Bui et al. (2005) these studies investigated mild chronic IOP elevation rather than severe acute pressure increase. Furthermore, the *in vivo* pressure application made it difficult to differentiate between the effect of mechanical and hypoxic stress related to impaired blood flow. In our study, the investigation of RGC functionality included the analysis of responses to full-field light stimuli. In future studies, the external light source within the experimental setup can be adjusted or replaced and a multitude of different light stimuli can be tested in order to investigate, e.g., contrast sensitivity and receptive field properties that have been proven to be affected by pressure stress (Pang et al., 2015; Sabharwal et al., 2017; Tao et al., 2019).

Although the RGC functionality remained stable during pressure stress, the bursting behavior of the cells was strikingly different. The burst analysis revealed a significantly higher incidence of bursts under a highly increased pressure of 90 mmHg. Furthermore, the change in the RGCs' bursting behavior was not reversible. The number of spikes in bursts remained high after pressure stress. However, increased pressure did not seem to affect all RGC types equally. The MEA

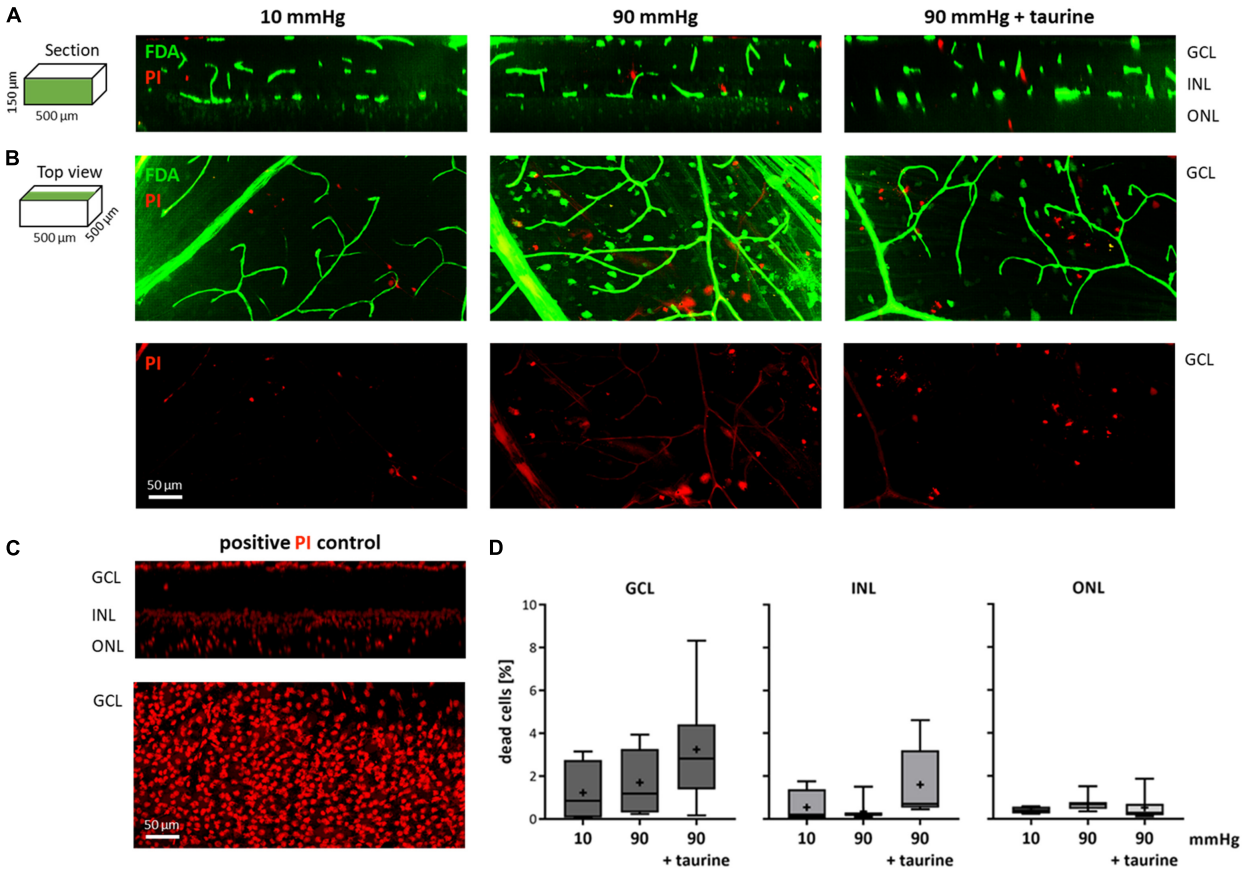

FIGURE 8 | Live/dead stained retinae after pressure stress analyzed *via* TPLSM. Retinae were live/dead double stained with FDA (green) and PI (red) and analyzed using a two photon microscope. Retinae that endured 10 mmHg (control), 90 mmHg, and 90 mmHg + taurine (1 mM) were analyzed. **(A)** Representative examples of sections through image stacks showing GCL, INL, and ONL are presented. **(B)** Representative examples of the top view of image stacks onto the GCL. **(C)** Representative section and top view of a retina after 4 h hypoxic stress (positive PI control). **(D)** Number of dead cells related to the number of dead cells in the positive PI control [%]. Data are presented as box and whisker (min to max) plots for GCL (dark gray), INL (gray), and ONL (light gray). Mean values are shown as + . No significant values were identified. One-way ANOVA with *post hoc* Tukey's test was performed with GraphPad Prism Software version 7. **(D)** $F(2, 17) = 1.863$, $p = 0.1855$; $F(2, 17) = 2.593$, $p = 0.1040$; $F(2, 17) = 0.6987$, $p = 0.5110$. $n_{retinae}$ = 4/group, n_{stacks} = 2/retina.

experiments with light stimulation revealed that the increase in bursts under pressure stress is carried by ON-, and ON-OFF RGCs, but not by OFF RGCs, suggesting that OFF RGCs are more resistant to pressure stress. Also the application of glutamate receptor antagonists DL-AP5 and CNQX resulted in an increase of bursts under pressure suggesting that the bursts were generated in the RGCs themselves and were independent of the glutamatergic input *via* AMPA/kainate and NMDA receptors.

Altered bursting behavior can also be seen in animal models of retinal degeneration. In *rd1* and *rd10* mice, bursts occur alongside of oscillatory LFPs affecting the retinal response properties after electrical stimulation (Jensen and Rizzo, 2008; Park et al., 2015). In healthy retinae, RGCs fire bursts in response to changes in the internal circuit or external visual stimuli. Bursts can improve the transmission of visual signals to the lateral geniculate nucleus and induce its synapse plasticity (Moore et al., 2011; Alitto et al., 2019). However, it still needs to be examined how the altered bursting behavior during and after high pressure stress affects the retinal functionality in the long term.

There was no significant change in the survival rate under pressure stress in none of the three investigated retinal layers. Overall, the highly increased pressure of 90 mmHg did not affect the retinal cells' survival, nor were any neuroprotective effects observed by the addition of 1 mM taurine, which was consistent with the outcome of the MEA recordings.

Other studies also proofed the resistance of retinal cells to sheer pressure stress. Osborne et al. (2015) showed that neither constant, nor fluctuating increased hydrostatic pressure (10–100 mmHg) caused significant changes in the survival rate of human RGCs in culture. The work of Aihara et al. (2014) showed that pressure increase (+ 15/30/90 mmHg) alone did not induce cell death in primary cultures of rat RGCs; however, the susceptibility to glutamate toxicity under pressure stress was increased. Consistent results were shown by histological examinations of rat retinae (Ishikawa et al., 2010): hydrostatic pressure of 50 mmHg and 75 mmHg induced axonal swelling in the NFL. The swelling was prevented by the addition of glutamate receptor antagonists. Therefore, the authors suggested that neural

degeneration under pressure stress is caused by an impaired glial glutamate metabolism.

For there was no significant impairment of the RGC survival rate under pressure stress, the investigation of the neuromodulating effect of taurine, rather than the neuroprotective effect, was of interest. The addition of taurine had no effect on the spontaneous RGC firing frequency, nor on the RGC response rate. However, the incidence of bursts during and after pressure stress was significantly altered by taurine: it caused a decrease of spikes in bursts during and after high pressure stress and therefore counteracted the effect of high pressure on the RGC bursting behavior.

A neuroprotective effect of taurine on RGCs has been shown in two different glaucomatous animal models (Froger et al., 2012, 2013). The survival rate of RGCs in DBA/2J mice and Long-Evans rats with episcleral vein occlusion was significantly increased under taurine supplementation. For the primary cells *in vitro*, taurine was added to the cell culture medium, and for the *in vivo* experiments, taurine was provided *via* the drinking water. In addition to these neuroprotective effects, the neuromodulating effects on RGCs shown here make taurine an interesting candidate for glaucoma treatment in the future.

Since hydrostatic pressure had only mild effects on the electrical activity of the retina and no effect on its survival rate, mechanosensitive receptors within the retinal tissue do not seem to play a role in reactions to acute pressure stress. However, using an *in vivo* rodent hypertension model, the transient receptor potential vanilloid 1 (TRPV1) channel was proven to be involved in RGC apoptosis induced by long pressure stress (+70 mmHg for 48 h), likely through the inflow of extracellular Ca^{2+} (Sappington et al., 2009). Furthermore, the expression of five of the six transient receptor potential (TRP) channel subfamilies and two piezo channels (Piezo1, Piezo2) was detected in the ONH (Choi et al., 2015).

Other models to investigate the effect of pressure stress on the retina are diverse and range from *in vitro* cell culture models to *in vivo* animal models with naturally or induced glaucomatous pathomechanisms. The effect of increased ocular pressure on retinal cells and explants in culture has been simulated with pressure chambers (Aihara et al., 2014; Osborne et al., 2015; Ishikawa et al., 2016) or hydrostatic pressure of liquid columns (Ishikawa et al., 2010). Elevated IOP *in vivo* has been induced *via* cannulation (Bui et al., 2005; Wang et al., 2021), microbead injection into the anterior chamber occluding the outflow of aqueous humor (Sappington et al., 2010; Frankfort et al., 2013; Pang et al., 2015; Park et al., 2019), hyaluronic acid (Moreno et al., 2005) or hypertonic saline injection (Kipfer-Kauer et al., 2010), and vein cauterization/photocoagulation (Garcia-Valenzuela et al., 1995; Ji et al., 2005; Pang et al., 2015). The optic nerve crush is another common glaucoma model, but it leads to ONH atrophy independent of the IOP level (Levkovitch-Verbin et al., 2000; Choi et al., 2015; Cameron et al., 2020). Apart from the cannulation method, by which the IOP can be adjusted reliably by the height of the liquid column, all other *in vivo* models fail to induce defined pressure levels and cause high rejection rates of animals when target pressure levels are not met. Moreover, measured effects can never be definitely attributed to the pressure stress alone. Although the influence of elevated IOP on blood flow is often avoided by checking retinal blanching or measuring the blood pressure, an impairment cannot be ruled out completely. These problems are also present in the DBA/2J mouse model (Anderson et al., 2006; Inman et al., 2006; Williams et al., 2013). The limitations of the *in vivo* models seem to be overcome in the *in vitro* models mentioned above; however, most of the studies have focused on histological and molecular investigations of the retina after pressure application rather than on the functionality.

The MEA-based pressure model presented here enables the analysis of the retinal functionality not only after, but also before and during pressure application. Experimental conditions can be precisely adjusted and the functional electrical activity of the retina can be recorded in real time. Furthermore, the effect of neuroprotective agents can easily be examined. However, the artificial conditions during MEA recordings limit the duration of an experiment to several hours. Therefore, the setup serves more as an acute model imitating conditions of glaucomatous attack rather than chronical IOP elevation.

Although high IOP is considered the main risk factor in glaucoma, we showed that the sheer mechanical stress of pressure does not seem to affect the retinal functionality in the acute model. In contrast, we showed that hypoxic stress has a dramatic effect on the RGCs' electrical activity and their survival rate (Ingensiep et al., 2021). Hypoxia can be induced *in vivo* by impaired blood flow under high IOP (Andreeva et al., 2014; Wiemann et al., 2021). The findings of our work help to better evaluate and understand the role of pressure stress in glaucoma next to other stressors, such as hypoxia.

DATA AVAILABILITY STATEMENT

The raw data supporting the conclusions of this article will be made available by the authors, without undue reservation.

ETHICS STATEMENT

The animal study was reviewed and approved by Institute of Laboratory Animal Science (Faculty of Medicine, RWTH Aachen University).

AUTHOR CONTRIBUTIONS

CI, KS, PW, and SJ contributed to conception and design of the study. CI performed the experiments, performed the data analysis, and wrote the manuscript. KS, PW, and SJ revised and edited the manuscript. SJ was responsible for funding acquisition. All authors contributed to the article and approved the submitted version.

FUNDING

This work was supported by the START program (Faculty of Medicine, RWTH Aachen University, project 122/18).

ACKNOWLEDGMENTS

We would like to thank Axel Honné and the team of the scientific workshop (*Wissenschaftliche Werkstatt*, University Hospital RWTH Aachen) for their great collaboration and the manufacturing of the pressure lid. We would also like to thank Dr. Michael Vogt of the Two-Photon Imaging Facility for his expertise in TPLSM and Anne Freialdenhoven (Department of Ophthalmology, University Hospital RWTH Aachen) for excellent assistance in the laboratory. The results presented here are part of the doctoral thesis of Claudia Ingensiep.

REFERENCES

Aihara, M., Chen, Y., Uchida, S., Nakayama, M., and Araie, M. (2014). Hyperbaric pressure and increased susceptibility to glutamate toxicity in retinal ganglion cells in vitro. *Mol. Vis.* 20, 606–615.

Alitto, H., Rathbun, D. L., Vandeleest, J. J., Alexander, P. C., and Usrey, W. M. (2019). The Augmentation of Retinogeniculate Communication during Thalamic Burst Mode. *J. Neurosci.* 39, 5697–5710. doi: 10.1523/JNEUROSCI.2320-18.2019

Ames, A. III, and Nesbett, F. B. (1981). In vitro retina as an experimental model of the central nervous system. *J. Neurochem.* 37, 867–877. doi: 10.1111/j.1471-4159.1981.tb04473.x

Anderson, M. G., Libby, R. T., Mao, M., Cosma, I. M., Wilson, L. A., Smith, R. S., et al. (2006). Genetic context determines susceptibility to intraocular pressure elevation in a mouse pigmentary glaucoma. *BMC Biol.* 4:20. doi: 10.1186/1741-7007-4-20

Andreeva, K., Zhang, M., Fan, W., Li, X., Chen, Y., Rebolledo-Mendez, J. D., et al. (2014). Time-dependent Gene Profiling Indicates the Presence of Different Phases for Ischemia/Reperfusion Injury in Retina. *Ophthalmol. Eye Dis.* 6, 43–54. doi: 10.4137/OED.S17671

Biswas, S., Haselier, C., Mataruga, A., Thumann, G., Walter, P., and Muller, F. (2014). Pharmacological analysis of intrinsic neuronal oscillations in rd10 retina. *PLoS One* 9:e99075. doi: 10.1371/journal.pone.0099075

Bui, B. V., Edmunds, B., Cioffi, G. A., and Fortune, B. (2005). The gradient of retinal functional changes during acute intraocular pressure elevation. *Invest. Opthalmol. Vis. Sci.* 46:421. doi: 10.1167/iovs.04-0421

Cameron, E. G., Xia, X., Galvao, J., Ashouri, M., Kapiloff, M. S., and Goldberg, J. L. (2020). Optic nerve crush in mice to study retinal ganglion cell survival and regeneration. *Bio. Protoc.* 10:3559. doi: 10.21769/BioProtoc.3559

Chen, H., Li, J., Liu, J., Liu, L., Liu, N., and Song, Y. Z. (2009). Effects of prenatal taurine on mRNA expression of PKA CREB signal pathway and glial cell line derived neurotrophic factor in fetal rat brains of intrauterine growth restriction. *Zhongguo Dang Dai Er Ke Za Zhi* 11, 923–926.

Choi, H. J., Sun, D., and Jakobs, T. C. (2015). Astrocytes in the optic nerve head express putative mechanosensitive channels. *Mol. Vis.* 21, 749–766.

Della Santina, L., Inman, D. M., Lupien, C. B., Horner, P. J., and Wong, R. O. (2013). Differential progression of structural and functional alterations in distinct retinal ganglion cell types in a mouse model of glaucoma. *J. Neurosci.* 33, 17444–17457. doi: 10.1523/JNEUROSCI.5461-12.2013

El Idrissi, A. (2008). Taurine increases mitochondrial buffering of calcium: role in neuroprotection. *Amino. Acids* 34, 321–328. doi: 10.1007/s00726-006-0396-9

El-Sherbeny, A., Naggar, H., Miyauchi, S., Ola, M. S., Maddox, D. M., Martin, P. M., et al. (2004). Osmoregulation of taurine transporter function and expression in retinal pigment epithelial, ganglion, and muller cells. *Invest. Ophthalmol. Vis. Sci.* 45, 694–701. doi: 10.1167/iovs.03-0503

Frankfort, B. J., Kareem Khan, A., Tse, D. Y., Chung, I., Pang, J. J., Yang, Z., et al. (2013). Elevated intraocular pressure causes inner retinal dysfunction before cell loss in a mouse model of experimental glaucoma. *Invest. Ophthalmol. Vis. Sci.* 54, 762–770. doi: 10.1167/iovs.12-10581

Froger, N., Cadetti, L., Lorach, H., Martins, J., Bemelmans, A. P., Dubus, E., et al. (2012). Taurine provides neuroprotection against retinal ganglion cell degeneration. *PLoS One* 7:e42017. doi: 10.1371/journal.pone.0042017

Froger, N., Jammoul, F., Gaucher, D., Cadetti, L., Lorach, H., Degardin, J., et al. (2013). Taurine is a crucial factor to preserve retinal ganglion cell survival. *Adv. Exp. Med. Biol.* 775, 69–83. doi: 10.1007/978-1-4614-6130-2_6

Garcia-Valenzuela, E., Shareef, S., Walsh, J., and Sharma, S. C. (1995). Programmed cell death of retinal ganglion cells during experimental glaucoma. *Exp. Eye Res.* 61, 33–44.

Gross, R. L., Hensley, S. H., Gao, F., and Wu, S. M. (1999). Retinal ganglion cell dysfunction induced by hypoxia and glutamate: potential neuroprotective effects of β-Blockers. *Surv. Ophthalmol.* 43, 162–170. doi: 10.1016/s0039-6257(99)00054-5

Howard, D. R., and Sawyer, D. C. (1975). Electroretinography of acute hypoxic and increased intraocular pressure status in the dog. *Am. J. Vet. Res.* 36, 81–84.

Inatani, M., Iwao, K., Inoue, T., Awai, M., Muto, T., Koga, T., et al. (2008). Long-term relationship between intraocular pressure and visual field loss in primary open-angle glaucoma. *J. Glaucoma* 17, 275–279. doi: 10.1097/IJG.0b013e31815c3ab7

Ingensiep, C., Schaffrath, K., Denecke, B., Walter, P., and Johnen, S. (2021). A multielectrode array-based hypoxia model for the analysis of electrical activity in murine retinae. *J. Neurosci. Res.* 99, 2172–2187. doi: 10.1002/jnr.24899

Inman, D. M., Sappington, R. M., Horner, P. J., and Calkins, D. J. (2006). Quantitative correlation of optic nerve pathology with ocular pressure and corneal thickness in the DBA/2 mouse model of glaucoma. *Invest. Ophthalmol. Vis. Sci.* 47, 986–996. doi: 10.1167/iovs.05-0925

Ishikawa, M., Yoshitomi, T., Zorumski, C. F., and Izumi, Y. (2010). Effects of acutely elevated hydrostatic pressure in a rat ex vivo retinal preparation. *Invest. Ophthalmol. Vis. Sci.* 51, 6414–6423. doi: 10.1167/iovs.09-5127

Ishikawa, M., Yoshitomi, T., Zorumski, C. F., and Izumi, Y. (2016). 24(S)-Hydroxycholesterol protects the ex vivo rat retina from injury by elevated hydrostatic pressure. *Sci. Rep.* 6:33886. doi: 10.1038/srep33886

Janaky, M., Grosz, A., Toth, E., Benedek, K., and Benedek, G. (2007). Hypobaric hypoxia reduces the amplitude of oscillatory potentials in the human ERG. *Doc. Ophthalmol.* 114, 45–51. doi: 10.1007/s10633-006-9038-5

Jensen, R. J., and Rizzo, J. F. III (2008). Activation of retinal ganglion cells in wild-type and rd1 mice through electrical stimulation of the retinal neural network. *Vision Res.* 48, 1562–1568. doi: 10.1016/j.visres.2008.04.016

Jeon, C. J., Strettoi, E., and Masland, R. H. (1998). The major cell populations of the mouse retina. *J. Neurosci.* 18, 8936–8946. doi: 10.1523/JNEUROSCI.18-21-08936.1998

Ji, J., Chang, P., Pennesi, M. E., Yang, Z., Zhang, J., Li, D., et al. (2005). Effects of elevated intraocular pressure on mouse retinal ganglion cells. *Vision Res.* 45, 169–179. doi: 10.1016/j.visres.2004.08.008

Kergoat, H., Herard, M. E., and Lemay, M. (2006). RGC sensitivity to mild systemic hypoxia. *Invest. Ophthalmol. Vis. Sci.* 47, 5423–5427. doi: 10.1167/iovs.06-0602

Kim, C. Y., Kuehn, M. H., Anderson, M. G., and Kwon, Y. H. (2007). Intraocular pressure measurement in mice: a comparison between Goldmann and rebound tonometry. *Eye* 21, 1202–1209. doi: 10.1038/sj.eye.6702576

Kipfer-Kauer, A., McKinnon, S. J., Frueh, B. E., and Goldblum, D. (2010). Distribution of amyloid precursor protein and amyloid-beta in ocular hypertensive C57BL/6 mouse eyes. *Curr. Eye Res.* 35, 828–834. doi: 10.3109/02713683.2010.494240

Lei, Y., Overby, D. R., Boussommier-Calleja, A., Stamer, W. D., and Ethier, C. R. (2011). Outflow physiology of the mouse eye: pressure dependence and washout. *Invest. Ophthalmol. Vis. Sci.* 52, 1865–1871. doi: 10.1167/iovs.10-6019/-/DCSupplemental

Leske, M. C., Connell, A. M., Wu, S. Y., Hyman, L., and Schachat, A. P. (1997). Distribution of intraocular pressure. The Barbados Eye Study. *Arch. Ophthalmol.* 115, 1051–1057. doi: 10.1001/archopht.1997.01100160221012

Leske, M. C., Heijl, A., Hussein, M., Bengtsson, B., Hyman, L., Komaroff, E., et al. (2003). Factors for glaucoma progression and the effect of treatment: the early manifest glaucoma trial. *Arch. Ophthalmol.* 121, 48–56. doi: 10.1001/archopht.121.1.48

Levkovitch-Verbin, H., Harris-Cerruti, C., Groner, Y., Wheeler, L. A., Schwartz, M., and Yoles, E. (2000). RGC death in mice after optic nerve crush injury: oxidative stress and neuroprotection. *Invest. Ophthalmol. Vis. Sci.* 41, 4169–4174.

Louzada, P. R., Paula Lima, A. C., Mendonca-Silva, D. L., Noel, F., De Mello, F. G., and Ferreira, S. T. (2004). Taurine prevents the neurotoxicity of beta-amyloid and glutamate receptor agonists: activation of GABA receptors and possible implications for Alzheimer's disease and other neurological disorders. *FASEB J.* 18, 511–518. doi: 10.1096/fj.03-0739com

Macaione, S., Ruggeri, P., De Luca, F., and Tucci, G. (1974). Free amino acids in developing rat retina. *J. Neurochem.* 22, 887–891. doi: 10.1111/j.1471-4159.1974.tb04313.x

Moore, B. D., Kiley, C. W., Sun, C., and Usrey, W. M. (2011). Rapid plasticity of visual responses in the adult lateral geniculate nucleus. *Neuron* 71, 812–819. doi: 10.1016/j.neuron.2011.06.025

Moreno, M. C., Marcos, H. J., Oscar Croxatto, J., Sande, P. H., Campanelli, J., Jaliffa, C. O., et al. (2005). A new experimental model of glaucoma in rats through intracameral injections of hyaluronic acid. *Exp. Eye Res.* 81, 71–80. doi: 10.1016/j.exer.2005.01.008

Osborne, A., Aldarwesh, A., Rhodes, J. D., Broadway, D. C., Everitt, C., and Sanderson, J. (2015). Hydrostatic pressure does not cause detectable changes in survival of human retinal ganglion cells. *PLoS One* 10:e0115591. doi: 10.1371/journal.pone.0115591

Osborne, N. N., Casson, R. J., Wood, J. P., Chidlow, G., Graham, M., and Melena, J. (2004). Retinal ischemia: mechanisms of damage and potential therapeutic strategies. *Prog. Retin. Eye Res.* 23, 91–147. doi: 10.1016/j.preteyeres.2003.12.001

Ou, Y., Jo, R. E., Ullian, E. M., Wong, R. O., and Della Santina, L. (2016). Selective vulnerability of specific retinal ganglion cell types and synapses after transient ocular hypertension. *J. Neurosci.* 36, 9240–9252. doi: 10.1523/JNEUROSCI.0940-16.2016

Pang, J. J., Frankfort, B. J., Gross, R. L., and Wu, S. M. (2015). Elevated intraocular pressure decreases response sensitivity of inner retinal neurons in experimental glaucoma mice. *Proc. Natl. Acad. Sci. USA* 112, 2593–2598. doi: 10.1073/pnas.1419921112

Park, D. J., Senok, S. S., and Goo, Y. S. (2015). Degeneration stage-specific response pattern of retinal ganglion cell spikes in rd10 mouse retina. *Annu. Int. Conf. IEEE Eng. Med. Biol. Soc.* 2015, 3351–3354. doi: 10.1109/EMBC.2015.7319110

Park, Y. H., Snook, J. D., Ostrin, E. J., Kim, S., Chen, R., and Frankfort, B. J. (2019). Transcriptomic profiles of retinal ganglion cells are defined by the magnitude of intraocular pressure elevation in adult mice. *Sci. Rep.* 9:2594. doi: 10.1038/s41598-019-39141-1

Pasantes-Morales, H., and Ordonez, A. (1982). Taurine activation of a bicarbonate-dependent, ATP-supported calcium uptake in frog rod outer segments. *Neurochem. Res.* 7, 317–328. doi: 10.1007/BF00965643

Quigley, H. A. (1996). Number of people with glaucoma worldwide. *Br. J. Ophthalmol.* 80, 389–393. doi: 10.1136/bjo.80.5.389

Quigley, H. A., and Broman, A. T. (2006). The number of people with glaucoma worldwide in 2010 and 2020. *Br. J. Ophthalmol.* 90, 262–267. doi: 10.1136/bjo.2005.081224

Sabharwal, J., Seilheimer, R. L., Tao, X., Cowan, C. S., Frankfort, B. J., and Wu, S. M. (2017). Elevated IOP alters the space-time profiles in the center and surround of both ON and OFF RGCs in mouse. *Proc. Natl. Acad. Sci. USA* 114, 8859–8864. doi: 10.1073/pnas.1706994114

Sanes, J. R., and Masland, R. H. (2015). The types of retinal ganglion cells: current status and implications for neuronal classification. *Annu. Rev. Neurosci.* 38, 221–246. doi: 10.1146/annurev-neuro-071714-034120

Sappington, R. M., Carlson, B. J., Crish, S. D., and Calkins, D. J. (2010). The microbead occlusion model: a paradigm for induced ocular hypertension in rats and mice. *Invest. Ophthalmol. Vis. Sci.* 51, 207–216. doi: 10.1167/iovs.09-3947

Sappington, R. M., Sidorova, T., Long, D. J., and Calkins, D. J. (2009). TRPV1: contribution to retinal ganglion cell apoptosis and increased intracellular Ca2+ with exposure to hydrostatic pressure. *Invest. Ophthalmol. Vis. Sci.* 50, 717–728. doi: 10.1167/iovs.08-2321

Tan, J., Ye, X., Xu, Y., Wang, H., Sheng, M., and Wang, F. (2011). Acid-sensing ion channel 1a is involved in retinal ganglion cell death induced by hypoxia. *Mol. Vis.* 17, 3300–3308.

Tao, X., Sabharwal, J., Seilheimer, R. L., Wu, S. M., and Frankfort, B. J. (2019). Mild Intraocular pressure elevation in mice reveals distinct retinal ganglion cell functional thresholds and pressure-dependent properties. *J. Neurosci.* 39, 1881–1891. doi: 10.1523/JNEUROSCI.2085-18.2019

Tham, Y. C., Li, X., Wong, T. Y., Quigley, H. A., Aung, T., and Cheng, C. Y. (2014). Global prevalence of glaucoma and projections of glaucoma burden through 2040: a systematic review and meta-analysis. *Ophthalmology* 121, 2081–2090. doi: 10.1016/j.ophtha.2014.05.013

Wang, A. Y. M., Wong, V. H. Y., Lee, P. Y., Bui, B. V., Dudczig, S., Vessey, K. A., et al. (2021). Retinal ganglion cell dysfunction in mice following acute intraocular pressure is exacerbated by P2X7 receptor knockout. *Sci. Rep.* 11:4184. doi: 10.1038/s41598-021-83669-0

Wiemann, S., Yousf, A., Joachim, S. C., Peters, C., Mueller-Buehl, A. M., Wagner, N., et al. (2021). Knock-Out of Tenascin-C ameliorates ischemia-induced rod-photoreceptor degeneration and retinal dysfunction. *Front. Neurosci.* 15:642176. doi: 10.3389/fnins.2021.642176

Williams, P. A., Howell, G. R., Barbay, J. M., Braine, C. E., Sousa, G. L., John, S. W., et al. (2013). Retinal ganglion cell dendritic atrophy in DBA/2J glaucoma. *PLoS One* 8:e72282. doi: 10.1371/journal.pone.0072282

Winkler, B. S. (1981). Glycolytic and oxidative metabolism in relation to retinal function. *J. Gen. Physiol.* 77, 667–692. doi: 10.1085/jgp.77.6.667

Conflict of Interest: The authors declare that the research was conducted in the absence of any commercial or financial relationships that could be construed as a potential conflict of interest.

Publisher's Note: All claims expressed in this article are solely those of the authors and do not necessarily represent those of their affiliated organizations, or those of the publisher, the editors and the reviewers. Any product that may be evaluated in this article, or claim that may be made by its manufacturer, is not guaranteed or endorsed by the publisher.

Copyright © 2022 Ingensiep, Schaffrath, Walter and Johnen. This is an open-access article distributed under the terms of the Creative Commons Attribution License (CC BY). The use, distribution or reproduction in other forums is permitted, provided the original author(s) and the copyright owner(s) are credited and that the original publication in this journal is cited, in accordance with accepted academic practice. No use, distribution or reproduction is permitted which does not comply with these terms.

Advantages of publishing in Frontiers

OPEN ACCESS
Articles are free to read for greatest visibility and readership

FAST PUBLICATION
Around 90 days from submission to decision

HIGH QUALITY PEER-REVIEW
Rigorous, collaborative, and constructive peer-review

TRANSPARENT PEER-REVIEW
Editors and reviewers acknowledged by name on published articles

Frontiers
Avenue du Tribunal-Fédéral 34
1005 Lausanne | Switzerland

Visit us: www.frontiersin.org
Contact us: frontiersin.org/about/contact

REPRODUCIBILITY OF RESEARCH
Support open data and methods to enhance research reproducibility

DIGITAL PUBLISHING
Articles designed for optimal readership across devices

FOLLOW US
@frontiersin

IMPACT METRICS
Advanced article metrics track visibility across digital media

EXTENSIVE PROMOTION
Marketing and promotion of impactful research

LOOP RESEARCH NETWORK
Our network increases your article's readership